

Государственное образовательное учреждение  
высшего профессионального образования  
**«Томский государственный университет  
систем управления и радиоэлектроники»**

## **ТЕМАТИЧЕСКИЙ РЕФЕРАТИВНЫЙ СБОРНИК № 4-2/1**

**“Radar Remote Sensing”  
(«Дистанционное зондирование в радиолокации»)**

Публикации в трудах конференций

Источник: *Digital Library IEEEExplore*

Язык: *английский*

Глубина поиска: *2009 – 2011 гг.*

Дата формирования: *март 2011 г.*

Составитель: *В.И. Карнышев*

**Томск – 2011**

## ТЕМАТИЧЕСКИЙ РЕФЕРАТИВНЫЙ СБОРНИК № 4-2/1

### "Radar Remote Sensing"

#### («Дистанционное зондирование в радиолокации»)

Публикации в трудах конференций

#### "3D Multiple Maneuvering Targets Tracking in Active and Passive Radar Composite Guidance"

Active and passive radar composite guidance has been developed into a promising technology for target tracking in the electronic counter measurements (ECM) environment. Based on the technology, this paper investigates the problem of 3D multiple maneuvering targets tracking in the presence of sea clutter and jamming. We present a set of algorithms and establish a complete tracking system composed of measurement generation, data association, track initiation, track filtering, track management, track correlation and missile guidance. The simulation results indicate that the proposed algorithms can offer significant tracking and anti-jamming performance. The ideas and methods presented will also bear important significance for developing similar tracking systems in practice. [C1]

#### "Determination of LIDAR Points Cloud Filtering Parameters Using Distance Image"

Filtering of LIDAR points cloud is the key of obtaining precise DEM and it has become a studying focus. Determination of the filtering parameters affects the results directly. Within this paper, it is proposed that making use of pixel position and grey information in distance image to guide determination of the filtering parameters like the block size and the threshold value. And the method is validated by a kind of filtering using the determined parameters. In experiment it is shown that this method is available. [C2]

#### "POLARSAR Image Classification Based on Polarimetric Decomposition and Generalized Discriminant Analysis"

In this paper, a new classification scheme of fully polarimetric SAR images is proposed. This is based on the joint use of the Freeman-Durden decomposition and generalized discriminant analysis, a new method for Feature extraction. After getting the powers of the three scattering mechanism components through Freeman-Durden decomposition, the Feature extraction algorithm is introduced to well exploit the information available in the full polarimetric coherency matrix. The experimental results show that using this exploited information as new features of Fisher classification, can provides fine performance and good compactness. [C3]

#### "Fusion of High Resolution Satellite SAR and Optical Images"

This paper proposes a methodology for fusion of high resolution satellite SAR and Optical Panchromatic images. The main objective of fusion is to bring together complementary information contained in SAR and Optical images. The paper discusses and illustrates the issues involved in merging and choosing of suitable approaches to overcome them. The choosing of proper fusion method was explained from the point of nature of SAR and Optical wave interaction with the surface and objective of fusion. Two methods are proposed in this paper one is based on Fourier filtering and the other is based on multiresolution pyramid. The methodologies are applied on Cartosat-1 Panchromatic and TerraSAR-X images. The results and evaluation of the fusion based on entropy are presented. [C4]

#### "SAR Automatic Target Recognition Based on Classifiers Fusion"

Synthetic aperture radar automatic target recognition (SAR ATR) remains a challenging problem in military and civil field. Much work has been done to improve the performance of SAR ATR systems, both in feature extraction and classifier designing. This paper designs a multiple classifier system to solve the target classification problem in the area of SAR ATR. The proposed multiple classifier system trains three classifiers on different feature sets using three leaning algorithms. The outputs of the three classifiers are combined through evidence combination rule and discounting operation of Dempster-Shafer theory of evidence. Experiments on MSTAR public data set demonstrate that the proposed multiple classifier system significantly outperforms single classifiers and also excels adaptive boosting with RBF network as base learner. [C5]

### "High Resolution Radar Imaging Based on Compressed Sensing and Fast Bayesian Matching Pursuit"

Recently the rapid imaging based on the compressive sensing (CS) theory have attracted increasing interests, which simultaneously sampling and compressing signals or images. Radar imaging based CS is a potential way to obtain the high-resolution radar images without the constraint of Nyquist sampling rate. In this paper, we proposed a radar remote-sensing imaging approach based on compressive sensing and fast Bayesian matching pursuit (FBMP) recovery algorithm. Some experiments are taken and the results indicate that an accurate reconstruction of high-resolution radar images are obtained, with fewer measurements than most its counterparts (e.g., MP, OMP, StOMP, GPSR), but resulting in lower normalized MSE (NMSE). Although BCS obtains lower NMSE than FBMP, simultaneously with higher time complexity and sparsity. [C6]

### "Roof Detection in Lidar Data"

Lidar is widely used in many fields in recent years. Consequently, research of feature extraction in lidar data has intensified. Roof of building as a stable line feature is widely used in many fields. But there is yet not a good algorithm to finish this work. In this paper, we propose a new method to extract roof of building. The roof is modeled by a symmetric exponential roof edge model and the altitude image which generated from original lidar point cloud data is smoothed by a low-pass filter ISEF which is optimal for the symmetric exponential model. And then an algorithm for roof detection and a grouping and fitting method are proposed for line feature extraction. In order to depress the effect of the noise a fusion method is used for multi-images. In the end of the paper the method is proved useful through the lidar data comes from Calgary University in the end of the paper. [C7]

### "A Novel Polarimetric CFAR Target Detection Method"

A new polarimetric synthetic aperture radar (PolSAR) image CFAR target detector is proposed in this paper. By introducing the inverse Gamma distribution which is extensively used in modeling, the distribution of polarimetric matched filter (PMF) metric, denoted as  $P_{G0}$ , is derived on the product model; Furthermore, a fast and exact parameter estimation method of  $P_{G0}$  distribution is presented using the "second kind statistics" based on the Mellin transform; Finally the formula of the CFAR detection threshold is deduced, and the target detection using the proposed constant alarm rate (CFAR) detector is performed on the RADARSAT-2 PolSAR data. Experimental results demonstrate the great efficiency of the  $P_G$  distribution and the corresponding parameter estimation method in data fitting of areas with different degree of homogeneity. Moreover, the successive CFAR detector can successfully complete the automatic target detection with low false alarm rate and high detection rate in complex clutter environment where the homogeneity of terrain varies sharply. [C8]

### "Cooperative Synthetic Aperture Radar Image Segmentation Using Learning Sparse Representation Based Clustering Scheme"

Based on a recent proposed and popular sparse representation based classifier (SRC), in this paper we presented a novel Learning Sparse Representation based Clustering (LSRC) scheme for Synthetic Aperture Radar (SAR) segmentation. LSRC introduces the examples-based dictionary learning technology in SRC to find a dictionary that is adaptable to sparsely representing samples, which is liable to provide more accurate approximation of samples and subsequently achieve higher classification accuracy rate. Moreover, for the intrinsic supervised nature of LSRC, we adopt an unsupervised-clustering cooperative approach to provide training samples for LSRC, in which some "good" samples with higher membership degrees are selected from the clustering result of K-means algorithm. Some experiments are taken on segmentation of both the texture images and SAR images to investigate the performance of our proposed method, and the results prove its superiority to its counterparts. [C9]

### "Ship Detection after Removal of Ambiguities by Using PolSAR Images"

Ambiguities in SAR image are very common phenomena. For maritime applications, as the high intensities of the ambiguities in low radar backscatter background of sea environments, they can be mistaken as targets and cause false alarms in ship detection. Thus, through the analysis of polarimetric characteristics of ships and ambiguities, we propose a ship detection method which applies the eigenvalue to differentiating the ship target and azimuth ambiguities. One set of Cband JPL AIRSAR polarimetric data covered Kojimawan Bay, Japan has been chosen to evaluate the method that can effectively remove false alarms caused by the azimuth ambiguities. [C10]

### "Multitask Learning and Sparse Representation Based Super-Resolution Reconstruction of

### **"Synthetic Aperture Radar Images"**

In earth observing remote sensing fields, to recognize objects whose size approaches the limiting spatial resolution scale especially in Synthetic Aperture Radar (SAR) images, spatial resolution enhancement is usually required. In this paper, we proposed a multi-task learning and K-SVD based Superresolution image restoration method where K-SVD algorithm is employed to learn a redundant dictionary from some example image patches. In order to learn more accurate dictionary and reduce the complexity of dictionary learning, multitask learning concept is adopted to learn multiple dictionaries from the samples classified by K-means clustering. Some experiments are taken to investigate the performance of our proposed method, and the visual result and numerical guidelines both prove its superiority to some start-of-art SRIR methods. [C11]

### **"Adaptive RFI Suppression Algorithm Based on CEMD for SAR Data"**

This paper proposes a novel adaptive filtering method based on complex empirical mode decomposition (CEMD) for narrowband radio frequency interference (RFI) suppression applied to SAR. This method decomposes the RFI contaminated signal into a finite and often small number of Intrinsic Mode Function (IMF). The sum of some selected IMF components is taken as reference input of adaptive filter based on the characteristics of CEMD. Experiment results show that CEMD provides an effective way to obtain reference input. The proposed method can effectively subtract RFI component from the RFI contaminated signal, which is the primary input of the adaptive interference canceller. The point-target simulation is used to show the working principle of the proposed algorithm. Experimental results based on SAR real data are also shown to verify the proposed algorithm. [C12]

### **"Considerations in measuring vital signs cross section with Doppler radar"**

This paper describes the different considerations and challenges in measuring human cardiopulmonary radar cross section (RCS). The effect of clutter on the received signal is explained as well as the importance of preserving baseband dc content for valid readings. The center estimation algorithm with dc-cancellation is presented as a solution to restore dc content in the baseband signals and to exclude clutter contribution. The far-field conditions for the target range are revisited. By modeling the human torso as a half-cylinder and assuming unity reflectivity, the ratio of the RCS of the back of the torso with respect to the front is a function of wavelength. At 2.4 GHz and for a chest breadth of 30 cm, the back is expected to have an RCS that is 10 times that of the front while the RCS of the side is expected to be 4 times smaller. [C13]

### **"Mathematical analysis of interpolation step of Omega-K Algorithm for GPR and its implementation"**

GROUND-penetrating radar (GPR) is a mature remote sensing technique employed by engineers and scientists to obtain information from subsurface structures. These structures range from manmade objects, such as buried utilities, pavements, and unexploded ordnance, to geological formations. GPR data collection may be viewed as a mapping from the object space  $(x,y,z)$ , characterized by the object's spatial location and reflectivity, to the image space. The image space may be viewed in the space-time domain  $(x,y,t)$ , where the recorded scattered signals are displayed as a function of lateral position and time, or in the Omega-K domain  $(k_x,k_y,f)$ , where the two image sets are related by spatial-temporal Fourier transforms (FTs). Additionally, data may be recorded in the space-frequency domain  $(x,y,f)$ , as would be the case with a frequency-domain GPR. Fourier transforms allow easy conversions between the three image domains. [C14]

### **"Advantages of Airborne Lidar Technology in Power Line Asset Management"**

Airborne lidar technology is widely accepted among power utility companies as the most efficient tool for acquiring high-density and high-accuracy geo-referenced spatial data for various applications essential to power line asset management. This paper describes the typical workflow in lidar data collection. It also describes further application steps in the traditional engineering analysis required for power utilities management, including catenary modeling for thermal up-rating and vegetation encroachment analysis. It will be shown that lidar data can have exceptional precision and accuracy, enabling tight-tolerance engineering calculations for power line efficiency modeling. The paper will also briefly discuss change detection in transmission and distribution wires themselves, the underlying surface terrain and surrounding vegetation throughout the transmission corridor, and how lidar technology can help to address monitoring issues. Finally, the performance advantages of airborne laser terrain mapper (ALTM) systems are discussed in the context of applications related to power line asset management. [C15]

### **"A Novel Image Based Multi-Channel SAR-GMTI Algorithm"**

A novel three-channel SAR-GMTI algorithm based on the compressed image rather than the azimuth-

uncompressed raw data is proposed, which employs the classical DPCA technique and FrFT. The chirp characteristics of DPCA signal of the moving target in the SAR image domain is investigated for the first time in this paper. The scheme introduce FrFT to detect the moving target and estimate the position, velocity and radial acceleration, which lead to a more overall description on motion parameters than that of the majority of estimation algorithms. The excellent anti-noise ability of FrFT and the ideal clutter cancellation of DPCA technique results in great GMTI performance during a clutter-rich and low SNR environment. The simulation results indicate the efficiency and availability of the novel algorithm. [C16]

### "Airport Detection in SAR Image Based on Perceptual Organization"

Being one of the key transportation targets, airport detection is of great importance in military and civil applications. In this paper we propose a new method based on perceptual organization for airport detection in large SAR image. Since the runways are the most obvious characteristic of the airport, we first design belief functions for the runway features, which include collinearity, proximity, width and texture similarity. Then we propose to use the DS-evidence theory for the fusion of all belief functions, which can serve as a criterion to decide whether the two region units can be grouped. The candidate airport can be found by grouped region growing and detected by airport knowledge. Experimental results showed the effectiveness of the proposed approach for airport detection in large complex SAR image. [C17]

### "One micron laser technology advancements at GSFC"

In recent years, lasers have proven themselves to be invaluable to a variety of remote sensing applications. LIDAR techniques have been used to measure atmospheric aerosols and a variety of trace species, profile winds, and develop high resolution topographical maps. Often it would be of great advantage to make these measurements from an orbiting satellite. Unfortunately, the space environment is a challenging one for the high power lasers that would enable many LIDAR missions. Optical mounts must maintain precision alignment during and after launch. Outgassing materials in the vacuum of space lead to contamination of laser optics. Electronic components and optical materials must survive the space environment, including a vacuum atmosphere, thermal cycling, and radiation exposure. Laser designs must be lightweight, compact, and energy efficient. Many LIDAR applications require frequency conversion systems that have never been designed or tested for use in space. For the last seven or eight years the National Aeronautical and Space Administration (NASA) has undertaken a program specifically directed at addressing the durability and long term reliability issues that face space-borne lasers (The Laser Risk Reduction Program-LRRP). [C18]

### "On-ground tests and measurements of the Passive Advanced Unit Synthetic Aperture (PAU-SA)"

This paper presents the current state of the Passive Advanced Unit Synthetic Aperture's instrument (PAU-SA), its installation in the transportation truck, and the preliminary tests that have been performed to verify the instrument's status. [C19]

### "Coupling polarimetric L-Band insar and airborne lidar to characterize the geomorphological deformations in the piton de la fournaise volcano"

Until recently the coarse resolution of topographic mapping acted as a break on understanding the forces and processes that shape the Earth's surface. However, active surface deformation is an important indicator for the earth crustal dynamics since it is directly linked to earthquakes, volcanic eruptions and landslides. Both airborne laser scanning systems (LiDAR) and spaceborne interferometric synthetic aperture radars (InSAR) have provided valuable information for many case studies requiring highresolution characterization of ground movement in relatively large areas to assess the threat and impact of natural hazards especially for volcanic eruptions. The Piton de la Fournaise volcano (Reunion Island, France) is one of the most active basaltic shield volcanoes in the world. It has reached an anomalous activity level in the past years with a major eruption occurring in April 2007. In this paper, we explore the statistical, spatial and temporal behavior of the L-Band backscattering coefficient at both HH and HV polarizations over different type of terrains in the Fournaise lava field as a function of the LiDAR intensity data. The correlation will be used in setting empirical models to correct for the L-Band phase distortion on ash and rough surfaces in volcanic terrains. [C20]

### "Fractal based filtering of SAR images"

In this paper an innovative fractal based filtering for the analysis of SAR images of natural surfaces is presented. Its definition is based on a complete direct imaging model developed by the authors. The application of this innovative algorithm to SAR images makes it possible to obtain a complete map of the fractal dimension of the observed scene. Significant results obtained on actual SAR data are shown in the last section of the paper. [C21]

### "3D imaging of ice sheets"

We developed and deployed, in July 2005, a wideband 8-channel synthetic aperture radar (SAR) at Summit Camp, Greenland (72.5783° N and 38.4596° W). The radar was designed to map internal layers, measure topography, and generate backscatter maps—all in a single pass. Information on ice thickness, bed topography and basal conditions is essential to the refinement of glaciological models of ice sheets, which are used to predict ice-sheet behavior (especially mass balance) and to select deep ice-core sites. This work focuses on the use of fine-resolution 3D imaging algorithms for combining all 8-channels to form cross-track image slices through the ice. As compared with traditional 2D depth sounding, these 3D images allow for the characterization of bed topography with very fine resolution. They also allow for the generation of strip-map SAR images with absolute geocoding without ground control points (these are unavailable at the bottom of the ice), and the ability to analyze the ice-sheet volume in 3D. Topography, backscattering, and 3D ice volume results are illustrated here. [C22]

### "Performance status of the wave scatterometer SWIM"

SWIM is a Ku-band radar designed for wave directional spectrum estimation. This radar operates at six incidence angles (from 0° to 10°) with a complete azimuth scanning covering a swath of 180 km. The phase B (addressing preliminary design) of SWIM is currently under finalization. In, the preliminary design and associated performance analysis have been published taking into account the first results of Phase B design. This paper is focused on the last performance assessment of this phase B for all the measurements performed by the SWIM instrument. [C23]

### "Robust estimation of pasture biomass using dual-polarisation TerraSAR-X imagery"

The efficient management of pasture is a key driver of profitability for New Zealand's pastoral dairy and meat industries. In this paper, we report results from a study that tests the viability of using short-wavelength imaging radar to estimate pasture biomass. We use images from the TerraSAR-X satellite, comparing the HH & HV and VV&HV dual-polarisation combinations. Several linear models have been tested for field-measured pasture biomass. The best model is a linear regression using backscatter from the HH&HV combination, resulting in a residual standard error of 317 kg/ha. This standard error is 61% less than the standard error for the VV&HV combination (511 kg/ha), which clearly suggests adopting the HH&HV model. A model for prediction of the pasture biomass rank percentile is somewhat less convincing than the model for the pasture biomass itself. Finally, a repeated measures analysis for the HH&HV pair, suggests invariance of the regression for pasture biomass over time, except for a possible outlier date 01 September 2008. [C24]

### "Physical optics-based method to compute the radar signature of complex objects over a sea surface"

In this paper, a model based on asymptotic methods is proposed in order to compute the scattered field from a complex maritime scene. The basic idea is to combine the geometrical optics and the physical optics technique. The sea surface is generated by using the Elfouhaily directional wave spectrum to obtain a realistic scene. Both the target and the sea surface are meshed with triangular patches in order to compute the scattered field. Simulated results are presented to validate this model through a simple configuration by comparisons with the method of moment. Then more complex scenes for different sea states and different kind of targets (PEC or inhomogeneous) are investigated. [C25]

### "Nasa's Laser Risk Reduction Program: A risk reduction approach for technology development"

The benefits of Earth Science (ES) laser instrumentation have been proven by decades of earth-science observations. Lasers allow remote sensing of earth-system variables such as sea elevation, atmospheric composition, wind profiles, cloud cover, ice mass, and vegetation canopy. Further, orbiting platforms provide a unique vantage point that allows laser measurements on a global scale. NASA implemented the Laser Risk Reduction Program (LRRP) to identify and address capability-gap areas where new devices or processes could yield high-reliability mission-ready parts, and to develop components needed to advance the state-of-the-art of laser-based instrumentation. This paper discusses LRRP's approach and the evolution of the program's developments from inception to their planned infusion into NASA's missions. It is the first part of a three-paper presentation (Program goals and organization; 1<sup>st</sup> developments and results at the Goddard Space Flight Center (GSFC); and 2<sup>nd</sup> developments and results at Langley Research Center (LaRC)) that summarizes LRRP's goals, formulation approach, management organization, and final results. [C26]

### "Synchronous retrieval of forest canopy cover by airborne LiDAR and optical remote sensing"

Forest canopy cover is retrieved Synchronous by the airborne LiDAR data and SPOT-5 HRG data, using the method of linear spectrum decomposition model combined with Li-Strahler geometric-optical model. First, the airborne LiDAR data is used to retrieve forest parameters and then the proportion of pixel not covered by crown or shadow K<sub>gof</sub> each pixel in the sample was calculated using Li-Strahler geometric-optical model, while the linear spectrum decomposition model is used to extract the proportion of pixel not covered by crown or shadow K<sub>gof</sub> each pixel in the whole imagery. [C27]

### "Next generation of multi beam rotating antenna on SWIM scatterometer"

In the frame of the development of the instrument SWIM (Surface Waves Investigation and Monitoring) on the CFOSAT program (Chinese French Oceanographic Satellite) funded by CNES, Thales Alenia Space is currently developing a new multi beam rotating antenna in Ku Band. This single reflector offset antenna includes a rotating feed comprising 6 beams. The SWIM instrument is the first ever space radar concept that is mainly dedicated to the measurement of ocean waves directional spectra and surface wind velocities through multi-azimuth and multi-incidence observations. Orbiting on a 500 km sun-synchronous orbit, its multiple Ku-band (13,575 GHz) beams illuminating from nadir to 10° incidence and scanning the whole azimuth angles (0-360°) provide with a 180 km wide swath and a quasi global coverage of the planet between the latitude of -80 and 80°. Such a wide range of observations requiring high range resolution (about 20 m on the ground) have led to design an instrument whose architecture and technology goes beyond what has been done on altimeter and scatterometer systems. At antenna subsystem level, multi-azimuth and multi-incidence observations requirements have led to design an ambitious antenna subsystem that rotates at 6 rotations per minute while transmitting RF signals towards 6 different beams in Transmit and Receive Modes. Thales Alenia Space started in January 2009 under CNES contract phase B studies on the design of this multi beam rotating antenna in order to contribute to the System Preliminary Design Review held successfully in January 2010. B Phase complementary activities are currently under progress to prepare the C/D Phase planned to start beginning of 2011. This paper aims at giving an overview of the SWIM antenna preliminary design and performances. [C28]

### "ESA Earth Observation educational tools contribution to the creation of awareness for World Heritage site conservation"

EO from space is a key tool to assess the effects of anthropogenic activities to our planet (e.g. deforestation, urban growth). It can provide measurements supporting the process of sustainable development, or observations allowing the detection of changes in the surface of our planet related to climate change. UNESCO and ESA have launched a call to all national and international space agencies, space research institutions and universities to make use of space technologies in order to assist developing countries in the monitoring of the World Heritage sites. ESA and UNESCO are also covering associated educational aspects by using all the results of the projects under implementation as educational material to support UNESCO's 'UN decade for education and sustainable development', within a common and joint strategy of education, targeting schools, universities and young professionals. This includes creating new tools for the creation of awareness and savoir-faire in the use of space technology for the conservation and preservation of the environment and for a sustainable development. Material derived from satellite images provided to decision makers is also being used to support teachers and school children from the surroundings of the World Heritage sites where the space partners of the 'Open Initiative' are working. In the frame of its educational activities for Earth Observation, ESA is creating particular modules oriented to UNESCO sites. All this material comes out of the different activities being implemented by partners of the ESA-UNESCO 'Open Initiative', in complete integration with the EDUSPACE programme of ESA, a platform and web-based tool for Earth Observation Education, in eight different languages, available for free to worldwide secondary schools teachers and students, aiming to provide schools with tools for teaching and learning. It offers an entry point to Earth Observation satellite data and software applications for training. The website is-- host to a multitude of didactical material inclusive high-resolution local and lower resolution global remote sensing satellite data in order to show students how to study the planet as a whole from space as well as the possibility of zooming into specific areas and natural features to investigate their behaviour over space and time. An image processing tool called LEOWorks (Learning Earth Observation), including a GIS, soon in open source, is made available for data analysis and image interpretation. New dedicated content, like case studies and projects dedicated to the monitoring of UNESCO archaeological sites and to sustainable development are presently under development. [C29]

### "A new global Snow Extent product based on ATSR-2 and AATSR"

The ESA project GlobSnow develops products and services for snow extent and snow water equivalent. The time series of Snow Extent (SE) products will cover the whole seasonally snow-covered Earth for the years 1995-2010 based on the optical sensors ERS-2 ATSR-2 and Envisat AATSR data. A laboratory processing

chain has been developed for testing and improving algorithms in an iterative process. The final version of the laboratory processing chain will function as a reference system for the implementation of an operational system for production of the full time series of products as well as near-real-time products produced on a daily basis. The first version of the SE product set spanning 15 years of the Northern Hemisphere is expected to be ready by the end of 2010 and will be made freely available. [C30]

#### **"The preliminary temporal analysis of ground deformations in the area of Dabrowski Coal Basin (south Poland)"**

In this work the preliminary temporal analysis of ground deformations in the area of Dabrowski Coal Basin was performed. In this region the intensive coal exploitation has been performed for about 200 years. The studied region covers the mining areas of seven coal mines. Moreover this area is crossed by many faults. In the described work the analysis concerned only the small, long lasting deformations that were detected using PSInSAR technique. The aim of this work was to analyze the changes in the deformations' trend between years 1992 and 2003 for each PS point. In order to perform this task the special algorithm was developed. It allows detecting maximum one (the most significant) trend change in the considered period of time. Performed analysis revealed that in the study area the changes of trend deformations occurred for about 40% of PS points. The spatial and temporal distribution of PS points with trend changes showed some regularity. This regularity may indicate the influence of coal exploitation on the values of small, long period deformations that were previously explained only by neotectonics movements. [C31]

#### **"Observational studies of atmospheric aerosols in the lower troposphere using multiple sensors"**

Atmospheric aerosols play a large role in the Earth's radiation budget, but their specific radiative forcing effects vary wildly depending upon species, altitude and geographic location. A suite of instruments has been developed and deployed at Montana State University in Bozeman for the purpose of conducting altitude-resolved atmospheric aerosol studies. [C32]

#### **"The BIOMASS mission-An ESA Earth Explorer candidate to measure the BIOMASS of the earth's forests"**

The European Space Agency (ESA) released a Call for Proposals for the next Earth Explorer Core Mission in March 2005, with the aim to select the 7th Earth Explorer (EE-7) mission for launch in the next decade. Twenty-four proposals were received and subject to scientific and technical assessment. Six candidate missions were selected and further investigated in the preliminary feasibility studies (Phase 0). One of these missions is BIOMASS, which has recently been selected to proceed to Phase-A. BIOMASS is a response to the urgent need for greatly improved mapping of global biomass and the lack of any current space systems capable of addressing this need. [C33]

#### **"Modeling lidar scene sparsity using compressive sensing"**

One of the major problems associated with LIDAR sensing is that significant amounts of data must be collected to obtain detailed topographical information about a region. Current efforts to solve this problem have focused on designing compression algorithms which operate on the collected data. These, however, require the collection of large amounts of data only to discard most of it in some transformed domain. Instead, compressive sensing has demonstrated that highly accurate signal reconstructions are achievable even when sampling below the Nyquist rate. Such sensing is clearly desirable for LIDAR range data compression if it can be achieved. One notes, however, that compressive sensing requires a priori knowledge of the sparsifying basis of the signal which is a major problem for LIDAR since that basis depends not only on the underlying scene complexity but also on the laser spot size and target distance. For these reasons, the goal of this research is to take the first steps in establishing a relationship between typical LIDAR scenes of varying complexity and the sparsity of the scene compressively sampled. [C34]

#### **"Metallic objects and oil spill detection with multi-polarization SAR"**

In this study, two innovative physically-based approaches have been developed to detect man-made metallic objects and oil slicks in polarimetric SAR data. They are based on the different sea surface scattering mechanisms expected with and without oil slicks and metallic objects. Experiments, accomplished over Single Look Complex (SLC) Level 1.1 quad-pol L-band ALOS PALSAR SAR data, demonstrate the effectiveness of the two approaches for oil slick and metallic target detection purposes and witness the capability of ALOS PALSAR data for such applications. [C35]

### "TerraSAR-X observations over the antarctic ice sheet"

An incoherent correlation approach is used to derive ice motion fields for outlet glaciers through the Transantarctic Mountains, Antarctica. High-resolution repeat-pass, left-looking-mode TerraSAR-X data from 2009 were analyzed. Detailed ice velocity patterns on the Nimrod glacier basin and Starshot glacier are presented.

[C36]

### "The snowscat ground-based polarimetric scatterometer: Calibration and initial measurements from Davos Switzerland"

The COld REgions Hydrology High-resolution Observatory (CoReH20) Mission proposes a dual frequency radar operating at 9.6 and 17 GHz utilizing VV and VH polarization [1]. By combining X and Ku-Band with both co and cross-polarization diversity it is possible to estimate the Snow Water Equivalent of dry snow. To support this proposed mission, ESA has sponsored the development of a ground-based coherent polarimetric scatterometer operating over the 9-18 GHz frequency range. ESA is supporting campaigns to acquire and process data using SnowScat for validation of Snow Water Equivalent (SWE) retrieval algorithms. [C37]

### "Infrared satellite precipitation estimate using waveletbased cloud classification and radar calibration"

We have developed a methodology to enhance an infrared-based high resolution rainfall retrieval algorithm by intelligently calibrating the rainfall estimates using space-based observations. Our approach involves the following four steps: 1) segmentation of infrared cloud images into patches; 2) feature extraction using a wavelet-based method; 3) clustering and classification of cloud patches; and 4) dynamic application of brightness temperature (Tb) and rain rate relationships, derived using satellite observations. The results show that using wavelet features along with other features increase the performance of rainfall estimate in terms of quantitative rain/no rain area estimates. In addition, using lightning data as a feature improves the estimates as well. [C38]

### "Atmospheric phase screen-estimation for PSInSAR applied to TerraSAR-X high resolution spotlight-data"

The PSInSAR technique, invented by Ferretti et. al. ten years ago, meanwhile has proven its capability for very precise measurement of surface deformations. To achieve this, the influence of the atmospheric phase screen (APS) has to be removed. We investigated the APS for two series of TerraSAR-X high resolution spotlight data of a scene in Bavaria. Our approach was to consider the APS as composed of a phase ramp, a part stratified with height and a turbulent component. We estimated the turbulent component via kriging. The variograms show for short distances a regime which is not visible for lower resolutions. In this paper we discuss the choice of appropriate variogram models with respect to our data. [C39]

### "Doppler effect and compensation in a Rotating Fanbeam Spaceborne Scatterometer"

Spaceborne Rotating Fanbeam Scatterometer, RFSCAT, has a wider continuous swath that can provide a large number of independent samples of Sigma0 for wind speed and direction retrieving. But the large swath and footprint result in a wideband Doppler frequency shift. For a low earth orbiting satellite, the maximum Doppler bandwidth between forward and backward echoes will be about 500 KHz. Even in a single echo of RFSCAT, the Doppler bandwidth is about 90 KHz, while in a pencil beam scatterometer the Doppler bandwidth is almost a single tone. A method of Doppler frequency compensation both on center frequency of transmitted pulses and signal processing section of the echoes are carried out and evaluated. [C40]

### "Potentials of a compact polarimetric SAR system"

The goal of this study is to show the potential of a compact-pol SAR system for vegetation applications. Compact-pol concept has been suggested to minimize the system design while maximize the information and is declined as the  $\pi/4$ ,  $\pi/2$  and hybrid modes. In this paper, the applications such as classification, Faraday rotation and soil moisture estimates are first reminded, then, biomass estimation from CP data is presented and a calibration procedure using external targets is proposed. Finally, the interferometry concept is added to assess the capabilities of a compact-pol system to retrieve vegetation height. [C41]

### "In-situ broadband soil measurements: Dielectric and magnetic properties"

This paper presents an in-situ method for measuring both electric and magnetic properties of Hawaiian volcanic soil for GPR applications in a broad frequency range from 50 MHz to 1GHz. For the in-situ probe, we combined two monopole antennas with parasitic elements into one piece to achieve reflection (S11) and transmission (S21)

measurements simultaneously. Finally, the in-situ probe has a shape of a multi-conductor TEM transmission line, which consists of five conducting rods, two ground plates and two coaxial feed connectors. In a typical measurement the in-situ probe is connected to a two ports vector network analyzer and system calibration is then performed to characterize the sample free device. The calibration is based on measurements of the S-parameters for sample free and sample loaded devices. A unique post processing algorithm has been developed to extract accurate constitutive parameters ( $\epsilon^*$   $\mu^*$ ) from the scattering parameters (S11, S21) of the soil probe, which will be discussed in this paper. The prototype in-situ soil probe and post processing algorithm were also tested by both numerical simulation and actual soils in volcanic red soil. The simulation results showed around 1 % of error over the operational frequencies between 100 MHz and 800 MHz. Actual measurement results conducted by the in-situ probe and developed algorithms were in very good agreement with those obtained by a laboratory method. Simulation and actual measurement data will be presented in this paper. [C42]

### "Building detection and height retrieval in urban areas in the framework of high resolution optical and SAR data fusion"

In this paper, we propose a symmetrized version of a semiautomatic processing chain, able to provide the simple 3D reconstruction of buildings in urban scenes, from high-resolution optical and SAR imagery. The new elaborated chain gives an equivalent part to the optical and SAR components, in order to fully exploit complementary information provided by proper building features in both images. First, the initial processing chain is reminded and completely illustrated on a studied scene on real data. Then, three points of improvements by process symmetrization are discussed: an augmentation of the detection rate in the footprint extraction step, an increase of the reliability attached to the estimated building heights and a joint improvement of the steps of building validation and qualification. It is shown that the appropriate combination of optical and SAR features, inside some processing steps, could give better results of reconstruction. [C43]

### "Remote sensing image synthesis"

For remote sensing data, the testing analysis tools is difficult since the ground-truth data are not available in many cases. To address this issue, a novel method for image synthesis is presented for use as a evaluation test-bed. Given the scale-dependent, non-stationary nature of remotely sensed data, a new modeling approach that combines a resolution-oriented hierarchical method with a regional label-oriented binary tree structure is introduced to synthesize such complex data. In this paper, we are proposing on first synthesizing a label field, which contains the complex structural characteristics, then synthesizing the texture based on the generated label field for a more accurate modeling. Experimental results using operational RADARSAT SAR sea-ice image data show that the proposed method is capable of modeling complex, nonstationary scale structures, thus making it well-suitable to produce reliable, realistic remote sensing imagery. [C44]

### "Estimation of building density using Terrasar-X-Data"

This study presents an approach towards the estimation of building density by utilizing the intensity data of the German space borne very high resolution SAR system TerraSAR-X. By using reference data we segmented a SAR scene of the city of Munich, Germany, on the scale of city blocks. Then we computed first order statistics and texture measures according to Haralick on the image objects. We used a random forests regression algorithm to establish the relationship between these features and the building density taken from reference data. The result is a promising coefficient of determination of 0.63. [C45]

### "RADARSAT-2 continuing system operations and performance"

This paper provides a status report for RADARSAT-2 system operations and performance now that two years of Routine Phase operations have been completed. Experience from the second year of operations is reviewed. System status, performance, and trends are described along with performance and achievements of the RADARSAT-2 operations functional groups. Normal operations now includes increased attention to orbital collision risk avoidance, and the RADARSAT-2 risk mitigation experience is summarized. In addition to meeting and maintaining specified performance requirements for the Routine Phase, the operations team has implemented a number of improvements to both the system and operations to provide enhanced performance. These include reduced tasking latency, enhanced beam modes, and further improved image quality. The improvements are described as part of the evolution of the mission capabilities along with some further planned enhancements. [C46]

### "Enhanced Cloud algorithm from collocated CALIPSO, CloudSat and MODIS global boundary layer lapse rate studies"

Coincident profile information from CALIPSO's lidar and CloudSat's radar offers a unique opportunity to map the vertical structure of clouds over the globe with accuracies never before realized. At Langley NASA, both CALIPSO and CloudSat are collocated with each MODIS 1-km pixel to create a new data set named C3M (Figure 1). A year (July 2006-June 2007) of C3M data is used to derive global lapse rate maps, as an enhancement to NASA Langley's CERES Cloud Property Retrieval System (CCPRS). The lapse rates are derived for boundary layer clouds using the the cloud-top temperature from Aqua MODIS level 1 data, skin temperature over ocean and surface temperature over land from the GMAO GEOS-4, and cloud-top height from CALIPSO. The derived global lapse rate maps are used to process a month of CERES-MODIS data to calculate cloud top heights, which are compared with CALIPSO cloud top height. The comparisons shows good agreement between CERES-MODIS and CALIPSO. [C47]

#### **"Oblique polarimetric SAR processor based on signal and interference subspace models"**

We develop a new SAR processor based on oblique projection. We take into account the scattering properties of the target and the interferences by using subspace models. To detect the target and to reject the interferences, we process images with the oblique projection of the received signal into the target subspace along the interference one. This new SAR processor is applied to realistic simulated data for FoPen (Foliage Penetration) application. [C48]

#### **"A Matchstick Model of microwave backscatter from a forest: A change of regime"**

In this paper we present a forest scattering scenario consisting of solely vertical stems. Stems are the primary volume stores of forests; this model therefore simplifies the forest make-up to represent these major scatterers. This model representation is known as the "Matchstick Model" and is used as a comparison to backscatter data resulting from the combination of macro-ecology with a numerical scattering model (RT2). The "Matchstick Model" provides SAR scattering trends based on equations for the Optical and Rayleigh scattering regimes and presents forest scattering as a combination of the two. Conclusions state that saturation is a consequence of basal area and thinning limitations and ultimately that backscatter is not directly proportional to stand volume, even in the simple case of a single layer of stems. [C49]

#### **"Multichannel Coherent Radar Depth Sounder for NASA Operation Ice Bridge"**

The Multichannel Coherent Radar Depth Sounder (MCoRDS) system was developed by the Center for Remote Sensing of Ice Sheets (CReSIS) to map the thickness of ice sheets. This radar system was used in Antarctica as one of the primary sensors for NASA's Operation Ice Bridge (OIB) during the fall of 2009. Compared to its predecessors, MCoRDS features several new capabilities which enabled it to successfully capture ice thickness measurements over multiple glaciers on an aerial platform. This paper will focus on the capabilities of MCoRDS and also provide a sample of the processed radar results. [C50]

#### **"Investigations into high resolution mapping of precipitation features utilizing the TRMM precipitation Radar"**

Precipitation measurements from the Tropical Rainfall Measuring Mission (TRMM) satellite's Precipitation Radar (PR) have been used to create high-resolution grids of precipitation features at a resolution of 0.05degrees. This grid size is on the order of a nominal PR instantaneous field of view (ifov) of 4.9km at nadir. Currently 12 years of data has been collected from the TRMM mission, resulting in sufficient sampling to begin these high-resolution studies. Precipitation fields at this resolution show detailed, local climatological features and comparisons with topographic data sets allow for the identification of potential problem areas in the retrieval algorithms. [C51]

#### **"DVB-T passive radar for vehicles detection in urban environment"**

Passive radar systems exploit non-cooperative transmitter to detect targets in areas of interest. Some of the main advantages of such systems with respect to conventional radars include low cost architectures, low energy requirements and potentially null probability of intercept. In this paper a low-cost solution for vehicles detection making use of passive radar concept is presented. A Software Defined Radio (SDR) solution and commercial antennas have been used to realize a DVB-T passive radar demonstrator. An analysis of the DVB-T signal is firstly presented together with a study of its capability as radar waveform. Afterwards an experimental setup is presented and analysed and finally some results of targets detection are shown. [C52]

#### **"Observation of a boat and its wake with a Dual-Beam along-track interferometric sar"**

The Dual-Beam Interferometer is an airborne instrument that combines two along-track interferometric synthetic aperture radars observing the surface below at different squints. This configuration allows retrieving vector

velocities of surface flows in a single aircraft pass. The system was designed by the University of Massachusetts and saw several deployments in the early 2000s. An imagery of a boat with a rather pronounced wake system captured during one of these flights is the subject of this paper. The velocity of the vessel is estimated based on the "train off the tracks" displacement in one of the looks. This estimate, which will be affected by uncertainty in target position due to smearing, is then used to remove unknown phase biases in the interferometric channels. Retrieved velocity variations are examined along cuts traversing the wake, with the focus on its narrow "turbulent" part. We find that the reconstructed velocities 150 m behind the boat are intuitively satisfying, but we are unable to fully account for the cross-wake component of velocity at 400 m behind the vessel. [C53]

#### "Wall-to-wall mapping of forest extent and change in Tasmania using ALOS PALSAR data"

Consistent estimation of carbon stocks at national level requires the integration of wall-to-wall, time-series satellite and in situ data of forest area, type and change. In this paper we demonstrate a consistent approach to the generation of wall-to-wall time-series mosaics using ALOS PALSAR data acquired over 2007 to 2009 for Tasmania, Australia. The project is part of a series of National Demonstrators initiated by the Group on Earth Observations (GEO) Forest Carbon Tracking (FCT) task that emphasize the contribution and operational use of satellite measurements for forest monitoring and national carbon accounting. Interoperability between optical and Synthetic Aperture Radar (SAR) derived forest measurements will also be demonstrated. The project will deliver a series of forest monitoring products and technical documentation, which will be made available as a guide to GEO member countries with a desire to develop their own national carbon accounting systems. [C54]

#### "Monitoring sea-ice and dry snow with GNSS reflections"

GPS reflected signals have become a source of opportunity for remote sensing of the Earth's surface. In this work, we present several capabilities of this technique in two different polar environments: Greenland and Antarctica. The first part is dedicated to the retrieval of sea-ice properties, giving emphasis to the study of the coherent phase for altimetric and roughness estimations, and polarimetric measurements for the determination of the ice salinity variation. The results show good agreement with a tide model and daily ice charts. On the second part, some preliminary results and analysis strategies to retrieve dry snow signatures are presented. [C55]

#### "AMSR and DFS synergy"

The Japan Aerospace Exploration Agency (JAXA), National Oceanic and Atmospheric Agency (NOAA), and Jet Propulsion Laboratory (JPL) are now proposing to launch the second satellite of the Global Change Observation Mission-W (GCOM-W2) carrying the Advanced Microwave Scanning Radiometer-3 (AMSR-3) together with Dual Frequency Scatterometer (DFS). This paper reviews sensor and science synergy of microwave scatterometers and radiometers. [C56]

#### "Logistic regression for detecting changes between databases and remote sensing images"

This paper studies database updating using optical and synthetic aperture radar images. Logistic regression is used to model the conditional probability of presence/absence of buildings given features extracted from the images. The logistic regression parameters are estimated using the maximum likelihood method. Binary hypothesis tests are then constructed from these estimates to detect changes between the optical/radar images and the existing database. The estimation and detection algorithms are evaluated using simulated and real data sets. [C57]

#### "Utilization of airborne multi-aspect InSAR data for the generation of urban ortho-images"

This paper addresses the generation of "true" RADAR ortho-images from highest resolution multi-aspect InSAR data. Due to the side-looking SAR imaging geometry, the well-known layover and shadowing effects prevent the production of truly rectified ortho-imagery from one image alone. Here, an approach for the reconstruction of Digital Surface Models of densely built inner city areas is proposed. Since in SAR interferometry each dataset pixel contains not only the interferometric phase needed for 3D reconstruction but also the corresponding amplitude or intensity value, respectively, the procedure can also be seen in the context of true ortho-rectification. [C58]

#### "Polarimetric sar image visualization and interpretation with covariance matrix invariants"

In this study we give short overview of polarimetric SAR image visualization with colors. By studying the color models and polarization visualization models we propose basic principles which should be followed when presenting polarimetric information in color. We show that for different polarimetric parameters, different color models should be used, and give guidelines for color model selection. We present also two visualization

schemes which are suitable for interpretation and browsing of large polarimetric SAR images. [C59]

### "Fully polarimetric ALOS PALSAR data applications for snow and ice studies"

In this study, the capability assessment of fully polarimetric L-band ALOS PALSAR data has been carried out for snow discrimination from other targets. Eigenvalue based polarization fraction value has been determined for assessing the capability of PALSAR data for snow discrimination. Radar snow index has been developed using polarization fraction and normalized third eigenvalue of coherency matrix. It has been found that radar snow index is more robust and simple to implement than supervised classification. [C60]

### "TanDEM-X commissioning phase status"

After the recent launch of the TanDEM-X satellite, the twin of TerraSAR-X, its demanding commissioning phase has started. On the one hand, it has to ensure the same monostatic operation performance as TerraSAR-X. On the other hand, the bistatic aspects have to be verified, which are essential for the acquisition of the global digital elevation model (DEM). This has to be done in a limited time period in order to keep the required nominal operation duration. This paper shows the summary of the commissioning phase activities and its running status. [C61]

### "Copyright"

The following topics are dealt with: SEAGRASS HABITATS; HIGH RESOLUTION DIFFERENTIAL SAR TOMOGRAPHY; FOREST COVER CHANGES; HYPERSPECTRAL IMAGERY CLASSIFICATION; REMOTE SENSING; GEOSPATIAL IMAGE ANALYSIS ALGORITHMS; SOIL MOISTURE; LAND USE CLASSIFICATION; WATER QUALITY; LAKE; RADIATIVE TRANSFER; CALIBRATION; VOLCANIC DEFORMATION; SEA SURFACE TEMPERATURE FRONT; and FLOOD MONITORING. [C62]

### "Physical-based models of speckle for high resolution SAR images"

In this paper we present a physical model for the description of the speckle in Synthetic Aperture Radar (SAR) images. The proposed model highlights the analytical dependence of the speckle characteristics on the surface roughness and the sensor parameters. The illuminated surface is represented using the fractal geometry. In addition, a SAR raw signal simulator able to generate SAR images whose speckle characteristics are coherent with the observed surface properties is presented. [C63]

### "Fetch limited sea scattering spectral model for HF-OTH skywave radar"

Sea Normalized RCS, and Doppler spectra have been revised for HF-OTH Clutter Modelling. The Hasselmann model is firstly introduced to predict the sea directional spectrum of fetch-limited sea and results have been compared with the Pierson-Moskowitz model used for large scale ocean remote sensing. Results show that the closed fetch-limited sea has lower NRCS compared with ocean for similar wind intensity and direction. For this reason RCS and Doppler spectra must be predicted taking into account of the fetch dimension. In future work we will generalize this interesting approach to fetch-limited wind, time-limited pulse, in order to show the waveform effect on Doppler spectrum. [C64]

### "Surface reference normalized radar cross section over land for the improvement of the TRMM PR algorithm"

The Tropical Rainfall Measuring Mission (TRMM) precipitation radar (PR) standard algorithm 2A21 produces the surface normalized radar cross section (NRCS) values under no rain conditions as functions of the incidence angle and surface physical parameters which affect surface scattering. These NRCS values are used as the reference values to calculate the path integrated attenuation (PIA) values in the surface reference technique (SRT) to perform the rain attenuation correction. This paper shows the relation between the land surface NRCS values and the three land surface physical parameters which are NDVI (Normalized Differential Vegetation Index), the surface roughness, and the soil moisture over the land for each of the incidence angles and tries to improve the methods to calculate surface reference NRCS values over the land. [C65]

### "Applications of polarimetric decomposition technology in a dried up lake evolution"

This paper presents fundamental reason to Lop Nur "Ear" feature based on polarimetric decomposition technology. Lop Nur is located at the east Tarim Basin in China, and in history, all the major rivers running in Tarim Basin converged to this lowest place. Lop Nur belongs to arid region, and satisfies penetration conditions for SAR signals. Through comparison between decomposed volume scattering contribution and sub-surface

salinity, it is found that subsurface properties (such as salinity) is the fundamental reason to "Ear" feature. And dynamic mechanism of geomorphology builds the relationship between surface and subsurface evolution processes, and indirectly unifies previous points on the reasons to formation of Lop Nur "Ear". Polarimetric technology is anticipated to be used to retrieve more information and to help extend applications in environment of arid region. [C66]

#### "Electromagnetic simulations of borehole radar for metal ore detection"

We perform finite difference time domain (FDTD) numerical simulation for metal ore detection by borehole radar. The ore-body model is adopted from a practical Ni-Cu-Pt ore body which is a magmatic deposit located in Sudbury, Canada. We design three boreholes along a cross-section perpendicular to the geological strike of the formation which is composed with overburden, ore zone, iron formation, peridotite, granite-gneiss, and sediments. We analyzed the simulated borehole radar profiles and found that some interfaces could be detected and some could not, also the ore zone is very absorptive to the wave. [C67]

#### "Development of spaceborne radar simulator by NICT and JAXA using JMA cloud-resolving model"

This study demonstrated preliminary results in diagnosis of the numerical model with reference to the TRMM/PR, examples of the GPM/DPR synthetic data, and application of the synthetic data to the algorithm development in the nonuniform beamfilling correction method. These were performed using a satellite radar simulation algorithm by the National Institute of Information and Communications Technology (NICT) and the Japan Aerospace Exploration Agency (JAXA) named as the Integrated Satellite Observation Simulator for Radar (ISOSIM-Radar) and a cloud-resolving model by the Japan Meteorological Agency (JMA-NHM). [C68]

#### "Reciprocal spectrum algorithm for radar imaging with frequency sampling waveform"

A radar imaging algorithm named reciprocal spectrum algorithm (RSA) is proposed in this paper to get higher resolution in azimuth direction with frequency sampling waveform. Theoretical analysis and simulation results show that the algorithm can give better performance than the tradition range Doppler algorithm (RDA) at the cost of peak value reduction at the object points in radar image. [C69]

#### "Scientific and engineering overview of the NASA Dual-Frequency Dual-Polarized Doppler Radar (D3R) system for GPM Ground Validation"

As an integral part of Global Precipitation Measurement (GPM) mission, Ground Validation (GV) program proposes to establish an independent global cross-validation process to characterize errors and quantify uncertainties in the precipitation measurements of the GPM program. A ground-based Dual-Frequency Dual-Polarized Doppler Radar (D3R) that will provide measurements at the two broadly separated frequencies (Ku- and Ka-band) is currently being developed to enable GPM ground validation, enhance understanding of the microphysical interpretation of precipitation and facilitate improvement of retrieval algorithms. The first generation D3R design will comprise of two separate co-aligned single-frequency antenna units mounted on a common pedestal with dual-frequency dual-polarized solid-state transmitter. This paper describes the salient features of this radar, the system concept and its engineering design challenges. [C70]

#### "A Study on Extraction of Man-Made Targets Using SVM Method from High Resolution PolInSAR Data"

This paper studies a man-made target extraction technique using SVM (Support Vector Machine) method from high resolution PolInSAR(polarimetric Interferometric synthetic aperture radar ) data. Fully polarimetric interferometric data in X band was acquired by a China-made airborne SAR system in January 2010, over the Linshui area in Hainan province. This study focuses on man-made targets extraction in Linshui area, where the ground survey allows the validation of the final extraction results. Different PolSAR (polarimetric SAR) and PolInSAR(polarimetric interferometric SAR) feature indicators, such as  $H/A/\alpha$ , based on the Pauli formalism or an optimal set of coherences are subsequently analyzed and the representatives of features are selected. In order to consider effect of man-made targets extraction with different feature indicators, the SVM method is investigated. The results based on PolSAR, PolInSAR and combined PolSAR and PolInSAR features are respectively compared, the best result is obtained via combining PolSAR and PolInSAR features. [C71]

#### "A New Approach on Topographic Feature Point Extraction of SAR Imagery"

The feature points extraction is a foundation for feature based SAR images registration, the quality of feature points directly determines the accuracy of registration. Current SAR feature points extraction algorithms are mainly shifted from optical image corresponding algorithms, accordingly feature points extracted with these

algorithms are not only impacted by the speckle noise, but also not able to describe topography features effectively, especially in the mountain regions, both disadvantages of these algorithms degrade seriously the accuracy of SAR image registration. In this paper, we present a new approach to extract those special feature points in the SAR imagery, the topographic feature points, with sub-pixel level through a novel topographic feature point detection algorithm which bases on the SAR imaging characteristics of the terrain. After the analysis of the geometric and scattering characteristics of topographic features in the SAR imagery, a topographic feature point detection algorithm is designed and implemented. During the procession, the SAR image is firstly filtered by a speckle suppression algorithm, then an improved Harris algorithm is used to extract feature points. Furthermore, non-topographic feature points extracted in former steps are removed by the topographic feature points detection algorithm proposed in this paper. Finally the topographic feature points which can reflect terrain characteristic are reserved. The experiment results indicate that the approach put forward in this paper is effective in extracting topographic feature points. [C72]

### "Multi-Temporal Polarimetric SAR and Optical Data Fusion for Land Cover Mapping in Southwest China"

Zhazuo area located in Guizhou Province of southwest China was selected as the test site of this study. Based on six polarimetric RADARSAT-2 images, this paper presents the analysis on polarimetric and temporal variation backscattering behavior of typical targets such as residential areas, farmlands, forests and water bodies within the test site. The multi-temporal polarimetric SAR data fusion, as well as SAR and optical data fusion was conducted to improve the land cover classification. The analysis shows that there are significant differences of polarimetric backscattering and temporal variation behavior among different land cover types. The fusion of the multi-temporal polarimetric SAR data highlights the significant reduction of speckle noises, better land cover discrimination and improved visual appearance of SAR image. The fusion of SAR images with QuickBird data efficiently improves the land cover classification. This study demonstrates that high-precision land cover thematic mapping with SAR data in combination with optical remote sensing image in cloudy and rainy areas is feasible. [C73]

### "Airborne LiDAR Strip Adjustment Based on Least Z-Difference Algorithm"

An airborne LiDAR system is an integration of GPS, INS and laserscanner. Because of errors of these instruments or sub-optimalities of the GPS/INS integration, points of neighboring laserscanner strips will usually show vertical and horizontal discrepancies. They can be corrected in a strip adjustment procedure. In this paper, least z-difference algorithm (LZD) is applied to the LiDAR strip adjustment. It estimates the transformation parameters between different strips, using the Generalized Gauss-Markoff model, minimizing the separation between the surfaces along the Z axis. Real data sets are used to validate the method. We study the need for using Gauss-Markoff model and the matching accuracy of our algorithm. Experimental results show that after correction the point clouds show much better alignment and the vertical matching error is less than 0.05m for idea data, while poor quality data the error is slightly larger. [C74]

### "Wind Field Retrieval over the Ocean by HH Polarization TerraSAR-X Data"

A new X-band wind field algorithm (XMOD) based on a linear approach is discussed in another paper to describe the relationship between normalized radar cross section (NRCS), wind speed, wind direction and incidence angle. But XMOD could only be applied with VV polarization SAR data. To be use the HH polarization SAR data, two C-band polarization ratio models were analysed and modified to X-band. To demonstrate the applicability of the two models, 10m height wind speeds were computed with XMOD from several VV/HH TerraSAR-X images and validated by QuikScat and DWD model results. In addition, the wind speeds were retrieved and compared to each other from the HH and VV polarization TerraSAR-X images of the same scene at the same time. [C75]

### "Identify Islands by Complex SAR Image"

The performance of interferometric synthetic aperture radar (INSAR)-based objects identifying in sea environment with clutter background is researched by many literatures, but most of them are mainly about detecting dynamic objects, such as ship targets. A new method is presented in this paper, which utilizes SAR image and point target analysis method to identify islands on sea surface in near and far range from mainland, especially for islets which can be confused with big ship or other objects such as floating, oil platform and so on. In the sea, either islands or islets is static objects, and other thing is dynamic characteristics, according to this characteristics, islands can be distinguished by spaceborne synthetic aperture radar (SAR) images joint point target analysis (PTA) method. The processing procedure includes three main phases: interferometric phase fringe, coherence evaluation, and sublook analysis. This method is applied with TerraSAR-X SSC image in

HONHKONG area. [C76]

### "A Methodology for Trees' Detection Using LiDAR Data in Urban Areas"

In this paper, we present an approach to detecting and locating trees using LiDAR point data. The motivation for this issue comes from urban planning and management, in which LiDAR data is used to obtain information of the cities. As for the echo characteristic of the LiDAR data is sensitive for the trees, we propose a three-step method for tree detection consisting of data- preprocessing, tree-points extraction and connectivity detection and merging, which make full use of the echo information for the LiDAR points to get the location of the trees in the urban areas. [C77]

### "Airborne LiDAR Data Strip Adjustment Based on Least Squares Matching and Independent Model"

As a new kind of remote sensing sensor, airborne LiDAR (Light detection and Ranging) has gained much attention by photogrammetry and remote sensing community. This paper focuses on the matching and strip adjustment of airborne LiDAR data. A multi-strip least squares matching (LSM) method was proposed, which adopts a combined feature called quasi-height including both the height and reflectance information. For strip adjustment which aims to eliminate the effect of geometric errors, an independent model was proposed. To validate the efficiency of the methods in this paper, a real project experiment is conducted and the discrepancies among different overlapping strips are obtained which are used for the strip adjustment. The adjustment results demonstrate the efficiency of this matching method and adjustment model. [C78]

### "Influence and Analysis of IMU Attitude Measurement Error on Laser Point Accuracy"

The emergence of airborne LIDAR system provides a new technical method for fast acquisition and processing of the spatial three-dimensional data. The limitations of traditional techniques are overcome by LIDRA, using of non-contact scanning data to obtain high-precision 3D data, it be able to work in all-weather, with a quickly scanning speed, strong real-time, all-digital processing and so on. The coordinates of laser pin-point can be obtained by calculating the spatial orientation vector of known points to the unknown point in LIDRA system. The composition of systems is very complex, so the laser point coordinates location will be affected by system error and accidental error of the LIADR system. The status quo of airborne laser scanning was briefly introduced in this paper. On the basis of airborne laser scanning system positioning principle, the impact of the pitch angle, roll angle, yaw angle and synthetic attitude error of IMU on laser point positioning accuracy was detailedly analyzed. After simulated calculations using IMU practical measurement accuracy presently, some useful conclusions were obtained, which have certain guiding significance for the understanding of airborne laser positioning accuracy and practical application. [C79]

### "Quantifying Human Indoor Activity Using a Software Radio-Based Radar"

Human activity quantification consists of computing a numerical or qualitative metric that indicates the amount of movement a person engaged in a given time interval. Such a metric has important applications in elderly care, wellness and healthcare given the strong empirical relation between a person's health and his or her activity level. This paper proposes and evaluates methods to quantify the level of human activity in an indoor environment using a continuous wave radar. An experimental evaluation is carried out using a flexible and low-cost software defined radar platform. Results showed a good correlation between the proposed metrics and the motion sequence performed by the subject suggesting that accurate activity quantification in indoor environments can be achieved using a few simple off-body sensors. [C80]

### "A Study on Removal of Radial Interference Echo with Weather Radar"

Electromagnetic disturbance (EMI) is an unpredictable event which often cause abnormal radar echo. EMI enables invariant radial interference echo (features such as sun-strobes) existing in certain directions in radar echo charts at many radar stations, the interference echo and the precipitation echo overlap in many regions. The paper key research has analyzed removal of interference echo which laps over precipitation echo, and an algorithm has been proposed. The radial interference echo could be distinguished from precipitation echo by analyzing their differences. According to the wave principle of superposition and the weather radar signal processing principle, the effective precipitation echo power was obtained by processing the echo power, thus disturbance was eliminated. The analyses results show that most of interference echo were detected and removed by the algorithm, especially in the overlap regions. It can eliminate radial interference echo and retain precipitation echo well at the same time. [C81]

### "A Novel Method for Linear Features Extraction from Raw LiDAR Point Clouds"

The paper proposes a novel method for automatic linear features extraction from raw LiDAR point clouds. Our method bases on the fact that facades of a building in urban area can reflect laser pulses since most of time the scanning angle of the laser scanner does not equal to zero degree. Experimental results show that our algorithm can extract linear features in urban area automatically with high accuracy. [C82]

### "A Speckle Reduction Method Based on Hyperspectral and SAR Image Fusion"

SAR images are affected by speckle noise which needs to be suppressed. An ideal speckle reduction method must smooth noise and preserve detail both. However, there is a tradeoff between such two goals for many methods. This paper proposes a speckle reduction method based on hyperspectral and SAR image fusion. It combines the coherent portions from MNF transformation for hyperspectral image and the SAR image. After radiance correction on the united data, the Correlation Simulating Analysis Model (CSAM) judge based SRSSHf filter is used to smooth the image, and the dark isolated points regarded as the remaining noise are eliminated. Experimental results on Radarsat-1 imagery show that the proposed method in this paper smoothes the noise and keeps the features both well. [C83]

### "Advances in vegetation management for power line corridor monitoring using aerial remote sensing techniques"

This paper presents a comprehensive discussion of vegetation management approaches in power line corridors based on aerial remote sensing techniques. We address three issues 1) strategies for risk management in power line corridors, 2) selection of suitable platforms and sensor suite for data collection and 3) the progress in automated data processing techniques for vegetation management. We present initial results from a series of experiments and, challenges and lessons learnt from our project. [C84]

### "Research on the Method of Airborne SAR Direct Geocoding Based on Correction of Systematic Error"

In this paper, a algorithm of airborne SAR Direct Geocoding based on correction of airborne SAR systematic error including slant range measurement error and time delay is put forward to improve the positioning precise, and POS/PPP technique is used to obtain radar phase center position data taking into account work efficiency. Many factors result in airborne SAR positioning accuracy, but main of them are slant range measurement error and time delay, if they couldn't be corrected precisely, the positioning accuracy won't be satisfactory. So this paper calculates the errors through some control points with P-band airborne SAR image of 2.5 meters resolution in mountain area of China (Xian, ShanXi), then we select eleven check points to make statistics. As a result, the horizontal accuracy is 12.6 meters, so the new algorithm on airborne SAR presented in this paper is efficient and practicable for airborne SAR Direct Geocoding in mountain area. [C85]

### "Application of ENVISAT ASAR Data to Rice Monitoring in Jiangsu Province, China"

Radar remote sensing technology has become an important method for stable and long-time rice monitoring for its capability to operate in all weather conditions. In this paper, the obtained main achievements on rice monitoring using ENVISAT ASAR data were reviewed and major results were summarized. The results showed that the multi-temporal and multi-polarization radar data has advantages in rice monitoring, especially in rice mapping and rice parameters estimation. A practical scheme for rice yield estimation was also summarized, showing prospect for radar data in rice production prediction. However, further studies are expected to develop a theoretical model for explaining the mechanism of radar interaction between rice plants and radar waves. [C86]

### "Coastal Radar WERA, a tool for Search and Rescue and oil spill management"

The HF-Coastal Radar "WERA" is a shore based remote sensing system to monitor ocean surface currents, waves and wind direction. This very reliable long range and high resolution monitoring system based on short radio wave radar technology. Due to the outstanding accuracy WERA can provide very valuable data to be assimilated into hydrographic models. In case of accidents in a distance of up to 200 km off the coast the real-time ocean surface current data can help Search and Rescue (SAR) operators. Presently, SAR tools are based on hydro-dynamical and atmospheric models to provide hindcast and forecast situations. Even if these oceanic numerical models are efficient to produce instantaneous maps of currents, the accuracy of derived Lagrangian trajectories often is not sufficient for search and rescue purposes. To improve these numerical models by means of realtime data it is essential that the quality of the assimilated data is very high and reliable. For this reason long term comparisons with buoy data for ground truthing and statistical analysis were carried out for more than two years. The resulting data availability (98,7 %) is outstanding and the data quality is as good as buoy data.

[C87]

### "Use of earth observation data and numerical modeling in the development of marine downstream services in Estonia"

The objective of the Global Monitoring for Environment and Security (GMES) is to provide, on a sustained basis, reliable and timely services related to environmental and security issues in support of public policy makers' needs. MyOcean is the implementation project of the GMES Marine Core Service (MCS), aiming at deploying the first concerted and integrated pan-European capacity for Ocean Monitoring and Forecasting ([www.myocean.eu.org](http://www.myocean.eu.org)). MyOcean develops upgraded European capabilities for reference marine information and provides a wide range of key ocean indicators. The MCS provides information to intermediate users who combine it with other forms of information and data to provide customized downstream services for end users. The end users range from wide public to special target groups. Downstream marine services in Estonia are built on in-situ real time and near real time measurements, satellite remote sensing imagery and numerical modeling. Two-day marine forecasts for the North-Eastern Baltic Sea are produced by 3D circulation model HIROMB-EST. The downstream service portfolio consists of following items. Real time sea level observations including history and two-day forecasts on 12 locations around the Estonian coast are available in the Internet. Sea surface temperature (SST) and salinity are complimented with near real time ferry-box observations on the cross-section between Tallinn and Helsinki. During cloud free sky SST charts are produced using MODIS (Moderate Resolution Imaging Spectroradiometer) imagery for the Gulf of Finland and Gulf of Riga. Illegal oil spills are detected from SAR imagery. The drift of the slick is simulated by Seatrack-Web and potential polluters are identified combining Seatrack Web and the Automatic Identification System (AIS). The monitoring of suspended particulate matter during harbor dredging is based on MODIS and MERIS (MEdium Resolution Imaging Spectrometer) data. The laboratory analyses of water samples are used for the-- calibration and validation of satellite products. The in situ measurements of vertical profiles of absorption and attenuation coefficients are used to determine the profiles of particle origin, concentration and size distribution. Operational ice extent monitoring using SAR data is rather widespread. Optical remote sensing imagery from MODIS and MERIS sensors complement SAR imagery. Ice concentration maps are produced using the histogram analysis of MODIS 250 m reflectance data. This data is used for model evaluation with the purpose to get reliable ice forecast from the HIROMB-EST model. Spectral optical remote sensing data from MERIS helps to identify different ice types. The determination of high spatial resolution marine and coastal wind from the Advanced Synthetic Aperture Radar (ASAR) is quite a novel application in the Estonian waters. Wind field data can be retrieved from ASAR C-band data and model results using CMOD algorithm. [C88]

### "Mosaic in g the ocean/terrestrial SRTM-DEM and making t he geomorphologic relief shading map"

Ocean and terra are the largest geomorphologic units on the earth, and there are essential differences between them. Hence, while we make the geomorphologic relief shading map, it is necessary to make the ocean/terrestrial geomorphologic relief shading map respectively. Then combining the ocean and terra map, we can get a whole geomorphologic map about the study area. However, the SRTM-DEM(Shuttle Radar Topography Mission-Digital Elevation Model) we get from USGS(United States Geological Survey) is clipped by SWBD(Shorelines and Water Bodies Database) coastline, so the coastline may be not accordance with the coastline we get about the study area. To solve this problem, we had to clip the DEM and patch the void data. Only in this way can we assure the DEM is accordance with the coastline. If the DEM is larger than the coastline, we can cut the spare parts by using the tool-extract by mask. However, if the DEM is smaller than the coastline, we have to patch the void data. This paper tries to find the best interpolating method to patch the void area according to the geomorphologic units. After that, we illustrate the processes of how to make the geomorphologic relief shading map by the software-Global Mapper. [C89]

### "Design and Implementation of Wireless FAEM System Based on the ZigBee and GPRS"

A wireless FAEM (facility agriculture environmental monitoring) system is presented by using ZigBee and GPRS technology, and the hardware realization and software flow are given too. By means of ZigBee wireless sensor module, the method can get together much information on soil humidity, Carbon dioxide, temperature, humidity and so on. Then such information is delivered to the remote control center through GPRS. Two kinds of internet technology can complement each other. During the latter part of the test, the wireless system can achieve the required operational performance: reliable data transmission as well as higher real-time system, and also reduce power consumption and overall system cost. [C90]

### "Monitoring Ground Subsidence in New Orleans with Persistent Scatterers Interferometry"

Ground subsidence and flooding are well publicized problems in the area of New Orleans, USA. Interferometric

Synthetic Aperture Radar (InSAR) has been applied by various research groups to study the ground subsidence in the area as an international effort supported by the Canadian Space Agency (CSA), National Aeronautics and Space Administration (NASA) and United States Geological Survey (USGS). This paper presents some of the work carried out at the Hong Kong Polytechnic University in contribution to this effort. 23 Radarsat-1 images acquired over a 2.5-year period from December 2004 to March 2007 are used in the PS-InSAR processing. Over 23,000 PS points are identified in the area based on both the amplitude and the coherence variations in the sequence of images. A network of PS points is then formed and used in the PS solution. The LAMBDA method is used to facilitate the determination of the phase integer ambiguities. The average subsidence rate along the direction of the radar illumination determined is 2.1 mm per annum. [C91]

### "Paddy Rice Identification Using Polarimetric SAR Data in Southern China"

Rice is one of the largest food grains in the world, providing food for more than one third of globe population. The radar remote sensing has been proved as an effective tool for rice mapping. With the emergence of spaceborne polarimetric SAR satellite, researches on polarization backscattering behavior and identification methods of paddy rice are of great significance and attract attention of remote sensing communities. Zhazuo Area located in Guizhou Province of southwest China was selected as the test site of this study. The RADARSAT-2 polarimetric data acquired at four dates were used to analyze the polarization backscattering behaviors and temporal variation characteristics of rice, and identification method for rice based on optimal polarization combination was established. This study shows that HH with HH/HV is the best polarization combination for rice identification under the adoption of linear polarization combination. [C92]

### "Soil Moisture Estimation over Jiangnan Plain Using ENVISAT ASAR Data"

Active microwave remote sensing techniques in the soil moisture inversion take advantages of their measurement on any weather conditions, strong capacity of penetrating the soil and their sensitivity to soil moisture content. This paper presents a method to estimate the soil moisture using ENVISAT ASAR data over Jiangnan plain in China. First of all, water-cloud model is used to eliminate the impact of the vegetation cover. Secondly a new combination roughness is introduced to describe the roughness of soil surface. Thirdly the effect of surface roughness is ruled out with the use of empirical model, and then the soil moisture inversion algorithm is achieved by programming. Finally, a contrast of the inversion result which is based on statistical method is made to discuss the logarithm relationship between backscattering coefficient and soil moisture. [C93]

### "The Application of Optimal Polarization Theory in Polarimetric SAR Change Detection"

In recent years, SAR is developing to multitemporal, multi-band, high resolution and full polarization. So the study of polarization SAR change detection technology is the trend of the SAR. The traditional change detection methods have disadvantages either low accuracy, serious noise or can't determine changes types. In order to improve the detection accuracy of polarization SAR data, a new change detection method is presented in this paper. Firstly, we use optimal polarization theory and optimization of polarimetric contrast enhancement (OPCE) theory to enhance change phenomenon respectively. Then, the probability relaxation iteration algorithm is made use of to extract change information automatically. This method can not only improve the accuracy, decrease noise, but also can determine the change type, it is a kind of ideal change detection method. [C94]

### "Subsidence Monitoring by Permanent Scatterers in InSAR: A Case Study of Yancheng City in Jiangsu"

The thesis adopts time series analysis of the SAR images in 10 phases up to 4-year span of Yancheng city area in Jiangsu province, by selecting the SAR image acquired on September 3, 2005 as the main image and the rest of the SAR images as vice images, interferometric processings are carried out and 9 interferograms consisting of the terrain and the deformation information are extracted. By dealing with the 9 difference interferograms with PS technology, terrain feature spatial distribution characteristics with stable electromagnetic reflecting characteristics are successfully ascertained. After temporal and spatial analysis of the 9 unwrapping interferograms, DEM error, atmospheric delay error in the main image and the vice image are obtained, thus the PS-point nonlinear distortion of the ground is extracted. Then by integrating analysis of ground deformation direction, reference datum, floor deformation positiveness and negativeness three aspects, the surface subsidence distributed situation in time and space of Yancheng city area are discovered. [C95]

### "The Application of Electric Field Data Combined with Other Observed Data in Lightning Warning"

The observation data of ground electric field is processed and theoretical simulation is combined with actual detection. The probability of lightning occurrence and warning time can be calculated due to the thunderstorm by choosing electric field intensity and variation of electric field as warning parameter. The process of a

thunderstorm will be analyzed by combining electric field data on net with lightning location data and radar echo data, which can effectively reflect the development of migration path of thunderstorm and monitor lightning activities within large area. It can provide some reference for extrapolating the migration path of lightning. [C96]

#### "The gauging-measuring system model with controllable retransmitter structure"

The model has been developed for the gauging-measuring mm-range system, which contains a retransmitter operating in near-zone remote sensing and has a controllable retransmitter structure. It has been shown that simulation allows getting the measurer signal parameters statistics for retransmitter parameters deviation from nominal values. [C97]

#### "Progress in the validation of dual-wavelength aerosol retrieval models via airborne high spectral resolution lidar data"

The Constrained Ratio Aerosol Model-fit (CRAM) technique is a method for making aerosol retrievals from dual-wavelength elastic scatter lidars which attempts to constrain the retrievals so as to be consistent with a number of aerosol models thought to characterize a variety of aerosol types observed around the world. The NASA Langley Research Center Airborne HSRL is an airborne high spectral resolution lidar capable of direct measurements of aerosol extinction and backscatter at 532 nm and having the capability for elastic backscatter measurements at 1064 nm. Aerosol measurements by HSRL during the TEXas Air Quality Survey/ Gulf of Mexico Atmospheric Composition and Climate Study (TEXAQS/GoMACCS) campaign are used to validate existing aerosol models critical to the application of CRAM, in particular to data from the Cloud-Aerosol Lidar with Orthogonal Polarization (CALIOP) lidar instrument on board the Cloud-Aerosol Lidar and Infrared Pathfinder Satellite Observations (CALIPSO) satellite. [C98]

#### "Focal plane approximation for near field interferometric radiometer imaging"

Applying synthetic aperture interferometric radiometer (SAIR) in near field imaging has been receiving great interest in the recent years. Because the traditional far-field Fourier imaging theory is not valid in near-field condition, developing the proper near-field imaging techniques is the major desirable objective of near field SAIR applications. This work is devoted to establish an effective near field imaging method still with traditional far-field plane antenna array. The discrete numerical inversion method with focal plane approximation is developed. The regularization method is also introduced to deal with the ill condition and measurement errors. [C99]

#### "Oil-slick observation using single look complex TerraSAR-X dual-polarized data"

In this study single look complex (SSC) TerraSAR-X dual-polarized data are firstly exploited for sea oil slick observation purposes. An electromagnetic model which, based on the Co-polarised Phase Difference between the HH and VV channels (CPD), allows describing the X-band sea surface scattering with and without surface slicks is proposed. Following this rationale, the polarimetric approach is firstly developed and applied to X-band Synthetic Aperture Radar (SAR) data in which both certified oil slicks and look-alikes are present. Experimental results demonstrate, for the first time, that X-band dual-polarimetric SAR data are suitable for sea oil slicks observation purposes and witness the paramount importance of the TerraSAR-X dual-polarimetric mode for such application. [C100]

#### "Simulation of Faraday rotation on longer wavelength spaceborne polarimetric InSAR"

The effects of Faraday rotation (FR) on longer wavelength (i.e. L or P-Band) spaceborne linearly full-polarized interferometry synthetic aperture radar (Pol-InSAR) processing are addressed. A model for linearly full-polarimetric InSAR data subject to Faraday rotation is investigated. Due to Faraday rotation, the received signal in each channel will be contaminated by backscattering signals from other polarimetric channels, which consequently reduce the coherence of the two single look complex SAR images received by the same channel for PolInSAR processing. The numerical simulation results are presented, which indicates that Faraday Rotation has significant impact on the coherence of the interferograms, especially for the spaceborne longer wavelength Pol-InSAR system. [C101]

#### "Prospects of new real-time radar applications for environmental remote sensing"

Remote sensing used to assess geophysical parameters on Earth is increasingly exploited and necessary for sustainable human life on Earth. A goal of using satellites to monitor changes and characteristics of Earth's surfaces is to further understanding of the planet and its systems, as well as understanding of how humans interact with and change the environment. Mostly underexploited, biomass detection via active radar remote sensing could provide a more thorough and in depth analysis of Earth. Upcoming NASA Earth monitoring

satellites cover a wide range of science products and applications, but little influence is put on the possibility of harnessing data from biomass reaction to radar pulse. In addition to the benefit of radar remote sensing in observing large areas at once, an added ability of transmitting detected frequencies in nearreal- time has potential to provide countless advantages. Direct Broadcast increases possibilities and practical uses for collected data. [C102]

#### "Simulation studies on data fusion algorithms for forest structure from lidar and SAR data"

The NASA's DESDynI mission will provide global systematic lidar point-sampling data and areal coverage of L-band SAR data with polarimetric capabilities for 3-D structural studies of vegetation. The combined use of lidar's direct sampling measurements and radar's global areal mapping capabilities creates a real opportunity to map global ecosystem structures and functions that link to carbon dynamics. However, the relationship of the lidar point-sample data and corresponding areal SAR data is yet to be established. In this study the data fusion algorithms for the estimation of parameters of forest structure from Lidar and SAR Data is investigated. The results show that SAR intensity data is sensitive to forest biomass which is less than 15kg/m<sup>2</sup>(or 150 ton/ha) and insensitive to the maximum forest height. Lidar data can be used to provide the information of forest height and the introduction of the information of forest height is helpful in the estimation of forest biomass. [C103]

#### "Case studies of automatic change detection using AVNIR-2 onboard ALOS"

This paper suggests a new automatic change detection approach using image-object-based contextual inference. The approach first detects changed areas, and then infers what happened there. The inference process uses knowledge based on a change detection process performed by humans. It enables flexible and intuitive description of the change detection process. In this paper, we describe the results of case studies on automatic change detection using the Advanced Visible and Near Infrared Radiometer type-2 (AVNIR-2) onboard the Advanced Land Observing Satellite (ALOS, nicknamed "Daichi"). [C104]

#### "Temporal snowpack density mapping using C-band multi-polarization ASAR data"

Radar remote sensing has great potential to determine the extent and properties of snow cover. Availability of spaceborne sensor dual-polarization C-band data of ENVISAT- ASAR can enhance the accuracy in measurement of snow physical parameters as compared to single polarization data measurement. This study shows the capability of C-band SAR data for estimating dry snow density over snow covered rugged terrain in Himalayan region. The snow density is an important parameter for the snow hydrology and avalanche forecasting related studies. An algorithm has been developed for estimating snow density, based on snow volume scattering and snow-ground scattering components. The radar backscattering coefficients of both HH and VV polarization and incidence angle are used as inputs in the algorithm to provide the snow dielectric constant which can be used to derive snow density using Looyenga's, semi empirical formula. Comparison was made between snow density estimated from algorithm using ENVISAT-ASAR HH and HH polarization data and the measured field value. The mean absolute error between estimated and measured snow density was found to be 24.38 kg/m<sup>3</sup>. [C105]

#### "A new polarization ratio model from C-Band RADARSAT-2 fine Quad-Pol imagery"

We propose two new analytical polarization ratio (PR) models based on the RADARSAT-2 Quad-Polarization (HH+VV+HV+VH) observations over the ocean. One is a function of incidence angle only and the other has additional dependence on wind speed. Comparisons are presented with theoretical and empirical PR models from the literature. The new PR model with wind speed and incidence angle dependence is shown to compare best with observed RADARSAT-2 data. An assessment of the PR model with only incidence angle dependence is given using CMOD algorithms and HH-polarized images. Results suggest that this PR model can accurately convert normalized radar cross sections (NRCS) in HH polarization to VV polarization and retrieve wind speeds from RADARSAT-1 or RADARSAT-2 HH polarization images. [C106]

#### "Lidar education at Georgia Tech"

The Georgia Tech Research Institute's atmospheric laser radar (lidar) team became involved in education projects starting in 2001, when we developed an eye safe lidar with undergraduate women at Agnes Scott College in Decatur, Georgia. We have initiated several other projects since that time, including short courses, an academic course at Georgia Tech, a lidar textbook, and a lidar system designed specifically for education. The lidar education program at GTRI is reviewed here with comments about future plans and prospects. [C107]

#### "Exploitation of the additive component of the polarimetric noise model for speckle filtering"

Ratio filters for speckle noise reduction in SAR imagery are recursive filters where the image structure is iteratively recovered from an initial oversmoothed image. We show that the MBPolSAR filter could be interpreted as a ratio filter applied to the off-diagonal terms of the covariance/coherency matrix. From this observation, we propose a new polarimetric ratio filter allowing us to recover the image structure from all the terms of the covariance matrix. In addition, we briefly look at how the additive noise component could also be exploited for the image structure extraction. Filtering results on both simulated and real PolSAR images are shown. [C108]

#### "SAR performance monitoring for TerraSAR-X mission"

The TerraSAR-X satellite features an advanced X-Band SAR based on the active phased array technology which allows flexible operation of Spotlight, Stripmap, and ScanSAR mode for various combinations and elevation angles. It combines the ability to acquire high resolution images for detailed analysis as well as wide swath images for overview applications. The SAR performance of the system is analysed with respect to geometric and radiometric parameters. Long-term monitoring of system parameters like instrument characteristics or SAR image quality confirms the continuous stability of the system. By launching a twin satellite TanDEM-X for global DEM acquisition, the TerraSAR-X mission is now supported by two satellites. The approach presented in the following shows how to keep the SAR performance for both satellites, TerraSAR-X and TanDEM-X. [C109]

#### "Using airborne & space lidars for large-area inventory"

NASA plans to launch two space lidar missions over the next decade, and at least one proposal for a space lidar is being considered by the European Space Agency. All designs call for single-beam or multi-beam profiling systems. These space ranging systems, like the ICESat/GLAS lidar that collected over 1.91 billion waveforms between January 2003 and October 2009, must necessarily be used as sampling tools to characterize vegetation cover and to estimate forest volume, biomass, and carbon globally. Recent investigations conducted by these authors have centered on developing, testing, and refining statistical approaches that can incorporate airborne and space lidar acquisitions to inventory large areas. [C110]

#### "Construction approach of integrated remote sensing systems based on the partial channels"

The principles of construction and technical implementation of multichannel integrated remote sensing systems based on the separate channels which work at splitted spectral bands were developed. [C111]

#### "Use of double frequency radar for measurement of reflectance-intensity dependence"

The results of study of double frequency method of remote sensing of liquid precipitation are presented for measurement of their intensity. Also the calculation algorithm of dependence of radar reflectance vs. rain intensity is described and main results of numerical simulation are discussed. [C112]

#### "Simulation research of microwave automatic clutter-cancellation in life-detection radar"

Clutter signal can bring interference to life-detection radar and reduce accuracy of recognition. This research attempts to resolve the problem in clutter jamming by simulation experiment. The automatic clutter-cancellation model is established according to theories and experiments are simulated on computer. The result suggests that the variation of auto-cancellation signal is not correlative with time and precision of the cancellation but amplitude and phase of the clutter signal. The result has instructive significance for the design of digital auto-cancellation circuit in life-detection radar. [C113]

#### "Doppler radar method for plasma structure investigation"

The stratified positive column of glowing discharge plasma was investigated using coherent homodyne measuring transmitter-receiver equipment. The estimation of absolute cross-section of stratified plasma creations was carried out experimentally. Frequency dependencies of a reflected signal from plasma creation have been presented. [C114]

#### "Radiophysics features of agrarian reference sites at base subsatellite landfill "skripai""

A complex of agrarian reference sites was organized. It serves for the operational calibration of space-based remote sensing sensors of different ranges, validation and verification obtained of its data. The second class weather station is located at the complex. A required number of reference points and calibration for all ranges, in particular, for service SAR, is provided. We give radiophysical characteristics of reference sites in the millimeter and centimeter wavelengths in relation to microclimatic data and the parameters of the infrastructure of agricultural vegetation. [C115]

### "Electrodynamic processes in the electrically active mesosphere"

The MF radar developed for remotely probing the near-Earth space environment and the technique for diagnosing plasma parameters in the electrically active mesosphere have enabled the determination of the basic electrodynamic characteristics of this region, which are required for achieving the fundamental physical understanding and can be used in practical applications (Sun-Earth connections, modeling the ionosphere as well as natural and anthropogenic global disturbances, near-Earth environment monitoring, earthquake predictions, and radio propagation forecasting). In particular, the average daily electric fields intrinsic to the mesosphere have been determined for the first time. [C116]

### "Water objects extraction from polarimetric SAR imagery based on blind source separation and morphological reconstruction"

The SOMMR nonlinear blind source separation (BSS) method is proposed for speckle noise suppression and water objects extracting from synthetic aperture radar (SAR) imagery based on self-organizing maps (SOM) neural networks and morphological reconstruction (MR). The multiplicative speckle noise and image data are separated from multipolarimetric imagery by means of SOM neural networks. Morphological reconstruction is employed to remove the residual noise. The experimental results using ENVISAT ASAR polarimetric imagery show that the proposed method can extract water objects accurately, and the speckle noise index is better than ICA and SOM method. [C117]

### "Fish-pond change detection based on short term time series of RADARSAT images and object-oriented method"

As an important type of wetlands, fish-pond provides a number of important ecosystem services. It was easily affected by human activities such as the change of cultivation structure. Tracking the fast change of fish-pond can obtain the information that the environment is impacted by human activities to what extent. In this study, we proposed a change detection procedure in order to delineate fast change fish-pond using high resolution, short term time series of SAR imagery. The procedure includes (1) SAR images preprocessing, (2) object extraction, (3) multi-temporal change characteristics analysis of fish-pond, (4) change objects classification, and (5) a final change results analysis. In this study, object-oriented method was adopted to extract and analyze the texture characteristics of fish-pond in the high spatial resolution of SAR data. Objects were generated with suitable scale parameters by means of multi-temporal segmentation approach according to the image features (including backscatter, difference and ratio of three temporal RADARSAT images, shape characters), and the changed objects were extracted through analyzing the shape index and contextual information generated by Definiens software. Six change types of fish-pond were achieved. The results indicate that high resolution SAR data can provide better information for fish-pond change detection in the study area, and the procedure proposed in this study can efficiently obtain the fast change objects with high accuracy between three short term time series SAR images, which are useful for the further classification. [C118]

### "Research on extracting the tree height based on LiDAR data"

In this paper, extraction of the forest tree height based on LiDAR (Light Detection and Ranging) data was studied. A simple algorithm was proposed to compensate the result computed by the DEMs of first return and last return. The satellite image download from the GoogleEarth was used to facilitate the analysis. The algorithm was tested with these data, and had been proved to be effective. Although the data we used was not suit for extracting tree height, LiDAR has great potential in this field. [C119]

### "Wetland cover information extraction research based on the multi-polar radar images and multi-spectrum optical images fusion"

The research takes Radarsat-2 multi-polarization radar images and ALOS multi-spectrum optical images for example, through the information filtering and extraction methods such as information quantity statistics and correlation matrix, we obtain the cognition of the spectral characteristics and detection performance of each polarization mode radar image, and select the optimal data for fusion and classification experiment. Using Brovey, PCA, HPF and Wavelet transformation methods to fuse, and adopting non-supervision, supervision and object-oriented method to carry out classification experiment, we explore the application of radar and optical remote sensing image fusion technology in the wetland area covers information extraction, which verifies the effectiveness and feasibility using radar and multi-spectral image fusion technology in the wetland cover information extraction. [C120]

### "Classifying multisensor images by support vector machine in Chongming Dongtan"

Optical remote sensing (ORS) technology has been extensively used for the investigation of the environment and resources. Considering it is heavily constrained by the weather conditions, especially in the coastal zone, the round-the-clock SAR (Synthetic Aperture Radar) data are chosen to compensate for the shortcomings of optical data. In this paper, we will use the fusion image of ASAR and TM to identify five land cover types in Chongming Dongtan. And the SVM algorithm is adopted because of its capability to take numerous and heterogeneous parameters into account. Results have been shown that the fusion data of SAR and ORS is particularly suited to account for the rainy and cloudy weather in coastal zone. And the SVM algorithm has attained a high level of classification performance with the overall accuracy 90.83%. [C121]

### "Airborne LiDAR strip adjustment based on LSM"

An airborne LiDAR system is an integration of GPS, INS, and laser scanner. Because of errors of these instruments or sub-optimalities of the GPS/INS integration, points of neighbouring laser scanner strips will usually show vertical and horizontal discrepancies. Currently the more common way for the reducing or ultimately eliminating discrepancies found in strip overlap areas is strip adjustment. Based on Microsoft Visual Studio 2008 C++ platform, a data-driven method of seven parameters conformal transformation for airborne LiDAR strip adjustment is realized in our paper, the algorithm improved Robert (2004) least squares surface matching algorithm, by introducing the Gauss-Markoff model, Acquired the unbiased minimum variance estimation for the unknown parameters. Real data sets are used to validate the method. We study the matching precision of different reference surface from two strips, the need for using Gauss-Markoff model and the matching accuracy. Experimental results show that after correction the point clouds show much better alignment and the vertical matching error is less than 0.05m. [C122]

### "Estimation of significant wave height from X-band marine radar images"

Radar images include abundant information about ocean waves. Sea state parameters and surface currents can be obtained by analyzing time series of radar images of the sea surface. Due to the non-linearity of the imaging mechanism of ocean waves, significant wave height ( $H_s$ ) can not be determined directly from radar images. Applying a method to infer the  $H_s$  from synthetic aperture radar (SAR) images, the  $H_s$  can be estimated from marine radar images. Comparing the  $H_s$  obtained by this method with buoy data, the results show that it is feasible to obtain reliable data of the  $H_s$  from marine radar images. [C123]

### "Bistatic SAR tomography: Processing and experimental results"

This paper presents across-track tomography applied to a bistatic geometry with fixed receivers. This kind of geometry can overcome some of the classical monostatic tomography limitations such as temporal decorrelation and irregular baseline distribution. The Remote Sensing Laboratory (RSLab) of the Universitat Politècnica de Catalunya (UPC) has implemented a SAR Bistatic Receiver for Interferometric Applications, SABRINA, with 4-channels. SABRINA has been used to carry out a bistatic tomographic experiment. The acquired data has been processed with different tomographic methods and their performances compared. [C124]

### "Estimation of pasture biomass and soil-moisture using dual-polarimetric X and L band SAR-accuracy assessment with field data"

This paper presents the results of a study conducted to relate X and L band polarimetric SAR backscatter to pasture soil moisture and biomass as part of an environmental monitoring program. Extensive field data was collected concurrently with satellite SAR data acquisition-including dry/wet above ground biomass, soil moisture, surface roughness profiles and EM-38 electromagnetic sensor data. This data is used for both electromagnetically modeling the surface to work out the theoretical backscatter as well as empirical fitting regression models to the recorded SAR data and validation of existing inversion models. [C125]

### "Diverse methods to monitoring volcanic deformation based on SAR interferometry"

In this paper, different methods for the detection of the deformation signal with SAR data based on persistent scatterer interferometry (PSI) are described. Two test sites have been selected. For experimental purposes, two corner reflectors (CRs) were installed in the Fogo volcano. The location, phase as well as intensity of corner reflectors were analyzed with 11 TerraSAR-X stripmap (TSX-SM) data. For algorithmic development and validation, four stacks of TerraSAR-X high resolution spotlight (TSX-HSL) data from the Stromboli volcano have been acquired and used for PSI processing. The PSI results of deformation and topography update are fused by using point matching method with Iterative Closest Point (ICP). This research is a part of the German volcano monitoring project Exupery, Work Package 2: 'Space based observation techniques'. [C126]

### "Breaking wave measurements with sar depolarized returns"

The wind generates a distribution of small slope waves and sporadic steep breaking events. Such double structure of the sea surface is expected to have a strong impact on the radar scattering from the ocean surface. The signature of the double structure is in the wind speed dependence of radar returns: linear for scattering from gentle waves and cubic for breaking contribution. The composite-surface Bragg resonance (CB) theory describes the former very well. Detection of the breaking contribution remains difficult. Here we show that the depolarized (de-pol) radar return exhibits the typical double structure, its wind speed dependence increases with wind speed from linear to cubic. The increased sensitivity of the de-pol returns in high winds is ideal for hurricane wind retrieval. The strong breaking connection offers an opportunity to measure wave breaking and the associated energy dissipation and area of foam coverage from space, their quantification is important in air-sea interaction and electromagnetic and electro-optical remote sensing. [C127]

### "Supporting precision agriculture with dual-polarimetric TerraSAR-X-yield prediction and identification of in-field variations to generate fertilizer prescription maps"

This paper presents studies carried out over 2 growing season in South Australia to evaluate the suitability of TerraSAR-X dual-polarimetric imagery for crop growth monitoring and yield prediction. End of season crops were observed in 2008 and significant correlation with yield was noted. Mid-season crops were observed in 2009 and due to the lower biomass no significant in field trends were observed in the SAR when compared with concurrently acquired ground NDVI sensor and multispectral optical data. Separability between different crop types is evident in both studies, but crop biomass has to be significant for any in-field variations to be apparent. [C128]

### "Estimation of building damage ratio due to earthquakes and tsunamis using satellite SAR imagery"

In order to expand the existing C-band SAR based damage estimation model into L-band SAR, this paper introduces a likelihood function to estimate severe damage ratio by earthquakes on the basis of dataset from JERS-1/SAR (L-band SAR) images observed the 1995 Kobe earthquake and its detailed ground truth data. The model is applied to JERS-1/SAR images taken over the tsunami affected areas by the 1993 Hokkaido Nansei-oki, Japan earthquake. [C129]

### "Operation icebridge: Using instrumented aircraft to bridge the observational gap between icesat and icesat-2"

Operation IceBridge, a six-year NASA mission, is the largest airborne survey of Earth's polar ice ever flown. Data collected during IceBridge will help scientists bridge the gap in polar observations between NASA's Ice, Cloud and Land Elevation Satellite (ICESat), in orbit from 2003 to 2009, and ICESat-2, planned for launch in late 2015, making IceBridge critical for ensuring a continuous series of observations. Operation IceBridge is using airborne instruments to map Arctic and Antarctic areas once a year, building on two decades of repeat airborne measurements of rapidly changing areas in the Arctic. Operation IceBridge is also producing critical data that cannot be measured from space such as ice thickness measurements. The first Operation IceBridge flights were conducted in boreal spring 2009 over Greenland and the boreal fall 2009 over Antarctica. Other smaller airborne surveys around the world are also part of NASA's Operation IceBridge campaign. [C130]

### "KaRIn-the Ka-band radar interferometer on SWOT: Measurement principle, processing and data specificities"

The principal instrument of the SWOT (Surface Water and Ocean Topography) altimetry mission is KaRIn, a Ka-band interferometric SAR system operating on near-nadir swaths on both sides of the satellite track. This article briefly describes the measurement principle, the processing steps and the specificities of the interferometric SAR data of KaRIn as compared to conventional spaceborne SAR systems. [C131]

### "Use of the merged dual-frequency radar altimeter backscatter data over China land surface"

It is a special way to investigate continental surfaces using radar altimeter, besides scatterometers and Synthetic Aperture Radar among the active microwave remote sensing sensors for the altimeter works at the nadir point of satellite and at dual-frequency, which can measure the backscatters from different layers instantaneously. The aim of this paper is to merge multi-radar altimeter dual-frequency backscatter measurements over land surface to achieve better spatial and temporal resolution. The 0.5°×0.5° merged altimetry backscatter maps between 66° N to 66° S over land surface every 6 days are generated in Ku, C, and S band for the period from January 2002 to June 2009. Temporal profiles of backscatters are examined for main land types (desert, forest, savanna) to

validate the dataset and to analyze radar response to land surface variability through 8 years. [C132]

### "Longtime monitoring of mine subsidence in Northern Moravia, Czech republic using different insar techniques"

In the undermined Northern Moravia region, the land is subsiding even more than a metre per year causing damages to many human-made objects. Such a fast subsidence is almost not possible to estimate using multitemporal radar interferometry techniques that were applied to ERS-2 data of 1996-2001. Classic differential radar interferometry approaches were successfully applied allowing to visually interpret the evolution of subsidence in the area using Envisat and ERS-1/2 images from years 1996-2009. Results of the radar interferometry usage have been compared with the levelling data. Because of several factors, most of the interferograms are decorrelated. These factors are depicted and several solution scenarios are pointed out. To overcome such limitations as a relatively strong vegetation cover in the area and to detect such a fast subsidence in small areas, the ALOS PALSAR images in fine resolution mode has been successfully used.

[C133]

### "Forest change detection from L-band satellite SAR images using iterative histogram matching and thresholding together with data fusion"

In this study, we assess the efficiency of using L-band satellite SAR for forest change monitoring, by applying a combination of change detection techniques to SAR backscatter intensity images acquired over Swedish forest. We use a bi-temporal change detection approach based on image rationing. Histogram based techniques are used both for radiometric normalization and thresholding. For a final classification step, we evaluate a data fusion based change detection method that exploits the spatial and spectral information from one or multiple SAR channels. Pre-applied filters are also evaluated as alternatives to tackle low resolution and speckle. HH and HV polarized Fine Beam Dual images, acquired 34 degrees off nadir (FBD34) by the Advanced Land Observing Satellite Phased Array type L-band Synthetic Aperture Radar (ALOS PALSAR), are used to find clear-cuts in Swedish boreal forest. Our results show that clear-cuts can be clearly extracted from L-band SAR data. [C134]

### "Spatial latency reduction in GPR processing using stochastic sampling"

Ground penetrating radar (GPR) is a promising technique for buried threat detection which provides a complimentary phenomenology to electro-magnetic induction (EMI) based sensing. However, many successful GPR-based buried threat detection algorithms require data collected both before and after an object of interest is encountered to make a declaration (typically this data is used to perform background normalization, or to adequately characterize the object's shape). Samples taken past an object of interest, but before a decision is made, constitute an algorithm's "spatial latency". For vehicular mounted antennae arrays, where vehicle stopping distance is a function of vehicle dynamics, driver responsiveness, and algorithmic spatial latency, reducing an algorithm's spatial latency can increase overall system safety and help keep operators out of harm's way. In this work we propose a stochastic sampling algorithm that can help reduce spatial latency for a wide range of GPR-based buried threat detection algorithms. [C135]

### "Optimal sensor positioning for ISAR imaging"

ISAR imaging is a powerful signal processing that allows obtaining images of non-cooperative targets. Such images are often used as input to classification and recognition systems since they contain useful two-dimensional features. Nevertheless, the interpretation of ISAR images remains problematic since the image plane cannot be defined by the user but it depends on the target's own motions and on the relative position of it with respect to the radar. In this scenario, the only degree of freedom that is controlled by the user is the position of the sensor. In this paper, the problem of selecting an optimal position of the sensor to maximise the probability of obtaining a desired image projection plane is addressed. Moreover, mathematical tools are derived that may assist the user in deciding where to place an ISAR sensor given a priori knowledge of the scenario.

[C136]

### "Topography effects on forest radar scattering, consequences on biomass retrieval"

Ground topography under vegetated area is liable to bring significant changes on radar backscattering and thereby on the associated standard retrieval algorithms dedicated to forest biomass. Within the framework of the ESA BIOMASS mission, this paper evinces the evolution of P-band polarimetric intensities with a tilted underlying ground. For that purpose, electromagnetic simulations have been achieved using our model MIPERS which theoretical specificities accounting for the topographic effects are herein described. Its originality lies mainly in the 3D characterization of the ground and the volume, as well as the coupling effects between both.

This description is followed by a sensitivity analysis in order to further-on quantify the possible consequences on biomass retrieval, conducted with the two standard approaches, namely the P-HV intensity technique and the Pol-InSAR one assuming the RVoG model. This investigation have been also undertaken for a better understanding of experimental data, particularly with the BioSAR and the TropiSAR airborne campaigns over boreal and tropical forests. [C137]

#### **"Processing of MEMPHIS millimeter wave multi-baseline InSAR data"**

This paper presents a processing method for multi-baseline interferometric data acquired with the MEMPHIS airborne sensor. The processing method ingests the SAR raw data from each receiver and extends up to the generation of digital elevation models (DEMs). Critical steps include the correction of the azimuth phase undulations, the multi-baseline processing and the phase-to-DEM conversion. Methods for resolving the various hurdles were adapted to the MEMPHIS sensor and are presented here. The results obtained for a data take over a test site near Zurich, Switzerland are shown; these results are in a good agreement with comparable LIDAR products. [C138]

#### **"Monitoring slow moving landslides in the Berkeley Hills with TerraSAR-X data"**

Large, slow moving landslides in the Berkeley Hills cause many damage and pose a potential threat to public safety due to the close proximity of the Hayward Fault. We have been using Differential SAR interferometry (DInSAR) and time-series analysis of SAR data to resolve the rates of the landslide motion. In this paper, we aim to interpret the new satellite TerraSAR-X data in this small landslides area. We have acquired both Stripmap data and Spotlight data. Standard InSAR method as well as Persistent Scatterer InSAR is utilized in the processing. [C139]

#### **"Development of an Off-The-Grid X-band radar for weather applications"**

The Student Led Test Bed (STB) is part of the NSF Engineering Research Center CASA and is currently focused in developing low-cost and low infrastructure radar networks to fill lower atmosphere gaps not covered by current technology. The first radar node, which is part of a small region radar network, will significantly improve the time and spatial resolution of the radar data measured for the lower atmosphere. This paper describes the development of an Off-The-Grid (OTG) X-band radar node that requires minimum infrastructure for its deployment and can operate using solar energy and wireless communication links. The OTG radar was developed for meteorological applications modifying a commercially available marine radar. Hardware modifications for meteorological purposes were performed as well as the design and implementation of a photovoltaic system to power the radar using solar energy. The system was moved to the Colorado State University (CSU)-CHILL National Weather Radar facility for a cross-calibration and system evaluation. Satisfactory results were obtained where it was demonstrated that the OTG radar can provide precipitation measurements with improved spatial and temporal resolution, both necessary to have better lower troposphere measurements. This OTG node is the first prototype of a low infrastructure X-band weather radar network to aid forecasts in the western region of Puerto Rico. [C140]

#### **"Advanced classification of UXO using fully polarimetric GPR and frequency-polarization features"**

The classification of buried UXO has been a difficult task due to the large amount of false alarms resulted from troublesome clutter objects. This paper closely examined scattering characteristics of such clutter objects by using numerical simulations. From the numerical study, we found that some clutter objects, which mainly causes the false alarms, produce multiple resonances at different frequencies and different polarizations. Based on these observations, we developed new classification algorithms which utilize the frequency-polarization dependent responses of complex targets in order to discriminate UXO-like objects from such trouble some clutters. The developed algorithms were tested by experiments in a test plot. In the test, the new classification algorithms clearly discriminated such clutters from UXO-like targets. In this paper, we present the simulation results for scattering characteristics of complex clutters and the new classification algorithm based on frequency-polarization dependent responses will be discussed. Finally, results from experimental verification will be presented. [C141]

#### **"Wide area assessment-Development and case study"**

Munitions response is a high priority issue for the Department of Defense (DOD). Over 3,600 munitions response sites (MRS) are in DOD's inventory of sites with potential military munitions and explosives of concern (MEC) contamination, including unexploded ordnance (UXO) and discarded military munitions (DMM). Because many of these sites are large in size (greater than 10,000 acres), the investigation and remediation of these sites could cost billions of dollars. To address this issue, a wide area assessment (WAA) process was developed to

quickly and cost effectively assess 100% of a site to reduce the footprint to only those areas with known MEC contamination (i.e. MRS). In this paper, we present a discussion of the origins of the WAA concept, a case study of its first large scale application, descriptions of the component technologies, and conclude with recommendations. [C142]

#### **"Model level fusion of edge histogram descriptors and gabor wavelets for landmine detection with ground penetrating radar"**

We propose a discriminative method for combining heterogeneous sets of features for the continuous hidden Markov model classifier. We use a model level fusion approach and apply it to the problem of landmine detection using ground penetrating radar (GPR). We hypothesize that each signature (mine or non-mine) can be characterized better by multiple synchronous sequences that can capture different and complementary features. Our work is motivated by the fact that mines and clutter objects can have different characteristics depending on the mine type, soil and weather conditions, and burial depth. Thus, different sets of specialized feature extraction mechanisms, may be needed to achieve high detection and low false alarm rates. In order to fuse the different modalities, a multi-stream continuous HMM that includes a stream relevance weighting component is developed. In particular, we modify the probability density function that characterizes the standard continuous HMM to include state and component dependent stream relevance weights. We generalize the Minimum Classification Error (MCE) objective function to include stream relevance weights and derive the necessary conditions to update all model parameters simultaneously. Results on a large collection of GPR alarms show that the proposed model level fusion outperforms the baseline HMM when each feature is used independently and when both features are combined with equal weights. [C143]

#### **"The microasar experiment on CASIE-09"**

During the summer of 2009, the Characterization of Arctic Sea Ice Experiment 2009 (CASIE-09) operated a small, unmanned aircraft system (UAS) over the Arctic Ocean for a number of long-distance flights from Svalbard Island. In addition to other instruments, the UAS carried a small C-band synthetic aperture radar (SAR) known as MicroASAR to image sea ice roughness at 1 m resolution. This paper briefly describes the SAR, its role in CASIE-09, and presents sample SAR image results. [C144]

#### **"Theoretical and practical design considerations for a small, multi-band SAR: The SlimSAR"**

The SlimSAR is a small, low-cost, Synthetic Aperture Radar (SAR) system and represents a new advancement in high-performance SAR. ARTEMIS employed a unique design methodology that exploits previous developments in designing the SlimSAR to be small, light, and flexible while consuming very little power. The system contains an L-Band core and uses block-converters to operate in a number of other bands. It also has the capability to operate in either deramp or direct-sampling mode and can collect data in two polarizations simultaneously. The flexible control software allows us to change the radar parameters in flight. Multi-frequency SAR provides day and night imaging through smoke, dust, rain, and clouds with the advantages of additional capabilities at different frequencies (i.e. dry ground and foliage penetration at low frequencies, and high-resolution change detection at high frequencies). [C145]

#### **"Advanced digital beamforming concepts for future SAR systems"**

This paper reviews advanced multi-channel SAR system concepts for the imaging of wide swaths with high resolution. Several novel system architectures employing both direct radiating arrays and reflector antennas fed by a digital array are introduced and compared to each other with regard to their imaging performance. In addition, innovative SAR imaging modes are proposed which enable the mapping of ultra-wide swaths with high azimuth resolution. The new techniques and technologies have the potential to enhance the imaging performance of future SAR systems by one order of magnitude if compared to state of the art SAR sensors like TerraSAR-X, ALOS, Radarsat-2 or Sentinel-1. [C146]

#### **"Surf zone surface displacement measurements using interferometric microwave radar"**

Vertically polarized backscattered power, Doppler velocity, and interferometric height were measured in the nearshore ocean region using a high-resolution imaging microwave radar. The interferometric surface displacement measurements are compared with normalized radar cross sections (NRCS) and Doppler velocities, and with in situ pressure sensor estimates of wave height. The rms uncertainty in the interferometric surface displacement is computed from the data. The interferometric surface displacement measurements are intuitively satisfying in that positive displacements are generally associated with pixels that have larger NRCS values. Interferometric surface displacements compare well with heights derived from in situ pressure sensors, and we provide some possible explanations for the differences. [C147]

### "Preliminary model for wind estimation from Cosmo/SkyMed X band SAR data"

In the paper we present a preliminary model for wind estimation from SAR data in X band. The data set we have used is composed of more than 300 Cosmo/SkyMed SAR images and the wind data obtained from the SeaWinds instrument on QuikSCAT. We have derived 18 parameters to express  $\sigma_{\text{oa}}$  as function of wind intensity, direction and Radar look angle. The preliminary validation results are encouraging although our data set needs to be extended in order to increase those conditions poorly represented. [C148]

### "Use of PALSAR polarimetric data for tropical forest stratification and comparison of simulated dual and compact polarimetric modes"

This paper presents a case study addressing the comparison between different SAR polarimetric mode for tropical forest stratification: Full polarimetry (FP), Dual Polarimetry (DP) and Compact Polarimetry (CP). These 2 latter modes are simulated using FP data acquired by the L band PALSAR sensor over 2 study sites. Cayenne in French Guyana and the Fazenda Saio Nicolau in Brazil. The classification approach used to evaluate each mode based on Support Vector Machine (SVM) algorithm shows the good capabilities of the FP mode to discriminate different kinds of vegetation. The choice of one DP mode that gives twice bigger swath than FP mode depends on the study classes. In this tropical environment the hh/hv existing mode seems to be a good choice and CP mode show a good alternative to all the actual DP modes. [C149]

### "Development of ALOS/PALSAR data on-demand processing and providing system on GEO Grid"

GEO Grid has been proposed by AIST in order to contribute to earth science. GEO Grid mainly provides satellite and field observation data related to earth science through data search service, data processing service and data providing service. Recently, we have developed ALOS PALSAR data on-demand processing and providing system as one of GEO Grid data providing system. The system allows users to easily search and quickly receive PALSAR products without careful considerations and advanced skills. There are two important points in the system. One is seamless connection between AIST and an external archive system. The other is that the system can provide calibrated PALSAR products according to observations using Corner Reflectors. As a future plan, OGC-CSW is applied to this system for data search service. [C150]

### "Ground penetrating radar measurements: Applications to synthetic data generation and target characterization"

Ground penetrating radar (GPR) is widely studied for detection of landmines and mine-like targets; GPR is particularly useful for detecting minimum metal mines which are harder to detect using traditional metal detection devices alone. In order to expand the phenomenology for GPR, careful measurements of homogeneous and heterogeneous soils with and without targets (landmine simulants and metal objects) are performed in a controlled environment. These measurements will aid in the development of models for soil response beyond the initial air-ground interface. Such explicit models for soil will increase the effectiveness of algorithms designed to discriminate between returns from targets and from naturally occurring geologic materials and interfaces. Furthermore, careful measurement of soil characteristics will enable comparison and refinement of models of soil with embedded targets developed in electromagnetic simulations (using finite-difference time-domain codes (FDTD), e.g.). [C151]

### "A Ku-band rotating fan-beam scatterometer: Design and performance simulations"

This paper introduces the design and simulation results of a Ku-band rotating fan-beam radar scatterometer for ocean surface wind vector measurement. It will be flown on a small satellite dedicated to provide data for investigation of the ocean wave and ocean surface wind vector interactions, along with another payload for measurement of directional ocean wave spectra by a real-aperture radar with multiple scanned pencil beams. Key issues about the design of a Ku-band rotating fan-beam radar scatterometer, and results of performance simulations are provided as well. The performance of the system is simulated by the absolute and relative specifications. For the absolute specifications, retrieval performances for both wind speed and wind direction are evaluated, with the maximum likelihood method being employed. For the relative specifications, the figures of merit (FOM) is simulated, for comparison with other Ku-band scatterometers and optimization of system parameters. Simulation results of both the  $\sigma^{\circ}$  precision and wind retrieval accuracies for different wind speed from 4m/s to 24m/s will be provided, which shows that SCAT can satisfy the performance requirements within most part of the swath. [C152]

### "A broad band lidar for precise atmospheric CO2 column absorption measurement from space"

Accurate global measurement of carbon dioxide column with the aim of discovering and quantifying unknown sources and sinks has been a high priority for the last decade. In order to uncover the "missing sink" that is responsible for the large discrepancies in the budget the critical precision for a measurement from space needs to be on the order of 1ppm. To better understand the CO<sub>2</sub> budget and to evaluate its impact on global warming the National Research Council (NRC) in its recent decadal survey report (NACP) to NASA recommended a laser based total CO<sub>2</sub> mapping mission in the near future. That's the goal of Active Sensing of CO<sub>2</sub> Emissions over Nights, Days, and Seasons (ASCENDS) mission-to significantly enhance the understanding of the role of CO<sub>2</sub> in the global carbon cycle. Our current goal is to develop an ultra precise, inexpensive new lidar system for column measurements of CO<sub>2</sub> changes in the lower atmosphere that uses a Fabry-Perot interferometer based system as the detector portion of the instrument and replaces the narrow band laser commonly used in lidars with a high power broadband source. This approach reduces the number of individual lasers used in the system and considerably reduces the risk of failure. It also tremendously reduces the requirement for wavelength stability in the source putting this responsibility instead on the Fabry-Perot subsystem. [C153]

#### **"Evaluation of two region based classifications in Tapajys National Forest using the ALOS/PALSAR polarimetric and interferometric coherences"**

The use of phase information present in complex multi polarized images may increase the classification results. Thus, the coherence is one attribute that may be extracted from these images and used to distinguish some land cover classes. Therefore, its discriminatory capability for land use and land cover classification is analyzed. The analysis is based on the classification results of a region classifier, which needs a segmented image as one input. The influence of this kind of image input is also evaluated using of two segmentation algorithms, the SegSAR and the SPRING region growing. Two ALOS/PALSAR images acquired over Tapajos National Forest in the Brazilian Amazon were classified. The classifications were quantified by the overall accuracy, the kappa values and its variance. The classification improvement using the coherence information with intensity images was noticed for every image set. [C154]

#### **"Integrating space-time processing into time-domain backprojection process for detection and imaging moving objects"**

This paper discusses a possibility to integrate space-time processing into the time-domain backprojection process. This combination allows detection as well as imaging moving objects. Two space-time techniques, Displaced Phase Center Antenna (DPCA) and Space-Time Adaptive Processing (STAP), are considered for this integration. Simulated results based on the LORA parameters demonstrate the efficiency of detection and imaging moving objects. [C155]

#### **"Use of 2D FDTD simulation and the determination of the GPR travel path angle for oblique B-scans of 2D geometries"**

Scattering from a subsurface point object, such as a reinforcing steel bar embedded concrete or a tunnel buried in sand, results in a B-scan contour that is essentially hyperbolic as the Ground Penetrating Radar (GPR) passes over the object. The shape of the hyperbola can be used to determine the angle at which the GPR traveled over the point object. This information is very useful in determining the orientation and size of an object such as reinforcing steel, buried utilities, and subsurface tunnels. A 2D Finite Difference Time-Domain (FDTD) method can be used to simulate the GPR B-scan when the geometry is invariant in the third dimension and the sensors are appropriately located. The shape of the hyperbola extracted from 3D simulation, analogous to field-collected data, can be compared to a library of hyperbolas extracted from 2D simulations and used to determine the angle of the GPR travel path from the cross-sectional plane. [C156]

#### **"How does dew affect L-band backscatter? analysis of pals data at the Iowa validation site and implications for smap"**

NASA's Soil Moisture Active Passive satellite mission will use both an L-band radiometer and radar to produce global-scale measurements of soil moisture. L-band backscatter is also sensitive to the water content of vegetation. We found that a moderate dew increased the L-band backscatter of a soybean canopy by 1 dB. Dew thus has the potential to add error to satellite observations of soil moisture. [C157]

#### **"Experimental validation of the Corbella's visibility function using HUT-2D and MIRAS"**

The Corbella's revision of the fundamental equation of the interferometric aperture synthesis radiometry is verified using airborne and spaceborne data. This experimental verification uses the measurements of the airborne instrument HUT-2D from the Aalto University (Helsinki), and the unique spaceborne microwave imaging

radiometer by aperture synthesis (MIRAS) from the ESA's Soil Moisture and Ocean Salinity (SMOS) mission. The data acquired with those sensors support the Corbella's revision of the visibility function. The revised function predicts that visibilities depend on the contrast between the target's brightness temperature and the backward noise of the receivers emitted through the antennas. [C158]

### "The Slope Imaging Multi-polarization Photon-counting Lidar: Development and performance results"

The Slope Imaging Multi-polarization Photon-counting Lidar is an airborne instrument developed to demonstrate laser altimetry measurement methods that will enable more efficient observations of topography and surface properties from space. The instrument was developed through the NASA Earth Science Technology Office Instrument Incubator Program with a focus on cryosphere remote sensing. The SIMPL transmitter is an 11 KHz, 1064 nm, plane-polarized micropulse laser transmitter that is frequency doubled to 532 nm and split into four push-broom beams. The receiver employs single-photon, polarimetric ranging at 532 and 1064 nm using Single Photon Counting Modules in order to achieve simultaneous sampling of surface elevation, slope, roughness and depolarizing scattering properties, the latter used to differentiate surface types. Data acquired over ice-covered Lake Erie in February, 2009 are documenting SIMPL's measurement performance and capabilities, demonstrating differentiation of open water and several ice cover types. ICESat-2 will employ several of the technologies advanced by SIMPL, including micropulse, single photon ranging in a multi-beam, push-broom configuration operating at 532 nm. [C159]

### "Electromagnetic infrastructure monitoring: The exploitation of GPR data and neural networks for multi-layered geometries"

In this paper, an inversion ANN-based algorithm for the estimation of geophysical properties (i.e. thickness and permittivity) of subsurface layers in stratified geometries is presented. The basic procedure for the analysis of GPR scans of single subsurface layers placed over a uniform background recently proposed by the authors has been here extended and inserted into a general framework where each stratum is recursively processed. [C160]

### "Towards Bayesian estimator selection for QuikSCAT wind and rain estimation"

The QuikSCAT scatterometer infers wind vectors over the ocean using measurements of the surface backscatter. During rain events the QuikSCAT observations are subject to rain contamination. Three separate estimators have been developed: wind-only, simultaneous wind and rain, and rain-only, which account for rain contamination in varying degrees. This paper introduces a Bayes estimator selection technique to adaptively choose a best estimator from among the three types of estimators at each measurement location. Bayes estimator selection is introduced from a general perspective after which it is applied specifically to QuikSCAT wind and rain estimation. Bayes estimator selection is demonstrated in a case study to illustrate improvements in wind and rain estimation which can be obtained. [C161]

### "Using airborne lidar to retrieve crop structural parameters"

Airborne LIDAR (Light Detection and Ranging) is an active remote sensing technique that measures the properties of scattered light to determine the range and intensity information of a distant target. Many studies have been reported on estimating a suite of forest characteristics such as fractional vegetation cover, leaf area index and canopy height using LIDAR data. The three characteristics of crop canopy also play key roles in vegetation radiative transfer models and yield estimation. But crops are so small and low that more than 95% pulses have ground hit, it is difficult to separate the crop and soil completely, so the methods used in forest may not be suitable for crops. In this paper, based on theoretical analysis, we propose a new method, trying to derive gap fraction of crop field using the airborne LIDAR intensity of ground hits, so we can manage to retrieve the fractional vegetation cover, LAI and the height of crop canopy. We choose corn field as study object, field validation shows that our method can accurately retrieve the three structural parameters of corn field. This study documents the great potential of LIDAR remote sensing for accurately characterizing crop canopies. [C162]

### "A revised geophysical model function for the advanced scatterometer (ASCAT) at NOAA/NESDIS"

The current ASCAT winds retrieval is based on the CMOD5.n geophysical model function (GMF) with the ASCAT wind data processor developed at the Royal Netherlands Meteorological Institute (KNMI). Recent validation of ASCAT wind retrieval reveals that high wind retrievals were underestimated as being compared to the operational QuikSCAT scatterometer. The goal in this paper is to improve ASCAT wind retrievals at high winds. In this paper we map the radar backscatter ( $\sigma_0$ ) as a function of extreme wind conditions as measured by an airborne scatterometer and adjusted the isotropic term in CMOD5.n to follow the aircraft GMF trend. The

geophysical model QuikSCAT wind inputs are improved for  $\sigma_0$  that calculated from QuikSCAT wind inputs are improved for  $\sigma_0$  approximately  $> -15$  dB and in very good agreement with the ASCAT  $\sigma_0$  measurement. The wind retrieval validations show wind speed rms error is improved at approximately wind speed  $> 12$  m/s and example mean wind composite from two winter seasons shows significant in detection of storm-force winds. [C163]

### "Segmentation of lakes from the local background on the surface of Titan using Cassini SAR images"

Synthetic Aperture Radar (SAR) images of Titan, the largest satellite of Saturn, reveal quasi-circular to complex features which are interpreted to be liquid hydrocarbon lakes. One of the major problems hampering the derivation of meaningful texture information from SAR imagery is the speckle noise. It overlays real structures and causes gray value variations even in homogeneous parts of the image. A filtering technique is applied to obtain the restored SAR images. Our method is based on probabilistic methods and regards an image as a random element drawn from a prespecified set of possible images. The TSPR (Total Sum Preserving Regularization) filter used here is based on a membrane model Markov random field approximation with a Gaussian conditional probability density function optimized by a synchronous local iterative method. The despeckle filter can be used as intermediate stage for the extraction of meaningful regions that correspond to structural units in the scene or distinguish objects of interest like lakes. [C164]

### "IMaging geodesy with TerraSAR-X"

We report on a method and experiments to achieve about 3 centimeters pixel location accuracy of TerraSAR-X SAR images. The method is based on atmospheric refraction corrections, Earth tide compensation and image correlation or the use of corner reflectors. Our method does not exploit the SAR phase and is therefore not subject to phase unwrapping problems or unknown phase offsets. [C165]

### "Development of the LiDAR data processing system for the rapid generation of the terrestrial information"

This paper present an improved application system which can generate the 2.5D or 3D terrestrial information like DSM, DEM rapidly using LiDAR data. To process and manipulate input LiDAR data, various function modules are contained in the developed system. It allows users to display LIDAR data using TINS and even allows users to analyze the data using a profile viewer. In addition, the system also allows users to save the processed data with LAS file format, ASCII format. [C166]

### "A multimodal Matching Pursuits Dissimilarity Measure applied to landmine/clutter discrimination"

The Matching Pursuits Dissimilarity Measure (MPDM) is an effective way to to compare signals that are sparsely approximated using a Matching Pursuits method. The CAMP algorithm uses an MPDM distance measure in Competitive Agglomeration clustering to model and classify signals. The MPDM approach can only compare signals originating from a single source. Many landmine detection systems use multiple sensors to make simultaneous measurements of the same region of interest. In this paper we propose a Multimodal MPDM that can be used with CAMP to fuse signals from multiple sensors. We demonstrate the effectiveness of the Multimodal MPDM over the single sensor MPDM in improving discrimination of landmines from clutter objects. [C167]

### "On radar sounding applications for Enceladean ice"

Due to the nature of observations taken by planetary spacecraft, many surface and atmospheric studies have been performed at the icy moons of the outer planets, which have left the many seemingly complex interior processes in these bodies left unexplored and unexplained. It is notably difficult to access the interior regions in which planetary formation and dynamics take place. This paper presents the possibility that radar measurements could contribute to the understanding of interior structure, particularly that of Enceladus, the small but notably dynamic icy moon of Saturn. The application of such radar may lead to discoveries concerning formation mechanisms and surface processes. Additionally, radar sounding will contribute measurements that aid in diagnosing the dynamics system at work in the subsurface-perhaps most notably, the source reservoir and/or dynamics of the observed water plume at the moon's south pole, in addition the moon's role as a whole in the Saturnian system. [C168]

### "The Hurricane Imaging Radiometer wide swath simulation and wind speed retrievals"

The knowledge of peak winds in hurricanes is critical to classification of hurricane intensity; therefore, there is a strong interest in the operational remote sensing of ocean surface winds for monitoring tropical storms and

hurricanes, especially those which threaten landfall. Presently, the airborne Stepped Frequency Microwave Radiometer (SFMR) is the state-of-the-art remote sensor for providing this information in real-time, during hurricane surveillance flights. However, for the future, NASA and NOAA are collaborating in the development of the Hurricane Imaging Radiometer (HIRAD), which is a prototype of the next-generation high-flying airborne instrument for monitoring hurricanes. This paper describes a realistic end-to-end simulation of HIRAD hurricane measurements while flying on an unmanned Global Hawk aircraft. The objective of this research is to develop baseline retrieval algorithms and provide a wind speed measurement accuracy assessment for the upcoming NASA hurricane field program, Genesis and Rapid Intensification Processes (GRIP), to be conducted in 2010.

[C169]

### "Three dimensional reconstruction of urban areas using jointly phase and amplitude multichannel images"

The aim of this paper is the three dimensional reconstruction of urban areas using Very High Resolution (VHR) images. The proposed innovative approach for the three dimensional reconstruction is based on the joint exploitation of both amplitude and interferometric phase images of a multichannel SAR system. The information provided by the amplitude data is added to the 3D reconstruction chain, considering that in urban areas edges of amplitude image are likely also present in the interferometric phase one and conversely. Differently from other works present in literature, the proposed technique exploits the amplitude image, not only to improve the phase regularization, but also to improve the phase unwrapping step. The results will show the effectiveness of the method. [C170]

### "The external calibration study for EarthCARE/CPR"

The Cloud Profiling Radar (CPR) is one of key sensors on EarthCARE for joint project between Europe and Japan. The CPR is developed by National Institute of Information and Communications Technology (NICT) in Japan and Japanese Aerospace Exploration Agency (JAXA). The CPR uses W-band frequency and large antenna diameter in order to obtain enough sensitivity. In other words, beam footprint becomes small but antenna scanning cannot be performed. Two external calibration methods are considered. The first method is external calibration using active radar calibrator (ARC). It is foreseen the difficulty to place exact location on sub-satellite track. The second method is external calibration using naturally distributed target, such as sea surface. We describe about test experiment for first method and statistical analysis using satellite data for second method as the feasibility study. [C171]

### "Quantifying the results of wind and rain on ifsar tree height estimation"

The horizontal and vertical (3D) structure of Earth's forested ecosystems are of great significance to their ecological functioning and societal uses. An IfSAR approach is one methodology whereby a forest's structure and height in particular can be successfully estimated. Critical to the successful estimation is a high correlation between multiple SAR images. Regardless of a forest's location on the Earth, wind and precipitation can significantly alter a forest's appearance to a SAR system operating in either the L or C bands and so too decrease this necessary correlation. In order to investigate and quantize the decorrelation induced by factors such as wind and rain, we have developed a model for the repeat-pass interferometric SAR response of a forest including the application of a wind field and / or a rain storm. The simulation consists of multiple interconnected parts including the generation of fractal tree geometries, a wind simulator to apply variable wind forces to the generated trees, an electromagnetic model to allow us to calculate a Single Look Complex value for the SAR return of the combined target, an image forming technique based on antenna array theory, and an image processing algorithm. Results present polarimetric coherence as a function of platform look angle, wind speed, and moisture content. An important feature of this research is the usage of a physically based realistic wind model that is based on measurements of wind effects on trees as well as realistic models of fluid flow and simple harmonic branch segment resonators. Allowing branches to bend and move out of the plane of the incident wind field enables our model to capture numerous features of a physical tree blowing in the wind. This realistic model is necessary for a realistic simulation of the effects that wind has on a given InSAR imaging system as expressed in this study by the interferometric coherence. [C172]

### "Preliminary result of polarization property analysis using fully polarimetric GB-SAR images"

Korea Institute of Geoscience and Mineral Resources (KIGAM) and Kangwon National University (KNU) ground-based synthetic aperture radar (GB-SAR) team has been developed a fully polarimetric and interferometric GB-SAR system over past several years. The objective of this paper is to investigate an application of the obtained fully polarimetric GB-SAR images and an effective polarimetric analysis method to extract polarization properties from different terrain targets as a preliminary study. We utilized an unsupervised classification method for

analyzing of a fully polarimetric GB-SAR image, in particular, Cloude and Pottier's method and a combined  $H/A/\alpha$  and the complex Wishart classifier method based on the  $H/A/\alpha$  polarimetric decomposition theorem. [C173]

#### "Four-component scattering power decomposition with rotation of coherency matrix"

In this presentation, a new decomposition scheme of first using a rotation of the coherency matrix followed by the four-component decomposition is presented. It is shown using airborne Pi-SAR data sets that oriented urban areas are clearly distinguished from volume scattering as double bounce objects by the rotation of coherency matrix. [C174]

#### "Accelerating InSAR raw data simulation on GPU using CUDA"

This paper describes a scalable parallel method for interferometric synthetic aperture radar (InSAR) raw data simulation on graphic processing unit (GPU) with common unified device architecture (CUDA). The advantages of the new method rely on the three contributions: GPU hardware provides lots of stream processors for threads calculating, CUDA software environment runs thousands of threads working in parallel for assigned task, raw data simulation adopts the fine-grained task parallelism. Compared with OpenMP, MPI and grid computing, the method not only improves the computational efficiency greatly, but also save the resources such as hardware, electric power and room space. The results show that the method not only ensures accuracy, but also be able to obtain the speedup about 30 times. [C175]

#### "AN SVM classifier with HMM-based kernel for landmine detection using ground penetrating radar"

We propose a landmine detection algorithm using ground penetrating radar data that is based on an SVM classifier. The kernel function for the SVM is constructed using discrete hidden Markov modeling (HMM). Typically, the kernel matrix could be obtained by defining an adequate similarity measure in the feature space. However, this approach is inappropriate as it is not trivial to define a meaningful distance metric for sequence comparison. Our proposed approach is based on HMM modeling and has two main steps. First, one HMM is fit to each of the  $N$  individual sequences. For each fitted model, we evaluate the log-likelihood of each sequence. This will result in an  $N \times N$  log-likelihood similarity matrix that will be adapted to serve as the kernel of the SVM classifier. In the second step, we train an SVM classifier to learn a decision boundary between the positive and negative samples. [C176]

#### "A physically-based approach to observe man-made metallic objects in dual-polarized SAR data"

An electromagnetic model to observe man-made metallic objects in dual-polarized SAR data has been developed. The model predicts that man-made metallic objects and sea surface, being characterized by completely different symmetry properties, call for a different and well-distinguishable HH-HV correlation. Following this rationale, a simple and very computer-time effective filtering technique has been developed to observe man-made metallic objects in full-resolution dual-polarized SAR data. Experiments accomplished over Single Look Complex (SLC) Fine Quad Polarization RADARSAT-2 SAR data confirm the effectiveness of the proposed approach. [C177]

#### "A novel three-step focusing algorithm for TOPSAR image formation"

This paper conducted thorough research to the theory of space-borne TOPSAR data processing. The time-frequency characteristic of TOPSAR mode signal was analyzed and discussed in detail by mathematic derivation combined with the TOPSAR factor. Based on the analysis, an efficient and precise three-step image formation algorithm was presented for TOPSAR image formation without data division, and the operation in every step was theoretically proved effective. The de-rotation operation in the first step and deramp operation in the third step are adopted to finish the stretch in both frequency and time domains respectively, by which the azimuth folding effects in the time and frequency domains are overcome. [C178]

#### "Image formation algorithm for bistatic forward-looking SAR"

The conventional monostatic SAR shows a limitation of achieving a high azimuth (angular) resolution if a forward-looking geometry is used. Bistatic SAR offers a possibility of the forward-looking formation image, e.g. one platform operates as a separated illuminator while another works in a forward-looking mode. In this special bistatic configuration, the forward-looking beam will introduce two problems. The first one is the significant Doppler shift, which will produce the range-azimuth coupling. The second one is that the targets located at symmetrically about the flight path of the forward-looking platform have the same antenna-to-target range which would cause the range migration ambiguity of the receiver. This paper will develop a mathematical model to

describe the Doppler characteristic of bistatic forward-looking SAR (BFLSAR). Based on this model, the previous bistatic point reference spectrum (BPTRS) can be applied. Using the BPTRS, a modified range-Doppler algorithm is proposed to handle the two problems and focus BFLSAR data in the azimuth-invariant configuration. Finally, simulation experiment is used to validate the proposed model and processing approach.

[C179]

### "Comparisons of rain rate and reflectivity between TRMM precipitation radar and Gosan S-band radar"

As a part of GPM joint Ground Validation (GV) projects with the US and international partnership, one of the Korea Meteorological Administration (KMA) S-band radar at Gosan, Jeju Island, South Korea has been selected in the Validation Network (VN). It performs the match-up of TRMM Precipitation Radar (PR) data with ground-based radar (GR) during August 2006 to May 2008 for the rain events on criteria of at least 25 % overlap of the PR swath and 25 % or more of the points in the overlap area indicating rain certain in the PR data. 60 events with these criteria during the period have been selected to compare the reflectivity only over 18 dBZ from both radars. Overall comparisons between GR and PR reflectivity roughly 1.37 dBZ low bias over 163,586 points. The results came out good quality and recently asked the TRMM Precipitation Processing System (PPS) to add the site to the daily TRMM site overpass coincidence table (CT) product. Rain rate comparisons between GR and PR show PR over estimate the rain rate in these events. [C180]

### "TropiSAR: Exploring the temporal behavior of P-Band SAR data"

The TropiSAR campaign has been conducted in August 2009 in French Guiana with the ONERA airborne system SETHI. The main objective of this campaign was to collect data to support the Phase A of the Earth Explorer candidate mission, Biomass. Several specific questions need to be addressed to answer the recommendations of the ESAC group and the data collection strategy has been constructed accordingly. The first part of the paper lists these specific questions. We then describe the selected test sites, followed by a summary on the radar instrument and the radar configuration (geometry and waveform). The data acquisition plan is provided and the temporal behaviour of the P-Band data is explored. [C181]

### "Retriveval of soll moisture under vegetation using Polarimetric Scattering Cubes"

Soil moisture inversion from polarimetric SAR data has attracted significant attention for the past twenty years. Comparing with the simple case of bare surface, it is extremely complicated for vegetated terrain to invert soil moisture because of a larger number of scattering mechanisms that contributes to the observation. In this paper, we show how polarimetric decomposition technique, which decomposes SAR observations into preferred scattering mechanisms, can be used for the inversion. The result leads us to give up the use of polarimetric decomposition because of an unknown attenuation ratio caused by the canopy. Then a new inversion algorithm using Polarimetric Scattering Cubes (PSC) is introduced with simulation results to show a sensitivity to physical parameter such as vegetation distribution. Finally, we also discuss how the technique should be implemented for the real SAR data. [C182]

### "Nowcasting rainfall fields estimated from specific differential phase"

This paper presents a preliminary evaluation of short-term prediction (nowcasting) of rainfall fields estimated from specific differential phase fields derived from Collaborative Adaptive Sensing of the Atmosphere X-band radar data. A Fourier-space, linear system-based nowcasting method used these rainfall fields as input to generate rainfall forecasts up to 20 min. The results show the extent to which specific differential phase-derived rainfall fields can be predicted and the utility of such predictions to be approximately 15 min. [C183]

### "Spatial spectrum of bistatic SAR with one fixed station"

Bistatic synthetic aperture radar (BSAR) with one fixed station (OF-BSAR) can be used in wide area surveillance, interferometry and etc. This paper analyzed the spatial spectrum of OF-BSAR. Analytical expressions of the spatial spectrum was given. Using this result, we can determine the resolution performance of OF-BSAR. [C184]

### "Land cover classification based on single-polarized VHR SAR images using texture information derived via speckle analysis"

Speckle is a SAR specific noise effect caused by constructive and destructive interference from multiple scattering within the resolution cell of the imaging radar system that superposes the true radiometric and textural information of SAR images as a grainy 'salt-and-pepper' pattern. Fully developed speckle basically follows

circular Gaussian image statistics. However, this assumption is not applicable for very high resolution SAR systems and for data showing sceneries with a significant amount of directional backscatter-e.g. urban areas. In those cases the multiple scattering processes within a resolution cell show-subject to the true structuring of the imaged area-rather a directional behavior than a random distribution. Consequently, the speckle is no longer fully developed. In our study we demonstrate how information on the local development of speckle can be used to differentiate between basic land cover types such as water, open land-meaning farmland, grassland and bare soil -, woodland and urban area in single-polarized, single-date VHR SAR images. The research is based on the analysis of a TerraSAR-X scene of Munich, Germany. [C185]

#### "Investigations on TOPS interferometry with TerraSAR-X"

This paper presents results on SAR interferometry with the so-called TOPSmode. The rationale to retrieve accurate interferometric products with such a mode is expounded, emphasizing the critical step of coregistering the pairs. Due to the particularities of the TOPS mode, a high Doppler-centroid is present at burst edges, demanding very high azimuth coregistration performance. A coregistration accuracy of one tenth of a pixel, as it is usually recommended with interferometric applications, will result in a large undesired azimuth phase ramp in the TOPS mode, above all at X-band. This paper presents two approaches based on the spectral diversity technique to estimate this offset with the required accuracy. Experimental results with repeat-pass TerraSAR-X data are shown to validate the proposed approach. [C186]

#### "Polarimetric scattering analysis for accurate observation of stricken man-made targets using a rotated coherency matrix"

This paper investigates polarimetric scattering features generated from man-made targets for accurately observing stricken residential area by making full use of quad. polarimetric SAR data set. First, we propose a simple improvement of the scattering power decomposition method by introducing a unitary rotation of the coherency matrix. It is found from the results of the POLSAR image analysis for a mountainous region including some stricken residential areas that by carrying out the rotation procedure, double-bounce scattering contribution can be enhanced even when the targets are oriented and/or set on small inclined ground plane. This peculiar scattering feature is utilized as a useful marker for precisely detecting man-made targets. To verify the generating and enhancing mechanism of the double-bounce scattering, we also carry out the Finite-Difference Time-Domain (FDTD) polarimetric scattering analysis for a simplified man-made target model. The dependency of the polarimetric scattering feature on the variation of squint angle is investigated. It is confirmed from the FDTD analysis for oblique squint angular range that by applying the rotation procedure before the scattering power decomposition, the double-bounce scattering contribution tends to be enhanced, and the volume scattering becomes small. [C187]

#### "ISAR imaging of an aircraft target USING ISDB-T digital TV based passive bistatic radar"

Passive bistatic radars (PBRs) exploit existing transmitters such as TV broadcasts as the source of illumination. PBR is consisted of two receivers, with one antenna pointed at the source and the other at the target, and the target range is determined by correlating the signal scattered by the target with the signal directly arrived at the receiver. Since PBR does not transmit any waveform, it consumes lower power, and no frequency allocation is required. We have conducted a field experiment exploiting terrestrial digital TV broadcast to assess the feasibility of ISAR (Inverse Synthetic Aperture Radar) observation based on PBR. The wide and flat spectrum of the OFDM signal and the small gap between the channels enables us to obtain high range resolution of up to several meters by exploiting multiple physical channels. Therefore, moderate resolution ISAR imaging is expected to be possible. In this paper, PBR based ISAR algorithm is briefly explained, and the first example of observed PBR based ISAR image of an aircraft target is shown. [C188]

#### "Performance and application of different image matching algorithms for investigating glacier and ice-shelf flow, permafrost creep and landslides"

This study focuses on evaluating image correlation methods for deriving surface velocity fields of glaciers, ice shelves, rockglaciers and landslides from both repeat optical and synthetic aperture radar (SAR) images. Firstly we show that low resolution MODIS images (250 m spatial resolution) can in fact be used for determining displacements on Antarctic ice shelves. In this particular case, orientation correlation operated in the frequency domain and using only the phase part of the signal performs better than normalized cross-correlation operated in the spatial domain. Secondly we demonstrate that for determining subpixel displacement when using normalized cross-correlation, image intensity interpolation before the matching process outperforms interpolation of the correlation peak after the matching. We also study methods for adaptively varying the matching template size in order to create the most reliable and accurate matches. The last part of the work shows some application

studies of glacier flow from optical and SAR images, rockglacier creep and land sliding. [C189]

#### "Mapping and change detection for boreal wetlands of North America based on JERS and PALSAR data"

We have been developing high-resolution thematic maps of wetlands throughout the North American boreal regions. We assemble a wetlands map for each region based on data collected during the late 1990s, then construct a second map based on data collected during the late 2000s. Comparison of the two maps then makes it possible to assess changes that have occurred over the course of the intervening decade.. [C190]

#### "High-resolution 3-D radar imaging using pseudo-random noise coded waveform"

In this paper, high-resolution 3-D radar imaging using a 3-step image formation procedure based on the Huggens-Fresnel's principle is analyzed and discussed. To achieve high spatial resolution, large antenna array is required. The array can be implemented with a synthesized antenna array, or a sparse antenna array. To achieve high range resolution, pseudo-random noise (PN) coded signal waveform is used. The ability of generating high-resolution 3-D imaging is verified by computer simulation. Numerical simulation shows the reconstructed 3-D radar image of an object. PN coded signal waveforms also has the advantage of noise immunity. Applications of the high resolution 3-D radar imaging can be in ground penetration radars, microwave medical imaging, and down-looking SARs. [C191]

#### "Improving hydrological forecasting using multi-source remote sensing data together with in situ measurements"

This paper describes the development of information systems and techniques for improving hydrological forecasting by applying satellite observations, weather radars, and in situ measurements from automatic monitoring stations. In the methodology developed and demonstrated, the observation data are accompanied with a detailed soil and land cover information. The information system is concerned with the following physical characteristics relevant to river discharges and flooding: snow water equivalent (SWE), cumulative amount of precipitation, fraction of snow covered area during the melting period (FSC), soil moisture, and soil frost. Feasibility of the multi-source information system is demonstrated in a pilot experiment for Finnish Lapland, using the hydrological forecasting system of the Finnish Environment Institute (SYKE) as an example of a typical operational distributed model. [C192]

#### "Ground penetrating radar for tunnel detection"

Ground penetrating radar (GPR) systems have important civil and military applications and can be used for surveying subsurface structures such as bunkers, tunnels and buried pipes. However, GPR systems for detecting deep tunnels still face many challenges, and their performance often depends on soil types, specific targets and subsurface geological features. This paper discusses challenges in tunnel detection and provides a useful and efficient procedure to develop system requirements and predict detection performance. [C193]

#### "Interpretation of buildings in high resolution sar images based on electromagnetic method"

High resolution SAR (Synthetic Aperture Radar) will provide an innovative tool for urban area applications. Nevertheless, interpretation of SAR image in urban area is far from solved by the increase of spatial resolution. It is usually difficult to establish a determined relationship between scattering centers in high resolution SAR images and the basic units of building targets. In order to thoroughly understand the backscattering behaviour of building targets in high resolution SAR images, a method of high resolution SAR imaging simulation based on electromagnetic model is proposed in this paper, which mainly includes 3-D model establishment for the building target, triangular facets partition, RCS prediction for each facet, and SAR imaging through coherent superposition of echo from each triangular facet. Through comparison of the simulated and the original SAR image, building scatter mechanisms in high resolution SAR images can be well interpreted. [C194]

#### "Tree height retrieval methods using POLInSAR coherence optimization"

This paper investigates to what extent interferometric coherence optimization in radar polarimetry improves the performance of forest height inversion method using POLInSAR measured data. Based on repeat pass E-SAR data and the corresponding ground measured forest stand heights, several available forest height inversion methods are validated and compared together with coherence optimization algorithms such as the iteration for the maximization of the magnitude difference (BF-mag) coherence optimization algorithm and phase diversity (PD) coherence optimization algorithm. The results show that coherence phase optimization can improve the performance of the tree height retrieval method based on coherence phase information, but can not improve the

performance of the retrieval method based on coherence amplitude information alone. Furthermore, an integrated inversion method, which combines coherence phase with coherence amplitude information and includes corresponding polarization coherence optimization and compensation of non-volume scattering decorrelation, is proposed and discussed. [C195]

#### "A comparison of estimated mixing height by multiple remote sensing instruments and its influence on air quality in urban regions"

Urban areas suffer from high pollutant loadings due to their proximity to emission sources as well as transported aerosols. Therefore it is essential to have an accurate technique for measuring the pollutants and evaluate their effect. Since the atmosphere mixing height (MH) defines the total volume available for the pollutant transport and dispersion, it is important that air-quality models can provide realistic estimates. This paper studies multiple instruments for MH determination and their potential for validating air-quality model forecasts such as WRF. In addition, use of automated PBL height retrieval using wavelet analysis is briefly described and long term statistical comparisons of MH and WRF mixing height are obtained. [C196]

#### "GPR evaluation test for humanitarian demining in Cambodia"

ALIS is a dual sensor for humanitarian demining, which is a combination of electromagnetic Induction sensor (EMI) and Ground Penetrating Radar (GPR), developed by Tohoku University, Japan. ALIS is equipped with a sensor tracking system using a CCD camera with image processing, which enables signal processing for subsurface imaging. Two sets of ALIS have been deployed in mine fields in Cambodia since 2009 and more than 50 buried landmines have been detected. We found that the Synthetic Aperture Radar processing (SAR processing) is effective not only imaging the buried objects, but also for reduction of clutter of soil. [C197]

#### "Tropospheric correction for InSAR using interpolated ECMWF data and GPS Zenith Total Delay from the Southern California Integrated GPS Network"

A tropospheric correction method for Interferometric Synthetic Aperture Radar (InSAR) was developed using profiles from the European Centre for Medium-Range Weather Forecasts (ECMWF) and Zenith Total Delay (ZTD) from the Global Positioning System (GPS). The ECMWF data were interpolated into a finer grid with the Stretched Boundary Layer Model (SBLM) using a Digital Elevation Model (DEM) with a horizontal resolution of 1 arcsecond. The output were converted into ZTD and combined with the GPS ZTD in order to achieve tropospheric correction maps utilizing both the high spatial resolution of the SBLM and the high accuracy of the GPS. These maps were evaluated for three InSAR images, with short temporal baselines (implying no surface deformation), from Envisat during 2006 on an area stretching northeast from the Los Angeles basin towards Death Valley. The RMS in the InSAR images was greatly reduced, up to 32%, when using the tropospheric corrections. Two of the residuals showed a constant gradient over the area, suggesting a remaining orbit error. This error was reduced by reprocessing the troposphere corrected InSAR images with the result of an overall RMS reduction of 15-68%. [C198]

#### "Remote sensing atmospheric CO<sub>2</sub> column abundance using an airborne pulsed laser sounder at 13 km altitude"

Accurate global measurements of tropospheric Carbon Dioxide abundance to the "parts per million" (ppm) level is required to better quantify processes that regulate CO<sub>2</sub> exchange between atmosphere, land and ocean. To measure CO<sub>2</sub> globally NASA has planned the ASCENDS mission, Active Sensing of CO<sub>2</sub> Emissions over Nights, Days and Seasons. We report on an airborne laser-based remote sensing instrument we have developed at NASA-GSFC as a candidate for the ACENDS mission. Preliminary analyses of data from initial flight testing to 13 km altitude indicates a CO<sub>2</sub> mixing ratio of 396 ppm from CO<sub>2</sub> column abundance where in situ sensors determine 390 ppm mixing ratio. [C199]

#### "Monitoring thickness change of the Dongkemadi Glacier on Qinghai-Tibetan Plateau using SRTM DEM and map-based topographic data"

In this paper we measured the long-term thickness change of the Dongkemadi Glacier (DG) on Tanggula Mountain, Qinghai-Tibetan Plateau, using the Shuttle Radar Topography Mission (SRTM) C-band data (2000) and a digital elevation model (DEM) generated from topographic map (1969). First we check the accuracy of SRTM DEM by comparison at 16 random independent points in surrounding non-glacier area below 5500m a.s.l., then we focus on an analysis of the glacier's surface thickness change features and a validation of the results using GPS survey data (2007) and DEM (1969) in Xiao Dongkemadi Glacier (XDG). The result shows XDG decreased by an average of 6.15m, or 0.20 m a<sup>-1</sup> between 1969 and 2000. We estimate the error of

annual thickness change rate to be on the order of 5% compared to the result of field measurement while Da Dongkemadi Glacier (DDG) decreased by an average of 20.74m or 0.67m a<sup>-1</sup> (1969-2000). [C200]

#### "Spaceborne-airborne bistatic radar for UAS navigation purposes: Preliminary analysis and strawman system identification"

The study of a novel navigation system for Unmanned Airborne System (UAS) based on bistatic Synthetic Aperture Radar (SAR) is presented. The innovative bistatic configuration builds on spaceborne radar transmitters and airborne receivers, the latter mounted in a forward-looking geometry. Such approach, impossible or extremely demanding with a monostatic approach, allows one to achieve dual information with two different radar working modes: imaging capability can be in fact coupled with the possibility of moving target indication. The study is particularly suited on one of the most common UAS platforms: a close range, medium takeoff weight, with an endurance of roughly 7 hours and cruise speed of about 50m/s, whose requirements have been identified. The finalization of the study is achieved by the definition of a strawman system concept with different approaches. Four options are identified, with different performance and system complications/challenges. The study herein reported was carried out under ESA contract 22449/09/F/MOS. [C201]

#### "Calibration accuracy enhancement in the field experiment with a ground-based scatterometer"

An improved field-measurement technique for enhancing the calibration accuracy of a ground-based scatterometer is proposed in this paper. The automatic two-dimensional (2-D) measurement of a calibration target, so-called '2-D target scanning technique (2DTST)', gives a precise alignment between a point calibration target and an antenna bore-sight. Averaging of the calibration-target measurements increases further the accuracy and reliability of the automatic alignment. The measurement results show that the correlation among the measurements is larger than 0.95 and the error-rate is below 5% at a frequency range from 9.4 GHz to 9.9 GHz. The evaluation of the calibration accuracy using the STCT (Single Target Calibration Technique) shows that 2DTST in the field experiment can secure the precise calibration accuracy within 0.5 dB for magnitude correction and 4° for phase correction. [C202]

#### "Evaluation of vegetation effect on the retrieval of snow parameters from backscattering measurements: A contribution to CoReH2O mission"

In preparation of the satellite mission CoReH2O, one of the three missions selected for scientific and technical feasibility studies within the Earth Explorer Programme of the European Space Agency, experimental and theoretical studies started in order to investigate backscatter properties of snow covered terrain and improve the methods for retrieval of snow physical properties from SAR data. The aim of this paper is to investigate the impact of vegetation in the retrieval of snow parameters from backscattering measurements. First a radiative transfer model, able to simulating scattering from a vegetated snow-covered terrain was developed and implemented. Lastly, a sensitivity analysis on snow and vegetation parameters was conducted for coniferous forest. Results confirm that with increasing biomass the sensitivity to SWE strongly decreases. Moreover when biomass is in the 0-150 m<sup>3</sup>/ha range a procedure to correct the vegetation effect in the SWE retrieval algorithm is suggested. [C203]

#### "Remote sensing research in undergraduate education: An international fieldwork perspective"

Institutions of higher education in the U.S. are increasing their use of project-based courses and experiential learning using projects or service in other countries. Project-based instruction provides students with an opportunity to make connections between the classroom and the world around them. Research suggests that fieldwork strongly enhances curriculum instruction and provides additional learning value to students. The goal of this grant was to increase the international content of existing curriculum by providing to students advanced skills in sampling design, geospatial statistics, and remote sensing for mapping and monitoring of crops and natural areas including semi-arid mountains, sub-tropical mountains, and tropical rain forests. This experience for the students has opened their eyes to new cultures and environments, allowed them to apply their classrooms skills in a real-world context and importantly to see how what they are learning is readily usable outside the classroom. [C204]

#### "Adapting the sir algorithm to ASCAT"

Scatterometers have been launched primarily to measure ocean winds. The value of scatterometer data is increased by application of the SIR (Scatterometer Image Reconstruction) algorithm. The SIR algorithm enhances the effective resolution of the scatterometer data to support its use for other studies. SIR has been used successfully on several scatterometers, including QuikSCAT. In this paper, we describe how the SIR

algorithm is adapted to ASCAT data. Using SZF data from ASCAT leads to the best resolution enhancement. SIR requires an estimate of the spatial extent for each measurement. We detail our method to estimate an approximate spatial response function for each ASCAT measurement. Finally, SIR parameters are tuned for use with ASCAT. [C205]

#### "Airborne Doppler Wind Lidar investigations of western Pacific typhoon genesis and evolution"

The first ever extensive study of tropical cyclones using Doppler Wind Lidars (DWL) was conducted in 2008 within the THORPEX Pacific Asian Regional Campaign. More than 100 hours of DWL profiles were obtained with an average spacing of 3 km. These wind profiles along with dropsonde temperature, moisture and wind profiles are being used to study the genesis and evolution of tropical cyclones. Initial investigations are focused upon the impact the DWL profiles have on numerical weather prediction. [C206]

#### "Synthetic aperture radar image analysis as a tool for validation of baroclinic internal wave 3D modeling in Algeciras Bay (Strait of Gibraltar)"

This paper presents the main results obtained from the application of synthetic aperture radar (SAR) sea surface image analysis to the validation of the baroclinic internal wave 3D modeling in the Strait of Gibraltar and Algeciras Bay. Appropriate SAR images, showing the occurrence of short-wavelength oscillations in the sea surface in this area, were selected and compared with the modeled spatial fields of the M2 free-surface elevation at the corresponding tidal stages, sometimes corrected for the consideration of neap or spring episodes. A good agreement between SAR images and model fields was found. The analysis of SAR images has showed to be a powerful tool for the study of the internal wave phenomena in the Strait of Gibraltar and Algeciras Bay, providing a holistic way for the validation of 3D model experiments in that matter. [C207]

#### "A distributed LiDAR processing model based on OWS and BPEL"

Traditional LiDAR post process is centralized. In centralized process model, data, process module and workflow can only be accessed within specific platform. This results in interoperability problem ranging from data sharing to functionality and workflow reuse. To tackle this problem, this paper proposes distributed process model for LiDAR post process. The distributed process model consists of interoperability solution on three aspects: data, process module and workflow. According to experiment, distributed LiDAR process model overcomes problems mentioned above. The process model and interoperability solution proposed in this paper can serve as reference to other geo-processing application. [C208]

#### "Coherent MIMO radar for GMTI"

In addition to imaging, coherent MIMO radars have a strong potential for detecting moving objects and estimating their parameters. This paper investigates different MIMO schemes based on spatial, waveform, and frequency diversity for their GMTI capability. The fully configurable MIMO radar MIRACLE X is taken as the baseline design for comparing the different approaches. [C209]

#### "Icesat lidar and global digital elevation models: applications to desdyni"

Geodetic control is extremely important in the production and quality control of topographic data sets, enabling elevation results to be referenced to an absolute vertical datum. Global topographic data with improved geodetic accuracy achieved using global Ground Control Point (GCP) databases enable more accurate characterization of land topography and its change related to solid Earth processes, natural hazards and climate change. The multiple-beam lidar instrument that will be part of the NASA Deformation, Ecosystem Structure and Dynamics of Ice (DESDynI) mission will provide a comprehensive, global data set that can be used for geodetic control purposes. Here we illustrate that potential using data acquired by NASA's Ice, Cloud and land Elevation Satellite (ICESat) that has acquired single-beam, globally distributed laser altimeter profiles ( $\pm 86^\circ$ ) since February of 2003. The profiles provide a consistently referenced elevation data set with unprecedented accuracy and quantified measurement errors that can be used to generate GCPs with sub-decimeter vertical accuracy and better than 10 m horizontal accuracy. Like the planned capability for DESDynI, ICESat records a waveform that is the elevation distribution of energy reflected within the laser footprint from vegetation, where present, and the ground where illuminated through gaps in any vegetation cover. The waveform enables assessment of Digital Elevation Models (DEMs) with respect to the highest, centroid, and lowest elevations observed by ICESat and in some cases with respect to the ground identified beneath vegetation cover. Using the ICESat altimetry data we are developing a comprehensive database of consistent, global, geodetic ground control that will enhance the quality of a variety of regional to global DEMs. Here we illustrate the accuracy assessment of the Shuttle Radar Topography Mission (SRTM) DEM produced for Australia, documenting spatially varying elevation biases of several meters in magnitude. [C210]

### "Geo-location error correction for Synthetic Aperture Radar image"

Spaceborne SAR (Synthetic Aperture Radar) image inherently contains geo-location errors which are caused by SAR image acquisition geometry, imaging mode, characteristics of reflectivity and image formation process. Since the geo-location error caused by SAR image acquisition geometry is inevitable, these errors should be considered and corrected during the image formation process. In this paper, a geo-location error correction method is presented to analyze and correct the azimuth skew and ground range non-linearity error, and orientation error. This scheme does not require the aids of GCP and DEM, and instead directly extract the key correction parameters from the SAR raw data. Using RADARSAT-1 image, a simulation is performed to evaluate the proposed geo-location algorithm. To analyze the effect of proposed correction method, the corrected SAR images are compared with the reference image by RMSE values. [C211]

### "Leaf area index (LAI) estimation based on vehicle-based laser scanning"

This paper proposes a novel approach for leaf area index (LAI) estimation based on vehicle-based laser scanning (VLS), which occurs as a state-of-the-art mapping technique. The method is advanced from the traditional terrestrial laser scanning (TLS), which has been primarily validated capable of predicting LAI. The associated schematic is to explore the correlations between VLS and TLS collections of the same trees. If positive, LAI can be retrieved with the related TLS data as reference. In this study, the consistency between the multi-echoes per pulse received by VLS and the single-echo per pulse recorded by TLS is further tackled, and LAI, thus, can be derived more accurately. The experiments based on the real-measured VLS and TLS data have validated the applicability of VLS for estimating LAI. [C212]

### "Dual-polarization performance of the phase-tilt antenna array in a casa dense network radar"

In this paper the evaluation of dual-polarized scanning performance of a large planar array antenna for a solid state radar for weather is discussed. The antenna array is designed to operate at 9.36 GHz  $\pm$ 50 MHz, and the transmission and reception mode is configured to work alternatively. The antenna array architecture based on a series-fed array configuration of Dual-Polarized Aperture Coupled Patch Antennas (DP-ACPA) was designed and implemented to achieve the required radar polarimetric performance at low cost. Measured patterns of the array in the elevation and azimuth plane are used to evaluate the two principal polarimetric radar parameters (Zdr and LDR) over the scanning range in azimuth plane. It is shown that the biases in the differential reflectivity due the cross-polarization of this antenna configuration are negligible in comparison with the biases produced for the mismatch antenna patterns (H and V). [C213]

### "Tandem-L: And innovative interferometric and polarimetric SAR mission to monitor earth system dynamics with high resolution"

Tandem-L is a proposal for an innovative interferometric and polarimetric radar mission that enables the systematic monitoring of dynamic processes on the Earth surface. Important mission objectives are global forest height and biomass inventories, large scale measurements of millimetric displacements due to tectonic shifts, and systematic observations of glacier movements. The innovative mission concept and the high data acquisition capacity of Tandem-L provide a unique data source to observe, analyze and quantify the dynamics of a wide range of mutually interacting processes in the bio-, litho-, hydro- and cryosphere. By this, Tandem-L will be an essential step to advance our understanding of the Earth system and its intricate dynamics. [C214]

### "Using AMSR-E land product to monitor the drought process in China"

This paper presents a method (drought index) to monitor the drought process in China. The method based on the relationship between drought and soil moisture change. Although the absolute value of soil moisture from AMSR-E land product is not accurate enough, but we can use the soil moisture change information in the temporal scale. The soil moisture product of AMSR-E from 2002 to present is used to build up the drought index. In each EASE-GRID grid, the smallest soil moisture value and the largest soil moisture value in the 8 years are defined to dry/wet edge points and the drought index of them are 0/100. With the two edge points, we can get drought index in each grid, each day. Using the former method, we represent 4 typical drought processes in China. Result show that the drought index from AMSR-E soil moisture product can brought out the development and distribution of drought process roughly. [C215]

### "A system trade model for the monitoring of coastal vessels using HF surface wave radar and ship automatic identification systems (AIS)"

Coastal nations have an interest in maritime domain awareness for applications in national security, coastal

conservancy, fishery and stewardship of the exclusive economic zones (EEZs) along their coastlines. Using our previously developed HF radar and AIS ship detection models we find signal to noise ratio (SNR) as a function of range, including ducted propagation for the AIS radio signals. We use these SNR estimates to find probability of detection  $P_d$  and then explore multiple systems and stations at variable spacings along the coast. Our example HF radar has significant power and aperture, similar to the Pisces radar. The AIS model is for high power (12.5 W) AIS and a significantly elevated receiver ( $\approx 250$  ft asl). A combined system of HF radar and AIS shows good capability ( $P_d > 0.9$ ) to ranges of  $\approx 125$  km for small ships and to 200 km for large ships. Considering a system of sites separated by 100 km we find that a  $P_{dof} > 0.9$  can be maintained to a distance off shore of 130 km even for small, 120 ton, ships. [C216]

#### "A concept for high performance reflector-based Synthetic Aperture Radar"

The success of current spaceborne Synthetic Aperture Radar (SAR) is boosting the performance requirement of next generation systems. In order to cope with the evolution of SAR the design of the new systems will need to meet higher requirements for spatial and radiometric resolution together with an increased availability. This tendency is recognized nearly independently of the application area and manifests itself through several study programs initiated by space agencies aiming at the design of future SAR systems. In this context the use of large reflectors combined with digital feed arrays for SAR is considered a possible alternative to planar array antennas. This paper suggests an X-band spaceborne SAR system utilizing a deployable reflector together with a digital feed array, analyzes its performance and highlights its advantages compared to other systems based on direct radiating arrays. [C217]

#### "Ocean wave field measurements using X-band Doppler radars at low grazing angles"

Ocean wave field observations using two types of Doppler radar systems are compared with time series measurements of the surface elevation at the USACE Field Research Facility (FRF) in Duck, NC. [C218]

#### "A polarimetric two-scale model for soil moisture retrieval"

A polarimetric two-scale surface scattering model employed to retrieve the surface parameters of bare soils from polarimetric SAR data is proposed. The scattering surface is considered as composed of slightly rough randomly tilted facets, for which the Small Perturbation Method holds. The facet random tilt causes a random variation of the local incidence angle, and a random rotation of the local incidence plane around the line of sight, which in turn causes a random rotation of the facet scattering matrix. Unlike other similar already existing approaches, our method considers both these effects. The proposed scattering model is then used to retrieve bare soil moisture and (large-scale) roughness from the co-polarized and cross-polarized ratios. The performances of the resulting retrieval algorithm is finally assessed by comparing obtained results to "in situ" measurements. To this aim, data from Little Washita campaign available in literature is employed. [C219]

#### "Microphysical retrievals of dual polarization and dual frequency ground radar for GPM ground validation"

A dual-frequency precipitation radar (DPR) will be deployed aboard GPM (Global Precipitation Measurement) core satellite in order to enhance our knowledge of precipitation microphysics. A ground based dual-frequency (Ku and Ka band) and dual-polarization radar D3R is being built to perform cross validation with GPM-DPR which helps provide insight into the physical basis of the retrieval algorithm. This paper is the follow up study of the author's previous paper where a new drop size distribution (DSD) retrieval algorithm was proposed. In this paper, the algorithm evaluation is extended to the complete region including rain, melting ice and ice based on simulation data. A possible method to classify the hydrometeor identification for dual-frequency and dual-polarization ground radar is also proposed which might be applied to D3R. [C220]

#### "Full wave analysis of VHF-UHF forest bistatic scattering mechanisms an investigation on the influence of electromagnetic coupling"

A 3D coherent scattering model simulating the interaction of electromagnetic waves with forests has been developed. It is obtained by means of a full wave approach, based on an integral representation of the electric field. A method of moments is used to solve the integral equation and compute the scattered fields related to the various scattering mechanisms as well as the contribution of tree-trunks and branches. This model is used here to evaluate the impact of electromagnetic coupling effects between a group of scatterers (which can be the branches and the trunk of a single tree, multiple tree-trunks, or multiple trees) for monostatic and/or bistatic radar configurations. To validate our model, we compare our simulation results with anechoic chamber measurements. [C221]

### "Estimation of the degree of polarization in compact polarimetry"

The degree of polarization (DoP) has long been recognized as one of the most important parameters characterizing partially polarized electromagnetic waves. This parameter can be effectively used to describe the information content of polarimetric images collected by synthetic aperture radar (SAR) systems. Estimation of DoP is standardly performed using four measurements. In SAR compact polarimetry (CP), however, only two measurements are available. In this paper, we develop maximum likelihood estimators of the DoP, in SAR CP modes, based on only two intensity images. We evaluate and compare the performance of these estimators for different CP modes on RADARSAT-2 polarimetric data, over various terrain types such as urban, vegetation, and ocean. [C222]

### "ALGAE: A fast algebraic estimation of interferogram phase offsets in space varying geometries"

This work deals with the estimation of terrain topography from multi-pass Synthetic Aperture Radar (SAR) interferometry (InSAR), focusing on the case where the variation of the system geometry within the imaged swath is relevant, as in airborne multi-pass interferometric campaigns. The space varying nature of the system geometry gives rise to a major issue in multi-pass InSAR analyses, in that it prevents from compensating for the presence of interferogram phase offsets by simply phase locking the data stack to a reference point, therefore hindering the retrieval of terrain topography. To cope with this issue properly we propose a novel approach that exploits the algebraic properties of the problem. Such an approach allows to cast the problem in terms of identification of a null space component for terrain topography, after which both topography and the interferogram phase offsets are quickly obtained without exploiting calibration points. [C223]

### "Extracting trees and structure parameters via integration of LIDAR data and ground imagery"

Detailed tree information, such as tree counts, tree heights, crown base heights, diameter at breast height (DBH), and tree biomass, is critical for the effective management and quantitative analysis of trees in urban area. Automatic detection of trees, and their parameters using light detection and ranging (LiDAR) data has been widely employed. However, at the single-tree level along road in urban area, LiDAR data depose the disadvantages such as space points, no texture information, so that the detailed tree parameters mentioned above cannot successfully be obtained at enough accuracy. This paper presented an integration of LiDAR data and ground mobile truck data. This development is driven by the fact that the information obtained from ground-mobile truck images can be substantially complemented by the data from LiDAR. [C224]

### "The RADARSAT-1 imaging performance, 14 years after launch, and independent report on RADARSAT-2 image quality"

This paper summarizes the calibration monitoring activities of the Canadian Space Agency (CSA) executed under the RADARSAT Program. The performance history of the RADARSAT-1 SAR since its commissioning in 1996 is reviewed, along with the calibration systems and methodologies used, in the context of the mission's thirteen-year calibration history. Independent image quality measurements for the privately-owned RADARSAT-2, launched in 2008, are also presented. It is shown that the calibration parameters of the RADARSAT-1 SAR have consistently been maintained within the mission's design goals and specifications, mostly thanks to payload stability and timely recalibrations performed using the calibration ground equipment. For RADARSAT-2, CSA's measurements report outstanding image quality levels. [C225]

### "Extraction of coastal wavefield properties from X-band radar"

The dynamic wave field in a high-energy coastal environment is investigated using frequency direction wave spectra obtained by nautical X-band radar imagery. Nautical radars are generally used for navigation and ship traffic control. Under various conditions (wind speed  $> 3\text{m/s}$ , significant wave height  $> 0.5\text{m}$ ), signatures of the sea surface (sea clutter) become visible in the near range (less than 3 nautical miles) of nautical radar images. Swell and wind sea waves become visible in nautical radar images as they modulate the sea clutter signal. Since standard X-band nautical radar systems scan the sea surface with high temporal and spatial resolution, they are able to monitor the sea surface in both time and space. The combination of the temporal and spatial wave information allows the determination of unambiguous directional wave spectra. Here, wave data collected from February-October 2005 at the US Army Corps of Engineers Field Research Facility (USACE-FRF) in Duck, North Carolina is presented. For the radar wave measurements the Wave and surface current Monitoring System WaMoS II was connected to a Furuno FR-7112 X-Band radar with a 6 feet open antenna and an update rate of 2.5s (24 rpm). The radar covers a range from 240m to 2160m from the antenna with a spatial resolution of 7.5m. The wave analysis was carried out over an area of 3.7 km<sup>2</sup> located in relative homogeneous bottom topography, off the near shore breaker bar system, in a water depth of 8m -10m. The WaMoS II wave measurements were

compared to those obtained from a pressure gauge array located in the same area. Earlier WaMoS II validations provide a general indicator of the quality of the measurement performance as they were carried out for standard integral wave properties over all existing wave systems such as mean or peak wave parameters. Here the XWaves ocean wave field analysis toolbox is used to compare data sets by means of a wave spectral partitioning analysis. This approach provides a more detailed validation especially for bi- and multi modal sea states, allows for a comparison of the heights, periods and directions of individual wind sea and swell components, and tracking the evolution of specific wave systems. Such analysis methods have been successfully applied in a variety of wave model validations. The data comparison was carried out for different sea state and wind conditions. Preliminary results of the data comparison show that the WaMoS II system captures the temporal evolution of the individual wind sea and swell wave components entering the surf zone. A statistical error analysis of the isolated wind sea and swell wave systems provides a quantitative assessment of WaMoS II performance in a coastal setting. [C226]

#### "Inferring the impact of radar incidence angle on soil moisture retrieval skill using data assimilation"

The impact of measurement incidence angle ( $\theta$ ) on the accuracy of radar-based surface soil moisture ( $\Theta_s$ ) retrievals is largely unknown due to discrepancies in theoretical backscatter models as well as limitations in the availability of sufficiently extensive ground-based  $\Theta$  observations for validation. Here, we apply a data assimilation-based evaluation technique for remotely-sensed  $\Theta$  retrievals that does not require ground-based soil moisture observations to examine the sensitivity of skill in surface  $\Theta$  retrievals to variations in  $\theta$ . Application of the evaluation approach to the TU-Wien European Remote Sensing (ERS) scatterometer  $\Theta$  data set over regional-scale ( $\sim 10002 \text{ km}^2$ ) domains in the Southern Great Plains (SGP) and Southeastern (SE) regions of the United States indicate a relative reduction in correlation-based skill of 23% to 30% for  $\Theta$  retrievals obtained from far-field ( $\theta > 50^\circ$ ) ERS observations relative to  $\Theta$  estimates obtained at  $\theta < 26^\circ$ . Such relatively modest sensitivity to  $\theta$  is consistent with  $\Theta$  retrieval noise predictions made using the TU-Wien ERS Water Retrieval Package 5 (WARP5) backscatter model. However, over moderate vegetation cover in the SE domain, the coupling of a bare soil backscatter model with a "vegetation water cloud" canopy model is shown to overestimate the impact of  $\theta$  on  $\Theta$  retrieval skill. [C227]

#### "Monitoring of collapsed built-up areas with high resolution SAR images"

A new concept for change detection algorithm for urban areas affected by earthquake is here presented. It is characterized as applicable to just one post-event amplitude Synthetic Aperture Radars (SAR) image and employs the inversion of sound scattering models already introduced in literature by the same authors. Aim of the algorithm is to try obtaining fast mapping of damaged areas and provide a first, even rough, evaluation of damage reported. In particular in this paper the overall block diagram chain and the algorithm rationale behind that framework are introduced and discussed in details. Some preliminary results are presented and the performance analyzed. New possible applications based on similar rationale are also commented. [C228]

#### "Estimation of sea ice thickness in the Arctic Sea using polarimetric parameters of C- and X-band space-borne SAR data"

In this study, we derived the relationship between target depolarization factor and physical parameters of sea ice in order to estimate the thickness using dual-polarization C- and X-band space-borne Synthetic Aperture Radar (SAR) data. The target depolarization factor, the cross-polarized ratio of C-band SAR data, which can explain the target depolarization effect, were strongly related to changes in surface roughness of thick First-Year Ice (FYI) and Multi-Year Ice (MYI), and were almost insensitive to variations in the surface dielectric constant of thick FYI and MYI and the incidence angle of C-band SAR data. This relationship showed a high correlation between target depolarization factor of C-band SAR data, the cross-polarized ratio, and thick FYI and MYI thickness. We validated the estimated method using RADARSAT-2 and TerraSAR-X data and ground-truth data acquired in the Arctic Sea off the northern coast of Greenland. [C229]

#### "SAR tomographic focusing by Compressive Sampling: Experiments on real data"

In this paper a 3-D SAR imaging technique based on Compressive Sampling is experimented on ERS 1-2 data. The technique is based on the sparsity property of the image to be focused along the elevation direction (i.e. only few scatterers with different elevation are present in the same range-azimuth resolution cell), exploits a reduced number of unevenly spaced acquisitions and allows an increased elevation resolution. Numerical results on real data are compared with those obtained by using Truncated Singular Value Decomposition (TSVD) techniques. [C230]

#### "Sea ice monitoring in the Baltic Sea using dual-pol C and L band SAR data"

Summary form only given. Monitoring of ice dynamics and ice type classification is an important task for understanding environmental changes as well as for safe winter navigation. SAR (Synthetic Aperture Radar) is a powerful spaceborne instrument to detect ridged ice regions as the radar backscatter is strongly influenced by geometrical properties of the ice surface. Data from polarimetric (or dual-pol) SAR sensors like Radarsat-2 and ALOS/Palsar enables to determine more precisely ice types as it contains more information about the ice surface geometry than single polarization images. Use of dual polarization SAR imagery also known as compact polarimetry has shown to be useful as it has reduced the complexity, cost and data rate of SAR image while preserving most of the capabilities of fully polarimetric image. A study for sea ice monitoring and characterization was carried out in the Baltic Sea from January to March 2009. The focus of current study was on enhanced monitoring of small scale changes/processes (ice types and dynamics) in the western Estonian archipelago sea. Secondary objective was to compare the backscatter characteristics at different frequencies (C-band and L-band) and polarizations (HH, HV, W) from various ice types (ridges, fast ice, water etc.) using data from different SAR sensors. Considering the objectives of the study high resolution SAR data from the following sensors was included: RADARSAT-2 (fine mode, HH/HV), ALOS/Palsar (fine mode, HH), ERS (image mode, W) and ASAR (wide swath, HH). Also optical remote sensing data from MODIS (Moderate Resolution Imaging Spectroradiometer) sensor was used to carry out non SAR dependent ice type classification. In addition to remote sensing imagery the meteorological data (wind measurements, air temperature, precipitation etc) from three different stations near the study area was analyzed to determine the cause of backscatter variations. A sea ice classification from C-band dual-pol Radarsat-2 imagery-- was performed. The classification on SAR image was based on entropy/alpha differences that were caused by ice type variations. Analysis showed that four ice types (level ice, fast ice, ridged ice, deformed ice and water) were identifiable from dual-pol data. Also two independent analyses that were performed on optical remote sensing imagery (MODIS) supported the classification results from Radarsat-2 data. Ice types were also determined from L-band SAR data and single polarization C-band data to characterize dependence of backscatter properties on surface type (roughness). The backscatter properties of ice types detected from RADARSAT-2 (C-band, HH/HV) were compared with single-pol data from Palsar L-band (HH), ERS (W), and ASAR (HH). Results showed that while C-band data was better for monitoring small scale ice deformations, the inclusion of L-band data improved significantly the analysis in snow covered ice regions in the coastal zone. The study provides additional information for enhanced ice monitoring in small areas (e.g. harbours, coastal zone) using high resolution data at multiple bands and polarizations. [C231]

#### "Inference of vertical soil moisture distribution using high-frequency CMP and reflection traveltime analysis"

High-frequency ground-penetrating radar (GPR) surveys were used to investigate temporal water content variations in a vertical soil column characterized by stratified clean sand deposits over multiple annual cycles. Reflection profiling and common-midpoint (CMP) soundings were coincidentally performed using 900 MHz antennas across a 2 m intensive monitoring profile. Our ability to identify fixed reflection events along a vertical soil profile permits inference of soil water flux across defined soil intervals in a non-invasive manner. Soil moisture contents were estimated from two-way traveltime measurements between seasonally coherent stratigraphic interfaces in the upper 2-3 m of soil. Interval thicknesses between stratigraphic interfaces were estimated from normal-moveout velocity analysis of coincidentally collected CMP soundings. Interval traveltimes from reflection profiles were then converted to wave velocity using the interval thickness estimates and a volumetric water content estimate using an appropriate petrophysical relationship. The GPR effectively characterized long (e.g., seasonal trends) and short-period (e.g., distinct wetting events) variations in vertical soil moisture distribution. [C232]

#### "Freshwater ground penetrating radar the significance of seasonal temperature variation"

Relatively high temperatures cause an increase in molecular motion as a result of weaker hydrogen bonding and a reduction in the tetrahedral geometry which in turn leads to depolarisation. Therefore a reduction in temperature aids the radar efficiency in several ways, increases the dielectric constant, reduces the velocity of the EM wave and reduces the effect of molecular vibration as a result of stronger bonds causing a reduction in depolarisation i.e. more efficient polarisation. [C233]

#### "2D and 3D GPR imaging and characterization of a carbonate hydrocarbon reservoir analogue"

We tested and adapted seismic attributes techniques on a 2-D and 3-D multi frequency GPR dataset to image the network of stratigraphic joints and fractures, the lithological variations and to characterize the rock mass based on the response to the radar wavefield measured in an abandoned limestone quarry. We applied semi-automatic horizon mapping techniques using manually picked seeds (control points) on selected attributes and automatic extrapolation both on inline and crossline, starting from seed positions. The results were integrated and validated with direct outcrop measures and allowed to image an hydrocarbon reservoir analogue in 3-D up

to a depth of over 10m below the topographic surface. [C234]

#### "Specified for air safety, monitoring atmospheric phenomena including the volcano dust"

This paper is an overview of methods and means for remote sensing of atmosphere based on backscattering of electromagnetic waves for prediction of dangerous weather phenomena zones along the route of the airplane. In addition to such traditional phenomena as turbulence, hail, icing-in-flight and thunderstorm, the approaches to distinguish areas of volcano dust is also included into consideration. [C235]

#### "Design of RF subsystem for Ku-band radar with synthesized bandwidth of 2GHz by using stepped-frequency chirp signal"

In this paper we introduce our work on developing a Ku-band 2GHz bandwidth RF subsystem based on Stepped frequency chirp signals (SFCS) including transmitter, receiver and frequency synthesizer, as well as experimental results. Very high resolution radar image for a moving train has been obtained by using the developed RF subsystem. [C236]

#### "Digital beam forming concepts with application to spaceborne reflector SAR systems"

The trend in the conception of future spaceborne radar remote sensing is towards the use of Digital Beam Forming (DBF) techniques. These systems will comprise multiple digital channels, where the analog-to-digital converter is moved closer to the antenna. This dispenses the need for analog beam steering and by this the use of transmit/receive modules for phase and amplitude control. Digital beam forming will enable Synthetic Aperture Radar (SAR) which overcomes the coverage and resolution limitations applicable to state-of-the-art systems. Moreover, new antenna architectures, such as reflectors, already implemented in communication satellites, are being reconsidered for SAR applications. This paper is dedicated to the digital signal processing aspects of such reflector based SAR systems. After introducing the hardware concepts the beam forming algorithms are presented and demonstrated by means of numerical simulations. [C237]

#### "Mapping thermal tufa deposits using GPR"

Tufa (freshwater calcareous) deposits can provide excellent targets for GPR exploration due to low clay content and low salinity. Widespread tufa deposits occur at the surface and in the shallow subsurface of Heber Valley, an alluvium-filled basin located in the Rocky Mountains of northern Utah (USA). A set of 200-MHz GPR profiles provides an unprecedented view of the internal structure of a tufa mound and its immediately surrounding platform. Our results indicate that features such as unconformities, caverns, disruptions due to voids, and "seismic" stratigraphic on-lap patterns can be mapped at high resolution. These patterns may be used to constrain interpretations of the episodic growth of a tufa system over geologic time. [C238]

#### "Using englacial radar attenuation to better diagnose the subglacial environment: A review"

The magnitude of the radar echo returned from beds underneath ice sheets has been used to identify subglacial lakes based on the prediction that wetter and flatter beds have larger reflectivities than dryer and/or rougher beds. Further quantitative diagnosis of the subglacial environment requires accurate correction for englacial dielectric attenuation, which is primarily a function of ice temperature and secondarily a function of ice chemistry. Models show that the attenuation contribution from chemistry (soluble ions) accounts for about one quarter of the attenuation averaged over the full ice thickness at Siple Dome and Vostok in Antarctica. These predictions suggest that a useful initial attenuation estimate across an ice sheet can be obtained simply with ice-temperature modeling. Methods for estimating attenuation from radar data are also reviewed, with an emphasis on the potential pitfalls of individual methods. Some discrepancies exist between attenuation estimated with ice-core data, temperature models, and radar data. We discuss strategies to improve these attenuation estimates. [C239]

#### "GPR research at the tomb of Zeynel Bey in Hasankeyf ancient city- Southeastern Turkey"

Hasankeyf is a town located along the Tigris River in the Batman Province in Southeastern Turkey. The tomb of Zeynel Bey ruled shortly over Hasankeyf- a rare example of its kind in Anatolia. We measured GPR data inside and around of the tomb of the Zeynel Bey to research buried archaeological remains. We imaged the results with interactive transparent 3D visualization and located archaeological remains with depth range. We determined the base structure and diffraction anomaly groups coming from a cemetery. Excavation in the tomb and around of it encouraged the new 3D image results and found a cemetery in the tomb. [C240]

#### "GPR investigation in different archaeological sites in Tuscany. Analysis and comparison of the

## obtained results"

In the last five years the collaboration between the Laboratory of Landscape Archaeology and Remote Sensing at the University of Siena and the Ground Remote Sensing Lab of the Institute of Technologies Applied to the Cultural Heritage (ITABC-CNR, Rome) produced several site prospection case histories. We focused our attention on a quite limited chronological range between late roman and the early medieval period. Chronology has a direct relationship with material culture and therefore with physical and chemical property of the archaeological stratification and of the context. We should emphasise that most of the site that has been surveyed has been also excavated or at least explored through archaeological sample excavation. The best results has been sistematically achieved through the integration with other methods as magnetic and resistivity systems. The paper will resume our experience, analyzing and comparing the different results, obtained in the sites characterised by late roman and early middle age features. [C241]

## "Radar subsurface sounding over the putative frozen sea in Cerberus Palus, Mars"

The area of Mars known as Cerberus Palus, suspected of harboring a frozen body of water, has been observed by the two subsurface sounding radar MARSIS and SHARAD. SHARAD data reveal subsurface interfaces at depths ranging from ~50 m to ~150 m which could be interpreted as either the bottom of an ice sheet lying over bedrock, or an interface between two lava flows. Echoes have been analyzed to estimate the dielectric properties of the surface layer, and results favor the interpretation that no ice is present in the area. [C242]

## "Imaging the subsurface structure of Planum Boreum with the Mars Reconnaissance Orbiter Shallow Radar"

We review prior mapping of the subsurface structure of Planum Boreum that was conducted with 2-D sounding data from the Shallow Radar (SHARAD) instrument onboard the Mars Reconnaissance Orbiter (MRO). Widespread reflections from basal and internal interfaces of the north polar layered deposits (NPLD) occur throughout the 1,000,000-km<sup>2</sup> area. A dome-shaped zone of diffuse reflectivity up to ~1 km thick underlies two-thirds of the NPLD. This zone is associated with a basal unit identified in image data as Amazonian sand-rich layered deposits. In other areas, the NPLD base is remarkably flat-lying and co-planar with the exposed surface of the surrounding Vastitas Borealis materials. Within the NPLD, radar-layer packets that extend throughout the deposits have been mapped as five units with a total volume of 821,000 km<sup>3</sup>, exclusive of the basal unit. Application of a 3-D imaging technique commonly used in processing seismic data to the polar grid of 2-D SHARAD observations is expected to yield an improved representation of the subsurface layering geometry and greatly reduce the effects of surface clutter. [C243]

## "Results of an experimental radar survey on the gornergletscher glacier system (Zwillingsgletscher), Valais, Switzerland"

A 775-m 200-MHz GPR traverse was surveyed in July 2009 over a portion of the Zwillingsgletscher branch of the Gornergletscher System, Valais, Switzerland. The survey line was approximately parallel to the glacial flow direction and situated in an area of prominent wave ogive formation. The traverse shows a well-developed pattern of scattering that is strongly folded into apparent troughs and ridges with the ridges commencing at 10-20 m depth. This pattern mimics the expected ogive structure. The origin of the scattering has not yet been confirmed, but is possibly related to an onset of warmer ice or to variations in rock or sediment content. [C244]

## "Potentialities of the Doppler spectrum of backscattered microwave signal in the problem of remote sensing of the sea surface"

Information about sea waves and the near surface wind speed is very important for meteorology. It is well-known that this information, in principle, can be obtained from a backscattered microwave signal. Evidently, the sea state determines both spectral and power characteristics of backscattered microwave signal. However, usually only a radar cross section is used for retrieval of the near surface wind speed. Considering only a radar cross section we lose the important information about the movement of sea surface that can be used for retrieval of key sea state parameters. In this paper the new description of a sea state is suggested and basic features of the microwave Doppler spectrum are discussed. We consider some features of various sea states and analyze their manifestation in the Doppler spectrum. [C245]

## "Application of double frequency radar for measurement of parameters of solid polydisperse aerosols"

In this paper the possibilities of application for double frequency remote sensing of solid aerosols are considered in the case of polydisperse medium. Use of double frequency sounding permits to evaluate effective aerosols

parameters with satisfactory accuracy for "narrow"  $\Delta r \leq 0.3$  and "wide"  $\Delta r \geq 4$  distribution law. The experiments with calibrated sand particles with "narrow" distribution law (as aerosols model) confirm the possibility of satisfactory evaluation of aerosol parameters. [C246]

### "Design of prospective spaceborne multi-aperture UWB polarimetric high performance SAR system"

Multi-aperture synthetic aperture radar (SAR) systems ensure high performance SAR imaging that is unachievable for conventional SAR. Application of modern technological capabilities in ultra-wide-band radar signals digital forming and processing (including optional modulation modes) enables realizing high performance characteristics and using operational flexibility of the SAR system. This report presents technical pattern and characteristics of the SAR, that is based on segmented polarimetric wide-band active phased array and multichannel digital subsystem for signal parameters control. The system uses technologies of 'multidimensional waveform encoding' for transmitted signal and 'digital beam forming' (DBF) for echoed signal receiving. The design main qualitative characteristics are estimated for multichannel remote sensing modes. [C247]

### "Experiment design framework for super-high resolution imaging with the geostar configured sensor array data"

In this work, we intend to address a novel look at the enhanced RS imaging with the mm-band array radar/SAR that employ the GeoSTAR sensor array geometry pursuing new descriptive experiment design regularization (DEDR) methodology that aggregates the concept of sensor array design with different methods for sensor system and reconstructive imaging method fusion, and report the simulation results of different DEDR-related GeoSTAR-adapted imaging techniques using the specialized elaborated software that we refer to as "Virtual Remote Sensing Laboratory" (VRSL). [C248]

### "Double frequency sounding of liquid precipitation"

Measurement of microstructure characteristics of precipitation is very important for study of process of their formation and progress. Use of the remote sensing methods is also quite interesting especially for measurement of particle size of liquid precipitation. That is why the double frequency method for measurement of particle dimensions is quite relevant. Peculiarity of liquid precipitation is dependence of their permittivity on temperature and operating wavelength. This fact essentially complicates application of double frequency method. So the goal of this paper is analysis of the method facilities in the frequency band, which is traditionally used for radio meteorology (8 mm and 3 cm). Experimental study of proposed approach was performed for single water drop by means of Doppler double frequency radar ( $\lambda_1=8$  mm and  $\lambda_2=3,2$  cm). The special measuring bench was developed for formation of drops with different sizes. The experimental data have good repeatability  $\leq 1\%$  and measurement error is about 30 %. Thereby performed experiments confirm possibility of use of double frequency method for estimation of effective drop size of liquid precipitation and their integral characteristics water content and intensity. [C249]

### "Comparative analysis of regression line fitting algorithms in blind method of mixed noise variance evaluation in radar images"

Radar images obtained by remote sensing systems as a rule are corrupted by mixed additive and multiplicative noise. To carry out high-efficiency filtering, the information about noise statistics in these images is required. However, in many practical situations such information is a priori unknown. Therefore methods able to evaluate variances simultaneously for both noise components are necessary. [C250]

### "SETHI flying lab: A tool for remote sensing applications"

This paper presents the new-generation test bench SETHI, developed by ONERA, the French Aerospace Lab. SETHI is a medium range platform dedicated to environmental, scientific and security applications. This paper presents the system architecture, the development state and the future capabilities planned. Before concluding, this paper displays a set of recent significant results covering three major applications: high spatial resolution image, change detection between two acquisitions, bio mass measurement in the tropical forest. [C251]

### "Robust detection in continuous-wave noise radar-experimental results"

In the paper the problem of target detection in continuous-wave noise radar in the presence of impulsive external noise is addressed. If received noise has distribution different than Gaussian, the classical correlation receiver does not provide the optimal results and the performance of the radar is seriously degraded. In order to restore the sensitivity lost due to the impulsive noise a robustification method is proposed. In the method a

nonlinear function is applied to the signal in order to remove the outliers. The method is verified on real-life signals. [C252]

#### "Study of double frequency method for remote sensing of liquid precipitations"

The peculiarities of double frequency method for remote sensing liquid precipitation are discussed in monodisperse approximation. The rigorous calculations of electromagnetic waves scattering by dielectric spheres and properties of radar cross section are considered. The limits of method application are discussed as well as results of experiments. [C253]

#### "Application of Autoregressive Model for Recognition of Meteorological Objects"

In the paper the results of development of recognition algorithm of meteorological objects by use of autoregressive model with spectrum-correlation signal processing of incoherent radar are presented. The radar hardware and experimental results on estimation of recognition efficiency are described. [C254]

#### "Technological challenges of a multifunction active phased array radar for weather, air traffic control and security applications"

By means of Active Phased Array techniques, an integrated target/weather surveillance at medium range, i.e. for Terminal Manoeuvre Area in the frame of ATC and regional weather monitoring, is possible and affordable provided that cost reduction for Transmit/Receive modules makes phased array radar affordable to civilian users. The MPAR (Multifunction Phased Array Radar) architecture allows a single equipment to satisfy different requirements for Air Traffic Control, Weather monitoring and analysis, and Security applications. The key techniques needed to achieve the required performance are (a) interleaving of functions by careful scheduling, (b) digital beam forming for target surveillance and (c) fast (electronic) scanning for the weather surveillance. The core technologies are of course those needed to implement at low cost the Transmit/Receive module (TRM), that in the proposed architecture may transmit a low peak power (order of one Watt), compatible with the low-cost requirement. [C255]

#### "Rank signal detection algorithms based on permutations of partial likelihood ratios"

This paper presents a new approach to design radar signal detection algorithms that are applicable when a priori information is limited. The problem is formulated as testing hypothesis on the kind of density function. A new method that uses ranks of partial likelihood ratios allows to adopt permutation test in a practical algorithm is suggested and researched. This approach gives a possibility to construct the rank detection algorithms, which are sensitive for the signal change for different situations, in the most simple and natural way. The results are useful for applications of signal detection in surveillance and remote sensing radar systems [C256]

#### "UWB radar for breath detection"

Using Breath Detection System can be detected breath rate and heart beating rate. System can be used for finding live human being behind nonmetallic obstacles. System was tested and showed good results in Test Polygon. [C257]

#### "Integrated geophysical methods for the knowledge of the urban layout of Hierapolis in Phrygia (Turkey)"

The paper concerns the various methods of geophysical prospecting (Ground Penetrating Radar, Magnetometry, Electrical Tomography) applied in Hierapolis of Phrygia, by the Italian Archaeological Mission, during the campaigns of 2007 and 2008. The integration between the different methods (in turn integrated with other exploration methods to the surface, as archaeological surveys and remote sensing from aerial platform and satellite), applied in areas of the city with different geological characteristics, allowed to retrieve important data on the urban layout in areas characterized by thick colluvial and alluvial deposits and in areas where there are extensive limestone formations that have formed recently and have incorporated the ancient remains. [C258]

#### "A IHS-WT remote sensing image fusion method based on dynamic weighting of regional multi-features"

This paper proposes a new IHS-WT method for remote sensing image fusion method with dynamic weighting of regional multi-features, based on the analysis of the advantages and disadvantages of classical IHS and wavelet transform fusion methods. It combines the advantages of the IHS transform and wavelet transform to achieve a better fusion result, the new I component can be obtained by fusing the wavelet coefficient data of the

histogram-matched panchromatic image and the I component through adaptive weights based on window region features. Experimental results indicate that the proposed method has apparent advantage in reservation of spectral information and spatial details enhancement than other methods. [C259]

#### "A temperature remote monitoring system of cable joint"

In order to monitor the temperature of cable joint, this paper designed a cable joint real-time temperature monitoring system based on GPRS which is integrated of computer technology, microcomputer control technology and digital sensor technology. It described the whole structure diagram of the system, and presented the hardware circuit and software design in detail. The system takes SCM as main control chip, adopts DS18B20 to build up the temperature measurement terminals, and uses the GPRS network as a wireless transmission network to realize wireless data transmission through the TCP/IP protocol management. Experimental results show that: the system have high accuracy, it is able to identify a variety of cable faults caused from overheating effectively and can meet the needs of cable temperature monitoring. [C260]

#### "Analysis of micro-doppler effect in SIMO radar"

SIMO (Single Input Multiple Output) radar system capitalizes on the receiving diversity, so it can obtain more information about the target and highly improve the target recognition capability of radar. In this paper, the micro-Doppler effect induced by rotation and vibration parts of target in SIMO radar system which transmitting single frequency signal are deduced respectively. Both the micro-Doppler effect induced by rotation and vibration are sinusoidal curves, but their amplitude vary with the selection of different receiving radar. In addition, the translation of the target's body will lead some horizontal shifts to the micro-Doppler curves with different value according to the selected receiving radar. Simulations are presented to validate the theoretic conclusions. [C261]

#### "Simulation and application of GPR in Artificial Freezing Engineering"

In Artificial Freezing Engineering(AFE), the distribution of freezing soil and its defects are important to engineering safety. Based on relative permittivity measured by vector network analyzer, electromagnetic models of artificial freezing walls were made. Then Ground Penetrating Radar (GPR) exploration of AFE was simulated by Time Domain Finite Element Method (TD-FEM) coupled with freezing temperature calculation. GPR were also used in AFE exploration. The research results show that GPR exploration and numerical simulation are in good accordance with each other. [C262]

#### "Remote control software development for a small airborne electronic support payload"

An unmanned aerial vehicle (UAV) electronic support payload (ESP) has been developed for the purpose of detecting and analyzing radar signals. The airborne payload control system (PCS) must be controlled from a ground control station (GCS) remotely through a wireless link. For the purpose, a control program, called Radar Signal Acquisition System (RSAS), has been designed, implemented and integrated with ESP. This paper introduces the ESP system, provides an overview of the general acquisition process, gives details on the RSAS and wireless link implementation using the Matlab scripting language, and finally presents some test results. [C263]

#### "Research on supervised classification of fully polarimetric SAR image using BP neural network trained by PSO"

Supervised classification of fully polarimetric SAR image using neural network is a common method nowadays. As an effective learning method of neural network, BP algorithm is the most widespread one in the neural network algorithms. However, BP network is easy to fall into local extremum and exists shortcomings such as the slow training process. To this end, this paper presents a method of supervised classification of fully polarimetric SAR image based on particle swarm optimization algorithm and BP algorithm. This method can improve BP algorithm using PSO and increase the convergence speed as well as the training accuracy of BP network. Experiment using fully polarimetric SAR image show that the supervised classification result of this method is better than the traditional BP algorithm classification result. [C264]

#### "The identification test of soil texture with ground penetrating radar"

The detection of soil texture needs nondestructive methods. Ground penetrating radar (GPR) develops fast in the fields of geological and agricultural survey in the recent years. To get a quantitative recognition of soil texture, experiments were designed with GPR of 500 MHz and 250 MHz frequency. Fine sand, sieved soil and natural soil were selected and tested indoors to acquire basic soil properties, amplitude attenuation characteristics and speed of electromagnetic wave. Compared to the experimental results outdoors, soil texture in the spots can be

identified and classified. The strong signal changes only happened at the surface of the medium. The study results also showed GPR could recognize silt loam and sand loam, which help us analyze the effects of soil texture on soil dielectric characteristics in the further research. [C265]

### "Evaluation of cloud liquid absorption models at 90 and 150 GHz"

The use of microwave observations in the frequency range of 90-150 GHz holds the promise to dramatically improve the retrieval of integrated liquid water in thin clouds due to the increased sensitivity of these frequencies to the presence of liquid water. One of the largest sources of retrieval uncertainty at these frequencies is the inaccuracy of liquid water absorption models at low temperatures. The purpose of this work is to assess the performance of four liquid water absorption models by comparing model simulations with measurements collected by a microwave high-frequency radiometer (MWRHF) located at the Atmospheric Radiation Measurement (ARM) Program Climate Research Facility (ACRF) in the Southern Great Plains, OK. Measurements at 90 and 150 GHz were collected during cloudy and cold conditions. In an attempt to isolate different sources of possible errors we give an assessment of the instrument calibration and compare clear-sky measurements with model simulations using an updated formulation for the water vapor continuum. With the help of a ceilometer and cloud radar we identified several cases of cold, thin liquid clouds and for those cases we independently retrieved liquid water path using infrared frequencies. The independently retrieved liquid water path was then used to compute brightness temperatures at 90 and 150 GHz with the four liquid absorption formulations. Simulation results were then analyzed and compared with observations. [C266]

### "Improved high wind speed retrievals using AMSR and the next generation NASA Dual Frequency Scatterometer"

Microwave scatterometer measurements are the standard for satellite ocean vector winds (OVW) measurements. Unfortunately, in extreme weather events, where high wind speeds are frequently associated with strong rain bands, precipitation can significantly degrade the OVW retrieval accuracy. This study addresses the feasibility of exploiting passive measurements to improve high wind speed retrievals for such extreme weather events. The Jet Propulsion Laboratory (JPL) has developed a conceptual design for a Dual Frequency Scatterometer (DFS) proposed to fly onboard the future Japan Aerospace Exploration Agency (JAXA) GCOM-W2 mission with the Advanced Microwave Scanning Radiometer (AMSR). These two instruments will provide a complimentary dataset of simultaneous and coincident active/passive measurements, which can correct for rain effects and thereby improve the OVW retrievals. End-to-end computer simulations are performed using the Weather Research and Forecasting (WRF) numerical weather model tuned to Hurricane Katrina (2005) for the 3D nature run (surface truth). Results show that the new OVW retrievals compare well to the nature run surface wind vectors and that this active/passive technique offers a robust option to extend the useful wind speed measurements range beyond the current operating scatterometers for future satellite missions. [C267]

### "AMSR-E observations of rain and flood events over vegetated areas of LA Plata basin"

This work analyzes AMSR-E signatures collected in two sites of La Plata basin, in South America. Within the wide Chaco forest, an area close to Las Lomitas meteorological station was selected. Here the forest is uniform, but not very dense, with biomass values in the range 70-120 t/ha. After strong rain events, appreciable variations of polarization index at C and X band were observed. As expected, the better dynamic range is obtained at C band. Also AMSR-E signatures collected during a strong flooding event in the Delta of Parana River were analyzed. Variations of polarization index are strong, as expected. Information about the water level in the river was made available by hydrometric stations. We selected specific pixels characterized by different kinds of land cover: agricultural fields, marshes, and planted forests. A significant correlation between polarization index (at various frequencies) and water level is proved. A flood monitoring algorithm based on AMSR-E brightness temperature difference is tested. Optical and radar data are used as ancillary input for calibration and validation proposes. [C268]

### "Radio frequency interferences investigation using the airborne L-band full polarimetric radiometer CAROLS"

In the present paper, different methods are proposed for the detection and mitigation of the undesirable effects of radio frequency interference (RFI) in microwave radiometry. The first of these makes use of kurtosis to detect the presence of non-Gaussian signals, whereas the second imposes a threshold on the standard deviation of brightness temperatures, in order to distinguish natural emission variations from RFI. Finally, the third approach is based on the use of a threshold applied to the third and fourth Stokes parameters. All of these methods have been applied and tested, with a CAROLS radiometer operating in the L-band, on data acquired during airborne campaigns made in spring 2009 over the South West of France. The performance of each, or of two combined

approaches is analyzed with our database. We thus show that the kurtosis method is well adapted to pulsed RFI, whereas the method based on the second moment is well adapted to continuous-wave RFI. [C269]

### **"An improved active/passive oceanic wind vector retrieval technique"**

This paper describes the advantages of combining passive and active microwave remote sensing observations for the purpose of ocean wind vectors retrievals. Previous studies have shown that a linear combination of horizontal and vertical polarized brightness temperatures contains a robust wind direction signal. In this paper, we present results from an end-to-end simulation of ocean measurements from a Ku-band (13.4 GHz) active/passive conical scanning satellite instrument. For this simulation, realistic wind fields from the NOAA National Center for Environmental Prediction (NCEP) numerical weather model were used to produce simultaneous brightness temperatures and radar backscatter measurements. These measurements were processed using a maximum likelihood estimation technique to yield ocean wind vector retrievals that were compared to NCEP fields. Results demonstrate significant improvements over simulated measurements for an active (radar scatterometer) sensor. [C270]

### **"Millimeter wave interferometric radiometry for passive imaging and the detection of low-power manmade signals"**

Millimeter wave detection and imaging is becoming increasingly important with the proliferation of hostile, mobile millimeter wave threats from both weapons systems and communication links. Improved force protection, surveillance, and targeting will rely increasingly on the interception, detection, geo-sorting, and the identification of sources, such as point-to point communication systems, missile seekers, precision guided munitions, and fire control radar systems. This paper describes the Naval Research Laboratory's (NRL) demonstration broadband passive millimeter wave (mmW) interferometric imaging system. In addition to limited active signal detection, the Ka-band system will provide the potential for detecting the passive signature of non-transmitting hostile systems along with a capability for meter-precision geolocation for imaged objects. The interferometer uses a distributed array of 12 antenna elements to synthesize a large aperture. Each antenna is packaged into an individual receiver, from which a baseband signal is recorded. The correlator is software-based, utilizing signal processing techniques for visibilities, and image formation via beamforming methods. [C271]

### **"GPR for large-scale estimation of groundwater recharge distribution"**

The Gnangara Mound, north of Perth, Western Australia, has been investigated using Ground-Penetrating Radar (GPR). Several hundred line-kilometers of GPR of common offset data have been acquired over an area of approximately 800 km<sup>2</sup>. The acquisition of these datasets was performed at two different center frequencies (50 and 250 MHz) in order to better resolve the complexity of the hydrogeological targets of interest which are water retentive layers found above the water table. These layers impede the recharge of the surficial aquifer and may have important impact on local ecosystems but also on the management of the ground water resource. The data presented here-in demonstrate the successful imaging of the regional water table and of these water retentive layers. For the first time, these data provide insight into the spatial distribution and the continuity of these water retentive layers and provide important information to be included in the flow modeling of the ground water in this region of the world. [C272]

### **"Recent deformation of Quaternary sediments in the northwest Canterbury Plains, New Zealand, as inferred from GPR and seismic data"**

A high-resolution seismic reflection survey in the northwest Canterbury Plains, New Zealand, has revealed a network of interconnected faults and folds underneath the seemingly undisturbed flat surface. Known rates of background seismicity in the larger area suggest ongoing deformation in the Plains, despite a lack of convincing surface expression. Ongoing deformation would be seen as disturbance of the uppermost Quaternary sediments. Unfortunately, the resolution of the seismic reflection data falls short in adequately imaging these uppermost sediments. Accordingly, we have collected > 31 kilometers of 50 MHz GPR data to provide complementary images of the uppermost Quaternary sediments. Final images show GPR-facies over the full depth range, indicative of braided river sediments. GPR images together with seismic refraction tomographic images also reveal locations where the youngest Quaternary sediments are deformed. Youngest deformation is observed only where folded Cretaceous-Tertiary and Permian-Triassic units come close to the surface. [C273]

### **"Mapping oil leak flow path using Step Frequency Radar: A case study"**

Leakage of oil from pipelines in an oil refinery often goes unnoticed until its contamination effect is seen in the polluted ground water. In one such case study in an Indian oil refinery, the oil leak from refinery was traced only

when neighbouring villagers complained of contaminated ground water. Since the source of leak was not known nor testing of leaked oil could reveal the source, this oil leak could not be arrested. In order to trace the source of oil leak, the GPR survey was done from the exit point outside the refinery and by following the flow path the survey was progressed inside the refinery campus on different benches. Finally after tracing around 700m long flow path, the particular plant was located from where leakage had originated and it was plugged. This paper describes the intricacies of GPR survey involved in this comprehensive exercise. [C274]

#### "Autonomous FMCW radar survey of Antarctic shear zone"

Radar survey of the Antarctic shear zone was conducted using an ultra-wideband (2-10 GHz) frequency modulated continuous wave (FMCW) radar. The radar was mounted on a sled and pulled by a robot that was specifically designed to operate in a harsh polar environment. Our FMCW radar had good penetration through Antarctic snow and we observed snow stratigraphy to a depth of 20 m. The radar images also revealed multiple crevasses in the shear zone. Our results demonstrate that autonomous survey using high frequency radar is feasible and safe approach for detecting hidden crevasses. [C275]

#### "GPR, ERT and CPT data integration for high resolution aquifer modeling"

It is widely accepted that an integrated characterization approach is necessary to define the geometry, internal structure, material distribution and water composition of aquifers. Multiple geophysical and hydrogeological data were measured in the sub-watershed surrounding a former unlined landfill: hydrogeological data in 25 direct push full-screen wells (slug tests, water conductivity, water levels), 21 km of GPR, 5 km of 2D electrical tomography and 30 cone penetration tests (CPT) with soil moisture resistivity (SMR). The 3D data integration in gOcad facilitates data interpretation and provides the basis for a detailed numerical groundwater flow and transport models. [C276]

#### "Applications of GPR in mineral resource evaluations"

Since the commercialisation of ground penetrating radar (GPR) in the 1970s, radar technology has been employed for niche applications in the mining industry. Although reliant on electrically resistive environments, GPR has gained acceptance in recent years as a standard exploration method for a number of deposit types, ranging from paleochannel delineation to iron ore mapping and kimberlite imaging. Numerous case studies have been published on GPR's applications to specific mineral exploration projects. Provided herein is an overview of commercialised GPR applications for surface mineral resource evaluations, covering examples of alluvial channels, nickel and bauxitic laterites, iron ore deposits, mineral sands, coal, kimberlite and massive sulphide examples. [C277]

#### "Water table detection by GPR in Sardon, Salamanca, Spain"

GPR was applied in the semi-arid Sardon catchment (Salamanca, Spain) in order to analyze the distribution of the water table depth with a high spatial resolution to serve as input in the parameterization of a hydrological model. We used a pulse radar with a single 200 MHz bowtie antenna combined with a differential GPS and a survey wheel for accurate positioning. Measurements were performed following a series of transects crossing perpendicularly the bed of the Sardon streams, which were dry during that period (September 2009). We measured the depth of the water table in several observation wells to interpret and validate the GPR data. A time domain reflectometry probe was used to estimate the shallow soil dielectric permittivity and corresponding wave propagation velocity along the transects. In general, the water table was visible in the GPR data, with depths ranging from about 2 to 3 meters. [C278]

#### "Advantages and restrictions of holographic subsurface radars"

Holographic subsurface radars (HSR) are not in common usage now; possibly because of the historical view amongst radar practitioners that high attenuation of electromagnetic waves in most media of interest will not allow sufficient depth of penetration. It is true that the fundamental physics of HSR prevent the possibility to change receiver amplification with time (i.e. depth) to adapt to lossy media (as is possible with impulse subsurface radar or ISR). However, use of HSR for surveying of shallow subsurface objects, defects, or inhomogeneities is an increasingly proven area of application. In this case HSR can record images with higher resolution than is possible for ISR images. This paper presents experiments with HSR imaging in media with different degrees of attenuation, and illustrates the principle of HSR through an optical analogy. [C279]

#### "Integrated GPR and archaeological investigations to study the site of Aquinum (Frosinone Italy)"

To enhance the knowledge finalised to the location and conservation of the unknown buried structures below the

actual studied levels, in the territory of the Ancient Aquinum (Frosinone, Italy), an integrated archaeological and ground remote sensing study has been developed during 2008-2009 and it is still in progress. Analysis of the historical and oblique aerial photographs, combined with topographical and archaeological field-walking surveys, allowed the preliminary interpretation of the main town-planning of Aquinum. To verify this preliminary interpretation an extensive geophysical surveys, employing Ground Penetrating Radar (GPR) method, has been made during 2008-2009. The obtained results indicate the good matching between the interpretation of aerial photographs and GPR images at different depths. The location, depth and size of the individuated archaeological structures were effectively estimated. Archaeological excavations made during the summer 2009, in a southern portion of the investigated area, have confirmed the results obtained with GPR method. [C280]

#### "Experimental investigation of different soil types for buried object imaging using impulse GPR"

Performance of electromagnetic sensors which are used to detect buried objects, is varied according to properties of soil. Most common sensor pair is EMI (Electromagnetic Induction) and GPR (Ground Penetrating Radar) for buried object detection systems. Besides the surface roughness and overlying vegetation, electrical conductivity ( $\sigma$ , (S/m)), electric permittivity ( $\epsilon$ , (F/m)), and magnetic susceptibility affects the detection performance of sensors. The electromagnetic properties of soil cause wave attenuation and change reflection coefficient of electromagnetic wave reflected from soil surface. For this reason, different soil types create various effects on sensor data, therefore performance of GPR and EMI sensors may decrease. Moreover, burial depth estimation can be performed if the soil properties are known exactly. This paper contains the effects of different soil types on impulse ground penetrating radar data, experimentally. [C281]

#### "Monitoring of seasonal influence on spatial distribution of moisture content at a natural Kanto loam site using ground wave of GPR"

Ground penetrating radar (GPR) ground wave was used at a natural Kanto loam (i.e. Andisol) site to examine the influence of seasonal variations on surface soil-moisture content. Kanto loam is a type of volcanic ash soil found widely distributed in Japan. In order to investigate the influence of surface soil conditions on GPR based estimates, the study site was divided in two zones: with and without vegetation. Measurements were conducted at regular intervals during a three month monitoring period. Results indicated that GW was sensitive to the surface soil conditions as well as to seasonal variations. A significant increase in moisture content was observed in the vegetated zone over that of the bare zone during a period of a day after precipitation (i.e. September 1st). It shows that in the vegetated zone moisture in plants themselves, including roots, stems, and leaves, affects GPR measurements, leading to higher moisture content than in the bare zone. However, the influence of vegetation was not found to have a large impact during periods of good weather. The effectiveness of surface soil conditions with seasonal variations on GPR-based moisture content provided a clear insight to agricultural management prospectives. This research confirmed that Kanto loam can be a good GPR site for noninvasive mapping of moisture content regardless of the presence of organic matter, silt, and clay content. [C282]

#### "A simple inversion model for the estimation of subsurface features of Mars poles"

Radar observations from Marsis have demonstrated that Martian Polar Layered Deposits (PLD's) are very transparent to radar waves. Thus, the sounder is able to detect the presence of subsurface reflections in the polar regions below the ice-rich layered deposits. The analysis of radar data makes it possible to gain information about some physical features of Mars surface. In this work an electromagnetic inversion model is used to characterize the shallower structures. This approach assumes that structure consists of layers with parallel plane interfaces and that the electromagnetic properties of the first layer are known a priori. Under these assumptions it is possible to estimate the dielectric permittivity of the subsurface structure. The inversion method has been tested in an area of South Pole and reconstruction results are shown. [C283]

#### "Attenuation of large bandwidth microwave signals in water and wet sand"

Large bandwidth microwave signals propagate in dispersive media as pulses that attenuate according to a non-exponential law. Although this is a direct consequence of wellknown theory of propagation in dispersive media, this fact is rarely acknowledged. The aim of this paper is an experimental study of this effect in fresh water and wet sand, both media of interest in Ground Penetrating Radar, which performances dramatically rely on capability of microwaves to propagate through soil. [C284]

#### "Surface, sub-surface mapping and geohazard identification and associated risk mitigation for power transmission"

Capture and analysis of remote sensing data of surface and sub-surface conditions can provide significant

logistical information for improved efficiencies and cost savings in transmission construction, upgrade, and maintenance programs. Cutting-edge LiDAR topographical mapping as well as sub-surface electro-magnetic and magnetic sensing datasets are practical tools for evaluation of surface and subsurface geologic-related hazards ('geohazards'), landslide and fault avoidance, alternate routing options, salinity/corrosion detection, determining construction feasibility and constraints including bedrock and overburden detection, encroachment discovery, and lightning strike mitigation. Resulting datasets can be placed into a GIS database as well as a three-dimensional visualization environment for complete design planning, asset management and future health modeling. [C285]

#### **"A novel approach to synthesize the range profile via predesigned stepped-frequency waveforms"**

In stepped-frequency radar systems, the phase error due to target motion in each burst make range profiles blur. Conventional technology, such as motion compensation, requires velocity estimation to eliminate the distortion of the synthetic range profile. However, it suffers a major drawback, namely that it is difficult to achieve real-time accurate estimation of the velocity of the target. A novel technology is presented to achieve a focused target range profile via predesigned stepped-frequency waveforms. By applying a new stepped frequency waveform, HRRP of the target can be obtained by the Fourier transform without any other process. The simulation results demonstrate the effectiveness of the proposed technology. [C286]

#### **"Single tree modeling and vegetation visualization using lidar data"**

Two applications of Lidar in three-dimensional visualization were proposed. The first one was single tree modeling. Regional-Maximum and K-means algorithm were used to isolate one single tree and its data points, and a SuperQuadric surface was fit as the silhouette of the tree's canopy. Then a geometric tree model was obtained with L-studio software. The second application was 3D vegetation visualization using DCM (Digital Canopy Model) to control the location of every single tree. DCM was calculated by subtracting DTM (Digital Terrain Model) from DSM (Digital Surface Model). DCM was a direct reflection of above-ground vegetation height, so it was used to determine whether a coniferous tree, deciduous tree or grass should be planted inside the DTM triangles. [C287]

#### **"Microwave FMCW Doppler radar implementation for in-house pervasive health care system"**

In recent years, the research in the area of ubiquitous healthcare has intensified. There are many technological advances regarding the development of unobtrusive sensors for cardiac and respiratory activity, but the current scenario is still far away from an everyday life fulfilled with ubiquitous healthcare systems. In this paper, it is described the usage of 24GHz microwave FMCW (frequency modulated continuous wave) Doppler radar (MDR) as one of the main components of a pervasive biomedical system that is part of an assistive environment for the people with less mobility or people with long term health condition. As parts of the present work, in this paper are mentioned the design and implementation of an assistive environment based on a MDR sensor, an experimental study concerning the microwave Doppler radar characteristics and remote sensing of heart rate and breath rate, based on acquisition and processing of the signals delivered by the used radar. [C288]

#### **"Vehicle relative movement estimation using microwave sensor"**

Microwave remote sensing based real vehicle movement estimator is under development. The application of this microwave sensor effectively increases the safety of traffic. The movement sensor provides further information about the estimation of the road-quality and the condition of shock-absorber, which are useful for the maintainer. [C289]

#### **"Multiprotocol transceiving, Formatting and Temperature monitoring FPGA based unit"**

The FCT (Formatting, Communications and Temperatures) electronic unit developed at INTA's radar laboratory as part of the X-Band synthetic aperture radar project (RBX SAR, see ref) is capable of receiving up to four channels of radar pulses and echoes at 1.5 Gbps line rates, with the use of aurora protocol on top of the Virtex 5 gigabit transceivers, format these data and send them to the system's storage unit (UAD) with a parallel protocol. In addition, the FCT communicates with other units through a VME bus. It also handles the memory map of the X-band transmitting unit, as well as translates the VME parallel bus communications to this unit to a 1.5 Gbps serial aurora protocol through optical fiber. Besides, the FCT monitors and stores temperature data gathered from different units of the radar system through a serial SMBus protocol, and manages access to these data through VME bus. Finally, with a second Virtex 5, it formats, decimates and filters the received radar echoes and sends them to the real time processing unit through a serial sFPDP protocol (1.0625 Gbaud). [C290]

#### **"Technical Analysis and Implementation Cost Assessment of Sigma-Point Kalman Filtering and**

### **"Particle Filtering in Autonomous Navigation Systems"**

The paper provides technical analysis and implementation cost assessment of Sigma-Point Kalman Filtering and Particle Filtering in autonomous navigation systems. As a case study, the sensor fusion-based navigation of an unmanned aerial vehicle (UAV) is examined. The UAV tracks a desirable flight trajectory by fusing measurements coming from its Inertial Measurement Unit (IMU) and measurements which are received from a satellite or ground-based positioning system (e.g. GPS or radar). The estimation of the UAV's state vector is performed with the use of (i) Sigma-Point Kalman Filtering (SPKF), (ii) Particle Filtering (PF). Trajectory tracking is succeeded by a nonlinear controller which is derived according to flatness-based control theory and which uses the UAV's state vector estimated through filtering. The performance of the remote sensing navigation system which is based on the aforementioned state estimation methods is evaluated through simulation tests. [C291]

### **"SAR imaging of forest structure at longer wavelengths"**

This paper is focused on the recovery of the vertical structure of forested areas from multi-baseline and multi-polarimetric SAR surveys at P-Band and L-Band. Baseline diversity provides sensitivity to the vertical structure of the vegetation layer, resulting in the possibility to yield Tomographic reconstructions of forested areas. Yet, far more information can be inferred basing on the joint exploitation of baseline and polarization diversity, which allows the decomposition of the SAR signal into ground-only and volume-only contributions. Ground-only contributions provide an easy and viable way to phase calibrate the data stack. Volume-only contributions, if correctly identified, allow a direct imaging of the vegetation layer. Results are shown basing on both P-Band and L-Band airborne data collected in the framework of the ESA campaign BioSAR 2008. The spaceborne case is also considered, basing on simulated BioMass data. [C292]

### **"Monitoring surface soil moisture and freeze-thaw state with the high-resolution radar of the Soil Moisture Active/Passive (SMAP) mission"**

An approach is described for retrieving surface soil moisture and freeze/thaw state using 3-km resolution L-band radar data of the planned Soil Moisture Active and Passive (SMAP) mission. SMAP radar backscatter coefficients are simulated using radar scattering models and land surface hydrology model output generated over the contiguous United States (CONUS). A Monte-Carlo simulation is performed to assess the error budget of the soil moisture retrievals in the presence of radar measurement error and error in surface roughness. The estimated soil moisture retrieval accuracy is better than 0.06 cm<sup>3</sup>/cm<sup>3</sup> for vegetation water content less than 1.2 kg/m<sup>2</sup> and soil moisture in the range of 0 to 0.3 cm<sup>3</sup>/cm<sup>3</sup>. The retrieval performance improves if radar speckle is reduced by additional observations (e.g., including both fore- and aft-scan data). It is currently assumed that the surface roughness is known with 10% error, but a time-series method is under development to estimate the roughness. The surface freeze/thaw state retrieval is simulated using a surface hydrology process model forced with climatology. The simulation illustrates a SMAP daily composite freeze/thaw product derived using a time-series algorithm applied to the SMAP high-resolution radar data. [C293]

### **"Ship detection using airborne SAR data acquired at X-band"**

During the last years, the interest in maritime surveillance has been growing up, and spaceborne SAR systems may contribute to the improvement of security and safety at sea. As such, to allow observation of non-cooperative boats with revisit times compatible with the objectives of reactivity of maritime surveillance, the solutions proposed by CNES (French Space Agency) in SAR domain concern a radar operating at very wide swath, which implies grazing conditions of acquisition. Under CNES initiative, an acquisition campaign using SETHI, the ONERA airborne SAR sensor, took place over the Mediterranean Sea, south of France, in February 2009. The main objective of this dedicated campaign was to perform very precise measurements of sea clutter and ship RCS for numerous conditions of acquisition so as to improve the understanding of radar backscattering specially at grazing angles: incidence up to 87°. [C294]

### **"Spotlight-mode synthetic aperture radar processing for high-resolution lunar mapping"**

During the 2008-2009 year, the Goldstone Solar System Radar was upgraded to support radar mapping of the lunar poles at 4 m resolution. The finer resolution of the new system and the accompanying migration through resolution cells called for spotlight, rather than delay-Doppler, imaging techniques. A new pre-processing system supports fast-time Doppler removal and motion compensation to a point. Two spotlight imaging techniques which compensate for phase errors due to (i) out of focus-plane motion of the radar and (ii) local topography, have been implemented and tested. One is based on the polar format algorithm followed by a unique autofocus technique, the other is a full bistatic time-domain backprojection technique. The processing system yields imagery of the specified resolution. Products enabled by this new system include topographic mapping through radar interferometry, and change detection techniques (amplitude and coherent change) for geolocation of the

NASA LCROSS mission impact site. [C295]

#### "OFDM waveforms for multistatic radars"

In this paper, the benefits of OFDM waveforms are analyzed for multistatic radar systems, where several radar stations cooperate in the same frequency band. The signal is coded over a 2D pattern, in the time and the frequency domains, using orthogonal Golay complementary sets derived from Reed-Muller codes. Binary data are also encoded in the signal. The obtained ambiguity and cross-ambiguity functions show that the OFDM signal structure is well adapted for radar applications. Transmitted waveforms have relatively low interference and sidelobe levels in the range and Doppler axis. [C296]

#### "The HF surface wave radar WERA. Part I: Statistical analysis of recorded data"

Surface wave (SW) over-the-horizon (OTH) radars are not only widely used for ocean remote sensing, but they can also be exploited in integrated maritime surveillance systems. This paper represents the first part of the description of the statistical and spectral analysis performed on sea backscattered signals recorded by the oceanographic WEllen RADar (WEERA) system. Data were collected on May 13th 2008 in the Bay of Brest, France. The data statistical analysis, after beamforming, shows that for near range cells the signal amplitude fits well the Rayleigh distribution, while for far cells the data show a more pronounced heavy-tailed behavior. The causes can be traced in man-made (i.e. radio communications) and/or natural (i.e. reflections of the transmitted signal through the ionosphere layers, meteor trails) interferences. [C297]

#### "Measurement of parameters of solid aerosols in polydisperse medium using double frequency radar"

In this paper the double frequency method for remote sensing of solid aerosols are considered in the case of polydisperse medium, when aerosols particles are distributed by lognormal law. The results of numerical simulation for two extreme cases- $\Gamma, B_{\text{inarrow}}$  and  $\Gamma, B_{\text{wide}}$  distribution law are presented and the limits of the method applicability are estimated. [C298]

#### "Application of AR model for radar recognition of meteorological objects"

The algorithm and measuring radar for recognition of meteorological objects are described. [C299]

#### "Improving geometric accuracy of optical VHR satellite data using Terrasar-X data"

The very high geometric accuracy of geocoded data of the TerraSAR-X satellite has been shown in several investigations. This precision has been reached fully automatically without any human interaction and is due to good sensor calibration, high accuracy of satellite position and the low dependency on the satellites attitude solution. High resolution optical images from space don't show this high geometric precision and need further ground control information, which is mainly due to insufficient attitude knowledge. Therefore TerraSAR-X data can be used as  $\Gamma, B_{\text{ground control}}$  to improve the exterior orientation and thereby the geometric accuracy of orthorectified optical satellite data. The technique used is the measurement of identical points in the images, either by manual measurements or through local image matching using adapted mutual information (MI) and to estimate improvements for the exterior orientation or Rational Polynomial Coefficients (RPCs). To be able to use this intensity based method, the radar data have to be filtered before starting the matching procedure. Through adjustment calculations falsely matched points are eliminated and an optimal improvement for the attitude angles is found. The optical data are orthorectified using these improvements and the available DEM. The results are very promising and compared using conventional ground control information from maps or GPS measurements. [C300]

#### "Simulation and Comparison of Two Kinds of Severe Convective Weather Processes"

Based on radar data and ground weather phenomenon, two kinds of severe convective weathers, hail and gale process and tornado process, are simulated by the model MM5. The simulated radar echo and actual radar echo are analyzed. Simulated micro-physics and dynamic characteristic are researched. The possible reasons of the difference with microphysical and dynamic characteristic between two kinds of severe convective weather are discussed. The results are as follows. (1) Simulated effect with two kinds of severe convective weather was good about the simulation of radar echo, so simulated radar echo had certain reliability. (2) That snow crystal was located above  $0^{\circ}\text{C}$  level is showed by the microphysical simulation of hail process. The isoline of wave band, comparatively with rain-water was crowded. The cloud-rain mainly distributed below  $0^{\circ}\text{C}$  level, and was scattered distribution. The rain distributed below and above  $0^{\circ}\text{C}$  level. That cloud water continuously distributed below  $0^{\circ}\text{C}$  level was showed by microphysical simulation of tornado process. The rainwater

distributed below 0Г,B°C level. The rainwater content distributed less below 0Г,B°C level, but mainly distributed above 0Г,B°C level, also the value was big, the isoline was crowded. The cloud ice content also presented scattered distribution. (3)The severe convective weather process corresponded to the strong lifting movement from the simulation of dynamic characteristic, but the region of strong lifting movement did not distribute specific position of the echo band. [C301]

### "Research on the Object-Extraction from Aerial LIDAR Dataset"

At present, object-extraction is one of the key problems of the data-procession to the aerial LIDAR dataset. The aim of this paper is to research the methods to classify and extract the object-points from the cloud points obtained by the aerial LIDAR system. In this paper, based on the different feature of elevation and intensity of different objects, the laser-points of buildings, vegetation and water are individually extracted. Then, several experiments are given to validate the effectivity of the object-extraction methods. [C302]

### "Inverse Modeling of 3D High Resolution Ground Deformation Maps Derived by Integrating GPS and DInSAR Data"

In this paper we present a strategy aimed to modeling large data set of 3D complex ground deformation patterns obtained by integrating sparse Global Positioning System (GPS) measurements of deformations and Differential Interferometric Synthetic Aperture Radar (DInSAR) maps of movements of the Earth's surface. The method used to integrate these two kinds of data to derive 3D ground deformation map, was the SISTEM (Simultaneous and Integrated Strain Tensor Estimation from geodetic and satellite deformation Measurements) one. In order to find the optimal model a Particle Swarm Optimization (PSO) algorithm is first used to locate optimal regions of complex search spaces. Then a derivative-based method, in particular the Gauss-Newton one, is used to refine results. The proposed strategy was tested on both synthetic and real datasets, the latter relevant to the Abruzzo region during the 2009 earthquake. [C303]

### "Estimating Large Area Evapotranspiration from MODIS Data"

Remotely sensed imagery of the Earth's surface via satellite sensors provides information to estimate the spatial distribution of evapotranspiration (ET) especially in a wide range. The Surface Energy Balance Algorithm for Land (SEBAL) was used to derive ET maps from Moderate Resolution Imaging Spectroradiometer (MODIS) images. However, SEBAL contains a simple adjustment procedure for the windspeed from only one meteorological station. The Hai river basin with 54 meteorological stations covers 318, 200 square kilometers and the weather conditions is not uniform across the satellite image of this huge basin. Therefore, the most appropriate solution is to separate an image into several subareas based on the weather condition, and operate SEBAL model separately, using different cold and hot pixels and weather data. But based on the above method, the process for calculating 24-hour evapotranspiration (ETdaily) for 365 days in 2007 is too difficult and complex. So we propose a simplified method to calculate the friction velocity by wind speed. The result shows that the simplified method can be used to predict ET by the comparison of ETdailypredicted for August 13, 2007 in Hai river basin by two different methods. [C304]

### "Parameters analysis for polarimetric SAR Based on classification accuracy"

As a multi-channel microwave remote sensing imaging radar system, polarimetric Synthetic Aperture Radar (SAR) enhances the information extraction ability for material scene in the observation area, in which the design and state monitoring for parameters play an important role in polarimetric SAR system and equipments management. This paper presents an analysis method for three typical polarimetric SAR system parameters: channel noise, polarization imbalance, and polarization isolation. We explore the polarimetric SAR image classification accuracy ratio and the relationship with three parameters above, review the statistic model of each parameter, and propose an analysis model between each parameter and the classification accuracy ratio measurement. By the polarimetric SAR image experiment, the comparative curve between each parameter and the influence on classification performance is obtained, which shows an application reference for polarimetric SAR system design and management. [C305]

### "Parameters extraction of crop based on PolSAR Data"

It is beneficial to extract the parameters of the objects by rich information of PolSAR (Polarimetric Synthetic Aperture Radar) data. With polSAR data of Radarsat-2, the polarimetric character of winter wheat in booting and milk stage is studied based on polarization theory. The results show that: there is a great difference between the polarimetric characters of two stages due to the change of wheat structure. Winter wheat growth can be retrieved by entropy, which changes in different way in the two stages. In booting stage, with LAI increasing, the scattering mechanism tends to be more complex. While in milk stage, with plant density increasing, the

scattering mechanism tends to be simpler. The eigenvalue of  $\lambda_2$  is a valuable parameter to retrieve soil moisture with crop cover. Results show the potential advantage of polarimetric radar. [C306]

### "Automatic target recognition of SAR images based on the fuzzy neural networks"

ATR (automatic target recognition), based on SAR (synthetic aperture radar) image, is crucial to the success of battlefield awareness and has become a very hot research topic. But many problems, which are caused by a great deal of missing, polluting, and superimposing of the signals, still generally exist in practical application, such as the low recognizing rate. How to recognize the useful signals from badly polluted images has become a difficult point in remote sensing image process. Thus, this paper will provide a way to recognize radar signal automatically by using the fuzzy neural networks. [C307]

### "SAR sensor employment planning for tactical aircraft"

In this paper, an attempt is made to define the features of SAR employment planning problem for tactical aircraft in military operations. General concepts for use of airborne SAR to find and locate targets are described and formulated into a parameter optimization problem. The utility and constraints of SAR imaging followed by weapon delivery are described, which rely on target characteristics, threat distribution, terrain and attack conditions. Then some approaches to solving the technique problem are described. Although the interests expressed in this paper are motivated by capabilities that might be afforded by manned aircrafts, the concepts are relevant for unmanned air vehicles conducting battle reconnaissance tasks equipped with SAR sensors. [C308]

### "Image Fusion Based on Multi-scale Kalman Filtering"

An image fusion algorithm, based on the Multiscale Kalman Filter (MKF), has been applied to combine remotely sensed data, acquired by radars having different resolutions and can improved information carried by each input image. The considered images have been acquired during the AIRSAR Mission and SIR-C/X-SAR Mission. The data have been co-registered to refer each pixel of each image to a common regular grid. The image fusion algorithm has been tested, and the merged images have been presented at different resolutions. A lineament detection algorithm based on the Hough transform, has been applied to the full resolution input data and to the full resolution merged data. The Golden Gate bridge has been detected in both images, but the computed probability of false alarm is lower in the case of the finest scale merged image than in the finest scale input image. This fact demonstrates that the knowledge provided by the coarser resolution data has been transferred to the merged image, improving the performance of the lineament detection algorithm. [C309]

### "Computational electromagnetic modeling & simulation of ultra wideband sub-surface sensors for the detection and imaging of buried objects using spatial and spectral diversity"

An enhanced remote sensing technique for the detection and identification of deeply buried objects is presented in this paper. A new RF Tomographic Technique is proposed for developing RF CAT Scans of buried objects using spectral and spatial diversity. This imaging technique uses an embedded ring of subsurface radiators as the source of strong underground radiated transmissions. Distributed surface-contact sensors are used to collect the tomographic data for relay to a remote control site. Three-dimensional numerical imaging algorithms have been developed to detect, image, and characterize deeply buried objects. Distributed transmitters and receivers significantly increase unwanted mutual coupling and EM emissions that interfere with signal reception; however, by embedding the transmitters underground, reduced mutual coupling and EM emissions, and improved signal-to-noise ratios, can be achieved. Simple 2D surface SAR experiments over deep mine shafts were performed to validate and verify (V&V) the 3D processing algorithms using 2D surface SAR sensor data. The WIPL-D CEM Code was used to model and simulate (M&S) the embedded and distributed sensors and to verify the significant enhancement in the received signal-to-noise ratio obtained by burying the radiating antennas. [C310]

### "Using the MicroASAR on the NASA SIERRA UAS in the Characterization of Arctic Sea Ice Experiment"

The MicroASAR is a flexible, robust SAR system built on the successful legacy of the BYU  $\mu$ SAR. It is a compact LFM-CW SAR system designed for low-power operation on small, manned aircraft or UAS. The NASA SIERRA UAS was designed to test new instruments and support flight experiments. NASA used the MicroASAR on the SIERRA during a science field campaign in 2009 to study sea ice roughness and break-up in the Arctic and high northern latitudes. This mission is known as CASIE-09 (Characterization of Arctic Sea Ice Experiment 2009). This paper describes the MicroASAR and its role flying on the SIERRA UAS platform as part of CASIE-09. [C311]

### "Analysis of image fusion and classification for high resolution SAR data on-line"

SAR and optical remote sensing image, with highly complementary characteristics, can enhance the integration of information utilization of remote sensing data. Adopting the new Cosmo-Skymed SAR high-resolution image data, we inhibit speckle impact using enhanced Lee filtering. Then we fused this image with a CBERS image using local use standard deviation based on wavelet packet method. Because of fully integrating the characteristics of each image, it can retain the spectral characteristics and details of properties to the maximum extent, improve signal-to-noise ratio, and be conducive to information extraction. The experiments show that the automatic classification accuracy significantly increased and classification Kappa coefficient increased from 0.47 to 0.93 after fusion of Cosmo-Skymed and CBERS02 data. Meanwhile, This paper employ a geospatial information processing concept model complied interoperable system framework and an implementation approach for accessing geospatial information openly by chaining individual service module to assemble complex geospatial processing and executing the processing model to deliver information. [C312]

### "Extraction of ionospheric clutter in HFSWR"

The two main applications of High frequency surface wave radar (HFSWR) are maritime surveillance of the Exclusive Economic Zone (EEZ) and the remote sensing of the sea. Ionospheric clutter strongly limits the detection capabilities of HFSWR. In order to analyze the effect of ionospheric clutter, a method based on image processing is proposed to extract ionospheric clutter. In this method, the Range-Doppler spectrum of radar echo was processed as image, and the color image segmentation technique was used to extract ionospheric clutter. By a preliminary analysis of the ionospheric clutter extract results, we can get that the average power of ionospheric clutter is big, and it occupies many Range-Doppler cells, and it has direction. The results provide a frame of reference for the ionospheric clutter assessment, suppression and frequency selectivity, etc. [C313]

### "A 5.8 GHz RFID-based data transmission system as an energy efficient solution for on-board monitoring"

This paper presents a wireless data transmission system based on the RFID concept designed initially for an enviroment typical in aeronautics. As a response to a growing interest into wireless monitoring of various parameters onboard of modern aircraft, the author performed several experiments that were aimed at verifying to what extent a low-complexity RFID-based data transmission solution can meet basic requirements related to the expected distance between sensors, as well as the possibility to realise an efficient data link when the sensors are not installed in the line-of-sight and the transmission must rely solely on wall reflections. The paper cncludes with a description of the results of the performed measurements. [C314]

### "Application of D-InSAR Technique for the Bam Earthquake"

The difference synthetic aperture radar interferometer (D-InSAR) is developed based on the synthetic aperture radar (InSAR) technique. It can be used to detect the earth surface deformation, fire hazard, earthquake and etc.. The imaging principle and data process procedure are introduced. The difference interfere process of the SAR data from Bam in Iran where earthquake happened on Dec. 26th, 2003 is implemented. The distinguish between the interferegrams before and after the earthquake is discussed. The phase image reflected the earth surface deformation arise from the earthquake is obtained. Thus the damaged area and the earthquake fracture zone position can be determined. Results show that the D-InSAR technique can be used to study the parameters of the earthquake and supply a new tool to help people to comprehensive the earthquake further. [C315]

### "Engineering design of the rain mode on an ocean-dedicating radar altimeter"

Satellite radar altimeters are fundamental tools in microwave remote sensing, but traditionally they were regarded as unsuitable for rain measurement. This paper designs a rain mode on an ocean-dedicating altimeter, taking China's forthcoming HY-2 ALT as a typical example. In rain mode the altimeter receives the surface and rain echoes simultaneously, so it can estimate the rain layer structure without losing surface topography information. The variable system parameters are designed to fulfill the task with very low hardware expenses. Some key issues are discussed in detail. To achieve the compatibility of measuring both surface and rain, an adaptive digital i/q demodulator is proposed, and receiver weighting is implemented to suppress the side-lobes. Constrained by echo power, altimeter can detect rains heavier than 6 mm/hr. [C316]

### "Predesign of the wind field measuring radar for FengYun-3E meteorological satellite"

Spaceborne microwave scatterometers have successfully provided global ocean surface wind field for two decades. Ocean wind data have become as a critical tool utilized daily by operational weather forecast and

warming centers around the world. However current scatterometers still can not satisfy the requirement of achieve ocean wind vectors in nearly all weather and all wind conditions. The wind field measuring radar (WIFIR) onboard Chinese FengYun-3E meteorological satellite is being developed to attempt to overcome their shortcomings. This paper describes the predesign of the WIFIR, including the mission requirements, system design, and performance analysis. [C317]

#### **"FPGA based IF digital receiver for the PARSAX-Polarimetric agile radar"**

An FPGA-based digital receiver has been developed to perform real-time processing for the PARSAX radar. It is a fully polarimetric FMCW radar with dual-orthogonal sounding signals, which has the possibility to measure all elements of the radar targets polarization scattering matrix simultaneously, in one sweep. This paper presents the design principles including the range profile interpretation, optimal parameters selection and processing gain analysis. A novel parallel deramping processing architecture suitable for FPGA implementation is introduced; the overall digital de-ramping processing has been implemented in one chip of FPGA and verified by experimental results. [C318]

#### **"Research on the spaceborne SAR image processing and feature extraction for ocean fronts detection"**

This paper discusses the interaction of short surface waves with shearing and converging current. On the basis of the spectral perturbations caused by the interaction, the influences of the interaction on the ocean surface wave spectral density and gradients are analyzed. A two-scale electromagnetic scattering model explains not only the interaction between short-wave and radar backscatter, but also the interaction between long-wave and radar backscattering. Then SAR imaging mechanism of ocean fronts is derived. In SAR images, the scale of ocean fronts is 2-3 orders larger than that of sea waves. Most of wave information is filtered out by the 2-D spatial spectrum analytics. Then the characteristic information of ocean fronts is extracted by digital image processing technology. Thus, information processing means by which characteristic information of ocean fronts can be extracted from SAR images is constructed. [C319]

#### **"Extraction of gap and canopy properties using LiDAR and multispectral data for forest microclimate modelling"**

The creation of gaps in forest canopies can dramatically change the microclimate and soil water balance which strongly influences the process of regeneration and biodiversity within forest ecosystems. Hence, understanding the microclimatic conditions in canopy gaps is a prerequisite in developing and improving techniques for forest management and conservation practices. However, information is scarce on how the size and shape of gaps and their spatial distribution affects the microclimate and soil water balance across forest stands. In the present study we investigated the potential for retrieving forest gap and canopy attributes from LiDAR and multispectral sensors in order to provide new opportunities for modelling forest microclimates. A spatially explicit microclimate model (FORGAP-BD) was developed which could be driven using inputs from remote sensing. The model was implemented for a study site in the broadleaved deciduous forest, Eaves Wood, UK in order to quantify the spatio-temporal dynamics of microclimates over an entire forest stand. [C320]

#### **"Aggregated convex regularization and variational analysis technique for enhancement of mm waveband remote sensing imagery"**

In this paper, the statistical Bayesian and descriptive regularization approaches for high resolution radar image formation is detailed in many works, where such approach is adapted to the sm and mm waveband remote sensing (RS) applications considered. [C321]

#### **"Airborne analysis and assessment of urban traffic scenes from LiDAR data-Theory and experiments"**

This paper investigates the theoretical background for LiDAR to monitor traffic from airborne platforms. An object moving with a velocity deviating from the assumptions incorporated in the scanning process will generally appear both stretched and sheared-motion artifacts. To study the impact of these deformations in airborne laser scanning (ALS) data, the analytic relations between an arbitrarily moving object and its conjugate in the ALS data have been examined and adapted to concrete airborne specifications. A complete scheme is proposed to analyze urban traffic in real-life situations. This scheme combines vehicle motion classification method successively with vehicle detection. Furthermore, the velocity of moving vehicles can be derived. The algorithmic performance was assessed with respect to reference data concurrently obtained by video camera. [C322]

### "Comparisons of speckle noise filtering methods on high resolution SAR image"

Numerous image processing methods to suppress the speckle noise in synthetic aperture radar (SAR) have been proposed. There is always a tradeoff between smoothing out speckle and preserving the useful spatial information (i.e. edge, texture). This paper proposed a novel index by integrating the evaluation of both speckle and edge preservation to evaluate the balance of the aforementioned two criteria. Some of the well-known adaptive speckle suppression filters are then compared and evaluated using two high resolution SAR datasets on heterogeneous areas. Experimental result shows that Kuan filter performance better in preserving image sharpness and detail while suppressing noise. [C323]

### "SAR and Landsat ETM+ image fusion using variational model"

Multispectral and synthetic aperture radar (SAR) image fusion is one of the most complex tasks to perform integration of multi-source remotely sensed imagery. Fusion of SAR and optical remote sensing image, with highly complementary characteristics, may contribute to a better understanding of the objects with the imaged scene and finally benefit to application such as precision farming/ agricultural. In this paper, we adopt a variational model to fuse SAR imagery and multispectral imagery. Experimental results on Cosmo-Skymed SAR and Landsat-7 Enhanced Thematic Mapper Plus (ETM+) satellite images of an urban area, demonstrate accurate spectral preservation, which is indicated by high correlation between original multispectral and fused bands. [C324]

### "Observation of Mixed-Layer Depth of Atmosphere with Lidar"

A Micro-pulsed lidar at 532 nm has been developed and used for routine observations of optical property of aerosol and the temporal-spatial evolution of the mixed-layer depth (MLD) of atmosphere. The mixed-layer depth of atmosphere is retrieved by seeking the absolute minimum of first derivative or second derivative of the range-squared- corrected lidar signal. Through 24 hours of continuous observation over Xi'an, the result shows that the lidar can clearly observe the diurnal variation of MLD of the Xi'an, which is of great importance for studying the proliferation of urban pollution and obtaining a complete meteorological status of the urban atmosphere. [C325]

### "Study of Double-Wavelength Airborne Lidar System Based on Ocean Red Tide Monitoring"

Am at monitoring and forecasting the red tide in real time, an double-wavelength airborne lidar system is proposed in this paper. The lidar system not only can use a infrared laser to detect the seawater scattering signal and gain the information about the red tise's density and size, but also can use a blue-green laser to detect the Brillouin scattering signal and deduce the temperature and salinity of the seawater. The infrared scattering signal can be detected by the infrared filter, at the sametime, the Brillouin scattering signal can be detected by a bromine molecule absorption cell and an iodine molecule absorption cell. Through simulating and analyzing the absorption spectrum of molecule absorption cell, it can gain the data of the laser center frequency, the laser monochromatic and stable frequency indexes, and the absorption spectrum of all filters in the system. The results show that our research can be used as forming the practical double-wavelength airborne lidar system. [C326]

### "A Method of 3D Building Boundary Extraction from Airborne LIDAR Points Cloud"

Building boundary is of great significance for building reconstruction and digital mapping. The emergence of airborne LIDAR technology makes rapid extraction of buildings possible. Based on the analysis of existing buildings extraction method, the article proposes an automatic method for extracting 3D building boundaries directly from airborne LIDAR points cloud, which consists of three steps: firstly, building points are segmented by a multi-resolution directional prediction filter method and roof points are then recognized by a series of refinement procedure; Secondly, TIN mode is built by roof points and initial boundaries are extracted by analysis of height differences among vertices and relationships between vertex and edge of TIN facets. Lastly, initial boundaries are regularized by a modified method for roofs with different shapes. Datasets with different roof types are selected to test the proposed approach and results show that it can correctly extract 3D buildings boundaries from discrete LIDAR points cloud. [C327]

### "Copyright page"

The following topics are dealt with: geoscience and remote sensing; skywave OTH radar; maritime surveillance; passive radar; phased arrays; radar clutter modelling; SAR; MIMO radar; ultra wideband radar; and radar imaging. [C328]

### "Resolution selective change detection in satellite images"

In this paper, we propose a novel method for unsupervised change detection in satellite images. A feature vector for each pixel is extracted using the multiresolution representation of the difference image which is computed from the multitemporal satellite images of the same scene acquired at different time instances. A metric for automatically estimating the number of resolution levels used in multiresolution analysis is proposed. The dimensionality of each feature vector is reduced using principal component analysis (PCA). The feature vectors are then classified into "changed" and "unchanged" classes using k-means clustering with  $k = 2$  to achieve a change detection map. Results are shown on real data and comparisons with the state-of-the-art techniques on advanced synthetic aperture radar (ASAR) images are provided. [C329]

### "Implementation of handheld remote sense image calibration system software"

This paper based on 4S(GPS, GPRS, GIS and RS technology in a integrated system) and designed a remote sense image calibration system by using a high precise GPS module which is integrated in the handheld client device. This article designed and realized a software architecture and a data storage and transfer model though the GPRS real-time network. The handheld devices based on 4S changed the poor efficiency way of the original remote sense image of the manual data acquisition, post-mapping and other operations. The efficiency of original system is also greatly enhanced by implement the digitization of external work system which is constituted on a collaborative platform within the inner work system. [C330]

### "On the optimal synthesis of ring symmetric shaped beams through uniformly spaced planar arrays"

This paper deals with the power pattern synthesis of circularly symmetric shaped beams via equispaced planar arrays. A computationally effective approach taking inspiration from results available in the linear array case and not exploiting global optimization schemes is presented and assessed. In particular, for a given number of radiating elements, the proposed procedure is able to state a priori whether the constraints can be fulfilled or not, and, in the affirmative case, to determine the needed excitation coefficients. An example of actual interest is shown and discussed. [C331]

### "Spaceborne SAR Systems and technologies"

With the launch and operation of Europe's first remote sensing satellite ERS-1 in the 90's, the usefulness and need of spaceborne SAR Systems has become obvious. Meanwhile, affordable 'state of the art' technology in modern active phase array antennas has drastically improved the SAR system agility and its image performance, such that also commercial and military application is of highest interest. [C332]

### "Development of a multi-frequency airborne radar instrumentation package for ice sheet mapping and imaging"

We have developed improved versions of three different radar systems and integrated them as an airborne instrumentation suite for sounding and imaging Polar ice sheets. The first instrument consists of a multi-channel, coherent, pulsed radar operating at VHF with up to 20 MHz bandwidth. This instrument is capable of sounding a few-kilometer thick ice while flying at altitudes up to 10 km above mean sea level. The second instrument is designed to operate at UHF using a burst of narrow-bandwidth signals to digitally synthesize a bandwidth of in excess of 300 MHz. This apparatus is used to measure internal layers of the ice sheet to a depth close to 100 m. The third component to the instrumentation package is based on a frequency-modulated continuous wave (FMCW) radar, which operates at microwave (Ku band) frequencies with up to 1 GHz of instantaneous bandwidth. This radar set is used to measure the ice sheet surface elevation profile with centimeter accuracy. We are presenting a description of each system, with emphasis on the VHF depth sounder. We also present sample field test results obtained during the 2009 austral summer season in Antarctica, as a validation of the performance of the instrument package. [C333]

### "Special session in honor Dr. Kiyo Tomiyasu"

This session is dedicated to the career of Dr. Kiyo Tomiyasu. His career includes technical accomplishments in microwaves, lasers, and remote sensing of the earth using satellite-borne radiometers, scatterometers, and synthetic radars. He has contributed much to MTT-S, and to IEEE, including awards and contributions to the IEEE Foundation. This special session will include invited speakers to recall activities associated with Dr. Tomiyasu, his contributions to the MTT-S AdCom and his technical accomplishments as witnessed by the speakers. Dr. Tomiyasu will receive the Thomas Alva Edison Medal at the IMS 2010 Plenary Session. This

special session in honor of Dr. Kiyo Tomiyasu will be recorded and CD-ROMs made available to the session attendees. [C334]

### "Active and passive THz systems for short-range imaging applications"

In this paper three different systems at 94 GHz for short-range imaging applications are presented; both active and passive methodologies are described. An analysis for each case is performed, determining the parameters which satisfy the field of view and resolution requirements. A T-shape interferometric radiometer is first exposed describing the implemented imaging algorithm, the overall system block diagram, and the images obtained from the simulations. The radiometric resolution estimate is calculated, specifying the minimum temperature the system is capable to detect in function of the system parameters. Then, a Mills-Cross based active system is presented; recovered images are shown, as well as the geometry employed in the setup performance. Finally, a reflectarray setup is described; presenting its geometry of exploration and operation principles. In addition a phase discretization analysis is performed for the case of 1 bit. For both active systems the minimum detectable Radar Cross Section, RCS, is computed. [C335]

### "Towards marine bloom trajectory prediction for AUV mission planning"

This paper presents an oceanographic toolchain that can be used to generate multi-vehicle robotic surveys for large-scale dynamic features in the coastal ocean. Our science application targets Harmful Algal Blooms (HABs) which have significant societal impact to coastal communities yet are poorly understood ecologically. Bloom patches can be large spatially (in kms) and unpredictable in their extent. To understand their ecology, we need to be able to bring back water samples from the 'right' places and times for lab analysis. In doing so, we target hotspots representative of intense biogeochemical activity for such sampling. Our approach uses remote sensing data to detect such hotspots using ocean color as a proxy, and advectively projects these patches spatio-temporally using surface current data from HF Radar stations. Experiments with satellite and Radar data sets are promising for large, coherent blooms. We show how these predictions can be used to select an appropriate sampling trajectory for an AUV. [C336]

### "Vision based collision avoidance by plotting a virtual obstacle on depth map"

Obstacle avoidance is an important task for autonomous navigation. The paper presents a simple vision based obstacle detection and avoidance algorithm for mobile robots. Using a monocular vision system, a depth map is created in which every pixel of the image captured by the robot is classified in one of the two categories- ground or obstacle. A virtual triangular obstacle is then created on the depth map. To avoid this obstacle, the robot is directed along its edge having the maximum magnitude of slope. A distinct feature of the proposed algorithm is that along with the position, it takes into account, how densely populated are the obstacles in the field of view and turns the robot in the direction offering less hindrance. The algorithm can be effectively deployed for situations involving environment exploration. The algorithm has been validated on a differential steering robot with an on-board camera, driven by a remote computer which guides the robot, based on the algorithm implemented in MATLAB®. The algorithm is tested under uniform indoor lighting conditions and avoids collision of obstacles in its path successfully. [C337]

### "Utilization of airborne and in situ data obtained in SGP99, SMEX02, CLASIC and SMAPVEX08 Field Campaigns for SMAP Soil Moisture Algorithm Development and Validation"

Field experiment data sets that include coincident remote sensing measurements and in situ sampling will be valuable in the development and validation of the soil moisture algorithms of the NASA's future SMAP (Soil Moisture Active and Passive) mission. This paper presents an overview of the field experiment data collected from SGP99, SMEX02, CLASIC and SMAPVEX08 campaigns. Common in these campaigns were observations of the airborne PALS (Passive and Active L- and S-band) instrument, which was developed to acquire radar and radiometer measurements at low frequencies. The combined set of the PALS measurements and ground truth obtained from all these campaigns was under study. The investigation shows that the data set contains a range of soil moisture values collected under a limited number of conditions. The quality of both PALS and ground truth data meets the needs of the SMAP algorithm development and validation. The data set has already made significant impact on the science behind SMAP mission. The areas where complementing of the data would be most beneficial are also discussed. [C338]

### "LFMCW SAR waveform generation with frequency nonlinearity suppression"

Linearly frequency modulated (LFM) signals are desired in many electronic systems. For example, linearly frequency modulated continuous wave (LFMCW) radar has the good performance of lightweight, cost-effective, and high-resolution imaging. However, the presence of frequency nonlinearity in the transmitted signal will result

in contrast range-resolution degradation. In this paper, the impact of frequency nonlinearities on LFM CW synthetic aperture radar (SAR) system is addressed, and one parallel direct digital synthesizer (DDS)-driven phase locked loop (PLL) frequency synthesizer to synthesize wideband LFM signals is designed, and an adaptive system nonlinearity compensation technique is employed. In this way, an example wideband LFM synthesizer with good performance frequency linearity is designed. [C339]

#### "Route planning for unmanned aerial vehicle based on threat probability and mission time restriction"

In this paper, a route planning approach for unmanned aerial vehicle (UAV) with mission time restriction is investigated. According to the types and the characteristic of threats in the battlefield environment, we analyse the relation between threat extent and threat probability, build the model of threats, improve A\* algorithm through design the cost valuation function of A\* algorithm and use the variable step length strategy, it improve the search efficiency, when the route planned in safety area can't satisfy UAV mission time require, the method that suitable adding threat probability to satisfy mission time restriction was adopted. The simulation results show that the approach was feasible, effective and can plan route that satisfy the mission time requirements of UAV. [C340]

#### "Micro-doppler extraction of vibrating target based on dual-channel ATI technique in SAR"

Aiming at extracting the time-varying micro-Doppler feature of the ground vibrating target within ground clutter environment, the method of micro-Doppler extraction based on dual-channel ATI technique is presented. The ATI technique is utilized to suppress the ground clutter, and preserve the interferometric signal of the vibrating target in the raw data domain, which is presented as a straight line along the azimuth direction. According to this feature, we can find out which range cell the signal locates at, and then by taking the time derivative of its phase, the micro-Doppler modulation can be obtained. Compared to the single-channel situation, there is no need to compensate for the Doppler shift caused by the radar's translation in advance, and we can obtain the micro-Doppler feature induced by the vibration in any direction, which will help to reduce the computation burden and improve the target detectability. Simulated results verify the validity of the proposed method. [C341]

#### "Data analysis of wind profiler radar(WPR) under three kinds of synoptic processes in spring on Donghai island of Zhanjiang"

Observations from the WPR located in Zhanjiang are used to analysis the characteristics of wind field and virtual temperature in boundary layer under three kinds of synoptic processes during 5th-12th April, 2010. The results show that: (1) The horizontal wind velocity first increased and then decreased with altitude in low level of spring fair weather over Zhanjiang, with maxima range of 7-16 m/s, and the velocity also first increased and then decreased, with maxima less than 20 m/s in the middle level, the wind velocity was increased with altitude in high level. The horizontal wind direction was easterly in low level and southwesterly in high level, and the direction veered with altitude accompanied by warm advection. It appeared varied velocity of downdraft except for the weak updraft at the altitude of 2500-4000m. (2) During the spring fog process, the wind velocity fluctuated around 5 m/s with easterly direction in the low level and increased with altitude above 1100m which up to 19 m/s with southeasterly direction, but the velocity turned decreasing apparently around 5500m, with wind direction veering with altitude accompanied by warm advection. (3) There were two downdraft areas during precipitation, the first one was under the height of 1000m, and the second one was at the mid-level of 3000m. Updraft appeared before the onset of precipitation, and the low level was dominated by downdraft airflow after the beginning of rainfall. At the beginning of rainfall, the horizontal wind velocity shook at mid- and low-level with wider fluctuation margin of 3-9 m/s. The wind velocity increased with altitude accompanied by single warm advection and the direction was easterly below the height of 1000m, and the wind direction became more volatile with height above 1000m with alternated appeared warm and cold advection. [C342]

#### "Research on DBF SAR system in near space"

In this paper, a SAR system with a method of Digital Beamforming(DBF) was offered, which can realize both wide swath and high resolution at the same time. This research is based on the Displaced Phase Centers Multiple system, which adopt the DBF method at the receive, and is combined with the properties and demands of near space., and through the optimization of the design and overall consideration of the antenna size,pulse repetition frequency(PRF) and the ambiguities etc, the analyzed results demonstrate that it is possible to get wide swath and high resolution, what'more, such a system combined with the advantage of the near space will create a great superiority, and is of great reference value of the near space development and applications. [C343]

#### "Monitoring manners research on the river ice in the Yellow River"

According to the current need of controlling ice disaster, three types automatic monitoring ice system are put forward, i.e. ice depth auto measurement system; ice depth probing system; unpiloted aircraft monitoring system. They can continuously and automatically monitor many parameters including ice thickness, water level under ice, air temperature, ice temperature, water temperature and get the ice images, drift ice velocity and the density of drift ice. The process of ice in Yellow River can be obtained by the continuous monitoring with remote images monitoring, radar detecting and unpiloted aircraft monitoring after selecting proper monitoring point. As a result, these monitoring manners provide theoretical support and technical parameters for improving ice disaster emergency monitoring techniques and conditions forecast. At the same time, the monitoring information offers more detailed support to decision maker. [C344]

#### **"Wind field retrieval over the ocean using X-band polarization SAR data"**

An X-band wind field algorithm (XMOD) based on a linear approach is discussed in our previous work to describe the relationship between normalized radar cross section (NRCS), wind speed, wind direction and incidence angle. To apply the XMOD to TerraSAR-X data acquired in HH polarization, the two C-band polarization models are analyzed and tuned to X-band TerraSAR-X data. To demonstrate the applicability of the two models, 10m height wind speeds were computed with XMOD from several VV/HH TerraSAR-X images and validated by QuikScat and DWD model results. In addition, the wind speeds were retrieved and compared to each other from the HH and VV polarization TerraSAR-X images of the same scene at the same time. [C345]

#### **"The use of HF radar surface currents for computing Lagrangian trajectories: Benefits and issues"**

Surface coastal currents mapped by a pair of high frequency ground-wave radars (HFR) have been used to predict Lagrangian trajectories in the proximity of Heron Island (Capricorn Bunker Group, Great Barrier Reef, Australia), and to compare with the current data measured by an Acoustic Doppler Current Profiler (ADCP) at three mooring stations. Overall the HFR and ADCP absolute current speeds showed a difference less than  $\pm 0.15$  m s<sup>-1</sup> for 68% of the observations. A good agreement between HFR (at a depth of 1.5 m) and ADCP (at a depth of 5.5 m) data were observed for the u-component (cross-shelf) which presented a stronger tidal signal, while a poor comparison was found for the v-component (north-south) more influenced by the south-easterly and northerly winds. The HFR allowed inclusion of not only the temporal, but also the spatial current variability in the tracking computation. This proved to be crucial because the Lagrangian trajectories were very sensitive to the starting position and time in the studied area, where the currents exhibit a large spatial variation imposed by tides, winds, large scale circulation and topography. One challenge in applying HFR data for Lagrangian tracking consists of estimating the missing values and including the effects of small scale fluctuations. [C346]

#### **"Mechanisms and system design of satellite interferometric Synthetic Aperture Radar altimeter"**

Satellite radar altimeter plays an important role in microwave remote sensing, but its performance and applications on non-ocean surfaces are constrained by its poor resolution. The along-track resolution of altimeters can be improved by the synthetic aperture technology, while the cross-track resolution can be improved by the interferometric technology. Although these two technologies are well-established in side-looking radars, relevant studies on nadir-looking radar are rather inadequate. This paper reviewed the backgrounds of the synthetic aperture altimeter and interferometric altimeter. Then the mechanisms of the Interferometric Synthetic Aperture Altimeter (INSAA) are analyzed, and a set of typical INSAA system parameters are designed, especially on the phase-wrapping problem and baseline-length issue. [C347]

#### **"Offshore petroleum exploration from space: A developing capability at Geoscience Australia"**

Natural seepage can generate hydrocarbon slicks on the sea surface that may provide petroleum explorers with direct evidence of oil and gas below the sea bed. Remote sensing has the potential to be used as a tool for detecting such sea surface slicks, thereby identifying areas in both producing and frontier basins that are prospective for hydrocarbons. We are developing a two-pronged, remote sensing-based approach for seepage slick studies in the Australian Marine Jurisdiction: 1) building a semiautomated processing and classification system in order to scan large numbers of Synthetic Aperture Radar scenes for potential natural slick targets, and; 2) investigating the potential of optical remote sensing as a diagnostic tool for further, targeted study. Using objected-oriented classification algorithms in a bulk processing environment, large Synthetic Aperture Radar data sets were able to be efficiently screened for potential natural oil slick targets. This processing system offers a range of outputs, including classification statistics for each scene studied, as well as geo-referenced shapefiles ready for analysis in Geographic Information System software, where it can be combined with ancillary data sets for contextual analysis. Our research into the potential for optical remote sensing to enable further diagnostic study of identified, potential targets has shown that there are several commercially available, space borne sensors able to detect the types of oils found throughout the Australian Marine Jurisdiction, but that oil type is

critical for this application. Further to this, we have developed an approach for performing a feasibility study of oil type versus sensor sensitivity prior to image data acquisition. [C348]

### "Study the feasibility of airborne LiDAR on areal earth's crust deformation surveying"

Depicting people haven't find out one efficacious method to rapidly survey the areal outburst geological disaster at present. Through analysing the characteristic and the status quo of the airborne LiDAR, the paper consider that airborne LiDAR can do it. In order to verify the feasibility of airborne LiDAR on areal earth's crust deformation surveying. First, the paper analyse the error cause and should adopte quality control measures. Then, adopte net-RTK to survey many of points three dimensions coordinate in five different terrain regions (flat, river, town, hill, mountainous region). Second, Use DEM by airborne LiDAR points cloud on 3000 m altitude to interpolate vertical coordinate on same position. Third, compute the different value between datum and processing statistics and analysis to the different values. Last, The paper draw a conclusion that airborne LiDAR on 3000 m altitude can use areal earth's crust deformation. [C349]

### "Further analysis of the modulation of high frequency radar spectra due to sea-induced antenna platform motion"

The scattering of high frequency electromagnetic waves from the ocean surface is considered for the case of the radiation source being a vertical pulsed antenna mounted on a floating platform while the receiving antenna is fixed on the shore. This represents a small extension to an earlier analysis by Walsh in which both the transmitting (TX) and receiving (RX) antennas were co-located on a floating platform and the effect of the sway was accounted for in the ocean cross section. It is known that additional features appear in the Doppler spectrum when the RX and TX antennas are permitted to sway slowly, and here a similar result is shown when only the TX antenna moves. It is seen in this case that the magnitude of the additional spectral features is reduced as compared to the case when both antennas are moving. As a motivation for continuing analytical work, a preliminary field result is depicted. [C350]

### "The Integrated Marine Observing System-delivering data-streams to support marine research and applications"

The Integrated Marine Observing System (IMOS) is funded by the Australian Government through the National Collaborative Research Infrastructure Strategy (NCRIS) and the Education Investment Fund (EIF) to deliver data-streams from the Oceans around Australia. IMOS aims to meet the needs of the research community, address issues of national importance and contribute to international ocean observing programs. The strategic focus of IMOS is on the role of the oceans in the climate system, and the impact of major boundary currents on the continental shelf, ecosystems and biodiversity. [C351]

### "Assimilation MODIS and HJ-1 Reflectance Images to Produce NDVI of High Spatial and Temporal Resolution"

NDVI time series represent vegetation changes on land surfaces in time and space. MODIS, revisiting the earth once or twice a day, provides time series NDVI, which is a big advantage in global change study. However, the 1-km resolution of MODIS is too low to quantify the changes of heterogeneous landscapes. HJ-1 30-m CCD sensor can show detailed spatial information, but is affected badly by the weather, which has limited its use in studying biophysical process evolving rapidly in growing season. In cloudy areas, the problem is compounded, only several images can be obtained in a year. In this study, a data assimilation method was used to combine the advantages of the high temporal information of MODIS and the high spatial information of HJ-1 CCD to generate high temporal and spatial resolution NDVI to meet the need of the applications requiring NDVI in time and space. The MODIS multi-year mean NDVI time series for each type of vegetation is used as background field, and HJ-1 NDVI of the corresponding type of vegetation is taken as observations. The uncertainties of the two kinds of data sources are also taken into account. In this paper, MODIS 16-day NBAR product and HJ-1 30-m reflectance images, which NDVI are derived from, are used to produce the 16-day NDVI at HJ-1 spatial resolution in Heihe River Basin, Gansu province, China, in 2009. And comparing the assimilated data with the filed data, the results show that, the assimilated data and ground data are in good agreement, so this method used in our study is feasible. [C352]

### "Coseismic Deformation of 2009 L'Aquila, Italy Earthquake Derived from Ascending and Descending ENVISAT/ASAR Images"

The Mw6.3 L'Aquila earthquake (in central Italy) occurred on 6 April 2009 and caused ground displacements. In order to study this earthquake mechanism, three tracks(track 079, 129, 401) ENVISAT/ASAR images, which

include ascending and descending data, were used to derive different line of sight directions coseismic deformation based on the technique of two pass differential interferometric synthetic aperture rada (D-InSAR). The coseismic deformation results are quite consistent with the GPS measurements, and the RMSs (root mean square) in LOS between GPS and coseismic deformation of three tracks are 15mm, 26mm, 20mm respectively. This demonstrates that the D-InSAR LOS deformation accuracy can reach centimeter's level here. These coseismic deformations show that the earthquake fault is right lateral fault, the strike is NW-ES direction, and the largest LOS deformations of the three tracks are -268mm, -233mm, -255mm respectively. [C353]

#### "A Novel Random Sampling Method for Radar Image Compression"

In this paper, we propose a process of the radar image data by Random sampling. The sampling rate is far lower than Nyquist-Shannon sampling theorem, which shows that image data can be reconstructed from an extremely small set of measurements than what is generally considered necessary. Compressive Sampling is considered for signals and images that are sparse in a wavelet basis. A low complexity compression method for high resolution image based on block partition in wavelet region is proposed. The image is partitioned into blocks in wavelet domain and then compressed separately with CS. The bit rates for each block is allocated according to the texture complexity of the block. The proposed method eliminates the "block effect" caused by traditional block partition in pixel domain, and solves the problem caused by traditional block partition that the areas with simple texture are good in reconstruction quality while those with complicated texture are too poor to be used because of the uneven distribution of texture complexity. The experimental results show that the compression performance of the proposed method is quite similar to the results obtained by global compression. This compression method is particularly suitable for the high resolution remote sensing image which sparse in a wavelet domain. [C354]

#### "Filtering of LIDAR Points by a Hierarchical Smoothing Method"

Being able to collect 3D information directly from objects, LIDAR makes it possible to generate Digital Terrain Models (DTMs) quickly. To extract ground points from LIDAR point clouds, the paper proposes one filtering method which detects ground points by a hierarchical smooth method. Firstly a reference surface is generated by hierarchical smoothing method; Secondly ground points can be extracted by buffer analysis based on the reference surface. Based on ground points, DTM can be quickly produced by an interpolating algorithm. In the experiment, datasets with complex topographical undulations and different point density are taken to evaluate the validity of the proposed method. And results show that the proposed method is efficient and has potential for practices. [C355]

#### "A New Image Segmentation Method for Individual Tree Recognition Based on Airborne LiDAR Data"

Data filtering and image segmentation are two crucial steps in individual tree information extraction based on airborne LiDAR data. In this paper, a new image segmentation method was proposed to isolate individual tree and extract tree height and size information of the tree crowns, which is the fusion of marker-controlled watershed segmentation and valley-following segmentation. This method can perform edge detection effectively compared to methods before because a special detection constraint was added into it. A real data test was given to testify its validation. [C356]

#### "Practicable Research on Suppressing Angular Glint Base on the Target's RCS Weights"

Aim at the problem of glint in amplitude-comparison monopulse radar, the text uses the target's RCS weights method to suppress glint. For the effect of the method, besides using the simulation of extended target, the text uses real data of amplitude-comparison monopulse radar to validate the algorithm, and explains the adjust when way used for real data, finally demonstrates the suppressing effect and advances the practicable way for use. [C357]

#### "A method for InSAR baseline refinement and its application"

Interferometric baseline plays a very important role in InSAR data processing, and it will directly affect the accuracy of interferometric result. In this article, three classical baseline estimation methods were described. By comparing and combining three methods, a new baseline estimation method and its flow were listed. RADARSAT-2 satellite image data and grid digital elevation model ASTER GDEM (30m resolution) in Kailuan area are used as sample data. By analyzing the differential interferometric results generated with different baseline estimation methods, it can be concluded that the new method used by this article is correct and feasible. [C358]

### "Modeling and simulation of position for the Stratospheric ISAR system"

There are many advantages to put the Inverse Synthetic Aperture Radar (ISAR) system up in the stratosphere. Compared with the Ground-based ISAR system, one problem of the Stratospheric ISAR system is the platform drifting. This paper established models for the different positions of the airship and investigated the effects of drifting on imaging. The results of simulations for Stratospheric ISAR system show effectiveness of the models.

[C359]

### "Application of integrated geological prediction in expressway tunnel"

Because of the complicated geological conditions of tunnel surrounding rocks, it is of necessity to operate geological prediction during tunnel construction. Geology analysis, seismic wave method (TSP was adopted) and GPR (ground penetrating radar) are used to make prediction in the construction of Gaojiabao Tunnel. The utilization of several prediction methods that can be seen as an integrated prediction system can avoid one-sided conclusion obtained by single method. Moreover, each conclusion can be checked and made up mutually. The application result shows that the prediction conclusions are relatively accurate, which can meet the needs of safe construction. [C360]

### "Deformation analysis of Wenchuan earthquake based on D-InSAR with image mode"

It is considerably destructive for Wenchuan earthquake. The derived deformation field is an effective way to retrieve the geophysical parameters and study the seismic mechanism. Numerous geodetic methods can be exploited for the earthquake deformation monitoring. In spite of the high accuracy and consistent temporal scale, the results of GPS measurements are discrete. Continuous deformation field can be derived from Interferometric Synthetic Aperture Radar (InSAR). For image mode (IM) has full resolution, we will use conventional InSAR to get deformation field of Wenchuan earthquake. First, the geolocation of Longmen Mountain areas was introduced. The process of IM interferometry was analyzed in detail. At last, the deformation field was derived with the extent of 100km<sup>4</sup>100km. The results revealed that it was not the largest deformation region at the earthquake focus. The closer you get to the fault zone, the larger deformation gradient of the heading wall it become. At the same time, IM Interferometry can not reveal deformation field because IM is too narrow to obtain the entire deformation field. With the application to IM interferometry in Wenchuan earthquake, it is significant for earth science research such as earthquakes and crustal motion. [C361]

### "High-resolution airborne SAR interferometry mapping application in Huashan mountain"

Interferometric synthetic aperture radar (SAR) data offer the opportunity to map the western area of China, acquired from the first Chinese multi-modes airborne SAR mapping system. DEM could be obtained through airborne interferometric pairs. Furthermore, the quality of the InSAR DEM may vary significantly depending on the local topography. Aims of the approach are to smooth the noisy InSAR data, to merge the different directions DEM from the complementary interferometric pairs, to eliminate effectively spurious terrain surface points, to generate an improved 3-D visualization of the InSAR DEM scene and finally to meet DEM product accuracy requirement based on the different topography condition with a scale of 1:50,000. [C362]

### "DInSAR for land subsidence monitoring using high resolution COSMO-SKYMED SAR Data: Preliminary results compared with ASAR"

DInSAR can map ground deformation phenomena over tens-of-kilometers-wide area with centimeter-scale accuracy level, and has been considered as a powerful tool. Because of the data availability, previous DInSAR applications were mainly based on ERS, JERS, ENVISAT ASAR, and RADARSAT-1 data with resolution coarser than 10m. Nowadays, several kinds of high resolution SAR data are available for DInSAR and there are high expectations for the application of these data. In this paper, COSMO-SkyMed SAR data and grid digital elevation model ASTER GDEM (30m resolution) are used as research data. COSMO-SkyMed SAR data are preliminary processed by DInSAR technique for land subsidence mapping of Tianjin and Beijing area. Meanwhile, the DInSAR results from COSMO-SkyMed and ASAR data are preliminary compared. COSMO images are more suitable to extract high-precision ground deformation information than ASAR images in civil application given precise orbit data. While COSMO data are suitable for deformation monitoring in a relatively small and important area, ASAR data are fit for regional survey. [C363]

### "SAR image target recognition based on NMF feature extraction and Bayesian decision fusion"

In this paper, a new approach of synthetic aperture radar (SAR) image target recognition based on non-negative matrix factorization (NMF) feature extraction and Bayesian decision fusion is presented for recognizing ground vehicles in MSTAR database. First, feature vectors are extracted from image chips by NMF algorithm. Support

vector machine (SVM) is used to classify the feature vectors. After multiple views of the same vehicle collected at different aspects are classified by SVM, the outputs are fused by Bayesian decision fusion algorithm and then the final classification decision is generated. We evaluate NMF algorithm and the Bayesian decision fusion approach. Experimental results indicate that there are significant target recognition performance benefits in the probability of correct classification when NMF algorithm is applied and three or more views are used for Bayesian decision fusion. [C364]

#### "Time domain numerical simulation of microwave backscattering from sea surface for radar remote sensing"

Time domain numerical simulation technique has been developed to understand microwave backscattering mechanisms and evaluate sea surface observation methods. Backscattering coefficients and Doppler spectra can be obtained by this simulation technique. Physical optics approximation is applied to calculate scattering electric fields. The validity of the simulation has been verified by comparing with the results of the experimental basin. The results indicate that the simulation technique is effective to calculate microwave backscattering from the water surface changing in time. As an application of the simulation, we have simulated microwave backscattering with a pulse Doppler radar to evaluate sea surface observation methods. Radar images of backscattering coefficient and Doppler velocity have been generated. The results of the simulation show that radar images of Doppler velocity are more effective than images of backscattering coefficient for sea surface observation. [C365]

#### "Simulation study of relationships between Doppler-polarimetric parameters at microwave remote sensing of precipitation"

This paper studies the relationships between recently introduced differential Doppler velocity and other parameters of radar signal reflected from rain. Analytical calculation and simulation methods are used mostly. The results are checked by measurements in special cases. Some possibilities to derive information on distributed object structure are shown. [C366]

#### "Bio-radiolocation method at chest wall motion analysis during tidal breathing"

Influence of chest wall surface motion in bio-radar signal during tidal breathing was researched. A high-speed camera and multi-frequency radar with signal step modulation were simultaneously applied. The model of chest motion during quite breathing was used. Pairwise correlation coefficients for all the markers on the chest wall given in the model were calculated. The correlation of data from high-speed camera and bio-radar was found. Two methods were compared. [C367]

#### "Backscattering of wide-band HF signals from evolving ocean-like surface: 2-D direct numerical simulations and analysis"

Direct numerical simulations are used to calculate wide-band HF radar backscatter from evolving ocean-like surfaces in 2-D space. With the attainable spatial resolution of about 15 m, the large-scale wave pattern is visible in range-time plots of backscatter magnitude. The double Fourier transform of the signal magnitude or power in range and time reveals strong harmonics located along the dispersion curve of the propagating long waves. The signature is not predicted by the 1st-order Small Perturbation Method, and considering the next, 2nd order is required. It is shown that the spectral components along the expected dispersion curves in the  $\omega$ - $K$  domain can be used to retrieve the deterministic wave height of the surface. [C368]

#### "The DESDynI synthetic aperture radar array-fed reflector antenna"

DESDynI is a mission being developed by NASA with radar and lidar instruments for Earth-orbit remote sensing. This paper focuses on the design of a large-aperture antenna for the radar instrument. The antenna comprises a deployable reflector antenna and an active switched array of patch elements fed by transmit / receive modules. The antenna and radar architecture facilitates a new mode of synthetic aperture radar imaging called 'SweepSAR'. A system-level description of the antenna is provided, along with predictions of antenna performance. [C369]

#### "Fractal based detection using blind box-counting method in high resolution radars"

Sea clutter refers to the radar returns from the sea surface. Accurate modelling of sea clutter and detection of low observable targets within sea clutter are major problems in remote sensing and radar signal processing applications. Recently fractal geometry is applied to the analysis of high range resolution radar sea clutters. The box-counting method is widely used to estimate fractal dimension but it has some drawbacks rarely considered in literature. We explain the problem of box size range and present a novel method to select an appropriate

range. [C370]

### "Monitoring open-pit quarries by interferometric radar for safety purposes"

A novel Ground Based Synthetic Aperture Interferometric radar was set up for slope stability monitoring in open pit quarries. It is a wide view angle system which is easily adapted to the typical geometry of a quarry, and it automatically generates interferometric DEMs of the area under investigation. The system was tested during a 40 days field survey in a stone quarry in Tuscany, Italy. [C371]

### "Possibilities of oil slick detection on the sea surface using radar"

Possibilities of oil films detection on the sea surface and distinction them from natural marine slicks and look-alikes phenomena are discussed. [C372]

### "Development of wideband crosshole and surface GPR for soil characterization: FDTD modeling and experiments"

Original wide band antennas dedicated to the imaging of the subsurface by crosshole or surface radar for civil engineering application have been developed. The challenge in the developments is twofold: in the case of crosshole radar, the design of a narrow antenna less than 61 cm wide working in the frequency band [0.5;1.5] GHz, and in the case of a surface radar the design of a compact antenna less than 55 cm long working in the frequency range [0.3;1] GHz. FDTD simulations have allowed to propose optimized antenna geometries and to model both types of transmission links in the presence of a layered soil representing a moisture gradient. A first measurement campaign performed in the frequency domain in a clay sand embankment has allowed to validate the theoretical developments associated with the crosshole radar and to extract the dielectric parameters (permittivity and attenuation coefficient) as a function of the depth. The experimental validation of the surface radar will further be made and the performances of both types of radars will be compared. [C373]

### "SAR imagery and Seatrack Web as decision making tools for illegal oil spill combating-a case study"

The number of marine pollution arising from illegal oil discharges from ship tank or bilge pumping is much greater than those spectacular ship accidents. Illegal spills are mainly detected on essential navigation routes. In every country, marine surveillance agencies are responsible for oil spill combating and on identification of illegal polluters. They rely on information that has been provided on potential oil spills by responsible institution. The first information is usually provided by satellite remote sensing. The decisions about oil combating action is taken based not only on SAR imagery, but checking confirmation from aerial surveillance and using oil spill modeling, also. SAR imagery and aerial surveillance does not provide information about the type of spilled oil, which is important input information for oil spill modeling. Different types of oil have different behavior in water and may affect the decisions about which oil combating activities should be taken. The aim of this study was to show how different type of oil behaves in water according to the Seatrack Web oil drift model, which is the main modeling tool of Estonian Border Guard who is responsible in oil combating. Current study is based on illegal oil spill accident that happened in the eastern Baltic Proper on 10 April 2010. Potential oil pollution was detected on SAR image at 9:08 UTC. Consecutive SAR image was obtained at 9:40 UTC showing no significant change of the slicks area and shape in such a short time. Oil pollution was also confirmed by aerial surveillance at 11:10 UTC. Report that was based on visual observations said that it was probably a bilge water, which started to vanish due to ship traffic. The pollution was also recorded by Side Looking Aperture Radar (SLAR). Seatrack Web model (STW) was used for the forecast of oil slick drift. The input of light and medium oil was chosen. The results showed rather different results about oil drift as well as about oil fate. In case of medium oil 20% of oil was expected to evaporate within a couple of hours and the rest stayed in water surface. In the case of light oil 20% was evaporated, but the rest of the oil was expected to disperse in to the water column and emerge on the surface in time to time. The light oil was simulated to drift to the NWW, while medium oil to the SW. Laboratory analyses of the sample that was taken at 14:30 UTC showed that heavy fraction of the oil (hydrocarbons C16-C36) was maintained in the water until then. In conclusion, this study shows that the information about the type of spilled oil is needed as soon as possible after the oil detection to make appropriate decision on oil combating activities. [C374]

### "Advancing coastal upwelling observations with use of SAR data: Case study from SE Baltic"

Nowadays exploitation of satellite data, mostly infrared and visible, became a regular practice for upwelling detection and analysis. At the same time these types of satellite data strongly depend on sun illumination conditions and cloud cover, with the latter being very limiting factor specifically for the Baltic Sea. In this case

SAR (Synthetic Aperture Radar) imagery not affected by clouds and with high spatial resolution can significantly contribute to upwelling observations. The aims of this study are to show how SAR complements both in situ and satellite optical data, and to examine general SAR limitations to observe sea surface temperature (SST) fronts associated with coastal upwelling. [C375]

#### "Brillouin amplification of weak Stokes signal from sea water with different salinities and temperatures"

A scheme is presented for amplifying weak Stokes signals from sea water with different salinities and temperatures by Brillouin amplification. CS<sub>2</sub> whose Brillouin shift is near to that of water's is chosen as amplifier medium. A frequency doubled Nd:YAG laser is used to produce singlemode pulses of 7.2-ns duration. Results show that weak Stokes signals arising from water in the temperature range of 2°C to 40°C and salinity range of 00/00 to 350/00 can be amplified efficiently at room temperature. Signal gains as high as 107 were achieved with input signal energy in the order of pJ in experiment. [C376]

#### "Experiments research on ocean surface wave detecting using Streak Tube Imaging Lidar"

Synthetic Aperture Radar (SAR) can acquire the ocean wave spectrum in the wide-range area, and it can recognize the complicated space structure of the ocean wave. However, because the wavelength of SAR is long, its space resolution is not enough to analyze the micro-scale wave of the ocean surface. In the paper, Streak Tube Imaging Lidar (STIL) is presented firstly to collect the 4-D image (3-D range image + 1-D intensity image) of the ocean surface wave, which has high space resolution and range accuracy. Through analyzing the 4-D image, the variance of height and coarseness of the small-scale wave can be computed. Therefore, the micro-changes of wave are obtained. The experiments were performed in Yellow Sea, China. The results state that STIL can collect the 4-D images of the ocean wave with high accuracy, which can be used to analyze the micro-scale wave. [C377]

#### "Design and development of a millimetre-wave novel passive ultrasensitive temperature transducer for remote sensing and identification"

The millimetre-wave passive temperature transducer consists of micro bimorph cantilevers (Au-Silicon) and split ring resonators, operating around 30 GHz. The temperature change causes a deflection on the bimorph cantilevers, thus results in a shift of resonant frequencies of the split ring structure. The design achieves sensitivity of 2.62 GHz/ $\mu$ m in terms of frequency shift response to cantilever deflection, corresponding to a sensitivity of 498 MHz/°C, three order of magnitude higher than existing sensors. In terms of deflection versus temperature, the material choices for the bimorph cantilevers can be varied and adapted to different applications including those operating in harsh environments. To demonstrate proof-of-concept, a scaled prototype operating around 3 GHz is presented with Radar Cross Section measurements for remote identification. [C378]

#### "Spectrum crowding and Cognitive Radar"

The ever increasing demand on remote sensing capabilities directly conflicts with the accelerating loss of spectrum allocation. Increased spectral awareness and waveform diversity can be applied to this problem through cognitive processing and control of modern radar. This paper motivates the development of essential technology for this purpose. [C379]

#### "CFAR detector using GIS information"

In order to realize the constant false alarm ratio (CFAR) processing, the adaptive threshold should be used in radar signal detection. The threshold of the CFAR detector can be calculated using the clutter of range bins nearby the cell under test. In the real world, the clutter environments is always non homogeneous, which result in the performance degradation of the CFAR detector. In this paper, the CFAR detector using geographic information system (GIS) is proposed. With the knowledge of the clutter environment, the performance of the CFAR detector can be improved remarkably. The IPIX radar data are used to validate that the CFAR detector using GIS information is outperform the other conventional CFAR detectors. [C380]

#### "Study on retrieval methods of soil water content in vegetation covering areas based on multi-source remote sensing data"

Fusion image of SAR (Radar-sat image) combined with visible spectrum remote sensing image (TM image) is used to extract soil and vegetation water content in arid oasis taking the delta oasis of Weigan and Kuqa rivers in Xinjiang as the study area. Based on the Normalized Difference Moisture Index extracted from homochromous visible spectrum remote sensing data, this thesis utilizes "water-cloud model" to wipe off vegetation influence

from total backscattering coefficient of radar data and sets up the relationship between soil backscattering coefficient and soil moisture. The Result shows that in arid and semi-arid area where the main crops are cotton and corn, the combination of C- band HH polarization radar data with visible image performs well in the study of removing vegetation influence while retrieving soil water content in medium vegetated areas. [C381]

#### "Waves in the Southern Great Barrier Reef"

A brief description of three different platforms (WAVEWATCH III, Acoustic Doppler Current Profiler mooring and HF ocean radar) with directional wave measurement capabilities is provided. Initial results of directional wave and wind patterns derived from observations within the southern Great Barrier Reef, Australia, show consistency with the WAVEWATCH III model. These early findings are promising for future wind-wave investigations and validation studies in this region. [C382]

#### "Doppler velocity dealiasing with millimeter wave radar RHI data"

Millimeter wave radar has a unique advantage on detecting cloud microphysical structure. However, it is easy to cause the velocity aliasing due to its short wavelength. Velocity dealiasing is an effective means of detecting wind field information with Doppler radar. This paper reviews the cause of velocity folding and proposed a human-machine interaction method aimed at millimeter wave radar in the RHI scanning. It is concluded that the algorithm is very efficient and can produce high quality velocity data. [C383]

#### "X-Band radar derived sea surface elevation maps as input to ship motion forecasting"

Nautical X-Band radars used for navigation can also be used to determine spectral and individual wave properties. The sea surface reflects the incident radar beams and wave fronts become visible as stripe like pattern of high back scatter on the radar screen. When connected to a conventional nautical X-Band radar, the Wave Monitoring System WaMoS II exploits this imaging of waves to detect full directional wave spectra and to derive statistical sea state parameters as well as surface currents. WaMoS II is continuously improved with new features being developed. In particular, the sea surface elevation maps derived by WaMoS II allow to investigate and describe the spatial and temporal development of 3D ocean surface waves. The European Joint Industry Project 'On board Wave and Motion Estimator (OWME)' used this measurement technique to provide the wave information that is required to predict periods of quiescent vessel motions. A task that offers valuable support for various offshore operations like e.g. the tensioning of a tanker or the landing of a helicopter. This contribution gives an overview of the overall OWME system design showing first validation results, focusing on the method to derive wave trains using the WaMoS II system. [C384]

#### "Signal and image processing applications in radar ocean observations"

Signal processing is quite intensive when dealing with radar sensors. In this paper, the ability of spaceborne radars for imaging ocean surface features is explained and some of the very actual results are shown through several illustrations. The aim of such means to watch the earth is to provide useful information on a global basis regardless of the weather conditions (especially clouds) and in daylight as well as at nighttime. In this context, the main mean of observation is, without any doubt the SAR or Synthetic Aperture Radar [1]. From a signal processing perspective, radar data and images are a very interesting domain of research. Indeed, they present non-gaussian, non-stationary and often non-linear characteristics, thus raising the challenge of their interpretation. We will first focus on the SAR signal processing and the mechanisms allowing a radar image of the ocean to be formed. Then we will detail some of the special characteristics when using SAR processing. Indeed this processing is done at the ground receiving station and present several very interesting challenges in terms of statistical behavior of the data and signal processing. The following section will deal with signal and image processing techniques aimed at achieving very high resolution spectral analysis, especially in 2D. Finally, we will present several of the main features that are detected and we will give some of the inferred parameters that can be measured and used by the oceanographic community. We will also, describe some of the environmental issues associated. [C385]

#### "A new class of microwave filters using vertically stacked coupled open loop resonators"

The design of microwave bandpass filters with compact circuit size has attracted tremendous research interests worldwide recently since the well-established traditional techniques do not satisfy this requirement. Development of advanced technology in emerging wireless communications such as multifunction ultra-wideband (UWB) systems, personal communication network WLAN, Bluetooth and remote sensing and imaging radars; demand ultra-high integrating density components and techniques. The bandpass filter should also be able to offer a good performance, constant group delay over the desired passband, high selectivity, wide band rejection, low insertion loss, low manufacturing cost and high reliability. [C386]

### "Validation of the AVTIS volcano imager radiometry-A comparison of infrared and millimetre wave thermal imagery"

The AVTIS remote sensing instrument is a custom built millimetre wave sensor that has been developed as a practical field tool for remote sensing of volcanic terrain at active lava domes. We present validation of the MMW radiometry of a volcanic scene by comparison with coincident infrared imagery. [C387]

### "Measurement of the complex dielectric constant of volcanic ash at millimetre wavelengths"

Methods for determining the dielectric permittivity of rock samples at millimetre wave frequencies have been investigated. A quasi-optical approach using pellets of powdered samples was found to work well, avoiding the dimensional restrictions of small waveguides. The permittivity of volcanic rock and ash samples was measured, providing valuable data for MMW radar remote sensing of terrain and ash clouds. [C388]

### "Digital module design of a satellite rain-compatible radar altimeter"

Satellite radar altimeters play an independent role in ocean remote sensing, while the authors exploited their potential in rain measurement. This paper designs the digital system of the rain mode in an altimeter. In rain mode the altimeter receives the ocean and rain echoes simultaneously, so it can retrieve the rain layer profile without losing surface topography information. An adaptive IF-digital I/Q demodulator is designed, and all of its components are considered in turn. Afterwards the algorithm of an ocean-rain compatible processor is designed to switch the altimeter in various operate modes. [C389]

### "Fused variational analysis technique for high-resolution reconstruction of remote sensing imagery"

In this study, we apply the robust error estimation theory as a basis to develop an appropriate procedure that performs the processing and enhancement of the remote sensing (RS) image contaminated by composite noise (additive and multiplicative) and degraded by the data acquisition system. The first reconstruction stage is performed using the Bayesian statistical estimators referred to as WCMAP { WCLS (Weighted Constrained Least Squares) and MAP (Maximum a Posteriori Probability) algorithms } which significantly increase the gain of image sharpness. Subsequently, we employ the isotropic diffusion and anisotropic diffusion methods for obtaining the optimal balance in reference to increasing the perceptual quality of RS images. The effectiveness of the proposed fused WCMAP method were evaluated through the comparative simulation of different RS image reconstructive. [C390]

### "Design of mobile robot system with remote control based on CAN-bus"

In order to realizing remote control and information collection quickly and reliably, the mobile robot with remote control is designed. In the paper, according to analysis of the overall structure, hardware circuit of the robot system is designed. Because the CAN2.0 standard only makes physical layer protocol and data link layer protocol, application layer protocol is ruled according to robot control system. In the last part of this paper, the software of master/slave computer is introduced in detail. The experiment shows that running performance of robot control system is balanced, efficient and has satisfied the practical demand. [C391]

### "Multitemporal polarimetric SAR data fusion for land cover mapping"

With the development of the polarimetric Synthetic Aperture Radar (SAR), the research on the land cover classification using SAR data has developed rapidly. But the classification accuracy is serious affected by the speckle noises on the SAR image. A new method which combines the advantages of multi temporal SAR data and quad-polarization SAR data was presented in this paper. A method of multitemporal SAR data fusion was used to eliminate the effect of the speckle noises on the SAR image. An area of 12 Ч 17 km was selected as test area. 6 multi temporal RADARSAT-2 images were used in this study to contact the land cover classification. The results show that different land cover type denote different backscattering mechanism and the backscattering coefficient value of different land cover type varies as function of time. Based on the fusion result of multi temporal polarimetric SAR data, the land cover classification was fulfilled and the results show this method can effectively distinguish the man-made buildings, forest, farm land and water. The speckle noise was obviously reduced and the visual appearance of the SAR fusion image well improved. [C392]

### "A study of PS-InSAR method for small area urban land subsidence"

Persistent Scatterers for SAR Interferometry (PS-InSAR) technique allows monitoring the temporal evolution of a deformation phenomenon at millimeter level, via the generation of mean deformation velocity maps and

displacement time series from a data set of acquired SAR images. However, the serious noises of multi-temporal SAR images make the selection of permanent scatters (PSs) difficult. In this paper, we propose a novel PS-InSAR method based on wavelet phase analysis to solve this problem by improving the quality of interferograms. Firstly, both the real parts and the imaginary parts of SAR interferograms are processed by wavelet decomposition. Secondly, the interferograms on every level are filtered by grads dependent adaptive filter and reconstructed. Finally, interferograms are processed to identify PSs by using two indices namely, amplitude disperse index and spatial correlation index, followed by an unwrap process to extract land subsidence information. We then use this method to process 12 ENVISAT SAR imgs covering Jiaxing city in Zhejiang province, China. The experimental results show its effectiveness in residuals and PSs identification and land subsidence extraction for plain urban area. [C393]

### **"Integration of LIDAR data and geological maps for landslide hazard assessment in the Three Gorges Reservoir area, China"**

The water storage and millions of immigrants work have a great impact on engineering geological condition which may cause slope instability in the Three Gorges Reservoir area, China. This paper presents regional assessment of landslide hazard from Zigui to Badong based on Light Detection and Ranging (LIDAR) data in combination with geological maps and landslides information of this area. Four essential parameters, including engineering rocks, slope, slope structure and water impact, are extracted from this data. The informative model is employed to create landslide hazard map. The result shows that informative model successfully identified the stable regions as well as instable reservoir banks. Reservoir water and engineering rocks are principle control on slope stability in this area. We also divided the study area into fourteen sections according to the landslide hazard map. [C394]

### **"Wetland mapping by using multi-band and multitemporal SAR images: A case study of Hong he National Natural Reserve"**

Wetland ecosystems have many important functions as the regional environment stabilization, natural species protection and ecological resources facility. Investigation and monitoring on wetland urgently need the application of remote sensing. The optional remote sensing technology is sometimes difficult to receive the data due to the bad weather, or in specific light conditions. However, radar remote sensing has a great potential for technical application in wetland mapping with its all-weather, all-time capabilities. And SAR scattering intensity is sensitive to the soil moisture of land cover and land change, therefore it is also helpful to the wetland research. In this paper, multi-band, multi-temporal SAR technique was used for wetland mapping. Unifies the SAR polarization characteristic, the backscattering characteristic of multi-temporal ENVISAT ASAR HH, HV, VV polarization data and ALOS PALSAR HH polarization data of different land use type and different vegetation type in Honghe National Natural Reserve (HNNR) were analyzed. The multi-temporal SAR data was used for vegetation classification research in decision tree classification method. And the authors use actual samples to do accuracy assessment in the way of computing confusion matrix. The result from this study shows that the improvement of water and marsh classification accuracy owes to the summer data, and the classification accuracy can be improved when we used the multitemporal data, HV polarization data in winter is more advantageous for forest map. The recognition rate of water, marsh and forest was relatively high. The classification of grass and bush had confusion. The classification accuracy of multitemporal SAR reached 79.55%. [C395]

### **"Vulnerability assessment of combined impacts of sea level rise and coastal flooding for China's coastal region using remote sensing and GIS"**

China's coastal region is physically and socio-economically vulnerable to accelerated sea-level rise and associated coastal flooding because of its low topography, highly developed economy and highly-dense population. In this study, we present a scenario of sea level rise and storm surge flooding along the China's coastal region over the next century and apply them to a digital elevation model (DEM) which acquired by the shuttle radar topography mission (SRTM) to illustrate the extent and spatial distribution to which coastal areas are susceptible to permanent inundation and episodic flooding due to storm events. To perform flood scenario analysis and vulnerability assessment, a method for producing several sets of data was implemented by combining remote sensing processing, the use of grid-based socio-economic data, and subsequent analysis using Geographical Information Systems (GIS). This analysis shows that inundation and coastal flooding will mainly occur in the major delta without the protection of dike systems. However, due to the concentration of population and economic activities in China's coastal region, societal and economic consequences of continued sea-level rise would be substantial. Finally, some suggestions are presented for decision-makers, and other concerned stakeholders to develop appropriate public policies and mitigation measures. [C396]

### **"InSAR analysis over Yellow River Delta for mapping water-level changes over wetland"**

Wetlands cover more than 4% of the Earth's land surface and include hydrologic and other process that are fundamental to understanding ecologic and climatic changes. It is very important for wetlands protection and re-construction to measure water level changes and consequently water-storage capacity changes in wetlands. Using VV polarization C-band and HH polarization L-band SAR data, combined with synchronous field measurement and investigation, this paper analyzes the difference of backscattering and interferometric coherence characteristics of different types of wetlands. After evaluating factors that influence interferometric coherence, the framework, for measuring water level changes using InSAR phase information, is presented in this paper. With obtained SAR data, this paper studies the InSAR-derived water level changes in Yellow-River Delta wetlands. The results show that the InSAR technology has a great potential in mapping water level changes in coastal wetlands, and InSAR-derived water level changes can supply unprecedented spatial details.

[C397]

### **"Precise SAR satellite orbit parameters determination based on Ground Control Points"**

Aim to solve the georeferencing problem of spaceborne SAR imagery, accounting for the orbit physics model and the impact of the earth perturbations, some description models such as four parameters model and polynomial model could be applied to determine the satellite orbit parameters. However the orbit state vectors solved by 5 satellite state vectors supplied by header file in SAR data files could hardly acquire precise orbit parameters, which would greatly effect on the accuracy of co-registration, phase unwrapping, baseline estimation and the generation of Interferogram and DEM (Digital Elevation Model). In this paper, combined with R-D (Range-Doppler) conformation equation and earth ellipsoid equation, which explicitly describe the relationship of corresponding pixel between the 2D image coordinate and the 3D cartographic coordinate of ground targets, an advanced orbit model algorithm by adding few GCPs (Ground Control Points) to improve satellite state vectors is presented. All the correlative formulas are deduced and the orbit parameters can then be iteratively determined through solving a linear equation set consisting of the error equations from all GCPs under Recursive Least Square (RLS) algorithm. The algorithm is tested on an ERS SCL (Single Complex Looked) scene with a series of simulation experiments and the improved orbit parameters and contrasted with accurate SAR orbit data supplied by DEOS institution of Delft University in Holland, which could be demonstrated of validity and stability.

[C398]

### **"Study on accurate estimation of baseline parameters of space-borne InSAR based on GCPs"**

The estimation of baseline parameters is an important step in SAR interferometry (InSAR) processing and applications, because its accuracy influences directly the quality of the final DEM generated from interferogram. In this paper, some classical methods of baseline parameters estimation, based respectively on precise orbit data, interferogram and Ground Control Points(GCPs), are summarized and compared. For it is recognized that the baseline parameters estimation based on GCPs is the most reliable method at present, this paper concentrate on researching optimizing model of several correction algorithms based on GCPs for baseline parameters. The approach is tested with ENVISAT ASAR data over the Dujiangyan region of Sichuan Province of China. Finally, the feasibility and rationality of the proposed method is showed by comparing the quality of DEM generated from interferogram with SRTM DEM. [C399]

### **"An improved filtering method for digital elevation models construction based on LiDAR"**

LiDAR (Light Detection and Ranging) is a positive remote sensing technology. In this paper, with analyzed the characteristic of LiDAR data and discussed the advantages of LiDAR data, we present an improved data filtering algorithm for LiDAR data. It is basing on the last return laser pulses and tries to design an fast pre-processing LiDAR point data with the purpose of DEM Modeling from LiDAR based point cloud data. The algorithm contains two times of filtering with different aims and data process strategies. Experiments of real terrain area are presented for testing efficiency and accuracy of this filtering method. [C400]

### **"Regional aboveground forest biomass estimation using airborne and spaceborne LiDAR fusion with optical data in the Southwest of China"**

Laser altimeter systems provide an accurate measurement of canopy height, the vertical structure of vegetation and the aboveground biomass (AGB). Airborne discrete return LiDAR (Light Detection and Ranging) was used operationally in many cases and some regions; spaceborne large footprint LiDAR (ICESat GLAS) has acquired over 250 million LiDAR observations over forest regions globally. The ICESat GLAS data have been used successfully for forest height and biomass in various sites. To estimate aboveground forest biomass in the Southwest of China, products from EOS MODIS and ENVISAT MERIS were used to expand the estimation from GLAS data. Airborne LiDAR data were collected along GLAS orbit to estimate forest height and biomass for

each GLAS footprint after training with 81 field measured plots. The  $R^2$  are 0.68 and 0.91 for field measured biomass and mean height estimation using airborne LiDAR data. Then the aboveground biomass was estimated from ICESat GLAS data using the equation trained by field data ( $R^2 = 0.47$ ,  $n=185$ ). EOS MODIS Vegetation Continuous Fields (VCF) product, enhanced vegetation index (EVI) product and ENVISAT MERIS Regional Land Cover product were used to generate 175 forest classes, which included five forest canopy density classes, five vegetation index classes, and seven forest cover types. Then we combined forest aboveground biomass derived from GLAS pulses footprint with 175 forest classes to generate a continuous aboveground forest biomass map of study area. Forest aboveground biomass was minimal at 43 Mg/ha, maximal at 133 Mg/ha, averaged at 78.9 Mg/ha in the study area. The results of predicted aboveground biomass were in agreement on the amount and distribution after comparison with reference data, which showed that the predict model for GLAS successfully captured the distribution of aboveground biomass. [C401]

#### "Determination of sedimentation rate of tidal flats at the Yangtze estuary, China, using multi-temporal Landsat TM images"

Remote sensing, combined with in situ surveying, is an effective tool for monitoring the tidal flats. Airborne light detection and ranging (LIDAR) or radar interferometry can be utilized to measure precisely the surface topographic change. However, neither the satellite-borne synthetic aperture radar (SAR) nor LIDAR is an effective way to obtain appropriate data on tidal flats, mainly because of the little opportunity of finding favorable tidal conditions. Therefore, the waterline method is, so far, the only useful approach to the practical application of satellite remote sensing to monitor the tidal flat environment. The 'waterline' is defined as the boundary between a water body and an exposed land mass in a remotely sensed image. Waterline method has been applied in analyzing the horizontal evolution of tidal flat, but such approach has seldom been used for vertical development. Sedimentation rate is an important factor describing the dynamic nature of tidal flat, so waterline method to determine multi-year mean sedimentation rate was reported at Chongming Dongtan Nature Preserve in Shanghai, China in this paper. The waterlines were extracted from multi-temporal Landsat TM images by unsupervised classification method and region growing algorithm. The mean sedimentation rates were calculated at four transects according to corresponding elevation measurements and waterlines with heights assigned by hydrodynamic model. The results showed that the evolution of the bed level was changed spatially in the cross-shore profiles. The peak of accretion rate occurred at different elevations of the four profiles. Sediment surface of all profiles showed a shoreward reduction from the maximum site to the high marsh, likely due to the shoreward decrease in water energy and submergence time as well as the protective effect of marsh vegetation. The offshore decrease may be related to hydrodynamic attenuation by vegetation and settling lag. A positive relationship was demonstrated--between the mean accretion rates and surface elevation of low marsh and mudflat ( $R^2 = 0.8106$ ). Spatial changes in sedimentation rate were also striking at the same elevations of different profiles, which could be attributed to differences in sediment distribution and hydrodynamics. The effects of tidal marshes on hydrodynamics and sedimentation were also related to the degree of shelter from water energy. The relationship between sedimentation rate and vegetation distribution was also discussed. [C402]

#### "Multi-spectral and SAR images fusion via Mallat and A trous wavelet transform"

The information which is contained in the multi-spectral and SAR images have different characteristic. Multi-spectral images contain a great deal of spectral information, whereas SAR images contain rich texture information, such as buildings and road network. SAR and TM images fusion based on the wavelet transform ensure the fusion image showing more spatial detail, not only conserving the spectral information of the multi-spectral images and reducing the distortions as well, but also highlighting the texture information of the SAR image. In this paper, the wavelet transform-based image fusion methods by using SAR and TM multi-spectral images are implemented by Mallat and a trous algorithms separately. Before the image fusion, both of the SAR and TM images have to be geographic coordinate registered in order to they having the same pixel size. In wavelet decomposition, the decomposition level is determined by statistical of entropy value. According to SAR and TM image fusion based on wavelet transform, it can be seen that the fusion image is greatly improved and both of spectral and textural information are enhanced. The value of entropy, variance, average gradient and correlation coefficients of the fusion image are analyzed for two different algorithms evaluation. By analyzing the results, It can be concluded that the image fusion by a trous wavelet transform has a good effect in experiment. [C403]

#### "A case study on co-seismic ground deformation of the Wenchuan earthquake using L-band and C-band SAR interferometry"

Synthetic aperture radar interferometry (InSAR) has been widely used for the co-seismic ground deformation monitoring. In this paper, The L-band SAR datasets acquired by ALOS PALSAR and C-band acquired by Envisat ASAR are tested respectively for monitoring the co-seismic ground deformation in the area of Dujiangyan, where

the Wenchuan Ms8.0 earthquake occurred on May 12, 2008. The displacement on line of sight has been acquired with two-pass DInSAR processing. It is also found that the C-band SAR data results generally have lower coherence over high vegetated and rugged areas, while the L-band SAR with comparatively longer wavelength is more suitable for monitoring the deformation where large displacement over a small spatial extent occurs and the mountainous terrain. However, current satellite radar interferometry, because of its single-frequency signal structure, is hard to measure ground deformation with large gradients as it produce very dense fringe patterns, which cause that the ground displacement deformed in the faults cannot be measured. Although the longer wavelength of the radar signal is less susceptible to high deformation gradients, loss of correlation often still occurs in the faults caused by earthquake. So it is necessary to propose techniques which can monitor large-gradient deformation and the data fusion methods of multi-source satellite SAR images. [C404]

#### "Effect of primary feed polarization on phase centre location of parabolic reflector antennas"

Knowledge of the phase centre location of the antenna is of great importance in various applications, such as global positioning system (GPS), remote sensing, radars, and virtual arrays. In parabolic reflectors, the phase centre is located at the center of the aperture plane when it is illuminated by a prime-focus point source feed having an axially symmetric pattern. It is clear that if one displaces the antenna phase centre, the apparent location of the antenna will move resulting in a virtual antenna. The virtual array antenna can be thought of as an antenna having multiple identical beams, with multiple displaced phase centre locations. Such a property is desirable in remote sensing applications, to allow multiple antenna representations. Multiple phase centre reflector antennas were studied in using a dual-mode feed horn as a primary feed. In this paper, the impact of the feed polarization on the phase centre location of offset reflector antennas will be addressed. The feed is a dual mode circular waveguide antenna operating at its fundamental mode,  $TE_n$ , and the higher order mode  $TE_{21}$ . It will be shown that the phase centre displacement can be controlled by simply changing the excitation amplitude and phase of each mode, as well as employing different mode orientations. In particular, the direction of the phase centre movement will depend on the polarization of each mode. [C405]

#### "A novel passive ultrasensitive RF temperature transducer for remote sensing and identification utilizing radar cross sections variability"

In this paper, a prototype of the novel SRR temperature sensor integrated into the passive multi-sensor identification sensing system is demonstrated as well as RCS measurements. [C406]

#### "Simulation of UWB echoes from ground based on CPML-FDTD"

In designing some UWB-IR (ultra-wideband impulse radio) devices, the effects of ground echoes must be taken into consideration. The dispersion of soil and roughness of ground surface are significant factors in ground echoes calculation. FDTD (finite difference of time domain) algorithms applied in ground echo simulation at present have the problems of slow speed or large errors. By using multi-pole Debye model as soil dielectric coefficients, and CPML (convolutional perfectly matched layer) as absorption boundary condition, a CPML-FDTD algorithm is derived in multi-pole Debye media. Simulations are carried out under different conditions, and comparison with non-PML FDTD algorithm proves the validity and efficiency of the proposed algorithm. [C407]

#### "CAROLS campaigns 2009: First Results"

The CAROLS, L band radiometer, is built and designed as a copy of EMIRAD II radiometer of DTU team. It is a Correlation radiometer with direct sampling and fully polarimetric (i.e 4 Stockes). It will be used in conjunction with other airborne instruments (in particular the C-Band scatterometer (STORM) and IEEE GPS system, Infrared CIMEL radiometer and one visible camera), in coordination with in situ field campaigns for SMOS CAL/VAL. The instruments are implemented on board the French research airplane ATR42. A scientific campaign with thirteen flights is realized over south-western France, Valencia site and Bay of Biscay (Atlantic Ocean) in spring 2009. In order to qualify the radiometer data, different types of aircraft movements were realized: circle flights, wing and nose wags. Simultaneously to flights, different ground measurements were made over continental surfaces and ocean. Results show a good quality of data. For continental surfaces, important Radio-Frequency Interferences (RFI) were observed over a large part of the studied region. [C408]

#### "Advances in waveguide-fed slot arrays"

Waveguide-fed slot arrays are employed in numerous radar, remote sensing, and communication applications in ground and space systems. Professor Elliott's significant contributions paved the way for the eventual maturity of the slot array antenna technology to the point that it is possible to design such systems in one pass without the need for any experimental data. The author worked in a research group headed by Prof. Elliott and centered at Hughes Aircraft Company, Canoga Park, CA in the early eighties. Later the author collaborated with Elliott in the

study of slot arrays for a decade with funding from the University of California and the Hughes Corporate office. Subsequent work was funded by many sponsors. This paper reviews the advances made in the field of slot arrays by the author in collaboration with colleagues and students. [C409]

### "DFT-UTD based MoM approach for an efficient analysis of scattering from large, finite arrays in the vicinity of scattering objects"

This paper presents an efficient hybrid method for analyzing scattering/radiation from electrically large arrays in the vicinity of nearby obstacles. Electrically large arrays are widely used in several applications such as radars, remote sensing systems, and modern communication systems. In general, these arrays radiate in the presence of nearby obstacles, such as an array on a mast. The proposed approach is based on the combination of a ray-field representation of the field radiated by electrically large arrays and a DFT (Discrete Fourier Transform) representation of nonuniform array current distribution. Realistic array current distributions are nonuniform even if the array is excited uniformly due to coupling among the array elements and coupling between array and scattering objects. DFT employment for expressing nonuniform array current distribution is a robust approach, since, for practical array current distributions most of the DFT coefficients are close to zero, except for a few significant terms. [C410]

### "The study on extracting of vessels information from the SAR satellite data"

The paper introduces satellite remote sensing technology used into marine traffic investigation, to detect and analyze actual marine traffic situation on a large scale. The paper introduces characteristics of SAR image and the procedure for extracting information of vessels based on the SAR Remote Sensing image. Vessel Detection Technology is studied based on multi-source space borne SAR data, after analyzing the characteristics of various types of vessels detection algorithm and combining with the needs of marine vessel detection and traffic investigation. According to the characteristics of SAR images, four methods of extracting ship information have been developed, including gravitational field, CFAR detection, PNN and adaptive algorithm. Taking the ERS-2 images as an example, the reliability and limitations of vessel information extracting from the satellite image is discussed. The study shows that satellite remote sensing provides a new and feasible method for marine vessel traffic investigation. At present, the technology has been developed and some tests have been carried out. However, some limitations in the system need further study, especially the impact of the sea state. [C411]

### "Remote sensing retrieval of soil moisture using ENVISAT-ASAR images: A case study in suburban region of Peking, China"

Soil moisture is a highly variable component of soil, and plays an important role in materials and energy exchanges between earth and atmosphere. It is also the basic parameter of crop growing and crop yield forecast. With the features of observing large area synchronously, timely, and economically, remote sensing technique makes dynamic soil moisture monitoring possible. Soil moisture remote sensing monitoring has 30 years history and many researches have been done home and abroad in this field, including visible and infrared remote sensing based NDVI methods, hyper spectral remote sensing based algorithm, and microwave remote sensing orientated methodology and so on. Among these methods, microwave has great advantage in retrieval soil moisture because of the characteristics of all-weather, penetrability and not affected by the cloud. Through study people found that microwave is one of the most effective methods in retrieval soil moisture in various technologies. This paper summarizes the major microwave sensors and the principle of microwave remote sensing, and introduces the microwave model and soil moisture algorithm. Based on ENVISAT Radar data, with suburban farmland (wheat and corn as the main crop) of Peking as the study area, we established the microwave scattering characteristics database of local exposed surface. We used the selected model to simulate the response characteristics of backscattering coefficient influenced by a variety of parameters, such as soil moisture, surface roughness, incidence angle, polarization, etc. Then we got the updated inversion empirical model of the exposed surface, and evaluated the accuracy of model with the actually surveyed data in the field. This article makes certain contributions to the active microwave soil moisture retrieval methods study, and provide a viable model for water resources decision-making support to the Peking municipal government. [C412]

### "Estimation of forest height, biomass and volume using support vector regression and segmentation from lidar transects and Quickbird imagery"

Lidar (light detection and ranging) remote sensing can accurately characterize forest vertical structure, such as canopy height, above-ground biomass (AGB) and timber volume; however, data acquisition is expensive. To reduce costs, one potential method is to integrate (small area) lidar transects and (large extent) optical imagery to estimate forest characteristics. Typically, multiple regression is used to link variables extracted from lidar transect data and optical imagery. Height information is then generalized from the area covered by lidar

transects to other areas without lidar coverage. However, multiple regression models may not fully capture the complex relationship between variables. Fortunately, Support vector regression (SVR) provides a solution to deal with such complex nonlinear problems. Using a case study in Vancouver Island, Canada, SVR was applied to generalize canopy height from lidar transect(s) to the entire study area (2601 ha) based on a segmented Quickbird image. Results show that: (i) compared to typical multiple regression models, the SVR models provided better results for estimating canopy height; (ii) by using only one lidar transect (i.e., 8.8% cover), the SVR model generates an average canopy height estimation error of 6.2 m-which is less than a British Columbia forest inventory height class (9.0 m); and (iii) the final model estimates have relatively high correlations with field data for forest canopy height ( $R^2$ : 0.81), AGB ( $R^2$ : 0.76) and volume ( $R^2$ : 0.64), while representing dramatically reduced acquisition costs. [C413]

### "Estimation of wetland aboveground biomass based on SAR image: A case study of Honghe National Natural Reserve in Heilongjiang, China"

Wetland is a significant component of the land ecosystems to discover the characteristics and ecological laws. Presently, a common method to estimate a regional wetland biomass is normally based on optical remote sensing images. The estimation of wetland biomass by Synthesize Aperture Radar (SAR) is a novel subject. As a new type sensor, SAR has advantages for wetland applications, therefore, it can be apply for generating some important information about wetland ecology and hydrology, especially with the complex ecological habitat of the transitional place between land and water, radar images can be significant tool for wetland biomass estimation. In this paper, as a case study of SAR application on Honghe National Natural Reserve (HNNR), the wet weight and dry weight field data of 28 quadrats of diverse vegetation in a growing season from the study area in 2009 were gathered, the ASAR image was acquired at the same time with field work. The backscattering coefficient of polarimetric radar and wet weight and dry weight data was taken as correlation variable, the fitting equations of regression models and water cloud model were built to estimate the wet weight and dry weight, a validation was made from 9 measured plots. The research shows the estimation of the wetland biomass by SAR image can be a supplement to optical image with a scientific significance in ecology studying. [C414]

### "Preliminary study on land use classification based on multi-source remotely sensed data fusion technology"

High spectral resolution, high spatial resolution and high temporal resolution are the development trend of modern remote sensing technology. In the case of same image data, it is difficult to obtain high spatial resolution and hyperspectral remote sensing data information simultaneously. This weakness can be remedied, the quality of the image can be improved and the useful thematic information also can be highlighted by fusion of remote sensing image which is from the different sensors. In this paper, Multiplicative Transform, Principal Component Transform and Brovey Transform had been used to fuse the high spatial resolution radar data- COSMO-SkyMed, IRS-P5 data and high spectral resolution data of multi-spectral image -IKONOS, image respectively. And then, the results of fusion accuracy used to land use classification had been evaluated. The results show that: (1) the standard deviation of the fused image by the multiplicative transformation of COSMO-SkyMed radar data and IKONOS multi-spectral data is 21.327 and the relevant index is 0.565675, so the quality of the fused image is the most optimal. The standard deviation of the fused image by the principal component transformation of IRS-P5 data and IKONOS multi-spectral data is 26.506 and the relevant index is 0.56842, which indicate that the quality of the fused image is the best. (2) The classification accuracy of using original image data is not high (the classification accuracy without visual correction is 68.75%). The accuracy classification which using fused image was apparently improved. The classification accuracy of the fused image (without visual correction) which by using the fused image of COSMO-SkyMed radar data and IKONOS multi-spectral data is higher than that of the fused image of IRS-P5 data and IKONOS multi-spectral data. The classification accuracy of former (without the visual correction) is 81.82%, and the classification accuracy of latter (without the visual correction) is 73.33%. It shows that the former is more conducive to extract the information of the thematic features. [C415]

### "Unsupervised classification for polarimetric Synthetic Aperture Radar image using the fuzzy possibilistic C-means clustering"

The polarimetric Synthetic Aperture Radar (POLSAR) image data has the problems of the noisy pixels and vague category boundaries because of its complex scattering mechanism and statistical property, which strongly influence the classification quality, while the fuzzy possibilistic C-means (FPCM) is robust in detecting the noisy pixels and modeling the uncertainty. Hence, we tried FPCM algorithm combined with the four scattering features (entropy (H), anisotropy (A), scattering angle ( $\alpha$ ) and total power (SPAN)) to classify the POLSAR data. The feasibility of this approach was tested on the JPL/AIRSAR POLSAR data, and the experiment result shows that the clustering algorithm can perform the classification more effectively in contrast to its counterparts FCM and PCM clustering algorithms. [C416]

### "LIDAR filtering based on morphological watershed and region growing"

The morphology watershed is an effective method of image segmentation. This filter algorithm is as follows: First, basing on elevation information, discrete data point cloud should be turned into a gray image, Then it be pre-filtered with morphological watershed, because of the excessive separate phenomena of watershed morphology, Finally we use the region growing to eliminate or reduce its negative effects. The algorithm does not need to interpolate original data, without iteration, and speed is good. Experimental results show that this filter process can be programmed to obtain the goal of automation and certain accuracy. [C417]

### "Digital terrain model extraction from airborne LiDAR data in complex mining area"

Airborne light detection and ranging (LiDAR) proved to be an adequate technique to deliver highly accurate 3D mass points of the surface. However, the surface of mining area is complex with steep slope, dense vegetation, artificial mining facilities and buildings, which is different from the flat surface of city. The main processing workflow for DTM generation from LiDAR includes points filtering and DEM interpolation. In this article, five methods for removing object points from LiDAR data in mining area were compared. These methods, including Adaptive TIN (ATIN), Elevation Threshold with Expand Window (ETEW), Maximum Local Slope (MLS), Mathematical morphology (MM), Iterative Polynomial Fitting (IPF), analyze data points based on variations of local slope, elevation and height difference between points and the interpolated surfaces. Complex mining area data set with various cliffs of quarry, trees, houses, roads and small reliefs were selected to test the filtering methods. The results show that all methods can effectively remove most object points in complex mining areas. The ATIN and MM filter generated the best result in sharp cliff area of a quarry, whereas the other algorithms tended to remove the steep edge of quarry and roads. Depending on the filtering parameters, each method experienced various omission or commission errors. Quantitative assessment shows the ATIN and IPF based on the height difference between points and surface perform better. DEM interpolation assessment experiments indicate that interpolation biases were minute. Global statistics show that Modified shepard's method, Spline and Radial basis function interpolation methods have the lowest errors in the study area. [C418]

### "Semi-supervised remote sensing image classification via maximum entropy"

Remote sensing image segmentation requires multi-category classification typically with limited number of labeled training samples. While semi-supervised learning (SSL) has emerged as a sub-field of machine learning to tackle the scarcity of labeled samples, most SSL algorithms to date have had trade-offs in terms of scalability and/or applicability to multi-categorical data. In this paper, we evaluate semi-supervised logistic regression (SLR), a recent information theoretic semi-supervised algorithm, for remote sensing image classification problems. SLR is a probabilistic discriminative classifier and a specific instance of the generalized maximum entropy framework with a convex loss function. Moreover, the method is inherently multi-class and easy to implement. These characteristics make SLR a strong alternative to the widely used semi-supervised variants of SVM for the segmentation of remote sensing images. We demonstrate the competitiveness of SLR in multispectral, hyperspectral and radar image classification. [C419]

### "Wireless tomography, Part I: A novel approach to remote sensing"

Wireless tomography, a novel approach to remote sensing, is proposed in Part I of this series. The methodology, literature review, related work, and system engineering are presented. Concrete algorithms and hardware platforms are implemented to demonstrate this concept. Self-cohering tomography is studied in depth. More research will be reported, following this initiative. [C420]

### "Active hyperspectral LIDAR methods for object classification"

We have studied the fusion of active hyperspectral and range (LIDAR) data to investigate the concept of an active hyperspectral LIDAR and its potential applications in the remote sensing of vegetation. We have built two prototype instruments using the newly developed supercontinuum laser technique providing a continuous spectrum, which has then been used both for combined hyperspectral and LIDAR or time-of-flight measurement. The preliminary results point out the potential of active hyperspectral methods in laser-based remote sensing applications: the combined topographic and spectral information, such as the normalized difference vegetation index (NDVI), can be used efficiently in automatic target identification and classification. [C421]

### "Detecting potential human activities using coherent change detection"

This paper describes detection and interpretation of temporal changes in an area of interest using coherent change detection in repeat-pass Synthetic Aperture Radar imagery, with the main goal of detecting subtle scene

changes such as potential human activities. Possibilities of introducing knowledge sources in order to improve the final result are also presented. [C422]

### "Support vector machine fusion of multisensor imagery in tropical ecosystems"

One of the major stakeholders of image fusion is being able to process the most complex images at the finest possible integration level and with the most reliable accuracy. The use of support vector machine (SVM) fusion for the classification of multisensors images representing a complex tropical ecosystem is investigated. First, SVM are trained individually on a set of complementary sources: multispectral, synthetic aperture radar (SAR) images and a digital elevation model (DEM). Then a SVM-based decision fusion is performed on the three sources. SVM fusion outperforms all monosource classifications outputting results with the same accuracy as the majority of other comparable studies on cultural landscapes. SVM-based hybrid consensus classification does not only balance successful and misclassified results, it also uses misclassification patterns as information. Such a successful approach is partially due to the integration of DEM-extracted indices which are relevant to land cover mapping in non-cultural and topographically complex landscapes. [C423]

### "SNR-dependent filtering for Time Of Arrival estimation in high noise"

Time of Arrival (ToA) estimation is a cornerstone of many of the remote sensing applications including radar, sonar, and reflective seismology. The conventional Matched Filter Maximum Likelihood (MFML) ToA estimator suffers from rapid deterioration in the accuracy as Signal to Noise Ratio (SNR) falls below certain threshold value. In this paper we suggest an alternative method for ToA estimation based on the fusion of measurements from biased estimators which are obtained using a pair of unmatched filters. Suboptimal but not perfectly correlated estimators are combined together to produce a robust estimator for ToA estimation in high noise. The unmatched filters pair is parameterized by a single parameter (phase shift) which is selected based on estimated SNR level. [C424]

### "Fusion of hyperspectral images and LiDAR data for civil engineering structure monitoring"

Investigation of civil engineering materials includes a wide range of applications that requires three-dimensional (3D) information. Complex structures shapes and formations within heterogeneous artificial/natural land covers under varying environmental conditions requires knowledge on the 3D status of the urban materials for better (visual) interpretation of polluted sources. Obtaining 3D information and merge them with aerial photography is not a trivial task. It is thus, strongly needed to develop new approaches for near real time analysis of the urban environment with natural 3D visualization of extensive coverage. The hyperspectral remote sensing (HRS) technology is a promising and powerful tool to assess degradation of urban materials in artificial structures by exploring possible chemical physical changes using spectral information across the VIS-NIR-SWIR spectral region (400-2500nm). This technique provides the ability for easy, rapid and accurate in situ assessment of many materials on a spatial domain within near real time condition and high temporal resolution. LiDAR technology, on the other hand, offers precise information about the geometrical properties of the surfaces within the study areas and can reflect different shapes and formations of the complex urban environment. Generating a monitoring system that is based on the integrative fusion between HRS and LiDAR data may enlarge the application envelop of each technology separately and contribute valuable information on urban runoff and planning. The aim of the presented research is to implement this direction and define set of rules for practical integration between the two datasets. A fusion process defined by integrative decision tree analysis includes spectral/spatial and 3D information is developed and presented. [C425]

### "Probabilistic robust hyperbola mixture model for interpreting ground penetrating radar data"

This paper proposes a probabilistic robust hyperbola mixture model based on a classification expectation maximization algorithm and applies this algorithm to Ground Penetrating Radar (GPR) spatial data interpretation. Previous work tackling this problem using the Hough transform or neural networks for identifying GPR hyperbolae are unsuitable for on-site applications owing to their computational demands and the difficulties of getting sufficient appropriate training data for neural network based approaches. By incorporating a robust hyperbola fitting algorithm based on orthogonal distance into the probabilistic mixture model, the proposed algorithm can identify the hyperbolae in GPR data in real time and also calculate the depth and the size of the buried utility pipes. The number of the hyperbolae can be determined by conducting model selection using a Bayesian information criterion. The experimental results on both the synthetic/simulated and real GPR data show the effectiveness of this algorithm. [C426]

### "Using Snakes with Asymmetric Energy Terms for the Detection of Varying-Contrast Edges in SAR Images"

Active contour methods like snakes, have become a basic tool in computer vision and image analysis over the last years. They have proven to be adequate for the task of finding boundary features like broken edges in an image. However, when applying the basic snake technique to synthetic aperture radar (SAR) remote sensing images, the detection of varying-contrast edges may not be satisfying. This is caused by the special imaging technique of SAR and the commonly known specklenoise. In this paper we propose the use of asymmetric external energy terms to cope with this problem. We show first results of the method for the detection of edges of tidal creeks using an ENVISAT ASAR image. These creeks can be found in the World Heritage Site "Wadden Sea" located at the German Bight (North Sea). [C427]

### "Fast Derivation of Soil Surface Roughness Parameters Using Multi-band SAR Imagery and the Integral Equation Model"

The Integral Equation Model (IEM) predicts the normalized radar cross section (NRCS) of dielectric surfaces given surface and radar parameters. To derive the surface parameters from the NRCS using the IEM, the model needs to be inverted. We present a fast method of this model inversion to derive soil surface roughness parameters from synthetic aperture radar (SAR) remote sensing data. The model inversion is based on two different collocated SAR images of different bands, the derivation of the parameters cannot be done using one band alone. The computation of the model and the model inversion are very time consuming tasks and therefore may be impractical for large remote sensing data. We present an approach that is based on a few model assumptions to speed up the computation of the surface parameters. We applied the algorithm to detect the correlation length of the surface for dry-fallen areas in the World Cultural Heritage "Wadden Sea", a coastal tidal flat at the German Bight (North Sea). The results are very promising and may be used for a classification of the area in future steps. [C428]

### "Vegetation management of utility corridors using high-resolution hyperspectral imaging and LiDAR"

This study examines the use of high spatial resolution hyperspectral imagery in combination with light detection and ranging (LiDAR) data and digital aerial imagery for vegetation management of utility corridors. Two different classification methods, i.e. the support vector machines (SVM) and the spectral angle mapper (SAM) were applied on the datasets to test their ability for discrimination of various vegetation species. The SVM classifier performed best with an overall accuracy of 83% applied on the hyperspectral imagery. With inclusion of the LiDAR data the accuracy could be increased to 92%. Power lines were extracted from the LiDAR data and the conductor clearance was calculated. The results were merged with the SVM classification and a species map of vegetation that could cause potential damage to the power lines was generated. The results of this study show that an improved approach for vegetation management of utility corridors can be achieved by combining the spatial and spectral information of multi-source datasets. [C429]

### "Thermal infrared radiosity and heat diffusion model verification and validation"

A radiosity model used for predicting effective hyperspectral emissivity spectra and radiant temperatures for rough surfaces has been developed. Here we compare the computer model results to analytic model results in order to verify that the computer model is working properly, and validate the model results by comparison to spectra measured in the field by an hyperspectral imaging spectrometer. We measured a cm-scale DEM of the test scene using a tripod-based LiDAR. The discrepancies between analytical and modeled values are less than 0.01%. Modeled emissivity spectra deviate from the measured by no more than 0.015 emissivity units. [C430]

### "Canopy vertical structure using MODIS Bidirectional Reflectance data"

Canopy spectral invariant variables, escape probability and recollision probability, are wavelength independent and intrinsic canopy structure properties. They provide a physical interpretation of the correlation between canopy architecture and multi-angle spectral data. The 500m Moderate resolution Imaging Spectroradiometer (MODIS) Bidirectional Reflectance Distribution Function (BRDF) product from study sites at Howland Forest, Maine are used to develop multivariate linear regression models to estimate canopy vertical structure using both escape probabilities and directional reflectance. These are compared with canopy height information which has been retrieved from the airborne Laser Vegetation Imaging Sensor (LVIS) at a finer scale spatial resolution. Both the escape probability and the directional reflectance approaches achieve similar results with correlation coefficients of 0.63-0.66. This suggests that the MODIS 500m BRDF data can be useful in extrapolating limited lidar information on canopy vertical structure to larger regional areas. [C431]

### "Identification of inclined buildings from aerial LIDAR Data for disaster management"

Airborne laser scanning has demonstrated a strong ability to obtain the location of collapsed buildings and the dimension and characteristic of their damage. This paper focuses on the identification of inclined buildings from aerial LIDAR Data which contains amount of noise and small details. To achieve the goal, several steps were carried out in the approach: Firstly, the building's roof was classified and majority of roof types were taken into account in our research; Secondly, a chosen algorithm was used to extract the roof facets of building and also the foundation, and it was proved to be robust to eliminate the noise and give a good result; Thirdly, the geometric axis line of a building was extracted; fourthly, a method was proposed to determining whether buildings are inclined. Finally, an experimental study was made to demonstrate the feasibility of the proposed solution on disaster management. [C432]

#### **"Geodesics-based topographical feature extraction from airborne Lidar data for disaster management"**

Hundreds of thousands of lives were lost in the natural disasters such as geological earthquakes, floods, landslides and mud-rock flow in every year. Nowadays, with the rapid development in airborne LiDAR techniques, extraction of the multi-scale topographical features from high-resolution topographic data acquired via airborne LiDAR would lead to fundamentally new understandings of earth essential to mapping flood, landslide and mud-rock flow hazards for decision makers. In this paper, we define topographic features in a multi-scale manner using a center-surround operator on Gaussian-weighted mean curvatures. These multi-scale topographical features would allow improved detecting, understanding and prediction of flood inundation, landslide and mud-rock flow likelihood. For example, experimental results identify that proposed method can be employed for detecting landslide. [C433]

#### **"The atmosphere correction in SBAS D-InSAR land subsidence monitoring application: A case study in Jiaxing-Huzhou plain, China"**

It is well know that atmospheric phase screen(APS) effect in Small Baseline Subset (SBAS) D-InSAR processing to obtain ground deformation in long time series leads to additional interferometry phase and the unreliable result. To solve the problem above, MODIS product provide a mean to stimulate atmospheric field of SAR data for reducing the APS effect in D-InSAR processing. In this paper, 12 ENVISAT ASAR images are used to process SBAS method and 6 MODIS MOD05\_L2 products are used to process atmosphere correction. A case study in the Jiaxing-Huzhou plain in Zhejiang province, China shows successfully stimulate the atmospheric field of SAR data and analysis its effect on SBAS application. [C434]

#### **"Large-scale, rapid detection method of surface subsidence in western mining area"**

In view of the character of mining disaster and the limitation of traditional methods of earth surface deformation monitoring in western mining area, an attempt at adopting InSAR techniques in dynamic deformation monitoring in west mining area has been developed. This paper takes Shaanxi Province Binchang mining area as study area, processes the SAR image by differential interference, obtains the deformation image of Binchang Coal Mining Area, This shows that the InSAR can rapid detect the surface subsidence areas in a large area (100 km<sup>4</sup>100 km). InSAR technology will be widely used in mining damage dynamic monitoring in western mining area. [C435]

#### **"SAR and multi-spectral image fusion based on feature additive integration"**

Fusion of SAR image and multi-spectral (MS) image can provide complementary information about the ground observed objects. This paper presents a fusion method of SAR and multi-spectral images based on the IHS transformation and phase congruence feature extraction. The IHS transform is firstly made to MS image to separate the intensity from the hue and saturation components. Then the phase congruence is calculated from intensity component of MS image and SAR image, which can provide an absolute measure of image features that is viewing-condition-independent and is invariant to change in illumination and magnification. According to both phase congruence values, the feature of SAR image is integrated into MS image. The experiments show that the fusion method proposed has a good performance. [C436]

#### **"Production and accuracy analysis of high quality TerraSAR-X DOM"**

The production and accuracy analysis of high quality TerraSAR-X DOM are presented. The main focus is given to how to control the accuracy of ortho-rectification framework. Two SpotLight scenes of 1 meter resolution images and two ScanSAR scenes of 3 meter resolution images in China are used as the experimental data. Based on the proposal ortho-rectification framework, the absolute accuracy of TerraSAR-X DOM can reach to less than three pixels. [C437]

### "SAR satellite image interpretation based on the multilayer level set approach"

Synthetic aperture radar, SAR, is a remote sensing way to explore the ground truth in day and night. How to interpret the given SAR images provides an import clue to study the characteristics of the imaged areas. However, the image interpretations for SAR images are difficult because of the effects of speckle signals shown in the images. In order to solve the problem, several algorithms have been proposed. The processed results show the proposed algorithms still have their own limits on reducing the effect of speckle signals. In this paper, the multilayer level set approach is employed to have the SAR images be grouped into several sub-regions such that the segmented regions are homogeneous. Based on this minimization of the energy, the multilayer level set method implicitly presents the regional boundaries as several nested level lines. By increasing iterations and preselected level values, these lines evolve close to the level boundaries based on the energy minimization. This method provides numerical stability and quick convergence. In order to implement the multilayer level set approach, several level values need to be established firstly. Those level values are determined with calculating the average values from the classified groups with applying K-means method. Based on the four-color theory, the multilayer level set method is able to generate an optimal piecewise continuous approximation for the SAR image such that each approximation sub-region is homogeneous. From the processed results, the multilayer level set approach can efficiently reduce the effect of the speckle signals, and quickly segment SAR images for further image interpretation. [C438]

### "Application of three-orbits D-InSAR technique on landslide displacement monitoring"

Landslide disaster has happened frequently in our country. Monitoring and early warning are the main means to effectively reduce the harm of landslide disaster. Different from the traditional method of monitoring, differential interferometry synthetic aperture radar (D-InSAR) measuring technique has the advantage of detecting and penetrating earth surface in all weather conditions and in all time, obtaining continuous and large-area deformation information. Taking the Jinpingzi Landslide of Jinshajiang valley as the research object. The monitoring technique of three orbits difference, the basic method of D-InSAR, is used to obtain surface deformation value. Research results show that the deformation value of Landslide boundaries is larger than the surrounding area, and the D-InSAR technology is a feasible approach for monitoring landslide. [C439]

### "Application of GIS and remote sensing techniques for water resources management"

Water is one of the most important natural elements on earth. Water quality directly and indirectly influences human lives and development. In this paper, a GIS-based system is designed to assist water resources professionals in making economical and efficient decision. GIS and remote sensing techniques are effectively used to replace, complement and supplement data collection in various facets of different kinds of water resources projects. This paper describes the design and implementation of a GIS-based system for water resources management. The system consists of five parts: Geographical Information System (GIS), the database, the mathematical model, the knowledge database and the user graphical interface. The system can help water resource manager to appreciate the potential of remote sensing capabilities for application in the management of precious water wealth. The system can dynamically monitor water and provide decision support for precious water management. It has obvious economic, environmental and social benefits. [C440]

### "Forecast hail by analysis radar image"

In this paper, we use a new way to find some information from radar image. We process the image by Hole-Full Cell Nerve Network (CNN) and then add the all data in the image. We can find there seems some relation between the number and hail shooting. We process more pictures. And gave more parameters to do so. Dug some data as information. At last we find some regular to distinguish the cloud with hail or not. It is a area be find. It will be hail shooting when the data come to the area. We find those are useful way for forecasting of hail. [C441]

### "Assessment of ASTER GDEM performance by comparing with SRTM and ICESat/GLAS data in Central China"

Recently, a new Global Digital Elevation Model (GDEM) from optical stereo data acquired by the Advanced Spaceborne Thermal Emission and Reflection Radiometer (ASTER) was released with the resolution of 1 arc sec. In this study, the performance of the new ASTER GDEM is assessed by comparing with SRTM (the Shuttle Radar Topography Mission) and point data from ICESat/GLAS (Ice, Cloud, and land Elevation Satellite/ Geoscience Laser Altimeter System). A 5°45' area (30°-35°N, 110°-115°E) with varied terrain was chosen as the study area. Standard DEM-to-DEM comparison, DEM-to-control-point comparison and visual analysis were used to evaluate the ASTER GDEM quality. The results show that the ASTER GDEM has much fewer voids

than SRTM V2 (the version 2 SRTM). The ASTER GDEM has lower elevations (approximately -5m) compared with SRTM, whereas the ASTER GDEM has higher elevations (approximately 15m) compared with ICESat/GLAS points. To the vertical accuracy, the results of the ASTER GDEM compared with SRTM V4 (the version 4 SRTM), SRTM V2 and ICESat/GLAS points are 39.55m, 25.99m, 33.99m at 95% confidence respectively, exceeding 20m estimated prior to the ASTER GDEM production. The poor accuracy may be related to the high terrain relief and high ratio of lower stack number of the ASTER GDEM in the study area. The ASTER GDEM shows better performance in the flat areas than that in the mountainous areas, and the accuracy improves with the increasing stack number. The ASTER GDEM has many artifacts including inland water noises and straight lines related to the irregular stack number boundaries, which are caused by the methodology to produce the ASTER GDEM. [C442]

#### **"Building extraction using dual-aspect high resolution SAR images"**

Interpretation of SAR image in urban area is far from solved with the increase of spatial resolution, and building extraction in SAR image has remained as a tough work. Typically, the outlines of buildings are usually not complete, and the geometric distortions further complicate the appearances of buildings in high resolution SAR images. Thus, in this paper, a strategy based on dual-aspect high resolution SAR images was proposed to extract complete footprint of buildings in urban area. Experiments prove that dual-aspect SAR images, especially with high resolution, are very useful for building extraction in urban areas. [C443]

#### **"Ortho-rectification of high-resolution SAR image in mountain area by DEM"**

Because of the side-looking imaging characteristics, the quality of Synthetic Aperture Radar (SAR) image is badly affected by variable terrain. Such terrain can introduce large displacements in the SAR image geometry that inhibits the collocation of SAR-derived quantities with geographically referenced information acquired from other sources. So it is necessary to eliminate such inherent geometric distortions by generating a radar ortho-imagery that corresponds to a well defined map projection. In this paper, aiming at the newest high-resolution SAR data-RADARSAT-2 and TerraSAR-X, an effective ortho-rectification method was studied in detail and the result showed this method could achieve high geo-location accuracy. [C444]

#### **"A fuzzy-logic-based approach for flood detection from Cosmo-SkyMed data"**

The Cosmo-SkyMed mission offers a unique opportunity to obtain radar images useful for flood mapping, being characterized by high revisit time, thanks to the four satellites that form its constellation. In the context of a study aiming at evaluating the usefulness of Earth Observation data for managing flood events, particularly focused on Cosmo-SkyMed, an algorithm to map flooded areas from synthetic aperture radar imagery has been developed. It employs also ancillary data as a land cover map and a digital elevation model. The approach is based on the fuzzy logic because such a theory allows us to exploit the theoretical knowledge about the radar return from inundated areas and to account for simple hydraulic considerations and contextual information. [C445]

#### **"Polarisation and mode combinations for ship detection using RADARSAT-2"**

RADARSAT-2 provides new opportunities for spaceborne monitoring of vessel traffic and fishing activities. A series of RADARSAT-2 data has been collected and analysed over Norwegian waters. ScanSAR and Standard Quad-pol images have been used in the analyses. The Norne field is used as a test site, because it is possible to image the same vessel under different conditions. The different polarisations and polarisation combinations are analysed. [C446]

#### **"Processing of bistatic TanDEM-X data"**

On June 21st, 2010, the German radar satellite TanDEM-X was launched and successfully placed in an orbit approaching the TerraSAR-X satellite until both systems will fly in close formation and will establish the only available bi-static interferometer in space. The primary TanDEM-X mission goal is to generate a global Digital Elevation Model (DEM) with a relative point-to-point height accuracy of 2 meters for moderate terrain at 12 m posting. For that purpose interferometric SAR data will be acquired over a period of 3 years in parallel to the operational running TerraSAR-X mission. Systematic processing of SAR raw data to so-called Raw-DEMs is performed by one single processing system, the Integrated TanDEM Processor (ITP). The final global DEM is then calibrated and mosaicked by a second system, the Calibration and Mosaicking Processor (MCP). The scope of this paper is to present an overview of ITP functionalities and to summarize the first processing results. [C447]

#### **"Peatland subsurface water flow monitoring using polarimetric L-band PALSAR"**

The potential of L-band PALSAR for monitoring water flow beneath the peat surface is demonstrated on a bog near Lac Saint Pierre (Canada). Two polarimetric ALOS acquisitions collected at spring and fall under different water conditions are used. The Touzi decomposition, which was shown to be very promising for peatland characterization using the C-band Convair 580 SAR, is applied. Like in, the information provided by the multi-polarization (HH, HV, and VV), the scattering type magnitude (the Cloude  $\alpha$  or the Touzi  $\alpha_s$ ), the single scattering eigenvalues and the entropy, cannot detect the presence of water underneath the peat surface. The Touzi scattering phase is shown to be the only target scattering decomposition parameter that can detect water flow variations beneath the peat surface. The fall acquisition that took place after two days rain permits demonstrating that the wave can penetrate deep into the acrotelm layer to detect the rain water that has sunk rapidly into the peat layer of high hydraulic conductivity. The spring acquisition at dry conditions permits better discrimination of poor fen from bog. The wave, which cannot detect deep water flow in the bog sublayer of low hydraulic conductivity (the catotelm), is more sensitive to the shallower fen subsurface water and this makes possible the separation of poor fen from shrub bog. The requirement for polarimetric PALSAR acquisition during summer is brought out for more effective exploitation of PALSAR unique long wavelength penetration capabilities in monitoring arctic peatland transformations related to climate change stress. [C448]

### "PolSAR images characterization through Blind Sources Separation techniques"

Since the backscattered signal in PolSAR images is intrinsically linked with the physical characteristics of the objects in the image, valuable information may be extracted therefrom. The paper focus is to propose a new physical characterization of the scattering target, inspired by the Blind Sources Separation techniques. [C449]

### "Accuracy of the engineering calibration of weather radars"

This paper provides a synopsis of the accuracy calculation for the engineering calibration of a weather radar system. The underlying meteorological radar equation is optimized in order to reduce the total uncertainty of the calibration. Special emphasis is given to the determination of the different uncertainties of the various measurements which are required for a system calibration. A spreadsheet for the calculation of the total uncertainty of the calibration is presented. [C450]

### "Fine structure of the upper ocean from high-resolution Terrasar-X imagery and In-Situ measurements"

We investigate small-scale features using SAR imagery, including sharp frontal interfaces, slicks of artificial and natural origin, and wakes of surface ships. Collection of the ground truth data helps in the understanding of the physical mechanisms behind the patterns visible in the image. [C451]

### "Texture estimation in sar images: The impact of scale and model order"

This paper discusses methods and parameter settings that help to estimate texture in SAR images. In general, this is a difficult task for SAR images that are characterized by speckle noise and which span a wide range of pixel magnitudes. We applied Gauss Markov Random Field (GMRF) models and Enhanced Model Based Despeckling (EMBD) to 1 meter resolution amplitude images of the German TerraSAR-X mission. The results demonstrate that one can find appropriate parameter combinations that allow robust texture estimation even for different types of target areas. [C452]

### "A new SAR sensor designed for micro-satellites"

Micro Satellites ( $\mu$ SATs) are good opportunities for small countries. This paper describes a new design of a SAR for a  $\mu$ SAT. The centre frequency and the SAR processing were optimized in a way to allow the realization of a simple but capable system that provides many interesting opportunities for researchers and allows participating to international environmental monitoring and control activities. The major points of the design are a frequency that allows some penetration through vegetation and a relative small antenna in length and width. A new SAR processing concept allows a medium swath-width and an acceptable resolution. A patent is pending. [C453]

### "An improved CSA for one-stationary BiSAR squint mode"

The purpose of this paper is to solve the imaging problems of one-stationary bistatic synthetic aperture radar (BiSAR) squint mode. Through the analysis of the target's two-dimensional spectrum, an improved chirp scaling algorithm (CSA) is got. It can deal with the space variability of this kind of BiSAR and the simulation is done to verify the validity and feasibility of this algorithm. [C454]

### "Coherent marine radar measurements of properties of ocean waves and currents"

Marine radars offer the capability to image ocean wave propagation by virtue of repetitive coverage of the same scene. With a typical 1.25-s rotation period, ocean wave frequencies of 0.4 Hz can be measured unambiguously. Imaged areas of the order of ten square kilometers, allow the dynamics and kinematics of ocean wave fields to be measured with higher azimuthal resolution than traditional oceanographic instruments, such as buoys or pressure sensors. Using the dispersion relation for shallow waves in coastal regions, ocean wave spectra and bathymetry can be estimated using non-coherent marine radars. The derivation of wave height or wave height spectra from marine radar imagery has had some success by relating the radar echo intensity imagery of waves to wave height using an empirically derived modulation transfer function (MTF). More recently, using a radar scattering model's dependence of the radar scattering cross section on long wave slope, good results are reported in deep water for shipboard experiments, where winds and waves are typically in the same direction. However, in coastal waters, offshore winds blowing in a direction other than that of the incoming wave field can produce enhanced roughness on the front face of waves, resulting in a modulation of the radar wave field image that is not wave height dependent. A coherent radar can overcome these limitations using the direct measurement of the radial component of orbital wave velocity, accounting for Bragg scatter velocity. Radial orbital velocity will maximize and minimize at similar locations on long wave profiles as do radar echo intensity, so wave patterns should look very similar for the two. Thus, analysis methods similar to those used in non-coherent radar studies should be applicable to coherent radar data as well. We present recent experimental results on the retrieval of coastal ocean wave and current properties due to a storm over the Outer Banks of North Carolina in November of 2009. [C455]

### "POL SAR image classification using BP neural network based on Quantum Clonal Evolutionary Algorithm"

POL SAR image classification plays an important role in remote sensing. POL SAR data are a type of mass data and have more independent features which can represent different physical significances than optical image. Therefore, POL SAR image classification is actually a high dimensional nonlinear mapping problem. Because of the nonlinear mapping function of BP neural network, it can be used to classify POL SAR image. But BP neural network classifier is sensitive to initial weights and thresholds. Quantum Clonal Evolutionary Algorithm (QCEA) can converge to an optimal value quickly and can be used to optimize the initial weights and thresholds of BP neural network. Therefore, in this paper, BP classifier based on QCEA was used for POL SAR image classification. Firstly, optimize the initial weights and thresholds of BP neural network using QCEA. Secondly, train the optimized BP neural network classifier by gradient descent algorithm. Finally, classify the POL SAR image using the trained classifier. The validity test is demonstrated using Danish EMISAR L-band fully polarimetric data of Foulum Area (DK), Denmark. The preliminary result indicates that this method can classify most of the areas correctly. [C456]

### "RPC modeling for spaceborne SAR and its application in radargrammetry"

The RPC (Rational Polynomial Coefficient) model can be used as a replacement sensor model for geo-coding spaceborne SAR data. A hybrid method, combining the L-curve and the IMCCV (Iteration method by correcting characteristic value) method, for solving ill-conditioned equations in the RPC model is proposed. The hybrid method can get higher accuracy at low cost of calculation time. Based on an example in Malaysia, the application for fast RPC geocoding for stereo radargrammetry is shown. [C457]

### "Data acquisition of vessel ISAR data with assistance of automatic identification system"

In the past, imaging of moving vehicles using the principle of inverse synthetic aperture radar (ISAR) has typically been applied to ground moving vehicles or air and space borne objects. Nowadays, demands to image moving vessels on sea come along for both military applications and coastal surveillance. New processing algorithms have to be developed to focus ISAR data of vessels because of the complicated three-dimensional rotational motion and the sea clutter. Experimental data have to be available for the development process. To be able to acquire these data, the airborne radar sensor PAMIR of Fraunhofer FHR has been extended by integrating a receiver for automatic identification system (AIS) messages, which supports the system with position information of the vessels on sea. The paper shows the hardware integration and software implementation. Benefits of the information gained from the received AIS messages are discussed and results of first acquired data are presented. [C458]

### "Aspects of multivariate statistical theory with the application to change detection"

This paper proposes a new method for change detection measurement including whole SAR imaging modes such as PolInSAR, partial PolInSAR and InSAR in a set of multi-temporal multidimensional SAR images. The

method is based on the special case of Kullback-Leibler (KL-divergence) test, known as Mutual Information. In order to develop an algorithm, firstly the joint distribution of PolInSAR data set, based on the second order statistics has been derived. Such a derivation accounts for the whole multi-temporal SAR images. Then the mutual information is used to measure the difference between the joint density of multi-temporal PolSAR data sets and their marginal density known as complex Wishart distribution. A comparison between the proposed and the other well-known change detection (e.g. cross correlation) technique is shown by means of real data, describing the advantages due to the fact that the proposed change detector involves almost every facet of the applied change detection. [C459]

#### **"Filtering and segmentation of polarimetric SAR images with Binary Partition Trees"**

A new multi-scale PolSAR data filtering technique, based on a Binary Partition Tree (BPT) representation of the data, is proposed. Different alternatives for the construction and the exploitation of the BPT for filtering and segmentation are presented. Results with simulated and experimental PolSAR data are presented to show the capabilities of the BPT-filtering strategy to maintain both spatial details and the polarimetric information. [C460]

#### **"A novel approach for redundant integration of finite differences and phase unwrapping on a sparse multidimensional domain"**

Phase unwrapping and integration of finite differences are key problems in several technical fields, among which SAR interferometry. In this paper we propose a general formulation for robust and efficient integration of finite differences and for phase unwrapping, which includes standard techniques methods as sub-cases. The proposed approach allows obtaining more reliable and accurate solutions by exploiting redundant differential estimates (not only between nearest neighboring points) and multi-dimensional information (e.g. multitemporal, multi-frequency, multi-baseline), or external data (e.g. GPS measurements). The method requires the solution of linear or quadratic programming problems, for which computationally efficient algorithms exist. The validation tests performed confirm the validity of the technique. [C461]

#### **"Building detection and height estimation from high-resolution insar and optical data"**

State-of-the-art satellite SAR sensors acquire data of one meter geometric ground resolution, airborne sensors achieve even higher resolutions. Nonetheless, layover and occlusion hamper interpretability of such data particularly in urban scenes. In order to overcome this drawback, we use additional information from aerial photos to detect buildings. Features are extracted from both data sets and introduced to a common feature vector followed by a classification into building sites and non-building sites with Conditional Random Fields (CRF). Furthermore, we show that the different sensor geometries of the SAR and the optical sensor may be used to estimate building heights. [C462]

#### **"SAR and optical images registration using shape context"**

Image registration is the process of overlaying two or more images of the same scene taken at different times, from different view points, and /or by different sensors. A novel feature-based multi-sensor image registration system is developed. The system consists of two new points: first, edge features are extracted from images, and the features are dilated to suppress some certain kinds of noise arising from groves; second, the preprocessed features are matched using the improved shape context. The shape context has been found to be robust in hand written digit and object recognition, and now it is introduced into remote sensing image matching after some adjustments. The developed system is successfully applied to register airborne optical and C-band SAR images in our experiments, and the results demonstrate its robustness and accuracy. [C463]

#### **"Radargrammetric improvements: A multi-window approach"**

This paper deals with the relevance of using stereoscopic radar images in order to retrieve the relief of terrain. Firstly, the basic characteristics of the radargrammetry are described. Thus, we present the results of the radargrammetric processing using the ZNCC procedure and applied to radar images. These images are recorded by the SIR-C mission over the French Alps. The results show that the image matching can fail, especially in foreshortened areas. So, we expose two different improvement methods using several correlation windows in order to cancel the reconstruction errors. The first improvement take advantage of a multi-window approach to combine information multiplying the correlation surfaces obtained for each correlation window size. The second improvement is based on another multi-window approach that makes it possible to get correlation windows adapted to the foreshortened areas. Finally, we combine these two improvement methods to show that it's possible to make the disparity map more reliable for the first step of the pyramidal scheme. [C464]

### **"InSAR time-series analysis for management and mitigation of geological risk in urban area"**

This work shows the capabilities of InSAR time series analyses to support civil protection activities in the framework of geological risk management and mitigation. We discuss the outcomes from an integrated analysis of conventional in situ investigations and observations with advanced InSAR analyses carried out for the test sites of Agrigento and Naro (Italy), affected by ground instability respectively due to landsliding and tectonic forces. The study of past ground deformations provided valuable insights into the spatial and temporal patterns and behaviors of these phenomena, helping local civil protection authorities to focus resources on the areas of maximum need and to identify the most appropriate mitigation measures to reduce the impacts on elements at risk. [C465]

### **"Roll invariant target detection based on PolSAR clutter models"**

Based on the Kennaugh-Huynen decomposition, the Target Scattering Vector Model (TSVM) allows to extract four roll-invariant parameters. Those parameters are necessary for an unambiguous description of the target scattering mechanism. The proposed method consists in applying the TSVM prior to the GLRT-LQ detector for the detection of any oriented target. [C466]

### **"Ice sheet anisotropy measured with polarimetric ice sounding radar"**

For polar ice sheets, valuable stress and strain information can be deduced from crystal orientation fabrics (COF) and their prevailing c-axis alignment. Polarimetric radio echo sounding is a promising technique to measure the anisotropic electromagnetic propagation and reflection properties associated with COFs. In this paper, fully polarimetric P-band data acquired with the airborne POLARIS system near the ice divide of the Greenland ice sheet are analyzed. Based on a simple electromagnetic model, these data are interpreted, and a pronounced birefringence is found. [C467]

### **"A tracking algorithm for GNSS reflected signals on sea surface"**

The observation of the ocean surface using electromagnetic sources of opportunity (GNSS signals for instance) has been a green research topic for several years. The Global Navigation Satellite System (GNSS) presents a powerful and useful technology for remote sensing, ocean surface monitoring and oceanography. Many experiments have been conducted to show the efficiency of the Global Positioning System (GPS) in applications such as ocean surface altimetry, wave height, surface current measurements, and current direction estimation [1]. Considering the GPS link as a passive sensor for ocean monitoring, we study in this paper the possibility of tracking GPS signal reflection footprints on the sea surface to improve the acquisition and the extraction of this signal. As an analogy to the classical problem of moving targets Radar tracking, we develop a tracking algorithm based on Kalman filtering. [C468]

### **"Assessment of airborne lidar data for instream flow type classification"**

The information of instream biotype, i.e., types, location, distribution, etc, are important for estuary environment management. Field observations carry out by ecology surveyor is the standard procedure to gather that information, which is time consuming and difficult to be applied to a large spatial extend. In this research, we propose using airborne for instream biotype classification. Texture of point clouds is the key to distinguish between flow types, and semi-variogram was employed for texture measurement of different flow types. The principle component analysis is then used for classification and data compression. The results show that the first principle components are closely related to the flow types considered in this study. [C469]

### **"An integrated approach to determine parameters of a 3D volcano model by using InSAR data with metamodel technique"**

In this paper, an integrated approach is presented to determine the suitable parameters of a magma-filled dyke, which causes observable deformation at the ground surface. By this approach, the finite element method (FEM) and metamodel techniques are combined. FEM is used to establish the numerical model of the dyke and to produce the data required to identify metamodel parameters. Parameter identification problems are also known as parameter estimation or inverse problems. The metamodel technique is employed to make the whole procedure efficient in the identification phase. The identification approach is carried out by a systematic routine based on particle swarm optimization (PSO) algorithm. The approach is tested with synthetic data generated by analytic models. Moreover, it has been also applied to Stromboli Volcano (Italy) as an example, and the ground deformation data is acquired by using interferometry SAR technique. With the approach, the parameters can be successfully estimated with acceptable degree of accuracy. The results also indicate that only one kind of geophysical data are not sufficient for solving such a complex problem. [C470]

### "A CHMT model based DE-speckling method for SAR image"

A coarse-classification based tying method for the Contourlet-domain Hidden Markov Tree model (CHMT) solution algorithm is proposed to speed up the parameters estimation; and a general SAR image filtering framework, to which any kind of shift-variant transform can be applied, is generated by applying together with the LOG Transform, mean rectification and cycle-spinning, etc. The proposed coarse classification based tying method for CHMT is applied to de-speckle the SAR image in the general framework, and the result is compared with those of some commonly-used filters. The visual effects and the statistical parameters indicate that the coarse-classification based tying method for CHMT is much faster than the other tying methods, and the CHMT based de-speckle method can achieve better result than some commonly-used filters. [C471]

### "Ship detection and measurement using the TerraSAR-X dual-receive antenna mode"

The detection of ships and the retrieval of parameters like vessel velocity, heading and size are important techniques for ocean and shore surveillance systems. Space borne SAR along-track interferometry (ATI) can detect ships for large areas and measure their velocity at the same time by means of interferometric phase. In this paper we report about first results of automatic ship detection using TerraSAR-X ATI. [C472]

### "Mean-shift and hierarchical clustering for textured polarimetric SAR image segmentation/classification"

Image segmentation and unsupervised classification are difficult problems. We propose to combine both. A clustering process is applied over segment mean values. Only large segments are considered. The clustering is composed of a mean-shift step and a hierarchical clustering step. The hierarchical grouping is based upon a powerful segmentation technique previously developed. The approach is applied on a 9-look polarimetric SAR image. Textured and non-textured image regions are considered. The K and Wishart distributions are used respectively. The unsupervised classification results can be very useful for image analysis and further supervised classification. The obtained region groups constitute an important simplification of the image. [C473]

### "Realization of the NASA Dual-Frequency Dual-Polarized Doppler Radar (D3R)"

This paper describes some of the novel technologies adopted in the realization of the NASA Dual-frequency Dual-polarized Doppler Radar (D3R) system for to be used by the GPM ground validation program. A description of the transceivers and major trades that lead to a solid-state architecture is presented. Other aspects enabling the design such as the waveform design and generation and the digital receiver is also described. Data measured from a similar power amplifier was used to estimate the expected range side lobe performance. An estimate of the expected sensitivity based on the transceiver parameters also presented. [C474]

### "Polarimetric SAR estimation based on non-local means"

During the past few years, the non-local (NL) means have proved their efficiency for image denoising. This approach assumes there exist enough redundant patterns in images to be used for noise reduction. We suggest that the same assumption can be done for polarimetric synthetic aperture radar (PolSAR) images. In its original version, the NL means deal with additive white Gaussian noise, but several extensions have been proposed for non-Gaussian noise. This paper applies the methodology proposed in PolSAR data. The proposed filter seems to deal well with the statistical properties of speckle noise and the multi-dimensional nature of such data. Results are given on synthetic and L-Band E-SAR data to validate the proposed method. [C475]

### "Polarimetric decomposition for forest biomass retrieval"

In this paper, the decomposition of fully polarimetric SAR data into three canonical scattering mechanisms is investigated with respect to forest biomass retrieval. It is demonstrated that the dominant backscattering contribution depends strongly on the frequency, incidence angle, and stand condition. The relation between in-situ biomass measurements and the individual decomposition components is examined. [C476]

### "Eigen decomposition parameter based forest mapping using Radarsat-2 PolSAR data"

In this paper, a set of polarimetric eigenvalue and eigenvector based parameters, e.g. entropy and anisotropy, are investigated for forest application. The correlation terms of the eigenvectors,  $\mu_1$  and  $\mu_2$ , are found to be better for forest mapping in both summer and winter using Radarsat-2 quad-polarimetric space borne SAR data. These are used to automatically identify forest class pixels from the volume scattering category of a Freeman-Durden Wishart unsupervised segmentation map. The algorithm scheme was developed and implemented using fully polarimetric Radarsat-2 SAR (PolSAR) data acquired in July and October and the validity was evaluated

using the ground reference data created from SPOT5 K-clustering classification map. [C477]

### **"Polarimetric SAR tomography of natural environments using hybrid spectral estimators"**

SAR tomography is the extension of conventional two dimensional SAR imaging principle to three dimensions. In order to improve the vertical resolution with respect to classical Fourier-based methods, high resolution approaches are used in this paper to perform SAR tomography. Both nonparametric spectral estimators, like beamforming and Capon and parametric ones, like MUSIC, maximum likelihood, are applied to real data sets and compared in terms of scatterer location accuracy and resolution. This paper addresses the discrimination of coherent scatterers presented in the natural environment and a joint approach of estimation and detection is proposed. [C478]

### **"An application of reciprocity to the numerical modeling of a GPR system"**

In this paper, a technique is developed to model ground penetrating radar interactions. It combines reciprocity with the results from a full numerical model and allows one to compute a large number of scattering responses simultaneously, provided the scatterers are small. The results of an example calculation are shown and compared with a full numerical model and a possible application is demonstrated. [C479]

### **"A portable 35 GHZ cross-track interferometer for topographic and surface change measurements"**

In the following, we present first results obtained from the design, construction and deployment of a 35 GHz fixed-point radar interferometer, that uses the principles of FMCW for generating a range resolving signal. Using a single transmit antenna and two receive, separated by an interferometric baseline, it is possible to determine phase differences between the two receive channels, and given the viewing geometry, to solve for the target topography. To test the system described in this short paper, it was deployed on a local mountain top, some 270m above the local terrain. With knowledge of the nominal topography (measured by the Shuttle Radar Topography Mission; SRTM), and sufficiently large interferometric height ambiguity, it is possible to solve for the topography, as seen at 35 GHz, and to monitor differences in the observed topography which may be due to differences in volume scattering, surface motion, and surface dielectric change. [C480]

### **"Mapping earthquake damage in VHR radar images of human settlements: Preliminary results on the 6th April 2009, Italy case"**

Automated earthquake damage assessment from post-event only remotely sensed data is highly desirable, especially when new generation, Very High Resolution (VHR) spaceborne data is concerned, lacking extensive pre-event archives. Though, most damage assessment method either rely on human interpretation or on pre-post-event comparison. In this paper we illustrate some possible tracks for investigating damage assessment on post-event only data, focusing on the 6th April 2009 Abruzzi, Italy earthquake and on related COSMO/SkyMed acquisitions. [C481]

### **"The analysis of surface deformation based on two-pass and three-pass D-InSAR"**

The Differential Synthetic Aperture Radar Interferometry (D-InSAR) is widely used in large-scale ground deformation monitoring such as crustal deformation, seismic changes, land subsidence, landslides, volcanic deformation, glacial movement. In this paper, The deformation analysis based on two-pass differential and three-pass differential InSAR is done. We have shown that the analytic results by the three-pass differential method is better. The quality of result may be effected in phase unwrapping in two different methods. The deformation fields obtained by two different differential methods have been compared with traditional methods. With the changes in topographic factor, climatic conditions and vegetation types, the coherence effect is different, results have been given. It is not easy that the strong coherence is satisfied in three SAR images in the same time. Therefore, the optimizing methods depend on the purpose of application and the characteristics of studied area. [C482]

### **"Topographic correction for biomass retrieval from P-band SAR data in boreal forests"**

The influence of the ground slope on radar backscatter has been proven to be greater for lower radar frequencies due to deeper canopy penetration. In this study, multiple heading, P-band SAR data of boreal forest in Sweden was used to find a model for topographic correction for improved biomass retrieval. Eleven models were tested and the best model was selected. The selected model was then used for biomass retrieval. Even by means of the most simplified approach, forest biomass could be established with a root-mean-square error of approximately 50 t/ha for HV and 66 t/ha for HH. [C483]

### "A new approach to modeling ice crystal aggregates and its implications for radar remote sensing"

Backscattering cross sections of model ice crystal aggregates are computed at 35.6 GHz using the generalized multiparticle Mie (GMM) method and compared against a commonly used equivalent dielectric model (also referred to as the "soft sphere" or the "bulk" model). It is shown that the bulk model underestimates the backscattering cross sections by 7 to 20 dB over aggregate sizes from 3 to 19 mm. This raises concerns about using bulk models for the interpretation of millimeter wave radar measurements of ice clouds and snow. [C484]

### "Processing and segmentation of COSMO-SkyMed images for flood monitoring"

In the framework of the application of remote sensing to civil protection from floods, the problem of the detection of flooded areas in high-resolution images is addressed in this paper. Specifically, the high-resolution multitemporal observation capability offered by the current COSMO-SkyMed synthetic aperture radar (SAR) constellation is exploited. This work is framed in the context of the "OPERA-Civil protection from floods" pilot project funded by the Italian Space Agency in cooperation with the Italian Department for Civil Protection. Several SAR image processing methods are presented in order to identify flooded areas after a flood event. Both fast-ready and detailed maps are obtained from a pair of multitemporal images of the monitored area. Experiments are presented with COSMO-SkyMed images related to a flood in the areas of Alessandria (Italy). [C485]

### "Extraction of typhoon-damaged forests from multi-temporal high-resolution polarimetric SAR images"

The purpose of this study is to extract the forests destroyed by typhoons and to quantitatively estimate the damage levels by using high-resolution polarimetric synthetic aperture radar (SAR) data. The study area is located in Tomakomai, Hokkaido, Japan. Two sets of data were acquired before and after the typhoon by the L-band airborne Pi-SAR (Polarimetric-interferometric SAR) with 3m Ч 3m resolution (4-look in azimuth direction). It was found that the values of RCS (Radar Cross Section) averaged over the whole image after the typhoon damage changed by -0.47 dB, 0.05 dB, and 0.64 dB at HH-, HV-, and VV-polarization respectively in comparison with those before the damage. To fully utilize the data, a scattering model of the linear combination of the cross- and co-polarization RCS changes was developed to estimate the damage levels. Similar analytical approaches were also applied using the three-component decomposition analysis. The changes in RCS of double-, volume- and surface scattering mechanisms after the damage were respectively 27.5 dB, -0.20 dB and -20.3 dB. Finally, by comparing the results with the ground survey data, the accuracies of 64.1% and 77.7% were obtained for the RCS and decomposition analyses respectively. [C486]

### "Relations between SAR tomography and full-waveform LIDAR for structural analysis of forested areas"

Active remote sensing techniques, like SAR tomography and full-waveform LIDAR, are able to capture the 3D reflectance function at or inside objects. They are therefore of special interest for analyzing forest environments. Research goals are the derivation and characterization of the different physical measurement aspects of data taken over forested areas, as well as establishing mutual relations in such a way that LIDAR data can be used to calibrate and correct 3D density data of SAR tomography. The paper outlines the phenomenology of forested areas in SAR tomograms and full-waveform LIDAR data and sketches a simple mathematical methodology for linking SAR and LIDAR reflection density profiles. [C487]

### "Optimal algorithms for spaceborne altimeter"

This paper is dedicated to new methods of space altimeter altitude and sea surface significant wave height (SWH) measuring. These methods are based on the fundamentals of Bayesian optimal measure method of a parameter. Optimal discriminators of the parameters are developed using the least square error of the estimate criteria, apart from others papers which mostly minimize the least square error of altimeter waveform fitting function. Potential measurement accuracy calculation results are also presented. [C488]

### "Morphological filtering of SAR interferometric images"

This paper proposes a new morphological filter for SAR interferograms. It is based on a modified version of alternate sequential filters with reconstruction (MASF), in which the structuring elements are adaptively defined according to the fringe directions. This provides a good fidelity to the fringe information while efficiently removing noise. Another feature of the proposed approach is to apply the filter on the original interferogram and on shifted version, to overcome the wrapping of the phase, and to combine the two results. The proposed filtering

technique is then tested on both simulated and real data with different levels of noise. It is also compared to previous techniques according to simplicity and noise reduction. [C489]

#### "Detection of salient features in surface current maps from dopplerized X-band radar"

The mapping of the near surface currents and their interaction with the spatial and temporal varying bottom topography is of high significance for the experimental analysis of morphodynamic processes in coastal areas and the monitoring the effectiveness of coastal protection actions. An efficient application is also the real-time monitoring of currents in harbours to pilot large vessels [8]. The next steps of this inquiry are the application of image processing methods to extract also, together with the orientation, length scales and spatial shifts of salient current features. The correlation with salient features of the bed topography will be analyzed further together with sea state images that can also be deduced from radar data. [C490]

#### "Quasar SBK accurate internal calibration"

A new compact fully polarimetric Ku band SAR system (SBK) is being developed by INTA radar Laboratory as an advanced payload for QUASAR project, which involves INTA new SAR developments for small platforms and UAV's. As an operative system, SBK shall allow precise calibration of the obtained data in order to achieve high products quality. The present paper shows SBK internal calibration concept focusing on internal calibration facility description, on ground characterization task overview and in flight calibration method. Furthermore, internal calibration accuracy estimation based on first prototypes measurements is also presented. [C491]

#### "Development and experiments of a passive SAR receiver system in a bistatic spaceborne/stationary configuration"

In this paper, the development of a stationary SAR receiver system using TerraSAR-X as transmitter is described. First the bistatic geometry and expected resolution are considered. After giving an overview of the hardware setup, the expected performance of the system is evaluated. The paper ends with the processed results of a measurement campaign performed in summer and fall 2009, and a comparison with the monostatic data acquired by the TerraSAR-X satellite. [C492]

#### "Automatic registration of sar and optical image based on multi-features and multi-constraints"

This paper proposes a two-stage registration method for SAR and optical images based on multi-features and multi-constraints. In the first stage, closed regions are extracted automatically to achieve the coarse mapping parameters as geometrical restriction. In the second stage, Harris corner points and cross-road features are extracted, and then correlation analysis and mutual information are utilized to match the corresponding control points. After that, multi-constraints are used to delete the false matched points. The retained ones are served as ground control points for registration. The experimental results show that the method can reduce the possibility of false matching effectively and the registration error is within one pixel. [C493]

#### "Beamwidth analysis for SAR processing of airborne depth-sounder data over ice sheets"

Information on the bedrock topography below the Greenland and Antarctic ice sheets is vital to developing models of future sea-level rise. To measure the topography, advanced data acquisition and processing techniques, including Synthetic Aperture Radar (SAR), are required. This work investigates the optimal beamwidth that would enable SAR processing to maximize the signal to noise ratio of the target. Platform height above the ice surface and bedrock roughness determine the optimal beamwidth. We found that for data collected at a "typical" altitude of 867 m, the optimal beamwidth is about 8°. In the high-altitude case, we found that beamwidth did not have a significant effect on the signal-to-noise ratio. This is probably related to scattering from the ice surface. [C494]

#### "DSM generation from very high optical and radar sensors: Problems and potentialities along the road from the 3D geometric modeling to the Surface Model"

The availability of new high resolution optical and radar spaceborne sensors offers new interesting potentialities for the acquisition of data useful for the generation of Digital Surface Models (DSMs). The accuracy level of DSM is strictly related both to the image orientation and to the matching process. As regards the image orientation, remote sensing community usually adopts two different types of models for High Resolution Satellite Imagery (HRSI): the physical sensor models and the generalized sensor models also called rigorous and Rational Polynomial Functions (RPFs) models respectively. In a scientific software developed by the research group of Geodesy and Geomatic Area of the University of Rome "La Sapienza" both rigorous and RPFs models are implemented, with a specific tool for the terrain-independent Rational Polynomial Coefficients (RPCs) generation;

the software manages the imagery acquired by several optical sensors (EROS A, Ikonos, QuickBird, Cartosat-1, WorldView-1, GeoEye-1) and by the Italian SAR constellation COSMO-SkyMed. In the same software a facility for image matching is embedded. The Area Base Matching (ABM) is used, combined with the orientation model re-parametrized in terms of RPCs. In the present work some examples of models application and DSM generation are analyzed and discussed. [C495]

#### "On the use of Support Vector Machines for land cover analysis with L-band SAR data"

This study investigates a new technique for land cover analysis by means of the Support Vector Machines. Intrinsic spatial variability within SAR images, beyond that caused by speckle, is of high interest for land cover characterization and classification. However, its use is still an ongoing issue due to its complex multi-scale nature. On the other hand, classification algorithms based on statistical learning methods such as the supervised Support Vector Machines (SVM) approach are implemented in a wide range of data mining applications. SVM can also be used as a technique for feature selection. In this paper, a new tool using the Recursive Feature Elimination SVM-based process (SVM-RFE) and the textural Haralick's parameters is introduced. The real contribution of textures within the land cover classification can be understood. A small set of textural parameters is determined at local scale while being optimal for the land cover discrimination. In this study, orthorectified 50m resolution data acquired by the L-band PALSAR/ALOS sensor are used. [C496]

#### "A new Bayesian source separation approach to blind decorrelation of SAR data"

In this paper, a novel approach for performing blind decorrelation of SAR data is proposed. A patch-wise computation of the point-spread function (PSF) is performed directly from the SAR data to account for spatial nonstationarities present in SAR. The problem of estimating the PSF is formulated as an additive source separation problem in the frequency domain, and is subsequently solved using a Bayesian least squares estimation approach based on a Fisher-Tippett log-scatter model. Experimental results using both simulated SAR data and real RADARSAT-2 SAR sea-ice data showed that the proposed decorrelation approach can successfully learn the correct PSF and significantly reduce the correlation in SAR data. [C497]

#### "SAR complex image analysis: A Gauss Markov and a multiple sub-aperture based target characterization"

In this paper we discuss Gauss-Markov Random Field (GMRF) based on multiple sub-aperture decomposition method for the analysis of targets in complex-valued high-resolution SAR data. Gauss-Markov Random Field (GMRF) model with a quadratic energy function as a parametric analysis parameterizes the spectrogram of the signal, whereas sub-aperture decomposition method exploits the holographic property of the spectrum at the cost of reducing resolution. This analysis helps to understand, characterize and analyze complex-valued SAR data and provides temptation to use complex-valued SAR data over detected data. [C498]

#### "MIMO SAR processing with azimuth nonuniform sampling"

This paper analyses ambiguity suppression caused by multiple-input multiple-output (MIMO) SAR azimuth nonuniform samplings. Two methods are analyzed: azimuth spectrum reconstruction algorithm and minimum mean square error (MMSE) imaging algorithm. The azimuth spectrum reconstruction algorithm can reconstruct the scene fine resolution, while the nonideal orthogonality of multi-channel encoding waveforms causes azimuth ambiguous in SAR imaging. The MMSE imaging algorithm can perfectly reconstruct, while it requires high SNR. [C499]

#### "Doppler processing of coherent radar backscatter for ocean surface wave measurements"

The technique for extracting wave period and wave direction from a navigation radar backscattering intensity is well developed but the determination of spectral density or wave height is hindered by the complex nature of the modulation transfer function. In contrast to backscattering intensity, Doppler velocity from coherent radar is the radial velocity of the scattering objects. Its oscillatory component is contributed by ocean waves. The spectral peak component of Doppler velocity is close to the peak wave period measured by a nearby buoy and the significant wave height can be accurately calculated. With radar range coverage on the order of ten dominant wavelengths, reliable assessment of peak wave period and significant wave height is achievable with radar data as short as one second. Wave direction can also be determined with a scanning system. [C500]

#### "Decomposition methods for the estimation of bare soil surface parameters using fully polarimetric SAR data 1"

This study wants to demonstrate that two different polarimetric target decomposition methods can improve SAR

data accuracy for estimating the parameters of bare soil surface. To achieve this goal, two experiments are conducted: (1) both Freeman and Cloude decomposition methods are performed on JPL/AIRSAR L-band fully polarimetric data; and (2) Advanced Integral Equation Model (AIEM) is used to simulate backscattering coefficients. The root mean square errors (RMSEs) of  $\sigma_{0hh}$ ,  $\sigma_{0vv}$  between original data and AIEM simulated data are 1.96 and 1.25 dB. However, if Cloude method is used to decompose original data, the RMSEs will be reduced to 1.45 and 1.14 dB, respectively; for Freeman method, the RMSEs are 1.64 and 1.35 dB. Therefore, polarimetric target decomposition compensation, especially Cloude method, can help to improve the accuracy of SAR data for estimating the parameters of bare soil surface. [C501]

#### "Effect of squint imaging on beam position design of space borne SAR"

Range migration of space borne SAR at large squint angle is much greater than the side-looking SAR, and longer echo receiving window is needed. Thus, the traditional beam position design method is invalid. In this paper, the method of drawing zebra map is improved by taking the range migration into consideration. The maximum and the minimum slant ranges during the synthetic time are derived. This paper also analyses the relation between the effective swath width and the range beam width at large squint angle. Simulation for X-SAR system proves that a given azimuth resolution limits the squint angle. STK and echo simulation are used to verify the validity of the improved beam position design method. [C502]

#### "A shadow percentage estimation method for Radar look angle selection in spaceborne INSAR application"

Spaceborne INSAR (Interferometric Synthetic Aperture Radar) is an important remote sensing tool for topographic mapping, while there are inevitably shadow areas in Radar images. Shadow area has no radar echo signal or low coherence SNR (signal noise ratio). In this paper, Shadow area percentage estimation according to Radar look angle is proposed. Digital elevation model of natural terrains and ascending and descending orbits are used in simulation. This estimation method is suitable for incidence angle considerations in the phase of INSAR system design. [C503]

#### "Radarsat Constellation, moving toward implementation"

The Canadian Space Agency initiated the development of a three-satellite SAR mission, known as the RADARSAT Constellation Mission (RCM), in 2005. The main objective of the mission is to assure C-band data continuity in the next decade, while allowing a greater use of data for operational applications by providing more persistent observation over Canada and better system reliability. The Phase B contract was awarded in November 2008 for a period of 16 months. The Space and Ground Segment Requirements reviews were held at the end of February 2009. The spacecraft and Ground Segment concepts were adopted and design decisions have been taken to allow preliminary design to proceed. A Payload and Bus Preliminary Design reviews were held in Fall 2009. A Mission Preliminary Design review was held in February 2010. The CSA is currently in phase C and preparing for the Critical Design Review. Several challenges, such as the implementation of the ship detection mode or the final selection of the launcher must be resolved and important decisions must be taken to allow the progress of the program toward full implementation. The first spacecraft will be built and tested as a proto-flight and launched in 2014. The following two spacecrafts will then be built and tested in parallel and launched in 2015. [C504]

#### "Canopy height, crown cover, and aboveground biomass maps for the southwestern United States from MISR, 2000 and 2009"

Red band reflectance factor data from NASA's Multiangle Imaging SpectroRadiometer (MISR) were used to create maps of woody plant canopy cover, fractional height, and aboveground biomass for the southwestern United States, via inversion of a geometric-optical (GO) model provided with reflectance magnitude and anisotropy via a Li-Ross bidirectional reflectance distribution model. Crown cover, canopy height, and biomass distributions are compatible with those seen in other data sets, although there are anomalies associated with the use of the same set of background prediction coefficients over the 10-year period. [C505]

#### "A study on the possibility of applying precursor waves to penetration imaging"

Precursor wave occurs when wideband electromagnetic pulse propagates through temporally dispersive and absorptive media. In this paper, the mechanisms of precursor wave generation and propagation in lossy and dispersive media are studied for radar pulses with different rise time and carrier frequencies. Simulation results are presented to discuss the possibility of precursor waves generated through dispersive media for radar imagery. [C506]

### "Investigation on moving target detection and velocity estimation with Triple-Channel MIMO-SAR"

Triple-Channel SAR system can detect moving target, and estimate its range velocity. However, the problems of blind velocity and velocity ambiguity still exist. To resolve these problems, Triple-Channel Multi-Input Multi-Output SAR (Triple-Channel MIMO-SAR) system, with a displaced phase center antenna (DPCA) and interferometry method based on matched Fourier Transform (MFT), is proposed in this paper, which could combine detection and estimation results of different working frequencies and obtain accurate Doppler frequency modulated rate estimation. Using this method, we can not only detect moving target and estimate its range velocity, but also resolve the problems of blind velocity and velocity ambiguity and get accurate azimuth velocity estimation. The effectiveness of this approach is validated by the computer simulation results. [C507]

### "Change detection in a multitemporal series of radar images"

In the literature, several works are led around the radar images especially the detection of the cartographic objects, the 3D reconstruction and the change detection. Concerning this last application, several techniques compete to ensure the best possible result. In this paper, we aim first at developing an automatic detection procedure to compare between similarity measures. Then we propose a change detection technique based on the fusion of two similarity measures. The first one is the Contrast (C) measure [1] and the second one is the Rayleigh Distribution Ratio (RDR) measure [2]. The proposed method has been validated on simulated data and then applied on three radar images. [C508]

### "Characterization of forest opacity using multi-angular emission and backscatter data"

This paper discusses the results from a series of field experiments using ground-based L-band microwave active/passive sensors. Three independent approaches are applied to the microwave data to determine vegetation opacity of coniferous trees. First, a zero-order radiative transfer model is fitted to multi-angular microwave emissivity data in a least-square sense to provide "effective" vegetation optical depth. Second, a ratio between radar backscatter measurements with a corner reflector under trees and in an open area is calculated to obtain "measured" tree propagation characteristics. Finally, the "theoretical" propagation constant is determined by forward scattering theorem using detailed measurements of size/angle distributions and dielectric constants of the tree constituents (trunk, branches, and needles). The results indicate that "effective" values underestimate attenuation values compared to both "theoretical" and "measured" values. [C509]

### "A new bistatic doppler measurement system with reduced contamination by sidelobe echoes"

A new bistatic Doppler measurement system with an array receiving antenna is proposed. In this system the spacing of receiving array elements is more than a wavelength (e.g. 10 wavelengths), and it leads to forming many sharp grating lobes. With these sharp lobes (beams) and some signal processing techniques like a digital beam forming, it can be expected that the effect of sidelobe contaminations, which is a serious problem of bistatic measurement, can be effectively reduced. [C510]

### "Autoregressive modeling of dechirped spotlight-mode sar rawdata in transform domain"

Raw data collected by synthetic aperture radar (SAR) is commonly assumed to be uncorrelated and with a zero-mean Gaussian distribution. In this paper, we show-both analytically and numerically-that the range-wise inverse Fourier transform of the dechirp-on-receive circular SAR data exhibits significant correlation in the azimuth direction. Moreover, we show that a block adaptive autoregressive model well represents the transformed SAR data. [C511]

### "An experiment for oil spill recognition using RADARSAT-2 image"

In this paper, an experiment that is oriented to discriminate between different oil slicks using polarimetric SAR image was introduced. Dark patches which often appear in SAR images such as biogenic slicks, atmospheric front, and crude oil with different chemical composition were identified according to the result of Eigenvector-Eigenvalue based Incoherent Target Decomposition. The experiment demonstrated that polarimetric SAR can be of great help in classifying of oil spills. [C512]

### "The characteristics of post-seismic surface deformation of the Wenchuan MS 8.0 earthquake from InSAR"

The D-InSAR technology is used to acquire four strips of post-seismic surface deformation of Wenchuan M8 earthquake of 2008 from the ALOS/PALSAR satellite data of Japan. The result covers the Yingxiu town, Wenchuan, Shifang, Maoxian county, Beichuan, Pingwu and Qingchuan county in Sichuan Province. Some post-

deformation characteristics is showed in the final result. Around Yingxiu town, the epicenter of main shock, a area of uplift is present with small amplitude 0-5cm at the northern wall of the causative fault, while relative subsidence took place with the amplitude 0-15cm on the other wall. Near Shifang county, there are slightly arranged concentric fringes, reflecting another subsidence area with amplitude 0-20cm. Around the Beichuan and Anxian county, there exists a relatively small uplift of an strip area with 0-5cm along the causative fault on its both side. A small area of dense concentric fringes(indicated by a rectangle box) appeared in 30km northeast of Qingchuan, which coincide with the locations of the aftershocks Ms6.1 of 5 Aug. 2008. On the lower wall, we can see another large uplift area of sparse concentric fringes located in more than 100km southeast of Qingchuan, because it is far from the causative fault, it's impossible so large deformation took place, and it should attribute to atmospheric component. the deformation characteristics of the whole area is complicated generally. [C513]

#### "Characterization of volume scattering of dry sand at millimeter-wave frequencies"

Fully polarimetric measurements of volume scattering contribution from dry layer of fine sand with smooth air/sand interface were performed at millimeter-wave frequencies. The measured radar response was compared to predictions made by the numerical solution of the DMRT model. Sand particles were modeled as spherical particles. The simulated response was able to predict the angular dependence of the data but was not able to predict accurately the absolute level, especially for the cross-polarized return. Furthermore, a simpler model, which was developed earlier for asphalt surfaces and is based on 1st order solution of RT for semi-infinite medium, was tested against the measured data. The model was not able to predict the angular dependence demonstrated by the measured data. [C514]

#### "Iceberg size and orientation estimation using SeaWinds"

From 1999 to 2009, the SeaWinds scatterometer has been used to detect and track large Antarctic icebergs on a daily basis. Here, we develop an automated estimation algorithm to supplement iceberg position reports with estimates of the iceberg's major axis length, minor axis length, and angle of orientation. A maximum-likelihood objective function that relates measured backscatter to model-based simulated backscatter is developed. The utility of the estimation approach is analyzed in simulation and via a case study of iceberg A22a. Subsequent results agree with and supplement reports compiled by the United States National Ice Center. [C515]

#### "Forest parameter retrieval from SAR data using an estimation algorithm applied to regrowing forest stands in Queensland, Australia"

The use of a non-linear estimation algorithm for retrieving the biomass and structure of vegetation from polarimetric Synthetic Aperture Radar (SAR) data is demonstrated for woody regrowth in Queensland, Australia dominated by *Acacia harpophylla* (Brigalow). By varying the size and density of trees and associated woody components (branches and trunks), multiple simulations of the backscattering coefficient ( $\sigma^0$ ) were performed based on the SAR simulation model of. Functions relating  $\sigma^0$  to these variables were subsequently used to generate spatial estimates from NASA JPL airborne SAR (AIRSAR) data. Above ground biomass was estimated from stem density and size measurements using available allometric relationships. The study demonstrates potential for retrieval of regrowth structure and biomass through nonlinear estimation. [C516]

#### "Forest biomass estimation in northeastern China using ALOS PALSAR data combined radiative transfer model"

Forest above ground biomass (AGB) is an important variable for evaluating ecosystem function and structure across landscape, which is necessary for studying forest productivity, carbon balance and nutrient allocation in forest ecosystem. In this study, a forest biomass estimate technique based on forest backscattering database is developed, and is used to retrieve AGB of Changbai mountain area from ALOS PALSAR dual-polarization data. The forest growth model and the 3D forest radar backscattering model were combined to build a forest multi-polarization radar backscattering database. Then forest AGB was estimated based on this database using statistic regression method and look up table (LUT) method. Two types of LUT searching methods (nearest distance and distance threshold) were used to find the accurate results. The biomass retrieved from forest inventory data was taken as ground truth to evaluate the inversion methods and the precision of the AGB estimation. The inversion results derived from PALSAR FBD data shows that both the statistical regression method and nearest distance LUT method underestimate forest aboveground biomass. The distance threshold LUT method gives the better biomass estimation compared with forest inventory data, the mean absolute error (MAE) of the whole research area is less than 10 Ton/ha. [C517]

#### "Validation of tie-point concepts by the DEM adjustment approach of TanDEM-X"

The aimed accuracies for the final TanDEM-X DEM of 10m absolute and 2m relative height error will be ensured by calibration data. One crucial data set for the relative accuracy is tie-points that connect adjacent DEM acquisitions in the approximately 4km-overlap-area with each other. In this paper an improved concept for tie-point candidates is presented that is based on averaging a larger region instead of comparing single points. This concept should be more robust against noise. It is validated by applying the DEM calibration on a simulated test area, as real TanDEM-X data was not yet available. Also, the DEM calibration will be validated for the first time on a larger "real" test site by applying the TanDEM-X processing scenario. [C518]

### "Road surface quality measurement using inexpensive radar"

The near surface dielectric characteristics of pavement can indicate the overall health of roadways and bridge decks. By performing simple and fast reflectometry measurements of the near surface, it may be possible to efficiently monitor large amount of critical civil infrastructure, and provide early alerts of the initial stages of damage. We demonstrate the variation with moisture content of surface reflected waves using a commercial-off-the-shelf 24 GHz FMCW radar. Initial experiments show that detectable amounts of water is absorbed in asphalt and concrete. The amount of absorbed water increases with micro- and macro-cracking, and this measurement will correlate with quantifiable changes in the observed return signal. [C519]

### "Bistatic SAR based on Terrasar-X and ground based receivers"

The paper presents the development of a ground based bistatic receiver using TerraSAR-X as a transmitter. The receiver subsystems like antennas, low-noise amplifiers, mixers, filters, synthesizers, etc. have been developed using low-cost monolithic devices in order to allow affordable deployment and at the same time offer final year students a challenging SAR engineering project. First raw data have been acquired on the Barcelona harbor area that has been focused producing geocoded images well matched with existing maps. A preliminary interferogram have been also produced. [C520]

### "Designing an Illegal Mining Detection System based on DinSAR"

Satellite Differential Radar Interferometry (DInSAR) has demonstrated its ability for monitoring mine-induced ground subsidence. However, it is still a challenging task to routinely identify all mining activities from the large-scale coverage interferogram, especially the illegal mines. In response to this challenge an underground mining detection system based on DInSAR is described. The system is tested over a dense mining area in Asia. With such a system it is hoped that the detection efficiency of illegal underground mining using DInSAR can be improved. [C521]

### "Automation of object extraction from LiDAR in urban areas"

Light Detection and Ranging (LiDAR) has become a valuable data source for urban data acquisition. This paper gives an overview about current trends in the automation of object extraction from LiDAR data. These trends are caused by the technical development of LiDAR sensors that enable the acquisition of point clouds at higher resolution as well as the recording of the full waveform of the returned signal, and by the adoption of processing techniques from the Computer Vision and Pattern Recognition communities. Triggered by these developments, new applications are being found for LiDAR data. [C522]

### "Dual-polarized, coherent microwave backscatter from rough water surfaces at low grazing angles"

We show that at low grazing angles, breaking wave effects are very important in HH polarized microwave backscatter from the ocean but less so at VV polarized backscatter. When the ocean surface is disturbed only by wind, breaking wave effects in VV backscatter are much smaller than Bragg scattering, even at low grazing angles. For HH polarization, on the other hand, breaking wave effects are very important at low grazing angles. In the presence of surface current gradients set up by internal waves, HH cross sections can exceed those at VV by as much as 10 dB near internal wave crests, indicating enhanced breaking wave effects that cannot be described as specular. Breaking effects are nearly as strong as Bragg effects in VV backscatter under these conditions. Spectral comparisons confirm these conclusions. [C523]

### "Quikscat backscatter sensitivity to landscape freeze/thaw state over ALECTRA sites in Alaska from 2000 to 2007: Application to SMAP validation planning"

The mapping of freeze/thaw state of the landscape is one of the main objectives of NASA's upcoming SMAP (Soil Moisture Active and Passive) mission. This study applies ALECTRA (Alaska Ecological Transect) biophysical network and QuikSCAT scatterometer data to evaluate some of the validation issues regarding the SMAP freeze/thaw measurements. Although the QuikSCAT data is at Ku-band frequency, rather than the L-band

of the SMAP instrument, the data is utilized due to its uniquely high temporal resolution over the ALECTRA sites. The results show that multiple temperature measurements representative of individual landscape (soil, snow cover, vegetation and atmosphere) elements and spatial heterogeneity within the satellite field-of-view are important for understanding the radar backscatter process and aggregate freeze/thaw signal. The backscatter temporal dynamics and relative contribution of these landscape elements to the freeze-thaw signal varies with land cover type, seasonal weather and climate conditions. [C524]

#### **"Advances in the integration of ALOS PALSAR and Landsat sensor data for forest characterisation, mapping and monitoring"**

Based on case studies undertaken in tropical forests in Brazil and Indonesia and subtropical woodlands in Australia, the paper highlights how data acquired by the Advanced Land Observing Satellite (ALOS) Phased Arrayed L-band Synthetic Aperture Radar (SAR) and Landsat sensors can be integrated to better quantify the extent, biophysical characteristics and/or dynamics of undisturbed, degraded and regenerating forests. The benefits of using time-series of Landsat sensor data to support the interpretation of ALOS PALSAR data and to identify areas with greatest potential for ecosystem recovery are conveyed. [C525]

#### **"A combined approach to detect urban features from multi-spectral and radar data"**

With increase of urban population, the cities have an impact more and more important on environment. Because of artificial surface, building morphology, economical activities, traffic several natural ecosystem are modified. To analyze this impact, the land covers/land uses have to be identified exactly in an urban area. To reach this objective, remote sensing represents an important and complete source of information. Joint use of radar and optical data allows improving results of classical classification to identify the cover mode. Re-sampled to 1m resolution, the difference between the two classifications is analyzed to detect the confusion in each class corresponding to a land cover/land use. Finally, a vector process allowed to transform the geometry of the results: a polygon aggregates several pixels. Combination of results is also possible with GIS functionalities like contains, intersect, cut, and permits to propose a land cover/ land use description on the study area. [C526]

#### **"Extension of the Target Scattering Vector Model to the bistatic case"**

The polarimetric information has been widely used to interpret the Synthetic Aperture Radar (SAR) scene. Hence, many decompositions have been introduced to extract polarimetric parameters with a physical meaning. Nevertheless, for most of them, the reciprocity assumption is assumed. For a bistatic PolSAR sensor, the cross-polarization terms of the scattering matrix are not equal. This paper presents a generalization of the Target Scattering Vector Model (TSVM) to the bistatic case. [C527]

#### **"Synergistic use of multi-temporal ALOS/PALSAR with SPOT multispectral satellite imagery for land cover mapping in the Ho Chi Minh city area, Vietnam"**

This paper discusses the synergistic use of multi-temporal ALOS/PALSAR and SPOT multi-spectral images for land cover classification in the Ho Chi Minh city area in Vietnam. Five PALSAR images and SPOT 2 multispectral image were used for classification. Integration of additional information such as interferometric coherence, textural data was also studied. Different combinations of multi-temporal SAR backscatter images, coherence data, SPOT multi-spectral bands, texture measures were generated and tested in order to determine the best combination, which gives the highest classification accuracy. Results indicate that the combination of SAR and optical images gives significantly higher classification accuracy than using a single type of data, and that the Support Vector Machine (SVM) classifier could outperform the Maximum Likelihood (ML) classifier in cases of classification of the combined datasets. [C528]

#### **"High resolution optical and sar image fusion for road database updating"**

This paper addresses the issue of cartographic database creation or updating using high resolution SAR and optical images. It proposes a processing chain to create or update road databases in urban environment. The approach is composed of two steps. First, if a database is available, the presence of each database object is checked in the images. Then, we verify if road hypotheses extracted from images should be included in the database. These two steps are conducted by extracting relevant features from the images in the neighborhood of the considered object. The object removal/inclusion in the database is based on a score obtained by the fusion of features in the framework of Dempster-Shafer evidence theory. [C529]

#### **"Real-time road traffic monitoring using a fast a priori knowledge based SAR-GMTI algorithm"**

Radar systems operating on high altitude platforms can provide traffic information over wide areas, independent

of sunlight illumination and weather conditions. In the paper, a novel a priori knowledge based ground moving target indication (GMTI) and parameter estimation algorithm applicable on single- as well as on multi-channel synthetic aperture radar (SAR) data is presented. Only the intersection points of the moving vehicle signals with the a priori known road axes, which are mapped into the range-compressed data domain, are evaluated. The algorithm needs low computational load and is hence well suited for real-time traffic monitoring applications.

[C530]

### "Three-dimensional deformation field caused by the Gaize earthquake by Multi-LOS DInSAR measurement technology"

This paper firstly presents the Multi-LOS DInSAR measurement result of the coseismic deformation field caused by the Gaize Ms6.9 mainshock and Ms6.0 aftershock in Tibet, China, and then obtain the 3D deformation field based on the 3D resolving mode. The characteristic analysis of coseismic deformation field shows the rupture of mainshock is majority normal, left-lateral striking with a little rotation; and the aftershock is typical normal rupture nature. The mainshock and aftershock had induced the east and west rupture(maybe buried) successively, and produced the east and west two subsiding centers. [C531]

### "The use of ALOS PALSAR imagery for Cerrado's land use and land cover mapping"

In Brazil, land use and land cover (LULC) mappings are obtained mainly from optical images. Radar data are also promising since they are independent of solar illumination and the microwave radiation can penetrate clouds and depict differences in canopy structures. This study analyzed the potential of ALOS PALSAR data for LULC mapping of Federal District of Brazil (FD). L-band, HH-, HV- and VV-polarized amplitude images from the end of wet season were processed through the image segmentation technique by growing region. The segments were exported into a geographical information system software package as shapefile format and then visually interpreted in the computer screen. The following classes were discriminated: consolidate urban areas; urban areas in consolidation; natural grasslands; Cerrado shrubland; croplands; gallery forest; indiscriminated forests: pasturelands; reforestations; and water reservoirs. Cerrado shrubland was the most representative mapping class of the study area, followed by consolidated urban areas and natural grasslands. [C532]

### "Spaceborne sar imaging of coastal ocean phenomena"

Synthetic aperture radar (SAR) observes the large-scale ocean surface wind field. With SAR instruments, we can actively monitor phenomena in the coastal ocean and marine atmospheric boundary layer at very high spatial resolution (on the order of tens of meters) in all weather conditions day and night. SAR observations are particularly useful in coastal regions where clouds are usually present, causing observation problems for visible and infrared sensors. SAR sensors onboard the RADARSAT-1/2, ENVISAT, ALOS, and other satellites can provide swath coverage of about 100 to 450 km, wide enough to cover oceanic and atmospheric meso-scale features. SAR has long been used to monitor the ocean surface wind field, vessel locations, oil spills, sea state, and sea ice at NOAA. In this paper, we present several case studies. [C533]

### "Ground topography estimation over forests considering Polarimetric SAR Interferometry"

The work detailed in this paper analyzes the topographic phase retrieval process on forested areas by means of Polarimetric Interferometric SAR data. On the basis of the Random Volume over Ground scattering model, an alternative implementation for the retrieval of the topographic phase, avoiding the bias introduced by the volumetric scattering components is presented. [C534]

### "SAR mapping technology and its application in difficulty terrain area"

In western China, there is a large area perennially covered by cloud, fog, ice, and snow. It is very difficult to acquire optical image for mapping in this area, so high resolution spaceborne synthetic aperture radar (SAR) images have to be used to make topographic maps. A scheme of SAR mapping technology is proposed in this paper. Digital elevation model (DEM) was extracted with stereo radargrammetry (StereoSAR), and topographic map was created with ideal SAR stereoscopic image pairs. Due to the difficult terrain, parallax edit under stereoscopic observation is used for improving matching result from stereo images. Ideal SAR stereoscopic image pairs generated with image simulation based on DEM are used for stereoscopic observation to extract topographic features. Ascending and descending image data were combined to solve the problem of lack of information caused by shadow and layover. Mapping experiment in western China shows that SAR data with resolution of 3-8 meters can be used to make topographic map at scale of 1:50,000 by the scheme of SAR mapping introduced in this paper. [C535]

### "Rice areas mapping using ALOS PALSAR FBD data considering the Bragg scattering in L-band SAR images of rice fields"

The objective of this paper is to assess the use of ALOS PALSAR FBD data to map rice growing areas. Image enhancement in backscattering in rice fields as a result of Bragg resonance scattering was found only at HH polarization since double-bounce scattering is a prerequisite to Bragg resonance scattering for radar backscatter from bunches of rice plants. A rice mapping method using HV images was developed and applied to Haian test site. Validation showed that rice mapping using L-band SAR is promising when cross-polarized data are available to cope with the Bragg resonance scattering effects. [C536]

### "Radar observations of wave field in littoral zone"

The dissipation of the wave energy in the littoral zone is significant for the coastal hydro- and sediment dynamics. In this presentation, a recently developed method is presented about the separate, simultaneous measurements of wave propagating field and of wave breakers' velocity, based on ground based, Doppler, X-band Radar observations. The kinetic energy of the wave field is calculated for the last 2 km of the N. Sea towards the shore, with high spatial resolution (7.5 m) and the rate of the dissipated is estimated. [C537]

### "Status of the Metop ASCAT soil moisture product"

Since December 2008 the European Organisation for the Exploitation of Meteorological Satellites (EUMETSAT) has been disseminating global 25 km ASCAT surface soil moisture data in near real-time (within 135 minutes after sensing) over its broadcast system EUMETCast. The ASCAT surface soil moisture product is thus the first truly operational satellite soil moisture product that may be used for Numerical Weather Prediction (NWP), flood forecasting and other time-critical applications. In this paper we provide information about the status of the ASCAT Level 2 soil moisture processor, review first published validation and application studies and discuss plans for further improvements. [C538]

### "Simulating and mitigating ionospheric effects in synthetic aperture radar"

The ionosphere is magnetized plasma that forms above the neutral atmosphere due to solar ionization of upper atmosphere constituents. It presents an obstacle to space based synthetic aperture radar (SAR) systems since it affects the radar signals traveling through it. Its impact can be split into two groups: uniform effects (those caused by a spatially uniform non-turbulent ionosphere) and nonuniform effects (those caused by irregularities in the ionosphere). In this paper, we present a method for simulating the uniform non-turbulent effects such as dispersion, group delay, Faraday rotation, and phase shift. This method is then validated using PALSAR data of Washington, DC. We also show the coherence in this scene after ionospheric effects are added. Finally, the model is used to predict the level of ionospheric effects in future space based SAR systems such as ALOS-2. [C539]

### "A specific methodology for atmospheric effect reduction on SAR interferograms"

Interferometric Synthetic Aperture Radar (InSAR) measurements are often biased due to atmospheric effects. Especially, the tropospheric water vapor engenders a delay of SAR signal propagation. In this paper, we propose a specific methodology for atmospheric effects correction on SAR interferograms. It is based on ancillary data collected from NOAA-AVHRR sensor. The specificity of the approach consists in its applicability where no ground truth GPS measurements are available neither for calibration nor for result validation. An adaptive validation demarche is also proposed. [C540]

### "Design considerations for a dual-frequency radar for sea spray measurement in hurricanes"

Over the last few years, researchers have determined that sea spray from breaking waves can have a large effect on the magnitude and distribution of the air-sea energy flux at hurricane-force wind speeds. Characterizing the fluxes requires estimates of the height-dependent droplet size distribution (DSD). Currently, the few available measurements have been acquired with spectrometer probes, which can provide only flight-level measurements. As such, in-situ measurement of near-surface droplet fluxes in hurricanes with these instruments is, at best, extremely challenging, if at all possible. This paper describes an airborne dual-wavelength radar profiler concept to retrieve the DSD of sea spray. [C541]

### "Spaceborne P-band SAR for BIOMASS mission"

In the frame of the BIOMASS mission promoted by ESA for evaluating and monitoring Earth biomass, the expected performance of a P-band SAR instrument based on very large Direct Radiating Array antenna is

addressed, as well as its architecture and the accommodation challenge on a platform. [C542]

### "Signal: SAR for ice, glacier and global dynamics"

SIGNAL is an innovative earth exploration mission proposal with the main objective to estimate accurately and repeatedly topography and topographic changes associated with mass change or other dynamic effects on glaciers, ice caps and polar ice sheets. Elevation measurements are complemented with glacier velocity measurements, providing valuable additional information for a better understanding of the hydrology of glacierized basins and of the Arctic and Antarctic water cycle. SIGNAL is capable of monitoring all critical regions with a high spatial resolution and an adequate revisit time. This paper gives an overview about the actual mission design status and provides a brief description of the topography (DEM-digital elevation map) self-calibration strategy and the estimated global interferometric performance. [C543]

### "Focusing general bistatic SAR data using frequency scaling"

This paper presents a method to focusing the general bistatic synthetic aperture radar (BiSAR) data. First, using the extended Taylor series, the general BiSAR data are transformed into the azimuth-invariant BiSAR one. Second, the monostatic frequency scaling algorithm is extended to the bistatic one. The numerical experiment indicates that our methodology is valid and the proposed algorithm can process the data of the general BiSAR. [C544]

### "Detecting depolarizing targets with satellite data: A new geometrical perturbation filter"

Target detectors using polarimetry are often focused on single (coherent) targets, since these are the ones that can be more simply characterized polarimetrically. The new proposed algorithm is aimed at the more difficult problem of partial target detection (i.e. targets with any degree of polarization). A new feature vector is defined starting from the coherency matrix, and then a perturbation method is performed. Starting from the partial target detection, a novel classification algorithm is proposed. The validation is carried out against fully polarimetric satellite data. In particular, X band TerraSAR-X and L band ALOS PALSAR are employed, providing significant agreement with the expected results and the supervised Wishart classifier. [C545]

### "A radar profiling algorithm designed for use with multiresolution radiometer measurements"

We have developed a radar profiling algorithm that can be incorporated into a larger radar+radiometer retrieval framework. The modular nature of the framework provides the opportunity to test the sensitivity of the retrieval to the inclusion of different measurements, retrieved parameters, and models for microwave scattering properties of hydrometeors. [C546]

### "Applicability of the iterative backward retrieval method for the GPM dual-frequency precipitation radar"

The dual-frequency precipitation radar (DPR) on the core satellite of the Global Precipitation Measurement (GPM) mission will measure the radar reflectivity factor in the Ku-band and Ka-band. A rain-rate retrieval algorithm that does not require surface reference was developed (called the MA04 method). However, MA04 cannot give the true solution in some cases of heavy rainfall. MA04 is a simplified version of the iterative backward retrieval method (IBRM) and the IBRM is equivalent to the forward retrieval method with a constraint. The purpose of this study is to clarify the essential conditions under which the IBRM and MA04 can give the true solution. [C547]

### "Airborne DInSAR time series at X-Band"

Differential SAR Interferometry (DInSAR) is a remote sensing technique which allows monitoring ground deformation with accuracy of the order of the transmitted wavelength by exploiting the phase difference (interferogram) of two temporally separated SAR images relevant to the same area. In addition, when more than two multi-pass acquisitions relevant to the same area are available, they can be properly combined by means of recent multitemporal DInSAR algorithms, in order to detect and follow the temporal evolution of ground deformation via the generation of spatially dense time series. Such a multitemporal DInSAR technique is nowadays developed and operative with space-borne SAR data, whereas specific problems may limit its application to airborne data. In this work, starting from the results already shown in previous works and relevant to an X-Band airborne DInSAR experiment carried out over the Perugia area (center of Italy) by using the OrbiSAR system, we carry out a DInSAR multitemporal analysis of data relevant to a 16 km (in azimuth) by 4 km (in range) region. [C548]

### "Potential and limitations of forward-looking bistatic SAR"

Bistatic synthetic aperture radar (SAR) operates with spatially separated transmit and receive antennas that are mounted on separated platforms. Provided that there is an overlap of both antenna footprints, the platforms can move with different velocities in arbitrary directions. A special configuration is given, when the receive antenna looks in forward direction, which is called bistatic forward-looking SAR. Besides the well known advantages of bistatic SAR like the increased information content of the data because of different RCS and scattering characteristics, such a configuration enables high resolution imaging in forward direction, which is not possible with conventional monostatic SAR systems. This paper analyzes a bistatic forward-looking configuration and demonstrates the capability and feasibility of imaging in forward or backward direction using the radar satellite TerraSAR-X as transmitter and the airborne SAR system PAMIR as receiver. [C549]

### "Tropical land cover change detection with polarimetric SAR data"

There is an increasing need for fast and accurate data on tropical land cover status, and a baseline for land cover monitoring. Remotely sensed SAR data are not sensitive to cloud cover and can be useful for such purpose. Polarimetric SAR data are available in orbital systems, such as RADARSAT-2, and still have to be tested for the classification of tropical land cover and the detection of land cover change, particularly forest conversion. This work presents a study of RADARSAT-2 polarimetric images, acquired in two different dates (September 2008 and October 2009), to assess their potential in classifying forest and non-forest classes in Brazilian Amazonia. SAR images were acquired following different orbit and incidence angles, which anticipated varied conditions for images interpretation and classes discrimination. The complex SAR data were classified based on the distance of Wishart, and information from field campaigns was used for the training and test samples. Classification results were compared to evaluate possibilities for change detection in the forest cover. Classification accuracy figures were around 80%. The use of RADARSAT-2 images allowed the mapping of land cover and land cover change, considering forest and non-forest classes. [C550]

### "Oil Spill statistics from SAR images in the North Eastern Baltic Sea ship route in 2007-2009"

A large number of illegal oil pollutions impose considerable threat to marine environment especially in marginal seas like the Baltic Sea. Illegal spills are mainly detected on essential navigation routes. The monitoring of Oil Spills (OS) using remote sensing imagery (SAR data) was performed on the northeastern Baltic Sea ship route. The pre-analyzed satellite images for detecting marine pollution were provided to marine surveillance agency in Estonia. Out of 137 detected potential pollutions 76 were confirmed by aerial surveillance missions within two-year period. OS were mainly of low confidence, had small area, low contrast with surrounding water and smeared edges. The entrance to the Gulf of Finland was classified as the area where illegal spills of oil and bilge water take place, mainly. Between 30-50% of actual oil pollutions are not detected by SAR. [C551]

### "COSMIC-2: The future of global navigation satellite system-remote observation (GNSS-RO) sensing"

COSMIC is a joint U.S.-Taiwan 6-microsatellite demonstration mission that was launched in April 2006. It is the world's first operational GPS radio occultation (RO) mission for global Earth weather forecast; climate monitoring; atmospheric, ionospheric, and geodetic research. The GPS-RO data has been demonstrated to be valuable to the climate, meteorology, and space weather communities. COSMIC has proven to increase the accuracy of the predictions of hurricane/typhoon behavior, significantly improve long-range weather forecasts, and monitor climate change with unprecedented accuracy. COSMIC will reach the end of its design life in 2011, and the critical capability it provides will begin to degrade as satellites become no longer operational. As a result, NOAA and NSPO intend to jointly develop and launch COSMIC-2, a high-reliability next generation follow-on system. COSMIC-2 is will provide the next generation of global navigation satellite system (GNSS)-RO data to users who critically rely on it. [C552]

### "The NANOOS Visualization System (NVS): lessons learned in data aggregation, management and reuse, for a user application"

The mission of NANOOS is to coordinate and support the development, implementation, and operations of a regional coastal ocean observing system (RCOOS) for the Pacific Northwest region, as part of the U.S. IOOS. A key objective for NANOOS is to provide data and user-defined products to a diverse group of stakeholders in a timely fashion, and at spatial and temporal scales appropriate for their needs. To this end, NANOOS developed the NANOOS Visualization System (NVS), which aggregates, displays and serves meteorological and oceanographic data, derived from buoys, gliders, tide gauges, HF Radar, meteorological stations and satellites, as well as model forecast information in such a way that it presents end users with a rich, informative and user

friendly experience. First released in November 2009, NVS has already undergone several significant updates. While its original focus and continued strength is on near-real-time (NRT) observations from stationary platforms (buoys, coastal stations, etc.), it has evolved to include other types of observations as well as forecast information. NVS integrates data from a wide diversity of providers across the region, ranging from county agencies, private industry and regional partnerships, to core IOOS federal programs, and state agencies and academic groups that are principal partners in NANOOS' Data Management and Communication (DMAC) efforts. Regional and national feedback confirms that NVS has been well received by ocean observing and stakeholder communities alike. This paper discusses, in detail, NVS 2.0, which was released in August 2010. In particular, we provide an in depth look at the database schema, metadata, data harvesting, and component communication. In addition, we discuss the NVS data management and communication approach in the context of the IOOS DMAC interoperability and standards-based efforts, highlighting the strengths and weaknesses of application-focused vs. strong-interoperability-focused approaches. Lessons learned both from technical and project management perspectives are also presented. Lastly, we discuss future plans for NVS. Anticipated improvements include automating asset metadata discovery and processing using IOOS standard protocols, and a NANOOS implementation of ERDDAP that will support NVS by replacing multiple, data-source-specific data harvesters with more generic and easier-to-maintain NERDDAP harvesters; and by enabling customized data subsetting and download capabilities that will be accessible through the NVS user interface. [C553]

### "Comparisons of a fully coherent and coherent-on-receive marine radar for measurements of wave spectra and surface currents"

A new coherent solid state marine radar has been developed for short range coastal ocean remote sensing applications. It has been applied to the measurement of coastal ocean currents and ocean wave spectra, examples of which are reported here. The radar is based on a standard marine radar package, but using a solid state power amplifier incorporated as part of the transceiver subassembly. The solid state transceiver subassembly was developed based on a SMA-connector component prototype that was reported on at the Oceans 2019 Biloxi meeting. A series of parallel tests were run with a prototype coherent-on-receive radar, which is based on modifications to a standard Koden marine radar. For the latter, the leakage signal of the transmitted pulse is used as the reference for realigning the phase of the received echo. Due to the non-coherent nature of magnetron sources used for marine radars, the pulse-to-pulse stability of the transmitted frequency of such a system creates problems with pulse-pair phase-differencing estimates of Doppler shifts. This effect creates a rather noisy Doppler image, and mean Doppler estimates over many rotations can be in error. Data were collected with the pair of radars during the passage of 2-m waves up to 13-s period at the FRF pier in Duck NC. We report on differences in Doppler estimates for the fully coherent and coherent-on-receive marine radars for data collected during this storm, comparing with FRF measurements of wave spectra and surface currents. [C554]

### "Front matter"

The following topics are dealt with: deep ocean survey; oceanographic instruments; optical communication system; data visualization; autonomous underwater vehicles; sonar signal processing; acoustic systems; SAR imagery; water quality sensor; deepwater horizon oil spill; and marine renewable energy. [C555]

### "Semi-Automatic Extraction of Ribbon Roads from VHR Remotely Sensed SAR Imagery"

Roads have very small backscattering coefficient for radio waves, thus they have low intensities on very high resolution (VHR) SAR imagery. Based on the above unique characteristic, mean angular texture signature (MATs) is proposed to track ribbon roads from VHR SAR images in this paper. Experiments demonstrate the proposed tracker can reliably extract most of roads from VHR SAR images. [C556]

### "Cascade SVM Based Oil Detection in SAR Images"

Synthetic aperture radar (SAR) is well adapted to detect ocean pollution independently from daily or weather conditions. Oil slicks have a specific impact on ocean wave spectra because the presence of oil slicks can induce a damping of the backscattering to the sensor and a damping of the energy of wave spectra. Thus oil slicks can be discernible from the radar image. Several algorithms are applied for local segmentation of oil slicks but most solutions are tailored for specific applications. This paper describes a multi-scale kernel-based fusion approach by using textural and statistical features. This cascade svm approach reduces the problems of speckle and sea clutter and preserves subtle variations of oil slicks. The experimental results carried out on SAR images prove the effectiveness of proposed approach. [C557]

### "What can HF radar contribute to the salvage of a grounded ship?"

The area around the grounding site of the Shen Neng 1 in Great Barrier Reef waters On 3 April 2010 was monitored by an HF radar and several Acoustic Doppler Profilers. The HF radar is shown to compare well with the Profilers at the mooring sites. The radar data was used to produce a time series of surface currents at the site during the grounding and throughout the subsequent salvage and clean-up. The spatial and temporal surface current maps are ideally suited for Lagrangian tracking of notional zero buoyancy water parcels starting from the grounding site. Lagrangian 'parcels' were released at two-hour intervals after the grounding in order to identify locations of flotsam or spills. Releases at two-hour intervals through a tidal cycle followed similar tracks until, on the fifth day, a significant change in the meso-scale meteorology and oceanography occurred. It is shown that the meso-scale change had a stronger control on the destination of 'parcels' than tides. HF radar has much to offer in nudging real-time hydrodynamic models used for predictions of currents during a maritime incident like this. [C558]

### "Integrated Coastal Observation Network (ICON) for real-time monitoring of sea-level, sea-state, and surface-meteorological data"

National Institute of Oceanography (NIO) has established an Integrated Coastal Observation Network (ICON) of in-house designed and developed Internet-accessible real/near-real time reporting cellular based sea-level, sea-state, and surface meteorological (Met) stations at several locations on the Indian coasts & Islands (<http://inet.nio.org>). Subsurface pressure sensors and downward-looking microwave radars are incorporated in the sea-level station network. Sea-level, Met, and surface wave parameters are acquired using dedicated Linux based data loggers and uploaded to an Internet server at 5-, 10- and 30-min intervals, respectively with the use of GPRS cellular modems. The sensors and data loggers are powered from sealed lead acid batteries, which are charged through solar panels. The ICON provides graphical presentation of sea-level information (observed sea-level, predicted tide, residual sea-level); significant wave height and wave direction; and Met information (vector-averaged wind speed & direction, barometric pressure, atmospheric temperature, solar radiation, relative humidity, and rainfall). Installation of sea-level sensors free from the influence of stilling-wells and long narrow tubes renders the measurements ideal for tsunami and storm-surge studies by preventing waveform distortion and non-linearity of largeamplitude short-period signals. The network maintains accurate time-stamp of the dataset through Internet-time synchronization using network time protocol (NTP). Real-time reporting capability of ICON yields several benefits, such as (i) remote monitoring of proper working condition of individual stations; (ii) implementation of repair/maintenance in the shortest possible time, thereby minimizing break in the time-series data stream; (iii) periodic arrival of data stream from all stations at a single central server, thus yielding backup for the data from all the stations; (iv) access to the latest in-situ information; (v) allows possible-- use of data with automated real-time running numerical models for operational forecast. In contrast to the limited bandwidth provided by INSAT transmitters, coastal observations at high bandwidth at significantly low cost have become realizable using cellular GPRS network. The NIO-network allows, Internet based real/near-real time tracking and monitoring of sea-level, sea-state, and meteorological conditions along the Indian coasts and islands and from almost anywhere-an issue of considerable practical significance during natural disasters such as storm, storm-surge, and tsunami. [C559]

### "Using a dynamic ocean surface to perform a geometric calibration of a bathymetric lidar"

A geometric calibration of an airborne lidar is an essential component to any bathymetric survey. A poorly-aligned system leads to erroneously reported depths, diminished system resolution and internally inconsistent point clouds. While most calibration procedures depend on the use of cultural features (like gabled roofs), one recently suggested methodology requires only a single broad, flat surface. Given the potential difficulty in identifying such a surface on land, this paper investigates the possibility of using the ocean surface instead. Simulations are performed to examine the anticipated influences of both surface waves and tidal variation. Finally, oceanic results are compared with the likely topographic alternative: using a narrow airport runway as the calibration surface. [C560]

### "Software beam forming for ocean radar WERA features and accuracy"

The WERA system (Wave RADar) is a shore based remote sensing system to monitor ocean surface currents, waves and wind direction. This long range, high resolution monitoring system based on short radio wave radar technology. The vertical polarised electromagnetic wave is coupled to the conductive ocean surface and follows the curvature of the earth. This over the horizon oceanography radar can pick up back-scattered signals from the rough ocean surface (Bragg effect) from ranges of up to 200 km. The direction in azimuth is defined by means of the phase of the incoming electro-magnetic wave. That means the accuracy of this measured azimuth strongly depends on the quality of this phase measurements. The described Software Beam Forming method combines best accuracy with the highest temporal resolution for ocean radar applications. Compared with other beam forming methods the flexibility of this method provides more degrees of freedom for the radar site planing

and makes it much easier to identify suited site locations. [C561]

### "Characteristics of internal waves in the South China Sea Observed by a shipboard coherent radar"

In 2005 and 2007, a coherent, X-band radar was deployed in the South China Sea on two different ships. In both cases, the two parabolic antennas of the radar were fixed at grazing angles of approximately  $2^\circ$  looking toward the bow of the ship. The radar transmitted and received through a single antenna but alternated between the two antennas approximately every half second. One antenna was horizontally polarized and the other was vertically polarized. The data were analyzed by computing normalized radar cross sections and scatterer velocities as a function of ground range and time. Surface signatures of the internal waves were obvious in both types of image and at both polarizations as regions of enhanced cross sections or scatterer velocities. The collected imagery showed that at least two different types of internal waves exist in the South China Sea: small, nearly sinusoidal trains of waves and large soliton-like waves. These different types travel at very different speeds and interact with each other. The small nearly sinusoidal waves travelled at phase speeds near 1 m/s that increased as the small wave trains were overtaken by the faster solitons. Combined with other shipboard measurements, the radar measurements yielded the widths, maximum velocities, and strain rates of the solitons as well as the dependence of phase speed on amplitude. When the speeds of both the ship and the solitons were removed, the measurements showed that soliton full-widths at half-maximum ranged from about 0.5 to 4.5 km. These widths showed a dependence on the amplitude of the soliton. The phase speeds of the solitons also depended on their amplitude, reaching 3 m/s in deep water but only about 1.2 m/s in shallow water. CTD profiles were used to estimate an interface depth for a two-layer fluid model of the propagation of the solitons. The phase speeds predicted by this model agreed well with the observed dependence of the soliton phase speed on amplitude in both shallow and deep water. [C562]

### "Modeling and simulation of sea surface radar observations"

This paper describes a methodology to model and simulate the reflectivity measured by radar observing a maritime environment. The simulation principle consists of reproducing the acquisition of a Real Aperture Radar (RAR) moving along its axis. Pulse after pulse, high range resolution profiles are successively computed by summing the contribution of backscatters comprised in the radar footprint. The scatterer contributions are calculated from typical statistical distribution estimation. The simulation output, called raw data, is the concatenation of time profiles (short time) successively obtained for each radar pulse (long time). A SAR algorithm is then applied in order to form a high resolution image. The generation of the sea surface is achieved by a multi-scale model. This approach takes into account phenomena at different scales (from long wave to small objects), all in interaction in a hydrodynamic environment. It is thus possible to focus locally on contributions considered as more significant. To improve the processing time some contributions can also be retrieved from Look-Up Tables. Hence, our method performs a realistic simulation of electromagnetic interactions in a maritime environment. [C563]

### "Microwave backscatter of ship signatures on SAR imagery"

Speckle characteristics was analyzed by computing the ENL (Equivalent Number of Looks) for sub images of 30 by 30 pixels from four RADARSAT-2 dual polarization products, two single look complex (SLC) products acquired in wide swath single beam mode with dual polarization of HH+HV and two ScanSAR Wide (SCW) products acquired in ScanSAR Wide beam mode with dual polarization of HH+HV, which lie in the sea area around Iberian Peninsula. The speckle analysis indicates that ENL value combined with the intensity value of the SAR image should be a feasible short cut to find ship signatures out of SAR image. Based on the ENL analysis of speckle characteristics, a data set for ship signature has been derived, from which the ship signature was measured by polarimetric synthesis since the polarimetric SAR signature is an effective way of utilizing the amplitude and phase information to characterize the polarization properties of microwave backscatter. Driven by the need for a realistic microwave backscatter of ship signature model, the detailed behavior of a single ship in different polarizations and different incidence angles will be investigated by the Ray-Optical method which was developed by Burkholder et al. The purpose of this paper is to pave the way for a further improved scatter matrix model. [C564]

### "Class-A semiconductor lasers for the transport and generation of optically carried RF analog signals for radar applications"

Class-A operation of VECSELs is obtained. Such shot noise limited sources are used for the transport of RF signals and the generation of radar local oscillators via two-frequency operation. [C565]

### "Surface current retrieval from TerraSAR-X data using Doppler measurements"

The purpose of this paper is to investigate the estimation of surface currents directly on stripmap TerraSAR-X data, as an alternative to Along Track Interferometry. The algorithm relies on efficient baseband magnitude-based Doppler estimation, preventing the estimate from possible biases like azimuth ambiguities and strong target reflections. The validation of the algorithm is made with acquisitions over the Elbe estuary river in Germany and the Eyjafjallajökull volcano in Iceland. [C566]

#### "Currents in rivers, coastal areas, and the open ocean from TerraSAR-X along-track InSAR"

Since the first presentation of a TerraSAR-X along-track InSAR (ATI) derived current field in November 2008, considerable progress has been made with the implementation and testing of various ATI modes of the instrument, improvements of data processing techniques, and test dataset acquisitions over a variety of test sites. Furthermore, receiving and processing capabilities for TerraSAR-X data have been established at the University of Miami's Center for Southeastern Tropical Advanced Remote Sensing (CSTARS), which will permit a complete processing and analysis of TerraSAR-X ATI-derived current fields at CSTARS in the future. We give an overview of these developments and show a few results of recent experiments. [C567]

#### "The propagating speed of internal solitary waves investigated by X-band radar near Dongsha island"

Shipboard X-Band radar images acquired on June 24th, 2009 are used to study internal solitary waves (ISWs) characteristics at northeast of the South China Sea (SCS). The studied images show one ISW in a packet. A methodology based on the Radon Transform (RT) technique is introduced to calculate internal wave parameters such as direction of propagation, internal wave velocity from backscatter image. The result shows that the ISW amplitude is more than 100 meters and it approximately propagates northwestward continent shelf at a speed of 3.04 m/s. Compared with the other researches, especially only with satellite remote sensing images, the ISW propagation speed we got seems higher than other results. A new explanation is presented among different remote sensing images. The periods of most internal waves at northeast of SCS acquired from SAR images aren't regular M2 tidal period ( $T = 12.4h$ ), but less than 12.4h. This may be the reason that the ISW propagation speed we got from X-band radar images is higher than others from SAR images. [C568]

#### "Spaceborne fully polarimetric time-series datasets for land cover analysis"

The objective of this paper is to make a review of the current status of the project entitled Evaluation of RADARSAT-2 quad-pol data for functional assessment of wetlands (Id6842), developed in the frame of the CSA-ESA SOAR-EU (Science and operational applications research for Europe) program by a consortium comprising I.E.T.R at the University of Rennes 1 and COSTEL-LETG at the University of Haute-Bretagne. The main objective of this project concerns in evaluating fully polarimetric RADARSAT-2 time-series datasets to delineate precisely effective and potential wetlands, map detailed vegetation distribution, identify agricultural practices and determine water cycle and waterlevels. [C569]

#### "Propagation of subinertial variations in the Soya Warm Current revealed by HF ocean radars"

Propagation of subinertial variations in the Soya Warm Current (SWC), which flows through the Soya Strait located between Hokkaido, Japan and Sakhalin Island, Russia, is investigated using data from HF ocean radars together with in situ observations, such as bottom-mounted acoustic Doppler current profilers (ADCPs) and coastal tide gauges. The subinertial variations with periods from 5 to 20 days were captured by the HF radars. The subinertial variations were significantly correlated with the meridional wind stress component over the region, suggesting that the sea level difference through the strait caused by wind-generated coastally-trapped waves on the east coast of Sakhalin and west coast of Hokkaido are considered to be a possible mechanism causing the subinertial variations in the SWC. Propagation of the subinertial variations was also clearly captured by the HF radars. The estimated phase velocity suggests that the subinertial variations propagate downstream along the coast as the 3rd-mode barotropic continental shelf waves. [C570]

#### "Multi-source SVM fusion for environmental monitoring in Marquesas archipelago"

Mapping plant species in montane tropical ecosystems needs the use of complementary information sources to be optimally accurate. In this paper, we study SVM fusion as a tool to classify several sources as optical, synthetic aperture radar and topographical ones. Our fusion scheme consists first in applying a single SVM on each individual data. Their outputs are then used for a SVM-based decision fusion to predict the final class membership of each sample. SVM fusion outperforms all mono-source SVM, our fusion method showing numerous successful traits. [C571]

### "Moving target refocusing algorithm for synthetic aperture radar images"

In the area of SAR imaging, it is of interest to be able to focus moving targets. In this paper, an algorithm for moving target focusing is presented. The algorithm is able to refocus a smeared moving target in a SAR image processed at one relative speed to the correct one%. The algorithm works in the frequency domain and is based on the Range Migration algorithm. The refocusing can be made on the whole SAR image or small sub images corresponding to physical areas of interest for the end user. By applying the algorithm to a small image, the computational cost is greatly reduced compared with using the full SAR image. The performance is illustrated by applying the algorithm to simulated SAR data according to the parameters for the LORA system. [C572]

### "Unsupervised classification of PolInSAR image based on Shannon Entropy Characterization"

In this paper, we propose a new method for unsupervised classification of polarimetric synthetic aperture radar interferometry (PolInSAR) images based on Shannon Entropy Characterization. Firstly, we use polarimetric H (entropy) and a parameters to classify the image initially. Then, we reclassify the image according to the span of Shannon Entropy Characterization. Finally, we fuse the results of the two previous steps and merge them to the specified number of clusters. The effectiveness of this method is demonstrated on CETC38 PolInSAR data and E-SAR PolInSAR data. [C573]

### "Noise analysis and restrain in the fusion process of remote sensing"

Considering the noise problem of multi-spectral images and SAR, several image noise models are described in this paper. The idea of non-negative matrix factorization and rough set are used to carry out the fusion experiment. Non-negative factorization is a matrix factorization method in the restrictive condition which all elements are non-factorization. The theory of rough set is mainly about the combination between knowledge and classification, which has an effect on de-noising aspect to the image noises. On the other side, the HIS and wavelet algorithm are adopted to the multi-spectral image fusion. It can not only hold more spectral information but also improve the spatial resolution greatly. The results from the experiment on the images specified the different types of noise, and get the conclusion in the help of some evaluation methods. [C574]

### "A Hybrid Polarimetric Decomposition Method Based on Combination of Scattering-Model and Eigenvector-Decomposition"

Polarimetric decomposition methods are divided into two basic categories: Scattering-model based decomposition and eigenvector-based decomposition. The former has a clear physical meaning but may lead to negative power coefficient, while the latter is the opposite. So, a hybrid Polarimetric decomposition method based on combination of these two methods is proposed, avoiding the negative power coefficient and retaining physical meaning to some extent. The preliminary results of the experiment confirmed that the proposed method is effective for analysis of polarimetric sar images. [C575]

### "Oil spill detection from polarimetric SAR image"

A new combined feature is proposed based on polarimetric features extraction. Moreover, a new oil spills detection method is developed based on the combined feature and max entropy segmentation. The application to NASA/JPL SIR-C data shows that the new combined feature and detection method are effective to oil spills detection. [C576]

### "A novel adaptive learning method for low-sidelobe step frequency waveform designing"

For a step frequency waveform, high range resolution can be achieved by inter-pulse synthesis processing and its sidelobe level can be controlled by weighting in frequency domain. However, high range sidelobe arise when the frequency steps is sparsely spaced. For this, low sidelobe can be obtained in two ways. One is by signal processing after receiving. And the other is to design the waveform with low sidelobe. In order to avoid the SNR loss, The latter is more effective. In this paper, a novel adaptive learning method is given. The method can adaptively adjust the frequencys by max sidelobe discrepancy between the matched filtering out of present and the ideal one. The result of simulation shows that it can approach the optimal frequencys for which the max sidelobe is lowest. [C577]

### "Point target reference spectrum of bistatic SAR with parallel flight paths"

The precise point target reference spectrum of bistatic SAR has been a difficult problem for a long time. Many of the current available algorithms have approximation during deducing. This paper deduces the precise expression in Doppler-Frequency domain with the configuration of parallel flight paths and constant velocity of each

platform. At last, simulations are given to demonstrate the good focusing performance. [C578]

#### "A 2-axis MEMS scanner for the landing laser radar of the space explorer"

We have developed a novel 2-axis MEMS scanner of the small laser radar for landing to the planet. The scanner has to overcome launching vibration and impact and can be used in harsh environment of the space. [C579]

#### "A novel polarimetric FM-CW radar system for laboratory remote sensing experiments"

With the advantage of compact, low cost and high resolution, the frequency-modulated continuous wave (FM-CW) radar equipped in airborne or unmanned aerial vehicles (UAVs) has been well applied to small-scale remote sensing measurements. To make laboratory experiment, our Key Laboratory of Wave Scattering and Remote Sensing Information (KLWSRSI) has developed a fully polarimetric FM-CW synthetic aperture radar (SAR) system. This system can be applied to analysis and demonstration of targets scattering mechanism and polarimetric radar imaging. [C580]

#### "A new two-dimensional millimeter wave imaging radiometer"

Synthetic aperture radiometer has the potential to meet the spatial resolution requirement of passive microwave remote sensing from space. This paper introduces a prototype of two-dimensional imaging radiometer at millimeter wave (MMW) band. A G Matrix calibration approach and an iterative gradient inversion method are presented to obtain the brightness temperature image. Total least squares (TLS) image processing algorithms for improving the brightness temperature image are also presented. Experimental results show that the proposed radiometer can give brightness temperature image of natural scenes and the image processing algorithms can improve image quality of the radiometer. [C581]

#### "Advances in numerical simulation of composite scattering from target above rough surface"

Study of radar echoes from the targets in environmental clutters has been of great interest in many applications. In this paper, research works on theoretical modeling and numerical simulations of composite electromagnetic scattering from target and rough surface are briefly reported. It includes GFBM/SAA, Hybrid KA-MoM, FEM with CMPL-DDM-TLQST, FDTD, and BART, developed in this Lab during recent years. GFBM/SAA: generalized forward backward method with spectral accelerate algorithm Hybrid KA-MoM: hybrid analytic Kirchhoff approximation and numerical method of moment FEM with CMPL, DDM and TLQST: finite element method with conformal perfectly matched layer, domain decomposition method, and two level quasistationary algorithm FDTD: finite difference time domain BART: bidirectional analytic ray tracing. [C582]

#### "An interpolation method for lack of DEM data area in tidal creeks based on neural network"

This paper researches an interpolation method for lack of LiDAR DEM data area in tidal creeks. The study area is tidal flats in the yellow sea radial sand ridges eastern China. Based on a large of tidal creeks surveying data, combined with topography and geomorphology laws, this research focuses on an interpolation method for lack of LiDAR DEM data area in tidal creek by neural network. The interpolation model structure is 2 hidden layers, 6 neurons in every layer. The calculated terrain of tidal creek that is lack of DEM data is very similar to the actual surveyed terrain. RMSE is 0.117m. R2 is 0.716. Residual distribution is normal. The study value is creative to repair the terrain where is lack of LiDAR DEM in tidal flats. [C583]

#### "TIDs in ionospheric F-region at Cusp latitude: Observations and numerical simulation"

Travelling Ionospheric Disturbances (TIDs) at Cusp latitude observed by EISCAT-Svalbard radar (ESR) were presented in this paper. Several representative cases were reported in detail, including a case of TIDs appearing at a broad altitude range (up to the topside of ionospheric F-region). Height profiles of wave number  $k$  were obtained in F-region using Maximum Entropy spectral Estimation (MESE) method when TIDs were monitored by various radar beams simultaneously. Simulation results indicated that TIDs observed at cusp latitude could be reasonable reproduced by carefully selecting AGW inputs. [C584]

#### "Scattering and emission models and simulations for lunar exploration"

This paper presents the research works on the modeling, data-image simulation and data validation for lunar exploration in both passive/active microwave remote sensing. As the first part, the works on Chinese Chang-E (CE-1) lunar program, including brightness temperature simulation ( $T_b$ ) of lunar surface media, CE-1 data validation and retrieval of lunar regolith layer thickness from multi-channel CE-1  $T_b$  data, and evaluation of

global inventory of Helium-3 in lunar regolith, are reported. As the second part of this paper, scattering modeling and numerical image simulations of the randomly cratered lunar surface/subsurface structures for synthetic aperture radar (SAR) imagery and high frequency (HF) radar range echoes are presented. [C585]

#### **"Imaging and reconstruction of a 3D complex target using downward-looking step-frequency radar"**

A technique of imaging and reconstruction for a three-dimensional (3D) complex-shaped Perfect Electric Conductor (PEC) target is developed using step-frequency radar observation synthesizing a two-dimensional aperture. The radar works in downward-looking spotlight mode moving within a 2D circular arc aperture to eliminate geometric distortions and shadowing effect, and the backscattered electrical fields in both the amplitude and phase are obtained. The three-dimensional fast Fourier transform (3D-FFT) algorithm is adopted for uniformly resampling data, which are acquired by interpolating the collected backscattering fields to quickly form a focus image. The bidirectional analytic ray tracing (BART) method [1] is applied to fast calculate the backscattering fields from the 3D complex target, e.g. a tank. Automatic reconstruction of the target is well demonstrated. As a validation, the scattering fields are also computed and compared using widely accepted software FEKO based on Physical Optics. [C586]

#### **"Search Aid System Based on Machine Vision and Its Visual Attention Model for Rescue Target Detection"**

The prompt search and rescue of lifesaving target is very important in the case that a marine casualty occurs. To detect the small target in the wide views over the sea, we have proposed a machine vision system to aid search and rescue on the sea, which combines remote sensing, radar, infrared with visual light technology. One of the detection methods in this system, which is based on visual attention mechanism, is proposed in this paper to find rescue target from visual light image. The color information, image intensity and other image properties are used to generate the feature maps that form the saliency map subsequently with the weighted integrating strategy. The experimental results show that the proposed method is efficient to detect the small target in cluttered ocean scene. [C587]

#### **"Using Remote Sensing Technology for Dynamic Monitoring of Poyang Lake Area and Capacity"**

This article base on more than 130 cloudless satellite imagery since 1983, and Poyang Lake water level data from hydrological site since 1993, computed analysis of Poyang Lake water area, established the remote sensing calculation model with Poyang area, demonstration of Poyang Lake area be increased at the same time with water level by XingZi station, and There are significant seasonal variations, Fitting out the curve of Poyang water level with area, and the water level with capacity, divided into two season section with spring and summer(January-July)and autumn and winter (August-December), provides important tools to study the water resource of Poyang Lake. [C588]

#### **"Pulse reduction method for circularly polarized synthetic aperture radar"**

Many types of data compression for SAR raw data have been developed during the past 30 years. Since most of them focus on reducing the number of bits required to store signal information onboard, the resulting complexity has been a great hindrance to the implementation of an efficient compression algorithm. We propose a new method of data compression that can be carried out onboard a small-sized platform. The method imposes no additional requirement on the antenna size by reducing the number of pulses needed to produce an image and compensating the missing pulses based on information provided from other pulses. The most complicated task of reconstructing the missing pulses can be performed in the ground station, not onboard the small platform. Because fewer pulses are needed, less power will be required for transmitting and receiving the pulses. This is advantageous for reducing the pulse repetition frequency (PRF), which normally becomes higher for smaller antennas. This method will be applied to our circularly polarized synthetic aperture radar (CP-SAR) system, which is currently being developed toward a mission onboard a microsatellite. [C589]

#### **"Emerging Trends of Computational Grid Based Near Real Time/Real Time Flood Assessment and Forecasting Models"**

From recent past, the computational Grid based flood assessment and forecasting models is getting emerged as an interdisciplinary integrated 'near real time/real time model'. Many such, Grid based flood assessment and forecasting model supports in logically integrating various components of flood related scientific simulations such as Metrological, Hydrological, Hydraulic, RADAR, LIDAR Remote Sensing, GIS, Satellite Communication and other technologies and derives the end result which can be straight away used by the disaster mitigation team member/end user. This paper mainly brings out the emerging technological trends observed in the fields of

computational Grid based flood assessment and forecasting models by surveying the flood forecasting model of 'Cross Grid' as well as the operational flood model of ESA Grid. Details reflecting the technology trends and simulation methods adopted by the 'GARUDA Grid' flood assessment experimental model have been given.

[C590]

#### **"Dynamical Weather Radar Beam Blockage Correction"**

Error of quantitative rainfall estimations due to partial or total weather radar beam blockage is important in complex orographic areas. A simple method named dynamical weather radar beam blockage correction different from the operational "look-up" table method is presented. The dynamical correction method is implemented with the multiplicative factor between two antenna elevation angles. Case study of quantitative rainfall estimation shows that the dynamical beam blockage correction is effective if the beam blockage azimuths are less than 10 degrees.

[C591]

#### **"Retrieval of oriented vegetation parameters based on experimental data of PolInSAR"**

Polarimetric SAR interferometry (PolInSAR) can be used to inversion of vegetation parameters and a two-layer coherent scattering model composed of a random volume over the ground is applied usually. However, the propagation of the electromagnetic waves is anisotropic because the extinction coefficients are highly polarization dependent, the random model is inapplicable. In this paper, a new vegetation model composed of an oriented volume over the ground is employed and experimental data about the true scene can be gained through the microwave anechoic chamber. Finally, the oriented vegetation parameters are retrieved by using three-stage method.

[C592]

#### **"Extraction of wetland combining with Radarsat and HJ data of Yellow River Delta"**

Wetland types of Yellow River Delta are various and serious phenomena of 'same object with different spectrum' and 'different object with same spectrum' is one of the reasons caused low classification accuracy. Combination with multi source images is an efficient method to mitigate this influence. In the paper, principal component transform was carried out to Radarsat four polarization data and the first principal component were fused with HJ images based on HIS, Brovey, PC and Wavelet transform. A maximum likelihood classifier was applied to extract wetland information of Yellow River Delta. The experiment results demonstrated that HIS transform performed well than the others and outstood the wetland information. The results also showed that the classification accuracies of HIS merged images and the stacked images were highest, through combining two different source data to make good use of information.

[C593]

#### **"RPC-based adjustment model for COSMO-SkyMed stereo slant/ground-range images"**

The use of stereoscopic SAR images offers an alternative to conventional stereo-photogrammetric survey for the generation of Digital Elevation Models (DEMs). Often the SAR ground-range form is more popular with the commercial users, since the pixel spacing on the ground is roughly the same for the different look-angle images. The different mathematical descriptions between the slant-range and ground-range products thus make the stereo modeling and adjustment a challenging objective to deal with. Previous work applied sensor model adjustment of range and timing parameters to SAR spotlight range images, promising 3-D mapping accuracies in the range of 2 m. However, this adopted the direct least squares method, which is too sensitive in the case of the ground-range images, making it less than optimal for SAR range images' stereo restitution. In this paper, an image based transformation (geometric correction) using a small number of control points (CPs) in cooperation with the Rational Polynomial Coefficient (RPC) model to improve the space intersection accuracy is proposed. The development of such an RPC-based adjustment method is first described, which is very practical to implement and can be applied to SAR slant- or ground-range products. By situating several well-distributed trihedral corner reflectors (CRs) within sites and imaging these sites using COSMO-SkyMed's stripmap (SM) mode, the modeling quality of the delivered slant- or ground-range products was validated, and the 3-D mapping potential was also assessed.

[C594]

#### **"Research on a self-powered wireless ultrasonic flow sensor system"**

A self-powered wireless ultrasonic flow sensor system has been designed and developed from a system level approach in this paper. By using small-sized hydroelectric generator as the source of power for commercial low power microcontrollers, energy harvesting circuitry, and GPRS transmitters, the sensor is capable of detecting water flow in water pipelines network. A major feature of this sensor system is its power-management unit, able to recharge batteries with energy harvested from the small-sized hydroelectric generator installed in water pipelines. It allows the sensor to sustain operation as a general-purpose wireless acquisition device for remote sensing in large coverage areas, where the power to run the devices is always a concern. In addition to

describing the overall architecture, hardware and software of the sensor, the paper also reports on the performance of the module in the water pipelines network, emphasizing the energy issues, crucial to obtain self-sustained operation. The testing was done in two stages: the first in the laboratory, to validate the management and solutions under particularly severe conditions, the second stage in a water pipelines network. The measurements about the behaviors of the sensor confirm that the hardware and software solutions proposed do indeed lead to good performance. [C595]

### "Closure monitoring in Potash Mines using LiDAR"

Underground soft rock mines are constantly deforming-this is a normal rock response to mining excavation. Once a mine opening has been excavated or cut, the opening begins to deform into the excavation. This rock displacement, or room closure, could occur quickly or much more slowly depending on the stress changes caused by mining pattern, rock mechanical properties and in-situ rock pressure. Of particular importance to Mining Engineers and Rock Mechanics specialists is the rate of this closure and where it is occurring within the mine. Room closure is traditionally measured using simple displacement transducers; these instruments give readings only at the points where they are installed. This paper proposes the use of Laser Range Finders (LRF) in generating 3D models of the mine areas where closure needs to be monitored. With this approach, closure can be measured at many points in the room, not just at individual instrumented stations. A procedure is presented using automatic scan registration to obtain a 3D model of an area using an inexpensive 3D LRF. Test results are presented from the Allan Potash Mine. It is shown that this procedure produces results consistent with a standard closure meter in a real mine environment. The difference between the average closure measured with LRF and the closure rod ranged from 3 millimetres to 13 millimetres (4% to 14% of total displacement change). [C596]

### "Retrieval of Ground Deformation Based on TS-DInSAR Technique"

Time series interferogram analysis is an upgrade of the traditional 2/3/4-pass differential interferometry, and has been widely used to map ground deformation associated with urban subsidence, landslide, earthquake and so on. This paper analyzes some key steps in TS-DInSAR processing, including selection of high-coherent points, extraction of linear deformation, separation nonlinear deformation phase and atmospheric phase. Finally, an experiment based on TS-DInSAR technique is conducted over Taiyuan area using totally 14 ENVISAT ASAR scenes in the time span of 2003-2007, and the result of derived deformation shows good agreement with the leveling data with mean square root error of 3.1mm, demonstrating that the TS-DInSAR technique is accurate and efficient in deformation mapping over urban areas. [C597]

### "Urban watershed management: Using remote sensing to implement Low Impact Development"

This paper discusses how remote sensing, specifically Light Detection and Ranging (LiDAR), was used to carry out a detailed Low Impact Development (LID) suitability estimate in an urban watershed. The research uses LiDAR as an accurate and efficient tool for identifying and quantifying LID retrofit locations. The results of the LiDAR analysis were run in a hydrologic model to determine the flood response to various LID implementation scenarios. The overall goal of the research project is to determine whether LID can effectively mitigate the flooding that is predicted to occur due to climate change. LID relies on runoff management measures that seek to control rainwater volume at the source by retaining and infiltrating rainwater. Multiple datasets derived from LiDAR were used to identify suitable LID retrofit locations in the Bowker Creek watershed in Victoria, BC, Canada. LiDAR-derived drainage vectors, Digital Elevation Models (DEM), and Digital Surface Models (DSM) were used in combination with existing GIS data in a selection process that strategically located facilities in areas that optimally reduced peak flow rates and met municipal criteria. [C598]

### "Full polarimetric SAR classification based on Yamaguchi decomposition model and scattering parameters"

The full polarimetric information of the target from polarized Synthetic Aperture Radar (POLSAR) enables us to implement recognition and classification of remote sensing images more effectively. Based on the analysis of typical polarized target decomposition and classification, the issue proposes a new scheme for iterative classification of polarimetric SAR image, which blends the outcomes of Yamaguchi decomposition and H/ $\alpha$  decomposition. This technique extracts four decomposition coefficients of four scattering mechanism components through Yamaguchi decomposition, the scattering entropy and angle through H/ $\alpha$  decomposition first; then the initial classification of the POLSAR images is done by the combination of the 6 parameters mentioned above. The final result is obtained by iterative classification due to coherence scattering matrix following wishart distribution. The effectiveness of this method plus less computation required is demonstrated by the experimental results of polarimetric SAR data. [C599]

### "Comparison between ETM+ imageries and ICESat-GLAS waveforms for forest classification"

The paper presents a method for classifying Light Detection And Ranging (LiDAR) full waveform data, using an artificial neural network (ANN) approach. The ANN classifier used was a multilayer perceptron trained through the generalized predefined learning rule functions. Compared with the unsupervised classification based on Landsat 7 ETM+ (Enhanced Thematic Mapper Plus) images, the ANN classifier was suitable to better represent the nonlinearity in the LiDAR waveforms dataset. The multilayer perceptron neural network has proved to be a very effective tool for the classification of waveforms data. The classification results show that forest classification accuracy for broadleaved forest and needleleaved waveforms using ANN classifier is better than the classification accuracy of ETM+ image based-unsupervised classifier. Whereas, the overall classification accuracy of testing datasets using ANN classifier with using waveform data without a prior class probabilities is lower than the unsupervised classifier based-image. [C600]

### "Modeling methods for tidal flat digital terrain based on neural network"

The purpose of this paper is to model tidal flat digital terrain. The study tidal flats are in the yellow sea radial sand ridges eastern China. Based on the regularity and variability characteristics of changeable tidal flats, combined with remote sensing and remote surveying technology and information, this research focuses on tidal flat digital terrain modeling by neural network. The model structure is 2 hidden layers, 11 neurons in every layer. The terrain calculated is very close to the terrain actual surveyed. RMSE is 0.1564 m. R2 is 0.95817. Residual distribution is normal. The study value is creative to get dynamic tidal flat terrain information fast and efficiently. [C601]

### "Study on remote sensing radiation transfer model"

In order to perform the remote sensing models' collaborative retrieval through different medium and different bands, the deep relationship of Radiation Transfer Equation (RTE) in different medium should be understood in advance. Therefore, the author deduced the "classical RTE" on the basis of the radiation transfer theory, and then analyzed the hidden relationship among the RTE in the atmosphere, soil, and water body. The results reveal that the difference of different medium's RTE mostly derives from the mathematical descriptions about their optical properties, and that these equations have great relevance with each other. Due to this, the "classical RTE" is just like an inner "bridge" to link different equations together. [C602]

### "The study of Range Doppler Algorithm in focusing Bistatic SAR"

Comparing to monostatic SAR, Bistatic SAR has specific advantages, such as the reduced vulnerability in military systems, additional information about the target and characteristics of signal. Nevertheless, it brings the complication of processing algorithms because of the range history of a Bistatic target is the sum of two hyperbolic range equations, which give a double square-root term in the range equation, and the traditional RD algorithms using in monostatic SAR can not apply for processing Bistatic SAR. This paper obtained the point target signal by establishing the echo signal model, then derived the approximate two-dimensional spectrum of echo signal by using POSP, and a Range Doppler Algorithm suitable for Bistatic SAR is presented. The algorithm is validated by the simulation experiments of point targets. [C603]

### "Earthquake-collapsed building extraction from LiDAR and aerophotograph based on OBIA"

Estimation of damages caused by a large earthquake is a major task in the post disaster mitigation process. To enhance the relief and rescue operation in the affected area it is required to receive rapid, accurate knowledge about the conditions of damaged area. Remote sensing techniques were proved to be useful to detect, identify and monitor the impact and effect of natural disasters in last decades. Recently emerging LiDAR data provide the height of the ground objects, which can be used for extracting the collapsed buildings in a complex urban environment. Using the aerophotographs and the normalized digital surface model (nDSM) extracted from LiDAR data, a method based on OBIA and SVM was developed to extract the earthquake-collapsed building. The test study in Haiti's capital, Port-au-Prince after 2010 Jan. 12 earthquake shows that the method can extract collapsed buildings with high accuracy. [C604]

### "Study on collaborative biohazard risk assessment system integrated with mobile GIS"

This article summarizes related factors about biohazard events, and extracts the main factors to determine the main parameters of agent spread model and hazard assessment model. Mobile terminal (PDA) is used for data acquisition and model calculation, in the mean time a variety of methods are adopted for collaborative communications with server station, ensuring the consistency of models and datas. The map of national administrative divisions, rivers and other relevant factors are incorporated to realize the dynamic visualization of

models, and establish the whole system of biohazard risk assessment models. This system improves emergency response capacity of biological hazards, and runs steadily and powerfully during working. [C605]

#### "QEM-based simplification of building footprints from Airborne LiDAR data"

This paper presents a QEM-based simplification approach for extracting and delineating building footprints from Airborne LiDAR data. Our approach consists of three steps: first of all, Digital Surface Model (DSM) is generated from the raw point cloud by using the interpolation method. Secondly, the potential points on building outlines have to be aggregated to form connected building blobs. Those blobs that exceed a certain size and have certain characteristics (e.g. consisting of planes) are supposed to be building candidates. In a third step these outlines are simplified to building footprints. The focus lies on taking the characteristics of buildings into account to produce a meaningful 2D building shape and simplifying different possibilities to generalize the building footprints. [C606]

#### "Extraction of frequent grouped sequential patterns from Satellite Image Time Series"

This paper presents an original data mining approach for extracting pixel evolutions and sub-evolutions from Satellite Image Time Series. These patterns, called frequent grouped sequential patterns, represent the (sub-)evolutions of pixels over time, and have to satisfy two constraints: firstly to correspond to at least a given minimum surface and secondly to be shared by pixels that are sufficiently connected. These spatial constraints are actively used to face large data volumes and to select evolutions making sense for end-users. Successful experiments on an optical and a radar SITS are presented. [C607]

#### "Soil moisture detection using KOMPSAT-5 SAR data"

The applicability of the KOMPSAT-5 (Korea Multi-Purpose Satellite-5) SAR on soil moisture detection is addressed in this paper. At first, the penetration into and reflection from bare soil surfaces at X-band are compared with those at L-band for homogeneous and inhomogeneous moisture profiles. The sensitivities of the X-band radar backscatter on soil moisture are examined for rough bare soil surfaces. Then the sensitivities of the X-band radar backscatter on the soil moisture of vegetated surfaces are also examined for various vegetation densities and incidence angles. The applicability of an X-band radar for soil moisture detection may be as good as L-band radar for bare soil surfaces. For vegetated surfaces, the soil moisture can be detected using an X-band radar at lower incidence angles, where the upper limit of the incidence angles depends on vegetation density. [C608]

#### "Generation of DEM by radargrammetric techniques"

Thanks to the signal processing applied to radar signal, radar systems can provide images with a very high resolution. With regard to these properties, one can estimate that radar images are used to get elevation terrain considering the basic characteristics of a radar image. This paper examines one way to produce DEM (Digital Elevation Models) from a mountainous area (the French Alps). So, we organize the discussion in three parts. First, we present the basic operations that the radargrammetric processing requires to be performed. So we deal with the different steps to obtain a DEM. Secondly, we expose two classical image matching improvements: the epipolar geometry and the pyramidal scheme. At the end, we present the results of DEM generation from a SIRC shuttle mission image pair and the way to improve these results. [C609]

#### "A comparative study of polarimetric and non-polarimetric lidar in deciduous-coniferous tree classification"

As an important active remote sensing tool in forest remote sensing, lidar is able to provide information on tree height, canopy structure, aboveground biomass, among other parameters. It has become desirable to be able to classify tree species using lidar data during recent years. Research has been performed using commercial non-polarimetric lidar in tree species classification, at either dominant species level or individual tree level. The objective of this research is to classify deciduous and coniferous trees using the newly developed polarimetric lidar system. Lidar data from five different tree species were collected in the field. These included ponderosa pine, Austrian pine, blue spruce, green ash and maple. Data were preprocessed and artificial neural network method was developed for classification. Data analysis demonstrated that the classification performance using polarimetric lidar data was far better than that using the non-polarimetric lidar data. [C610]

#### "National ecological observatory network (NEON) airborne remote measurements of vegetation canopy biochemistry and structure"

The National Ecological Observatory Network (NEON) is a continental-scale research platform for discovering,

understanding and forecasting the impacts of climate change, land-use change, and invasive species on ecology. Site-based flux tower and field measurements will be coordinated with high resolution, regional airborne remote sensing observations. This data combined with satellite observations, national data sets and ecosystem models will extend site-based and regional coverage to the continental scale. The NEON Airborne Observation Platform (AOP) will carry remote sensing instrumentation designed to achieve sub-meter to meter scale ground resolution to bridge scales from organism and stand scales to the scale of satellite based remote sensing. The capability of the airborne system will be well beyond existing systems in its ability to produce quantitative information about ecosystem structure and functioning covering nearly 2 million hectares each year for 30 years or more. [C611]

#### "The inversion of crop height based on small-footprint waveform airborne lidar"

Due to limited vertical resolution, the waveform of vegetation whose height is relatively low will superpose on soil waveform. Therefore, lidar full-waveform data were mainly used in forestry, but no research in the crop. In this paper, in order to derive crop height, a gaussian decomposition algorithm based on transmitting waveform is adopted to distinguish the crop waveform from soil waveform, and to extract peak location and pulse width from raw waveform data, proving it is a reliable and highly accurate decomposition algorithm. Moreover, the decomposition algorithm lays the proper foundation for obtaining other crop biophysical parameters. [C612]

#### "Extraction of building's geometric axis line from LiDAR data for disaster management"

Fast and reliable building damage analysis is crucial for survivors rescue and disaster management when a destructive natural disaster occurs which helps to limit life losses. For this purpose, a method was developed in this paper to extract building's geometric axis line from aerial LiDAR data which helps to do further building damage analysis like to identify inclined buildings. To extract building's geometric axis line, several steps were carried out such as segmentation of buildings, extraction of roof facets, fitting of mean roof plane and getting main roof. The aerial LiDAR data was captured over the area of Port-au-Prince, Haiti which contains numerous of inclined buildings. The results demonstrate the feasibility and effectiveness of the proposed approach to identify inclined building for damage management. [C613]

#### "Mapping of wind-thrown forests using satellite SAR images"

The study focuses on investigation and evaluation of wind-thrown forest mapping using satellite remotely sensed data from three synthetic aperture radar (SAR) sensors. The study is carried out at Remningstorp, a test site in the south of Sweden dominated by coniferous forest, where trees were manual felled to simulate wind-thrown forest. The satellite data consisted of time series of HH polarized SAR images acquired by the Advanced Land Observing Satellite (ALOS) Phased Array type L-band Synthetic Aperture Radar (PALSAR), Radarsat-2 (C-band) and TerraSAR-X (X-band). The results from visual interpretation of SAR images acquired before and after the simulated wind-throw together with corresponding ratio images show that ALOS PALSAR HH polarized intensity images are not able to detect wind-thrown forest, probably due to too coarse spatial resolution. In contrast, the wind-thrown forest is clearly visible in the Radarsat-2 and TerraSAR-X HH polarized images, implying that it may be possible to develop a new application using these SAR data for mapping of wind-thrown forests. [C614]

#### "Full exploitation of the SBAS-DInSAR algorithm in active seismogenetic scenarios"

We perform a full exploitation of the Differential SAR Interferometry (DInSAR) algorithm referred to as Small Baseline Subset (SBAS) technique to investigate long term surface deformation occurring in extended, seismogenetic areas. To this aim we benefit of the SBAS technique capability to work in multi-frame and multi-sensor scenarios in order to improve the spatial and temporal coverage, as well as to employ new generation SAR sensors to increase the temporal sampling of the retrieved time series. In this work we apply the SBAS algorithm to analyze the temporal evolution of the detected displacements affecting three different seismogenetic scenarios by means of deformation time series retrieved through data acquired by European (ERS-1/2, ENVISAT) and Italian (COSMO-SkyMed) satellites. In particular, we focus on the analysis of the deformation patterns associated with the activity of the San Andreas (SAF, California, USA), the North Anatolian (NAF, Turkey) and the Paganica (PF, Abruzzo, Central Italy) Faults. The achieved results provide a clear idea of the surface deformation retrieval capability of the SBAS procedure. [C615]

#### "Scatterometer image reconstruction from aperture-filtered samples"

This paper considers sampling and reconstruction theory with application to scatterometer image reconstruction. Backscatter imaging is approached as the inversion of a noisy aperture-filtered sampling operation. A reconstruction estimator based on maximum a posteriori probability (MAP) estimation is proposed to recover the

conventional samples from noisy aperture-filtered samples. Examples from the SeaWinds scatterometer and the Advanced Wind Scatterometer (ASCAT) are presented. [C616]

### "Radargrammetry of high resolution synthetic aperture radar onboard KOMPSAT-5"

This paper reports the preliminary results on the study of radargrammetry especially for a high-resolution satellite synthetic aperture radar system. Theoretical configurations for radargrammetry in terms of coverage, orbit selection, incidence angles, height sensitivity of parallax and height resolution of DEM were calculated according to the proposed orbit characteristics and the imaging modes of KOMPSAT-5 SAR. Possible imaging strategies and mission scenarios for coverage versus rapidity are suggested for a future mission dedicated to radargrammetry. [C617]

### "Fusion of LiDAR data and orthoimage for automatic building reconstruction"

Recent years LiDAR data is widely used for constructing 3D terrain models which provide realistic impressions of the urban environment. This paper presents an automatic method for extracting 3D building model by the fusion of LiDAR data, 2D building outlines and orthoimage. 2D building outlines is generated by classifying the LiDAR data to terrain and off-terrain points, then detecting building edges points through step-structure detector and generalization. 2D building boundaries are added on the DSM (Digital Surface Model) from LiDAR data to generate complex buildings by using CSG with the Boolean operations of union, intersection and differences. [C618]

### "Compressive sensing for high resolution differential SAR tomography-the SL1MMER algorithm"

Differential SAR tomography extends the synthetic aperture principle into the elevation and time directions for 4-D imaging. With modern meter-resolution space-borne SAR systems like TerraSAR-X (TS-X), systematic tomographic imaging of urban infrastructure and its deformations becomes feasible. We demonstrate the potential of TS-X data for this purpose and introduce several novel concepts. Since building deformation in general is nonlinear, e.g. due to thermal dilation, we start from a tomographic system formulation that is general enough to allow for the inclusion of motion models (linear, periodic, etc.). By appropriate warping of the time axis we map the motion model function to become linear and lead to a peak in the spectral domain. For the differential tomographic inversion itself we propose a 2-D compressive sensing (CS) based approach-"SL1MMER". We demonstrate the super-resolution power and the robustness of SL1MMER both with simulated and with real data. We also show that it provides an attractive compromise between parametric and non-parametric methods. A full reconstruction of a building complex and its seasonal deformation from a stack of TS-X spotlight data is finally presented. [C619]

### "Building extraction from VHR multi-spectral images using rule-based object-oriented method: A case study"

Object-oriented classification has been demonstrated a promising method for large-scale detailed urban structure mapping using very high-resolution space-borne or airborne remote sensing images. In the paper, the object-oriented classification method for building extraction using pan-sharpened IKONOS multi-spectral images was applied to roof mapping combined with Lidar data. The scheme to produce the vector polygon database of buildings includes the following steps: (1) image pre-processing and derivation of secondary inputs to image segmentation and classification procedures; (2) segmentation of processed data layers into image objects; (3) classification of image objects; (4) export classified map objects and average building height data; and (5) polygon generalization and/or geometrical regularization. The experimental result is visually satisfactory and may suit overall investigations of building development. [C620]

### "Retrieval of Aerosol optical thickness and size distribution from PARASOL in Pearl River Delta area"

AOTs(Aerosol optical thicknesses) and aerosol size distribution functions in Pearl River Delta area are derived from PARASOL (Polarization and Anisotropy of Reflectances for Atmospheric Science coupled with Observations from a LIDAR)multi-directional, multi-spectral polarized signals. Based on analyzing the products of AERONET(Aerosol Robotic Network), aerosol size distribution function and complex refractive index over Pearl River Delta area are received. After that, the particular aerosol model is abstracted. The land surface polarized contribution is calculated using semi empirical model as a function of surface type and NDVI, and the pure atmospheric contribution is computed with a radiative transfer code. Compared with the products of the ground-based AERONET, the derived AOTs are underestimated against AERONET measurement. The retrieved size distribution for the radii bigger than 0.2 micron is also underestimated due to that polarization is insensitive to

coarse model aerosol. [C621]

### "Contribution of Cosmo/SkyMed data into PRIMI: A pilot project on marine oil pollution. results after one year of operations"

In this paper we present the Pilot Project PRIMI, designed to provide information on marine oil spills, and its validation campaign, held in august 2009, conducted with the oceanography ship Urania. During the experiment CosmoSkyMed has provided an extraordinary contribution supplying almost any day images over the area inspected by the ship and in some cases also images requested with short notice. [C622]

### "First experiments of sector interpolated SAR tomography"

SAR Tomography (Tomo-SAR) is an experimental advanced coherent data combination mode allowing full 3-D imaging of volumetric and layover scatterers from a multibaseline (MB) synthetic aperture radar (SAR) data stack. However, the linear Fourier-based Tomo-SAR is generally affected by unsatisfactory imaging quality due to a typically low number of baselines with irregular spatial distribution. Recently, to improve the elevation focusing technique, a sector interpolation approach has been proposed by the authors, in which a set of uniform baseline data is recovered from the available non-uniform one by exploiting the a priori information about the extension of a height sector which contains the scatterers. In this work, first experiments are presented of sector interpolated Tomo-SAR carried out with real spaceborne MB SAR data acquired over the Cinecitta area of the city of Rome. [C623]

### "The COSMO SKYMED constellation turn on the l'aquila earthquake: Dinsar results of the morfeo project"

On April 6th 2009 a Mw=6.3 earthquake struck the area around the city of L'Aquila in Italy. SAR systems have been proven to be valuable sensors for analyzing the effect of earthquakes and monitoring post-seismic displacements. Due to the low deformation rate, the study of post-seismic events requires the use of a multi-temporal InSAR approach. COSMO/SKYMED is a constellation of SAR sensors of 4 X-band sensors operative also for the civilian use. Thanks to the availability of a stack of ascending acquisitions, ad hoc programmed by ASI on the area stricken by the earthquake, it was possible to provide post-seismic deformation maps by using two different multi-temporal interferometric approaches: the SPINUA and SBAS techniques. The work is carried out in the framework of the MORFEO project dedicated to the monitoring of the landslides risk by means of Earth Observation data. The displacement maps related to the post-seismic activity are presented and commented. The results clearly show the potentiality of the COSMO/SKYMED constellation use for emergency monitoring. [C624]

### "Towards fully automatic generation of land cover maps from polarimetric and metric-resolution SAR data"

Information mining from heavy SAR images is considered from the point of view of the procedure automatization. Two schemes based on Neural Networks are evaluated, one based on the Self Organizing Map method exploiting polarimetric information and oriented to land cover classification, the other based on the Pulse-Coupled Neural Networks aiming at characterizing the imaged buildings. [C625]

### "Statistics of depolarization ratio from an airborne backscatter lidar"

An important cloud optical property derived from elastic backscatter lidars is depolarization ratio because it is used to determine cloud phase. Statistics and trends of volume depolarization ratio were analyzed for four years, 2003-2007, of Cloud Physics Lidar data during five projects of varying geographic locations and meteorological seasons. The volume depolarization ratio was computed using the parallel and perpendicular polarized 1064 nm channels. The majority of the cloud layers yielded a volume depolarization ratio between 0.3 and 0.6 with the volume depolarization ratio frequency distribution centered at 0.45 for ice clouds and 0.05 for water clouds. On average for ice clouds, volume depolarization ratio increased significantly as temperatures decreased. No trend for water clouds was observed, since all water particles are in theory spherical. [C626]

### "Soil dielectric and senisitivity analysis for subsurface imaging applications based on distributed Sensor Networks"

The concept of a subsurface imaging technique based on Unattended Ground Sensor Networks operating in the VHF range using ultra-wideband waveforms was recently proposed in. In this approach a forward model for realistic subsurface environment based on the Dyadic Green's function for a stratified medium and an inversion

technique using an ultra-wideband near-field focusing were presented. Simulation results showed that very good lateral and depth resolution could be achieved. Before carrying out an experiment to test the proposed technique, three vital aspects of the work which are imposed by practical limitations are investigated and presented in this paper. First, the sensitivity analysis to assess the signal penetration depth in realistic subsurface environments for various frequencies is performed. Analysis of the frequency requirements of the inversion as they relate to depth resolution is also analyzed. A semi-analytic soil dielectric model originally devised for microwave frequencies is extended to VHF and validated using measurement results available in literature. [C627]

#### **"The Semi-Analytic Mode Matching algorithm for GPR wave scattering from multiple complex objects buried in a dielectric half space"**

The Semi-Analytic Mode Matching (SAMM) algorithm is a quick and efficient computational method that can model wave scattering from multiple objects in half spaces. This algorithm relies heavily on the appropriate choice of coordinate scattering centers (CSCs) for its modal expansions. Here, the radius of curvature method of finding CSCs is extended to "tune" the CSC loci. Because the CSC locations are essentially frequency independent and independent of the dielectric contrast between scatterer and background, it is worthwhile to analyze carefully particular scattering object shapes and store the optimal CSC locations for future use. Scattering from multiple targets buried within half spaces can be constructed from simpler simulations of the individual targets taken independently in uniform media-combining these initial simulations correctly can greatly reduce overall computational time and increase robustness in full simulations. Excellent results are found comparing SAMM and Finite Difference Frequency Domain (FDFD) for multiple 2D scattering objects 0.1-15 wavelengths in size located beneath half spaces. [C628]

#### **"Integrating object-oriented image analysis and decision tree algorithm for land use and land cover classification using RADARSAT-2 polarimetric SAR imagery"**

Traditional pixel-based classification methods yield poor results when applied to SAR imagery because of the presence of speckle and limited information in backscatter coefficients. A novel classification method, integrating polarimetric target decomposition, object-oriented image analysis, and decision tree algorithms, is proposed for the classification of polarimetric SAR data (PolSAR). The polarimetric target decomposition is aimed at extracting physical information related to the scattering mechanism of targets for the classification of scattering data. The main purposes of the object-oriented image analysis are delineating objects and extracting various spatial and textural features. The decision tree algorithm provides an efficient way to select features and create a decision tree for the classification. A comparison between the proposed method and the Wishart supervised classification was made. The overall accuracies of these two methods were 89.34% and 79.36%, respectively. The results show that the proposed method is an effective method for the classification of PolSAR data. [C629]

#### **"Maximum Likelihood texture tracking in highly heterogeneous PolSAR clutter"**

This paper introduces a generalisation of the conventional Maximum Likelihood (ML) texture tracking algorithm in the context of highly heterogeneous PolSAR clutter. The statistical criterion is defined in both uncorrelated and correlated texture cases. Some results on simulated data are computed and an application on temperate glaciers velocity estimation is processed. Finally, some additional improvements are performed: an adaptative sliding windows is set and a basic Bayes inference for flow model constraint is added. [C630]

#### **"Estimating rice growth parameters using X-band scatterometer data"**

In this study, we constructed an X-band automatic scatterometer system and analyzed scattering characteristics of paddy rice over the whole period of rice growth from transplanting to harvesting. The backscattering coefficients were calculated from the measured data at incidence angle  $45^\circ$  and full polarization (HH, VV, HV, VH) by applying the radar equation and compared with rice growth data such as plant height, stem number, fresh and dry weight and Leaf Area Index (LAI) that were collected at the same time of each scatterometer measurement. Based on the analysis of the relation between backscattering coefficients at X-band and rice growth parameters, we predicted the rice growth parameters using the radar backscattering data. Relationship between measured and estimated grain dry weight using the X-band backscattering coefficients (VV-polarization) is highly correlated ( $R^2=0.94^{***}$ ). Results from this study show that backscattering coefficients X-band appear effective to estimate rice growth parameters. [C631]

#### **"Optimal parameter estimation in heterogeneous clutter for high resolution polarimetric SAR data"**

This paper presents a new estimation scheme for optimally deriving clutter parameters with high resolution

POLSAR data. The heterogeneous clutter in POLSAR data was described by the Spherically Invariant Random Vectors model. Three parameters were introduced for the high resolution POLSAR data clutter: the span, the normalized texture and the speckle normalized covariance matrix. The asymptotic distribution of the novel span estimator is also investigated. The proposed method is tested with airborne POLSAR images provided by the ONERA RAMSES system. [C632]

### "Review of Observing System Simulation Experiments to evaluate the potential impact of lidar winds on weather prediction"

Observing System Simulation Experiments (OSSEs) are an important tool for evaluating the potential impact of proposed new observing systems, as well as for evaluating trade-offs in observing system design, and in developing and assessing improved methodology for assimilating new observations. Extensive OSSEs have been conducted at NASA/GSFC and NOAA/AOML in collaboration with Simpson Weather Associates and operational data assimilation centers over the last 25 years. These OSSEs determined correctly the quantitative potential for several proposed satellite observing systems to improve weather prediction prior to their launch, and evaluated trade-offs in orbits, coverage, and accuracy for space-based wind lidars. In this paper, we summarize OSSE methodology and present results from OSSEs to assess the potential impact of lidar winds. [C633]

### "Shallow water bathymetry with an incoherent X-band radar using small (smaller) space-time image cubes"

The approach most commonly used in bathymetry by "depth inversion" starts by transforming a space-time cube of ocean surface images into a wavenumber-frequency spectrum. The depth is determined by fitting the shallow water gravity wave dispersion equation to the 3D spectrum. The depth error using this method is inversely proportional to the image cube size. Very large image cubes are required for accurate bathymetry. Typical cube dimensions are on the order of 250 m Ч 250 m Ч 100 s. A new algorithm, originally developed for satellite images, can achieve the same accuracy with much smaller cubes, on the order of 100 m Ч 100 m Ч 10 s. This paper describes a test of this algorithm on low grazing angle radar data. The algorithm offers the potential for rapid near shore bathymetry surveys using marine X-band radars flown on aircraft. [C634]

### "Combining GIS and InSAR data for 3D building reconstruction"

Today space-borne high resolution SAR sensors (e.g., TerraSAR-X, TanDEM-X, SAR-Lupe or Cosmo-SkyMed) provide SAR images up to spatial resolutions of 1-3m and even better in spotlight modes. Hence, one major issue of these missions is the development of methods to automatically derive detailed cartographic information from their data. Especially, the analysis of rural and urban areas is on demand in case of disasters (e.g., earthquakes), where active remote sensing systems are highly attractive. Here, an important issue is the development of automatic methods for damage assessment or change detection, in general. For that it is advisable to combine existing GIS data with current SAR data. In this paper an approach for 3D building reconstruction is presented, based on information fusion by utilizing GIS and InSAR data. Thereby, the GIS data are providing the 2D building footprints and the acquired InSAR data the height information. An InSAR simulation step and the subsequent assessment between the real and simulated InSAR phase data enables the extraction of the current building shape. [C635]

### "Characterization of the scattered field by an urban area in the X-frequency band for bistatic and monostatic radar configurations"

The application of the ray-tracing technique in combination with the asymptotic method Uniform Theory of Diffraction (UTD) for an analysis of the electromagnetic (EM) wave propagation in urban areas is presented. The frequency of the study is in the X-frequency band from 8 to 12 GHz but can be applied for Ku-band and a three-dimensional model of the geometry is proposed. The transmitter and receiver can be separated to present both bistatic and monostatic configurations. At the end of the work, we evaluate the amplitude and the phase of the far field diffracted by urban scenarios. [C636]

### "Burst mode to strip-map mode SAR interferometry of ALOS PALSAR"

A complete processing flow is proposed to implement burst mode to strip-map mode interferometry for ALOS PALSAR data. The processing flow is applied to an interferometric pair comprised of FBD (High Resolution mode [Dual polarization], belonging to strip-map mode) and WB1 (Wide observation mode, belonging to burst mode) mode of PALSAR. Interferometric products including differential interferometric phase and DEM are generated. The evaluation of these products shows satisfactory precision. [C637]

### "Study of snowmelt impact on SST and TSM fields in the coastal zone of Barents Sea"

Spatial and temporal variations of SST and biological fields were observed in the coastal area off Novaya Zemlja, Barents Sea. Focus is on the relation between SST and biological parameters. The variations of snowmelt runoff from land (glaciers and river runoff) were estimated using SAR imagery. A relation between snowmelt input from land and ocean Chl a as well as TSM concentration was observed based on a case study. The data showed that the TSM and Chl a concentration increased significantly ~30 days after the snowmelt over land started to increase. [C638]

### "Assimilation of D-InSAR and sub-pixel image correlation displacement measurements for coseismic fault parameter estimation"

In this paper, 2 data fusion strategies from SAR images are investigated through application to measurement of displacement field due to the Kashmir earthquake (Mw=7.6, 2005). Firstly, the 3D displacement field at the Earth's surface is retrieved by a linear inversion, using the measurements from sub-pixel image correlation and differential interferometry. In addition to the generalized least square method, a fuzzy approach is applied to represent the measurement uncertainty. Secondly, the geometry of the fault is optimized by a non linear inversion, using the same measurements. The inter-comparisons between strategies and approaches are performed in order to highlight the advantages and disadvantages of each strategy and approach. [C639]

### "Bistatic Radar Cross Section of a complex target on sea surface"

This paper deals with modeling interaction between Electro-Magnetic (EM) wave and the complex target. The first objective is to estimate monostatic and bistatic Radar Cross Section (RCS) of a complex target. The second objective is to present a new approach to compute the RCS of complex target (typically a boat). The target is modeled in 3D using computer aided design (CAD) to generate triangular facet meshing, as does CATIA software. From the triangular mesh, we propose to implement a parallelepiped mesh technique. This new mesh approach allow to introduce more precisely target in its environment and can be used in remote sensing domain. [C640]

### "Analyzing tomographic SAR data of a forest with respect to frequency, polarization, and focusing technique"

In this paper, two fully-polarimetric tomographic SAR data sets of a forested area, at L-band and P-band, are analyzed with respect to the localization of scattering sources and scattering mechanisms. In particular, the 3D SAR data is examined regarding the performance of three different tomographic focusing techniques multilook standard beamforming, robust Capon beamforming, and MUSIC, as well as for both, the two frequency bands and the different polarimetric channels. [C641]

### "Radiometric performance of the Advanced Wind Scatterometer radar ASCAT"

The Advanced Wind Scatterometer (ASCAT) instrument [1 & 2] is one of the instruments carried by the ESA / EUMETSAT METOP satellites (METOP A, B & C). The ASCAT is a six-beam radar instrument designed to measure wind fields over the oceans; the instrument also provides useful data for ice and land applications. The radiometric performance of the ASCAT carried by METOP-A is estimated and discussed. [C642]

### "An innovative spaceborne radar concept for global maritime surveillance: Description and performance demonstration"

The paper describes an alternative concept to conventional SAR instruments for ship detection over all ocean surfaces. The concept is specifically oriented for ship detection, and not for land or sea imaging. It allows wide swath coverage (as high as 1000 km). It exhibits high detection performances of small ships even in adverse sea states conditions. Its power consumption is reduced allowing a permanent operation all along the orbit. At least, it uses already developed and low cost technologies. [C643]

### "X-band backscatter map generation using TerraSAR-x data"

The goal of this work is the generation of an X-Band backscatter map by assembling images acquired by the TerraSAR-X mission. Global backscatter data is required for accurate performance estimation and instrument commanding inside the TerraSAR-X and TanDEM-X missions. Moreover, many scientific applications can be based on the analysis of backscatter behavior and evolution. The complete ground coverage will be achievable with TanDEM-X mission data. An interpolator, that allows the estimation of the backscatter for any required polarization and incidence angle from the available data, has been implemented. In this paper, the backscatter

map generation algorithm will be presented, together with the first obtained results, generated using TerraSAR-X data. Moreover, the validity of the interpolation models will also be discussed, presenting the preliminary results of a statistical analysis of backscatter from TerraSAR-X data. [C644]

#### **"Change detection in urban areas with high resolution SAR images using second kind statistics based G0 distribution"**

This paper presents a SAR image change detection algorithm for urban areas which mainly contains three steps: (i) modeling the Synthetic Aperture Radar (SAR) image by G0 distribution; (ii) generating a change map by computing the Kullback-Leibler divergence; (iii) masking the change map to obtain the final change areas. We propose to use the second kind statistics based parameter estimation method via Mellin transform to figure out the three parameters of G0 distribution. Experiment results indicate the second kind based G0 distribution model outperforms the moment based methods and can achieve a satisfactory result. [C645]

#### **"A generalized logical format for inter-calibrated brightness temperatures for the global precipitation measurement mission"**

An important aspect of the GPM mission is the merging of precipitation data from multiple radiometers on different satellites. This requires that each radiometer be consistently calibrated and that each be intercalibrated with a mission reference standard. For GPM the reference standard is to be the core satellite carrying a dual frequency precipitation radar and a well calibrated conically scanning radiometer. This paper describes a common format for representing these intercalibrated brightness temperatures which will be used for all radiometer products from GPM partner satellites. The use of common formats ensures that users obtain all the required information and also facilitates the rain retrieval algorithm code preparation as it can always expect to have the data that it needs for the retrieval. [C646]

#### **"A review of ionospheric effects in low-frequency SAR-Signals, correction methods, and performance requirements"**

Ionospheric signal distortions are commonplace in low-frequency space-borne SAR observations and can lead to the degradation of SAR data quality and data consistency if no signal compensation is applied. In this paper we will give an overview of the problem of ionospheric influence in SAR, PolSAR, and InSAR data. We will characterize the spatiotemporal signal properties of ionospheric signals, introduce a selection of currently available correction methods, and present a list of performance requirements to be met by ionospheric correction. [C647]

#### **"Impact of the wave number estimation in Underground Focusing SAR images"**

This work studies the impact estimating soil wave number in Underground Focusing SAR imaging for tunnel detection applications. It is demonstrated that poor underground imaging results when wave refraction at the ground surface is neglected, but that incorporating refraction with sufficiently high estimates of soil dielectric constant produce clear target images. Using a wrong wave number for the soil incorrectly predicts the tunnel's depth, but gives positive identification of its transverse and extent. [C648]

#### **"Glaciermonitoring: Correlation versus texture tracking"**

Synthetic aperture radar (SAR) images provide scattering information which can be used under any weather conditions for glacier monitoring. Our purpose is to estimate a displacement field characterizing at each position the local speeds and orientations of the glacier displacement. Recent proposed methods build a vector field by tracking patches between two SAR images co-registered on static areas and sensed at different times. The tracking is performed either by evaluating the correlations or the similarities from one acquisition to the other. We propose to estimate locally the displacement vectors by using either the maximum correlation or a maximum likelihood estimator. This local estimation is then refined to provide a sub-pixelic result. The efficiency of both methods are compared. [C649]

#### **"A non-local approach for SAR and interferometric SAR denoising"**

Recently, non-local approaches have proved very powerful for image denoising. Unlike local filters, the non-local (NL) means introduced in decrease the noise while preserving well the resolution. In the proposed paper, we suggest the use of a non-local approach to estimate single-look SAR reflectivity images or to construct SAR interferograms. SAR interferogram construction refers to the joint estimation of the reflectivity, phase difference and coherence image from a pair of two co-registered single-look complex SAR images. The weighted-maximum likelihood is introduced as a generalization of the weighted average performed in the NL means. We propose to

set the weights according to the probability of similarity which provides an extension of the Euclidean distance used in the NL means. Experiments and results are presented to show the efficiency of the proposed approach. [C650]

### "Data visualization and analysis tools for the Global Precipitation Measurement (GPM) Validation Network"

The Validation Network (VN) prototype for the Global Precipitation Measurement (GPM) mission compares data from the its predecessor Tropical Rainfall Measuring Mission (TRMM) satellite's Precipitation Radar (PR) to ground radar (GR) measurements from U.S. and international operational weather radars. This prototype is a major component of the GPM Ground Validation System (GVS). The VN provides a means for the precipitation measurement community to identify and resolve significant discrepancies between the GR observations and similar satellite observations. The VN prototype is based on research results and computer code Liao et al. [1]. Morris and Schwaller [3] describe the VN prototype and initial results in detail. This paper describes software tools that have been developed for visualization and statistical analysis of the original and volume matched PR and GR data. [C651]

### "New trends in SAR tomography"

In this paper a comparison between two techniques developed to recover layover solution in SAR images is presented. SAR Statistical Tomography and Compressive Sensing techniques are described and analyzed in order to provide a set of instruments for 3D SAR imaging able to tackle different scattering mechanisms in layover areas and to recover height reconstruction of an observed scene. The performances of the two techniques are compared on simulated data and some conclusions are drawn. [C652]

### "Monitoring tree farms and coastal environments using RADARSAT-2 PolSAR data"

This paper addresses the feasibility of using RADARSAT-2 fine Quad-Pol mode to monitor coastal environment and young tree growth. It will be shown that interferometric coherence may not be high enough for the height estimation of young trees at C-band, but polarimetric sensitivity could be used for tree and crop classification. For coastal environment, we found that polarimetric signature of oyster farm reveals the effect of double bounce scattering and the orientation angle effects. [C653]

### "Ultra-wideband radar measurements of snow thickness over sea ice"

An ultra-wideband, frequency modulated, continuous wave radar working from 2.0 to 6.5 GHz was designed, built and tested at the Center for Remote Sensing of Ice Sheets (CReSIS) at the University of Kansas to measure snow thickness over sea ice. Improvements and modifications to the existing radar, compared to previous versions, allow for snow thickness measurements from fast-moving, long-range aircraft. Over the past year, the radar has recorded snow thickness measurements over sea ice in the Arctic and Antarctic oceans as part of NASA's Operation Ice Bridge. [C654]

### "Effects of surface roughness on sea ice freeboard retrieval with an Airborne Ku-Band SAR radar altimeter"

Results from two years of the CryoSat Validation Experiment (CryoVEx) over sea ice in the western Arctic Ocean are presented. The estimation of freeboard, the height of sea ice floating above the water level, is one the main goals of the CryoSat-2 mission of the European Space Agency (ESA) in order to investigate sea ice volume changes on an Arctic wide scale. Freeboard retrieval requires precise radar range measurements to the ice surface, therefore we investigate the penetration of the Ku-Band radar waves into the overlying snow cover as well as the effects of sub-footprint-scale surface roughness using airborne radar and laser altimeters. We find regional variable penetration of the radar signal at late spring conditions, where the difference of the radar and the reference laser range measurement never agrees with the expected snow thickness. In addition, a rough surface can lead to biases of the airborne validation dataset, since the radar overestimates the amount of open water and thin ice as well the freeboard of heavy ice deformation zones. [C655]

### "Overview of SMOS Level 2 Ocean Salinity processing and first results"

SMOS (Soil Moisture and Ocean Salinity), launched in November 2, 2009 is the first satellite mission addressing the salinity measurement from space through the use of MIRAS (Microwave Imaging Radiometer with Aperture Synthesis), a new two-dimensional interferometer designed by the European Space Agency (ESA) and operating at L-band. This paper presents a summary of the sea surface salinity retrieval approach implemented in SMOS, as well as first results obtained after completing the mission commissioning phase in May 2010. A large number

of papers have been published about salinity remote sensing and its implementation in the SMOS mission. An extensive list of references is provided here, many authored by the SMOS ocean salinity team, with emphasis on the different physical processes that have been considered in the SMOS salinity retrieval algorithm. [C656]

### "Characteristic analysis of vehicle target in Quad-Pol Radarsat-2 SAR images"

Radarsat-2 satellite offers general users the Quad-Pol SAR image service with a resolution of 8 meters, which provides valuable data source for the research of traffic vehicles monitoring on Quad-Pol SAR images. According to the vehicle target in such new SAR images, this paper put forward a target characteristic analysis method, which is a combination of target RCS measurement and polarization decomposition. Moreover, it choose the large trucks as an example, give out a conclusion of characteristic analysis of vehicle targets through the on-site synchronous experimental data obtained at different incident angle. Thus provides the research foundation for further exploration of realizing the traffic monitoring with space-born Quad-Pol SAR images. [C657]

### "Rotated dihedral and volume scattering behavior in cross-polarimetric SAR"

In this study we analyze Radarsat-2 quadruple polarization (quad-pol) mode data acquired over the Everglades wetlands in south Florida. We analyzed the phase information of each polarization mode independently, and obtained similar fringe patterns representing water level changes in all four interferograms. It is surprising, because common scattering theories indicate that cross-polarization (cross-pol) observations reflect volume scattering due to the interaction of the radar signal with upper sections of the vegetation. However, our cross-pol interferometric observations suggest that the cross-pol signal reached the water surface and scattered back to the satellite by a rotated dihedral double bounce mechanism. Based on these new observations, we developed a new scattering formulation that accounts also for double bounce component in cross-pol. [C658]

### "Polarimetric and interferometric applications in a bistatic hybrid SAR mode using Terrasar-X"

A lot of bistatic experiments have recently been performed by different researchers to show the differences between monostatic and bistatic SAR. The acquired data was needed to verify the developed bistatic processing algorithms. To extend the conventional bistatic SAR experiments, we investigated whether bistatic systems can be used in the field of bistatic interferometry and polarimetry, also shown by [3]. For this purpose we have used our stationary receiver system together with TerraSAR-X as transmitting satellite. This paper describes the experiments and shows some results we obtained using single and repeat pass SAR configurations. [C659]

### "Calibration system stability plans for a long-term Ecological Airborne remote sensing project"

The National Ecological Observatory Network (NEON) Airborne Observation Platform (AOP) will fly an imaging spectrometer, small footprint waveform LiDAR and high-resolution digital camera to observe both the human drivers of climate change and the biological consequences of environmental change at a continental scale. The project is planned for a 30-year period. To be meaningful as an ecological climate data record, the AOP data set must have a continuous and consistent calibration effort. This paper briefly describes plans for the development of a robust calibration and validation plan to ensure data continuity from instrument-to-instrument, flight-to-flight, and year-to-year over the lifetime of the NEON project. [C660]

### "3D velocity model and ray tracing of antenna array GPR"

Migration is an important signal processing method that can improve signal-clutter ratio and reconstruct subsurface image. Diffraction stacking migration and Kirchhoff migration sum amplitudes along the migration trajectory, which generally is hyperbolic. But when the ground surface varies acutely, the migration trajectory is not hyperbolic. To computer the migration trajectory need the technique of ray tracing. We introduce a method of ray tracing based on 3D velocity model. Firstly, we build the 3D velocity model depending on the estimation of both ground surface topography and velocities. Then we compute the travel time between transmitter, receiver and each subsurface scattering point, and search the propagation ray depending on the Fermat's principle. The method is tested by an experiment data acquired by the stepped-frequency (SF) CMP antenna GPR system. The target is a metal ball that is buried under a sand mound. A nice result of ray tracing is shown in the case. [C661]

### "Progressive spatial clustering of content-based satellite imagery retrieval results"

The ProgressiveDBSCAN algorithm allows for the progressive clustering of results from a geospatial information retrieval system. Results can be clustered by a combination of both their spatial and non-spatial attributes. The benefit of this clustering is that users are able to sort through the results returned from a geospatial information retrieval system in a spatial context. No longer are results from disparate locations presented to the user, but

instead compact spatial clusters are displayed. There is a 98% reduction in the spatial distance between consecutive CBIR results and the spatial distance between the compact clusters; this leads to more efficient analysis of results by reducing the amount of time users spend context switching while on average only adding a few seconds to the query time. [C662]

### "Modification of slant range model and imaging processing in GEO SAR"

In this paper, considering the relative motion between satellite and earth during signal propagation time, the accurate analysis method for propagation slant range is presented in geosynchronous SAR. Furthermore, the difference between accurate analysis method and 'Stop-and-Go' assumption is analytically obtained. Meanwhile based on the derived accurate slant range model, it is found that the corresponding range migration correction and azimuth reference function must consider the high order term, and therefore the modified SPECAN algorithm is proposed. The simulation results verify the correctness of 'Stop-and-Go' assumption error derivation and SPECAN algorithm modification. [C663]

### "Operational evaluation of damages in flooded areas combining Cosmo-SkyMed and multispectral optical images"

The management of a flood event requires singling out the affected area, quantifying the damages and programming an effective rescue plan. This requires rapid and easy access to all the geographical and observational information available for the target area. Optical imagery allow the identification of land uses, critical infrastructures and the extraction of important information to quantify the actual vulnerability of the area. In this case, the main advantage of satellite imagery is the much higher refresh rate with respect to classical in-situ surveys. When floods occur, the detection of flooded areas allowed by SAR observations such as those provided by Cosmo-SkyMed, helps in rapid and effective evaluation of the damage and organization of the management of the crisis. Here we present an integrated system developed by the team of the Italian Space Agency pilot project "Opera". The system allows the end user to integrate multispectral high resolution imagery and Cosmo-SkyMed products, in a 3-D environment, providing all the tools to virtually survey the observed area and extract quantitative information for many features relevant to the emergency management. The system has been tested in real time on a prolonged flooding event occurred in January 2010 in the Shkoder plain in Albania. [C664]

### "A target tracking method with a single antenna using time-reversal UWB radar imaging in a multipath environment"

UWB (Ultra Wide-Band) radar systems are promising imaging tools covering a variety of application fields including surveillance systems. UWB radar technology can provide advanced capabilities for current surveillance systems. An imaging algorithm for UWB radars, the TR (Time-Reversal) method enables high-resolution imaging in a multipath environment. Conventional TR methods have been applied to antenna array systems while our previous work proposed a TR method with a low-cost single antenna-based system. In this study, we propose a radar system with a single antenna on a vehicle in a multipath environment. This vehicle is assumed to get close to a moving target by adaptively tracking the target location. Some numerical simulation results show that the proposed low-cost system works well in a multi-path environment. [C665]

### "ISAR imaging of maneuvering targets via matching pursuit"

An algorithm based on matching pursuit (MP) technique is proposed for inverse synthetic aperture radar (ISAR) imaging of maneuvering targets. The received ISAR echo is decomposed into many basis sub-signals that are generated by discretizing the target spatial domain and synthesizing the ISAR data for every discretized spatial position, and then the ISAR imaging problem is converted into the sub-signal selection problem. The basis sub-signals that indeed contribute to the ISAR echo are selected by using the MP technique, and the projection coefficients of the ISAR echo on the selected basis sub-signals represent the ISAR image. In the case of unknown rotation rate of the target, the true rotation rate is obtained by combining the MP technique with the maximum contrast search. Numerical examples show that the proposed algorithm can produce high resolution and remove sidelobe artifacts. [C666]

### "A method to estimate Snow Water Equivalent using multi-angle X-band radar observations"

Active microwave sensors, especially high-frequency radar systems, are highly sensitive to snow pack parameters, including Snow Water Equivalent (SWE). With the availability of several X-band space-borne SAR systems, the study attempts to make use of multiple-angle SAR observations and develop relevant SWE inversion algorithms. Analysis was carried out based on parameterized scattering models for both soil surface and snowpack. It is found that the backscattering signals at two incident angles are well correlated for both soil

surface and snowpack; and snow optical thickness can be well defined and estimated through snow volume scattering at two different angles. The snow and soil parameters can be estimated through two pairs of adjacent observations. The technique was tested using theoretical simulated database. Initial analysis shows that current technique needs to be further improved and a better estimation of single scattering albedo is needed. [C667]

### "Monitoring time-dependent volcanic dynamics at Long Valley Caldera using InSAR and GPS measurements"

Continuous monitoring Long Valley Caldera since the late 1970s, including data from seismic and geodetic networks has shown renewed episodic unrest activities with accelerated uplift separated by reduced uplift, no activity or slow deflation. We examine the time-dependent behaviors at Long Valley Caldera in 1996-2009 by integrating InSAR and continuous GPS (CGPS) measurements. The ERS-1/2 radar data between 1992 and 2008 and reprocessed three-component continuous GPS (CGPS) data from Long Valley GPS network in 1996-2009 were combined to invert for source geometry and volume change in the following deformation episodes: 97-98 uplift, 02-03 uplift, 04-07 slow subsidence, and 07-09 slow uplift. Our results show that all post-2000 events locate in the shallow depth range of ~7-9 km and have nearly identical source location, suggesting that these events are caused by the same partial melt magma source at the mid-crustal level. All three events are characterized by the low volume change, in comparison with previous 1997-1998 inflation event that has much larger volume change and steeper source geometry. If we regard post-2000 events as proxy for future eruption hazard, the inferred source dynamics (e.g., mid-crustal location and low volume change) from these post-2000 events suggest that the probability for near-term eruption is low. Our study demonstrates that CGPS, along with InSAR, are important tools in monitoring time-dependent source process at the active volcano region. [C668]

### "Spurious signal in measurement of the third Stokes parameter from space at L-band"

Spurious spikes in the third Stokes parameter have been observed in numerical simulations of the signal expected from the L-band radiometers to be flown as part of the Aquarius instrument. These signals are present over scenes with large contrast such as land water boundaries and are due to cross polarization coupling and the relatively large footprint of the antennas. [C669]

### "Individual tree species classification using structure features from high density airborne lidar data"

The paper investigated the advantage of high density airborne LiDAR data for improving species classification of individual tree. The investigation is comprised of two stages, feature extraction and classification. Several feature metrics were derived from LiDAR data, most of which were to characterize the vertical structural properties of difference species. Some other metrics were calculated statistically from intensity and return number information. A supervised decision tree algorithm was applied on the extracted features to perform both feature selection and classification. Two classification themes were carried out: classification of coniferous and deciduous trees, and classification of five species. Experiment was conducted in Canadian boreal forests dominated by mature trees. The results demonstrated LiDAR derived vertical profile metrics are capable for species classification either to separate coniferous and deciduous or to separate multiple species. The best overall classification accuracy is 81.7% validated by using the test data from the same ecosystem as the training data. [C670]

### "On the use of transponder measurements for high precision assessment and calibration of polarimetric Radarsat-2"

An independent assessment and calibration of polarimetric RADARSAT-2 (RS2) are conducted using transponder measurements extracted from uncalibrated data collected at various incidence angles between 20° and 40°. It is shown that RS2 antenna is highly isolated (better than -32 dB), and only crosschannel relative phase correction is required to provide calibrated data that meet comfortably the CEOS Cal-Val requirements. To take full advantage of the excellent RS2 performance in terms of low noise floor (-38 dB), transponder measurements are used for high precision assessment of RS2 calibration parameters. It is shown that the antenna cross-talks are stable with incidence angle, and only one transmitter-receiver distortion matrix is required for accurate calibration of the 20 modes of RS2 (Right looking) from 20° to 40°. A new method based on high precision transponder measurements is introduced for polarimetric RS2 calibration. Data collected at various incidence angles are used to validate the calibration. Transponder measurements using calibrated data indicate a residual cross-talk lower than -43 dB. The residual cross-channel error is lower than 0.3 dB in radiometry, and 5° in phase. [C671]

### "Biomass retrieval based on UAVSAR polarimetric data"

Parameters of vegetation spatial structure have important effect on the carbon cycle and biodiversity of the

ecosystems. How to estimate above-ground biomass is still a problem need to be worked out. In this paper we tried to use UAVSAR datasets to discuss the relation between backscattering coefficient and local incidence angle in different forest types. By the relation, a method based on scattering mechanism for correcting radiometric distortion caused by large range of incidence angle is developed. Biomass retrieval is based on incidence angle correction. The result shows good correlation between biomass and backscattering coefficient in 1 ha scale. [C672]

#### **"The Cloudsat Education Network: Scientifically significant collaborative research between students and scientists"**

The CloudSat Education Network (CEN) is the primary education and public outreach component of the CloudSat mission. Approximately 116 schools in 16 countries around the world participate in the CEN, and are recruited from schools in the GLOBE program. Students and teachers in the CEN make atmospheric observations of temperature, precipitation, and crucially, of cloud type and cloud cover amount (including photographs of cloud observations), using a modified GLOBE Atmosphere protocol as a guide for observations. CEN observations are taken coincident with CloudSat overpasses, providing coincident spaceborne- and student surface observations. A preliminary comparison study using CEN-collected observations of cloud type during the period from 2007-2008 compared the observed cloud types to those retrieved using the CloudSat 2B-CLDCLASS product. In this preliminary study, there were 227 coincidental measurements between CEN schools and CloudSat overpasses, with an agreement rate of approximately 66% between the surface observers and satellite observations. [C673]

#### **"A nonlocal approach for SAR image denoising"**

Speckle reduction is a key step in several SAR image processing procedures. In this paper, a new despeckling technique based on the "nonlocal" denoising filter BM3D [1] is presented. The filter has been modified in order to take into account SAR image characteristics. The experimental results, conducted on both synthetic and real SAR images, confirm the potential of the proposed approach. [C674]

#### **"Global laser pulse reflectance at 1064 nm of snow and land surfaces from the Glas satellite Lidar"**

During the development of the Geoscience Laser Altimeter System (GLAS), launched in 2003, it was understood that the values of surface pulse reflectance was an important design parameter for satellite laser altimeters and that the magnitude of observed pulse reflectance would have valuable applications. Thus a significant effort was made to obtain calibrated surface pulse reflectance from GLAS measurements. In this paper we describe the calibration and atmospheric correction procedures and present global measurement results for earth surface laser pulse reflectance. [C675]

#### **"PSI analyses of land subsidence due to economic development near the city of Hangzhou, China"**

In this work we mapped the spatial and temporal patterns of the land subsidence near the city of Hangzhou, China by PSI analysis with 49 scenes of ERS-1/2 SAR images acquired from 1992 to 2006 to detect and retrieve the subsidence due to economic development. The main reason of land subsidence in Hangzhou is groundwater exploitation, which is necessary for the rapid economic development, especially in China. Xiaoshan Economic and Technological Development Zone was approved as a state-level development zone by the State Council in May, 1993. Since then the zone has been suffering land subsidence. There have been more than 300 overseas-funded enterprises with investors from 26 countries and regions by the year 2006. The development of this area can be divided into three periods according to its pace: construction period (1993-1996), stable increase period (1996-2001) and high-speed period (2001-2006). [C676]

#### **"C- and Ku-band (at 5.6GHz and 13.6GHz), dual-frequency, multi-polarization, short pulse, combined scatterometer-radiometer system for low altitude platform, vessel and aircraft applications"**

In this paper C-, and Ku-band, dual frequency, multi-polarization, combined, short-pulse scatterometer-radiometer system is described, for short (from low altitude platform), middle (from vessel) and long (from aircraft) distance remote sensing applications for water surface, soil and land snow cover's microwave reflective and emissive characteristics simultaneous and spatially coincident measurements. [C677]

#### **"Change detection for earthquake damage assessment in built-up areas using very high resolution optical and SAR imagery"**

Information on the impact of catastrophic events (e.g. earthquakes) can be derived from suitable satellite imagery by comparing data from a chosen reference before the event (pre-event) to imagery acquired shortly after the event (post-event). In this paper, we propose a novel method that detects buildings destroyed in an earthquake using pre-event very high resolution (VHR) multispectral and post-event detected VHR synthetic aperture radar (SAR) imagery. The core concept of the proposed method is the evaluation of the presence of the predicted undamaged building SAR signature in the post-event SAR scene. The decision if a building belongs to the damaged or undamaged building class is performed with a Bayesian classifier, trained either in a supervised or unsupervised manner. We show the results of the proposed method using VHR TerraSAR-X and COSMO-SkyMed, as well as VHR optical data for a subset of the town of Yingxiu, China, which was heavily damaged in the 2008 Sichuan earthquake. [C678]

#### **"Investigation of forest height retrieval using SRTM-DEM and ASTER-GDEM"**

Interferometric SAR (InSAR) data have been used to measure canopy height. Polarimetric interferometric SAR (PolInSAR) data can be used to derive canopy height without using ground surface elevation data. But in most cases, only single polarization InSAR data are available and the elevation of ground surface in the forested areas is needed to get the height of the scattering phase center. On contrary, the elevation of canopy surface is relatively easy to obtain by Stereo imagery. In this study the feasibility of the estimation of forest height using SRTM-DEM and ASTER-GDEM was investigated. The ASTER-GDEM was firstly resampled to the pixel size of SRTM-DEM (3 arc-second) and then was registered to SRTM-DEM using the points selected from their aspect maps. The results showed that the registration is necessary because the geolocation error at east-west direction is about half of the pixel size. The relationship between the forest height and the elevation difference was analyzed. The results showed that the elevation difference between registered ASTER-GDEM and SRTM-DEM is positively correlated with the forest height. Although there are some problems when the terrain is rough, it provides us a way to estimate the height of mature forest in flat terrain. [C679]

#### **"A phase screen simulator for predicting the impact of small-scale ionospheric structure on SAR image formation and interferometry"**

We describe the SAR Scintillation Simulator (SAR-SS), a new phase screen model for simulating the impact of small-scale ionospheric structure on SAR image formation and interferometry. We compare simulated and observed PALSAR imagery over Brazil, and our preliminary findings show that SAR-SS can reproduce the essential features of azimuthal streaking and contrast degradation caused by small-scale structure in the ionosphere. [C680]

#### **"Coherent scatterer in forest environment: Detection, properties and its applications"**

In this paper, the first detection result of coherent scatterers (CSs) in forest environment is addressed. As a scatterer associated with CS, the dihedral structure consists of the tree-trunk like a vertical cylinder and the ground surface is assumed. The potential of CSs as being the phase stable scatterers as permanent scatterers will be also demonstrated with P-&L-band Pol-InSAR datasets acquired in repeat-pass InSAR mode over boreal forest test site by German Aerospace Center's E-SAR airborne system. [C681]

#### **"Modeling attenuation of melting hydrometeors with a method based on volume integral equations"**

The attenuation of spheroidal melting hydrometeors is simulated in C-, Ku- and Ka-band utilizing a microphysical melting layer model. The scattering properties are obtained with Mie scattering solution. In C-band the polarimetric radar parameters are computed utilizing a method based on volume integral equation. Polarization difference is detectable, but reflectivity values are regularly smaller than those calculated with Mie solution. This is dependent on the process of formatting the particle structure according to the change in liquid water mass fraction. [C682]

#### **"Accurate focusing of single-pass airborne InSAR data at L-band"**

Long wavelength airborne single-pass InSAR systems call for very accurate SAR focusing and motion compensation algorithms. We have analyzed 3 different techniques and evaluated their performance using real data acquired with an L-band single-pass interferometer in Canada. Time domain backprojection with terrain-dependent motion compensation shows the best performance with results close to the theoretically expected values. [C683]

#### **"Rotation and scale invariant template matching applied to buried object discrimination in GPR data"**

In this study, a template matching approach to buried object discrimination problem is proposed over ground penetrating radar (GPR) B-scan images. The technique is scale invariant, which compensates for the change in the swinging speed of the detector. It is also rotation invariant to some extent, which reduces the number of templates to be used by compensating for the change in the scanning direction. The algorithm is tested on real GPR data and results are observed to be promising. [C684]

### "Mapping urban subsidence with TerraSAR-X data by PSI analysis"

With a spatial resolution of up to 1 m, the German radar satellite TerraSAR-X has significantly improved the applicability of spaceborne SAR interferometry (InSAR) technique for fast ground motion monitoring due to its high spatial resolution and short time interval. In this work we present the first Permanent Scatterer Interferometry analysis with TerraSAR-X data for urban subsidence mapping in Tianjin city in China. Totally 17 scenes strip mode SAR images have been collected from Feb to Oct 2009 to perform the PSI analysis. The resulted average subsidence velocity demonstrates the ability of high resolution data for detailed monitoring of urban subsidence. Comparison between PSI result of TerraSAR-X and ENVISAT show the potential of TerraSAR-X data for urban motion as well as large scale manmade linear infrastructure monitoring. [C685]

### "Landslide detection by indices of LiDAR point-cloud density"

The deliverables of an airborne LiDAR survey usually include all points, ground points, digital surface models (DSM) and digital elevation models (DEM). Indices of point clouds tested in this study include density of all points, density of ground points, density of only returns, and density of multiple returns. Shallow landslides are the most common landslides triggered by torrential rainfalls and explicit fresh scars after rainfall events. Multiple returns in forest area give the possibility of differentiating landslide scars from vegetated lands. Classification results from the indices derived from these four kinds of densities are verified by the result obtained by manual interpretation of the derived nDSM images. The experiment is carried out using the dataset obtained in I-Lan County after Typhoon Kalmaegi on 17 July 2008. The results show that a proper definition of the parameters for the indices is most critical for the detection of shallow landslides. [C686]

### "3D subsurface visualization by suppressing ground reflection and direct wave with bistatic GPR"

A ground reflection and a direct wave which propagates directly from a transmitting antenna to a receiving antenna are often arisen as issues especially for a ground penetrating radar (GPR) to monitor a near-surface region. In this paper, a 3D subsurface radar image by suppressing those components with a bistatic GPR system is presented. A relative permittivity of a ground surface is measured at the beginning, and a Brewster angle is estimated from that value. Then, the transmitting antenna is located to match an incident angle with the Brewster angle. In this case, the ground reflection does not occur, and all the energy penetrates into the ground. The direct wave is suppressed with an f-k filter which works automatically from position information of the antennas. An experimental result gives the 3D subsurface image without the ground reflection and the direct wave under a condition that a landmine model is buried at a depth of 10cm in a dry sand. [C687]

### "Studies of radio frequency interference at L-band using an airborne 2-D interferometric radiometer"

Potential radio frequency interference (RFI) sources at L-band include L-band radars; mobile, navigation and other satellite services; and various land services. We have collected data using our airborne L-band interferometric HUT-2D radiometer in order to support the ESA SMOS mission. We participated in April-May 2008 in ESA's rehearsal campaign for SMOS satellite validation activities in Germany and Spain. Additional data have been collected in Finland. Two basic categories of RFI have been observed: (1) Point-wise weak sources that do not saturate the HUT-2D instrument, and (2) strong sources that totally saturate the sensor over a large area. [C688]

### "Tidal current measurement with TerraSAR-X Along-Track Interferometry"

In this paper we describe new achievements of surface current measurements obtained by space-borne Along-Track Interferometry (ATI). We show how tidal currents can be mapped using the TerraSAR-X satellite and adequate dual-channel SAR data processing techniques. We present results from tidal currents at the Orkney Islands that clearly demonstrate the potential and suitability of the method. [C689]

### "Environmental monitoring with the imaging MIMO radars MIRA-CLE and MIRA-CLE X"

Several applications need imaging sensors for environmental monitoring which can continuously observe an area in a 24/7 mode independently from the weather and other atmospheric obscuration like dust and smoke. Imaging

MIMO radar fulfills these requirements and enables the opportunity of low-cost and robust imaging systems by synthesizing many virtual antennas out of just a few real ones. MIRA-CLE is a fully configurable and expandable experimental MIMO radar in Ka-band while MIRA-CLE X works in X-band and is intended to be a low-cost experimental system for long range applications. This paper presents both MIMO radar systems and shows and discusses first imaging results of MIRA-CLE X. [C690]

### "Modular Radar Core for airborne and space applications"

The development of Radar Core electronics for any airand spaceborne radar units has a long space heritage at EADS in Friedrichshafen. It encompasses the spaceborne radars SIR-C/ X-SAR, SRTM, TerraSAR-X, TanDEM-X, and the oncoming PAZ mission and many airborne missions. These missions demonstrated successfully the high end radar electronics performances. EADS initiated a product development program called SmartRadar (Scalable modular aerospace radar technology) for the next generation airborne and space radars. The Radar Core development is one step in the SmartRadar development road map at EADS. To summarise the status of the development: the new hardware and related software have been flown in a demonstration flight campaign in summer 2009. For this campaign the frequency band was chosen to be at XBand to use an available Reflector Antenna and Travelling Wave Tube Amplifier (TWT) and Front end equipment. Synthetic Aperture Radar (SAR) image results are of very good quality and performance parameters analysed from the recorded raw data match or exceed the chosen design parameters. [C691]

### "Integration of InSAR and GIS for an estimation of ground subsidence susceptibility"

Ground subsidence susceptibility at a coal mine by integration of L-band SAR measurements and a subsidence hazard model incorporated in GIS was estimated. A subsidence hazard map was constructed using JERS-1 SAR data from the early 1990s and the subsidence hazard model. A certainty factor analysis was employed for estimating the relative weights of four control factors influencing coal mine subsidence. The relative weight of each factor was then integrated to generate a subsidence hazard index (SHI) by a fuzzy combination operator. The hazard map was validated by comparison with subsidence observed by ALOS PALSAR interferometry in 2007-2008. The results showed a good agreement between the predicted locations vulnerable to subsidence and the actual subsidence occurrences with an accuracy of about 72.5%. These results showed that the map produced by integration of InSAR and GIS can be used to predict and monitor coal mine subsidence hazards, especially in remote regions. [C692]

### "Using lidar to estimate the capacity for storm water recycling and solar energy collection"

In this paper two lidar applications are addressed so that the data from large-scale airborne laser scanning of three New South Wales towns and the University of New South Wales can be used to estimate the capacity for storm water recycling and solar energy collection. The building outlines in each of these surveyed areas are extracted using the lidar point cloud to provide an accurate measurement of the total area of roofing within each region. The accurate area measurements are used with simple modelling equations to calculate the amount of rainfall runoff that could be collected and solar energy that could be produced, during an average year. The final results show the potential savings that could be produced each year if these towns and the university campus became more water and energy conscious. [C693]

### "Advances in the generation of deformation time series from SAR data sequences in areas affected by large dynamics"

We propose advances on the generation of deformation time series in areas affected by large deformation dynamics, where the exploitation of the differential SAR phase can be strongly limited by severe misregistration errors or by very high fringe rates. First, to overcome the former issue, we present an extension of the amplitude-based Pixel-Offset (PO) analyses by applying the Small BAseline SubSet (SBAS) strategy, in order to move from the investigation of single (large) deformation events to that of dynamic phenomena. Secondly, to handle the high fringe rate interferograms, we subtract from them properly generated synthetic deformation models allowing us to reduce the fringe rate, thus helping the phase unwrapping step. The proposed approaches have been tested on ASAR-ENVISAT data acquired on Galapagos Islands and validated via continuous GPS measurements. [C694]

### "Microwave remote sensing for marine monitoring: An example of Enteromorpha prolifera bloom monitoring"

The bloom of algae called Enteromorpha prolifera posed a potential threat to the Olympic sailing competition in June 2008. Synthetic Aperture Radar (SAR) technology plays an irreplaceable role in algal blooming monitoring.

Based on the analysis of various influence factors, a procedure for E.P. detection is proposed. In this paper, multi-temporal SAR images especially with short time interval, currents datum from buoys and wind products retrieved from SeaWinds scatterometer have been employed for E.P. dynamic monitoring and drift trend analysis. The result of analysis shows SAR, currents and wind datum are available for forecasting the trend of the E.P. drift. [C695]

#### "Monostatic calibration of both TanDEM-X satellites"

The primary object of the TanDEM-X mission is to generate a highly accurate digital elevation model (DEM) with never achieved accuracy on global scale. But in addition to this bistatic TanDEM-X mission the monostatic TerraSAR-X mission have to be operated in parallel with both satellites. Consequently the second satellite TDX, successfully launched in June 2010, has to achieve the same accuracy and performance as those of the first satellite TSX, already in-flight since 2007. Thus, the monostatic calibration of the second satellite TDX is performed according to the same strategy based on effective and exact calibration techniques successfully demonstrated by the first satellite TSX. The paper discusses the calibration results of the first satellite TSX derived two years after launch by an extended re-calibration campaign executed in summer 2009, and presents first results of the second satellite TDX. But it has to be mentioned, the main calibration activities of TDX will start three weeks after launch, i.e. after uploading of this paper. [C696]

#### "Towards an improved wind and rain backscatter model for ASCAT"

The ASCAT scatterometer measures the backscatter from the ocean surface with which it infers the near-surface wind vector. When rain is present in the observation area the wind-induced backscatter is modified by the rain. This paper uses co-located observations from TRMM PR to model the effects of rain on the ASCAT observed backscatter. Two model types are considered, a phenomenological rain model and a lumped effect rain model which are comparable for most rain rates. For low rain events the ASCAT observed backscatter due to rain is not substantial, however for moderate to high rains the rain-induced backscatter from the ocean surface can be significant, and for extreme rain rates the atmospheric scattering and attenuation are dominant. [C697]

#### "Gulf stream thermal fronts detected by synthetic aperture radar"

Our objective is to detect ocean surface features, specifically oceanic thermal fronts, through analysis of SAR (synthetic aperture radar)-derived wind stress fields. Fine-resolution measurements of near-surface wind speeds over the Gulf Stream region of the Northwest Atlantic were made using SAR images collected by RADARSAT-2. Linear statistical relationships between the wind stress curl and divergence to the crosswind and downwind components of the sea surface temperature (SST) gradient field were used to derive a new method for detecting Gulf Stream thermal fronts from Synthetic Aperture Radar (SAR) imagery. In particular, sea surface temperature front features, as suggested by corresponding AVHRR and MODIS images, are evident in both of the wind stress curl and divergence fields. [C698]

#### "Ultra-rapid optronic processor for instantaneous ENVISAT/ASAR scene observation"

This paper introduces a real-time compact optronic SAR processor that has the capability to generate ENVISAT/ASAR image swaths of 100 km  $\times$  100 km in 10 seconds exhibiting slant plane sampling distances of 4 meters in azimuth and 1 meter in range. It may be instantaneously reconfigured to process data from any of the 7 ASAR image swath modes. In this respect, numerous SAR image sets may be produced immediately on-demand without bottleneck. A rapid SAR processor that also provides fine ground sampling distances in both azimuth and range directions could provide benefits for such applications as ship detection, landslide and flood monitoring, snow and ice coverage and glacier monitoring. [C699]

#### "Automated Polar ice thickness estimation from radar imagery"

This work focuses on automating the task of estimating Polar ice thickness from airborne radar data acquired over Greenland and Antarctica. This process involves the identification and accurate selection of the ice sheet's surface location and interface between the ice sheet and the underlying bedrock for each measurement. Identifying the surface and bedrock locations in the radar imagery enables the computation of ice sheet thickness, which is important for the study of ice sheets, their volume, and how they may contribute to global climate change. The time-consuming manual approach requires sparse hand-selection of surface and bedrock interfaces by several human experts, and interpolating between the selections to save time. [C700]

#### "Building height extraction via a deterministic approach using a TerraSAR-X data stack"

A method for building height determination via a deterministic approach is tested using three TerraSAR-X images

from Barcelona, Spain. Using this method, the height of a building wall can be determined based on the strength of the double-bounce backscattering. The approach requires knowledge of the material properties of the measured building wall and the area in near range of the building wall. For certain test buildings the approach provides good results, while for other buildings the results are erroneous. [C701]

#### "Rain effect on polarimetric SAR observation"

The purpose of this paper is to consider the radio wave propagation of Polarimetric SAR in rain and to verify the influence of rain quantitatively. We assume the Polarimetric SAR observation model in non-spherical rain drop environments and evaluate the influence of rain at 5.405, 9.65 and 13.9GHz by calculating the rain distortion matrix with parameters of rainfall rate and the rain drop canting angle. The results show that the rain attenuation, the attenuation difference between horizontal and vertical polarization, and the cross-polarization factor increase as the frequency and rainfall rate increase, and they depend on the rain drop canting angle and the incident angle. [C702]

#### "Global trends in remote sensing of human settlements"

Advances in both airborne and spaceborne remote sensing systems have provided a range of tools for monitoring and managing human settlements. In particular the availability of very high spatial resolution satellite systems has dramatically increased access to high quality two-dimensional spatial information, while laser profilers and interferometric synthetic aperture radar have allowed acquisition of the third dimension. Over the past 100 years sensor systems have changed dramatically, from early airborne cameras that imaged only small parts of an urban area on a project return basis, to very high resolution spaceborne systems, covering a wide spectral range, with regular return periods down to a few weeks or days. This paper provides a brief history of urban remote sensing, followed by an examination of the properties of current systems and their acquired data, some processing methods and urban applications. It concludes with an overview of future developments. [C703]

#### "CRInSAR for landslide deformation monitoring: A case in threegorge area"

Landslide in threegorge area is a severe geohazard threatening many people. Conventional differential SAR interferometry (DInSAR) and Persistent Scatterers for SAR interferometry (PSInSAR) technique are unsuitable for landslide deformation monitoring in this area due to temporal and lack of natural phase stable point targets. The method of DInSAR using corner reflectors (CRInSAR) is a powerful tool in the vegetation area. The procedure of DInSAR using corner reflectors (CRInSAR) used by this paper is briefly introduced. Using ENVISAT ASAR time series data, the deformation of 12 corner reflectors (CR) in Shuping landslide are analyzed. As to the CR with slow creep deformation, the CRInSAR results are reliable. But as to the CR with nonlinear accelerated deformation, our CRInSAR method still needs to be enhanced. [C704]

#### "Support vector machines regression for estimation of forest parameters from airborne laser scanning data"

Estimation of forest stand parameters from airborne laser scanning data relies on the selection of laser metrics sets and numerous field plots for model calibration. In mountainous areas, forest is highly heterogeneous and field data collection labour-intensive hence the need for robust prediction methods. The aim of this paper is to compare stand parameters prediction accuracies of support vector machines regression and multiple regression models. Sensitivity of these techniques to the number and type of laser metrics, and use of dimension reduction techniques such as principal component and independent component analyses are also tested. Results show that support vector regression was less accurate but more stable than multiple regression for the prediction of forest parameters. [C705]

#### "The Soil Moisture Active Passive (SMAP) mission L-Band radar/radiometer instrument"

The Soil Moisture Active/Passive (SMAP) mission is a NASA mission identified by the NRC "decadal survey" to measure both soil moisture and freeze/thaw state from space. The mission will use both active radar and passive radiometer instruments at L-Band. In order to achieve a wide swath at sufficiently high resolution for both active and passive channels, an instrument architecture that uses a large rotating reflector is employed. The active radar will further utilize SAR processing in order to obtain the sub-footprint resolution necessary for the geophysical retrievals. The SMAP radiometer uses a more conventional real-aperture resolution, albeit with a significantly larger antenna than flown before. Both the SMAP radar and radiometer must address the effects of radiofrequency interference (RFI). [C706]

#### "Extraction of area-averaged orientation angle from POLSAR measurement"

We have shown that area-averaged structure orientation angles relative to incident angle of POLSAR in urban area can be estimated from argument of correlation coefficient of circularly-polarized observation bases. It is quite interesting that by this approach we can estimate area-averaged urban parameters even if we can not distinguish them from conventional received signal component intensity map due to lack of spatial resolution.

[C707]

#### "Stap based ground moving target detectability in the airborne/spaceborne array radar"

A space-time adaptive processing (STAP) can be effective in detecting the ground moving targets from the airborne/spaceborne moving platform in the severe ground clutter and jammer environments. In this paper, the characteristics of target, ground clutter and jammer signals are analyzed and designed the adaptively weighted clutter notch filter in two dimensional spatial and temporal azimuth angle-Doppler domains. The simulation is performed for ground moving target detection by rejecting both clutter and jammer simultaneously through the STAP processing. The probability of target detection is investigated depending on the SNR and the minimum detectable velocity (MDV) in the given false alarm rate. The simulation results show that the MDV can be ideally achieved up to 2 m/s ~ 3 m/s at the 90 % of detection probability in the given false alarm rate of 10<sup>-3</sup> and 10<sup>-6</sup>. This technique may be applied for the surveillance and traffic monitoring of moving vehicle on the road. [C708]

#### "Quantification of the topographic slope from radar satellite imagery"

A specificity of Synthetic Aperture Radar (SAR) scenes is to display geometric distortions depending on both the system of acquisition and its relation with the topography. Establishing the geometric relationship between the radar sensor parameters and the related surface deformation should therefore provide quantitative information on the topographic surface. Here, we propose a new technique for the computation of the terrain slope, which is based on the quantification of the geometric deformation generated during the acquisition of a SAR scene. The method uses a pair of radar scenes consisting of an orthorectified image and another in slant-range geometry to compute the local topographic slope of a reference ground segment identified on both images. Computed slope values using ENVISAT-ASAR and TerraSAR-X images and compared with measurements taken in the field in the Djebel En Negueb anticline located in south-central Tunisia reach 3° with both data. [C709]

#### "Deformation in Hawaii's volcanoes obtained from a ScanSAR-to-stripmap Small BASeline Subset technique"

We investigate the displacement phenomena affecting Mauna Loa and Kilauea volcanoes at Big Island (Hawaii, USA), by applying an advanced ScanSAR-to-stripmap differential Synthetic Aperture Radar Interferometry (InSAR) approach. The implemented method, based on the application of the well-known Small BASeline Subset (SBAS) technique, allows the generation of LOS mean deformation velocity maps and corresponding time series, leading us to characterize the complex deformation of Mauna Loa and Kilauea volcanoes. The presented analysis relies on the use of a SAR dataset composed by 49 ASAR ENVISAT satellite images, relevant to both stripmap and ScanSAR operational modes, acquired on descending orbits (track 200) from January 2003 to September 2008. Moreover, in order to assess the quality of the proposed combined ScanSAR-to-stripmap approach, we perform a comparison between the achieved DInSAR results and the LOS-projected GPS displacement measurements. [C710]

#### "Analysis of the effect of radio frequency interference on interferometric phase"

The P-band ultra wideband synthetic aperture radar shares the band with other services, as for example TV broadcast and telecommunications transmitter stations, means distortion by radio frequency interference (RFI) to the SAR. It's well known the performance of UWB-SAR is degraded due to the existence of radio frequency interference. This paper describes the problems of RFI in InSAR, and analyses the effect of RFI to interferometric phase based on simulation. [C711]

#### "Shadow region imaging algorithm using array antenna based on aperture synthesis of multiple scattered waves for UWB radars"

Ultra-wide band (UWB) pulse radar has a definite advantage over optical ranging techniques, as to applicability to the harsh optical environment, such as the dark smog, or strong back-light. We have already proposed the extended Synthetic Aperture Radar (SAR) algorithm employing the multiple scattered waves, which aims at enhancing the reconstructible region of the target boundary including the shadow. However, it still suffers from the shadow region in the case of the target with a sharp inclination or deep concave boundary, because it assumes the antenna scanning whose real aperture size is too small. To resolve this difficulty, this paper proposes an extension algorithm using the array antenna model. While this extension is quite simple, the

effectiveness of the proposed method is nontrivial regarding to the expansion of the imaging range. The results from numerical simulations verify that our method remarkably enhances the visible range of target surfaces without a priori knowledge of target shapes or a preliminary observation of its surroundings. [C712]

#### **"Electromagnetic scattering from arbitrary random rough surfaces using stabilized extended boundary condition method (SEBCM) for remote sensing of soil moisture"**

In this paper, the stabilized extended boundary condition method (SEBCM) is developed based on the classical EBCM to solve both 2D and 3D electromagnetic scattering from arbitrary random rough surfaces. The SEBCM gives accurate full wave solutions over large range of surface roughnesses and medium losses, which are far beyond the validity range of analytical methods, and perform with much higher efficiency than numerical methods. These properties make SEBCM a competitive forward model in the inverse problem for soil moisture retrieval from radar measurements. [C713]

#### **"Code sequence selection for SAR radiometric calibration"**

It is an important significance for SAR radiometric calibration accuracy to select a proper code sequence about active coded transponder (ACT), in the process of active coding radiometric calibration using synthetic aperture radar (SAR). According to the principle of active coding radiometric calibration, a signal processing model of active coded reflected signals is proposed in this paper. And  $m$  sequences, Gold sequences and random sequences are studied. Simulation experiments with the compression of SAR azimuth signals are carried out. [C714]

#### **"2D uesprit superresolution SAR imaging algorithm"**

One of the driving forces of the development of SAR image formation has been to obtain better and better image resolution. Conventional radar imaging methods based on Fourier transform provide good resolution as long as the backscattered data is available over a large bandwidth and a sufficient aspect region. The paper proposes a 2D Unitary ESPRIT superresolution SAR imaging method exploiting that the SAR image in phase history domain is a band-pass function with a main frequency support domain. Thus, the problem of superresolution SAR imaging is transformed to solve sinusoid harmonic estimation, which can be solved by 2D Unitary ESPRIT. From the experiments using simulation and measured data, we can see better resolution obtained by the method of the paper than the FFT method. [C715]

#### **"SAR focusing of P-band ice sounding data using back-projection"**

SAR processing can be applied to ice sounder data to improve along-track resolution and clutter suppression. This paper presents a time-domain back-projection technique for SAR focusing of ice sounder data. With this technique, variations in flight track and ice surface slope can be accurately accommodated at the expense of computation time. The back-projection algorithm can be easily parallelized however, and can advantageously be implemented on a graphics processing unit (GPU). Results from using the back-projection algorithm on POLARIS ice sounder data from North Greenland shows that the quality of data is improved by the processing, and the performance of the GPU implementation allows for very fast focusing. [C716]

#### **"A test statistic for high resolution polarimetric SAR data classification"**

Modern SAR systems have high resolution which leads the backscattering clutter to be non-Gaussian. In order to properly classify images from these systems, a non-Gaussian noise model is considered: the SIRV model. A statistical test of equality of covariance matrices is used to classify pixels, taking into account the critical region of the test which rejects the likeliness of a covariance matrix to any of the class centers. This test is applied on experimental data obtained with the ONERA RAMSES system in X-band. The results show a good separation between natural and man-made areas of the image. [C717]

#### **"Investigating co-seismic deformation of the 2008 Wenchuan earthquake with ALOS SCANSAR interferometric observations"**

On May 12th, 2008, a destructive earthquake of magnitude 8.0 struck Wenchuan. The seismic region is located at the transition zone between Qinghai-Tibet Plateau and the Sichuan Basin, which has a complex geological tectonic background. In this paper, we intend to investigate the Wenchuan earthquake using the Differential Interferometric SAR (D-InSAR) technique. Due to the large scale of the crustal deformation affected by the disastrous earthquake, SCANSAR images show more advantages than conventional strip-map mode images. And taking account the vegetation conditions, the L band images are suitable than the C band images for our study. Therefore, we choose to use ALOS SCANSAR interferometric observations to obtain a preliminary co-

seismic displacement field of the Wenchuan earthquake. [C718]

#### "Evaluation of the influence of the polarimetric calibration process on the H/A/ $\alpha$ decomposition"

The objective of this article is to evaluate the influence of the cross-talk and channel imbalance calibration on the estimation of the entropy and the  $\alpha$  images. Few studies can be found in SAR literature concerning the influence of the polarimetric image calibration process on the target decomposition methods and their consequences on the characterization and discrimination of different ground targets. This influence is illustrated here by using a methodology based on an L-band fully polarimetric SAR data acquired by the SIPAM (Amazon Protection System) airborne R99-SAR over two areas of study, located in the Brazilian Amazon Forest and urban area regions. [C719]

#### "Analysis and compensation for motion errors in FMCW SAR data"

In this paper, we present a motion error model for a Frequency-Modulated Continuous-Wave (FMCW) SAR system, and analyze the characteristics of the intrapulse motion error. Furthermore, we develop an effective compensation approach to handle motion errors based on our previous result. Finally, we validate the formulated signal model and compensation method by using simulated FMCW SAR data. [C720]

#### "The extended SBAS technique for generating full resolution ERS/ENVISAT deformation time-series"

In this work we extend the Small Baseline Subset (SBAS) Differential SAR Interferometry approach to allow the generation of deformation time-series by processing long sequences of ERS-1, ERS-2 and ENVISAT SAR data at the full spatial resolution scale. Our idea is to avoid the generation of ERS/ENVISAT cross-interferograms, severely affected by noise phenomena, and to consider single-platform interferograms only (i.e. ERS/ERS and ENVISAT/ENVISAT interferograms), that are properly combined by applying the SVD-based SBAS approach. The presented results, achieved on two datasets relevant to the Napoli Bay area and to the Murge region (Italy), confirm the effectiveness of the presented technique and demonstrate the relevance of deformation analysis carried out at the scale of single buildings with more than 15 years of ERS and ENVISAT acquisitions. [C721]

#### "Multi-frequency and polarimetric measurements of snow microwave reflection and emission by C- and Ku-band, combined scatterometer-radiometer systems"

In this paper the results of simultaneous and spatially coincident, dual-frequency (at C- and Ku-band), multi-polarization measurements will be represented, of bare soil and snow microwave reflective (radar backscattering coefficient) and emissive (brightness temperature) characteristics angular dependences at 5.6GHz and 15GHz. [C722]

#### "Progressive SAR imaging technique"

A progressive SAR imaging technique is proposed as a novel SAR raw data processing scheme in this paper. Different from the classic SAR imaging algorithms which focus the SAR raw data as a whole regardless of the backscattering signal, the novel scheme discriminates the backscattering signal and chooses the proper ones to be focused progressively according to some application context while the others will be discarded. The new scheme makes the SAR imaging algorithm not only focus the energy back to the scattering points but also form an image more suitable for some special applications. In this paper, a realization of the scheme is presented via Atomic Decomposition (AD)[1]-[3]. AD helps estimate the parameters of backscattered signal of a scattering point and detach it from the raw data. With the parameters, the backscattering-signal can be reconstructed and focused. Targets or scatter-points in the scene will be imaged progressively in a sequence of their energy due to the greedy nature of matching pursuit employed during AD. Therefore, the contents in the final SAR image can be controlled by an energy threshold. Besides the interested targets can be extracted easily from the background clutter and this may be helpful for the SAR image understanding. [C723]

#### "Evaluation of the self-consistency principle for calibration of the CASA radar network using properties of the observed medium"

The Center for Collaborative and Adaptive Sensing of the Atmosphere (CASA) has deployed a Distributed, Adaptive and Collaborative Sensing (DCAS) network of four radars in central Oklahoma. The radars operate at the X-band frequency and are capable of polarimetric and Doppler measurements. The radar network is being evaluated for Quantitative Precipitation Estimation (QPE). QPE algorithms based on radar power measurements (e.g. Z-H and ZDR) require bias correction. The polarimetric self-consistency principle is applied to the CASA radar data to estimate any bias in ZH. Results show a ZH calibration accuracy of 0.6 dBZ or less for two the

analyzed events. ZHbias estimates from the self-consistency principle in rainfall are compared and validated with ZHbias estimated from the comparison of the X-band and the S-band radars' data. Comparison of the two approaches shows a difference in the ZHbias estimation of 0.61 dBZ or less and validates the use of the self-consistency principle in rainfall for the absolute radar calibration of the CASA radars. [C724]

#### "A novel range migration algorithm of GEO SAR echo data"

The key problem of the imaging processing in geosynchronous earth orbit (GEO) SAR system is the space-variance of the Doppler parameters, which will result in the defocus of the SAR image with classical imaging algorithm. In this paper, a Modified Range Migration Algorithm (RMA) is proposed to overcome the space-variance of Doppler parameters by compensating the velocity change along the location of the target. Furthermore the simulation results fully verify the effectiveness of derived algorithm after velocity compensation. [C725]

#### "An overview of recent advances in Polarimetric SAR information extraction: Algorithms and applications"

Recent advances in Polarimetric SAR information extractions are reviewed. Papers published in IEEE Transactions on Geoscience and Remote Sensing and IGARSS proceedings over the last five years were included. We found that PolSAR technology has reached a certain degree of maturity. The availability of high-resolution multi-frequency PolSAR data from space borne and airborne SAR systems will stimulate significant PolSAR applications. [C726]

#### "CASA dual-doppler system"

Conventional radar networks are limited at warning against low-altitude wind hazards such as tornadoes and micro-bursts due to the combined effects of their long range, far spacing, and Earth's curvature. The Collaborative Adaptive Sensing of the Atmosphere (CASA) Engineering Research Center aims to solve these limitations through dual-Doppler systems operating in densely-spaced short range radar networks. The CASA test bed radar network incorporate the Distributed Collaborative Adaptive Sensing (DCAS) model in order to optimize scanning and retrieval for fast Doppler wind field products. Under the DCAS environment, fast coordinated sector scans are made by each radar based on weather detection and competitive end-user needs. The retrieval subsystem then makes the best pair selection for dual-Doppler synthesis based on optimal beam-crossing angles for target areas. Together, they create a fast, accurate, and robust dual-Doppler system suitable for weather emergency warnings. [C727]

#### "PS-InSAR time series analysis for measuring surface deformation before the L'Aquila earthquake"

L'Aquila area has a high topography and complex geological structures, and is covered with thick vegetation and snow in areas of high topography. To monitor the characteristics of crustal deformation in this region before the 2009 L'Aquila earthquake, we apply StaMPS software to analyse 20 descending ASAR images acquired between September 2003 and March 2007 and 39 ascending ASAR images acquired between February 2003 and March 2009. In this paper, two mean LOS deformation velocity maps are acquired for this area, which reveal the same deformation pattern. Several deformation gradient in this area can be clearly identified, furthermore, we discover that most faults in this region may strike approximately NW-SE and dip  $< 90^\circ$  to SW. We also draw the conclusion that descending SAR images are superior to ascending ones in monitoring crustal deformation with InSAR in this region. [C728]

#### "Extracting structural land cover components using small-footprint waveform lidar data"

Previous work has shown the ability of waveform LiDAR sensors to accurately describe various land cover types [1] and biomass estimates made in the field [2]. What is lacking, however, is a way to describe the different structural components that are embedded in the digitized backscattered energy from the LiDAR pulse. This study aims to extract structural components from waveform LiDAR data in terms of woody, herbaceous, and bare ground components from data collected over a savanna environment in and around Kruger National Park (KNP), South Africa. These components are comprised of metrics extracted from the waveforms and validated using biomass measurements made in field plots. Different size windows around plot centers, 3  $\times$  3 pixels and 9  $\times$  9 pixels (resulting in 1.5m and 4.5 m footprint, respectively), were used to examine scale effects of larger footprints. It was found that composite waveforms resembling plot sizes (9  $\times$  9) most often are able to describe more than 80% of the woody biomass variability across the entire study site, and individually for two of the three land uses within the area. However, the herbaceous component of the waveform did not correlate well with the field measurements, while the bare ground component was verified visually in a side-by-side comparison with

optical imagery. [C729]

#### **"Assessment of compact polarimetry over different tropical environment and dataset"**

This paper presents different radar polarimetric modes over different study sites in Tropical environment: Full polarimetry (FP), Dual Polarimetry (DP) and Compact Polarimetry (CP). By using SVM classification, we show the capabilities of each polarimetric mode linked to the scattering model assumption of the fully polarimetric reconstruction for CP mode proposed by Souyris et al.. We are focused on 3 study sites which have different landscape: Tubuai in French Polynesia (AIRSAR data), the Fazenda Saio Nicolau in Brazil and Cayenne in French Guyana (PALSAR data). It shown that the reflection symmetry assumption may not be verified due to spatial heterogeneity or due to the definition of the study classes. Even if the choice of the DP modes is strongly dependant of the study site, the CP mode have shown equivalent or better overall accuracy than the other DP modes, particularly when the study area are very homogeneous. [C730]

#### **"A study on different PS-like methods for subsidence in Tianjin, China"**

In this paper, the methods, primary PS-like method and Stanford Method for PS (StaMPS) are both studied and used to monitor the subsidence in Tianjin area. PS (Permanent Scatter) technique is possible to avoid many of the limitations of conventional DInSAR by analyzing just certain pixels which behave like point scatters and retain good correlations. Several PS-like methods have been developed and practiced by many researchers. StaMPS is a relatively new PS-like method, which uses spatial correlation of interferogram phase to find a network of stable pixels in almost all terrain without prior knowledge of temporal variations in the deformation. 17 ENVISAT SLC data for Tianjin area are used, covering from April 2003 to March 2006. The SLC scene acquired on Nov-05-2004 is chose as the master. And the results of the two methods are compared. By using the primary PS-like method and StaMPS, the subsidence field in Tianjin area has been mapped. As to PS selection, the primary PS-like method needs less input parameters and easier to understand than StaMPS. For deformation value calculation, StaMPS is good at evaluating non-linear subsidence history. [C731]

#### **"Scansar signal processing and image quality enhancement with fitted-geometry doppler surface"**

In this paper, an efficient and relatively high quality ScanSAR processor is implemented based on SPECAN algorithm. The role of the accurate Doppler parameter estimation is described with regard to the processed SAR images. A method of extracting the essential Doppler parameters with high precision is introduced and its performance is verified. For this purpose, we have adopted a Doppler surface fitted-geometry method and demonstrated how it can contribute to the improved Doppler parameter estimation. [C732]

#### **"Assessment of tree and crown heights of a maritime pine forest at plot level using a fullwaveform UltraViolet Lidar prototype"**

This study aims to determine the potential of a new lidar prototype with an ultraviolet laser and a medium footprint for retrieving forest parameters. The lidar is embedded on an ultra-light aircraft. The choice of the Landes forest in southwestern France as study area was made regarding the flat topography of the area and the stand height consistency. We chose three plots from different stands (different height characteristics) and compared the lidar derived metries to field measurements. To derive metries from lidar data, we summed the lidar waveforms within a plot and calculated derived reflectance profiles to correct the lidar signal from the occlusion effect. We then retrieve plot mean total and mean crown base heights measurement from reflectance profiles. We obtain a good consistency of the lidar measurements compared to field measurements, even if we noticed the existence of a 5 to 10% bias probably linked to the lidar sampling strategy. [C733]

#### **"Remote sensing applications for petroleum resource exploration in offshore basins of China"**

In this paper, a new approach for detecting and analyzing sea surface slicks caused by hydrocarbon seepage of offshore petroleum accumulations has been developed. This approach uses remote sensing radar technology and geophysical exploration techniques and has been developed based on hydrocarbon seepage theory. In this study, Synthetic Aperture Radar (SAR) data were used as the main data source. These data were integrated with gravity data inversed from satellite altimeter data, geophysical abnormal data from airborne magnetic data, and geological data of oil-and gas-bearing basins. Using the geographical information system, the oil and gas accumulating areas were outlined by the prospect models. This approach for the exploration and evaluation for offshore petroleum accumulations has been applied to two study areas in offshore petroleum basins in China: the Bohai Sea and Pearl River Mouth basins. By comparing the drilling outcomes and relative materials, our results show that the application of this integrated method is very effective. [C734]

### "A network based attenuation correction system for networked dual polarization radar observations"

Electromagnetic waves backscattered from a common volume in networked radar systems are attenuated differently along the different paths. A network based attenuation correction system for a network of dual polarization radars can be developed by combining the conventional network approach and the conventional differential propagation phase based attenuation correction technique. The network based attenuation correction system proposed here has been evaluated by data from the Adaptive Sensing of the Atmosphere (CASA) Integrated Project 1 (IP1) radars, which is a radar network that can observe a weather event simultaneously by multiple radars in different locations. The preliminary results show that the network based attenuation correction algorithm retrieves reflectivity and differential reflectivity properly. [C735]

### "Taxi: A versatile processing chain for experimental TanDEM-X product evaluation"

TanDEM-X is a high-resolution interferometric radar mission with the main goal of providing a global digital elevation model (DEM) of the Earth surface by means of single-pass X-band SAR interferometry. It is, moreover, the first genuinely bistatic spaceborne SAR mission, and, independently of its usual quasi-monostatic configuration, includes many of the peculiarities of bistatic SAR. An experimental, versatile, and flexible interferometric chain has been developed at DLR Microwaves and Radar Institute for the scientific exploitation of TanDEM-X data acquired in non-standard configurations. The paper describes the structure of the processing chain and focusses on some essential aspects of its bistatic part. Some experimental results performed with TerraSAR-X demonstrate the flexibility of the implemented processor. [C736]

### "Retrieval of raindrop shape-size relation using dual polarization radar measurements"

Dual polarization radar measurements of rainfall parameters are based on the assumption of a mean shape-size relationship of raindrops. This paper focuses on retrieving and interpreting the mean raindrop shape-size relation from polarimetric radar observations. A procedure to retrieve the drop shape-size relation that governs the polarimetric radar observations of reflectivity ( $Z_h$ ) differential reflectivity ( $Z_{dr}$ ) and specific differential propagation phase ( $K_{dp}$ ) is presented. The mean drop shape-size relations retrieved from measurements collected by the NCAR SPOL radar during three campaigns are analyzed to explore whether the natural raindrop shape-size relation can be described by a unique model. [C737]

### "GNSS illuminator based high range resolution algorithm in space-surface bistatic SAR"

Space-surface bistatic synthetic aperture radar (SS-BSAR) has gained more and more researcher's interests. In this paper, we focus on improving range resolutions of GNSS illuminator based SS-BSAR with the method of spectrum synthesis of ultra-wide-band (UWB). Narrow bandwidth signals, such as GPS P code, can be spliced into a wider signal. Simulation results show that it can effectively increase signal processing bandwidth, improve range resolution and target recognition capabilities. [C738]

### "RADAR and AIS sensors constellation for global maritime surveillance"

In the frame of SAMSON study (a Feasibility study of a space-based maritime surveillance system), funded by CNES, several concepts for a dual sensor RADAR + AIS (Automatic Identification System) constellation have been addressed. One of them supported by Thales Alenia Space is described in this paper. Its interest for global maritime surveillance is discussed. The constellation performance is presented in terms of revisit time and detection probability for each sensor before data fusion processing. Instruments are described as well as the proposed satellite concept. [C739]

### "Morphological-based source extraction method for HFSW radar ship detection"

In this contribution, High Frequency Surface Wave (HFSW) radars are considered for target detection. These systems, commonly used for oceanographic purposes, are of interest in maritime surveillance because of their long range detection capabilities. Unfortunately, the received signals are strongly polluted by different noises. To improve target detection a method based on Morphological Component Analysis (MCA) is investigated. Shortly, this paper introduces HFSW radars and gives an overview of the MCA. Then, numerical results from simulated data illustrate the MCA-based target detection method. Comparisons with classical detection methods based on CFAR techniques (GOCA-CFAR and GOOS-CFAR) are proposed through Receiver Operating Characteristics (ROC) curves. [C740]

### "Polinsar forestry applications improved by modeling height-dependent temporal decorrelation"

We model the temporal decorrelation in volumetric media imaged by a repeat-pass SAR interferometer by using a temporal correlation function that varies with depth. An expression of this function is proposed and based on

the Brownian motion of the canopy and soil elements. The spatial and temporal correlation terms are merged in a single coherence model that includes a large class of decorrelation effects, such as those induced by changes in the structure of the medium. We discuss the effects of the temporal correlation function and its implications on the parameters estimation using the POLINSAR random volume over ground model. [C741]

### "A dual-frequency SAR mosaic of the Amazon"

The development and availability of accurate landcover information is critical to the ecological science questions [Cerri, et al., 1995; Hall, et al., 1995], such as defining the rate and extent of deforestation within the Amazon. This need can only be met by techniques that are sensitive to phenomena at the scale of the landscape patch and can be efficiently applied in a consistent fashion over very large regions. For example, estimation of Amazonia's carbon budget will require a large-scale mosaic of the location and spatial extent of landcover types, forest regrowth biomass, and selective logging. Vegetation type and surface condition exert control over carbon and trace gas fluxes. Estimates of the biotic carbon pool are also important since carbon accumulation rates vary not only with vegetation types but with successional stage and management practices as well. Both the extent and carbon accumulation rates of regenerating tropical forest are poorly known. If the ages of forest disturbance can be established (i.e., from the Landsat time series), then the SAR-derived estimates of aboveground biomass can be used to estimate annual sequestering of carbon. Though these data were acquired at higher resolution, it is possible to use this data to map landcover, biomass and selective logging at a spatial scale of 100m for the Amazon basin. [C742]

### "Multi-frequency and polarimetric measurements of bare and vegetated soils microwave reflection and emission by C- and Ku-band, combined scatterometer-radiometer systems"

In this paper the results of simultaneous and spatially coincident, multi-frequency, polarimetric, spatio-temporally collocated measurements of bare, dry vegetated and ash covered soils microwave reflective (radar backscattering coefficient) and emissive (brightness temperature) characteristics angular dependences at ~5.6GHz and ~15GHz are presented. During these experiments the observed area was set ablaze and multi-frequency, multi-polarization, microwave active and passive measurements at 300 incidence angle were continued for smock, fire and ash situations. For these measurements C-, and Ku-band, polarimetric, combined scatterometric-radiometric systems were used, set jointly on a mobile buggy moving along the measuring platform. Structures, operational features and the main technical characteristics of the utilized systems are presented too. The paper has an aim as well to attract attention of interested researchers and to invite them to perform their own or joint researches using available devices and facilities. [C743]

### "Polarimetric and structural properties of forest scenarios as imaged by longer wavelength SARs"

SAR data gathered from forested areas collect contributions coming from the vegetation layer, from the ground below and from other scattering mechanisms (SMs). Multi-baseline data allow a tomographic analysis thus retrieving information about the vertical structure of the target. Multi-polarimetric acquisitions enrich the data, providing ways to identify the targets basing on their electromagnetic properties. The joint exploitation of multi-polarimetric and multi-baseline data suggests the possibility of linking the estimation of the vertical structure of different SMs with their polarimetric signature. A formal framework in which this task can be accomplished is provided by the Algebraic Synthesis (AS) technique, which extends the concepts within PolInSAR through the assumption of the Sum of Kronecker Products (SKP) structure. By assuming the presence of two SMs (for example ground and volume scattering), the SKP assumption leads to a cross dependence between the polarimetric and interferometric coherences, in that ground structure is shown to be related to volume polarimetry, and dually volume structure is shown to be related to ground polarimetry. The aim of this paper is to investigate the implications of this cross relation. Experimental results will be shown basing on a data-set of multi-polarimetric and multi-baseline SAR images at P-band acquired by DLR's E-SAR over the Krycklan catchment, in northern Sweden, in the framework of the ESA campaign BioSAR 2008. [C744]

### "Processing for airborne interferometric SAR data with high squint"

A novel approach for the highly squinted airborne InSAR data processing is presented. Using the IMU data to resolve the PRF ambiguity and moving azimuth windows according to the Doppler centroid varying in the different range, as well as combining the auto-registration imaging algorithm, such approach not only can compensate the squint effect and motion error directly at the imaging processing stage, but also can improve the coherence and restrain the interferometric phase error of the image-pair. The simulative and practical results indicate that the proposed approach is very suitable for the processing of the data with a high squint for a dual-antenna airborne InSAR system with its efficiency in improving the image quality and enhancing the interferogram and coherence. [C745]

### "Comparison of crop classification capabilities of spaceborne multi-parameter SAR data"

With the arisen spaceborne multi-parameter Synthetic Aperture Radar (SAR) systems, such as Envisat ASAR, TerraSAR-X, ALOS PALSAR, and RADARSAT-2, the interest of crop mapping has been increasing. The present study compares the capabilities of the multi-parameter SAR in discriminating the main crop types by object-based classification in Haian county of Jiangsu province, South China. Two kinds of information, SAR intensity based and SAR statistical properties based are used for Maximum Likelihood Classification (MLC) and Minimum Distance Classification (MDC) respectively. The results show that, the L-band SAR can uniquely identify mulberry from dry-land crops, such as maize and vegetable and C-band SAR has some advantages in mapping rice. Specifically, the polarimetric RADARSAT-2 data can identify the rice with accuracy about 75% ~ 80% which is similar as the result from X-band TerraSAR-X Spotlight data but higher than that from C-band dual-polarization Envisat ASAR data. Nevertheless, both of X- and C-band can hardly separate the mulberry from the other dry-land crops. [C746]

### "A biomass estimate over the harvard forest using field measurements with radar and lidar data"

The National Research Council's decadal survey recommended DESDynI as one of the high priority missions for NASA. The mission envisions an InSAR/Lidar instrument for observing ecosystem structures on global scales with high spatial resolutions. Consistent and highly resolved global maps of biomass and carbon stocks require highly accurate observations of vegetation, in fact it is expected that such accuracies would require a combination of the high vertical precision of Lidar observations and the large spatial extent of SAR/InSAR measurements. Here we analyze radar backscatter data along with biomass estimates from a field campaign conducted in the Harvard forest in Massachusetts, USA. [C747]

### "A high accuracy method for interference fringes suppression in SAR distributed targets' raw data simulation"

Interference fringes will be generated in SAR image when distributed targets' echo signal is simulated because of the uniform model of targets. The fringes can be suppressed by adding random height in space or random phase on backscatter coefficient of the distributed targets. However, the former method will introduce location error and the latter method will increase speckle noise twice in simulated image. In this paper, we develop a high accuracy method for fringes suppression based on targets' position randomizing and RCS re-sampling via bilinear interpolation. The validation of method is successfully proved by simulation results and the performance of the method is discussed on accuracy and computational complexity at the end of this paper. [C748]

### "Analysis of the correlation properties of digital satellite signals and their applicability in bistatic remote sensing"

This paper presents a study of relevant correlation properties of signal transmitted from commercial communication satellites in order to evaluate their potential use as "signal of opportunity" for bistatic remote sensing. The ambiguity function for the XM radio satellites was computed analytically from published information on the modulation schemes and bandwidth, under the assumption that the data modulation is random. The model was then experimentally tested by recording the received signals from these satellites. Next, a cross-correlation waveform for digital signal reflected from random rough surface was simulated. Scattering model that were originally developed for Global Navigation Satellite System (GNSS-R) signals was applied to the modified simulator to incorporate the derived ambiguity function. The simulator was then used to generate synthetic waveform with a realistic signal to noise ratio (SNR). Retrieval algorithms for ocean surface roughness and reflectivity that were derived originally for GNSS-R, were applied to these simulated signals. Non-linear least square methods were applied to invert a scattering model and estimate the slope variances of the probability density function (PDF), which best fits the measurements of the reflected XM signal waveform. The SNR for the experimental data was found to be within 0.5dB of the theoretically calculated SNR. [C749]

### "A fully polarimetric borehole radar based numerical modelling: Fully polarimetric response to synthetic fractures and "fluid substitution""

A fully polarimetric borehole radar system with four combinations of dipole and cylindrical slot antennas was developed to acquire fully polarimetric data sets in drilled boreholes. To better understand the fully polarimetric response to subsurface fractures with different roughness, in this study, synthetic fractures with different roughness are generated on a computer via fractal theory based simulation techniques. Quantitative assessment for the roughness of synthetic fractures is possible by use of three main parameters: the fractal dimension, the rms roughness at a reference length, and a length scale describing the degree of mismatch between the two fracture surfaces, allowing future detailed study of mechanical and transport properties of fractures and fully

polarimetric radar response on them. Next, a 3D sub-grid FDTD numerical simulation is used to synthesize fully polarimetric data sets with synthetic fractures as primary reflectors. Based on the synthetic data sets, it is possible to evaluate the applicability of different radar polarimetry analysis approaches to physical characterization of subsurface fractures in future. [C750]

#### "Mapping tropical forest using ALOS PALSAR 50m resolution data with multiscale GLCM analysis"

PALSAR orthorectified HH and HV produced at 50m resolution is used for analysis. Since only two bands (HH and HV) have been limited in land cover discrimination, textures have been used as additional information for classification. This research derives second-order textures at different spatial resolutions and compares second-order textures at multiple scales to demonstrate their contributions in land cover classification. The discriminating capability of texture features is derived by the transformed divergence on several selected regions of interest. Optimum combination of backscattering and textures are used as input data into a supervised multi-resolution maximum likelihood classification. It is found that by including the texture information, the overall classification accuracy is improved by 10%. [C751]

#### "Ship detection with RadarSat-2 Quad-Pol sar data using a notch filter based on perturbation analysis"

Target detection of marine feature is a major topic for the security and monitoring of coastlines. Synthetic Aperture Radar (SAR) has been shown to be particularly useful for this application because of its all-weather and night capability. In this paper a new ship and iceberg detection methodology is described. The algorithm proposed is based on a perturbation analysis in the target space recently developed and published by the authors, which was focused on land based target detection. The algorithm can be considered to be a negative filter focused on sea. Consequently, all the features which have a polarimetric behaviour different from the sea are detected. To demonstrate and validate the technique two RadarSat Fine Quad-Pol mode scenes were acquired off the south coast of the UK at Portsmouth harbour. An extensive ground truth campaign was also conducted that was coincident with these acquisitions. Portsmouth is one of the busiest harbours in the UK and this afforded the opportunity to capture a wide range of vessel sizes and types for analysis. [C752]

#### "Contextual remote-sensing image classification by support vector machines and Markov random fields"

In the framework of remote-sensing image classification support vector machines (SVMs) have recently been receiving a very strong attention, thanks to their accurate results in many applications and good analytical properties. However, SVM classifiers are intrinsically noncontextual, which represents a severe limitation in image classification. In this paper, a novel method is proposed to integrate support vector classification with Markov random field models for the spatial context, and is validated with multichannel SAR and multispectral high-resolution images. The integration relies on an analytical reformulation of the Markovian minimum-energy rule in terms of a suitable SVM-like kernel expansion. Parameter-optimization and hierarchical clustering algorithms are also integrated in the method to automatically tune its input parameters and to minimize the execution time with large images and training sets, respectively. [C753]

#### "Pose estimation for ISAR image classification"

This paper presents aircraft target recognition (ATR) system using Inverse Synthetic Aperture Radar (ISAR) images. Knowing the pose of the target can improve the ATR performance (recognition rate and computational complexity). So, we propose in this paper a new pose estimator from ISAR images, based on the axis of symmetry and the similarity measure. The method proposed is compared with several approaches proposed recently in the literature, such as 2-D Continuous wavelet Transform and Hough transform. Once the pose of target is estimated, the classification is finally performed by K-Nearest Angle (KNA) classifier which insert the pose information into image retrieval task. [C754]

#### "Analysis of geosar dual-band InSAR data for peruvian forest"

At present there is no consensus as to which remote sensing technologies are appropriate for tropical forest biomass estimation. Cloud cover in the tropics and biomass saturation suggest that a combination of low-frequency SAR and interferometry (either PolInSAR or dual-band interferometric SAR DBInSAR) could provide a solution. Tropical forest biomass recovery using X-P DBInSAR has been demonstrated from an airborne platform using the X-P DEM height difference. This height is known to be considerably lower than the tree height as a result of penetration of microwaves into the canopy that can be significant even at X-band. We model the penetration using the RVOG model and show that in the strong attenuation approximation the interferometric

coherence magnitude can be used to estimate penetration depth. We compare the model with GeoSAR DBInSAR observations of Peruvian forest, and, by comparison with LiDAR data, show that the GeoSAR Xband interferometric height can be corrected towards the upper canopy using knowledge of the coherence magnitude combined with the high-frequency "X-RVOG" model. We employ the corrected height with a biomass inversion equation derived from plot samples covered in the Peru campaign and generate a map of above ground forest biomass. [C755]

#### "Predictive quantization of dechirped spotlight-mode SAR raw data in transform domain"

Synthetic aperture radar (SAR) systems collect large volumes of data that must be transmitted to a ground station for storage and processing. However, given the limited bandwidth of the downlink channel it is imperative that SAR data be compressed before transmission. While it is commonly believed that raw SAR data is uncorrelated, it is shown in that the inverse Fourier transform of spotlight-mode SAR exhibits non-negligible correlation that can be exploited in a predictive quantization scheme. In this paper, we propose two predictive quantization algorithms-transform-domain block predictive quantization (TD-BPQ), and transform-domain block predictive vector quantization (TD-BPVQ)-to encode dechirp-on-receive spotlight-mode SAR raw data. Experimental results indicate that, on average, TD-BPQ and TD-BPVQ outperform the well known block adaptive quantization (BAQ) by 5 and 6 dB, respectively. [C756]

#### "Z-R relation for snowfall using two small doppler radars and snow particle images"

Snowfall data was simultaneously recorded by two small Doppler radars, two high sensitive snow gages and an image processing system with high accuracy at short time interval. The snowfall rate  $R$  was measured with two gauges and radar reflectivity factor  $Z$  was measured using small bistatic X-band radar and monostatic K-band radar. The images of falling snow particles were used to obtain size distribution. Since all the measurements were located in a small area, it can be said that the obtained data corresponds well to others, and it is possible to analyze Z-R relation in detail. The relationships between two radar reflectivity factors and snowfall rate were investigated and compared to the characteristics of snow particles. [C757]

#### "Characterization of affected areas of the 2008 Iwate-Miyagi, Japan, earthquake using SAR intensity images"

SAR images obtained before and after a natural disaster are considered to be useful for emergency response due to its all-weather and sunlight-independent characteristics. Recently, the spatial resolutions of SAR systems have been improved significantly. In this paper, SAR intensity images acquired before and after the 2008 Iwate-Miyagi, Japan, earthquake from ALOS/PALSAR (L-band) and TerraSAR-X (X-band) are employed to investigate the radar backscattering characteristics for various acquisition and surface conditions. The spatial resolution, radar frequency, flight path, and incidence angle were shown to affect SAR backscattering echo, depending on surface materials and roughness. It is also observed that the difference of the backscattering coefficients at the pre- and post-event times gets large and their correlation coefficient becomes small at the locations of landslides and slope failures. [C758]

#### "SAR data collection over rain forests at VHF- and UHF-band"

Radar imaging of tropical vegetation at VHF- and UHF-band has been performed using the airborne SAR sensors CARABAS-II and LORA, respectively. The acquired data set is limited to HH-polarized registrations only. The area mapped exhibits a rough terrain with dramatic topographic variations, mostly covered by dense tropical rain forests. Multiple illumination directions spanning  $360^\circ$  were adopted in the data collection for both sensors to overcome the shadowing due to the high relief topography. For each heading, the SAR images generated, adjacent in azimuth and from all imaging passes, were calibrated and geocoded separately and then merged into a mosaic representing the full ground coverage. A first output from the forest backscatter analysis indicates a 12 dB lower level at VHF-band at an incidence angle of about  $70^\circ$ . However, this preliminary result is based on one sample point only, where the investigated forested area was located on a fairly flat ground surface. [C759]

#### "Application of the moving target detection by focusing technique in civil traffic monitoring"

This paper presents an application of the moving target detection by focusing technique (MTDF) in civil traffic monitoring. The experimental results based on simulations show that the basic civil traffic monitoring can be solved using MTDF using a single-channel airborne SAR system. With an assumption of known moving directions of vehicles, MTDF allows detecting, estimation of speed, and finally reconstructing a SAR image of the vehicles of interest. In this study, the focusing approach of MTDF is based on ultrawideband chirp scaling (UCS) algorithm. [C760]

### "Esprit-based scattering power decomposition by using modified volume scattering model"

The scattering power decomposition for POLSAR data is one of the powerful tools in the radar polarimetry. There are several model-based decomposition techniques. However, since the number of independent observables in POLSAR images is limited, these techniques require several assumptions to obtain unique solution. The authors have proposed an alternative technique with POL-InSAR dataset. By using the POL-InSAR dataset, we can increase the number of observables. However, selection of volume scattering component was still a problem. Recently, Dr. Arie et. al., proposed a generalized volume scattering model, and applied it to the POLSAR dataset with the adaptive non-negative eigenvalue decomposition technique. In this report, we apply the model to the ESPRIT-based POL-InSAR decomposition technique and verify the estimation performance experimentally. [C761]

### "Multi-Channel RADAR Depth Sounder (MCRDS) signal processing: A distributed computing approach"

In response to problems surrounding measuring ice sheet thickness in high attenuation areas of Greenland and the Antarctic, the Center for the Remote Sensing of Ice Sheets (CReSIS) created a Multi-Channel RADAR Depth Sounder (MCRDS). The MCRDS system was used to measure ice thicknesses of up to five kilometers in depth. This system produced large datasets, which required greater processing capabilities in the field. The purpose of this project was to test processing performance on a 32-core cluster through distributed computing resources. Testing involved a six-node cluster with an attached storage array and use of the CReSIS Synthetic Aperture RADAR Processor (CSARP) through the MATLAB Distributed Server Job Manager. Performance testing was derived from average run times collected once CSARP jobs completed. The run times were then compared using an ANOVA test with a five percent significance level. [C762]

### "Application of KOMPSAT-5 data for emergent oil spill monitoring"

In this paper, we discussed the functionalities of KOMPSAT-5 from the emergency response perspective to oil spill detection, describing its technical abilities in terms of maneuverability, system response time, image quality, and damping ratio. The damping ratio at the X-band was higher than that at other available frequencies, which increased the probability of oil spill detection from SAR data. However, the detection of oil spills depends significantly on the wind condition and the presence of look-alikes. Oil spill detection algorithm for KOMPSAT-5 estimates wind information directly from SAR data, and is expected to enhance the detection capability. [C763]

### "Snow wetness retrieval inversion modeling for C-band and X-band multi-polarization SAR data"

This paper is concerning the estimation of snow wetness from multi-polarization SAR data. In this paper, microwave interaction with snow covered terrain and different scattering mechanism from snowpack and their backscattering model for developing inversion algorithm with wet snow conditions are described in order to estimate snow wetness. SAR data processing and field measurement of snow parameters are also discussed. In this study, snow wetness has been measured with a dielectric moisture meter with synchronous satellite passes over the part of snow covered Indian Himalayan region (e.g. Dhundi observatory in Himachal Pradesh, India). [C764]

### "Random noise SAR based on compressed sensing"

Recent theory of compressed sensing (CS) suggested that exact recovery of an unknown sparse signal can be achieved from few measurements with overwhelming probability. In this paper, we combine CS technology with a random noise SAR and proposed the concept of random noise SAR based on CS. The block diagram of the radar system and the collected data processing procedure was presented. Theoretic analysis show that the sensing matrix of the random noise SAR exhibits good restricted isometry property (RIP). When the target scene is sparse or sparse in any basis, the random noise radar based on CS can get high accuracy image by collecting far less amount of echo data than traditional noise radar does. The conclusions are all demonstrated by simulation experiments. [C765]

### "An improvement for the unsupervised Wishart Freeman classification with fully polarimetric SAR data"

In this paper, we proposed an improvement for the Wishart Freeman classification, which is based on the Wishart distance measurement and the estimation algorithm of the number of clusters for fully polarimetric SAR data. Our experimental results show the effectiveness of the proposed method. [C766]

### "Deployment of the ASCAT calibration transponders"

The METOP-A Advanced Scatterometer Radar has stringent radiometric requirements requiring regular, accurate, calibration. The specified stability of 0.2 dB or better is too demanding for targets such as rain forest or simple corner reflectors, so three highly stable return signal sources have been precisely sited to give accurate measures of the beam patterns over the satellite repeat cycle. The Scatterometer is required to provide full coverage over all the oceans, so the three calibration transponders have been installed in Turkey, as the Black Sea and Eastern Mediterranean are not used in the ASCAT programme. [C767]

### "Effect of the polarization on SISAR imaging and feature recognition in forward scattering radar"

In this paper, the effect of the polarization and the multipath on shadow inverse synthetic aperture radar (SISAR) imaging is analyzed respectively in forward scattering radar (FSR). The multi-polarization and the multipath imaging results of targets, based on SISAR, are discussed respectively. In addition, the target forward scattering (FS) RCS under multi-polarization conditions are also obtained using CST simulation software to research the effect of multi-polarization on moving target feature recognition in FSR. [C768]

### "Automatic image classification of landslides improved with terrain roughness indices in various kernel sizes"

Using spectral-only information for landslides classification is usually confusing with houses, roads, and other bare lands because these ground features have similar spectral patterns on images. The terrain roughness can be measured by significant wavelengths; some studies have linked the relationships between terrain roughness and the landslide by using numerical analyses of topography data. In this study, airborne LiDAR data of 1m grid are used to explore the possibility of improvement of landslide classification, the LiDAR-derived data include DEM slope and terrain roughness indices including diversity, dominance and relative richness with different grid size data are used to improvement classification accuracy. The improvement of accuracy when including DEM slope is 22% in producer's accuracy and 27% in user's accuracy. The accuracy of diversity, dominance and relative richness indices all are improved when kernel sizes enlarge in Maximum Likelihood and Mahalanobis Distance algorithms. [C769]

### "Comparison of alternative image representations in the context of SAR change detection"

This article compares four different alternative image representations in the context of a structure-based change detection. The framework is taken from the already published Curvelet-based change detection approach. Only the transform step is modified by inserting three additional transforms: the Laplacian pyramid, the Wavelet and the Surfacelet transform. The results of the change detection are compared to the single pixel difference image in order to find the representation that best illustrates the underlying structures. The Curvelet transform again turns out to be very powerful in describing man-made objects and landscapes. [C770]

### "Microphysical retrieval from dual frequency precipitation radar board GPM"

Global Precipitation Measurement (GPM) is poised to be the next generation observations from space after Tropical Rainfall Measuring Mission (TRMM). The GPM mission concept is centered on the deployment of a core observatory satellite with an active dual-frequency radar (DPR), operating at Ku and Ka bands. The DPR is expected to improve our knowledge of precipitation processes relative to single-frequency radar on microphysics retrievals. Hydrometeor classification method is a key part of any microphysical retrieval algorithm. This paper is focused on the hydrometeor classification method which might be applied to GPM DPR and maps the results to Zdr- DFR plane to cross verify with the pixel based hydrometer identification method. In addition a comparison is made between the DSD retrieval algorithm proposed by the author and other existing algorithm. [C771]

### "Investigations on the full polarimetric PALSAR data to discriminate macrophytes species in the Amazon floodplain wetland"

The purpose of this work is to evaluate the capacity of full polarimetric L band data to discriminate macrophyte species in Amazon wetland. Fieldwork was carried out almost simultaneously to the acquisition of the full polarimetric PALSAR data. Coherent and incoherent attributes were extracted from the image, and macrophyte morphological variables were measured on the ground. The image attributes and the macrophyte variables were compared in order to evaluate their application for discriminating macrophytes species. The findings suggest that polarimetric information could be adopted to discriminate plant species based on morphology, and that estimation of plant biomass and productivity could be improved by using the polarimetric information. [C772]

### "On the feasibility of tsunami detection using satellite-based sea surface roughness measurements"

Observations of tsunamis away from shore are critical for improving early warning systems and understanding of tsunami generation and propagation. Using analysis already applied to the 2004 Sumatra-Andaman tsunami, we positively identify the 2010 Chilean tsunami in satellite altimeter measurements of sea surface roughness. Use of radar backscattering strength measurements from satellite altimeters would be impractical for tsunami detection and early warning purposes due to the limited temporal and spatial resolution. On the other hand, it is likely that tsunami-induced changes in sea surface roughness are observable with other types of space- and airborne sensors that sense sea surface roughness over much wider swaths. With this in mind, we explore the feasibility of using existing instruments and technology as the basis for a tsunami detection and early warning system.

[C773]

### "Generic object recognition in high resolution SAR images"

This paper presents a non-parametric modeling scheme for high resolution SAR data, based on Short Time Fourier Transform which is able to integrate the radiometrical and morphological properties of the data, for object recognition, scene and target indexing, addressing the problem of large data base queries and information retrieval.. The method is assessed by using a Bayesian Support Vector Machine image search engine based on a hierarchical learning model. The method allowed for the recognition of over 30 different classes, both homogeneous and heterogeneous urban objects with high levels of details. Qualitative and quantitative measures for evaluation are presented and discussed. [C774]

### "A ground-based Arc-scanning synthetic aperture radar (ArcSAR) system and focusing algorithms"

KIGAM and KNU are developing a ground-based Arc-scanning SAR system (ArcSAR) mounted on a truck. The system achieves the coherent integration of radar returns from ground targets by the circular motion of the antennae attached to the end of an extendable arm. Precise control of antenna position and the extended coherent-integration-length enable the formation of high-resolution, high-precision and phase-preserving SAR images. Based on the Polar Format Algorithm, two SAR-focusing algorithms were developed for the data acquired from two different scanning modes of this unique system: the scan mode and the spot mode. [C775]

### "A filtering approach to improve deformation accuracy using large baseline, low coherence DInSAR phase images"

Phase noise in an interferogram hinders the accuracy and reliability of interferometric synthetic aperture radar (InSAR) measurements, including deformation estimation and topographic mapping. The Goldstein filter is one of the most commonly used interferogram filters to reduce the effects of phase noise. In this paper, we present a modification to the Goldstein interferogram filter such that the maximum value for the filtering parameter alpha is set to greater than 1 over less coherent areas so that aggressive filtering is implemented on incoherent areas. We also discuss the combined use of estimated coherences from linear and non-linear filters to deal with the coherence saturation due to the strong filtering, which is crucial in generating InSAR deformation products.

[C776]

### "Log-polar and polar image for recognition targets"

We describe in this paper, data processing algorithms applied on radar image in order to extract feature descriptors and then to perform recognition task. Several kinds of descriptors can be used to acquire information about target characteristics from radar images such as ISAR (Inverse Synthetic Aperture Radar) images. This paper presents two types of vector descriptors extracted via two kinds of transformed images so-called polar and log-polar images obtained respectively from the polar and log-polar mapping. In order to guarantee the invariance of some geometrical transformation, additional processing are proposed. In this paper, we present the polar and log-polar transformations and then the classification scheme adapted on correspondent polar and log-polar templates. In the classification step, log-polar and polar mapping results are compared using adapted classification scheme. [C777]

### "Random Forests for building detection in polarimetric SAR data"

Building detection from Synthetic Aperture Radar (SAR) images states a particular important as well as difficult problem. The high-resolution which is necessary to distinguish single buildings as well as the geometric and dielectric properties of dense urban areas cause most assumptions to fail, that are commonly made in SAR data analysis. This paper proposes the usage of Random Forests for building detection from high-resolution Polarimetric Synthetic Aperture Radar (PolSAR) imagery. Random Forests can handle high-dimensional input and therefore a large set of different features, they are known to lead to good classification performance in terms

of robustness and accuracy, and are nevertheless seldomly applied to analysis of PolSAR images in general and building detection in particular. This paper presents first results of Random Forests when applied to a building detection task and shows their successful applicability. [C778]

#### **"Effects of forest disturbances on forest structural parameters retrieval from lidar waveform data"**

The effect of forest disturbance on the lidar waveform and the forest biomass estimation was demonstrated by model simulation. The results show that the correlation between stand biomass and the lidar waveform indices changes when the stand spatial structure changes due to disturbances rather than the natural succession. This has to be considered in developing algorithms for regional or global mapping of biomass from lidar waveform data. [C779]

#### **"Composite scattering from electric-large target over randomly rough surface in numerical approaches"**

Numerical study of radar echoes from the targets in environmental clutters has been of great interest in many applications. In this paper, the bidirectional analytic ray tracing (BART) method for composite scattering from three-dimensional (3D) electrically large complex target above a randomly rough surface is reported. Analytic tracing of polygon ray tubes in bidirectional tracing is developed to precisely calculate the illumination and shadowing of facets, which exempt large patches of the target from any finer meshing. It significantly reduces the complexity relevant to the target electric-size. Numerical examples of angularly composite scattering from a three-dimensional electrically large, e.g., a ship-like target over a randomly rough surface are presented and discussed. [C780]

#### **"Towards an operational daily soil moisture index derived from combination of MODIS, ASAR and AMSR-E data"**

This work aims at deriving a methodology for calculation of a soil moisture index based on the apparent thermal inertia (ATI) approach. For the processing, MODIS images have been exploited which have a higher resolution (1 km) if compared with METEOSAT images and are suitable for the ATI calculation. Furthermore, the approach considers the soil moisture estimates derived from SAR sensors and use them to calibrate the information coming from the optical data. The main advantage of this approach is to transform a soil moisture index derived from optical images in soil moisture values by using a comparison between spatial distributed data. In order to make the calibration more robust and consider the variability from different areas, three main test sites have been chosen located in Italian regions with different meteorological and landscape characteristics. In case of anomalous values due to the not appropriate acquisition time, AMSR-E soil moisture data are used as prior information in order to improve the estimates. [C781]

#### **"Deriving soil moisture with the combined L-band radar and radiometer measurements"**

In this study, we develop a combined active/passive technique to estimate surface soil moisture with the focus on the short vegetated surfaces. We first simulated a database for both active and passive signals under SMAP's sensor configurations using the radiative transfer model with a wide range of conditions for surface soil moisture, roughness and vegetation properties that we considered as the random orientated disks and cylinders. Using this database, we developed 1) the techniques to estimate surface backscattering and emission components and 2) the technique to estimate soil moisture with the estimated surface backscattering and emission components. We will demonstrate these techniques with the model simulated data and its validation with the airborne PALS image data from the soil moisture SGP'99 and SMEX'02 experiments. [C782]

#### **"Recent advances in the development of the open source Toolbox for Polarimetric and Interferometric Polarimetric SAR Data Processing: The PolSARpro v4.1.5 Software"**

The objective of this paper is to make a review of the current status of the PolSARpro v4.0 Software (Polarimetric SAR Data Processing and Educational Toolbox), developed under contract to ESA. The objective of this current project is to provide Educational Software that offers a tool for self-education in the field of Polarimetric SAR data analysis at University level and a comprehensive suite of functions for the scientific exploitation of fully and partially polarimetric multi-data sets and the development of applications for such data. The PolSARpro v4.0 Software establishes a foundation for the exploitation of Polarimetric techniques for scientific developments and stimulates research and applications developments using PolSAR and PolInSAR data. [C783]

#### **"Characterization of ENVISAT multipolarization SAR data with bidimensional statistics"**

This paper is about evaluating the interest between studying directly dual images statistical indices and the use of statistical indices build from two SAR multipolarization images. We show an original way of using this kind of images by using two dimensionned statistical calculation in a Markov random field classification. We present results of our segmentation on urban, forest and mangrove areas. Those results are computed from ENVISAT ASAR data in HH and VV polarizations in a tropical context, near Libreville. [C784]

#### "Interferometric processing algorithms of TanDEM-X data"

The purpose of this paper is to provide an algorithmic overview of the interferometric processing embedded in the Integrated TanDEM-X Processor (ITP), settled to the generation of the raw digital elevation model (DEM). The main processing blocks are described, with a focus on the spectral matching of the azimuth spectra, the high-precision coregistration, the dual-baseline phase unwrapping and the geocoding of the products. The robustness of the algorithms is demonstrated through a dual-pass TerraSAR-X scenario. [C785]

#### "Extrapolation of LiDAR for forest structure estimation using SAR, InSAR, and optical data"

One of the most fundamental new technical challenges of a DESDynI spaceborne mission is the fusion of the several sensor modalities-LiDAR, SAR, InSAR, and Optical-in order to accurately estimate desired 3D Vegetation structures and biomass parameters at their point of intersection and to extrapolate them over continuous areas. The objective of this paper is to use both our simulation models and measured dataset to develop and validate fusion and extrapolation methods while simulating DESDynI-type missions. We use existing datasets to develop and validate our fusion and extrapolation approach, which involves using our four sensor simulators, including our fractal-based tree geometry generator, in tandem with our in-house parameter estimation software which performs fusion and retrieval functions. We then use existing field and radarlidar-VNIR data for the Boreas southern study area to validate our simulators in this region and construct a large set of boreal trees for use in our fusion and extrapolation processes. [C786]

#### "Estimation of sea ice concentration in the Sea of Okhotsk using PALSAR polarimetric data"

The objective of this research is mainly in estimating sea ice concentration from Phased-Array L-band SAR (PALSAR) polarimetric data. This paper shows the results of estimating sea ice concentration from PALSAR data acquired from 2008 to 2010. The AMSR-E sea ice concentration data are also used to verify the result of sea ice concentration derived from PALSAR data. The difference in two sea ice concentrations was found especially in AMSR-E low concentration area. The high resolution backscattering and scattering entropy images give us an idea that there is some difficulty in AMSR-E to detect thin sea ice in the Sea of Okhotsk. [C787]

#### "Application of aspect angle normalized polsar images for urban building detection"

Variation in the building aspect angle, defined as the angle between the flight direction of a satellite (azimuth direction) and the vertical wall of a building, is a significant cause of accuracy reduction in building detection and terrain classification from Polarimetric Synthetic Aperture POLSAR (POLSAR) images. However, the existing building detection methods usually are effective for the buildings with a limited aspect angle range. Considering the relationship between the aspect angle of the building and the orientation angle shift, an aspect angle normalization method is introduced to remove the disadvantageous influences caused by the aspect angle. From a comparison between the double-bounce building detection results of the original and aspect angle normalized RadarSat-2 data acquired in Beijing, China, buildings with any aspect angle can be detected effectively from aspect angle normalized data. [C788]

#### "Progressive change detection in time series of SAR images"

The aim of this paper is to present a general framework for change detection in a time series of radar images, for an operational purpose and in the context of environmental monitoring. The change detection procedure is turned into the framework of detecting a random signal into the noise; the detection of this signal leads to the detection of a change in the time series. This framework is based on a non-parametric detection method that assume a sparse representation of the data. When using radar images, the speckle noise invalidates the hypothesis of sparsity. Then a pre-processing technique is required to provide an appropriate sparse representation of data, whatever the initial noise characteristics. The paper focuses on the change indicator, based on recursive median filtering, yielding a piecewise regular representation of a scene obtained by spreading the statistically most reliable pixel values over the image. The recursive median filtering leads to simple change indicators that are more efficient than the Kullback-Leibler change indicator when using small analyzing sliding window. Furthermore, it induces an simple extension to perform progressive change characterization through a multi-temporal filtering approach. Results are shown with a two-date change detection from RADARSAT images and from a time series of ERS and ENVISAT images. [C789]

### "Merging multi-track PSI result for land subsidence mapping over very extended area"

The Permanent Scatterer Interferometry (PSI) technique is usually applied for surface deformation mapping at local area from 1 up to a maximum of 100 km<sup>2</sup>. Although the ability to provide deformation map of regional area exceeding 10,000 km<sup>2</sup>, the processed area of interest is mostly limited to SAR acquisitions in a single satellite track and frame. In this work we present the study of merging multi-track PSI results for land subsidence monitoring over very extended area. Apart from the description of the PSI method used for long strip SAR data processing, datum connection of multiple adjacent tracks, including conversion of a common coordinate system and the connection of the PSI derived velocity maps are demonstrated. The application of the proposed method to monitor large coverage land subsidence in the central North China Plain (NCP) is described. The presented results obtained by merging 3 adjacent tracks of ENVISAT ASAR data acquired between Jan, 2007 and Dec, 2009, with a coverage of 2004260km<sup>2</sup> are very significant and indicate the effectiveness and potential of this technique for land subsidence mapping over very extended area. [C790]

### "Unsupervised change detection with very high-resolution SAR images by multiscale analysis and Markov random fields"

Change detection represents an important tool in environmental monitoring and disaster management. Here, a novel unsupervised change-detection method is proposed for very high-resolution SAR images, by integrating wavelet multiscale feature extraction, Markov random fields for contextual modeling, and generalized Gaussian models. Experiments with COSMO-SkyMed data remark the effectiveness of the method as compared with previous methods. [C791]

### "Orthogonal polarimetric SAR processor based on signal and interference subspace models"

We develop a new SAR processor based on several orthogonal projections. We take into account the scattering properties of the target and the interferences by using subspace models. To detect the target without detecting the interferences, we process images from the orthogonal projection of the received signal into the target subspace and from the orthogonal projection of the received signal into a part of the interference subspace. We can combine these two images to firstly detect the target and to secondly reduce interference. This new SAR processor is applied to realistic simulated data for FoPen (Foliage Penetration) application. [C792]

### "Target detection above rough surfaces in microwave imaging using Compressive Sampling"

A subspace extraction approach for detection of targets embedded in the clutter is presented in this work. Subspace extraction approach that makes use of both Compressive Sampling and Principal Component Analysis (PCA) is presented in this paper. Inverse Synthetic Aperture Radar (ISAR) Imaging measurement data is used to validate the proposed approach. Experimental results of targets above rough surface with intermediate roughness are presented. Results showed the dimensionality of an intermediate scale rough surface is generally larger than the dimensionality of the finite size targets. Results showed that by compressing the dimensionality through compressive sampling and extracting the principal components, significant improvement in target subspace extraction can be achieved. [C793]

### "Overview of KOMPSAT-5 program, mission, and system"

Korea Aerospace Research Institute (KARI) are developing the KOMPSAT-5 system of which primary payload is X band Synthetic Aperture Radar (SAR). The program overview, mission and system characteristics of KOMPSAT-5 are described in this paper. [C794]

### "UWB electromagnetic borehole logging tool"

Based on a theoretical model of the geosteering borehole logging tool, which operates the broadband pulse, we demonstrate the possibility of detecting an interface between oil- and water-saturated layers in the oil-gas formation. [C795]

### "Temporal analysis of the magma supply system beneath the Okmok caldera by Interferometric Synthetic Aperture Radar and statistical seismology"

The temporal characteristics of the magma supply system beneath the Okmok caldera is examined using Interferometric Synthetic Aperture Radar (InSAR) and statistical seismology. Surface deformation produced by a shallow magma chamber is studied through time series analysis of InSAR imagery acquired between 1995 and 2008 by the ERS-1/2 satellites. A spherical source model (Mogi Source) is utilized to simulate the deformation

pattern produced by the shallow magma chamber's fluctuating geometry. Statistical seismology provides an independent estimate of the magma chamber's depth to reduce the non-uniqueness of the Mogi source model solutions. Seismic results show that a shallow magma chamber is located approximately 4.0 km below the caldera floor. InSAR imagery indicates the chamber has expanded continuously between 1997 and 2008. Modeling results suggest that magma replenishment has occurred at an average rate of approximately  $7.0 \pm 10^{-3} \text{ km}^3/\text{year}$  and that the volume within the chamber returned to its pre-1997 eruption state by June 2008. [C796]

#### "Development of a signal processing subsystem for a spaceborne rotating, fan-beam scatterometer"

This paper introduces an on-board signal processing subsystem of a spaceborne rotating fan-beam scatterometer in China. The subsystem processes returned signal after downconversion to intermediate frequency. To reduce the data stream downlinked from the satellite, the final data bins are summed into 34 energy slices, each with a range resolution of 10 km. Then a simulation process is adopted to analyze the Doppler effects due to the motion of the spacecraft, and to generate the Doppler compensation table and the bin summation table. This method is also used to analyze the measurement variance  $K_{pc}$  of each detected slice. Finally, the coefficients of the expression of  $K_{pc}$  are presented. [C797]

#### "Investigation of cirrus clouds using the calipso lidar data"

Cirrus clouds normally exist in the upper troposphere and sometimes extend into the stratosphere. Unlike low altitude clouds that have a cooling effect on solar radiation through scattering, cirrus clouds scatter only a small amount of solar radiation and prevent a large quantity of long-wave radiation from leaving the earth-atmosphere system. Cirrus clouds are globally distributed and are composed almost exclusively of non-spherical ice crystals. Tropopause cirrus tends to occur over regions of intense convective activity like equatorial Africa and South America, which are sites for vigorous continental convection, and the western Pacific, which is a site of significant oceanic convection. Few instruments can deduce the global presence of cirrus clouds. The Cloud-Aerosol Lidar and Infrared Pathfinder Satellite Observations (CALIPSO) satellite mission provides comprehensive observations of cloud vertical structure on a near-global scale. [C798]

#### "Monitoring environmental conditions in Muuga harbor using Envisat MERIS and ASAR data"

Environmental conditions were monitored using in situ measured inherent optical properties and water sampling together with remote sensing imagery (MERIS and ASAR) in Muuga Bay, Baltic Sea. Simultaneous monitoring using different methodologies gave detailed overview of suspended matter (SPM) load into the water column during the dredging operations. MERIS FRS data enabled to receive the distribution of SPM on water surface. The measurements of inherent optical properties revealed the particle concentration on vertical scale. Backscattering from the ASAR data was in correlation with oil products determined from water samples when ballast water discharge was detected during field sampling. [C799]

#### "Monitoring of thawing process using envisat asar global mode data"

Due to the high temporal sampling rate of ASAR Global Monitoring mode, it has an application potential for analyzing seasonal changes in permafrost environment. The objective of the study is to develop a robust method for monitoring freeze/thaw cycles beyond threshold approaches. In order to use ASAR GM time-series for analyzing freeze/thaw states, a least square fitting of piecewise step function is introduced in this paper. An experiment result for Siberian permafrost area near Yakutsk illustrates that it can be a promising approach in monitoring permafrost ecosystems. [C800]

#### "Monitoring flooded area fraction in floodplains of Parana basin using passive and active microwave systems"

Over the past two decades, orbital passive microwave systems have proven to be sensitive to flood condition in large floodplains. This sensitivity is rooted in the well differentiated emission properties of calm water with respect to non-flooded land of any kind. In this paper, AMSR-E observations of an herbaceous wetland area on the Parana River sub-basin were analyzed during the 2009-10 timeframe when this region was affected by a strong and long lasting flooding. Evident effects on the difference between vertically and horizontally polarized brightness temperatures ( $\Delta T$ ) were observed at C-band. The fraction of vegetated flooded area was estimated by applying an improved algorithm which uses ENVISAT ASAR data at specific dates to calibrate AMSR-E temporal series. Also, using a theoretical emission model, the behavior of  $\Delta T$  flooded is discussed. [C801]

#### "What is the information content of TRMM precipitation radar for determining radiometer"

### observations and vice versa?"

Both the space borne radar and the radiometer suite on the TRMM satellite observe the same column of precipitation and derive rain rates, however at different spatial resolutions. The observations from TRMM PR and TMI are fundamentally different measurements. While the radar provides a backscatter measurement resolved in the vertical direction, the radiometer is a passive instrument obtaining integrated observations over the full depth of the cloud. In addition, they respond to different physical mechanisms. Nevertheless, they observe the same precipitation medium and retrieve the same output products. Therefore, it begs the question, what type of information about radiometric observations can be directly retrieved from radar observations. This question can be further focused and stated as: To what extent can one predict the radiometric observations from radar observations? This question can be answered in several ways, and one of them is an informational theoretic approach using neural networks which is described in this paper. [C802]

### "Detection of land subsidence in Beijing, China, using Interferometric Point Target Analysis technique"

Land subsidence in Beijing is supposed to be caused by over-exploitation of ground water, which is leading to a rapid decline of water levels, drying out clay layers that finally result in land subsidence. The Interferometric Point Target Analysis (IPTA) is an advanced method to monitor vertical motion of the land surface over time. IPTA identifies backscattering objects, named as coherent points or points targets, at the ground surface that persistently reflect radar radiation emitted by the SAR antenna. The core component of the IPTA technique is the iterative estimation of phase differences for all measurement points over the sets of the SAR data using a linear model. In this paper, IPTA technique was used to retrieve the phase history, extract the linear deformation information from interferometry phase and weaken atmosphere phase delay in Beijing. 20 ENVISAT ASAR images acquired between June-18-2003 and March-14-2007 have been selected. The intention of this article is to demonstrate how IPTA technique could be used to extract valuable information in Beijing area. [C803]

### "KOMPSAT-5 spotlight SAR processor using FSA with calculation of effective velocity"

In KOMPSAT-5 program, Korea Aerospace Research Institute has made SAR imaging chain analysis tool to evaluate imaging system of KOMPSAT-5. The tool consists of a simulator and a processor. The simulator simulates observation of a scene by the operational mode of KOMPSAT-5 and generates SAR raw data. The processor generates an image of the scene. This paper is about the second part of processing the simulated raw data that is acquired by the step steering sliding spotlight mode of KOMPSAT-5. For this observation mode, dechirp on receive is operated in receiving the echoes. So, extended frequency scaling algorithm is used to process the raw data in order to directly handle the dechirped data. This paper mainly contributes for the accuracy of effective velocity. The effective velocity criterions for range and azimuth processing allows that the processor uses only one scene center effective velocity in range processing and several ones in azimuth processing. In this paper, a method to increase the accuracy of calculation of effective velocity is also proposed. Simulation result shows that the proposed method is valid. [C804]

### "Fusion: A fully ultraportable system for imaging objects in nature"

To improve satellite-derived estimates of terrestrial plant production and exchange of CO<sub>2</sub>, water, and energy with the atmosphere, scientists need to consider ecosystem composition, structure, function, and health. This can be accomplished through the fusion of Light Detection And Ranging (LiDAR) data, which can provide 3D information about the vertical and horizontal distribution of vegetation and hyperspectral remote sensing, which can inform us about variations in biophysical variables (e.g., photosynthetic pigments) and responses to environmental stressors (e.g., heat, moisture loss). Satellite observations from upcoming Decadal Survey missions will provide NASA with the unique opportunity to fuse LiDAR data from ICESat-II, DESDynI, and LIST with hyperspectral and thermal imagery from HypSIRI and GEO-CAPE. This synergy will augment and enhance the individual science objectives of decadal survey missions, and will allow scientists the opportunity to develop 3D models of plant canopies that better describe global cycling of carbon, water and energy. Multiple NASA's Earth Science Focus Areas are served by this science, including carbon cycle and ecosystems; water and energy cycle; and climate variability and change (i.e., ecosystem responses and feedbacks to climate change). One of the major obstacles to the development of data fusion algorithms is the availability of accurately co-registered data of similar grain size. This is often the case when instruments are flown on different platforms and at different times during a field campaign. We believe that "instrument fusion" is a prerequisite to "data fusion", and we have developed a system that integrates a full-waveform LiDAR, narrow band hyperspectral imager, and broad band thermal imager in a single, compact and portable instrument package that could be readily deployed on a number of observation platforms. FUSION will provide accurate co aligned datasets that are needed for: (i) calibration and validation of satellite-derived land products; (ii) development of data fusion algorithms; and (iii) combine observations from multiple sensors to characterize ecosystem composition, structure, function, and

health. [C805]

#### "A new algorithm for wind speed at low incidence angles using TRMM Precipitation Radar data"

Large datasets from crossovers of Precipitation Radar (PR) and buoy observations clearly demonstrate that ocean PR backscatter correlates with both the near-surface wind speed and the sea surface wave slope. Multi-incidence angles PR data are used to retrieve surface wave slope parameter and normalized nadir backscatter. After that, an empirical wind speed model was developed based on those two parameters that attenuates the surface tilting effect. The inversion is defined using a multilayer perceptron neural network with radar-derived backscatter and surface wave slope parameter as inputs. Results show the root mean square errors between retrieved wind speeds and in situ buoy observations is 1.36m/s, bias is nearly zero, revealing good agreements in wind speed estimations. [C806]

#### "Approach for volcanic surveillance using satellite-borne microwave radiometer data"

Volcanic surveillance is one of the practical fields for remotesensing technology. Monitoring of thermal anomalies on volcanoes by infrared radiometer and detection of slight landsurface deformations around volcanoes by interferometry of synthetic aperture radar (SAR) are good examples. However, an infrared radiometer is a little nervous for clouds which cover volcanoes, and interferometry of SAR also has a weakness that the time resolution becomes low in exchange for high spatial resolution. Meanwhile, focusing on microwave radiometer, we know it is less affected by clouds than infrared radiometer. Its time resolution is also higher than interferometry of SAR. Therefore, microwave radiometer can become a promising tool for volcanic surveillance. But, a new methodology to compensate its coarse spatial resolution is essential. It was a serious problem. [C807]

#### "A study on anomalous signal detection using HMM for ELF electromagnetic wave"

A seismic radiation emitted from the earth's crust is useful for predicting earthquakes. The electromagnetic (EM) wave in the Extremely Low Frequency (ELF) band have been observed at many places in Japan. In this paper, we propose the anomalous signal detection method based on HMM whose input vector is the amplitude density distribution of an EM wave. The amplitude density distribution is calculated from the image of an EM wave data. The optimal scale of an image to calculate an amplitude density distribution and the optimal number of states of HMM are investigated to achieve an accurate detection. [C808]

#### "Application of TerraSAR-X data to the monitoring of urban subsidence in the city of Murcia"

This paper presents an analysis of the performance of TerraSAR-X for subsidence monitoring in urban areas. The city of Murcia has been selected as a test-site due to its high deformation rate and the set of extensometers deployed along the city that provide validation data. The obtained results have been compared with those obtained from ERS/ENVISAT data belonging to the same period and validated with the in-situ measurements. [C809]

#### "Research on interferometric deformation detection for geosynchronous SAR"

The nadir track of geosynchronous satellite can be "figure-8", circular or ellipse track which could be produced with appropriate orbit parameters. In this paper, the characteristics of the interferometric deformation detection for geosynchronous SAR with circular aperture are analyzed. The connection between the interferometric phase and the deformation of repeat pass geosynchronous SAR is derived, and its potential to get three-dimensional 3D deformation measurement is interpreted. [C810]

#### "MVM based SAR image processing for ship pose estimation"

As an essential approach of SAR image interpretation, a good pose estimation calls for two conditions: an accurate extraction of the scattering centers and a thorough exploration of the structural information among them. The article focuses on these two topics successively. Firstly, the power spectrum estimation methods are recommended to improve the scattering center resolution and the Minimum Variance Method (MVM) is chosen for its sidelobe suppressing ability and signal model independence. With the segmented MVM image, the axis extraction problem is then solved by a new strategy, namely the Angle Entropy of Radon transform (AER) strategy. Data from computational electromagnetics are used for experiments. It is shown that the MVM image shows better morphologic feature than the Fourier ones (both original and Hanning-windowed), and the AER strategy achieves more accurate and robust estimation compared with the edge-based Hough transform (HT) technique. [C811]

### "Lidar integrated airborne imaging spectroscopy for root disease detection and measurement of foliar chemistry"

Root disease is a serious concern for the softwood timber industry. This paper reports on the development of a root disease detection procedure that applies lidar integrated with imaging spectrometer data. Chlorophyll-a was found to be significantly affected by the disease in a needle level study[I]. Chlorophyll-a was estimated from canopy reflectance through partial least squares regression and achieved an R2value of 0.82. Continuum removal metrics, which proved to be good estimators at the needle level where found to be insufficient at the canopy level. Through the union of decreased stand density and decreased foliar chlorophyll, potential disease sites were identified in the Greater Victoria Watershed District test site. [C812]

### "Submerged dunes and breakwater embayments mapped using wave inversions of shore-mounted marine X-band radar data"

Surveying very shallow coastal areas, particularly around coastal defences, can be a logistically difficult and time consuming process. A marine-radar based bathymetry mapping technique has been used to remotely map the embayments around a series of shore-parallel breakwaters at Sea Palling on the south east coast of England during the LEACOST2 project. The duration of the deployment spanned over 2 years, with the aim of observing any evolution of bathymetric features over that timescale while providing a clear indication of the spatial variability of wave and current patterns contributing to such evolution. The embayments generated by the shore parallel breakwaters at that site are resolved and a field of subtidal dunes with a wavelength of the order of 200m and amplitude around 1m located in approximately 6-10m of water were within the radar field of view and are evident in the remotely sensed bathymetry. Comparisons between bathymetric data obtained using conventional survey techniques and the radar based technique are presented together with measurements of tidal currents mapped using the same remote sensing method and compared with ADCP data during a storm event. [C813]

### "Field test of KOMPSAT-5 Calibration Equipment"

Korea Aerospace Research Institute (KARI) is developing the KOMPSAT-5 (K-5, the fifth of KOREA MultiPurpose SATellite) system of which primary payload is X-band Synthetic Aperture Radar (SAR). K-5 CALVAL (Calibration & Validation) activities must be important tasks for successful operation. The field test of K-5 Calibration Equipments can support a direction of CALVAL activities during not only IOT (In-Orbit Test) phase but also normal operation phase. [C814]

### "High resolution D-INSAR measurement for land subsidence"

In this paper, a study area of subsidence in the city of Taiyuan has been investigated using TerraSAR-X high resolution data and D-INSAR technique. In order to determine the accurate location and shape of each subsidence center, a time series of differential interferograms has been first generated and applied to preliminary location determination and rough subsidence rate estimation for each subsidence center, then the time series analysis of persistent scatterers including single point objects and highly coherent surface pieces for each subsidence center has been used for accurate positioning of subsidence center and precise subsidence rate estimation. [C815]

### "Preliminary results of a low-frequency 3D-sar approach for glacier volume mapping"

First experimental results with a low-frequency, ultra wideband (UWB) radar for estimating the height of glacier beds are illustrated. We use a 3-dimensional Time-Domain Back-Projection (TDBP) algorithm which incorporates the influence of the refractivity of ice to reconstruct the glacier bed of the Aletsch Glacier in the Swiss Alps using several CARABAS data sets. As the results indicate, the proposed method underlines the ability of low-frequency Synthetic Aperture Radar (SAR) to penetrate into glacier ice and thus, to map glacier volumes on a large scale even with only few, suboptimal data acquisitions. [C816]

### "Application of conventional marine radars for measuring ocean wave fields in shallow water conditions"

This work presents the estimation of wave field properties derived from X-band marine radar measurements taken close to coastal locations, where the wave fields are affected by the finite water depth conditions. The work is focused on the detection of individual waves and their related characteristics, such as the estimation of the local and instantaneous wave envelope derived from the wave elevation fields estimated from X-band marine radar time series. [C817]

### "Multispectral classification of remote sensing imagery for archaeological land use analysis: Prospective study"

Much of human history can be traced through the impacts of human actions upon the environment. The use of remote sensing technology offers the archeologist the opportunity to detect these impacts which are often invisible to the naked eye. The extraction of remote sensing signatures from a particular geographical region allows the generation of geophysical signature maps; this can be achieved using an accurate and recently developed multispectral image classification approach based on pixel statistics for the class description, which is referred to as the Weighted Pixel Statistics method. This paper presents the prospective study of the effectiveness that this approach provides for supervised segmentation and classification of sensed archaeological signatures for land use analysis. The results obtained with this study uses real multispectral scenes obtained with remote sensing techniques (high-resolution synthetic aperture radar) to probe the efficiency of the classification technique. [C818]

### "Directional-adaptive despeckling for high-resolution SAR"

In this study, an iterative maximum a posteriori (MAP) approach using a Bayesian model of Markov random field (MRF) was proposed for despeckling images that contains speckle. Image process is assumed to combine the random fields associated with the observed intensity process and the image texture process respectively. The objective measure for determining the optimal restoration of this "double compound stochastic" image process is based on Bayes' theorem, and the MAP estimation employs the Point-Jacobian iteration to obtain the optimal solution. In the proposed algorithm, MRF is used to quantify the spatial interaction probabilistically, that is, to provide a type of prior information on the image texture and the neighbor window of any size is defined for contextual information on a local region. However, the window of a certain size would result in using wrong information for the estimation from adjacent regions with different characteristics at the pixels close to or on boundary. To overcome this problem, the new method is designed to use less information from the neighbors located in the direction to an adjacent different region and more information from the neighbors located in the inner region of same characteristics. It can reduce the possibility to involve the pixel values of adjacent region with different characteristics. [C819]

### "Signal analysis and modeling of wind turbine clutter in weather radars"

Lately, the continuing expansion of wind energy industry has led to the installation of several wind farms which are often in the vicinity of the weather radars. This is a source of growing concern for the weather radar community since wind turbines interfere with the normal operation of the weather radars. The wind turbine tower can drive the receivers into saturation and the Doppler shift from the moving blades can introduce errors in the estimation of wind speed, reflectivity and rainfall rates. The radar cross-section of the wind turbines has a large temporal and spatial variation which poses additional difficulties for traditional clutter filtering algorithms. This paper presents a first-order theoretical model of the radar signature of a wind turbine that can be helpful in deducing its unique features to be incorporated in filtering out the wind turbine clutter. A comparison with the observations from an S-band radar is made later in the paper. [C820]

### "Triple collocation-A new tool to determine the error structure of global soil moisture products"

Recently Triple Collocation (TC) was adopted for soil moisture application. Results from a first application indicated that the method could be useful to estimate global error patterns. Here we test the method with new data sets. The results show that the method is robust and that it allows to derive objective error estimates. [C821]

### "Automatic exclusion of surface deformation in InSAR DEM generation using differential radar interferometry"

The Digital Elevation Models (DEMs) are an important source of topographical data for many scientific and engineering applications. Where topographical data are unavailable, global coverage elevation data sets, typically DEMs from remotely sensed data, are the main sources of such information. Interferometric SAR (InSAR), is a useful method for low-cost, relatively precise and wide-coverage surface DEM generation. However, ground deformation should somehow be excluded from InSAR-based DEM generation. To identify surface deformation areas, the so-called Differential InSAR (DInSAR) is a commonly used method. In this paper, the authors propose a two-step DEM generation method: the ground deformation area detection using DInSAR technique and deformation area exclusion in InSAR DEM generation by detected mask. [C822]

### "GPM Microwave Imager design, predicted performance and status"

The Global Precipitation Measurement (GPM) Microwave Imager (GMI) Instrument is being developed by Ball Aerospace and Technologies Corporation (Ball) for the GPM program at NASA Goddard. The Global Precipitation Measurement (GPM) mission is an international effort managed by the National Aeronautics and Space Administration (NASA) to improve climate, weather, and hydro-meteorological predictions through more accurate and more frequent precipitation measurements. The GPM Microwave Imager (GMI) will be used to make calibrated, radiometric measurements from space at multiple microwave frequencies and polarizations. GMI will be placed on the GPM Core Spacecraft together with the Dual-frequency Precipitation Radar (DPR). The DPR is two-frequency precipitation measurement radar, which will operate in the Ku-band and Ka-band of the microwave spectrum. The Core Spacecraft will make radiometric and radar measurements of clouds and precipitation and will be the central element of GPM's space segment. The data products from GPM will provide information concerning global precipitation on a frequent, near-global basis to meteorologists and scientists making weather forecasts and performing research on the global energy and water cycle, precipitation, hydrology, and related disciplines. In addition, radiometric measurements from GMI and radar measurements from the DPR will be used together to develop a retrieval transfer standard for the purpose of calibrating precipitation retrieval algorithms. This calibration standard will establish a reference against which other retrieval algorithms using only microwave radiometers (and without the benefit of the DPR) on other satellites in the GPM constellation will be compared. The instrument has completed the Critical Design Review phase of the program. The design of the instrument is complete. We describe the instrument and predict the performance of the GMI instrument. The instrument interfaces have been finalized and the design completed. The final mechanical and electrical interfaces are described. The mechanical interface was specifically designed to provide isolation from the spacecraft and allow accommodation on future low inclination spacecraft. An electrical interface was added coming from the spacecraft that allows the GMI integration to be blanked during Dual Precipitation Radar pulses. The implementation of this blanking is described. The instrument is currently in the flight production phase. Status and initial test results on the flight hardware are presented. [C823]

#### "Multiresolution despeckling of VHR SAR images based on MRF segmentation"

In this work, maximum a posteriori (MAP) despeckling, implemented in the multiresolution domain defined by the undecimated discrete wavelet transform (UDWT), will be carried out on very high resolution (VHR) SAR images and compared with earlier multiresolution approaches developed by the authors. The MAP solution in UDWT domain has been specialized to SAR imagery. Every UDWT subband is segmented into statistically homogeneous segments and one generalized Gaussian (GG) PDF (variance and shape factor) is estimated for each segment. This solution allows to effectively handle scene heterogeneity as imaged by the VHR SAR system. Segmentation exploits a Tree Structured Markov Random Field (TSMRF), which is a low complexity MRF segmentation that allows the estimation of the number of segments and the segmentation itself to be carried out at same time. Experiments performed on a single-look VHR X-band SAR images demonstrate that the segmented approach is effective whenever the classical circular Gaussian model of complex reflectivity may no longer hold. [C824]

#### "Potential of mapping soil moisture by combining radar backscatter modeling and PolSAR decomposition"

The purpose of this study is to evaluate the capability of the Oh backscattering model in combination with the Freeman Durden decomposition to estimate soil moisture over agricultural fields from fully polarimetric RADARSAT-2 C-band SAR responses. Initially, soil moisture multi-polarization retrieval was accomplished by using a look-up table (LUT) approach applied to the Oh model. Two methods were considered: the multi-polarization method and the one-unknown configuration. Of the two methods, results showed that the HH-HV inversion provided the best estimates. In the second phase, the Freeman Durden decomposition was applied to the polarimetric data. The conceptual approach for retrieving soil moisture using the surface scattering component of the total power was implemented in a LUT inversion. The algorithm attempts to minimize the difference between measured single scattering power obtained by applying the Freeman Durden decomposition and simulated total power using Oh model. When compared with the multi-polarization approach, this polarimetry-based method improves the accuracy of soil moisture estimates. [C825]

#### "Evaluation of system polarization quality for polarimetric SAR imagery and target decomposition"

The quality of polarimetric synthetic aperture radar (PolSAR) imagery and its polarimetric decompositions depends on the accuracy of polarimetric observations of the SAR system and its calibration. Polarization distortions on the polarimetric measurement can be incurred due to nonideal system polarization quality and propagation factors, such as channel imbalance, cross-talk, and Faraday rotation at lower frequencies. All these distortions have varying impacts on different target types as well as different decomposition methods. In this paper, we assess the polarization quality of the PolSAR system in the context of polarimetric imagery analysis and quantify the various effects of polarization distortions on polarization target decompositions. A generic metric

is defined to measure the polarization purity of the system. Considering the fact that target decomposition plays an important role in imagery analysis, we apply several widely used decomposition methods to showcase the polarimetric system requirement based on the defined metric. [C826]

#### **"Imaging algorithm and experimental demonstration of rotating scanning interferometric radiometer"**

Recently, a new concept of rotation scanning synthetic aperture interferometric radiometer (RS-SAIR) has been receiving more and more attentions for its advantage of much simpler configuration with looser requirements of antenna elements. In this article, we investigate the imaging theory of RS-SAIR, and introduce the pseudo-polar FFT algorithm to deal with the polar u-v samples. It only involves 1D interpolation and 1D FFT routine that guarantee a high accuracy and computation efficiency. The sampling strategy and aliasing effect of RS-SAIR are studied with this imaging algorithm. Numerical simulations are provided to validate the associate theory. Finally we develop a 5-elements RS-SAIR instrument and carry out rotating scanning imaging experiment successfully. The first imaging results consist with the expectation. [C827]

#### **"Comparing data of two airborne L-band radiometers with different spatial resolution over a heterogeneous land surface"**

This paper describes a first attempt of comparing data of the two airborne L-band radiometers EMIRAD and HUT-2D over land surface. While HUT-2D is an imaging system with a high spatial resolution, EMIRAD delivers data averaged over a relatively large footprint but can be considered to be more stable. The Upper Danube catchment, located mostly in Southern Germany, is one of two major test sites in Europe for the calibration and validation activities for the Soil Moisture and Ocean Salinity (SMOS) mission launched by the European Space Agency (ESA). For the study presented in this paper, the radiometric measurements collected during the SMOS Validation Rehearsal Campaign 2008 in the Upper Danube catchment are used. The results suggest that differences between the measurements are mainly controlled by temperature effects and can be limited by implementing a temperature correction in the processing of HUT-2D data. [C828]

#### **"The bistatic electromagnetic signature of heterogeneous sea surface: Study of the hydrodynamic phenomena"**

In this article, we carried out a preliminary study on the hydrodynamic effect (non-linear) produced by the breaking of a coastal wave on the scattering coefficient (in horizontal and vertical polarization) in the bi-static configuration (forward propagation). We calculated in X-band (10 GHz)  $\sigma_{HH}$  and  $\sigma_{VV}$  of a series of oceanic surfaces (different phases of construction of a breaking wave ( $\theta_i = -20^\circ$ )) then we studied the different characteristics for each scattering coefficients. In this first study we considered that the maritime surface is the perfect conductor. [C829]

#### **"Contribution of small-scale correlated fluctuations of the microstructural properties of a spatially extended geophysical target under the assessment of radar backscatter"**

The study of the collective effects of radar scattering from an aggregation of discrete scatterers randomly distributed in a space is important for a better understanding of the origin of the backscatter from spatially extended geophysical targets (SEGT). We consider the microstructural irregularities of SEGТ as the essential factor that affects radar backscatter. To evaluate their contribution, this study uses the "slice" approach: particles close to the front of an incident radar wave are considered to reflect incident electromagnetic waves coherently. The radar equation for a SEGТ is derived. The equation includes contributions to the total backscatter from correlated small-scale fluctuations in the slice's reflectivity. The correlation contribution changes in accordance with an idea proposed earlier by Smith (1964) based on physical consideration. The slice approach applied allows parameterizing the features of the SEGТ's inhomogeneities. [C830]

#### **"Characteristics of rough surface parameters estimated from measured surface profile of finite length"**

Estimation of roughness parameters of soil surface is one of the important problems in the field of radar remote sensing. In order to estimate these parameters from measured surface height-profile, data samples with sufficiently long record length are required for accurate estimation. In an actual measurement situation, however, it is difficult to get the surface height-profile in pure form because a bias and inclination of the data are unknown. In this study, we present a method for estimation of the bias and inclination from measured surface height-profile and reveal the effect of the accuracy on the parameter estimates. [C831]

#### **"Target detection performance analysis for airborne passive bistatic radar"**

For a ground-based/airborne passive bistatic radar, its performance is dependent on the geometrical configuration and the passive transmit signal attributes. Theoretical power budget and ambiguity function analysis using a ground-based non-cooperative transmitter of opportunity with a passive bistatic radar being airborne but stationary (airship, etc.) had shown that target detection performance is limited by the strong direct path coupling signal. In comparison, the bistatic ground clutter power is significantly lower and even more so for noise power. For the passive radar to perform satisfactorily, sufficient attenuation must be provided for the direct path and strong ground clutter signals, corresponding to increasing the height of the target peak on the ambiguity function pedestal. In addition, performance could also be improved by increasing the time-bandwidth product (assuming no target migration issues), which lowers the pedestal of the ambiguity function of the strong direct path interfering signal. [C832]

### "Building detection and radar footprint reconstruction from single VHR SAR images"

The development of methods for the automatic detection and reconstruction of building radar footprints from single very high resolution (VHR) synthetic aperture radar (SAR) images is a difficult task for two main reasons: i) the very high complexity of VHR SAR images; and ii) the need to develop efficient algorithms that can be applied to large images in order to be used in real applications. In this paper we present a novel method for automatic building detection, which also reconstructs the 2D radar footprint of the detected buildings. The method is based on the extraction of a set of low-level features from the images and on their combination in more structured primitives. Then the semantic meaning of primitives is used for the definition of building candidates and for the radar footprint reconstruction. In order to process large VHR SAR images, the method has been implemented on a computer cluster. We demonstrate the effectiveness of the method using a large TerraSAR-X spotlight scene. [C833]

### "Unsupervised nonparametric classification of polarimetric SAR data using the K-nearest neighbor graph"

Polarimetric SAR classifications are often based on assumptions about the shape of clusters in the data space. Such a scheme will fail for nonlinear structures in the feature space, unless the classification algorithm has the capacity to describe cluster shapes in sufficient generality. Existing polarimetric SAR classification methods are faced by this exact problem: typically they initialize clusters in the Cloude-Pottier parameter space [1], further optimizing them in the coherency matrix space [2, 3]. Methods using K-means [2] or agglomeration [3] require clusters that are spherical, or compact and well separated, respectively. In the Cloude-Pottier space, these requirements are not met, so initialization in the Cloude-Pottier space cannot be consistent with optimization by K-means or agglomeration. This paper sets out to address this problem, by implementing a new data-driven clustering approach, for arbitrarily shaped clusters. It is applied to quad-polarisation data, demonstrating the new methodology's potential for forest land-cover type discrimination. [C834]

### "Development of a three-element interferometer at 50–56 GHz for Geostationary Interferometric Microwave Sounder (GIMS)"

The Geostationary Interferometric Microwave Sounder (GIMS) is a new concept imaging radiometer proposed by CSSAR, aiming for China's next generation geostationary meteorological satellite (FY-4M). The concept of GIMS is based on aperture synthesis with a rotating circular thinned array. A three-element interferometer has been developed and tested to investigate the feasibility of the GIMS system design. A full-scale ground-based demonstrator with 27 elements is also under development, which is defined as a minimum system intended to fulfill the threshold application requirements. In this paper, the preliminary results of these activities will be reported. [C835]

### "High-resolution mapping of fluvial landform change in arid environments using terrasars-X images"

The high resolution acquisition mode of TerraSAR-X provides a new dimension in fluvial landform change detection. Here we analyzed high resolution (5 m) coherence images with temporal baselines of up to a year from the Palpa Valley in the hyper-arid coastal desert of southern Peru. The results provide evidence that this sensor is suitable for mapping the land surface changes caused by erosion and sedimentation following rainfall and runoff events in bare desert landscape units. [C836]

### "Implementation of a low cost, lightweight X-band antenna with integrated SiGe RF electronics"

This paper presents an organic, lightweight X-band antenna array with integrated silicon germanium (SiGe) low noise amplifiers (LNA) and 3-bit phase shifters (PS). The SiGe LNAs and PSs were successfully integrated onto an 841 lightweight antenna stack-up utilizing a multilayer liquid crystal polymer (LCP) substrate. Successful

comparisons of the measured and simulated results verify a working antenna array with a return loss of around 10 dB across the frequency band of 9.25 GHz-9.75 GHz. A comparison of radiation patterns for the 841 antenna with integrated SiGe LNA and the 841 antenna with integrated SiGe LNA and PS show a 16 dB and 25 dB increase in gain, respectively. The ultimate goal is to develop an airborne X-band radar capable of a beam steering of at least  $\pm 40^\circ$  through utilization of low power highly integrated SiGe electronics on a low cost multi-layer organic platform. This paper represents the first successful demonstration of a building block prototype (i.e., a fully integrated, high gain X-band antenna with SiGe LNAs and SiGe phase shifters) that can be expanded to a complete active phased array for remote sensing applications in X-band. [C837]

#### "Improvement of ship detection accuracy by sar multi-look cross-correlation technique using adaptive CFAR"

This paper describes a novel technique to improve the accuracy of ship detection by synthetic aperture radar (SAR). The methodology is to apply the algorithm of constant false alarm rate (CFAR) to the coherence images produced by multi-look cross-correlation (MLCC) of sub-images. The experiment was carried out in the Tosa bay, Kochi, Japan using three known fishing boats and the simultaneous data acquired by the Phased Array L-band SAR (PALSAR) on board of the Japanese Land Observing Satellite (ALOS) at four different modes. The inter-look coherence images were found to fit best to Gamma distribution, and using this distribution function, CFAR was applied to the coherence image. The results showed substantial improvement in signal to noise ratio and false alarm rate as compared with the coherence image alone. In the followings, the principle of MLCC-CFAR and experimental procedure are summarized, and the results are discussed. [C838]

#### "Japanese hyper-multi spectral mission"

The hyperspectral and the multispectral (hyper-multi spectral) mission is the Japanese next generation space-borne radiometer development project. This project is a heritage from ASTER launched in December 1999. The performance of the hyperspectral radiometer is 30m ground sampling distance, 30km swath width, 10nm and 12.5nm wavelength distance for VNIR and SWIR respectively, over 450@620nm and 300@2,100nm of the signal to noise (S/N) ratio. The performance of the multispectral radiometer is 5m ground sampling distance, 90km swath width, over 200 for all bands of S/N ratio. This project will be launched on ALOS-3 of JAXA in FY2014. The panchromatic sensor with stereo viewing will also be installed on ALOS-3. [C839]

#### "Automatic ship detection in sar images using aegir"

Aegir is an automatic ship detection tool developed at FFI. Now it analyses the different polarisation channels independently. The goal is to fuse the channels before the analysis starts, and to detect the ships in the fused channels. When dual-polarised data is available it is possible to look at the channels individually and combined. When fully polarised data is available, it is also possible to use the scattering matrix and decompose it in different ways. [C840]

#### "Bistatic SAR along track interferometry with multiple fixed receivers"

This paper presents an along-track interferometry (ATI) study for a bistatic or multistatic SAR configuration with fixed ground receivers. This technique can be useful for sea current estimation or for any problem of Ground Motion Target Indicator (GMTI). The proximity of the ground receivers to the scene allows to be very sensitive to velocities with small baselines. This paper also proposes a multibaseline approach for ATI able to differentiate among different velocity contributions in the same resolution cell. At the end of this paper, some results over real acquired bistatic data will be presented and discussed. The data have been acquired using the C-band SAR Bistatic Receiver for INTERferometric Applications (SABRINA) and ESA's ENVISAT satellite, as a transmitter of opportunity. [C841]

#### "Radar retrieval of subsurface parameters for layered media with nonsmooth interfaces"

The solution to the inverse problem for a three-layer medium representing a large class of natural subsurface structures is developed in this paper using radar data. The retrieval of the layered medium parameters is accomplished as a sequential nonlinear optimization starting from the top layer and progressively characterizing the layers below. The optimization process is accomplished by an efficient iterative technique built around the solution of the forward scattering problem. The forward scattering process is formulated by using the Extended Boundary Condition Method (EBCM) and constructing reflection and transmission matrices for each interface. These matrices are then combined into the generalized scattering matrix for the entire system, from which radar scattering coefficients are then computed. To be efficiently utilized in the inverse problem, the forward scattering model is simulated over a wide range of unknowns to obtain a complete set of subspace-based equivalent closed form models that relate radar cross section coefficients to the sought-for parameters including dielectric

constants of each layer and separation of the layers. The inversion algorithm is implemented as a modified conjugate-gradient-based nonlinear optimization. It is assumed that multifrequency radar measurements are available from tower-mounted or airborne platforms, for example at typical radar frequencies of L-band and P-band (UHF). It is shown that this technique results in accurate retrieval of surface and subsurface parameters, even in the presence of noise. [C842]

#### **"Combined active and passive measurements of snow, bare and vegetated soils microwave reflective and emissive characteristics by Ka-band, combined scatterometer-radiometer system"**

In this paper the results spatio-temporally collocated measurements of bare, dry vegetated and ash covered soils microwave reflective (radar backscattering coefficient) and emissive (brightness temperature) characteristics angular dependences at ~37GHz are presented. During the experiment with dry vegetated soil the observed area was set ablaze and microwave active and passive measurements at 300 incidence angle were continued for smock, fire and ash situations. For these measurements Ka-band, polarimetric, combined scatterometric-radiometric system was used, set on a mobile buggy moving along the measuring platform. Structures, operational features and the main technical characteristics of the used system are presented too. The paper has an aim as well to attract attention of interested researchers and to invite them to perform their own or joint researches using available devices and facilities. [C843]

#### **"A new scalloping filter algorithm for scansar images"**

Due to its specific way of scanning over multiple sub-swaths of a radar image, a ScanSAR (scanning synthetic aperture radar) cannot sample Doppler histories continuously like a regular SAR in stripmap mode. This can cause an artifact known as azimuthal scalloping, a wave-like modulation of the image intensity in azimuth direction. Although the problem is theoretically understood, many ScanSAR images of ocean scenes continue to exhibit scalloping. This hampers their use for applications such as wave and wind retrievals. We have developed an efficient descloping algorithm that can be applied to such images as a post-processing tool. We describe how it works and show examples. [C844]

#### **"Geometric refinement of road networks using network snakes and SAR images"**

In this paper, a new approach for the geometric refinement of road networks using network snakes and SAR images is presented. Network snakes are based on the well-known active contour models, but in addition to the image energy and internal energy the topology is introduced into the optimization process. This graph-based active contour method enables a complete topological and shape control during the object delineation. The method is applied to the geometric refinement of road networks to improve and correct GIS-databases as a basis for traffic navigation or infrastructure planning purposes. The proposed approach is either able to deal with roads from a database as initialization in an automatic system or, alternatively, within an interactive framework to derive a geometrically optimized road network. The derived results using SAR images are evaluated with reference data to demonstrate the benefit and transferability of network snakes. [C845]

#### **"Characterization of full surface roughness in agricultural soils using groundbased LiDAR"**

Microwave emission and scattering models require the parametrization of surface roughness. Traditionally this has been achieved by sampling the surface in transects. In this work, roughness is characterized from 3D surface models derived from ground-based LiDAR. The dataset consist 18 surfaces with varying roughness characteristics. 2D profiles extracted from the surface model constitute the baseline to compare to traditional profiling methods. It was found that sampling using profiles produces an underestimation of the RMS<sub>h</sub> by 25-63% and an even more severe underestimation in the correlation length that can reach up to an order of magnitude difference. From the 17,178 2D extracted profiles it was determined a significant sensitivity of the roughness parameters to the detrending methods, as well as a poor fit between the experimental ACF and the exponential and Gaussian models. Finally, methodologies to detrend quasi-periodic surfaces and the decomposition of surface at different scales are proposed and illustrate the advantage of having a 3D representation. [C846]

#### **"Multi beam joined estimation for persistent scatterer interferometry"**

The persistent scatterer interferometry (PSI) is a powerful technique to monitor the line of sight (LOS) deformation with Millimeter accuracy in urban areas. Nowadays, this technique is well established for the sensors ERS and Envisat/ASAR. Nevertheless, the availability of high resolution SAR sensors enables new applications which require new estimation principles. Application test cases for the sensor TerraSAR-X were demonstrated already. However, the high resolution data are not really fully exploited at the moment. This paper

describes a newly developed PSI estimation principle which improves the spatial resolution by the support of distributed scatterers and increases the temporal sampling by the joint estimation of different beams. The prototyped technique needs to cope with the different projections of the horizontal and vertical deformation components onto the line of sight (LOS). Basically, this allows the inversion of the beam's observation equation and finally retrieves the vertical and horizontal deformation components. [C847]

#### "Iterative calibration of relative platform position: A new method for SAR baseline estimation"

Baseline calibration is needed in most of SAR interferometry processing. An iterative optimization of baseline with constrain of relative platform position is presented in this paper. The SAR passes which gives inaccurate platform position is successfully detected and calibrated using this algorithm. After processing, new estimated baseline improves the quality of interferogram. Existence of reference Digital Elevation Model (DEM) error and atmospheric phase screen (APS) can also be detected from the convergence value. This method is based on a reversed concept of platform position estimation from interferometric result. Validation of method performed on multiple SAR images over Singapore. [C848]

#### "Multibaseline gradient ambiguity resolution to support Minimum Cost Flow Phase Unwrapping"

The TanDEM-X Mission has as primary objective to generate a high resolution global Digital Elevation Model. This paper proposes a new method for multibaseline Phase Unwrapping which is the critical point of this generation. We propose to combine both Minimum Cost Flow (MCF) and Maximum a Posteriori (MAP) estimation. The latter is used to solve phase gradient ambiguities. The problem is posed as an energy minimization one and solved using Belief Propagation (BP) which is an iterative process. Nevertheless, although very good results are obtained on loopy graphs, it is not guaranteed to converge. Thus, phase unwrapping of the most accurate interferogram is finally performed with the MCF algorithm and takes as input the unwrapped gradients. [C849]

#### "Context-dependent landmine detection with ground-penetrating radar using a Hidden Markov Context Model"

Context-dependent approaches to landmine detection have been developed in recent years to exploit the sensitivity of ground-penetrating radar (GPR) to changes in environmental conditions. Previous approaches to context-dependent fusion have only considered the special case of statistically independent observations. This work proposes the use of Hidden Markov Models, trained on the GPR background, for modeling the context of observation sequences. The performances of context-dependent fusion using two statistical context models were compared in an experiment with field data. One approach utilized a Hidden Markov Context Model (HMCM), and the other utilized a Gaussian mixture. Experimental results illustrated that the HMCM improved performance of context-dependent fusion. These results suggest that spatial dependencies are an important source of contextual information for landmine detection that warrants further investigation. [C850]

#### "Ka-band SAR interferometry studies for the SWOT mission"

The primary objective of the National Research Council (NRC) Decadal Survey recommended SWOT (Surface Water and Ocean Topography) Mission is to measure the water elevation of the global oceans, as well as terrestrial water bodies (such as rivers, lakes, reservoirs, and wetlands), to answer key scientific questions on the kinetic energy of ocean circulation, the spatial and temporal variability of the world's surface freshwater storage and discharge, and to provide societal benefits on predicting climate change, coastal zone management, flood prediction, and water resources management. In this paper, we present the overall concept of the SWOT mission, as well as the scientific rationale, objectives and development status of the technology items currently under development. [C851]

#### "Advanced techniques and new high resolution SAR sensors for monitoring urban areas"

In the last years MultiDimensional (3D and 4D) Synthetic Aperture Radar (SAR) techniques, also known as SAR tomography and differential SAR tomography, are emerging in the field of coherent combination of multibaseline/multitemporal SAR data. With respect to the classical differential interferometric processing, these techniques improve the capability of detection and monitoring of the ground targets. Moreover they were proven to be effective in resolving the signal interference due to the layover effect, that may occur in areas with high density of scatterers located on vertical structures, such as urban areas. Beside the development of these advanced techniques the new generation of sensor, such as TerraSAR-X and COSMO-SKYMED with very high spatial resolution offer new perspectives in the imaging and monitoring of urban areas. In this paper we address the application of the SAR tomography to real spaceborne data. Particularly, we show and discuss the first results of the application of this technique to high resolution TerraSAR-X data. [C852]

### "Monitoring grasslands with radarsat 2 quad-pol imagery"

Radarsat 2 quad polarization imagery has been used to study the effectiveness of polarimetric radar to monitor the extent and health of prairie grasslands in southern Alberta, Canada. In this report of preliminary findings, the imagery is shown to be effective in the separation of cropped lands from rangelands, and in the separation of native grasslands and improved pastures. Classification was more accurate using Freeman-Durden decomposition parameters than using Cloude-Pottier parameters. Incidence angle differences were noted and use of multiple angles in classification improved accuracy. In a second part of the study, it was shown that polarimetric imagery was capable of identifying weeds and brush growing in native rangeland, and in separating different kinds of brush and weeds. Validated sample sets were too small to allow proper accuracy assessment, but a 'performance metric' showed that accuracy would be improved by use of multiple incidence angles, and by the use of Freeman-Durden or coherency matrix parameters. [C853]

### "Electromagnetic characteristics of simple targets embedded in chiral multilayer structures"

The scattering properties of a chiral stratified multilayer structure having an printed planar electric dipole are addressed in this paper. In order to obtain the scattered fields the method of moments in spectral domain is applied. The dipole scattering is characterized by the radar cross section (RCS), the polarimetric response, the  $\alpha$ -angle from Cloude-Pottier's target decomposition theorem and the directivity function. The results point out that all parameters are sensible to variations on the chiral layer admittance. The chiral layer impinges a rotation on the polarization plane of linearly incident wave for all frequency analyzed. [C854]

### "Improved hurricane active/passive simulated wind vector retrievals"

Microwave scatterometers are the standard for satellite ocean vector winds (OVW) measurements, and they provide the major source of global ocean surface winds observations for scientific and operational applications. A major challenge for Ku-band scatterometry missions is to provide reliable retrievals in the presence of precipitation, particularly in extreme ocean wind events that are usually associated with intense rain. This paper explores the advantages of combining dual frequency (C- and Ku-band) scatterometer measurements and passive microwave observations to improve high wind speed retrievals. For this study, a conceptual design proposed by the Jet Propulsion Laboratory for a Dual Frequency Scatterometer (DFS) to fly onboard the future Japan Aerospace Exploration Agency (JAXA) GCOM-W2 mission with the Advanced Microwave Scanning Radiometer (AMSR) was adopted. A computer simulation that combines the DFS and AMSR measurements was used to develop an artificial neural network OVW retrieval algorithm. The Weather Research and Forecasting (WRF) numerical weather model of Hurricane Katrina (2005) was used as the nature run (surface truth), and simulated OVW retrievals demonstrate that this new technique offers a robust option to extend the useful wind speed measurements range beyond the current operating scatterometers for future satellite missions. [C855]

### "Forest structure from longer wavelength SARs"

In this paper we address three topics related to SAR Tomography of forest scenarios at P-Band. In first place we discuss the role of pulse bandwidth, which is shown to play a critical role as for the capability of the Tomographic system to separate ground and canopy contributions. Accordingly, vertical resolution depends not only on baseline aperture, but also on pulse bandwidth. Another factor to be accounted for is phase calibration, as the quality of the vertical focusing carried out by SAR Tomography is strictly related to the condition that phase contributions due to platform motion or atmospheric propagation are properly compensated for. Finally, multiple scattering phenomena are likely to occur at longer wavelengths, resulting in Tomographic techniques not being suffice for the aim of discriminating ground and volume scattering. The three points above are here discussed in light of the results achieved in the framework of the ESA campaign BioSAR 2008. The analysis has been carried out by exploiting the Algebraic Synthesis technique, which provides a theoretical framework to decompose the SAR signal into ground-only and volume-only contributions. Ground-only contributions provide an easy and viable way to phase calibrate the data stack. Volume-only contributions, if correctly identified, allow a direct Tomographic imaging of the vegetation layer. The impact of pulse bandwidth is tackled by assuming a Common Band Filtering approach, which results in a vertical resolution improvement by a factor 2. [C856]

### "DESDynI lidar for solid earth applications"

As part of the NASA's DESDynI mission, global elevation profiles from contiguous 25 m footprint Lidar measurements will be made. Here we present results of a performance simulation of a single pass of the multi-beam Lidar instrument over uplifted marine terraces in southern Alaska. The significance of the Lidar simulations is that surface topography would be captured at sufficient resolution for mapping uplifted terraces features but it will be hard to discern 1-2m topographic change over features less than tens of meters in width. Since Lidar

would penetrate most vegetation, the accurate bald Earth elevation profiles will give new elevation information beyond the standard 30-m DEM. [C857]

**"Studies of the influence of rainfall upon scatterometer estimates for sea surface stress: Applications to boundary layer parameterization and drag coefficient models within tropical cyclone environments"**

The use of satellite scatterometers to probe the winds in and near strong tropical cyclones (TCs) is a valuable tool for both numerical weather prediction (NWP) and weather forecasters. The presence of widespread rain in these storms complicates the estimation of surface winds from the satellite. Improvements in the techniques to infer surface winds from the satellite observations, which remove the effects of rain contamination at the ocean surface, will improve the modeling efforts as they pertain to the prediction of TC intensity. This study will demonstrate the use of collated and simultaneous high-resolution rain measurements obtained from nearby Next-Generation Radar (NEXRAD) and NASA Quick Scatterometer (QuikSCAT) measurements, respectively. Through the application of the National Oceanic and Atmospheric Administration (NOAA)/Atlantic Oceanographic and Meteorological Laboratories (AOML)/Hurricane Research Division (HRD) TC wind analysis (H\*WIND; Powell and Houston [1996] ), we will study the dependence of a surface normalized radar cross-section (NRCS) on the TC wind-speed and rain-rate. The objective is to better observe and understand the dependence of the drag coefficient upon the surface stress across a wide range of conditions and spatial scales within these storms. [C858]

**"Semantic segmentation of Polarimetric SAR imagery using Conditional Random Fields"**

The paper proposes a fast and accurate semantic segmentation approach for a large Polarimetric SAR (PolSAR) image using Conditional Random Fields (CRFs). It efficiently incorporates the polarimetric signatures, texture and intensity features into a unite CRFs model, and employs a fast max-margin training method for parameters learning. Experiments on RadarSat-2 PolSAR data in Flevoland test site demonstrate that our approach achieves precise segmentation results with a few well-selected training samples. [C859]

**"A MIMO technique for enhanced clutter selectivity in a multiple scattering environment: Application to HF surface wave radar"**

The significance of multiple scattering processes whereby unwanted Doppler-spread energy can contaminate HF/SWR remote sensing measurements has recently been reported. In this paper we present the results of quantitative calculations of the extent of the contamination, and then outline a solution based on the adoption of MIMO radar concepts which have been applied successfully in HF skywave radars. [C860]

**"Detection of rapid land subsidence of civil constructions with TerraSAR-X interferometry"**

The TerraSAR-X SAR system provides high spatial resolution and geometric accuracy imagery which supports well the mapping of the 3-D structure of large-scale civil infrastructure and its motions (4-D). In this work, we investigated the potential of TerraSAR-X observations for monitoring rapid land subsidence induced by reclamation activities. A case study was conducted in Hong Kong Disneyland Theme Park (DTP) at the Penny's Bay, one of the largest land reclamation projects worldwide. A total of 16 TerraSAR-X scenes were used in a small-baseline PSI method for retrieving residual reclamation settlement in the study area. The preliminary results indicate that a remarkably high density of high coherent point targets (>2,500 PS point/km<sup>2</sup>) was identified in the reclamation area and a large land subsidence rate on the order of 35 cm/yr could be detected in the center of reclaimed land. The high detail level of deformation filed as well as the high sensitivity regarding rapid residual settlement makes TerraSAR-X interferometry a remarkable potential Earth Observation technique to enable the detection of ground deformation related to the large-scale infrastructure development in reclaimed land. [C861]

**"One-day interferometry results with the COSMO-SkyMed constellation"**

COSMO-SkyMed is a Dual-Use (Civilian and Defence) End-to-End Earth Observation System aimed at establishing a global service supplying provision of data, products and services relevant to a wide range of applications, such as Risk Management, Scientific and Commercial Applications and Defence Applications. The system consists of a constellation of four LEO mid-sized satellites, each equipped with a multi-mode high-resolution SAR operating at X-band. Three out of four COSMO-SkyMed satellites have been successfully launched, while the remaining satellite will be deployed within 2010. The first two satellites have been launched in 2007 while COSMO-SkyMed-3 has been launched on October 25th 2008. Since its launch COSMO-SkyMed-3 has been put in an orbital position at 67,5° from COSMO-SkyMed-2, in the so-called "one-day interferometry

configuration". Since then COSMO-SkyMed-2 and COSMO-SkyMed-3 are providing a interferometric pairs for a wide range of applications. [C862]

### "Estimation and compensation of ionospheric delay for SAR interferometry"

For spaceborne SAR (Synthetic Aperture Radar) systems, the dispersive effects of the ionosphere on the propagation of the SAR signal can be a significant source of phase error. While at X-band frequencies the effects are small, current and future L-band systems would benefit from ionospheric compensation. We consider two ways to estimate the ionospheric delay in SAR signals and evaluate them on L-band ALOS-PALSAR acquisitions. [C863]

### "Phase retrieval in SAR interferograms using diffusion and inpainting"

A high-contrast inpainting scheme based on the Complex Ginzburg-Landau equation recently applied successfully to image restoration is applied to SAR interferograms to improve their quality and therefore final quality of Digital Elevation Models (DEMs). The new technique attempts to recover the phase values in low coherence regions through diffusion and inpainting. After phase unwrapping low coherence regions are masked and discarded and a Complex Ginzburg-Landau (CGL) inpainting scheme is applied to regions where phase values are missing. We demonstrate that the residues reduce and the proposed algorithm leads to a higher Signal-to-Noise Ratio (SNR) if compared with MCF algorithm. The restoration technique has been applied to ERS-1 and ERS-2 data sets acquired on July 1995. Results appear to be very promising: the proposed algorithm provides good performances especially in presence of strong noise level and low coherence areas with relatively small dimensions. [C864]

### "A modified wind vector retrieval algorithm for polarimetric scatterometer"

Experiments and theoretical analysis demonstrate that the polarimetric scatterometer has the potential in enhancing the accuracy of the wind vector retrieval. However, currently, there is no special wind vector retrieval algorithm for the polarimetric scatterometer. Based on the distribution characteristic of the objective function, a modified wind vector retrieval algorithm was designed for the conically scanning polarimetric scatterometer in this paper. Simulation experiments indicated that this algorithm could further improve the retrieval precision of the polarimetric scatterometer in comparison with the traditional algorithm, especially in the nadir- and outer-swath. By extending the wind direction range for the first and second ambiguity in the nadir- and outer-swath, the algorithm can effectively reduce the uncertainty of the wind direction solutions with error magnitude of 0° to 15°. Up to 2° improvement in wind direction retrieval can be achieved in the nadir track. [C865]

### "Status, results, potentiality and evolution of COSMO-SkyMed, the Italian Earth Observation constellation for risk management and security"

COSMO-SkyMed is a Dual-Use program, devoted to produce both civilian and military applications, and as such it is required to have a fast response time, to manage conflicts and to optimize resources. In order to provide operational continuity to COSMO-SkyMed mission, the Italian Space Agency (ASI) and Italian Ministry of Defense (It-MoD) are conceiving the next generation of the system. The new system, called "COSMO-SkyMed Seconda Generazione" (CSG), starting from the well established design of the first generation, will provide the end user with outstanding characteristics consolidating its position in the frame of SAR Systems. After a description of the current COSMO-SkyMed unique in-orbit performances, functionalities and Dual-Use operations, with examples of data already acquired in the last few years, the paper will introduce the CSG mission describing the main features and capabilities that will drive the design of the new system. [C866]

### "Disaster mapping from medium spatial resolution alos palsar images"

All-day and all-weather Synthetic Aperture Radar (SAR) can measure both intensity and phase of the reflected signal. The backscattering coefficients measured by SAR reflect the backscatter characteristics of surface targets. Changes happened to a target's surface roughness, geometric and structural characteristics will result in the change of its backscattering intensity recorded in SAR image. The 2008 Wenchuan earthquake, China have caused widely distributed geological disasters, such as landslides, mudfloods and barrier lakes, which resulted in the difference between pre- and post-earthquake SAR images. Comparison between the pre- and post-earthquake SAR intensity images will reveal the damage information. In this study, PALSAR Level 1.0 data acquired for the Wenchuan earthquake were used to analyze the geological disasters. Results show that medium spatial resolution SAR data, such as 10 m resolution ALOS PALSAR data, especially when both pre- and post-earthquake images are available, are useful in revealing the distribution of landslides and barrier lakes. [C867]

### "Performance analysis of atmospheric correction in InSAR data based on the Weather Research and Forecasting Model (WRF)"

The influence of the turbulent atmosphere is seen as the main performance limitation for high-quality Interferometric Synthetic Aperture Radar (InSAR) techniques in ground deformation monitoring applications. Atmospheric correction using numerical weather prediction (NWP) models is widely seen as a promising emerging technology for mitigation of atmospheric signals. First results showed promising capabilities for correction of stratified delay yet have revealed limited performance for modeling and mitigating turbulent atmospheric water vapor signals from SAR [1, 2]. This paper presents an integration of InSAR observations with predictions from the high-resolution Weather Research and Forecasting Model (WRF). Special focus is put on investigating improvements in the weather model parameterization to achieve enhanced performance in atmospheric correction. First, a statistical analysis of the quality of absolute delay predictions is presented based on a comparison of vertically integrated WRF delays with radiosonde measurements. Second, the performance of WRF for atmospheric correction of InSAR data is analyzed by comparing WRF phase delay maps to SAR interferograms and analyzing structure functions and variances of the residual atmospheric delay signal. Here, significant improvements could be achieved through modifications of the WRF model parameterization, which are highlighted in Section 3.2. From our study, we conclude that the performance of latest generation high-resolution NWP models can be significantly improved if the setup and parameterization of the model domain is optimized. [C868]

### "The mathematic model of multipath error in airborne interferometric SAR system"

In airborne two-antenna interferometric SAR system, the returned pulse may be reflected by parts of the aircraft platform into the antennas, and this is called multipath effect which will cause oscillating phase errors and hence height errors. This paper presents a theoretical model to compute the multipath error. In this model the multipath phase error is a function of look angle or ideal phase, and the unknown parameters of the model can be estimated from distributed targets with known elevation. On the basis of the model, a method and processing procedure can be used to correct multipath error effectively, and this paper illustrates its successful application to interferometric SAR data collected by Institute of Electronics, Chinese Academy of Sciences. [C869]

### "The NASA Soil Moisture Active Passive (SMAP) mission: Overview"

The Soil Moisture Active Passive (SMAP) mission is one of the first Earth observation satellites being developed by NASA in response to the National Research Council's Decadal Survey. Its mission design consists of L-band radiometer and radar instruments sharing a rotating 6-m mesh reflector antenna to provide high-resolution and high-accuracy global maps of soil moisture and freeze/thaw state every 2-3 days. The combined active/passive microwave soil moisture product will have a spatial resolution of 10 km and a mean latency of 24 hours. In addition, the SMAP surface observations will be combined with advanced modeling and data assimilation to provide deeper root zone soil moisture and net ecosystem exchange of carbon. SMAP is expected to launch in the late 2014-early 2015 time frame. [C870]

### "Multi-baseline along track SAR interferometric systems for ground moving target indication"

In this paper we analyze the performance of ground moving target detection by means of single-baseline and dual-baseline along track interferometric synthetic aperture radar (SAR) systems, obtained using a generalized likelihood ratio test (GLRT). Detection performance are evaluated in terms of probability of detection and probability of false alarm using data simulated with TerraSAR-X parameters. [C871]

### "Comparison of Beijing-Tianjin Intercity Railway deformation monitoring results between ASAR and PALSAR data"

First comparison experiments by different datasets were done to estimate the subsidence pattern of China Beijing-Tianjin Intercity Railway roadbed in Tianjin area in this paper. The multi-baseline differential synthetic aperture radar interferometry technique was used to give the subsidence monitoring. During the period of middle 2008 to middle 2009, the experiment results show that the roadbed is relative stable during the first year running of the Intercity Railway. And the comparison analyses show that both experiment results give the same subsidence rate pattern along the roadbed corridor, meanwhile the PALSAR results give better railway imaged but larger subsidence velocity standard deviation. [C872]

### "Geophysical Characters for Archaeology in the Ancient City of JinYang, China"

The ancient city relics in Jinyang have a long history, and Jinyang is a very important burial region of ancient culture. It has abundant relics with unique burial forms under the ground. Due to the wide measured range of the

target layers and target articles which is from centimeters to meters, and the different requests of the resolution, we take the method combining with the high density resistivity technique (HDRT) and geophysical prospecting radar (GPR) to carry through geophysical testing exploration on several ancient culture layers and target areas of relics in Jinyang. In this paper, we have collected a rich knowledge of the geophysical characters, which has laid a solid foundation of geophysical exploration for archaeological study on the ancient city relics in Jinyang. [C873]

#### "Preliminary analysis on characteristics of co-seismic deformation field of the Gkrzk earthquake (Ms6.9) from ascending and descending pass ASAR radar interferometry"

We process the ascending and descending mode ASAR radar data that covers the same area using 2-pass D-InSAR technology, and get the co-seismic deformation field, which provides us information on the seismic activity in the study area, in LOS direction of the GeҒ, BırzeҒ, Bi (Tibet) earthquake (Ms 6.9), which happened on 9 January 2008, followed by 40 aftershocks including the largest one on 16 January 2008. The result shows that it is double earthquakes caused by two buried normal faults. The LOS deformation is from -46.0 cm to 11.4 cm by descending interferometry pair, and -47.8 cm by ascending interferometry pair. [C874]

#### "Regularization of Complex SAR Images Using Markov Random Fields"

This paper presents despeckling and information extraction using non-quadratic regularization. The novelty of this paper is that instead of the Gaussian prior model a Gauss-Markov random field model is chosen, because it can efficiently model textures in the images. The iterative procedure consists of noise-free image and texture parameter. The experimental results show that the proposed method satisfactorily removes noise form synthetic and real SAR images and is comparable with the state of the art methods using objective measurements on synthetic SAR images. [C875]

#### "Comparison of ALOS PALSAR RVI and Landsat TM NDVI for forest area mapping"

The objective of this research is to investigate the effectiveness of the radar vegetation index (RVI) derived from ALOS PALSAR full polarimetric data for forest area mapping. Comparison was made between RVI and NDVI of Landsat TM data. After examining of the index maps and the corresponding histograms, forest/non-forest segmentation was performed by unsupervised classification and by threshold method. The results show that RVI is much better in this kind of application. Considering the data acquisition capability, full polarimetric SAR data are quite promising for forest monitoring. [C876]

#### "Improvement of Bandelets in cost function and coding strategy for SAR image compression"

Synthetic aperture radar (SAR) data collections can cover large areas at high resolution, generating massive amounts of data. Many existed transform-based compression techniques can effectively reduce the costs of storage and transmission with slight loss of information. As a new developed multi-resolution geometry analysis tool, Bandelet can make full use of intrinsic geometry regularity of images and exhibit enormous potential in image compression. In this paper, we propose a low complexity Bandelet transform for SAR image compression. A new cost function is defined to determine the optimal geometric flows in each dyadic squared sub-block of images, and an optimization of low frequency component followed by EBCOT coding of the Bandelet coefficients are employed. Some experiments are taken on some Ku-band SAR images came from Sandia National Laboratories and the results show the superiority of our proposed method over JPEG2000 and the second generation Bandelet in PSNR, ENL and EPI. [C877]

#### "Turbo-like Iterative Thresholding for SAR image recovery from compressed measurements"

Compressive sensing (CS) has attracted many researchers since it offers a novel paradigm that one can acquire sparse signals at a sub-Nyquist rate without information losses. In J. Ma, April 2009, S. Bhattacharya et al, Aug 2007, and G. Rilling et al, 2009, the authors have presented some schemes for CS application on remote sensing imaging, some of which are related to SAR. CS remote sensing imaging includes two steps: on-board encoding imaging and off-line decoding recovery. Based on the on-board encoding imaging scheme proposed in J. Ma, April 2009, this paper focuses on the off-line decoding recovery algorithm. We proposed a turbo-like iterative residual thresholding algorithm (RTIT) to decode the compressed SAR data with approximately sparse property. The experimental results show that it outperforms the state-of-the-art iterative thresholding algorithm (IT). [C878]

#### "Application of spaceborne SAR imagery in monitoring green algae"

Synthetic Aperture Radar (SAR) satellite image is first used to monitor dramatically growing green algae near Qingdao coastal in 2008. The system played important role in ensuring Qingdao 2008 Olympic Sailing

Competition. Based on imagery statistic analysis, the influences of radar parameter on detection performance are evaluated. A processing method which used in practice is presented. Processing results consist with field observation data well, which validate the feasibility of the method. [C879]

#### "PALSAR interferometry for urban subsidence monitoring: An experiment in Shanghai area"

In this paper, we apply the Advanced Land Observing Satellite (ALOS) PALSAR data to study the urban subsidence condition in Shanghai, China. The baseline condition, troposphere delay, DEM accuracy mainly limit the capability of PALSAR interferometry, and the influences are evaluated. Six interferograms are analysed in this research, based on D-InSAR technology. We introduce a polynomial to fit the orbit error in each interferogram. After that we use a weighed interferogram stacking method to reduce the influence of atmospheric delay, and to evaluate the mean deformation rate as well. [C880]

#### "Relationship between SAR and biomass derived from LiDAR in Mountain areas"

In this paper, the response of ALOS (the Advanced Land Observing Satellite) PALSAR (the Phased Array type L-band Synthetic Aperture Radar) data to the forest biomass was analyzed in the Qilian Mountain area within Gansu province, western China. Due to not enough field biomass, the Light Detection and Ranging (LiDAR) data were used to extract biomass in a 20 m ГrB— 20 m cell. Then, the relationship between PALSAR backscattering coefficient in HH and HV polarization and LiDAR-derived forest above-ground biomass was analyzed. The result showed that at each biomass level, the range of backscatter coefficient in HH and HV polarization was very big and there was no obvious relationship between SAR backscatter coefficient and biomass in pixel scale, while after averaging backscatter coefficients in different biomass level, the backscatter coefficient in HV polarization increased with the increase of forest biomass and following one logarithm equation. The reason may be that forest structure is complex at pixel scale, while the average value partly removes the forest structure difference. [C881]

#### "An automatic bridge detection technique for high resolution SAR images"

In this paper, an approach for detecting bridges over water bodies from high resolution SAR images is presented. It consists of two steps: water extraction and bridge detection. A method based on porosity combined with an edge mending algorithm utilizing canny edges is used to extract water bodies firstly. By considering the ubiety of bridges and water bodies, the candidate bridge regions are detected. Then the candidate bridge regions are confirmed on the basis of the geometric characteristics of bridges. Finally bridges are detected in confirmed bridge regions according to geometric characteristics of bridges and water extraction result. The proposed approach has been tested with SAR images that have a spatial resolution of 1 m. The experimental results show that our method can detect bridges effectively. [C882]

#### "Precision evaluation and characteristics analysis of the coseismic deformation field of the 12th may 2008 Wenchuan Ms8.0 earthquake"

Based on the improved DInSAR technology, this paper obtained the whole coseismic deformation field of the Wenchuan Ms 8.0 earthquake by 128 frames of Level1.0 data of ALOS PALSAR. By comparing with the continuous GPS survey results, the precision of coseismic deformation field was estimated as about 9.5 cm, better than half-wavelength of L-band. The whole coseismic deformation stripe has a total length of about 300 km, which encircles the NE-trend seismic ruptures, and is mostly distributed within 19-100 km from the fault rupture. The spatial distribution of coseismic deformation gradually narrows down from southwest to northeast, owing to the fact that the seismic energy gradually decayed along the NE-trend from Yingxiu where the seismic fracture begins to Qingchuan where it ends. There is a weak coherence zone near the seismic rupture relating to strong displacements, such as landslide, mud and rock flow, etc. And this weak coherence zone obviously extends wider in south Beichuan than in north Beichuan, which is corresponding to the fact that two parallel rupture faults exist in south Beichuan while only one exists in north Beichuan. The 471-track deformation is produced mainly by Qingchuan Ms 6.4 dextral-strike aftershock and other strong aftershocks, and therefore its deformation field is discontinuous with adjacent tracks. As a whole, northwest plate-Bayankala Block was uplifted, while southeast plate-rigid Sichuan Basin subsided, and both sides of the seismic rupture were uplifted. But there exist one subsided zone 10-30 km away from the rupture in the Bayankala Block. Synthetically analysis shows that, under the effect of the huge eastward pushing force from Tibet, the Bayankala Block was resisted by the rigid Sichuan Basin when it thrust along the high-angle seismic rupture, and then its east margin bent to form a subsided zone to absorb and release the strong eastward thrusting force. [C883]

#### "Dynamic reconfigurable storage and pretreatment system of SAR signal processing using Nios II architecture"

Because of synthetic aperture radar (SAR) is a powerful remote sensing technique, there has been growing interest in using SAR to obtain high resolution image. Modern high- performance SAR requires advanced and sophisticated signal processing technique to get high-quality image products. Meanwhile, the semiconductor technologies are updated day after day, programmability and flexibility are the trend of current electronic system, and it leads to the advent of system-on-chip (SOC). The Nios II, a soft-core processor integrated in Altera FPGA chip, is characterized by its flexibility and programmability. In this paper, a dynamic reconfigurable storage and pretreatment system of SAR signal processing is designed and realized based on the Nios II soft- core processor. The proposed architecture takes advantage of the embedded CPU to control all the peripherals, highly increased the efficiency of the design. [C884]

#### "Segmentation of dual polarized SAR imagery of the west of China based on evidence theory"

Most areas in the west of China are mountains covered by cloud and mist all the year. Therefore mapping by negative remote sensing could not satisfy the requirements of thematic map. SAR is an alternative approach. Among single, dual and quad polarized imagery, dual polarized one is a compromised choice taking cost and information into account. A new algorithm based on the theory of evidence for dual polarized SAR images of west China is proposed in this paper. Firstly we get a single channel image from original dataset by PWF (Polarimetric whiten filter), and then over-segment the image. Secondly the borderlines of each segment are adjusted by fusing two evidences, pixels' values and the values of their neighbourhood by applying evidence theory. Finally initial segments are merged based on evidence combination. In this paper, not only each channel but also the mean of neighbour areas is considered as a piece of evidence. In order to eliminate the factor of hypsography, the ratio of different polarization was added as a new piece of evidence. The experimental results of dual-polarimetric SAR images in Hengduan Mountain of West China show that the proposed algorithm performs better than traditional algorithm when noise rich images are processed because it is less sensitive to speckle noise so edge information is better reserved and it reduce the influence of hypsography. [C885]

#### "The detection and information compensation of SAR layover based on R-D model"

The traditional method of detecting Radar layover is firstly calculating the local radar angle of the image pixel points, then comparing the local radar angle of adjacent pixels to determine the size of Radar layover region. But this method is of low efficiency towards a complete radar images. This article is being launched to detect Radar layover areas through the region growing algorithm and compensate gray information of the detected area with SAR image simulation on the basis of the semi-empirical Backscattering model and R-D(Range-Doppler)model, with the radar noise finally added in radar layover area. The final tests verify it is effective to solve the problem of missing information in the layover area of radar orthophotos. [C886]

#### "A Flow to Generate DEM from Lidar Data"

To consume less time and less memory, this paper presents a flow to generate DEM from Lidar data. Firstly the flow labels non-ground points based on multi-echo information. Secondly by the relativity among neighbor points, the flow labels many other non-ground points. After these two up-to-down steps, many non-ground points have been eliminated, which has reduced the amount of the Lidar points successful. At last, the flow use filtering arithmetic based on scan lines to get DEM. This paper comes to a conclusion that both the flow and algorithm are feasible by using them to disposing laboratory data. [C887]

#### "Fast Processing of Airborne LiDAR Data and Imagery"

This paper presents a fast processing flow of airborne LiDAR data and imagery which acquired by Leica ALS50-II. On the one hand, position and orientation system (POS) data are converted to approximate exterior orientation parameters (EOP). On the other hand, the light detection and ranging (LiDAR) point cloud can generate digital elevation model (DEM) after filtering. Then mosaic can be generated quickly using collinearity equations with imagery, DEM and approximate EOP. The results of experiment show that this method is effective and efficiency. [C888]

#### "Retrieval of Three-Dimensional Wind Field of Typhoon by SVVP Method"

Typhoons landing in China have caused severe calamity and loss in past years. Therefore, disaster prevention and reduction, and life and possession protection are very important and to be imperative under the circumstances. Many Doppler radar covering extensive areas are erected along the coast of Southeastern China, and they are crucial for monitoring and warning of severe weather. The radial velocity information received by Doppler radar can be recovered to real wind field by some retrieval method, which is important for the research on wind field structure and development and evolvement of typhoons. Velocity volume processing (VVP) is one of

the mainly used methods for wind field retrieval. However, VVP method is disturbed by ill-conditioned matrix in calculation, leading to great error and thus its application is too much limited. Step velocity volume processing (SVVP) is an improved VVP method. It efficiently overcomes the ill-conditioned matrix problem in VVP method, and can acquire exact horizontal wind, horizontal shear, vertical wind, etc. In this paper, it is attempted to retrieve the three-dimensional wind field of typhoon by SVVP method. According to the retrieval experiments on simulated and real typhoon radial velocity data, we focus on the retrieval validity and feasibility of the vertical wind. [C889]

### "Cramer-Rao Bound-Based Evaluation of Texture Extraction from SAR Images"

SAR images are affected by speckle which is a coherent process modelled as a multiplicative noise. It makes the automatic image classification difficult. Thus, many methods have been developed to remove speckle from SAR images while preserving the useful information of the image such as texture. This paper presents an evaluation of texture extraction parameter estimation methods using Cramer-Rao lower bound (CRLB). The first evaluated method is model-based despeckling (MBD) algorithm, which uses Gauss-Markov random fields as prior. The second one is the maximum a posteriori auto-binomial method (MAP-ABM), which rather uses auto-binomial model as prior. The evaluation has been carried out using simulated SAR data. In here, data with increasing number of looks have been used in order to study 1) how the estimated parameters approach the real one, and 2) how their variances get closer to CRLB. The experimental results show the superiority of MBD parameter estimation. Both MBD and MAP-ABM provide the most robust texture parameters when the number of look is between 3 and 4. [C890]

### "Damage Assessment Based on SAR Image Analysis: Flood Scenario for Romanian Eastern Carpathian Region"

When natural disasters occur, it is necessary for the authorities to make fast and effective decisions in order to prevent the occurrence of more damage, as well as to find solutions for the affected population that needs to be relocated. Satellite imagery can prove to be a useful instrument in decision support during emergency situations of such nature (floods), and especially SAR data, due to its all weather capabilities. This paper makes an assessment of the utility of satellite radar products (TerraSAR-X and Radarsat) in the frame of emergency situations management. A real case study is presented, where radar data were processed by human specialists on one hand, and automatically on the other hand, using an intelligent information extraction system. [C891]

### "Soil Moisture Estimation with TerraSAR-X: With Dubois Empirical Model"

This paper presents a possibility of supervision against leaks in artificially made river canals, which can be done by estimating soil moisture content with TerraSAR-X synthetic radar aperture images. For soil moisture estimation problem an empirical model was used, which estimates dielectric constant and later on this can be transformed into soil water moisture content. [C892]

### "The application of power density spectrum estimation on synthetic aperture radiometer"

Aperture synthetic is a technique for overcoming the limitation that a large antenna aperture places on passive microwave remote sensing from space. This is an interferometric technique in which pairs of small antennas are used together with signal processing to achieve the solution of a single large aperture antenna. In this technique, the product of the signal from each pair of antennas is measured using a correlation radiometer. The complex product is recorded for pairs of antennas at many different spacings. The spacing is called a baseline and both the magnitude and orientation of the distance between the antennas is important. Once the place and the number of antennas are determined, the complex products are determined. In this paper, we get more complex products by the method of power density spectrum estimation to improve the temperature sensitive. [C893]

### "Key technology analysis of sub-millimetre wave seeker"

The paper introduces the characteristics and the main applications of sub-millimetre wave. The technology development status of SMMW in home and abroad are also introduced. The characteristics of sub-millimetre wave seeker and the problems which are needed to be solved are specified. Both key technology and investigative difficulties of sub-millimetre wave seeker are analyzed. The influence of target movement towards SMMW chirp is analyzed. The analysis result proves that velocity compensation must be carried out before signal processing of SMMW-chirp is implemented. [C894]

### "Research on phase shift in mono-pulse angle tracking system"

Phase shift in angle tracking system leads to a decline of tracking precision. In terms of mono-pulse angle

tracking system based on amplitude comparison of sum signal and difference signal with digital phase comparison technology, the paper analyzes the system phase shift and discusses the effect of it on angle tracking. Then, two methods to compensate phase shift are introduced with their efficiency verified by experimental data. [C895]

### **"Statistical analysis to assess building damage in 2008 Wenchuan earthquake from multi-temporal SAR images"**

The statistical approaches, i.e. K-distribution and Getis statistics, are applied to ALOS PALSAR image for assessing the building damage caused by Wenchuan earthquake in 2008. As a proposed image analysis, a simulated image with random bright squares, as building objects, is firstly presented for analysis of the K-distribution and Getis statistics. Then, these statistics are applied to two ALOS PALSAR images acquired before and after the Wenchuan Earthquake to assess building damage level. Results of K-distribution and Getis statistics show that the damage level might reach 93% and 81%, respectively. [C896]

### **"The Practice of an Automatic Registration System Based on Contour Features and Wavelet Transform for Remote Sensing Images"**

Image registration is an inevitable problem arising in many image-processing applications whenever two or more images of the same scene have to be compared pixel by pixel. The increased volume of satellite images has reinforced the need for automatic image registration methods. In this paper, two new feature-based approaches to automated image-to-image registration are presented. The characteristic of the first approach is that it combines an invariant moment shape descriptor with improved chain-code matching to establish correspondences between the potentially matched regions detected from the two images. This method works well for image pairs in which the contour information is well preserved. For the registration of the optical images with synthetic aperture radar (SAR) images, we propose another method based on the wavelet transform, this second method uses spectral information of the images and their local wavelet transform modulus maxima to extract a set of control points. The experimental result demonstrates the robustness, efficiency and accuracy of the two algorithms. [C897]

### **"Detection scene analysis for high frequency radar"**

Suffering from multiform time-variant and fluctuant clutter in High Frequency Radar (HFR), uniform target detection, tracking and clutter mitigation methods will result in false alarm or missing alarm. To select optimized detection and clutter mitigation method in the region of interesting, a method maximizing the separability of the resultant classes in amplitude of range-Doppler map is used for segmentation in multi-level detection background. Statistical and qualitative analysis is operated on the result of clutter extraction. Real data indicated that the proposed method can extract clutter region and adapt for various echo spectral maps for HFR as well, which can offer more accurate prior knowledge for target detection and clutter mitigation. [C898]

### **"A new wavelet based algorithm for estimating respiratory motion rate using UWB radar"**

UWB signals have become attractive for their particular advantage of having narrow pulse width which makes them suitable for remote sensing of vital signals. In this paper a novel approach to estimate periodic motion rates, using ultra wide band (UWB) signals is proposed. The proposed algorithm which is based on wavelet transform is used as a non-contact tool for measurement of respiration motion rate. Compared with traditional contact measurement devices, experimental results utilizing a 3.2 GHz bandwidth transceiver, demonstrate 99% similar results. The standard deviation of the proposed algorithm for 30 independent experiments has obtained 19% for respiration motion. [C899]

### **"Research on application of unmanned aerial vehicles borne SAR"**

Synthetic Aperture Radar (SAR) has become one of the most important military equipments. And based on the virtues such as zero-casualty, low observable ability and low price, the field of unmanned aerial vehicles SAR(UAV-SAR) now gets more and more attention. This paper gives the summarization of UAV-SAR, introduces the foreign applications of UAV-SAR, both advantages and problems (as well as the countermeasures) are analysed in detail. At last, this paper shows the trend of UAV-SAR development in the future. [C900]

### **"C-Band multi-polarimetric SAR and the flight experiment of land and sea"**

The C-Band multi-polarization SAR system has a wide range of applications in the earth observation field, and it can be applied to ocean observing, crop monitoring, mapping and other fields. The application flight experiment is introduced, and some SAR image, inversion results of land, sea are presented. [C901]

### "SAR Image Segmentation Based on Immune Genetic Algorithm and Gaussian Mixture Models"

In this paper, an effective synthetic aperture radar image segmentation method is proposed. Gaussian mixture models optimized by greedy expectation maximization algorithm are applied. The immune genetic algorithm is employed to initialize greedy expectation maximization algorithm and search the optimal values in the whole range, instead of general k-means algorithm, which is different from the traditional algorithm. Experimental results show our method can get better results for target segmentation. It can effectively segment the object from SAR images and inhibit speckle noise. [C902]

### "Research on Database Storage of Large-Scale Terrestrial LIDAR Data"

Generally speaking, a large number of point-cloud data will be generated in the process of collecting 3D structure information of large building using the 3D LIDAR technology. Based on analyzing raw files content and form 3D laser scanning point-cloud data is reorganized and a storage mean of large-scale point-cloud data which is by data stream means is presented in this paper. The data is stored in Oracle 11g database in the SecureFile (BLOB) form. ODP.NET is selected as the database access interface, C# as experimental programming language. Database design model and stored procedure of large-scale 3D laser scanning point-cloud data is introduced. The study gives a new idea and research direction for applications and developments based on large-scale 3D laser scanning data. [C903]

### "Doppler-polarimetric radar system for recognition of distributed objects"

This paper considers Doppler-polarimetric radar methods in application to observing distributed targets. Examples of typical distributed targets are meteorological objects. For instance, among wide variety of meteorological objects, such targets as clouds with precipitation are considered. Developed mathematical models of Doppler-polarimetric reflections from distributed targets as rain and clouds are discussed. Phenomenological and mathematical aspects of the relationships between different Doppler-polarimetric measurable variables and parameters of the object under observation such as its microstructure and dynamic properties of scatterers inside the resolution volume are considered. Implementation of Doppler-polarimetric approach, which requires significant processing power, in reasonable devices is considered. [C904]

### "Linear FM radar operating in the Tera-Hertz regime for concealed objects detection"

Sub-millimeter and terahertz waves maintain reasonable penetration depth in certain common materials, such as cloth, plastic, wood, sand and soil. Therefore, THz radiation can detect concealed weapons since many non-metallic, non-polar materials are transparent to this type of radiation (and are not transparent to visible radiation). Target compounds such as explosives and illicit drugs have characteristic THz spectra that can be used to identify these compounds. Investigation, design and development of a sub-millimeter wave remote sensing RADAR system for homeland security applications are presented. The RADAR, operating at 330 GHz is based on transmission of a frequency modulated continuous wave (FMCW) and aimed at detection of concealed objects for ranges up to 20 m. The system consists of 2 horn-lens antennas integrated with a homodyne transceiver. The synthesized linear FM signal with a frequency span of 200 MHz at X-band is multiplied by a factor of 32 to generate the transmitted Tera-Hertz wave. Using a splitter, the signal is fed to an antenna and to a local oscillator port of a second harmonic balanced mixer. As a result, an intermediate frequency signal is obtained, containing the information on the target. Distance measurements were made by performing data acquisition and signal processing commercial programs, resulting in a range resolution better than 1 cm. Preliminary Tera-Hertz imaging was also carried out to perform a three-dimensional image of the object. [C905]

### "Design and fabrication of MMW module for 94 GHz radar sensor applications"

We present design and fabrication of a 94 GHz radar sensor module. The 94 GHz sensor module has four components including 94 GHz single balanced diode mixer part, waveguide VCO (voltage controlled oscillator) part, magic tee part and bias PCB part. The 94 GHz single balanced diode mixer is developed on Duroid RT 5880 substrate with DC 1346 Schottky diode. The mixer has advantage of good conversion loss at high LO power and isolation characteristic. 94 GHz single balanced diode mixer has advantage of comparatively easy fabrication. The waveguide VCO consist of GaAs Gunn diode, varactor diode, two-bias post and cavity. The waveguide VCO is operated at 94 GHz. The magic tee has four waveguide arm regions with standard WR-10 and divides output power from VCO. Transmission frequency of 94 GHz MMW sensor module is 93.607 ~ 94.727 GHz. Bandwidth is 1.12 GHz. 2% linearity range is 680 MHz. Power is 11.03 ~ 11.47 dBm. Conversion loss about -7 dB at IF 500 MHz. [C906]

### "Comparison of Reflection and Transmission Method and Metal Back Method Measurement of Dielectric properties of transformer oil using free space microwave measurement system in 8-12 GHz frequency range"

Nondestructive, non-contact and real time evaluation of dielectric properties of low-loss liquids is important for applications such as service-aged transformer oil, biomedical, remote sensing and design of radar absorbing material. Free-space methods (which are nondestructive and non-contact) were developed a measurement of dielectric properties of transformer oil at microwave frequencies. Transmission and Reflection method and Metal Back Method are developed for measurements using free space microwave measurement system (FSMM). FSMM system consists of spot focusing horn lens antennas, mode transitions, coaxial cables and vector network analyzer (VNA). Dielectric constants and loss factors were measured for new transformer oil. It is observed that metal-back method is suitable for dielectric measurement of transformer oil compared to Transmission and Reflection method. [C907]

### "Multi-modal Registration of SAR and Optical Satellite Images"

Frequently the need arises to combine remotely sensed data taken from different sensors for improved interpretation of an imaged area. However, before this multi-sensor data fusion can be performed the image data must first be registered geometrically. In this paper we investigate the use of an information-theoretic similarity measure known as cross-cumulative residual entropy (CCRE) to perform the registration of SAR imagery and optical data. An affine transformation is implemented in the registration procedure to account for geometric errors other than simple translation and rotation. The results of our experiments showed that the CCRE registration algorithm performed satisfactorily and provided a significant improvement over the standard mutual-information based technique. [C908]

### "Design and simulation analysis of polarimetric interferometric synthetic aperture radar"

Polarimetric SAR interferometry (POLINSAR) is a very promising technique by combining polarimetric technique and interferometric technique. It can be applied to the area of remote sensing and measurement of structure over forest terrain. At present, many POLINSAR systems were developed, and the first POLINSAR prototype in China is also developed by 38th Research Institute of CETC. Lots of data are acquired by these systems, so POLINSAR techniques have been studied as hot research topics in the area of SAR remote sensing in recent years. In this paper, we introduce design of the POLINSAR prototype and demonstration of system parameters, and we also study coherence and elevation precision by computer simulation. [C909]

### "Road extraction in remote sensing images based on Nonsubsampled Contourlet Transform"

A new method for automated road extraction in remote sensing images is proposed based on Nonsubsampled Contourlet Transform (NSCT). Due to the advantages of multi-scale, multi-direction and translation invariance, NSCT is much efficient for the capture of linear singularity of road target. A pixel-wised feature extraction algorithm is given first based on the analysis of the NSCT coefficient responses for the road target. Final results can be achieved by the simple fuzzy C-means clustering and the postprocessing steps. Experimental results demonstrate that our method outperforms other methods such as Gabor wavelet in accuracy, localization and false detection. [C910]

### "A beam-splitting approach to measuring microwave backscattering coefficient ( $\sigma^\circ$ ) and its application"

This article attempts to use the beam-splitting approach to measure the microwave backscattering coefficient ( $\sigma^\circ$ ) of blank concrete samples, cobble surface samples of different sizes and others, and observe the variation laws of incident angle. This approach, low-cost and stable in performance, is able to overcome the cross talk between emitting and receiving antennas lying side by side, and result in the strict coincidence between incident beams and scattered ones. This approach and its results offer an experimental means of SAR remote sensing calibration and image interpretation. [C911]

### "Plenary session"

The forest-land use carbon source is still the major area of uncertainty in determining the global carbon budget. Methods to map forest and non-forest areas with precision using optical remote sensing in the tropical world is extremely difficult due to cloud cover. Time series satellite derived radar data provide the opportunity to map forest change and forest degradation in a consistent and quantifiable manner for input into forest carbon assessment models. Recent work with GEOSAR an airborne radar dataset has resulted in biomass estimations being retrieved directly from multi-band X and P band interferometric (height) and polarimetric (class) information.

While the methods still need verification using ground based estimates of biomass, the potential exists to map biomass and greatly assist in the estimation of carbon sequestration and carbon emissions in tropical regions.

[C912]

### "SAR image retrieval based on Gaussian Mixture Model classification"

SAR image retrieval, lacking of well performance recently due to the particularity of SAR image, has drawn more and more attention with the increasing volume of SAR data and the dramatically enlarging application range of SAR image. This paper considers both the characteristic of content-based image retrieval (CBIR) and SAR image, proposing a novel SAR image retrieval method. The proposed method can be divided into two parts: image classification and matching. Firstly we use Gaussian Mixture Model (GMM) to gain a precise result of classification, and then we get the retrieval results through the integrated region matching (IRM) algorithm. Experimental results show that the proposed method can retrieve SAR images which contain all kinds of surface features effectively. [C913]

### "Urban change detection using coherence and intensity characteristics of multi-temporal SAR imagery"

Change detection using multi-temporal SAR images is one of the most important applications of remote sensing technology. A new method for unsupervised change detection in urban area with multi-temporal SAR images is proposed in this paper. The method operates in two steps: change measures computation and unsupervised 2-D thresholding. In the first step, two change measures, backscattering intensity variation and long-term coherence variation, are defined. In the second step, an unsupervised 2-D thresholding technique based on maximum 2-D Fuzzy entropy criterion is introduced, which is performed on the two difference images derived from the two change measures to produce an accurate change-detection map with two classes  $\Gamma, B_i$  change  $\Gamma, B_i$  and  $\Gamma, B_i$  non-change  $\Gamma, B_i$ . The parameters of Fuzzy entropy are optimized by genetic algorithm (GA). The effectiveness of the new method is validated by four ERS SAR images of Nanjing area acquired in 1997 and 1999. [C914]

### "Parameter assessment for texture feature quality evaluation in SAR ocean image"

Synthetic Aperture Radar (SAR) is increasingly used in the ocean remote sensing. Thus the assessment for SAR ocean image quality evaluation has become an important issue. Texture features are very common in SAR ocean images. In this paper, a set of parameters aimed at such characters is raised. Then these parameters are applied to evaluate texture features in two SAR images which contain internal waves information. [C915]

### "A MTRC correction algorithm in Bistatic ISAR"

In conventional ISAR system, when the requested resolution of radar is high, while the size of target is large, it will cause the Migration Through Resolution Cell (MTRC), it will also exist the same problems in Bistatic ISAR systems. This paper analyzes and discusses the reason of causing MTRC particularly in the module of Bistatic ISAR, and compares it with the situation in Mono ISAR systems. And then a correction algorithm based on Keystone transformation is presented in the paper, which eliminates the MTRC in the target imaging. Finally, some simulation results are given to validate the validity of the algorithm. [C916]

### "Micro-Doppler analysis of vibrating target in bistatic radar"

Bistatic radar is gaining more and more interest by the radar community over the last years, and Micro-Doppler information is regarded to be the unique features of radar's targets. In this paper, a geometric of bistatic radar and vibrating target is constructed. Then in bistatic radar system, the Micro-Doppler information reduced by vibrating structure of target is analysis via Gabor-Transform. Then we get that vibrating parts and the relationship between target and radar will modulate the micro-Doppler frequency. Lastly the simulation results validate the conclusions. [C917]

### "Fast compressive sensing radar imaging based on smoothed l0 norm"

Compressive sensing technique has been shown capable of reducing the number of data samples beyond the Nyquist theorem, and achieving perfect reconstruction of the original signal. Because of its compressed sampling ability, compressive sensing has been found many applications in imaging, remote sensing conversion and many other fields. Although several kinds of radar imaging arithmetic were proposed, but the reconstructed speed arithmetic are slow. In this paper, we propose a faster compressive sensing radar imaging arithmetic based on smoothed l0 norm. Simulation experiments conformed that the algorithm has faster reconstruct speed and well reconstruct quality compared with other algorithm. [C918]

### "Scattering and image simulation for reconstruction of 3D PEC objects concealed in a dielectric box"

A new approach of imaging reconstruction of concealed targets from multi-angular scattering is presented. As the broadband stepped-frequency radar transmits planar wave from different azimuthal directions around the target, the backscattered electrical fields in both the amplitude and phase are obtained. The two-dimensional (2D) fast Fourier transform (FFT) algorithm for spline interpolation is adopted for uniformly sampled back scattering fields. Then, 2D images of a dielectric box with and without the concealed targets can be numerically simulated. The concealed targets can be well identified from the imaging reconstruction. [C919]

### "Polarimetric sscattering for information retrieval of SAR imagery"

This paper presents an overview of recent research progress in WSRS on theoretical modeling of the terrain surface for polarimetric scattering simulation and Mueller matrix solution, mono-static and bistatic SAR image simulation, new parameters for unsupervised surface classification based on de-orientation approach, DEM inversion, change detection from multi-temporal SAR images, and reconstructions of buildings from multi-aspect SAR images etc. [C920]

### "A new change detection algorithm for SAR images"

Speckle noise of Synthetic aperture radar (SAR) image and the azimuth sensitivity for imaging obstruct the interpretation and applications for SAR images. But it is very much remote sensing source because it can acquire data under all-day and all weather. Texture features reflect the spatial property of ground objects. If texture features change, in general the ground object does so. Therefore, this paper deep analyzes SAR image texture feature and proposes a new multi-temporal SAR image change detection algorithm, which is called by texture features fusion voting (TFFV) algorithm. Finally, the airborne SAR image data tests the method and experimental results indicate that the presented methods are feasible. [C921]

### "The Rapid Generation of DOM for Geophysical Applications"

Orthophoto have some features, such as informative, rich content, and intuitive truth. This paper discusses how to rapidly produce orthophoto in the situation of flight pattern of aero geophysical. Thiessen polygon method used to build sampling area and automatically generate orthophoto of measurement area, it's not need to carry on manually edge processing. Given the characteristic of mass data about magnanimous images, we proposed the method of demonstration, roam, and zoom of magnanimous image based on pyramid memory scheduling strategy of piecemeal and graduation. [C922]

### "A Study of Land Subsidence by Radar Remote Sensing at Datong Jurassic & Carboniferous Period Coalfield"

At Datong coalfield, the heavy mining activities in its jurassic & carboniferous coal seams has caused very serious adverse effects to the local geological environment, such as soil avalanche, landslide, mud-rock flow, surface settlement, surface crack, surface gangue stack, surface deformations and subsidence. Moreover, as coal mining causes groundwater leakage, excessive groundwater exploitation has greatly intensified surface settlement in Datong City. The paper uses 8 cognominal ERS-1/2 SAR data frames obtained during 1992 to 2003 period, obtained 84 deformation fields. Of the 84 sites for preliminary interference, 44 sites belong to mining subsidence, 23 urban subsidences and 17 landslides. The total coverage area of deformation amounts to 1824.4 km<sup>2</sup>, which is almost equivalent to the total area of the Datong coalfield. [C923]

### "An Improved Automatic Ship Detection Method in SAR Images"

This paper provides an improved automatic ship detection algorithm, which uses two-parameter CFAR algorithm based on Gauss-distribution to process the homogeneous imaging local area, and uses two-parameter CFAR algorithm based on K-distribution to process the heterogeneous imaging local area again. This improved algorithm keeps both the ability of traditional two-parameter CFAR algorithm' good features, such as small computation quantity, easy to implement and so on, and the detection accuracy in complex sea conditions at the same time. [C924]

### "A Novel Deformable Model for Urban Vegetation Detection Using LiDAR Data"

This paper presents a new approach to creating variational level set model for vegetation detection combining 3D irregular point clouds and aerial image simultaneously acquired by LiDAR light scanning and imaging device. Firstly, a fundamental statistical level set framework is built which integrates texture information to improve the

quality of vegetation detection. Then, several derived products directly or indirectly from LiDAR raw point cloud data, like DTM(digital terrain model,) nDSM(normalized digital surface model) and local roughness capable of describing 3D texture feature of vegetation, are used to construct a novel energy term in relation to height and roughness of non-terrain objects, in order to make up the disadvantages caused by insufficient information only from remote sensing image. This model can well fuse spectral feature, height and roughness information of objects from different sensors. Experiments on pairs of LiDAR Aerial image and 3D point cloud data are carried out, and conclusions can be drawn that our model can effectively separate various vegetation categories including grass and tree in urban area from other land covers, including buildings, noises, ground etc., and alleviate various influences caused by occlusions or spectral inhomogeneity. [C925]

### "Forest Reconstruction Using Point Cloud Data of Airborne LIDAR"

Computer modeling and visualization of forest landscape recently becomes a hot topic, whose study can benefit such fields as virtual reality, ecology, forest management, physical geography and botany, etc. It is a problem to get the 3D model of the forest quickly and accurately. In this article, the placement of the trees and terrain are derived automatically from airborne lidar data. 3D structure of the trees is also extracted from lidar data. Combining these feature and AMAP software, 3D model of the tree is created. [C926]

### "The Design of the Remote Water Quality Monitoring System Based on WSN"

To resolve the problem of the manual analytical method adopted in water quality detection with bad real-time character, this paper introduces a novel kind of remote water quality measuring and monitoring system based on WSN. It has used wireless sensor network based on the ZigBee to realize the water quality parameter remote probing and the real-time monitoring function. Users can observe the current or historical water quality status easily, and it provide a reasonable basis for the further breeding plan. This system has a simple architecture, and isn't confined by the geographical position. According to the test results, this system can run stably. And its operation is convenient. [C927]

### "Water Objects Extraction from Polarimetric SAR Imagery Based on Sequential Nonlinear Filtering and Independent Component Analysis"

A new method is proposed for speckle noise suppression and water objects extracting from synthetic aperture radar (SAR) imagery based on sequential nonlinear filtering and independent component analysis. The distribution of SAR image data with multiplicative speckle noise is non-Gaussian and its parameters are unknown. Logarithmic quantification is utilized to transform multiplicative speckle noise to independent additive noise. Speckle noise and image data are separated from multi-polarimetric imagery, and the components with the least speckle index are chosen as the object component automatically by means of ICA while the specific distribution of SAR imagery is unnecessary. Water objects are extracted from the separated object component imagery based on sequential nonlinear filtering according to their lightness and region shape features. The experimental results using ENVISAT ASAR polarimetric imagery show that the proposed method can extract water objects rapidly and accurately. [C928]

### "A novel digital beam-forming concept for spaceborne reflector SAR Systems"

The trend in the conception of future spaceborne radar remote sensing is towards the use of digital beam-forming techniques. These systems will comprise multiple digital channels, where the analog-to-digital converter is moved closer to the antenna. This dispenses the need for analog beam steering and by this the use of transmit/receive modules for phase and amplitude control. Digital beam-forming will enable synthetic aperture radar (SAR) which overcomes the coverage and resolution limitations applicable to state-of-the-art systems. Moreover, new antenna architectures, such as reflectors, already implemented in communication satellites, are being reconsidered for SAR applications. This paper introduces a new digital beam-forming radar concept based on the combination of a reflector with a digital feed array. For a system example the SAR performance is estimated. Finally a novel digital signal processing approach, exploiting the signal properties of the transmitted waveform, is presented. [C929]

### "Usage of electromagnetic fields of antropogenic irradiation sources for remote sensing of atmosphere"

Examined the possibility of usage of anthropogenic irradiation sources such as television centers, navigation artificial satellites for diagnosis of atmospheric processes (troposphere refraction, dangerous meteorological phenomenon). The methods of troposphere refraction estimation on UHF field propagation factor at over-the-horizon path using radio setting and raising of GPS system navigation satellites are proposed. [C930]

### "Status, results and perspectives of the Italian Earth Observation SAR COSMO-SkyMed"

COSMO-SkyMed is a Dual-Use program, devoted to produce both civilian and military applications, and as such, it is required to have a fast response time, to manage conflicts and to optimize resources. This paper provides a description of the current COSMO-SkyMed unique in-orbit performances, functionalities and Dual-Use design, implementation and operations, comparing them with other RADAR remote sensing Systems. In this context examples and potentialities of the data already acquired and catalogued are given and discussed. Following that the paper summarizes: 1) The lesson learnt and the needs evolution up to now collected from the Scientific, Technological and User Communities, also through the experiments performed in the frame of the current utilization phase; 2) The evolution that is planned for the 2nd generation of the COSMO-SkyMed System to provide the involved Civilian and Defence Communities with adequate imagery capabilities and global performance. In particular are discussed: 3) The new/improved architectures and technologies necessary in the Space as in the Ground Segments to provide new/improved operative modes, performances, applications, interoperability and modularity features, life-cycle costs, et cetera; 4) The implementation plan of the necessary technical improvements; 5) The COSMO-SkyMed 2nd Generation development and deployment plan. [C931]

### "Machine learning in remote sensing data processing"

Remote sensing data processing deals with real-life applications with great societal values. For instance urban monitoring, fire detection or flood prediction from remotely sensed multispectral or radar images have a great impact on economical and environmental issues. To treat efficiently the acquired data and provide accurate products, remote sensing has evolved into a multidisciplinary field, where machine learning and signal processing algorithms play an important role nowadays. This paper serves as a survey of methods and applications, and reviews the latest methodological advances in machine learning for remote sensing data analysis. [C932]

### "DDV-novel Doppler-polarimetric technique for remote sensing of precipitation"

This paper presents results of Doppler-polarimetric radar signal modelling and real data processing that show correlation between Differential Doppler Velocity (DDV) and parameters of rain including rain microstructure and turbulence in rain. Reasonability to use DDV as one of informative parameters in recognition neural network system is checked. [C933]

### "Evaluation of beam-forming algorithms for automotive OFDM signal based radar"

In this paper the applicability of beam-forming algorithms in radar systems operating with OFDM signals is investigated. It is shown that beam-forming techniques can be directly applied to the output of an OFDM radar processor in order to calculate two-dimensional radar images in distance and azimuth. With a dedicated system model including a realistic road scenario propagation simulator, the performance of different algorithms in typical automotive radar scenarios is analyzed for 24 GHz ISM applications. [C934]

### "Application of ASAR PSI technology to ground deformation detection in mega-cities of the Pearl River Delta Region in China"

In this study, we present the application of Persistent Scatterer Interferometry (PSI) technology with ENVISAT (European satellite) Advanced Synthetic Aperture Radar (ASAR) images to detect the ground deformation in the Guangzhou urban area and Hong Kong International Airport (HKIA). A map of ground deformation rates in Guangzhou with scattered points shows that the maximum subsidence (rise) rate is up to -26 to -20  $\text{mma}^{-1}$  (-16 to 21  $\text{mma}^{-1}$ ), implying the study area as an active zone of the ground deformation. Based on the point targets, a contour map of ground deformation rates was then generated. The map indicates that three major subsidence zones are located in the middle-west, east, and southwest of Guangzhou urban area, respectively. Six ground collapse accidents that occurred in Guangzhou during 2007-2008, within these subsidence zones, qualitatively validated the results. In the case of detecting ground deformation in HKIA, the ground truth data provided by the Airport Authority Hong Kong were used to correct the model, which is then applied to analyze the systematic errors existing in ASAR PSI-detected ground deformation rates. 2250 corrected ASAR PSI-detected points of annual ground deformation rates were used for the statistical analysis. The obtained results agree the Gaussian distribution well in our case studies. [C935]

### "Registration of LiDAR data through stable surface matching"

The accuracy of final LiDAR points on ground depends on various factors including GPS/IMU position and orientation, laser range and scan angle measurements. As a result, the adjacent overlapping swaths or flight strips fail to match with each other. Surface matching is a common procedure used to relatively register the LiDAR data and reduce the mismatch between the overlapping strips. However, in case of smooth topography

with fewer features, classical registration algorithms render poor results. This paper presents a modified registration technique for the optimal relative registration of LiDAR data over a flat terrain with fewer features. In this method, the feature samples used in the algorithm are selected depending on their geometric stability. The points from overlapping strips are matched through iteratively closest point (ICP) method based on minimizing point to plane normal distance. [C936]

#### "Impact analysis and appraisal of Tangjiashan Barrier Lake by spatial information technology"

Tangjiashan Barrier Lake is one of the most dangerous induced disasters in the great Wenchuan Earthquake. In this paper, spatial information such as synthetic aperture radar, Multi-spectrum remote sensing imagery and DEM is utilized to fast acquire characteristic parameters of Barrier Lake, such as storage capacity in different water level, the retain ability and the flood area, etc. The impact analysis and appraisal of Tangjiashan Barrier Lake are available by overlay between spatial information and calculation of the hydrodynamics model. Several hydrodynamics model computations are worked out according to different scheme and different assumed water level. The spatial information overlaid by calculational results demonstrates disaster's space-time distribution of Tangjiashan Barrier Lake's break. The result shows that the spatial information processing method will provide information in a fast and accurate manner for the Barrier Lake monitoring. It will provide an early warning to the government and provides a valuable reference for decision-maker as well. [C937]

#### "Sevastopol range for measuring radar, thermal and laser properties of surface ships (1979-1991)"

Described in this paper is the history of creation of Sevastopol ground for testing radar, heat and laser properties of surface crafts. The review of the testing ground activity and biography of its research supervisor D.Sc. Ye. Shtager is presented. The questions regarding researches noncompletion because of the USSR collapse are discussed. [C938]

#### "Title page"

The following topics are dealt with: radioengineering research; microwave amplifiers; oscillator; receive devices; solid state devices; CAD/CAM; O-type microwave devices; DRO microwave devices; M-type devices; gyrodevices; wireless access networks; telecommunication systems; information technologies; antenna arrays; antenna elements; passive devices; microstrip devices; SHF-devices; semiconductor materials technology; microwave microscopy; nanotechnology; nanomaterials; nanoelectronics; quantum devices; very high power microwave electronics; chaotic oscillations; chaos generators; microwave devices measurement; microwave signals measurement; technological processes control; nondestructive testing; ecological applications; medical applications; radioastronomy; atmosphere research; remote sensing; and radar systems theory. [C939]

#### "Development of integrated typhoon remote sensing application system based on .NET and ArcGIS Engine"

The use of remote sensing to monitor and forecast typhoon (a severe weather system) rapidly and efficiently, is one of the prerequisites for disaster prevention and mitigation. Yet so far there only have been a few simple systems focusing on single function of typhoon's analysis in the fields of meteorological operations, but still lack a comprehensive and integrated remote sensing application-oriented platform for typhoon that combines all kinds of data in various formats and most analysis functions. The integrated typhoon remote sensing application system newly developed by utilizing .NET and ArcGIS Engine has effectively integrated remote sensing data of different satellites and different sensors such as FY2C, NOAA, FY3A etc, and radar data, spatial geographical data as well as various kinds of thematic data related to typhoon, and capably provide with professional analysis functions such as determination of typhoon's location, type and intensity, diagnosis of typhoon's structure, analysis of typhoon's track, along with rainfall estimation, as well as auxiliary analysis functions such as image processing, geographic navigation, thematic mapping and numerical weather prediction. This paper highlights the methods of software analyzing, framework and database designing adopted in object-oriented integrated typhoon remote sensing application system development and functions-realizing methods based on components. The module of typhoon disaster assessment needs to be further developed to improve the system. [C940]

#### "Denoising of SAR Images Based on Wavelet Packet"

The SAR remote sensing images are interfered by noises during the detection and transmission, a method based on wavelet packet and level dependent adaptive threshold is proposed in this paper. By using this method, the SAR images can be decomposed in a more elaborate method compared to the traditional wavelet transform, and the noises in the SAR images are eliminated by the adaptive threshold method. The experiment results show that this method can reduce the noises efficiently. The PSNR and the subjective vision of the results have better performances than the result of traditional wavelet transform method. [C941]

### "Design and Implementation of Mobile GeoSpatial Information System for Public Health Emergency"

As mobile devices like personal digital assistant (PDA) or handheld PC (HPC) are rapidly developing and the wireless Internet is increasingly used, interests in the mobile geospatial information system are gradually expanded. Nowadays, the outbreak of emergent public health events can be heard more often than before and make lots of people ill in a short time. How to deal with the events much more rapidly and efficiently are the main factors needed to be considered. With the development of mobile devices and wireless network, according to the characteristics of emergent public health event, the authors have designed and implemented a mobile geospatial information system based on PDA for public health emergency. The platform integrates the technologies of geographic information system (GIS), Global Positioning System (GPS), global system for mobile communication (GSM) and general packet radio service (GPRS). Based on platform, the paper conducts an experimental case study of HFRS (hemorrhagic fever with renal syndrome) fieldwork, and test the effectiveness and usefulness of field survey based on mobile collaboration. [C942]

### "Calculation and Analysis of Typical Coastal Low-Tide Marks Based on Lidar Data"

Coastal Zone is the current research hotspot. But it is difficult to accurately designate the inter-tidal coastal zone because the low-tide mark is underwater for a long time and difficult to be established. Light Detection and Ranging (Lidar) can quickly, directly and accurately detect elevation information of real surface and ground; The high-resolution aerial image synchronously accessed with Lidar can notably present characteristics of, so it is convenient for accurately locating and extracting features; we can acquire the average tide difference of coastal zone according to years of tidal information. With the support of geographic information system and remote sensing technology, this paper establishes a model for extracting the low-tide mark based on Lidar data and the high-resolution aerial image simultaneously received. The main contents of the model are: (1) Extract the average high-tide mark and water-mark from the high-resolution aerial image in ArcGIS; (2) Generate DEM using Lidar data, and then derive gradients from the generated DEM. (3) Calculate the average tide difference according to tidal information. Finally, based on the above three parameters, reckon the projected average low-tide mark position. [C943]

### "Identification of sand dredges in Yangtze River based on ASAR remote sensing data"

This paper wants to explore a key technique of identifying and locating the sand exploitation ships using ASAR images. Chenglingji of Yangtze River is selected as the research region. One software module was developed with the IDL (Interactive Data Language) which is a facing matrix, simple visual language. This paper researches on some key techniques based on ASAR images such as filtering and noise reduction, the process of image based on morphology, edge detection, region growth, extraction of ship's shape feature and so on. Comparing with the field monitoring results, this method can achieve 80%-90% accurateness. [C944]

### "New spatial measures of terrain dynamics derived from time series of lidar data"

We anticipate that multiyear lidar surveys, currently focused on vulnerable coastal areas, will soon become a common resource for monitoring and analysis of various aspects of regional terrain change. We propose raster based measures for mapping and quantification of discrete and continuous terrain changes by introducing novel concepts, such as core and envelope surfaces, contour evolution band, and evolution regression slope map that can provide insights into the spatial aspects of terrain dynamics and changes in structures. The methodology is applied to a section of North Carolina coast where multiyear time series of lidar data is already available. Dynamics of bare dune and beach systems, changes in structures and vegetation growth are mapped and quantified to evaluate the proposed approach. [C945]

### "Wireless interrogation techniques for a passive pressure micro-sensor using an EM transducer"

In this communication, the new and latest results relative to an original passive electromagnetic micro-sensor for wireless pressure monitoring application are presented. This micro-sensor uses the electromagnetic transduction principle. The sensing element is a flexible high resistivity silicon membrane located above a coplanar quarter-wavelength resonator operating in Ka-band. From the measurement of the resonant frequency the pressure applied on the membrane can be derived. This completely passive and wireless pressure telemetry micro-sensor has been designed, fabricated and characterized, thereby eliminating the need for contact, signal processing circuits, or power supplies to be contained within the sensor. Measurement results under real working conditions, obtained from a specific RF/pressure bench are reported and reveal a very good sensitivity of 370 MHz/bar in Ka-band. Moreover, for the first time, we propose to use a frequency-Modulated Continuous-Wave (FMCW)

radar system for the remote determination of the pressure data via the electromagnetic micro-sensor. This attractive concept of radar interrogated micro-sensor based on electromagnetic transducer is discussed and illustrated. [C946]

### "Welcome to EuRAD 2009"

It is my pleasure, as conference chairman, to welcome you to the 6th European Radar Conference (EuRAD 2009) being held in Roma as part of the European Microwave Week (EuMW). EuRAD started six years ago thanks to a wonderful idea of our Dutch colleagues and friends from IRCTR and Delft University and in particular to the determination of prof. Leonard Ligthart. Since then, EuRAD has grown into one of the largest European and worldwide recognised radar events, both in terms of quality (guaranteed by a rigorous, peer review of a substantial abstract) and of quantity: in fact, the number of proposed contributions has steadily increased during six years. This year, in spite of the present international financial crisis, we have received 189 submissions to this conference, with more than 18% increase with respect to the very successful EuRAD 2008 edition. EuRAD submissions are now about 15% of the whole EuMW, making this conference the second largest of the EuMW and with an increase of its duration of more than two full days. The accepted papers are organised into twelve oral sessions plus four Focused Sessions and one common session EuMC/EuRAD (summing up to eighty-three podium presentations), complemented by a poster session. Moreover, five invited papers of wide interest are presented in the Opening and Closing sessions. This year, I feel that the strong reduction in the number of parallel sessions will enhance the benefit for the attendees. The programme covers a wide range of radar topics including Radar Subsystems and Technology, Signal Processing, Design and Evaluation, Systems and Applications; two focused sessions are dedicated to Space Radars and their Environmental Remote Sensing applications, one to Space-Time Adaptive Processing and one to Passive Radar, while the common session with EuMC is dedicated to through-the wall radar imaging. In addition to that, the programme includes other "hot" topics such as ultra wide band radar, multilateration-, interception/analysis of radar signals, new radar waveforms and OFDM radar, sea and OTH radar, phased arrays and more, with a wide and updated overview on the most recent advances in radar technology and applications. [C947]

### "Inversion of wavelet coefficients in oil spills detection in radar images for environment risk reduction in Adriatic Sea"

Problem of oil spills detection is involvement of dark colors. Dark colors are close to 0 and cannot be detected by image differencing. The paper presents an idea to overcome the detection problem for oil spills. By using DWT, the idea is to remove parts of the signal which represent main structures such as coastlines and increase noise. Wavelet analysis in real time, for oil spills, has been applied to an inverted image. Then the so called frame differencing technique is applied. The benefits of using the proposed method is the reduction of risk for environment pollution, prevention of environment danger, tracking of pollution spread, and help in crisis management. The proposed method can be combined with VTS for narrow seas such as the Adriatic Sea. [C948]

### "Lidar measurements on aerosol characteristics at the tropical stations Trivandrum (8.33° N, 77° E) and Gadanki (13.5° N, 79.2° E)"

Lidar has proven to be an effective instrument for obtaining high resolution profiles of atmospheric aerosols. In this work we present the characteristics of the atmospheric aerosols derived using the range dependent lidar ratio values at the two tropical stations namely Trivandrum (8.330N, 77.0E), India and Gadanki (13.50N, 79.20E), India. Summer aerosol properties at the two stations are studied and compared. The nature and optical properties of aerosols are found to be different at the two stations and shows temporal and altitude variability. [C949]

### "Optical properties of cirrus clouds during monsoon over Indian subcontinent"

The monsoon water cycle is the lifeline to over 60% of the world's population. The precipitation of the clouds in the monsoon season depends on the microphysical properties of the clouds. The effect of aerosol on cirrus clouds is being looked into through this work as an effort to study the role of aerosol on Indian Monsoon. The microphysical properties of high altitude clouds were obtained from the ground based lidar experiments at a low latitude station in the Indian subcontinent. Measurements during the Indian monsoon period from the inland station National Atmospheric Research Laboratory (NARL) Gadanki (13.5° N, 79.2° E), Tirupati, India were used for the investigation. The seasonal variation of depolarization characteristics of the cirrus clouds were analyzed. The results obtained over a period of one year from January 2002 to December 2002 were presented. [C950]

### "Remotely Operated and Autonomous Mapping System (ROAMS)"

The development of a relatively low cost mobile 3D mapping robot prototype named ROAMS (Remotely Operated and Autonomous Mappings Systems) which enables rapid generation of high resolution 3D maps of indoor/outdoor environments is presented. The Robotic system generates 3D maps using a video registered Lidar scanning system integrated with a multiple degree of freedom actuator. This vehicle is also used as a test platform for conducting studies and real-time experiments on autonomous operations. Environmental awareness sensors in combination with a long range wireless communications system is used to enable remote operation and monitoring of ROAMS. Techniques for improving the resolution and point distribution of Lidar data through the use of video images and actuator speed control are also investigated and presented. [C951]

### "Multi-element arrays for LADAR"

Remote optical sensing using laser radiation is being increasingly deployed for both military and civilian applications. The technique, commonly known as LADAR or LIDAR, uses an optical range finder to determine relative displacement and velocity. LADAR can also be used to measure the environment, for example atmospheric turbulence or pollution. In addition, smart cameras are emerging, where a conventional 2-D image is supplemented with distance information to give a complete 3-D picture, with applications in autonomous vehicles and collision avoidance systems. [C952]

### "Compact high power DPSS laser with very low RIN and phase noise for 1550nm wavelength band"

The performance of analog photonic systems is strongly affected by laser power and noise. There are two components to the noise, intensity noise and phase noise. The phase noise directly impacts linewidth and can also be converted to intensity noise via wavelength sensitive components. [C953]

### "Research of the aeroplane intelligent localization methods based on Synthetic Aperture Radar imagery"

Synthetic aperture radar (SAR) presents prominent advantages, such as working in all-time and all weather condition, which makes it locate the aeroplane more advantageous. First, the article discusses the effect on aircraft location caused by factors such as topographic relief while SAR imaging. Then, proposes a method that calculates the aeroplane's spatial position based on the multi-angular cone model after images matching are finished between different SAR images. The experiments verify the high-precision location of aircraft with more than 4 matching points provided, which spells itself the fitting tool in positioning aircraft with scarce image matching points. [C954]

### "Oil Spill Identification in Marine SAR Images Based on Texture Feature and Fuzzy Logic System"

A model based on texture feature and fuzzy logic algorithm was constructed to discriminate oil spills from look-alike phenomena in the SAR images. Statistics texture feature of SAR images were extracted and used as the input parameters in the fuzzy logic system. The texture features consisted of entropy second order, angular second moment, contrast and inverse difference moment of dark objects. The system analyzed 38 SAR images with 77 oil spills and 52 look-alikes, and provided the probability of a dark object to be an oil spill. The remaining 26 processed SAR images, which were not included in the training, were used to test the system. The result showed that 80.5% of the oil spills were correctly classified. It seemed that the texture features and fuzzy logic system were effective in identifying oil spills on marine SAR images. [C955]

### "Application of Two-Pass D-InSAR in Chengdu Region's Deformation Measurement in Wenchuan Earthquake"

On the 12th May 2008, an earthquake with 8.0 Ms shook a large area of the Sichuan Province in China. The epicenter of the devastating earthquake was located in Wenchuan, 80 kilometers west-northwest of Chengdu, the capital of Sichuan Province. A lot of scholars have used various remote sensing images and other techniques to detect the disaster. Differential synthetic aperture radar interferometry (D-InSAR) is an advanced technique for monitoring large-scale terrain deformation with mm accuracy. This paper described the application of two-pass D-InSAR in mapping the co-seismic surface deformation caused by the Wenchuan earthquake including the interferometric data processing workflow and results. Chengdu region's deformation measures at roughly 140 mm in our study, which is relative rather than absolute. DInSAR applied to a terrain deformation measurement has been proven as an effective tool to detect displacements. [C956]

### "Precise positioning with wireless sensor nodes: Monitoring natural hazards in all terrains"

Prediction, assessment, and mitigation of surface-affecting natural hazard processes such as landslides, avalanches, earthquakes, and floods call upon geoscientists to rapidly deploy instruments and accurately characterize these earth processes, often with little lead time and under dangerous working conditions. Affected areas may have heavy tree canopies, or high atmospheric dust loads (volcanic eruptions), precluding the use of traditional location techniques like Global Positioning System (GPS). The proliferation of inexpensive radio systems provides a technology that has the potential to redefine the approach to rapid characterization of hazardous earth processes. The research effort described in this paper developed and demonstrated an inexpensive, cooperative radar-like technology for precise distance measurement between intelligent radio nodes. [C957]

#### "Analysis of land cover/use over Penang Island, Malaysia by using ALOS PALSAR data"

Microwave Remote sensing data have been widely used for detecting and analyzing land cover/use feature in our environment. The objective of this project is to investigate the use of multi-polarized data of ALOS-PALSAR data for land cover/use mapping. ASF MapReady programs from Alaska satellite Facility Geographical Institute at the University of Alaska Fairbanks was used for the preprocessing of ALOS-PALSAR data. Standard supervised classification techniques such as the maximum likelihood, minimum distance-to-mean, and parallelepiped were chosen for the ALOS-PALSAR images in land cover mapping. Some filtering and enhancement methods were applied to reduce speckle noise and to contrast the images. The ALOS-PALSAR data was classified into four categories, such as forest, urban, water and open land. The ALOS-PALSAR data training areas were choose based on optical satellite imagery. The land cover information was extracted from the digital data using PCI Geomatica 10.1 software package. The classification accuracy was used to evaluate the best performing data combination. This study indicates that the land cover/use of Penang Island, Malaysia can be mapped accurately using ALOS PALSAR data. [C958]

#### "Improvement of classification accuracy integrating C- and X-band synthetic aperture radar data"

Remote sensing for the monitoring of agricultural crops has been widely used in the past. Synthetic aperture radar (SAR) system, for its characteristics of all-weather, all-day image obtain capacity, is an attractive source of information for agriculture crop classification applications, particularly in regions where cloud cover is a problem. The accuracy with which crops can be classified is dependent on a range of sensor properties, including the SAR operating configuration. This paper focuses on the effect of integrating C- and X-band SAR data on the improvement of classification accuracy. The study was carried out on Yucheng Ecological Experimental Station (China). Radarsat-2 and TerraSAR-X data were acquired, and during the satellite overpass, the ground investigation was implemented. Support vector machine classifier was used to classify the image based on the backscattering coefficients and texture features. The classification was conducted separately on Radarsat-2, TerraSAR-X and the integrating of the two. The performance of single band SAR was not acceptly good, but the integrating of the two had a great increase on classification accuracy (more than 10%). With different frequency we would get more information about the earth surface. Integrating of multiband of SAR data was a dependable way to improve classification accuracy. [C959]

#### "Sentinel 1-the future GMES C-band SAR mission"

The ESA Sentinels constitute the first series of operational satellites responding to the Earth Observation needs of the EU-ESA Global Monitoring for Environment and Security (GMES) programme. The GMES space component relies on existing and planned space assets as well as on new complementary developments by ESA. This paper describes the Sentinel-1 mission, an imaging synthetic aperture radar (SAR) satellite constellation at C-band. It provides an overview of the mission requirements, its applications and the technical concept for the system. [C960]

#### "Out-of-sequence measurement processing for an automotive pre-crash application"

In this paper, the merits of incorporating out-of-sequence measurements (OOSM) into a Pre-Crash application are investigated. When an imminent front crash is detected by the Pre-Crash system, the algorithm activates a reversible seat belt tightening system. This paper points out that simple buffering is not applicable in most time critical applications such as Pre-Crash. It is crucial to have sufficiently accurate tracking information without any buffering delays, especially in urban traffic scenarios. Furthermore, the existing OOSM algorithm from Bar-Shalom [1] for the 1-step-lag case is extended to support Joint Probabilistic Data Association (JPDA). A comprehensive evaluation on simulated as well as on real sensor data is presented. [C961]

#### "The Study of Image Fusion Method Based on Wavelet-Packet Transform"

Based on the IHS transform and wavelet packet transform, a scheme of remote-sensing images fusion aiming at

protecting image's spectral characteristics is made in this paper. This scheme makes best use of the information in remote-sensing images to be fused and prevents the loss of image information. Through the experiment using SAR image and TM image, all the spectral characteristics, the textural feature and the spatial quality of image have been improved. [C962]

### "Detection of objects inside water exploiting the Brillouin precursors"

In a dispersive medium, the appearance of the steady-state part of the signal is preceded by oscillations known as precursors. This is due to the interrelated effects of phase dispersion and frequency dependent attenuation. The propagation properties of the precursors are different from the steady-state part of the pulse which makes them suitable for many applications. An example of these interesting properties is the non-exponential attenuation rate of the Brillouin precursor inside a Debye medium. Exploiting this property, it is suggested that an input pulse consisting of two mutually delayed Brillouin precursors would be a "near optimal" excitation in terms of the attenuation inside triply distilled water. Evidently, this optimized pulse is promising for remote sensing applications, aimed at detecting objects inside lossy dispersive media such as moist soil and water. In such cases, the optimized pulse can overcome the high loss of the medium and contribute to the detection of objects further inside the dispersive medium. In this paper, Finite-Difference Time-Domain (FDTD) simulations are employed to evaluate the usefulness of the optimized pulse for remote sensing applications, by modeling its scattering from objects inside water. [C963]

### "Doppler Radar for planetary safe descent and landing"

This paper discusses some basic requirements for a Doppler Radar intended to provide critical measures to be used for safe descent and landing on planets. Some considerations are briefly developed in order to establish a preliminary design of such a radar. [C964]

### "Candidate scatterometer concepts for the Post-EPS mission"

Post EUMETSAT Polar System (Post-EPS) is the next generation meteorological polar satellites system of EUMETSAT, a joint ESA-EUMETSAT development programme currently in phase 0, to replace MetOp system in the 2018-2020 time frame. Post-EPS is a mandatory programme addressing the need to continue EPS to provide, first of all, observations for operational meteorology and climate monitoring, and in addition, environmental services covering ocean, atmosphere, land and biosphere, and natural disasters. According to these objectives, the Scatterometry (SCA) mission has to provide ocean surface wind vectors, which are an important input to global and regional Numerical Weather Prediction (NWP) and also models of the ocean surface waves. The SCA instrument is conceived with the objectives of ensuring continuity of past spaceborne scatterometer missions. Their heritages (ASCAT, SeaWinds, etc.) have been fully exploited in SCA design and has directly led to the identification of the SCA candidate concepts. The direct comparison of the performance for past scatterometry missions and the SCA requirements shows that SCA performance would be in line with the ASCAT radiometric performance, while significantly exceeding ASCAT in terms of geometric parameters (horizontal resolution and accuracy). This paper presents the preliminary instrument concepts that have been investigated during the on-going phase 0 study. [C965]

### "Spatial relationship of F-region field-aligned irregularities and medium-scale traveling ionospheric disturbances observed with the MU radar and all-sky airglow imagers"

We report simultaneous observations of medium-scale traveling ionospheric disturbances (MSTIDs) and field-aligned irregularities (FAIs) in the F region by using two all-sky airglow imagers and the MU radar in Japan. MSTIDs propagating southwestward were observed in 630-nm airglow images on the night of June 16, 2004. During this MSTID event, FAIs in the F region were observed by making multibeam measurements with the MU radar. We found that FAIs with intense (weak) signal-to-noise ratio (SNR) coincided with the airglow depletion (enhancement) caused by the MSTIDs. This result indicates that the FAIs could be generated by the gradient drift instability at the airglow depletion region. [C966]

### "Cloud profiling radar on earthcare satellite"

The design and current status of EarthCARE/CPR are described in this report. Basic design of CPR will be confirmed in this year, and engineering model development and testing will be done this year and the next year. In parallel with the development activity of CPR, algorithm development activity is in progress. The data from CPR is expected to contribute to reveal the detailed information of clouds and to the studies on global warming. It is also expected the continuation of cloud observation from CloudSat data that was launched in 2006[4]. [C967]

### "Performance evaluation of adaptive scan with wide-band noise modulation for spaceborne rain radar based on simulation"

The adaptive scan technique using wide-band noise modulation is applied for the simulation of rainfall observation for spaceborne rain radar in a no-rain area. The accuracy of this method is discussed based on a simulation using rainfall data observed by TRMM (Tropical Rainfall Measuring Mission) Precipitation Radar (PR). [C968]

### "DEM Extraction from LIDAR Data by Morphological Gradient"

Digital elevation model (DEM) is essential for most geographic information system (GIS) applications and topographic analysis. The technology of airborne light detection and ranging (LIDAR) provides a powerful support for generating high-resolution DEM. DEM extraction from LIDAR data includes filtering and DEM reconstruction. Recent years witnessed many kinds of filters designed and developed. However, filtering is still a practicably difficult, especially for scene complex area. In this paper, a new method of DEM extraction from LIDAR data based on morphological gradient is proposed. Firstly, point clouds are divided by an index mesh. Then, the morphological gradient of each point is calculated using the method suitable for filtering. And, objects are removed gradually by choosing some points based on gradients to carry on an improved opening operation iteratively. Finally, DEM is three-dimensional reconstructed through interpolating by inversing distance to a power. This method is tested with 15 sample data sets which are released by ISPRS and compared with other filtering methods qualitatively and quantitatively. The experimental results show that this method has high robustness in all kinds of complex scenes, which can reduce the nonessential computation as well as the possibility that all types of error happen. So the method has good adaptability and practicability. [C969]

### "Visualization of water vapor distribution in the lower atmosphere using two lidars"

Water vapor distribution in the lower atmosphere was observed using two optical lidars (ceilometer) set up at the distance of 3.1 km. Range height indicator (RHI) display was constructed from two time series data measured by each lidar. The instruments were also included small vertical radar and snowfall gauge. All the data were displayed on the same coordinate system to compare the profiles with time synchronization. To examine horizontal distribution of water vapor (cloud) widely, conventional weather radar was also used. Combination of all these instruments and methods will be potent system for understanding lower atmospheric structure. [C970]

### "Airborne GPS reflectometry from low altitude aircraft"

This work is intended to develop a software-defined Global Positioning System (GPS) receiver specifically designed to process reflected GPS signal off the ground or the ocean surface for purpose of remote sensing. A set of airborne campaign was conducted to evaluate the performance of the prototype GPS reflectometry receiver. The reflected signal was tracked in open-loop manner using the so called delay mapping receiver. The result shows that the prototype receiver was capable of providing altimetric measurements with a precision level of the order of few meters with an unknown system bias which should be estimated. [C971]

### "Forest parameters inversion using Polarimetric and Interferometric SAR data"

In this paper we discuss some aspects of the forest height estimation using Polarimetric and Interferometric (POLINSAR) SAR data. Three main issues limit the inversion of the POLINSAR coherence from repeat-pass POLINSAR systems: temporal decorrelation, terrain slope distortions and effects of wave penetration. We show that, if temporal decorrelation is not severe, the distortions due to terrain slope can be removed and the wave penetration can be compensated using the predictions of the scattering simulator PolSARProSIM. A detailed procedure that applies to any POLINSAR data is presented and illustrated using ALOS/PALSAR data and the SRTM digital elevation model (DEM). [C972]

### "Quantitative study of the Eco-water indices based on remote sensing"

Eco-water is defined as a transformation of precipitation, which is deposited by vegetation layer, humiliated vegetation layer and soil layer. It plays an important role in the water-cycle system. As potential factors on Eco-water and Eco-water layer are different from one season to another, multi-temporal and multi-type remote sensing data, measured spectrum and the routine observation were applied to construct the indices for Eco-water and its inversion model. The four Eco-water indices, including Vegetation Canopy Interception Content, Vegetation Water Content Index, Soil Moisture Index and Eco-water Storage Index, were calculated. The results show that the RS information model can reflect the real soil moisture. The dissertation brings forward the Eco-water Remote Sensing quantitative study based on vegetation layer. The vegetation-based calculation model for Eco-water with quantitative remote sensing technology, which has been identified in the dissertation, possesses

significant science affect and practical value; and it can not only advance the methods of Eco-environment study, but also promote the research on water-resources transformation and water-cycle, also enlarge the domains of remote sensing applications. [C973]

#### **"Preliminary results of the Passive Advanced Unit Synthetic Aperture (PAU-SA)"**

This paper presents the current state and preliminary results of the Passive Advanced Unit Synthetic Aperture's instrument (PAU-SA) validation tests. The performed test has been focused on the implementation of the PAU-SA's interface in order to test extended source simulations. Moreover, the currently status of the hardware instrument is presented. [C974]

#### **"C-band D-InSAR and field data for calibrating a groundwater flow and land subsidence model"**

Differential Synthetic Aperture Radar Interferometry (D-InSAR) is a powerful technique used for detecting and measuring surface deformation with sub-centimetre accuracy. Using C-band data from three different satellites, the D-InSAR technique is used to calibrate a coupled groundwater flow and land subsidence numerical model. Additionally, D-InSAR results from different sensors are compared and contrasted. When comparing D-InSAR results with extensometers and water levels, a direct correlation is noticed. For all D-InSAR image pairs, large baselines, atmospheric effects, temporal decorrelation, and vegetative cover were limiting factors in obtaining a maximum number of usable interferograms. The total maximum subsidence for a point location in the valley between November 2003 and May 2008 is approximately 40 cm reaching a maximum total subsidence of over 2.0 metres since 1962. When contrasting the ENVISAT ASAR and RADARSAT-1 data, subsidence rates were similar yet the distribution had significant differences. Additionally, ENVISAT's shorter baselines led to more accurate results. [C975]

#### **"Forest parameter retrieval using a general repeat-pass polarimetric interferometric vegetation model"**

This paper concerns forest parameter retrieval from multi-temporal polarimetric interferometric SAR data. A two-component polarimetric interferometric model, designed for geophysical parameter retrieval, is presented for volumetric media over the ground. It is founded on a scattering model based polarimetric decomposition and the random volume over ground (RVoG) PolInSAR inversion technique. For forest vegetation observed at L-band, this model accounts for the ground topography, canopy layer and total tree heights, mean wave attenuation in the canopy, tree morphology in the form of orientation distribution and effective shapes of the branches, surface scattering contribution, and double-bounce ground-trunk interactions. A parameter retrieval framework is developed for repeat-pass acquisitions which aims to estimate and to compensate temporal decorrelation. The parameter estimation performance is evaluated on real airborne L-band SAR data in the repeat pass mode. [C976]

#### **"Variable wind influence on InSAR imagery of forests"**

The horizontal and vertical (3D) structure of Earth's forested ecosystems are of great significance to their ecological functioning and societal uses. An InSAR approach is one methodology whereby a forest's structure and height in particular can be successfully estimated. Critical to the successful estimation is a high correlation between multiple SAR images. Regardless of a forest's location on the Earth, wind can significantly alter a forest's appearance to an L-band SAR system and so decrease this necessary correlation. In order to investigate the wind-induced decorrelation, we have developed a model for the repeat-pass interferometric SAR response of a forested area taking into account wind effects. The simulation consists of multiple interconnected parts including static tree geometry's generation, a wind simulator to apply to a static tree, and an electromagnetic model to allow us to calculate the interferometric SAR response. The static tree geometry generation process generates a pseudo-random tree based on a given DNA file which specifies a species specific structure. This geometry is then modified by the wind simulator producing snapshots of tree-geometry as a function of time. Each snapshot is then used in the interferometric SAR simulator to synthesize the wind-blown geometry's InSAR response. Results present coherence as a function of wind speed and forest structure. An important feature of this research is the usage of a physically based realistic wind model that is based on measurements of wind effects on trees as well as realistic models of fluid flow and simple harmonic branch resonators. Allowing branches to bend and move out of the plane of the incident wind field enables our model to capture numerous features of a physical tree blowing in the wind. This realistic model is necessary for a realistic simulation of the effects that wind has on a given InSAR imaging system. [C977]

#### **"Modeling surface-flow characteristics in glaciated landscapes"**

Geographic Information Systems (GIS) hydrologic modeling techniques are used to better understand the

surface-flow characteristics in the Prairie Pothole Region (PPR) of North America. This research uses an airborne Interferometric Synthetic Aperture Radar (IFSAR)-derived digital terrain model (DTM) as a base for developing a hydrologically-correct DEM and derivative products. The IFSAR DTM is assessed for accuracy and ability to resolve wetland features. A wetland mask is developed to selectively fill the DTM and from it products such as wetland catchments and drainage linkages are derived and interpreted. Study sites in the PPR are two surveyed and closely monitored wetland complexes, Crystal Springs and Orchid Meadows in Deuel County, South Dakota, USA. [C978]

#### **"Parametrization of integrated hydrological model of Nam Co lake catchment on Tibetan Plateau using synergy of SAR and optical data"**

Understanding of exchange processes over Tibetan Plateau including hydrological cycle is becoming increasingly important since their influence on the formation of the Asian monsoon system is known. Tibetan Plateau is source area for main Asian rivers that are of crucial importance for downstream communities of China, India, Bangladesh, Pakistan and SE Asia. Accurate and up-to date information of the characteristics and the current trend of these changes, provided by modern satellite systems like TerraSAR-X, are thus needed. The study area is delimited by the watershed of Nam Co basin on Tibetan Plateau in Tibet Autonomous Region of China approximately 100 km NNW from Lhasa. The no-outlet basin of the lake offers an excellent example of landscape unit characteristic for Tibetan Plateau where all exchange processes between land and atmosphere can be studied. Hydrologic modeling of Nam Co basin will be supported by complex interpretation of TerraSAR-X data that will provide whole set of hydrologic parameters. The TerraSAR data will be processed in synergy with other available microwave and optical remote sensing data sets. Basic extracted variables will be thus transformed into meaningful hydrological parameters. Data evaluation will take into account various aspects of landscape qualities with respect to water cycle. Variability of lake level, seasonal changes of soil moisture, influence of wetlands, lake icing and snow melt will be estimated. The synergetic approach to interpretation of TerraSAR-X data will benefit from major advantages of the high spatial resolution, the fast repetition cycle and the full-polarimetric capabilities in combination with high resolution optical data (RapidEye, QuickBird, Kompsat-2, ASTER, Landsat etc.) and digital elevation models. [C979]

#### **"Measurement and analysis of paddy field by polarimetric GB-SAR"**

Polarimetric ground-based synthetic aperture radar (GB-SAR) measurements in a paddy field and its analysis results are presented. The measurements were carried out three times before and after an ear emergence of rice, and SAR images of full polarimetric components are reconstructed from the acquired dataset. By using those images, a sensitivity of a polarimetric component and a frequency range due to the ear emergence is discussed. Then, we could confirm that HH component of C-band is the most sensitive parameter although HV and VV components do not give significant changes. Especially, HH component of 5-6 GHz and 6-7 GHz show 10 dB increases after the ear emergence. Moreover, Freeman decomposition is applied to the SAR images. And, increases of a surface scattering component and a double bounce component in a same frequency range with the increase of HH component can be observed. [C980]

#### **"Independent component analysis of polarimetric SAR data for separating ground and vegetation components"**

In this study, the use of independent component analysis (ICA) to separate the ground and vegetation scattering components from polarimetric, synthetic aperture radar (SAR) data is presented. In vegetation covered terrain, the backscattered signal is a composite of both a ground scattering component and a vegetation scattering component. The FastICA algorithm is customized and applied to both simulated and field data. The improved customized algorithm is found to work better than the standard FastICA algorithm. It is also shown that noise and depolarization limit the ability of ICA to separate the different scattering components. The technique is applied to field data from the Glen Afric region in Scotland and produces results consistent with other radar metrics obtained from that region. [C981]

#### **"Developing new spectral indices for karst rocky desertification monitoring in Southwest China"**

Karst rocky desertification is a special kind of land desertification developed under violent human impacts on the vulnerable eco-geo-environment of karst ecosystem. The fractional cover of photosynthetic vegetation (PV), non-photosynthetic vegetation (NPV), bare soil and exposed bedrock are key indicators of the extent and degree of land degradation in karst region. The vegetation fractional cover can be estimated approximately from remote sensing with vegetation indices. However, the vegetation indices cannot be easily applicable to all land cover types. In this study, we developed new spectral indices, karst rocky desertification synthesis indices (KRDSI), were then designed based on tied-spectrum permutation and unique spectral characteristics of main land cover

types. Comparing with the use of traditional vegetation indices and LSU, the KRDSI was more consistent with the field measurement of main land cover fractions. Our study indicates that KRDSI is a useful tool for karst rocky desertification monitoring with remotely sensed data. [C982]

#### "Woody cover and heterogeneity in the Savannas of the Kruger National Park, South Africa"

The woody vegetation of the Kruger National Park varies greatly in species composition, biomass and cover at regional scales. This study focuses on woody (tree and shrub) cover as a defining characteristic of savannas. We combine field measurements, optical and radar remote sensing to map woody cover across the whole of the Kruger Park at medium resolution (90 m). We also explore relationships between the mapped woody cover, climate, soil, topography, fire and herbivory. The spatial and temporal variability of woody cover is significant for Park managers in support of priorities relating to maintenance of structural and biotic heterogeneity. We derive a product that quantifies the spatial heterogeneity in woody cover within 1-km cells. [C983]

#### "Hardware-accelerated edge detection for polarimetric synthetic aperture radar data"

From the literature review, there are two constant false alarm rate detectors for detecting edges in multi-look fully polarimetric synthetic aperture radar (POLSAR) imagery, namely the likelihood ratio edge detector and the Roy's largest eigenvalue-based edge detector. In the latter approach, one major restriction is the computation complexity, i.e. in the context of the chosen C language-based implementation. Thus, in this paper, a novel hardware-based architecture is presented to improve the processing time for the Roy's largest eigenvalue-based edge detection. The algorithm was implemented in a field-programmable gate array (FPGA) with an accelerated solution targeting data rates of up to 1 Gb/s. Its performance was examined using nine-look NASA/JPL C-band data and evaluated in terms of processing speed and accuracy as compared to the C language-based implementation on a personal computer (PC) with a Core™ i7 2 Duo processor clocked at 2.2 GHz. [C984]

#### "Real time monitoring of flooded areas by a multi-temporal analysis of optical satellite data"

Optical sensors aboard meteorological satellites are an excellent tool to monitor floods and support the flood risk management cycle, mainly thanks to their high temporal resolution, which allow us to obtain real time and frequently updated information on environmental changes. The RST (Robust Satellite Techniques) approach, an automatic change detection scheme, has been already applied using AVHRR (Advanced very High Resolution Radiometer) and MODIS (Moderate Resolution Imaging Spectroradiometer) data to detect and monitor flooded areas. Results achieved have shown its capability in automatically identify flooded areas with a low rate of false alarms, also discriminating permanent water from actual inundated areas. In this paper, in order to further assess the reliability and the sensitivity of the proposed approach in different conditions of observation, the RST methodology has been used to analyze the July 2007 and October 2008 floods occurred in the South Africa and Algeria regions. [C985]

#### "SETHI, the ONERA airborne SAR sensor, and his low frequency capability"

SETHI is the airborne SAR system developed by the ONERA, the French Aerospace Lab dedicated to civilian application. This new SAR system was designed to explore the science applications of radar remote sensing; it can operate over a wide range of frequency bands (X, L and UHF/VHF) and it has polarimetric and interferometric capabilities. In this paper, we will more specifically illustrate the low frequency capability of this new airborne SAR system and provide some results obtained with the system. [C986]

#### "Integrating remote sensing and ancillary data for regional ecosystem assessment: Eucalyptus grandis agro-system in KwaZulu-Natal, South Africa"

The ability of various ecosystems to perform vital functions such as biodiversity production, and water, energy and nutrient cycling depends on the ecosystem state, i.e. health. Ecosystem state assessment has been a topic of intense research, but has reached a point at which accurate large scale (e.g. regional to global scale) modelling and monitoring are hindered by limitations in conventional assessment methods such as direct field sampling, modelling from environmental drivers such as temperature, precipitation and available nutrients, and modelling from remote sensing data. The Ecosystem-Earth Observation (Eco-EO) research group at the Council for Scientific and Industrial Research (CSIR), South Africa has highlighted the need in remote sensing research for an integrated sensing approach at the systems level. This perspective is based on the assumption that a modelling approach that exploits the strength of the various techniques (in situ environmental variables, direct field observation and remote sensing data) could potentially improve the assessment of ecosystem state at various geographic scales. In this light, the Eco-EO research group has embarked on an agro-system state assessment project since 2007 as a first step towards the implementation of the integrated modelling approach for various ecosystems. The agro-system consists of a monoculture forest plantation of Eucalyptus grandis

situated in KwaZulu-Natal, South Africa. This paper presents preliminary results from the KwaZulu-Natal E. grandis experimental study. [C987]

#### "An a-contrario approach for unsupervised change detection in radar images"

This paper presents a new approach for unsupervised change detection in pairs of Synthetic Aperture Radar (SAR) images. As changes to detect can have various sizes and intensities which are a priori unknown in most applications, we propose a multiscale approach without considering any a priori information. Using multiscale series of a cumulant-based Kullback-Leibler divergence (CKLD) measure computed between two dates, changes are characterized as areas where the CKLD values vary a lot when the scale varies. In a probabilistic a-contrario framework, a measure of meaningfulness of such an evolution through scale is derived, leading to a criterion free of parameter. Results are presented using a pair of SAR images acquired before and after the volcanic eruption of the Nyiragongo in January 2002 (Congo), showing the robustness of the method with respect to the number of false alarms. [C988]

#### "An approach to SAR tomography with limited number of tracks"

In SAR tomography, the available information in the height direction is limited by the number of different tracks that can be acquired in practice. To counterbalance this limitation, electromagnetic scattering models, properly exploiting the available a priori information, should be used, the  $\Gamma$ ,  $B$  few  $\Gamma$ ,  $B$  possible acquisitions should be accurately selected, and processing algorithms, guaranteeing the reliability of the results, should be employed. We present an approach for the reconstruction of the vertical reflectivity distribution of vegetated areas facing the above three points. In particular, an eigenvalue optimization procedure is exploited to design an  $\Gamma$ ,  $B$  optimal  $\Gamma$ ,  $B$  constellation to be flown, the peculiar features of ground and canopy are accounted for and an effective global optimization algorithm is used to enhance the reliability. The approach is tested with both simulated and real data acquired by the E-SAR system of DLR over the Dornstetten forest test-site. [C989]

#### "Estimation and correction of ionospheric induced phase errors in SAR images using Coherent Scatterers"

Coherent Scatterers (CSs) are usually detected in SAR data using spectral correlation techniques, by evaluating multilook images in the range direction. The first part of the paper demonstrates an alternative way to detect CSs by exploiting their inherent strong phase stability along frequency. The main advantage of the technique is the absence of a spatial average (necessary in the original procedure), which avoids loss of resolution. The second part of this work illustrates the use of CSs for the estimation and correction of phase errors along the synthetic aperture. Such source of errors may be originated by different effects as platform motion and atmospheric or ionospheric disturbances. For the correction of one and two-dimensional phase errors addressed here, a CSs based autofocus procedure was implemented and applied to simulated and real data. [C990]

#### "DEM production utilizing stereo technology of TerraSAR-X data"

This paper describes the generation of digital elevation models (DEMs) with stereo technologies. We developed this method, and applied it to high-resolution TerraSAR-X data. The generated DEM was evaluated quantitatively using airborne DEM. It showed that the vertical accuracy was dependant on the land cover, and almost satisfied the objective specification in flat area. [C991]

#### "A polarimetric vegetation model to retrieve particle and orientation distribution characteristics"

A simple vegetation model for polarimetric covariance and coherency matrix elements is presented. The model aims to represent vegetation characteristics which are observable by radar polarimetry, including the average particle scattering anisotropy, the main orientation of the volume, the degree of orientation randomness in the volume, and the terrain slopes. The goal of this approach is to quantify these parameters and to enable their estimation in a remote sensing parameter inversion framework. The retrieval of parameters related to effective particle shapes in the polarization plane and the orientation distribution characteristics is evaluated on real SAR data acquired by DLR's E-SAR system at L-band. [C992]

#### "Neural network algorithm and backscattering model for biomass estimation of wetland vegetation in Poyang Lake area using Envisat ASAR data"

Poyang Lake is the largest freshwater lake in China with an area of about 3000 km<sup>2</sup>. Its wetland ecosystem has a significant impact on China's environment change. In this paper, we discuss the neural network algorithms (NNA) to retrieve wetland vegetation biomass using the alternating polarization Envisat ASAR data. Two field measurements were carried out coincident with the satellite overpasses at this area through the hydrological

cycle from April and November. Training data of the neural network are generated by the Michigan Microwave Canopy Scattering (MIMICS) model which is often used for the tree canopy. We modified the model to make it applicable to herbaceous wetland ecosystems. The model input parameters are defined according to the wetland circumstance. NNA retrieval results are validated with ground measured data. The inversion results show the NNA combined with MIMICS model is capable of performing the retrieval with good accuracy. Finally, the trained neural network is used to estimate the overall biomass of Poyang Lake wetland vegetation. [C993]

### "Comparison of L- and P-band biomass retrievals based on backscatter from the BioSAR campaign"

With the continued threat of global warming, the need to obtain consistent and accurate measurements of the carbon stored in forests is strong. L- and P-band SAR backscatter data have shown to be sensitive to forest biomass, which in turn is coupled to the stored carbon. In this paper a biomass retrieval method is developed for L- and P-band using data from the BioSAR campaign conducted in Sweden during the spring 2007 over hemi-boreal forest. The results show that the use of L-band data gives an underestimation of biomass for stands with high biomass; while for P-band no such underestimation is seen. RMSEs are found to be 30-40% of the mean biomass for L-band and about 25% for P-band for stands with biomass ranging from 10 to 290 tons/ha. [C994]

### "Tropical forest biomass recovery using GeoSAR observations"

Tropical forests host some 40% of the world's above-ground vegetation biomass. Tropical forest biomass estimation from remote sensing is a key issue for REDD and carbon market credit allocation and monitoring. At present there is no consensus on the appropriate remote sensing technologies for tropical forest areas. Cloud cover in the tropics and biomass saturation suggest that a combination of low-frequency SAR and interferometry (either PolInSAR or dual-band interferometric SAR DBInSAR) can provide a solution. The airborne GeoSAR collects X-band and P-band InSAR data simultaneously, at a rate of 288 sq km / minute, and is used for wide-area mapping. Tropical forest biomass recovery using X-P DBInSAR and P-band backscattering cross section has been demonstrated from an airborne platform. The technique is applied to GeoSAR data of tropical forests. We show that GeoSAR X-P interferometric data alone may be used to recover tropical forest biomass, removing ambiguity associated with variation in ground conditions. The effects of terrain slope on biomass recovery are discussed. Airborne observation would yield only a "snapshot" of biomass and carbon stocks. We suggest that a combination of GeoSAR observation with PALSAR data for forest/non-forest classification, plus natural sequestration modelling, should provide an accurate measure of tropical forest biomass temporal variation at high-spatial resolution. [C995]

### "Study on the influence of drought to crop growth based on SAR remote sensing"

This paper aims to get the relationship between drought and crop growth. By investigating synthetic aperture radar (SAR) backscattering coefficients, HH- and VV- polarization were found different due to influence from canopy, because of strong attenuation of the VV- polarization by the vertically oriented wheat stems. In small incidence angle, HH is sensitive to soil moisture, while VV is more sensitive to canopy. Two classes of crop with low and high soil moisture are investigated by Г,Віwater-cloudГ,Ві model with vegetation descriptor vegetation water mass (VWM). Parameters of the model show that in drought the crop growth will be worse. This research presents that it is possible to study the influence of drought to wheat growth with small incidence angle of C-band SAR. [C996]

### "A combination of particle filter, matrix pencil and region growing techniques for phase unwrapping in SAR interferometry"

This work presents an improved InSAR phase unwrapping (PU) method based on a combination of a particle filter, a region growing technique and a matrix pencil based local slope estimator. The better performance of this new solution when compared against some representative traditional methods and the previous particle filter PU approaches is justified and illustrated with results obtained from synthetic and real data. [C997]

### "Enhancing complex interferograms by anisotropic diffusion"

In this paper a new algorithm for interferometric phase restoration is presented. Firstly, a continuous framework for anisotropic phase diffusion is stated. A tensorial based metric allows directional control. The periodic continuous structure of the phase representation is accounted for. Secondly, this framework is adapted for interferometric phase filtering. Progressive re-estimation of directionality avoids directional bias. Isotropy and anisotropy are adaptively combined with a constant overall diffusion rhythm, so that the degree of regularization is the same regardless of the underlying topography. Robust estimation minimizes the spread of outliers. Results

on both synthetic and TerraSAR-X data are provided. [C998]

#### "Simulation of dual-channel SAR-GMTI for velocity estimation and compensation"

The velocity and acceleration of the ground moving target can cause the target position to be displaced and defocused in the SAR image. In this paper, the displacement compensation scheme is presented to correct the displaced position and defocused moving target image in the DPCA based SAR-GMTI system. The influence of the ground moving target due to the velocity and acceleration is analyzed in range and azimuth directions, and its compensation method is presented with the simulation results. The performance of the proposed method is compared with respect to the estimated velocity and defocused quantity in both range and azimuth directions. [C999]

#### "Morphological operators applied to X-band SAR for urban land use classification"

This study provides an assessment of the potential for using contextual information with TerraSAR-X backscattering images in classifying urban land-use. Due to the lack of multi-frequency data, a contextual analysis was carried out to extract geometrical information of objects/classes within the images. Anisotropic morphological filters were applied to the backscattering image using a multi-scale approach. A range of different spatial domains were investigated by neural network pruning. The final map of land-use composed of seven different classes of interest was obtained using a Multi-Layer Perceptron neural network with an accuracy of 0.91 in terms of K-coefficient. [C1000]

#### "Ship detection and recognition in high-resolution satellite images"

Nowadays, the availability of high-resolution images taken from satellites, like Quickbird, Orbview, and others, offers the remote sensing community the possibility of monitoring and surveying vast areas of the Earth for different purposes, e.g. monitoring forest regions for ecological reasons. A particular application is the use of satellite images to survey the bottom of the seas around the Iberian peninsula which is flooded with innumerable treasures that are being plundered by specialized ships. In this paper we present a GIS-based application aimed to catalog areas of the sea with archeological interest and to monitor the risk of plundering of ships that stay within such areas during a suspicious period of time. [C1001]

#### "Detection and radiation area estimation of anomalous environmental electromagnetic wave related to earthquake precursor"

Anomalous radiation of environmental electromagnetic (EM) wave is reported as a portent of earthquake. We are observing environmental electromagnetic waves in ELF band all over Japan. Our goal is to predict earthquakes by detecting anomalous EM radiation. We have proposed various detection methods of anomalous radiation. However, the earthquake prediction requires the estimate of EM radiation area in addition to the detection of anomalous radiation. If the EM radiation area can be estimated, we can obtain information about the occurrence area of possible future earthquake. In this paper, we propose the method of detection and area estimation in the anomalous EM radiation by using cross-correlation in magnetic field azimuth. We apply the proposed method to the observed signals before the large earthquake that occurred in the past, and we detect an anomalous radiation and estimated the EM radiation area. [C1002]

#### "A revised radiometric normalisation standard for SAR"

Improved geometric accuracy in SAR sensors implies that more complex models of the Earth may be used not only to geometrically rectify imagery, but also to more robustly calibrate their radiometry. Current beta, sigma, and gamma nought SAR radiometry conventions all assume a simple flat as Kansas flat Earth ellipsoid model. We complement these simple models with improved radiometric calibration that accounts for local terrain variations. In the era of ERS-1 and RADARSAT-1, image geolocation accuracy was in the order of multiple samples, and tiepoint-free establishment of the relationship between radar and map geometries was not possible. Newer sensors such as ASAR, PALSAR, and TerraSAR-X all support accurate geolocation based on product annotations alone. We show that high geolocation accuracy, combined with availability of high-resolution accurate elevation models, enables a more robust radiometric calibration standard for modern SAR sensors that is based on gamma nought normalised using an Earth terrain-model. [C1003]

#### "Effect of linear array elements spacing on angle imaging performance of downward-looking 3D-SAR"

This paper presented the 3D-SAR with linear array antennas (LAA) which could, in contrast to conventional single-channel 2D-SAR, create the real 3D resolution cells to avoid geometric distortions. Except for

conventional side-looking mode, 3D-SAR with LAA can be operated in downward-looking mode which can avoid shadowing effects. The relation between the LAA elements spacing and the elevation angular ambiguity is derived, and the maximal distance between individual antenna elements allowed to avoid elevation angular ambiguity is deduced in this paper. The demonstration of the feasibility of the 3D-SAR with LAA and the relation between elements spacing and elevation angular ambiguity are analyzed by simulation in the last part of this paper. [C1004]

#### **"Research on the relationship between satellite attitude stability and interferometric performance"**

Attitude stability is a very important design parameter to synthetic aperture radar (SAR) satellite platform. The mathematical expression of distributed satellite SAR system impulse response function with attitude jitter is studied using paired echo theory. The effect of attitude stability on interferometric performance is confirmed according to the change of peak sidelobe ratio (PSLR) and integrated sidelobe ratio (ISLR). The constraint relationship is given between three-axis attitude jitter and interferometric performance. Through computer simulation, the relationship curve is obtained to verify the conclusion. The study in this paper provides an important theoretical basis for the integrated design of distributed satellite SAR system. [C1005]

#### **"Interferometric SAR calibration with area calibration site of same height"**

Aimed at the interferometric calibration problem for the Dual-antenna Airborne InSAR, Considering Ground Control Points (GCPs) are limited, calibration site of area with same height such as flat terrain is advanced. A scheme of establishing parameters bias and building Digital Elevation Model (DEM) is designed. Some airborne InSAR data, derived by Institute Of Electronics, Chinese Academy Of Sciences (IECAS), were used to do calibration experiments with the proposed processor. Their results demonstrated it is efficient. [C1006]

#### **"Large scale land subsidence monitoring with a reduced set of SAR images"**

In this work we presented the first experimental results of land subsidence mapping for large areas by using Coherent Point Target SAR interferometry with a reduced set of images in the North China Plain (NCP). Since the limitations of the classical Permanent Scatterer InSAR (PSI) for short temporal span surface deformation monitoring due to the dependency on large volumes data availability, we combine the classical PS InSAR and Small Baseline Subset (SBAS) technique in the data processing chain for large coverage InSAR data processing with a reduced set images. The starting point of our study is the generation of small baseline interferograms of the continuous frames in the same track. Following that, each stack of interferograms are processed with CPT InSAR so as to minimize the effect of phase ramp caused by inaccuracy baseline estimation. For large scale land subsidence mapping, all the mean velocity map are merged into a long strip and the subsidence rate of each coherent point are retrieved. The algorithm are tested with 15 ENVISAT ASAR images collected during the period from Jun, 2007 to Nov, 2008 with an extent of 100 ГfB— 400 km<sup>2</sup> in the NCP for land subsidence mapping. The presented results indicates the large scale land subsidence in central NCP and demonstrates the effectiveness the approach. [C1007]

#### **"Motion measurement errors analysis for the "one-active" LASAR"**

The influences of the motion measurement errors (MMEs) to the 3D SAR imaging are analyzed based on the "one-active" LASAR system in this paper. Firstly, the principle and the spatial ambiguity function (AF) of the "one-active" LASAR are introduced. Then the 3D MMEs are introduced according to three forms: the 3D velocity errors and the 3D acceleration errors, the sine vibration errors and the array vibration errors. The 3D SAR system's maximum allowable MMEs are obtained and the influences of the 3D MMEs to the 3D AF are analyzed by the numerical simulation. Finally, the ground experiments and its results are presented, which validate the feasibility of the "one-active" LASAR. [C1008]

#### **"Hyperimage concept: Multidimensional Time-Frequency Analysis applied to SAR imaging"**

This paper deals with the analysis of non-stationary scatterers in SAR images. Indeed, SAR imaging makes the assumptions that the scatterers are isotropic and white in the emitted frequency band. However, new SAR applications use a large bandwidth and a strong angular excursion. These assumptions become obsolete and the behavior of scatterers becomes non-stationary. The basic tool to study non-stationary signals is the time-frequency analysis. Recent studies based on multidimensional Time-Frequency Analysis describing the angular and frequency behavior of scatterers has highlighted anisotropic and dispersive behavior of bright points. This paper generalizes the hyperimage concept to study scatterers. Multidimensional Time-Frequency distributions are tested on simulations, then they are applied to very high resolution SAR images and show some scatterers are anisotropic and dispersive. [C1009]

### "A pattern recognition system for extracting buried object characteristics in GPR images"

In this work, we present a pattern recognition system for the automatic analysis of ground penetrating radar (GPR) images. This system comprises pre-processing, segmentation, object detection, object material recognition, and object dimension estimation stages. Object detection is done using an unsupervised strategy based on genetic algorithms (GA) which allows to localize linear/hyperbolic patterns in GPR images. Object material recognition is approached as a classification issue, which is solved by means of a support vector machine (SVM) classifier. Dimension estimation is formulated within a Gaussian process (GP) regression approach. Results on synthetic images, representing random exploration scenarios, are reported and discussed.

[C1010]

### "Supervised classification by neural networks using polarimetric time-frequency signatures"

In radar imaging, the assumption is made that scatterers are white in the emitted frequency band and isotropic for all direction of observation. Nevertheless, new capacities in radar imaging, using a wideband and a large angular excursion, make these hypotheses not valid. Time-frequency analysis highlight this point of view and show some scatterers are anisotropic and/or dispersive. This information source can be completed by radar polarimetry. This paper suggests a supervised classification of scatterers using neural networks based on polarimetric time-frequency signatures. This method is applied here on anechoic chamber data, however can be generalized to SAR or circular SAR imaging. [C1011]

### "Analysis of the effect of crown structure changes on backscattering coefficient using modeling and SAR data"

Stand level forest canopy structure such as the size, density, and distribution of the branches and leaves may have a strong effect on radar backscatter. In this study, several broad-leaf (birch) stands and needle stands (larch) with different growing stages and different canopy structures are established using parametric and stochastic L-system. Stands with 10, 30, 50 years and with 10, 40, 100 years, which correspond to young, mid-age and mature birch and larch stands respectively, are simulated according to field measurements. To stands with the same age, the above ground biomass is almost the same. Then different 3D birch and larch crown architectures faithful to the real stand are generated using L-system, which provide realistic and detailed canopy biometric data for radar model. The radar model used here is an improved 3D forest radar backscatter model based on Radiative Transfer Theory, which considers tree crown distribution and multiple scattering from canopy during backscattering calculation. In this paper, total 60 stands with 30ГrB—30m area, namely three stand ages, ten canopy structures and two species, are simulated and analyzed at C-, L-band with different polarizations. Simulation results show that the backscatter coefficient is sensitive to the canopy structure, particularly at C-band and L-band HV polarization. The discrepancy between birch and larch stands with the same tree age is distinct. The crown structure effect to the C-band is more obvious than L-band because of its short wavelength. Then the simulation results of L-HH, C-HH and C-HV polarizations are compared with JERS-1, ASAR data of Changqing forest farm located at DaXinAnLing, northeast of China, which shows good correspondence. [C1012]

### "Urban areas characterization from polarimetric SAR images using Hidden Markov Model"

Scatterers in synthetic aperture radar (SAR) images exhibit high dependence on scatterer-sensor orientations. This phenomenon is prevalent in urban areas. This paper applies hidden Markov model (HMM) to characterize the dependence and model the variations with respect to orientation. Buildings in high resolution SAR images of urban areas are studied. Buildings regions are divided into several discrete classes according to their orientation angles. We model the variations of scatterers characteristics throughout the subapertures using HMM. Subapertures are generated using wavelet packet decomposition. The experimental results show that HMM is efficient in building detection and orientation angle identification. HMMs trained using different feature sets are investigated. The evolution of scatterer states in subapertures are obtained from the HMM inference. [C1013]

### "Bayesian building extraction from high resolution polarimetric SAR data"

Building extraction from high resolution Synthetic Aperture Radar (SAR) images can benefit from modelling the interaction of several elements in urban scene. This paper proposes a Bayesian approach to exploit the interplay. The appearances of buildings in SAR images are dependent on their orientation angles. We estimate the orientation angles of buildings by supervised learning. The knowledge of other object classes could contribute to the building detection. We extract surface evidence of major object classes. The integration of angle estimation, building detection and surface classes provides promising results. [C1014]

### "Speckle reduction of SAR images using sure-based adaptive Sigmoid thresholding in the wavelet

### domain"

Synthetic aperture radar (SAR) images are corrupted by speckle noise due to random interference of electromagnetic waves. The speckle degrades the quality of the images and makes interpretation, analysis and classification of SAR images harder. Therefore, some speckle reduction is necessary prior to the processing of SAR images. The speckle noise can be modeled as multiplicative i.i.d. Rayleigh noise. Sveinsson and Benediktsson [1996], proposed an adaptive sigmoid thresholding method for SAR images in the wavelet domain. The coefficients thresholding for this method is based on the choice of parameters in the sigmoid thresholding function. They were chosen according to a visual appreciation, i.e., by an ad hoc method. We propose to select these parameters by minimizing an estimate of square error between the clean image and the denoised one. The key point is that we have in our proposal computable, statistically unbiased, MSE estimate-Stein's Unbiased Risk Estimate (SURE)-that depends on the noisy image alone, not on the clean image. We apply the proposed method on an SAR images, both simulated and real data. [C1015]

### "A preliminary study of target contour extraction based on scattering mechanism using polarimetric SAR images"

Finding the target contour information from a remote sensing image is one of the fundamental steps for image analysis. Conventional target contour extraction methods are usually based on the statistics information of the image. In this paper, using the maximum return value of the normalized scattering matrix derived from full-polarized Synthetic Aperture Radar (PolSAR), the relationship between the contour of targets and their corresponding dominate scattering type is preliminary researched. Then a novel target contour information extraction method based on the physical scattering mechanism of terrain targets is proposed, which is more effective and adaptable due to the scattering mechanism of terrain targets do not depend on the radar backscattering intensity, but its proportion among different polarizations. After applying to E-SAR airborne data, the results show that this method has a good capability to extract the target contour information. [C1016]

### "Oil slick spot detection using K-distribution model of the sea background"

A new method is proposed to get the segmentation threshold and detect the dark spot in oil-spill images. The method is inspired from the  $\Gamma, \text{Bi}$ -distribution model of sea background, which is widely accepted to describe the ocean clutter. By comparing the histograms of oil-spill region and the sea background, it is found that the oil slicks break the  $\Gamma, \text{Bi}$ -distribution model, but there is still some information unchanged-the relative probability ratios among the pixel values in 95%~99% CDF extent, which is used to deduce the original  $\Gamma, \text{Bi}$ -distribution model. Finally, the intersection of the original histogram of the oil spill image and the deduced sea background PDF is selected to be the threshold. Experiment in RADARSAT-2 image shows the effectiveness of the method. [C1017]

### "Resolution enhancement of SAR image using a multiframe super resolution technique"

This paper proposes a SAR image resolution enhancement method employing a multiframe super resolution technique. The super resolution process providing high robustness by local iterative operations is adopted in consideration with orbit deviations of a satellite and temporal changes. At first, offset functions between SAR images are estimated by co-registration with sub-pixel order. An initial high resolution image is simply produced by enlarging a master SAR image. The high resolution image is iteratively modified while the total error between simulated and original SAR images is larger than tolerance. Processing results of the resolution enhancement using ALOS PALSAR images are shown. [C1018]

### "An accuracy assessment of ML texture tracking algorithm over multitemporal SAR images"

In this paper, the accuracy assessment of the recently proposed Maximum Likelihood (ML) texture tracking algorithm is discussed. Its comparison with the well known texture tracking technique, i.e., Normalized Incoherent Cross Correlation (NICC), has also been investigated in the case of the presence of multiplicative noise structure. [C1019]

### "Speckle reduction of TerraSAR-X imagery using TV segmentation"

The nonsubsampled contourlet transform (NSCT) is a new image representation approach that has sparser representation at both spatial and directional resolution and thus captures smooth contours in images. On the other hand, wavelet transform has sparser representation of homogeneous areas. In this paper, we are going to use the three combinations of undecimated wavelet and nonsubsampled contourlet transforms that was used in for denoising of TerraSAR-X images. Two of the methods use the undecimated wavelet transform to de-noise homogeneous areas and the nonsubsampled contourlet transform to denoise areas with edges. The

segmentation between homogeneous areas and areas with edges is done by using total variation segmentation. The third method is a linear averaging of the two denoising methods. A thresholding in the wavelet and contourlet domain is done by non-linear functions which are adapted for each selected subband. The non-linear functions are based on sigmoid functions. Simulation results suggested that these denoising schemes achieve good and clean images. [C1020]

#### "A study on GPP inversion of different ecosystems by remote sensing and impact factors comparison"

Light use efficiency model is one of the method to retrieval regional scale Gross Prime Productivity (GPP). Absorbed Photosynthetic Active Radiation (APAR) and Light use efficiency are the main parameters of this kind of model. At the same time, light use efficiency is affected by air temperature and precipitation. In this article, one of the Light use efficiency model is used to retrieval daily GPP of the Chinese five typical ecosystem experimental station in 2003. The inversion results are compared with MOIDS NPP product and station measurement data. Based on the different air temperature and precipitation condition of the different station, it also analyses the sensitivity of parameters. [C1021]

#### "Level 1 algorithm development of spaceborne dual-frequency precipitation radar (DPR) for GPM"

Global Precipitation Measurement (GPM) started as an international mission and follow-on mission of the TRMM project to obtain more accurate and frequent observations of precipitation. The accurate measurement of precipitation will be achieved by the Dual-frequency Precipitation Radar (DPR) installed on the GPM core satellite. DPR consists of two radars, which are Ku-band (13.6 GHz) precipitation radar (KuPR) and Ka-band (35.5 GHz) radar (KaPR). Level 1 algorithm, which calculates engineering values, for processing the products of each KuPR and KaPR will be developed based on the PR level 1 algorithm. Japan Aerospace Exploration Agency (JAXA) is developing level 1 algorithm. Housekeeping (HK) and science telemetry data of the DPR is basically similar to that of PR except for pulse repetition frequency (PRF) and noise sampling. DPR will use variable PRF (VPRF) technique to obtain higher sensitivity under the limited resources on the spacecraft. Sampling methods of noise for each angle are different between PR and DPR. The information of VPRF table and noise sampling will be added to level 1 products of KuPR and KaPR. KaPR sampling simulation experiment using TRMM PR was carried out for half-day on 15 March 2007 to get the same geometry data of KaPR scanning in order to create synthetic data of level 1 products for development of higher-level algorithms of DPR and examine to make the best use of them in the critical design, operation and algorithm development for DPR. It successfully finished and we could get the simulation data with same geometry of KaPR scanning. [C1022]

#### "A long-term trend observed in TRMM/PR monthly rainfall products and an evaluation of sampling error by a bootstrap method"

This study examines the trend in the 7-year monthly rainfall amounts (September 2001-August 2008) observed by the TRMM Precipitation Radar (PR). It is shown that the monthly rainfall amounts averaged in the range of 35°S to 35°N (PR observation range) tend to increase slightly over this period. This tendency can be considered to be affected by sampling errors due to the narrow observation swaths of the PR, in addition to natural variations. Therefore, this study developed the method of evaluating the sampling errors by a bootstrap method using the actual data observed by the PR. We examined the trend in the averaged rainfall amounts during 7 years considering the simulated sampling errors. As a result, the positive trend was significantly detected, even when sampling error was removed. From this, it can be concluded that this positive trend is highly likely to be due to natural variations. [C1023]

#### "Observation of mesoscale eddies by using SAR data complemented with optical remote sensing and in situ measurements"

Mesoscale eddies were observed in the Baltic Sea using optical remote sensing, SAR imagery and high resolution in situ measurement from an autonomous system on a passenger ferry. Comparison between SAR data and in situ measurements was carried out to analyze the manifestation of sea surface temperature differences and biological surface slicks on SAR imagery. Correlation between radar backscatter and biological parameters (chlorophyll a and turbidity) was observed. Locations of upwelling related cold eddies and low temperature areas were clearly detectable on radar imagery as well. Therefore, SAR data complemented with in situ measurements enables to observe the evolution of mesoscale eddies in case there is no optical remote sensing data available (i.e. under cloud cover). [C1024]

#### "Electromagnetic wave scattering from ocean surface at low grazing angles"

Bragg scattering is widely recognized as the dominant mechanism at moderate incident angles, by which the ocean surface backscatters microwave radiation. In this paper we have shown that the validity domain of the Bragg/composite surface theory can be extended to low grazing angles by taking into account the contribution of second order scattering effects into the first order at small scale. An improved two scale model (TSM) has been investigated at low grazing angles for (radar frequencies) L-, C- and Ku-band with wind speeds of 7 m/s and 15 m/s. It is observed that for higher wind speeds the intensity of  $\Gamma_{\text{HH}}$  increases up to 8 dB. In backscattering configuration predictions of the model are compared with the experimental data at Ku-band. Comparison shows good agreement at higher wind speeds. Finally, we use the improved TSM to predict the sea scattering in bistatic configuration and compare the results with classical TSM. [C1025]

#### "Improving rainfall estimation from ground based radar measurements using neural networks"

Neural network is a nonparametric method to represent the relationship between radar measurements and rainfall rate. The performance of neural network based rainfall estimation is subject to many factors such as the representativeness and sufficiency of the training dataset, the generalization capability of the network to new data, seasonal changes, and regional changes. Improving the performance of the neural network in real time context is of great interest. In this paper, the goal is to improve rainfall estimation based on Radial Basis Function (RBF) neural networks. The principal components analysis (PCA) technique is used to reduce the dimensionality of the training dataset. Reducing the dimensionality of the input training data will reduce the training time as well as reduce the network complexity. More importantly, the small scale uncertainty will be removed during PCA such that the network is less likely overfitted. In addition,  $\Gamma_{\text{Rain/No Rain}}$  detection is performed using an adaptive neural network running simultaneously with the rainfall estimation neural network. The  $\Gamma_{\text{Rain/No Rain}}$  detection can eliminate those  $\Gamma_{\text{No Rain}}$  data inputs from the training set. [C1026]

#### "Combined Ku and Ka band observations of precipitation and retrievals for GPM Ground validation"

The dual-frequency precipitation radar (DPR) aboard the GPM (Global Precipitation Measurement) core satellite is expected to improve our knowledge of precipitation processes. Ground validation is an integral part of all satellite precipitation missions which helps provide insight into the physical basis of the retrieval algorithm. A dual-frequency (Ku and Ka band) and dual-polarization ground radar will be built in near future to perform cross validation with GPM. This paper presents a new algorithm to retrieve parameters of the drop size distribution from this dual-frequency and dual-polarization ground. The method is based on combination of DFR (dual frequency ratio) and dual-polarization approach. Attenuation correction is solved within the retrieval process. The proposed algorithm is evaluated based on simulated Ku and Ka band realistic observations, for rain, melting layer and ice parts. [C1027]

#### "Mapping and monitoring urban growth on wetlands in humid tropical context using earth observation technology: Case study of Mangrove zones around Douala in Cameroon"

Douala, the economic capital of Cameroon, is the hub of the Country in terms of Commercial, industrial, transport, fishing, agricultural, craft activities and the tourism industry. As typical of most tropical metropolis, Douala with 1.5 million inhabitants has a rapid annual population growth rate of more than 5 per cent. The spatial expansion of Douala has been greatly deterred and handicapped by its peninsular environment made up principally of a plane topography that is surrounded by the Atlantic Ocean, River Wouri and a Mangrove ecosystem. This Mangrove occupies a surface area of 2700 Km<sup>2</sup> along the Fringes of Littoral Cameroon, and typical of brackish humid environments. The main objective of this work was to show how the advance radar processing technique can enable important information to be extracted to characterize mangroves found in the west and south of Douala. This all-weather capability of radar waves is one of the main advantages of imaging radars compared to optical sensors. The Interferometric Land-Use (ILU) technique is useful for quickly assessing of the suitability of an interferometric pair for discrimination between different land use types around the Douala city. [C1028]

#### "A high speed microwave interferometer used for monitoring Stromboli volcano"

This work reports on the results obtained with a high speed ground based radar interferometer applied to the monitoring of the explosive activity of Stromboli volcano, Italy. The sensor illuminated a few craters below the summit distinguishing among them according to their distances from the sensor. The sampling rate allowed tracking the craters' movements even while they were erupting providing information about both the area affected from the deformation and its extent. Radar data were compared with seismic signals from the permanent monitoring network. The comparison demonstrated that the radar interferometer is a powerful device for retrieving ground deformation before and after an explosive event. In particular, eruptions were clearly

identified from the observation of peculiar characteristics of the amplitude, phase and coherence data. [C1029]

### "ERS-ENVISAT Tandem cross-interferometry coherence estimation"

ERS-ENVISAT cross-interferometry is a unique tool for a number of applications since it combines a short repeat-pass interval (28 minutes) with a long perpendicular baseline (2 km). Temporal decorrelation effects are limited and the sensitivity to topographic features is strongly enhanced. In this contribution the focus is on problems encountered during the coherence estimation in ERS-ENVISAT cross-interferometry. Because of the ERS-2 Doppler Centroid variations the azimuth common band available is often only a relatively small fraction of the PRF. Similarly, in the case of not ideal baselines, the common range bandwidth is often much smaller than the chirp bandwidth. Furthermore, high phase gradients in the cross-interferograms can significantly affect the coherence estimates. In our contribution we propose methodologies to reduce these problems in the coherence estimation. [C1030]

### "Monitoring of *Enteromorpha prolifera* in Qingdao marine by exploiting the synergy of active and passive remote sensing data"

In late June 2008, *Enteromorpha prolifera* (E.P) bloomed in Qingdao marine, including Qingdao Olympic Sailing Center. The large scale and the fast extending speed of the E.P bloom were rare in history. The E.P bloomed just before Beijing 2008 Olympics, so it attracted the most attention around the world. Monitoring E.P from remote sensing data has the advantages of rapidness, wide coverage, low cost. But commonly used optical remote sensing is easily affected by cloud, which limits the monitoring timelines. In this paper, the theory of E.P monitoring from optical remote sensing and SAR remote sensing were analyzed. Then, the technical routes of E.P monitoring by exploiting the synergy of active and passive remote sensing data were presented. Because the SAR images are not affected by cloud, the timelines can be increased exploiting the by synergy of active and passive remote sensing data. MODIS and RADARSAT were used to monitor E.P. The monitoring results were used to analyze the beginning and spread of E.P. The monitoring results from MODIS and RADARSAT were compared. [C1031]

### "QA for satellite sea surface temperatures using the ISAR ship-borne radiometric system"

Satellite measurements of global sea surface temperature (SST) distribution are increasingly recognised to have great importance for understanding changes in the world's climate, as well as for operational forecasting of the oceans and atmosphere. If satellite-derived SSTs are to provide the basis of an essential climate variable (ECV) it is necessary to establish methods for independently verifying their quality. Previously the validation of satellite SST products has been performed by comparison with sea temperatures measured by contact thermometers on the hulls of moored or drifting buoys or of ships. Such sensors operate below the sea surface, within the top few metres of the water column, recording what is now referred to as SSTdepth. Infrared radiometers on satellites measure the temperature of the surface skin of the ocean, referred to as SSTskin. However, significant uncertainties are introduced when validation is based on comparisons between SSTdepth and SSTskin because the sea temperature is not uniform across the skin and the upper few metres, especially but not only because of diurnal variability. Such uncertainties can be eliminated by using in situ SSTskin measurements as the basis for a satellite SST validation approach which genuinely compares like with like. This paper describes the principles and results of such a system which has now been in place for five years. It has been used to validate SST measurements from the Advanced Along Track Scanning Radiometer (AATSR) on Envisat. Within the collaborative approach developed by the Group for High Resolution SST (GHRSSST) for merging of complementary data from different satellites, the primary role of AATSR data is to provide a reference for bias adjustment of other data. Precise validation of AATSR measurements is therefore essential for maintaining the quality of other GHRSSST products. [C1032]

### "Remote sensing and geological mapping for a groundwater recharge model in the arid area of Sebt Rbrykine: Doukkala, western Morocco"

Pressure has recently been put on the water resources of Doukkala region (western Morocco) due to the development of agricultural and industrial activities, associated with strong demographic expansion. Doukkala's water resources must be better managed and remote sensing provides effective techniques for such an objective. This research illustrates the use of remote sensing for mapping the regional geology, surface hydrology and hydrogeology of the Sebt Rbrykine, regarded as a groundwater recharge zone for the populated plains of Doukkala. A moderate resolution DEM (30 m pixels) was needed for the hydrological and geomorphological characterization. Derivative products from DEM will also be useful for environmental studies and assessing possible impacts of climate change. Multi-sensor remotely sensed datasets were used to produce several thematic map layers at 1:100 000 scale (lithologies, geological structures, and drainage). These maps

allowed the characterization of the regional aquifers and aquicludes for a better understanding of groundwater circulation. [C1033]

### **"Bounding the number of relevant objects in automotive environment perception systems"**

Multi-sensor data fusion systems for environment perception in the automotive domain are regarded as a promising instrument for obtaining dependable vehicular context information. Sensor data from remote sensing devices like radar or laserscanners is transmitted via intra-car networks to electronic control units (ECU) that enable an intelligent, context sensitive vehicle behavior depending on the current traffic situation. Although new bus systems, such as Flexray, offer increased data rates, the communication resources need to be utilized efficiently. In order to do so, two aspects have to be considered: (1) The size of a single object description and (2) the overall number of perceivable objects. In this paper we focus on the latter of the two aspects. We created a flexible discrete event simulation framework that allows for an in-depth analysis of various aspects of environment perception systems. Our simulation covers scenarios consisting of different sensor-sets, traffic scenarios, fusion benefits, and algorithms for context perception. Using this framework we were able to limit the number of objects a single sensor is allowed to perceive and analyze the impact of this limitation on the overall system performance without such restrictions. Our findings include: (1) Bounding the number of relevant objects to a number between 4-8 does not affect the false negative ratio of the system, (2) the overall error and false positive error ratio does not increase by bounding the number of relevant objects, (3) in safety-relevant environment perception systems the number of relevant objects can be reduced even further without compromising the system integrity, and (4) bounding the number of objects at an early stage of signal processing is superior to a reduction at a late stage of signal processing. [C1034]

### **"General automation test system based on the cooperation of software and hardware"**

In this paper, we use virtual instruments (VI) and commercial off-the-shelf (COTS) technique to construct a portable general automatic test system (ATS). The system's function were realized by using PXI based modular architecture in its automatic test equipment (ATE). While its test program set (TPS) was compiled on the basis of the graphical development platform-LabVIEW8.2. By using powerful data acquisition (DAQ) function and excellent multi-board-synchronization ability of the PXI, the ATS system can satisfy various demands of automatic test perfectly. The system has already been used in the department as vehicle rush repair equipment. This paper also mentions the implementation aspects of a general ATS in the field of the microwave remote sensing radar (MRSR) testing. [C1035]

### **"An automatic registration and mosaicking system based on contour features and wavelet transform for remote sensing images"**

Image registration is an inevitable problem arising in many image-processing applications whenever two or more images of the same scene have to be compared pixel by pixel. The increased volume of satellite images has reinforced the need for automatic image registration methods. In this paper, two new feature-based approaches to automated image-to-image registration are presented. The characteristic of the first approach is that it combines an invariant moment shape descriptor with improved chain-code matching to establish correspondences between the potentially matched regions detected from the two images. This method works well for image pairs in which the contour information is well preserved, such as the optical images from Landsat and Spot satellites. For the registration of the optical images with synthetic aperture radar (SAR) images, we propose another method based on the wavelet transform, this second method uses spectral information of the images and their local wavelet transform modulus maxima to extract a set of control points. The experimental result demonstrates the robustness, efficiency and accuracy of the two algorithms. [C1036]

### **"Classification of convective and stratiform types of rain and their characteristics features at a tropical location"**

The effect of rain attenuation in high frequency signals need proper understanding of the variation of drop size distribution (DSD) separately in convective and stratiform rain due to different characteristics. This paper presents the analysis of variation of vertical rain rate profile for these two types from micro rain radar observations as well as the variation of DSD at ground using disdrometer, of an event observed over Ahmedabad. The bright band signature in vertical rain rate profile is used for rain classification as well as the rain classification based on ground based DSD model is also attempted. The results highlight a rain classification scheme based on lognormal DSD parameter. It is also found that large drops size is more in convective cases associated with high rain rate. It is also observed that for lower rain rates, convective cases have smaller number of bigger drops than stratiform types of rain of same rain intensity. The information will be of importance for classification for rain and rain attenuation study. [C1037]

### "Recent advances in fully polarimetric space-SAR sensor design and its applications"

With the un-abating global population increase our natural resources are stressed as never before, and the global day/night monitoring of the terrestrial covers from the mesosphere to the lithosphere becomes all the more urgent. Microwave radar sensors are ideally suited for space imaging because those are almost weather independent, and microwaves propagate through the atmosphere with little deteriorating effects due to clouds, storms, rain, fog and haze. Globally humidity, haze and cloudiness are increasing at a rather rapid pace, whereas only 20 years ago all of those covered only 48% of the globe, today those have increased to about 62% and within another 20 years may exceed 80% for irreversible reasons; thus optical remote sensing from space especially in the tropical and sub-tropical vegetated belts will become rather ineffective, and microwave remote sensing technology must now be advanced strongly and most rapidly because operationally it is more rapidly available especially for disaster mitigation assistance. [C1038]

### "Vehicular communication and safety in realization of intelligent transport system"

Attempts are made in realization of the trend noticed for smart vehicle in terms of vehicular safety and communication. A Doppler radar is established at the Laboratory and tested on road for vehicular detection. In order to improve the detection performance further and more meaningful, range, classification of vehicles, angle of arrival information are also required to be measured. Additionally communication part is also embedded into the system. The embedded system design is almost finalized. The end to end simulation efforts are going on. Parts of the implementations are also tried. With this kind of challenging efforts, the authors will like to converge two important fields of electronics 'remote sensing' and 'mobile communication' together in intelligent vehicular operation. [C1039]

### "Variational model-based 3d building extraction from remote sensing data"

In this paper, we introduce a variational framework towards automatic 3D building reconstruction from optical and Lidar data. Multiple 3D competing building priors are considered under a recognition-driven way. These models, under a certain hierarchical representation, describe the space of solutions and under a fruitful synergy with an inferential procedure recover the observed scene's geometry. Our formulation allows the cue with the higher spatial resolution to constrain properly the boundaries detection procedure ensuring, in this way, optimal results in terms of accuracy. Such an integrated approach is defined in a variational context, solves segmentation in both spaces, addresses fusion in a natural manner and allows multiple competing priors to determine the pose and 3D geometry from the observed data. Very promising experimental results demonstrate the potentials of our approach. [C1040]

### "Geodesic neighborhoods for piecewise affine interpolation of sparse data"

We propose an interpolation method for sparse data that incorporates the geometric information of a reference image. The idea consists in defining for each sample a geodesic neighborhood and then fit a model (affine for instance) to interpolate at the current point. In the field of remote sensing for urban areas, two widely used techniques are laser range scanning (LIDAR) and stereo photogrammetry. Both techniques have a common drawback, for a variety of reasons the information they provide is sparse or incomplete. But in both cases it is fair to assume that a high resolution image of the scene is available, and we propose in this paper a diffusion algorithm that takes into account the geometry of the image  $u$  to refine the range data. This allows us to interpolate the data set while respecting the edges of  $u$ . The core of the algorithm is a fast method for computing geodesic distances between image points, which has been successfully applied to colorization by Yatziv et al. and supervised segmentation by Bai et al. The geodesic distance is used to find the set of points that are used to interpolate a piecewise affine model in the current sample. This first interpolation result is refined by merging the obtained affine patches using a greedy Mumford-Shah like algorithm. The output is a piecewise affine interpolation of the data set that respects both the given data and the radiometric information provided by  $u$ . [C1041]

### "A polarimetric sea surface backscattering model"

An extended Bragg scattering model, for fully polarimetric SAR data, is here proposed for describing sea surface scattering. Moreover, the model is considered to examine the scattering contributions from sea surface and detected dark areas due to the presence of anthropogenic and biogenic slicks. Experiments are conducted on fully polarimetric C- and L-band SAR data. [C1042]

### "MIMO radar waveform design: a divergence-based approach for sequential and fixed-sample size tests"

A multi-frame, multiple-input, multiple-output radar detection problem is considered here. Different waveform design strategies are inspected for both fixed-sample size and sequential test. The unified treatment of the two cases is a direct consequence of the divergence-based merit function used in the optimization process. It is proved that no strategy is uniformly optimal, and that the diversity order is limited by the available energy budget. [C1043]

### "Classifying urban landscape in aerial LiDAR using 3D shape analysis"

The classification of urban landscape in aerial lidar point clouds is useful in 3D modeling and object recognition applications in urban environments. In this paper, we introduce a multi-category classification system for identifying water, ground, roof, and trees in airborne lidar. The system is organized as a cascade of binary classifiers, each of which performs unsupervised region growing followed by supervised, segment-wise classification. Categories with the most discriminating features, such as water and ground, are identified first and are used as context for identifying more complex categories, such as trees. We use 3D shape analysis and region growing to identify  $\Gamma, \text{B}^i \text{planar} \Gamma, \text{B}^i$  and  $\Gamma, \text{B}^i \text{scatter} \Gamma, \text{B}^i$  regions that likely correspond to ground/roof and trees respectively. We demonstrate results on two urban datasets, the larger of which contains 200 million lidar returns over 7km<sup>2</sup>. We show that our ground, roof, and tree classifiers, when trained on one dataset, perform well on the other dataset. [C1044]

### "Classification of water regions in SAR images using level sets and non-parametric density estimation"

This paper presents a semi-supervised algorithm for the classification of water regions in SAR images. The proposed technique is based on region based level sets and non-parametric estimation of the probability density function (PDF) of the pixel intensities. The level set framework allows automatic topology adaptation and provides the regularization while the PDF's are estimated in each region using Parzen windows. Using non-parametric density estimation gives the method the flexibility to be used with different kinds of SAR data. To illustrate the performance of the proposed algorithm, the method is applied to the problems of river mapping and coastline extraction in real amplitude SAR images. [C1045]

### "High range resolution directional borehole radar for 3-D fracture delineation"

Directional borehole radar was developed for detection of three-dimensional (3-D) target localization in single-hole radar measurement. Phase differences among four dipole elements of receiving circular array uniquely determine an azimuth direction of a reflected wave. Receiving voltages of dipole elements are measured by optical electric field sensors whose high electrical isolation feature enables data acquisition of highly correlated signal between the channels. Besides, a switching unit to control resonant frequency of dipole elements was newly developed to reduce mutual coupling between the dipole elements. Laboratory experiments have demonstrated that approximately 30% frequency bandwidth enlargement is achieved by the switching operation without been affected by the mutual coupling in air. The directional borehole radar system was tested in a field test site in Kamaishi-Mine in Japan. All the boreholes available in this test site is filled with water and past borehole radar surveys conducted in this test site revealed presence of complex fracture system. Cross-hole and single-hole borehole radar measurement were conducted to clarify the performance of the resonant switching control and also to detect 3-D geometrical structure of fractures in this test site. 3-D analysis of data acquired by the directional borehole radar in a single-hole measurement clarified azimuth orientation fractures up to a range distance of 15 m with a range resolution less than 1 m. High reliability of the result was inferred from the fact that individual fracture pattern in a reflection profile showed a consistent color along the depth and also high repeatability of the result was obtained by repeating measurements. [C1046]

### "Adaptive scan-on-receive based on spatial spectral estimation for high-resolution, wide-swath Synthetic Aperture Radar"

Intensive research is currently ongoing in the field of Smart Multi-Aperture Radar Techniques (SMART) for high-resolution wide-swath Synthetic Aperture Radar (SAR) imaging. This work investigates the possibility of applying direction of arrival estimation methods to spaceborne SMART SAR systems, that employ receive beam steering. In particular, a new algorithm based on the actual spatial distribution of the received signal power is proposed. The performance of the algorithm is evaluated by Monte Carlo simulations and compared with that of the conventional scan-on-receive approach, in different operational scenarios. The Cramer Rao Lower Bound is also reported as a benchmark on the performance. [C1047]

### "Focusing Synthetic Aperture Sonar (SAS) data with the Omega-K technique"

Synthetic Aperture Radar (SAR) and Sonar (SAS) systems provide high resolution reflectivity maps of the imaged scene by coherently combining the echoes collected along a virtual array of receivers. A peculiarity of SAS systems is that the echoes are often collected by moving a short real array of hydrophones to avoid range ambiguity. In this paper we present a modification of the standard wavenumber focusing algorithm widely used in SAR data processing to make it suitable for focusing bi-static SAS data. An autofocusing technique is then exploited to estimate and compensate for the deviation of the platform trajectory from the rectilinear one. [C1048]

#### **"Coherent multi-frequency-band resolution enhancement for synthetic aperture radar"**

This paper presents a method whereby the range resolution of multi-frequency-band SAR systems can be enhanced. If multiple signals are coherent and cover disjoint frequency bands, they can be combined into a single signal which can be processed using slightly modified SAR processing algorithms, resulting in an image with a range resolution enhanced by the sum of the constituent bandwidths. [C1049]

#### **"A statistical study of wind field distribution within extra-tropical cyclones in North Pacific ocean from 7-years of QuikSCAT wind data"**

In this paper we used QuikSCAT measurements over extratropical storms that reached hurricane force (HF) wind strength in the North Pacific over a period of 7 cold seasons from 2001-2008 to study the average wind speed distribution within these intense cyclones. During this period a total of 225 cyclones with HF winds were identified and tracked in the North Pacific. December proved to be most active month with 56 separate storms reaching HF strength over the 7 year period. The peak activity was found to be over the western portion of the ocean basin. The Pacific cyclones appear to have preferred tracks and have an average heading of  $\sim 50^\circ$  from north. The average storm motion was found to be  $\sim 24$  knots. Most hurricane force events last between 6-24 hours. 50% of the 12 hour events occurred during December and 75% of the 30 hour events occurred during November and December. [C1050]

#### **"The combined effect of surface rain and wind on scatterometer observations of surface roughness"**

The wind stress on the sea surface is closely related to the sea surface roughness. When rain impacts affect this roughness, we need to learn the consequences for the air-sea momentum exchange. Our data shows that areas of highest winds correlate closely with the heaviest rainfall. Changes in the sea surface radar cross section from the combined effects of wind and rain, on scales of tens of kilometers, are being studied using the QuikSCAT scatterometer and simultaneous NEXRAD three-dimensional measurements of rain within Hurricane Ike. Buoy, NOAA HRD H\*Winds and related data provide the additional wind information. From the remote sensing perspective, these results will show the dependence of the sea surface radar cross section, at Ku-band, as a function of the rainrate, wind speed and relative direction, and polarization. At this microwave frequency the surface backscatter is controlled by the centimeter-scale roughness, but at these high wind speeds the simple models based on Bragg scattering are not useful. In order to study the air-sea interaction that is related to surface fluxes (e.g., momentum, sensible heat, and latent heat) during rain events, extended experimental investigations are needed. Heavy rain in the boundary layer changes the profiles of wind and stratification which alter the surface stress and turbulent heat fluxes. The wind driven rain also creates roughness properties that need to be modeled in order to interpret the Ku-band NRCS at the two polarizations, When high winds also exist ( $>20$  m/s), the interaction is complicated by sea spray. [C1051]

#### **"UAE mapped attenuation at RF frequencies (UAE-MARF)"**

This paper develops both theoretical and experimental models for the prediction of attenuation and reflectivity of satellite signals at Ku-band in the UAE. The theoretical model gives a detailed study on the effect of the attenuation and the reflectivity due to the increase of the frequency or the density of different hydrometers. The experimental model, which is based on actual measurements obtained from NASA, was used to extract the required precipitation radar (PR) products. By applying the image analysis techniques on the PR data for one whole year (2000), a graphical representation of attenuation at Ku-band in the UAE was obtained. Results of this paper are vital for the successful design of satellite TV broadcast systems in the UAE operating at Ku-band. [C1052]

#### **"Modeling and validation of GPR wave scattering with the Semi-Analytic Mode Matching algorithm: Choosing optimal coordinate scattering centers"**

Choosing the coordinate scattering centers (CSCs) for the Semi-Analytic Mode Matching (SAMM) algorithm is a critical and heretofore unexplored aspect of this method, necessary for the ultimate goal of simulating full 3D

scattering. Establishing the locations at which modes originate is essential for accurate modeling of electromagnetic fields with SAMM. Six test scattering objects are investigated, and the CSCs are found for each by considering the radii of curvature at each  $\Gamma_i$  fitting point on the objects' perimeters. Additional CSCs are needed for scattering objects which have long  $\Gamma_i$  flat regions. Excellent results are found comparing SAMM and Finite Difference Frequency Domain (FDFD) for 2D scattering objects several wavelengths in size. [C1053]

### "Radar radome and its design considerations"

Radar plays a significant role in managing air and sea transportation, monitoring a certain areas, surveying, remote sensing, predicting weather, and defense. To protect the Radar against environmental factors, a radome is required. In this paper, we present some design considerations for constructing a Radome. Based on experience in building the ISRA LIPI Radar, the Radome designs are presented. Measurement results on the effects of Radome to the Radar performance are also presented. [C1054]

### "Remote sensing based season calendar for Indian districts using MODIS data"

Seasonal characteristics and crop growth information is of great utility for crop management. The primary occupation in India being agriculture, it is important to devise quick and reliable methods that will help in making decisions affecting agricultural practices at a macro level more efficiently. In this paper, the authors have devised an algorithm to derive a seasonal calendar from the time series data of a moderate resolution satellite, MODIS which is one step short of producing a crop calendar. The method proposed involves filtering time series data using Local Maximum Fitting, finding maximum and minimum points on the time series profile, calculating phenological parameters namely start of season, mid of season, end of season and seasonal amplitude and finally clustering these phenological parameters to obtain a cluster center which is representative of a particular season/cropping practice. The initial results are promising as they are similar to the information available in the form of handouts of the regions under study. A full scale validation involving field visits and comparison with statistical data from government sources will prove the utility of this product. Nevertheless, this work demonstrates the utility of time series MODIS data for obtaining phenological parameters. [C1055]

### "3D SAR focusing for subsurface point targets"

In this work we develop a methodology for imaging subsurface point targets using a single-pass strip-map synthetic aperture radar (SAR). The point targets are embedded in an arbitrary homogeneous half space, and are located at arbitrary depths. It is assumed that the radar frequency is low enough and system sensitivity high enough to allow the required two-way penetration depth to target. The succession of steps required to form the image of the subsurface point targets are described, including the estimation of the subsurface wave velocity, estimation of the depth of the point target, and the modified range and azimuth filters to achieve optimum resolution. The theoretical approach is described and results are presented for a range of point target depths, subsurface velocities, and radar system parameters. It is found that with the assumptions made it is possible to image the point targets in 3D with good range, azimuth, and depth accuracy. [C1056]

### "Innovative and efficient strategy of calibrating Sentinel-1"

In the frame of the GMES program, the main objective of the Sentinel-1 mission is to ensure the continuity of SAR data acquisitions for SAR applications in C-band for global earth monitoring. But in contrast to SAR systems already existing in C-band like ASAR/ENVISAT or RADARSAT-2, high demands on the radiometric accuracy are made. Thus, product quality is of paramount importance and the success or failure of the mission depends essentially on the method of calibrating the entire Sentinel-1 system in an efficient way. This paper describes the strategy and the method of calibrating Sentinel-1. [C1057]

### "A neural network electromagnetic approach for GPR pavement diagnostic: A preliminary study"

In this paper, a preliminary study, based on GPR data analysis by means of artificial neural networks, for automatic pavement diagnostic is addressed. The proposed solving solution models the pavement as a multi-layered medium composed of N parallel homogenous layers, which are separately analyzed through a recursive procedure able to reconstruct their permittivity and thickness. The basic processing module of the whole procedure, is here presented. [C1058]

### "Efficient configurations of SAR sensors for improved range resolution"

In this paper an innovative technique for ground range resolution improvement in Multiple Input Multiple Output (MIMO) SAR systems is presented. The technique allows to achieve a maximum theoretical range resolution improvement factor greater than the number of operating SAR sensors, by exploiting both the monostatic and

the bistatic acquisitions. The effectiveness of the proposed technique is validated over a simulated dataset. [C1059]

### "Analysis of Sentinel-1 mission capabilities"

The Sentinel-1 mission is designed to be a source of continuous and reliable collection of C-band SAR imagery. Requirements for Sentinel-1 end to end system, as part of the complete family of GMES Sentinels, guarantee continuity of C-band SAR data and products availability to operational entities who exploit satellite radar imagery since ERS 1 operations. Typical drivers for current- and future-generation Remote Sensing LEO satellite missions are fast target access capabilities and short on-board data latency in order to speed up the operations of data download and products' delivery to the end-users. On the other hand complete or almost complete Earth surface coverage is also required from the system. Satellite orbit and sensor swath determine the access capability so that the mission timeliness performance can only improve at the cost of increasing the number of satellites (constellation concept). SAR power demand limits the satellite operational duty cycle implying the need for trade-off between frequent acquisition of the same targets and extension of acquisition surface coverage. A balance between fast access/response to (or frequent revisit of) a few regions of interest and maximization of geographical coverage within the satellite orbit repeat cycle is thus needed when none of the above goals prevail as the main mission driver. Sentinel-1 applies a new operational mission concept; SAR acquisitions by Sentinel-1A (and Sentinel-1B when the constellation will be deployed) are designed according to pre-defined operational sequences to ensure: 1. continuous and systematic acquisition of data all along the mission time (to maximize mission return and system exploitation efficiency); 2. a growing archive of ?world-wide extended? data; 3. maximum extension of coverage after any orbit repeat cycle (175 orbits in 12 days); 4. minimum possible revisit time on few selected regions (North Atlantic Maritime Transport zones, Europe and Canada) but also; 5. possibility to include and perform, as an additional mission capability, sporadic data acquisitions coming from asynchronous user orders submitted to the system following for example requests for specific imagery during emergency occurrences. The mission analysis process performed to define in detail the above operational concept is outlined in this paper and results are presented. [C1060]

### "FDBAQ a novel encoding scheme for Sentinel-1"

Modern operational and/or high resolution SAR satellite missions impose stringent requirements on on-board data compression such as a higher data reduction ratio, more flexibility, and faster data throughput. A novel approach is flexible dynamic block adaptive quantization (FDBAQ). This method outperforms currently used block adaptive quantization with respect to Signal-to-Noise-Ratio related to the compression ratio. The FDBAQ method allows bit rate programmability with non-integer rates. This allows the SAR information throughput to be optimized for different types of targets and down-link scenarios using a tradeoff between thermal and quantization noise. [C1061]

### "Sentinel 1: Interferometric applications"

Here we report recent applications that extend the range of feasibility of InSAR: imaging subsurface fluid flow, estimating flow properties such as permeability, and tracking the integrity of water defense structures. [C1062]

### "2-1/2 Dimensional bi-static GPR propagation and scattering modeling of roadways and tunnels with projected 2D FDTD"

Subsurface sensing modalities such as Ground Penetrating Radar (GPR) are increasingly being used to assess the condition of aging civil infrastructure by evaluating deterioration within roadways and bridges, and to monitor the security of national borders by the detection of underground tunnels. The need to address these issues is intensifying and, while valuable data are collected using nondestructive evaluation there is urgency for improved understanding and analysis. Simulation of GPR investigations to search for defects in bridges and the presence of underground tunnels can help to understand and analyze real world data. Three-dimensional simulations consider the full geometry of an area. When the geometry is relatively invariant in the third dimension, 2-1/2D simulations can capture most of the 3D scattering and account for bi-static transmitters and receivers located out of the cross-sectional plane. Additionally, comparison of 3D simulation results to a library of 2D results may help to indicate the angle of GPR travel from the cross-sectional plane. [C1063]

### "Physical limitations on detecting tunnels using Underground Focusing Spotlight Synthetic Aperture Radar"

This work studies the concept of Underground Focusing Spotlight Synthetic Aperture Radar (UF-SL-SAR) systems for tunnel detection applications. A general formulation for generating UF-SL-SAR imaging in realistic,

randomly rough ground is developed by focusing in space and frequency at subsurface points by considering rays refraction at the nominal ground surface. Imaging results are presented for two soil scenarios: dry sand and moist clay loam. It is demonstrated that the tunnel is successfully imaged only for the sand case. [C1064]

### "InSAR monitoring of landslides using RADARSAT"

In this study we used both differential and corner reflector InSAR techniques to monitor landslides at different geological sites in Canada and China. Our results show the differential InSAR maps are necessary and simple first steps in understanding regional landslide motion at these sites. In the case of our Canadian site the corner reflector results compares well with our D InSAR results. [C1065]

### "ASI-Volcanic Risk System (SRV): A pilot project to develop EO data processing modules and products for volcanic activity monitoring, first results"

The ASI-SRV (Sistema Rischio Vulcanico) project is devoted to the development of an integrated system based on EO and Non EO data to respond to specific needs of the Italian Civil Protection Department (DPC). ASI-SRV provides the capability to import many different EO and Non EO data into the system, it maintains a repository where the acquired data have to be stored and generates selected products which will be functional to the different volcanic activity phases. The processing modules for Radar and EO Optical sensors data allow to estimate a number of parameters which include: surface thermal proprieties, gas, aerosol and ash emissions and to characterize the volcanic products in terms of composition and geometry, surface deformations in terms of displacements and velocity. All the generated products are related to Italian actives volcanoes and three test sites have been chosen to demonstrate the capability of this integrated system: Vesuvio, Campi Flegrei (Campania region) and Etna (Sicilia region). In this paper the first results obtained by means of modules developed within the ASI-SRV project and dedicated to the processing of EO historical series are presented. [C1066]

### "The medium resolution soil moisture dataset: Overview of the SHARE ESA DUE TIGER project"

To address the needs of the hydrological community for medium resolution soil moisture dataset an approach developed at the TU WIEN for the coarse resolution ERS/METOP datasets has been transferred to medium resolution SAR data. This work was performed within the ESA Tiger Innovator project SHARE and introduces an operational soil moisture monitoring service for the region of the Southern African Development Community (SADC) and Australia. The data from the ASAR onboard ENVISAT operating in Global Mode (GM) with 1 km spatial resolution were implemented for the dataset generation that provides twice weekly measurements and captures highly variable soil moisture patterns. Several validation and application studies were summarized in this paper that demonstrated the ability of ASAR Global Mode (GM) Soil Moisture for global soil moisture monitoring. The dataset can be accessed via <http://www.ipf.tuwien.ac.at/radar/share/>. [C1067]

### "Sentinel-1 mission overview"

The ESA Sentinels constitute the first series of operational satellites responding to the Earth Observation needs of the EU-ESA Global Monitoring for Environment and Security (GMES) programme. The GMES space component relies on existing and planned space assets as well as on new complementary developments by ESA. This paper describes the Sentinel-1 mission, an imaging synthetic aperture radar (SAR) satellite constellation at C-band. It provides an overview of the mission requirements, its applications and the technical concept for the system. [C1068]

### "Light scattering by thin curved dielectric surface and cylinder"

Light scattering properties from curved surface and cylinder are important in the area of propagation and remote sensing. The radar cross sections (RCS) of a dielectric thin curved surface and cylinder are obtained by employing a quasi-static approximation. The method is applicable to the electromagnetic (EM) scattering in general. However, the simulated results emphasize light scattering, i.e. the RCS displayed rather than the electric field. The results are complemented by numerical calculations. [C1069]

### "Temperature, color and deformation monitoring of volcanic regions in New Zealand"

There are many examples around the world where satellite based remote sensing has been used to successfully monitor different stages of volcanic activity. This paper describes some of the methods used and their results for monitoring two active volcanoes in New Zealand-Mt Ruapehu and Raoul Island. A time series of ASTER night-time thermal images has been successfully used to assess crater lake temperature variability; Hyperion hyperspectral imagery was tested for crater lake color monitoring with inconclusive results; and interferograms

using ALOS PALSAR data were generated of Mt Ruapehu for the purpose of mapping deformation patterns. These data provide information for baseline monitoring, as no major volcanic activity was evidenced over the duration of the study. [C1070]

#### "ACO algorithm processing multisensor data for urban land cover"

A novel ant colony optimization (ACO) algorithm takes inspiration from the coordinated behavior of ant swarms finding the shortest way from their nests and the food source, which has been applied on many research areas for solving optimization problems, but it has seldom been used in remote sensing data processing. ACO algorithm has many potential advantages in remote sensing data processing, such as it does not assume an implicit assumption for processing dataset, it can take into account of contextual information, it has strong robustness, and it can combine different sources of data. This paper represents an application of the combination of Landsat TM data and Envisat ASAR data based on ACO algorithm for land cover classification. The classification results based on ACO algorithm were compared with MLC and C4.5, the experimentation results and analysis indicate that the ACO algorithm can provide a new efficient approach for land cover classification using multi-source of remote sensing data. [C1071]

#### "Automatic 3D building reconstruction from airborne LiDAR measurements"

A framework which includes six major components has been developed to reconstruct 3D building models from airborne LiDAR measurements. The application of the framework to both commercial and adjacent residential areas shows that the proposed methods identified building patches well, and reconstructed 3D building models effectively. The entire process is highly automatic and requires little human aid, which is very useful for processing voluminous LIDAR measurements. [C1072]

#### "InSAR interferogram detail-compensating filtering method based on the stationary wavelet transform"

Speckle is an inherent characteristic of InSAR (Interferometric Synthetic Aperture Radar) interferogram, it affects the accuracy of prediction and evaluation of urban Geology and Geohazards, so it is necessary to carry out interferogram filtering to suppress the effect of speckle. However, there is a contradiction between speckle reduction and keeping the details of the interferogram in current methods of interferogram filtering. Using the difference idea and the character of the wavelet transform, we propose InSAR interferogram detail-compensating filter method based on the stationary wavelet transform. And an experiment is made on the partial interferogram generated by two SAR images of Bam earthquake with this method. As a result, not only can the new method suppress the speckle effectively, but also it can maintain details of interferogram well by compensating the details, and it reduces the number of residual points greatly. [C1073]

#### "Fast InSAR multichannel phase unwrapping for DEM generation"

In this paper, a method to solve the multichannel phase unwrapping problem is presented. MAP approach together with Markov Random Fields have proved to be effective, allowing to restore the uniqueness of the solution without introducing external constraints to regularize the problem. The idea is to develop a fast algorithm to unwrap the interferometric phase in the multichannel configuration, which is, in the main time, able to provide the global optimum solution. To reach this target, an a priori model based on Total Variation is used together with optimization algorithm based on graph-cut technique. The proposed approach has been tested both on simulated and real data. The obtained results show the effectiveness of our approach. [C1074]

#### "Space-borne high resolution SAR tomography: experiments in urban environment using TS-X Data"

Synthetic Aperture Radar (SAR) tomography aims at retrieving the 3-D reflectivity from multi-pass SAR data. It is essentially a spectrum estimation problem. As a consequence, complex values of a specific range cell in a SAR image stack as a function of baseline are closely related to the Fourier transform of the reflectivity function in the elevation direction. The new generation of SAR satellites, like TerraSAR-X, allow for the first time the building up of high-resolution SAR data stacks on a regular basis. TerraSAR-X in its high resolution spotlight mode provides data with 0.6 m slant range resolution. It has already been shown that persistent scatterer interferometry (PSI) benefits enormously from this new quality of data. The data stacks used for PSI in urban areas can also be used to derive tomographic information. This paper presents the first demonstration of space-borne high resolution tomographic reconstruction of multiple scatterers in a resolution cell situation in urban areas. Different spectrum estimation strategies such as the Singular Value Decomposition (SVD) and Nonlinear Least Squares estimation (NLS) are evaluated and compared using both simulated data and TerraSAR-X spotlight data over Las Vegas

with special consideration of the difficulties caused by sparse and irregular samples. The nuisance of ill-conditioning is investigated and regularization tools are utilized to overcome this problem. For validation, the spectrum estimation results with TerraSAR-X data are compared to the plausible ground truth. In a second step of processing model selection criteria such as the Bayesian Information Criterion (BIC), Akaike information criterion (AIC) and Minimum Description Length criterion (MDL) are implemented on the spectral estimates to determine the number of scatterers inside a resolution cell. The probability of correctly detecting the number of scatterers and the accuracy of the corresponding elevation estimates are evaluated from simulated data.- Additionally, model selection results with TerraSAR-X data are analyzed. Finally, SAR tomography, as a straightforward extension to PSL is integrated into DLRs PSI-GENESIS processor to support deformation estimation and solve the ambiguity due to multiple scatterers inside a resolution cell. First processing results using TerraSAR-X data are presented that confirm the capability of space-borne high resolution SAR tomography for resolving multiple targets within the same azimuth-range cell and to map the 3-D scattering properties of the illuminated scene. [C1075]

#### "An object-based two-stage method for a detailed classification of urban landscape components by integrating airborne LiDAR and color infrared image data: A case study of downtown Houston"

By exploiting high resolution airborne LiDAR data along with color infrared aerial photographs, this research aims to quantify the urban landscape components using an object-based two-stage method in the case of downtown Houston, Texas, USA. The urban landscape components will be identified and classified by integrating spectral information from color infrared aerial photograph and surface geometric information from airborne LiDAR data. In first stage, the color near-infrared aerial photographs are used to segment the scene into image objects. Then, these objects are classified into three broad categories-impervious surface, vegetation, and water surface, based on their spectral and two-dimensional spatial attributes. In the second stage, the normalized Digital Surface Model derived from airborne LiDAR data is introduced into analysis. Two indicators, relative height and roughness, of each vegetation object from the first stage are calculated, and the threshold values are determined to separate vegetation into lawns, shrubs/hedges, and trees. Next, a series of image processing steps are applied to the nDSM to further classify the impervious surface objects into skyscrapers, high-rise buildings, ordinary buildings, streets, highways, and open spaces. The overall classification accuracy is evaluated as high as 94.10%, and the Kappa coefficient is 92.91%. This research suggests that the combination of morphological information of LiDAR data and spectral information from image data renders a powerful tool for a detailed investigation of urban landscape structure. [C1076]

#### "Advanced interferometric techniques for monitoring urban areas"

This paper addresses techniques for the imaging and monitoring of urban areas via advanced interferometric analysis. We discuss the multidimensional SAR imaging techniques and an approach for the generation of long term time series from multisensor data. Results of the application to real ERS and Envisat data are presented. [C1077]

#### "Urban dynamic change detection using interferometric SAR in Southeast China"

Synthetic aperture radar is the only instrument that can provide consistent remote sensing data for south China with persistent cloud cover and rain. In this paper, the potential of multi-temporal ERS and ENVISAT-1 SAR data for land cover/land use classification and urban change detection was investigated at a test area in Fuzhou city, the capital of Fujian province in southeastern China. Both SAR backscatter intensity characteristics and interferometric data were analyzed. A parcel-based approach has been implemented to overcome the limitations and weaknesses of traditional image processing methods for feature extraction from gray images. Two methods were carried out in the urban dynamics change detection: one was post-classification comparison, and the other one was multi-temporal image ratioing. The results from both classification and urban change detection were validated by field survey data and showed promising application of ESA SAR data in southeastern China, where clouds and rains persist. [C1078]

#### "SAR interferometry atmospheric mitigation from GPS water vapor retrieval in Hong Kong"

Continuously observed GPS data and meteorological observations spanning rainy summer from May to August and covering entire Hong Kong were processed in this paper. Zenith Total delay (ZTD) and corresponding Precipitable Water Vapor(PWV) were retrieved from above observations and validated by tropospheric product from IGS and Radiosondes observations. Differential two-way Radar Line of Sight (LOS) slant atmospheric phase map was then obtained from GPS PWV through Universal Kriging Prediction and Niell Mapping Function with azimuth asymmetry consideration. In our designed experiment, the acquired Radar atmospheric phase map was used to calibrate the 35-day interval HK ASAR Interferogram and comparatively analyze the feasibility of

such mitigation. Additionally, Coherent Point (CP) targets from Radar Image were extracted to perform deterministic assessment for the improvement of atmospheric mitigation on InSAR from GPS water vapor. The result demonstrated that atmospheric mitigation from GPS PWV could reduce the InSAR residual atmospheric noise under 1 cm for 88% coherent points in HK. The technique would to some extent break through the bottle neck of atmospheric de-correlation in case of small SAR image amount in hazard emergency monitoring in Hong Kong. [C1079]

### "Urban structuring using multisensoral remote sensing data: By the example of the German cities Cologne and Dresden"

The urban landscape is a highly complex and small-structured, heterogeneous area as a result of permanent human settlement. Urban structure is scale-dependant and can be expressed on various levels of detail by satellite imagery. Very high resolution satellite (VHR) sensors are capable of mapping and monitoring cities-on house/block level-with their high degree of landcover diversity. However, detection of morphological features such as shape and elevation of single objects is performed much better when a digital surface model (DSM)-e.g. derived by airborne laserscanning-is incorporated. An object-oriented methodology for the joint analysis of optical satellite data and a digital surface model is presented for the classification of the urban morphology in terms of urban structural types. These are spatial units-mostly on block level-with aggregated information on the classified single features like landcover/landuse and urban fabric. Hence, a hierarchical, modular segmentation and classification workflow is implemented to extract the required information. The methodology is applied on two study areas in the cities of Cologne and Dresden, Germany, and a validation of the capability of the potential for transferability of the rulebase is shown. [C1080]

### "Potential and status of high-resolution remote sensing information applied in urban planning in China"

This paper discussed several facets of remote sensing information applying in urban planning in China. It emphasized the application and development process for high resolution remote sensing information during the last years, including new satellite-borne and airborne high resolution optical and Synthetic Aperture Radar (SAR) remote sensing data sources. And, the corresponding application questions about application history and status, main data processing flow, advantages and questions, the development potential in future and so on were discussed in detail. [C1081]

### "Point cloud segmentation towards urban ground modeling"

This paper presents a new method for segmentation and interpretation of 3D point clouds from mobile LIDAR data. The main contribution of this work is the automatic detection and classification of artifacts located at the ground level. The detection is based on Top-Hat of hole filling algorithm of range images. Then, several features are extracted from the detected connected components (CCs). Afterward, a stepwise forward variable selection by using Wilk's Lambda criterion is performed. Finally, CCs are classified in four categories (lampposts, pedestrians, cars, the others) by using a SVM machine learning method. [C1082]

### "The second-order monostatic HF radar cross section incorporating antenna barge motion"

The second-order HF radar ocean cross section is derived for the case of the transmitting and receiving antenna undergoing platform (i.e. barge) motion. The derivation for electromagnetic patch scatter begins with a general expression for the bistatically received second-order electric field. Based on an assumption that the ocean surface can be described as a Fourier series with coefficients being zero-mean Gaussian random variables, the second-order monostatic radar cross section is developed. The derivation for the hydrodynamic patch scatter follows from an earlier first-order analysis. The second-order HF radar cross section is found to consist of Bessel functions, and no singularity exists in the new electromagnetic coupling coefficient. Simulation results depict the effects of barge motion under a variety of sea states. It is evident that first-order effects spread into the second-order region and thus could have detrimental effects on wave measurement schemes. [C1083]

### "Biomedical innovation lessons learned during the MCAMS discovery process"

The remote sensing device developed by noninvasive medical technologies, Inc. (NMT), and the integration of several other innovations that create the multiple casualty assessment management system (MCAMS) is a modern day example of technology created to transform physiological data into valuable medical knowledge. Spanning the course of four years, the MCAMS project has yielded multiple innovations and patents. The lessons learned from the discovery process; conceptualization through implementation present an example framework for biomedical system innovation. The Multiple Casualty Assessment Management System is the

integration of remote biosensor monitors reporting objective data to redundant receivers that can seamlessly move across the care continuum. The conceptualization process was the most protracted phase of this innovation. Each development stage, from proof of concept to prototype, evaluation, reconceptualization, and finally implementation has been fraught with its own challenges. The key to assuring success in the innovative biomedical process has been focus on the central concern: the patient-the need. While the conceptualization stage was focused on defining relative advantage, throughout the course of the discovery process it was important to reflect on this definition, reevaluate and redefine it. During the development phases of proof of concept and prototype important innovation characteristics were addressed in regard to innovation compatibility and complexity. For example the innovation idea may be compatible with saving lives however the concept of operations was so complex or arduous that it became incompatible with innovation success. Challenges as complex as radar design offer huge advances in biomedical science, however it is simply the Idquoon/offrdquo switch that the end user references the most frequently. Using the MCAMS development process as an example of how to utilize Roger's theory of innovation diffusion, each diffusion characteristic will be considered as a part of the biomedical development process; relative advantage, compatibility, complexity, observability and trialability. The author also asserts that current technological tools should include innovation adaptability as a predictor of successful diffusion. [C1084]

### "SAR interferometry for long term deformation mapping using SBAS method: A case study in Nanjing area"

Synthetic aperture radar interferometry (InSAR) is a novel remote sensing technique to measure earth surface deformation, it is capable of obtaining dense information related to the deformation of a large area quickly, economically and effectively. However, Conventional InSAR technique is easily suffered from both spatial and temporal decorrelation which limits its application, especially for long term deformation mapping. In this paper, a Small Baseline Subset (SBAS) InSAR approach, which generates interferograms between two SAR images with small spatial baseline was presented, this approach can reduce both spatial and temporal decorrelation for long term deformation using a data set of SAR images acquired subsequently; deformation maps and displacement time series of the Nanjing City, P. R. China was generated with SBAS approach. Results of 13 differential interferograms generated by 8 SAR images in Nanjing from August 1996 to April 2000, demonstrate its efficiency. [C1085]

### "A comparison of AIRSAR and SPOT imagery for land cover mapping"

There are two main types based of remote sensing which is known as optical based and radar based. This study related to investigation of the use of AIRSAR imagery compare to SPOT imagery for land cover mapping purpose. Covering the Muda Merbok area as a case study, 10 meters resolution of airborne (AIRSAR imagery) and 20 meters resolution of optical based (SPOT imagery) which has been resample into 10 meters resolution output were used. The imageries used were at same year 2000. Both imageries had been processed by using ENVI (for AIRSAR imagery) and ERDAS IMAGINE (for SPOT imagery). The synthesize or decompress data, slant to ground range conversion, mask pixels of extreme values, antenna pattern correction and speckle removing were among the steps in AIRSAR data processing. For SPOT imagery the general steps like geocoding, subset, clumps, eliminate and recode were used. The supervised classifications for both images were performed to produce the classification maps. From these two images processing, comparison between both of the images were performed and then the land cover mapping for AIRSAR and SPOT were produced. It is found that land cover mapping based from the AIRSAR imagery is also reliable for land cover mapping compared to SPOT imagery. [C1086]

### "Information assessment for polarimetric SAR intensity images"

Polarimetric synthetic aperture radar (SAR) systems generate data, which have different information content in each polarimetric band. In analyzing the intensity information of multi-polarimetric SAR images (without taking into account phase information) two key issues were addressed. First, the mutual information and the entropy are used to assess the information difference between the polarimetric bands. Second, the image restoration method for full polarimetric SAR images can be evaluated with the information theory and a statistical method of minimum mean squared error estimation. This method was used to find the amount of information in an image as a function of spatial frequencies. A priori information about the power spectrum of an image and a point spread function of SAR system was applied. Statistical quality measures as well as the amount of information show good performances for polarimetric image restoration. [C1087]

### "Orthorectification of TerraSAR-X Images Based on Precise Orbit Information"

This paper describes a method for the orthorectification of TerraSAR imagery. Being an effective earth

observation technique, the synthetic aperture radar (SAR) systems supply extremely detailed radar images, day and night, under all weather conditions. EADS Astrium 's new radar satellite TerraSAR-X was launched in June 2007, which provides earth observation data of unprecedented quality, with a resolution of up to one meter and the error of orbit information up to 0.2 m, for increasingly diversified commercial as well as for scientific applications. This paper describes a method for the orthorectification of TerraSAR imagery. The correction method is based on a rigorous orbital/attitude model. The result from testing the method demonstrates the possibility to orthorectify TerraSAR imagery to sub-pixel accuracy. This research makes the well technique foundation of using high resolution satellite-borne SAR to update topographic map of scale 1:50,000 in Western China. [C1088]

### "Fast evaluation for speckle feature in urban SAR images"

Coherent speckle is an important feature in Synthetic Aperture Radar (SAR) image. Testing the property of speckle is effective for urban SAR image performance evaluation. Through correlation analysis for speckle measures, this paper proposes a measurement for speckle feature based on parametric hypothesis test. Firstly selects homogeneous areas in tested SAR image with manual mode and estimates the ENL of each area. In contrast with the speckle feature in sampled image from population, secondly utilizes the u-parametric hypothesis test to measure the quality of speckle. Finally obtains the result that accepts the null hypothesis or rejects it. Experiments of Japan Pi-SAR and East China Research Institute of Electronic Engineering (ECRIEE) SAR images in urban areas show the measurement could distinguish those tested images where speckle property is in accordance with the coherent imaging principle, which is one of the vital requirements for post processing technology of SAR imagery. [C1089]

### "Three-dimension information extracting from high resolution airborne Synthetic Aperture Radar images"

According to the geometric imaging characteristics of airborne Synthetic Aperture Radar (SAR) system, the methods of extracting three dimension information for some typical ground objects with height have been described in this paper, including image preprocessing, height information extracting of buildings and trees, the final visualization and so on. And, the test result provided a practical reference for the application of urban and town area with high-resolution airborne SAR images. [C1090]

### "A modified method for relevance feedback in high-resolution SAR image retrieval system based on SVM"

Relevance feedback (RF) is an importance technique in CBIR (Content-Based Image Retrieval) systems to bridge the semantic gap between low-level visual features (eg. color, shape, texture) and high-level human perception. One of the most frequently used methods to do RF is Support Vector Machine (SVM), which has a good generalization ability in pattern recognition. But when the training data is insufficient, the performance of SVM may drop dramatically. In this paper, we proposed a method to alleviate the small sample problem in SVM based RF by using a new piecewise similarity measure function and ensemble learning. We compared our method with standard SVM based RF on a high-resolution SAR (Synthetic Aperture Radar) image database, the experiment results show that our method has a better performance and prove that it's an effective algorithm for RF. [C1091]

### "Building extraction in urban scenes from high-resolution InSAR data and optical imagery"

Modern space borne SAR sensors provide geometric resolution of one meter, airborne systems even higher. In data of this kind many features of urban objects become visible, which were beyond the scope of radar remote sensing only a few years ago. However, layover and occlusion issues inevitably arise in undulated terrain and urban areas because of the side-looking SAR sensor principle. In order to support interpretation, SAR data are often analyzed using additional complementary information provided by maps or other remote sensing imagery. The focus of this paper is on building extraction in urban scenes by means of combined InSAR data and optical aerial imagery. [C1092]

### "Coherent stacking with TerraSAR-X imagery in urban areas"

The German radar satellite TerraSAR-X was launched in June 2007. It is one of the first satellites to continuously provide space-borne high resolution radar imagery with a slant range resolution in the order of 0.6 m times 1.1 m for civil applications. The sensor, the mission design, the orbit concept, and the SAR processor (TMSP) perfectly support interferometric applications. Naturally, DLR's operational interferometric system GENESIS has been adapted to exploit the innovative high resolution data. Algorithm updates have been proven

indispensable due to the more complicated spectral characteristic of the data introduced by the spotlight acquisition mode. Also, the high spatial resolution requires that radargrammetric effects, i.e. local parallaxes, be considered in interferometric processing. [C1093]

### "Automatic recognition of man-made objects in SAR images using support vector machines"

Over the past two decades the remote sensing technology is applied in a large scale in environmental research and policy, i.e. water pollution monitoring and conservation of soil, etc. The methods for recognition of man-made objects in remote sensing images are providing capabilities for mapping and monitoring crucial objects or sites in environmental management, i.e. hazardous chemicals storerooms, oil depots, etc. However, the task of recognizing key man-made objects from large images is time consuming and complex. In the paper we aim at developing an automatic and fast image processing method for the recognizing man-made objects in synthetic aperture radar (SAR) images, which is a supervised learning approach based on support vector machines. Firstly, a sample image data set which contains several classes of interested man-made objects is manually extracted from SAR images. Then we train the image data set by least squares support vector machines. After cross-validation and an exhaustive grid search, a model that can predict target label of data instances in the testing set is obtained. Finally we can implement classification in random image set using above prediction model and recognize the man-made objects. This approach needs no a priori knowledge, and only a set of train examples for the learning step is needed. [C1094]

### "DEM reconstruction in urban scenario"

In this paper a method to handle layover regions in SAR images is presented. Layover occurs when multiple radar echoes collapse in the same resolution cell; presented approach is addressed to resolve the different echoes in order to allow a proper Digital Elevation Model generation, with particular attention to urban scenario. The problem is approached using a statistical modeling of the layover phenomenon and a classical statistical estimation technique. Some cases of study on realistically simulated SAR data are presented, showing the effectiveness of the method. [C1095]

### "Surface subsidence and ground fissures activity monitoring based on D-InSAR: A case of Datong city"

The Synthetic Aperture Radar Interferometry technique has become one of geological disaster monitoring tools, for its economical, efficient, high-precision and large-scale surface deformation monitoring capacities. Datong is a well-known historical and cultural city, which is also a major energy bases and known as "town of coal" reputation in China. Since 1980s, with the development of industry and agriculture the amplitude of groundwater withdrawal has increased year by year, which lead to serious surface subsidence and ground fissures hazards in this city, even active up-to-date. Presently, 10 ground fissures with a total length of 34.5 km can be found in Datong region. However, the city-level spirit leveling only carried out during years of 1988-1993 to monitor the surface subsidence, and ceased later on. So in this paper, we collect 8 scenes of Envisat SAR data covering Datong city to monitor the subsidence evolution during Jan. 2005 to Feb. 2008. The interferometric pairs are set according to the principles that temporal and geometric baseline limits. Finally, we obtain the annual and accumulated subsidence amounts. The study shows that the land subsidences in Datong are greatly correlated with the groundwater withdrawal and seasonal variation. And some new subsidence cones are located at new economic and technological development zones of Datong city. Thirdly, ground fissures deformation in Datong is controlled by the regional tectonic activity and also affects the land subsidence in its surroundings. [C1096]

### "Building extraction by fusion of LIDAR data and aerial images"

It is well known that geometric filters for points cloud can only go so far when removing above-ground phenomena for it's difficult to determine whether a laser point has hit a special object when only spatial analysis is included. And comparing to the discrete points cloud, the high quality, large-coverage images provided by aerial cameras is a very important advantage of photogrammetry, which can be a very important complement data source to the points cloud. And by a process of spectral imagery LIDAR composite, points cloud can be fused with accurate spectral images provided by aerial CCD cameras on the same board. And the points cloud, with both high quality of reflection and geometric properties, can be filtered by integrating the reflectivity and geometric method. In this paper, the measurement characteristics and advantages of reflectivity of laser scanning and CCD cameras for the classification of return points are analyzed, and a building extraction method, integrating the geometric feature and reflectivity information of the return's intensity and the spectral range of CCD camera are presented. In which, the vegetation points are filtered by spectral attributes initially, and then points belonged to the building walls are segmented by a area attributes after constructing the return points'

voronoi diagram; and building surface points are filtered by plane-fitting clustering method. [C1097]

### "Urban DEM generation from airborne Lidar data"

Digital surface model (DSM) can be acquired from airborne Lidar (light detection and ranging) directly. But for the production of digital elevation model (DEM) from the point cloud, the filtering of the point cloud should be carried out in order to remove points representing surface of non-ground objects. According to the deficiencies of slope based method and characteristics of Lidar data in urban area, a novel filtering algorithm for Lidar data that combining slope based method and region growing is presented in this paper. This method can improve precision and efficiency of filtering, and is very suitable for Lidar data of complex urban area. Experiment results show that the proposed method can remove objects in complex urban area effectively and rapidly. [C1098]

### "Assessment of urban tree shade using fused LIDAR and high spatial resolution imagery"

Advancements in high spatial resolution remote sensing technologies including multispectral satellite (Quickbird, IKONOS) and active airborne sensors (LIDAR-Light Detection and Ranging) are enabling detailed analysis of physical features across the urban environment. Often these datasets have been applied in isolation, however by fusing these technologies significant added benefit can be gained. Specifically, LIDAR data enables highly accurate extraction of three dimensional urban structures such as buildings, trees, and the underlying terrain; while multispectral data can provide accurate estimates of surface cover type. In this paper we present a technique to model and map seasonal solar radiation effects related to urban trees by integrating structural and spectral data. Results indicate that across the study area (The District of North Vancouver) trees reduce incoming potential solar radiation in summer by 4.38 MJm-2day-1(24%) and in winter by 0.28 MJm-2day-1(13%). In addition, solar radiation is decreased by 0.2 MJm-2day-1(11%) in winter when deciduous tree species are removed. Finally, solar radiation is summarized by urban land use and results suggest that radiation in developed regions is most affected by tree shading in single-family residential areas (3.5 MJm-2day-1) and least affected in commercial areas (1.22 MJm-2day-1). [C1099]

### "Assessing the utility of DMSP/OLS night-time images for characterizing indian urbanization"

Urbanization, that is the movement of population from rural to urban locations, is a process that has been occurring for hundreds of years, but is increasingly prevalent in today's world. In 2008 most of the global population was resident in urban areas. It has been predicted that in the coming years, an increasing number of people will be living in cities; especially in the developing countries within in Asia and Latin America. This study considers the case of India, the second most populated country in the world, with a present total population exceeding 1 billion. It focuses on the state of Maharashtra (including the mega-city of Mumbai and its surrounds-the largest in India with a population of approximately 18.1 million). The Defense Meteorological Satellite Program (DMSP) Operational Linescan System (OLS) is a spaceborne system that detects visible light and thermal emissions of the earth at night. The data is collected nightly, on a global basis. The aim of this paper is to correlate the values obtained from the radiance calibrated DMSP/OLS night-time images of 2001 with population data. The spatial resolution of DMSP/OLS images is approximately 1 Km. This paper asks the question over what range of spatial scales does DMSP/OLS have utility in retrieving metrics of urbanization. [C1100]

### "Water feature extraction from aerial-image fused with airborne LIDAR data"

An innovative method to extract water feature from aerial-image is introduced in this paper. This approach extracts water feature from coarse to fine considering laser spectral bands of current existing airborne LIDAR systems and the spectral characteristic of these bands. Quad-edge based incremental inserting algorithm is used to construct the TIN (Triangulation Irregular Network) from LIDAR points. According to the triangulate features of different objects, area-analysis is performed to extract water triangles from TIN. Water triangles depict the water location of aerial-image. Then buffering is performed to extend the area of water triangle and to uptake the whole water-related points cloud data. Raster calculation is used here to obtain the rough water feature. Then, Mean-Shift algorithm is used to reclassify the rough water feature and to obtain the precise water. Finally, the feasibility of the approach is verified using comparison between two ordinary methods and the approach proposed in this paper. [C1101]

### "Road tracking by circular template matching from high resolution remotely sensed imagery"

Template matching has been brought effective results in road tracking. Actually, the shape of template plays a very important role. In this paper, a novel circular template is utilized to search the center points of the road. The circular template is not necessary to rotate for the isotropy of template when searching the optimal road axis point, which means less computation. At the same time, least square matching method is employed to trace the

road trajectory. The main purpose of the paper is to propose a circular template that improves the performance value of tracking road axis. Experiments show that the circular template matching method (CTM) is more efficient than the rectangular template matching (RTM). [C1102]

#### "Mining area subsidence monitoring using multi-band SAR data"

In this work, DInSAR technique has been applied to the monitoring of mining induced land subsidence in many areas. In this paper, the DInSAR technique is used to process the space borne SAR data including C band ENVISAT ASAR and L band JERS, PALSAR SAR data to derive the temporal land subsidence information in Fengfeng coal mine area, Hebei province in China. Since JERS do not have precise orbit, an orbit adjustment must be accomplished before the DInSAR interferogram was formed. We designed an images coregistration method based on the imaging geometry of interferometric SAR, and an external DEM. We analyzed 8 differential interferograms derived from JERS SAR, PALSAR, ENVISAT ASAR data. In our analysis, the DInSAR results were compared with leveling data that show high consistency. The characteristics of phase pattern on these C band and L band deformation interferograms were compared; we can notice that in most situations, the obtained deformation pattern on the surface is not the same of L and C band. And at last the feasibility and limitations in mining subsidence monitoring with DInSAR were analyzed. The experimental result shows that both C band and L band can accomplish monitoring mining area subsidence, but C band has more restrict conditions of its perpendicular baseline. In order to get a satisfactory outcome in mining area subsidence by DInSAR method, the time series of SAR images of every visit period and SAR deformation interferograms should be archived. [C1103]

#### "Monitoring ground subsidence in mining area using spaceborne InSAR technology"

A case study of InSAR application to monitor the ground subsidence of colliery area in Fengfeng coal mining area, Hebei Province, China is investigated in this paper. Using the data of ENVISAT ASAR and JERS SAR, the interferometric results of this area are derived. At the same time as acquisition of ENVISAT ASAR data, field leveling measurement in this area was carried out, and the historical excavation data were collected as well. A synthetic comparison is done between the results of D-InSAR and leveling measurement. The comparison shows that the D-InSAR subsidence results are consistent with the field measurement results and the historical excavation data. Finally, some ideas and suggestions about InSAR applications to deformation monitoring in mining areas and mining industrial cities are given based on this case study and other applications. [C1104]

#### "Monitoring urban subsidence with coherent point target SAR interferometry"

Spaceborne SAR interferometry (InSAR) is a well known microwave remote sensing technique which has been applied for topography mapping and ground motion monitoring by exploiting phase difference from SAR data acquisition with relevant large spatial scale and high precision. The developed Permanent Scatterers Interferometry (PSI) is a further step of InSAR technique which offers a convenient processing framework that enables the use of all data acquisitions. It aims to bypass the problem of geometric and temporal decorrelation by considering long term coherent point. Furthermore, by using a large number of data, atmospheric signal is estimated and compensated for. We present in this work the development of an improved PSI, called Coherent Point Target InSAR, for land subsidence velocity field estimation in urban area as well as rural area in China. A series of case studies demonstrate the ability of CPT InSAR for monitoring ground subsidence field with relevant large spatial extent as well as small area. [C1105]

#### "Ground settlement monitoring from temporarily persistent scatterers between two SAR acquisitions"

We present an improved differential interferometric synthetic aperture radar (DInSAR) analysis method that measures motions of scatterers whose phases are stable between two SAR acquisitions. Such scatterers are referred to as temporarily persistent scatterers (TPS) for simplicity. Unlike the persistent scatterer InSAR (PS-InSAR) method that relies on a time-series of interferograms, the new algorithm needs only one interferogram. TPS are identified based on pixel offsets between two SAR images, and are specially coregistered based on their estimated offsets instead of a global polynomial for the whole image. Phase unwrapping is carried out based on an algorithm for sparse data points. The method is successfully applied to measure the settlement in the Hong Kong Airport area. The buildings surrounded by vegetation were successfully selected as TPS and the tiny deformation signal over the area was detected. [C1106]

#### "A method of deriving features of building from LIDAR point clouds in urban area"

This research paper aims at extracting features, especially the plane feature, of building from Light Detection And Ranging (LiDAR) point clouds in Urban Area, and with these features and information to build the model of object. Unlike modeling object in other fields, such as reverse engineering, surfaces of building usually consist of

abundant big and plane surfaces which are significant features. In urban area, most buildings can be simplified to the models that are made up of approximate plane surfaces to which features of buildings refer, in this paper. Among these surfaces, there are distinct points and intersection lines (the edges and vertices of the building object). Plane detection, surface adjacency relations restoration, model parameter calculation, and model reconstruction constitute the main research of extracting geometric features and modeling the object. In this contribution, some examples of deriving information from the point clouds are presented to demonstrate the method. And, the results prove that when the geometric information of vertices, edges and normal lines of the plane surface, together with the topological relations (Surface adjacency relations) among them, is derived from the point cloud data, the model, representing building in this paper, can be built effectively. Equally significant, models generated from this method, while occupying less memory space, can store more comprehensive structural information, and have a better exhibit effect. And this method can provide three dimensional data of buildings from point cloud data in applications like GIS, navigation and virtual city. [C1107]

#### **"Non-parametric multiple level set model for efficient image classification in urban areas"**

Multispectral remotely sensing imagery with high spatial resolution, such as QuickBird, IKONOS satellite imagery or Aerial imagery, especially in urban scenes, often perform spectral variations and rich details within a category, resulting in a poor accuracy of classification. To seek an efficient solution, this paper presents a non-parametric and variational multiple level set model by a joint use of Aerial image and two products, digital terrain model (DTM) and digital surface model (DSM), directly or indirectly derived from raw LiDAR (Light Detection And Ranging) 3D point cloud data. Proposed model is to minimize an energy function. The energy includes two terms. First term is mainly image-based energy which introduces Parzen Window density estimation technique in the multiple level set framework. To make up the disadvantages brought by only multispectral image-based classification scheme mentioned above. A novel energy constraint term is added by combining elevation information of objects derived from LiDAR raw point cloud. Thus, a closely integrated and effective classification model under variational level set framework has formed. Finally, comparative experiments on a pair of Aerial image and LiDAR point cloud data have demonstrated the our proposal can obtain more accurate and detailed classification than that of relevant methods only depending on spectral information of image. [C1108]

#### **"A detailed comparison between two fast approaches to urban extent extraction in VHR SAR images"**

This work is devoted to the comparison of two algorithms for human settlement map extraction from VHR SAR data. The two approaches have been recently proposed in literature, but extensive comparison of their performance in different situation and in different areas of the world was not available yet. The first approach is based on the computation of local statistical indexes to detect "seed areas", which in turn are used to train a texture-based settlement detection procedure. The second approach is based directly on a textural feature, data range, and shows usually less precise, but equally useful results. In this work the two approaches are compared on a range of different SAR sensors, and a discussion of their relative performances for different spatial resolutions and radar frequencies is provided. Reference settlement extents are obtained from maps provided by global mapping projects. [C1109]

#### **"BREC: The Built-up area RECOgnition tool"**

This paper presents the overall structure and some examples of use for BREC (Building RECOgnition tool) software, developed by the Remote Sensing Group at the University of Pavia. The software allows detecting the characteristics of built-up areas at different scales, from urban extent delineation to individual building recognition, depending on the remote sensing data in input and their spatial resolution. A set of different tools for classification, feature extraction, and data fusion at the feature level have been developed and can be suitably combined to achieve the best results. All of them have been optimized for the analysis of urban areas and human settlements, and can be applied to both optical and radar images. [C1110]

#### **"Segment-based urban block outlining in high-resolution SAR images"**

While analysing remotely sensed images of urban areas, in many cases an at least approximate knowledge of block partition is useful for specialising operations over areas within which a certain degree of homogeneity can be assumed. Unfortunately, though, this information is not always accessible in a reasonable time or with a reasonable effort, or even in some cases a GIS of the city is not available at all. Automatic extraction of block boundaries becomes thus an interesting means of obtaining such information. City blocks are usually separated by major urban roads; this paper presents a preliminary work on the use of a linear feature extractor, originally developed for road network extraction, as a tool to partition a very high resolution SAR scene acquired over an urban area. [C1111]

### "Fast compression and access of LiDAR point clouds using wavelets"

To compress, access, visualize and analyze large 3D point clouds, they are often converted to Digital Surface Models, either as raster grids or Triangulated Irregular Networks. This paper proposes an approach, which works directly on the points as they were recorded during data capture. There is usually a strong correlation between successively recorded points. This correlation is used to compress the point clouds using wavelet transforms. The characteristics of wavelet coefficients are used to access areas of progressively higher resolution and quality. The detail coefficients can also be used for 3D analysis and reconstruction. [C1112]

### "The application of remote sensing technology in monitoring environmental disasters of mining cites"

Aiming at the increasingly serious pollution and ecological damage in mining cites, environmental information urgently are urgently needed to provide basis and decision-making for the economic transition of mining cites. This article describes main environmental problems existing in mining cites, as well as ways of monitoring these major environmental problems, such as the Landsat TM images are used in Land use dynamic monitoring, High Spectrum Images are used in the extracted vegetation monitoring, and the water quality change is monitored by the way of NOAA / AVHRR. Particularly, the effectual way of the Interferometric Synthetic Aperture Radar (InSAR) landslides monitoring is introduced, which is well applied to the opencast mine of Haizhou and Fushun in China with this technology. Differential interferometry using Synthetic Aperture Radar (SAR) is a powerful technology for detecting surface deformation of ground. Surface deformation can be analyzed from different phase of micro-wave between two observed data by SAR. The accuracy of measurement is less than plus-and-minus 1 cm. Achieved research results will provide early warning of environment disasters, rapid & real-time information and interpretation means for the mining cites. [C1113]

### "Automatic registration of SAR and optics image based on multi-features on suburban areas"

Image registration, the process of estimating the optimal correspondence relation between two or more images taken at different time, from different viewpoint or by different sensors, is essential for a variety of applications in remote sensing, computer vision, pattern recognition and medicine, etc. It is a prerequisite for accomplishing high level tasks such as sensor fusion, surface reconstruction, change detection, and object recognition. In order to realize the automatic registration between Synthesize Aperture Radar(SAR) and Optical images, in this paper, an automatic registration algorithm based on different features is proposed. This method is proposed according to characteristic of image of remote sensing. Patches, edge and point features are used in our paper to registry. The evaluation of the image registration accuracy proves that the stratified registration algorithm based on multi-features proposed in this paper work well in automatic registration of SAR image and optical image with pixel accuracy. [C1114]

### "Analysis of active ground subsidence zones in Guangzhou city using ASAR Persistent Scatterer Interferometry"

A Persistent Scatterer Interferometry (PSI) technology is used to detect ground deformation from ASAR images acquired from 2007-2008 in the urban area of Guangzhou in South China. To obtain active ground subsidence zones a great value filter method is developed to extract characteristic points with great values. Based on the ground deformation rate maps of the study area, a thematic map of the active ground subsidence zones is generated. To interpret the distribution of active ground subsidence zones, a local geological map of faults and rock type information is used to generate a series of thematic maps. The results show that geological faults, rock distribution, over-development, and underground engineering projects may be four factors leading to the distribution of the active ground subsidence zones in the study. [C1115]

### "An automatic method on detecting image control points from SAR imagery based on Optical Image Patches"

In this paper, we propose a novel procedure of detecting control points from SAR image based on Optical Image Patches procedure. The method presented here is a three-step procedure. In the first stage, a local image patch from the SAR image is estimated from the geo-information of the SAR image and the GCP geo-coordinate, and the local patch is performed an affine transformation by using the four geo-coordinates of the SAR image in advance. In the second stage, the NCC procedure is performed on the GCP and the preprocessed local SAR image patch to find the candidate image control point(ICP). In the third stage, the pairs of ICP and GCP are refined, and the false pairs are discarded by the RANSAC algorithm. Experiments on SAR-Optical satellite images demonstrate the reliability and effectiveness of the presented method. [C1116]

### "The utilization of SAR remote sensing and GIS technology to delineate urban extent in North China"

Urban environments represent one of the most dynamic regions on earth. In order to obtain more frequently updated and spatially detailed data on urban phenomena, remote sensing satellites can serve as a valuable instrument. With its ability to image the Earth's surface in nearly all weather conditions, together with its high spatial resolution, synthetic aperture radar (SAR) represents a very powerful observation tool for monitoring geophysical resources globally. SAR images with high resolution have proven their usefulness for land description and scene analysis. The goal of this study was the development of a temporally and spatially robust approach towards an automated identification of built-up areas based on RADARSAT imagery. In our work, the urban extent distributed in the major part of North China was extracted and delineated. By visual inspection, the resulting map of urban extent was acceptable. [C1117]

### "Supervised land-cover classification of TerraSAR-X imagery over urban areas using extremely randomized clustering forests"

This study investigates the impact of the use of scattering intensity and texture features derived from TerraSAR-X intensity images on urban land cover classification accuracy, in combination with the Extremely Randomized Clustering Forests as the visual codebook former and classifier. We propose a multi-orientation ratio descriptor to represent the features of each SAR image patch effectively, and introduce a graph cut optimization based Markov Random Field smoothing processing to reduce block boundary effects due to patch-based classification method. We compare our classification results using one or all features together on 1 m resolution TerraSAR-X images and show that the reasonableness of the proposed descriptor and the effectiveness of the Extremely Randomized Clustering Forests classifier. [C1118]

### "A classification method for building detection based on LiDAR point clouds"

Building detection using LiDAR data is a popular topic in LiDAR data processing. The object classification can play an important role in the detection. In this paper, a new algorithm based on LiDAR point clouds is developed to resolve the object classification difficulties in the case of trees close to buildings. Compared with other algorithms, the methods can work effectively due to use the combination of height texture and regular geometric element. The experiment results is also given and discussed to improve the validity of the proposed algorithm. [C1119]

### "Design of an AMC plane for a unidirectional, low-profile tulip-loop antenna"

The ways of converting a wide band, electrically small in size, bi-directional quasi magnetic antenna into a unidirectional one are investigated. The purpose is to develop a magnetic wall parallel to the antenna which provides low-profile unidirectional designs, without sacrificing the bandwidth too much. Initial attempts to preserve the wide bandwidth caused some problems like pattern splitting at the broadside of the antenna and this problem has been solved by introducing an aperiodic AMC. An operational bandwidth for a VSWR less than 2 of 44% in the X-band is achieved. The total height of AMC and the antenna is  $\lambda/6.2$  at  $f_{min}$  and  $\lambda/4$  at  $f_{max}$ . [C1120]

### "The Global Road Extraction Approach from Synthetic Aperture Radar Images"

The extraction of road networks from synthetic aperture radar imagery is of fundamental importance for geospatial applications. The methods basically go through the steps such as road sharpening, road finding, road tracking and road linking. In this paper, a new global approach to road detection that is motivated by Kohonen neural network is proposed. It makes the joint of the roads more fluent and reduces detection errors. The computer simulation results show the highest extraction quality from the real SAR images. [C1121]

### "Wave Simulation of SAR Signal for Two-Dimensions Sea Surface"

The paper describes a synthetic aperture radar (SAR) image simulation for ocean surface. It's In order to study the SAR image of the ocean wave and the wave modulation of the RCS (radar cross section). The simulation is based on the velocity bunching (VB) theory and is developed in the Matlab programming language. The software has been conceived and implemented modularly and its use can also assist microwave remote sensing courses. The way is an available method of studying the sea surface wave image by SAR. [C1122]

### "Cancellation of range ambiguities with block coding techniques"

This paper presents radar signaling schemes for cancellation of late time arriving echos. Signal reflections

arriving delayed at the radar when the radar has already emitted a next pulse result in range ambiguities and materialize as potential false targets. In this work we propose pulse block coding techniques to distinguish echo reflections originating through the recently emitted pulse and those impending from subsequent pulses. The methods introduced require only simple matched filtering operations at the receiver and permit usage of arbitrary waveforms with potential for waveform diversity gains. [C1123]

### "Systolic array implementations for real time enhancement of remote sensing imaging"

In this paper, we propose a hardware/software (HW/SW) co-design approach for near real time implementation of high-resolution reconstruction of remote sensing (RS) imagery using systolic arrays as coprocessors. The proposed design is based on a field programmable gate array (FPGA) and implements the image enhancement/reconstruction tasks in an efficient concurrent processing architecture with systolic arrays that meets the (near) real time imaging systems requirements in spite of conventional computations. The software design is aimed at the algorithmic-level decrease of the computational load of the large-scale SAR image enhancement tasks. The innovative algorithmic idea is based on the concept of descriptive regularization (DR) approach. Finally, we report and discuss the results of the hardware/software co-design implementation in a Xilinx Virtex-4 XC4VSX35-10ff668 for reconstruction of large scale real world RS images of 512 times 512 pixel format. [C1124]

### "Sea Wind Power Energy Evaluation by HF Radar System"

This paper presents a remote sensing method for wind energy measurement and evaluation on sea surface, which can be used for the investigation of wind farm. It provides a valid proof for building wind plants or monitoring wind farms on the sea surface. The wind speed and direction can be derived from radar echo spectrum as well as wind profile, and it can cover a large area (thousands of square-kilometers) and measure wind simultaneously. It provides a real-time, all-weather remote sensing measurement and it is a new method for wind evaluation comparing to conventional methods. [C1125]

### "UHF Radar Designed for Inshore Wave Watcher and Ocean Power Application"

This paper presents a remote sensing method for the measurement of inshore wave energy, which can be used for the investigation of some regional coast for building wave power plants and monitoring the waves near dykes. It is designed to operate at UHF channel, and it is a portable and low power system, it can measure the movement of sea surface simultaneously without probing into the water. The field test on the beach of Zhujiajian Island proved that the system can be used successfully. [C1126]

### "Radar cross-section modeling of marine vessels in practical oceanic environments for high-frequency surface-wave radar"

Models of the Teleost marine vessel and the Bonn express cargo freighter are developed for generation of monostatic and bistatic radar cross section (RCS) returns for high-frequency surface-wave radar (HFSWR). Simulated monostatic RCS values are in good agreement with measured values at 4.1 MHz, thus additional investigations, to model varied practical situations may also be of interest. Specifically, the effects of pitch and roll and ship displacement (due to cargo container loading) are studied. Results show that the monostatic RCS of the Teleost can vary by more than 10 dB for a 10deg roll or a 15deg pitch incline. These results also suggest that the monostatic RCS of the Teleost has a null at broadside at the radar frequency of 7 MHz likely due to the resonant scattering of the A-frame mast and antenna structures. In addition, by modeling the Bonn Express with a full load and varied displacement, a very good agreement between the measured and simulated RCS can be observed. [C1127]

### "Application of passive microwave data in estimating freeze-thaw dates of a small lake"

Our method uses coarse resolution passive microwave data to estimate freeze-thaw dates of soil in the region surrounding the lake. Using the soil freeze-thaw dates we then determine a high probability window of days during which the lake freeze-thaw dates may occur. This paper mainly focuses on using passive microwave data to estimate this high probability window of days for the freeze and the thaw seasons of a lake. The importance of this project in our broader research goal of estimating freeze-thaw dates for small lakes can be explained as follows. Given a classifier that can classify SAR images of small lakes into "ice" and "no-ice" images (a parallel research project that we are involved in), we demonstrate that using passive microwave data to estimate the window will improve the practical use of the classifier in detecting freeze-thaw dates of the lake, by reducing the number of datasets required (using only the datasets that fall within the window). By reducing the number of SAR datasets required for the algorithm we reduce both financial and computational cost of the classification algorithm. This in turn will make the method more affordable and

improve the usability of the classification algorithm to keep track of lake freeze-thaw dates for a larger number of lakes. The passive microwave data collected, results obtained till date and related literature will be discussed in this paper. [C1128]

### "Development and integration of the aquarius scatterometer processor/control electronics for achieving high measurement accuracy"

The upcoming Aquarius sea-surface salinity mission has tight requirements on backscatter measurement accuracy and stability at L-band frequencies (1.26 GHz). These requirements have driven the development of new capabilities in the radar's backend detector electronics, which are the focus of this paper. Topics include the development of flight-grade hardware aboard the scatterometer for radio frequency interference (RFI) detection and mitigation, and analog/digital electronics design techniques that reduce system noise and yield highly linear power detection over a wide dynamic range. We also summarize the approach taken to test the scatterometer's processing and control functions at the level of the integrated Aquarius flight instrument, and present some recent results from the integrated testing campaign. [C1129]

### "Bistatic radar probing of planetary surfaces"

Bistatic radar provides a simple, cost-effective way to obtain survey information about planetary surfaces on scales important to landers and rovers. The centimeter-scale waves interact most strongly with surface structure on similar and slightly larger scales yielding estimates of rms surface slopes  $\zeta$  and material dielectric constant  $\epsilon_{\text{psiv}}$  (which can be related to density). Recent experiments in the Mars north polar region show an unusually heterogeneous surface with some segments having  $\zeta$  less than 0.2deg. The dielectric constants appear to vary only between 1.8 within the polar cap (snow) and 3-4 outside (sand). Uplink experiments (transmissions from ground to spacecraft) have been successfully conducted using Mars Odyssey; future possibilities include spacecraft-to-spacecraft experiments. [C1130]

### "RFI study for the SMAP radar"

The Soil Moisture Active/Passive (SMAP) mission has the scientific objective of measuring both soil moisture and freeze/thaw state from space. The mission will make both active radar and passive radiometer measurements at L-band in order to retrieve soil moisture. Some studies, however, indicated that these measurements are susceptible to radio frequency interference (RFI) in several geographic locations. As SMAP is a global mission and its mission life is 3 years, it is crucial for SMAP to understand the RFI over the whole globe and its temporal behavior. There will be impacts to the instrument system design and ground data processing in order to mitigate RFI. In this paper, strategies and procedures for performing this RFI study will be presented, and some results utilizing the RFI observed in the ALOS PALSAR data are described. The nature of the observed RFI is characterized and suggests some bands are relative free of RFI. The SMAP radar system will use a 1 MHz bandwidth, which can be placed within these suggested frequencies. The ALOS PALSAR data covers 28 MHz within the 80 MHz allocated for active L-band remote sensing. In addition, an initial analysis with UAVSAR data, which uses the entire 80 MHz allocation, indicates the relative severity of RFI over the whole band. An algorithm to remove RFI is suggested and its performance is shown for some data from ALOS PALSAR and UAVSAR. [C1131]

### "Accuracy of reflectivity estimated from profiling radars"

In this study, the accuracy of reflectivity measured using vertically pointing profiling radars is investigated. Interesting, while disdrometer observations are used to absolutely calibrate profiling radars, this study quantifies that disdrometers have significantly larger random measurement uncertainty than profiling radars. Using observations from a S-band profiling radar during the tropical warm pool international cloud experiment (TWPICE), reflectivity uncertainties of rainfall were found to be about 0.25 dBZ for 9-second dwell times and about 0.1 dBZ for 60-second dwell times. It was also found that the reflectivity uncertainty was dependent on both the signal-to-noise ratio and the number of velocity channels in the Doppler velocity power spectrum above the noise threshold. This lead to the reflectivity uncertainty for snow which has narrower velocity spectra than rain to increase to 0.4 and 0.2 dBZ for 9- and 60-second dwell times, respectively. [C1132]

### "First design investigations on a fully-electronic microwave imaging radiometer system"

Present applications of microwave remote sensing systems are spread out widely. One topic for using the frequency range 1-300 GHz is the domain of security and reconnaissance. Examples are, the observation of sensitive areas or the performance of personal security checks in order to find hidden weapons or explosives, both being an important mean in our world of a growing international terrorism. The imaging capability of hidden

objects is one of the main advantages of microwave remote sensing, because of the given penetration of electromagnetic waves through dielectric materials in this frequency domain. The physical effect used in passive microwave sensing relies on the thermal radiation of objects above a temperature of 0 K. The intensity of this radiation depends on the surface characteristics, the chemical and physical composition, and the temperature of the material. So it is possible to discriminate objects having different material characteristics like ceramic weapons or plastic explosives with respect to the human body. Considering the use of a people scanning system in airports, railway stations, or stadiums, it is important that passive microwave imaging devices have no exposure on the scanned object, like active devices do. Especially for highly frequent passed security gateways it is important to have a high through-put rate in order to minimize the queue time. Consequently fast imaging systems are necessary. In the following the conceptual idea of a fully-electronic microwave imaging radiometer system is introduced. [C1133]

#### **"An innovative multimode millimeter wave radar for Moon remote sensing"**

Since 2004, afterwards the US announcement, a renewed spirit of exploration has pushed space agencies in the world to promote new programs and studies devoted both to return to the Moon and to prepare a human mission toward Mars. Main objectives of this new phase of the space exploration is to collect as many as possible science data of the two planetary bodies and to acquire and test the technological basis on which to found the human challenge to the red planet. Within this context, Italy through the Italian Space Agency has recently funded a study for Moon remote sensing named MAGIA (Italian acronym standing for mission for lunar altimetry, gravimetry and geochemistry), and currently carried out by Rheinmetall Italy as prime contractor. The mission foresees the development of different payloads for Moon study, including an innovative radar-altimeter-radiometer (RAR) operating at millimeter wavelengths (95 GHz). This paper, after introducing the MAGIA mission, focuses on the preliminary activity, currently ongoing, of radar designing and dimensioning along with the trade-off carried out. [C1134]

#### **"Comparison and integration of GPS and DInSAR deformation time-series"**

We compare the surface deformation measurement capability of the small BAseline subset (SBAS) DInSAR technique and of the continuous Global positioning system (GPS). The analysis is focused on the Los Angeles (California) test area where different deformation phenomena occur and a large amount of SAR data, acquired by the European remote sensing satellite (ERS) sensors, and of continuous GPS measurements is available. Our analysis shows that the SBAS technique allows to achieve an estimate of the single displacement measurements, in the radar line of sight (LOS), with a standard deviation of about 5 mm, which is comparable with the LOS-projected GPS data accuracy. A final discussion on the complementariness and integration of SAR and GPS measurements is provided. [C1135]

#### **"A Collaboration Mobile System for Epidemiology Investigation in the Wenchuan Earthquake-Stricken Area"**

Communication is one of the major issue for the epidemiology investigation in the area affected by Wenchuan earthquake. A collaborative mobile system has been designed for the field epidemiology event investigation and disposal for it. To get more stable communication between field and indoor groups, provide more information to field investigators and experts, we designed a star communication topology. Because of the different networks and different terminals, an asymmetric client/server network has been designed for the collaboration between field and indoor workfellows. A prototype system has been implemented and tested in the Wenchuan earthquake stricken area, the results show the system works well and is very useful for field work and collaboration. [C1136]

#### **"Orthogonal multicarrier phased coded signal for netted radar systems"**

Orthogonal multicarrier radar waveforms have been designed for netted radar systems, where several radar stations are active simultaneously. The waveforms are phase-coded using orthogonal Golay complementary sets, derived from Reed Muller codes. These codes constrain the PMEPR of the signal to a maximum a 3 dB. Besides, ambiguity functions and cross-ambiguity functions with low sidelobes have been obtained. The possibility to encode data relative to the transmitter configuration (position, direction of the beam,...) in the radar waveform is also demonstrated. [C1137]

#### **"A signal level simulator for netted radar waveforms evaluation"**

When evaluating the performances of radar waveforms, it is crucial to understand how the signal is affected by multiple interactions with the environment and the system hardware. Analysis of complex radar systems, such as multistatic and netted designs (see Fig. 1) is often intractable without the application of a dedicated radar simulation system. Recent research into radar simulation has focused primarily on synthetic aperture radar (SAR)

systems and is not entirely applicable to traditional radar systems concerned with the location and tracking of remote targets. A complete simulator has been designed for the accurate simulation of raw returns in complex, multistatic and netted radars and is applicable to pulsed and continuous wave (CW) systems, and both active and passive radar systems. The flexible simulator for multistatic radars (FERS) can be used to simulate radar systems with arbitrary waveforms and arbitrary numbers of receivers, transmitters and scatterers. In this paper, algorithms for the simulation of raw radar return signals are presented, based on interpolation and modification of the transmitted signal and modelling of the radar hardware and environment. The algorithms are expected to be especially valuable for the simulation of emerging radar technologies, such as Passive Coherent Location (PCL), netted radar and phased array radar. Preliminary results, presented in this paper, suggest that these algorithms can simulate physical systems with excellent accuracy. [C1138]

#### "Advances in tactical laser radar"

Laser radar has enjoyed significant advances over the past decade. Novel sensor topologies, compact laser illuminators, and advanced signal processing have enabled the construction of low power, portable 2-D and 3-D laser vision systems. The applications of such systems range from surveillance, targeting, weapons guidance, and remote scene measurement, to target identification and atmospheric characterization. This paper serves to assemble some recent significant examples of laser radar in the context of emergent tactical applications. Strengths and limitations of competing topologies are also examined. [C1139]

#### "Low-noise detector with RFI mitigation capability for the Aquarius L-band scatterometer"

The upcoming Aquarius sea-surface salinity mission has tight requirements on backscatter measurement accuracy and stability at L-band frequencies (1.26 GHz). These requirements have driven the development of new capabilities in the scatterometer's backend detector electronics, which are the focus of this paper. Topics include the development of flight-grade hardware aboard the scatterometer for radio frequency interference (RFI) detection and mitigation, and analog/digital electronics design techniques used to reduce system noise and achieve highly linear power detection over a wide dynamic range. We also summarize the approach taken to test the scatterometer's processing and control functions at the level of the integrated Aquarius flight instrument, and present some recent results from the integrated testing campaign. [C1140]

#### "Automated cyclone tracking using multiple remote satellite data via knowledge transfer"

Cyclone tracking using a single orbiting satellite in a continuous manner is impractical as it has limited spatial and temporal coverage. One solution is to use multiple orbiting satellites for cyclone tracking. However, data from some orbiting satellites do not provide features as useful as other satellites in identifying cyclones. Moreover, satellite data containing strong cyclone discriminating features may be affected by coarse temporal resolution and object occlusion. In this paper, we propose a knowledge transfer methodology based on a Kalman filter for cyclone tracking using multiple satellite data sources containing a mixture of strong and weak features. This approach minimizes the negative effect of coarse temporal resolution and occlusion if only the satellite data containing strong cyclone discriminating features were used. Experimental results are presented to demonstrate the feasibility and usefulness of our knowledge transfer approach for cyclone tracking. [C1141]

#### "LIDAR versus satellite-measured optical thickness of a wildfire aerosol"

A dual UV, Rayleigh/nitrogen Raman LIDAR system was developed for the purpose of profiling aerosols at vertical ranges between 0.025 and 5 km. The 355 nm LIDAR was operated in El Segundo, California during June and July 2008, during a period of intense wildfire activity in Northern California. From the two independent measurements we calculated the particle backscatter, and using the humidity-corrected LIDAR backscatter-to-extinction ratios given by Ackermann we calculated aerosol optical thickness (AOT) profiles. Preliminary validation studies revealed that under most conditions the calculated LIDAR AOT data agreed with total AOT measured from a collocated sun photometer, except for cases when high-altitude smoke from wildfires was present. To account for high-altitude smoke, a two-layer atmospheric model was assumed, where the lower layer's AOT was calculated using the backscatter-to-extinction method and the high-altitude AOT was found through direct attenuation of the Raman signal. A comparison of AOT measurements from the ground-based LIDAR and the MODIS (Aqua and Terra) overpasses was then performed during the peak period of transport of smoke from Northern California, between 19 June 2008 and 2 July 2008. While the LIDAR and Sun Photometer were found to be in good agreement, it was found that the MODIS overpasses consistently indicated a larger AOT. [C1142]

#### "Precision column CO<sub>2</sub> measurement from space using broad band LIDAR"

In order to better understand the budget of carbon dioxide in the Earth's atmosphere it is necessary to develop a

global high precision understanding of the carbon dioxide column. To uncover the missing link that is responsible for the large discrepancies in the budget as we presently understand it, calculation has indicated that measurement accuracy of 1 ppm is necessary. Because typical column average CO<sub>2</sub> has now reached 380 ppm this represents a precision on the order of 0.25% for these column measurements. No species has ever been measured from space at such a precision. In recognition of the importance of understanding the CO<sub>2</sub> budget to evaluate its impact on global warming the National Research Council in its decadal survey report to NASA recommended planning for a laser based total CO<sub>2</sub> mapping mission in the near future. [C1143]

#### "Range estimation algorithms comparison in simulated 3-D flash LADAR data"

Range estimation algorithms have been applied to simulated 3-D flash laser radar data to test for accuracy and bias. Simulated data is modeled after hit mode performance of the Advanced Scientific Concepts 3-D flash laser radar camera. Hit mode is a mode of operation that stores buffered samples into memory only after a set number of photoelectrons have been observed by the detector. In hit mode, waveforms may not be centered within the range gate and may not contain the true peak of original waveform. Under these conditions traditional range estimation techniques could prove ineffective. A peak estimator, matched filter, and maximum likelihood estimator were tested for performance as waveforms shift position within the range gate. This paper suggests the best scenario for implementing each algorithm and shows the overall effectiveness of the matched filter when incorporated in the time domain. 1000 trials with noise were conducted for each waveform position and performance was judged based on mean square error and standard deviation of the range estimations. [C1144]

#### "Waveform diversity and knowledge based signal processing in distributed radar"

The asymmetric threat of the twenty-first century is presenting a challenge for the information and sensors domain. The intelligent aggregation of information and sensor data in real-time is required. The use of waveform and geometric diversity along with knowledge based signal processing in distributed radars and heterogeneous sensors is necessary. Three example cases are presented illustrating how to intelligently aggregate information and sensor data for delivering the desired effects to the asymmetric threat. [C1145]

#### "Full polarimetric GPR antenna system aboard the ExoMars rover"

A full polarimetric antenna system on board the ExoMars rover is part of the Experiment "Water Ice and Subsurface Deposit Observations on Mars" (WISDOM). The WISDOM-Experiment is a Ground Penetrating Radar (GPR) selected to be part of the Pasteur payload aboard the rover of the ExoMars mission. The Pasteur Panoramic Instruments (wide angle camera PANCAM, infrared spectrometer MIMA and WISDOM) will perform large-scale scientific investigations at the sites the Rover will visit. Among these instruments, WISDOM is the only that can provide a view of the subsurface structure prior to drilling. WISDOM has been designed to characterize the shallow subsurface structure of Mars. WISDOM will for the first time give access to the geological structure, electromagnetic nature, and, possibly, hydrological state of the shallow subsurface by retrieving the layering and properties of the buried reflectors. It will address important scientific questions regarding the planet's present state and past evolution. The measured data will also be used to determine the most promising locations to obtain underground samples with the drilling system mounted on board the rover. The instrument's objective is to get high-resolution measurements down to 2 m depth in the Martian crust. The radar is a gated step frequency system covering a frequency range from 500 MHz to 3 GHz. The radar is fully polarimetric and makes use of an ultra wideband antenna system based on Vivaldi antenna elements. The paper describes requirements, design and realization of the WISDOM antenna system accommodated on the ExoMars rover. Simulated and measured antenna performance is compared in this paper. Test measurements performed in permafrost regions on earth will be shown in the presentation. [C1146]

#### "A study of a potential venus radar topography mission"

Radar has been shown to be the best way to view the surface of Venus as was demonstrated by Pioneer Venus Orbiter, Veneras 15 and 16, and Magellan Missions. Each of these missions progressively increased our knowledge of the surface and it has been nearly twenty years since Magellan covered nearly all the surface with SAR images from 120 to 300 m resolution. Advances in technology including onboard processing and high rate down links now make it possible to propose a mission that would create a data set of the topography of Venus at 50 m resolution posting and 5 m height accuracy. Other modes of the radar, using the same hardware, would yield 6 m resolution images of small (10 km by 10 km) areas. This paper describes one point design. [C1147]

#### "Combining a rain microphysical model and observations: Implications for radar rainfall estimation"

A bin-model was used to characterize the signature of dynamical microphysical processes on Z-R relationships used for radar rainfall estimation. The sensitivity analysis performed shows that coalescence is the dominant

microphysical process for low to moderate rain intensity regimes ( $R < 20 \text{ mm h}^{-1}$ ), and that rain rate in this regime is strongly dependent on the spectral properties of the DSD (i.e. the shape). For high intensity rainfall ( $R > 20 \text{ mm h}^{-1}$ ), collision-breakup dynamics dominate the evolution of the raindrop spectra. Analysis of the time-dependent Z-R relationships produced by the model suggests convergence to a universal Z-R relationship for heavy intensity rainfall. Conversely, the model results show that Z-R relationships severely underestimate reflectivity in the light rainfall regime. [C1148]

#### "Interferometric absolute phase determination with TerraSAR-X wideband SAR data"

Wideband SAR systems such as TerraSAR-X bring the range resolution down to the order of the carrier wavelength. This opens the possibility to determine not only the fractional phase of SAR interferograms, but also the absolute phase value including the unknown number of integer phase cycles. This possibility enormously helps all interferometric applications such as DEM generation or land surface motion determination. Here we review the basic theory of such processing techniques and show a number of recent results from an ESA study aimed at developing an operational system. Furthermore we show how such techniques can be optimized by the use of customized dasiasplit-bandwidthpsila chirp signals in place of the standard chirps used in contemporary SAR systems. [C1149]

#### "Recent experiments in Ocean remote sensing with bistatic radar using Navigation Satellite Signals"

This paper will present results from a recent airborne campaign to collect and analyze reflected Global Navigation Satellite System (GNSS-R) signals. The objective of this experiment was to test the GNSS Instrument for Multistatic and Occultation Sensing (GISMOS) and provide additional data for comparison of GNSS-R sea roughness retrievals with in situ measurements. Raw sampled data from the direct GPS signal (using a conventional navigation antenna) and the reflected signal (both right and left-hand circularly polarized nadir antennas) were recorded at both the L1 (1575.42 MHz) and L2 (1227.6 MHz) frequencies. These signals were post-processed using a software-defined radio. Low cost consumer gaming processors were reprogrammed to efficiently generate Delay-Doppler maps (DDMs). A scattering model was then fit to these DDMs in order to estimate the upwind and cross-wind slope variances and the principal axis direction. Initial results suggest a sensitivity to wind direction. [C1150]

#### "Next-generation spaceborne Cloud Profiling Radars"

One of the instruments recommended for deployment on the Aerosol/Cloud/Ecosystems (ACE) mission is a new advanced Cloud Profiling Radar (ACE-CPR). The atmospheric sciences community has initiated the effort to define the scientific requirements for this instrument. Initial studies focusing on system configuration, performance and feasibility start from the successful experience of the Cloud Profiling Radar on CloudSat Mission (CS-CPR), the first 94-GHz nadir-looking spaceborne radar which has been acquiring global time series of vertical cloud structure since June 2, 2006. In this paper we address the significance of CloudSat's accomplishments in regards to the design and development of radars for future cloud profiling missions such as EarthCARE and ACE. [C1151]

#### "CoReH2 O-Cold Regions Hydrology High-resolution Observatory"

The COld REgions Hydrology High-resolution Observatory (CoRe-H2O) satellite mission has been selected for scientific and technical studies within the ESA Earth Explorer Programme. The mission addresses the need for spatially detailed snow and ice observations in order to improve the representation of the cryosphere in climate models and to improve the knowledge and prediction of water cycle variability and changes. CoRe-H2O will observe the extent, water equivalent and melting state of the snow cover, accumulation and diagenetic facies of glaciers, permafrost features, and sea ice types. The sensor is a dual frequency SAR, operating at 17 GHz and 9.6 GHz, VV and VH polarizations. This configuration enables the decomposition of the scattering signal for retrieving physical properties of snow and ice. [C1152]

#### "A ground-based real-aperture radar instrument for differential interferometry"

Radar differential interferometry was initially developed using satellite SAR sensors due to the requirements for precise control and knowledge of the interferometric baseline. The development of ground-based radar imaging systems extends this technology to obtain essentially continuous deformation measurements at high spatial resolution. Applications requiring near real-time deformation measurements such as monitoring of landslides, glaciers, and mining can benefit from this technology. We describe a real-aperture ground-based radar system operating at 17.2 GHz developed by Gamma Remote Sensing. Results for observations of landslides, glaciers and a dam in the Alps are presented. Sources of positional and deformation error including decorrelation and

atmospheric phase delay along with strategies for reduction of these errors are discussed. [C1153]

### "Integrated atmospheric profiling for satellite communication"

Future satellite communication will put a strong demand on the use of high frequencies. In such case the satellite signal will be more susceptible to small scale properties of the atmosphere it is passing through. To understand and predict this impact long term experiments are needed. This paper describes the state-of-the-art of ground based remote sensing of clouds. The work is based on experiments at the Dutch multi-instrumental CESAR research site for atmospheric processes. [C1154]

### "Scatterometer and ScanSAR soil moisture observations of the contiguous United States"

Soil moisture has been identified as a land surface parameter of great importance in various fields of application. Based on long-term time series data of various radar sensors, change detection methods for scatterometer and ScanSAR data are presented. After data processing and model parameter estimation, individual radar backscatter measurements are compared to references describing location specific backscatter conditions representing dry and wet surface soil moisture. Using exponential filtering, also profile soil moisture can be calculated. The method have been implemented in a fully automatic data processing chain for soil moisture retrieval for ERS-1/2 and MetOp ASCAT data and Envisat ASAR ScanSAR data. Various validation studies showed good agreement between the remotely sensed soil moisture products and reference data. [C1155]

### "Using satellite radar data to map and monitor variations in Great Lakes ice cover"

Satellite-borne radars, including synthetic aperture radar (SAR) and scatterometer data, are used to classify and map Great Lakes ice cover and to derive freeze-up date, breakup date, and ice cover duration. These are important indicators of regional climatic conditions. [C1156]

### "The green Sahara: Climate change, hydrologic history and human occupation"

Archaeology can provide insight into interactions of climate change and human activities in sensitive areas such as the Sahara, to the benefit of both disciplines. Such analyses can help set bounds on climate change projections, perhaps identify elements of tipping points, and provide constraints on models. The opportunity exists to more precisely constrain the relationship of natural solar and climate interactions, improving understanding of present and future anthropogenic forcing. We are beginning to explore the relationship of human occupation of the Sahara and long-term solar irradiance variations synergetic with changes in atmospheric-ocean circulation patterns. Archaeological and climate records for the last 12 K years are gaining adequate precision to make such comparisons possible. We employ a range of climate records taken over the globe (e.g. Antarctica, Greenland, Cariaco Basin, West African Ocean cores, records from caves) to identify the timing and spatial patterns affecting Saharan climate to compare with archaeological records. We see correlation in changing ocean temperature patterns ~ contemporaneous with drying of the Sahara ~6 K years BP. The role of radar images and other remote sensing in this work includes providing a geographically comprehensive geomorphic overview of this key area. Such coverage is becoming available from the Japanese PALSAR radar system (Paliou, et. al., 2007), which can guide fieldwork to collect archaeological and climatic data to further constrain the climate change chronology and link to models. Our initial remote sensing efforts concentrate on the Gilf Kebir area of Egypt. [C1157]

### "The tandem-L mission proposal: Monitoring earth's dynamics with high resolution SAR interferometry"

Tandem-L is a proposal for an innovative interferometric and polarimetric radar mission that enables the systematic monitoring of dynamic processes on the Earth surface. Important mission objectives are global forest height and biomass inventories, large scale measurements of millimetric displacements due to tectonic shifts, and systematic observations of glacier movements. The innovative mission concept and the high data acquisition capacity of Tandem-L provide a unique data source to observe, analyze and quantify the dynamics of a wide range of mutually interacting processes in the bio-, litho-, hydro- and cryosphere. By this, Tandem-L will be an essential step to advance our understanding of the Earth system and its intricate dynamics. This paper provides an overview of the Tandem-L mission concept and its main application areas. Performance predictions show the great potential of Tandem-L to acquire a wide range of bio- and geophysical parameters with high accuracy on a global scale. Innovative aspects like the employment of advanced digital beamforming techniques to improve performance and coverage are discussed in detail. [C1158]

### "RADARSAT-1 deformation time-series generation by using the SBAS-DInSAR algorithm"

We have extended the deformation time-series generation capability of the small baseline subset (SBAS) DInSAR algorithm to the SAR data collected by the RADARSAT-1 sensor. The selected SBAS algorithm relies on conventional multi-look interferograms characterized by small temporal and spatial baseline values. We present in this work the first results achieved by exploiting the implemented RADARSAT-1 SBAS-DInSAR processing chain. The investigated test site is the area of New Orleans and its surroundings, for which a RADARSAT-1 archive of 27 acquisitions, spanning the time interval between December 2004 and March 2007, has been processed. The presented results demonstrate the effectiveness of the RADARSAT-1 SBAS-DInSAR processing chain. [C1159]

#### "Cold region hydrology high-resolution observatory (CoReH2 O): A new microwave earth explorer core mission candidate"

The CoReH2O mission focuses on spatially detailed observation of global snow, ice and water cycle parameters using a SAR at X- and Ku-bands in regions where snow and ice play a major role in the water and energy cycles as well as in biospheric processes. Two parallel industrial studies at phase 0 level have been awarded respectively to Astrium GmbH and Thales Alenia Space-Italy. This paper presents the resulting system concepts as elaborated by the industrial teams. The result of the phase 0 has been presented to the user community in January 2009 in Lisbon together with other Earth Explorer candidates for further down-selection. If successfully selected after phase 0 and phase A, CoReH2O will be launched during 2016. [C1160]

#### "Ground validation of satellite measurements of precipitation with C-band polarimetric radar"

Ground validation is an essential part of all satellite precipitation missions aiming to describe clouds and precipitation parameters. It helps to characterize errors, quantify measurement uncertainty, and provide insight into the physical and statistical basis of the retrieval algorithms. Dual-polarization weather radar is a very powerful tool for many important issues of the validation process. This paper presents various aspects considered to develop C-band dual-polarization weather radar products specifically tailored for ground validation of precipitation satellite measurements. Examples are provided by case studies observed with the CNR-ISAC Polar 55C radar operating in Rome (Italy). [C1161]

#### "The combined effect of surface rain and wind on scatterometer observations of surface roughness"

Changes in the sea surface roughness from the combined effects of wind and rain, on scales of tens of kilometers, are being studied using the QuikSCAT scatterometer and simultaneous NEXRAD three-dimensional measurements of rain within Hurricane Claudette. Buoys, NOAA HRD H\*Winds and related data provide the additional wind information. From the remote sensing perspective, these results will show the dependence of the sea surface radar cross section, at Ku-band, as a function of the rainrate, wind speed and relative direction, and polarization. At this microwave frequency the surface backscatter is controlled by the centimeter-scale roughness, but at these high wind speeds the simple models based on Bragg scattering are not useful. In order to study the air-sea interaction that is related to surface fluxes (e.g., momentum, sensible heat, and latent heat) during rain events, extended experimental investigations are needed. Heavy rain in the boundary layer changes the profiles of wind and stratification which alter the surface stress and turbulent heat fluxes. The wind driven rain also creates roughness properties that need to be modeled in order to interpret the Kuband NRCS at the two polarizations. When high winds also exist (>20 m/s), the interaction is complicated by sea spray. [C1162]

#### "THE TanDEM-X Mission: Overview and status"

TanDEM-X (TerraSAR-X add-on for digital elevation measurements) is an innovative spaceborne radar interferometer mission that will be launched in autumn 2009. This paper gives an overview of the TanDEM-X mission concept, summarizes the basic products, illustrates the achievable performance, and provides some examples for new imaging modes and applications. [C1163]

#### "A scatterometer for XOVWM, the Extended Ocean Vector Winds Mission"

This paper presents a designs for a scatterometer satisfying the performance requirements set by the National Research Council Decadal Review in its description of the Extended Ocean Vector Winds Mission (XOVWM). Our design consists of a Ku and C-band pencil-beam scatterometer system coupled with an X-band polarimetric radiometer. Multiple frequencies allow us to achieve all winds and all-weather capabilities, and we achieve high spatial resolution thanks to an onboard SAR processor. We present examples of significant improvements in performance that can be achieved by this next-generation system compared with current ocean vector winds instruments. [C1164]

### "The TropSat mission: An observatory for mesoscale convective system processes in the global tropics"

A satellite mission is proposed to provide frequent, high-resolution measurements of surface winds, rain, and temperature profiles to support critical observations of mesoscale convective systems (MCS) over the global tropical oceans. The proposed mission includes an innovative active/passive microwave system coupled with IR cloud top measurements for multi-layer atmosphere observations. The TropSat system will provide frequent, high-resolution measurements of the near-surface wind vector and rain rate over the tropical oceans. The sensor design is based on the proven technology of SeaWinds but includes key innovations and an integral radiometer. The main sensor will include: (1) dual-band (C- and Ku-band) and dual beam (inner/outer beams) operation (C- and Ku-band) at multiple polarizations and (2) ground-based post processing to achieve the desired high spatial resolution. Backscatter measurements over land can support vegetation and climate change studies. This paper provides a brief description of the TropSat mission, discusses various instrument and mission tradeoffs, and presents performance estimates to demonstrate the feasibility of the mission concept. [C1165]

### "Coastal wind field and sea state measured by TerraSAR-X"

TerraSAR-X (TSX) is a high resolution right looking radar satellite, launched on June 15, 2007. TSX carries a high frequency X-band SAR sensor that can be operated in different modes (coverage and resolution) and has quad polarization and dual receive antenna mode used for along track interferometry (ATI) experimental acquisitions. [C1166]

### "Simultaneous observations of a tropical cyclone from dual-pol TerraSAR-X and ground-based weather radar"

Recent advances in Synthetic Aperture Radar (SAR) technology have revived meteorological applications with this type of radar. SARs are designed for surface imaging, but now that several X-band, multi-polarization SAR satellites are in orbit, the attenuation and backscatter change caused by precipitation can be better studied. The results presented here demonstrate some of the possibilities by analyzing observations from dual-polarization (HH, VV) TerraSAR-X acquisitions over central Florida during and after Tropical Storm Fay on August 19, 2008. Simultaneously, WSR-88D ground weather radars in Melbourne and Tampa Bay, FL collected reflectivity and radial velocity data from the storm where a strong precipitation cell is roughly co-located with severe attenuation in the SAR image. The SAR measurements are explained quantitatively by simultaneous ground radar observations. In addition, polarization analysis comparing the SAR image a subsequent TerraSAR-X acquisition 11 days later shows the impact of the storm over the entire image. [C1167]

### "BIOMASS: A P-band SAR earth explorer core mission candidate"

The greatest uncertainties in the global carbon cycle involve estimating how carbon dioxide is taken up by land. The BIOMASS mission aims to improve the present assessment and future projection of the terrestrial carbon cycle by providing consistent global maps of forest biomass and forest area, forest disturbances and recovery with time, and the extent and evolution of the forest flooding. The BIOMASS primary objectives can be achieved through P-band (435 MHz) synthetic aperture radar (SAR) observations of global forest cover. Two parallel industrial studies at phase 0 level were awarded respectively to Astrium GmbH and Thales Alenia Space Italy. This paper presents the resulting system concepts as elaborated by the industrial teams. The result of the phase 0 was presented to the user community in January 2009 in Lisbon together with other Earth Explorer candidates for further down-selection. If successfully selected after phase 0 and phase A, BIOMASS will be launched during 2016. [C1168]

### "Picosecond pulse generation on CMOS: Design beyond transistor limits"

Nonlinear transmission media can be used for high amplitude, narrow pulse generation. We developed the theory of pulse generation in one- and two-dimensional transmission lattices. We used a conventional CMOS process to fabricate these lattices. Using these structures, it is possible to generate signals with a bandwidth of more than the cut-off frequency of the fastest transistor on the same process. We showed a 2-D nonlinear lattice that can generate pulses as narrow as 1 psec with an amplitude of more than 3V by using nonlinear constructive interference in a conventional 130 nm CMOS process. [C1169]

### "Tm:germanate fiber laser for planetary water vapor atmospheric profiling"

The atmospheric profiling of water vapor is necessary for finding life on Mars and weather on Earth. The design and performance of a water vapor lidar based on a Tm:germanate fiber laser is presented. [C1170]

### "SMOS image reconstruction algorithm: Extension of the band limited approach to the fully-polarimetric mode of MIRAS"

It is now well established that synthetic aperture imaging radiometers (SAIR) promise to be powerful sensors for high-resolution observations of the earth at low microwave frequencies. Within this context, the European Space Agency is currently developing the SMOS mission devoted to the monitoring of soil moisture and ocean salinity at global scale from Lband space borne radiometric observations obtained with a two-dimensional interferometer. This contribution is concerned with the reconstruction of radiometric brightness temperature maps from interferometric measurements. It extends the concept of band-limited resolving matrix to the case of the processing of full-polarimetric data. [C1171]

### "Filter of LIDAR Data Based on Multi-Resolution and Directional Elevation Tolerance"

Based on studying the principle of wavelet multi-resolution analysis, this paper takes Wavelet into the LIDAR filtering, by making use of pyramid-delaminating theory, the fast organization of raw DSM data comes true, while the computing speed increases and the filtering speed improves. At the same time, by considering the directional elevation tolerance of the whole region in the process of filtering threshold selection, judgement makes better accordance with terrain, and the precision of filtering is improved. At last, experiment is carried out on DSM data obtained by LIDAR, the result proves the validity and advantage of the advanced filtering method. [C1172]

### "A multi-functional fiber laser lidar for Earth Science & Exploration"

A multi-pixel laser altimeter using pseudo-random-noise-modulated fiber lasers has been developed under a NASA Instrument Incubator Program. We will present the instrument design, field campaign results and implementations for Earth Science Decadal Missions and Exploration. [C1173]

### "Remote detection of aluminum and trace methane using mobile femtosecond laser system of T&T Lab"

We report two remote sensing experiments of aluminum in the winter time and trace methane in the summer time using the mobile femtosecond laser facility T&T (Terawatt & Terahertz) designed by the Defence R&D Canada-Valcartier (DRDC-Valcartier). This system is similar in many respects to Teramobile, the Franco-German laser system. In the first experiment, we demonstrated the feasibility of remote filament-induced breakdown spectroscopy of aluminum targets in an open field in the winter season of Quebec-city when the outside temperature was as low as -20degC. The fluorescence signals are detected in a LIDAR configuration with aluminum target located up to 60 meters. In the second experiment in the summer season, we remotely detected trace methane in the open field during daytime (with strong sun light) up to 20 meters. [C1174]

### "Modified PN codes for laser remote sensing measurements"

We describe a modified pseudo noise code for laser remote sensing measurements. Our experiments show it improves receiver signal to noise ratio and time resolution and is well suited for lasers with limited peak power. [C1175]

### "Design of Wireless Environmental Monitoring Data Acquisition System Based on Cortex"

Remote environmental monitoring often has the characteristics of monitoring points widely distributed, large numbers, long distance, individual collection points in remote areas, etc. In the past, the manner of remote environmental monitoring data acquisition that staff operate in person on the spot is extremely inconvenient. In order to solve the problems produced in the manner above, we design the Cortex-M3-based wireless environmental monitoring data acquisition system, which has the following excellent features: It adopts a high cost-performance chip based on Cortex-M3 core; Pre-terminal, integrated into a circuit board, has small volume, take up less space, and can work without any special requirements for the environment; System can automatically restart; Power supply designed for the system can reduce the interference on the circuit from external AC voltage, and lower the interference from high frequency entering through power supply; It can be applied to multi-channel data acquisition information monitoring system. [C1176]

### "Achieving the Real-time rectification of remote sensing data based on 4S integration in handset"

This article introduced the design and implementation of real-time correcting remote sensing data based on the handset witch integrated 4S functions. Introduced the function and status quo of the 4S integrated system, given the development environment and related technologies of the 4S integrated handset correcting remote sensing data, explored the design method of the system's hardware and software. Using appropriate optimization

algorithm to load remote sensing data fast, using GIS map overlay to collect real-time high-precision GPS geo-data, it can collect real-time, accurate mass of GPS information, achieve the accurate corrective of the remote sensing map, then send the corrected real-time data to the center through GPRS module with embedded TCP/IP protocol. Combined with the advance of the WINCE system and the integrated development environment EVC perfect supports for the GDI interface, it can facilitate the design of correcting system, easy operation for user, become an extremely important field of the handheld device in field prospect. [C1177]

#### "Interpretation target pattern of a buried basic object on Surface Ground Penetrating Radar system"

Surface ground penetrating radar (GPR) is the one of radar technology that is widely used on many applications. It is non-destructive remote sensing method to detect underground buried objects. However, the output target is only hyperbolic representation. This research tries to enhance GPR capability by representing the visual/pattern of the detected target. GPR data of many basic objects (with circular, triangular and rectangular cross-section) are classified and extracted to generate data training model as a unique template for each type basic object. The pattern of object under test will be known by comparing its data with the training data using a decision tree method. A simple powerful algorithm to extract feature parameters of object which based on linear extrapolation is proposed. The result shown that tested buried basic objects can be correctly interpreted. [C1178]

#### "SEC: Stochastic Ensemble Consensus Approach to Unsupervised SAR Sea-Ice Segmentation"

The use of synthetic aperture radar (SAR) has become an integral part of sea-ice monitoring and analysis in the polar regions. An important task in sea-ice analysis is to segment SAR sea-ice imagery based on the underlying ice type, which is a challenging task to perform automatically due to various imaging and environmental conditions. A novel stochastic ensemble consensus approach to sea-ice segmentation (SEC) is presented to tackle this challenging task. In SEC, each pixel in the SAR sea-ice image is assigned an initial sub-class based on its tonal characteristics. Ensembles of random samples are generated from a random field representing the SAR sea-ice imagery. The generated ensembles are then used to re-estimate the sub-class of the pixels using a weighted median consensus strategy. Based on the probability distribution of the sub-classes, an expectation maximization (EM) approach is utilized to estimate the final class likelihoods using a Gaussian mixture model (GMM). Finally, maximum likelihood (ML) classification is performed to estimate the final class of each pixel within the SAR sea-ice imagery based on the estimated GMM and the assigned sub-classes. SEC was tested using a variety of operational RADARSAT-1 and RADARSAT-2 SAR sea-ice imagery provided by the Canadian Ice Service (CIS) and was shown to produce successfully segmentation results that were superior to approaches based on K-means clustering, Gamma mixture models, and Markov Random Field (MRF) models for sea-ice segmentation. [C1179]

#### "IceSynth: An Image Synthesis System for Sea-Ice Segmentation Evaluation"

An ongoing challenge in automatic sea-ice monitoring using synthetic aperture radar (SAR) is the automatic segmentation of SAR sea-ice images based on the underlying ice type. Given the intractability of obtaining ground-truth segmentation data from polar regions, the evaluation of automatic SAR sea-ice image segmentation algorithms is generally limited to tests using real SAR imagery based on pseudo-ground truth data (e.g., manual segmentations) and simple synthetic tests using basic shape primitives. As such, it is difficult to evaluate automatic segmentation algorithms in a systematic and reliable manner using realistic scenarios. To tackle this issue, a novel image synthesis system named IceSynth is presented, which is capable of generating a variety of synthetic sea-ice images that are representative of real SAR sea-ice imagery. In IceSynth, SAR sea-ice textures for each ice type are synthesized via stochastic sampling based on non-parametric local conditional texture probability distribution estimates. A stochastic sampling approach based on non-parametric local class probability distribution estimates is used to generate large-scale sea-ice structures of various ice types based on ice classification priors extracted from real SAR sea-ice imagery. Experimental results show that IceSynth is capable of generating realistic-looking SAR sea-ice images that are well-suited for performing objective evaluation of SAR sea-ice image segmentation algorithms. [C1180]

#### "SAR Image Processing Based on Fast Discrete Curvelet Transform"

Curvelet transform is a new kind of multiscale analysis algorithm which is more suitable for image processing, as compared with Wavelet it can better analysis the line and curve edge characteristics, and it has better approximation precision and sparsity description, also has good directivity. This paper introduces that remote sensing image speckle reduction based on Curvelet transform. Synthetic Aperture Radar (SAR) image is easily polluted by speckle noise, which can affect further processing of SAR image. This paper put forward method of SAR image speckle deduction based on Fast Discrete Curvelet Transform (FDCT). This method firstly transform SAR image to Curvelet domain by using FDCT, and get the Curvelet coefficient, then estimate the Curvelet

coefficient threshold of different scale and direction by using adaptive threshold method, treatment on Curvelet coefficient with hard threshold and soft threshold respectively, and the last recovery the original image by using IFDCT. This paper uses this method to single-look SAR image and compare with Wavelet de-noising method, the result shows that the effect of Curvelet flitting is better than Wavelet flitting, and the soft threshold is better than hard threshold. [C1181]

### "Application of the Marine Oil Spill Surveillance by Satellite Remote Sensing"

Oil spill accidents are seen relatively frequent and becomes a severe threat to coastal and marine ecosystems and water quality. Thus, active surveillance and rapid response to marine oil spills is important and essential to environment protection. So, this paper lays emphasis on the research of monitoring the marine oil spills for application by satellite remote sensing especially SAR. Imaging characteristics of satellites and image-forming principle of oil spill information in remote sensing images are analyzed at first. Then how to monitor the marine oil spills by satellite remote sensing and how to identify and detect marine oil spills information in SAR images are discussed mainly. Through the practical applications examples of the marine oil spill surveillance by satellite remote sensing in oil spill accidents of oil tanker "Hebei Spirit", the method this paper proposed is proved to be very effectively and feasibly for the fast response and detection to oil spills especially in the waters near Bohai sea of China. Finally future development of marine oil spill surveillance is suggested with conclusion. [C1182]

### "Developments of GNSS Radio Occultation for Sounding Atmosphere"

Compared to traditional radiosonde and radar probing, the Global Navigation Satellite System radio occultation (GNSS RO) is a powerful tool for atmospheric sounding, which have many traits such as no calibration, all-weather, almost uniform global coverage, high precision and vertical resolution. In this paper, investigative actuality which we make use of GNSS RO technique get atmosphere parameters like temperature, air pressure and humidity is introduced. At the same time, development direction of GNSS RO in the weather domain is put forward, undoubtedly, it will boost up use of GNSS RO technique for global climate. [C1183]

### "Performance of evaluation methods in image fusion"

Many algorithms and software tools have been developed for fusing panchromatic and multispectral datasets in remote sensing. Also, a number of methods has been proposed and developed for the comparative evaluation of fusion results. To this date, however, no papers have been published that analyze effectiveness and quality of the evaluation techniques. In our study, methods that evaluate fusion quality are tested for different images and test sites. This analysis shows that in most cases the tested methods perform well, but are sometimes inconsistent with visual analysis results. [C1184]

### "Monitoring Co-seismic Deformation Fields of Bam Earthquake Using D-InSAR Technique"

The Mw=6.5 Bam earthquake, taking place on 26th December 2003 in Iran, caused severe surface deformation. This paper described that it used the differential interferometric SAR (D-InSAR) technique and ENVISAT ASAR data to monitor the Bam co-seismic deformation fields. Firstly, it introduced the principle of D-InSAR and the method to select proper D-InSAR data pairs. Then we used ENVISAT ASAR data to carry out D-InSAR test in the Bam earthquake. We successfully got the Bam co-seismic deformation field. The shape and location of the fault caused by the Bam earthquake was also found in the coherence maps. The test proved that D-InSAR technique is a powerful tool to measure surface deformation and to study earthquake. [C1185]

### "Using LiDAR Data Visualization to Investigate Origin of Uphill-Facing Scarps in Mountains, Alaska"

Light Detection and Ranging (LIDAR) is a fast method for sampling the earth's surface with a high density and high accuracy point cloud that is used to generate high density and high accuracy Digital Elevation Models (DEMs) and DSMs. In this research we obtained airborne LIDAR elevation data with spatial resolution of 1 m to reveal new details of mountain block morphology and structure to investigate the origin of uphill facing scarps. Quaternary fault scarps occur in several mountain blocks in the western Saint Elias and Eastern Chugach Mountains of southern Alaska. Possible mechanisms for formation of these scarps include deformation caused by active folding, or deformation caused by gravitational loading and strong ground motion during earthquakes. The field observations and LIDAR visualization lead us to propose a three-stage model for flexural toppling. Failure is by flexural toppling, with rotation and shearing of bedding planes under the influence of gravity where bedding dips steeply into the mountain side. Down-slope bending of bedding surfaces may initiate formation of a basal sliding surface beneath the toppled beds, leading to landsliding down slope. However, horizontal acceleration caused by strong ground motion enhances the probability of failure by flexural toppling, especially in the upper

parts of mountain slopes, where ground motion is amplified. [C1186]

### "Application Study of PS-DInSAR Technique Fusing Multi-metadata in Urban Ground Deformation Survey"

PS-DInSAR technique fusing multi-metadata and its basic flow are expounded considering limitations of conventional D-InSAR in atmospheric delay and space-time decoherence. It is held that multi-metadata helps to weaken the influence of systematic error and improve the surveying precision and model steadiness of PS-DInSAR. Tianjing City is surveyed in PS-DInSAR fusing ENVISAT ASAR from 2003 to 2007, GPS, SRTM3-DEM and leveling data, which greatly weakens the influence of atmospheric delay, space-time decoherence and systematic error. The precise deformation of the studied area in that period is obtained. [C1187]

### "Airborne measurements of CO<sub>2</sub> column absorption using a pulsed wavelength-scanned laser sounder instrument"

We have demonstrated airborne measurements of CO<sub>2</sub> column absorption at 1571.4 nm from 10 km altitudes with a wavelength-scanned lidar using a pulsed diode-seeded EDFA transmitter and a photon counting receiver. [C1188]

### "Atomic oxygen detection using radar REMPI"

We use a microwave scattering based resonantly enhanced multi-photon ionization scheme for monitoring the concentration of oxygen atoms in a flame. This technique allows for remote investigation of concentration of atomic species with nanosecond resolution. [C1189]

### "Synthetic aperture imaging at optical wavelengths"

Optical implementations of synthetic aperture imaging techniques provide a method of overcoming the platform constrained diffraction limit for optical imaging systems. We discuss progress in applying these methods to outdoor imaging demonstrations. [C1190]

### "Performance enhancement of pulsed solid state power amplifier using Drain Modulation over Gate Modulation"

The study was conducted to compare the RF parameters of pulsed solid state power amplifier using drain modulation and gate modulation and thereby to analyze the impact of modulations on the pulsed performance. To establish this, the C-band pulsed SSPA is designed, fabricated and tested at 5.35 GHz frequency with 225 MHz bandwidth using two different methods of modulation techniques, implemented on electronic power conditioner. The performance of two modulation techniques is compared for different RF parameters. The test results of drain and gate modulated pulsed solid state power amplifier are discussed at length for identical dc operating conditions and based upon the measured performances, conclusion are derived. This pulsed microwave solid state power amplifier can be used by pulsed RADAR community for the development of space borne RADAR like synthetic aperture radar, altimeter etc. for microwave remote sensing applications. [C1191]

### "Automatic reconstruction of cities from remote sensor data"

In this paper, we address the complex problem of rapid modeling of large-scale areas and present a novel approach for the automatic reconstruction of cities from remote sensor data. The goal in this work is to automatically create lightweight, watertight polygonal 3D models from LiDAR data (Light Detection and Ranging) captured by an airborne scanner. This is achieved in three steps: preprocessing, segmentation and modeling, as shown in Figure 1. Our main technical contributions in this paper are: (i) a novel, robust, automatic segmentation technique based on the statistical analysis of the geometric properties of the data, which makes no particular assumptions about the input data, thus having no data dependencies, and (ii) an efficient and automatic modeling pipeline for the reconstruction of large-scale areas containing several thousands of buildings. We have extensively tested the proposed approach with several city-size datasets including downtown Baltimore, downtown Denver, the city of Atlanta, downtown Oakland, and we present and evaluate the experimental results. [C1192]

### "A Study on Quantitative Radar Rainfall Measurements by the Method of Set-pair Analysis"

This paper introduces the basic principles of Set-pair Analysis, and presents a method of applying Set-pair Analysis in determining the two parameters of  $Z \sim I$  relationship of radar rainfall measurement. This method is then applied in the Baillianhe catchment. After a comparative study between the Set-pair Analysis and the

traditional method of CTF, a conclusion is made that, compared with the traditional method of CTF, the parameters selected by Set-pair Analysis can produce better rainfall results. It can not only improve the precision of the total accumulated rainfall, but also decrease the bad effect that the irrational radar reflectivity and actual measured rainfall data pairs brought to parametric optimization. At the same time, it improves the fitting precision of the rational data, which consequently improves the rationality of the two parameters. [C1193]

### "New approach of imagery generation and target recognition based on 3D LIDAR data"

Light Detection and Ranging (LIDAR) sensor is an advanced technology of 3D-measurement with high accuracy. The processing of 3D point cloud data collected via LIDAR sensor is of topical interest for 3D target recognition. In this paper, a new approach of imagery generation and target recognition based on 3D LIDAR data is presented. The raw 3D point cloud data are transformed and interpolated to be stored in 2D matrix. The target imagery is generated and visualized by means of height-gray mapping principle proposed in paper. For different poses of target, the affine invariable moments of target imagery are selected as features for recognition because of its invariance in rotation, scaling, translation and affine transformation. BP neural network algorithm and Support Vector Machine (SVM) algorithm are utilized as method of target classification and recognition. The recognition results by two algorithms are compared against and analyzed detailedly. The new method had been applied into target recognition in outdoor experiments. Different types of targets are classified and the rate of correct recognition is greater than 95%. Through outdoor experiments, it can be proven that this new method is applied to the field of 3D target recognition effectively and stability. [C1194]

### "Rapid Calculation Research on Water Area Extraction from ASAR Image"

Flooded area is a piece of the most important information we have got to know in flood supervision and disaster evaluation. And water area extraction is one of the decisive preconditions in confirming the size of flooded areas. With the appearance of remote sensing technology, people could extract the water areas from the space, and the radar images gotten from the flooded area provide us the exact size of water areas. However, the speed of water area extraction affects flood evaluation directly, which matters a lot to the rescue work after flood. To shorten the extracting time of water areas, parallelization process is used as one of the most efficient ways. Based on some normal methods frequently used in water area extraction, such as threshold method, NDVI, and so on, a new way is put forward, that is, to use Self-organized Feature Map to extract the water areas from ASAR images automatically and accurately, and then to analyze the SOM calculation flows to find out what influences the extraction speed, finally to optimize the calculation by using parallel I/O of parallel file system and the asynchronous parallel model of I/O hidden strategy. All of the above enhances the calculation speed so as to ensure that the subsequent flood evaluation and rescue work can be carried out as soon as possible. [C1195]

### "Design and application of dielectrically scaled double-ridged horn antennas for biomedical UWB radar applications"

Ultra-wideband sensing begins to play an important role in biomedical diagnostic systems. Promising and relevant applications include remotely monitored vital functions as well as the characterization of tissues and organs. The acquisition of such physiological signatures requires small and radiation-efficient antennas, designed for ultra-wideband frequency operation. We have developed physically small and adjustable double-ridged horn antennas with which we could demonstrate the specific advantages of miniaturized, dielectrically matched sensor elements in a direct mode compared to remote sensor applications. As a logical consequence of these results, we have considered to replace the lossy high-permittivity liquid by low-loss high-permittivity solid ceramic material to improve the degree of miniaturization and the radiation efficiency further. Some unexpected peculiarities related to this approach are discussed. [C1196]

### "Close range hyperspectral and lidar data integration for geological outcrop analysis"

The use of spatial data collection techniques in geology has increased significantly in recent years, with methods such as laser scanning (lidar) becoming popular. However, the remote mapping of rock properties within the geological outcrops remains a major challenge. This study develops a workflow for combining and utilising ground based hyperspectral and laser scanning data. This workflow is presented for two case studies, each with different geological settings and mineral composition. Multiple hyperspectral and lidar scans were acquired to gain both spectral and geometric data. Mixture Tuned Matched Filtering was utilised to extract and map geological features from the spectral images, resulting in thematic images. This combination of geometrically accurate lidar data and spectral mapping of lithology has significant implications for the improved collection of geological data. [C1197]

### "High resolution current & bathymetry determined by nautical X-Band radar in shallow waters"

The wave and current monitoring system WaMoS II is a remote sensing system based on a nautical X-Band radar generally used for navigation and ship traffic control. It has been used in recent years to monitor sea state information from moored platforms, coastal sites and moving vessels. A nautical radar can scan the sea surface over a large area (~ 10 km<sup>2</sup>) with a high spatial (~7.5 m) and temporal resolution (~2s). Directional wave spectra and standard sea state parameters such as significant wave height, peak wave period and direction can be derived by analyzing the sea surface image sequences. Using the temporal and spatial evolution of the sea surface wave images it is also possible to determine high resolution current and bathymetry information. In the paper a brief introduction into the measuring principle of WaMoS II is given and results of a high resolution current and bathymetric mapping technique for shallow water areas (<20 m) are presented. For validation these results are compared with model data and in-situ measurements. [C1198]

### "Simulation of the radar observation of a sea patch using the TLM electromagnetic method"

We propose the simulated rendition of the observation of a variety of small sea patches by radar. These patches include a random sea surface of variable state, with possibly the presence of a manufactured, metallic object in its middle. The simulation in itself draws upon two different techniques which are combined: for the free-space propagation, a simple geometrical ray tracing method is used. On the other hand, we rely on a discrete calculation of the propagation of the electromagnetic waves in the vicinity of the sea surface, using the TLM method. Different aspects of this particular electromagnetic method are discussed in this paper. The originality of the approach is the combination of a geometrical calculation with a discrete, exact computation, each of them being devoted to a precise part of the simulation. Further matter in the article extends onto the explanation of some techniques developed for the need of our study, presentation and annotation of some results along with computation times, and overall discussion. [C1199]

### "HF radar role in an integrated ocean observing system"

The Australian Coastal Ocean radar Network (ACORN) is a monitoring network of HF radars which are being installed around Australia under a National Collaborative Research Infrastructure Strategy (NCRIS). It is a five-year project, at the end of which there will be five pairs of radar stations and one triplet installed and operating, enabled by the central pool of funding for the Integrated Marine Observing System (IMOS) which is a part of NCRIS, and augmented by funding from other sources. At each chosen site there is a pair (or triplet) of radar stations, mounted on the shore, which receive radar echoes from the rough sea. The two stations provide a triangulation which enables the data analysis software to extract surface currents, wave heights and directional wave spectra over the coastal ocean. The NCRIS strategy is to support research into coastal dynamics and exchange between the open ocean and the continental shelf. Research is being undertaken into the use of maps of surface currents, well resolved in time and space, in mixing of different bodies of water, physical connectivity between reefs and islands, and nowcasting and short-term forecasting of surface currents. There is potential for application of the data to management of coastal marine resources, and in marine safety areas. Real-time maps of surface currents and the prospect of short-term forecasting have the potential to reduce search areas in coastal waters and to make pollution/spill mitigation more effective. With the establishment of HF radar monitoring stations like those in ACORN, there is growing opportunity for researchers around the world to access data from well curated archives to carry out basic research on physical oceanography, or applications research without having direct access to the measuring facility. One of the features of IMOS is to establish such an archive which is easy to access and free to research users. This feature brings the ACORN HF radars into GEOSS for coastal processes and dynamics. [C1200]

### "Optical design for in-line typed compact lidar"

An in-line typed lidar optics for short range atmosphere sensing and gas detection was designed. Restricting the receiver's field of view, the signal-to-noise ratio of the in-line typed lidar echo had little change within the measurement range. [C1201]

### "Simulation of morphological measurement system based on FM-CW"

The morphological measurement simulation system based on FM-CW is built and tested. The result of 10 km imaging experiments shows that the range accuracy can reach 1.00 m and that the system has achieved the design goal. [C1202]

### "An application of Geographical Information System and Remote Sensing techniques for detection of oil spill"

Oil spill has become critical in some countries, especially for countries that have seas or oceans like Iraq, Malaysia and others. The situation is caused damage the environment and polluted the water. To reduce environment damage and protect life in water, plants and soil near to disaster area. Study and analysis should be carried out. The causes and factors that lead to the disaster of oil spill should be studied or investigated. Geographical Information System and Remote Sensing can be used to analyze this problem. The aim of the study is to apply Geographical Information System (GIS) and Remote Sensing techniques to determine location and to map oil spill area using Radarsat data. [C1203]

#### **"Hyperspectral data analysis of nitrogen fertilization effects on winter wheat using spectrometer in North China Plain"**

This article presents results from hyperspectral analysis for winter wheat (*Triticum Aestivum* L.) in the North China Plain during a research study in 2006. In the first part the focus was set on canopy spectral reflectance during the vegetation period under different N supplies. Four different experiments with variable N-inputs and winter wheat cultivars were set up in the study area of Huimin County, Shandong Province. Spectral reflectance data and agronomic data like biomass, plant height, N-uptake and LAI were collected at different phenological stages. In the second part of the study a spectral and agronomic library was set up. For this purpose, spectral reflectance was related to agronomic parameters. The results indicated significant difference in spectra characteristics, cultivars and N-inputs. Vegetation indices like NDVI, HNDVI, RVI, HVI, OSAVI and MCARI2 had the best performance in estimating agronomic parameters among the vegetation indices evaluated. [C1204]

#### **"LiDAR-guided analysis of airborne hyperspectral data"**

This paper describes a new framework to the collection and fusion of multisensor airborne LiDAR and hyperspectral data. We describe a data fusion philosophy that provides a spatially precise positioning of hyperspectral data based on discrete first and last return LiDAR data. Three dimensional objects defined by the LiDAR data are then used to sample optimal spectra for subsequent analysis. The sampled spectra retain their positioning metadata and so can be mapped back into geographic space for further analysis. While the paper presents this philosophy within the context of a species classification, other analytical analysis can be performed. [C1205]

#### **"Development of fiber-based CW modulation DIAL system for CO<sub>2</sub> monitoring"**

We have demonstrated the fiber-based CW modulation hard-target Differential Absorption Lidar (DIAL) system for CO<sub>2</sub>sensing. It is shown that stable CO<sub>2</sub>concentration measurement corresponding to 4 ppm(rms) can be realized. [C1206]

#### **"ROSE: development and demonstration of a "Mobile Response Observatory" prototype for subsea environmental monitoring"**

ROSE project was aimed at defining and studying a system for monitoring polluting wrecks based on the deployment of a set of subsea stations integrated in an acoustic network and communicating with shore through a wireless link. The project scope also comprised the building of a prototype system intended for a near shore demonstration of limited duration. This system comprises: two floating measuring stations anchored at sea bottom, a relay buoy and the operating shore station. Station sensors are shared in pollutant sensors and environmental parameter sensors. The prototype system is fitted with: hydrocarbon fluorometer, CTD sensor, back scattering meter, dissolved O<sub>2</sub> sensor and ADCP profiler. The system was deployed in Bay of Douarnenez, at 25 meter during 2.5 months in summer 2006. This deployment enables to draw experience return on at sea operations and system behaviour, data acquisition by the various sensors and operation of the communication system. [C1207]

#### **"Sediment modeling based on radar observed surface hydrodynamics"**

The work we present is an analytical method to estimate the tidal current induced bottom shear stress. The method is based on radar remote sensing measurements and in situ data. The results of the method are irrotational maps of the bottom shear stress and the initiation of motion. [C1208]

#### **"An approach for tracking oil slicks by using active contours on satellite images"**

This paper describes a process for achieving oil spill detection in satellite images acquired after tanker accidents. These images have been treated with image processing techniques, such us image equalization, image binarization and morphological operations, to obtain the residue segmentation. Once the oil slick is segmented and localized in the image, an active contour is generated around it and fitted to it. The active

contour provides useful information about the shape and localization of the oil spill, even providing an estimation of the deformation and the displacement that it could suffer over the time. This information could allow the evolution of residues dumped at sea to be tracked. The validity of this process is demonstrated using several ENVISAT-ASAR images acquired over several regions (Spanish, Philippine and Korean coasts), in which a tanker accident has occurred and as a consequence oil spillage has taken place. [C1209]

### "Sea surface current retrievals using ASAR WVW acquisitions"

In this paper, we present an algorithm aimed at extracting ocean surface current information from SAR acquisitions based on wind information. The acquisitions used to test this algorithm are the Wave Mode Ocean Wave Spectra products, called WVW acquisitions, from ASAR, the C-Band SAR onboard ENVISAT. Parts of this method have already been tested with monthly means. We show here using buoy measurements that this method is able to yield the radial component of sea surface currents. These results will be used as a complement to sea surface current data gathering. [C1210]

### "Web-based GIS dedicated for marine environment surveillance and monitoring"

Maritime and port areas throughout the world are exposed to many different hazards, like pollution, terrorism and natural disasters. Early detection, identification and preparation of appropriate response strategies is especially important in the case of semi-enclosed Basins like the Southern Baltic Sea, mainly due to the marine ecosystems' continuous absorption of pollutants including oil, heavy metals and chemicals. Many of those agents are characterised by great toxicity and cause devastation of the natural environment. The recent development in the information technology provides the means and possibilities for much faster and more efficient access to survey data, allowing their remote, nearly real-time management, processing and visualisation. Several approaches and techniques of measurements are available in marine environment monitoring. These consist of direct sampling, airborne and satellite imagery, hydrological measurements using CTD probes, remote sensing with the use of electromagnetic waves, acoustic methods based on the data acquired by multi-beam and side-scan sonars and single-beam echosounders. The acquisition, processing, integration and visualisation of various kinds of data constitutes an important problem in the context of development of applications supporting littoral environment management. These methods are not easily suited for monitoring threat levels for maritime Critical Infrastructures (CI) like ports and shipyards. However, this field has also been explored, using specialised modules like CARVER2trade or similar systems now easily available not only commercially. The presented system integrates data from all of the aforementioned sources as well as others, like live radar feed and oil spill spread simulation results. The data from the investigated marine region is presented in the form of multiple, time-varying layers, rendered in up to three dimensions. The system allows authenticated end users to remotely view these layers in a geo- graphic context while also providing interactive features like oil spill spread animation and tools for layer query. The CI threat sensing element of the system is being developed in cooperation with the City of Gdansk. The system's application for monitoring water pollution as well as processing, integration and visualisation of various kinds of background and sensor data has been reported recently. The presented system consists of several modules, or subsystems, namely the Data Integration and Adaptation module, the Remotely Accessible GIS and third-party simulation engines, connected through the interface for Simulation Modules. The Data Integration and Adaptation module is developed using the Microsoft .NET platform and the ESRI ArcGIS Engine, which is a set of GIS objects with application programming interfaces (APIs) for COM, .NET, Java, and C++. To provide a common and efficient solution for geospatial data serving via the TCP/IP protocol, the system utilises the ArcSDE application server that facilitates storing and managing spatial data (raster, vector, and survey) in an underlying database. ArcGIS Engine MapControl and GlobeControl components provide a standard set of GIS functionalities like map viewing, zooming and panning for twodimensional and three-dimensional imaging respectively. Interfaces to various external sensors were implemented during the development of the system. The Web-GIS module was developed entirely with the use of Open-Source technology. It utilizes the established GeoServer technology for serving Open Geospatial Consortium's (OGC) standard Web Map Service (WMS) layers and Apache Web Server as the HTTP proxy. Data processing is done by means of custom Java 2 Platform Standard Edition servlets running within the Tomcat Servlet Engine. The browser-independent DHTML client is built with help of the Openlayers Javascript library. The Interface for Simulation Modules allows third-party applications to provide data directly into the Spati [C1211]

### "On the influence of positioning errors on tomography-based sonar imaging systems"

The receiver signal of sonar systems consists of the sum of reflected signals stemming from many scatterers. The resolution of sonar imaging systems depends in range direction on the bandwidths of the transmitter signal and in angular direction on the beamwidth of the receiver antenna. Tomography is a very promising method to improve the resolution of such sonar systems in angular direction. Basically, tomography relies on an appropriate fusion of sonar images of a scene derived from different spatial positions and thus under different viewing angles.

Obviously, knowledge of the exact antenna position during acquisition of the different basic images is substantial for achieving high quality tomography reconstructions. Positioning errors, i.e. differences between real antenna locations and assumed (measured) antenna positions, causes blurring of the reconstructed image of the scene. In this paper the aforementioned image degradations are demonstrated by means of simulation results. Furthermore, basic ideas to reduce the problems caused by positioning errors are presented for a forward looking sonar with tomographic signal processing. [C1212]

#### **"Detection and classification of offshore artificial objects in TerraSAR-X images: First outcomes of the DeMarine-DEKO project"**

The project DEKO (Detection of artificial objects in sea areas) is integrated in the DeMarine-Security project and focuses on the detection and classification of ships and off shore artificial objects relying on TerraSAR-X as well as on RapidEye optical images. The DEKO project has been started in Mai 2008. The main expected outcomes of the DEKO project are 1/ the definition of concepts for GMES downstream services based on the obtained results, 2/ the development of new detection and classification algorithms for the analysis of ships and off shore artificial objects and 3/ the validation of the results w.r.t. the sensor acquisition parameters. This paper presents preliminary results obtained in the early stage of the DEKO project like the state of the art on ship detection and classification in SAR images, the currently implemented detection and classification algorithms as well as the first results obtained for ship detection in TerraSAR-X images. [C1213]

#### **"Accuracy and reliability of ocean current and wave monitoring with the coastal radar "WERA""**

The WERA system (Wave RADar) is a shore based remote sensing system to monitor ocean surface currents, waves and wind direction. WERA is using the lowest noise FMcw technique to provide highest temporal and fine spatial resolution for time critical applications. The vertical polarised electromagnetic wave is coupled to the conductive ocean surface and will follow the curvature of the earth. This over the horizon oceanography radar can pick up back-scattered signals (Bragg effect) up to ranges of more than 200 km. Publications about the results from systems installed all over the world have proved the accuracy of the WERA system. The reliability of these ocean data was studied for more than 2 years at a permanent WERA installation at the French coast near Brest. [C1214]

#### **"Issues and preliminary results in oil spill detection using optical remotely sensed images"**

An approach to oil spill detection is presented using optical satellite images. Features from SAR literature are studied. Different statistical and neural network-based classifiers are used in order to perform a supervised automatic classification and their performances are compared. The promising results achieved on the collected dataset encourage a further analysis of the potential of the optical oil spill detection approach. [C1215]

#### **"Monitoring river estuaries and coastal areas using TerraSAR-X"**

Morphological changes in coastal areas, especially in river estuaries, are of high interest in many parts of the world. A new X-band radar on board the TerraSAR-X satellite gives access to spatial resolution as fine as 1 m. In Spotlight (SL) mode, resolution is down to 1.7 m in azimuth, with 10 times 10 km coverage. Spotlight is the best choice to monitor river estuaries, river channels, and bathymetry. Stripmap (SM) mode with a resolution down to 3.3 m and a swath width around 30 km is a perfect tool to investigate morphological features, such as coastline changes or wadden sea areas. ScanSAR (SC) mode with a resolution as fine as 18 m and spatial coverage of 150 times 100 km is also used for remote sensing of coastal region and open seas. Several polarization modes allow better separation of land and water areas. For assessing the suitability of remote sensing satellite data (TerraSAR-X) to detect morphological changes, the highly morphodynamic area of the river Elbe estuary has been chosen. Morphological changes related to sedimentation, erosion and redeposition is shown by analysing in-situ data. Moreover, bottom topography retrieval can be quite efficiently demonstrated by using TerraSAR-X data compared to 1 arc-minute global relief model (ETOPO1). [C1216]

#### **"Utilization of ASAR wave mode data for shipping safety"**

Safety of shipping is a growing concern. The causes of shipping casualties are various, while over 30% of the casualties are due to bad weather. Heavy sea state and severe weather conditions have caused the loss of more than 200 large cargo vessels within 20 years between 1981 and 2000. Remote sensing techniques, particularly the active microwave radar provides global sea surface observations for detecting heavy sea state and bad weather independent of clouds and sunlight and therefore it can contribute to shipping safety. A dataset of synthetic aperture radar (SAR) images spans nearly two decades since the launch of ERS-1 in 1991 for operational observations. When no other operations are requested, ERS-1, 2 SAR and ENVISAT ASAR can collect data as small images of 10 km times 5 km size every 200 km or 100 km along the satellite's orbit. This

kind of data is called SAR wave mode data and can be acquired continuously and globally over the sea surface. Using the integral wave parameters derived from SAR wave mode data, global sea state statistics can be carried out. In the present paper, significant wave height and zero upcrossing wave periods derived from ASAR wave mode data using the CWAVEENV empirical algorithm are compiled into a global wave atlas. Wave steepness is a crucial parameter for shipping safety. By using integral wave parameters derived from ASAR wave mode data, wave steepness is calculated and compiled to the global wave atlas as well. [C1217]

#### **"High-resolution current measurements from space with TerraSAR-X along-track InSAR"**

The German satellite TerraSAR-X, launched in 2007, carries an advanced synthetic aperture radar (SAR) with a variety of standard and experimental modes of operation, including along-track interferometry (ATI) capabilities for direct line-of-sight target velocity measurements. The potential of TerraSAR-X for high-resolution imaging of surface current fields has been discussed in several publications. In this paper we show first results based on actual TerraSAR-X ATI data, explain our data processing procedure, and give an update on the status of the instrument and on upcoming developments. [C1218]

#### **"Research on Land Use Supervision by Using High Resolution and Fully Polarizations Sar Data"**

Land is an important and fundamental natural resource which the mankind depends on for existence. Governor wants a better and cheaper mechanization to supervise land usage. The predominant source of remote intelligence for monitoring land change activities, remote sensing satellites especially Synthetic Aperture Radar (SAR)satellites are finding a niche on this arena. The high resolution and fully polarization SAR data provide a new mode for land use supervision. This paper aims to systematically analyze the SAR date representative applications in agriculture, forestry,urban planning and so on. [C1219]

#### **"Application of Mathematical Morphology to automatically extract roads on radar images"**

The new constellation of remote sensing satellite COSMO/SkyMed will guarantee a combination of spatial and temporal resolution never reached by previously systems. The full exploitation of this system can allow the development of new applications, like these aiming at providing insight into the magnitude of a disaster and a detailed assessment of the damages as required by first responders for planning relief actions. [C1220]

#### **"An investigation of urban water automatic extraction based on texture and imaging knowledge from high resolution SAR images"**

Extracting water body information with SAR images is distinctive and important. Especially for high-resolution SAR images, it's hard to extract water accurately because of Speckle Noises, so a Gabor filtering method related to the image texture is proposed. Firstly, frequency spectrum analysis method was used to identify the wedge and ring characters of image texture, and the period and directional parameters of the texture distribution were computed. Based on these characters, Gabor filter were constructed in order to filter the frequency spectrum of the multi-texture image, and best filter parameters were selected. After the filtering in frequency domain, components of corresponding texture were acquired by transforming the filtered frequency spectrum image to time domain image. The test results of terra SAR image indicate that the water body extraction method is good. [C1221]

#### **"Tile mapping of urban area extent in VHR SAR images"**

At the high resolutions attainable with the new generation space-borne sensors, the focus moves increasingly from spectral characteristics to geometric features. This trend is even more evident for urban areas which tend to show an unpaired concentration of linear features with respect to any other land cover. This naturally applies to both optical and radar images, and suggests one may use local concentration of linear features to gauge the presence of urban structures. In this paper we exploit a linear feature extractor to map the extent of urban areas in very high resolution optical and SAR images. [C1222]

#### **"Airborne laser scanner point clouds strip adjustment aided by photogrammetry"**

Airborne LIDAR has obtained more and more attention, especially in the field of 3-D city modeling, surveying and mapping. Laser Scanner Point Clouds strip adjustment plays a very important role in the processing and application of Airborne LIDAR. In this paper, some conventional algorithms of the airborne laser scanner point clouds strip adjustment are reviewed and contrasted, then a new method using the photogrammetric images and relative information such as the EOP (exterior orientation parameters) and IOP (interior orientation parameters)and VLL (Vertical Line Locus) based on object space matching method is introduced. A certain dataset which contains two strips of laser point clouds and the same region photogrammetric images is used to

implement the algorithm. The result of experiment validates this method and future work and research direction is discussed. [C1223]

### "Geometric processing of QuickBird stereo imagery with high building data in megapolis"

Much research work has been done concerning the geometric accuracy for High-Resolution Satellite Imagery (HRSI), the conclusion regarding this respect in photogrammetric society is that Ground Control Points (GCPs) are necessary for the accurate geo-positioning to get meter or sub-meter positioning accuracy. But most existing publications are about the horizontal positioning determination rather than vertical direction. This paper aims to evaluate the geo-positioning capability in vertical direction for HRSI and analyze the influence of GCPs vertical distribution to that of the final vertical accuracy. The study is performed in Shanghai, China, the typical metropolis, using a pair of across-track QuickBird stereo imagery, within a relatively small but representative area filled with very high buildings to provide height difference for GCPs and Independent Check Points (ICPs). A new accuracy evaluation scheme in vertical direction is put forward and employed in the assessment. Processed with the Rational Function Model (RFM) and its accuracy improvement models in image space, some relations are found between the GCPs height and obtainable ICPs vertical accuracy in different height ranges, discussions and conclusions are presented in the end. [C1224]

### "Low-resolution urban area outlining in satellite SAR images"

Urban areas represent a vital and highly dynamic environment, and monitoring their growth provides important input to decision and policy makers at large scale. Detection and outlining of urban areas from satellite sensors, though less precise, is faster than any on-site data collection. Various techniques have been proposed to classify urban areas, based on their typical features like textural features or backscatter intensity. In this paper a fuzzy-connectedness technique proposed for coastline detection, based on interferometric coherence and backscatter intensity, has been tested and adapted to urban area boundary detection. The modified method appear to be suitable for urban area extraction at ERS-like resolutions, for which long historical records are available allowing to reconstruct urban area growth in the past. [C1225]

### "Post-earthquake landslide detection and early detection of landslide prone areas using SAR"

High-resolution synthetic aperture radar (SAR) played an important role in the disaster management efforts after the Wenchuan Earthquake on May 12, 2008. SAR data was used for damage assessment, risk monitoring, and for the continuous monitoring of the so-called quake lakes. Landslides, triggered by the earthquake and the aftershocks, devastated large areas, killing thousands of people. Landslides formed natural dams, blocking rivers and leading to 34 so-called quake lakes, endangering millions of inhabitants and rescue workers downstream. SAR, amongst other sensor systems, was used to detect landslides and monitor those quake lakes. SAR can also assist the risk analysis by early surveying landslide prone areas and supporting the risk management and disaster reduction approaches. [C1226]

### "Monitoring terrain motion in China by means of spaceborne SAR images"

In this work we recall a recently developed processing chain (called Quasi-Permanent Scatterers -QPS-technique) that, by analyzing all possible interferometric pairs in a given SAR data-set and by evaluating the spatial interferometric coherence, is able to exploit partially coherent targets to estimate the ground motion. The technique has been successfully applied in the Badong site in China for retrieving the local DEM and for individuating active landslides. The possibility of processing effectively short-term coherent scatterers will turn out particularly useful to process series of high-resolution SAR data with short repeat-cycles. [C1227]

### "Steps towards a new technique for automated registration of pre- and post-event images"

With the continuing increase in the number of images collected every day from different sensors, automated registration of multisensor/multispectral images has become a very important issue. This is especially true when pre- and post-event image comparison is concerned: for this particular application, the requirement of obtaining the earliest possible post-event image imposes the use of data potentially showing strongly different characteristics with respect to the pre-event image. Non-homogeneous image pairs require robust automatic registration techniques. Resolution-independent, feature-based registration is naturally preferred over correlation-based registration but finding correct and sensible feature point sets to be matched is still an open problem today. In this paper we propose to use intersection points of extension off longest linear features found in the images. The fixed points are then matched using a modal matching approach. The procedure is illustrated and results over a set of high-resolution SAR images are presented and discussed. [C1228]

### "Data Fusion towards building roof reconstruction based on CSR approach"

3D building modeling has emerged as a focus of research as well as development for many urban planning and geo-information related applications. To its most abstract form on geometric level, 3D building roofs are regarded as the fundamental elements to present outlines of 3D building models. The emphasis of this study is to demonstrate a novel algorithm of building roof reconstruction, termed CSR (Construct-Shape-Refine). The proposed algorithm aims at reconstructing building roof models purely by employing 3D line features or integrating 3D and 2D line features from existing data. In particular, the latter integration involving fusion from multiple data sources strengthens the reliability as well as the precision of 3D building roofs. The CSR approach is characterized through three stages. Geometric inferences are imposed at the stage of Construct where topological relationship of the 3D line features is established while 3D coordinates of roof corners are adjusted and estimated through Shape processes, apart from compensating the hidden boundaries, if any. The efficiencies of two fusion streams, including fusion of 3D line features that result from different sources or fusing 3D line features with photogrammetric line features, are gained as promoting the building roof quality via Refine workflow. Experiments of the Construct-Shape stages show that the proposed method is independent of building roof types, however constrained in polygons under current consideration, as well as whether 3D line features are complete for both successful and efficient performance of building roof reconstruction on a 3D line feature basis. Moreover, the Refine stage offers more up-to-date and satisfactory building roof reconstruction results as compared to the situation when only one single data set is considered. [C1229]

### "Automatic road extraction from LIDAR data based on classifier fusion"

The ultimate goal of pattern recognition systems in remote sensing is to achieve the best possible classification performance for recognition of different objects such as buildings, roads and trees. From a scientific perspective, the extraction of roads in complex environments is one of the challenging issues in photogrammetry and computer vision, since many tasks related to automatic scene interpretation are involved. Roads have homogeneous reflectivity in LIDAR intensity and the same height as bare surface in elevation. Proposed method in this paper is based on combining multiple classifiers (MCS) is one of the most important topics in pattern recognition to achieve higher accuracy. Majority Voting and Selective Naive Bays are two methods that used for fusion of classifiers. [C1230]

### "A multi-agent method for automatic building recognition based on the fusion of Lidar range and intensity data"

Lidar has proved to be a promising data source for various mapping and 3D modeling of buildings in urban areas. Therefore, many researchers have been trying to study and develop automatic building recognition algorithms based on Lidar data. But, according to the complicated relationships between buildings and other objects in urban areas, especially trees and vegetations, the performance of obtained results from most of these algorithms is still dependent to several assumptions and simplifications. In this paper a multi-agent methodology has been proposed for automatic building recognition based on the fusion of textural and spatial information extracted from Lidar range and intensity data. The evaluation of obtained results confirms the high capabilities of this proposed multi-agent algorithm to decrease the conflicts in the field of automatic building recognition in complex urban areas. [C1231]

### "Inversion of leaf area index for invasive plant using ENVISAT ASAR"

In this paper, leaf area index LAI retrieval of invasive plant species from C-band synthetic aperture radar (SAR) data was demonstrated to be feasible via experiment. Taking an invasive plant of spartina alterniflora in Dongtan of Chongming island, Shanghai, China as example, a specific method that inversion LAI of invasive plant from the ENVISAT dual-polarization Advanced Synthetic Aperture Radar (ASAR) imagery would be presented in the paper. In the experimental test, the functional relationship model between the LAI values and backscattering ratio values was at first built and the model parameters were then objectively calculated by fitting, using simulated LAI values according to published research work and backscattering ratio values converted from the ENVISAT ASAR images. Moreover, it is confirmed in our study that it is being computably functional relationship between the LAI and the image pixel for either HH polarization mode image or VV polarization mode of ENVISAT ASAR image. The experimental conclusions are finally revealed that: 1) The 2-polynomial fitting is better than the 1-polynomial for both HH polarization mode image and VV polarization mode in approximation degree; 2) The difference of using the 1-polynomial fitting and the 2-polynomial fitting as adopting the HH polarization mode image is larger than the one as adopting the VV polarization mode image; 3) Adopting the HH polarization mode image is more effective than adopting the VV polarization mode image in inversion LAI for invasive plant from ENVISAT ASAR image; and 4) the related coefficient between the LAI and backscattering ratio corresponding to ENVISAT ASAR image were acquired up to 0.7100 in the HH polarization mode and 0.6657 in the VV polarization mode. [C1232]

### "An approach to urban surface features identification using Pushbroom Hyperspectral Imager"

The hyperspectral data can identify the complicated urban surface features which can't be identified using the multispectral data because of their lots of continuous bands in a narrow band width. The goal of this paper was to perform the urban surface features identification based on airborne Pushbroom Hyperspectral Imager (PHI) data. At first, some preprocessing of PHI data from original data, such as atmospheric correction and geometry calibration has been done. Then, the endmembers were located and identified using the n-d Visualizer on the pixels determined from pixel purify index (PPI) which was run on the Minimum Noise Fraction (MNF) transform result. The most crucial step is the matching between the target spectra and the reference spectra. In this paper, four matching algorithms were introduced and analyzed such as the spectral angle measure (SAM), the spectral correlation measure (SCM), the Euclidean distance measure (ED) and the spectral information divergence (SID). SAM and SID were used and compared in the target area. At last, the validation of the identification results was done and the error of the SID method was analyzed. The result indicated that water, vegetation and buildings can be identified exactly and the asphalt road can't be distinguished from the buildings because their spectra are similar in PHI image. To be concluded, SID is a more effective algorithm for the spectral matching than SAM in that it can identify the minute difference of the surface features and there are too many isolated pixels in the SAM algorithm. [C1233]

### "Object-based level set model for building detection in urban area"

This paper studies an new approach to creating a variational level set model for buildings detection by combining LiDAR point clouds and Aerial image data. The level set model introduces an object-based image analysis technique. Firstly, a fundamental object-based level set framework is built by neighbor analysis of remote sensing image. Then, several derived products directly or indirectly from LiDAR raw point cloud data, like nDSM and absolute roughness data, are used to construct a novel energy term in relation to height and roughness of non-terrain objects, in order to make up the disadvantages caused by insufficient information only from remote sensing image. Thus, a closely combined model for buildings extraction has formed. The model can well fuse spectral feature, height and roughness information of objects from different sensors. Finally, experiments on pairs of Aerial image and LiDAR 3D point cloud data are carried out, and conclusions can be drawn that our model can effectively separate various small or high building in urban area from other land covers, including trees, grass, ground etc., and alleviate those influence caused by shadow, occlusions or spectral inhomogeneity. [C1234]

### "Fuzzy samples retrieval: A method of SAR image retrieval in urban areas"

As the retrieval entrance, description of retrieval objects plays an important role in CBSIR (Content-Based SAR (Synthetic Aperture Radar) Image Retrieval) systems. Most of the CBSIR systems take one Region of Interest (ROI) from the original image, which contains the retrieval object, as the retrieval entrance. Besides, freehand sketch retrieval methods are used extensively in CBOIR (Content-Based Optical Image Retrieval). But when the retrieval objects are fuzzy in SAR image, methods mentioned above are no longer applied because speckle noises make the description of retrieval objects unfeasible. In this paper, a method is proposed to describe the retrieval objects in SAR image, which is called Fuzzy Samples Retrieval (FSR). In the experiments FSR is compared with the retrieval based on ROI of original image and freehand sketch sample, the results show that FSR has a better performance in CBSIR systems. [C1235]

### "Object extraction based on 3D-segmentation of LiDAR data by combining mean shift with normalized cuts: Two examples from urban areas"

In this work, we have looked into the problem of urban analysis using airborne LiDAR data based on the strategy of classification by segmentation. Segmentation is a key and hard step in the processing of 3D point clouds, which is not perfectly solved in view of different applications. A new 3d segmentation method incorporating the advantages of nonparametric and spectral graph clustering is presented here to facilitate the task of object extraction in urban areas. This integrated method features local detection of arbitrary modes and globally optimized organization of segments concurrently, thereby making it particularly appropriate for partitioning raw airborne LiDAR data of urban areas into segments approximating semantic entities. Two examples in urban areas-flyover and vehicle are chosen as interest objects to be extracted by a classification-based step. The approach has been tested on LiDAR data of dense urban areas, and the results that are obtained have been compared with manual counts and showed us the efficiency and reliability of the strategy. [C1236]

### "Construction and visualization of photo-realistic three-dimensional digital city"

This paper presents systematic approaches to create photo-realistic three-dimensional (3D) digital city systems. In the created 3D digital city systems, prismatic and polyhedral building models are constructed from assorted remote sensing and spatial datasets, including topographic maps, aerial and satellite images, airborne and ground-based LIDAR point clouds. Close-ranged digital photographs and video sequences are used to generate facade texture images for photo-realistic texture mapping of the constructed building models. High performance visualization algorithms based on Level of Detail (LOD) processes are also implemented for real-time, interactive exploration and applications. A few applications of the constructed 3D digital cities to urban development evaluation, environmental simulation, hazard mitigation and crime scene reconstruction are presented to demonstrate the usability of the developed 3D digital city system. [C1237]

#### **"A study of land subsidence with PS-InSAR method based on wavelet phase analysis"**

By estimating the phase information of stable natural reflectors or permanent scatterers of a set of SAR images, Persistent Scatterers for SAR Interferometry (PSInSAR) can be used to obtain the land subsidence information at millimeter level while the serious noises of multi-temporal SAR images which make it difficult. In this study, we study the influence of PS-InSAR method based on wavelet phase analysis to the PSs selection and surface deformation monitoring. We then use the method to process ENVISAT SAR images covering Jiaxing city in Zhejiang province in China. The experiment results have shown its effectiveness. [C1238]

#### **"Statistical characterization and modeling of high resolution COSMO/SkyMed SAR images over urban areas"**

As less attention has been devoted to land scattering in high-resolution SAR, especially satellite image, a comprehensive statistical analysis of COSMO/SkyMed SAR data is carried out in this paper. The images of different land types (such as bare soil, grassland, water, forestland, urban area and farmland) are analyzed by means of histogram, kurtosis and covariance estimation. As the experimental data over urban areas show impulsive characteristics that correspond to underlying heavy-tailed distributions which are clearly non-Rayleigh, some alternative distributions have been suggested and discussed such as the Weibull, lognormal, Gamma and K-distribution. Furthermore, the Alpha-stable distribution is introduced for modeling SAR images over urban areas. And by comparing with other amplitude distribution models, its performance is demonstrated to be better than others. [C1239]

#### **"Observation of urban heat island using airborne thermal sensors"**

As a basic study on urban heat island, the surface temperature of the central Tokyo, Japan is investigated using images obtained by airborne thermal sensors. Thermographies were taken from a helicopter on August 7, 2007, both in the daytime and at night. Using these thermal images, the variation of surface temperature can be observed in a detailed manner. Although the road surface and building roofs shows very high temperature, vegetation and water bodies show much lower temperature. The temperature at night also shows significant variation depending on the surface material and the sunlight condition in the daytime. Ground based verification of surface temperature was also carried out using a handheld thermal sensor. Based on these observations, detailed variations of temperature on various urban earth surfaces were revealed. [C1240]

#### **"Mobile mapping system and computing methods for modelling of road environment"**

Mobile mapping is a new way of efficiently collecting three-dimensional data from the road environment. Mobile mapping systems are cost efficient and robust technique to acquire information about even highly dynamic environments like highways and urban streets, where the data collection has previously been laborious and even dangerous for the staff performing the surveying. The dynamic mobile mapping systems could access the site with less risk to the personnel and with less need for road closures. The need for high resolution and details captured in to the data for street and road inventories, or city modelling, are the main reasons for the rapid adoption of the mobile mapping techniques in these fields. Lidar based mobile mapping system produces three-dimensional points from the surrounding objects. Typically, two-dimensional profiling scanner is mounted on the system and the third dimension is achieved by the movement of the vehicle. The characteristics of the obtained point cloud depend largely on the sensor arrangement and the sensor properties. The ROAMER, a single-scanner system for road environment mapping presented in this paper, is able to use various tilted scanning planes for the point acquisition with 120 kHz point measurement frequency and up to 48 Hz profile measurement rate. The relative point precision for the system is estimated to be a few millimetres, but is eventually defined absolutely by the accuracy of the navigation solution that could be provided in real-time, or more reliably through post-processing. We believe that in the future, lidar based mobile mapping will be used considerably for urban and road environment modelling, as well as in many other applications in the fields of construction, forestry, railways, and even in environmental modelling and monitoring e.g. hydrology and glaciology. In urban context,

the main applications of these models could include urban and environmental planning, road safety assessment, road construction planning and navigation. [C1241]

#### "Study of residents information extraction in SAR image based on texture features"

This paper focuses on the topic of extracting residential properties information based on texture features in low or moderate resolution SAR image, because the residential area has characters of high bright and regular texture in that scale image. Firstly, filtering the noises of the SAR image by using the FROST algorithm; secondly, obtaining a binary image which contains the residential information by threshold processing; thirdly extracting texture features based on the gray-level co-occurrence matrix and the texture features such as entropy, variance and correlation are selected according to actual situation, then the selected images are combined into a multiband image; Finally, the multi-band image multiplies the binary image and gets a new image, then classifying it by unsupervised classification, connecting the break points by using the morphology algorithm, a boundary of residential areas is obtained. As results, both the theoretical analyses and the experimental results indicate that this method is very efficient in extracting the residential information. [C1242]

#### "Seasonal displacements in upper-middle alluvial fan of Chaobai River, Beijing, China, observed by the permanent scatterers technique"

Miyun-Huairou-Shunyi area, located on the upper-middle alluvial fan of Chaobai River, is the largest groundwater source region of Beijing, China. The study area is approximately equal to 479 km<sup>2</sup> and covers three counties. The area includes one ground-water sub-basin, named Chaobai River, which is filled with unconsolidated alluvial deposits that comprise the aquifer system. Groundwater constituted about 66% of the municipal water supply in this region. Groundwater withdrawals had not exceeded the natural recharge between 1989 and 1992. During a period of low runoff and extensive ground-water extractions from about 1993 to 2006, ground-water levels fell as much as 25.6 m. Extensive groundwater use in upper-middle alluvial fan of Chaobai River has resulted in the continual decline of piezometric levels associated with the environment consequences of land subsidence. [C1243]

#### "Multi-source SAR remote sensing data for emergency monitoring to Wenchuan Earthquake damage assessment"

Synthetic Aperture Radar (SAR) has significant advantages in disaster monitoring that are all weather, independent of illumination imaging capabilities and strong stereoscopic sense. SAR technology played irreplaceable role in rapid response to Wenchuan Earthquake monitoring and damage assessment. With multi-source and multi-temporal high resolution SAR images, we conduct rapid, systematic and serial observations regarding to town damage and secondary disaster in Wenchuan Earthquake area. And based on special SAR image characteristics of building damage conditions, distributions and scopes of landslides and dammed lakes, we carried out rapid quantitative evaluation and built corresponding interpretation symbols. The detection reports and achievements are presented to related apartments of country and rescue teams, supplying full and accurate scientific basis about emergency service and disaster relief. [C1244]

#### "A novel twin-horn feed for multi-beam remote sensing reflector antenna"

Multibeam reflector antennas attract more interest nowadays with the ever increasing requirements of spaceborne. It features two sets of feeds located in the focal plane to generate two scanning beams. The twin-horn structure is employed to better receive remote sensing signals reflected. The far-field pattern of the reflector antenna illuminated by the measured twin-horn feed pattern is also obtained, and the simulation results match well with the design goals. [C1245]

#### "Radio channel simulations using multiple scattering center models"

A stochastic approach to model scattering effects of complex objects in comprehensive system simulation scenarios has been used in a simple and consistent way. In the given example the system simulation complexity is thereby reduced from appr. 100000 triangles per vehicle object down to 80 triangles plus additional bistatic RCS table look-ups. Consequently, detailed deterministic analyses of radio channel signal variations can be carried out for critical communication or sensing systems in an efficient and accurate way. Significant deviations can be observed, as expected, particularly at the shadow boundaries for grazing incidence. It should be mentioned that for larger scenarios and rather low number of observation points a system level ray tracing instead of the ray launching is expected to bring performance benefits. Nevertheless, a good approximation of the results obtained with the much more complex polygonal models has been proven. [C1246]

### "Satellite electronic attack of enemy air defenses"

Satellite electronic attack on enemy air defense radars is a pioneering use of orbiting radar emitters that were once used for remote sensing. Electronic attack is not the same as remote sensing, so a detailed design analysis of candidate space radar systems is required. The shuttle radar topographic mapper mission (SRTM) seems perfectly capable of electronic attack based upon ongoing engineering analysis. The electromagnetic propagation path is narrowly evaluated to answer the basic critique, "space too far away". This evaluation establishes critical limits for key parameters: (1) number of satellites required in the enemy's field of view, (2) transmitter power, (3) transmitter gain, (4) transmitter bandwidth, and (5) assumed losses resulting in burnthrough ranges for various assumed design parameters. [C1247]

### "Refractivity Estimation from Radar Sea Echos"

This paper addresses the problem of estimating parameters of the height-dependent index of refraction over the sea surface. The parabolic approximation for numerical solution of the wave equation is used to formulate the forward model. Refractivity estimation is performed by a modified genetic algorithm (MGA). Simulation results are presented which demonstrate the ability of this approach to estimate refractivity parameters with high precision, which is likely to provide an effective method for the estimation of the duct effects from radar sea echoes. [C1248]

### "Novel ultrasensitive millimeter-wave pressure transducer utilizing a Si membrane and a stacked-patch configuration"

A new highly sensitive radio frequency pressure transducer has been designed to operate in the millimeter wave frequency range that can be seamlessly integrated with other RF circuits in the LTCC multilayer packaging technology. The resonator consists of a stacked-patch based on LTCC multilayer packaging technology, having an air cavity embedded by a silicon (Si) diaphragm that deflects due to pressure change. Furthermore, the RF transducer presented here, operating in two frequency bands between 30-55 GHz, serves as both a wireless communications link and a remote sensing differential pressure indicator. This device can simultaneously simplify the design process, reduce the device's size, and reduce power consumption of the sensor at device level, providing a sensitivity of 116 MHz/ $\mu\text{m}$  with respect to the diaphragm deflection due to pressure change. The pressure inside the air cavity can be calibrated to detect differential pressure anywhere from zero to several bars. The transducer can be directly employed in a typical remote sensing / radar system without the need for additional circuits such as transceivers required in traditional wired transducers. Thus, it significantly reduces the power consumption and greatly minimizes the sensor. Due to its high sensitivity and portability, in future work the RF transducer design will be modified to use multilayer organics, such as LCP so that it may be utilized as wireless implantable sensors for biomedical applications and conformal structural health monitoring devices. A prototype of the RF transducer will also be presented to demonstrate the operation of the device. [C1249]

### "A dual-polarized cylindrical array antenna for aerial vehicles"

An X-band conformal array antenna designed for the use of unmanned aerial vehicles with polarimetric radars/sensors is presented. The array antennas mounted on the cylinder with various curvature radii are experimentally studied. The array can be easily placed on the aircraft fuselage or payload due to its ultra-thin and ultra-lightweight characteristics. It should have potential applications in radar surveillance, remote sensing, and wireless communications. [C1250]

### "CRBs for the Joint Estimation of TOA and AOA in Wideband MISO and MIMO Systems: Comparison with SISO and SIMO Systems"

We derive the CRBs (Cramer Rao bound) for the joint estimation of the TOA (time of arrival) and the AOA (angle of arrival) in wideband (WB) MISO (multiple input single output) and MIMO (multiple input multiple output) systems. We consider both cases of orthogonal and non-orthogonal transmitted signals. We compare the CRBs obtained in SISO (single input single output), SIMO (single input multiple output), MISO and MIMO systems under the assumption that the total transmitted energy is the same for all systems. We show that SIMO and MIMO are equivalent for TOA estimation, and MISO and SISO as well when the transmitted signals are orthogonal. For non-orthogonal signals, MIMO is better than SIMO, and MISO is better than SISO when the received signals are constructive. For AOA estimation, we show that MIMO is better than SIMO and SIMO is better than MISO when the transmitted signals are orthogonal. For non-orthogonal signals, MIMO is much better when the received signals are constructive. The CRBs obtained for non-orthogonal signals are very sensitive to the angle. Numerical results obtained in a typical scenario are provided. [C1251]

### "Low Relative Humidity Layer Observation with Micro Pulse Lidar in Qingdao"

A low backscattering intensity layer with clear boundary was found with an eye-safe, compact Micro Pulse Lidar (MPL) system in Qingdao (120.33, 36.07). This layer was also found from the energy monitor channel signal of the High Resolution Spectral Lidar (HRSL) system. From radiosonde data we found this layer had low relative humidity (RH) and the RH kept as a constant. Also the radiosonde data showed there was an obvious temperature inversion in low atmosphere which blocked aerosol transport. Jinan(117.55, 36.70) in Shandong province, China and west coast of Korea were two low RH centers. Similar phenomena were also found in many other days, especially in autumn. But the reasons caused to the low RH area need further research. [C1252]

### "Meteorological Visibility Measurements by a Micro Pulsed Lidar during the 2006 Qingdao International Sailing Regatta"

Meteorological visibility is a basic parameter for aeronautical, seafaring, expressway and military operations. In most domestic and overseas meteorological departments, the method to measure visibility is by eyeballing, which lacks criteria and objectivity. Among the instruments for visibility measurement, lidar is a powerful tool by directly collecting the backscattering laser light from the atmosphere. During the 2006 Qingdao International Sailing Regatta, atmospheric horizontal visibility was measured by an eye-safe Micro-pulsed lidar (MPL) which was developed by the Ocean Remote Sensing Laboratory (ORSL) of the Ocean University of China (OUC) in Xiaomai island (36deg3'9.91"N, 120deg25'37.10"E) from August 18 to 29, 2006. Klett method was used for processing the data measured from MPL. In this 12 days period, the visibility ranges from 1km to 30 km, covering many different weather conditions. The MPL operated stably at all times including the continual measurement from August 21 to 23, 2006 for both days and nights. Simultaneous eye observation data from Qingdao Meteorological Bureau were obtained for comparison. Visibility results of MPL system show good agreement with the eye observations data, with a correlation coefficient of 0.88. Experiments and comparisons successfully prove the capability and feasibility of the MPL system for atmospheric visibility. [C1253]

### "Rain rate retrieval by processing the observations of the 85V and 85H GHz channels of the SSM/I and TMI passive microwave sensors"

We present a new methodology, which provides the sea surface rain rate by inverting the 85 GHz channel measurements (TB) of the SMM/I and TMI microwave radiometers. This high frequency channel has the advantage of a spatial resolution close to the size of rain cells. We used a neural network whose inputs were the vertical and horizontal polarized 85 GHz TBs, the output being the rain rate. The learning dataset was made of downscale ECMWF atmospheric parameters and the corresponding brightness temperatures computed through the use of the radiative transfer equations. The computed rain rate compared well with the standard SSM/I algorithm both at global and regional scales. The comparison with the rain rates retrieved by TRMM radar, with similar pixel areas, showed a correlation coefficient higher than 0.97. A major difficulty was finding suitable observations to validate our results. [C1254]

### "Stimulated Brillouin threshold reduction by core microstructuration in multifilament core fibers"

High power fiber amplifiers producing long pulses ( $> 50\text{ns}$ ) with narrow linewidth ( $< 1\text{MHz}$ ) have many applications in remote sensing and Lidar systems. In this regime, the output power is usually limited by stimulated Brillouin scattering (SBS). We have recently demonstrated erbium-ytterbium doped multifilament core (MFC) fibers for amplification of narrow linewidth pulses with high ( $> 1\text{ kW}$ ) SBS threshold and  $M^2 \sim 1.3$ . In this new fiber structure, the core is composed of 37 erbium-ytterbium filaments surrounded by fluorine doped silica. [C1255]

### "A novel 2 $\mu\text{m}$ laser source for CO<sub>2</sub> DIAL"

Laser specifications for a spaceborne sensitive measurement of CO<sub>2</sub>, by differential absorption LIDAR (DIAL) at 2.05  $\mu\text{m}$ , have been derived in terms of output energy, frequency stability and beam quality. To achieve such operation, single longitudinal mode (SLM) operation and fine frequency control is needed. In previous work, the authors have developed an optical parametric oscillator based set-up for the detection of species (CO<sub>2</sub>, CH<sub>4</sub>, N<sub>2</sub>O) with very low oscillation threshold. In this work, the range of operation of the previous device was extended to 2  $\mu\text{m}$  range. It was demonstrated that using a type II PPLN based doubly resonant optical parametric oscillator (DROPO) in a master oscillator power amplifier (MOPA) configuration, energy levels in the tens of mJ range can be obtained, while maintaining both high spectral and spatial performances. High efficiency and high beam quality performances have been demonstrated recently in OPO/OPA configurations. [C1256]

### "Autonomous planetary exploration using LIDAR data"

In this paper we present the approach for autonomous planetary exploration developed at the Canadian Space

Agency. The goal of this work is to autonomously navigate to remote locations, well beyond the sensing horizon of the rover, with minimal interaction with a human operator. We employ LIDAR range sensors due to their accuracy, long range and robustness in the harsh lighting conditions of space. Irregular triangular meshes (ITMs) are used for representing the environment providing an accurate yet compact spatial representation. In this paper a novel path-planning technique through the ITM is introduced, which guides the rover through flatter terrain and safely away from obstacles. Experiments performed in CSA's Mars emulation terrain that validate our approach are also presented. [C1257]

### "Evaluation of QuikSCAT wind vector performance with respect to field measurements for the Bulgarian part of the Black Sea"

Winds over the ocean play an important role in meteorology, oceanography and climatology. They affect air-sea variations in heat, humidity, gases and particles, regulating the crucial relation between the ocean and the atmosphere that establishes and supports the climate on regional and global scale. Therefore, the knowledge of wind fields over the oceans is essential for global weather forecast purposes. Furthermore, the accurate forecasting of ocean surface winds contribute to good wave forecasts, which provide informativeness and safety in marine industry, navigation and other human activities in open and off-shore seas. The sources of surface observations that are generally used to make analyses of winds over the oceans not always can provide data with temporal and spatial regularity. These gaps can be filled in with wind data registered by satellite sensors like NASA's QuikSCAT satellite radar scatterometer. It provides on operational basis wind vector measurements over global oceans with considerable reliability and sufficient time frequency. The standard operational QuikSCAT wind vector product has a spatial resolution of 25 km times 25 km. However, the recent measurement methodology of QuikSCAT allows for wind vector retrievals at better spatial resolution of 12.5 km. In the present paper the performance of the latest QuikSCAT Level 2B (L2B) 12.5 km wind product was evaluated with respect to wind data acquired from meteorological station mounted on a fixed earth gas exploration platform "Galata" in the western Black Sea. The QuikSCAT satellite occupies a sun-synchronous, near-polar orbit with altitude of 803 km above the Earth and with local equator crossing time at the ascending node of 6.00 a.m. +/-30 min and swath width of 1800 km. The mission requirements of QuikSCAT SeaWinds Scatterometer for wind measurements are an accuracy of plusmn2 m/s in speed for the range 3-20 m/s and plusmn20deg RMS in wind direction for wind speed ranging from 3-30 m/s. On the other hand, the Galata platform is located on the Bulgarian shelf, 26 km off cape Galata to the east of city of Varna. The satellite sensor measurements of wind speed and direction were validated against anemometer observations co-located in time and space to the satellite pass in 2007 for winter (January-February) and summer (June-July) periods. The QuikSCAT wind vector processing algorithm estimates the wind speed on 10 m level above the sea surface. To make the satellite wind speed data comparable to those derived from the anemometer, the latter were recalculated to 10 m level applying a correction to every measurement. The validation of scatterometer data of wind speed and direction for both abovementioned time periods was performed by statistical analysis including calculation of RMSE, bias and correlation. The results indicate a good agreement between satellite and in situ data for moderate winds (3-15 m/s). Estimated coefficients of correlation R are 0.88 and 0.96 for wind speed and wind direction, respectively. The highest RMS error was found for the light winds with speed less or equal to 3 m/s. The study results have confirmed the reliability of QuikSCAT L2B wind vector product for the western Black Sea conditions, which imply on its further use for meteorological, oceanographic, and climate researches and forecasts in regions of sparse in situ data such as the Black Sea. [C1258]

### "A glimpse to future commercial spy satellite systems"

Over the past decade the commercial remote sensing industry has experienced significant technological change and improved market penetration. New sensor Technologies in space systems offer new information capabilities. The development of high-resolution commercial satellites which is better than 1 meter black and white and 2.5 meter multispectral has opened new data and new collection methodologies to the ultimate information customer. Future commercial spy satellite programs are linked, connected to military systems. The objective is to show how governments mix and harmonize the capabilities inside the country to supply the national demands in the frame of security and intelligence as well as commercial use. According to the reports published to public the usage of satellite imagery as commercial or military applications are approximately equal. Influencing the development and construction of the next generation of commercial remote sensing satellites is the purpose of the NextView procurement of U.S. The national space program in United States along with the President's directive created a new era in space industry and market. The high resolution imaging industry was born in 1994, when president Clinton issued a national policy granting companies licenses to build and launch the satellites. The new directive presumably will go a long way toward supporting two U.S. companies. There was a tremendous hunger for high resolution satellite imagery and the US firms were ready to fulfill the needs. In early Spring 1999 Director of Central Intelligence and Deputy Defense Secretary approved the commercial imagery initiative proposed by NRO. The goal of the plan was to satisfy general imagery requirements through

commercial vendors, while keeping more advanced imagery systems under government control. In July 1999 the CIA and DOD approved the \$1 billion multi-year budget for the initiative, which is part of the Future Imagery Architecture. Half of this amount had already been included in the NRO and NIMA budgets for 2001 through 2005. What new capabilities will arise during the next decade? A substantial thrust is doing things faster and cheaper rather than bigger and better. The military is developing new techniques for building reconnaissance satellites that can be launched on short notice as needs arise. The industry will expand the use of non-visible portions of the spectrum that are particularly infrared and microwave, increase the number of active sensors such as lidar and radar, and improve our spatial and temporal sampling. Particularly important will be new technologies for linking sensors through wireless and traditional means into sensor networks. This will allow the information to be combined so as to support rapid decisions in complex situations. In addition, the output of one or several sensors can be used to trigger observations from others, or even to rapidly reconfigure the other sensors so as to optimize observations of an event. What will remote sensing be like a decade from now? The competing forces of increased business demand, limited government resources, and advancing technological capability will play out over this time period. The rapidly growing consumer needs will introduce a new and somewhat unpredictable factor. The future promises to be bright, but it won't happen on its own. The full paper will discuss the details of future needs and plans of commercial remote sensing satellites and their sensors. Albeit the future demands are not only key factor for intelligence the manufacturers around the world will show the countries' capabilities to build up future space programs under the national defence. The next few years will prove interesting as the business potential of constellations for remote sensing is fully realized. [C1259]

### **"Building extraction and 3D reconstruction in urban areas from high-resolution optical and SAR imagery"**

In this paper, we propose to investigate the joint use of high-resolution optical and SAR data, for building extraction and 3D reconstruction in large urban areas. A sequence of methods providing, in a semi-automatic way, the building detection and reconstruction is presented. Potential building footprints are first extracted on an optical image by a two-phases process (coarse detection and boundaries refinement). The framework of fusion with SAR data is then developed. A first step of registration allows us to get a fine superposition of optical and SAR building features. Then, we show how to take benefit from the introduction of SAR data: The proposed methodology, based on the optimization of criteria referring to building SAR characteristics, allows us to simultaneously deal with the building presence validation and with the height retrieval. [C1260]

### **"PSInSAR Analysis over the Three Gorges Dam and urban areas in China"**

In this work we present the results achieved within the Dragon project, cooperation program between the European Space Agency (ESA) and the National Remote Sensing Center of China (NRSCC), about monitoring the terrain motion in urban areas, measuring the city growth rate and analyzing the stability of big manmade structures. Among the processed areas, we report here the main results we obtained in the test sites of Shanghai, Tianjin and Three Gorges. The techniques that have been used to process the data are classical SAR interferometry (InSAR), Permanent Scatterers (PSInSAR) and a combination of coherent-uncoherent analysis. Particular attention is worth to be paid to the analysis of the Three Gorges Dam, biggest hydroelectric plant in the world, in which stability and characteristics of its scattering structures have been studied. [C1261]

### **"Persistent scatterer pairs (PSP) technique and high resolution SAR interferometry in urban areas"**

We have recently proposed a new approach, named persistent scatterer pairs (PSP), for the identification and the analysis of persistent scatterers in series of full resolution SAR images. In this technique, atmosphere phase artefacts are effectively eliminated by exploiting their spatial correlation, but without using model based interpolations to remove orbital and atmospheric phase artefacts. This approach allows efficiently identify the persistent scatterers, and to retrieve the corresponding terrain height and displacement velocity. [C1262]

### **"Remote Sensing of Human Body by Stepped-Frequency Continuous-Wave"**

Remote sensing of human body is very useful in many services. The micro-Doppler characteristic of human body can be detected to identify life target. In this paper, another new theoretical method to obtain the range and Doppler frequency of human body is proposed in which multiple periods stepped-frequency continuous-wave signal and moving target indication (MTI) filter are adopted. The simulation results illustrate the validity of this method and present the detection of the target range and the vibration frequency of heart beating and breathing. [C1263]

### **"POLARIS: ESA's airborne ice sounding radar front-end design, performance assessment and first results"**

This paper addresses the design, implementation and experimental performance assessment of the RF front-end of an airborne P-band ice sounding radar. The ice sounder design comprises commercial-of-the-shelf modules and newly purpose-built components at a centre frequency of 435 MHz with 20% relative bandwidth. The transmitter uses two amplifiers combined in parallel to generate more than >128 W peak power, with system >60% PAE and 47 dB in-band to out-of-band signal ratio. The four channel receiver features digitally controlled variable gain to achieve more than 100 dB dynamic range, 2.4 dB noise figure, 160 ns receiver recovery time and -46 dBc 3rd order IMD products. The system comprises also, a digital front-end, a digital signal generator, a microstrip antenna array and a control unit. All the subsystems were integrated, certified and functionally tested, and in May 2008 a successful proof-of-concept campaign was organized in Greenland. The system detected the bedrock under 3 km of ice, and internal layers were mapped up to 1.3 km. [C1264]

#### **"An update on multi-channel digital receiver development for the phased array radar at the National Weather Radar Testbed"**

This paper describes the beginning states of a new project that will digitize radar signals coming from eight channels on the phased array antenna at the National Weather Radar Testbed (NWRT) in Norman, Oklahoma. At the current time, a single-channel digital receiver is operational to mimic the current capability. The multi-channel digital data will foster a new generation of adaptive/fast scanning techniques and space-antenna/interferometry measurements, which will then be used for improved weather forecasting via data assimilation. Differing from the conventional rotating radar, the phased array is suited for multi-mission capabilities so that a variety of targets may be observed simultaneously with a high degree of fidelity. The development of a multi-channel receiver will be the catalyst and an enabling tool for research in this area for the next decade. This collaborative project, which involves scientists and engineers from the University of Oklahoma and the National Severe Storms Laboratory in Norman, is the result of a recently funded a grant from the National Science Foundation (as described in the Acknowledgement section of this paper). [C1265]

#### **"Point Scatterer Model for RCS prediction using ISAR measurements"**

A New Point Scatterer Prediction Model is presented in this paper to predict RCS of an aircraft model using Inverse Synthetic Aperture Radar (ISAR) images of the aircraft.. The ISAR images are provided by Defense Agency of Sweden and Saab inc. for each 15 degrees in horizontal plane. RCS is predicted for each aspect angle by taking superposition of the dominant point scatterers whose locations and strength are calculated from these ISAR images and simulation results are given with measurement results of the same aircraft model. [C1266]

#### **"Synthetic aperture radar using spread spectrum modulation"**

An X-band SAR is developed, being upgraded and tested. It uses solid state electronics and phase modulated impulses. The first results using corner reflectors prove the concept. [C1267]

#### **"SAR and Infrared Image Fusion Using Nonsubsampled Contourlet Transform"**

To utilize the separate advantage of the Synthetic Aperture Radar (SAR) and infrared images, in this paper, a fusion method based on the nonsubsampled contourlet transform is proposed for SAR and infrared image fusion. Simulation experiments show that this method can yield fusion image with better visual quality than discrete wavelet transform and the obtained fusion image can preserve much information of edges and textures of SAR and infrared images. [C1268]

#### **"An internal calibration scheme for polarimetric Synthetic Aperture Radar system"**

Two important aspects of internal calibration of polarimetric Synthetic Aperture Radar (SAR) are discussed, that is, system gain calibration and individual Transmit/Receive Module (TRM) calibration. System gain variation is measured utilizing the internal calibration loop. Dualchannel TRM gain and phase calibration is carried out using Orthogonal Phase Coding (OPC), in which signal of individual TRM is phase-encoded according to a set of orthogonal codes in order to be separated from the composite calibration signal of all TRMs. Calibration results are developed both theoretically and through simulation in the case of TRM failure. A crosstalk model is used to investigate the effect of imperfect isolation between the two polarization channels of each TRM on the calibration error. [C1269]

#### **"CSIR-NLC mobile LIDAR for atmosphere remote sensing"**

A mobile LIDAR (Light Detection And Ranging) system is being developed and employed for atmosphere remote sensing at the Council for Scientific and Industrial Research (CSIR) National Laser Centre (NLC), Pretoria (25.45

S; 28.16 E), South Africa. In this paper, we describe the results obtained using the CSIR-NLC mobile LIDAR in a 23 hour field campaign at the University of Pretoria. [C1270]

### "Characterization of soil surface roughness from terrestrial laser scanner data"

The surface roughness parameters commonly used as inputs to forest radar backscatter models are the root mean square heights (RMS)  $s$  and auto-correlation length  $l$ . These parameters were traditionally estimated from a one-dimensional surface profile with limited length. The complexity of natural surfaces makes it very difficult to explicitly describe the soil roughness. Terrestrial Laser Scanner (TLS) provides a new approach for the characterization of soil surface roughness. In this paper we address the issue of soil roughness characterization from terrestrial laser scanner data. The RMS height  $s$  was calculated using TLS data and compared with field measurements. The results showed that the proposed method can be used to make soil roughness measurement so long as the data sampling frequency was high enough. The relationship between required sampling frequency and the wave length of Microwaves was derived. In addition to the soil roughness parameters, a high resolution three dimensional digital elevation model (DEM) was constructed. [C1271]

### "Spectral ratio lidar for objects detection"

In this paper a new technique of objects measurement based on spectral ratio lidar system has been proposed and developed to make horizontal-path laser measurements of objects. The two or more wavelengths laser transmitter operates within and adjacent to the sensitive bands exhibited by the characteristics of each object, the result could be used to establish inversion models of the laser transmitting backscatter signals. The application value and the key techniques of the spectral lidar are analyzed. The laser spectral ratio model is established and the lidar system is designed, the lidar measurements were down to testify its feasibility. Also issues to approach the final goal of this new technique are discussed. [C1272]

### "Estimation of seismic intensity due to the 2008 Wenchuan Earthquake"

The great earthquake that occurred in Sichuan, China on May 12, 2008 claimed about 70, 000 precious lives. It is necessary to quickly pinpoint the areas where extensive damage is expected when such a big earthquake occurs and quickly input limited resources. As an attempt to instantaneously pinpoint the areas where extensive damage is expected, we classified landform of Sichuan Province, China using SRTM-3 and estimated the amplification factor and distribution of seismic intensity of Great Wenchuan Earthquake(2008) based on our results. [C1273]

### "The January 2002 eruption of Nyiragongo volcano (DRC) captured by InSAR"

On 17th January 2002, Nyiragongo erupted along an approximately 20 km long fracture network extending from the volcano to the city of Goma and its airport. The event was captured by InSAR data from the ERS-2 and RADARSAT-1 satellites acquired in three different geometries. These data show complex ground displacements, with several overlapping fringe patterns, associated to a combination of sources of magmatic and tectonics origins. A combination of 3D numerical modeling and inversions is used in order to interpret these displacements. Synthetic tests indicate that with one to three INSAR geometries, the best fit and mean models are within the confidence intervals whether the source of displacements is a single dike, a dike combined with a west dipping normal fault or a dike combined with an ellipsoid. Increasing the number of InSAR geometries makes the confidence intervals smaller and the inversions faster. At this stage of the study, only the area close to the eruptive fissures was analyzed assuming displacements were caused by a single dike. The best-fit dike model obtained with a simultaneous inversion of the three InSAR geometries is subvertical, and has a low overpressure. Both characteristics are consistent with the rift context. [C1274]

### "Earthquake intensity estimation and damage detection using remote sensing data for global rescue operations"

In order to support global rescue operations, we propose a new earthquake damage detection method based on a combination of both the result estimated by using earthquake information (magnitude, location of source, detailed ground conditions, and distance attenuation equation), and change detection using multi-temporal SAR data. First, to find collapsed buildings and houses on the earth's surface, we adopt a difference image calculated from multi-temporal SAR images observed before and after the earthquake. Next, to estimate seismic intensity and probability of destruction caused by the earthquake, we apply an earthquake engineering model. Finally, damaged area is calculated using a logical AND of difference image and the destruction probability. In order to show that we can obtain a damage detection map which corresponds with the actual damage of houses, we applied the method to simulations of the 2008 Sichuan earthquake in China. [C1275]

### "Radar signal retrodiffusion by water surface"

To prepare the future altimetry space missions at Ka band, a measurement campaign has been done with ONERA BUSARD platform and DRIVE radar. Particularity of the campaign was the use of steep incident angles, in Ka band, with a SAR instrument. Area of interest was the Camargue region in south of France. Three flights were planned on dry, wet and sea surfaces. In this paper, we describe the context of the campaign, and sensor's configuration that has been used. We then present the areas that have been measured and expose an example of aircraft's trajectory. Finally, we present some results as SAR images that have been acquired and some extracted backscattering coefficient profiles, figured as a function of the incident angle. Nadir backscattered levels are close to the literature values, and specular behavior is found on pond surfaces while more diffuse returns are observed over sea surfaces. [C1276]

### "Finite difference model for modeling sea surface current from RADARSAT-1 SAR data"

This study introduces a new approach for modelling sea surface current variation using synthetic aperture radar (SAR). SAR Doppler frequency shift was computed by the ambiguous estimation and Wavelength Diversity Ambiguity Resolving algorithm (WDAR) and Multi Look beat Frequency (MLBF) RADARSAT-1 SAR standard mode data. In situ current measurements have been collected by using wave rider buoy (AWAC). The current velocity then estimated by conversation of residual Doppler Centroid by performing second order polynomial model. The second-order accurate dispersive Lax-Wendrof was used to determine the spatial variation of sea surface current in RADARSAT-1 SAR data. The study shows that there is a significant relationship between in situ current measurements and sea surface current estimated by WDAR and MLBF techniques. The high accuracy is shown with mean root mean square error (RMSE) of  $\Gamma_B \pm 0.11$  m/s. It can be concluded that the integration between WDAR and MLBF techniques and Euler finite element model is good tool for modelling sea surface current variation in RADARSAT-1 SAR images. [C1277]

### "Sea surface simulation for SAR remote sensing based on the fractal model"

Based on the fractal ocean surface model, electromagnetic scattering model under Kirchhoff Approximation and the raw signal simulation procedure of dynamic scene based on time domain, the sea surface of the SAR remote sensing has been simulated. The images of the wave and complex fractal sea surface are in accordance with the hydrodynamic modulation, the tilt modulation and the velocity bunching modulation. The simulation has been developed in the Matlab programming language. [C1278]

### "Automated extraction of building geometric features from raw LiDAR data"

In recent years, with new services expected, such as navigation systems, location based services, and augmented reality, the need for automatically, efficient 3D building reconstruction systems becomes more urgent than ever. As a new spatial information technology, airborne LiDAR is widely used for the acquisition of 3D objects on the earth. The automatic reconstruction of 3D buildings from airborne LiDAR data has been a topic of research for decades. However the lack of 3D building reconstruction methods is still the bottleneck for the further development of airborne LiDAR. Since the 3D geometry feature is extremely important for many applications such as urban planning, car navigation, or environment monitoring etc., this paper introduces an automated method for implementing building geometric features extraction from raw LiDAR data in details. The outlines of 3D buildings are generated by using discrete curvature analysis according to the building geometry features. In the experiment, 3D building models are automatically reconstructed by using a model-driven approach according to their geometry features derived from raw LiDAR data. [C1279]

### "Simulation of 3D laser systems"

This paper deals with modeling of new optical non-conventional imaging with laser systems. In this paper, we present the simulation of the 3D ladar sensor including physics based modeling of laser backscattering from complex rough targets, reflectance modeling of porous occluders, development of 3D scenes and reconstruction algorithms for identification. We shall focus on tomography algorithms for reconstructing optical three-dimensional scenes. [C1280]

### "3D coastal bathymetry reconstruction using TOPSAR data"

Coastal bathymetry is considered to provide key parameters for coastal engineering and coastal navigation. In this paper we address the question of reducing the effect of speckle on the accuracy of depth determination in coastal waters using TOPSAR multi-polarized data without needing to include any sounding data values. In doing so, two three-dimensional surface models, the Volterra model and a fuzzy B-Spline model, which construct a global topological structure between the data points, were used to support an approximation to the

real surface. The statistical differences between real bathymetry map, CVVband and LHHband showed that the best reconstruction of coastal bathymetry was obtained with polarised L and C bands SAR acquired with HH and VV polarizations, respectively. With 10 m spatial resolution of TOPSAR data, bias of -0.04 and the standard error mean of 0.05 m in depth determination was obtained with LHHband. [C1281]

#### "Analysis of the mean raindrop shape model for dual polarization radar rainfall estimation"

Information about the shape of raindrops is critical for estimating rainfall rate with dual polarization radar. As described in the literature, the relation describing drop oblateness as a function of its equivolumetric diameter is nonlinear. There are several relations that express the shape-size dependence as nonlinear fourth-order polynomials. In fact, there is still no consensus regarding the most appropriate equation to use to describe the shape-size relation. Moreover, while non-linear equations are important for studying raindrop shape, it is not clear that they are needed to estimate an integral quantity such as rainfall rate. The validity of using a simple equivalent linear shape-size model based on the principle of the mean value theorem for estimating rain from dual polarization radar measurements is examined. Proposed rain algorithms based on the estimation of the drop shape are compared with algorithms that assume specific a-priori fixed drop shape-size relations expressed by a fourth order polynomial. Reconstructed rain and radar measurement profiles obtained from real radar observations were used to this purpose. Results show that the proposed rain algorithms perform better or at least equal to the algorithms derived assuming a priori fixed shape-size models, demonstrating that the prevailing model directly derived from data is suitable for rainfall retrieval purposes. [C1282]

#### "A unified polarimetric approach for SAR sea oil slick observation"

In this study, a novel unified theoretical framework to describe the polarimetric sea surface scattering with and without surface slicks, entirely based on the Mueller scattering matrix, is proposed. Dealing with slick-free or weak-damping-slick-covered sea surface a Bragg scattering mechanism is expected, while, a non-Bragg scattering mechanism is expected in case of oil-covered sea surface. Following this rationale, the Mueller scattering matrix is physically read in terms of slick-free and slick-covered sea surface scattering mechanisms, through the analysis of some Mueller based polarimetric descriptors, i.e. the degree of polarization, the statistics of the phase difference and the pedestal height. Experiments accomplished on Level 1.1 full polarimetric L-band ALOS PalSAR data confirm the effectiveness of the proposed approach. [C1283]

#### "Spatially adaptive classification of hyperspectral data with Gaussian processes"

Automated classification of land cover types based on hyper-spectral imagery often involves a large geographical area, but class labels are available for only small portions of the entire area. Moreover, the spectral signature of the same land cover class may vary substantially over different locations. When a classifier is trained on a specific geographical location and applied to other areas, it often performs poorly because of such spatial variation of spectral signatures. In this paper, we propose a novel framework for classification of hyper-spectral data: a Gaussian-Process Maximum-Likelihood (GP-ML) model where the mean of each spectral band is spatially modeled using a Gaussian process. Our framework provides a practical and effective way to model spatial variations of high dimensional data such as hyperspectral images for classification problems. [C1284]

#### "Topography of sand covered bedrock using two-frequency airborne interferometric SAR measurements"

This paper presents the application of Interferometric Synthetic Aperture Radar (InSAR) to estimate the height of the sand layer on top of the bedrock in deserts. This is anticipated to greatly increase the efficiency of oil field search and can have several applications for environmental and archaeological studies. The extension of InSAR processing to estimate the covered bedrock height through an iterative algorithm is introduced. The sensitivity of the proposed algorithm to system errors is investigated and its application to a common type of sand dunes is also presented. [C1285]

#### "Investigation on the applications of decorrelation analysis in Polarimetric SAR Interferometry"

Interferometric coherence is a key quantity in Polarimetric SAR Interferometry (Pol-InSAR), but it is usually decreased (named decorrelation) by the decorrelation sources, such as polarization type, volume scatterers, instrument settings and processing errors. The analysis of decorrelation has been used to system performance assessment and vegetation parameter estimation. This paper presents two other applications of the decorrelation analysis. One is the derivation of Pol-InSAR system and processing requirements. It is based on quantitative expressions of the decorrelation as a function of system and processing parameters. The other is compensation of the decorrelation that cannot be eliminated by optimizing system and processing parameters. It is implemented by using dual-baseline Pol-InSAR data. The Pol-InSAR requirement on noise equivalent

backscattering coefficient and the compensation of temporal decorrelation are shown to demonstrate and validate these two applications respectively. [C1286]

### "Recent developments in the MODTRAN® atmospheric model and implications for hyperspectral compensation"

Recent developmental efforts involving in the MODTRAN® atmospheric radiative transport model and derivative codes have led to advancements with important implications for hyperspectral imaging. New MODTRAN® features include (a) direct computation of diffuse transmittance and spherical albedo data, (b) two options for computing multiple line-of-sight (MLOS) radiances using a single DISORT scattering calculation for each spectral wavelength or channel and (c) enhancements to the treatment of Earth's curvature effects on scattered radiances. [C1287]

### "Application of SAR remote sensing data to lithological mapping: A case study in railway geological survey"

The interpretation and application of optic remote sensing images, including aerial photos and satellite images, had become the indispensable tool for railway engineering geological survey. But microwave remote sensing images, mainly SAR images, were rarely used in the application. In the paper, SIR-C SAR remote sensing data were used to identify different rocks and survey the lithological distribution around Qinghe River in the north part of Xinjiang Province. Firstly, the multi-frequency and multi-polarization data were used to produce the false color composite image for visual interpretation and lithological mapping by remote sensing digital image processing and enhancement. Secondly, the various backscattering data of containing abundant information about rock's characteristics were input into the computer Neural Network Classifier. The overall accuracy of lithological classification is 62.6%. [C1288]

### "Fast extracting and change detection of dammed lakes using highresolution SAR images: A case study of Tangjiashan Dammed Lake"

Wenchuan Earthquake has caused many huge landslides in the rivers in Sichuan Province. Synthetic Aperture Radar (SAR) technology played an irreplaceable role in rapid response to Wenchuan Earthquake monitoring and damage assessment. In this paper, Tangjiashan Dammed Lake was taken as a case study area for fast extracting and change detection with continuously acquired multi-temporal high-resolution SAR images. By June 12, 2008, we had identified dozens of dammed lakes in the area heavily affected by the Wenchuan Earthquake using high-resolution SAR images. In order to make a scientific evaluation of the disaster situation and provide efficient and instantaneous rescue action in the future, an effective method was developed for rapid extraction and change detection of dammed lakes. [C1289]

### "Using permanent scatterer InSAR to detect land subsidence and ground fissures: A case study in Xi'an city"

The Permanent Scatterers (PSs) SAR Interferometry has become an operational tool in the context of spaceborne SAR interferometry for monitoring surface deformation with millimetric accuracy. In this contribution we presented a case study in Xi'an city for land subsidence monitoring and ground fissures detection by using PS InSAR. We applied a linear regression model to retrieval land subsidence velocity by using a series interferometric phase of the coherent target. For the displacement of ground fissures monitoring, which caused by the nonuniform displacement of land subsidence and fault motion, a time series interferometric analysis of coherent target has been carried out to retrieve the history of displacement. The results archived from ENVISAT ASAR images acquired from 2005 to 2008 has demonstrated the distribution and the magnitude of the land subsidence and ground fissures. We compared the result from PS InSAR with the field surveying data and the results shown good agreement. [C1290]

### "Monitoring of snow cover properties during the spring melting period in forested areas"

As space-borne C-band SAR observations are used for monitoring the snow cover during the spring melt period, temporal changes in backscatter from forest cover disturb the mapping of snow cover. This paper presents an analysis of snow backscattering properties in eight test areas situated around weather stations. Test areas represent open and forested landscapes in Northern Finland. Analyses are carried out using an extensive multitemporal ERS-2 C-band SAR data set from the snow melt period. We validate the (1) forest backscattering model for forest compensation, (2) TKK fractional snow-covered area (SCA) method with in situ observations and (3) inversion of a combined forest/snow/ground backscattering model in an application to yield estimates of the relative changes of snow wetness during full snow cover conditions. The results show that the semi-empirical

TKK backscattering model describes the average C-band backscattering properties of all test regions well as a function of forest stem volume. Comparison of SCA estimation results with available ground truth data also shows a good performance. The retrieved relative snow wetness values agree well with temperature observations. [C1291]

#### "The PARIS in-orbit demonstrator"

Mesoscale ocean altimetry remains being a challenging area for satellite observations. Conventional nadir looking radar altimeters can make observations only along the satellite ground track and many of them are needed to sample the sea surface at the required spatial and temporal resolutions. The Passive Reflectometry and Interferometry System (PARIS) using GNSS reflected signals was proposed as a means to perform ocean altimetry along several tracks simultaneously spread over a wide swath. The present paper describes such an instrument specially conceived to fully exploit the GNSS signals for best altimetric performance, and to provide multi-frequency observations to correct for the ionospheric delay. Instrument calibration strategy is also discussed. Furthermore an in-orbit demonstration mission is proposed that would prove the expected altimetric accuracy suited for mesoscale ocean science. [C1292]

#### "Connecting the dots between laser waveforms and herbaceous biomass for assessment of land degradation using small-footprint waveform LiDAR data"

Measurement and management of vegetation biomass accumulation in ecosystems typically involves extensive field data collection, which can be expensive and time consuming, while leaving the user with relatively crude inputs to intricate biomass models. Light detection and ranging (LiDAR) remote sensing, which provides extensive height measurements of terrain and vegetation, has become an effective alternative to characterize vegetation structure. In this paper, we report on ongoing efforts at developing signal processing approaches to model herbaceous biomass using a new generation of airborne laser scanners, namely full-waveform LiDAR systems. Structural and statistic-based feature metrics are directly derived from LiDAR waveforms at the pixel level and related to plot-level field data. Initial results reveal a definite correlation between the LiDAR waveform and herbaceous biomass. Ongoing research focuses on the links between fractional cover estimated from imaging spectroscopy and woody biomass. [C1293]

#### "A technique to derive the spatial distribution of rain intensity from NWP data"

Numerical weather predictions provided by world meteorological organizations like ECMWF are unique sources of valuable information about the meteorological situation on a global scale. This paper introduces a technique to derive the spatial distribution of rainfall rate for a given area and time interval, in terms of complementary cumulative distribution function,  $PS(R)$ , from the knowledge of the corresponding total rain amount,  $M_t$ , and of the ratio between convective and total rain amounts  $\Gamma_{\text{CB}}$ . The performance of the method is tested against a large database of radar derived rain field data, from which both the inputs to the algorithm and the associated output  $PS(R)$ s are obtained. [C1294]

#### "A discrete interferometric model for a layer of random medium"

This paper presents a discrete interferometric model of random media. The forest is modeled by characterizing tree trunks, branches and leaves with randomly oriented, lossy dielectric particles whose area and orientation in a layer of random medium are prescribed. The model result is compared to the theoretical result in the literature and good agreement is found. [C1295]

#### "The coherent microwave emission of freezing soil: Experimental research and model simulation"

Interference effect happens in layered medium. The brightness temperature oscillation has been observed during the freezing process of over-saturated soil, which could be explained by interference effect and a three layer coherent model. The modeled BT is qualitatively in consistent with the measurement. It is shown that the interference must be considered when measuring frozen soil with ground based microwave radiometer especially when using the frequency is low. [C1296]

#### "Synthetic retrieval of aerosol optical depth and surface reflectance using Terra and Aqua platforms in semi-arid regions"

Aerosol quantitative retrieval from remote sensing over land surface is still a challenging task, especially for bright land areas such as desert, urban, coast, arid and semi-arid regions. A new aerosol optical depth (AOD) and surface reflectance remote sensing retrieval model is developed by exploiting a kernel-driven BRDF (Bidirectional Reflectance Distribution Function) model and the SYNTAM (Synergy of TERRA and AQUA

MODIS) model, which considered the surface BRDF effect while retrieving AOD. After applying this new model to Terra and Aqua MODIS data in the Heihe River Basin of China, AOD and surface reflectance of this region are retrieved. Results show that the multiple correlation coefficient ( $R^2$ ) between retrieved AOD from MODIS and in situ measurements of CIMEL CE318 Sun-photometers is 0.92 at 0.55/ $\mu\text{m}$ . Using ASD Field Spec spectral radiometer measurements to validate retrieved surface reflectance, the RMSE values for band 1~3 are lower than 0.06. [C1297]

#### "Snow density estimation using Polarimetric ASAR data"

Remote sensing of radar polarimetry has great potential to determine the extent and properties of snow cover. Availability of spaceborne sensor dual polarimetric C-band data of ENVISAT-ASAR can enhance the accuracy in measurement of snow physical parameters as compared to single fixed polarization data measurement. This study shows that the capability of C-band SAR data for estimating dry snow density over snow covered rugged terrain in Himalayan region. The study area lies in Beas, Chandra and Bhaga catchments of Himachal state (India). For this investigation, the main assumptions are that the snow is dry and at C-band, total backscattering coefficient comes from snowpack and snow ground interface. An algorithm for estimating snow density has been developed based on snow volume scattering and snow-ground scattering components. Snow density estimation algorithm requires HH and VV polarization combination data. The radar backscattering coefficients of both HH and VV polarization and incidence angle are given as input to the developed algorithm. Finally, the algorithm gives the snow dielectric constant which can further be related to snow density using Looyenga's semi empirical formula. Comparison was done between algorithm estimated snow density and field value of snow density in the study region. The mean absolute error between estimated and measured snow density was 21.3 kg/m<sup>3</sup>. [C1298]

#### "Study on tobacco spatial agglomeration pattern based on remote sensing and GIS methods in Henan province, China"

Industry spatial agglomeration is a world-wide phenomenon. As the raw material of tobacco industry, tobacco is the only economic crop which is intensive produced in China at present. The statistic data is used to analyze the regional specialization and agglomeration of tobacco planting industry, but the spatial pattern of tobacco sown area is always neglected. In this paper, Henan province is chosen as the study area, and the distribution pattern of tobacco sown area has been studied using RS and GIS methods. According to the analysis of phenology characters of crops, the tobacco sown area and its growing condition were monitored using two-temporal data, which was in Jan and June 2008 respectively. Then the tobacco sown area of each county was calculated and tobacco patch was derived using ARCGIS 9.0. According to the result, the regional Geordie coefficient which indicates industry agglomeration distribution status and the fragmentation index were studied. Results showed the higher regional Geordie coefficient means the higher planting scale at present, but does not totally equal the higher level of aggregation. The fragmentation index of tobacco sown area shows different trend. So both the economic coefficient and the fragmentation index should be considered during discussing the aggregation level. In order to increase the development potential of Henan tobacco industry, it should increase the planting scale of the central part of Henan province. [C1299]

#### "Survey of landslide activity and rockglaciers movement in the Swiss Alps with TerraSAR-X"

Four TerraSAR-X stripmap mode scenes acquired during the late summer of 2008 in the Oberwallis region in the Swiss Alps have been interferometrically analyzed for the survey of the activity of unstable slopes. Differential interferometry was applied using a high precision external Digital Elevation Model (DEM). Position, extent, contour, and approximate velocity of unstable slopes were determined for a large area. Selected results representing rockglacier movement and landslide activity are discussed and compared with in-situ information and interferograms derived from ENVISAT ASAR, JERS-1 SAR and ALOS PASLSAR data. This application strongly benefits from the higher spatial resolution of the TerraSAR-X data in comparison to the C- and L-band sensors used in the past, because many of the instabilities are of relatively small size. [C1300]

#### "Passive real-time localization through wireless sensor networks"

The rapid progress of wireless communication and embedded systems has made wireless sensor networks a valuable backbone for numerous applications, mainly with monitoring purposes. In this field, the need for location aware systems has growth rapidly in the last few years. Most research efforts have been done in node localization but less attention has been paid on the localization and tracking of passive (that do not belong to the network infrastructure) objects. In this paper, the problem of passive object localization is dealt with an innovative methodology based on support vector machine exploiting the received signal strength indicator measured by the nodes. Some preliminary results chosen from the assessment of the proposed approach are presented. [C1301]

### "On sensitivity of Kuroshio modeling in the Luzon Strait with ERS-1/2 wind field forcing"

In this presentation, it is studied that the response of the Kuroshio to forcing provided by three wind products: Comprehensive Ocean-Atmosphere Data Set (COADS); Hellerman & Rosenstein objective analysis data set (HR) and observations made by the ERS radar scatterometer. The sea surface currents of the Kuroshio in the Luzon Strait in winter and summer simulated by the Princeton Ocean Model with the three kind of wind fields are compared with the 20-year (1984-2003) mean surface drifter tracks from MEDs/GTS (Marine Environmental Data Service/Global Telecommunications System, Canada). The simulated surface currents from COADS and ERS wind fields are found to be closer to the mean surface drifter tracks in winter. However, the surface current from HR wind field cannot present the surface current pattern of the drifter tracks. And the model results from ERS wind field show a more accuracy surface current which can be seen from the remote sensing data analyzed by Yuan and Han (2006). In summer, the three wind products all can provide a good wind stress and the surface currents from them show the major features of the current field patterns of the drifter tracks. The distribution of the eddies driven by the three kind of wind fields are analyzed in winter and summer time, respectively. [C1302]

### "A vegetation correction methodology applied for soil moisture retrieval from C-band radar observations"

This research presents a methodology to correct backscatter ( $\Gamma_{\text{Bio}}$ ) observations for vegetation effects. The proposed methodology is based on the concept that the ratio between the surface scattering over the total amount of scattering ( $\Gamma_{\text{Bisurfaceo}}/\Gamma_{\text{Bisoilo}}$ ) is affected only by the vegetation and can be described as a function of the vegetation water content. The data set used in this study was collected at USDA's Optimizing Production Inputs for Economic and Environmental Enhancement (OPE3) experimental site in Beltsville, Maryland (USA) over a corn growth cycle in 2002 and includes C-band (4.75 GHz) HH- and VV-polarized observations acquired at incidence angles of 15, 35 and 55 degrees. During this period the corn crops reached peak biomass of 6.6 kg m<sup>-2</sup> and a soil moisture range varying from 0.02 to 0.26 cm<sup>3</sup>cm<sup>-3</sup>. The results show that through application of the proposed vegetation correction methodology the soil moisture retrieval accuracy can be improved from 0.033 to 0.032 cm<sup>3</sup>cm<sup>-3</sup>, 0.049 to 0.033 cm<sup>3</sup>cm<sup>-3</sup>, and 0.079 to 0.047 cm<sup>3</sup>cm<sup>-3</sup> at incidence angles of 15, 35 and 55 degrees, respectively. [C1303]

### "Microwave satellite data applied for agriculture area-Case study-Poland"

The radar data have been used for establishing the proper crop information system in Poland. The objective of the study is to find an efficient method of crop classification based on satellite microwave data and to find the relationship of different soil-vegetation parameters on backscatter. There is a large demand of microwave images as due to often cloud effect these satellite data are available during a certain growth season. Wielkopolska region located in western Poland was selected for the research works. This region, characterized by intensive agricultural practices and diversified agricultural pattern, was equipped with ground truth information, which enabled to make properly the whole classification process. [C1304]

### "Combined use of Cassini Radar active and passive measurements to characterize Titan morphology"

This paper focuses on the Titan surface parameters retrieval with emphasis on a combination of passive and active microwave measurements from Cassini spacecraft on the areas characterized by large liquid surfaces and neighboring land areas. The methodology consists of a combination of direct modeling and inversion algorithms. First, these surfaces have been described by means of a double layer model which considers an upper liquid hydrocarbons layer and a lower layer compatible with the radar response of the neighboring areas. This model is introduced into a Bayesian framework for the purpose of inferring the likely ranges of some parameters, in particular the optical thickness of the hypothesized liquid hydrocarbons layer and the wind speed. Second, the optical thickness information is used as an input to a forward radiative transfer model calculation to obtain simulated brightness temperatures. Comparison of the observed and computed brightness temperatures allows addressing the consistency of the observations from the two instruments. [C1305]

### "Study on the backscattering characteristic of typical earth substances in northwest of China"

The S-band and C-band FM-CW land-based radar scatterometers were used to measure the backscattering coefficient of a variety of typical earth substances in northwest of China, including: bare soil, frozen soil, bulrush and maize etc. under the different time and different wave band and different polarized condition. First of all, the measurement principle and performance parameters of scatterometer were introduced, the detailed experimental plans and measurements specifications were developed. Based on them, the various units of measurement were

completed successfully. The measurement process of scatterometer was briefly introduced in this work. according to different scattering mechanisms, features are divided into two categories: surface scattering and volume scattering, and analyzed these Scattering Characteristics and the reasons for these differences; combining with the corresponding earth substances scattering model, quantitative studying a function between the backscattering coefficient and surface parameters, getting different surface parameters of features by inversion, and analysis of a variety of influencing factors by comparing the measured datas. [C1306]

#### **"A new blended snow product using visible, microwave and scatterometer satellite data"**

For this blended product, snow cover extent, snow water equivalent (SWE) and snowmelt are mapped and measured globally on a daily or near-daily basis, initially at a resolution of 25 km, utilizing Moderate Resolution Imaging Spectroradiometer (MODIS), Advanced Microwave Scanning Radiometer for NASA's Earth Observing System (AMSR-E) passive microwave data and QuikSCAT scatterometer data. A snow algorithm referred to as the Air Force, NASA Snow Algorithm (ANSA) has been developed, and is still being fine tuned, to derive the above stated snow parameters. The algorithm results have thus far been evaluated in the lower Great Lakes area of North America, in Colorado (Cold Lands Project Experiment sites) in portions of Finland, and eastern Turkey. [C1307]

#### **"Establishing field and base camp servers for remote sensing of ice sheets in ilulissat, Greenland"**

The University of Indiana and Elizabeth City State University are working with the Center for Remote Sensing of Ice Sheets (CReSIS) to develop and deploy cyberinfrastructure grid computing resources and synthetic aperture radar (SAR) data storage capabilities for Greenland and Antarctic fieldwork. This paper will detail the Summer 2008 efforts of the Polar Grid team to configure and establish field and base camp servers. The base camp system consists of one eight-core server, three raid arrays with 34 terabytes (TB) of total storage in a RAID 10 configuration (13 TB useable), a custom designed compact peripheral control interface (CPCI) system, and 80 TB of external storage in the form of 40 two TB MyBook external hard drives. The field camp system also consisted of one eight-core server, but did not contain the raid arrays. Multiple SATA hard drives were used to store the data. [C1308]

#### **"Derivation of glacier velocity from SAR and optical data with feature tracking"**

Monitoring temperate glacier activity has become more and more necessary for economical and security reasons and as an indicator of the local effects of global climate. The most studied variable in ice dynamics in the literature is ice velocity. From remotely sensed images, mainly two types of methods have been used for the estimation of glacier flow velocities: feature tracking and differential interferometry (DInSAR). In this paper velocities of the Keqikaer glacier are acquired from ALOS (Advanced Land Observing Satellite) optical and SAR data respectively with feature tracking. We show that different window size in correlation calculation of feature tracking leads to different flow field. We also developed a new method to determine the best window size, and the method is testified by the two kinds of data. [C1309]

#### **"High-compacted FM-CW SAR for boarding on small UAVs"**

In this paper a compact, lightweight, low power consumption airborne SAR sensor able to be fitted in an UAV is presented. The Air-Based Remote Sensing (ARBRES) system is based on the previous experience acquired in developing GB-SAR sensors for subsidence and landslide monitoring. Prior to the in-flight evaluation of the developed SAR, different tests were performed boarding the hardware on a car to evaluate its performance. After this debugging step, tests of the system in an airborne platform were carried out and the results are presented. GPS and INS systems are used to record the aircraft position, velocity, and attitude for future Motion Compensation (MoCo) Techniques. [C1310]

#### **"Coseismic surface deformation caused by the Wenchuan M8 earthquake from InSAR data analysis"**

The D-InSAR technology is used to aquired seven belts of coseismic surface deformation of Sichuan M8 earthquake of 12 May 2008 from the ALOS/PALSAR satellite data of Japan. The result covers Yinxu, Dujiangyan, Wenchuan, Moxian, Beichuan, Pingwu and Qingchuan county, each 500 km in north-south and 70 km in east-west. The investigation indicates that the surface rupture zone caused by the earthquake coincides the Beichuan-Yingxiu fault, extending from nearby the epicenter southwest of the Yingxiu town to north of the Suhe, Qingchuan county for about 230 km. The northwest wall of the seismogenic fault has uplifted, exhibiting a dominant thrust motion. The maximum relative LOS displacement at the epicenter reaches 260 cm. A swell of LOS 120-180 cm displacements is present from Beichuan to Pingtong. Another uplifted belt of displacements 70-80 cm occurs nearby north of Suhe, Qingchuan. Around Ya'an and Mount Emeishan, and from Shehong to north

of Chongqing, there is a large area of subsidence. In Chongqing and its south is seen a small uplifted area of 20-30 cm. From Qingchuan, eastward to Guangyuan and Ningqiang, uplift amplitudes are 60-70 cm. The whole area of the deformation filed is fairly large, even in the Sichuan basin occurs surface deformation of different degrees. [C1311]

### "Constellations: A new paradigm for earth observations"

The last decade has seen a significant increase in the number and the capabilities of remote sensing satellites launched by the international community. A relatively new approach is the launching of heterogeneous satellites to form constellations. Constellations provide scientists a capability to acquire science data, not only from specific instruments on a single satellite, but also from instruments on other satellites that fly in close proximity. Constellation design is driven primarily by science requirements. Scientists from each member satellite choose the orbit that enables their science and concurrent observations with the other satellites. Although the satellites are controlled by different organizations around the world, the teams cooperate and coordinate operations to ensure safety. This paper presents the benefits of joining an on-orbit constellation and ideas for the longterm evolution of constellations. [C1312]

### "Potentials of RADARSAT-2 data to monitor freezing/thawing cycles over agricultural lands in Canada"

The target decompositions technique of Freeman-Durden is used to monitor freeze/thaw cycles, with fully polarimetric RADARSAT-2 images acquired over agricultural areas. In this paper is presented a preliminary analysis of the scattering mechanisms derived from three RADARSAT-2 acquisitions during the fall of 2008, over agricultural sites located in Saskatchewan, Ontario and Quebec. AMSR-E brightness temperatures data is also used in the analysis. Contrary to expectations, results indicate that surface scattering represents the main contribution to the signal over frozen soils. [C1313]

### "The results of preliminary measurements of snow and water ice microwave reflection and emission angular dependences at 5, 6GHz"

In this paper structural and operational features of C-band, dual-polarization, combined scatterometer-radiometer system and the results of preliminary, spatio-temporally collocated measurements of land snow cover's and experimental pool water surface ice cover's microwave reflective (radar backscattering coefficient) and emissive (brightness temperature) characteristics angular dependences at ~5.6 GHz are presented. [C1314]

### "Evaluating snow depth in Western China based on passive microwave remote sensing"

In order to evaluate the accuracy of snow water equivalent (SWE) inversion algorithm for passive microwave sensor Advanced Microwave Scanning Radiometer-Earth Observing System (AMSR-E) in Western China, we compared SWE got from AMSR-E daily SWE product with the ground measurements from 15 meteorological stations in Tibetan plateau. The results show AMSR-E overestimate SWE in this regions and the RMSE is 21mm Tibetan plateau. Through incorporating snow fraction factor, a new empirical algorithm estimate snow depth and SWE have been developed in Tibet. This new algorithm appeared higher accuracy than AMSR-E. Due to complex topography, shallow patchy snow and frozen grounds covered at the Tibetan Plateau, this technique didn't show good results. In future we will focus on how to evaluate and eliminate the effects of these factors quantitatively on SWE retrieval. [C1315]

### "The glacier movement estimation and analysis with InSAR in the Qinghai-Tibetan plateau"

The glacier is important factor in climatological and hydrological investigations, especially in the western China. Glacier changes are among the clearest signals of on-going warming trends existing in nature. In view of environmental changes, combined with the high thermal sensitivity of earth's mountain glaciers, especially in Qinghai-Tibetan Plateau, is of growing interest. SAR systems have an important ability to observe the earth's surface, independent of cloud conditions. Particularly, the SAR interferometry provides a useful tool for monitoring the velocity of glacier movement. For accurate measurement of glacier movement with InSAR data, the suitable method of retrieving velocity of glacier motion need be considered for the different type of glaciers in case of the difference of the characteristics of surface and movement velocity. In this paper, we use the SAR interferometry to derive the movement of several types of glaciers and analyze the characteristics of different glaciers type, such as continental glacier, sub-continental glacier and maritime glacier, and demonstrate the method and results for the glacier motion in the Qinghai-Tibetan plateau. [C1316]

### "Sea ice concentration and type analysis from dual pol Radarsat-2 and Modis images in the Baltic"

## Sea"

A sea ice classification technique is introduced. The classification was performed on Radarsat-2 dual polarization image (07.02.2009) and MODIS images (09.02.2009) that covered coastal area in the western part of Baltic Sea. The classification on SAR image was based on Shannon entropy differences that occur on various ice types. Analysis showed that four ice types (water, fast ice, ridged ice and deformed ice) were identifiable. Also two independent analysis were performed on MODIS image. The spectral classification enabled to separate ridged ice regions and fast ice areas. Using histogram analysis ice concentration map was created. The analysis of Modis image enabled to identify regions where water was covering ice surface. The same phenomena was also detected from SAR data. [C1317]

## "Ground based SAR survey of Basal interface at NEEM drill site"

In August of 2008 a radar survey was conducted at the NEEM site in Greenland. An example echogram showing internal layers all the way to the bed, a digital elevation map around the drill site, and a side looking synthetic aperture radar image will be presented. The echogram appears to show a fairly continuous Eemian layer where predicted by modeling. Additionally the area around the drill site is very flat although some slope variation is observed. Finally side looking SAR images show reflected power variations that need more analysis to determine their source. [C1318]

## "Experimental results with bistatic SAR tomography"

This paper gives a quick overview of inversion methods for bistatic tomographic processing. The methods are tested over simulated and real data. The real data has been acquired from a set of indoor experiments carried out in the Radiation Laboratory (RadLab), at the University of Michigan. A scale model with a house, some trees and a rough surface on the ground has been built to reproduce an urban scenario. [C1319]

## "Study on bistatic SAR ocean wave imaging mechanism"

In order to develop bistatic SAR ocean investigation, the first issue is the study of bistatic SAR ocean surface imaging mechanism. And velocity bunching mechanism is a SAR inherent modulation. Thus, the intensity expression in the bistatic SAR image plane is derived in this paper. The expression describes quantitatively the displacement of the scatter elements in the image plane and a degradation in radar resolution in azimuthal direction. In addition, a bistatic SAR linear velocity bunching transfer function is obtained in the linear parameter regime. Finally, this paper analyzes qualitatively the effects that various platform observation conditions have on the bistatic SAR linear imaging range of wave spectrum. [C1320]

## "A new calculation method of NuSAR for translational variant bistatic SAR"

Processing bistatic SAR image all through numerical calculation is the concept of NuSAR. In this paper, the block scheme of NuSAR is modified to handle the translational variant case. Then a new calculation method of NuSAR is provided, which saves half of the memory compared with the existing calculation method. The provided new NuSAR is practical and can handle the spaceborne-airborne configuration. [C1321]

## "Monitoring a tunneling in an urbanized area with Terrasar-X interferometry-Surface deformation measurements and atmospheric error treatment"

We present results from a deformation monitoring to demonstrate potential and limitations of TerraSAR-X interferometry to measure vertical displacements due to the tunneling of main sewerage pipes along the river Emscher in Germany. In spite of higher sensitivity for deformation gradients the potential for deformation monitoring benefits from high spatial and temporal resolution of the TerraSAR-X data. We analyzed a large stack of TerraSAR-X stripmap scenes to derive regional pattern of vertical displacements with differential SAR Interferometry and small-scale displacements and deformation of objects (infrastructure and houses) in time series of SAR-scenes with Persistent Scatterer Interferometry (PSI). First results from PSI are promising with a great number of detected PS. We show deformation measurements with Artificial Corner Reflectors. Short-time interferograms (11 or 22 days) show high coherence for large areas and therefore are likely less infected by unwrapping errors. Atmospheric errors are important for X-Band SAR. Expected deformation in our application is in the range of mm to cm, similar to tropospheric delay features in their spatial and temporal extent. The atmospheric phase screen in PSI and stacking procedures are smoothing the nonuniform deformation history of progressing tunneling. [C1322]

## "Investigation of Radarsat-2 and Terrasar-X data for river ice classification"

To date, monitoring of river ice using remote sensing has mainly focused on the use of mono-polarized and multi-polarized C-band radar data only. In this paper, Support Vector Machine (SVM) classifications using polarimetric parameters are tested to identify types of river ice. Classification algorithms are validated on the newly available C-band Radarsat-2 and X-band Terrasar-X data to investigate the potential of this new imagery, acquired in winter 2009. An electromagnetic model is improved to simulate the polarimetric response of a river ice cover to understand the interactions of the radar signal with the ice cover. At C-band, using dual-polarized data over mono-polarized data increases by 23.9% the final classification producer accuracy. Furthermore, the best producer accuracy is 91.6% when using dual-pol data at C-band, which stand for a gain of 2.2% compared to dual-pol data at X-band. [C1323]

#### "Multi-thematic exploitation of TerraSAR-X images in the context of the kalideos reference datasets"

This paper presents the use of TerraSAR-X images in the context of the Kalideos programme, which aims at providing the user community with time series of multi-spectral (optical and radar) and multi-resolution remote sensing imagery. 120 TerraSAR-X acquisitions are scheduled for three distinct thematics: volcano monitoring (Reunion island site), sugarcane crop monitoring (Reunion island site) and forest monitoring (Arcachon/Landes forest site). We describe here the advancement of these studies, focusing on sugarcane crop monitoring which is the most advanced one. These studies will serve as typical examples of multi-thematic use of TerraSAR-X imagery and demonstrate the relevance of TerraSAR-X imagery for the development of scientific reference datasets. [C1324]

#### "A fast numerical method for scattering from dielectric rough surfaces"

In this paper we propose a fast numerical method for EM scattering from one-dimensional dielectric rough surfaces. we first employ a new impedance matrix splitting scheme for the associated iterative system. We further develop a block operation method to accelerate computation, which transform a  $2N \Gamma B \rightarrow 2N$  problem to a  $N \Gamma B \rightarrow N$  one. Due to block operation, run time can be saved about 1/3. Through extensive numerical simulation, our proposed method has demonstrated much improved speed over FBM, and considerably improved convergence behavior over FBM-SA. [C1325]

#### "Development of a simple scattering model for vegetation canopies and examination of its validity with scatterometer measurements of green-onion fields"

A simple scattering model for radar backscattering from vegetated surfaces is developed based on the radiative transfer technique. The number of input parameters of the model is minimized to simplify the scattering model. The validity of the model is examined by comparison between the computation outputs and scatterometer measurements for the backscattering coefficients of green-onion (scallion) fields. [C1326]

#### "Numerical modeling of a spiral-antenna GPR system"

To better study the ground penetrating radar (GPR) problem, an important step is to develop an accurate simulation of the fields induced by the radiating antennas. In this work, a finite-difference time-domain (FDTD) model of a spiral-antenna GPR system was developed and verified against measurements of a prototype system. The paper discusses difficulties in modeling the antenna elements and presents evidence that the model properly predicts the response of the antennas to scatterers in the presence of the ground. [C1327]

#### "A GPS signal based numeric range migration algorithm of space-surface bistatic SAR"

In this paper, we present a new numeric bistatic range migration algorithm (RMA), specifically designed for GPS signal based space-surface bistatic SAR(SS-BSAR). It can be applied to any arbitrary trajectory BSAR imaging system. Based on the principle of stationary phase and the geometric relationship of the SS-BSAR, a two dimensional (2-D) precise analytic response expression of point targets in frequency domain is deduced first. Then a numeric RMA is proposed which match function and interpolation function are derived numerically. The proposed RMA can process wide SAR scene at once and the shape distortion can be corrected at the same time. Simulation results illustrate the validity of the proposed approach. [C1328]

#### "Chirp scaling algorithm for parallel bistatic SAR data processing"

This paper discusses parallel bistatic synthetic aperture radar (SAR) processing using chirp scaling algorithm. The key step is to use an analytical form of the signal spectrum derived by the geometry-based bistatic formula (GBF) method. With the above formula, a chirp scaling (CS) algorithm is proposed for azimuth-shift-invariant bistatic SAR processing. The presented algorithm can well resolve the range variation of motion through range

cell(MTRC) for bistatic SAR, and requires no interpolate; it requires only FFTs and complex multiplies, these attributes lead to efficient implementations of FFT-based signal processors and high speed parallel processors; it can be used for high resolution image formation. [C1329]

#### "Hybrid of the method of moments/ Monte Carlo technique and a surface scattering model for estimating the radar backscatters OF harvested farm fields"

The method of moments/Monte Carlo technique is used to numerically compute the Mueller matrix for radar backscattering from stem-cut cluster sections of a harvested farm field, and a semi-empirical surface scattering model is employed for estimating the radar backscatter of a rough soil surface. The full-wave numerical technique and the surface scattering model are combined to compute the Mueller matrix and consequently the backscattering coefficients of a harvest farm field. This hybrid technique is verified comparing the numerical computations with the experimental measurements for the backscattering coefficients of harvested rice fields. [C1330]

#### "Assessment of urban extent and imperviousness of Cape Town using TerraSAR-X and Landsat images"

The worldwide urban growth leads to an increase in impervious surface, which in turn has many negative consequences for the environment. For an assessment of these phenomena in this study first TerraSAR-X radar data are classified using a knowledge-based approach to detect the extent of urban areas. Subsequently within this area the percentage of imperviousness is estimated by using a Support Vector Regression model with optical Landsat images and high resolution aerial pictures. These methods were developed for urban areas in Germany and transferred to Cape Town, South Africa. The overall accuracy of the settlement detection is 82.3 % and the mean error of the percentage of imperviousness is 14.1 % with a local regression model. It was also possible to apply a model generated for the German city of Munich for Cape Town but the absolute mean error increased to 32.8 %, indicating the necessity to further improve the radiometric adjustment. [C1331]

#### "On the accuracy of scatterers LOS rotation estimation procedures in radar polarimetry"

The Line-of-Sight (LOS) rotation angle of scatterers can be estimated using polarimetric radar measurements. Exact estimation is unrealistic since noise and clutter are almost always present in the data. The paper presents the derivation of an approximated distribution, mean bias and variance analysis, of the scatterers LOS rotation angle using polarimetry, when estimated for the high-coherent (quasi-deterministic) scattering case. Example of scatterers fulfilling such condition are the so-called Coherent Scatterers (CSs). [C1332]

#### "Validation of RADARSAT-2 Polarimetric SAR measurements of ocean waves"

Four C-band fully polarimetric synthetic aperture radar (POLSAR) images of ocean waves from the RADARSAT-2 SAR are used to measure ocean slopes and wave spectra. A new technique has been developed to measure wave slopes in the SAR azimuth and range directions. The POLSAR ocean wave parameter measurements were validated with in situ observations from an NOAA National Data buoy Center (NDBC) buoy. The results show that wave parameters measured using the new method are in good agreement with in situ NDBC measurement products. [C1333]

#### "Cross-comparison and validation of MODIS AQUA cloud mask by using CLOUDSAT and CALIPSO datasets"

This paper presents a cross-comparison of the data acquired by the MODIS, CLOUDSAT and CALIPSO sensors in order to understand the limit of the developed cloud-mask algorithm and to provide a quantitative validation assessment by using exclusively remotely sensed data. The comparison has been carried out by considering both the cloud mask and the intermediate levels such as the brightness temperatures and the reflectance values for different channels from which the cloud mask is derived. The preliminary analysis indicates a general good agreement among the different sources. A main underestimation of cloud cover is present on the sea and especially for high thin clouds. First results indicate that in order to increase the cloud cover accuracy the threshold for the intermediate levels (brightness temperature and reflectance values) may be changed by taking into account also the cloud vertical profiles. [C1334]

#### "Polarimetric analysis over African savanna woodland using ALOS/PALSAR"

This paper presents polarimetric analysis over African Savanna woodland using ALOS/PALSAR to investigate the trend between backscatter and biomass levels. An extensive field inventory was carried out combining Differential GPS and conventional topographic mapping techniques. Geographic position, basal diameter and

height of trees in sampled plots were measured. Plot level biomass quantities were obtained using established allometry for the region. Geocoded ALOS/PALSAR level 1.1 and 1.5 data is checked for accuracy against existing geospatial data for the case study area. Sigma nought, Freeman and Pauli component are extracted for the sampled plots to investigate the relationship between biomass, volume and double bounce scattering. Finally a comparison of sigma nought, Freeman and Pauli components is carried out to analyze trend against volume and double bounce scattering. [C1335]

### "Backscatter and interferometry for estimating above-ground biomass of sparse woodland: A case study in Belize"

Tropical savannas cover 20% of the Earth's land surface and are important ecosystems in the global carbon cycle due to their high productivity. This paper evaluates the use of SAR for estimating above-ground biomass of the woody vegetation in heterogeneous tropical savanna woodland in Belize, Central America. Single-pass shortwave InSAR data used are X-band (Intermap) and C-band (AIRSAR and SRTM). L- and P-band SAR backscatter data are from AIRSAR. Results show that SAR backscatter has a relatively low correlation to above ground biomass in the sparse savanna woodlands. Retrieved canopy heights from both X- and C-band InSAR give a better representation of the spatial distribution of AGB, but cannot be used to estimate biomass directly due to the heterogeneity of the canopy. [C1336]

### "Geological mapping in the zone of Chotts, Tunisia, using ALOS sensors"

The three sensors onboard the Advanced Land Observing Satellite (ALOS) are the Phased Array L-band Synthetic Aperture Radar (PALSAR), the Panchromatic Remote-Sensing Instrument for Stereo Mapping (PRISM), and the Advanced Visible and Near-Infrared Radiometer type 2 (AVNIR-2). Each of them has been evaluated for the geological mapping of the Zone of Chotts, Tunisia. Both the endoreic basins and the surrounding ranges have been studied. The 10 m-resolution AVNIR-2 sensor is a good trade-off for geological mapping. The 2.5 m-resolution PRISM sensor with its stereoscopic capability is very useful for the detailed study of sedimentary layers. Copolarized radar data are relevant for the study of the flat itself but the C-band is more accurate for sensing the roughness of the finer sediments (sand veneers, evaporites, etc.). The HV polarization is suitable for identifying the presence of halophytic plants that fringe the upper part of the flat. [C1337]

### "Extraction of traffic flows and surface current information using Terrasar-X Along-track interferometry data"

TerraSAR-X offers different possibilities for Along-track Interferometry (ATI) SAR data acquisition. This enables to test new SAR applications for the detection and measurement of moving ground objects from space. In this paper we demonstrate space-borne traffic flow measurements using TerraSAR-X ATI data and an automatic traffic data extraction processor. The obtained results evidence the potential of space-borne SAR for this particular application. The traffic information can be derived in near-real time, which underlines the practicability of the method. Another application of TerraSAR-X ATI is the measurement of water surface currents, of which we also show a first example. [C1338]

### "Analysis of first Terrasar-X along-track InSAR-derived surface current fields"

The potential of the along-track interferometric SAR (along-track InSAR, ATI) modes of TerraSAR-X for high-resolution imaging of surface current fields has been discussed in several publications. In this paper we show first results based on actual TerraSAR-X ATI data, explain our data processing procedure, and give an update on the status of the instrument and on upcoming developments. [C1339]

### "Curvelet-based change detection for man-made objects from SAR images"

In this article we present a technique for fast and robust change detection based on the curvelet transform. The curvelet transform is a two dimensional further development of the well-known wavelet transform that reconstructs the original image by ridge-like features, called ridgelets, in different scales, directions and positions. Geocoded SAR amplitude images from TerraSAR-X are compared by differentiating the coefficients of both images in the curvelet coefficient domain. Before the difference image is transformed back to the spatial domain, the influence of the single ridgelets on the resulting image can be manipulated to suppress noise and to intensify structures. Two examples were chosen to show the potential of this approach: a construction site in Germany and an open cast mining area in Chile. Our prototype version is able to compare time series without any interaction of an operator so that the implemented algorithms can easily be embedded into an automatic processing chain. [C1340]

### "Synergetic use of multi-temporal ALOS PALSAR and ENVISAT ASAR data for topographic/land cover mapping and monitoring at national scale in Africa"

The use of Synthetic Aperture Radar (SAR) data in large parts of the African countries, in particular for those close to the equator, is often *conditio sine qua non*, simply due to the fact that optical data are severely hampered by clouds, especially during the raining (corresponding to the crop) season. The objective of this paper is to present a methodology-and the related results-for the generation of land cover maps and changes over large areas by fusing single-date or interferometric ALOS PALSAR Fine/Dual Beam data with multi-temporal ENVISAT ASAR Image Mode/Alternating Polarization intensity. In synthesis, the method is based on data fusion by exclusively considering-in the prior knowledge-based classifier that requires neither user-defined parameters nor reference samples-the data characteristics and related acquisition modes. Results clearly show that the synergetic use enables the reliable identification of key land cover types (in particular cropped areas, bare soil areas, forestry, forest clear cut, forest burnt areas, water bodies) and their evolution over time, providing basic information on the land cover status. Finally, it is shown that using the same 46-days interferometric ALOS PALSAR data set, a Digital Elevation Model (DEM) with higher quality than the Shuttle Radar Topographic Mission (SRTM) one can be generated in those nearly equatorial-non dense forest-regions.

[C1341]

### "Exploitation of ALOS-PALSAR SAR full-polarimetry data to the mapping of an African region"

Due to their large scale of observation and their relatively high revisiting frequency, spaceborne SAR systems offer interesting possibilities for the systematic monitoring of land cover. Several techniques have been developed to analyze land cover areas from single-polarization spaceborne SAR data, based on the statistical properties of the reflectivity of such complex media and its spatial variations (texture). The reduced resolution of the data, compared to the airborne SAR case, is a particularly limiting factor. Polarization diversity offers an interesting and powerful alternative mean to characterize land cover areas. In this paper, we propose to use polarimetric SAR acquired by the ALOS sensor at L band, to monitor land cover of an African region. [C1342]

### "Wiener prediction-based change detection for locating mines in multilook SAR imagery"

In this paper, we present a Wiener-based change detection method and compare its performance with several other methods for a pair of multi-look synthetic aperture radar (SAR) images of the same scene. We implement and compare several techniques which vary in complexity. Among the simple methods that are implemented are differencing, Euclidean distance, and image ratioing. These methods require minimal processing time, with little computational complexity, and incorporate no statistical information. We also implemented methods which incorporate second order statistic calculations in making a change decision in efforts to mitigate false alarms arising from the speckle noise, misregistration errors, and nonlinear variations in SAR images. These methods include a Wiener prediction-based method, Mahalanobis distance measure and subspace projection method. We compare the performance of these methods using multi-look SAR images containing several targets (mines). We present results in the form of receiver operating characteristics (ROC) curves. [C1343]

### "Preliminary Terrasar-X observations for temperate glaciers on the Chamonix Mont Blanc test site"

Due to their high temporal variability, monitoring temperate glaciers by in-situ measurements is quite hazardous. The new TerraSAR-X (TSX) sensor provides high resolution SAR data which can be acquired every 11 days in the same configuration and can cover the whole surface of several glaciers in a studied area. Their potential for temperate glacier monitoring by remote sensing has to be investigated. This paper presents some early results on the Argentière/Bière glacier test site in the Mont Blanc massif to estimate the surface velocity using some texture tracking methods. After having evaluated the Differential Interferometric SAR (DInSAR) potential with TSX Stripmap data, correlation and Maximum Likelihood (ML) based methods are performed on the texture variable extracted from the Spherically Invariant Random Vectors (SIRV) estimation scheme. [C1344]

### "Comparison of helicopter-borne thin sea ice thickness profiles with polarimetric signatures of dual-pol Terrasar-X data"

In this paper first results of a sensitivity study using dual polarimetric TerraSAR-X data for ice thickness estimation are presented. The sea ice thickness reference data set was measured, coincident to the SAR data take, by means of a helicopter-borne EM sounding device on April 28, 2008 in the Russian Arctic. For some of the signatures, namely the complex correlation coefficient, a relation to ice thickness could be found that is theoretically predicted for L-band SAR. The first results show, that the new generation of polarimetric space borne SAR sensors like TerraSAR-X may open a new opportunity for thin sea ice thickness monitoring from space. [C1345]

### **"Radio base network and tomographic processing for real time estimation of the rainfall rate fields"**

In this paper, we propose a novel remote sensing method that is adequate for rainfall rate measurements in real time by means of tomographic processing applied to power attenuation measurements made across the microwave links defined by radio base station networks for mobile communication systems. A description of the tomographic algorithms we developed is presented together with some simulation results. These concern rainfall rate estimation applying such algorithms to the current radio base station arrangement over the city of Florence, Italy, while the rainfall field is simulated through weather radar data. [C1346]

### **"The use of ALOS PALSAR for supporting sustainable forest use in southern Africa: A case study in Malawi"**

Malawi is facing a forest loss crisis with demand far outstripping sustainable supply. Recent projections suggest that there will be no primary forest left in Malawi by 2020. One possibly method to support forest protection has come from the proposed introduction of REDD (Reductions in Emissions from Deforestation and Degradation) schemes into the next international climate protocol. This study aims to assess the ability of ALOS PALSAR for providing biomass estimates in miombo woodland in Malawi. No correlation has been found between ALOS PALSAR backscatter and a number of different forest parameters including biomass, stem diameter at 1.3 meters (dbh), stem volume, and the BCI (Biomass Consolidation Index). [C1347]

### **"L-band and C-band InSAR studies of African volcanic areas"**

Radar interferometry has proven to be a very suitable, low-cost and accurate tool to measure surface displacements. We investigate several data fusion or time-series analysis strategies which aim to mitigate C-band InSAR restrictions for volcano deformation monitoring applications. The focus is on active African volcanic areas. Firstly, data fusion of C-band ENVISAT/ASAR and L-band ALOS/PALSAR sensors helps the determination of a rifting event sequence that took place in summer 2007 in Lake Natron area. The second strategy investigated is a new Wavelet Based InSAR time series applied on ERS-2 data covering the Nyiragongo-Nyamulagira area. It allows new ground displacements identifications outside the local rift valley. Lastly, PALSAR Quad-Pol POLInSAR applicability is explored for La Palma Island. [C1348]

### **"Synthetic aperture radar data employed for soil moisture estimation in the Piketberg region, South Africa"**

Information on the distribution of surface soil moisture is important for a number of applications. Due to the high temporal and spatial variability, and consequently the cost of monitoring by field observations, a means of remote monitoring of soil moisture content using remote sensing data is needed. The aim of this study was to test soil moisture retrieval algorithms based on synthetic aperture radar data (SAR). This includes the use of Envisat ASAR and ALOS PALSAR data, which was provided by the European Space Agency. Both linear regression and multiple-polarization models were applied for soil moisture quantification. The results could not be validated due to a lack of distributed field-based measurements but were compared to rainfall figures over the same period. Though inconclusive, the results suggest that the techniques show promise in their ability to quantify surface soil moisture. [C1349]

### **"Results and analysis of hybrid bistatic SAR experiments with spaceborne, airborne and stationary sensors"**

Bistatic SAR is a promising and useful supplement to a classical monostatic SAR system. Since transmitter and receiver are spatially separated, additional information of a scene may be provided. Further, as shadowing, layover, and foreshortening depend on the bistatic geometry, which can be quite different to the monostatic case, they can contribute to image analysis and classification. The transmitter and receiver are located on different platforms, which may either be close together or hundreds of kilometers apart. Typical platforms are satellites, UAVs, aircrafts, and towers. This paper presents recent bistatic SAR experiments with spaceborne, airborne, and stationary sensors, which have been conducted at FHR or in cooperation with Defence Research & Development Canada. Image results are presented and analyzed with respect to scattering behavior and resolution and compared to monostatic images. [C1350]

### **"New processing approach and results for bistatic TerraSAR-X/F-SAR spaceborne-airborne experiments"**

Following the success of the first bistatic spaceborne-airborne experiment between TerraSAR-X and F-SAR carried out in November 2007, DLR has performed a second bistatic experiment in July 2008 with new

challenging acquisitions. Furthermore, the existing bistatic processing chain has been updated with two significant improvements: a) clock offset synchronisation is now performed without the use of reference targets, and b) SAR imaging is done using a fast focussing technique. The new SAR imaging algorithm, based on the fast factorised backprojection algorithm, has proved very good focussing qualities while dramatically reducing (up to a factor 100 with respect to direct backprojection) the overall computational load. The new processing chain is tested using the image of the first TerraSAR-X experiment. Results of a dualpol acquisition performed during the second TerraSAR-X/F-SAR experiment and showing the first dual-pol bistatic spaceborne-airborne images are also presented in this paper. [C1351]

#### **"Repeat-pass interferometry using a fixed-receiver and ERS-2/ENVISAT as transmitters of opportunity"**

The presented work discusses the processing of repeat-pass interferometric data acquired with SABRINA (SAR Bistatic Receiver for INterferometric Applications), where the receiver is fixed and the baseline is due to the two different satellite orbits. The paper addresses the particularities of bistatic interferometry like the coregistration of the images and the decorrelation factors affecting the interferometric phase. Theoretical developments are complemented with the first repeat-pass results. The characteristics of the scene and the 35 days temporal baseline have caused the interferogram to be severely affected by the temporal decorrelation. This first result opens the discussion of what kind of targets are seen in a bistatic geometry and which of them can be coherent along time. [C1352]

#### **"TerraSAR-X observations of the recovery glacier system, Antarctica"**

We present a comparison of 1997 RADARSAT Antarctic Mapping Project (RAMP) SAR data with 2008-09 TerraSAR-X observations of a tributary glacier that is part of the Recovery Glacier drainage network in Coates Land Antarctica. The Recovery Glacier system is of scientific interest because of its role in discharging East Antarctic ice to the sea and because it has been subsequently learned that the flow of the glacier is likely controlled by the presence of subglacial lakes near the onset of faster glacier flow. [C1353]

#### **"Determination of variations in glacier surface movements through high resolution interferometry; Bylot Island, Canada"**

Interferograms were generated from 10 TerraSAR-X image pairs, with the objective of obtaining estimates of winter surface motion for a slow-moving polythermal arctic glacier. Flow directions were computed using both ascending and descending-pass interferograms for each period, with the median value being adopted as the final direction. The weighted average flow was computed, with weighting based on the inverse of the difference between the ascending and descending-pass displacement estimates for each date. This study uses multiple interferograms with different imaging geometries to provide estimates of down-glacier flow. The methodology adopted minimizes the effects of glacier / satellite track alignment and those resulting from vertical motion of the glacier surface. Current velocities were compared with flow estimates derived from a 1992 ERS-1 image pair. The velocities were similar over most of the glacier, but current velocities were found to be 30% to 50% lower on the lower glacier. [C1354]

#### **"Bistatic experiment with the UWB-CARABAS sensor-First results and prospects of future applications"**

Bistatic SAR experiments are in focus in recent years. We will present first results of an airborne bistatic experiment conducted 2007 in Switzerland with the Swedish ultrawideband sensor CARABAS, operating at 28-73 MHz (UWB). The acquired bistatic data include HH and HV polarization with different bistatic elevation angles, various transmitting flight tracks-including non-linear tracks-and fixed receiving antennas (horizontal and vertical) installed on a mountain top. We will place an emphasis on the processing, improving and evaluating of the data and give an overview of future applications which are made feasible by this bistatic dataset. [C1355]

#### **"Estimation of snow water equivalent using a parameterized snow model"**

Snow Water Equivalent (SWE) is a crucial parameter in the studies of hydrology and climatology. Estimating SWE by using high-resolution radar systems, especially those capable of providing high-frequency observations, is an important task in the microwave studies. In this paper, a parameterized snow scattering model was first developed to provide the model basis for the snow inversion problems. A scheme based on the parameterized model, analysis on the depolarization factor as well as the scattering and extinction relationships between X and Ku-band snow backscattering signals was then developed for SWE inversion. Initial evaluation on the technique was made through theoretically simulated database. The estimated SWE is found to be well correlated with

simulated SWE with an acceptable accuracy. [C1356]

### "Performance analysis of a cross-frequency detector of pulsed sinusoidal RFI in Microwave Radiometry"

The performance of a cross-frequency detector against pulsed sinusoidal Radio Frequency Interference (RFI) is analyzed theoretically. The effects of duty cycle and RFI strength are examined, and the detection performance of the cross-frequency algorithm is compared with that achieved by pulse and kurtosis detectors. The performance loss that occurs in the cross-frequency algorithm when an RFI source is not centered in a frequency channel is also quantified, and a computationally simple model for this loss is described. [C1357]

### "Sea ice SAR classification based on edge features"

In addition to the areal backscattering, the information in sea ice SAR images is in the edges. Here we propose some novel features for sea ice SAR classification. The features are mainly based on the information extracted from the edges detected by an edge detection algorithm, and segment edges at segment boundaries. [C1358]

### "Contribution of the inter-channel polarimetric coherence for soil classification"

Fully polarimetric SAR (POL-SAR) images provide a large amount of information through the four channels HH, VV, HV and VH. They proved to be useful in many applications such as delimiting homogenous areas. Such large amounts of data require robust processing algorithms with minimal supervision and low complexity, especially for classification purposes. Most existing classification algorithms (H/A/alpha for instance) use combinations of some or all the channels as features for classification. In this paper, we present a new approach for polarimetric images classification. We are interested in the information of the inter-channel polarimetric coherence as a feature element for the classification algorithm. The coherence information is known for being used in multi-temporal acquisitions for its advantage of detecting changes in the scenes during time. It is commonly used in interferometry. We want to profit from this information in the case of polarimetric images in order to take advantage of the multi-channel property of the data. This coherence classification approach (reading images, computing the coherence and the classification) will be implemented within the OTB (ORFEO ToolBox), the free software which is dedicated especially for remote sensing imagery processing. The approach is tested using images acquired by the CV-580 airborne near Ottawa, Ontario, Canada. [C1359]

### "Retrieval of snow parameters from Ku-band and X-band radar backscatter measurements"

Techniques for the retrieval of snow properties from Ku- and X-band radar backscatter measurements were investigated. The work contributes to feasibility studies for the CoReH2O satellite mission of ESA for which a dual frequency SAR, operating at Ku-band (17.2 GHz) and X-band (9.6 GHz), VV and VH polarizations, is proposed. A main parameter to be measured is the snow water equivalent (SWE). For the retrieval of SWE it is necessary to separate the backscatter contributions of the snow volume and the background target and to account for effects of snow grain size. The current version of the SWE retrieval algorithm applies the maximum likelihood approach matching radiative transfer forward computations with measured backscatter data. An application example for SWE retrieval is shown for the Cold Land Processes Experiment (CLPX-II) in Alaska, using Ku-band data of the NASA-JPL PolScat and X-band data of the TerraSAR-X satellite as input. [C1360]

### "Comparison with CLPX II airborne data using DMRT model"

In this paper, we considered a physical-based model which use numerical solution of Maxwell Equations in three-dimensional simulations and apply into Dense Media Radiative Theory (DMRT). The model is validated in two specific dataset from the second Cold Land Processes Experiment (CLPX II) at Alaska and Colorado. The data were all obtain by the Ku-band (13.95 GHz) observations using airborne imaging polarimetric scatterometer (POLSCAT). Snow is a densely packed media. To take into account the collective scattering and incoherent scattering, analytical Quasi-Crystalline Approximation (QCA) and Numerical Maxwell Equation Method of 3-D simulation (NMM3D) are used to calculate the extinction coefficient and phase matrix. DMRT equations were solved by iterative solution up to 2ndorder for the case of small optical thickness and full multiple scattering solution by decomposing the diffuse intensities into Fourier series was used when optical thickness exceed unity. It was shown that the model predictions agree with the field experiment not only co-polarization but also cross-polarization. For Alaska region, the input snow structure data was obtain by the in situ ground observations, while for Colorado region, we combined the VIC model to get the snow profile. [C1361]

### "Detailed structural characterisation of the savanna flux site at Skukuza, South Africa"

A detailed structure and composition dataset has been assembled for a 200 m ГrB— 200 m area surrounding

the eddy covariance flux measurement tower near Skukuza in the Kruger National Park. The information includes (by species) individual stem mapping, biomass and leaf area, canopy cover and height. Several different techniques were used for most of the attribute estimates, allowing a comparison of methods and an estimation of their accuracy. At the same time that the in situ information was collected (April 2008) using manual, photographic and ground-based laser scanning techniques, hyperspectral reflectance and lidar canopy structure information was gathered at 0.5 m resolution for this patch and a larger surrounding area, using the Carnegie Airborne Observatory sensors. The site has a nine-year record of water, energy and CO<sub>2</sub> fluxes, phenology and various other ecological measurements. Initial findings relating to measurement techniques and basic structural parameters for the site are presented. The intention is to make the data available as a standard calibration site for remotely sensed products. [C1362]

#### "Tree cover, tree height and bare soil cover differences along a land use degradation gradient in semi-arid savannas, South Africa"

High resolution airborne hyperspectral and discrete return LiDAR data were used to assess bare soil and tree cover differences along a land use transect consisting of state-owned, privately-owned conservation areas, and communal areas in South African savannas. The results show that tree cover is higher in conservation areas as compared to communal areas where local people use fuel wood for personal consumption. Low impact communal sites (limited use) tend to have higher tree cover than higher impacted communal sites. Generally communal areas have altered tree height distribution but in diverse way depending on the geology or the level of human utilization. Bare soil cover was generally found to be quite low (< 10%) in all different land uses, suggesting that the degradation level in communal areas might not be as high as generally perceived. [C1363]

#### "Three-dimensional woody vegetation structure across different land-use types and -land-use intensities in a semi-arid savanna"

Factors influencing woody savanna vegetation structure across a land-use gradient of intensity (highly and lightly utilized communal rangeland) and type (national protected area, private game reserve and communal rangelands) were investigated. Small-footprint discrete return LiDAR data (1.12 m point spacing) from the Carnegie Airborne Observatory (CAO) 'Alpha system' were used to measure three-dimensional vegetation structure across the different treatments. A volumetric pixel (voxel) approach was used to characterise the vertical distribution of LiDAR returns, i.e., vegetation density, in one metre increments for comparison using descriptive statistics across the land-use type and intensity gradient. Vegetation structure in the national protected area was most similar to the lightly utilized rangelands, and the private game reserve was most similar to the highly utilized rangelands with low levels of structural diversity present. Current trends in structural diversity can be related to harvesting, regeneration, herbivory and fire. [C1364]

#### "Advanced paris altimeter based on delay compensation of Doppler Waveforms"

Measuring ocean mesoscale variability is one of the main objectives of next generation satellite altimeters. Among the alternative solutions proposed to overcome the limitations of conventional altimeters, the PARIS concept has been proposed, which exploits GNSS signals reflected from the ocean surface and allows performing altimetry along several points simultaneously over a wide swath with sub-decimeter accuracy in spatial scales of 50-100 Km. The present paper proposes to adopt for a PARIS altimeter a multilook unfocused Doppler processing in order to improve height precision and accuracy. The proposed processing concept is a simplified extension to PARIS of the delay/Doppler processing adopted in conventional radar altimetry. The analyses reported in the paper show that, for open access GPS L5 navigation signal, an improvement of height precision up to 30% could be achieved without modifications to the RF front-end. [C1365]

#### "Comparing wind speed retrievals from GPS reflectometry with SFMR surface wind speeds in Hurricane Ike (2008)"

Recently, a compact system, able to record raw GPS intermediate frequency (IF) samples has been designed and tested by the research group at the CU/Aerospace Engineering Sciences Department. Such an approach provides the most fundamental measurement, enabling the most advanced and complete post-processing, with data volumes on the order of 1GB/minute. In 2008 this system was flying on board the NOAA WP-3D aircraft which collected research-mission data on Hurricane Ike. During two flights there was collected about 800 GB of raw data for flight legs that transverse the hurricane eye and away from it. After the flights the correlation waveforms for both direct and reflected signals were retrieved from the raw data for all available satellites and sea surface roughness estimates were produced. Those retrievals were compared with the Step Frequency Microwave Radiometer (SFMR) measurements of the surface wind speed. As expected, the data show a high sensitivity of the GPS bistatic radar signals to ocean surface roughness. However, the system of swells

generated by various parts of the hurricane complicates the picture and makes the problem of wind retrieval non-trivial. [C1366]

### "Simulation of GNSS-R returns for delay-DOPPLER analysis of the ocean surface"

We present a new approach to the retrieval of sea surface roughness using GNSS-R. The steps through the simulation of the whole end-to-end microwave scattering of GNSS signals from the sea surface are explained, with emphasis on how to generate a linear sea surface and to implement the Kirchhoff Approximation (KA), as the large-scale part of the full scattering model. We illustrate some examples of radar cross sections calculated using the Kirchhoff scattering model, and how they change with respect to different polarizations. Their variations with geometry, sea state and spatial resolution are investigated and discussed. [C1367]

### "Temporal variation of simulated rice backscattering of S-band HJ-1 SAR"

Rice is a major food supply in the southeast of China, which is very important for this region's rapid and sustainable development. Synthetic Aperture Radar (SAR) provides a powerful tool for rice monitoring in these regions because of its all-weather, day-and-night imaging and canopy penetration capabilities. HJ-1 small satellite constellation of China has been designed for environment and disaster monitoring, and HJ-1-C satellite has a SAR system working in S-band with incidence varying from  $31^\circ$  to  $40^\circ$ , VV polarization. Scattering model is helpful to better understand the temporal behavior of rice backscatter in S-band before HJ-1 SAR satellite is launched. In this paper, Zhaoqing test site in Guangdong province was selected as the test site, and 9-temporal field measurements acquired during the rice growing period in 1997 were used for analysis. Then rice backscattering and seasonal variation in S-band and VV polarization were simulated and analyzed based on radiative transfer model and ground measurements. [C1368]

### "Automated change detection using Synthetic Aperture Sonar imagery"

When resurveying a seafloor area of interest during change detection operations, an automated method to match found bottom objects with objects detected in a previous survey allows the surveyor to quickly sort new objects from old. The change detection system developed at the Naval Research Laboratory contains modules for automatic object detection, feature matching using shadow outlining, scene matching using control-point matching, and visualization capabilities. This system was developed for sidescan sonar surveys using instrumentation such as the high-frequency Marine Sonic Technology sidescan sonar. In this paper, the authors describe modifications to the sidescan-based system required to perform change detection using Synthetic Aperture Sonar (SAS) bottom imagery. [C1369]

### "Surveying coastal ship traffic with LANDSAT"

A semi-automated algorithm was developed to detect ships in LANDSAT 7 images. The algorithm combines multispectral and pattern recognition methods to discriminate ships from ocean clutter. Automated processing enables us to process a large number of images and gather a statistical picture of ship traffic patterns. As a test case we applied the algorithm on 54 LANDSAT images in the area of Jacksonville, FL, from the period 1999-2003. The area and time period are the same as an earlier ship traffic study by Ward-Geiger et al. using ship reports in the Mandatory Ship Reporting System (MSRS). The similarities between the two studies suggest that LANDSAT is a good alternative for surveying nearshore ship traffic. [C1370]

### "USACE National Coastal Mapping Program and the next generation of data products"

The U.S. Army Corps of Engineers (USACE) has been monitoring coastal change for decades. Each coastal district has the duty to maintain the federal navigation channels to insure safe passage for commercial and private vessels. In addition to these navigation channels, monitoring coastal change and regional sediment management rank high in both importance and financial expenditures. Acoustic boat surveys have been and will continue to be a viable way to accomplish these goals. For the past 15 years these surveys efforts have been assisted by the Joint Airborne Lidar Bathymetry Technical Center of expertise (JALBTCX). The JALBTCX has in-house survey capability using the U.S. Naval Oceanographic Office's Compact Hydrographic Airborne Rapid Total Survey (CHARTS) system. The CHARTS system collects bathymetric lidar, topographic lidar, RGB imagery, and hyperspectral imagery. CHARTS is mounted on a Beech King Air 200 which provides a platform capable of surveying the federal navigation projects and the areas between to support regional sediment management. In 2004, USACE Headquarters funded JALBTCX to map the sandy shoreline of the continental U.S. on a recurring basis. This mapping effort falls under the National Coastal Mapping Program (NCMP). In addition to the NCMP, JALBTCX performs emergency response surveys following natural disasters. Since 2004, JALBTCX was surveyed after every category 2 (or greater) hurricane that makes land fall within the U.S. As the survey capabilities increase it becomes more difficult for the local engineers to process the large volumes of data

and the demand for analysis ready products became a necessity. JALBTCX took on this challenge and is currently delivering a suite of products to meet the needs. With the addition of new sensors, JALBTCX has also been able to develop new data fusion products to assist in monitoring the engineering, economic, and environmental changes to the coastal zone. [C1371]

#### **"Sub-canopy ground characteristics retrieval of PolinSAR using spectral analysis technique"**

The advances in Polarimetric SAR Interferometry (PolInSAR) techniques provide a promising way to recover ground characteristics such as sub-canopy soil moisture and roughness using SAR data. Spectral analysis techniques have been applied to extract the vegetation and building parameters. Yamada et al proposed the ESPRIT algorithm to estimate vegetation height; Sauer et al apply the spectral analysis techniques to estimate building heights and extract physical properties from Multi-baseline (MB) PolinSAR data. In these applications, the parameters are mainly estimated from the phase information or phase center, but the validity of the sub-canopy soil backscattering or reflectivity estimation from polarimetric spectral analysis technique is not investigated. In this paper, the ground scattering center is first located by polarimetric MUSIC algorithm and then the ground reflectivity is recovered using a polarimetric least-square method. The validity of the polarimetric spectral analysis technique for the sub-canopy ground reflectivity estimation is demonstrated using simulated and real SAR data. [C1372]

#### **"The RADARSAT Constellation Mission: Meeting the government of Canada'S needs and requirements"**

In this paper, we describe the high level RADARSAT Constellation Mission (RCM) concept and how it is being designed to meet Government of Canada user requirements. The constellation concept is designed primarily as a wide area monitoring system, offering medium resolution information on a daily basis, as well as high resolution imaging functionality. We briefly discuss the unique capabilities of the constellation particularly related to coverage and revisit as it pertains to meeting the needs of each of the three Core Use Area applications. Finally, we outline the approach and activities being undertaken in the development of a Data Utilization Plan to ensure that the Canadian user departments and agencies will be ready to use data from the RCM on Day 1 of the launch of the first satellite. [C1373]

#### **"Modeling the multidimensional & fiscal impacts of storm surge & sea level rise: A compelling view through a powerful interactive 4D data integration, analysis and visualization tool"**

Nearly one third of the world's population live in coastal areas, and ten of the fifteen most populous cities in the world lie on a coast. Inhabitants of the Low Elevation Coastal Zone (LECZ)-defined as the contiguous area along the coast that is less than 10 meters above sea level-make up 10% of the world's population and 13% of the world's urban population. Sea level rise, coastal inundation and associated shoreline retreat have emerged as one of the primary threats to these populations and the resources located near the coastal fringe. To meet the needs of governments, planners and managers, researchers are continually faced with the challenge of integrating large volumes of complex environmental and spatial-temporal data. Typically the spatial and temporal components of data sets are underutilized because methods for effectively handling these data have not been available. To address these issues, Eonfusion, a 4-Dimensional software solution, is easily incorporated into the geospatial workflow to significantly enhance the ease with which we can now integrate and explore complex spatially and temporally variant data sets. This paper explores case studies along prominent coastal regions in which, as example, models are developed to predict the impact of rising sea levels on low-lying coastal areas focusing on: (1) Coastal Inundation (2) Coastal Vulnerability (3) Property Devaluation. The inundation is spatially modeled as a function of time and enables the visualization of sea level rise scenarios to assess the extent and impact. The coastal vulnerability mapping highlights the analytical power of Eonfusion, through the efficient integration of inundation and vulnerability models to demonstrate the universal application of the software to the field of climate change research. The third model fuses the cadastral layer and a simple property valuation model to complete the scenario, thus demonstrating a powerful pathway for the estimation and visualization of the impact of these climate change events. The data for these case studies include: (1) Sea level rise scenarios from IPCC stage 4 (2) LIDAR Elevation Data (3) Cadastral Parcels and Value Indicators (4) Storm Surge Information (5) Vulnerability Mapping. The processing steps required to integrate, analyze and visualize these models are: (1) Generation of 3D terrain model from LIDAR data (2) Adjustments for any Height Data (AHD) discrepancies (3) Integrate IPCC sea level rises and storm surges into Sea level rise timeseries (4) Identification of sinks using Eonfusion API application (5) Calculate inundation levels and tipping points at which sinks get filled (6) Fuse Cadastre and value model with 3D surface-value decreases as % of title flooded (7) Airphoto drape (8) Set up visualization scene with integrated graph for all scenarios. The outcomes from this work include the identification of powerful pathways through the employment of new visualization and spatial-temporal analysis tools for: (1) Dynamic scenario based modeling for assessing cost and environmental impacts from climate

change; (2) The provision of a mechanism enabling the visualization of the complex spatial and temporal patterns from a wide range of data derived empirically and from models. This enables key stakeholders to rapidly assess scenarios and their likely impacts (3) Modeling of this type could be used in a number of areas including fire, flood, tsunami, hurricanes, etc. [C1374]

#### "HFR surface currents observing system in lower Chesapeake Bay and Virginia coast"

Surface currents are measured using high frequency (25 MHz and 5 MHz) radar in the lower Chesapeake Bay and offshore in the Mid-Atlantic. The data have become quite reliable and of high quality over the past couple of years. This paper describes the existing system, the dataset, the quality of data and some examples of how it is being used. It also presents results of recent analysis of mean currents within the lower Bay. [C1375]

#### "Underwater optical ranging: A hybrid LIDAR-RADAR approach"

A hybrid LIDAR-RADAR system is applied to optical ranging in order to achieve centimeter-type range accuracy over the distance of meters with high range resolution. The experiment is performed for NIR 830 nm, red 660 nm, green 532 nm using photomultiplier tube, interference filter, RF demodulator. An optical wavelength in the NIR region helps to protect the system against the effects of changing turbidity levels of water because NIR wavelengths absorb quickly in clean water without being affected by scattering, the components that make total attenuation. The modulation frequency of 66 MHz for NIR wavelength allowed a theoretical maximum range measurement of 1.71 m within the unambiguous range, which drops to 1.61 cm at 70 Mhz. A scheme involving chaotic modulation techniques (CLIDAR) will be studied in future. [C1376]

#### "Evaluating connectivity between marine protected areas using CODAR high-frequency radar"

To investigate the connectivity between central California marine protected areas (MPAs), back-projections were calculated using the network of high-frequency (HF) radar ocean surface current mapping stations operated along the California coast by the member institutions of the Coastal Ocean Currents Monitoring Program with funding provided by California voters through Propositions 40 & 50 and administered by the State Coastal Conservancy. Trajectories of 1 km resolution grids of water particles were back-projected from ten MPAs each hour, out through 40 days in the past, from each day in 2008, producing a map of where surface waters travel over a 40-day period to reach the MPAs-and visualizations of the length of time the waters travel along these paths. By comparing the travel times of those back-projected track-points that crossed between MPA regions, the connection time between MPAs along the State's central coast was assessed. Repeating these calculations resulted in a connectivity matrix between the MPAs in the region, and may be useful for assessing connectivity for the important invertebrate and fish larvae that are restricted to the surface ocean during a fraction of their lifecycle. [C1377]

#### "Target coherence analysis using canonical correlation decomposition for SAS data"

This paper analyzes the connection between the canonical correlations of sonar signals captured using two linear hydrophone arrays and the spatial coherence of the sources that are observed. Analysis of this connection allows for the use of a canonical correlation decomposition (CCD) framework for performing synthetic aperture sonar (SAS)-like processing. In particular, it can be used to extract correlation features of the targets in the frequency domain, which can then be used as a measure for target detection and classification. Results on real and simulated data indicate that coherence patterns are different in the presence of a target when compared to background clutter, and this pattern also changes as a function of the number of sensors on the array. [C1378]

#### "Simulated OVW retrievals in tropical cyclones for the next generation Dual Frequency Scatterometer"

The purpose of this study is to investigate the potential of the next generation Dual Frequency Scatterometer (DFS) proposed to fly onboard the Japanese Aerospace Exploration Agency (JAXA)/GCOM-W2 future mission to measure surface ocean vector winds. An end-to-end simulation was performed to retrieve ocean vector winds in extreme weather conditions, where high winds are usually associated with high rain rates. Both C-and Ku-bands DFS active measurements were combined in the retrieval algorithm. The simultaneous observations of JAXA's Advanced Microwave Scanning Radiometer (AMSR) were used to passively model both the atmospheric attenuation and rain volume backscatter to correct for rain effects and to further improve the retrievals range for tropical cyclones beyond that exhibited by the current operating scatterometers. [C1379]

#### "Coincident observations, with QuikSCAT and ASCAT, of the effects of rain-induced sea surface stress during hurricanes Gustav and Ike"

The use of satellite scatterometers to probe the winds in and near strong storms and hurricanes is a valuable tool for weather forecasters. The presence of widespread rain in these storms makes the estimates of surface winds from the satellite data problematic. A motivating question here is: "Is there a substantial influence of rain on the air-sea momentum exchange in Hurricanes". Satellite scatterometer measurements were made for Hurricane Gustav (C-Band), which affected New Orleans on September 1 and Hurricane Ike (Ku-band) which impacted the Texas coastline near Houston, on September 13, 2008. The NEXRAD rain reflectivity images (available every 6 minutes) show that there was wide rain coverage throughout these storms. The sustained surface wind estimates from NOAA/ AOML/ HRD show a maximum of 90 kts, and a wide inhomogeneity even within 50 km areas. The broad swath coverage of the NEXRAD radar enables us to select and compare NRCS effects in both rain and non-raining areas. The methodology to be presented here demonstrates how the atmospheric influence can be removed to observe the total surface NRCS. [C1380]

#### "Fusion of hyperspectral and lidar remote sensing data for the estimation of tree stem diameters"

The estimation of stem diameters can be very useful in the study of forests, as together with height and tree specie, it is one of the most important parameters used in forest inventories. In this paper a system for the estimation of stem diameters with LIDAR and hyperspectral data (both separately and combined in a data fusion framework) is presented. An analysis on the effectiveness of these data in the estimation process and on the accuracy and robustness of different estimation algorithms is presented. Experimental results point out the effectiveness and the properties of the proposed system. [C1381]

#### "Case studies of frozen ground monitoring using PALSAR/ALOS data"

Frozen ground is a sensitive indicator of how our home planet is changing. In the meantime, new spaceborne SAR systems have been launched, such as the polarimetric PALSAR sensor onboard ALOS in January 2006. In this paper, the relevance of L-band polarimetric SAR data for extracting information on frozen ground is presented. Dealing with ground assessments, the necessity for a validated Electromagnetic (EM) model is of importance. The adequation between Oh's po-larimetric EM model and PALSAR data is first studied over agricultural bare fields in Hokkaido, Japan. The assessment of residual liquid water can be realized by means of bare soil EM backscattering model. Over natural wildland area, an approach is proposed in order to tackle the effect of the vegetation or other irrelevant effects. The monitoring of permafrost active layer is performed over the ANWR, Alaska. [C1382]

#### "Polarimetric ice sounding at P-band: First results"

For polar ice sheets valuable stress and strain information can be deduced from the crystal orientation fabric (COF) and its prevailing c-axis alignment. Polarimetric radio echo sounding is a promising technique to measure the anisotropic electromagnetic propagation and reflection properties associated with the COF. In this paper, dual-polarized P-band data acquired with the airborne POLARIS system near the ice divide of the Greenland ice sheet are analyzed. The internal layers in the uppermost few hundred meters of the ice sheet look the same at HH and VV polarizations, whereas the layering differs further down. Accordingly, the magnitude of the complex HH-VV correlation coefficient decreases with depth and, interestingly, the phase gives evidence of polarization dependent reflection and birefringence effects. [C1383]

#### "CASA Phased Array Radar System description, simulation and products"

This paper discusses the systems architecture of the CASA Phased Array Radar System, the Phase-Tilt Escan Radar System, for deployment in a CASA DCAS network of low power, solid-state phased array radars. The paper highlights the high-level system's architecture accompanied by measured data from the subsystems. [C1384]

#### "Hierarchical segmentation of Polarimetric SAR images using heterogeneous clutter models"

In this paper, heterogeneous clutter models are introduced to describe Polarimetric Synthetic Aperture Radar (PolSAR) data. Based on the Spherically Invariant Random Vectors (SIRV) estimation scheme, the scalar texture parameter and the normalized covariance matrix are extracted. If the texture parameter is modeled by a Fisher PDF, the observed target scattering vector follows a KummerU PDF. Then, this PDF is implemented in a hierarchical segmentation algorithm. Segmentation results are shown on high resolution PolSAR data at L and X band. [C1385]

#### "Parametric versus non-parametric complex image analysis"

In this paper we compare parametric and non-parametric method for the analysis of complex valued high-

resolution SAR data. Gauss-Markov Random Field (GMRF) model with a quadratic energy function as a parametric analysis parameterizes the spectrogram of the signal, whereas nonlinear short time Fourier transform (STFT) method, the method based on time frequency analysis (TFA) as a non-parametric approach exploits the signal's non-stationarity in the time-frequency domain for information extraction. This comparative analysis helps to understand, characterize and analyze complex valued SAR data. [C1386]

#### **"Selectable target detector using the polarization fork"**

A new target detection methodology is described that makes novel use of the polarization fork of the target. The mathematical formulation is general and can be applied to any kind of single target as long as its expression in the target space is known. Aim of this paper is to present a standard procedure to set the detector parameters for any target of interest. The algorithm makes use of the Gram-Schmidt ortho-normalization in order to set the appropriate basis for the polarimetric space. Validation against real data shows significant agreement with the expected results based on the theoretical description. [C1387]

#### **"Parameter-free clustering: Application to fawns detection"**

Many fawns and other wild animals are killed by mowing machines every year. To prevent them from being killed or injured, a sensor system is being developed to detect the fawns hidden in meadows under mowing. Beside a microwave radar system, two cameras (thermal infrared and RGB) take a picture at the mower's current location. This contribution focuses on the compression-based algorithm that will be adopted to detect the locations containing a fawn hiding in the grass: such approach, being parameter-free, allows performing a fully unsupervised clustering by exploiting the intrinsic properties of data compression to estimate the amount of shared information between two images. [C1388]

#### **"Surface parameters retrieval from alluvial fan in Ejina area of Inner Mongolia using multi-polarization SAR data"**

This paper presents the method of retrieving surface parameters of alluvial fan using multi-polarization SAR data based on Genetic Algorithm combined with backscattering models. The comparison of simulated results and field measurements shows that the method is efficient for surface parameters retrieval from alluvial fan. This method presented that the cross function of surface parameters inversion could be variable with the amount of data acquired. The data used for surface parameters inversion must be more than two scenes. The more data could generate the more accurate results. Then the surface parameters of alluvial fan in Ejina area of Inner Mongolia were estimated using ENVISAT ASAR and ALOS PALSAR data. The estimation results shows the ground surface of Ejina alluvial fan is very flat, so the range of its roughness is small, and the root mean squared heights in most party of the alluvial fan are no more than 1.0cm. The roughness in the area along Heihe River is big, and it is very small in the other areas far from Heihe River. The estimation result of soil moisture shows this area is very arid, and the soil volume moisture in most party is no more than 10%. [C1389]

#### **"Surface velocity and variations of outlet glaciers of the Patagonia Icefields by means of TerraSAR-X"**

An incoherent amplitude correlation approach is used to derive ice motion fields of three major outlet glaciers of the Patagonia Icefields. High resolution repeat pass TerraSAR-X data of 2008 and 2009 were analyzed. The strong gradients in ice velocity of the terminus of San Rafael glacier, ranging from 2 to 16 m d<sup>-1</sup>, were captured well. Significant acceleration of the ice flow and losses in mass were observed for Upsala glacier. [C1390]

#### **"Mapping Canadian wetlands using L-band radar satellite imagery S"**

Previously, we have developed a robust algorithm for mapping boreal wetlands using L-band satellite radar imagery, and in particular have used the method to produce a complete vegetated wetlands map of Alaska using the JERS radar data. In this work, we apply this algorithm to produce a static map of Canadian wetlands from the 1997-98 era JERS radar data at 100-m resolution, to be followed in the future by 2007-era ALOS/PALSAR maps. [C1391]

#### **"Airborne imaging differential optical absorption spectroscopy: Trace-gas measurements from the suburbs to the sub-continent"**

A remote sensing instrument for high-resolution measurement of two dimensional trace-gas distributions from an aircraft has been built. The instrument has been tested during three measurement campaigns over the South African High-veld region. The resolution achieved is less than 100 metres, allowing point sources to be clearly identified. Measurements have been interpreted with respect to emission flux and oxidation of species in the

atmosphere. The high speed of the aircraft also allows measurements to be made on a regional scale. [C1392]

#### "A toolbox dedicated to the analysis of airborne SAR sea clutter data"

The characterization of the sea clutter spatial and statistical properties is a challenging problem for improving the detection performances of any radar system confronted with strong sea clutter perturbations. On the one hand, the use of radar scatterometry made it possible to precisely determine the behavior of the sea surface backscattering coefficient and to confirm electromagnetic models. On the other hand, the imaging of the ocean by radar has been studied extensively and has led to a mature theory of synthetic aperture radar (SAR) imaging of the ocean. Nevertheless the manipulations of SAR data are handicapped by the size of data. In order to analyze SAR data, we need a very flexible tool well adapted to these data. This paper briefly presents the inner functioning of a software (i.e. the different choices of class organization and how it is convenient to use them) based on a multilook philosophy (spectral sub bands processing) and on Octave script. Then we specify the type of operations and processings, we can perform using this software. Two examples of use are presented which show the easiness of use of this software. [C1393]

#### "SUMATRA, a W-band SAR for UAV application"

Based upon most recent advances in millimeterwave technology, especially monolithic integrated low noise or medium power HEMT amplifiers and an integrated receiver containing an LNA, Mixer and IF Amplifier, a miniaturized experimental radar at 94 GHz was designed with the aim to be used on board of a remotely piloted model aircraft. This highly advanced front-end technique was combined with off-the-shelf model aircraft hardware and miniaturized GPS and data transmission equipment which is readily available. Goal of the project is to demonstrate, that using modern 94-GHz front-end technique combined with achievable back-end components it is possible to set up a versatile SAR system usable for a wide range of remote sensing applications at medium range. The paper describes the current state of the research project SUMATRA-94 and gives some perspectives for future applications. [C1394]

#### "Study of vegetable Okra by microwave remote sensing at X- band"

Okra commonly known as lady finger is one of the important vegetable cultivated in India. Today Remote sensing is an important tool for monitoring the crop production. For this purpose we use bistatic microwave scatterometer working at X-band (9.5 GHz). Biomass factor and leaf area index is calculated within this period. Scattering coefficient (s) and their dependence on look angle were analyzed. In this way by using the Biomass, Leaf area index and scattering coefficient an idea is developed which is helpful for radar sensors and also helpful for the production monitoring of this vegetable. [C1395]

#### "Measuring Synthetic Aperture Radar target differences with stochastic distances"

Synthetic Aperture Radar (SAR) imagery plays a central role as a source of unique data for Geographic Information Systems. These data sets provide complementary information to that provided by optical and infrared sensors as, for instance, Landsat TM, CBERS-2, IKONOS and SPOT, to name a few. SAR sensors capture information about the target roughness and its dielectric properties, and their imaging capabilities are able to penetrate clouds, fog, rain and even some types of land cover as, for instance, forest canopies. A major issue related to the use of SAR images is their statistical behavior. It is well known that classical Gaussian and additive models do not hold for such data. The multiplicative model (MM) has been extensively tested with success, and it is able to explain phenomenological aspects of the image formation. One of the most important distributions related to the MM is the  $GF, B^\circ$  law. The  $GF, B^\circ$  distribution, as all other laws related to the MM, greatly departs from the Gaussian model. This paper assesses the SAR image discrimination capabilities of selected parametric methods based on divergences measures, when compared to the nonparametric Kolmogorov-Smirnov testing methodology. The importance of the Triangular and Arithmetic-Geometric distances is quantified with respect to the Kullback-Leibler parametric and Kolmogorov-Smirnov non-parametric classical distances by means of Monte Carlo simulation. [C1396]

#### "Compact polarimetry mode at low frequency for vegetation applications"

Global warming is now known to be the major environmental issue mankind will have to face in the next decade. Monitoring of vegetation and biomass is clearly an essential piece of information required at all levels ranging from the scientific studies to understand and forecast, to the political actors and government leaders responsible for drafting remediation policies and evaluating their impact. Microwave remote sensing with the low-frequency SAR technique can provide a useful characterization of forest (spatial coverage, species, density, height...) at a global scale, relying on the all-weather imaging capabilities of SAR linked with the significant penetration of the low-frequency EM wave in the canopy. The published techniques for forest characterization from low frequency

SAR data include radiometry inversion, polarimetric inversion based on the anisotropy parameters and PolInSAR Random Volume Over Ground inversion. In this paper, we will more specifically concentrate on the PolSAR technique and the impact of ionospheric effect. [C1397]

### "Combining modern spectral estimation with Time-Frequency representation"

With Joint Time-Frequency Analysis (JTFA), one can estimate the speed of moving targets from Synthetic Aperture Radar (SAR) images. These targets are usually compact. JTFA estimation of water surface speeds is more difficult since the radar returns are weak and generated by Bragg scattering patches, randomly distributed within the radar's footprint, both in time and space. To increase the signal strength, JTFA is applied to multiple range lines, which requires a generalization of the Time-Frequency representation (TFR). To do this, modern spectral estimation (MSE) techniques, which depend on estimating the data covariance matrix, are weaved into the framework of a TFR. The resulting TFR formed along azimuth-lines naturally integrates the data across multiple range-lines. We discuss and illustrate this technique on simulated data and then apply it to estimate the speed of moving water in a single-phase center SAR image. This method also enhances the signal-to-clutter ratio (SCR). [C1398]

### "The Sentinel-1 radar mission: status and performance"

The ESA Sentinels constitute the first series of operational satellites responding to the Earth Observation needs of the EU-ESA Global Monitoring for Environment and Security (GMES) programme. The GMES space component relies on existing and planned space assets as well as on new complementary developments by ESA. This paper describes the Sentinel-1 mission, an imaging synthetic aperture radar (SAR) satellite constellation at C-band. It provides an overview of the mission requirements, its applications and the technical concept for the system. [C1399]

### "Study on Astronomical Solar Radiation over Rugged Terrain Using DEM Data"

This paper is based on a distributed model for calculating daily astronomical solar radiation with a resolution of 90 m GfB— 90 m SRTM (Shuttle Radar Topography Mission) DEM. We use a ray-tracing method and integral by subparagraph to calculate the conditions of terrain shading information, and through an integral way to make a visualization of astronomical solar radiation. The result shows that the geographical and topographical factors make a visible effect on the spatial distribution of astronomical solar radiation over a rugged area. [C1400]

### "Automated 3D object identification using Bayesian networks"

3D object reconstruction from images involves two important parts: object identification and object modeling. Human beings are very adept at automatically identifying different objects in a scene due to the extensive training they receive over their lifetimes. Similarly, machines need to be trained to perform this task. At present, automated 3D object identification process from aerial video imagery encounters various problems due to uncertainties in data. The first problem is setting the input parameters of segmentation algorithm for accurate identification of the homogeneous surfaces in the scene. The second problem is deterministic inference used on the features extracted from these homogeneous surfaces or segments to identify different objects such as buildings, and trees. These problems would result in the 3D models being overfitted to a particular data set as a result of which they would fail when applied to other data sets. In this paper, an algorithm for using probabilistic inference to determine input segmentation parameters and to identify 3D objects from aerial video imagery is described. Bayesian networks are used to perform the probabilistic inference. In order to improve the accuracy of the identification process, information from Lidar data is fused with the visual imagery in a Bayesian network. The imagery is generated using the DIRSIG (Digital Imaging and Remote Sensing Image Generation) model at RIT. The parameters of the airborne sensor such as focal length, detector size, average flying height and the external parameters such as solar zenith angle can be simulated using this tool. The results show a significant improvement in the accuracy of object identification when Lidar data is fused with visual imagery compared to that when visual imagery is used alone. [C1401]

### "GPRS Based Guard Robot Alarm System Design"

This paper presents a practical approach to design guard robot alarm system using GPRS technology. GPRS offers an interesting communications infrastructure for remotely accessing, controlling and interacting with robots in an integrated and highly portable manner, particularly in recent years the GPRS network provides wireless access of internet for mobile phone which becomes the most important and common terminal equipment. Therefore, in this paper the alarm information is designed to send to the user's mobile phone, and add man-made intervention to the system, thus achieves a more convenient and reliable alarm system. The system mainly consists of two parts: detection of abnormal and dangerous situation in domestic environment and sending the

alarm information as MMS form to the user's phone via GPRS networks. Finally experiments show that the alarm system can accurately send alarm information to the user's mobile phone. The system is low-cost, flexible, reliable, and can be widely used. [C1402]

### "Review and Comparison: Building Extraction Methods Using High-Resolution Images"

This paper gave a review of building extraction methods using high-resolution images, and introduced three methods in detail. The comparison of extraction results are taken from two aspects, which are overall accuracy and extraction rate. It is reported that the building extraction based on Dempster-Shafer theory is the most robust method, because it can receive high accuracy in those two aspects. [C1403]

### "Performance Study of the Robust Bayesian Regularization Technique for Remote Sensing Imaging in Geophysical Applications"

In this paper, a performance study of a methodology for reconstruction of high-resolution remote sensing imagery is presented. This method is the robust version of the Bayesian regularization (BR) technique, which performs the image reconstruction as a solution of the ill-conditioned inverse spatial spectrum pattern (SSP) estimation problem with model uncertainties via unifying the Bayesian minimum risk (BMR) estimation strategy with the maximum entropy (ME) randomized a priori image model and other projection-type regularization constraints imposed on the solution. The results of extended comparative simulation study of a family of image formation/enhancement algorithms that employ the RBR method for high-resolution reconstruction of the SSP is presented. Moreover, the computational complexity of different methods are analyzed and reported together with the scene imaging protocols. The advantages of the remote sensing imaging experiment (that employ the BR-based estimator) over the cases of poorer designed experiments (that employ the conventional matched spatial filtering as well as the least squares techniques) are verified through the simulation study. Finally, the application of this estimator in geophysical applications of remote sensing imagery is described. [C1404]

### "Three Dimension Wind Retrieval of Single-Doppler Radar Data with Improved VVP Method"

Theoretically, three dimension (3D) wind field and the other kinematical parameters could be retrieved by the volume velocity processing (VVP) method using single-Doppler weather radar volume data. However, ever since the theory was brought forward, it has never been fully and truly applied to practice due to the large vertical speed error. This research has found that the ill coefficient matrix of the linear equations is the key obstacle in retrieving the vertical speed field and other parameters. Based on the numerical analysis theory, the feasible algorithm has also been studied as an attempt to solve the ill matrix problem in linear equations. Numerical experiments have also been conducted with single-Doppler radar data, and the retrieval results are verified with dual-Doppler radar data observed in HUBEX\_IOP. The research results show that the better retrieval of three dimension wind field can be obtained with the improved VVP method. Especially, the retrieval of vertical speed is obviously much better than that of the previous studies, and consistent with the real vertical wind speed of severe weather. [C1405]

### "Bistatic HF ocean radar: Errors and limitations"

Bistatic HF ocean radars are being proposed as a useful option when planning the layout of coastal stations for mapping sea surface currents. Monostatic HF ocean radar stations measure the components of the vector currents which are radially towards or away from the stations. The combination of the radials from one point on the sea surface to each station can be combined to produce the familiar surface current maps, which are the primary product from HF ocean radars. If the monostatic radars were also operating in bistatic mode, then components of the vector current are measured in the direction of the normal to each ellipse which represents a signal path length from the transmitter to the scattering point (on the ellipse) and on to the receiver. Stylised pictures of this geometry show that these surface current components are directed towards the general area of the midpoint between the transmitter and the receiver, and can be useful in reducing errors by providing extra, redundant, information in the calculation of the re-constituted vectors. Errors in determining the location of the scattering point in bistatic radar observations in some circumstances lead to degradation of the accuracy of the currents which can be detected. In this paper we consider two effects: the effect of receiver beamwidth; and the effect of receiver bandwidth. [C1406]

### "Next generation use of high power and bandwidth in the NE Pacific-A component of the NSF Ocean Observing Initiative"

This paper will present the unique opportunities of integrating the existing Integrated Ocean Observing System (IOOS) technologies with the capabilities of OOI RSN and the resulting significant enhancement to IOOS HF

Radar coverage along the Oregon and Washington coastlines. [C1407]

### "A history of reflector antenna development: Past, present and future"

The purpose of a reflector antenna is to confine most of the electromagnetic energy over a distributed aperture into a focal plane for communication or energy transfer; whereas, the purpose of this article is to focus a good portion of the history of reflector antenna development over a large time frame-including present and future-into a few pages. [C1408]

### "Coherent microwave marine radars for deterministic wave profile mapping, decameter-scale coastal current mapping and ocean wave spectra measurements"

Two different approaches in development of a coherent marine radar for ocean remote sensing applications have been designed, assembled, and tested: a fully coherent radar (COHrad) and a coherent-on-receive radar (CORrad). These radars operate similar to standard marine radars, with rotation revisit rates of either 0.4 or 0.8 Hz, suitable for measuring ocean wave frequencies of half these values. They allow repetitive maps of radial velocity, primarily orbital wave velocity of ocean waves, and thus can provide a map of ocean wave height directly, without the need for a modulation transfer function as is used with non-coherent radars. When averaging of a large set of consecutive images, slower time scale phenomena can be mapped, such as mean area currents and localized rip current features. Two radars illuminating a common area could thus provide the vector current field for all such processes in that area. A string of such radars along a coast with overlapping coverage could provide continuous coastal maps of ocean currents. A description of both radars is provided, the signal processing involved, and some preliminary examples of displays that are available for data from these systems. [C1409]

### "Coherent microwave marine radar measurements of directional ocean wave spectra and mean radial current fields"

Results of measurements of ocean waves using a coherent marine radar are presented. Data were collected in a coastal environment, at the U.S. Army Corps of Engineers Field Research Facility, Duck, N.C. Measurements of ocean wave spectra derived from maps of radial components of orbital wave velocity are used to measure directional ocean wave spectra, using three-dimensional FFT algorithms. Wave height spectra can be derived directly from such measurements, without the need for a modulation transfer function (MTF) that is used for traditional marine radars. The MTF approaches can suffer from wind speed variability and wind-wave relative direction effects, and are typically robust only for equilibrium wind-wave conditions. A discussion is presented of how one might use such data to provide a real time wave profile map of the coverage area. Such a map of wave height profiles is useful in ship motion response prediction for real-time applications such as safe helicopter landings under high sea conditions. [C1410]

### "Interferometric measurements using redundant phase centers of synthetic aperture sonars"

Interferometric sonars with multiple horizontal rows of elements have been used routinely to produce swath bathymetry. However, interferometric sonars are larger more complex, and consume more power than arrays with a single row of elements. Synthetic aperture sonar (SAS) systems often require the use of redundant phase centers (RPC), where the aft sonar element positions overlap in space with the forward element positions of the previous ping. Considering that a vehicle carrying a SAS array would likely have non-zero pitch, the use of RPC provides sonar data from receivers at the same along-track position with some vertical displacement. This data is similar to that of interferometric systems with the exception that the distance between receiver pairs can vary with vehicle motion and the received signals are not collected concurrently. This paper evaluates the possibility that an interferometric capability could be achieved using RPC data collected from a SAS system consisting of a single horizontal row of elements. An error analysis was conducted to determine the effect of errors in relative receiver position on swath bathymetry. Results show that errors in receiver vertical displacement result in similar percent errors in elevation. Therefore, errors in swath bathymetry can be reduced by designing the array to increase vertical displacement between RPC pairs. Results also show that increasing vertical displacement between RPC pairs can also reduce the impact of data phase measurement errors on swath bathymetry. Swath bathymetry measurements are very sensitive to errors in across-track displacements, but the predictable nature and scale of the error may indicate that accurate across-track displacements could be calculated from phase measurements. Swath bathymetry images produced from data acquired by an existing SAS consisting of a single horizontal row of elements are shown and illustrate viability of the technique depending on the required resolution of the system. [C1411]

### "The airborne SAR-system: SETHI airborne microwave remote sensing imaging system"

SETHI, the airborne SAR system developed by the ONERA, the French Aerospace Lab., integrates a new frequency band radar: the UHF-VHF component. Thanks to its new payload, SETHI can operate over a wide range of frequency bands from UHF-VHF, to X including L-Band and has polarimetric and interferometric capabilities. We describe in this paper the pod-based SAR-system SETHI and its associated numeric remote control. Then we describe the UHF-VHF validation campaign and as a conclusion the first polarimetric SAR results. [C1412]

#### "Electromagnetic wave scattering from sea and bare soil surfaces based on an improved two-scale model"

Remote sensing applications require developing accurate models to predict radar backscattering from rough surfaces. An improved two-scale model to calculate the electromagnetic backscattering coefficients from sea and bare soil surface is investigated. The sea surface calculations are made by assuming the surface height spectrum of Elfouhaily et al. whereas the roughness of soil surface is approximated by Gaussian spectrum. The simulation results are compared with the published experimental data from ocean surface at Ku-band and for soil surface at L-band. Fairly good agreements are found for the fixed physical surface roughness parameters on these frequency bands specially, for cross polarizations. It is observed that as the roughness of the surface increases the intensity of SHH increases at low grazing angles. [C1413]

#### "HFSW radar model and evaluation of a multiscale source extraction approach for target detection"

High Frequency radar, which is based on surface wave propagation, is an important tool to remotely measure sea state. It can also be used to detect targets far beyond the conventional microwave radar coverage. The goal of our project is to investigate this detection capability. In this way, the received power by the system in presence of targets has been modeled leading to a Range-Doppler image. This model can be used for different purpose like, for example, the (theoretical) evaluation of target detection algorithms. In this contribution, a multiscale source extraction method is also proposed as a detection technique and some first results illustrate its capabilities. [C1414]

#### "Recent advances in SAR remote sensing: "Multimodal POLinSAR imaging with applications to remote sensing of the terrestrial covers and the monitoring of environmental stress changes""

Land cover monitoring is one of the most potential applications of Polarimetric Synthetic Aperture Radar (POLSAR) sensing and so is Repeat-Pass Polarimetric-Interferometric SAR (RP-DIFF-POL-IN-SAR) stress-change assessment by air/high-altitude/space-borne SAR sensor deployment. Provided fully polarimetric SAR information can be made available, a plethora of novel POLSAR matrix decomposition methods can be implemented for recovering rather precise scattering contributions from isolated and distributed scattering scenarios, and so can rather exact environmental changes from consecutive repeat-pass observations at 1 m resolution from air and from space. With the recent launches of the fully polarimetric satellites JAXA-ALOS (PAL-SAR-L-Band), the DLR TerraSAR-X (X-Band) and of RADASAT-2 (C-Band), a new era in space imaging of the terrestrial terrain and ocean surfaces has arrived providing unforeseen advantages. [C1415]

#### "A tutorial on design and analysis of waveguide-fed slot array antennas"

This tutorial gives a detailed presentation on the design and analysis of waveguide-fed slot arrays. Examples of application of such arrays in radar, communications and remote sensing systems will also be discussed. [C1416]

#### "ONERA DRIVE project"

Future UAV employment in the civilian areas of surveillance and communication relays can be conceived now at short term range. Flight tests for such applications have already been done and validated UAV interest. In the domain of remote sensing, and more precisely imagery, many payload configurations may be used in UAV operations, but compared to sensors working in other spectral regions (such as optical or infrared sensors), radar sensor has the main advantage to be able to operate in all-weather condition. [C1417]

#### "Scientific requirements and feasibility on an L-band mission dedicated to measure surface deformation"

DLR is currently studying a space borne mission based on two L-band satellites to map Earth surface deformation and vegetation structure from space. In this study the scientific requirements for deformation measurements are collected, traded off versus technical feasibility and a mission concept is investigated that provides a global monitoring capability of geo-tectonic threats. [C1418]

### "Mission design and performance for systematic deformation measurements with a spaceborne SAR system"

Tandem-L is an L-band SAR satellite mission currently under study at DLR. It is intended to serve a number of geophysical applications in several domains, like solid Earth, ecosystems and cryosphere. The various applications compete for the system resources and the mission design optimization requires that a performance model is developed for each application in order to allow motivated choices. We describe the adopted approach for deformation measurements, which is based on recent formulations of the Cramer-Rao bound for multi-image SAR interferometry and on the a-posteriori combination of the measurements from different lines of sight. We also discuss the limitations that the use of a reduced set of interferograms would entail. [C1419]

### "Deformation monitoring using the ALOS/PALSAR"

Because of the higher interferometric coherence, ALOS/PALSAR data are often used for monitoring the deformation caused by the disaster events (i.e., earthquakes, volcanoes, land subsidence by water and oil pumping, land slide, etc) using the interferometric data analysis. JAXA has been a member of the international charter, and responds to the charter calls for the emergency call. In this paper we will introduce the responses to the charter call events and the data examples generated and distributed to the disaster event as the interferometric SAR products. [C1420]

### "Improving sea states monitoring of nautical radar using dispersion relation of nonlinear ocean waves"

The purpose of this study is to discuss the influence of nonlinearity upon X-band radar observations. For simplicity, the analytical dispersion relationship of finite amplitude ocean wave theory was applied and discussed. We found that the shallow water dispersion relation curve covers more ocean wave energy than deep water and linear dispersion relationship. However, the shallow water dispersion relationship filter can not derive the ocean spectrum from radar image spectrum. The accurate measurement of ocean wave amplitude and water depth may be contributed to the results. More data are needed to analyze the reasons. [C1421]

### "COSMO-SkyMed contribution in oil spill monitoring of the Mediterranean Sea"

High resolution Cosmo-SkyMed SAR images are used for oil spill detection and ship identification on the Mediterranean Sea, in the framework of PRIMI Pilot Project currently developed by Italian Space Agency (ASI). The system consists of four components, two of them devoted to the analysis of the SAR and Optical satellites images for the slicks detection, an oil spill forecast subsystem and a central archive that provides web-gis services; a preliminary version of the system is already operational. Besides the slicks relevant information and detected ships on the analyzed scene, the system also provides meteorological and oceanographic information. The architecture of the system, the operational scenario and the preliminary results are presented. [C1422]

### "18 Years of interferometry, as seen from POLIMI"

The progressive expansion of the applications of Synthetic Aperture Radar from airborne or satellite platforms is due to its capabilities of imaging through clouds and during the nights; further, the coherent character of the images has allowed the onset of interferometry, namely the use of the phases of the radiation. The goal of this contribution is to recollect some episodes of the development of the technology, as viewed from our observatory, namely the Politecnico di Milano. Inevitable bias will follow. [C1423]

### "Stable Coherent Area in SAR interferometry"

Synthetic aperture radar images have been a tool of interest in many land cover studies for their night and day, all weather conditions operability. The classic InSAR technique is often limited by temporal and geometrical decorrelation, especially in the context of long time series analysis. Indeed, one of the major drawback of radar images is that some surfaces such as vegetated areas have a varying backscattering coefficient over time. While two images are acquired in multipass interferometric mode, this leads to a partial or sometimes complete loss of correlation of the data. This paper deals with coherence measurements based on 83 ERS images of a large area which is particularly remarkable due to the temporal stability of its interferometric coherence. This area is located on the Serre-Poncon dam, France. Longitudinal observations based on seven years frame ERS interferograms show an expected complete loss of coherence of the scene over vegetated and mountainous areas, excepted on the Serre-Poncon dam for which coherence degree remains high despite the long time span between these acquisitions. An experimental qualitative analysis is lead on the measured coherence of this Stable Coherent Area (SCA). As classic coherence estimators are biased on small averaging windows, a specific method is thus

proposed to improve the results, by measuring the global coherence of the dam. This requires a compensation of the topographic and orbital phase components. [C1424]

### "Analyzing radar backscatter of land within the TRMM footprint using high resolution SAR"

Spaceborn precipitation radars acquire atmospheric measurements using beams that scan through nadir. Naturally, the reflection from the surface is typically quite strong, especially at nadir. This surface observation can be used to estimate the attenuation caused by precipitation provided there is a reasonable value of the non-attenuated surface return leading to an estimate of the rain rate. Over land, the backscatter characteristics are usually very dynamic and change in the presence of water due to its high dielectric constant. In addition, the viewing geometry results in very large beam footprints on the ground containing highly variable scattering mechanisms. Using a high resolution Synthetic Aperture Radar, the surface characteristics within this footprint can be examined with respect to how precipitation changes the backscatter. This research investigates both of these radar types, plus ground based weather radars, to quantitatively analyze surface dynamics within the footprint of a precipitation radar. [C1425]

### "3-D characterization of buildings in a dense urban environment using L-band Pol-InSAR data with irregular baselines"

Diverse spectral estimations methods, i.e. MUSIC, Maximum Likelihood (ML), Weighted Subspace fitting (WSF), are proposed and applied to the estimation of building height dense urban environments and to the retrieval of scatterers' physical properties. Compared to other estimators, the polarimetric WSF estimator is optimally model adaptive and results in reduced sidelobes induced by irregularly sampled baselines. [C1426]

### "Impact studies of AMSR-E ocean surface wind speed data in NWP at JMA"

The impact of assimilation of Advanced Microwave Scanning Radiometer for the Earth Observing System (AMSR-E) ocean surface wind speed data was investigated in Japan Meteorological Agency (JMA) global four dimensional variational data assimilation system. Japan Aerospace Exploration Agency (JAXA) produces ocean surface wind speed data from AMSR-E measurements as a standard level 2 product using 37 GHz vertical and horizontal polarized channels in no rainy area. As a research product, all weather ocean surface wind speed data are also produced by including AMSR-E low frequency (6.925 and 10.65 GHz) information. AMSR-E all weather ocean surface wind speed data were utilized in this study. A case study of cyclone Nargis in Myanmar 2008 was performed to examine the impact of microwave imager radiance data and AMSR-E all weather ocean wind speed data. Although there were no significant improvements in the cyclone track forecast by adding all weather ocean wind speed data, the assimilation of the data inside the cyclone strengthened the intensity and the maximum wind speed in the forecast realistically. [C1427]

### "Modeling of roughness effects on electromagnetic waves propagation above sea surface using 3D parabolic equation"

This paper deals with effects of sea surface roughness on electromagnetic waves propagation in a three-dimensional domain. The 3D Parabolic Equation method is used to solve the wave equation. A new approach is presented to model the propagation above rough sea surface. Numerical results of electromagnetic waves propagation are presented to highlight the sea surface roughness influence. [C1428]

### "Comparison between electromagnetic scattering by a rain induced sea surface roughness and field data"

Scattering cross-sections for a rough sea surface in presence of wind and rain are simulated at oblique incidences and for various environmental conditions. They are compared with Ku-band radar signatures available from the literature. [C1429]

### "On the value of high-resolution weather models for atmospheric mitigation in SAR interferometry"

Atmospheric delay is one of the major error sources in In-SAR, hindering the accurate monitoring of ground motion. Here we use the WRF (Weather Research and Forecasting) weather model to hindcast atmospheric delays at SAR acquisition times over both mountainous and flat regions. The performance of the model is evaluated by comparing it to interferograms formed using acquisitions with short temporal baselines (Г,Ві4 months). Our results show that for flat regions the model not only misestimates atmospheric delay in magnitude and location but also largely underestimates the (horizontal) spatial variation (turbulent mixing) of the delay. In mountainous areas it can model the height dependent (vertical stratification) part of total delay correctly in some cases but not always. By removing the height dependent part we find again that the model may underestimate

the spatial variation of the delay. Therefore, we conclude that the WRF weather model is in general not reliable for the operational mitigation of atmospheric delay in interferograms. [C1430]

### "RADARSAT-2 initial system operations and performance"

Following launch on SOYUZ in December, 2007, the RADARSAT-2 Satellite went through intensive Launch and Early Orbit Phase (LEOP) appendage deployment and attitude configuration activities. The first SAR data, including a remarkable Quad Pole image of Greenland, was acquired on-board on Day 4 of the mission as part of an extensive system commissioning campaign. The initial period of system operations saw introduction of a new high resolution imaging mode, demonstration of rapid tasking capabilities, successful operation through the first annual eclipse season, implementation of a new regulatory framework for control of user access to imagery, and continuous system improvement through tuning and enhancement of performance and to improve operations robustness. This paper provides a summary of the achievements and status of system operations and performance. Comparisons with pre-launch expectations, specifications, and plans are made to draw lessons from the flight experience. Plans for sustaining and enhancing system operations performance are outlined. [C1431]

### "Image quality and calibration of RADARSAT-2"

RADARSAT-2 has 177 operational imaging modes. Versions of each of these modes are available either for left- or right-looking imaging, and most modes allow images to be generated for any of the four linear polarization combinations (HH, VV, HV, VH). To support these modes there are currently 1816 sets of beam coefficients and 16 digitized pulse forms stored on the spacecraft. The radar employs a number of SAR techniques besides the established Stripmap and ScanSAR of RADARSAT-1, including alternating transmit polarization, Dual-Receive (separately on the two antenna wings) and Stitched Pulse. All these factors that provide the versatility for the system also increase the complexity of the task to establish and maintain image quality and calibration. This paper covers work that was undertaken to achieve an efficient image quality and calibration campaign during the first four months of the mission, and to maintain and upgrade imaging capabilities and quality since that period. [C1432]

### "Polarization plane rotation effects on SAR polarimetric attributes"

The polarization plane rotation effects on SAR polarimetric attributes are analyzed. This analysis is carried out by simulating a polarimetric SAR image containing four regions with different electric characteristic. The simulation process is based on an electromagnetic scattering model. Employing a rotation model is generated a image set having 361 images, where each image has its polarization plane rotated by a different angle. From all images of the set are computed the covariance matrix and six polarimetric attributes of each image region and compared with their correspondent parameter in the image without rotation. From this evaluation it could be seen that the rotation angle influences differently all polarimetric attributes. The effects of rotation angle can lead to a misunderstanding of the target scattering mechanism. [C1433]

### "Microwave scattering behaviour analysis of typical targets with SAR image"

As the high resolution radar satellite's has been successfully launched, its ability of the typical target's recognition monitor enhances a lot. This article mainly does analysis based on the RADARSAT2 quad-polarimetric data, compared scattering properties of typical target feature with two temporal full polarized data, and used the measured data to drive MIMICS (Michigan Microwave Canopy Scattering model) model and carry on the multi-wave band full polarization backscattering simulation about the farmland and forest. Then we carried on the comparison between X, C band SAR image gain's actual scattering value and simulation value in order to infer the typical target feature' scattering properties rule of S band. With anticipation of HJ-1-C satellite soon launched by China and then we can carry on the comparison with the fact. Along with the full polarized data's development, the typical target feature's scattering properties analysis will be more perfect. [C1434]

### "Correction of target data taking into consideration the troposphere refractivity"

In presented paper the aspects of correction of target data are discussed. It is proposed to determine the atmosphere refractivity and correct the distance and angles of target which are measured with microwave radar. The determination of atmosphere refractivity it is proposed to carry out with the measurements of phase progression of microwave on a separate testing link. The phase progression adequately represents the atmosphere refractivity. [C1435]

### "COSMO-SkyMed mission status: Three out of four satellites in orbit"

COSMO-SkyMed is a Dual-Use (Civilian and Defence) end-to-end Earth Observation System aimed at establishing a global service supplying provision of data, products and services relevant to a wide range of applications, such as Risk Management, Scientific and Commercial Applications and Defence Applications. The system consists of a constellation of four LEO mid-sized satellites, each equipped with a multimode high-resolution SAR operating at X-band. Three out of four COSMO-SkyMed satellites have been successfully launched, while the remaining satellite will be deployed within 2010. COSMO-1 and COSMO-2 completed their Commissioning phase to test, verify and qualify the overall System and from the 1st of August both satellites are in the operational phase. The third satellite is performing its commissioning and it is expected to enter in operation in the second half of 2009. In this paper will be presented the current status of the mission and future objectives. [C1436]

#### "Sea surface transport derived by frequent revisit time series of COSMO SkyMed SAR data"

The surface transport of 'SAR detectable' features on sea is accurately estimated by couples of overlapping COSMO SkyMed ScanSAR images acquired with a very short time lag (below the hour). Tests performed with the two satellites constellation during 2008 (4 operative by 2010) provided pairs of overlapping images with a time shift of 48 minutes and with a repeat time from 12 to 24 h. The short time lag acquisition has two advantages: the first is that the pair of overlapping images is a sort of time derivative from which an accurate estimate of the surface transport can be extracted, the second is that the deformation of the 'tracked features' in the short time interval is minimal and a large number of objects can be tracked, even with the only automated processing. The sea surface transport is a crucial data in case of marine emergencies and the accurate estimate greatly improves the surveillance and the forecasting capability. Overlapping and short time lagged SAR imagery provide surface transport data of detectable objects with all-weather conditions. [C1437]

#### "Swell influence on ocean surface roughness and radar scattering from the ocean surface"

Swell effects of surface roughness spectral properties, including their wind speed dependence and modification of components characterizing Bragg resonance and surface tilting in radar application, are investigated. Computations of radar cross sections are performed with four different spectral models with various degrees of swell consideration. Swell impact on the resulting radar return is illustrated. [C1438]

#### "TanDEM-X DEM calibration: Correction of systematic DEM errors by block adjustment"

This paper gives an overview of the DEM adjustment within the TanDEM-X mission. The DEM adjustment estimates residual, systematic height offsets and deformations of each single interferometric DEM acquisition. The challenge of calibrating the TanDEM-X DEMs lies in the magnitude of the systematic errors: these errors are in the same order like the random error of about 2 m. For the estimation of the corrections a least-squares adjustment of adjacent, overlapping interferometric DEMs over a certain earth region is described in this paper. Adjustment results on simulated DEM data are shown to validate the approach. The tests are carried out for different dense ground control point configurations. Further the improvements by a combined adjustment of the two coverages are demonstrated. [C1439]

#### "Processing system and algorithms for the TanDEM-X mission"

In 2009, the German radar satellite TerraSAR-X will be supplemented with the TanDEM-X satellite to form the first bi-static single pass interferometer in space. TanDEM-X will fly close to TerraSAR-X in a controlled helix configuration for 3 years to jointly acquire interferometric SAR data in bistatic mode. The primary TanDEM-X mission goal is to generate a global Digital Elevation Model (DEM) with a relative point-to-point height accuracy of 2 meters for moderate terrain at 12 m posting. This paper outlines the SAR data workflow from quality check screening through to bistatic focusing and interferometric processing to raw DEM generation. [C1440]

#### "Ensuring globally the TanDEM-X height accuracy: Analysis of the reference data sets ICESat, SRTM and KGPS-tracks"

The TanDEM-X mission will derive a global digital elevation model (DEM) with satellite SAR interferometry. Height references play an important role to ensure the required height accuracy of 10 m absolute and 2 m relative for 90% of the data. In this paper the main height reference data sets ICESat (for DEM calibration), SRTM (for phase unwrapping) and kinematic GPS-Tracks (KGPS-for DEM verification) are analyzed regarding to their accuracy. For the ICESat data a reliable quality measure is developed. For SRTM an improved version adjusted to reliable ICESat data is presented and a concept for collecting and evaluating decimeter-precise kinematic GPS tracks is proposed. [C1441]

### "3D topography and forest recovery from an L-BAND single-pass airborne PolInSAR system"

Polarimetric InSAR (PolInSAR) using repeat-pass L-Band has generated interest in recent years because of its potential for extraction of forest height and of bare-earth topography beneath the canopy. However temporal decorrelation remains a problem. In previous papers a single-pass system has been demonstrated which removes the temporal issue. In this paper we extend the single-pass PolInSAR work previously described and show results for forests in which tree height maps and corresponding DTMs have been generated and compared to lidar truth. [C1442]

### "Retrieval of soil moisture with airborne and satellite microwave sensors"

Experimental campaigns with airborne and satellite microwave sensors have been carried out on an agricultural area in Northern Italy with the main purpose of gathering a suitable set of data to validate two operational algorithms developed to retrieve soil moisture from passive and active microwave sensors at different spatial scales. The algorithms will be used in a pilot project based on the use of Earth observation data in forecasting and monitoring the risk of floods and landslides. Radiometric data have been collected with the airborne IFAC instruments and the AMSR-E, while ENVISAT/ASAR images have been acquired for high resolution estimate of soil moisture at field scale. [C1443]

### "Extrapolation of airborne polarimetric and interferometric SAR data for validation of bio-geo-retrieval algorithms for future spaceborne SAR missions"

This paper describes a methodology to extrapolate spaceborne quality SAR image products from long wavelength airborne polarimetric and interferometric SAR data. The methodology is applied to E-SAR data of DLR, partially acquired under ESA contract especially for the development and validation of bio/geo-retrieval algorithms in forested regions. For this purpose not only system (sensor) related parameters are altered, but also those relating to the propagation path (ionosphere) and to temporal decorrelation. Examples for future spaceborne products are presented and the potential of Pol-InSAR methods for the retrieval of forest heights from these data is discussed. [C1444]

### "Impact of atmospheric water vapor on the design of a Ku band geosynchronous SAR system"

We consider a geosynchronous Ku band system, and the defocusing effects due to the temporal and spatial variability of the atmospheric water vapor. Due to the very slow formation of the spatial chirp (minutes or even hours), the temporal change of the local water vapor content could be significant, thus preventing a correct image focusing and the formation of a coherent image. Using GPS and ground based radar data, we estimate and model the spatial temporal correlation function of the water vapor delay. Then, for a given spatial scale, we estimate the maximum time within which the temporal evolution of the water vapor should be carried out, to be able to track its temporal evolution. This requisite constrains both the EIRP and the apparent velocity of the satellite. Then, we evaluate the possibilities of real time ground motion analyses, as a function of the spatial and temporal resolution and the EIRP. [C1445]

### "Quantitative analysis of stripmap and spotlight SAR interferometry with COSMO-SkyMed constellation"

This work is focused on the phase validation of interferograms obtained by combining COSMO-SkyMed SAR images acquired by a single satellite (temporal baseline coincident with the orbital repeat cycle) or even by two satellites of the SAR constellation in equi-phased configuration on the orbital plane (temporal baseline: 8 days), thus minimizing the temporal decorrelation. Both qualitative and quantitative analyses have been therefore carried out for HI (HIMAGE: stripmap, single polarization) and S2 (enhanced spotlight) imaging modes, in order to proof whether or not COSMO-SkyMed constellation is well suited for SAR interferometry. [C1446]

### "The OPERA project: EO-based flood risk management in Italy"

This paper illustrates some applications of COSMO-SkyMed (CSK) observations for rapid mapping of flooded areas and damages in small to medium size catchments. The results presented here have been obtained within the framework of the project "OPERA Civil protection from floods" funded by the Italian Space Agency and run by a team of scientific research centres and private companies. The project aims to the systematic evaluation of the added value of the use of Earth Observation techniques into operational flood prediction chains. Due to the specific geomorphology of Italy, the focus is mainly on flash floods on small sized river catchments. Monitoring and modelling processes at proper space-time scales in this environment raise several issues to be solved, compared to applications in larger river basins. Here we address some related to the suitable use of CSK imagery. [C1447]

### "Using COSMO-SkyMed data for flood mapping: Some case-studies"

The COSMO-SkyMed mission is expected to give a fundamental contribution for flood mapping, because of the high revisit time and throughput achieved by the four satellites that form the constellation. To study the potentiality of COSMO-SkyMed radar data for this purpose, two inundation events are analyzed in this paper, namely the flood occurred in Myanmar in May 2008 and the event that took place in the city of Alessandria (Italy) in April 2009. For the first event, two radar images were considered, one temporally close to the peak of the event, and the other one acquired one week later. As for the Alessandria flood, a time series of images was available, so that an attempt to monitor the temporal evolution of the inundation was accomplished. [C1448]

### "Attenuation margin requirements in a networked radar system for observation of precipitation"

In recent years, it becomes increasingly possible to move the operating frequency of weather radar systems from non-attenuating lower frequencies, such as at S-band, to attenuating higher frequencies, such as at X-band. However, wave is more easily extinct in rain at higher frequencies in which case there will be missing observations. Therefore, rain attenuation is one of the important metrics in radar system design and an extra attenuation margin needs to be applied to the allocation of power budget to meet the required sensitivity. The NSF Engineering Research Center (ERC) for Collaborative and Adaptive Sensing of the Atmosphere (CASA) is advancing a new sensing paradigm using networked short-range radar systems to avoid problematic earth curvature blockage. The CASA ERC has developed a networked radar test bed-Integrated Project 1 (IP1)-in southwestern Oklahoma, using 4 X-band radar of 40 km range to cover an area of 7, 000 km<sup>2</sup>. In this paper the attenuation margin performance are analyzed in the network context and the metric to design a networked radar system is formed. [C1449]

### "Differential Reflectivity (ZDR ) calibration for CASA radar network using properties of the observed medium"

The Center for Collaborative and Adaptive Sensing of the Atmosphere (CASA) has deployed a Distributive, Adaptive and Collaborative Sensing (DCAS) network of four radars in central Oklahoma working as a closed-loop system since 2006. The radars operate at the X-band frequency and are capable of polarimetric and Doppler measurements. The radar network is being evaluated for Quantitative Precipitation Estimation (QPE). QPE algorithms based on radar power measurements (e.g. ZHand ZDR) require bias correction. ZDRcalibration is required prior to any application of the self-consistency principle. Two different methods were evaluated for ZDRbias correction. The intrinsic properties of dry aggregated snow present above the melting layer and light rain measurements close to the ground are used for the study. Results show a ZDRcalibration accuracy of 0.2 dB or less for both analyzed events when both methods are compared. [C1450]

### "Coverage comparison of short range radar networks vs. conventional weather radars: Case study in the northwestern United States"

The West Coast of Washington and the NE and SW comers of Wyoming are regions of the contiguous United States where NEXRAD coverage is incomplete. One approach to addressing these gaps is to install additional NEXRAD-class radars. Another potential approach is to install small radar networks of the type being investigated in the CASA project. This paper compares these two approaches. We provide a meteorological and user-need assessment of present radar coverage in these regions (based on a recent feasibility study led by J. Brotzge) as well as an objective assessment of the radar-coverage that would be achieved using the large radar and small radar approaches. For this evaluation we consider two classes of radar: long-range radars having similar attributes to the WSR-88D (i.e., 10 cm wavelength, >250 km maximum range, 1 degree beamwidth, -500 kW peak power); and short-range radars having attributes similar to those operating in CASA's Oklahoma prototype network (i.e., 3 cm wavelength, 40 km maximum range, 2 degree beamwidth). We first establish the number of both types of radar that would be needed to provide coverage over a given rectangular ground-domain. Next, we quantify the coverage-versus-altitude for both weather-event detection and precipitation estimation over these regions, considering the blockage caused by both the curved earth and the local terrain. [C1451]

### "Analysis of SAR image time-series with a time-frequency method"

Time-frequency analysis (TFA) is an efficient tool to jointly detect point scatterers in SAR images and determine their backscattering properties. In this paper, we focus on TFA in multi-image context (for instance, interferometric stacks or multi-temporal series). A new TFA algorithm is proposed based on Г,ВispectrogramsГ,Вi which are 4D hyper images representing the behaviour of each pixel with respect to range and azimuth frequencies. Spectrograms are analyzed in a multi-image context: they are combined to select pixels with stable

behaviour over time (persistent scatterer detection) or unstable behaviour (change detection). Spectrograms characterize short term variations, whereas, in this paper, we characterize long term variations based on spectrogram properties. Preliminary results obtained with Spotlight interferometric TerraSAR-X images are discussed. [C1452]

### "3D analysis of scattering effects based on Ray Tracing techniques"

The side-looking geometry of SAR sensors hampers the interpretation of SAR images of urban areas. Simulation tools for illuminating 3D models of man-made objects by means of a virtual sensor support the interpretation of scattering effects by providing artificial images in the azimuth-range plane. In this paper, a simulation approach is presented which extends SAR simulation to three dimensions in order to focus detected intensity contributions in azimuth, range and elevation. Based on the simulation output, a concept for creating scatterer histograms displaying the number of scatterers within one resolution cell is introduced. Methods for analyzing simulated elevation data by means of selected slices are presented for an urban test site. Eventually, the number of scatterers extracted for a selected pixel by tomographic analysis, using a stack of spotlight TerraSAR-X images, is confirmed by results provided by the simulator. [C1453]

### "Satellite ground deformation measurements: An on-demand GRID-InSAR processing system exploiting the SBAS algorithm"

We present the results of the first experiment to plug the Small Baseline Subset (SBAS) DInSAR algorithm into a GRID-based system; the key idea is to combine the robustness of the exploited advanced interferometric SAR approach with the high computing capability provided by a GRID environment. In particular, we have exploited the low-resolution SBAS algorithm and we benefited of the availability of the ESA Grid Processing-on-demand environment. The presented results, carried out on ENVISAT data, provide an overview of the main characteristics of the implemented SBAS-GRID processing solution. [C1454]

### "Joint SAR imaging and DEM reconstruction from multichannel layover-affected SAR data"

In this paper a methodology for the reconstruction of height profile of earth surface starting from layover affected Synthetic Aperture Radar data is presented. The proposed approach is based on classical statistical estimation techniques, in particular using Maximum Likelihood Estimator, together with a Gaussian model for the point target response. Multi-channel configuration has been exploited in order to solve the solution ambiguity and to increase the reconstruction accuracy. The performances of the proposed estimator have been evaluated in comparison with the Cramer Rao Lower Bounds for the considered model, showing the effectiveness of the method. The height reconstruction procedure has been tested on a simulated realistic scenario, providing interesting and promising results. [C1455]

### "RADARSAT-1 AND -2 government calibration activities"

This paper examines the calibration activities assumed by the Canadian government within the RADARSAT program, from RADARSAT-1 commissioning in 1996 to the current period, more than one year into the RADARSAT-2 mission. Concepts, operations and results of the RADARSAT-1 calibration plan are reviewed, including the eleven-year image quality measurement history. Government calibration monitoring activities and results for RADARSAT-2 are also presented, indicating that image quality and calibration measurements are better than the specifications. [C1456]

### "RADARSAT constellation, project objectives and status"

The RADARSAT Constellation is an evolution of the RADARSAT program with the objective of assuring C-band data continuity in the next decade with improved operational use of Synthetic Aperture Radar (SAR) and improved system reliability. This paper describes mission's main objectives and user requirements, as well as its concept and current status. [C1457]

### "Monitoring turbidity and suspended sediment concentration of coastal and inland waters using satellite data"

A method for retrieving water turbidity and suspended sediment concentration of inland and near-shore coastal waters using high resolution remote sensing satellite data is described. Backscattering coefficient at the near infrared band is first derived from the satellite images using a quasi-analytical algorithm after applying a simple atmospheric correction routine. A turbidity map is obtained by applying an empirical relation derived from laboratory experiments to convert the backscattering coefficient to nephelometric turbidity units (NTU). This method can be operationalized for global water quality monitoring using currently operating satellite sensors such

as those on Landsat, SPOT and Terra / Aqua MODIS. [C1458]

### "Evaluation of the single reference image snow-covered area estimation method for the boreal forest zone"

Spaceborne Synthetic Aperture Radar (SAR) data have been utilized for regional scale snow-covered area (SCA) monitoring for several years. Different methods have been developed and demonstrated for different geographical regions. A method utilizing a single reference image for SCA estimation has been shown to function well on mountainous and non-forested regions. For the boreal forest zone a method using two reference images and a forest compensation procedure has been previously utilized. The single reference image method is evaluated here for the boreal forest zone and its performance is compared with the Helsinki University of Technology (TKK) SCA method that is specifically developed for boreal forest regions. The SCA evaluations are carried out using Radarsat-1 data for the snow-melt seasons of 2004-2007. The SCA estimation accuracies for the radar-based methods are determined using optical satellite based SCA data as reference. The results show that SCA estimation using a single reference image is usable for the boreal forest zone, although the accuracy is significantly weaker than that of the TKK-developed, boreal forest specific SCA method. The best accuracy obtained shows a root-mean-square error (RMSE) of 0.176 for the single reference image method and an RMSE of 0.123 for the TKK SCA method. [C1459]

### "Tomographic 3D reconstruction from airborne circular SAR"

The study of data acquired over a circular trajectory has raised an increasing interest in the SAR community. Two main reasons summarize the interest in such geometry. First, sub-wavelength resolution can be achieved, as the targets in the spotted area are observed under a 360° aperture. Second, the use of the information from different azimuthal directions allows one to obtain information of the scene in the third dimension, making possible a 3D target reconstruction. In any case, both applications require certain target reflectivity homogeneity. This paper shows several processing results and analyzes the potentials and limitations of circular SAR to perform tomography of semi-transparent media. Special processing aspects, like the estimation of residual motion errors due to inaccuracies in the navigation data, are also addressed. Data acquired at L-band by DLR's E-SAR system are used to demonstrate the high resolution and tomographic imaging capabilities of circular SAR. The results include the tomogram of a Luneburg lens, as well as preliminary results over man-made targets and vegetation. [C1460]

### "Development of X-band airborne polarimetric and interferometric SAR with sub-meter spatial resolution"

These days, the space-borne SAR becomes one of the powerful instruments to observe the earth surface. On the other hand, a airborne SAR is also important for development of SAR system and analysis technique. Moreover, airborne SAR is able to make immediate observation of disaster area. The National Institute of Information and Communications Technology (NICT) has been developing the new airborne synthetic aperture radar: Pi-SAR2 since 2006. The Pi-SAR2 is an airborne X-band polarimetric and cross-track interferometric SAR with sub-meter spatial resolution. The spatial resolution is measured less than 0.5m using some corner reflectors. The Pi-SAR2 system were completed and began the operation in autumn 2008. [C1461]

### "INTASAR Program"

This paper describes the INTASAR Program of Spanish National Institute for Aerospace Technology (INTA) which goal is to research in Synthetic Aperture Radar technology area. INTASAR constitutes an INTA's long-term program, which basis is the development of airborne SAR prototypes, working presently in three complementary lines: SAR prototypes on-board CASA-212 platform, SAR developments in small platforms and participation in PAZ Program-Spanish radar satellite. [C1462]

### "Use of Cosmo-SkyMed data for seismic risk management in the framework of the ASI-SIGRIS project"

The scope of the SIGRIS pilot project is the development of an infrastructure to provide value-added information services for the seismic risk management, using satellite Earth Observation data. The project is funded by the Italian Space Agency (ASI) and will exploit Cosmo-SkyMed SAR data to generate various information products to support the activities of the Italian Civil Protection Department. We show the first achievements of the project obtained using Cosmo-SkyMed imagery to generate products for the April 6th, 2009 L'Aquila earthquake in Central Italy. [C1463]

### "TerraSAR-X and RADARSAT-2 for crop classification and acreage estimation"

This research outlines a preliminary assessment of the use of TerraSAR-X data for classifying agricultural crop land in Canada. X-Band data were able to identify crops (pasture-forage, soybeans, corn and wheat) to accuracies of 95% once a post-classification filter was applied. These accuracies were achieved using six TerraSAR-X images from 2008 and a decision-tree classification algorithm. Acquisitions began only mid-season and consequently a second full season TerraSAR-X data set is being collected in 2009. C-Band classification accuracies were about 10% lower in comparison. These results clearly demonstrate the potential of X-Band data for crop identification. [C1464]

### "F-SAR-DLR's new multifrequency polarimetric airborne SAR"

The Microwaves and Radar Institute of the German Aerospace Center (DLR) is known for consistent work on the field of airborne synthetic aperture radar and its application. In April 2008 the 20th anniversary of the maiden flight of the well-known E-SAR system was celebrated. E-SAR has been maintained well over the time. It provided valuable knowledge to the science community, especially in the past 10 years. However, it became more and more obvious that a technological renewal was inevitable. Consequently the development of a new SAR system was put on line under the name 'F-SAR'. [C1465]

### "RBX: The new X-band radar from INTA"

This paper describes the architecture and main characteristics of the new synthetic aperture radar system which is being developed at Spanish National Institute of Aerospace Technology. The new prototype will support submetric resolution and interferometric and polarimetric capabilities, similar to other research SAR systems. The system architecture was designed taking into account an easy upgrade procedure and a continuous mount and dismount requisite. Hence, the system has just a few units and external interconnections. In addition, a feature which focused a significant design effort was data quality, thus the system supports calibration procedures like calibration loops or the acquisition of a replica from the transmitted signal. [C1466]

### "Full-resolution adaptive differential tomography"

Recently, a new interferometric mode crossing the differential SAR interferometry and multibaseline SAR tomography concepts, termed differential SAR tomography, has been proposed. Its potentials, coming from the joint elevation-velocity resolution capability of multiple scatterers, have been demonstrated both theoretically and with real data. Processing is cast in a two-dimensional baseline-time spectral analysis framework, with sparse sampling. The use of adaptive two-dimensional spectral estimation has been shown to allow joint baseline-time processing with reduced sidelobes and enhanced elevation-velocity resolution. However, this method requires coherent multilooking processing, thus does not produce a range-azimuth full resolution differential tomographic product. In this work a new single-look adaptive differential tomographic processor is presented, to allow range-azimuth full resolution together with the good elevation-velocity sidelobe and resolution capabilities of adaptive processing. Simulated results are reported for different baseline-time acquisition patterns, both monostatic and multistatic, and different motion conditions of layover scatterers. [C1467]

### "Methods of analysis of atmospheric aerosols from future spaceborne high spectral resolution lidar data"

The limitations of single wavelength elastic scatter lidar with regard to retrieving various optical or microphysical properties of the observed aerosols are well known. Typical retrieval methodologies rely on elastic scatter information at at least two wavelengths, together with either temporally or geographically inferred estimates of the extinction-to-back-scatter ratio  $S_a$ , or aerosol model parameters which constrain the solution in such a way as to be consistent with the optical properties of commonly observed aerosol types. High spectral resolution lidars (HSRL) now facilitate unambiguous, direct measurement of aerosol extinction and backscatter profiles, greatly augmenting the level of information available for determining aerosol type or other relevant parameters. In this paper, we explore a methodology for using HSRL data at one wavelength to facilitate retrievals from traditional elastic scatter data at other wavelengths. Further, we extend the scope of the technique to improving aerosol models used to constrain retrievals from multi-wavelength elastic scatter lidars. We explore this methodology in the context of currently available HSRL technology as well as anticipated future spaceborne HSRL systems. [C1468]

### "SAR altimeter retracker performance bound over water surfaces"

This paper provides the theoretical limit for the performance of a Maximum Likelihood Estimation (MLE) DDA re-tracker for different Significant Wave Height (SWH) conditions based on Cramer-Rao Lower Bound (CRLB)

analysis. [C1469]

### "A radar suite for ice sheet accumulation measurements and near-surface internal layer mapping"

Many satellite, airborne, and in situ observations have been made to better understand the mass balance of the ice sheets. Satellite missions such as GRACE, ICESat, and Cryosat provide broad coverage, but are only capable of collecting data at relatively coarse temporal and spatial resolutions. Satellite observations alone are not sufficient to fully understand all mechanisms responsible for changes in the overall ice sheet mass balance. While these are sufficient over much of the interior of the ice sheet, to understand and model the dynamics of fast flowing glaciers and the margins of the ice sheet, finer resolution data are required. Airborne platforms, especially autonomous platforms, allow for key regions of the ice sheets to be measured with fine-resolution remote sensing instruments. These platforms provide more accurate ice thickness estimates, internal layer mapping, and ice-bedrock interface imaging. To address this gap in the observations, we are designing and developing an instrumentation suite to be deployed on crewed and uncrewed aircrafts. Here we will focus on two radars in the instrumentation suite: an accumulation radar and a radar altimeter. The altimeter will be capable of measuring surface elevation and near-surface internal layers to a depth of about 10 m. The accumulation radar will be capable of measuring internal layers to a depth of about 100 m. A previously developed 150 MHz radar depth sounder/imager will be used to map layers below 100 m, as well as the ice-bedrock interface. This radar is beyond the scope of this paper. Field data collection using these systems will be performed simultaneously, providing a fine-resolution characterization of the ice sheet from surface to bedrock. The altimeter provides annual and short-term information on the accumulation, while the accumulation radar provides information on the decadal scale variability. The depth sounder provides information on the century scale variability. Initial data collection occurred during the early spring 2009 Greenland field season; additional data collection will continue during future campaigns both in Greenland and Antarctica. System refinements will allow for this suite to be deployed on uncrewed aerial vehicles (UAVs), also being developed at the Center for Remote Sensing (CRSIS) at the University of Kansas. [C1470]

### "Mapping aurora activity with SAR-a case study"

Auroral physics is an exceedingly rich and complex subject. However, due to a lack of high resolution data of ionospheric activity during auroral events, not all phenomena in the high latitude ionosphere are fully understood. Recent research has proven that L-band SAR data is significantly affected by the ionosphere and can be used for mapping its activity. With this paper we will prove and unambiguously verify the potential of L-band SAR to capture auroral activity. We will present examples of aurora signatures mapped from ALOS PALSAR data and will verify the results from SAR with observations provided from ground based measurements. [C1471]

### "Dependence of P-band interferometric height on forest parameters from simulation and observation"

GeoSAR is a unique dual-band, interferometric SAR (DBInSAR) sensor capable of collecting single-pass, X-band (VV) and P-band (HH) interferometric data simultaneously. In this paper we examine the dependence of the P-band HH interferometric phase centre height upon forest and terrain parameters. We develop a simple model for P-band GeoSAR observations, and use the model to show how the elevation in P-band HH phase centre height above true ground height is related to the volume-to-ground scattering ratio. GeoSAR is not fully-polarimetric, but records cross-polar (HV) returns at P-band (although not interferometrically). We conjecture that these returns are dominated by direct-volume scattering and related to the direct-volume HH backscatter. We use this relationship to model the dependence of the P-band HH DTM height upon the HV/HH ratio, and the difference in X-band DEM with P-band DTM heights. The relationships are examined using simulated forest InSAR data, and a model is proposed for ground-height and tree-height estimation using DBInSAR that does not require full polarimetry. [C1472]

### "Global atmospheric aerosol optical depth retrievals over land and ocean from AATSR"

Aerosol radiative forcing is a major unknown in climate modelling. Owing to the large spatial and temporal variability exhibited by atmospheric aerosol concentrations remote sensing is the only feasible way to obtain global measurements. The ATSR-2 (1995-2002) and AATSR (2002-) radiometer instruments together provide one of the longest available, well calibrated datasets of satellite radiance measurements. The algorithm presented here enables the retrieval of aerosol optical depths (AODs) from these data over a wide variety of surface types including ocean, vegetated land surfaces, and desert. This paper demonstrates the potential for retrievals based on ATSR-2 and AATSR data to reveal spatial and temporal signals in AOD from 1995 onwards. AODs based on AATSR data are validated against surface-based measurements and 6-year time series of regional monthly composites are presented. [C1473]

### "Estimation of target motion and 3D target geometry using multistatic ISAR movies"

Inverse synthetic aperture radar (ISAR) is one of the radar techniques used to observe two-dimensional images of a remotely based target using radio waves. If we keep observing the target and consecutively generate multiple ISAR images, which we call ISAR movie, the target image varies considerably due to the motion of the target. The authors have proposed an algorithm for reconstructing three dimensional target shape from an ISAR movie; however, the algorithm requires a priori knowledge of the relative motion of the target. In this paper, we propose a novel method that estimates the relative motion and the three dimensional shape of the target using multistatic ISAR movie. [C1474]

### "Time series of polarimetric and interferometric observations of TerraSAR-X data over rice fields in Spain"

The objective of this work is to investigate the coherent co-polarized behavior of rice plants during the growing stages and to explore their information content for rice monitoring at high frequencies recently available through new SAR satellite missions. Time series of dual-pol TerraSAR-X images have been acquired during the whole cultivation period over a rice site in Spain. Among different observations, the backscattering coefficients at HH and VV channels and the HH/VV ratio have confirmed to show a temporal variation that has a significant correlation with the development of the plants during the vegetative and reproductive phenological phases. In addition, the information content of the HHVV complex coherence and a dual polarimetric target decomposition is investigated and discussed. All the information layers investigated are contributing to the discrimination of rice fields from other crop types. Finally, interferograms computed with pairs of successive images (11 days separation) have been preliminary tested. [C1475]

### "Chirp scaling based detection of moving targets in SAR images"

A moving target detection and high-resolution focusing scheme is presented for single-channel SAR systems. The moving target focusing is made of a bank of Chirp Scaling Algorithms (CSA), each one matched to a different along-track target velocity component, thus allowing to produce a high-resolution image of the target itself. The effectiveness of the proposed technique is shown with reference to a sample dataset obtained from a SAREX-92 image. [C1476]

### "SRAL, a radar altimeter designed to measure a wide range of surface types"

The SRAL (Sar Radar ALtimeter) instrument is the core instrument of the topography mission carried on -board the Sentinel-3 satellite which is to be launched in 2013. A detailed overview of this instrument (on -going C/D phase) is given in terms of mission requirements, architecture and modes, budgets/performances and equipments. [C1477]

### "The relationship between radar backscatter cross section and ocean wave parameters at low incidence angles"

Using collocated data set of Tropical Rainfall Mapping Mission (TRMM) precipitation radar (PR) and buoy wind and wave measurements, we study the relationship between the Ku-band radar backscatter cross section ( $\Gamma_{Bi}\Gamma, B^\circ$ ), radar incidence angle ( $\Gamma, Bi$ ), the buoy measured near surface wind speed in 10m ( $U_{10}$ ), significant wave height (SWH), wave steepness ( $\Gamma, Bi$ ), and wave age ( $\Gamma B_u$ ). Sensitivity analysis of those parameters shows there is a nodal point at incidence angle about  $11\Gamma, B^\circ$  for radar backscattering, which exhibits not only low sensitivity to wave parameters but also an overall low variability. Tabular empirical functions relating PR  $\Gamma_{Bi}\Gamma, B^\circ$  to each single wave parameters for incidence angles from nadir to  $18\Gamma, B^\circ$  are developed. The dependence of  $\Gamma_{Bi}\Gamma, B^\circ$  on a single wave parameter in a fixed incidence angle is not unique, so multi-parameter functions of PR  $\Gamma_{Bi}\Gamma, B^\circ$  are also investigated. Those multi-parameter functions can be used to retrieve wave parameter from radar backscatter with other wave parameters measurements. An example of empirical tabular model function relating wave steepness to PR  $\Gamma_{Bi}\Gamma, B^\circ$  in terms of  $\Gamma, Bi$  and  $U_{10}$  is firstly developed from collocated buoys and PR measurements. [C1478]

### "Measurements of ocean wave spectra with vertical polarization X-band radar image sequences"

Ocean wave parameters, such as significant wave height, can be computed from wave spectrum. Ordinarily X-band nautical radar can produce the three dimensional wave number frequency image spectra from a time series of radar images with a 3-D FFT algorithm. The fundamental image spectrum is related to the surface wave spectrum by the modulation transfer function (MTF). To determine the modulation transfer function, the field experiment for vertically polarized X-band nautical radar is carried out at Zhangzi Island. This paper presents the

results of an experimental study by in-situ data analysis with existing inverting modeling method aimed at estimating the vertically polarized modulation transfer function, which can minimize the difference between the image spectra from radar images and spectra from buoy, and measuring the sea parameters using ocean wave spectra for two polarizations. [C1479]

#### **"Polarimetric SAR interferometry for forest application at P-band: Potentials and challenges"**

This paper presents the impact of simulation parameters according to the potential future space-borne mission BIOMASS (P-band) in polarimetric and interferometric SAR (Pol-InSAR) inversion performance. Forest height inversion is obtained from the simulated data sets (bandwidth, NESZ and ambiguities) generated from DLR E-SAR (Experimental Synthetic Aperture Radar) airborne SAR data. For this study two campaign data sets (BioSAR 2007 / INDREX-II) have been selected and investigated. The several comparative results of Pol-InSAR between airborne data and the simulated data (incl. bandwidth, NESZ and range/azimuth ambiguities) will be shown and discussed. [C1480]

#### **"Advances in unsupervised ship detection with multiscale techniques"**

This paper constitutes an example of analysis proving that new satellite borne full polSAR data is favorable for automatic ship detection purposes. In particular, this paper is based on a multiscale method for automatic ship enhancement based on the wavelet transform on single channel data and it proposes its extension to full polSAR images. Then, the enhancement of contrast of the ships with respect to the background sea reached with the method proposed is compared to that obtained by the classical polarization entropy. [C1481]

#### **"Ship detection in the Brazilian coast using TerraSAR-X SAR images"**

Extensive Brazilian coast and a growing up maritime vessel traffic lead to research better ancillary methods to control ship's flow. Orbital SAR imagery is an important tool, especially due to its ability to work day and night and clouds coverage doesn't interfere often. At present study, some well-known ship detection concepts are investigated, applying them to TerraSAR-X (TSX) ScanSAR images (16 m resolution), in VV and HH polarization. Statistical parameters are estimated and trough Kolmogorov-Smirnov test K-distribution fit to TSX images is checked. Algorithm detection based on Constant False Alarm Rate (CFAR) concept is applied and its performance is verified. Incidence angle, CFAR's windows size and Probability of False Alarm (PFA) influence are further analysed. Finally, we discuss some operational issues about near-real-time image delivery and the delay impact on a surveillance system or on an urgency request. [C1482]

#### **"Ship detection from polarimetric sar images"**

SAR image from sea can constantly contain ships and their ambiguities in azimuth and range directions. For maritime applications, the ambiguities are visible due to their strong intensities in a low backscattering background of sea environment. Thus, the ambiguities can be often mistaken as ships and cause false alarms. Many approaches have been proposed for reducing the azimuth ambiguities in single channel SAR image. This paper analyzed scattering mechanisms of the azimuth ambiguities for PolSAR images and proposed a method for detecting ships from PolSAR images. By using eigenvector-eigenvalue decomposition, three eigenvalues can be used to differentiate ship targets, azimuth ambiguities and sea clutter. One C-band JPL AIRSAR polarimetric data have been chosen to evaluate the method. The experimental results show that the proposed method can effectively reduce false alarms caused by the azimuth ambiguities. [C1483]

#### **"Multifrequency theoretical simulations of backscattering from flooded areas"**

This paper investigates the sensitivity of backscattering coefficient to variations of soil moisture and flooding for two kinds of crops, such as wheat and maize, and for deciduous forests. Investigations are based on model simulations at L and C band, VV and HH polarization. At L band, a significant sensitivity to flooding effects is observed for all vegetation covers. At C band, the sensitivity is still acceptable for wheat, while for maize it is present only in case of non uniform cover. For forests, the performance of C band is poor. [C1484]

#### **"Improvement of bare surface soil moisture estimation with L-band dual-polarization radar"**

This study demonstrates a new algorithm development for estimating bare surface soil moisture using dual-polarization L-band backscattering measurements. Through our analyses on the numerically simulated surface backscattering database by Advanced Integral Equation Model (AIEM) with a wide range of soil moisture and surface roughness conditions, we found that the relative difference of the overall surface roughness parameters at the different co-polarizations can be well estimated through a roughness index. This new finding leads to an algorithm on estimation of bare surface soil moisture. We will demonstrate the theory and techniques of this

algorithm through the AIEM simulated database and validate it with two field ground scatterometer experimental data. The results indicate that bare surface soil moisture can be estimated quite well with only co-polarized backscattering signals. It provides a solid support for Soil Moisture Active and Passive mission (SMAP). [C1485]

### "Operational approach for ship detection and classification"

The necessity to control all the activities within the marine environment is nowadays vital for most official authorities. Besides protecting the ecosystem and providing safety and surveillance along the transportation corridors, illegal immigration and sustainable economic activities are also issues to cover. Since early nineties, a lot of efforts have been devoted to develop monitoring systems based on transponders (VMS or AIS). Such systems use active on-board devices to track ship positions via satellite communications. Despite of their great performance, the experience has shown, however, that this approach does not have the required independency and other alternatives are necessary. Among them, the one gathering more benefits is the integration of remote sensing, specially Synthetic Aperture Radar (SAR), with operational transponders. Certainly, this solution provides redundancy, 7/24 and all-weather monitoring capability, independently from the targets to track. [C1486]

### "Monitoring land subsidence within the Venice Lagoon with SAR interferometry on Trihedral Corner Reflectors"

Before the summer of 2007 58 square Trihedral Corner Reflectors (TCR) were installed in salt marshes within the Venice Lagoon where anthropogenic structures completely lack or few constructions are scattered at a distance from one another too large to reliably resolve the radar phase ambiguity on ERS and ENVISAT interferometric point target analysis. An optimal TCR network has been established taking into account the location of  $\Gamma, B_{\text{natural}}, B_i$  point targets in ERS and ENVISAT SAR interferometric analyses and keeping to a value of about 1 km the maximum distance between the TCR or between an  $\Gamma, B_{\text{artificial}}, B_i$  and the adjacent  $\Gamma, B_{\text{natural}}, B_i$  reflectors. In this contribution we discuss the set-up of the TCR, their backscattering intensity response on ENVISAT ASAR and TerraSAR-X images, and the approach followed to measure the ground displacement in areas of particular interest within the Venice Lagoon. [C1487]

### "Experiences in optical and SAR imagery analysis for damage assessment in the Wuhan, may 2008 earthquake"

The Sichuan Earthquake on the 12th of May 2008, and the extensive rescue operations following this tragic event, proved the value of high-resolution optical and radar remote sensing during the emergency response. Optical data provide a fast and simple way to value  $\Gamma, B_{\text{at glance}}, B_i$  damages while radar sensors can deliver images independent of weather conditions, day and night, and thus in principle can represent a mean to obtain a damage map in the immediate aftermath of an event, providing precious information for intervention planning. On the other hand, SAR data is far more difficult to interpret than optical data both to the expert and non-expert. In this paper we present a case study of damage assessment on the Sichuan earthquake experimenting the use of very high resolution data from both worlds, discussing preliminary results and perspectives. [C1488]

### "Evaluating VHF-band SAR autofocus algorithms using a forest backscatter model"

The objective of this paper is to assess the accuracy of an autofocus method developed for the Fast Factorized Back-Projection (FFBP) algorithm in simulated scenarios. We specifically address the question whether correlation measurements between subimages will suffice in the focusing process in one arbitrary merging step. A forest clutter model is used together with a model of the impulse responses to simulate two SAR sub-images of a forest. Correlation is used for sub-image matching and residual displacement errors are compiled using simulation. We conclude that the matching error increases with increased number of trees per resolution cell but can be restored with a larger image size in the correlation measurements. We also conclude that the autofocus method will be successful. [C1489]

### "INTA's developments for UAS and small platforms: QUASAR"

This paper will outline the objectives and mission, general features and roadmap and will give a brief description of the two main prototypes of QUASAR (Quicklook Unmanned Aerial SAR), the main project in Synthetic Aperture RADAR for small platforms carried out by the Spanish National Institute for Aerospace Technology. QUASAR is planned be released as a functional demonstrator in 2011 and as complete, operative and deliverable high resolution Ku-band SAR with ground segment station for mission planning, image formation and data exploitation system in 2013. [C1490]

### "GPU-based framework for distributed interactive 3D visualization of multimodal remote sensing"

## **data"**

Interactive visualization of remote sensing data allows the user to explore the full scope of the data sets. Combining and comparing different modalities can give additional insight. In this paper, we present a 3D visualization framework for interactive exploration of remote sensing data. Data from different modalities can be combined into a single view. The visualization can be distributed across multiple graphics processing units and/or hosts, allowing interactive exploration of remote sensing data in virtual reality systems. [C1491]

## **"SBAS-InSAR analysis of surface deformation at Mauna Loa and Kilauea volcanoes in Hawaii"**

We investigate the deformation of Mauna Loa and Kilauea volcanoes, Hawai'i, by exploiting the advanced differential Synthetic Aperture Radar Interferometry (InSAR) technique referred to as the Small Baseline Subset (SBAS) algorithm. In particular, we present time series of line-of-sight (LOS) displacements derived from SAR data acquired by the ASAR instrument, on board the ENVISAT satellite, from the ascending (track 93) and descending (track 429) orbits between 2003 and 2008. For each coherent pixel of the radar images we compute time-dependent surface displacements as well as the average LOS deformation rate. Our results quantify, in space and time, the complex deformation of Mauna Loa and Kilauea volcanoes. The derived InSAR measurements are compared to continuous GPS data to assess the quality of the SBAS-InSAR products. [C1492]

## **"SAR interferometry and Speckle tracking approach for glacier velocity estimation using ERS-1/2 and TerraSAR-X spotlight high resolution data"**

Glacier retreat and advance is general phenomenon in Himalayan region due to change in climatic conditions. For quantifying the global warming effects on local scale glacier system monitoring and estimating its dynamic geophysical parameters viz. movement and volume change are important. In this study glacier movement estimation is attempted in north western Himalayan region using spaceborne InSAR technique, which is based on preserving the coherence between two acquisitions of the same scene. It is observed that ERS-1/2 tandem data give high correlation over Gangotri glacier and Siachen glacier and movement in LOS direction is deciphered. However, with the use of SAR Speckle tracking method two dimensional (Azimuth and range directions) velocities of glaciers can be obtained. In this study attempt has been made to measure 2-D velocity components of Gangotri glacier. New generation TerraSAR-X (TS-X) high resolution spotlight mode (HS), single look slant range complex (SSCs) data of 28th August, 2008, 08th September, 2008, 19th September, 2008 and 30th September, 2008 are exploited for this study. Interferogram, coherence image and intensity image are generated. It is observed that Interferometric SSC data of 28th August, 2008 and 08th September, 2008 give some fringes outside glacier area and complete decorrelation is shown on the Gangotri glacier due to high movement of glacier. [C1493]

## **"Polarized point scatterers: An algorithm for detection using ALOS-PALSAR data"**

This paper deals with a new class of localized point targets we call polarized point scatterers (PPS). They can be detected from Quadpol SAR data by using a two-dimensional filter, employing an eigenvalue/alpha threshold. They can then be used to estimate the dielectric constant of the target using a simple scattering model. We first consider the basic performance of the filter based on selection of thresholds and data window size to keep false alarms to a desired low level. We then illustrate application of the filter to sample data sets from the ALOS-PALSAR archive, showing its important application to urban areas. [C1494]

## **"Scattering component decomposition for POL-InSAR dataset and its applications"**

The three-component scattering model decomposition based on the scattering mechanisms corresponding to single-bounce, double-bounce, and volume scattering, is one of the powerful tools to classify terrain for fully polarimetric SAR data. However, the conventional scattering component decomposition technique with POLSAR image requires several assumptions to obtain a unique solution. This paper presents scattering component decomposition technique with Pol-InSAR image pair. The proposed technique based on the ESPRIT can decompose without any assumptions when a suitable set of candidates for volume scattering covariance matrix is prepared. In this report, we show the concept of the proposed method with the POL-InSAR image pair and the role of the ESPRIT in the volume scattering estimation. Experimental results of SIR-C/X-SAR are also provided as an example. [C1495]

## **"Detection and analysis of urban areas using ALOS PALSAR polarimetric data"**

Due to their large scale of observation and their relatively high revisiting frequency, spaceborne SAR systems offer interesting possibilities for the systematic monitoring of urban areas. Several techniques have been developed to analyze urban areas from single-polarization spaceborne SAR data, based on the statistical

properties of the reflectivity of such complex media and its spatial variations (texture). The reduced resolution of the data, compared to the airborne SAR case, is a particularly limiting factor. Polarization diversity offers an interesting and powerful alternative mean to detect and characterize urban areas. In this paper, we propose to use po-larimetric SAR acquired by the ALOS sensor at L band, to monitor urban areas. The proposed technique uses three complementary approaches to discriminate urban structures using detectors adapted to the complex polarimetric features of this medium, to isolate specific coherent responses from a Time-Frequency analysis of the coherent SAR signal, and finally to characterize built-up areas from the coherence properties of their Polarimetric and Interferometric SAR (POL-inSAR) response. [C1496]

#### "Capon/APES based SAR processing: Practical considerations"

This paper discusses the use of Capon's Minimum Variance Method (MVM) and Amplitude and Phase EStimation APES spectral estimation algorithms to SAR range-azimuth focusing. The rationale of the algorithms is explained. An implementation of a Capon or APES processing chain is described. Results using RADARSAT-2 Quad Pol data over Barcelona are used to qualitatively study the real-life performance of these algorithms. [C1497]

#### "Calibration of spaceborne polarimetric SAR data using a genetic alogrithm"

Calibration method for spaceborne polarimetric SAR data using a genetic algorithm is discussed in this paper. Recently some satellites which have polarimetric synthetic aperture radar were launched, and the polarimetric data analysis techniques are being developed for terrain classification, forest biomass and soil moisture estimations, etc. Thus, polarimetric calibration becomes an important issue for accurate polarimetric analysis. However, typical polarimetric calibration methods have some restrictions. For example, Freeman method requires the polarimetric data which satisfy reflection symmetry and does not estimate cross-talks. Thus, it is desired that a polarimetric calibration method is needed to estimate all polarimetric calibration parameters by using polarimetric data without considering reflection symmetry. In this report, a polarimetric calibration technique based on a genetic algorithm (GA) is proposed. This proposed method can estimate cross-talks, channel imbalances and Faraday rotation angle using one trihedral corner reflector and the measured polarimetric SAR data with non-reflection symmetry. [C1498]

#### "A new approach to improve the accuracy of baseline estimation for spaceborne radar interferometry"

The 'baseline' is one of the most important parameters in Interferometric Synthetic Aperture Radar (InSAR). The quality of InSAR products is significantly affected by the accuracy of baseline estimation. In this paper, a new approach to improving the baseline estimation is proposed. The main advantage of estimating baseline by the proposed method is that the calculation can be performed without the need for phase unwrapping and ground control points (GCPs). The final result shows that a better differential interferogram can be generated using the proposed baseline estimation method. [C1499]

#### "Polarimetric signatures and classification of tropical land covers"

Polarimetric signatures for different tropical land covers were extracted from RADARSAT-2 data. Subsequently, the data were classified. The objective of this work was to assess the potential of RADARSAT-2 polarimetric C band data on land cover mapping. RADARSAT-2 data were acquired over Tapajos National Forest, a tropical forest reserve in Brazil, and surroundings, in September 2008. A field campaign was conducted during the same week of the SAR data recording. Polarimetric signatures for the different land covers were extracted for co- and cross-polarised bands and results indicated the variety of scattering mechanisms in the study area. Following that, the coherence and covariance matrices were used for the Freeman-Durden target decomposition, which decomposed the image targets in new bands representing the main scattering mechanism in the resolution cells-corner reflection, volumetric and superficial. Data were later classified by a k-means-Wishart classifier. The bands representing volumetric and superficial scattering helped discriminating vegetated and non-vegetated areas. Classification accuracy reached around 80% for forest and pasture/bare soil classes. For the remaining classes, the classification accuracy results did not reach 50%. [C1500]

#### "Karst forest type discrimination in southwest China using spaceborne polarimetric SAR data"

Karst forest physiognomy occupy a large area of Guizhou, southwest China. It is a rare forest resource in the earth and urgently needed to carry out protection. Due to synthetic aperture radar (SAR) data's ability to acquire images through clouds, it was tested as an alternative to optical data to map changes of land use/land cover, to estimate biophysical parameters of vegetation types, and to detect deforestation. The main goal of this paper is to analyze the potential of the spaceborne full polarimetric data in distinguishing the different types of forest in

southwest China. Different polarimetric target decompositions, such as eigenvector-based decomposition (Cloude-Pottier's decomposition and Touzi Decomposition) and scattering model-based decomposition (Freeman decomposition), were used in this paper to extract forested areas from the scene. To further divide the extracted forested area into deciduous and coniferous forest., Supervised polarimetric classification procedures based on Freeman decomposition is presented in this paper. [C1501]

### **"The ALOS PALSAR mosaic over the African continent-A reference baseline dataset for forest- and land cover change monitoring"**

Within the framework of the ALOS Kyoto & Carbon Initiative, the European Commission Joint Research Centre (JRC) is in charge for the generation of a 50 m pixel spacing L-band SAR mosaic over the African continent. The mosaic is generated from full resolution (20 m), dual polarisation (HH + HV) ALOS PALSAR data, acquired from June through October 2007. The mosaic is scheduled for release in the autumn of 2009, and will be made available free of charge to scientific users worldwide through the JRC and JAXA. This paper provides a brief overview of the K&C Initiative, and a short description of the procedures employed by the JRC for the Africa mosaic generation. [C1502]

### **"Polarimetric coherence optimization for interferometric differential applications"**

In this paper, the potentials of polarimetric coherence-optimization techniques for differential interferometric SAR (DInSAR) applications are examined. For this purpose, the cutting-edge approaches available in the literature are considered. First, synthetic PolSAR data simulating homogeneous distributed scatterers are employed to demonstrate the convergence of the optimized differential phase to the deformation phase information. Then, real X-band ground-based PolSAR acquisitions concerning an urban environment are analyzed. The relation between optimum coherences and corresponding optimum phase in terms of deformation on retrieval is carefully analyzed using two zero-baseline fully-polarimetric data sets. In the end, general conclusions about the advantages and drawbacks of the alternative maximization approaches are drawn. [C1503]

### **"Determination of scattering mechanisms inside rice plants by means of PCT and high resolution radar imaging"**

3-D high-resolution radar images have been produced for a mature rice crop sample by using wide-band fully polarimetric data collected at the EMSL, JRC-Ispira (Italy). These images have been compared with the 1D vertical density profiles produced by the Polarization Coherence Tomography technique on the same rice sample. In order to obtain a 1D vertical reflectivity profile from the 3D SAR images, several slices at certain ground-range positions have been selected and then all the horizontal cross-range contributions have been summed up. As expected, very similar qualitative results are obtained when comparing these profiles with the PCT ones. The ground exhibits the highest response for all three polarization channels up to C-band, and also for the HH channel at X-band. In addition, at X-band the VV channel decreases significantly at ground level but the HV channel remains high. Finally, an important contribution from the upper layers is observed at C-band and more notably at X-band for all three polarization channels. [C1504]

### **"Multisensor SAR analysis for forest monitoring in boreal and tropical forest environments"**

For many aspects of the human life the world's forests are crucial. Only microwave remote sensing provides the means of all day weather independent monitoring of those pristine areas. Multi-temporal ENVISAT ASAR and ALOS PALSAR data for mapping boreal forest in central Siberia proved to be quite successful in diverse research projects. So far, TerraSAR-X High Resolution Spotlight images have been effectively used in the verification process of the resulting land cover area maps. Part of this knowledge will be transferred within the framework of the Remote Sensing Survey of the next global Forest Resources Assessment. Altogether 350 TerraSAR-X scenes all over the cloudy tropics will be analysed in a project called FRA-SAR 2010. The combined analysis of ALOS PALSAR, ENVISAT ASAR and TerraSAR-X on five areas inside the project will foster the expertise on forest structure parameters. [C1505]

### **"Local, nonlinear adaptive co-registration of master and slave interferometric SAR complex image data for high quality digital elevation map generation"**

Interferometric synthetic aperture radar (InSAR) is a key technology in geoscience. In the generation of a digital elevation map (DEM), the elimination of singular points (SPs) is the most important process besides the phase unwrapping (PU). A SP means a point where the phase rotation is not zero in the interferogram obtained by InSAR. What yields the SPs? One reason is a big cliff actually existing in the observation region. Empirically, such cliff-generated SP pairs (positive and negative SPs) are located at a distance from each other. Contrarily,

other SP pairs, which make up the majority of the SPs, emerge closely to each other. Such close pairs arise from the autointerference caused by the diffraction in electromagnetic-wave propagation including the local permittivity fluctuation effect related to moisture vapor density in the air and other effects. We call the former the global SPs, while we do the latter the local SPs. [C1506]

### "SWIM: A state of the art multi-incidence beams Ku-band waves scatterometer to go beyond current radar systems"

The instrument SWIM (Surface Waves Investigation and Monitoring) on the CFOSAT program (Chinese French Oceanographic Satellite) is a state of the art radar for several reasons. At first, SWIM is the first ever space radar concept that is mainly dedicated to the measurement of ocean waves directional spectra and surface wind velocities through multi-azimuth multi-incidence observations. Orbiting on a 500 km sun-synchronous orbit, its multiple Ku-band (13, 575 GHz) beams illuminating from nadir to  $10\Gamma, B^\circ$  incidence and scanning the whole azimuth angles ( $0-360\Gamma, B^\circ$ ) provide with a 180 km wide swath and a quasi global coverage of the world between  $-80$  and  $80\Gamma, B^\circ$ . Secondly, such a wide range of observations requiring high range resolution (about 20 m on the ground) have led to design an instrument whose architecture and technology goes beyond what has been done on altimeter and scatterometer systems. The global coverage and the reduction of telemetry budgets have required to perform onboard range compression. The variety of signals at different incidences, the impact of the complex moving geometry of observation and the required real-time signal processing have led to propose onboard complete digital range compression on backscattered 320 MHz bandwidth signals. Finally, multi-azimuth multi-incidence observations requirements have led to design a complex antenna subsystem that rotates at 6 rounds per minute while transmitting high power RF signals towards tunable directions. [C1507]

### "Atmospheric water vapor effects on spaceborne interferometric SAR imaging: Comparison with ground-based measurements and meteorological model simulations at different scales"

Spaceborne Interferometric Synthetic Aperture Radar (InSAR) is a well established technique useful in many land applications, such as monitoring tectonic movements and landslides or extracting digital elevation models. One of its major limitations is the atmospheric variability, and in particular the high water vapor spatial and temporal variability, which introduces an unknown delay in the signal propagation. On the other hand, these effects might be exploited, so as InSAR could become a tool for highresolution water vapor mapping. This paper describes the approach and some preliminary results achieved in the framework of an ESA funded project devoted to the mitigation of the water vapor effects in InSAR applications. Although very preliminary, the acquired experimental data and their comparison give a first idea of what can be done to gather valuable information on water vapor, which play a fundamental role in weather prediction and radio propagation studies. [C1508]

### "Boreal forest height estimation with SAR interferometry and laser measurements"

In this paper we summarize the results of FINSAR campaign, which was arranged to evaluate X- and L-band SAR interferometric and polarimetric SAR techniques for Boreal forest. The main emphasis of the work was on L-band polarimetric interferometry and forest height estimation. Also X-band interferometry and coherence tomography for X- and L-band, phase center height, extinction coefficient of forest and several other aspects of polarimetric interferometry were studied with help of ancillary measurements. Our results show that L-band polarimetric SAR interferometry can estimate well Boreal forest height. Also X-band interferometry shows good potential in height estimation. When accurate ground model is available, tree height can be estimated even by using one polarization interferometry. SAR appears to be more accurate in forest height measurement than forest inventory database, but not as accurate as laser measurement. [C1509]

### "A novel STAP algorithm using sparse recovery technique"

A novel STAP algorithm based on sparse recovery technique, called CS-STAP, were presented. Instead of using conventional maximum likelihood estimation of covariance matrix, our method utilizes the echo statistics on spatial-temporal plane, which is extracted from sample data of only ONE training range cell with Compressed Sensing techniques, to construct a new estimator of covariance matrix, and build the optimal detector based on it. Full description of CS-STAP is given. Numerical result on real data has provided the evidence for great potential of CS-STAP as a effective approach when clutter is non-stationary because it need much less training data compared with common STAP methods. [C1510]

### "A linear Kalman filter approach for estimation of a vehicle's motion parameters using range-Doppler tracking and road information"

For the processing of ISAR images of curving vehicles, the accurate knowledge of the target position as well as the aspect angle rate is essential. Especially when the targets are non-cooperative, there are no measurements like GPS positions available. This paper presents a Kalman filter based algorithm which fuses radar measurements of distance and velocity in line of sight with road information. The result is a set of parameters containing target position, velocity and acceleration, each in Cartesian coordinates. The aspect angle can then be obtained by calculating the angle between target velocity vector and the slant range vector. [C1511]

#### "GRLT detection of moving target by along track SAR interferometric systems"

In this paper we consider the problem of the detection of a ground moving target using Synthetic Aperture Radar Along Track Interferometric (AT- InSAR) systems. We propose a method exploiting a Generalized Likelihood Ratio Test (GRLT) and based on a Gaussian model for the target response. We also derive the log-likelihood ratio probability density function in closed form, both in the hypothesis of presence of target and absence of target. Numerical results based on simulated data are presented. [C1512]

#### "NDSA measurements between two LEO satellites in Ku and K bands for the tropospheric water vapor estimate: Performance evaluation at global scale"

In this work we present a software simulator for the performance evaluation of the NDSA (Normalized Differential Spectral Absorption) method at global scale assuming a realistic satellite orbital plane with two counter rotating satellite. The software tool processes atmospheric vertical profiles (pressure, temperature, water and liquid contents). The software simulator accounts for the main disturbance effects: scintillation impairments, thermal noise at the receiver and defocusing. The microwave propagation in atmosphere is simulated by means of the MPM93 model. Performance results about NDSA measurements at global scale for a single day at 17.25 and 20.20 GHZ are presented and discussed. [C1513]

#### "Rough thin pavement thickness estimation by GPR"

In civil engineering, usually the methods used to estimate the thickness of thin pavements consider flat interfaces for simplification. In this paper, the roughness of the surfaces is taken into account. First, the amplitudes of the first two echoes from the rough thin pavement are calculated from a rigorous electromagnetic method, the PILE method. A comparison is then made with the flat interface case, and their differences in the electromagnetic backscattering are highlighted. Eventually, the influence of the pavement roughness on the pavement thickness estimation is investigated by using the Maximum Likelihood Method. [C1514]

#### "Processing multiple SAR modes with baseband azimuth scaling"

This paper presents an efficient phase preserving processor for the focusing of data acquired in sliding spotlight, TOPS (Terrain Observation by Progressive Scans) and ScanSAR imaging modes. They share in common a linear variation of the Doppler centroid along the azimuth dimension, which is due to a steering of the antenna (either mechanically or electronically) throughout the data take for the first two modes, and due to the burst mode in the ScanSAR case. Existing approaches for the azimuth processing can become inefficient due to the additional processing to overcome the folding in the focused domain. In this paper an azimuth scaling approach is presented to perform the azimuth processing, whose kernel is the same for all three modes. Data acquired by TerraSAR-X in sliding spotlight, TOPS and ScanSAR modes are used to validate the developed algorithm. [C1515]

#### "Directional wave spectrum estimation by SWIM instrument on CFOSAT"

SWIM is a Ku-band radar designed for wave directional spectrum estimation. This radar operates at six incidence angles (from  $0^\circ$  to  $10^\circ$ ) with a complete azimuth scanning. SWIM is currently in Phase B (concept and design phase). In the preliminary design and associated performance analysis have been published taking into account the end of Phase A design. This paper is focused on the performance assessment of the SWIM instrument based on the new developments which occur during Phase B. In addition, major reviews have been carried out on the performance analysis. [C1516]

#### "Forest biomass retrieval from lidar and radar"

The use of lidar and radar instruments to measure forest structure attributes such as height and biomass are being considered for future Earth Observation satellite missions. Combined use of lidar sampling data and complete global coverage of L-band SAR data for vegetation 3D structure mapping requires some new data processing and fusion technologies. In this study, the potential information on biomass from a lidar waveform and the required lidar samples for reliable biomass estimation were investigated using both model and real data.

First, the Laser Vegetation Imaging Sensor (LVIS) data was used to generate an above-ground biomass map of the study site. The map was considered to represent the true biomass of the area. Then random samples were taken from the biomass image and the correlation between biomass and co-located SAR signature was studied. The proper model was used to extend the biomass from lidar samples into all forested areas in the study area. The new biomass map was compared with the original biomass map derived from LVIS data. The results showed the potential of the combined use of lidar samples and radar imagery for forest biomass mapping.

[C1517]

#### "Forest parameter mapping based on lidar and SAR data"

Vegetation spatial structure including plant height, biomass, vertical and horizontal heterogeneity, is an important factor influencing the exchanges of matter and energy between the landscape and atmosphere, and the biodiversity of ecosystems. Estimation of boreal forest canopy height is an extremely urgent research because it is essential for understanding ecosystems changing by human activities and climate change. Data from lidar and radar contain information relevant to different aspects of the biophysical properties of the vegetation canopy. GLAS (Geoscience Laser Altimeter System) and ALOS PALSAR data were used to test the combined use of lidar samplings and radar images for canopy height and stand biomass mapping in our test area. The result showed that maximum tree height and biomass in gLAS footprints can be predicted by GLAS waveform data. By using these sampling data parameters retrieval models using SAR data only can be developed. These models were applied to the entire SAR image, and the results were assessed using large-scale forest inventory data.

[C1518]

#### "An operational algorithm for snow cover mapping in hydrological applications"

An operational algorithm to produce snow cover maps from remote sensing data in the Italian Alps has been implemented in the framework of the Italian national project PROSA to contribute timely information to civil protection from floods and landslides. The algorithm can generate maps in presence of cloud cover by combining optical data from MODIS and SAR data from ENVISAT/ASAR. It has been validated on a wide area in North Italy by comparing the algorithm output with ground measurements. [C1519]

#### "A web application with visual SAR processor for education"

In this paper, a web application with a visual SAR processor is proposed in consideration of educational use and computer system environment. A system structure of the web application employs Ajax technology and object oriented software components. The main window of a client computer consists of view area, scene selection tab, tool panel, vertical and horizontal scroll bars. The processor can generate intermediate complex and map-projected images from raw SAR data using the range-Doppler method. An example of the educational use is demonstrated by compositing orthorectified images generated from a pair of ALOS PALSAR data observed by ascending and descending orbits. [C1520]

#### "GSOC's Scatterometry GNSS receiver for ocean remote sensing: Design and initial results"

The department of Space Flight Technology at the DLR's German Space Operations Center (GSOC) is currently developing a new Reflectometry/Scatterometry GNSS receiver for ocean remote sensing. This new instrument is being designed to be used in several conditions ranging from terrestrial applications to spaceborne GNSS experiments. One of its key features is the ability to compute at different scales a Delay Doppler Map (through time multiplexing the Doppler space) on one reflection event at a time using a 3ГfB—3 fully digitally steerable antenna array. Another feature is to perform digital beamforming of the incoming downconverted digitized GPS signal after IF carrier and C/A demodulation. This significantly reduces the technical requirements and costs of the analog RF front-end chain and the computation bandwidth at the FPGA respectively. A prototype version of this Scatterometry GNSS receiver is being developed as a proof of concept, using the Namuru II board as development platform. [C1521]

#### "ALOS-PALSAR polarimetric SAR data to observe sea oil slicks"

In this study an electromagnetic approach is proposed for exploiting polarimetric information for sea oil slick observation in L-band ALOS PALSAR full polarimetric SAR data. The problem is tackled from an electromagnetic viewpoint by describing the sea surface scattering mechanism with and without oil slicks. Following this rationale, a filtering technique, based on the Mueller scattering matrix, is applied to detect oil slicks in full polarimetric SAR data. Successively, the filtering results are verified by the analysis of the slick-free and slick-covered pedestal height and polarimetric entropy (H). Experiments, accomplished on a meaningful set of Level 1.1 L-Band ALOS PALSAR full polarimetric data, demonstrate the effectiveness of the proposed approach. [C1522]

### "Data processing frame for airborne SAR prototype development"

Since 1993 The National Institute of Aerospace Technology (INTA) has been working on the Synthetic Aperture Radar (SAR) program based on airborne SAR prototypes with increasing complexity development. In this frame, flexible data processing tools are needed as ground support, to allow the complete prototypes operation. This paper outlines the data processing framework of Radar laboratory. High level SAR processing environment is described. Different tasks and developments built in SAR data processing are introduced in several tools (data take campaigns design, performance assessment estimation, system configuration, product generation and data analysis). This group of tools performs the data processing core for the INTA SAR prototypes. New processing tools to cover specific needs for the new SAR prototypes developments in this laboratory are also introduced.

[C1523]

### "Antenna pointing measurement for spaceborne SAR based on sign-MLCC algorithm"

Dual-antenna single-pass synthetic aperture radar interferometry needs alignment of both antenna beams to achieve the best interferometric performance. Meanwhile, geosynchronous synthetic aperture radar, potentially used for global earthquake prediction and many other attractive applications, also requires antenna pointing control system to steer the radar antenna to illuminate desired territory, otherwise, even slight deviation from ideally boresight direction can cause a great variation of footprint position, because of the large slant range from the radar to mapped area. In principle, it is possible to measure antenna pointing information directly; however, measurement uncertainties will limit the accuracy. Thus it is feasible to resort to received radar data to measure the antenna pointing. This paper concentrates on the antenna pointing measurement using onboard Doppler centroid estimator, and furthermore, to drive pitch and yaw angles to steer the antenna pointing. In order to realize real-time onboard processing, a novel Doppler centroid estimation algorithm, called sign-MLCC, is presented here, utilizing the phase information of the received signal and the arcsine law by analyzing the sign alone, then evaluation of the algorithm is discussed. Finally, simulations are shown to prove the validity and reliability of the proposed method. [C1524]

### "Flood disaster monitoring with ALOS/PALSAR observation"

We investigate an effective algorithm to identify flood-inundated area with ALOS/PALSAR observations. Radar cross section from water surface is generally smaller than that from ground surface without water, which derives larger differences of radar cross section in flood-inundated area because there is no water in this area before disaster. Variances of differences in  $3\sigma_{\text{dB}} - 3$  pixels are also enough to identify flood-inundated area, and more effective algorithm to identify flood-inundated area will be obtained by taking radar cross section differences and variances of differences into account. [C1525]

### "Automatic target recognition of aircraft models based on ISAR images"

In this paper, we present a system for aircraft automatic target recognition (ATR) using inverse synthetic aperture radar (ISAR) and based on knowledge discovery from data process adapted to radar domain. We propose a method for target shape extraction from ISAR images based on the combination of two methods, SUSAN modified and active deformable contours via level set. In the second part of this work, we propose to fuse two commonly used shape descriptors algorithms based on moments invariant and Fourier descriptors. We have investigated the impact of the information fusion on the recognition rate. The classification scheme is ensured using support vector machine (SVM) classifier. Several combination strategies are compared at score/decision/feature level. Experimental results of the proposed method are provided and discussed. [C1526]

### "A first validation experiment for a Multi-Chromatic Analysis (MCA) of SAR data starting from SLC images"

The Multi-Chromatic Analysis uses interferometric pairs of SAR images processed at range sub-bands and explores the phase trend of each pixel as a function of the different central carrier frequencies to perform absolute topographic measurements. The previous work on the subject has started demonstrating the practical feasibility of the technique by using a set of SAR data collected by the airborne AES-1 radar-interferometer and by focusing the sensor raw data. The present work verifies the reliability of MCA procedures starting from SLC images, tests the robustness of MCA methods with respect to the total processed bandwidth and, provides first indications on the use of TerraSAR-X satellite data. [C1527]

### "Near real time oil spill detection and monitoring using satellite optical data"

Timely detection and continuously updated information are fundamental in reducing the ecological impact of the different sources of sea pollution. Satellite remote sensing, especially from meteorological platforms having a

high temporal resolution and an easy data delivery, can be profitably used for a near real time sea monitoring. Recently, a new methodology for oil spill detection and monitoring, based on the general Robust Satellite Technique (RST) approach, has been proposed. This technique has shown, by using AVHRR Thermal Infrared (TIR) data, a good capability in automatically detect, with high level of reliability, oil spill presence. In this paper, such an approach has been exported for the first time to MODIS TIR data. Preliminary results obtained for an oil spill event occurred during Lebanon war in 2006, are shown and discussed. [C1528]

#### **"Comparison with L-, C-, and X-band real SAR images and simulation SAR images of spilled oil on sea surface"**

In recent years, the oil spill detection over sea surface and similar oil material filtration are attracting much attention from the ecological point of view, and synthetic aperture radar (SAR) is considered as an effective way of monitoring such phenomenon due to the day-and-night and all weather observation capability. In this paper, results of the oil slick detection experiment by multi-frequency space borne SARs are reported. On December 7, 2007, an oil tanker was wrecked in the Yellow Sea off the Korean west coast, spilling over 12, 000 tons of crude oil, and causing considerable damage on the coastal environment. In order to analyze the impact of the oil spill, we acquired 4 sets of multi-frequency spaceborne SAR images, including TerraSAR-X X-band data, ENVISAT ASAR and RADARSAT-1 C-band data, and ALOS-PALSAR L-band data. We also computed, as a preliminary study, the backscatter radar cross section (RCS) based on the physical optics model at three microwave frequencies for different wave damping ratios by oil slick. In this paper, we describe the present status of the study on oil slick detection, and suggest the possible future direction to be taken. [C1529]

#### **"Automated information extraction from high resolution SAR images: TerraSAR-X interpretation applications"**

High resolution remote sensing SAR images-such as the image data acquired by the German TerraSAR-X mission-contain a variety of details that have to be extracted by automated processing in order to fully exploit and understand the image content. In particular, the interpretation of man-made structures that are typical of built-up or agricultural areas poses a number of challenges including parameterized image focusing during routine processing, careful despeckling, descriptor and feature extraction, and final classification including specific scattering and 3D effects. Therefore, we propose a set of general sequential as well as dedicated application-dependent processing steps that allow user-oriented classification of high resolution SAR images. We will also report on actual classification results and experiences. [C1530]

#### **"Speckle reduction and edge detection for TerraSAR-X single-look dual-polarization imagery"**

Preliminary work on speckle reduction and edge detection of TerraSAR-X single-look dual-polarization (HH and VV polarizations) spotlight data is reported. A speckle reduction approach is introduced based on a beta-distributed sample squared radius. The performance of the speckle reduction approach was benchmarked against the boxcar filter and assessed with respect to the degree of speckle reduction, radiometric preservation as well as image feature retention. For detecting edges in TerraSAR-X single-look dual-polarization speckled imagery, a constant false alarm rate (CFAR) detector is presented in this paper based on the Wilks' lambda. The applicability of the edge detector for TerraSAR-X single-look single-polarization intensity data is also discussed. [C1531]

#### **"Spotlight SAR processor by using extended frequency scaling"**

Frequency scaling algorithm (FSA) is generally used as a spotlight synthetic aperture radar (SAR) processor. FSA can directly process dechirped raw data. However, the plain algorithm itself is purposed for a single target because the formula of the algorithm is for a target. This paper presents a method to process a sliding spotlighted scene with FSA. Extended frequency scaling algorithm (EFSA) is used for focusing a point target in this paper. In order to get a focused scene of high quality image, effective velocity and Doppler centroid need to be very accurate for each target. Test has been done with a step steering sliding spotlight simulated raw data. [C1532]

#### **"Kernel regression-based background predicting method for target detection in SAR image"**

Target detection with SAR image is one of important research topics in remote sensing. In this paper, a kernel regression-based predicting method is proposed for target detection in SAR image. Badly speckle noise and background clutter are two main factors which make the target detection with SAR image difficult. In the proposed method, the kernel regression on local image is used to exactly predict the background interferences and make Gaussian assumption in conventional detector better followed after kernel regression-based prediction

and suppression of background clutter. Thus, final CFAR detection is performed on the background clutter-removed SAR image. Experiments conducted on real SAR image show that the proposed algorithm can effectively predict and suppress background clutters, and greatly improve the performance of the conventional CFAR detector. [C1533]

### "PSLR estimation considering clutter background from SAR image data"

Synthetic aperture radar (SAR) image performance can be quantified by the impulse response function (IRF) resulting from a ground reference-point scatterer. Since the level of clutter background surrounding the point scatterer affects not only the shape of the IRF but also the relative magnitude of the peak-to-sidelobe ratio (PSLR) of the IRF, the PSLR can be an important measure for SAR image quality evaluation. In this letter, a new PSLR estimation scheme for SAR image quantification is presented by taking into account the various groups of clutter backgrounds. In order to give a realistic clutter effect in the simulation, a group of clutter data extracted from a real SAR image is individually superimposed into an ideal IRF. Then, a clutter-containing IRF is analyzed with respect to the level of PSLR affected from a various group of clutter background. As expected, simulation result shows that the average PSLR varies from 0.4 dB to 2.0 dB over the various clutter backgrounds surrounding a reference point scatterer, which is well represented by the realistic clutter background compared to the ideal PSLR. [C1534]

### "Combined metal detector and ground-penetrating radar sensor experiments in a variety of soil conditions"

Landmine detection is a hazardous operation. To reduce the human casualties during landmine detection, unmanned ground vehicles (UGV) can be used. There are many landmine detection modalities that can be used with a UGV. However, the ground-penetrating radar (GPR) and the metal detector (MD; electromagnetic induction sensor) are fast and may be the most reliable means of landmine detection. In addition, GPR and MD sensors can easily be packaged in one sensor head. It is also easy to configure the sensor heads in an array. To combine GPR and MD sensor data, a series of experiments has been performed. The GPR and MD combined sensor is scanned over a 2 m ГfB— 2 m ГfB— 1 m soil box at a constant height. The soil box contains stony sand and a landmine, which is buried at 200 mm depth when measured from the surface of the ground to the top of the landmine. The control parameters for the experiments are sensor height and soil moisture. The sensor height is varied from 40 mm to 100 mm with 20 mm increment from the soil. The soil moisture conditions considered in the experiments are dry and wet. The stony sand used in the experiments contains rocks with approximately 100 mm diameter scattered in a random manner and a brick placed 200 mm apart horizontally from the landmine. The GPR and MD responses are recorded for all control parameter combinations and later analyzed. The GPR images are generated using time-domain back projection (TDBP) algorithm. The GPR images and MD responses are compared for the soil conditions and sensor heights. A combination algorithm, which enhances GPR images using MD responses, is also presented. [C1535]

### "Calibration of the high performance airborne SAR system (Pi-SAR2)"

NICT (National Institute of Information and Communications Technology, Japan) have developed a high performance airborne SAR system (Pi-SAR2) since 2006, as a successor to the Pi-SAR (X-band). Pi-SAR2 has polarimetric and interferometric functions with high spatial resolution of 0.3-0.6 m in along track (azimuth) direction and 0.3-0.5 m in cross track (slant-range) direction at X-band. In this paper we report the ground based calibration experiment using active radar calibrators (ARC) and corner reflectors (CR) in conjunction with the Pi-SAR2 test flight. [C1536]

### "Transpolarizing trihedral measurement using UPC X-band GB-SAR"

The use of a transpolarizing surface placed on one side of a trihedral corner reflector (TCR) as polarimetric calibrator is presented in this paper. The transpolarizing-TCR presents a high back-scattered cross-polar response. This structure has been tested at 9.65 GHz (X-band) with the help of the UPC GB-SAR system. [C1537]

### "Accuracy assessment of the first high-resolution IFSAR campaign over the coorong region of South Australia"

This paper discusses the vertical accuracy assessment of a high resolution digital elevation model and associated orthorectified radar imagery Apogee and Intermap Technologies are collecting in the Murray-Darling Basin region of Australia. This dataset will form the geospatial foundation upon which further remote sensing and field survey information resides forming a single uniform dataset which is consistent over large areas. A new

highly accurate geoid will also be generated to ensure the accuracy and consistency of the data. [C1538]

#### "SAR raw signal simulation based on GPU parallel computation"

In this paper we present a raw signal simulator based on GPU parallel computation for synthetic aperture radar. We describe a mathematical model of SAR simulation based on FFT in detail and implement it through GPU parallel computation. GPU has a better performance in complex calculation than CPU. It supports parallel computation and raises the speed of algorithms. At the last part of this paper, a simulation comparison is given. The result shows that the simulator base on GPU parallel computation improves the efficiency of algorithm. It is very useful when the algorithm consumes large amount of CPU time. [C1539]

#### "SAR target recognition based on sub-block statistical features extracted from the Gabor filtered image"

A method for SAR target recognition using low-frequency sub-band and Gabor filter sub-block statistical feature is proposed. The sub-band image extracted from the pre-processed SAR image is filtered by Gabor filter on different directions and scales. The each filtered sub-band image is divided into different sub-blocks and the statistical features derived from every sub-block of all filtered sub-band images are regarded as the target recognition feature, which can be used to recognize the targets with SVM. The proposed method is validated on MSTAR dataset for 3-type SAR target recognition. [C1540]

#### "An imaging method and the correction of distortion for Spaceborne-airborne bistatic SAR"

Because of the great speed difference between the transmitter and the receiver of the spaceborne/airborne bistatic SAR (SA-BiSAR), the bistatic angle changes with time, which makes the geometric structure of the SAR system no longer invariant, and the imaging result distort seriously and dissimilarly. In order to solve this problem the geometric model of the SA-BiSAR is established in this paper at first. Then based on the analysis to cause the image distortion, a correction method for bistatic SAR distortion named Inverse-Projection is brought up. The simulation results demonstrate that this method can work well for spaceborne/airborne configuration. [C1541]

#### "Anti-jamming techniques for synthetic aperture radar"

Excellent performance of SAR has aroused deep study of jamming techniques. This paper first discusses present jamming techniques and their shortcomings, then gives methodology of classifying ECCM of SAR, and at the same time, gives principle and results of signal design method, which combines orthogonal codes and random initial phase at each pulse, the method leads to disability of jamming to finish match filtering of both range and azimuth. Finally this paper points out that beamforming technique is a potential method for the future of ECCM of SAR. [C1542]

#### "The effects of multi-path scattering on the SAR image of cylinder cavity"

In this paper, the effects of multi-path scattering mechanisms on SAR image is deduced through range Doppler algorithms (RDA). The conclusion that the cloud phenomenon appeared due to the multi-path scattering mechanisms is detained. Through the analysis, the cloud caused by the multi-path in the down range is corresponding to focus mechanisms and the cloud appeared azimuth is non-focus. At last, the shooting and bouncing ray (SBR) technique is employed to calculate the scattering of the cylinder cavity and by combining with range Doppler algorithms (RDA), the SAR image of a cylinder cavity with underside closed is precisely given, considering the effects of the multi-path scattering mechanisms in different azimuth. [C1543]

#### "SAR raw singal simulation accounting for antenna attitude variations"

An efficient SAR raw signal simulator accounting for antenna attitude variations is presented here, based on the 2-dimensional Fourier domain formulation of SAR raw signal in presence of antenna beam pointing errors. It can meet the requirements of InSAR system simulation to deal with the extended scenes. The validity limit is analyzed to show that this algorithm is suit for the simulation of practical systems. [C1544]

#### "Sea-clutter analysis at multiple wavelengths (L, C, X) for target-clutter contrast assessment in littoral waters"

This study is aimed at quantifying the statistics and nature of sea-clutter as seen from spaceborne platforms and assessing the target-clutter contrast in the Adelaide harbor area of South Australia. To this end a series of images in mixture of polarizations were collected over this area in typical wide area surveillance mode-ScanSAR single polarization images from TerraSAR-X, Dual-Polarization Wide Beam images from RadarSAT-2 and Full

and Dual Polarization images from ALOS-PALSAR. Synchronized with the acquisitions (dawn/dusk orbit of SAR satellites) video over flights with a low light camera were performed to record the sea-state. AIS data was collected for the information on the large vessels and meteorological buoy readings for surface wind, wave height and swell were noted. [C1545]

#### "RADARSAT-1 deformation time-series analysis based on the SBAS-DInSAR algorithm"

We extend the Small Baseline Subset (SBAS) algorithm to generate deformation time-series from SAR data acquired by the Canadian Space Agency (CSA) RADARSAT-1 sensor. The proposed approach is mostly oriented to the investigation of large scale deformation events with relatively low spatial resolutions (of about 100 ГрВ— 100 m), and is based on the use of conventional multi-look interferograms with small temporal and spatial baseline separations. With respect to the original SBAS approach, several improvements are required to take into account the inaccuracies on the knowledge of the RADARSAT-1 orbital parameters, and of the significant fluctuations of the dop-pler centroid values over each single SAR scene. This work is aimed to present the first results achieved by applying the implemented RADARSAT-1 SBAS processing chain to an archive of SAR scenes, acquired in the time interval from 2000 to 2003 over, and relevant to the Hawaii Island area. The presented results markedly confirm the effectiveness of the implemented RADARSAT-1 SBAS processing chain. [C1546]

#### "Comparison of precipitation effects in space-borne X- and Ka-band SAR imaging"

As the operating frequencies of SAR-systems are increasing, the visible distortions due to precipitation in SAR-images are becoming more frequent. This holds especially for the case of convective rain events. The German space-borne satellite TerraSAR-X has delivered a series of measurement examples, which were used to study precipitation effects in SAR-images. Based on these valuable data takes and simultaneous weather radar measurements, a quantitative estimation of precipitation effects in SAR-images is presented. In a further step, an attempt is made to extrapolate the observed effects to systems operating at higher nominal frequency-bands, i.e. Ka-band, being taken under consideration for future SAR-systems. [C1547]

#### "Modelling and analysis of rain effect on Ka-band single pass InSAR Performance"

The adoption of Ka-band for performing SAR interferometry is considered very promising since it could provide the possibility to embark the full instrument within a single satellite. However, one of the major concerns of the effectiveness of spaceborne Ka-band radars is the impact of the atmosphere, and, in particular of precipitation on the instrument performance and availability. This paper analyzes the impact of precipitation on the performance of Ka-band across-track InSAR. In order to assess the rain impact on the InSAR random height error, the paper proposes an extended form of the interferogram coherence. The paper shows that, for the reference instrument configuration investigated, a random height error compatible with HRTI-3 specification can be met under moderate rain condition. [C1548]

#### "Airborne D-InSAR at X-band: Results with the complete repeat-pass processing methodology"

This paper presents the interferometric airborne repeat-pass mode results at X-band after applying a complete residual motion compensation (MoCo) strategy. The data were acquired, over the Perugia area, Italy, by the OrbiSAR sensor from OrbiSat, Brazil, and the first X-Band D-InSAR results were published, where a space-invariant topography-dependent MoCo was applied after focusing with smoothed elevation model. Now, in this paper, we apply to the same X-band data the precise topography- and aperture-dependent (PTA) MoCo and the weighted phase curvature autofocus (WPCA) to account for high-order residual motion errors. We compare the differential interferograms and coherence map obtained after PTA-WPCA to the formerly results. The results show improvement in the interferometric accuracy after PTA-WPCA processing. The need of such complete processing chain for narrowband systems is discussed. [C1549]

#### "SAR tomography from sparse samples"

Three dimensional (3-D) Synthetic Aperture Radar (SAR) image formation provides the scene reflectivity estimation along azimuth, range and elevation co-ordinates. For 3-D image focusing multiple signals, acquired along different orbits, are required. The practical application of the focusing methods requires that non-uniformly spaced acquisition orbits have to be considered. In this paper we propose a technique exploiting the Compressive Sampling theory, and assuming that the image to be focused has a sparse representation along the elevation directions, which amounts to suppose that only few point-like scatterers with different elevation are present in the same range-azimuth resolution cell. Numerical results on simulated data show the good performance of the method. [C1550]

### "Space-borne high resolution tomographic interferometry"

SAR tomography (TomoSAR) is a way of overcoming the limitations of standard 2-D imaging by achieving focused 3D images. Its capability of 3-D reflectivity reconstruction and multiple scatterers separation has been demonstrated in the urban environment in absence of significant deformation. In this paper, an example which reveals the distortion of 3-D reconstruction result by coupled deformation information is presented. Differential SAR Tomography (or 4-D SAR focusing), a new interferometric mode crossing differential SAR interferometry and the 3-D multi-baseline tomography concepts, are implemented. In this paper, space-borne high resolution differential SAR tomography is demonstrated using TerraSAR-X high resolution spotlight data. High resolution SAR is proven to be very attractive for city mapping. [C1551]

### "Fusion of multisource data sets from agricultural areas for improved land cover classification"

An approach for spectral-spatial classification of multisource remote sensing data from agricultural areas is addressed. Mathematical morphology is used to derive the spatial information from the data sets. The different data sources (i.e., SAR and multispectral) are classified by support vector machines (SVM). Afterwards, the SVM outputs are transferred to probability measurements. These probability values are combined by different fusion strategies, to derive the final classification result. Comparing the results based on mathematical morphology the total accuracy increased by 6% compared to the pure-pixel classification results. Moreover the transfer of the SVM outputs into probability values and the subsequent fusion further increases the classification accuracy, resulting in an accuracy of 78.5%. [C1552]

### "Fusion of high resolution optical and SAR images with vector data bases for change detection"

This paper addresses the issue of cartographic database creation or update using high resolution SAR and optical images. In cartographic applications, objects of interest are mainly buildings and roads. This paper proposes a processing chain to update building databases. The approach is composed of two steps. First, the presence of each database object is checked in the images. Then, we verify if objects coming from an image segmentation should be added in the database. To do those two steps, features are extracted from images in the neighborhood of the considered object. The object removal/inclusion in the database is based on a score obtained by the fusion of features in the framework of Dempster Shafer evidence theory. [C1553]

### "High resolution mapping of soil moisture by SAR: Data integration and exploitation of prior information"

Two different approaches to deal with the problem of estimating soil moisture content from SAR data in the presence of vegetation are presented. They exploit also the information about the biomass provided by ancillary optical data. The first method is suitable for sparse vegetation and is founded on the application of the well-known water cloud model. As for dense vegetation canopy, we have designed a model that expresses the variation of the component of the backscattering coefficient due to the soil characteristics as a function of the variations of the measured backscattering coefficient and of the biomass, assuming the availability of a time series of radar and optical data. To carry out the soil moisture retrieval, a multi-temporal inversion algorithm, based on the Bayesian MAP criterion, has been developed. It integrates all the samples of the time series of SAR data corrected for the vegetation effects. The approaches were evaluated on two case studies; the first one concerning an ENVISAT/ASAR observation of an agricultural site located in Northern Italy. The second test was performed on the AirSAR data collected during the SMEX02 experiment. The comparison between the estimated soil moisture contents and the in situ measurements has given encouraging results. [C1554]

### "Use of radar images for the development of a propagation oriented space-time rain model"

The propagation of electromagnetic waves through the atmosphere at frequencies above 10 GHz is strongly influenced by oxygen, water vapor, clouds and, even more heavily, by rain. The scarcity of worldwide reliable rainfall data has pushed towards the development of models that could adequately reproduce real rain fields. This contribution presents the analysis of some spatial and temporal characteristics of rain cells for rainfall modeling purposes, based on an extensive database of weather radar images. The results obtained in this study are of key importance in the development of advanced cellular space-time rainfall models. [C1555]

### "Toward a GUI remote sensing environment built over OTB"

The need for fast and reliable remote sensing algorithms is continuously growing. Remote sensing libraries are scarce and sometimes are difficult to use. The Orfeo Toolbox (OTB) is one such library that stands apart with its robust development scheme and programming concepts. Not all remote sensing researchers have a strong programming background. Programmers need to find ways of giving easier access to desired algorithms without

the need of cumbersome programming overhead. This paper compares the actual parameter management class of OTB with a proposed dynamic graphical interface to replace it. The programming concepts used will first be presented. This work will lead to creating a visual programming environment for OTB. [C1556]

### "Overview of the PolSARpro V4.0 software. the open source toolbox for polarimetric and interferometric polarimetric SAR data processing"

The objective of this paper is to make a review of the current status of the PolSARpro v4.0 Software (Polarimetric SAR Data Processing and Educational Toolbox), developed under contract to ESA by a consortium comprising I.E.T.R at the University of Rennes 1, AELc, DLR-HR and Dr mark Williams from Adelaide. The objective of this current project is to provide Educational Software that offers a tool for self-education in the field of Polarimetric SAR data analysis at University level and a comprehensive suite of functions for the scientific exploitation of fully and partially polarimetric multi-data sets and the development of applications for such data. The PolSARpro v4.0 Software establishes a foundation for the exploitation of Polarimetric techniques for scientific developments and stimulates research and applications developments using PolSAR and PolInSAR data. [C1557]

### "Multi-resolution target scattering decomposition for urban feature characterization using polarimetric SARs"

Urban areas include features (buildings) of coherent scattering as well as areas such as parks that manifest partially coherent scattering due to the significant natural variability in the scattering properties. While high-resolution coherent target decomposition (CTD) can be used for characterization of buildings, incoherent target scattering decomposition (ICTD) is more suitable for analysis of partially coherent targets [11]. In contrast to CTD, ICTD preserves the polarimetric information of the latter at the expense of the requirement for use of coarse-resolution for unbiased estimation of ICTD parameters [9]. The Touzi decomposition [10], [15] permits a unified roll invariant decomposition of both coherent and partially coherent scattering. In this paper, a multi-resolution technique is introduced to adapt the Touzi decomposition to the coherence nature of target scattering. The multi-resolution mixture CTD-ICTD decomposition is validated using polarimetric Convair 580 SAR data collected over Ottawa city. Implications on the use of the new multi-resolution decomposition for the unified analysis of coherent and partially coherent target scattering are discussed. [C1558]

### "Edge-preserving classification of high-resolution remote-sensing images by Markovian data fusion"

Very high spatial resolution (HR) data provide plenty of detailed information about the ground on a regular basis for applications such as urban planning, precision farming, or damage assessment after environmental disasters. The complex nature of HR observations, especially when acquired over urban/artificial environments, makes the accurate discrimination of distinct thematic classes a difficult task. In the present paper, a novel technique is proposed for supervised classification of multispectral HR images, based on the key-idea to fuse through a Markov random field (MRF) the information conveyed by user-defined thematic classes, subclasses related to the spectral responses of different ground materials, and spatial edges. The method is validated by experiments on IKONOS images. [C1559]

### "Building detection by fusion of optical and SAR features in metric resolution data"

In this paper, we propose to jointly use optical and SAR features issued from satellite images with metric resolution, to deal with the problem of building detection and height retrieval. In a first part, a process described in previous works for building boundary extraction, is briefly exposed and illustrated on a Quickbird urban scene. In a second part, the framework of fusion with SAR data is developed. After the steps of feature projection and registration, a new method for building height estimation is proposed. This one is based on a Likelihood criterion optimization and is built on the scheme "height hypothesis characteristic areas generation energy minimization". Such an approach refers to the adequation between a potential building signature and the real signature, effectively present on the SAR image and defined by characteristic building areas such as layover, shadow, roof and ground/wall echo. This height retrieval process is tested on simulated and real (TerraSAR-X) data. [C1560]

### "General framework on change detection in a sparse domain"

The paper presents a general framework for change detection in radar images, for an operational purpose and in the context of environmental monitoring. This framework is based on a processing which provides highly sparsifiable representations of data. This processing is called turbo-median and is a combination of the sample median robustness and the turbo principle for iteratively correcting errors. The turbo-median processing of a

scene is an homogenized representation based on an iterative median and which consists in spreading the statistically more robust measurements of the scene under consideration over the size of the image representing this scene. It allows for reducing the change detection problem into the problem of detecting a signal, with unknown distribution, in additive noise. [C1561]

#### "A study of forest vertical structure estimation using coherence tomography coupled to a macro-ecological scattering model"

In this paper we combine a macro-ecology forest model with a numerical scattering code to estimate the vertical scattering profile of L-band penetration into forests. We use these simulations to show that structure has an important impact on interferometric coherence and hence on height retrievals based on single baseline polarimetric interferometry. We conclude with some suggestions for dual baseline extensions to allow for better height and structure estimation in future sensors. [C1562]

#### "Estimation of forest vertical structure parameter by means of multi-baseline Pol-InSAR"

In this paper the impact of vertical forest structure on model based Pol-InSAR forest height inversion is discussed. For different scenarios appropriate extensions of the RVoG model are proposed and possible inversion schemata are suggested and validated against experimental data and ground measurements. [C1563]

#### "The Orfeo Toolbox remote sensing image processing software"

Orfeo Toolbox, OTB, is a remote sensing image processing library developed by CNES, the French Space Agency. OTB is distributed as open source software and is therefore available for any remote sensing scientist or processing chain developer. This paper describes the main features of OTB, how it can be used and the expected evolutions in the coming months. [C1564]

#### "An evaluation of PolSAR speckle filters"

Speckle suppression in PolSAR images is an important step for the extraction of meaningful information from PolSAR images, especially for homogeneous extended targets. It has been shown that insufficient noise filtering resulting in low equivalent number of look (ENL) values will increase bias on incoherent polarimetric parameters such as the Cloude-Pottier parameters. In addition, meaningful high-frequency information, such as edges and point targets must be preserved. Adaptive filters have been the most successful in reaching a good compromise between noise suppression and detail preservation. A large set of artificial PolSAR images, which ground truth are realizations of Markov random fields, has been generated. Performance metrics are focusing on speckle suppression (ENL), edge preservation, relative errors on polarimetric parameters and point target preservation. [C1565]

#### "The effect of orientation angle compensation on polarimetric target decompositions"

The orientation angle of scattering media affects the polarimetric radar signatures. This paper investigates the effect of orientation compensation on polarimetric target decompositions including Pauli decomposition, Freeman and Durden decomposition and Yamaguchi decomposition. The Cloude and Pottier decomposition is excluded, because entropy, anisotropy and alpha angle are rotational invariant. We will show that after the orientation compensation, the volume scattering power is consistently decreased, while the double bounce power has increased. The surface scattering power is relatively unchanged, and the helicity power is rotational invariant. All these characteristics can be explained by the compensation effect on the nine elements of the coherency matrix. This analysis reveals that, contrary to the general perception, the 4-component component decomposition by Yamaguchi et al. does not use complete information of the coherency matrix. Only six quantities are included-one more than the Freeman/Durden decomposition under the assumption of reflection symmetry. [C1566]

#### "Analysis and observation of polarimetric scattering behavior in wetland area"

This paper proposes a simple monitoring technique for water area change in wetland environment based on POLSAR image analysis. From the results of the image analysis by utilizing fully or quad. polarimetric SAR data set, it is found that strong double-bounce scattering can be observed at the vicinity of the boundary region between water area and the surrounding emerged-plants area. This peculiar scattering feature is utilized as a useful marker for estimating the water area change. To verify the generating mechanism of the double-bounce scattering, the Finite-Difference Time-Domain (FDTD) polarimetric scattering analysis is also carried out for a simplified water-emergent boundary model. The dependency of the polarimetric scattering feature on the variation of the radar incident angle, the change of the biomass and material parameters of the surrounding emerged-plants is investigated. Resultantly, it is confirmed from the detailed FDTD analysis that by using the

proposed technique, one can estimate the true water area change in wetland and its surrounding area in all seasons. [C1567]

### "Integration of RADARSAT-2 ScanSAR and AWiFS for operational agricultural land use monitoring over the Canadian prairies"

Agriculture plays an important role in the global economy, and sustainability of this sector is critical for world food security. Annual information on agricultural land use (crop inventory) would permit efficient and effective delivery of agricultural programs that support sustainability of this resource. Previous research has revealed encouraging results on using space borne satellite data (Landsat, SPOT) for crop mapping at the regional scale. Given Canada's large land mass, for operational crop monitoring satellite data with a wide swath and moderate spatial resolution are needed. This study presents the results on integrating RADARSAT-2 ScanSAR data with AWiFS data to improve crop identification. This study demonstrates that multi-temporal AWiFS data can produce an adequate crop classification, with an overall accuracy of 83%. The addition of ScanSAR data increases the overall classification accuracies. The radar contribution is most pronounced during the earlier season. [C1568]

### "CSIR-NLC mobile LIDAR-first scientific result"

In this paper, we present the obtained first scientific results from CSIR-NLC mobile LIDAR (Light Detection And Ranging) and its validation/comparison with other ground and space-borne measurements. The LIDAR results are compared using aerosol measurements from the Stratosphere Aerosol Gas Experiment (SAGE) and Optical depth derived from sun-photometer employed under AEROSOL ROBOTIC NETWORK (AERONET). [C1569]

### "FullAnalyze: A Research tool for handling, processing and analyzing full-waveform lidar data"

Full-waveform (FW) lidar systems provide range profiles of the Earth topography. They are acquired from airborne platforms or from satellites. Many applications derive from the use of such data, from the extraction of 3D point clouds to the inversion of vegetation profiles. Nevertheless, handling range profiles is much more difficult than handling 3D point cloud. The aim of this paper is to present a research tool based on opensource libraries that can process and visualize such data. We focused our work on the implementation on the 2D/3D interface that gives the possibility to visualize the interaction between the lidar electromagnetic waves and the Earth topography. Moreover, this tool integrates several processing steps of FW Lidar data. [C1570]

### "SAR monitoring of suburban areas based on an electromagnetic scattering model"

Cylindrical-shape tanks are typical of any suburban area and often contain dangerous gases or fluids. In this paper, we suggest a way to monitor them by means of high resolution Synthetic Aperture Radar (SAR) images and a scattering model able to quantitatively consider how the radar signal interacts with this kind of structures and how they appear in the SAR images. Adopting the model, geometrical information as the tank height is retrieved from the SAR images in a non-conventional way that is exploiting the information content contained in the double reflection contribution to the radar cross section. Results are compared with more traditional methods and discussed. [C1571]

### "Simulation and optimization of the performance of space-borne radar ocean wave spectrometer"

In this paper, a simulation method is presented to analyze and to optimize the performance of a real aperture radar system for measuring oceanic directional wave spectra, taking into account of data processing parameters. The results show that spaceborne radar ocean wave spectrometer (SB-ROWS) can measure spectra of fully developed waves with significant wave heights (SWH) over approximately 2.0 meter and swell surface under low wind conditions. The minimum detectable wavelength in the study is about 40 m. The wavelength resolution for a wavelength of 200 m is better than 30 m, and the directional resolution after averaging is better than 20°, B°. [C1572]

### "Polarimetric analysis of the dependency of backscattering from ocean surface on wind direction"

The dependencies of the backscattering from the ocean surface on the wind direction are analyzed by using the Pi-SAR under weaker wind condition (5 m/s) than the former analysis under stronger wind as 14 m/s. In the X-band HH polarization, the dependency of the normalized cross section (NRCS) on wind direction depends on the incidence angle, differently from the former analysis. In the X-band VV polarization, the NRCS represents weak incidence angle dependency as same with the former analysis. As a result, the dependency of the polarization ratio (PR) in the X-band on the wind direction also depends on the incidence angle. In the L-band, the dependencies of the NRCS and the PR are also weak, same as the former analysis. [C1573]

### "The development of a C-band Advanced Scatterometer (ASCAT) geophysical model function at NOAA/NESDIS"

Validation of the ASCAT wind vectors show that the ASCAT wind speed errors are within 2 m/s RMS error for wind speeds up to 15 m/s, however they exhibit an increasing low bias beyond 15 m/s. An examination of the ASCAT ГБИ0 revealed some additional sensitivity at the higher wind speeds that was not adequately represented by the current geophysical model function (GMF). A revised GMF is empirically derived using a near-real-time QuikSCAT as a surface truth. A new DC term in the GMF is derived and replaced in the operational CMOD5.5 GMF. Validation of the revised GMF shows that the wind speed retrievals are closer to QuikSCAT for wind speeds > 15 m/s than the operational retrievals, while wind direction retrievals remain the same for all wind speeds as expected. [C1574]

### "Using HF surface wave radar and the ship Automatic Identification System (AIS) to monitor coastal vessels"

We compare the ship detection capabilities of the automatic identification system AIS (installed on some ships) and coastal, surface wave HF radars, showing how to use both systems together to enhance ship detection performance in coastal regions. Practical reasons to want better real-time awareness of the location, velocity and type of vessels along coasts include vessel safety, protection of the coastal environment and national security. Our model for the HF radar aspect uses an example radar with significant power and aperture, similar to the Pisces radar. The AIS model is for the high power (12.5 W) AIS unit and a significantly elevated receiver (~ 250 ft asl). The HF system shows good capability to ranges of ~ 150 km for small ships to 250 km for large ships. The AIS system shows excellent capability out to a typical horizon of ~ 50 km with irregular coverage beyond using ducted propagation to several hundred km and more. Use of both systems allows monitoring of both AIS and non-AIS equipped ships and enhances probability of detection for situations where both systems are functional. [C1575]

### "PALSAR CALVAL updated 2009 and change detections at the forest and the Polar regions"

This paper describes the updated results of the PALSAR CALVAL activity conducted for last three years using the PALSAR calibration archives and the connected ground truth data. The results show that PALSAR has pretty good stabilities on the geometric and radiometric accuracies. Using PALSAR data, change detection on the forest in Indonesia and the polar regions (North Pole region, Antarctica region, and Greenland region) are in progress tracking the change of the sigma-naught and/or the phases. [C1576]

### "First assessment of the permanent scatterer linear displacement model in airborne InSAR time series"

This paper presents the very first assessment of the permanent scatterer (PS) technique for airborne data. A data set of 14 SAR images at L-band, acquired over the Oberpfaffenhofen area on the same day with the E-SAR system of the German Aerospace Center (DLR), is used for the first airborne time series analysis with PS. The paper shows the importance of mitigating the residual motion errors through the use of precise motion compensation strategy before PS analysis. The target velocity and DEM error results are obtained by a periodogram-based estimation considering the linear displacement model. Due to the small number of images in our data set, the displacement velocity and DEM error results are presented on a PS basis. Target structures related to selected reliable PSs are shown and the corresponding periodograms highlighted. [C1577]

### "Surface manifestations of non-tidal internal waves in the north-eastern Black Sea as viewed by satellite sensors"

In present paper the satellite remote sensing data (obtained by Envisat ASAR, Terra and Aqua MODIS, and NOAA AVHRR instruments) is used to study coastal dynamics of the north-eastern Black Sea. Surface manifestations of internal wave (IW) packets were registered in ASAR images of the sea surface. Possible factors leading to the generation of non-tidal IWs are determined on the basis of joint analysis of available satellite remote sensing data of the sea surface in microwave, visual and IR ranges complemented by contact measurements. A mechanism of IW generation is suggested. The coherence between occurrence of IW surface manifestations and location of the density pycnocline layer is established. [C1578]

### "Exploiting Markov random fields in Microwave tomography"

3D microwave tomography is an ill-posed and nonlinear inverse problem whose reconstruction performances may be impaired from the complexity of the scenario to be considered in the real world applications. The joint

adoption of convenient regularization schemes and a suitable rewriting and linearization of the pertinent scattering model can allow to achieve satisfactory solutions in many cases of practical interest. In this communication, an innovative inversion approach which takes definite advantage from the joint use of the linearized contrast source-extended Born model (CS-EB), and from a Markov random field (MRF) based regularization scheme is proposed. [C1579]

### "Scale decomposition of precipitation patterns and nowcasting in a high-resolution X-band radar network"

Shortterm weather forecasting (nowcasting) performance can be improved by spatially filtering radar images of precipitation patterns and either predicting only those precipitation scales most representative of pattern motion or removing unpredictable scales after prediction. Previous research has shown that improvement in nowcasting precision can be obtained by first applying an elliptical spatial filtering procedure to observed WSR-88D Vertically Integrated Liquid water data to predict larger-scale features believed to better represent the motion of precipitation patterns. Another study used the wavelet transform to develop measures of predictability at each scale and designed adaptive wavelet filters to remove perishable scales from predicted continental-scale reflectivity data. This study investigated the adaptation of both approaches and Fourier filtering to examine the effects of scale filtering on nowcasting performance using a spectral-based nowcasting method and high-resolution Collaborative Adaptive Sensing of the Atmosphere radar reflectivity data. [C1580]

### "Uncertainty in scatterometer derived vorticity"

A more versatile and robust technique is developed for determining area averaged surface vorticity based on vector winds from swaths of remotely sensed wind vectors. This technique is discussed in detail and compared to two previous studies that focused on early development of tropical systems. The error characteristics of the technique are examined in detail. Specifically, three independent sources of error are explored: random observational error, truncation error and representation error. Observational errors are due to random errors in the wind observations, and determined as a worst-case estimate as a function of averaging spatial scale. The observational uncertainty in vorticity averaged for a roughly circular shape with a 100 km diameter, expressed as one standard deviation, is approximately  $0.5 \text{ } \Gamma/\text{s}$  for the methodology described herein. Truncation error is associated with the assumption of linear changes between wind vectors. Uncertainty related to truncation has more organization in QuikSCAT data than observational uncertainty. On 25 km and 50 km scales, the truncation errors are very large. The third type of error, representation error, is due to the size of the area being averaged. This type of error is analogous to over-smoothing. Tropical and sub-tropical low pressure systems from three months of QuikSCAT observations are used to examine truncation and representation errors. Representation error results in a bias of approximately  $1.5 \text{ } \Gamma/\text{s}$  for area averaged vorticity calculated on a 100 km scale compared to vorticity calculated on a 25 km scale. The discussion of these errors will benefit future projects of this nature as well as future satellite missions. [C1581]

### "Velocity estimation of moving targets on the sea surface by azimuth differentials of simulated-SAR image"

Since the change in Doppler centroid according to moving targets brings alteration to the phase in azimuth differential signals, one can measure the velocity of the moving targets using this. In this study, we will investigate theoretically measuring velocity of an object from azimuth differential signals by using range compressed data which is the interim outcome of treatment from the simulated Synthetic Aperture Radar (SAR) Raw data of moving targets considering sea clutter. Also, it will provide evaluation for the elements that affect the estimation error of velocity from a single SAR sensor. In the concrete, by making RADARSAT-1 simulated image, the research includes comparisons for the means of velocity measurement classified by directions of movement as in the four following cases. 1. A case in which the object that becomes the target exists independently, 2. When there is a tidal current of 1 m/s, 3. When there exists moving targets of different velocity on the azimuth, 4. When the target is contiguous to the land where it has high back scatter factor. As a result, when the object, which becomes the target, independently exists on SAR image in the range of 128 pixels, the velocity of object could be measured with high accuracy. However, when there existed other moving targets in the range of 128 pixels or when the target was contiguous to the land of high back scatter factor, the velocity was in error by 10% at the maximum. This is because in the process of assuming the target's location, an error occurred due to the disturbed signals affected by the scatterers. [C1582]

### "Weather hazard interpretation and nowcast by radar"

A method for modeling and tracking convective clouds within radar images is presented. An object modeling approach is used, based on the extraction of grayscale skeletons from 2-dimensionnal cross-section of 3-

dimensional radar data. Grayscale skeletons are appropriate shape descriptors for non-rigid and heterogeneous objects, in which gray-level local maxima correspond to regions of interest. The modeling scheme is enhanced by linking meta-data to some chosen points of the skeleton; this provides a good representation of the weather scene in terms of hazards for an aircraft. Skeletons are stored within a graph structure and tracked among successive pictures by means of relaxation labeling processes. The deduced advection field is used to nowcast the clouds evolution. Preliminary results are satisfying concerning advection forecast. [C1583]

#### "Observing littoral waves by Doppler radar"

The offshore observation of the wavefield with coherent radar systems consist a common practice for the study of the electromagnetic waves probing the sea surface waves and for the extraction of information of the sea waves. In this investigation, a Dopplerized, horizontally polarized, nautical radar is utilized for the monitoring of the wavefield evolution in the littoral zone. The radar datasets are globally unique and cover different geophysical conditions; therefore the impact of the bathymetry on the Doppler spectra is discussed, the horizontal velocity towards the shore is calculated and the properties of the radar deduced quantities are compared with in situ measurements. [C1584]

#### "Comparison of Gaussian and Rayleigh noise models in inversion of subsurface parameters of layered rough surfaces using simulated annealing"

This work addresses the noise sensitivity of the simulated annealing method in inversion of subsurface parameters of layered rough surfaces to measurement noise. We consider two different noise models and assess the noise response of the inversion algorithm for each of the models. Conclusions are made based on the calculated average and standard deviation of the output error in the retrieved model parameters. [C1585]

#### "Target tracking enhancement using a Kalman filter in the presence of interference"

In this paper we present a new target tracking enhancement system that uses a Kalman filter in the presence of interference. If the radar (seeker) is affected by different types of interference, this will affect the missile trajectory towards the target and may cause inaccurate tracking. In the new system a six-state Kalman filter is utilized to perform the tracking task and to carry out smoothing to the corrupted trajectory. This also provides good information about the target velocity in three dimensions which is very important information about the target. A three dimensional scenario between target (with high manoeuvre) and missile is used to illustrate the performance of the system in the case when (i) no interference is present and (ii) interference is present. The performance of the filtered trajectory using the Kalman tracker will be assessed for different guidance methods: including (i) proportional navigation (ii) pure pursuit and (iii) constant bearing. The Kalman improvement for the tacking for the three guidance method will be analysed. [C1586]

#### "Classification of a reference image using auxiliary images"

This work does an extension of the Maximum A Posteriori (MAP) multidimensional image classification for the case that each image in a set of images can have different number of predominant classes. These different classes can be related to the sensor characteristics, which can detect different aspects of the same scene. In the proposed classification processes one image of the image set is choose as the reference image to be classified and the others images are considered complementary information. Simulations of two SAR amplitude images are used to evaluate the classification method. [C1587]

#### "Airborne radar depth sounding of fast flowing glaciers"

Sea-level rise will affect populations worldwide with considerable and lasting consequences in the not-too-distant future. Accurate measurement of fast flowing outlet glaciers in Greenland and Antarctica are of vital importance to ice sheet models that predict the course of sea-level rise. The Center for the Remote Sensing of Ice Sheets (CReSIS) has developed a suite of tools designed for use with data collected by CReSIS depth sounding radar platforms. This suite includes algorithms for removing clutter and noise from coherent radar data, and the results show successful sounding of some of these fast-flowing glaciers for the first time. [C1588]

#### "Accuracy improvement of maximum likelihood inversion of forest height with PolInSAR"

Polarimetric synthetic aperture radar interferometry (PolInSAR) technique has been intensively used for extracting forest heights. Among the forest height inversion algorithms, maximum-likelihood estimate computes the maximum-likelihood estimate of the vegetation parameters based directly on the sample coherency matrix. The estimation of the sample coherency matrix is of great importance in this inversion process. A coherency matrix estimation method with adaptive averaging window derived from coherence region shape parameters is

presented. Then the estimated coherency matrices are applied in the maximum likelihood inversion algorithm. In order to confirm the validity of the proposed method, simulated L-band PolInSAR data provided by ESA is used. Experiment results suggest that this method can help improve the accuracy of maximum likelihood inversion of forest heights. [C1589]

#### "Use of neural networks and SAR interferometry for the automatic retrieval of tectonic parameters"

The basic idea of this paper relies on the concurrent exploitation of the capabilities of neural networks and SAR interferometry for the characterization of a seismic source and the estimation of its geometric parameters. When a moderate-to-strong earthquake occurs we can apply SAR Interferometry (InSAR) technique to compute a differential interferogram. The earthquake has been generated by an active, seismogenic, fault having its own specific geometry. Therefore each differential interferogram contains in principle information concerning the geometry of the seismic source the earthquake comes from. To perform the inversion operation an approach based on neural networks can be considered. The paper illustrates such a methodology and its assessment on experimental data. [C1590]

#### "TerraSAR-X Dual Receive Antenna mode-Channel reconstruction and impact on the GMTI performance"

TerraSAR-X is a high resolution synthetic aperture radar (SAR) satellite which provides the option to split the antenna in along-track direction and sample two physical channels separately. This so-called dual receive antenna (DRA) mode is implemented by use of a Magic-T hybrid junction which provides the sum and difference channel data instead of the fore and aft channel data. One way to exploit this spatial degree of freedom is to reconstruct the fore and aft channel data in the processing. The critical issue with the fore and aft channel reconstruction is the fact, that for space-based radar systems very high precision calibration is required. This is even more difficult since the wide bandwidth pulses employed by the radar makes the receive hardware transformation frequency dependent. In this paper a fore and aft channel reconstruction approach is described based on an estimation of the receive hardware transformation matrix by use of internal calibration pulses and calibration beams. The quality gain of the fore and aft channel reconstruction is demonstrated with experimental data and results on the ground moving target indication (GMTI) capability are shown. [C1591]

#### "Multi-path correction model for multi-channel airborne SAR"

This paper analyzes the multi-path component effect in the airborne SAR context, proposing a model as an approach to correct the generated disturbances in the processed phase and amplitude images. The method assumes along-track interferometric or polarimetric data to estimate the unknowns of the model. Airborne data acquired by the F-SAR system of DLR are used to evaluate the performance of the proposed approach. [C1592]

#### "Digital beam-forming for spaceborne reflector- and planar-antenna SAR-A system performance comparison"

The trend in the conception of future spaceborne radar remote sensing is clearly towards the use of digital beam-forming techniques. These systems will comprise multiple digital channels, where the analog-to-digital converter is moved closer to the antenna. This dispenses the need for analog beam steering and by this the used of transmit/receive modules for phase and amplitude control. Digital beam-forming will enable Synthetic Aperture Radar (SAR) which overcomes the coverage and resolution limitations applicable to state-of-the-art systems. On the other hand, new antenna architectures, such as reflectors, already implemented in communication satellites, are being considered for SAR applications. The paper compares the system architecture and SAR performance of a planar and a reflector antenna SAR. [C1593]

#### "Three-component decomposition for polarimetric SAR"

An improved three-component decomposition for polarimetric SAR data is proposed in this paper. The reasons of the emergence of negative powers in the Freeman decomposition have been analyzed, and two improvements are included. Firstly, the deorientation process is applied to the coherency matrix before it is decomposed into three scattering components. Then, the coherency matrix with the maximal polarimetric entropy, i.e., the unit matrix is used as the new volume scattering model instead of the original one adopted in the Freeman decomposition. The E-SAR polarimetric data acquired over the Oberpfaffenhofen area in Germany are applied for experiment to demonstrate the effectiveness of the new model. [C1594]

#### "Statistical characterization of the Sinclair matrix: Application to polarimetric image segmentation"

This paper focuses on the flexibility of a multidimensional model of probability density function (pdf) to describe

distribution of complex data in polarimetric SAR images. This model is based on Copulas Theory for characterizing the dependence between the polarimetric channels (HH, VV, HV, VH). This corresponds to finding a model based on multidimensional copulas to describe the behavior of the target vector. The advantage in using copulas theory is to extend correlation concept to a wider dependence one, which may be non-linear, especially when processing high-resolution data. So, from this point of view, the model is more flexible than the classical Wishart distribution since no speckle filtering is required as preprocessing step to model accurately the pdfs. The other advantage of copulas is to split dependence concept and marginal distributions. Then, this multidimensional characterization may be linked to pdf which are not necessary of circular Gaussian law. So, specific parametric distribution may be chosen to fit each component (modulus and phase) of the Sinclair matrix. It yields a flexible model, for characterizing statistical behavior of the polarimetric SAR data, that may be derived to produce a segmentation algorithm. [C1595]

#### "Analysis of ASAR/Envisat polarimetric backscattering characteristics of Doñana national park wetlands"

Doñana National Park wetlands, in southwest Spain, undergo yearly cycles of inundation and drying out. These cycles, together with great extensions of annual helophytes, make of Doñana a rapidly changing environment. 43 ASAR/Envisat images of Doñana in HH, VV and HV polarizations were acquired throughout the hydrological year 2006/07 with the aim to monitor in detail an entire flooding cycle. The images were ordered in the seven ASAR swaths to achieve high observation frequency. Backscattering temporal signatures of two main land cover types were obtained in the three polarization configurations and six ASAR swaths. Polarimetric behavior of the signatures is analyzed with the aid of extensive site data, such as a precise digital elevation model and continuous records of water level and meteorological parameters. Conclusions on the feasibility to discriminate emerged versus flooded land are derived for the different incidence angles, land cover types and phenological stages. [C1596]

#### "Salient features of the radar nodes in the Puerto Rico tropical weather testbed"

A tropical weather testbed, inspired by the CASA IP1 radar network, is to be constructed on the western coast of the island of Puerto Rico. This new radar network testbed will address Quantitative Precipitation Estimation (QPE) in a tropical environment. The testbed will consist of three low-power, short-range, dual polarized X-band Doppler radars. Special considerations were taken in the design of the radar, as related to the tropical seaside environment of the proposed site locations, where high temperatures, humidity, and elevated salinity in the air are common. The goal of the network is to study tropical weather events in the lower 2 km of the troposphere, where reduced accuracy of precipitation estimates by conventional weather radar can occur. This paper will describe the characteristics of the network radar nodes. [C1597]

#### "Model-based statistical analysis of PolSAR data"

In this paper, we consider statistical analysis of PolSAR data in the framework of the multivariate product model. The complex scattering vector is here considered as a double stochastic circular Gaussian variable, in which the variance is linearly scaled by a common stochastic scaling factor  $z$ . The scaling factor is associated with texture. We discuss various parametric probability density functions for  $z$ , and indicate how model parameters can be estimated from data by a simple moment based method. Experimental analysis shows that for some surface covers, certain texture distributions fit better than others. Then, polarimetric covariance matrix data analysis is addressed in the framework of product models, and we propose a processing scheme which perform image segmentation using a stochastic EM approach. [C1598]

#### "PolSAR and PolInSAR model based information estimation"

Speckle for multidimensional SAR data may be modeled as the combination of multiplicative and additive noise sources. As demonstrated, the use of this noise model does not corrupt the estimation of physical information from PolInSAR data. The definition of a model based PolInSAR filter allows also the computation of relative errors for estimated heights of forested areas from PolInSAR data. [C1599]

#### "Estimation and segmentation in non-Gaussian POLSAR clutter by SIRV stochastic processes"

In the context of non-Gaussian polarimetric clutter models, this paper presents an application of the recent advances in the field of Spherically Invariant Random Vectors (SIRV) modelling for coherency matrix estimation in heterogeneous clutter. The complete description of the POLSAR data set is achieved by estimating the span and the normalized coherency independently. The normalized coherency describes the polarimetric diversity, while the span indicates the total received power. Based on the SIRV model, a new maximum likelihood distance measure is introduced for unsupervised POLSAR segmentation. The proposed method is tested with

airborne POLSAR images provided by the RAMSES system. [C1600]

### "A three-dimensional imaging algorithm for tomography SAR"

The three-dimensional image quality of tomography SAR is limited by the non-uniform track distribution in repeat-pass data acquisition. In order to overcome the drawbacks of known methods caused by the non-uniform track distribution, a new three-dimensional imaging approach is proposed based on backprojection for tomography SAR in this paper. Raw data of tomography SAR in X-band is simulated and three-dimensional image is achieved. The imaging result is analyzed, and simulation results confirm the validity of the proposed method. [C1601]

### "An assessment of ALOS L-band polarimetry for land-use monitoring in Malawi"

In this paper we investigate the advantages of using full quadpol low frequency radar imaging data for large area land-use classification and forest biomass estimation. We employ multiple PALSAR data sets over test sites in Malawi, Africa, where we have extensive in-situ measurements and ground campaigns for validation. We show how L-band PLR modes show great potential for quantitative land use applications and important sensitivity to above ground biomass. [C1602]

### "Decadal change in northern wetlands based on differential analysis of JERS and PALSAR data"

We have been developing a continental-scale map of the North American boreal wetlands based on L-Band SAR imagery collected in 1997-1998 by the Japanese Earth Resources Satellite (JERS). The map currently covers the entire state of Alaska, identifying up to nine wetlands classes and two uplands classes. We have also recently obtained and classified a region of L-Band SAR imagery collected in 2007 by the Advanced Land Observing Satellite (ALOS) Phased Array L-Band SAR (PALSAR). Herein, we compare the results of the PALSAR classification to those of the JERS classification in order to detect changes in wetlands type or extent during the decade-long interval between the two sets of SAR imagery. [C1603]

### "Semi-supervised learning for classification of polarimetric SAR-data"

Supervised learning algorithms are important methods to automatically interpret image data in general as well as PolSAR data in particular. However, they suffer from the need of a training set, which has to contain manually labelled data. Un-supervised methods do not demand this kind of data, but cannot be directly used to assign user-defined class labels to image regions. This paper proposes a semi-supervised method to overcome both shortcomings. The data is analysed by an un-supervised clustering algorithm under the usage of all available information. Simultaneously each pixel is classified by a supervised method using the information available at the current phase of clustering. [C1604]

### "An end-to-end error model for classification methods based on a SAR intensity ratio"

This paper aims at defining the expression of the probability of error of classification methods using a Synthetic Aperture Radar (SAR) intensity ratio as a classifier. The two SAR intensities involved in this ratio can be measurements from different dates, polarizations or possibly also frequency bands. Previous works provided a baseline expression of the probability of error addressing the two-class problem with equal a priori class probabilities and no calibration error. This study brings up a novel expression of the error, providing the possibility to assess the effect of class probabilities and calibration errors. The effect of calibration errors such as channel gain imbalance and radiometric stability is assessed in the general case. Results indicate that channel gain imbalance is generally not a decisive parameter, but that radiometric stability is more critical in methods based on the temporal change. This error model can be used to test the impact of other SAR system parameters (time-lapse between repeat-pass orbits, ambiguity ratio, number of looks) and constitutes a tool for the design of future SAR missions and for the development of robust classification methods using existing SAR instruments. [C1605]

### "Detection of double scatterers in SAR Tomography"

Multi-Dimensional (3D/4D) SAR imaging (SAR Tomography and Differential SAR Tomography) allows the localization and monitoring of ground scatterers, even interfering in the same azimuth-range pixel. Indeed, the presence of multiple scatterers has shown to affect even the performances of high resolution radar systems. In this paper we discuss two strategies for the detection of interfering scatterer pairs. The first one is based on the extension of the GLRT test already proposed for the detection of single scatterers, the second one is based on the BIC criteria commonly used in the context of model order selection. Performances of the two decision schemes are evaluated on simulated data. [C1606]

### **"An algebraic approach to ground-volume decomposition from multi-baseline PolInSAR data"**

In this paper, an algebraic methodology is described for the separation of ground and volume contributions basing on multi-baseline and multi-polarimetric acquisitions. As a result, a new general procedure is defined that encompasses single-baseline PolInSAR as a special case, and allows to proceed to ground/volume separation not only through model based approaches, but also through model free and hybrid approaches. Furthermore, it will be shown that such a methodology yields the best solution in the Least Square sense. [C1607]

### **"Multi-baseline POL-inSAR statistical techniques for the characterization of distributed media"**

This paper presents principles and robust techniques to estimate physical parameters of natural environments using Multi-Baseline Polarimetric and Interferometric SAR (MB-POL-inSAR) data. The first part of this paper concerns the abstract topic of MB-POL-inSAR coherence optimization. The second part is dedicated to the general estimation of the coherence line model parameters [1]. It is demonstrated that the line parameters can be estimated in an analytical and robust way by using the whole available POL-inSAR information. [C1608]

### **"K-way tree classification based on semi-greedy structure applied to multisource remote sensing images"**

In this paper we present a new supervised classification method, referred to as the k-way tree semi-greedy (KTSG) classifier, for the classification of multisource remote sensing images. The generalized positive Boolean function (GPBF) classifier scheme is recently proposed based on minimum classification error (MCE) criteria to improve classification performance. It makes use of MCE criteria to apply positive and negative samples as training parameters. Unfortunately, the classification performance of GPBF is limited when the number of classes increases. This is occurred in training phase by the unbalanced numbers of positive and negative samples caused by the use of a large number of classes. The proposed KTSG overcomes this drawback by modifying the scheme from the perception of pattern-node based semi-greedy (bottom-up scheme used in GPBF) to the conception of region-based semi-greedy (also known as the top-down scheme in KTSG). It is organized by a k-way tree in which every node is composed of a set of k-dimensional positive and negative labeled samples as represented as a percentage, i.e. the corresponding ratio of number of a specific (positive) class samples to the total number of the other (negative) classes. It iteratively divides the d-dimensional hyperplane into 2d subspaces according to the centroids of the labeled (training) samples of all classes. The statistical ratios between different classes are then compared as a basis for stopping the new subspace separation and identifying which subspace belongs to which class. By delivering both positive and negative samples of different classes to KTSG learning modules, KTSG outperforms GPBF and traditional classifiers in terms of classification accuracies. The effectiveness of the proposed KTSG is evaluated by fusing MODIS/ASTER airborne simulator (MASTER) hyperspectral images and airborne synthetic aperture radar (AIRSAR) images for land cover classification during the Pacrim II campaign. [C1609]

### **"Aspects of 3D tomography for multiple-pass spotlight-mode airborne SAR"**

Three-dimensional SAR tomography makes use of radar data acquired at different depression angles to synthesise an aperture in elevation and thereby undo layover and resolve along height. Focusing on one tomographic method appropriate to a spotlight-mode airborne collection system, the details of spatial bandwidth usage and point-spread function are described, and the phase modulation effects of the initial two-dimensional image formation stage are analysed in terms of the impact on the tomographic processing. Finally, an adaptive beamforming approach is investigated for the improvement of height resolution. [C1610]

### **"Subsatellite experiments in the north-eastern part of the Black Sea"**

Space-time variability of current field characteristics, surface waves, and parameters of the near-surface atmospheric layer above the shelf zone of the Black Sea in the Gelendzhik-city region are studied. A joint analysis of the field measurement data obtained on August, 2007, September, 2008 and of the synchronous SAR images made by the Envisat satellite of the European Space Agency is carried out. [C1611]

### **"Non-linear internal waves in the Banda Sea on satellite synthetic aperture radar and visible images"**

Comprehensive study of non-linear internal waves (IWs) in the Banda Sea was carried out. IWs were detected on quick look and full-resolution SAR images acquired by ERS-1, ERS-2, Envisat and ALOS as well as on Terra and Aqua MODIS and Landsat ETM images. IWs were generated by a sill between Alor and Atauro Islands in Ombai Strait connecting the Banda Sea with the Savu Sea. The IWs form packets, propagating northward into

the Banda Sea and have the classic appearance of rank ordered non-linear waves that depress the pycnocline. The length of the wave packets reached 100 km and more and packets could consist of 15-20 and more solitons. The maximum wavelength was approximately 12-15 km. The phase speeds of the waves varied from approximately 2.2 m s<sup>-1</sup> to 3.1 m s<sup>-1</sup> for the leading solitons in the packets. Wave crests in the packets formed semicircles, the length of which exceeded 350 km. [C1612]

#### "Classification of polarimetric SAR data over wet and arid regions of India"

Polarimetric SAR data from ALOS PALSAR, SIR-C and ENVISAT ASAR over wet and arid regions were processed for classification and soil moisture estimation. HH and HV dual polarized ALOS PALSAR could classify wetlands of Mumbai coastal area with an accuracy of 96%, whereas fully polarized SIR-C data over Kolkata gave 92% accuracy. The accuracies are based on selected training areas and not based on test areas. ALOS PALSAR could clearly discriminate water, mangrove forest and ocean water. With Dual polarized data, discrimination between Ocean water and wetlands is not possible. Several features in arid data can also be classified using PALSAR data in addition to the estimation of soil moisture. [C1613]

#### "Soil moisture and vegetation height retrieval using GNSS-R techniques"

Global Navigation Satellite Signals Reflections (GNSS-R) techniques are currently being used for remote sensing purposes retrieving geophysical parameters over different types of surfaces. Over the ocean, sea state information can be retrieved to improve the ocean salinity retrieval. Furthermore, over land these techniques can be used to retrieve soil moisture. This paper presents the theoretical and experimental results of using GNSS-R to retrieve soil moisture when vegetation is present. The particular technique being applied in this study is the Interference Pattern Technique (IPT) that measures the interference pattern of the GPS direct and reflected signals, after reflecting over the surface. [C1614]

#### "Combining SAR and optical features in a SVM classifier for man-made structures detection"

The increasing quality of satellite images has generated interests in extracting man-made structures in urban areas, such as buildings and roads. A classification adapted to urban areas can help to identify these structures. In this paper, SAR information are used to improve land-cover classification. We proposed a classification process using both radar and optical data, a segmentation and a classification with Support Vector Machines (SVM). [C1615]

#### "Polarimetric scattering feature estimation for accurate vegetation area classification"

This paper proposes an accuracy improvement of the vegetation area classification based on the POLSAR image analysis, when vegetation and man-made areas are both included in the radar target region. Here we introduce a simple compensate polarimetric marker, T13 or T31, to accurately distinguish the unexpected scattering from the obliquely oriented man-made targets and the complex volume scattering generated from vegetation area. T13 or T31 is the (1, 3) or (3, 1) elements of the  $3 \times 3$  averaged coherency matrix ( $[T]$ ), and has not been effectively utilized in the general scattering power decomposition scheme. By appropriately utilizing T13(T31), one can extract only the vegetation area from the mixed target region. It is verified from the detailed analysis that the proposed marker T13(T31) works well not only for Pi-SAR data but also for ALOS/PALSAR data. [C1616]

#### "Multiple scatterers identification in complex scenarios with adaptive differential tomography"

In the last few years, the interest is increasing in the interferometric processing of multibaseline/multitemporal SAR data from complex urban or infrastructure areas. In order to locate and monitor a high number of ground structures with the lowest signal misinterpretation, the identification, i.e. the detection and height and deformation velocity estimation, of both single and multiple layover scatterers is an important step. This issue is addressed here by extensively experimenting the technique of adaptive differential tomography, a recent interferometric framework which allows to resolve multiple moving scatterers at different heights in the same SAR cell. To this aim, adaptive differential tomography is augmented with an automated information extraction algorithm. The technique has been applied to real C-band spaceborne data over an urban area. Corresponding results are discussed. [C1617]

#### "On the ability of the ERS scatterometer to detect vegetation properties"

The ability of the active microwave remote sensing to complement existing optical vegetation indices has been explored by variety of studies. To demonstrate these complementarities, we investigate synergies between the slope parameter from the ERS scatterometer (ERS-SCAT) and the Normalized Difference Vegetation Index

(NDVI). While the NDVI is strongly linked to the absorption of photosynthetically active radiation (PAR), the active microwave signal has the ability to penetrate partially a vegetation canopy, bouncing back from its stalks and stems and so returning a signal (i.e. backscatter) that is influenced by the canopy structure. While this interaction is rather complicated and not fully understood, this study suggests the ability of the ERS-SCAT slope parameter to differentiate between varieties of structural vegetation properties and complement so to existing optical vegetation indices. [C1618]

#### **"A preliminary study on deforestation monitoring in Sumatra Island by PALSAR"**

An L-band normalized radar cross section (NRCS) characteristic derived from the Phased Array L-band Synthetic Aperture Radar (PALSAR) 50-m resolution dual-polarization mosaic and the land cover database in Riau province, Sumatra Island, represent that HV signals of natural forests are 2-3 dB larger than those of cleared and many plantations, indicating the usefulness of HV measurements for the detection of new deforestation. The 2007 and 2008 mosaic series, in fact, elucidates 3dB decreases in the HV channel for major deforested areas. On the other hand, HH shows no significant changes. 46-day repeat ScanSAR observations clarify common HH signal changes for the deforestation: they once increase departing from the annual cycle of natural forests and reach a peak in a rainy season. The result suggests the availability of the ScanSAR-derived HH time series for near-real-time deforestation monitoring. A HH signal variation on an acacia plantation cycle represents a similar characteristic to that for the deforestation: HH anomalously increases during the subsequent rainy season after the plantation. The increase level depends on an incidence angle, suggesting the dominance of surface scattering component over young acacia areas. With analogy with deforestations, it is suggested that the incidence angle dependency seems to be considered for the deforestation monitoring by ScanSAR. [C1619]

#### **"Investigation of multiple frequency polarimetric SAR signal backscattering from tidal flats"**

The tidal flats are largely developed along the western and southern coast of Korean peninsula. The simulation results of tidal flats through analytical scattering models could not be fully assessed by using only surface roughness (RMS height and correlation length) and soil moisture. The tidal flats are usually saturated with saline sea water and partially covered with remnant water in depressions. This may cause lower backscatters in SAR images due to the partial specular reflection. [C1620]

#### **"Techniques and examples for the 3D reconstruction of complex scattering situations using TerraSAR-X"**

The German radar satellite TerraSAR-X was launched in June 2007. Since then, it is continuously providing high resolution space-borne radar data which are perfectly suitable for sophisticated interferometric applications. I.e. the mission concept and the SAR sensor support the coherent stacking of radar scenes which is the basis for advanced processing techniques e.g. Persistent Scatterer Interferometry (PSI) and SAR tomography. In particular, the short repeat cycle of eleven days and the highly reproducible scene repetition of the spotlight acquisitions support the stacking and consequently the time series analysis of the radar data. Furthermore, the sensor's orbital tube is precisely controlled to be in the order of 200 m which basically allows to utilize the baseline spread of the stacked acquisitions. However, this small spread is actually limiting the resolution in the SAR tomography. Interferometric applications could be demonstrated already in a very early stage of the TerraSAR-X mission. Because the resolution is 0.6 m in slant range and 1.1 m in azimuth in the high resolution spotlight mode the PSI and the SAR tomography processing results were impressive. Urban areas and single buildings could be mapped from space in three dimensions. Even the structural stress of single buildings caused by thermal dilation could be demonstrated. However, extended layover areas are caused by typical buildings and as a consequence complicated scattering situations need to be resolved. DLR's operational In-SAR processing system GENESIS had already been adapted to cope with the new sensor modes of TerraSAR-X and their new specific spectral characteristics. Now, the new image characteristics e.g. the extended layover areas and the long time coherent distributed scatterer need better to be supported. Subject is to optimally exploit the available information e.g. the radar reflectivity. Several algorithms of the processing system can take advantage of this, e.g. the scatterer-configuration detection. As a matter of fact, the scatterer configuration has now become a very important characteristic for each resolution cell. It influences e.g. the estimation data extraction, the estimation of the 3D location and basically the estimation precision. A typical resolution cell can be composed of a single dominant point scatterer surrounded by clutter, two or more dominant point scatterers in clutter and of distributed scatterers with a specific phase stability over time. The paper provides technical details and a processing example of a newly developed algorithm to retrieve the 3D location of point scatterers from the scene's intensity which finally also provides the information on the scatterer configuration in a resolution cell. [C1621]

#### **"Method of persistent scatterer pairs (PSP) and high resolution SAR interferometry"**

Synthetic aperture radar (SAR) interferometry is an effective technology for detection and monitoring of slow terrain movements with millimetric resolution. This information is extracted by means of complex techniques from the phase of the signal, which is wrapped modulo  $2\pi$  and affected by noise and systematic terms. We have recently proposed a new method, named persistent scatterer pairs (PSP), aimed at overcoming some limitations of standard persistent scatterer interferometry (PSI) techniques. The method is characterized in that it works only with pairs of nearby pixels both for selecting and analyzing the persistent scatterers (PS), thus being intrinsically not affected by artifacts slowly variable in space, like those depending on atmosphere or orbits. Moreover, the method does not require an initial selection of PS based on the radar backscattered amplitude. In this work, after resuming the main ideas of the PSP method, we show some results obtained in extensive applications with ERS/ENVISAT data, and the first results obtained with high resolution COSMO-SkyMed images. [C1622]

#### "Monitoring slow ground movements around Tunis City by different SAR interferometric measures"

This paper presents an application of DInSAR techniques for the assessment of ground subsidences around Tunis City. A longterm analysis using two interferometric techniques were carried out to attempt reliable measurements. In this work, some aspects of interferometric processing softwares are reviewed and possible improvements are proposed in order to get better results. The convergence of the two different interferometric techniques done simultaneously and independently confirms results accuracy. [C1623]

#### "Urban dynamic change detection in southeastern China based on interferometric SAR"

Synthetic Aperture Radar is the only instrument that can provide consistent remote sensing data for south China with persistent cloud cover and rain. In this paper, the potential of multi-temporal ERS, ENVISAT-1 and PALSAR data for land cover/land use classification and urban change detection was investigated at a test area in Fuzhou city, the capital of Fujian province in southeastern China. Both SAR backscatter intensity characteristics and interferometric data were analyzed. Two methods were carried out in the urban dynamics change detection: one was post-classification comparison, and the other one was multi-temporal image ratioing. The results from both classification and urban change detection were validated by field survey data and showed promising application of PALSAR and ESA SAR data in southeastern China. [C1624]

#### "Preliminary measurements of bare soil and waved water surface microwave reflection and emission angular dependences at 5, 6GHz"

In this paper structural and operational features of C-band, dual-polarization, combined scatterometer-radiometer system and the results of preliminary, spatio-temporally collocated measurements of bare soil and waved pool water surface microwave reflective (radar backscattering coefficient) and emissive (brightness temperature) characteristics angular dependences at ~5.6 GHz are presented. [C1625]

#### "Multiple Crop Yield prediction using dual-polarimetric TerraSAR-X stripmap imagery"

This paper presents the results of an experiment carried out to relate the yield from various crops to TerraSAR-X dual polarimetric imagery. X-band wavelength has higher sensitivity to smaller crop structures, especially stem and head density making it suitable for relating yield to backscatter. The coherent dual-polarimetric mode of TerraSAR-X was also used to emphasize the volume scattering through dual-polarimetric entropy/alpha decomposition. Good correlations to yield data as gathered by harvester telemetry were obtained. [C1626]

#### "Paleoterrain model of the Yamato Marsh, Palm Beach County, Florida"

A modeling technique has been produced by combining remote sensing with geologic history for building a paleoterrain model that enables visualization of topography prior to anthropogenic development. The model's foundation is comprised of LIDAR data and stratigraphic sequences for describing the local geologic history. The Yamato Marsh, located in Palm Beach County, Florida, is a paleowatershed that was chosen for this study. The paleoterrain model of the marsh site can be utilized further in understanding land-use impacts on the surrounding environment. In conclusion, the final model of the Yamato Marsh successfully offers insight as well as a glimpse at a geomorphic feature that no longer exists. [C1627]

#### "Pulse Coupled Neural Network for automatic features extraction from COSMO-SkyMed and TerraSAR-X imagery"

In this paper we test an unsupervised neural network approach for extracting features from very high resolution X-band SAR images. The purpose of this study is buildings recognition in images of low density urban areas, acquired by COSMO-SkyMed and TerraSAR-X satellites, by means of Pulse Coupled Neural Network (PCNN), a relatively novel unsupervised algorithm based on models of the visual cortex of small mammals. The features

retrieved from geo-referenced SAR images are compared against the ground truth provided by corresponding optical images. The accuracy yielded by PCNN is quantitatively evaluated and critically discussed, also in comparison with commonly used feature extraction techniques. [C1628]

### "Operational applications of RADARSAT-2 for the environmental monitoring of oil slicks in the Southern Gulf of Mexico"

PEMEX has used RADARSAT-1 operationally for the environmental monitoring of oil slicks in the Southern Gulf of Mexico for almost a decade (2000-2008). In this time RADARSAT-1 data has become fully integrated into PEMEX's environmental response strategy. To move towards the future; PEMEX decided to transition to RADARSAT-2 when the data became commercially available in April 2008. The purpose of this paper is to discuss the steps made in the move from RADARSAT-1 to RADARSAT-2 and how the advanced capabilities of RADARSAT-2 have improved operational processes. [C1629]

### "Unsupervised segmentation of agricultural regions using TerraSAR-X images"

The framework of this study is focused on automatic fast recognition of agricultural interest for TerraSAR-X images. The intended goal is to label regions in an image as fast as possible, into classes significant for a given application, like crop classification. First, a filtering technique is applied to obtain the restored image. Then, two different methods of unsupervised segmentation are used. The Otsu's method which is based on the optimum threshold of histogram and the k-means method which is based on the Euclidean distance. [C1630]

### "A study on land cover classification based on HJ-1 CCD image"

Remote sensing technique has become one of the most effective means to acquire land cover information. The CCD cameras onboard the environment and disaster monitoring and forecasting satellite constellation (HJ-1 satellites) are advanced in spatial resolution, image coverage and revisit frequency. Thus, it can be very efficient to do land cover classification using their images. Taking Zhongshan County in Guangxi province as the study area, this paper studies on the best method of land cover classification based on HJ-1 CCD image and other assistant data. In order to test the general applicability of this land cover classification method, this paper also applies the method to another place. [C1631]

### "Mapping and monitoring clear-cuts in Swedish forest using ALOS PALSAR satellite images"

This study presents results for observing forest changes in Sweden using multi-temporal L-band satellite data and is a part of the JAXA's ALOS Kyoto and Carbon Initiative. An extensive dataset of images acquired by the Advanced Land Observing Satellite Phased Array type L-band Synthetic Aperture Radar (ALOS PALSAR) is investigated for clear-cut detection in boreal forests in northern Sweden (Lat. 64°14' N, Long. 19°50' E). Strong forest/non-forest contrast and temporal consistency were found for the Fine Beam Dual HV-polarized backscatter during unfrozen conditions. Thus, a simple thresholding algorithm that exploits the temporal consistency of pair-wise HV-backscatter measurements has been developed for clear-cut detection. When applied to an image pair acquired during favorable weather conditions, the detection algorithm identified 76% of the clear-cut pixels within a reference layer, with zero erroneously detected pixels. With further refinement the developed methodology can be an option to present operational alternatives for clear-cut detection. [C1632]

### "Fusion of ALOS Palsar and Landsat ETM data for land cover classification and biomass modeling using non-linear methods"

This work demonstrates the utility of reduced resolution ALOS PALSAR data for biomass mapping and land cover classification over the tropical forests of Indonesia. This study is important because we processed the ALOS PALSAR mosaic, which is made freely available within K&C initiatives project and will be updated regularly. We first used 38 sample plots collected on the ground during dry season in September 2004, to develop a tree diameter (dbh)-biomass model. The HH, HV, HV/HH and HH-HV backscatters of ALOS PALSAR data allowed the empirical estimation of forest above ground biomass (AGB). Each band of PALSAR data was separately used to estimate the biomass, and we found HV band resulted in better correlation with the AGB compared to other SAR bands. Validation of the prediction results was carried out by comparing the biomass estimates with those predicted from an existing allometric equation. Optical data are sensitive to the physical properties of the reflectors whereas SAR data are more influenced by the geometric properties of the scatterers. Therefore, the second part of this study concerned the integration of mosaic SAR textures and ETM data for land cover classification. The classification was conducted using ETM data and variations of ETM, SAR bands, and SAR textures calculated using GLC Matrix. The image classifications were carried out using a Machine Learning based classifier, so-called Support Vector Machine (SVM), and a conventional Maximum Likelihood

method. An ensemble of neural networks method using Kalman filter and scaled conjugate gradient algorithm was applied. The classification accuracy was assessed using confusion matrices and Kappa statistics. We show that the introduction of SAR textures significantly enhanced the classification accuracies. This study showed that the joint processing of SAR and multispectral data increased the accuracies of biomass estimation and landuse classifications. The efficiency of the method at medium spatial resolutions allows its application of global datasets. [C1633]

#### "Forest type discrimination using polarimetric Radarsat 2 data"

In the south of China, synthetic aperture radar (SAR) provides a powerful tool for forestry inventory because of its all-weather and all-day capabilities. Nevertheless previous single or dual polarization SAR data cannot meet the requirements of forest type classification. Polarimetric SAR data contained more information of targets and in this paper we investigated the capability of polarimetric Radarsat 2 data for forest type discrimination. Taking Zhazuo forest farm of Guizhou Province as study area, an 8-temporal field experiment was designed and used for polarimetric backscattering signatures analysis based on MIMICS model. Then two-temporal polarimetric Radarsat 2 data was analyzed to extract polarimetric variables for forest species discrimination, and then polarimetric decomposition and classification were carried out. Experiments prove that forest type can be discriminated using polarimetric Radarsat 2 data, but it is not very effective for forest species identification mainly due to the spatial resolution limitation. Polarimetric SAR data with higher resolution and more complicated classification methods are needed in the future. [C1634]

#### "Backscatter properties of multitemporal TerraSAR-X data and the effects of influencing factors on burn severity evaluation, in a mediterranean pine forest"

TerraSAR-X dual-polarized (HH and HV polarization) backscatter data have been investigated to assess the temporal backscatter stability of a burn scar in Spain. Analysis of the main factors influencing burn severity evaluation has been also carried out. The temporal stability of the backscatter was strong, unburned areas showing differences of less than 0.6 dB. For increasing burn severity the backscatter varied by up to 2 dB in highly burned areas located on slopes tilted towards the sensor. Heavy rainfall or moist vegetation increased the backscatter up to 1 dB. Steeper look angles resulted in significantly higher backscatter coefficients for HH polarization, while for HV polarization only marginal increase was observed. Association strength between backscatter and burn severity estimates improved with the size of the multi-look window, at the expenses however of spatial resolution. Even better results could be achieved at higher spatial resolution by applying a multi-temporal speckle filtering algorithm. [C1635]

#### "Retrieval of suspended sediment concentration in the Pearl River Estuary from MERIS using support vector machines"

With the rapid industrialization and urbanization, more and more solid have been emitted into the Pearl River Estuary. The suspended sediment concentration is one of the most important water quality parameters. With in-situ optical data and suspended sediment data collected on four cruises from 2004 to 2006 in the Pearl River Estuary, analysis shows that with the increasing of the total suspended sediment (TSM) concentration, the intensive bands which have the best correlation relationship with the TSM concentration shift from Rrs(620) to Rrs(778). When the mean suspended concentration is 14.5 g.m<sup>-3</sup>, the Rrs(620) has best correlation with the suspended concentration. However, when the mean suspended concentration becomes more than 40g.m<sup>-3</sup>, the most correlated band shifts to 778nm. It seems that all of the Rrs(620), Rrs(665), Rrs(681), Rrs(708), Rrs(753), Rrs(760), Rrs(778) may be the most sensitive band for the different TSM concentration. This work investigates the possibility of using a new universal approximator-support vector machines (SVMs)-as the nonlinear transfer function between TSM concentration and remote sensing reflectance in the Pearl River Estuary. Experimental results show that the SVM performs better result than general empirical algorithms or the piecewise algorithm. The correlation coefficient between the in-situ and modeled TSM of the test dataset is 0.91 and the root mean squared error (RMSE) is 0.145. The algorithm based on the SVM is applied to MERIS satellite data in January 31, 2007. The distribution of TSM concentration was obtained and it shows that the algorithm could be a useful tool for the study of TSM distribution in Pearl River estuary. [C1636]

#### "Derivation of surface soil moisture using multi-angle ASAR data in the middle stream of Heihe river basin"

Radar remote sensing has shown its potential for retrieving soil moisture from soil surfaces. Since the backscattering process is also influenced by soil roughness, the characterization of this roughness is crucial for an accurate estimation. The algorithm proposed in this investigation aiming to obtain the roughness parameters for every SAR pixel which could facilitate the derivation of soil moisture in virtue of multi-angle ASAR images,

and combined with a semi-empirical calibration for the correlation length. An application of the means was performed in the middle reaches of the Heihe river basin and achieved satisfactory results (RMSE less than 6 vol %). [C1637]

#### "Use of Radarsat-2 images to develop a scaling method of soil moisture over an agricultural area"

Our objective is to describe and evaluate the spatial variability of the surface soil moisture at small scales using Radarsat-2 images acquired over an agricultural area. To reach this aim, a geostatistical analysis is applied to up scale the soil moisture from ground measurements to the resolution of radar images and also from retrieving soil moisture at different spatial resolution. To conduct this study, four RADARSAT-2 images acquired at different modes during the summer of 2008 over agriculture fields located in Saskatoon (Saskatchewan, Canada) were used. The available data are ground measurements of soil moisture, surface roughness and vegetation characteristics. The comparison between retrieval and ground soil moisture showed average absolute relative errors of about 35% and 55% for fine and ScanSAR mode images respectively. Indeed, a weak amelioration was obtained from the up scaling of the ground soil moisture data to the spatial scale of the different radar image. [C1638]

#### "Detection subsurface hyper-saline soil in Lop Nur using full-polarimetric SAR data"

This paper presents the research results about Lop Nur using full-polarimetric technology. Lop Nur Lake is one of the driest places in the world and finally lost its last drop of water in 1972. It is well known for its  $\Gamma_{\text{B}}\text{E}\Gamma_{\text{B}}$  feature in optical remote sensing images. Likewise,  $\Gamma_{\text{B}}\text{E}\Gamma_{\text{B}}$  feature is shown in Synthetic Aperture Radar (SAR) images, and even larger because of penetration effect. With the penetration capability SAR is capable of detecting the subsurface targets and materials, especially in arid environment. As for SAR images, both C-band and L-band, there are two key features about Lop Nur area. One is the whole Lop Nur area is high-bright that means the backscattering is much stronger than other sites, such as Gobi, desert and so on. The other feature is the  $\Gamma_{\text{B}}\text{E}\Gamma_{\text{B}}$  pattern formation. polarimetric analysis about these two questions will be conducted based on past research results and field investigations. [C1639]

#### "Subsurface microwave remote sensing and scattering modelling on hyper-saline soil: Example of Lop Nur"

Subsurface microwave remote sensing is a direction of Synthetic Aperture Radar (SAR) research. With the penetration capability, SAR is capable of detecting the subsurface targets and materials, especially in arid environment. Lop Nur Lake is located at the east of Tarim Basin in Xinjiang province of China, which is described as  $\Gamma_{\text{B}}\text{D}\text{ry core}\Gamma_{\text{B}}$  of the world, and it can provide conditions for SAR penetration. This paper presents preliminary analysis about Lop Nur, and gives out an abstract subsurface structure about it. Then, the major scattering processes are concluded and a two-layer scattering model is developed. Based on parameters of soil samples, some rules about Lop Nur evolution will be figured out. With Genetic Algorithm (GA), an inversion procedure is constructed. All the attempts are viewed as the basis of future comprehensive interpretation about Lop Nur phenomenon. [C1640]

#### "Research on oil spill identification based on texture features-a case study of "Hebei Spirit" accident"

For single-band and single-polarized SAR, its capability to monitor oil spill is limited based on image intensity. Texture features are suggested to improve accuracy of oil spill surveillance. Texture measures, extracted from GLCM (gray-level co-occurrence matrices), are analyzed, which indicates that mean, contrast, variance, entropy, and dissimilarity are effective for oil identification. SAR image is characterized by high resolution and speckle noise, which limits pixel-based approaches. In this paper, object oriented image analysis is used to extract oil slick. This algorithm typically incorporates both spectral and spatial information in the image segmentation phase. Results indicate that texture features extend features of interested objects, and help to improve oil spill surveillance. [C1641]

#### "A new algorithm for the phase unwrapping of interferogram stacks"

Phase unwrapping is a key step in DInSAR stack analysis: it allows restoring the phase values starting from the restricted ones to extract the deformation time series of the observed area. Most of the available interferogram stack phase unwrapping techniques unwrap each interferogram separately. Based on a strategy proposed in the literature, in this work we discuss an unwrapping procedure that exploits both the temporal and spatial characteristics of the interferogram stack. In particular we propose a technique that allows carrying out a temporal unwrapping step with a generic set of interferograms. The validation of our method is carried out by

processing simulated data. [C1642]

### "Bayesian restoration of interferometric phase through biased anisotropic diffusion"

In this paper a new Bayesian algorithm for interferometric phase restoration is presented. Based on a non-linear anisotropic extension of Orientation Diffusions, the inherent directionality of the fringe structure is introduced into its prior model. It also accounts for the periodicity of the phase representation. A fidelity term derived from the anisotropic metrics and the InSAR phase statistics deviates diffusion towards the acquired phase value. It acts as an adapted likelihood of the diffused phase. Hence, phase restoration is a trade-off between directionality and reconstruction fidelity, prior and likelihood. Results are provided on a High Resolution Spotlight scene acquired by TerraSAR-X. [C1643]

### "InSAR permanent scatterers selection using SAR SVA filtering"

Permanent scatterers (PS) approach allows the identification of radar targets not affected by decorrelation noise then suitable for reliable SAR interferometric measurements. This paper introduces a new technique allowing the selection of stable scatterers based on adaptive SVA (Spatially Variant Apodization) filtering. Indeed, SVA filters identify SAR pixels with strong reflectivity (maximum of the mainlobe) over a long temporal series of interferometric SAR images which is the main feature of Permanent Scatterers pixels. A comparison between PS candidates pixels and selected SVA pixels is discussed in this study. [C1644]

### "One-dimensional radar interferometry for line infrastructure"

Here we present an efficient algorithm to analyze the deformation behavior of line infrastructure, such as water defense structures and railways, using radar interferometric time series. Due to the limited amount of pixels and the consistent reflection properties, a detailed analysis can be performed. By considering neighboring pixels, the influence of a large part of error sources is reduced. However, the strong correlation between pixels should be considered. The algorithm is applied to dikes in the Netherlands, showing global as well as local deformation effects. [C1645]

### "A GPU based time-domain raw signal simulator for interferometric SAR"

A novel GPU based time-domain raw signal simulator for InSAR is proposed in this paper to exploit the parallel computation of GPU using CUDA language. This simulator combines the advantages of both time-domain and frequency-domain InSAR simulator, i.e., it considers the baseline oscillation and real orbit, and it is also very efficient. Experimental results show the effectiveness of the simulator in varieties of conditions. [C1646]

### "Needs and applications for data mining in large series of remotely sensed images"

Recent years have shown an increase in image availability at decreasing cost, as focus changed from  $\Gamma, B_{\text{maximum profit}}, B_i$  to  $\Gamma, B_{\text{maximum use}}, B_i$ . This puts analysis and mining of time series of images within reach of a wider audience, promoting development of suitable techniques. This paper focuses on four generic types of mining of large series of images: a) presence and location; b) temporal patterns; c) spatio-temporal patterns; d) moving objects. For each type it is described which group of algorithms are used for mining and how uncertainty can be modeled. The four generic types can be used to find adequate algorithms for data mining and to describe uncertainty for new applications. Further developments are to be expected for tracking of fast moving objects, image mining of mixed archives and irregular time steps. Communication tools for uncertainty in image mining, targeted at users outside the geo-information sciences should be further developed. [C1647]

### "Damage analysis of 2008 Wenchuan earthquake using SAR images"

On May 12, 2008, Wenchuan earthquake (Ms 8.0) occurred in Sichuan, Southwestern China. This catastrophe caused severe damage of constructions in urban and rural areas, and fundamental infrastructure, such as those facilities of factories, electrical power, telecommunication and transportation, etc. The earthquake also resulted in many geological phenomena, i.e. landslide, debris flow, landslide lakes, etc. which also triggered off damage and threat. The airborne campaigns were performed after the earthquake with high-resolution SAR system for rescue and relief effort and damage assessment. In this study, damage of various facilities was described and analyzed using airborne SAR images acquired during the campaigns. The results were verified with ground truth investigation. The results showed the role of SAR data in earthquake damage assessment. [C1648]

### "Using geometric accuracy of TerraSAR-X data for improvement of direct sensor orientation and ortho-rectification of optical satellite data"

The very high geometric accuracy of geocoded data of the TerraSAR-X satellite has been shown in several investigations. It is due to the fact that it measures distances which are mainly dependent on the position of the satellite and the terrain height. If the used DEM is of high accuracy, the resulting geocoded data are very precise. This precision can be used to improve the exterior orientation and thereby the geometric accuracy of optical satellite data. The technique used is the measurement of identical points in the images, either by manual measurements or through local image matching using mutual information and to estimate improvements for the attitude data through this information. By adjustment calculations falsely matched points can be eliminated and an optimal improvement can be found. The optical data are orthorectified using these improvements and the available DEM. The results are compared using conventional ground control information from GPS measurements. [C1649]

#### "Calibration of radargrammetric DEMs from RADARSAT-2 high-resolution and fine-quad modes"

The new high-resolution and full polarimetric modes of RADARSAT-2 are evaluated for digital elevation model (DEM) generation using stereo-radargrammetry with Toutin's 3D physical model. The stereo-radargrammetric DEMs were evaluated with accurate Lidar data. Results on a test site north of Québec City, Canada showed good accuracy: (2 m 1Г,В horizontal and vertical) for Ultra-Fine mode (better than the resolution), and 5 m and 11 m (1Г,В horizontal and vertical, respectively) for the Fine-Quad polarimetric mode (about the resolution). [C1650]

#### "Fusion of SAR and optical data for urban extent extraction improvement"

This paper presents two methods to fuse SAR and optical data for urban extent extraction. The two methodologies build over single sensor's procedure in order to improve the efficiency of the characterization of the urban environment when more data is available. Results over Pavia and Al Fashir conform the effectiveness of the proposed procedures. [C1651]

#### "Analysis of multi-temporal land observation at C-band"

The availability of reliable land cover information is crucial for a wide range of applications, like for example monitoring of land use change and land degradation as well as administrative matters in global, regional and local scales. In this paper the potential of SENTINEL-1 C-band SAR data for land cover applications, e.g. generating level-2 land cover classification products has been investigated. Therefore, the planned short revisit and dual polarization concept of SENTINEL-1 has been simulated using multi-temporal ERS-2 and ENVISAT ASAR AP C-band backscatter intensity data. For classification, several multi-temporal metrics and the minimum amount of SAR data acquired during one growing season have been analyzed to derive five basic land cover classes with accuracies greater than 85%. [C1652]

#### "Exploring the potential of MODIS visible and thermal channels in monitoring and assessing the impact of desalination plant discharges in the Arabian Gulf"

Sea water desalination has experienced an unprecedented growth in the GCC countries to meet the ever growing demand of water for household consumption as well as for industrial and agricultural purposes. However, the current technologies used in water desalination are also accompanied by negative environmental impacts especially on the surrounding marine ecosystems. Since major seawater desalination plants are located by the shoreline, the main environmental considerations in desalination are water intakes and sea outfall discharges. We intent through this study to evaluate the potential of current polar orbiting satellites in evaluating the impact of desalination plant discharges, usually used to dispose of brine waste stream, on surrounding ecosystems and water quality. The objective of this project is to develop an automated approach for monitoring water quality and temperature (thermal properties) surrounding the discharges of desalination plants in the UAE coastal areas. Visible and thermal measurements provided by MODIS sensors on board of Terra and Aqua satellites are used in this project. The first four bands (visible) and band 31 & 32 (thermal) were selected. Future multi-spectral data from DubaiSat-1 (5-m resolution) will be also used to detect small changes in water color that cannot be detected with the MODIS data (250 m). [C1653]

#### "Land subsidence monitoring and Flood Simulation using multitemporal digital elevation models"

The over capacity use of the ground water usually results in the serious problems of land subsidence along the southwestern area in Taiwan. Therefore, how to monitor the land subsidence effectively will be an important study issue. The digital elevation models (DEMs) obtained by photogrammetry and remote sensing technologies provides more extensive height information on regular grids than traditional ground-based methods. However, it is not easy to perform the analysis of land subsidence when using the different DEM data sets with different resolution and accuracy. In this study, the least squares collocation (LSC) is proposed to adjust the low-precise

DEM data to high-precise leveling observations. The experimental results showed that the systematic errors of DEM data can be reduced using LSC, than the corrected DEM data can reveal more information of land subsidence in local areas. [C1654]

#### "Soil moisture retrieval from HUT-2D synthetic aperture radiometer data"

We have studied usage of our airborne L-band 2-D synthetic aperture radiometer HUT-2D for estimation of soil moisture. Measurements were conducted over three sites in Northern and Southern Finland in August 2007. Good results were achieved for bare soil and low vegetation, whereas soil moisture retrieval for forested areas requires further studies. [C1655]

#### "Soil moisture estimation using a multi-angular modified three component polarimetric decomposition"

In this paper a modified three component polarimetric decomposition incorporating multi-angular acquisitions is developed to estimate soil moisture under vegetation cover over agricultural areas. The approach is applied on fully-polarimetric L-band data acquired by DLR's airborne E-SAR sensor in the frame of the OPAQUE campaign conducted in May 2008 in the Weißeritz catchment area, near Dresden, Germany. The results for the estimated soil moisture from the overlapping area of the flight strips demonstrate a significant increase of the inversion rate, if more than one acquisition is used. The inverted soil moisture values are validated against in situ measurements for five test fields with different crop types resulting in an RMSE of approximately 7vol.% for different incidence angle constellations. Finally the results show how topographic effects in the soil moisture retrieval can be compensated by multi-angular constellations. [C1656]

#### "Polarimetric analysis from compact-pol measurements: Potential and limitation"

Global warming is now known to be the major environmental issue mankind will have to face in the next decade. Monitoring of vegetation and biomass is clearly an essential piece of information required at all levels ranging from the scientific studies to understand and forecast, to the political actors and government leaders responsible for drafting remediation policies and evaluating their impact. Microwave remote sensing with the low-frequency SAR technique can provide a useful characterization of forest (spatial coverage, species, density, height...) at a global scale, relying on the all-weather imaging capabilities of SAR linked with the significant penetration of the low-frequency EM wave in the canopy. The published techniques for forest characterization from low frequency SAR data include radiometry inversion, polarimetric inversion based on the anisotropy parameters and PolInSAR Random Volume Over Ground inversion. In this paper, we will more specifically concentrate on the PolSAR technique and the impact of ionospheric effect. [C1657]

#### "Microwave soil moisture retrieval under trees using a modified tau-omega model"

During 2007-2009 field experiments have been conducted using the ComRAD microwave truck instrument system with a goal of optimizing microwave soil moisture retrieval algorithms for small to medium deciduous and coniferous trees. A joint effort of NASA / GSFC and George Washington University, ComRAD consists of a quad-polarized 1.25 GHz radar and a dual-polarized 1.4 GHz radiometer sharing the same antenna. In the current study, ComRAD microwave data and ground truth measurements of soil moisture, temperature, soil texture, and vegetation water content and geometry statistics have been used to assess whether the zero-order tau-omega model can be employed successfully to retrieve soil moisture under tree canopies using effective values for tau (the vegetation opacity) and omega (the single scattering albedo). In addition, the tau-omega model has been modified to include a first-order scattering term, which will be discussed in a companion paper. [C1658]

#### "Waveform considerations for dual-polarization Doppler weather radar with solid-state transmitters"

Adequate sensitivity of weather radars using low-powered solid-state transmitter is achieved by using pulse compression waveforms. However, pulse compression waveforms have drawbacks of blind zone and range side lobes. In this paper, we present a methodology to address the major challenges in designing the waveforms for an X-band dual polarization Doppler radar operating with a solid-state transmitter. Here, frequency diversity wideband waveforms are proposed to mitigate low sensitivity of solid-state transmitters and the range eclipsing problem associated with pulse compression. An analysis of the performance of pulse compression using mismatched compression filters is reported. The performance of the proposed system is also quantified using signal and system simulations. [C1659]

#### "Detecting V-Storms using Meteosat Second Generation SEVIRI image and its applications: A case study over Western Turkey"

The present study focused on storm top observations utilizing the Meteosat Second Generation (MSG) data. The Spinning Enhanced Visible and Infrared Imager (SEVIRI) instrument aboard MSG provides image data with high spatial resolution (approximately 3 km) and high temporal resolution (15 minutes). This study used the thunderstorm event of 5 November 2007 over the Çiğli town in Western Turkey to provide an analysis of the enhanced-V satellite signature using MSG data. This signature was an important indicator of severe weather which can be used during weather warning operations to augment radar information. [C1660]

#### "Distributed targets detection based on local spectral histograms and agents"

To detect the distributed targets in SAR images of the sea, an algorithm based on local spectral histograms (LSH) and agents is proposed. The filter banks consist of the intensity filter and 36 Gaussian derivative filters at 6 orientations and 3 scales. After picking out the background images of the sea, the distribution of the difference value based on LSH is obtained. Given a probability, a threshold is achieved which will be used in judging behavior of the agent. Then an agent system is proposed, and a group of behaviors are introduced, including judging, moving, communicating, breeding, inheriting and dying behaviors. So the detection could be performed through the evolution of the agents. Several examples show that our algorithm is effective for different distributed targets. [C1661]

#### "Cloud amount and aerosol characteristic research in the atmosphere over Hubei province, China"

Although the Cloud-Aerosol Lidar with Orthogonal Polarization (CALIPSO) has been widely used in aerosol research, the classification of aerosol and cloud still presents some problems. The traditional classification method used by NASA is probability distribution functions (PDFs), but in reality, when we want to realize this algorithm, we find it is difficult to describe the multi-modal distribution of cloud backscatter coefficients. Further, because ice cloud and dust aerosol have some similar properties, it is not easy to identify them. In this paper, we introduce a classification method which is based on a support vector machine (SVM), and we add another characteristic. Then according to the result of classification inversion of the aerosol characteristic, the height of cloud top, at the same time, is combined with CloudSat data to calculate other cloud characters. These data will be helpful for further climate research. [C1662]

#### "Uncertainties in phase and frequency estimation with a magnetron radar: Implication for clear air measurements"

Radar systems with a drifting transmitter frequency (such as those employing magnetron transmitters) typically use an Automatic Frequency Control system to keep the receiver down-conversion settings tuned to the transmitted frequency. This paper presents a method to incorporate the Automated Frequency Control information in measurements affected by changing receiver frequency down-conversion settings, such as phase measurements to obtain change in refractivity fields. [C1663]

## СПИСОК ЛИТЕРАТУРЫ

- C1. Fan Bo. 3D Multiple Maneuvering Targets Tracking in Active and Passive Radar Composite Guidance. / Fan Bo, Qin Yu-liang, Wang Jian-tao, Xiao Huai-tie, Huang Pu-jian. // 2011 International Workshop on Multi-Platform/Multi-Sensor Remote Sensing and Mapping (M2RSM). - Xiamen, 10-12 Jan. 2011. - P. 1-6. ↑
- C2. Hui Wang. Determination of LIDAR Points Cloud Filtering Parameters Using Distance Image. / Hui Wang, Peng-cheng Li, Jun Liu, Li-yong Wang. // 2011 International Workshop on Multi-Platform/Multi-Sensor Remote Sensing and Mapping (M2RSM). - Xiamen, 10-12 Jan. 2011. - P. 1-4. ↑
- C3. Zheng-rong He. POLSAR Image Classification Based on Polarimetric Decomposition and Generalized Discriminant Analysis. / Zheng-rong He, Zhi Liu, Fan Wang, Yong-chang Chen. // 2011 International Workshop on Multi-Platform/Multi-Sensor Remote Sensing and Mapping (M2RSM). - Xiamen, 10-12 Jan. 2011. - P. 1-4. ↑
- C4. Chandrakanth R. Fusion of High Resolution Satellite SAR and Optical Images. / Chandrakanth R., Saibaba J., Varadan G., Raj P.A. // 2011 International Workshop on Multi-Platform/Multi-Sensor Remote Sensing and Mapping (M2RSM). - Xiamen, 10-12 Jan. 2011. - P. 1-6. ↑
- C5. Xin Yu. SAR Automatic Target Recognition Based on Classifiers Fusion. / Xin Yu, Yukuan Li, Jiao L.C. //

2011 International Workshop on Multi-Platform/Multi-Sensor Remote Sensing and Mapping (M2RSM). - Xiamen, 10-12 Jan. 2011. - P. 1-5. ↑

C6. Min Wang. High Resolution Radar Imaging Based on Compressed Sensing and Fast Bayesian Matching Pursuit. / Min Wang, Shuyuan Yang, Yanyan Wan, Jing Wang. // 2011 International Workshop on Multi-Platform/Multi-Sensor Remote Sensing and Mapping (M2RSM). - Xiamen, 10-12 Jan. 2011. - P. 1-5. ↑

C7. Hanyun Wang. Roof Detection in Lidar Data. / Hanyun Wang, Cheng Wang, Shengyong Hao. // 2011 International Workshop on Multi-Platform/Multi-Sensor Remote Sensing and Mapping (M2RSM). - Xiamen, 10-12 Jan. 2011. - P. 1-5. ↑

C8. Wang Na. A Novel Polarimetric CFAR Target Detection Method. / Wang Na, Liu Li, Hu Canbin, Kuang Gangyao, Jiang Yongmei. // 2011 International Workshop on Multi-Platform/Multi-Sensor Remote Sensing and Mapping (M2RSM). - Xiamen, 10-12 Jan. 2011. - P. 1-6. ↑

C9. Shuyuan Yang. Cooperative Synthetic Aperture Radar Image Segmentation Using Learning Sparse Representation Based Clustering Scheme. / Shuyuan Yang, Junlin Zhu, Zailin Hu, Min Wang, Licheng Jiao. // 2011 International Workshop on Multi-Platform/Multi-Sensor Remote Sensing and Mapping (M2RSM). - Xiamen, 10-12 Jan. 2011. - P. 1-6. ↑

C10. Changcheng Wang. Ship Detection after Removal of Ambiguities by Using PolSAR Images. 2011 International Workshop on Multi-Platform/Multi-Sensor Remote Sensing and Mapping (M2RSM). - Xiamen, 10-12 Jan. 2011. - P. 1-4. ↑

C11. Shuyuan Yang. Multitask Learning and Sparse Representation Based Super-Resolution Reconstruction of Synthetic Aperture Radar Images. / Shuyuan Yang, Zhizhou Liu, Min Wang, Fenghua Sun, Licheng Jiao. // 2011 International Workshop on Multi-Platform/Multi-Sensor Remote Sensing and Mapping (M2RSM). - Xiamen, 10-12 Jan. 2011. - P. 1-5. ↑

C12. Yu Chunrui. Adaptive RFI Suppression Algorithm Based on CEMD for SAR Data. / Yu Chunrui, Zhang Yongsheng, Dong Zhen, Liang Diannong. // 2011 International Workshop on Multi-Platform/Multi-Sensor Remote Sensing and Mapping (M2RSM). - Xiamen, 10-12 Jan. 2011. - P. 1-5. ↑

C13. Kiriazi J.E. Considerations in measuring vital signs cross section with Doppler radar. / Kiriazi J.E., Boric-Lubecke O., Lubecke V.M. // 2011 IEEE Radio and Wireless Symposium (RWS). - Phoenix, AZ, 16-19 Jan. 2011. - P. 426-429. ↑

C14. Sharma Shrikant. Mathematical analysis of interpolation step of Omega-K Algorithm for GPR and its implementation. / Sharma Shrikant, Jena Paramananda, Kuloor Ramachandra. // 2011 International Conference on Communications and Signal Processing (ICCSP). - Kerala, India, 10-12 Feb. 2011. - P. 46-50. ↑

C15. Ussyshkin R.V. Advantages of Airborne Lidar Technology in Power Line Asset Management. / Ussyshkin R.V., Theriault L., Sitar M., Kou T. // 2011 International Workshop on Multi-Platform/Multi-Sensor Remote Sensing and Mapping (M2RSM). - Xiamen, 10-12 Jan. 2011. - P. 1-5. ↑

C16. Liu A. A Novel Image Based Multi-Channel SAR-GMTI Algorithm. / Liu A., Li Chen, Fei Zhao, Gangyao Kuang. // 2011 International Workshop on Multi-Platform/Multi-Sensor Remote Sensing and Mapping (M2RSM). - Xiamen, 10-12 Jan. 2011. - P. 1-4. ↑

C17. Wang Wei. Airport Detection in SAR Image Based on Perceptual Organization. / Wang Wei, Liu Li, Hu Canbin, Jiang Yongmei, Kuang Gangyao. // 2011 International Workshop on Multi-Platform/Multi-Sensor Remote Sensing and Mapping (M2RSM). - Xiamen, 10-12 Jan. 2011. - P. 1-5. ↑

C18. Heaps W.S. One micron laser technology advancements at GSFC. 2010 IEEE International Geoscience and Remote Sensing Symposium (IGARSS). - Honolulu, HI, 25-30 July 2010. - P. 3110-3113. ↑

C19. Ramos-Perez I. On-ground tests and measurements of the Passive Advanced Unit Synthetic Aperture (PAU-SA). / Ramos-Perez I., Bosch-Lluis X., Camps A., Valencia E., Rodriguez-Alvarez N., Vall-Ilossera M., Forte G. // 2010 IEEE International Geoscience and Remote Sensing Symposium (IGARSS). - Honolulu, HI, 25-30 July 2010. - P. 3114-3117. ↑

C20. Heggy E. Coupling polarimetric L-Band insar and airborne lidar to characterize the geomorphological

deformations in the piton de la fournaise volcano. / Heggy E., Sedze M., Bretar F., Jacquemoud S., Rosen P.A., Wada K., Staudacher T. // 2010 IEEE International Geoscience and Remote Sensing Symposium (IGARSS). - Honolulu, HI, 25-30 July 2010. - P. 1911-1913. ↑

C21. Di Martino G. Fractal based filtering of SAR images. / Di Martino G., Iodice A., Riccio D., Ruello G., Zinno I. // 2010 IEEE International Geoscience and Remote Sensing Symposium (IGARSS). - Honolulu, HI, 25-30 July 2010. - P. 2984-2987. ↑

C22. Paden J. 3D imaging of ice sheets. / Paden J., Allen C., Gogineni P. // 2010 IEEE International Geoscience and Remote Sensing Symposium (IGARSS). - Honolulu, HI, 25-30 July 2010. - P. 2611-2613. ↑

C23. Tison C. Performance status of the wave scatterometer SWIM. / Tison C., Amiot T., Enjolras V., Hauser D., Rey L., Souyris J.C., Castillan P. // 2010 IEEE International Geoscience and Remote Sensing Symposium (IGARSS). - Honolulu, HI, 25-30 July 2010. - P. 4170-4173. ↑

C24. McNeill S.J. Robust estimation of pasture biomass using dual-polarisation TerrASAR-X imagery. / McNeill S.J., Pairman D., Belliss S.E., Dalley D., Dynes R. // 2010 IEEE International Geoscience and Remote Sensing Symposium (IGARSS). - Honolulu, HI, 25-30 July 2010. - P. 3094-3097. ↑

C25. Rochdi M. Physical optics-based method to compute the radar signature of complex objects over a sea surface. / Rochdi M., Baussard A., Khenchaf A. // 2010 IEEE International Geoscience and Remote Sensing Symposium (IGARSS). - Honolulu, HI, 25-30 July 2010. - P. 2976-2979. ↑

C26. Torres-Martinez E. Nasa's Laser Risk Reduction Program: A risk reduction approach for technology development. / Torres-Martinez E., Heaps W.S., Singh U.N. // 2010 IEEE International Geoscience and Remote Sensing Symposium (IGARSS). - Honolulu, HI, 25-30 July 2010. - P. 3106-3109. ↑

C27. Chunxiang Cao. Synchronous retrieval of forest canopy cover by airborne LiDAR and optical remote sensing. / Chunxiang Cao, Min Xu, Yunfei Bao, Hao Zhang. // 2010 IEEE International Geoscience and Remote Sensing Symposium (IGARSS). - Honolulu, HI, 25-30 July 2010. - P. 2660-2663. ↑

C28. Lorenzo J. Next generation of multi beam rotating antenna on SWIM scatterometer. / Lorenzo J., Demeestere F., Brossier J., Pouyez S., Enjolras V., Rey L., Amiot T., Tison C., Castillan P. // 2010 IEEE International Geoscience and Remote Sensing Symposium (IGARSS). - Honolulu, HI, 25-30 July 2010. - P. 3478-3481. ↑

C29. Sarti F. ESA Earth Observation educational tools contribution to the creation of awareness for World Heritage site conservation. / Sarti F., Hernandez M., Bigot J.C., Dransfeld S., Orient A.R. // 2010 IEEE International Geoscience and Remote Sensing Symposium (IGARSS). - Honolulu, HI, 25-30 July 2010. - P. 90-93. ↑

C30. Solberg R. A new global Snow Extent product based on ATSR-2 and AATSR. / Solberg R., Wangenstein B., Amlien J., Koren H., Metsajmaki S., Nagler T., Luoju K., Pulliainen J. // 2010 IEEE International Geoscience and Remote Sensing Symposium (IGARSS). - Honolulu, HI, 25-30 July 2010. - P. 1780-1783. ↑

C31. Porzycka S. The preliminary temporal analysis of ground deformations in the area of Dabrowski Coal Basin (south Poland). / Porzycka S., Le, sniak A. // 2010 IEEE International Geoscience and Remote Sensing Symposium (IGARSS). - Honolulu, HI, 25-30 July 2010. - P. 903-905. ↑

C32. Repasky K.S. Observational studies of atmospheric aerosols in the lower troposphere using multiple sensors. / Repasky K.S., Nehrir A.R., Hoffman D.S., Thomas M., Carlsten J.L., Shaw J.A. // 2010 IEEE International Geoscience and Remote Sensing Symposium (IGARSS). - Honolulu, HI, 25-30 July 2010. - P. 2583-2586. ↑

C33. Scipal K. The BIOMASS mission-An ESA Earth Explorer candidate to measure the BIOMASS of the earth's forests. / Scipal K., Arcioni M., Chave J., Dall J., Fois F., LeToan T., Lin C., Papathanassiou K., Quegan S., Rocca F., Saatchi S., Shugart H., Ulander L., Williams M. // 2010 IEEE International Geoscience and Remote Sensing Symposium (IGARSS). - Honolulu, HI, 25-30 July 2010. - P. 52-55. ↑

C34. Castorena J. Modeling lidar scene sparsity using compressive sensing. / Castorena J., Creusere C.D., Voelz D. // 2010 IEEE International Geoscience and Remote Sensing Symposium (IGARSS). - Honolulu, HI, 25-30 July 2010. - P. 2186-2189. ↑

- C35.** Nunziata F. Metallic objects and oil spill detection with multi-polarization SAR. / Nunziata F., Li X., Migliaccio M., Montuori A., Pichel W. // 2010 IEEE International Geoscience and Remote Sensing Symposium (IGARSS). - Honolulu, HI, 25-30 July 2010. - P. 2765-2768. ↑
- C36.** Floricioiu D. TerraSAR-X observations over the antarctic ice sheet. / Floricioiu D., Jezek K., Eineder M., Farness K., Abdel Jaber W., Yague-Martinez N. // 2010 IEEE International Geoscience and Remote Sensing Symposium (IGARSS). - Honolulu, HI, 25-30 July 2010. - P. 2614-2617. ↑
- C37.** Werner C. The snowcat ground-based polarimetric scatterometer: Calibration and initial measurements from Davos Switzerland. / Werner C., Wiesmann A., Strozzi T., Schneebeli M., Majtzer C. // 2010 IEEE International Geoscience and Remote Sensing Symposium (IGARSS). - Honolulu, HI, 25-30 July 2010. - P. 2363-2366. ↑
- C38.** Mahrooghy M. Infrared satellite precipitation estimate using waveletbased cloud classification and radar calibration. / Mahrooghy M., Anantharaj V.G., Younan N.H., Petersen W.A., Turk F.J., Aanstoots J. // 2010 IEEE International Geoscience and Remote Sensing Symposium (IGARSS). - Honolulu, HI, 25-30 July 2010. - P. 2345-2348. ↑
- C39.** Even M. Atmospheric phase screen-estimation for PSInSAR applied to TerraSAR-X high resolution spotlight-data. / Even M., Schunert A., Schulz K., Soergel U. // 2010 IEEE International Geoscience and Remote Sensing Symposium (IGARSS). - Honolulu, HI, 25-30 July 2010. - P. 2928-2931. ↑
- C40.** Di Zhu. Doppler effect and compensation in a Rotating Fanbeam Spaceborne Scatterometer. / Di Zhu, Xiaolong Dong, Wenming Lin, Yun R. // 2010 IEEE International Geoscience and Remote Sensing Symposium (IGARSS). - Honolulu, HI, 25-30 July 2010. - P. 1089-1091. ↑
- C41.** My-Linh Truong-Loi. Potentials of a compact polarimetric SAR system. / My-Linh Truong-Loi, Dubois-Fernandez P., Pottier E., Freeman A., Souyris J.-C. // 2010 IEEE International Geoscience and Remote Sensing Symposium (IGARSS). - Honolulu, HI, 25-30 July 2010. - P. 742-745. ↑
- C42.** Hyoung-sun Youn. In-situ broadband soil measurements: Dielectric and magnetic properties. / Hyoung-sun Youn, Loon Yip Lee, Iskander M. // 2010 IEEE International Geoscience and Remote Sensing Symposium (IGARSS). - Honolulu, HI, 25-30 July 2010. - P. 4483-4486. ↑
- C43.** Sportouche H. Building detection and height retrieval in urban areas in the framework of high resolution optical and SAR data fusion. / Sportouche H., Tupin F., Denise L. // 2010 IEEE International Geoscience and Remote Sensing Symposium (IGARSS). - Honolulu, HI, 25-30 July 2010. - P. 3660-3663. ↑
- C44.** Ying Liu. Remote sensing image synthesis. / Ying Liu, Wong A., Fieguth P. // 2010 IEEE International Geoscience and Remote Sensing Symposium (IGARSS). - Honolulu, HI, 25-30 July 2010. - P. 2467-2470. ↑
- C45.** Schmidt M. Estimation of building density using Terrasar-X-Data. / Schmidt M., Esch T., Klein D., Thiel M., Dech S. // 2010 IEEE International Geoscience and Remote Sensing Symposium (IGARSS). - Honolulu, HI, 25-30 July 2010. - P. 1936-1939. ↑
- C46.** Hillman A. RADARSAT-2 continuing system operations and performance. / Hillman A., Rolland P., Pe,riard R., Luscombe A., Chabot M., Chen C., Martens N. // 2010 IEEE International Geoscience and Remote Sensing Symposium (IGARSS). - Honolulu, HI, 25-30 July 2010. - P. 3228-3231. ↑
- C47.** Sun-Mack S. Enhanced Cloud algorithm from collocated CALIPSO, CloudSat and MODIS global boundary layer lapse rate studies. / Sun-Mack S., Minnis P., Kato S., Yan Chen, Yuhong Yi, Gibson S., Heck P., Winker D., Ayers K. // 2010 IEEE International Geoscience and Remote Sensing Symposium (IGARSS). - Honolulu, HI, 25-30 July 2010. - P. 201-204. ↑
- C48.** Brigui F. Oblique polarimetric SAR processor based on signal and interference subspace models. / Brigui F., Thiron-Lefevre L., Ginolhac G., Forster P. // 2010 IEEE International Geoscience and Remote Sensing Symposium (IGARSS). - Honolulu, HI, 25-30 July 2010. - P. 4027-4030. ↑
- C49.** Brolly M. A Matchstick Model of microwave backscatter from a forest: A change of regime. / Brolly M., Woodhouse I.H. // 2010 IEEE International Geoscience and Remote Sensing Symposium (IGARSS). - Honolulu, HI, 25-30 July 2010. - P. 3295-3298. ↑

- C50.** Lei Shi. Multichannel Coherent Radar Depth Sounder for NASA Operation Ice Bridge. / Lei Shi, Allen C.T., Ledford J.R., Rodriguez-Morales F., Blake W.A., Panzer B.G., Prokopiack S.C., Leuschen C.J., Gogineni S. // 2010 IEEE International Geoscience and Remote Sensing Symposium (IGARSS). - Honolulu, HI, 25-30 July 2010. - P. 1729-1732. ↑
- C51.** Kidd C. Investigations into high resolution mapping of precipitation features utilizing the TRMM precipitation Radar. / Kidd C., Kwiatkowski J., Nesbitt S. // 2010 IEEE International Geoscience and Remote Sensing Symposium (IGARSS). - Honolulu, HI, 25-30 July 2010. - P. 2337-2340. ↑
- C52.** Capria A. DVB-T passive radar for vehicles detection in urban environment. / Capria A., Petri D., Martorella M., Conti M., Dalle Mese E., Berizzi F. // 2010 IEEE International Geoscience and Remote Sensing Symposium (IGARSS). - Honolulu, HI, 25-30 July 2010. - P. 3917-3920. ↑
- C53.** Toporkov J.V. Observation of a boat and its wake with a Dual-Beam along-track interferometric sar. / Toporkov J.V., Hwang P.A., Sletten M.A., Frasier S.J., Farquharson G., Perkovic D. // 2010 IEEE International Geoscience and Remote Sensing Symposium (IGARSS). - Honolulu, HI, 25-30 July 2010. - P. 1940-1943. ↑
- C54.** Mitchell A.L. Wall-to-wall mapping of forest extent and change in Tasmania using ALOS PALSAR data. / Mitchell A.L., Milne A., Tapley I., Lowell K., Caccetta P., Lehmann E., Zheng-Shu Zhou. // 2010 IEEE International Geoscience and Remote Sensing Symposium (IGARSS). - Honolulu, HI, 25-30 July 2010. - P. 1230-1233. ↑
- C55.** Fabra F. Monitoring sea-ice and dry snow with GNSS reflections. / Fabra F., Cardellach E., Nogues-Correig O., Oliveras S., Ribo S., Rius A., Belmonte-Rivas M., Semmling M., Macelloni G., Pettinato S., Zasso R., D'Addio S. // 2010 IEEE International Geoscience and Remote Sensing Symposium (IGARSS). - Honolulu, HI, 25-30 July 2010. - P. 3837-3840. ↑
- C56.** Ebuchi N. AMSR and DFS synergy. / Ebuchi N., Liu W.T. // 2010 IEEE International Geoscience and Remote Sensing Symposium (IGARSS). - Honolulu, HI, 25-30 July 2010. - P. 1812-1814. ↑
- C57.** Chabert M. Logistic regression for detecting changes between databases and remote sensing images. / Chabert M., Tournet J.-Y., Poulain V., Inglada J. // 2010 IEEE International Geoscience and Remote Sensing Symposium (IGARSS). - Honolulu, HI, 25-30 July 2010. - P. 3198-3201. ↑
- C58.** Schmitt M. Utilization of airborne multi-aspect InSAR data for the generation of urban ortho-images. / Schmitt M., Stilla U. // 2010 IEEE International Geoscience and Remote Sensing Symposium (IGARSS). - Honolulu, HI, 25-30 July 2010. - P. 3937-3940. ↑
- C59.** Praks J. Polarimetric sar image visualization and interpretation with covariance matrix invariants. / Praks J., Hallikainen M., Koeniguer E.C. // 2010 IEEE International Geoscience and Remote Sensing Symposium (IGARSS). - Honolulu, HI, 25-30 July 2010. - P. 2035-2038. ↑
- C60.** Venkataraman G. Fully polarimetric ALOS PALSAR data applications for snow and ice studies. / Venkataraman G., Singh G., Yamaguchi Y. // 2010 IEEE International Geoscience and Remote Sensing Symposium (IGARSS). - Honolulu, HI, 25-30 July 2010. - P. 1776-1779. ↑
- C61.** Gonzalez J.H. TanDEM-X commissioning phase status. / Gonzalez J.H., Bachmann M., Hofmann H. // 2010 IEEE International Geoscience and Remote Sensing Symposium (IGARSS). - Honolulu, HI, 25-30 July 2010. - P. 2633-2635. ↑
- C62.** {no data available}. Copyright. 2010 IEEE International Geoscience and Remote Sensing Symposium (IGARSS). - Honolulu, HI, 25-30 July 2010. - P. ii. ↑
- C63.** Di Martino G. Physical-based models of speckle for high resolution SAR images. / Di Martino G., Iodice A., Riccio D., Ruello G. // 2010 IEEE International Geoscience and Remote Sensing Symposium (IGARSS). - Honolulu, HI, 25-30 July 2010. - P. 2980-2983. ↑
- C64.** Paladini R. Fetch limited sea scattering spectral model for HF-OTH skywave radar. / Paladini R., Dalle Mese E., Berizzi F., Garzelli A., Martorella M., Capria A. // 2010 IEEE International Geoscience and Remote Sensing Symposium (IGARSS). - Honolulu, HI, 25-30 July 2010. - P. 4177-4180. ↑
- C65.** Okamoto K. Surface reference normalized radar cross section over land for the improvement of the

TRMM PR algorithm. / Okamoto K., Komukai J., Shige S., Manabe T. // 2010 IEEE International Geoscience and Remote Sensing Symposium (IGARSS). - Honolulu, HI, 25-30 July 2010. - P. 1316-1318. ↑

C66. Yun Shao. Applications of polarimetric decomposition technology in a dried up lake evolution. / Yun Shao, Huaze Gong, Guojun Wang, Aimin Cai. // 2010 IEEE International Geoscience and Remote Sensing Symposium (IGARSS). - Honolulu, HI, 25-30 July 2010. - P. 4499-4502. ↑

C67. Sixin Liu. Electromagnetic simulations of borehole radar for metal ore detection. / Sixin Liu, Junfeng Zhou, Junjun Wu, Zhaofa Zeng. // 2010 IEEE International Geoscience and Remote Sensing Symposium (IGARSS). - Honolulu, HI, 25-30 July 2010. - P. 2992-2994. ↑

C68. Kubota T. Development of spaceborne radar simulator by NICT and JAXA using JMA cloud-resolving model. / Kubota T., Eito H., Aonashi K., Hashimoto A., Iguchi T., Hanado H., Shimizu S., Yoshida N., Oki R. // 2010 IEEE International Geoscience and Remote Sensing Symposium (IGARSS). - Honolulu, HI, 25-30 July 2010. - P. 1304-1307. ↑

C69. Gaohuan Lv. Reciprocal spectrum algorithm for radar imaging with frequency sampling waveform. / Gaohuan Lv, Kaizhi Wang, Xingzhao Liu, Wenxian Yu, Guozhong Chen, Junli Chen. // 2010 IEEE International Geoscience and Remote Sensing Symposium (IGARSS). - Honolulu, HI, 25-30 July 2010. - P. 4683-4685. ↑

C70. Chandrasekar V. Scientific and engineering overview of the NASA Dual-Frequency Dual-Polarized Doppler Radar (D3R) system for GPM Ground Validation. / Chandrasekar V., Schwaller M., Vega M., Carswell J., Mishra K.V., Meneghini R., Cuong Nguyen. // 2010 IEEE International Geoscience and Remote Sensing Symposium (IGARSS). - Honolulu, HI, 25-30 July 2010. - P. 1308-1311. ↑

C71. Lijun Lu. A Study on Extraction of Man-Made Targets Using SVM Method from High Resolution PolInSAR Data. / Lijun Lu, Jixian Zhang, Guoman Huang. // 2010 International Conference on Multimedia Technology (ICMT). - Ningbo, 29-31 Oct. 2010. - P. 1-5. ↑

C72. Bin Pan. A New Approach on Topographic Feature Point Extraction of SAR Imagery. / Bin Pan, Peng Chen, Ming Cong. // 2010 International Conference on Multimedia Technology (ICMT). - Ningbo, 29-31 Oct. 2010. - P. 1-4. ↑

C73. Maosong Xu. Multi-Temporal Polarimetric SAR and Optical Data Fusion for Land Cover Mapping in Southwest China. / Maosong Xu, Zhongsheng Xia, Fengli Zhang, Kun Li, Chou Xie. // 2010 International Conference on Multimedia Technology (ICMT). - Ningbo, 29-31 Oct. 2010. - P. 1-4. ↑

C74. Liying Wang. Airborne LiDAR Strip Adjustment Based on Least Z-Difference Algorithm. / Liying Wang, Weidong Song. // 2010 International Conference on Multimedia Technology (ICMT). - Ningbo, 29-31 Oct. 2010. - P. 1-5. ↑

C75. Yongzheng Ren. Wind Field Retrieval over the Ocean by HH Polarization TerraSAR-X Data. / Yongzheng Ren, Mingxia He, Lehner S. // 2010 International Conference on Multimedia Technology (ICMT). - Ningbo, 29-31 Oct. 2010. - P. 1-4. ↑

C76. Jia YouLiang. Identify Islands by Complex SAR Image. / Jia YouLiang, Ma HuaShan. // 2010 International Conference on Multimedia Technology (ICMT). - Ningbo, 29-31 Oct. 2010. - P. 1-4. ↑

C77. Hongchao Ma. A Methodology for Trees' Detection Using LiDAR Data in Urban Areas. / Hongchao Ma, Chunjing Yao. // 2010 International Conference on Multimedia Technology (ICMT). - Ningbo, 29-31 Oct. 2010. - P. 1-4. ↑

C78. Jianwei Wu. Airborne LiDAR Data Strip Adjustment Based on Least Squares Matching and Independent Model. // 2010 International Conference on Multimedia Technology (ICMT). - Ningbo, 29-31 Oct. 2010. - P. 1-4. ↑

C79. Han Yun. Influence and Analysis of IMU Attitude Measurement Error on Laser Point Accuracy. / Han Yun, Cheng Xin-wen, Sun Hua, Zhao Li-jian. // 2010 International Conference on Electrical and Control Engineering (ICECE). - Wuhan, 25-27 June 2010. - P. 1196-1199. ↑

C80. Godana B. Quantifying Human Indoor Activity Using a Software Radio-Based Radar. / Godana B., Leus G., Barroso A. // 2010 First International Conference on Sensor Device Technologies and Applications (SENSORDEVICES). - Venice, 18-25 July 2010. - P. 38-43. ↑

- C81. Zhou Jiao. A Study on Removal of Radial Interference Echo with Weather Radar. / Zhou Jiao, Gao Yuchun. // 2010 International Conference on Multimedia Technology (ICMT). - Ningbo, 29-31 Oct. 2010. - P. 1-5. ↑
- C82. Hongchao Ma. A Novel Method for Linear Features Extraction from Raw LiDAR Point Clouds. / Hongchao Ma, Chunjing Yao. // 2010 International Conference on Multimedia Technology (ICMT). - Ningbo, 29-31 Oct. 2010. - P. 1-3. ↑
- C83. Qiang Zhou. A Speckle Reduction Method Based on Hyperspectral and SAR Image Fusion. / Qiang Zhou, Peng Gong, Ziqi Guo. // 2010 International Conference on Multimedia Technology (ICMT). - Ningbo, 29-31 Oct. 2010. - P. 1-5. ↑
- C84. Zhengrong Li. Advances in vegetation management for power line corridor monitoring using aerial remote sensing techniques. / Zhengrong Li, Walker R., Hayward R., Mejias L. // 2010 1st International Conference on Applied Robotics for the Power Industry (CARPI). - Montreal, QC, 5-7 Oct. 2010. - P. 1-6. ↑
- C85. Zhanjun Song. Research on the Method of Airborne SAR Direct Geocoding Based on Correction of Systematic Error. / Zhanjun Song, Jixian Zhang, Guoman Huang, Zheng Zhao, Jujie Wei. // 2010 International Conference on Multimedia Technology (ICMT). - Ningbo, 29-31 Oct. 2010. - P. 1-4. ↑
- C86. Gengkang Yu. Application of ENVISAT ASAR Data to Rice Monitoring in Jiangsu Province, China. / Gengkang Yu, Shenbin Yang, Xiaoyan Zhao, Shuanghe Shen. // 2010 International Conference on Multimedia Technology (ICMT). - Ningbo, 29-31 Oct. 2010. - P. 1-3. ↑
- C87. Valentin M. Coastal Radar WERA, a tool for Search and Rescue and oil spill management. / Valentin M., Helzel T., Mariette V., Thomas N. // 2010 IEEE/OES US/EU Baltic International Symposium (BALTIC). - Riga, 24-27 Aug. 2010. - P. 1-4. ↑
- C88. Raudsepp U. Use of earth observation data and numerical modeling in the development of marine downstream services in Estonia. / Raudsepp U., Uiboupin R., Sipelgas L., Lagemaa P., Kouts T., Lips U. // 2010 IEEE/OES US/EU Baltic International Symposium (BALTIC). - Riga, 24-27 Aug. 2010. - P. 1-11. ↑
- C89. Zhou Zengpo. Mosaic in g the ocean/terrestrial SRTM-DEM and making t he geomorphologic relief shading map. / Zhou Zengpo, Cheng Weiming. // 2010 International Conference on Computer Application and System Modeling (ICCSM). - Taiyuan, 22-24 Oct. 2010. - Vol. 9. - P. V9-653-V9-657-653. ↑
- C90. YanRu Xue. Design and Implementation of Wireless FAEM System Based on the ZigBee and GPRS. / YanRu Xue, Min Liu. // 2010 International Conference on Electrical and Control Engineering (ICECE). - Wuhan, 25-27 June 2010. - P. 2726-2728. ↑
- C91. Jiangping Long. Monitoring Ground Subsidence in New Orleans with Persistent Scatterers Interferometry. / Jiangping Long, Xiaoli Ding. // 2010 International Conference on Multimedia Technology (ICMT). - Ningbo, 29-31 Oct. 2010. - P. 1-5. ↑
- C92. Kun Li. Paddy Rice Identification Using Polarimetric SAR Data in Southern China. / Kun Li, Yun Shao, Fengli Zhang. // 2010 International Conference on Multimedia Technology (ICMT). - Ningbo, 29-31 Oct. 2010. - P. 1-4. ↑
- C93. Lina Xu. Soil Moisture Estimation over Jiangnan Plain Using ENVISAT ASAR Data. / Lina Xu, Jiong Li, Ruiqing Niu. // 2010 International Conference on Multimedia Technology (ICMT). - Ningbo, 29-31 Oct. 2010. - P. 1-4. ↑
- C94. Hao Hongmei. The Application of Optimal Polarization Theory in Polarimetric SAR Change Detection. / Hao Hongmei, Zhang Yonghong. // 2010 International Conference on Multimedia Technology (ICMT). - Ningbo, 29-31 Oct. 2010. - P. 1-3. ↑
- C95. Bo Wang. Subsidence Monitoring by Permanent Scatterers in InSAR: A Case Study of Yancheng City in Jiangsu. / Bo Wang, Suozhong Chen, Hongyan Yi, Lei Mao. // 2010 International Conference on Multimedia Technology (ICMT). - Ningbo, 29-31 Oct. 2010. - P. 1-6. ↑
- C96. Zhu Hao. The Application of Electric Field Data Combined with Other Observed Data in Lightning Warning. / Zhu Hao, Yang Zhongjiang, Yang Tianqi. // 2010 International Conference on Multimedia Technology

(ICMT). - Ningbo, 29-31 Oct. 2010. - P. 1-4. ↑

C97. Velichko D.A. The gauging-measuring system model with controllable retransmitter structure. / Velichko D.A., Velichko S.A. // 2010 20th International Crimean Conference Microwave and Telecommunication Technology (CriMiCo). - Sevastopol, 13-17 Sept. 2010. - P. 1023-1024. ↑

C98. McPherson C. Progress in the validation of dual-wavelength aerosol retrieval models via airborne high spectral resolution lidar data. / McPherson C., Reagan J., Hostetler C., Hair J., Ferrare R. // 2010 IEEE International Geoscience and Remote Sensing Symposium (IGARSS). - Honolulu, HI, 25-30 July 2010. - P. 1714-1717. ↑

C99. Zhang C. Focal plane approximation for near field interferometric radiometer imaging. / Zhang C., Wu J., Liu H., Yan J.Y. // 2010 IEEE International Geoscience and Remote Sensing Symposium (IGARSS). - Honolulu, HI, 25-30 July 2010. - P. 3118-3121. ↑

C100. Velotto D. Oil-slick observation using single look complex TerraSAR-X dual-polarized data. / Velotto D., Migliaccio M., Nunziata F., Lehner S. // 2010 IEEE International Geoscience and Remote Sensing Symposium (IGARSS). - Honolulu, HI, 25-30 July 2010. - P. 3684-3687. ↑

C101. Haizhong Ma. Simulation of Faraday rotation on longer wavelength spaceborne polarimetric InSAR. / Haizhong Ma, Jie Chen, Xunjun Yin. // 2010 3rd International Congress on Image and Signal Processing (CISP). - Yantai, 16-18 Oct. 2010. - Vol. 5. - P. 2255-2259. ↑

C102. Franklin A.G. Prospects of new real-time radar applications for environmental remote sensing. / Franklin A.G., Coronado P.L. // 2010 IEEE International Geoscience and Remote Sensing Symposium (IGARSS). - Honolulu, HI, 25-30 July 2010. - P. 1914-1917. ↑

C103. Sun G. Simulation studies on data fusion algorithms for forest structure from lidar and SAR data. / Sun G., Ni W., Ranson K.J. // 2010 IEEE International Geoscience and Remote Sensing Symposium (IGARSS). - Honolulu, HI, 25-30 July 2010. - P. 3287-3290. ↑

C104. Hashimoto S. Case studies of automatic change detection using AVNIR-2 onboard ALOS. / Hashimoto S., Onosato M., Tadono T., Hori M., Moriyama T. // 2010 IEEE International Geoscience and Remote Sensing Symposium (IGARSS). - Honolulu, HI, 25-30 July 2010. - P. 3644-3647. ↑

C105. Singh G. Temporal snowpack density mapping using C-band multi-polarization ASAR data. / Singh G., Venkataraman G., Yamaguchi Y., Park S.E. // 2010 IEEE International Geoscience and Remote Sensing Symposium (IGARSS). - Honolulu, HI, 25-30 July 2010. - P. 1784-1787. ↑

C106. Biao Zhang. A new polarization ratio model from C-Band RADARSAT-2 fine Quad-Pol imagery. / Biao Zhang, Perrie W., Hwang P.A., Yijun He. // 2010 IEEE International Geoscience and Remote Sensing Symposium (IGARSS). - Honolulu, HI, 25-30 July 2010. - P. 1948-1951. ↑

C107. Gimmestad G. Lidar education at Georgia Tech. / Gimmestad G., West L. // 2010 IEEE International Geoscience and Remote Sensing Symposium (IGARSS). - Honolulu, HI, 25-30 July 2010. - P. 87-89. ↑

C108. Foucher S. Exploitation of the additive component of the polarimetric noise model for speckle filtering. / Foucher S., Farage G., Lopez-Martinez C. // 2010 IEEE International Geoscience and Remote Sensing Symposium (IGARSS). - Honolulu, HI, 25-30 July 2010. - P. 312-315. ↑

C109. Brajutigam B. SAR performance monitoring for TerraSAR-X mission. / Brajutigam B., Rizzoli P., Gonzalez C., Weigt M., Schrank D., Schulze D., Schwerdt M. // 2010 IEEE International Geoscience and Remote Sensing Symposium (IGARSS). - Honolulu, HI, 25-30 July 2010. - P. 3454-3457. ↑

C110. Nelson R. Using airborne & space lidars for large-area inventory. / Nelson R., Stehl G., Holm S., Gregoire T., Naesset E., Gobakken T. // 2010 IEEE International Geoscience and Remote Sensing Symposium (IGARSS). - Honolulu, HI, 25-30 July 2010. - P. 2463-2466. ↑

C111. Prudyus I.N. Construction approach of integrated remote sensing systems based on the partial channels. / Prudyus I.N., Zubkov A.N., Sumyk M.N., Lazko L.V., Mymrikov D.A., Yankevych R.V. // 2010 20th International Crimean Conference Microwave and Telecommunication Technology (CriMiCo). - Sevastopol, 13-17 Sept. 2010. - P. 1219-1220. ↑

- C112.** Voitovych O.A. Use of double frequency radar for measurement of reflectance-intensity dependence. / Voitovych O.A., Linkova A.M., Khlopov G.I., Khomenko S.I. // 2010 20th International Crimean Conference Microwave and Telecommunication Technology (CriMiCo). - Sevastopol, 13-17 Sept. 2010. - P. 1185-1186. ↑
- C113.** Yang Zhang. Simulation research of microwave automatic clutter-cancellation in life-detection radar. / Yang Zhang, Zhao Li, Teng Jiao, Hao Lv, Jianqi Wang. // 2010 3rd International Conference on Biomedical Engineering and Informatics (BMEI). - Yantai, 16-18 Oct. 2010. - Vol. 5. - P. 2098-2100. ↑
- C114.** Khomenko S.I. Doppler radar method for plasma structure investigation. / Khomenko S.I., Khorunzhiy M.O., Kuleshov A.N., Yefimov B.P. // 2010 20th International Crimean Conference Microwave and Telecommunication Technology (CriMiCo). - Sevastopol, 13-17 Sept. 2010. - P. 1025-1026. ↑
- C115.** Atroshenko L.M. Radiophysics features of agrarian reference sites at base subsatellite landfill "skripai". / Atroshenko L.M., Gorobets N.N., Kazachenko L.M., Onischenko A.A., Rokhmanov N.Y., Safronova L.P. // 2010 20th International Crimean Conference Microwave and Telecommunication Technology (CriMiCo). - Sevastopol, 13-17 Sept. 2010. - P. 1210-1211. ↑
- C116.** Garmash K.P. Electrodynamic processes in the electrically active mesosphere. / Garmash K.P., Gritchin A.I., Martynenko S.I., Rozumenko V.T., Tyrnov O.F. // 2010 20th International Crimean Conference Microwave and Telecommunication Technology (CriMiCo). - Sevastopol, 13-17 Sept. 2010. - P. 1181-1182. ↑
- C117.** Dong Wang. Water objects extraction from polarimetric SAR imagery based on blind source separation and morphological reconstruction. / Dong Wang, Weifeng Zhou, Wei Fan, Xingwei Jiang, Ping Qin. // 2010 3rd International Congress on Image and Signal Processing (CISP). - Yantai, 16-18 Oct. 2010. - Vol. 3. - P. 1028-1032. ↑
- C118.** Kai Liu. Fish-pond change detection based on short term time series of RADARSAT images and object-oriented method. / Kai Liu, Bin Ai, Shugong Wang. // 2010 3rd International Congress on Image and Signal Processing (CISP). - Yantai, 16-18 Oct. 2010. - Vol. 5. - P. 2175-2179. ↑
- C119.** Pei Wang. Research on extracting the tree height based on LiDAR data. 2010 3rd International Congress on Image and Signal Processing (CISP). - Yantai, 16-18 Oct. 2010. - Vol. 5. - P. 2236-2239. ↑
- C120.** Jianmin Wang. Wetland cover information extraction research based on the multi-polar radar images and multi-spectrum optical images fusion. / Jianmin Wang, Fanshuai Meng, Huan Yu. // 2010 3rd International Congress on Image and Signal Processing (CISP). - Yantai, 16-18 Oct. 2010. - Vol. 5. - P. 2298-2301. ↑
- C121.** Li-hua Wang. Classifying multisensor images by support vector machine in Chongming Dongtan. / Li-hua Wang, Yun-xuan Zhou, Xing Li. // 2010 3rd International Congress on Image and Signal Processing (CISP). - Yantai, 16-18 Oct. 2010. - Vol. 5. - P. 2134-2138. ↑
- C122.** Liying Wang. Airborne LiDAR strip adjustment based on LSM. / Liying Wang, Zhengjun Liu, Weidong Song, Haitao Li. // 2010 3rd International Congress on Image and Signal Processing (CISP). - Yantai, 16-18 Oct. 2010. - Vol. 6. - P. 2727-2731. ↑
- C123.** Feng Wang. Estimation of significant wave height from X-band marine radar images. / Feng Wang, Jian Wang, Shujuan Wang. // 2010 3rd International Congress on Image and Signal Processing (CISP). - Yantai, 16-18 Oct. 2010. - Vol. 5. - P. 2172-2174. ↑
- C124.** Duque S. Bistatic SAR tomography: Processing and experimental results. / Duque S., Lopez-Dekker P., Merlano J.C., Mallorqui J.J. // 2010 IEEE International Geoscience and Remote Sensing Symposium (IGARSS). - Honolulu, HI, 25-30 July 2010. - P. 154-157. ↑
- C125.** Dhar T. Estimation of pasture biomass and soil-moisture using dual-polarimetric X and L band SAR-accuracy assessment with field data. / Dhar T., Menges C., Douglas J., Schmidt M., Armston J. // 2010 IEEE International Geoscience and Remote Sensing Symposium (IGARSS). - Honolulu, HI, 25-30 July 2010. - P. 1450-1453. ↑
- C126.** Xiaoying Cong. Diverse methods to monitoring volcanic deformation based on SAR interferometry. / Xiaoying Cong, Eineder M., Gernhardt S., Minet C. // 2010 IEEE International Geoscience and Remote Sensing Symposium (IGARSS). - Honolulu, HI, 25-30 July 2010. - P. 661-664. ↑

- C127.** Hwang P.A. Breaking wave measurements with sar depolarized returns. / Hwang P.A., Biao Zhang, Perrie W. // 2010 IEEE International Geoscience and Remote Sensing Symposium (IGARSS). - Honolulu, HI, 25-30 July 2010. - P. 1952-1955. ↑
- C128.** Dhar T. Supporting precision agriculture with dual-polarimetric TerraSAR-X-yield prediction and identification of in-field variations to generate fertilizer prescription maps. / Dhar T., Menges C., Gray D., Douglas J., Wilksch L. // 2010 IEEE International Geoscience and Remote Sensing Symposium (IGARSS). - Honolulu, HI, 25-30 July 2010. - P. 1446-1449. ↑
- C129.** Matsuoka M. Estimation of building damage ratio due to earthquakes and tsunamis using satellite SAR imagery. / Matsuoka M., Koshimura S., Nojima N. // 2010 IEEE International Geoscience and Remote Sensing Symposium (IGARSS). - Honolulu, HI, 25-30 July 2010. - P. 3347-3349. ↑
- C130.** Studinger M. Operation icebridge: Using instrumented aircraft to bridge the observational gap between icesat and icesat-2. / Studinger M., Koenig L., Martin S., Sonntag J. // 2010 IEEE International Geoscience and Remote Sensing Symposium (IGARSS). - Honolulu, HI, 25-30 July 2010. - P. 1918-1919. ↑
- C131.** Fjш. KaRIn-the Ka-band radar interferometer on SWOT: Measurement principle, processing and data specificities. / Fjш, toft R., Gaudin J.-M., Pourthie N., Lion C., Mallet A., Souyris J.-C., Ruiz C., Koudogbo F., Duro J., Ordoqui P., Arnaud A. // 2010 IEEE International Geoscience and Remote Sensing Symposium (IGARSS). - Honolulu, HI, 25-30 July 2010. - P. 4823-4826. ↑
- C132.** Le Yang. Use of the merged dual-frequency radar altimeter backscatter data over China land surface. / Le Yang, Hejuan Du, Hongzhang Ma, Qinhua Liu. // 2010 IEEE International Geoscience and Remote Sensing Symposium (IGARSS). - Honolulu, HI, 25-30 July 2010. - P. 1454-1457. ↑
- C133.** Milan L. Longtime monitoring of mine subsidence in Northern Moravia, Czech republic using different insar techniques. / Milan L., Eva J. // 2010 IEEE International Geoscience and Remote Sensing Symposium (IGARSS). - Honolulu, HI, 25-30 July 2010. - P. 3331-3334. ↑
- C134.** Pantze A. Forest change detection from L-band satellite SAR images using iterative histogram matching and thresholding together with data fusion. / Pantze A., Fransson J.E.S., Santoro M. // 2010 IEEE International Geoscience and Remote Sensing Symposium (IGARSS). - Honolulu, HI, 25-30 July 2010. - P. 1226-1229. ↑
- C135.** Torrione P. Spatial latency reduction in GPR processing using stochastic sampling. / Torrione P., Collins L. // 2010 IEEE International Geoscience and Remote Sensing Symposium (IGARSS). - Honolulu, HI, 25-30 July 2010. - P. 3354-3357. ↑
- C136.** Martorella M. Optimal sensor positioning for ISAR imaging. 2010 IEEE International Geoscience and Remote Sensing Symposium (IGARSS). - Honolulu, HI, 25-30 July 2010. - P. 4819-4822. ↑
- C137.** Villard L. Topography effects on forest radar scattering, consequences on biomass retrieval. / Villard L., Borderies P., Le Toan T., Koleček T., Albinet C. // 2010 IEEE International Geoscience and Remote Sensing Symposium (IGARSS). - Honolulu, HI, 25-30 July 2010. - P. 60-63. ↑
- C138.** Magnard C. Processing of MEMPHIS millimeter wave multi-baseline InSAR data. / Magnard C., Meier E., Small D., Essen H., Brehm T. // 2010 IEEE International Geoscience and Remote Sensing Symposium (IGARSS). - Honolulu, HI, 25-30 July 2010. - P. 4302-4305. ↑
- C139.** Ling Lei. Monitoring slow moving landslides in the Berkeley Hills with TerraSAR-X data. / Ling Lei, Yinqing Zhou, Jingwen Li, Burgmann R. // 2010 IEEE International Geoscience and Remote Sensing Symposium (IGARSS). - Honolulu, HI, 25-30 July 2010. - P. 230-232. ↑
- C140.** Pablos-Vega G.A. Development of an Off-The-Grid X-band radar for weather applications. / Pablos-Vega G.A., Colom-Usta, riz J.G., Cruz-Pol S., Trabal J.M., Chandrasekar V., George J., Junyent F. // 2010 IEEE International Geoscience and Remote Sensing Symposium (IGARSS). - Honolulu, HI, 25-30 July 2010. - P. 1077-1080. ↑
- C141.** Hyoun-sun Youn. Advanced classification of UXO using fully polarimetric GPR and frequency-polarization features. / Hyoun-sun Youn, Evans M., Kobashigawa J., Iskander M. // 2010 IEEE International Geoscience and Remote Sensing Symposium (IGARSS). - Honolulu, HI, 25-30 July 2010. - P. 3374-3377. ↑

- C142.** Foley J. Wide area assessment-Development and case study. / Foley J., Hodgson J. // 2010 IEEE International Geoscience and Remote Sensing Symposium (IGARSS). - Honolulu, HI, 25-30 July 2010. - P. 3370-3373. ↑
- C143.** Missaoui O. Model level fusion of edge histogram descriptors and gabor wavelets for landmine detection with ground penetrating radar. / Missaoui O., Frigui H., Gader P. // 2010 IEEE International Geoscience and Remote Sensing Symposium (IGARSS). - Honolulu, HI, 25-30 July 2010. - P. 3378-3381. ↑
- C144.** Long D.G. The microasar experiment on CASIE-09. / Long D.G., Zaugg E., Edwards M., Maslanik J. // 2010 IEEE International Geoscience and Remote Sensing Symposium (IGARSS). - Honolulu, HI, 25-30 July 2010. - P. 3466-3469. ↑
- C145.** Zaugg E.C. Theoretical and practical design considerations for a small, multi-band SAR: The SlimSAR. / Zaugg E.C., Edwards M.C., Margulis A. // 2010 IEEE International Geoscience and Remote Sensing Symposium (IGARSS). - Honolulu, HI, 25-30 July 2010. - P. 126-129. ↑
- C146.** Krieger G. Advanced digital beamforming concepts for future SAR systems. / Krieger G., Younis M., Gebert N., Huber S., Bordonì F., Patyuchenko A., Moreira A. // 2010 IEEE International Geoscience and Remote Sensing Symposium (IGARSS). - Honolulu, HI, 25-30 July 2010. - P. 245-248. ↑
- C147.** Farquharson G. Surf zone surface displacement measurements using interferometric microwave radar. / Farquharson G., Frasier S.J., Raubenheimer B., Elgar S. // 2010 IEEE International Geoscience and Remote Sensing Symposium (IGARSS). - Honolulu, HI, 25-30 July 2010. - P. 2428-2431. ↑
- C148.** Nirchio F. Preliminary model for wind estimation from Cosmo/SkyMed X band SAR data. / Nirchio F., Venafrà S. // 2010 IEEE International Geoscience and Remote Sensing Symposium (IGARSS). - Honolulu, HI, 25-30 July 2010. - P. 3462-3465. ↑
- C149.** Lardeux C. Use of PALSAR polarimetric data for tropical forest stratification and comparison of simulated dual and compact polarimetric modes. / Lardeux C., Niamen D., Routier J.B., Giraud A., Frison P.L., Pottier E., Rudant J.P. // 2010 IEEE International Geoscience and Remote Sensing Symposium (IGARSS). - Honolulu, HI, 25-30 July 2010. - P. 1855-1858. ↑
- C150.** Takeyama Y. Development of ALOS/PALSAR data on-demand processing and providing system on GEO Grid. / Takeyama Y., Kodama S., Nakamura K., Matsuoka M., Yamamoto N. // 2010 IEEE International Geoscience and Remote Sensing Symposium (IGARSS). - Honolulu, HI, 25-30 July 2010. - P. 2315-2317. ↑
- C151.** Schwartz N.R. Ground penetrating radar measurements: Applications to synthetic data generation and target characterization. / Schwartz N.R., Zaghloul A.I. // 2010 IEEE International Geoscience and Remote Sensing Symposium (IGARSS). - Honolulu, HI, 25-30 July 2010. - P. 3362-3365. ↑
- C152.** Xiaolong Dong. A Ku-band rotating fan-beam scatterometer: Design and performance simulations. / Xiaolong Dong, Di Zhu, Wenming Lin, Heugang Liu, Jingshan Jiang. // 2010 IEEE International Geoscience and Remote Sensing Symposium (IGARSS). - Honolulu, HI, 25-30 July 2010. - P. 1081-1084. ↑
- C153.** Georgieva E.M. A broad band lidar for precise atmospheric CO2 column absorption measurement from space. / Georgieva E.M., Heaps W.S., Huang W. // 2010 IEEE International Geoscience and Remote Sensing Symposium (IGARSS). - Honolulu, HI, 25-30 July 2010. - P. 649-652. ↑
- C154.** Scofield G.B. Evaluation of two region based classifications in Tapajys National Forest using the ALOS/PALSAR polarimetric and interferometric coherences. / Scofield G.B., Dutra L.V., da Costa Freitas C., Siqueira S.J., Anna S., Silva D.L.A. // 2010 IEEE International Geoscience and Remote Sensing Symposium (IGARSS). - Honolulu, HI, 25-30 July 2010. - P. 3426-3429. ↑
- C155.** Vu V.T. Integrating space-time processing into time-domain backprojection process for detection and imaging moving objects. / Vu V.T., Sjojgren T.K., Pettersson M.I. // 2010 IEEE International Geoscience and Remote Sensing Symposium (IGARSS). - Honolulu, HI, 25-30 July 2010. - P. 4106-4109. ↑
- C156.** Belli K. Use of 2D FDTD simulation and the determination of the GPR travel path angle for oblique B-scans of 2D geometries. / Belli K., Rappaport C., Udall C., Hines M., Wadia-Fascetti S. // 2010 IEEE International Geoscience and Remote Sensing Symposium (IGARSS). - Honolulu, HI, 25-30 July 2010. - P. 4721-4724. ↑

- C157.** Hornbuckle B.K. How does dew affect L-band backscatter? analysis of pals data at the Iowa validation site and implications for smap. / Hornbuckle B.K., Rowlandson T.L., Russell E., Kaleita A., Logsdon S., Kruger A., Simon Yueh, De Roo R.D. // 2010 IEEE International Geoscience and Remote Sensing Symposium (IGARSS). - Honolulu, HI, 25-30 July 2010. - P. 4835-4838. ↑
- C158.** Martin-Porqueras F. Experimental validation of the Corbella's visibility function using HUT-2D and MIRAS. / Martin-Porqueras F., Kainulainen J., Martin-Neira M., Corbella I., Oliva R., Castro R., Barbosa J., Gutierrez A. // 2010 IEEE International Geoscience and Remote Sensing Symposium (IGARSS). - Honolulu, HI, 25-30 July 2010. - P. 4286-4289. ↑
- C159.** Dabney P. The Slope Imaging Multi-polarization Photon-counting Lidar: Development and performance results. / Dabney P., Harding D., Abshire J., Huss T., Jodor G., Machan R., Marzouk J., Rush K., Seas A., Shuman C., Xiaoli Sun, Valett S., Vasilyev A., Yu A., Yunhui Zheng. // 2010 IEEE International Geoscience and Remote Sensing Symposium (IGARSS). - Honolulu, HI, 25-30 July 2010. - P. 653-656. ↑
- C160.** Caorsi S. Electromagnetic infrastructure monitoring: The exploitation of GPR data and neural networks for multi-layered geometries. / Caorsi S., Stasolla M. // 2010 IEEE International Geoscience and Remote Sensing Symposium (IGARSS). - Honolulu, HI, 25-30 July 2010. - P. 4717-4720. ↑
- C161.** Owen M.P. Towards Bayesian estimator selection for QuikSCAT wind and rain estimation. / Owen M.P., Long D.G. // 2010 IEEE International Geoscience and Remote Sensing Symposium (IGARSS). - Honolulu, HI, 25-30 July 2010. - P. 1331-1334. ↑
- C162.** Yaokui Cui. Using airborne lidar to retrieve crop structural parameters. / Yaokui Cui, Kaiguang Zhao, Wenjie Fan, Xiru Xu. // 2010 IEEE International Geoscience and Remote Sensing Symposium (IGARSS). - Honolulu, HI, 25-30 July 2010. - P. 2107-2110. ↑
- C163.** Soisuvann S. A revised geophysical model function for the advanced scatterometer (ASCAT) at NOAA/NESDIS. / Soisuvann S., Jelenak Z., Chang P.S., Qi Zhu. // 2010 IEEE International Geoscience and Remote Sensing Symposium (IGARSS). - Honolulu, HI, 25-30 July 2010. - P. 1335-1338. ↑
- C164.** Bratsolis E. Segmentation of lakes from the local background on the surface of Titan using Cassini SAR images. // 2010 IEEE International Geoscience and Remote Sensing Symposium (IGARSS). - Honolulu, HI, 25-30 July 2010. - P. 906-909. ↑
- C165.** Eineder M. IMaging geodesy with TerraSAR-X. / Eineder M., Xiaoying Cong, Minet C., Steigenberger P., Fritz T., Jaber W.A. // 2010 IEEE International Geoscience and Remote Sensing Symposium (IGARSS). - Honolulu, HI, 25-30 July 2010. - P. 4827-4830. ↑
- C166.** SeungJoon Kwon. Development of the LIDAR data processing system for the rapid generation of the terrestrial information. / SeungJoon Kwon, SungWoong Shin. // 2010 IEEE International Geoscience and Remote Sensing Symposium (IGARSS). - Honolulu, HI, 25-30 July 2010. - P. 3902-3904. ↑
- C167.** Glenn T.C. A multimodal Matching Pursuits Dissimilarity Measure applied to landmine/clutter discrimination. / Glenn T.C., Wilson J.N., Ho K.C. // 2010 IEEE International Geoscience and Remote Sensing Symposium (IGARSS). - Honolulu, HI, 25-30 July 2010. - P. 4200-4203. ↑
- C168.** Walker C.C. On radar sounding applications for Enceladean ice. / Walker C.C., Liemohn M.W., Parkinson C.D. // 2010 IEEE International Geoscience and Remote Sensing Symposium (IGARSS). - Honolulu, HI, 25-30 July 2010. - P. 4522-4525. ↑
- C169.** Amarin R.A. The Hurricane Imaging Radiometer wide swath simulation and wind speed retrievals. / Amarin R.A., Jones L., Johnson J., Ruf C., Miller T.L., Uhlhorn E. // 2010 IEEE International Geoscience and Remote Sensing Symposium (IGARSS). - Honolulu, HI, 25-30 July 2010. - P. 4290-4293. ↑
- C170.** Shabou A. Three dimensional reconstruction of urban areas using jointly phase and amplitude multichannel images. / Shabou A., Tupin F., Ferraioli G., Pascasio V. // 2010 IEEE International Geoscience and Remote Sensing Symposium (IGARSS). - Honolulu, HI, 25-30 July 2010. - P. 4831-4834. ↑
- C171.** Horie H. The external calibration study for EarthCARE/CPR. / Horie H., Ohno Y., Takahashi N. // 2010 IEEE International Geoscience and Remote Sensing Symposium (IGARSS). - Honolulu, HI, 25-30 July 2010. - P. 1895-1898. ↑

- C172.** Benson M. Quantifying the results of wind and rain on ifsar tree height estimation. / Benson M., Pierce L., Sarabandi K. // 2010 IEEE International Geoscience and Remote Sensing Symposium (IGARSS). - Honolulu, HI, 25-30 July 2010. - P. 3275-3278. ↑
- C173.** Moon-Kyung Kang. Preliminary result of polarization property analysis using fully polarimetric GB-SAR images. / Moon-Kyung Kang, Kwang-Eun Kim, Hoonyol Lee, Seong-Jun Cho, Jae-Hee Lee. // 2010 IEEE International Geoscience and Remote Sensing Symposium (IGARSS). - Honolulu, HI, 25-30 July 2010. - P. 4019-4022. ↑
- C174.** Yamaguchi Y. Four-component scattering power decomposition with rotation of coherency matrix. / Yamaguchi Y., Sato A., Sato R., Yamada H., Boerner W.-M. // 2010 IEEE International Geoscience and Remote Sensing Symposium (IGARSS). - Honolulu, HI, 25-30 July 2010. - P. 1327-1330. ↑
- C175.** Zhang Fan. Accelerating InSAR raw data simulation on GPU using CUDA. / Zhang Fan, Wang Bing-nan, Xiang Mao-sheng. // 2010 IEEE International Geoscience and Remote Sensing Symposium (IGARSS). - Honolulu, HI, 25-30 July 2010. - P. 2932-2935. ↑
- C176.** Hamdi A. AN SVM classifier with HMM-based kernel for landmine detection using ground penetrating radar. / Hamdi A., Missaoui O., Frigui H. // 2010 IEEE International Geoscience and Remote Sensing Symposium (IGARSS). - Honolulu, HI, 25-30 July 2010. - P. 4196-4199. ↑
- C177.** Nunziata F. A physically-based approach to observe man-made metallic objects in dual-polarized SAR data. / Nunziata F., Migliaccio M., Brown C.E. // 2010 IEEE International Geoscience and Remote Sensing Symposium (IGARSS). - Honolulu, HI, 25-30 July 2010. - P. 3007-3010. ↑
- C178.** Yang Wei. A novel three-step focusing algorithm for TOPSAR image formation. / Yang Wei, Li Chunsheng, Chen Jie, Wang Pengbo. // 2010 IEEE International Geoscience and Remote Sensing Symposium (IGARSS). - Honolulu, HI, 25-30 July 2010. - P. 4087-4090. ↑
- C179.** Wang R. IMage formation algorithm for bistatic forward-looking SAR. / Wang R., Loffeld O., Nies H., Peters V. // 2010 IEEE International Geoscience and Remote Sensing Symposium (IGARSS). - Honolulu, HI, 25-30 July 2010. - P. 4091-4094. ↑
- C180.** Jun-Dong Park. Comparisons of rain rate and reflectivity between TRMM precipitation radar and Gosan S-band radar. / Jun-Dong Park, Mi-Lim Ou, Morris K.R., Schwaller M.R. // 2010 IEEE International Geoscience and Remote Sensing Symposium (IGARSS). - Honolulu, HI, 25-30 July 2010. - P. 4698-4700. ↑
- C181.** Dubois-Fernandez P. TropiSAR: Exploring the temporal behavior of P-Band SAR data. / Dubois-Fernandez P., Oriot H., Coulombeix C., Cantalloube H., Ruault du Plessis O., Le Toan T., Daniel S., Chave J., Blanc L., Davidson M., Petit M. // 2010 IEEE International Geoscience and Remote Sensing Symposium (IGARSS). - Honolulu, HI, 25-30 July 2010. - P. 1319-1322. ↑
- C182.** Arie M. Retrieval of soil moisture under vegetation using Polarimetric Scattering Cubes. / Arie M., van Zyl J.J., Kim Y. // 2010 IEEE International Geoscience and Remote Sensing Symposium (IGARSS). - Honolulu, HI, 25-30 July 2010. - P. 1323-1326. ↑
- C183.** Ruzanski E. Nowcasting rainfall fields estimated from specific differential phase. / Ruzanski E., Chandrasekar V. // 2010 IEEE International Geoscience and Remote Sensing Symposium (IGARSS). - Honolulu, HI, 25-30 July 2010. - P. 4694-4697. ↑
- C184.** Junjie Wu. Spatial spectrum of bistatic SAR with one fixed station. / Junjie Wu, Jianyu Yang, Yulin Huang, Haiguang Yang. // 2010 IEEE International Geoscience and Remote Sensing Symposium (IGARSS). - Honolulu, HI, 25-30 July 2010. - P. 4095-4098. ↑
- C185.** Esch T. Land cover classification based on single-polarized VHR SAR images using texture information derived via speckle analysis. / Esch T., Schenk A., Thiel M., Ullmann T., Schmidt M., Dech S. // 2010 IEEE International Geoscience and Remote Sensing Symposium (IGARSS). - Honolulu, HI, 25-30 July 2010. - P. 1875-1878. ↑
- C186.** Prats P. Investigations on TOPS interferometry with TerraSAR-X. / Prats P., Marotti L., Wollstadt S., Scheiber R. // 2010 IEEE International Geoscience and Remote Sensing Symposium (IGARSS). - Honolulu, HI, 25-30 July 2010. - P. 2629-2632. ↑

- C187.** Sato R. Polarimetric scattering analysis for accurate observation of stricken man-made targets using a rotated coherency matrix. / Sato R., Yamaguchi Y., Yamada H. // 2010 IEEE International Geoscience and Remote Sensing Symposium (IGARSS). - Honolulu, HI, 25-30 July 2010. - P. 746-749. ↑
- C188.** Suwa K. ISAR imaging of an aircraft target USING ISDB-T digital TV based passive bistatic radar. / Suwa K., Nakamura S., Morita S., Wakayama T., Maniwa H., Oshima T., Maekawa R., Matsuda S., Tachihara T. // 2010 IEEE International Geoscience and Remote Sensing Symposium (IGARSS). - Honolulu, HI, 25-30 July 2010. - P. 4103-4105. ↑
- C189.** Haug T. Performance and application of different image matching algorithms for investigating glacier and ice-shelf flow, permafrost creep and landslides. / Haug T., Debella-Gilo M., Karstensen J., Kajajb A. // 2010 IEEE International Geoscience and Remote Sensing Symposium (IGARSS). - Honolulu, HI, 25-30 July 2010. - P. 3636-3639. ↑
- C190.** Whitcomb J. Mapping and change detection for boreal wetlands of North America based on JERS and PALSAR data. / Whitcomb J., Moghaddam M., McDonald K., Podest E., Chapman B. // 2010 IEEE International Geoscience and Remote Sensing Symposium (IGARSS). - Honolulu, HI, 25-30 July 2010. - P. 1371-1373. ↑
- C191.** Chen V.C. High-resolution 3-D radar imaging using pseudo-random noise coded waveform. 2010 IEEE International Geoscience and Remote Sensing Symposium (IGARSS). - Honolulu, HI, 25-30 July 2010. - P. 718-721. ↑
- C192.** Kajrnaj J. Improving hydrological forecasting using multi-source remote sensing data together with in situ measurements. / Kajrnaj J., Huttunen M., Metsajmaki S., Vehvilainen B., Podsechin V., Pulliainen J., Lemmetyinen J., Kuitunen T., Rauste Y., Berglund R. // 2010 IEEE International Geoscience and Remote Sensing Symposium (IGARSS). - Honolulu, HI, 25-30 July 2010. - P. 1749-1752. ↑
- C193.** Kuloglu M. Ground penetrating radar for tunnel detection. / Kuloglu M., Chen C. // 2010 IEEE International Geoscience and Remote Sensing Symposium (IGARSS). - Honolulu, HI, 25-30 July 2010. - P. 4314-4317. ↑
- C194.** Fengli Zhang. Interpretation of buildings in high resolution sar images based on electromagnetic method. / Fengli Zhang, Yun Shao, Zi Wan, Xiao Zhang. // 2010 IEEE International Geoscience and Remote Sensing Symposium (IGARSS). - Honolulu, HI, 25-30 July 2010. - P. 2727-2730. ↑
- C195.** Huanmin Luo. Tree height retrieval methods using POLInSAR coherence optimization. / Huanmin Luo, Erxue Chen, Jian Cheng, Xiaowen Li. // 2010 IEEE International Geoscience and Remote Sensing Symposium (IGARSS). - Honolulu, HI, 25-30 July 2010. - P. 3259-3262. ↑
- C196.** Chuen-Meei Gan. A comparison of estimated mixing height by multiple remote sensing instruments and its influence on air quality in urban regions. / Chuen-Meei Gan, Wu Y.H., Gross B.M., Arend M., Moshary F., Ahmed S. // 2010 IEEE International Geoscience and Remote Sensing Symposium (IGARSS). - Honolulu, HI, 25-30 July 2010. - P. 730-733. ↑
- C197.** Sato M. GPR evaluation test for humanitarian demining in Cambodia. 2010 IEEE International Geoscience and Remote Sensing Symposium (IGARSS). - Honolulu, HI, 25-30 July 2010. - P. 4322-4325. ↑
- C198.** Lojfgren J.S. Tropospheric correction for InSAR using interpolated ECMWF data and GPS Zenith Total Delay from the Southern California Integrated GPS Network. / Lojfgren J.S., Bjojrndahl F., Moore A.W., Webb F.H., Fielding E.J., Fishbein E.F. // 2010 IEEE International Geoscience and Remote Sensing Symposium (IGARSS). - Honolulu, HI, 25-30 July 2010. - P. 4503-4506. ↑
- C199.** Allan G.R. Remote sensing atmospheric CO2 column abundance using an airborne pulsed laser sounder at 13 km altitude. / Allan G.R., Hasselbrack W., Riris H., Abshire J.B., Weaver C., Jianping Mao, Xiaoli Sun, Andrews A.E. // 2010 IEEE International Geoscience and Remote Sensing Symposium (IGARSS). - Honolulu, HI, 25-30 July 2010. - P. 2595-2598. ↑
- C200.** Qiang Xing. Monitoring thickness change of the Dongkemadi Glacier on Qinghai-Tibetan Plateau using SRTM DEM and map-based topographic data. / Qiang Xing, Zhen Li, Jianmin Zhou. // 2010 IEEE International Geoscience and Remote Sensing Symposium (IGARSS). - Honolulu, HI, 25-30 July 2010. - P. 1769-1771. ↑
- C201.** Renga A. Spaceborne-airborne bistatic radar for UAS navigation purposes: Preliminary analysis and

strawman system identification. / Renga A., Graziano M.D., D'Errico M., Moccia A., Menichino F., Vetrella S., Accardo D., Corrado F., Cuciniello G., Nebula F., Del Monte L. // 2010 IEEE International Geoscience and Remote Sensing Symposium (IGARSS). - Honolulu, HI, 25-30 July 2010. - P. 3474-3477. ↑

C202. Ji-Hwan Hwang. Calibration accuracy enhancement in the field experiment with a ground-based scatterometer. / Ji-Hwan Hwang, Seong-Min Park, Yisok Oh. // 2010 IEEE International Geoscience and Remote Sensing Symposium (IGARSS). - Honolulu, HI, 25-30 July 2010. - P. 1100-1103. ↑

C203. Macelloni G. Evaluation of vegetation effect on the retrieval of snow parameters from backscattering measurements: A contribution to CoReH2O mission. / Macelloni G., Brogioni M., Montomoli F., Fontanelli G., Kern M., Rott H. // 2010 IEEE International Geoscience and Remote Sensing Symposium (IGARSS). - Honolulu, HI, 25-30 July 2010. - P. 1772-1775. ↑

C204. Storie C.D. Remote sensing research in undergraduate education: An international fieldwork perspective. / Storie C.D., Bugden-Storie J. // 2010 IEEE International Geoscience and Remote Sensing Symposium (IGARSS). - Honolulu, HI, 25-30 July 2010. - P. 1114-1117. ↑

C205. Lindsley R.D. Adapting the sir algorithm to ASCAT. / Lindsley R.D., Long D.G. // 2010 IEEE International Geoscience and Remote Sensing Symposium (IGARSS). - Honolulu, HI, 25-30 July 2010. - P. 3402-3405. ↑

C206. Emmitt G.D. Airborne Doppler Wind Lidar investigations of western Pacific typhoon genesis and evolution. 2010 IEEE International Geoscience and Remote Sensing Symposium (IGARSS). - Honolulu, HI, 25-30 July 2010. - P. 2591-2594. ↑

C207. Gonza. Synthetic aperture radar image analysis as a tool for validation of baroclinic internal wave 3D modeling in Algeciras Bay (Strait of Gibraltar). / Gonza, Iez C.J., Lopez L., Gomez-Enri J., Gomez J.J., Alvarez O., Bruno M., Macanes R., Villares P. // 2010 IEEE International Geoscience and Remote Sensing Symposium (IGARSS). - Honolulu, HI, 25-30 July 2010. - P. 952-954. ↑

C208. Lingjun Kang. A distributed LiDAR processing model based on OWS and BPEL. / Lingjun Kang, Qunrong Wu, Ying Yuan. // 2010 IEEE International Geoscience and Remote Sensing Symposium (IGARSS). - Honolulu, HI, 25-30 July 2010. - P. 3628-3631. ↑

C209. Cerutti-Maori D. Coherent MIMO radar for GMTI. / Cerutti-Maori D., Klare J. // 2010 IEEE International Geoscience and Remote Sensing Symposium (IGARSS). - Honolulu, HI, 25-30 July 2010. - P. 1085-1088. ↑

C210. Carabajal C.C. Icesat lidar and global digital elevation models: applications to desdyni. / Carabajal C.C., Harding D.J., Suchdeo V.P. // 2010 IEEE International Geoscience and Remote Sensing Symposium (IGARSS). - Honolulu, HI, 25-30 July 2010. - P. 1907-1910. ↑

C211. Song S.H. Geo-location error correction for Synthetic Aperture Radar image. / Song S.H., Rho S.H., Jung C.H., Kwag Y.K. // 2010 IEEE International Geoscience and Remote Sensing Symposium (IGARSS). - Honolulu, HI, 25-30 July 2010. - P. 3406-3409. ↑

C212. Yi Lin. Leaf area index (LAI) estimation based on vehicle-based laser scanning. / Yi Lin, Hyyppa J. // 2010 IEEE International Geoscience and Remote Sensing Symposium (IGARSS). - Honolulu, HI, 25-30 July 2010. - P. 3422-3425. ↑

C213. Salazar J.L. Dual-polarization performance of the phase-tilt antenna array in a casa dense network radar. / Salazar J.L., Knapp E.J., McLaughlin D.J. // 2010 IEEE International Geoscience and Remote Sensing Symposium (IGARSS). - Honolulu, HI, 25-30 July 2010. - P. 3470-3473. ↑

C214. Krieger G. Tandem-L: And innovative interferometric and polarimetric SAR mission to monitor earth system dynamics with high resolution. / Krieger G., Hajnsek I., Papathanassiou K., Eineder M., Younis M., De Zan F., Huber S., Lopez-Dekker P., Prats P., Werner M., Shen Y., Freeman A., Rosen P., Hensley S., Johnson W., Villeux L., Grafmueller B., Werninghaus R., Bamler R., Moreira A. // 2010 IEEE International Geoscience and Remote Sensing Symposium (IGARSS). - Honolulu, HI, 25-30 July 2010. - P. 253-256. ↑

C215. Wu Shengli. Using AMSR-E land product to monitor the drought process in China. / Wu Shengli, Zhu Xiaoxiang. // 2010 IEEE International Geoscience and Remote Sensing Symposium (IGARSS). - Honolulu, HI, 25-30 July 2010. - P. 3894-3897. ↑

- C216.** Vesecky J.F. A system trade model for the monitoring of coastal vessels using HF surface wave radar and ship automatic identification systems (AIS). / Vesecky J.F., Laws K.E., Paduan J.D. // 2010 IEEE International Geoscience and Remote Sensing Symposium (IGARSS). - Honolulu, HI, 25-30 July 2010. - P. 3414-3417. ↑
- C217.** Younis M. A concept for high performance reflector-based Synthetic Aperture Radar. / Younis M., Patyuchenko A., Huber S., Krieger G., Moreira A. // 2010 IEEE International Geoscience and Remote Sensing Symposium (IGARSS). - Honolulu, HI, 25-30 July 2010. - P. 249-252. ↑
- C218.** Lyzenga D. Ocean wave field measurements using X-band Doppler radars at low grazing angles. / Lyzenga D., Nwogu O., Trizna D., Hathaway K. // 2010 IEEE International Geoscience and Remote Sensing Symposium (IGARSS). - Honolulu, HI, 25-30 July 2010. - P. 4725-4728. ↑
- C219.** Iodice A. A polarimetric two-scale model for soil moisture retrieval. / Iodice A., Natale A., Riccio D. // 2010 IEEE International Geoscience and Remote Sensing Symposium (IGARSS). - Honolulu, HI, 25-30 July 2010. - P. 1265-1268. ↑
- C220.** Le M. Microphysical retrievals of dual polarization and dual frequency ground radar for GPM ground validation. / Le M., Chandrasekar V., Lim S. // 2010 IEEE International Geoscience and Remote Sensing Symposium (IGARSS). - Honolulu, HI, 25-30 July 2010. - P. 2349-2352. ↑
- C221.** Bellez S. Full wave analysis of VHF-UHF forest bistatic scattering mechanisms an investigation on the influence of electromagnetic coupling. / Bellez S., Roussel H., Dahon C. // 2010 IEEE International Geoscience and Remote Sensing Symposium (IGARSS). - Honolulu, HI, 25-30 July 2010. - P. 2547-2550. ↑
- C222.** Shirvany R. Estimation of the degree of polarization in compact polarimetry. / Shirvany R., Chabert M., Tourneret J.-Y. // 2010 IEEE International Geoscience and Remote Sensing Symposium (IGARSS). - Honolulu, HI, 25-30 July 2010. - P. 722-725. ↑
- C223.** Tebaldini S. ALGAE: A fast algebraic estimation of interferogram phase offsets in space varying geometries. / Tebaldini S., Gatti G., Mariotti d'Alessandro M., Rocca F. // 2010 IEEE International Geoscience and Remote Sensing Symposium (IGARSS). - Honolulu, HI, 25-30 July 2010. - P. 2622-2624. ↑
- C224.** Xuemei Gong. Extracting trees and structure parameters via integration of LIDAR data and ground imagery. / Xuemei Gong, Daiyong Wei, Guoqing Zhou. // 2010 IEEE International Geoscience and Remote Sensing Symposium (IGARSS). - Honolulu, HI, 25-30 July 2010. - P. 2703-2706. ↑
- C225.** Srivastava S. The RADARSAT-1 imaging performance, 14 years after launch, and independent report on RADARSAT-2 image quality. / Srivastava S., Cote S., Muir S., Hawkins R. // 2010 IEEE International Geoscience and Remote Sensing Symposium (IGARSS). - Honolulu, HI, 25-30 July 2010. - P. 3458-3461. ↑
- C226.** Hessner K. Extraction of coastal wavefield properties from X-band radar. / Hessner K., Hanson J.L. // 2010 IEEE International Geoscience and Remote Sensing Symposium (IGARSS). - Honolulu, HI, 25-30 July 2010. - P. 4326-4329. ↑
- C227.** Crow W.T. Inferring the impact of radar incidence angle on soil moisture retrieval skill using data assimilation. / Crow W.T., Wagner W., Naeimi V. // 2010 IEEE International Geoscience and Remote Sensing Symposium (IGARSS). - Honolulu, HI, 25-30 July 2010. - P. 1261-1264. ↑
- C228.** Guida R. Monitoring of collapsed built-up areas with high resolution SAR images. / Guida R., Iodice A., Riccio D. // 2010 IEEE International Geoscience and Remote Sensing Symposium (IGARSS). - Honolulu, HI, 25-30 July 2010. - P. 2422-2425. ↑
- C229.** Jin-Woo Kim. Estimation of sea ice thickness in the Arctic Sea using polarimetric parameters of C- and X-band space-borne SAR data. / Jin-Woo Kim, Duk-jin Kim, Byong Jun Hwang. // 2010 IEEE International Geoscience and Remote Sensing Symposium (IGARSS). - Honolulu, HI, 25-30 July 2010. - P. 2402-2405. ↑
- C230.** Budillon A. SAR tomographic focusing by Compressive Sampling: Experiments on real data. / Budillon A., Evangelista A., Schirizzi G. // 2010 IEEE International Geoscience and Remote Sensing Symposium (IGARSS). - Honolulu, HI, 25-30 July 2010. - P. 3785-3788. ↑
- C231.** Uiboupin R. Sea ice monitoring in the Baltic Sea using dual-pol C and L band SAR data. / Uiboupin R.,

Sipelgas L. // 2010 IEEE/OES US/EU Baltic International Symposium (BALTIC). - Riga, 24-27 Aug. 2010. - P. 1-2. ↑

C232. Steelman C.M. Inference of vertical soil moisture distribution using high-frequency CMP and reflection traveltime analysis. / Steelman C.M., Endres A.L. // 2010 13th International Conference on Ground Penetrating Radar (GPR). - Lecce, 21-25 June 2010. - P. 1-6. ↑

C233. Parker R. Freshwater ground penetrating radar the significance of seasonal temperature variation. 2010 13th International Conference on Ground Penetrating Radar (GPR). - Lecce, 21-25 June 2010. - P. 1-6. ↑

C234. Forte E. 2D and 3D GPR imaging and characterization of a carbonate hydrocarbon reservoir analogue. / Forte E., Pipan M., Casabianca D., Di Cuia R., Riva A. // 2010 13th International Conference on Ground Penetrating Radar (GPR). - Lecce, 21-25 June 2010. - P. 1-7. ↑

C235. Yanovsky F. Specified for air safety, monitoring atmospheric phenomena including the volcano dust. 2010 11th International Radar Symposium (IRS). - Vilnius, 16-18 June 2010. - P. 1-4. ↑

C236. Zhang Yunhua. Design of RF subsystem for Ku-band radar with synthesized bandwidth of 2GHz by using stepped-frequency chirp signal. / Zhang Yunhua, Zhang Xiangkun, Zhai Wenshuai, Shi Xiaojin, Gu Xiang, Jiang Jingshan. // 2010 11th International Radar Symposium (IRS). - Vilnius, Lithuania, 16-18 June 2010. - P. 1-4. ↑

C237. Huber Sigurd. Digital beam forming concepts with application to spaceborne reflector SAR systems. / Huber Sigurd, Younis Marwan, Patyuchenko Anton, Krieger Gerhard. // 2010 11th International Radar Symposium (IRS). - Vilnius, Lithuania, 16-18 June 2010. - P. 1-4. ↑

C238. McBride J.H. Mapping thermal tufa deposits using GPR. / McBride J.H., Faust D.L., Guthrie W.S., Nelson S.T. // 2010 13th International Conference on Ground Penetrating Radar (GPR). - Lecce, 21-25 June 2010. - P. 1-6. ↑

C239. Matsuoka K. Using englacial radar attenuation to better diagnose the subglacial environment: A review. / Matsuoka K., MacGregor J.A., Pattyn F. // 2010 13th International Conference on Ground Penetrating Radar (GPR). - Lecce, 21-25 June 2010. - P. 1-5. ↑

C240. Kadioglu S. GPR research at the tomb of Zeynel Bey in Hasankeyf ancient city- Southeastern Turkey. / Kadioglu S., Akyol A.A., Kadioglu Y.K., Ekincioglu E.E. // 2010 13th International Conference on Ground Penetrating Radar (GPR). - Lecce, 21-25 June 2010. - P. 1-4. ↑

C241. Campana S. GPR investigation in different archaeological sites in Tuscany. Analysis and comparison of the obtained results. / Campana S., Piro S. // 2010 13th International Conference on Ground Penetrating Radar (GPR). - Lecce, Italy, 21-25 June 2010. - P. 1-6. ↑

C242. Orosei R. Radar subsurface sounding over the putative frozen sea in Cerberus Palus, Mars. / Orosei R., Cartacci M., Cicchetti A., Noschese R., Federico C., Frigeri A., Flamini E., Holt J.W., Marinangeli L., Pettinelli E., Phillips R.J., Picardi G., Seu R., Plaut J.J. // 2010 13th International Conference on Ground Penetrating Radar (GPR). - Lecce, 21-25 June 2010. - P. 1-4. ↑

C243. Putzig N.E. Imaging the subsurface structure of Planum Boreum with the Mars Reconnaissance Orbiter Shallow Radar. / Putzig N.E., Phillips R.J., Campbell B.A., Foss F.J. // 2010 13th International Conference on Ground Penetrating Radar (GPR). - Lecce, 21-25 June 2010. - P. 1-6. ↑

C244. McBride J.H. Results of an experimental radar survey on the gornergletscher glacier system (Zwillingsgletscher), Valais, Switzerland. / McBride J.H., Rupper S.B., Ritter S.M., Tingey D.G., Quick A.M., McKean A.P., Jones N.B. // 2010 13th International Conference on Ground Penetrating Radar (GPR). - Lecce, 21-25 June 2010. - P. 1-6. ↑

C245. Karaev V. Potentialities of the Doppler spectrum of backscattered microwave signal in the problem of remote sensing of the sea surface. / Karaev V., Kanevsky M., Meshkov E. // 2010 International Kharkov Symposium on Physics and Engineering of Microwaves, Millimeter and Submillimeter Waves (MSMW). - Kharkiv, 21-26 June 2010. - P. 1-3. ↑

C246. Khlopov G. Application of double frequency radar for measurement of parameters of solid polydisperse

aerosols. / Khlopov G., Knoechel R., Linkova A., Tepljuk A., Schuenemann K. // 2010 International Kharkov Symposium on Physics and Engineering of Microwaves, Millimeter and Submillimeter Waves (MSMW). - Kharkiv, 21-26 June 2010. - P. 1-3. ↑

C247. Kovalenko A. I. Design of prospective spaceborne multi-aperture UWB polarimetric high performance SAR system. / Kovalenko A. I., Riman V. V., Shishanov A. V., Vnotchenko S. L. // 2010 11th International Radar Symposium (IRS). - Vilnius, Lithuania, 16-18 June 2010. - P. 1-3. ↑

C248. Shkvarko Y.V. Experiment design framework for super-high resolution imaging with the geostar configured sensor array data. / Shkvarko Y.V., Espadas V.E. // 2010 International Kharkov Symposium on Physics and Engineering of Microwaves, Millimeter and Submillimeter Waves (MSMW). - Kharkiv, 21-26 June 2010. - P. 1-3. ↑

C249. Linkova A. Double frequency sounding of liquid precipitation. 2010 International Kharkov Symposium on Physics and Engineering of Microwaves, Millimeter and Submillimeter Waves (MSMW). - Kharkiv, 21-26 June 2010. - P. 1. ↑

C250. Zabrodina V.V. Comparative analysis of regression line fitting algorithms in blind method of mixed noise variance evaluation in radar images. / Zabrodina V.V., Abramov S.K., Abramov K.D. // 2010 International Kharkov Symposium on Physics and Engineering of Microwaves, Millimeter and Submillimeter Waves (MSMW). - Kharkiv, 21-26 June 2010. - P. 1. ↑

C251. Bruyant Jean-Paul. SETHI flying lab: A tool for remote sensing applications. 2010 11th International Radar Symposium (IRS). - Vilnius, Lithuania, 16-18 June 2010. - P. 1-4. ↑

C252. Malanowski M. Robust detection in continuous-wave noise radar-experimental results. / Malanowski M., Kulpa K. // 2010 11th International Radar Symposium (IRS). - Vilnius, 16-18 June 2010. - P. 1-4. ↑

C253. Khopov G. Study of double frequency method for remote sensing of liquid precipitations. / Khopov G., Khomenko S., Linkova A., Voitovych O. // 2010 11th International Radar Symposium (IRS). - Vilnius, 16-18 June 2010. - P. 1-3. ↑

C254. Bezruck V.M. Application of Autoregressive Model for Recognition of Meteorological Objects. / Bezruck V.M., Belov Y.N., Voitovych O.A., Netrobenko K.A., Tikhonov V.A., Rudnev G.A., Khlopov G.I., Khomenko S.I. // 2010 11th International Radar Symposium (IRS). - Vilnius, 16-18 June 2010. - P. 1-3. ↑

C255. Galati G. Technological challenges of a multifunction active phased array radar for weather, air traffic control and security applications. / Galati G., Pavan G., Scopelliti S., Infante L. // 2010 11th International Radar Symposium (IRS). - Vilnius, 16-18 June 2010. - P. 1-4. ↑

C256. Bokal Zhanna. Rank signal detection algorithms based on permutations of partial likelihood ratios. / Bokal Zhanna, Sinitsyn Rustem. // 2010 11th International Radar Symposium (IRS). - Vilnius, Lithuania, 16-18 June 2010. - P. 1-4. ↑

C257. Levitas Boris. UWB radar for breath detection. / Levitas Boris, Matuzas Jonas. // 2010 11th International Radar Symposium (IRS). - Vilnius, Lithuania, 16-18 June 2010. - P. 1-3. ↑

C258. Scardozzi Giuseppe. Integrated geophysical methods for the knowledge of the urban layout of Hierapolis in Phrygia (Turkey). 2010 13th International Conference on Ground Penetrating Radar (GPR). - Lecce, Italy, 21-25 June 2010. - P. 1-6. ↑

C259. Chengyun Liu. A IHS-WT remote sensing image fusion method based on dynamic weighting of regional multi-features. / Chengyun Liu, Zhenxue Chen, Faliang Chang, Jianguang Xu, Bingkun Yin. // 2010 8th World Congress on Intelligent Control and Automation (WCICA). - Jinan, 7-9 July 2010. - P. 6089-6093. ↑

C260. Wencheng Wang. A temperature remote monitoring system of cable joint. / Wencheng Wang, Lei Wang. // 2010 2nd International Conference on Signal Processing Systems (ICSPS). - Dalian, 5-7 July 2010. - Vol. 1. - P. V1-690-V1-694-690. ↑

C261. Xian-jiao Liang. Analysis of micro-doppler effect in SIMO radar. / Xian-jiao Liang, Qun Zhang, Meng Zhu, Ying Luo. // 2010 2nd International Conference on Signal Processing Systems (ICSPS). - Dalian, 5-7 July 2010. - Vol. 2. - P. V2-343-V2-346-343. ↑

- C262.** Song Lei. Simulation and application of GPR in Artificial Freezing Engineering. / Song Lei, Zhang Xiaojun, Li Haipeng, Zhang Houquan. // 2010 13th International Conference on Ground Penetrating Radar (GPR). - Lecce, 21-25 June 2010. - P. 1-4. ↑
- C263.** Poliakov E. Remote control software development for a small airborne electronic support payload. / Poliakov E., Wu C., Lee J.P.Y., Antar Y.M.M. // 2010 14th International Symposium on Antenna Technology and Applied Electromagnetics & the American Electromagnetics Conference (ANTEM-AMEREM). - Ottawa, ON, 5-8 July 2010. - P. 1-4. ↑
- C264.** Jie Yu. Research on supervised classification of fully polarimetric SAR image using BP neural network trained by PSO. / Jie Yu, Yan Li, Zhong Shan Zhang, Jing Chao Jiang. // 2010 8th World Congress on Intelligent Control and Automation (WCICA). - Jinan, 7-9 July 2010. - P. 6152-6157. ↑
- C265.** Ping Wang. The identification test of soil texture with ground penetrating radar. / Ping Wang, Zhenqi Hu, Junguo Yang, Fang Wang, Mingjie Gao. // 2010 International Conference on Advances in Energy Engineering (ICAEE). - Beijing, 19-20 June 2010. - P. 81-84. ↑
- C266.** Cadeddu M.P. Evaluation of cloud liquid absorption models at 90 and 150 GHz. / Cadeddu M.P., Turner D.D. // 2010 11th Specialist Meeting on Microwave Radiometry and Remote Sensing of the Environment (MicroRad). - Washington, DC, 1-4 March 2010. - P. 171-176. ↑
- C267.** Laupattarakasem P. Improved high wind speed retrievals using AMSR and the next generation NASA Dual Frequency Scatterometer. / Laupattarakasem P., Alsweiss S., El-Nimri S., Jones W.L., Veleva S., Stiles B.W., Rodriguez E., Gaston R.W. // 2010 11th Specialist Meeting on Microwave Radiometry and Remote Sensing of the Environment (MicroRad). - Washington, DC, 1-4 March 2010. - P. 134-139. ↑
- C268.** Ferrazzoli P. AMSR-E observations of rain and flood events over vegetated areas of LA Plata basin. / Ferrazzoli P., Rahmoune R., Grings F., Douna V., Parmuchi G., Salvia M., Karszenbaum H. // 2010 11th Specialist Meeting on Microwave Radiometry and Remote Sensing of the Environment (MicroRad). - Washington, DC, 1-4 March 2010. - P. 63-66. ↑
- C269.** Parde. Radio frequency interferences investigation using the airborne L-band full polarimetric radiometer CAROLS. / Parde, M., Zribi M., Fanise P., Dechambre M., Boutin J., Reul N., Tenerelli J., Hauser D., Kerr Y. // 2010 11th Specialist Meeting on Microwave Radiometry and Remote Sensing of the Environment (MicroRad). - Washington, DC, 1-4 March 2010. - P. 300-305. ↑
- C270.** Alsweiss S.O. An improved active/passive oceanic wind vector retrieval technique. / Alsweiss S.O., Laupattarakasem P., Jones W.L. // 2010 11th Specialist Meeting on Microwave Radiometry and Remote Sensing of the Environment (MicroRad). - Washington, DC, 1-4 March 2010. - P. 226-229. ↑
- C271.** Dowgiallo D.J. Millimeter wave interferometric radiometry for passive imaging and the detection of low-power manmade signals. / Dowgiallo D.J., Twarog E.M., Rauen S., Lazio J.T., Peters W.M., McGlothlin N.R., Helmboldt J.F., Gaiser P.W. // 2010 11th Specialist Meeting on Microwave Radiometry and Remote Sensing of the Environment (MicroRad). - Washington, DC, 1-4 March 2010. - P. 211-216. ↑
- C272.** Strobach E. GPR for large-scale estimation of groundwater recharge distribution. / Strobach E., Harris B.D., Dupuis J.C., Kepic A.W., Martin M.W. // 2010 13th International Conference on Ground Penetrating Radar (GPR). - Lecce, 21-25 June 2010. - P. 1-6. ↑
- C273.** Carpentier S.F.A. Recent deformation of Quaternary sediments in the northwest Canterbury Plains, New Zealand, as inferred from GPR and seismic data. / Carpentier S.F.A., Dorn C., Doetsch J.A., Campbell F.M., Horstmeyer H., Green A.G., Kaiser A.E., Campbell J., Pettinga J., Nobes D.C., Finnemore M., Jongens R. // 2010 13th International Conference on Ground Penetrating Radar (GPR). - Lecce, 21-25 June 2010. - P. 1-5. ↑
- C274.** Jha P.C. Mapping oil leak flow path using Step Frequency Radar: A case study. / Jha P.C., Balasubramaniam V.R., Sandeep N., Sivaram Y.V. // 2010 13th International Conference on Ground Penetrating Radar (GPR). - Lecce, 21-25 June 2010. - P. 1-6. ↑
- C275.** Koh G. Autonomous FMCW radar survey of Antarctic shear zone. / Koh G., Lever J.H., Arcone S.A., Marshall H., Ray L.E. // 2010 13th International Conference on Ground Penetrating Radar (GPR). - Lecce, 21-25 June 2010. - P. 1-5. ↑

- C276.** Be. GPR, ERT and CPT data integration for high resolution aquifer modeling. / Be, langer C., Giroux B., Gloaguen E., Lefebvre R. // 2010 13th International Conference on Ground Penetrating Radar (GPR). - Lecce, 21-25 June 2010. - P. 1-6. ↑
- C277.** Francke J. Applications of GPR in mineral resource evaluations. 2010 13th International Conference on Ground Penetrating Radar (GPR). - Lecce, 21-25 June 2010. - P. 1-5. ↑
- C278.** Mahmoudzadeh M.R. Water table detection by GPR in Sardon, Salamanca, Spain. / Mahmoudzadeh M.R., Lambot S., Frances A.P., Mohammed A.A., Lubczynski M. // 2010 13th International Conference on Ground Penetrating Radar (GPR). - Lecce, 21-25 June 2010. - P. 1-5. ↑
- C279.** Razevig V.V. Advantages and restrictions of holographic subsurface radars. / Razevig V.V., Ivashov S.I., Vasiliev I.A., Zhuravlev A.V., Bechtel T., Capineri L. // 2010 13th International Conference on Ground Penetrating Radar (GPR). - Lecce, 21-25 June 2010. - P. 1-6. ↑
- C280.** Ceraudo G. Integrated GPR and archaeological investigations to study the site of Aquinum (Frosinone Italy). / Ceraudo G., Piro S., Zamuner D. // 2010 13th International Conference on Ground Penetrating Radar (GPR). - Lecce, Italy, 21-25 June 2010. - P. 1-5. ↑
- C281.** Nazli H. Experimental investigation of different soil types for buried object imaging using impulse GPR. / Nazli H., Bicak E., Sezgin M. // 2010 13th International Conference on Ground Penetrating Radar (GPR). - Lecce, 21-25 June 2010. - P. 1-5. ↑
- C282.** Pallavi B. Monitoring of seasonal influence on spatial distribution of moisture content at a natural Kanto loam site using ground wave of GPR. / Pallavi B., Saito H., Kato M. // 2010 13th International Conference on Ground Penetrating Radar (GPR). - Lecce, 21-25 June 2010. - P. 1-5. ↑
- C283.** Lauro S.E. A simple inversion model for the estimation of subsurface features of Mars poles. / Lauro S.E., Mattei E., Pettinelli E., Orosei R., Soldovieri F. // 2010 13th International Conference on Ground Penetrating Radar (GPR). - Lecce, 21-25 June 2010. - P. 1-4. ↑
- C284.** Pieraccini M. Attenuation of large bandwidth microwave signals in water and wet sand. / Pieraccini M., Barucci A., Mecatti D., Macaluso G., Atzeni C. // 2010 13th International Conference on Ground Penetrating Radar (GPR). - Lecce, 21-25 June 2010. - P. 1-6. ↑
- C285.** Hitchcock C. Surface, sub-surface mapping and geohazard identification and associated risk mitigation for power transmission. / Hitchcock C., Mitchell T., Amine D. // 2010 IEEE PES Transmission and Distribution Conference and Exposition. - New Orleans, LA, USA, 19-22 April 2010. - P. 1-7. ↑
- C286.** Jiemin Hu. A novel approach to synthesize the range profile via predesigned stepped-frequency waveforms. / Jiemin Hu, Weidong Jiang, Yaowen Fu, Jing Ning. // 2010 2nd International Conference on Computer Engineering and Technology (ICCET). - Chengdu, 16-18 April 2010. - Vol. 5. - P. V5-363-V5-366-363. ↑
- C287.** Jun Guo. Single tree modeling and vegetation visualization using lidar data. / Jun Guo, Zheng Niu. // 2010 2nd International Conference on Advanced Computer Control (ICACC). - Shenyang, 27-29 March 2010. - Vol. 5. - P. 1-5. ↑
- C288.** Postolache O. Microwave FMCW Doppler radar implementation for in-house pervasive health care system. / Postolache O., Madeira R.N., Giraio P.S., Postolache G. // 2010 IEEE International Workshop on Medical Measurements and Applications Proceedings (MeMeA). - Ottawa, ON, April 30 2010-May 1 2010. - P. 47-52. ↑
- C289.** Dudas L. Vehicle relative movement estimation using microwave sensor. / Dudas L., Micskei T., Seller R., Kazi K. // 2010 15th International Conference on Microwave Techniques (COMITE). - Brno, 19-21 April 2010. - P. 109-112. ↑
- C290.** de Porras Bernacer R. Multiprotocol transceiving, Formatting and Temperature monitoring FPGA based unit. 2010 VI Southern Programmable Logic Conference (SPL). - Ipojuca, 24-26 March 2010. - P. 147-150. ↑
- C291.** Rigatos G.G. Technical Analysis and Implementation Cost Assessment of Sigma-Point Kalman Filtering and Particle Filtering in Autonomous Navigation Systems. 2010 IEEE 71st Vehicular Technology Conference

(VTC 2010-Spring). - Taipei, 16-19 May 2010. - P. 1-5. ↑

C292. Tebaldini S. SAR imaging of forest structure at longer wavelengths. / Tebaldini S., d'Alessandro M.M., Rocca F. // 2010 IEEE Radar Conference. - Washington, DC, 10-14 May 2010. - P. 811-815. ↑

C293. Seungbum Kim. Monitoring surface soil moisture and freeze-thaw state with the high-resolution radar of the Soil Moisture Active/Passive (SMAP) mission. / Seungbum Kim, van Zyl J., McDonald K., Njoku E. // 2010 IEEE Radar Conference. - Washington, DC, 10-14 May 2010. - P. 735-739. ↑

C294. Angelliaume S. Ship detection using airborne SAR data acquired at X-band. / Angelliaume S., Martineau P., Peyret J., Oriot H., Foix V., Durand P., Souyris J.C. // 2010 IEEE Radar Conference. - Washington, DC, 10-14 May 2010. - P. 657-660. ↑

C295. Harcke L. Spotlight-mode synthetic aperture radar processing for high-resolution lunar mapping. / Harcke L., Weintraub L., Sang-Ho Yun, Dickinson R., Gurrola E., Hensley S., Marechal N. // 2010 IEEE Radar Conference. - Washington, DC, 10-14 May 2010. - P. 1260-1264. ↑

C296. Paichard Y. OFDM waveforms for multistatic radars. 2010 IEEE Radar Conference. - Washington, DC, 10-14 May 2010. - P. 1187-1190. ↑

C297. Maresca S. The HF surface wave radar WERA. Part I: Statistical analysis of recorded data. / Maresca S., Greco M., Gini F., Grasso R., Coraluppi S., Thomas N. // 2010 IEEE Radar Conference. - Washington, DC, 10-14 May 2010. - P. 826-831. ↑

C298. Linkova A. Measurement of parameters of solid aerosols in polydisperse medium using double frequency radar. 2010 International Conference on Modern Problems of Radio Engineering, Telecommunications and Computer Science (TCSET). - Lviv-Slavske, 23-27 Feb. 2010. - P. 77. ↑

C299. Bezruk V. Application of AR model for radar recognition of meteorological objects. / Bezruk V., Belov E., Voitovych O., Netrebenko K., Tikhonov V., Rudnev G., Khlopov G., Khomenko S. // 2010 International Conference on Modern Problems of Radio Engineering, Telecommunications and Computer Science (TCSET). - Lviv-Slavske, 23-27 Feb. 2010. - P. 93. ↑

C300. Reinartz P. Improving geometric accuracy of optical VHR satellite data using Terrasar-X data. / Reinartz P., Muller R., Suri S., Schwind P. // 2010 IEEE Aerospace Conference. - Big Sky, MT, 6-13 March 2010. - P. 1-10. ↑

C301. Zhou Houfu. Simulation and Comparison of Two Kinds of Severe Convective Weather Processes. / Zhou Houfu, Guo Pinwen, Zhai Jing. // 2010. ICCMS '10. Second International Conference on Computer Modeling and Simulation. - Sanya, Hainan, 22-24 Jan. 2010. - Vol. 1. - P. 243-247. ↑

C302. Guoning Zhang. Research on the Object-Extraction from Aerial LIDAR Dataset. / Guoning Zhang, Jie Yu, Qin Yan. // 2010. ICCMS '10. Second International Conference on Computer Modeling and Simulation. - Sanya, Hainan, 22-24 Jan. 2010. - Vol. 4. - P. 299-302. ↑

C303. Nunnari G. Inverse Modeling of 3D High Resolution Ground Deformation Maps Derived by Integrating GPS and DInSAR Data. / Nunnari G., Spata A., Puglisi G., Guglielmino F., Bonforte A. // 2010. COMPENG '10. Complexity in Engineering. - Rome, 22-24 Feb. 2010. - P. 135-137. ↑

C304. Xiaochun Zhang. Estimating Large Area Evapotranspiration from MODIS Data. / Xiaochun Zhang, Jingwei Wu. // 2010 Asia-Pacific Power and Energy Engineering Conference (APPEEC). - Chengdu, 28-31 March 2010. - P. 1-4. ↑

C305. Wang Xiaojun. Parameters analysis for polarimetric SAR Based on classification accuracy. / Wang Xiaojun, Li Hao, Wu Yonghui, Yan Shusheng, Li Lianhua. // 2010 International Conference on Image Analysis and Signal Processing (IASP). - Zhejiang, 9-11 April 2010. - P. 268-271. ↑

C306. Aimin Cai. Parameters extraction of crop based on PolSAR Data. / Aimin Cai, Yun Shao, Huaze Gong. // 2010 International Conference on Image Analysis and Signal Processing (IASP). - Zhejiang, 9-11 April 2010. - P. 12-15. ↑

C307. Han Ping. Automatic target recognition of SAR images based on the fuzzy neural networks. / Han Ping,

Gao Shan. // 2010 The 2nd IEEE International Conference on Information Management and Engineering (ICIME). - Chengdu, 16-18 April 2010. - P. 102-104. ↑

C308. Nan Wang. SAR sensor employment planning for tactical aircraft. / Nan Wang, Yuan Li, Yanlong Bu, Jing Chen. // 2010 The 2nd International Conference on Computer and Automation Engineering (ICCAE). - Singapore, 26-28 Feb. 2010. - Vol. 5. - P. 603-608. ↑

C309. Zhao Tongzhou. Image Fusion Based on Multi-scale Kalman Filtering. / Zhao Tongzhou, Wang Yanli, Wang Haihui. // 2010 Second International Workshop on Education Technology and Computer Science (ETCS). - Wuhan, 6-7 March 2010. - Vol. 3. - P. 207-215. ↑

C310. Norgard J. Computational electromagnetic modeling & simulation of ultra wideband sub-surface sensors for the detection and imaging of buried objects using spatial and spectral diversity. / Norgard J., Musellman R., Drozd A. // 2010 Asia-Pacific Symposium on Electromagnetic Compatibility (APEMC). - Beijing, 12-16 April 2010. - P. 544-547. ↑

C311. Zaugg E. Using the MicroASAR on the NASA SIERRA UAS in the Characterization of Arctic Sea Ice Experiment. / Zaugg E., Long D., Edwards M., Fladeland M., Kolyer R., Crocker I., Maslanik J., Herzfeld U., Wallin B. // 2010 IEEE Radar Conference. - Washington, DC, 10-14 May 2010. - P. 271-276. ↑

C312. Zhang Deng-hui. Analysis of image fusion and classification for high resolution SAR data on-line. / Zhang Deng-hui, Zhang Han-kui, Xie Bin, Huang Zhao-quan, Yu Le, Cao Yun-yun. // 2010 2nd International Conference on Education Technology and Computer (ICETC). - Shanghai, 22-24 June 2010. - Vol. 1. - P. V1-267-V1-271-267. ↑

C313. Shang Shang. Extraction of ionospheric clutter in HFSWR. / Shang Shang, Zhang Ning, Li Yang. // 2010 2nd International Conference on Industrial Mechatronics and Automation (ICIMA). - Wuhan, China, 30-31 May 2010. - Vol. 2. - P. 296-299. ↑

C314. Kopyt Pawel. A 5.8 GHz RFID-based data transmission system as an energy efficient solution for on-board monitoring. 2010 18th International Conference on Microwave Radar and Wireless Communications (MIKON). - Vilnius, Lithuania, 14-16 June 2010. - P. 1-4. ↑

C315. Peng Shurong. Application of D-InSAR Technique for the Bam Earthquake. / Peng Shurong, Wang Xueqin, Liu Dan. // 2010 International Conference on Intelligent Computation Technology and Automation (ICICTA). - Changsha, 11-12 May 2010. - Vol. 1. - P. 746-749. ↑

C316. Xu Xi-Yu. Engineering design of the rain mode on an ocean-dedicating radar altimeter. / Xu Xi-Yu, Liu He-Guang, Liu Peng. // 2010 International Conference on Microwave and Millimeter Wave Technology (ICMMT). - Chengdu, 8-11 May 2010. - P. 1719-1722. ↑

C317. Yin Honggang. Predesign of the wind field measuring radar for FengYun-3E meteorological satellite. / Yin Honggang, Dong Xiaolong. // 2010 International Conference on Microwave and Millimeter Wave Technology (ICMMT). - Chengdu, 8-11 May 2010. - P. 1228-1230. ↑

C318. Zongbo Wang. FPGA based IF digital receiver for the PARSAX-Polarimetric agile radar. / Zongbo Wang, Krasnov O.A., Lighthart L.P., van der Zwan F. // 2010 18th International Conference on Microwave Radar and Wireless Communications (MIKON). - Vilnius, 14-16 June 2010. - P. 1-4. ↑

C319. Zhang Bentao. Research on the spaceborne SAR image processing and feature extraction for ocean fronts detection. / Zhang Bentao, Chen Biao, Gao Guoxing. // 2010 International Conference On Computer and Communication Technologies in Agriculture Engineering (CCTAE). - Chengdu, 12-13 June 2010. - Vol. 2. - P. 473-476. ↑

C320. Latif Z.A. Extraction of gap and canopy properties using LiDAR and multispectral data for forest microclimate modelling. / Latif Z.A., Blackburn G.A. // 2010 6th International Colloquium on Signal Processing and Its Applications (CSPA). - Mallaca City, 21-23 May 2010. - P. 1-5. ↑

C321. Shkvarko Y.V. Aggregated convex regularization and variational analysis technique for enhancement of mm waveband remote sensing imagery. / Shkvarko Y.V., Tuxpan J., Santos S.R. // 2010 International Kharkov Symposium on Physics and Engineering of Microwaves, Millimeter and Submillimeter Waves (MSMW). - Kharkiv, 21-26 June 2010. - P. 1-3. ↑

- C322.** Wei Yao. Airborne analysis and assessment of urban traffic scenes from LiDAR data-Theory and experiments. / Wei Yao, Hinz S., Stilla U. // 2010 IEEE Computer Society Conference on Computer Vision and Pattern Recognition Workshops (CVPRW). - San Francisco, CA, 13-18 June 2010. - P. 75-82. ↑
- C323.** Wei Zhang. Comparisons of speckle noise filtering methods on high resolution SAR image. / Wei Zhang, Jinzhong Yang, Le Yu. // 2010 International Conference On Computer and Communication Technologies in Agriculture Engineering (CCTAE). - Chengdu, 12-13 June 2010. - Vol. 3. - P. 202-204. ↑
- C324.** Wei Zhang. SAR and Landsat ETM+ image fusion using variational model. / Wei Zhang, Le Yu. // 2010 International Conference On Computer and Communication Technologies in Agriculture Engineering (CCTAE). - Chengdu, 12-13 June 2010. - Vol. 3. - P. 205-207. ↑
- C325.** Li Wang. Observation of Mixed-Layer Depth of Atmosphere with Lidar. / Li Wang, Jiandong Mao, Yufeng Wang, Ming Wang, Dengxin Hua. // 2010 Symposium on Photonics and Optoelectronic (SOPO). - Chengdu, 19-21 June 2010. - P. 1-4. ↑
- C326.** Lin Hong. Study of Double-Wavelength Airborne Lidar System Based on Ocean Red Tide Monitoring. / Lin Hong, Liang Kun. // 2010 Symposium on Photonics and Optoelectronic (SOPO). - Chengdu, 19-21 June 2010. - P. 1-4. ↑
- C327.** Xu Jing-zhong. A Method of 3D Building Boundary Extraction from Airborne LIDAR Points Cloud. / Xu Jing-zhong, Wan You-chuan, Yao Fang. // 2010 Symposium on Photonics and Optoelectronic (SOPO). - Chengdu, 19-21 June 2010. - P. 1-4. ↑
- C328.** {no data available}. Copyright page. 2010 IEEE Radar Conference. - Washington, DC, 10-14 May 2010. - P. 1. ↑
- C329.** Celik T. Resolution selective change detection in satellite images. / Celik T., Curtis C.V. // 2010 IEEE International Conference on Acoustics Speech and Signal Processing (ICASSP). - Dallas, TX, 14-19 March 2010. - P. 970-973. ↑
- C330.** Kaihua Xu. Implementation of handheld remote sense image calibration system software. / Kaihua Xu, Jian Chen, Rui Wang, Yuhua Liu. // 2010 2nd International Conference on Future Computer and Communication (ICFCC). - Wuhan, 21-24 May 2010. - Vol. 2. - P. V2-664-V2-668-664. ↑
- C331.** Morabito Andrea F. On the optimal synthesis of ring symmetric shaped beams through uniformly spaced planar arrays. / Morabito Andrea F., Lagana Antonia R., Isernia Tommaso. // 2010 Proceedings of the Fourth European Conference on Antennas and Propagation (EuCAP). - Barcelona, Spain, 12-16 April 2010. - P. 1-5. ↑
- C332.** Heer C. Spaceborne SAR Systems and technologies. / Heer C., Fischer C., Schaefer C. // 2010 IEEE MTT-S International Microwave Symposium Digest (MTT). - Anaheim, CA, 23-28 May 2010. - P. 538-541. ↑
- C333.** Rodriguez-Morales F. Development of a multi-frequency airborne radar instrumentation package for ice sheet mapping and imaging. / Rodriguez-Morales F., Gogineni P., Leuschen C., Allen C., Lewis C., Patel A., Byers K., Smith L., Shi L., Panzer B., Blake W., Crowe R., Gifford C. // 2010 IEEE MTT-S International Microwave Symposium Digest (MTT). - Anaheim, CA, 23-28 May 2010. - P. 157-160. ↑
- C334.** Horton J. B. Special session in honor Dr. Kiyo Tomiyasu. 2010 IEEE MTT-S International Microwave Symposium Digest (MTT). - Anaheim, CA, USA, 23-28 May 2010. - P. 1. ↑
- C335.** Abril J. Active and passive THz systems for short-range imaging applications. / Abril J., Nova E., Capdevila S., Broquetas A., Torres F., Jofre L. // 2010 Proceedings of the Fourth European Conference on Antennas and Propagation (EuCAP). - Barcelona, Spain, 12-16 April 2010. - P. 1-4. ↑
- C336.** Das J. Towards marine bloom trajectory prediction for AUV mission planning. / Das J., Rajany K., Frolov S., Pyy F., Ryany J., Caron D.A., Sukhatme G.S. // 2010 IEEE International Conference on Robotics and Automation (ICRA). - Anchorage, AK, 3-7 May 2010. - P. 4784-4790. ↑
- C337.** Aggarwal A. Vision based collision avoidance by plotting a virtual obstacle on depth map. / Aggarwal A., Kukreja A., Chopra P. // 2010 IEEE International Conference on Information and Automation (ICIA). - Harbin, 20-23 June 2010. - P. 532-536. ↑

- C338.** Colliander A. Utilization of airborne and in situ data obtained in SGP99, SMEX02, CLASIC and SMAPVEX08 Field Campaigns for SMAP Soil Moisture Algorithm Development and Validation. / Colliander A., Chan S., Yueh S., Cosh M., Bindlish R., Jackson T., Njoku E. // 2010 11th Specialist Meeting on Microwave Radiometry and Remote Sensing of the Environment (MicroRad). - Washington, DC, 1-4 March 2010. - P. 43-48. ↑
- C339.** Wen-Qin Wang. LFM CW SAR waveform generation with frequency nonlinearity suppression. 2010 Second IITA International Conference on Geoscience and Remote Sensing (IITA-GRS). - Qingdao, 28-31 Aug. 2010. - Vol. 1. - P. 380-383. ↑
- C340.** Wang Xinzeng. Route planning for unmanned aerial vehicle based on threat probability and mission time restriction. / Wang Xinzeng, Ci Linlin, Li Junshan, Yu Ning. // 2010 Second IITA International Conference on Geoscience and Remote Sensing (IITA-GRS). - Qingdao, 28-31 Aug. 2010. - Vol. 1. - P. 27-30. ↑
- C341.** Wei Zhang. Micro-doppler extraction of vibrating target based on dual-channel ATI technique in SAR. / Wei Zhang, Chuangming Tong, Qun Zhang, Xiao Zhang. // 2010 Second IITA International Conference on Geoscience and Remote Sensing (IITA-GRS). - Qingdao, 28-31 Aug. 2010. - Vol. 1. - P. 422-425. ↑
- C342.** Xu Feng. Data analysis of wind profiler radar(WPR) under three kinds of synoptic processes in spring on Donghai island of Zhanjiang. / Xu Feng, Niu Shengjie, Wang Jing, Zhang Yu, Yue Yan-yu, Zhao Li-juan, Xu Dan. // 2010 Second IITA International Conference on Geoscience and Remote Sensing (IITA-GRS). - Qingdao, 28-31 Aug. 2010. - Vol. 1. - P. 287-290. ↑
- C343.** Zeng Yejuan. Research on DBF SAR system in near space. / Zeng Yejuan, Dai Yuehua. // 2010 Second IITA International Conference on Geoscience and Remote Sensing (IITA-GRS). - Qingdao, 28-31 Aug. 2010. - Vol. 1. - P. 129-132. ↑
- C344.** Deng Yu. Monitoring manners research on the river ice in the Yellow River. / Deng Yu, Zhang Baosen. // 2010 Second IITA International Conference on Geoscience and Remote Sensing (IITA-GRS). - Qingdao, 28-31 Aug. 2010. - Vol. 1. - P. 111-113. ↑
- C345.** Yongzheng Ren. Wind field retrieval over the ocean using X-band polarization SAR data. / Yongzheng Ren, Mingxia He, Lehner S. // 2010 Second IITA International Conference on Geoscience and Remote Sensing (IITA-GRS). - Qingdao, 28-31 Aug. 2010. - Vol. 1. - P. 43-46. ↑
- C346.** Mantovanelli A. The use of HF radar surface currents for computing Lagrangian trajectories: Benefits and issues. / Mantovanelli A., Heron M.L., Prytz A. // OCEANS 2010 IEEE-Sydney. - Sydney, NSW, 24-27 May 2010. - P. 1-6. ↑
- C347.** Xu Xi-Yu. Mechanisms and system design of satellite interferometric Synthetic Aperture Radar altimeter. / Xu Xi-Yu, Liu He-Guang, Yang Shuang-Bao. // 2010 Second IITA International Conference on Geoscience and Remote Sensing (IITA-GRS). - Qingdao, 28-31 Aug. 2010. - Vol. 2. - P. 209-211. ↑
- C348.** Wettle M. Offshore petroleum exploration from space: A developing capability at Geoscience Australia. / Wettle M., Daniel P.J., Logan G.A., Thankappan M. // OCEANS 2010 IEEE-Sydney. - Sydney, NSW, 24-27 May 2010. - P. 1-7. ↑
- C349.** Shi Jian-qing. Study the feasibility of airborne LiDAR on areal earth's crust deformation surveying. / Shi Jian-qing, Jiang Ting-chen. // 2010 Second IITA International Conference on Geoscience and Remote Sensing (IITA-GRS). - Qingdao, 28-31 Aug. 2010. - Vol. 1. - P. 193-197. ↑
- C350.** Walsh J. Further analysis of the modulation of high frequency radar spectra due to sea-induced antenna platform motion. / Walsh J., Ryan B., Gill E., El Khoury J. // OCEANS 2010 IEEE-Sydney. - Sydney, NSW, 24-27 May 2010. - P. 1-4. ↑
- C351.** Moltmann T. The Integrated Marine Observing System-delivering data-streams to support marine research and applications. / Moltmann T., Proctor R., Hill K., McGowen M. // OCEANS 2010 IEEE-Sydney. - Sydney, NSW, 24-27 May 2010. - P. 1-8. ↑
- C352.** Cai Wenwen. Assimilation MODIS and HJ-1 Reflectance Images to Produce NDVI of High Spatial and Temporal Resolution. / Cai Wenwen, Song Jinling, Wang Jindi, Xiao Zhiqiang. // 2010 6th International Conference on Wireless Communications Networking and Mobile Computing (WiCOM). - Chengdu, 23-25 Sept. 2010. - P. 1-4. ↑

2010. - P. 1-4. ↑

**C353.** Yongzhe Wang. Coseismic Deformation of 2009 L'Aquila, Italy Earthquake Derived from Ascending and Descending ENVISAT/ASAR Images. / Yongzhe Wang, Ziqiang Ou, Jianjun Zhu, Xiaoyan Dong, Xuemin Xing, Yafu Yang. // 2010 6th International Conference on Wireless Communications Networking and Mobile Computing (WiCOM). - Chengdu, 23-25 Sept. 2010. - P. 1-3. ↑

**C354.** Liang Zhang. A Novel Random Sampling Method for Radar Image Compression. / Liang Zhang, Ming-Sheng Chen, Lei Xu, Xian-Liang Wu. // 2010 6th International Conference on Wireless Communications Networking and Mobile Computing (WiCOM). - Chengdu, 23-25 Sept. 2010. - P. 1-4. ↑

**C355.** Xu Jing-zhong. Filtering of LIDAR Points by a Hierarchical Smoothing Method. / Xu Jing-zhong, Wan You-chuan. // 2010 6th International Conference on Wireless Communications Networking and Mobile Computing (WiCOM). - Chengdu, 23-25 Sept. 2010. - P. 1-4. ↑

**C356.** Tang Feifei. A New Image Segmentation Method for Individual Tree Recognition Based on Airborne LiDAR Data. / Tang Feifei, Liu Xing, Zhang Yali, Ruan Zhimin. // 2010 6th International Conference on Wireless Communications Networking and Mobile Computing (WiCOM). - Chengdu, 23-25 Sept. 2010. - P. 1-4. ↑

**C357.** Zhou Zhen-yu. Practicable Research on Suppressing Angular Glint Base on the Target's RCS Weights. / Zhou Zhen-yu, He Zhi-yi, Zhao Xin, Luo Ye. // 2010 6th International Conference on Wireless Communications Networking and Mobile Computing (WiCOM). - Chengdu, 23-25 Sept. 2010. - P. 1-5. ↑

**C358.** Hong-Li Zhao. A method for InSAR baseline refinement and its application. / Hong-Li Zhao, Jing-Hui Fan, Xiao-Fang Guo. // 2010 Second IITA International Conference on Geoscience and Remote Sensing (IITA-GRS). - Qingdao, 28-31 Aug. 2010. - Vol. 2. - P. 161-164. ↑

**C359.** Lu Ye. Modeling and simulation of position for the Stratospheric ISAR system. / Lu Ye, Jing Xiaojun, You Siqing, Qi Zhaoqun, Sun Songlin. // 2010 Second IITA International Conference on Geoscience and Remote Sensing (IITA-GRS). - Qingdao, 28-31 Aug. 2010. - Vol. 1. - P. 525-528. ↑

**C360.** Sheng Chen. Application of integrated geological prediction in expressway tunnel. / Sheng Chen, Jiahua Shu, Qiaosen Luj, Guichun Zhu. // 2010 Second IITA International Conference on Geoscience and Remote Sensing (IITA-GRS). - Qingdao, 28-31 Aug. 2010. - Vol. 1. - P. 540-543. ↑

**C361.** Jiang Ting-Chen. Deformation analysis of Wenchuan earthquake based on D-InSAR with image mode. / Jiang Ting-Chen, Wang Xiu-Ping. // 2010 Second IITA International Conference on Geoscience and Remote Sensing (IITA-GRS). - Qingdao, 28-31 Aug. 2010. - Vol. 1. - P. 189-192. ↑

**C362.** Zheng Zhao. High-resolution airborne SAR interferometry mapping application in Huashan mountain. / Zheng Zhao, Jixian Zhang, Guoman Huang, Fenfen Hua, Shucheng Yang, Shaoping Deng. // 2010 Second IITA International Conference on Geoscience and Remote Sensing (IITA-GRS). - Qingdao, 28-31 Aug. 2010. - Vol. 2. - P. 571-574. ↑

**C363.** JingHui Fan. DInSAR for land subsidence monitoring using high resolution COSMO-SKYMED SAR Data: Preliminary results compared with ASAR. / JingHui Fan, HongLi Zhao, Xiaofang Guo. // 2010 Second IITA International Conference on Geoscience and Remote Sensing (IITA-GRS). - Qingdao, 28-31 Aug. 2010. - Vol. 2. - P. 157-160. ↑

**C364.** Huan Ruohong. SAR image target recognition based on NMF feature extraction and Bayesian decision fusion. / Huan Ruohong, Pan Yun, Mao Keji. // 2010 Second IITA International Conference on Geoscience and Remote Sensing (IITA-GRS). - Qingdao, 28-31 Aug. 2010. - Vol. 1. - P. 496-499. ↑

**C365.** Yoshida T. Time domain numerical simulation of microwave backscattering from sea surface for radar remote sensing. / Yoshida T., Chang-Kyu Rheem. // OCEANS 2010 IEEE-Sydney. - Sydney, NSW, 24-27 May 2010. - P. 1-6. ↑

**C366.** Yanovsky F.J. Simulation study of relationships between Doppler-polarimetric parameters at microwave remote sensing of precipitation. / Yanovsky F.J., Glushko D. // 2010 European Radar Conference (EuRAD). - Paris, Sept. 30 2010-Oct. 1 2010. - P. 148-151. ↑

**C367.** Korchagina D.A. Bio-radiolocation method at chest wall motion analysis during tidal breathing. /

Korchagina D.A., Alekhin M.D., Anishchenko L.N. // 2010 European Radar Conference (EuRAD). - Paris, Sept. 30 2010-Oct. 1 2010. - P. 475-478. ↑

C368. Toporkov J.V. Backscattering of wide-band HF signals from evolving ocean-like surface: 2-D direct numerical simulations and analysis. / Toporkov J.V., Sletten M.A. // 2010 European Radar Conference (EuRAD). - Paris, Sept. 30 2010-Oct. 1 2010. - P. 9-12. ↑

C369. Chamberlain N. The DESDynI synthetic aperture radar array-fed reflector antenna. / Chamberlain N., Ghaemi H., Giersch L., Harcke L., Hodges R., Hoffman J., Johnson W., Jordan R., Khayatian B., Rosen P., Sadowy G., Shaffer S., Shen Y., Veilleux L., Wu P. // 2010 IEEE International Symposium on Phased Array Systems and Technology (ARRAY). - Waltham, MA, 12-15 Oct. 2010. - P. 381-386. ↑

C370. PourNejatian N.M. Fractal based detection using blind box-counting method in high resolution radars. / PourNejatian N.M., Nayebi M.M. // 2010 European Radar Conference (EuRAD). - Paris, Sept. 30 2010-Oct. 1 2010. - P. 407-410. ↑

C371. Mecatti D. Monitoring open-pit quarries by interferometric radar for safety purposes. / Mecatti D., Macaluso G., Barucci A., Noferini L., Pieraccini M., Atzeni C. // 2010 European Radar Conference (EuRAD). - Paris, Sept. 30 2010-Oct. 1 2010. - P. 37-40. ↑

C372. Ermakov S. Possibilities of oil slick detection on the sea surface using radar. / Ermakov S., da Silva J.C.B., Magalhaes J.M., Sergievskaya I. // 2010 European Radar Conference (EuRAD). - Paris, Sept. 30 2010-Oct. 1 2010. - P. 13-16. ↑

C373. Sagnard F. Development of wideband crosshole and surface GPR for soil characterization: FDTD modeling and experiments. / Sagnard F., Rejiba F., Froumentin M. // 2010 European Microwave Conference (EuMC). - Paris, 28-30 Sept. 2010. - P. 332-335. ↑

C374. Anderson S. SAR imagery and Seatrack Web as decision making tools for illegal oil spill combating-a case study. / Anderson S., Uiboupin R., Verjovkina S., Raudsepp U. // 2010 IEEE/OES US/EU Baltic International Symposium (BALTIC). - Riga, 24-27 Aug. 2010. - P. 1-6. ↑

C375. Kozlov I. Advancing coastal upwelling observations with use of SAR data: Case study from SE Baltic. / Kozlov I., Dailidienė I., Kudryavtsev V. // 2010 IEEE/OES US/EU Baltic International Symposium (BALTIC). - Riga, 24-27 Aug. 2010. - P. 1-2. ↑

C376. Wei Gao. Brillouin amplification of weak Stokes signal from sea water with different salinities and temperatures. / Wei Gao, Di Sun, Jianyi Li, Guiyuan Cao, Entao Li, Zhiwei Lu, Weiming He. // 2010 10th Russian-Chinese Symposium on Laser Physics and Laser Technologies (RCSLPLT) and 2010 Academic Symposium on Optoelectronics Technology (ASOT). - Harbin, July 28 2010-Aug. 1 2010. - P. 139-142. ↑

C377. Jianfeng Sun. Experiments research on ocean surface wave detecting using Streak Tube Imaging Lidar. / Jianfeng Sun, Jian Gao, Jingsong Wei, Qi Wang. // 2010 10th Russian-Chinese Symposium on Laser Physics and Laser Technologies (RCSLPLT) and 2010 Academic Symposium on Optoelectronics Technology (ASOT). - Harbin, July 28 2010-Aug. 1 2010. - P. 228-231. ↑

C378. Thai T.T. Design and development of a millimetre-wave novel passive ultrasensitive temperature transducer for remote sensing and identification. / Thai T.T., Chebila F., Mehdi J.M., Pons P., Aubert H., DeJean G.R., Tentzeris M.M., Plana R. // 2010 European Microwave Conference (EuMC). - Paris, 28-30 Sept. 2010. - P. 45-48. ↑

C379. Wicks M. Spectrum crowding and Cognitive Radar. 2010 2nd International Workshop on Cognitive Information Processing (CIP). - Elba, 14-16 June 2010. - P. 452-457. ↑

C380. Xie Hongsen. CFAR detector using GIS information. / Xie Hongsen, Zou Kun. // 2010 Second IITA International Conference on Geoscience and Remote Sensing (IITA-GRS). - Qingdao, 28-31 Aug. 2010. - Vol. 2. - P. 272-274. ↑

C381. Zhang Ying. Study on retrieval methods of soil water content in vegetation covering areas based on multi-source remote sensing data. 2010 Second IITA International Conference on Geoscience and Remote Sensing (IITA-GRS). - Qingdao, 28-31 Aug. 2010. - Vol. 2. - P. 369-372. ↑

- C382.** Jaffre. Waves in the Southern Great Barrier Reef. / Jaffre, J.B.D., Heron M.L., Middleditch A., Steinberg C.R., Durrant T.H. // OCEANS 2010 IEEE-Sydney. - Sydney, NSW, 24-27 May 2010. - P. 1-4. ↑
- C383.** Lixue Song. Doppler velocity dealiasing with millimeter wave radar RHI data. / Lixue Song, Ming Wei. // 2010 Second IITA International Conference on Geoscience and Remote Sensing (IITA-GRS). - Qingdao, 28-31 Aug. 2010. - Vol. 2. - P. 216-218. ↑
- C384.** Reichert K. X-Band radar derived sea surface elevation maps as input to ship motion forecasting. / Reichert K., Dannenberg J., van den Boom H. // OCEANS 2010 IEEE-Sydney. - Sydney, NSW, 24-27 May 2010. - P. 1-7. ↑
- C385.** Garelo R. Signal and image processing applications in radar ocean observations. 2010 10th International Conference on Information Sciences Signal Processing and their Applications (ISSPA). - Kuala Lumpur, 10-13 May 2010. - P. 810-818. ↑
- C386.** Hashemi S.-K. A new class of microwave filters using vertically stacked coupled open loop resonators. 2010 IEEE International Conference on Wireless Information Technology and Systems (ICWITS). - Honolulu, HI, Aug. 28 2010-Sept. 3 2010. - P. 1-4. ↑
- C387.** Macfarlane D.G. Validation of the AVTIS volcano imager radiometry-A comparison of infrared and millimetre wave thermal imagery. / Macfarlane D.G., Robertson D.A., James M.R. // 2010 35th International Conference on Infrared Millimeter and Terahertz Waves (IRMMW-THz). - Rome, 5-10 Sept. 2010. - P. 1-3. ↑
- C388.** Rogers A.B. Measurement of the complex dielectric constant of volcanic ash at millimetre wavelengths. / Rogers A.B., Macfarlane D.G., Robertson D.A. // 2010 35th International Conference on Infrared Millimeter and Terahertz Waves (IRMMW-THz). - Rome, 5-10 Sept. 2010. - P. 1-2. ↑
- C389.** Xu Xi-Yu. Digital module design of a satellite rain-compatible radar altimeter. / Xu Xi-Yu, Liu He-Guang, Liu Peng. // 2010 International Symposium on Signals Systems and Electronics (ISSSE). - Nanjing, 17-20 Sept. 2010. - Vol. 2. - P. 1-3. ↑
- C390.** Tuxpan-Vargas J. Fused variational analysis technique for high-resolution reconstruction of remote sensing imagery. / Tuxpan-Vargas J., Santos-Arce S. // 2010 7th International Conference on Electrical Engineering Computing Science and Automatic Control (CCE). - Tuxtla Gutierrez, 8-10 Sept. 2010. - P. 351-356. ↑
- C391.** Chenggang Zhao. Design of mobile robot system with remote control based on CAN-bus. / Chenggang Zhao, Xiangke Han. // 2010 International Conference on Computer, Mechatronics, Control and Electronic Engineering (CMCE). - Changchun, 24-26 Aug. 2010. - Vol. 2. - P. 103-105. ↑
- C392.** Xie Chou. Multitemporal polarimetric SAR data fusion for land cover mapping. / Xie Chou, Shao Yun, Wan Zi, Zhang Fengli. // 2010 18th International Conference on Geoinformatics. - Beijing, 18-20 June 2010. - P. 1-5. ↑
- C393.** Fan Wang. A study of PS-InSAR method for small area urban land subsidence. / Fan Wang, Zhaoquan Huang, Le Yu, Lifan Zhou, Dengrong Zhang. // 2010 18th International Conference on Geoinformatics. - Beijing, 18-20 June 2010. - P. 1-6. ↑
- C394.** Ye R.Q. Integration of LIDAR data and geological maps for landslide hazard assessment in the Three Gorges Reservoir area, China. / Ye R.Q., Niu R.Q., Zhao Y.N., Jiang Q.Y., Wu T., Deng Q.L. // 2010 18th International Conference on Geoinformatics. - Beijing, 18-20 June 2010. - P. 1-5. ↑
- C395.** Anqi Wang. Wetland mapping by using multi-band and multitemporal SAR images: A case study of Hong he National Natural Reserve. / Anqi Wang, Demin Zhou, Huili Gong. // 2010 18th International Conference on Geoinformatics. - Beijing, 18-20 June 2010. - P. 1-5. ↑
- C396.** Jie Yin. Vulnerability assessment of combined impacts of sea level rise and coastal flooding for China's coastal region using remote sensing and GIS. / Jie Yin, Shiyuan Xu, Jun Wang, Haidong Zhong, Yingjie Hu, Zhane Yin, Kangfasheng Wang, Xinjian Zhang. // 2010 18th International Conference on Geoinformatics. - Beijing, 18-20 June 2010. - P. 1-4. ↑
- C397.** Xie Chou. InSAR analysis over Yellow River Delta for mapping water-level changes over wetland. / Xie Chou, Shao Yun, Wan Zi. // 2010 18th International Conference on Geoinformatics. - Beijing, 18-20 June 2010. -

P. 1-5. ↑

**C398.** Bin Pan. Precise SAR satellite orbit parameters determination based on Ground Control Points. / Bin Pan, Ling Liu. // 2010 18th International Conference on Geoinformatics. - Beijing, 18-20 June 2010. - P. 1-5. ↑

**C399.** Yong Du. Study on accurate estimation of baseline parameters of space-borne InSAR based on GCPs. / Yong Du, Songlin Yang, Hongyun Shi. // 2010 18th International Conference on Geoinformatics. - Beijing, 18-20 June 2010. - P. 1-4. ↑

**C400.** Yongquan Li. An improved filtering method for digital elevation models construction based on LiDAR. / Yongquan Li, Xiangxi Dai, Mingxiao Wang, Zhizhou Huang. // 2010 18th International Conference on Geoinformatics. - Beijing, 18-20 June 2010. - P. 1-5. ↑

**C401.** Kebiao Huang. Regional aboveground forest biomass estimation using airborne and spaceborne LiDAR fusion with optical data in the Southwest of China. / Kebiao Huang, Yong Pang, Qingtai Shu, Tian Fu. // 2010 18th International Conference on Geoinformatics. - Beijing, 18-20 June 2010. - P. 1-6. ↑

**C402.** Zongsheng Zheng. Determination of sedimentation rate of tidal flats at the Yangtze estuary, China, using multi-temporal Landsat TM images. / Zongsheng Zheng, Yunxuan Zhou, Xing Li, Runyuan Kuang. // 2010 18th International Conference on Geoinformatics. - Beijing, 18-20 June 2010. - P. 1-6. ↑

**C403.** Nianlong Han. Multi-spectral and SAR images fusion via Mallat and A trous wavelet transform. / Nianlong Han, Jinxing Hu, Wei Zhang. // 2010 18th International Conference on Geoinformatics. - Beijing, 18-20 June 2010. - P. 1-4. ↑

**C404.** Hongyun Shi. A case study on co-seismic ground deformation of the Wenchuan earthquake using L-band and C-band SAR interferometry. / Hongyun Shi, Songlin Yang, Qulin Tan. // 2010 18th International Conference on Geoinformatics. - Beijing, 18-20 June 2010. - P. 1-4. ↑

**C405.** Pour Z.A. Effect of primary feed polarization on phase centre location of parabolic reflector antennas. / Pour Z.A., Shafai L. // 2010 IEEE Antennas and Propagation Society International Symposium (APSURSI). - Toronto, ON, 11-17 July 2010. - P. 1-4. ↑

**C406.** Thai T.T. A novel passive ultrasensitive RF temperature transducer for remote sensing and identification utilizing radar cross sections variability. / Thai T.T., Chebila F., Mehdi J.M., Pons P., Aubert H., DeJean G.R., Tentzeris M.M., Plana R. // 2010 IEEE Antennas and Propagation Society International Symposium (APSURSI). - Toronto, ON, 11-17 July 2010. - P. 1-4. ↑

**C407.** Wang Quanmin. Simulation of UWB echoes from ground based on CPML-FDTD. / Wang Quanmin, Chen Bin, Guo Gang, Huang Kedi. // 2010 3rd IEEE International Conference on Computer Science and Information Technology (ICCSIT). - Chengdu, 9-11 July 2010. - Vol. 3. - P. 524-527. ↑

**C408.** Zribi M. CAROLS campaigns 2009: First Results. / Zribi M., Parde M., Hauser D., Fanise P., Boutin J., Albergel C., Calvet J.C., Crapeau M., Dechambre M., Kerr Y., Baeza E.L., Mialon A., Reverdin G., Ruis A., Saleh K., Wigneron J.P. // 2010 11th Specialist Meeting on Microwave Radiometry and Remote Sensing of the Environment (MicroRad). - Washington, DC, 1-4 March 2010. - P. 49-54. ↑

**C409.** Rengarajan S.R. Advances in waveguide-fed slot arrays. 2010 IEEE Antennas and Propagation Society International Symposium (APSURSI). - Toronto, ON, 11-17 July 2010. - P. 1-4. ↑

**C410.** Cetin R. DFT-UTD based MoM approach for an efficient analysis of scattering from large, finite arrays in the vicinity of scattering objects. / Cetin R., Civi O.A., Nepa P. // 2010 IEEE Antennas and Propagation Society International Symposium (APSURSI). - Toronto, ON, 11-17 July 2010. - P. 1-4. ↑

**C411.** Yuhui Fu. The study on extracting of vessels information from the SAR satellite data. / Yuhui Fu, Hui Ma, Zhaolin Wu. // 2010 International Conference on Intelligent Control and Information Processing (ICICIP). - Dalian, 13-15 Aug. 2010. - P. 266-270. ↑

**C412.** Xuhua Cai. Remote sensing retrieval of soil moisture using ENVISAT-ASAR images: A case study in suburban region of Peking, China. / Xuhua Cai, Huili Gong, Xiaojuan Li, Lin Zhu. // 2010 18th International Conference on Geoinformatics. - Beijing, 18-20 June 2010. - P. 1-4. ↑

- C413.** Gang Chen. Estimation of forest height, biomass and volume using support vector regression and segmentation from lidar transects and Quickbird imagery. / Gang Chen, Hay G.J., Yanlian Zhou. // 2010 18th International Conference on Geoinformatics. - Beijing, 18-20 June 2010. - P. 1-4. ↑
- C414.** Yao Ye. Estimation of wetland aboveground biomass based on SAR image: A case study of Honghe National Natural Reserve in Heilongjiang, China. / Yao Ye, Chunping Zhou, Yonghua Sun, Demin Zhou. // 2010 18th International Conference on Geoinformatics. - Beijing, 18-20 June 2010. - P. 1-6. ↑
- C415.** Jinliang Wang. Preliminary study on land use classification based on multi-source remotely sensed data fusion technology. / Jinliang Wang, Xiaohua Wang, Jun Hu, Yinxia Gao. // 2010 International Conference on Environmental Science and Information Application Technology (ESIAT). - Wuhan, 17-18 July 2010. - Vol. 2. - P. 5-9. ↑
- C416.** Jie Yu. Unsupervised classification for polarimetric Synthetic Aperture Radar image using the fuzzy possibilistic C-means clustering. / Jie Yu, Hongxia Ke, Zhongshan Zhang, Yan Li. // 2010 International Conference on Environmental Science and Information Application Technology (ESIAT). - Wuhan, 17-18 July 2010. - Vol. 2. - P. 72-75. ↑
- C417.** Cheng Xinwen. LIDAR filtering based on morphological watershed and region growing. / Cheng Xinwen, Li Chunfu, Peng Jing, Zhao Na, Zhang Huili. // 2010 International Conference on Environmental Science and Information Application Technology (ESIAT). - Wuhan, 17-18 July 2010. - Vol. 2. - P. 559-562. ↑
- C418.** Haiyang Yu. Digital terrain model extraction from airborne LIDAR data in complex mining area. / Haiyang Yu, Xiaoping Lu, Xiaosan Ge, Gang Cheng. // 2010 18th International Conference on Geoinformatics. - Beijing, 18-20 June 2010. - P. 1-6. ↑
- C419.** Erkan A.N. Semi-supervised remote sensing image classification via maximum entropy. / Erkan A.N., Camps-Valls G., Altun Y. // 2010 IEEE International Workshop on Machine Learning for Signal Processing (MLSP). - Kittila, Aug. 29 2010-Sept. 1 2010. - P. 313-318. ↑
- C420.** Qiu R.C. Wireless tomography, Part I: A novel approach to remote sensing. / Qiu R.C., Wicks M.C., Li L., Hu Z., Hou S.J., Chen P., Browning J.P. // 2010 International Waveform Diversity and Design Conference (WDD). - Niagara Falls, ON, 8-13 Aug. 2010. - P. 000244-000256. ↑
- C421.** Kaasalainen S. Active hyperspectral LIDAR methods for object classification. / Kaasalainen S., Suomalainen J., Hakala T., Yuwei Chen, Raikkonen E., Puttonen E., Kaartinen H. // 2010 2nd Workshop on Hyperspectral Image and Signal Processing: Evolution in Remote Sensing (WHISPERS). - Reykjavik, 14-16 June 2010. - P. 1-4. ↑
- C422.** Milisavljevic. Detecting potential human activities using coherent change detection. / Milisavljevic, N., Closson D., Bloch I. // 2010 2nd International Conference on Image Processing Theory Tools and Applications (IPTA). - Paris, 7-10 July 2010. - P. 482-485. ↑
- C423.** Pouteau R. Support vector machine fusion of multisensor imagery in tropical ecosystems. / Pouteau R., Stoll B., Chabrier S. // 2010 2nd International Conference on Image Processing Theory Tools and Applications (IPTA). - Paris, 7-10 July 2010. - P. 325-329. ↑
- C424.** Apartsin A. SNR-dependent filtering for Time Of Arrival estimation in high noise. / Apartsin A., Cooper L.N., Intrator N. // 2010 IEEE International Workshop on Machine Learning for Signal Processing (MLSP). - Kittila, Aug. 29 2010-Sept. 1 2010. - P. 427-431. ↑
- C425.** Brook A. Fusion of hyperspectral images and LiDAR data for civil engineering structure monitoring. / Brook A., Ben-Dor E., Richter R. // 2010 2nd Workshop on Hyperspectral Image and Signal Processing: Evolution in Remote Sensing (WHISPERS). - Reykjavik, 14-16 June 2010. - P. 1-5. ↑
- C426.** Huanhuan Chen. Probabilistic robust hyperbola mixture model for interpreting ground penetrating radar data. / Huanhuan Chen, Cohn A.G. // The 2010 International Joint Conference on Neural Networks (IJCNN). - Barcelona, 18-23 July 2010. - P. 1-8. ↑
- C427.** Seppke B. Using Snakes with Asymmetric Energy Terms for the Detection of Varying-Contrast Edges in SAR Images. / Seppke B., Dreschler-Fischer L., Hujbbe N. // 2010 20th International Conference on Pattern Recognition (ICPR). - Istanbul, 23-26 Aug. 2010. - P. 2792-2795. ↑

- C428.** Seppke B. Fast Derivation of Soil Surface Roughness Parameters Using Multi-band SAR Imagery and the Integral Equation Model. / Seppke B., Dreschler-Fischer L., Heimig J.-A., Wengenroth F. // 2010 20th International Conference on Pattern Recognition (ICPR). - Istanbul, 23-26 Aug. 2010. - P. 3931-3934. ↑
- C429.** Frank M. Vegetation management of utility corridors using high-resolution hyperspectral imaging and LiDAR. / Frank M., Zhihong Pan, Raber B., Lenart C. // 2010 2nd Workshop on Hyperspectral Image and Signal Processing: Evolution in Remote Sensing (WHISPERS). - Reykjavik, 14-16 June 2010. - P. 1-4. ↑
- C430.** Danilina I. Thermal infrared radiosity and heat diffusion model verification and validation. / Danilina I., Gillespie A.R., Smith M., Balick L., Abbott E. // 2010 2nd Workshop on Hyperspectral Image and Signal Processing: Evolution in Remote Sensing (WHISPERS). - Reykjavik, 14-16 June 2010. - P. 1-4. ↑
- C431.** Zhuosen Wang. Canopy vertical structure using MODIS Bidirectional Reflectance data. / Zhuosen Wang, Schaaf C.B., Philip L., Knyazikhin Y., Schull M.A., Strahler A.H., Myneni R.B., Chopping M. // 2010 2nd Workshop on Hyperspectral Image and Signal Processing: Evolution in Remote Sensing (WHISPERS). - Reykjavik, 14-16 June 2010. - P. 1-4. ↑
- C432.** Shen Yonglin. Identification of inclined buildings from aerial LIDAR Data for disaster management. / Shen Yonglin, Wu Lixin, Wang Zhi. // 2010 18th International Conference on Geoinformatics. - Beijing, 18-20 June 2010. - P. 1-5. ↑
- C433.** Zhi Wang. Geodesics-based topographical feature extraction from airborne Lidar data for disaster management. / Zhi Wang, Huiying Li, Lixin Wu. // 2010 18th International Conference on Geoinformatics. - Beijing, 18-20 June 2010. - P. 1-5. ↑
- C434.** Fan Wang. The atmosphere correction in SBAS D-InSAR land subsidence monitoring application: A case study in Jiading-Huzhou plain, China. / Fan Wang, Zhaoquan Huang, Lifan Zhou, Dengrong Zhang. // 2010 18th International Conference on Geoinformatics. - Beijing, 18-20 June 2010. - P. 1-5. ↑
- C435.** Yun Gong. Large-scale, rapid detection method of surface subsidence in western mining area. / Yun Gong, Caiping Meng. // 2010 18th International Conference on Geoinformatics. - Beijing, 18-20 June 2010. - P. 1-4. ↑
- C436.** Li Yan. SAR and multi-spectral image fusion based on feature additive integration. / Li Yan, Zhan Zhao, Hong Xie. // 2010 18th International Conference on Geoinformatics. - Beijing, 18-20 June 2010. - P. 1-4. ↑
- C437.** Li Yan. Production and accuracy analysis of high quality TerraSAR-X DOM. / Li Yan, Zhen Li. // 2010 18th International Conference on Geoinformatics. - Beijing, 18-20 June 2010. - P. 1-5. ↑
- C438.** Yishuo Huang. SAR satellite image interpretation based on the multilayer level set approach. / Yishuo Huang, Shang-Yuh Lin, Shengmin Wu. // 2010 18th International Conference on Geoinformatics. - Beijing, 18-20 June 2010. - P. 1-6. ↑
- C439.** Mowen Xie. Application of three-orbits D-InSAR technique on landslide displacement monitoring. / Mowen Xie, Jiehui Huang, Guijie Wang, Xiangyu Liu, Qiang Fu. // 2010 International Conference on Environmental Science and Information Application Technology (ESIAT). - Wuhan, 17-18 July 2010. - Vol. 4. - P. 46-50. ↑
- C440.** Lejiang Guo. Application of GIS and remote sensing techniques for water resources management. / Lejiang Guo, Lei Xiao, Xuanlai Tang, Zhe Hu. // 2010 International Conference on Environmental Science and Information Application Technology (ESIAT). - Wuhan, 17-18 July 2010. - Vol. 2. - P. 738-741. ↑
- C441.** Wen-Xia Xu. Forecast hail by analysis radar image. / Wen-Xia Xu, Guo-Dong Li, Fei-Jia Liao. // 2010 International Conference on Machine Learning and Cybernetics (ICMLC). - Qingdao, 11-14 July 2010. - Vol. 2. - P. 730-734. ↑
- C442.** Guosong Zhao. Assessment of ASTER GDEM performance by comparing with SRTM and ICESat/GLAS data in Central China. / Guosong Zhao, Huaiping Xue, Feng Ling. // 2010 18th International Conference on Geoinformatics. - Beijing, 18-20 June 2010. - P. 1-5. ↑
- C443.** Fengli Zhang. Building extraction using dual-aspect high resolution SAR images. / Fengli Zhang, Yun Shao, Xiao Zhang. // 2010 18th International Conference on Geoinformatics. - Beijing, 18-20 June 2010. - P. 1-

5. ↑

C444. Zi Wan. Ortho-rectification of high-resolution SAR image in mountain area by DEM. / Zi Wan, Yun Shao, Chou Xie, Fengli Zhang. // 2010 18th International Conference on Geoinformatics. - Beijing, 18-20 June 2010. - P. 1-6. ↑

C445. Pierdicca N. A fuzzy-logic-based approach for flood detection from Cosmo-SkyMed data. / Pierdicca N., Pulvirenti L., Chini M., Guerriero L., Ferrazzoli P. // 2010 IEEE International Geoscience and Remote Sensing Symposium (IGARSS). - Honolulu, HI, 25-30 July 2010. - P. 4796-4798. ↑

C446. Hannevik T.N. Polarisation and mode combinations for ship detection using RADARSAT-2. 2010 IEEE International Geoscience and Remote Sensing Symposium (IGARSS). - Honolulu, HI, 25-30 July 2010. - P. 3676-3679. ↑

C447. Breit H. Processing of bistatic TanDEM-X data. / Breit H., Fritz T., Balss U., Niedermeier A., Eineder M., Yague-Martinez N., Rossi C. // 2010 IEEE International Geoscience and Remote Sensing Symposium (IGARSS). - Honolulu, HI, 25-30 July 2010. - P. 2640-2643. ↑

C448. Touzi R. Peatland subsurface water flow monitoring using polarimetric L-band PALSAR. / Touzi R., Gosselin G. // 2010 IEEE International Geoscience and Remote Sensing Symposium (IGARSS). - Honolulu, HI, 25-30 July 2010. - P. 750-753. ↑

C449. Totir F. PolSAR images characterization through Blind Sources Separation techniques. / Totir F., Vasile G., Bombrun L., Gay M. // 2010 IEEE International Geoscience and Remote Sensing Symposium (IGARSS). - Honolulu, HI, 25-30 July 2010. - P. 4039-4042. ↑

C450. Gekat F. Accuracy of the engineering calibration of weather radars. / Gekat F., Hille M., Niese H., Pool M. // 2010 IEEE International Geoscience and Remote Sensing Symposium (IGARSS). - Honolulu, HI, 25-30 July 2010. - P. 1096-1099. ↑

C451. Soloviev A. Fine structure of the upper ocean from high-resolution Terrasar-X imagery and In-Situ measurements. / Soloviev A., Maingot C., Fujimura A., Fenton J., Gilman M., Matt S., Lehner S., Velotto D., Brusch S. // 2010 IEEE International Geoscience and Remote Sensing Symposium (IGARSS). - Honolulu, HI, 25-30 July 2010. - P. 1944-1947. ↑

C452. Datcu M. Texture estimation in sar images: The impact of scale and model order. / Datcu M., Espinoza-Molina D., de Miguel A., Schwarz G. // 2010 IEEE International Geoscience and Remote Sensing Symposium (IGARSS). - Honolulu, HI, 25-30 July 2010. - P. 2844-2847. ↑

C453. Braun H.M. A new SAR sensor designed for micro-satellites. 2010 IEEE International Geoscience and Remote Sensing Symposium (IGARSS). - Honolulu, HI, 25-30 July 2010. - P. 213-215. ↑

C454. Zeng Dazhi. An improved CSA for one-stationary BiSAR squint mode. / Zeng Dazhi, Wang Rui, Long Teng, Zeng Tao. // 2010 IEEE International Geoscience and Remote Sensing Symposium (IGARSS). - Honolulu, HI, 25-30 July 2010. - P. 1577-1580. ↑

C455. Trizna D. Coherent marine radar measurements of properties of ocean waves and currents. 2010 IEEE International Geoscience and Remote Sensing Symposium (IGARSS). - Honolulu, HI, 25-30 July 2010. - P. 4737-4740. ↑

C456. Bin Zou. POLSAR image classification using BP neural network based on Quantum Clonal Evolutionary Algorithm. / Bin Zou, Huijun Li, Lamei Zhang. // 2010 IEEE International Geoscience and Remote Sensing Symposium (IGARSS). - Honolulu, HI, 25-30 July 2010. - P. 1573-1576. ↑

C457. Xueyan He. RPC modeling for spaceborne SAR and its application in radargrammetry. / Xueyan He, Xiaohong Wei, Lu Zhang, Balz T., Mingsheng Liao. // 2010 IEEE International Geoscience and Remote Sensing Symposium (IGARSS). - Honolulu, HI, 25-30 July 2010. - P. 3600-3603. ↑

C458. Berens P. Data acquisition of vessel ISAR data with assistance of automatic identification system. 2010 IEEE International Geoscience and Remote Sensing Symposium (IGARSS). - Honolulu, HI, 25-30 July 2010. - P. 122-125. ↑

- C459.** Erten E. Aspects of multivariate statistical theory with the application to change detection. / Erten E., Reigber A., Hellwich O. // 2010 IEEE International Geoscience and Remote Sensing Symposium (IGARSS). - Honolulu, HI, 25-30 July 2010. - P. 1960-1963. ↑
- C460.** Alonso-Gonzalez A. Filtering and segmentation of polarimetric SAR images with Binary Partition Trees. / Alonso-Gonzalez A., Lopez-Martinez C., Salembier P. // 2010 IEEE International Geoscience and Remote Sensing Symposium (IGARSS). - Honolulu, HI, 25-30 July 2010. - P. 4043-4046. ↑
- C461.** Costantini M. A novel approach for redundant integration of finite differences and phase unwrapping on a sparse multidimensional domain. / Costantini M., Malvarosa F., Minati F. // 2010 IEEE International Geoscience and Remote Sensing Symposium (IGARSS). - Honolulu, HI, 25-30 July 2010. - P. 1565-1568. ↑
- C462.** Wegner J.D. Building detection and height estimation from high-resolution insar and optical data. / Wegner J.D., Ziehn J.R., Soergel U. // 2010 IEEE International Geoscience and Remote Sensing Symposium (IGARSS). - Honolulu, HI, 25-30 July 2010. - P. 1928-1931. ↑
- C463.** Lei Huang. SAR and optical images registration using shape context. / Lei Huang, Zhen Li, Rui Zhang. // 2010 IEEE International Geoscience and Remote Sensing Symposium (IGARSS). - Honolulu, HI, 25-30 July 2010. - P. 1007-1010. ↑
- C464.** Fayard F. Radargrammetric improvements: A multi-window approach. / Fayard F., Meric S., Pottier E. // 2010 IEEE International Geoscience and Remote Sensing Symposium (IGARSS). - Honolulu, HI, 25-30 July 2010. - P. 3604-3607. ↑
- C465.** Cigna F. Insar time-series analysis for management and mitigation of geological risk in urban area. / Cigna F., Del Ventisette C., Liguori V., Casagli N. // 2010 IEEE International Geoscience and Remote Sensing Symposium (IGARSS). - Honolulu, HI, 25-30 July 2010. - P. 1924-1927. ↑
- C466.** Bombrun L. Roll invariant target detection based on PolSAR clutter models. / Bombrun L., Vasile G., Gay M., Ovarlez J., Pascal F. // 2010 IEEE International Geoscience and Remote Sensing Symposium (IGARSS). - Honolulu, HI, 25-30 July 2010. - P. 2511-2514. ↑
- C467.** Dall J. Ice sheet anisotropy measured with polarimetric ice sounding radar. 2010 IEEE International Geoscience and Remote Sensing Symposium (IGARSS). - Honolulu, HI, 25-30 July 2010. - P. 2507-2510. ↑
- C468.** Tay S. A tracking algorithm for GNSS reflected signals on sea surface. / Tay S., Coatanhay A., Maussang F., Garelo R. // 2010 IEEE International Geoscience and Remote Sensing Symposium (IGARSS). - Honolulu, HI, 25-30 July 2010. - P. 3821-3824. ↑
- C469.** Yu-Li Lin. Assessment of airborne lidar data for instream flow type classification. / Yu-Li Lin, Chi-Kuei Wang. // 2010 IEEE International Geoscience and Remote Sensing Symposium (IGARSS). - Honolulu, HI, 25-30 July 2010. - P. 930-933. ↑
- C470.** Hao Zhang. An integrated approach to determine parameters of a 3D volcano model by using InSAR data with metamodel technique. / Hao Zhang, Xiaoying Cong, Eineder M., Bletzinger K.-U. // 2010 IEEE International Geoscience and Remote Sensing Symposium (IGARSS). - Honolulu, HI, 25-30 July 2010. - P. 1648-1651. ↑
- C471.** Deng Lei. A CHMT model based DE-speckling method for SAR image. / Deng Lei, Zhao Wenji, Hu Deyong, Hu Zhuowei, Cao Gaoming. // 2010 IEEE International Geoscience and Remote Sensing Symposium (IGARSS). - Honolulu, HI, 25-30 July 2010. - P. 1569-1572. ↑
- C472.** Suchandt S. Ship detection and measurement using the TerraSAR-X dual-receive antenna mode. / Suchandt S., Runge H., Steinbrecher U. // 2010 IEEE International Geoscience and Remote Sensing Symposium (IGARSS). - Honolulu, HI, 25-30 July 2010. - P. 2860-2863. ↑
- C473.** Beaulieu J. Mean-shift and hierarchical clustering for textured polarimetric SAR image segmentation/classification. / Beaulieu J., Touzi R. // 2010 IEEE International Geoscience and Remote Sensing Symposium (IGARSS). - Honolulu, HI, 25-30 July 2010. - P. 2519-2522. ↑
- C474.** Vega M. Realization of the NASA Dual-Frequency Dual-Polarized Doppler Radar (D3R). / Vega M., Carswell J., Chandrasekar V., Schwaller M., Mishra K.V. // 2010 IEEE International Geoscience and Remote Sensing Symposium (IGARSS). - Honolulu, HI, 25-30 July 2010. - P. 2523-2526. ↑

Sensing Symposium (IGARSS). - Honolulu, HI, 25-30 July 2010. - P. 4815-4818. ↑

C475. Deledalle C.-A. Polarimetric SAR estimation based on non-local means. / Deledalle C.-A., Tupin F., Denis L. // 2010 IEEE International Geoscience and Remote Sensing Symposium (IGARSS). - Honolulu, HI, 25-30 July 2010. - P. 2515-2518. ↑

C476. Sauer S. Polarimetric decomposition for forest biomass retrieval. / Sauer S., Kugler F., Seung-Kuk Lee, Papathanassiou K. // 2010 IEEE International Geoscience and Remote Sensing Symposium (IGARSS). - Honolulu, HI, 25-30 July 2010. - P. 4780-4783. ↑

C477. Yang Li. Eigen decomposition parameter based forest mapping using Radarsat-2 PolSAR data. / Yang Li, Wen Hong, Fang Cao, Erxue Chen, Goodenough D.G., Hao Chen, Peng Wang, Richardson A. // 2010 IEEE International Geoscience and Remote Sensing Symposium (IGARSS). - Honolulu, HI, 25-30 July 2010. - P. 4784-4787. ↑

C478. Yue Huang. Polarimetric SAR tomography of natural environments using hybrid spectral estimators. / Yue Huang, Ferro-Famil L., Reigber A. // 2010 IEEE International Geoscience and Remote Sensing Symposium (IGARSS). - Honolulu, HI, 25-30 July 2010. - P. 146-149. ↑

C479. McFadden M. An application of reciprocity to the numerical modeling of a GPR system. / McFadden M., Scott W.R. // 2010 IEEE International Geoscience and Remote Sensing Symposium (IGARSS). - Honolulu, HI, 25-30 July 2010. - P. 4709-4712. ↑

C480. Siqueira P. A portable 35 GHz cross-track interferometer for topographic and surface change measurements. / Siqueira P., Vedantham H., Swochak T. // 2010 IEEE International Geoscience and Remote Sensing Symposium (IGARSS). - Honolulu, HI, 25-30 July 2010. - P. 4811-4814. ↑

C481. Dell'Acqua F. Mapping earthquake damage in VHR radar images of human settlements: Preliminary results on the 6th April 2009, Italy case. / Dell'Acqua F., Gamba P., Polli D. // 2010 IEEE International Geoscience and Remote Sensing Symposium (IGARSS). - Honolulu, HI, 25-30 July 2010. - P. 1347-1350. ↑

C482. Qu Ning-ning. The analysis of surface deformation based on two-pass and three-pass D-InSAR. / Qu Ning-ning, Zhu Guang, Zhao Xi-an, Jing Chang-feng, Lv Jing-guo. // 2010 IEEE International Geoscience and Remote Sensing Symposium (IGARSS). - Honolulu, HI, 25-30 July 2010. - P. 4561-4563. ↑

C483. Soja M.J. Topographic correction for biomass retrieval from P-band SAR data in boreal forests. / Soja M.J., Sandberg G., Ulander L.M.H. // 2010 IEEE International Geoscience and Remote Sensing Symposium (IGARSS). - Honolulu, HI, 25-30 July 2010. - P. 4776-4779. ↑

C484. Botta G. A new approach to modeling ice crystal aggregates and its implications for radar remote sensing. / Botta G., Aydin K., Verlinde J. // 2010 IEEE International Geoscience and Remote Sensing Symposium (IGARSS). - Honolulu, HI, 25-30 July 2010. - P. 2353-2354. ↑

C485. Dellepiane S. Processing and segmentation of COSMO-SkyMed images for flood monitoring. / Dellepiane S., Angiati E., Vernazza G. // 2010 IEEE International Geoscience and Remote Sensing Symposium (IGARSS). - Honolulu, HI, 25-30 July 2010. - P. 4807-4810. ↑

C486. Haipeng Wang. Extraction of typhoon-damaged forests from multi-temporal high-resolution polarimetric SAR images. / Haipeng Wang, Ouchi K., Ya-Qiu Jin. // 2010 IEEE International Geoscience and Remote Sensing Symposium (IGARSS). - Honolulu, HI, 25-30 July 2010. - P. 3271-3274. ↑

C487. Jutzi B. Relations between SAR tomography and full-waveform LIDAR for structural analysis of forested areas. / Jutzi B., Thiele A., Meyer F., Hinz S. // 2010 IEEE International Geoscience and Remote Sensing Symposium (IGARSS). - Honolulu, HI, 25-30 July 2010. - P. 3267-3270. ↑

C488. Grishchkin B.Y. Optimal algorithms for spaceborne altimeter. / Grishchkin B.Y., Baskakov A.I. // 2010 IEEE International Geoscience and Remote Sensing Symposium (IGARSS). - Honolulu, HI, 25-30 July 2010. - P. 640-642. ↑

C489. Re. Morphological filtering of SAR interferometric images. / Rejichi S., Chaabane F., Tupin F., Bloch I. // 2010 IEEE International Geoscience and Remote Sensing Symposium (IGARSS). - Honolulu, HI, 25-30 July 2010. - P. 1581-1584. ↑

- C490.** Seemann J. Detection of salient features in surface current maps from dopplerized X-band radar. / Seemann J., Cysewski M., Ziemer F., Heineke M., Riethmujller R. // 2010 IEEE International Geoscience and Remote Sensing Symposium (IGARSS). - Honolulu, HI, 25-30 July 2010. - P. 4741-4744. ↑
- C491.** Castillo Mena J. Quasar SBK accurate internal calibration. / Castillo Mena J., Cuerda Munoz J.M., Larranaga Sudupe J.R. // 2010 IEEE International Geoscience and Remote Sensing Symposium (IGARSS). - Honolulu, HI, 25-30 July 2010. - P. 2864-2867. ↑
- C492.** Reuter S. Development and experiments of a passive SAR receiver system in a bistatic spaceborne/stationary configuration. / Reuter S., Behner F., Nies H., Loffeld O., Matthes D., Schiller J. // 2010 IEEE International Geoscience and Remote Sensing Symposium (IGARSS). - Honolulu, HI, 25-30 July 2010. - P. 118-121. ↑
- C493.** Zhenhua Wang. Automatic registration of sar and optical image based on multi-features and multi-constraints. / Zhenhua Wang, Junping Zhang, Ye Zhang, Bin Zou. // 2010 IEEE International Geoscience and Remote Sensing Symposium (IGARSS). - Honolulu, HI, 25-30 July 2010. - P. 1019-1022. ↑
- C494.** Smith L. Beamwidth analysis for SAR processing of airborne depth-sounder data over ice sheets. / Smith L., Paden J., Leuschen C., Gogineni S. // 2010 IEEE International Geoscience and Remote Sensing Symposium (IGARSS). - Honolulu, HI, 25-30 July 2010. - P. 4596-4599. ↑
- C495.** Crespi M. DSM generation from very high optical and radar sensors: Problems and potentialities along the road from the 3D geometric modeling to the Surface Model. / Crespi M., Capaldo P., Fratarcangeli F., Nascetti A., Pieralice F. // 2010 IEEE International Geoscience and Remote Sensing Symposium (IGARSS). - Honolulu, HI, 25-30 July 2010. - P. 3596-3599. ↑
- C496.** Longepe N. On the use of Support Vector Machines for land cover analysis with L-band SAR data. / Longepe N., Rakwatin P., Isoguchi O., Shimada M., Uryu Y. // 2010 IEEE International Geoscience and Remote Sensing Symposium (IGARSS). - Honolulu, HI, 25-30 July 2010. - P. 3263-3266. ↑
- C497.** Wong A. A new Bayesian source separation approach to blind decorrelation of SAR data. / Wong A., Fieguth P. // 2010 IEEE International Geoscience and Remote Sensing Symposium (IGARSS). - Honolulu, HI, 25-30 July 2010. - P. 4035-4038. ↑
- C498.** Singh J. SAR complex image analysis: A Gauss Markov and a multiple sub-aperture based target characterization. / Singh J., Soccorsi M., Datcu M. // 2010 IEEE International Geoscience and Remote Sensing Symposium (IGARSS). - Honolulu, HI, 25-30 July 2010. - P. 1585-1588. ↑
- C499.** Yueguan Lin. MIMO SAR processing with azimuth nonuniform sampling. / Yueguan Lin, Bingchen Zhang, Wen Hong, Yirong Wu, Yang Li. // 2010 IEEE International Geoscience and Remote Sensing Symposium (IGARSS). - Honolulu, HI, 25-30 July 2010. - P. 4652-4655. ↑
- C500.** Hwang P.A. Doppler processing of coherent radar backscatter for ocean surface wave measurements. / Hwang P.A., Sletten M.A., Toporkov J.V., Trizna D.B. // 2010 IEEE International Geoscience and Remote Sensing Symposium (IGARSS). - Honolulu, HI, 25-30 July 2010. - P. 4733-4736. ↑
- C501.** Weilin Yuan. Decomposition methods for the estimation of bare soil surface parameters using fully polarimetric SAR data 1. / Weilin Yuan, Qiming Qin, Shihong Du, Xinyi Shen, Hongbo Jiang, Yan Ma, Shixiong Liu. // 2010 IEEE International Geoscience and Remote Sensing Symposium (IGARSS). - Honolulu, HI, 25-30 July 2010. - P. 1273-1276. ↑
- C502.** Wang Zhiqian. Effect of squint imaging on beam position design of space borne SAR. / Wang Zhiqian, Li Chunsheng, Yu Ze, Zhang Yongqiang, Yang Wei. // 2010 IEEE International Geoscience and Remote Sensing Symposium (IGARSS). - Honolulu, HI, 25-30 July 2010. - P. 4648-4651. ↑
- C503.** Yu Wang. A shadow percentage estimation method for Radar look angle selection in spaceborne INSAR application. / Yu Wang, Xing-dong Liang. // 2010 IEEE International Geoscience and Remote Sensing Symposium (IGARSS). - Honolulu, HI, 25-30 July 2010. - P. 1481-1484. ↑
- C504.** Colinas J. Radarsat Constellation, moving toward implementation. / Colinas J., Se,guin G., Plourde P. // 2010 IEEE International Geoscience and Remote Sensing Symposium (IGARSS). - Honolulu, HI, 25-30 July 2010. - P. 3232-3235. ↑

- C505.** Chopping M. Canopy height, crown cover, and aboveground biomass maps for the southwestern United States from MISR, 2000 and 2009. / Chopping M., Shimada S., Bull M., Martonchik J. // 2010 IEEE International Geoscience and Remote Sensing Symposium (IGARSS). - Honolulu, HI, 25-30 July 2010. - P. 56-59. ↑
- C506.** Xiaojian Xu. A study on the possibility of applying precursor waves to penetration imaging. / Xiaojian Xu, Penghui Chen. // 2010 International Conference on Electromagnetics in Advanced Applications (ICEAA). - Sydney, NSW, 20-24 Sept. 2010. - P. 843-846. ↑
- C507.** Gao Han. Investigation on moving target detection and velocity estimation with Triple-Channel MIMO-SAR. / Gao Han, Li Jingwen, Yang Wei. // 2010 IEEE International Geoscience and Remote Sensing Symposium (IGARSS). - Honolulu, HI, 25-30 July 2010. - P. 4636-4639. ↑
- C508.** Benzid S. Change detection in a multitemporal series of radar images. / Benzid S., Deledalles C., Abdelfattah R., Chaabane F., Tupin F. // 2010 IEEE International Geoscience and Remote Sensing Symposium (IGARSS). - Honolulu, HI, 25-30 July 2010. - P. 1473-1476. ↑
- C509.** Kurum M. Characterization of forest opacity using multi-angular emission and backscatter data. / Kurum M., O'Neill P.E., Lang R.H., Joseph A.T., Cosh M.H., Jackson T.J. // 2010 IEEE International Geoscience and Remote Sensing Symposium (IGARSS). - Honolulu, HI, 25-30 July 2010. - P. 2051-2054. ↑
- C510.** Kawamura S. A new bistatic doppler measurement system with reduced contamination by sidelobe echoes. / Kawamura S., Hanado H., Sugitani S., Nakagawa K. // 2010 IEEE International Geoscience and Remote Sensing Symposium (IGARSS). - Honolulu, HI, 25-30 July 2010. - P. 4150-4153. ↑
- C511.** Ikuma T. Autoregressive modeling of dechirped spotlight-mode sar rawdata in transform domain. / Ikuma T., Naraghi-Pour M., Lewis T. // 2010 IEEE International Geoscience and Remote Sensing Symposium (IGARSS). - Honolulu, HI, 25-30 July 2010. - P. 4640-4643. ↑
- C512.** Wei Tian. An experiment for oil spill recognition using RADARSAT-2 image. / Wei Tian, Yun Shao, Junna Yuan, Shiang Wang, Yang Liu. // 2010 IEEE International Geoscience and Remote Sensing Symposium (IGARSS). - Honolulu, HI, 25-30 July 2010. - P. 2761-2764. ↑
- C513.** Xiaogang Song. The characteristics of post-seismic surface deformation of the Wenchuan MS 8.0 earthquake from InSAR. / Xiaogang Song, Xinjian Shan, Chunyan Qu, Yufei Han, Guifang Zhang, Limin Guo, Guohong Zhang. // 2010 IEEE International Geoscience and Remote Sensing Symposium (IGARSS). - Honolulu, HI, 25-30 July 2010. - P. 1210-1213. ↑
- C514.** Nashashibi A.Y. Characterization of volume scattering of dry sand at millimeter-wave frequencies. / Nashashibi A.Y., Sarabandi K., Al-Zaid F., Alhumaidi S. // 2010 IEEE International Geoscience and Remote Sensing Symposium (IGARSS). - Honolulu, HI, 25-30 July 2010. - P. 3067-3069. ↑
- C515.** Stuart K.M. Iceberg size and orientation estimation using SeaWinds. / Stuart K.M., Long D.G. // 2010 IEEE International Geoscience and Remote Sensing Symposium (IGARSS). - Honolulu, HI, 25-30 July 2010. - P. 2394-2397. ↑
- C516.** Clewley D. Forest parameter retrieval from SAR data using an estimation algorithm applied to regrowing forest stands in Queensland, Australia. / Clewley D., Lucas R.M., Moghaddam M., Bunting P., Dwyer J., Carreiras J. // 2010 IEEE International Geoscience and Remote Sensing Symposium (IGARSS). - Honolulu, HI, 25-30 July 2010. - P. 1238-1241. ↑
- C517.** Zhifeng Guo. Forest biomass estimation in northeastern China using ALOS PALSAR data combined radiative transfer model. / Zhifeng Guo, Wenjian Ni, Guoqing Sun. // 2010 IEEE International Geoscience and Remote Sensing Symposium (IGARSS). - Honolulu, HI, 25-30 July 2010. - P. 1497-1500. ↑
- C518.** Huber M. Validation of tie-point concepts by the DEM adjustment approach of TanDEM-X. / Huber M., Gruber A., Wessel B., Breunig M., Wendleder A. // 2010 IEEE International Geoscience and Remote Sensing Symposium (IGARSS). - Honolulu, HI, 25-30 July 2010. - P. 2644-2647. ↑
- C519.** Rappaport C. Road surface quality measurement using inexpensive radar. / Rappaport C., Holbrook D., Adams C., Busuioc D., Doughty J. // 2010 IEEE International Geoscience and Remote Sensing Symposium (IGARSS). - Honolulu, HI, 25-30 July 2010. - P. 4318-4321. ↑

- C520.** Broquetas A. Bistatic SAR based on Terrasar-X and ground based receivers. / Broquetas A., Fortes M., Siddique M.A., Duque S., Merlano J.C., Lopez-Dekker P., Mallorqui J.J., Aguasca A. // 2010 IEEE International Geoscience and Remote Sensing Symposium (IGARSS). - Honolulu, HI, 25-30 July 2010. - P. 114-117. ↑
- C521.** Zhe Hu. Designing an Illegal Mining Detection System based on DinSAR. / Zhe Hu, Linlin Ge, Xiaojing Li, Rizos C. // 2010 IEEE International Geoscience and Remote Sensing Symposium (IGARSS). - Honolulu, HI, 25-30 July 2010. - P. 3952-3955. ↑
- C522.** Rottensteiner F. Automation of object extraction from LiDAR in urban areas. 2010 IEEE International Geoscience and Remote Sensing Symposium (IGARSS). - Honolulu, HI, 25-30 July 2010. - P. 1343-1346. ↑
- C523.** Plant W.J. Dual-polarized, coherent microwave backscatter from rough water surfaces at low grazing angles. 2010 IEEE International Geoscience and Remote Sensing Symposium (IGARSS). - Honolulu, HI, 25-30 July 2010. - P. 4729-4732. ↑
- C524.** Colliander A. Quikscat backscatter sensitivity to landscape freeze/thaw state over ALECTRA sites in Alaska from 2000 to 2007: Application to SMAP validation planning. / Colliander A., McDonald K., Zimmermann R., Linke T., Schroeder R., Kimball J., Njoku E. // 2010 IEEE International Geoscience and Remote Sensing Symposium (IGARSS). - Honolulu, HI, 25-30 July 2010. - P. 1269-1272. ↑
- C525.** Lucas R.M. Advances in the integration of ALOS PALSAR and Landsat sensor data for forest characterisation, mapping and monitoring. / Lucas R.M., Armston J., Carreiras J., Nugroho N., Clewley D., de Grandi F. // 2010 IEEE International Geoscience and Remote Sensing Symposium (IGARSS). - Honolulu, HI, 25-30 July 2010. - P. 1851-1854. ↑
- C526.** Long N. A combined approach to detect urban features from multi-spectral and radar data. / Long N., Simonetto E., Bocher E. // 2010 IEEE International Geoscience and Remote Sensing Symposium (IGARSS). - Honolulu, HI, 25-30 July 2010. - P. 1469-1472. ↑
- C527.** Bombrun L. Extension of the Target Scattering Vector Model to the bistatic case. 2010 IEEE International Geoscience and Remote Sensing Symposium (IGARSS). - Honolulu, HI, 25-30 July 2010. - P. 4047-4050. ↑
- C528.** Hai Tung Chu. Synergistic use of multi-temporal ALOS/PALSAR with SPOT multispectral satellite imagery for land cover mapping in the Ho Chi Minh city area, Vietnam. / Hai Tung Chu, Linlin Ge. // 2010 IEEE International Geoscience and Remote Sensing Symposium (IGARSS). - Honolulu, HI, 25-30 July 2010. - P. 1465-1468. ↑
- C529.** Poulain V. High resolution optical and sar image fusion for road database updating. / Poulain V., Inglada J., Spigai M., Tournet J., Marthon P. // 2010 IEEE International Geoscience and Remote Sensing Symposium (IGARSS). - Honolulu, HI, 25-30 July 2010. - P. 2747-2750. ↑
- C530.** Baumgartner S.V. Real-time road traffic monitoring using a fast a priori knowledge based SAR-GMTI algorithm. / Baumgartner S.V., Krieger G. // 2010 IEEE International Geoscience and Remote Sensing Symposium (IGARSS). - Honolulu, HI, 25-30 July 2010. - P. 1843-1846. ↑
- C531.** Shunying Hong. Three-dimensional deformation field caused by the Gaize earthquake by Multi-LOS DInSAR measurement technology. / Shunying Hong, Xuhui Shen, Xiaogang Song, Xinjian Shan, Zhirong Liu, Yaqiong Dai, Chunli Kang, Feng Jing. // 2010 IEEE International Geoscience and Remote Sensing Symposium (IGARSS). - Honolulu, HI, 25-30 July 2010. - P. 765-768. ↑
- C532.** Sano E.E.S. The use of ALOS PALSAR imagery for Cerrado's land use and land cover mapping. / Sano E.E.S., Santos E.M., Meneses P.R. // 2010 IEEE International Geoscience and Remote Sensing Symposium (IGARSS). - Honolulu, HI, 25-30 July 2010. - P. 1458-1460. ↑
- C533.** Xiaofeng Li. Spaceborne sar imaging of coastal ocean phenomena. / Xiaofeng Li, Pichel W., Xiaofeng Yang. // 2010 IEEE International Geoscience and Remote Sensing Symposium (IGARSS). - Honolulu, HI, 25-30 July 2010. - P. 1956-1959. ↑
- C534.** Lo. Ground topography estimation over forests considering Polarimetric SAR Interferometry. / Lopez-Martinez C., Alonso A., Fabregas X., Papathanassiou K.P. // 2010 IEEE International Geoscience and Remote Sensing Symposium (IGARSS). - Honolulu, HI, 25-30 July 2010. - P. 3612-3615. ↑

- C535.** Jixian Zhang. SAR mapping technology and its application in difficulty terrain area. / Jixian Zhang, Shucheng Yang, Zheng Zhao, Guoman Huang. // 2010 IEEE International Geoscience and Remote Sensing Symposium (IGARSS). - Honolulu, HI, 25-30 July 2010. - P. 3608-3611. ↑
- C536.** Feilong Ling. Rice areas mapping using ALOS PALSAR FBD data considering the Bragg scattering in L-band SAR images of rice fields. / Feilong Ling, Zengyuan Li, Erxue Chen, Xin Tian, Lina Bai, Fengyu Wang. // 2010 IEEE International Geoscience and Remote Sensing Symposium (IGARSS). - Honolulu, HI, 25-30 July 2010. - P. 1461-1464. ↑
- C537.** Flampouris S. Radar observations of wave field in littoral zone. / Flampouris S., Seemann J., Ziemer F. // 2010 IEEE International Geoscience and Remote Sensing Symposium (IGARSS). - Honolulu, HI, 25-30 July 2010. - P. 948-951. ↑
- C538.** Wagner W. Status of the Metop ASCAT soil moisture product. / Wagner W., Bartalis Z., Naeimi V., Park S., Figa-Saldana J., Bonekamp H. // 2010 IEEE International Geoscience and Remote Sensing Symposium (IGARSS). - Honolulu, HI, 25-30 July 2010. - P. 276-279. ↑
- C539.** Roth A.P. Simulating and mitigating ionospheric effects in synthetic aperture radar. / Roth A.P., Huxtable B.D., Chotoo K., Chotoo S.D. // 2010 IEEE International Geoscience and Remote Sensing Symposium (IGARSS). - Honolulu, HI, 25-30 July 2010. - P. 2892-2895. ↑
- C540.** Abdelfattah R. A specific methodology for atmospheric effect reduction on SAR interferograms. / Abdelfattah R., Chokmani K., Chaabane N. // 2010 IEEE International Geoscience and Remote Sensing Symposium (IGARSS). - Honolulu, HI, 25-30 July 2010. - P. 1637-1640. ↑
- C541.** Esteban-Fernandez D. Design considerations for a dual-frequency radar for sea spray measurement in hurricanes. / Esteban-Fernandez D., Durden S.L., Chaubell J., Cooper K.B. // 2010 IEEE International Geoscience and Remote Sensing Symposium (IGARSS). - Honolulu, HI, 25-30 July 2010. - P. 2896-2899. ↑
- C542.** Ramongassie S. Spaceborne P-band SAR for BIOMASS mission. / Ramongassie S., Castiglioni S.K., Lorenzo J., Labiole E., Baudasse Y., Svara C., Luigi C., Heliere F., Mangenot C., Klooster K.V., Fonseca N., Diez H., Belot D. // 2010 IEEE International Geoscience and Remote Sensing Symposium (IGARSS). - Honolulu, HI, 25-30 July 2010. - P. 2880-2883. ↑
- C543.** Borner T. Signal: SAR for ice, glacier and global dynamics. / Borner T., De Zan F., Lopez-Dekker P., Krieger G., Hajnsek I., Papathanassiou K., Villano M., Younis M., Danklmayer A., Dierking W., Nagler T., Rott H., Lehner S., Fugen T., Moreira A. // 2010 IEEE International Geoscience and Remote Sensing Symposium (IGARSS). - Honolulu, HI, 25-30 July 2010. - P. 2884-2887. ↑
- C544.** Feng Li. Focusing general bistatic SAR data using frequency scaling. / Feng Li, Tao Zeng, Teng Long. // 2010 IEEE International Geoscience and Remote Sensing Symposium (IGARSS). - Honolulu, HI, 25-30 July 2010. - P. 1589-1592. ↑
- C545.** Marino A. Detecting depolarizing targets with satellite data: A new geometrical perturbation filter. / Marino A., Cloude S., Woodhouse I. // 2010 IEEE International Geoscience and Remote Sensing Symposium (IGARSS). - Honolulu, HI, 25-30 July 2010. - P. 1847-1850. ↑
- C546.** Munchak S.J. A radar profiling algorithm designed for use with multiresolution radiometer measurements. / Munchak S.J., Kummerow C. // 2010 IEEE International Geoscience and Remote Sensing Symposium (IGARSS). - Honolulu, HI, 25-30 July 2010. - P. 102-105. ↑
- C547.** Seto S. Applicability of the iterative backward retrieval method for the GPM dual-frequency precipitation radar. / Seto S., Iguchi T. // 2010 IEEE International Geoscience and Remote Sensing Symposium (IGARSS). - Honolulu, HI, 25-30 July 2010. - P. 106-109. ↑
- C548.** Perna S. Airborne DInSAR time series at X-Band. / Perna S., Wimmer C., Moreira J., Fornaro G. // 2010 IEEE International Geoscience and Remote Sensing Symposium (IGARSS). - Honolulu, HI, 25-30 July 2010. - P. 2868-2871. ↑
- C549.** Walterscheid I. Potential and limitations of forward-looking bistatic SAR. / Walterscheid I., Espeter T., Klare J., Brenner A.R., Ender J.H.G. // 2010 IEEE International Geoscience and Remote Sensing Symposium (IGARSS). - Honolulu, HI, 25-30 July 2010. - P. 216-219. ↑

- C550.** Servello E.L. Tropical land cover change detection with polarimetric SAR data. / Servello E.L., Kuplich T.M., Shimabukuro Y.E. // 2010 IEEE International Geoscience and Remote Sensing Symposium (IGARSS). - Honolulu, HI, 25-30 July 2010. - P. 1477-1480. ↑
- C551.** Anderson S. Oil Spill statistics from SAR images in the North Eastern Baltic Sea ship route in 2007-2009. / Anderson S., Raudsepp U., Uiboupin R. // 2010 IEEE International Geoscience and Remote Sensing Symposium (IGARSS). - Honolulu, HI, 25-30 July 2010. - P. 1883-1886. ↑
- C552.** Cook K. COSMIC-2: The future of global navigation satellite system-remote observation (GNSS-RO) sensing. / Cook K., Wilczynski P. // 2010 IEEE International Geoscience and Remote Sensing Symposium (IGARSS). - Honolulu, HI, 25-30 July 2010. - P. 3825-3828. ↑
- C553.** Mayorga E. The NANOOS Visualization System (NVS): lessons learned in data aggregation, management and reuse, for a user application. / Mayorga E., Tanner T., Blair R., Jaramillo A.V., Lederer N., Risien C.M., Seaton C. // OCEANS 2010. - Seattle, WA, 20-23 Sept. 2010. - P. 1-9. ↑
- C554.** Trizna D.B. Comparisons of a fully coherent and coherent-on-receive marine radar for measurements of wave spectra and surface currents. OCEANS 2010. - Seattle, WA, 20-23 Sept. 2010. - P. 1-5. ↑
- C555.** {no data available}. Front matter. OCEANS 2010. - Seattle, WA, 20-23 Sept. 2010. - P. 1-151. ↑
- C556.** Xiaofeng Sun. Semi-Automatic Extraction of Ribbon Roads from VHR Remotely Sensed SAR Imagery. / Xiaofeng Sun, Yingcheng Li, Xiangguo Lin. // 2010 Chinese Conference on Pattern Recognition (CCPR). - Chongqing, 21-23 Oct. 2010. - P. 1-4. ↑
- C557.** Bo Hua. Cascade SVM Based Oil Detection in SAR Images. / Bo Hua, Wang Xiaofeng, Ma Fulong. // 2010 International Conference on E-Product E-Service and E-Entertainment (ICEEE). - Henan, 7-9 Nov. 2010. - P. 1-4. ↑
- C558.** Heron M.L. What can HF radar contribute to the salvage of a grounded ship?. / Heron M.L., Mantovanelli A., Steinberg C., King B. // OCEANS 2010. - Seattle, WA, 20-23 Sept. 2010. - P. 1-4. ↑
- C559.** Prabhudesai R.G. Integrated Coastal Observation Network (ICON) for real-time monitoring of sea-level, sea-state, and surface-meteorological data. / Prabhudesai R.G., Joseph A., Agarwadekar Y., Mehra P., Kumar K.V., Luis R. // OCEANS 2010. - Seattle, WA, 20-23 Sept. 2010. - P. 1-9. ↑
- C560.** Gonsalves M.O. Using a dynamic ocean surface to perform a geometric calibration of a bathymetric lidar. OCEANS 2010. - Seattle, WA, 20-23 Sept. 2010. - P. 1-9. ↑
- C561.** Helzel T. Software beam forming for ocean radar WERA features and accuracy. / Helzel T., Kniephoff M. // OCEANS 2010. - Seattle, WA, 20-23 Sept. 2010. - P. 1-3. ↑
- C562.** Plant W.J. Characteristics of internal waves in the South China Sea Observed by a shipboard coherent radar. / Plant W.J., Keller W.C., Hayes K., Chatham G. // OCEANS 2010. - Seattle, WA, 20-23 Sept. 2010. - P. 1-7. ↑
- C563.** Ghaleb A. Modeling and simulation of sea surface radar observations. / Ghaleb A., Even S., Garelo R., Chapron B., Pinel N., de Beaucoudrey N., Comblet F., Parenthoen M., Pottier E. // OCEANS 2010. - Seattle, WA, 20-23 Sept. 2010. - P. 1-7. ↑
- C564.** Bo Wang. Microwave backscatter of ship signatures on SAR imagery. / Bo Wang, Chapron B., Mercier G., Garelo R. // OCEANS 2010. - Seattle, WA, 20-23 Sept. 2010. - P. 1-5. ↑
- C565.** Bretenaker F. Class-A semiconductor lasers for the transport and generation of optically carried RF analog signals for radar applications. / Bretenaker F., Sagnes I., Baili G., Alouini M., Morvan L., Dolfi D. // 2010 IEEE Topical Meeting on Microwave Photonics (MWP). - Montreal, QC, 5-9 Oct. 2010. - P. 39-41. ↑
- C566.** Rossi C. Surface current retrieval from TerraSAR-X data using Doppler measurements. / Rossi C., Runge H., Breit H., Fritz T. // 2010 IEEE International Geoscience and Remote Sensing Symposium (IGARSS). - Honolulu, HI, 25-30 July 2010. - P. 3055-3058. ↑
- C567.** Romeiser R. Currents in rivers, coastal areas, and the open ocean from TerraSAR-X along-track InSAR.

/ Romeiser R., Suchandt S., Runge H., Graber H. // 2010 IEEE International Geoscience and Remote Sensing Symposium (IGARSS). - Honolulu, HI, 25-30 July 2010. - P. 3059-3062. ↑

**C568.** Haibin Lv. The propagating speed of internal solitary waves investigated by X-band radar near Dongsha island. / Haibin Lv, Yijun He, Hui Shen, Limin Cui, Chang-e Dou. // 2010 IEEE International Geoscience and Remote Sensing Symposium (IGARSS). - Honolulu, HI, 25-30 July 2010. - P. 4705-4708. ↑

**C569.** Marechal C. Spaceborne fully polarimetric time-series datasets for land cover analysis. / Marechal C., Pottier E., Hubert-Moy L., Corgne S., Allain-Bailhache S., Meric S. // 2010 IEEE International Geoscience and Remote Sensing Symposium (IGARSS). - Honolulu, HI, 25-30 July 2010. - P. 859-862. ↑

**C570.** Ebuchi N. Propagation of subinertial variations in the Soya Warm Current revealed by HF ocean radars. / Ebuchi N., Fukamachi Y., Ohshima K.I. // 2010 IEEE International Geoscience and Remote Sensing Symposium (IGARSS). - Honolulu, HI, 25-30 July 2010. - P. 3051-3054. ↑

**C571.** Pouteau R. Multi-source SVM fusion for environmental monitoring in Marquesas archipelago. / Pouteau R., Stoll B., Chabrier S. // 2010 IEEE International Geoscience and Remote Sensing Symposium (IGARSS). - Honolulu, HI, 25-30 July 2010. - P. 2719-2722. ↑

**C572.** Sjojgren T.K. Moving target refocusing algorithm for synthetic aperture radar images. / Sjojgren T.K., Vu V.T., Pettersson M.I. // 2010 IEEE International Geoscience and Remote Sensing Symposium (IGARSS). - Honolulu, HI, 25-30 July 2010. - P. 4110-4113. ↑

**C573.** Wei Yan. Unsupervised classification of PolInSAR image based on Shannon Entropy Characterization. / Wei Yan, Wen Yang, Ying Liu, Hong Sun. // 2010 IEEE 10th International Conference on Signal Processing (ICSP). - Beijing, 24-28 Oct. 2010. - P. 2192-2195. ↑

**C574.** Cui Ni. Noise analysis and restrain in the fusion process of remote sensing. / Cui Ni, Zequn Guan. // 2010 IEEE International Conference on Intelligent Computing and Intelligent Systems (ICIS). - Xiamen, 29-31 Oct. 2010. - Vol. 3. - P. 490-495. ↑

**C575.** Huajie Chen. A Hybrid Polarimetric Decomposition Method Based on Combination of Scattering-Model and Eigenvector-Decomposition. / Huajie Chen, Liang Zeng, Yuesong Lin. // 2010 Chinese Conference on Pattern Recognition (CCPR). - Chongqing, 21-23 Oct. 2010. - P. 1-5. ↑

**C576.** Wang Wenguang. Oil spill detection from polarimetric SAR image. / Wang Wenguang, Lu Fei, Wu Peng, Wang Jun. // 2010 IEEE 10th International Conference on Signal Processing (ICSP). - Beijing, 24-28 Oct. 2010. - P. 832-835. ↑

**C577.** Wei Yinsheng. A novel adaptive learning method for low-sidelobe step frequency waveform designing. / Wei Yinsheng, Yang Siliang. // 2010 IEEE 10th International Conference on Signal Processing (ICSP). - Beijing, 24-28 Oct. 2010. - P. 2096-2099. ↑

**C578.** Li Ning. Point target reference spectrum of bistatic SAR with parallel flight paths. / Li Ning, Wang Luping. // 2010 IEEE 10th International Conference on Signal Processing (ICSP). - Beijing, 24-28 Oct. 2010. - P. 2075-2078. ↑

**C579.** Mita M. A 2-axis MEMS scanner for the landing laser radar of the space explorer. / Mita M., Mizuno T., Ataka M., Toshiyoshi H. // 2010 International Conference on Optical MEMS and Nanophotonics (OPT MEMS). - Sapporo, 9-12 Aug. 2010. - P. 111-112. ↑

**C580.** Haipeng Wang. A novel polarimetric FM-CW radar system for laboratory remote sensing experiments. / Haipeng Wang, Ya-Qiu Jin. // 2010 9th International Symposium on Antennas Propagation and EM Theory (ISAPE). - Guangzhou, Nov. 29 2010-Dec. 2 2010. - P. 662-665. ↑

**C581.** Yuanyuan Liu. A new two-dimensional millimeter wave imaging radiometer. / Yuanyuan Liu, Lu Zhu, Shan Wang. // 2010 9th International Symposium on Antennas Propagation and EM Theory (ISAPE). - Guangzhou, Nov. 29 2010-Dec. 2 2010. - P. 679-681. ↑

**C582.** Ya-Qiu Jin. Advances in numerical simulation of composite scattering from target above rough surface. 2010 9th International Symposium on Antennas Propagation and EM Theory (ISAPE). - Guangzhou, Nov. 29 2010-Dec. 2 2010. - P. 806-809. ↑

- C583.** Zhu Ang. An interpolation method for lack of DEM data area in tidal creeks based on neural network. / Zhu Ang, Ding Xianrong, Li Qing, Cheng Ligang, Zhang Jiajia, Ge Xiaoping, Huang Bi. // 2010 2nd International Conference on Information Science and Engineering (ICISE). - Hangzhou, China, 4-6 Dec. 2010. - P. 6440-6443. ↑
- C584.** Cai Hongtao. TIDs in ionospheric F-region at Cusp latitude: Observations and numerical simulation. / Cai Hongtao, Yin Fan, Ma Shuyin, Wei Qingyan. // 2010 9th International Symposium on Antennas Propagation and EM Theory (ISAPE). - Guangzhou, Nov. 29 2010-Dec. 2 2010. - P. 415-417. ↑
- C585.** Ya-Qiu Jin. Scattering and emission models and simulations for lunar exploration. 2010 9th International Symposium on Antennas Propagation and EM Theory (ISAPE). - Guangzhou, Nov. 29 2010-Dec. 2 2010. - P. 560-563. ↑
- C586.** Junwen Dai. Imaging and reconstruction of a 3D complex target using downward-looking step-frequency radar. / Junwen Dai, Ya-Qiu Jin. // 2010 9th International Symposium on Antennas Propagation and EM Theory (ISAPE). - Guangzhou, Nov. 29 2010-Dec. 2 2010. - P. 892-896. ↑
- C587.** Ran Xin. Search Aid System Based on Machine Vision and Its Visual Attention Model for Rescue Target Detection. / Ran Xin, Ren Lei. // 2010 Second WRI Global Congress on Intelligent Systems (GCIS). - Wuhan, 16-17 Dec. 2010. - Vol. 2. - P. 149-152. ↑
- C588.** Lei Sheng. Using Remote Sensing Technology for Dynamic Monitoring of Poyang Lake Area and Capacity. / Lei Sheng, Zhang Xiu-ping, Xu Xin-fa, Fu Qun. // 2010 Fourth International Conference on Genetic and Evolutionary Computing (ICGEC). - Shenzhen, 13-15 Dec. 2010. - P. 856-859. ↑
- C589.** Wissan V. Pulse reduction method for circularly polarized synthetic aperture radar. / Wissan V., Setiadi B., Bayuaji L., Sumantyo J. T. Sri, Kuze H. // 2010 Asia-Pacific Microwave Conference Proceedings (APMC). - Yokohama, Japan, 7-10 Dec. 2010. - P. 1324-1327. ↑
- C590.** Manavalan M. Emerging Trends of Computational Grid Based Near Real Time/Real Time Flood Assessment and Forecasting Models. / Manavalan M., Chattopadhyay S., Mangala M., Rao Y.S. // 2010 3rd International Conference on Emerging Trends in Engineering and Technology (ICETET). - Goa, 19-21 Nov. 2010. - P. 471-475. ↑
- C591.** Zhang Yaping. Dynamical Weather Radar Beam Blockage Correction. / Zhang Yaping, Cheng Minghu. // 2010 International Conference on Digital Manufacturing and Automation (ICDMA). - ChangSha, 18-20 Dec. 2010. - Vol. 1. - P. 593-596. ↑
- C592.** Xingzhao Liu. Retrieval of oriented vegetation parameters based on experimental data of PolInSAR. / Xingzhao Liu, Jie Ren, Linxi Zhang, Chufeng Hu. // 2010 3rd IEEE International Conference on Broadband Network and Multimedia Technology (IC-BNMT). - Beijing, 26-28 Oct. 2010. - P. 1150-1153. ↑
- C593.** Chen Liang. Extraction of wetland combining with Radarsat and HJ data of Yellow River Delta. / Chen Liang, Liu Xuegong, He Houjun, Han Lin. // 2010 International Conference on Audio Language and Image Processing (ICALIP). - Shanghai, 23-25 Nov. 2010. - P. 1614-1618. ↑
- C594.** Zhen Li. RPC-based adjustment model for COSMO-SkyMed stereo slant/ground-range images. / Zhen Li, Guo Zhang, Hong-bo Pan, Qiang Qiang. // 2010 IEEE International Conference on Progress in Informatics and Computing (PIC). - Shanghai, 10-12 Dec. 2010. - Vol. 1. - P. 593-597. ↑
- C595.** Chunyan Ma. Research on a self-powered wireless ultrasonic flow sensor system. / Chunyan Ma, Gengxin Li. // 2010 IEEE International Conference on Progress in Informatics and Computing (PIC). - Shanghai, 10-12 Dec. 2010. - Vol. 1. - P. 522-526. ↑
- C596.** Errington A.F.C. Closure monitoring in Potash Mines using LiDAR. / Errington A.F.C., Daku B.L.F., Prugger A. // IECON 2010-36th Annual Conference on IEEE Industrial Electronics Society. - Glendale, AZ, 7-10 Nov. 2010. - P. 2823-2827. ↑
- C597.** Guangtong Sun. Retrieval of Ground Deformation Based on TS-DInSAR Technique. / Guangtong Sun, Yonghong Zhang, Hongan Wu. // 2010 2nd International Conference on Information Engineering and Computer Science (ICIECS). - Wuhan, 25-26 Dec. 2010. - P. 1-4. ↑

- C598.** Jensen C.A. Urban watershed management: Using remote sensing to implement Low Impact Development. / Jensen C.A., Quinn R.J., Davis T.H. // 2010 Third International Conference on Infrastructure Systems and Services: Next Generation Infrastructure Systems for Eco-Cities (INFRA). - Shenzhen, 11-13 Nov. 2010. - P. 1-6. ↑
- C599.** Yang Han. Full polarimetric SAR classification based on Yamaguchi decomposition model and scattering parameters. / Yang Han, Yongshe Shao. // 2010 IEEE International Conference on Progress in Informatics and Computing (PIC). - Shanghai, 10-12 Dec. 2010. - Vol. 2. - P. 1104-1108. ↑
- C600.** Hongbo Wu. Comparison between ETM+ imageries and ICESat-GLAS waveforms for forest classification. / Hongbo Wu, Yanqiu Xing. // 2010 2nd International Conference on Information Science and Engineering (ICISE). - Hangzhou, China, 4-6 Dec. 2010. - P. 1088-1092. ↑
- C601.** Li Qing. Modeling methods for tidal flat digital terrain based on neural network. / Li Qing, Ding Xianrong, Zhu Ang, Cheng Ligang, Kang Yanyan, Ge Xiaoping, Zhang Jing. // 2010 2nd International Conference on Information Science and Engineering (ICISE). - Hangzhou, China, 4-6 Dec. 2010. - P. 6716-6719. ↑
- C602.** Pengfei Yin. Study on remote sensing radiation transfer model. / Pengfei Yin, Qiu Yin. // 2010 2nd International Conference on Information Science and Engineering (ICISE). - Hangzhou, China, 4-6 Dec. 2010. - P. 6957-6959. ↑
- C603.** Wang linyu. The study of Range Doppler Algorithm in focusing Bistatic SAR. / Wang linyu, Zhao hongfang. // 2010 2nd International Conference on Information Science and Engineering (ICISE). - Hangzhou, China, 4-6 Dec. 2010. - P. 7077-7080. ↑
- C604.** Yu Haiyang. Earthquake-collapsed building extraction from LiDAR and aerophotograph based on OBIA. / Yu Haiyang, Cheng Gang, Ge Xiaosan. // 2010 2nd International Conference on Information Science and Engineering (ICISE). - Hangzhou, China, 4-6 Dec. 2010. - P. 2034-2037. ↑
- C605.** Liang Guo. Study on collaborative biohazard risk assessment system integrated with mobile GIS. / Liang Guo, Jianhua Gong, Xiangwang Wei, Youfu Xu. // 2010 2nd International Conference on Information Science and Engineering (ICISE). - Hangzhou, China, 4-6 Dec. 2010. - P. 6938-6941. ↑
- C606.** Zhi Wang. QEM-based simplification of building footprints from Airborne LiDAR data. / Zhi Wang, Hui-Ying Li, Li-Xin Wu. // 2010 IEEE International Geoscience and Remote Sensing Symposium (IGARSS). - Honolulu, HI, 25-30 July 2010. - P. 1186-1189. ↑
- C607.** Julea A. Extraction of frequent grouped sequential patterns from Satellite Image Time Series. / Julea A., Me,ger N., Rigotti C., Doin M.-P., Lasserre C., Trouve, E., Bolon P., La,za,rescu V. // 2010 IEEE International Geoscience and Remote Sensing Symposium (IGARSS). - Honolulu, HI, 25-30 July 2010. - P. 3434-3437. ↑
- C608.** Yisok Oh. Soil moisture detection using KOMPSAT-5 SAR data. / Yisok Oh, Soon-Gu Kwon, Ji-Hwan Hwang. // 2010 IEEE International Geoscience and Remote Sensing Symposium (IGARSS). - Honolulu, HI, 25-30 July 2010. - P. 1250-1253. ↑
- C609.** Fayard F. Generation of DEM by radargrammetric techniques. / Fayard F., Meric S., Pottier E. // 2010 IEEE International Geoscience and Remote Sensing Symposium (IGARSS). - Honolulu, HI, 25-30 July 2010. - P. 4342-4345. ↑
- C610.** Songxin Tan. A comparative study of polarimetric and non-polarimetric lidar in deciduous-coniferous tree classification. / Songxin Tan, Haider A. // 2010 IEEE International Geoscience and Remote Sensing Symposium (IGARSS). - Honolulu, HI, 25-30 July 2010. - P. 1178-1181. ↑
- C611.** Johnson B.R. National ecological observatory network (NEON) airborne remote measurements of vegetation canopy biochemistry and structure. / Johnson B.R., Kuester M.A., Kampe T.U., Keller M. // 2010 IEEE International Geoscience and Remote Sensing Symposium (IGARSS). - Honolulu, HI, 25-30 July 2010. - P. 2079-2082. ↑
- C612.** Mengwei Zhou. The inversion of crop height based on small-footprint waveform airborne lidar. / Mengwei Zhou, Qinhua Liu, Qiang Liu, Qing Xiao, Bo Zhong. // 2010 IEEE International Geoscience and Remote Sensing Symposium (IGARSS). - Honolulu, HI, 25-30 July 2010. - P. 1190-1193. ↑

- C613.** Yonglin Shen. Extraction of building's geometric axis line from LiDAR data for disaster management. / Yonglin Shen, Zhi Wang, Lixin Wu. // 2010 IEEE International Geoscience and Remote Sensing Symposium (IGARSS). - Honolulu, HI, 25-30 July 2010. - P. 1198-1201. ↑
- C614.** Fransson J.E.S. Mapping of wind-thrown forests using satellite SAR images. / Fransson J.E.S., Pantze A., Eriksson L.E.B., Soja M.J., Santoro M. // 2010 IEEE International Geoscience and Remote Sensing Symposium (IGARSS). - Honolulu, HI, 25-30 July 2010. - P. 1242-1245. ↑
- C615.** Manzo M. Full exploitation of the SBAS-DInSAR algorithm in active seismogenetic scenarios. / Manzo M., Berardino P., Bonano M., Casu F., Lanari R., Manconi A., Manunta M., Pepe A., Pepe S., Sansosti E., Solaro G., Tizzani P., Zeni G. // 2010 IEEE International Geoscience and Remote Sensing Symposium (IGARSS). - Honolulu, HI, 25-30 July 2010. - P. 1206-1209. ↑
- C616.** Williams B.A. Scatterometer image reconstruction from aperture-filtered samples. / Williams B.A., Long D.G. // 2010 IEEE International Geoscience and Remote Sensing Symposium (IGARSS). - Honolulu, HI, 25-30 July 2010. - P. 1835-1838. ↑
- C617.** Hoonyol Lee. Radargrammetry of high resolution synthetic aperture radar onboard KOMPSAT-5. 2010 IEEE International Geoscience and Remote Sensing Symposium (IGARSS). - Honolulu, HI, 25-30 July 2010. - P. 1246-1249. ↑
- C618.** Hui-Ying Li. Fusion of LiDAR data and orthoimage for automatic building reconstruction. / Hui-Ying Li, Sheng-Bo Chen, Zhi Wang, Wen-Hui Li. // 2010 IEEE International Geoscience and Remote Sensing Symposium (IGARSS). - Honolulu, HI, 25-30 July 2010. - P. 1194-1197. ↑
- C619.** Xiao Xiang Zhu. Compressive sensing for high resolution differential SAR tomography-the SL1MMER algorithm. / Xiao Xiang Zhu, Bamler R. // 2010 IEEE International Geoscience and Remote Sensing Symposium (IGARSS). - Honolulu, HI, 25-30 July 2010. - P. 17-20. ↑
- C620.** Qulin Tan. Building extraction from VHR multi-spectral images using rule-based object-oriented method: A case study. / Qulin Tan, Qingchao Wei, Fei Liang. // 2010 IEEE International Geoscience and Remote Sensing Symposium (IGARSS). - Honolulu, HI, 25-30 July 2010. - P. 2754-2756. ↑
- C621.** Zhe Jiang. Retrieval of Aerosol optical thickness and size distribution from PARASOL in Pearl River Delta area. / Zhe Jiang, Liangfu Chen, Minghui Tao, Lin Su. // 2010 IEEE International Geoscience and Remote Sensing Symposium (IGARSS). - Honolulu, HI, 25-30 July 2010. - P. 1145-1148. ↑
- C622.** Nirchio F. Contribution of Cosmo/SkyMed data into PRIM: A pilot project on marine oil pollution. results after one year of operations. / Nirchio F., Pandiscia G., Ruggieri G., Santoleri R., Pinardi N., Trivero P., Castellani C., Tataranni F., Masini A., Adamo M., Archetti R., Biamino W., Bignami F., Bohm E., Borasi M., Nardelli B.B., Cavagnero M., Colao F., Colella S., Coppini G., Debettio V., De Carolis G., De Dominicis M., Forneris V., Fontebasso F., Griffa A., Iacono R., Lombardi E., Marullo S., Manzella G., Mercatini A., Napolitano E., Pisano A., Reseghetti F., Sorgente R., Sprovieri M., Terranova G., Volpe G., Zambianchi E. // 2010 IEEE International Geoscience and Remote Sensing Symposium (IGARSS). - Honolulu, HI, 25-30 July 2010. - P. 4799-4802. ↑
- C623.** Lombardini F. First experiments of sector interpolated SAR tomography. / Lombardini F., Pardini M. // 2010 IEEE International Geoscience and Remote Sensing Symposium (IGARSS). - Honolulu, HI, 25-30 July 2010. - P. 21-24. ↑
- C624.** Bovenga F. The COSMO SKYMED constellation turn on the l'aquila earthquake: Dinsar results of the morfeo project. / Bovenga F., Candela L., Casu F., Fornaro G., Guzzetti F., Lanari R., Nitti D.O., Nutricato R., Reale D. // 2010 IEEE International Geoscience and Remote Sensing Symposium (IGARSS). - Honolulu, HI, 25-30 July 2010. - P. 4803-4806. ↑
- C625.** Pratola C. Towards fully automatic generation of land cover maps from polarimetric and metric-resolution SAR data. / Pratola C., Del Greco M., Del Frate F., Schiavon G., Solimini D. // 2010 IEEE International Geoscience and Remote Sensing Symposium (IGARSS). - Honolulu, HI, 25-30 July 2010. - P. 3102-3105. ↑
- C626.** Yorks J.E. Statistics of depolarization ratio from an airborne backscatter lidar. / Yorks J.E., McGill M.J., Hlavka D.L., Hart W.D. // 2010 IEEE International Geoscience and Remote Sensing Symposium (IGARSS). - Honolulu, HI, 25-30 July 2010. - P. 2579-2582. ↑

- C627.** Dagefu F.T. Soil dielectric and senisitivity analysis for subsurface imaging applications based on distributed Sensor Networks. / Dagefu F.T., Sarabandi K. // 2010 IEEE International Geoscience and Remote Sensing Symposium (IGARSS). - Honolulu, HI, 25-30 July 2010. - P. 1839-1842. ↑
- C628.** Morgenthaler A.W. The Semi-Analytic Mode Matching algorithm for GPR wave scattering from multiple complex objects buried in a dielectric half space. / Morgenthaler A.W., Rappaport C.M. // 2010 IEEE International Geoscience and Remote Sensing Symposium (IGARSS). - Honolulu, HI, 25-30 July 2010. - P. 4713-4716. ↑
- C629.** Zhixin Qi. Integrating object-oriented image analysis and decision tree algorithm for land use and land cover classification using RADARSAT-2 polarimetric SAR imagery. / Zhixin Qi, Yeh A.G.-O., Xia Li, Zheng Lin. // 2010 IEEE International Geoscience and Remote Sensing Symposium (IGARSS). - Honolulu, HI, 25-30 July 2010. - P. 3098-3101. ↑
- C630.** Harant O. Maximum Likelihood texture tracking in highly heterogeneous PolSAR clutter. / Harant O., Bombrun L., Vasile G., Ferro-Famil L., Gay M. // 2010 IEEE International Geoscience and Remote Sensing Symposium (IGARSS). - Honolulu, HI, 25-30 July 2010. - P. 4031-4034. ↑
- C631.** YiHyun Kim. Estimating rice growth parameters using X-band scatterometer data. / YiHyun Kim, SukYoung Hong, Eunyoung Choe, Hoonyol Lee. // 2010 IEEE International Geoscience and Remote Sensing Symposium (IGARSS). - Honolulu, HI, 25-30 July 2010. - P. 1258-1260. ↑
- C632.** Vasile G. Optimal parameter estimation in heterogeneous clutter for high resolution polarimetric SAR data. / Vasile G., Pascal F., Ovarlez J., Zozor S., Gay M. // 2010 IEEE International Geoscience and Remote Sensing Symposium (IGARSS). - Honolulu, HI, 25-30 July 2010. - P. 855-858. ↑
- C633.** Atlas R. Review of Observing System Simulation Experiments to evaluate the potential impact of lidar winds on weather prediction. 2010 IEEE International Geoscience and Remote Sensing Symposium (IGARSS). - Honolulu, HI, 25-30 July 2010. - P. 2587-2590. ↑
- C634.** Abileah R. Shallow water bathymetry with an incoherent X-band radar using small (smaller) space-time image cubes. / Abileah R., Trizna D.B. // 2010 IEEE International Geoscience and Remote Sensing Symposium (IGARSS). - Honolulu, HI, 25-30 July 2010. - P. 4330-4333. ↑
- C635.** Thiele A. Combining GIS and InSAR data for 3D building reconstruction. / Thiele A., Hinz S., Cadario E. // 2010 IEEE International Geoscience and Remote Sensing Symposium (IGARSS). - Honolulu, HI, 25-30 July 2010. - P. 2418-2421. ↑
- C636.** Ngoc Truong Minh Nguyen. Characterization of the scattered field by an urban area in the X-frequency band for bistatic and monostatic radar configurations. / Ngoc Truong Minh Nguyen, Lautru D., Roussel H. // 2010 IEEE International Geoscience and Remote Sensing Symposium (IGARSS). - Honolulu, HI, 25-30 July 2010. - P. 2999-3002. ↑
- C637.** Cunren Liang. Burst mode to strip-map mode SAR interferometry of ALOS PALSAR. / Cunren Liang, Qiming Zeng, Xia Cui, Jian Jiao. // 2010 IEEE International Geoscience and Remote Sensing Symposium (IGARSS). - Honolulu, HI, 25-30 July 2010. - P. 4023-4026. ↑
- C638.** Uiboupin R. Study of snowmelt impact on SST and TSM fields in the coastal zone of Barents Sea. / Uiboupin R., Arino O. // 2010 IEEE International Geoscience and Remote Sensing Symposium (IGARSS). - Honolulu, HI, 25-30 July 2010. - P. 4212-4215. ↑
- C639.** Yan Y. Assimilation of D-InSAR and sub-pixel image correlation displacement measurements for coseismic fault parameter estimation. / Yan Y., Trouve, E., Bissierier A., Mauris G., Galichet S., Pinel V., Pathier E. // 2010 IEEE International Geoscience and Remote Sensing Symposium (IGARSS). - Honolulu, HI, 25-30 July 2010. - P. 3664-3667. ↑
- C640.** Bennani Y. Bistatic Radar Cross Section of an complex target on sea surface. / Bennani Y., Khenchaf A., Comblet F., Ali-Yahia A. // 2010 IEEE International Geoscience and Remote Sensing Symposium (IGARSS). - Honolulu, HI, 25-30 July 2010. - P. 2543-2546. ↑
- C641.** Frey O. Analyzing tomographic SAR data of a forest with respect to frequency, polarization, and focusing technique. / Frey O., Meier E. // 2010 IEEE International Geoscience and Remote Sensing Symposium (IGARSS). - Honolulu, HI, 25-30 July 2010. - P. 150-153. ↑

- C642.** Wilson J.J.W. Radiometric performance of the Advanced Wind Scatterometer radar ASCAT. / Wilson J.J.W., Anderson C., Figa Saldana J., Bonekamp H. // 2010 IEEE International Geoscience and Remote Sensing Symposium (IGARSS). - Honolulu, HI, 25-30 July 2010. - P. 1092-1095. ↑
- C643.** Richard J. An innovative spaceborne radar concept for global maritime surveillance: Description and performance demonstration. / Richard J., Enjolras V., Schoeser C., Angelliaume S., Durand P. // 2010 IEEE International Geoscience and Remote Sensing Symposium (IGARSS). - Honolulu, HI, 25-30 July 2010. - P. 257-259. ↑
- C644.** Rizzoli P. X-band backscatter map generation using TerraSAR-x data. / Rizzoli P., Brautigam B., Wollstadt S., Mittermayer J. // 2010 IEEE International Geoscience and Remote Sensing Symposium (IGARSS). - Honolulu, HI, 25-30 July 2010. - P. 3450-3453. ↑
- C645.** Zili Shan. Change detection in urban areas with high resolution SAR images using second kind statistics based G0 distribution. / Zili Shan, Chao Wang, Hong Zhang, Fan Wu. // 2010 IEEE International Geoscience and Remote Sensing Symposium (IGARSS). - Honolulu, HI, 25-30 July 2010. - P. 4600-4603. ↑
- C646.** Stocker E.F. A generalized logical format for inter-calibrated brightness temperatures for the global precipitation measurement mission. / Stocker E.F., Stout J., Kummerow C., Berg W. // 2010 IEEE International Geoscience and Remote Sensing Symposium (IGARSS). - Honolulu, HI, 25-30 July 2010. - P. 844-846. ↑
- C647.** Meyer F. A review of ionospheric effects in low-frequency SAR-Signals, correction methods, and performance requirements. 2010 IEEE International Geoscience and Remote Sensing Symposium (IGARSS). - Honolulu, HI, 25-30 July 2010. - P. 29-32. ↑
- C648.** Quivira F. Impact of the wave number estimation in Underground Focusing SAR images. / Quivira F., Martinez-Lorenzo J.A., Rappaport C.M. // 2010 IEEE International Geoscience and Remote Sensing Symposium (IGARSS). - Honolulu, HI, 25-30 July 2010. - P. 4310-4313. ↑
- C649.** Deledalle C.-A. Glaciermonitoring: Correlation versus texture tracking. / Deledalle C.-A., Nicolas J.-M., Tupin F., Denis L., Fallourd R., Trouve, E. // 2010 IEEE International Geoscience and Remote Sensing Symposium (IGARSS). - Honolulu, HI, 25-30 July 2010. - P. 513-516. ↑
- C650.** Deledalle C. A non-local approach for SAR and interferometric SAR denoising. / Deledalle C., Tupin F., Denis L. // 2010 IEEE International Geoscience and Remote Sensing Symposium (IGARSS). - Honolulu, HI, 25-30 July 2010. - P. 714-717. ↑
- C651.** Morris K.R. Data visualization and analysis tools for the Global Precipitation Measurement (GPM) Validation Network. / Morris K.R., Schwaller M.R. // 2010 IEEE International Geoscience and Remote Sensing Symposium (IGARSS). - Honolulu, HI, 25-30 July 2010. - P. 847-850. ↑
- C652.** Baselice F. New trends in SAR tomography. / Baselice F., Budillon A., Ferraioli G., Pascasio V., Schirinzi G., Evangelista A. // 2010 IEEE International Geoscience and Remote Sensing Symposium (IGARSS). - Honolulu, HI, 25-30 July 2010. - P. 25-28. ↑
- C653.** Jong-Sen Lee. Monitoring tree farms and coastal environments using RADARSAT-2 PolSAR data. / Jong-Sen Lee, Ainsworth T.L., Yanting Wang, Kun-Shan Chen, Chih-Tien Wang. // 2010 IEEE International Geoscience and Remote Sensing Symposium (IGARSS). - Honolulu, HI, 25-30 July 2010. - P. 3134-3137. ↑
- C654.** Panzer B. Ultra-wideband radar measurements of snow thickness over sea ice. / Panzer B., Leuschen C., Patel A., Markus T., Gogineni S. // 2010 IEEE International Geoscience and Remote Sensing Symposium (IGARSS). - Honolulu, HI, 25-30 July 2010. - P. 3130-3133. ↑
- C655.** Hendricks S. Effects of surface roughness on sea ice freeboard retrieval with an Airborne Ku-Band SAR radar altimeter. / Hendricks S., Stenseng L., Helm V., Haas C. // 2010 IEEE International Geoscience and Remote Sensing Symposium (IGARSS). - Honolulu, HI, 25-30 July 2010. - P. 3126-3129. ↑
- C656.** Font J. Overview of SMOS Level 2 Ocean Salinity processing and first results. / Font J., Boutin J., Reul N., Spurgeon P., Ballabrera J., Chuprin A., Gabarro, C., Gourrion J., Henocq C., Lavender S., Martin N., Martinez J., McCulloch M., Meirold-Mautner I., Petitcolin F., Portabella M., Sabia R., Talone M., Tenerelli J., Turiel A., Vergely J.L., Waldteufel P., Yin X., Zine S. // 2010 IEEE International Geoscience and Remote Sensing Symposium (IGARSS). - Honolulu, HI, 25-30 July 2010. - P. 3146-3149. ↑

- C657.** Bo Zhang. Characteristic analysis of vehicle target in Quad-Pol Radarsat-2 SAR images. / Bo Zhang, Hong Zhang, Chao Wang, Fan Wu, Yi-xian Tang. // 2010 IEEE International Geoscience and Remote Sensing Symposium (IGARSS). - Honolulu, HI, 25-30 July 2010. - P. 3142-3145. ↑
- C658.** Sang-Hoon Hong. Rotated dihedral and volume scattering behavior in cross-polarimetric SAR. / Sang-Hoon Hong, Wdowinski S. // 2010 IEEE International Geoscience and Remote Sensing Symposium (IGARSS). - Honolulu, HI, 25-30 July 2010. - P. 3138-3141. ↑
- C659.** Nies H. Polarimetric and interferometric applications in a bistatic hybrid SAR mode using Terrasar-X. / Nies H., Behner F., Reuter S., Loffeld O., Wang R. // 2010 IEEE International Geoscience and Remote Sensing Symposium (IGARSS). - Honolulu, HI, 25-30 July 2010. - P. 110-113. ↑
- C660.** Kuester M.A. Calibration system stability plans for a long-term Ecological Airborne remote sensing project. / Kuester M.A., Johnson B.R., Kampe T.U., McCorkel J. // 2010 IEEE International Geoscience and Remote Sensing Symposium (IGARSS). - Honolulu, HI, 25-30 July 2010. - P. 593-595. ↑
- C661.** Xuan Feng. 3D velocity model and ray tracing of antenna array GPR. / Xuan Feng, Wenjin Liang, Qi Lu, Cai Liu, Lili Li, Lilong Zou, Sato M. // 2010 IEEE International Geoscience and Remote Sensing Symposium (IGARSS). - Honolulu, HI, 25-30 July 2010. - P. 4204-4207. ↑
- C662.** Klaric M. Progressive spatial clustering of content-based satellite imagery retrieval results. / Klaric M., Scott G., Shyu C. // 2010 IEEE International Geoscience and Remote Sensing Symposium (IGARSS). - Honolulu, HI, 25-30 July 2010. - P. 36-39. ↑
- C663.** Cheng Hu. Modification of slant range model and imaging processing in GEO SAR. / Cheng Hu, Feifeng Liu, Wenfu Yang, Tao Zeng, Teng Long. // 2010 IEEE International Geoscience and Remote Sensing Symposium (IGARSS). - Honolulu, HI, 25-30 July 2010. - P. 4679-4682. ↑
- C664.** Angiati E. Operational evaluation of damages in flooded areas combining Cosmo-Skymed and multispectral optical images. / Angiati E., Boni G., Candela L., Castelli F., Dellepiane S., Delogu F., Pintus F., Rudari R., Serpico S.B., Traverso S., Versace C. // 2010 IEEE International Geoscience and Remote Sensing Symposium (IGARSS). - Honolulu, HI, 25-30 July 2010. - P. 2414-2417. ↑
- C665.** Sakamoto T. A target tracking method with a single antenna using time-reversal UWB radar imaging in a multi-path environment. / Sakamoto T., Sato T. // 2010 IEEE International Geoscience and Remote Sensing Symposium (IGARSS). - Honolulu, HI, 25-30 July 2010. - P. 3319-3322. ↑
- C666.** Gang Li. ISAR imaging of maneuvering targets via matching pursuit. / Gang Li, Hao Zhang, Xiqin Wang, Xiang-Gen Xia. // 2010 IEEE International Geoscience and Remote Sensing Symposium (IGARSS). - Honolulu, HI, 25-30 July 2010. - P. 1625-1628. ↑
- C667.** Jinyang Du. A method to estimate Snow Water Equivalent using multi-angle X-band radar observations. / Jinyang Du, Jiancheng Shi, Chuan Xiong. // 2010 IEEE International Geoscience and Remote Sensing Symposium (IGARSS). - Honolulu, HI, 25-30 July 2010. - P. 3774-3776. ↑
- C668.** Zhen Liu. Monitoring time-dependent volcanic dynamics at Long Valley Caldera using InSAR and GPS measurements. / Zhen Liu, Danan Dong, Lundgren P. // 2010 IEEE International Geoscience and Remote Sensing Symposium (IGARSS). - Honolulu, HI, 25-30 July 2010. - P. 665-668. ↑
- C669.** Le Vine D.M. Spurious signal in measurement of the third Stokes parameter from space at L-band. / Le Vine D.M., Dinnat E.D., Jacob S.D., Abraham S., de Mattheaïs P. // 2010 IEEE International Geoscience and Remote Sensing Symposium (IGARSS). - Honolulu, HI, 25-30 July 2010. - P. 3772-3773. ↑
- C670.** Jili Li. Individual tree species classification using structure features from high density airborne lidar data. / Jili Li, Baoxin Hu, Gunho Sohn, Linhai Jing. // 2010 IEEE International Geoscience and Remote Sensing Symposium (IGARSS). - Honolulu, HI, 25-30 July 2010. - P. 2099-2102. ↑
- C671.** Touzi R. On the use of transponder measurements for high precision assessment and calibration of polarimetric Radarsat-2. / Touzi R., Hawkins R.K., Co,te, S. // 2010 IEEE International Geoscience and Remote Sensing Symposium (IGARSS). - Honolulu, HI, 25-30 July 2010. - P. 4847-4850. ↑
- C672.** Zhiyu Zhang. Biomass retrieval based on UAVSAR polarimetric data. / Zhiyu Zhang, Guoqing Sun, Lixin

Zhang, Zhifeng Guo, Wenli Huang. // 2010 IEEE International Geoscience and Remote Sensing Symposium (IGARSS). - Honolulu, HI, 25-30 July 2010. - P. 604-607. ↑

C673. Rogers M. The Cloudsat Education Network: Scientifically significant collaborative research between students and scientists. / Rogers M., Vane D. // 2010 IEEE International Geoscience and Remote Sensing Symposium (IGARSS). - Honolulu, HI, 25-30 July 2010. - P. 84-86. ↑

C674. Parrilli S. A nonlocal approach for SAR image denoising. / Parrilli S., Poderico M., Angelino C.V., Scarpa G., Verdoliva L. // 2010 IEEE International Geoscience and Remote Sensing Symposium (IGARSS). - Honolulu, HI, 25-30 July 2010. - P. 726-729. ↑

C675. Spinhirne J.D. Global laser pulse reflectance at 1064 nm of snow and land surfaces from the Glas satellite Lidar. / Spinhirne J.D., Palm S.P. // 2010 IEEE International Geoscience and Remote Sensing Symposium (IGARSS). - Honolulu, HI, 25-30 July 2010. - P. 646-648. ↑

C676. Dapeng Yan. PSI analyses of land subsidence due to economic development near the city of Hangzhou, China. / Dapeng Yan, Daqing Ge, Jin Yang, Ling Zhang, Yan Wang, Xiaofang Guo. // 2010 IEEE International Geoscience and Remote Sensing Symposium (IGARSS). - Honolulu, HI, 25-30 July 2010. - P. 2410-2413. ↑

C677. Arakelyan A. C- and Ku-band (at 5.6GHz and 13.6GHz), dual-frequency, multi-polarization, short pulse, combined scatterometer-radiometer system for low altitude platform, vessel and aircraft applications. / Arakelyan A., Hambaryan A., Karyan V., Hovhannisyan G., Grigoryan M., Arakelyan A., Simonyan M., Poghosyan T., Poghosyan N. // 2010 IEEE International Geoscience and Remote Sensing Symposium (IGARSS). - Honolulu, HI, 25-30 July 2010. - P. 4470-4473. ↑

C678. Brunner D. Change detection for earthquake damage assessment in built-up areas using very high resolution optical and SAR imagery. / Brunner D., Bruzzone L., Lemoine G. // 2010 IEEE International Geoscience and Remote Sensing Symposium (IGARSS). - Honolulu, HI, 25-30 July 2010. - P. 3210-3213. ↑

C679. Wenjian Ni. Investigation of forest height retrieval using SRTM-DEM and ASTER-GDEM. / Wenjian Ni, Zhifeng Guo, Guoqing Sun, Hong Chi. // 2010 IEEE International Geoscience and Remote Sensing Symposium (IGARSS). - Honolulu, HI, 25-30 July 2010. - P. 2111-2114. ↑

C680. Carrano C.S. A phase screen simulator for predicting the impact of small-scale ionospheric structure on SAR image formation and interferometry. / Carrano C.S., Groves K.M., Caton R.G. // 2010 IEEE International Geoscience and Remote Sensing Symposium (IGARSS). - Honolulu, HI, 25-30 July 2010. - P. 162-165. ↑

C681. Iribe K. Coherent scatterer in forest environment: Detection, properties and its applications. / Iribe K., Papathanassiou K., Hajnsek I., Sato M., Yokota Y. // 2010 IEEE International Geoscience and Remote Sensing Symposium (IGARSS). - Honolulu, HI, 25-30 July 2010. - P. 3247-3250. ↑

C682. von Lerber A. Modeling attenuation of melting hydrometeors with a method based on volume integral equations. / von Lerber A., Piepponen T., Koskinen J., Moiseev D., Kestilä A., Tyynelä J., Nousiainen T., Koistinen J., Sihvola A., Ylä-Oijala P., Praks J., Hallikainen M., Pulliainen J. // 2010 IEEE International Geoscience and Remote Sensing Symposium (IGARSS). - Honolulu, HI, 25-30 July 2010. - P. 2355-2358. ↑

C683. Schwabisch M. Accurate focusing of single-pass airborne InSAR data at L-band. / Schwabisch M., Mercer B., Qiaoping Zhang, Wei Huang. // 2010 IEEE International Geoscience and Remote Sensing Symposium (IGARSS). - Honolulu, HI, 25-30 July 2010. - P. 2625-2628. ↑

C684. Yoldemir A.B. Rotation and scale invariant template matching applied to buried object discrimination in GPR data. / Yoldemir A.B., Sezgin M. // 2010 IEEE International Geoscience and Remote Sensing Symposium (IGARSS). - Honolulu, HI, 25-30 July 2010. - P. 3366-3369. ↑

C685. Daqing Ge. Mapping urban subsidence with TerraSAR-X data by PSI analysis. / Daqing Ge, Yan Wang, Ling Zhang, Xiaofang Guo, Ye Xia. // 2010 IEEE International Geoscience and Remote Sensing Symposium (IGARSS). - Honolulu, HI, 25-30 July 2010. - P. 3323-3326. ↑

C686. Jin-King Liu. Landslide detection by indices of LiDAR point-cloud density. / Jin-King Liu, Wei-Chen Hsu, Mon-Shieh Yang, Yu-Chung Shieh, Tian-Yuan Shih. // 2010 IEEE International Geoscience and Remote Sensing Symposium (IGARSS). - Honolulu, HI, 25-30 July 2010. - P. 3960-3963. ↑

- C687.** Hayashi N. 3D subsurface visualization by suppressing ground reflection and direct wave with bistatic GPR. / Hayashi N., Sato M. // 2010 IEEE International Geoscience and Remote Sensing Symposium (IGARSS). - Honolulu, HI, 25-30 July 2010. - P. 4592-4595. ↑
- C688.** Hallikainen M. Studies of radio frequency interference at L-band using an airborne 2-D interferometric radiometer. / Hallikainen M., Kainulainen J., Seppänen J., Hakkarainen A., Rautiainen K. // 2010 IEEE International Geoscience and Remote Sensing Symposium (IGARSS). - Honolulu, HI, 25-30 July 2010. - P. 2490-2491. ↑
- C689.** Suchandt S. Tidal current measurement with TerraSAR-X Along-Track Interferometry. / Suchandt S., Runge H., Romeiser R., Tous-Ramon N., Steinbrecher U. // 2010 IEEE International Geoscience and Remote Sensing Symposium (IGARSS). - Honolulu, HI, 25-30 July 2010. - P. 2432-2435. ↑
- C690.** Klare J. Environmental monitoring with the imaging MIMO radars MIRA-CLE and MIRA-CLE X. / Klare J., Saalman O., Wilden H., Brenner A.R. // 2010 IEEE International Geoscience and Remote Sensing Symposium (IGARSS). - Honolulu, HI, 25-30 July 2010. - P. 3781-3784. ↑
- C691.** Zahn R. Modular Radar Core for airborne and space applications. / Zahn R., Kirscht M., Weidmann K. // 2010 IEEE International Geoscience and Remote Sensing Symposium (IGARSS). - Honolulu, HI, 25-30 July 2010. - P. 677-680. ↑
- C692.** Jong-Kuk Choi. Integration of InSAR and GIS for an estimation of ground subsidence susceptibility. / Jong-Kuk Choi, Joong-Sun Won, Sang-Wan Kim, Ki-Dong Kim, Joo-Hyung Ryu, Hong-Rhyong Yoo. // 2010 IEEE International Geoscience and Remote Sensing Symposium (IGARSS). - Honolulu, HI, 25-30 July 2010. - P. 4588-4591. ↑
- C693.** Conway D. Using lidar to estimate the capacity for storm water recycling and solar energy collection. / Conway D., Samsung Lim. // 2010 IEEE International Geoscience and Remote Sensing Symposium (IGARSS). - Honolulu, HI, 25-30 July 2010. - P. 4545-4548. ↑
- C694.** Casu F. Advances in the generation of deformation time series from SAR data sequences in areas affected by large dynamics. / Casu F., Manconi A., Pepe A., Manzo M., Lanari R. // 2010 IEEE International Geoscience and Remote Sensing Symposium (IGARSS). - Honolulu, HI, 25-30 July 2010. - P. 2618-2621. ↑
- C695.** Shiang Wang. Microwave remote sensing for marine monitoring: An example of *Enteromorpha prolifera* bloom monitoring. / Shiang Wang, Fengli Zhang, Yun Shao, Wei Tian, Huaze Gong. // 2010 IEEE International Geoscience and Remote Sensing Symposium (IGARSS). - Honolulu, HI, 25-30 July 2010. - P. 4530-4533. ↑
- C696.** Schwerdt M. Monostatic calibration of both TanDEM-X satellites. / Schwerdt M., Gonzalez J.H., Bachmann M., Schrank D., Schulz C., Dojring B. // 2010 IEEE International Geoscience and Remote Sensing Symposium (IGARSS). - Honolulu, HI, 25-30 July 2010. - P. 2636-2639. ↑
- C697.** Owen M.P. Towards an improved wind and rain backscatter model for ASCAT. / Owen M.P., Long D.G. // 2010 IEEE International Geoscience and Remote Sensing Symposium (IGARSS). - Honolulu, HI, 25-30 July 2010. - P. 2531-2534. ↑
- C698.** Perrie W. Gulf stream thermal fronts detected by synthetic aperture radar. / Perrie W., Tao Xie. // 2010 IEEE International Geoscience and Remote Sensing Symposium (IGARSS). - Honolulu, HI, 25-30 July 2010. - P. 2426-2427. ↑
- C699.** Marchese L. Ultra-rapid optronic processor for instantaneous ENVISAT/ASAR scene observation. / Marchese L., Doucet M., Harnisch B., Suess M., Bourqui P., Legros M., Desnoyers N., Guillot L., Mercier L., Savard M., Martel A., Chateaufneuf F., Bergeron A. // 2010 IEEE International Geoscience and Remote Sensing Symposium (IGARSS). - Honolulu, HI, 25-30 July 2010. - P. 685-687. ↑
- C700.** Reid M.A. Automated Polar ice thickness estimation from radar imagery. / Reid M.A., Gifford C.M., Jefferson M., Akers E.L., Finyom G., Agah A. // 2010 IEEE International Geoscience and Remote Sensing Symposium (IGARSS). - Honolulu, HI, 25-30 July 2010. - P. 2406-2409. ↑
- C701.** Kang Liu. Building height extraction via a deterministic approach using a TerraSAR-X data stack. / Kang Liu, Balz T., Mingsheng Liao. // 2010 IEEE International Geoscience and Remote Sensing Symposium (IGARSS). - Honolulu, HI, 25-30 July 2010. - P. 2920-2923. ↑

- C702.** Yasuma H. Rain effect on polarimetric SAR observation. / Yasuma H., Fukuchi H. // 2010 IEEE International Geoscience and Remote Sensing Symposium (IGARSS). - Honolulu, HI, 25-30 July 2010. - P. 2047-2050. ↑
- C703.** Forster B. Global trends in remote sensing of human settlements. 2010 IEEE International Geoscience and Remote Sensing Symposium (IGARSS). - Honolulu, HI, 25-30 July 2010. - P. 1339-1342. ↑
- C704.** Jinghui Fan. CRInSAR for landslide deformation monitoring: A case in threegerge area. / Jinghui Fan, Hongli Zhao, Pengfei Tu, Yi Wang, Xiaofang Guo, Daqing Ge, Guang Liu. // 2010 IEEE International Geoscience and Remote Sensing Symposium (IGARSS). - Honolulu, HI, 25-30 July 2010. - P. 3956-3959. ↑
- C705.** Monnet J.-M. Support vector machines regression for estimation of forest parameters from airborne laser scanning data. / Monnet J.-M., Berger F., Chanussot J. // 2010 IEEE International Geoscience and Remote Sensing Symposium (IGARSS). - Honolulu, HI, 25-30 July 2010. - P. 2711-2714. ↑
- C706.** Spencer M. The Soil Moisture Active Passive (SMAP) mission L-Band radar/radiometer instrument. / Spencer M., Wheeler K., White C., West R., Piepmeier J., Hudson D., Medeiros J. // 2010 IEEE International Geoscience and Remote Sensing Symposium (IGARSS). - Honolulu, HI, 25-30 July 2010. - P. 3240-3243. ↑
- C707.** Komatsu Y. Extraction of area-averaged orientation angle from POLSAR measurement. / Komatsu Y., Aso Y., Fukuchi H. // 2010 IEEE International Geoscience and Remote Sensing Symposium (IGARSS). - Honolulu, HI, 25-30 July 2010. - P. 4051-4054. ↑
- C708.** Jung J.S. Stap based ground moving target detectability in the airborne/spaceborne array radar. / Jung J.S., Jung Kim, Kwag Y.K. // 2010 IEEE International Geoscience and Remote Sensing Symposium (IGARSS). - Honolulu, HI, 25-30 July 2010. - P. 4632-4635. ↑
- C709.** Dhont D. Quantification of the topographic slope from radar satellite imagery. / Dhont D., Pajot E., Rudant J. // 2010 IEEE International Geoscience and Remote Sensing Symposium (IGARSS). - Honolulu, HI, 25-30 July 2010. - P. 4584-4587. ↑
- C710.** Pepe A. Deformation in Hawaii's volcanoes obtained from a ScanSAR-to-stripmap Small Baseline Subset technique. / Pepe A., Ortiz A.B., Bonano M., Lanari R., Lundgren P., Rosen P.A. // 2010 IEEE International Geoscience and Remote Sensing Symposium (IGARSS). - Honolulu, HI, 25-30 July 2010. - P. 769-772. ↑
- C711.** Bin Ding. Analysis of the effect of radio frequency interference on interferometric phase. / Bin Ding, Mao Sheng Xiang, Xing Dong Liang. // 2010 IEEE International Geoscience and Remote Sensing Symposium (IGARSS). - Honolulu, HI, 25-30 July 2010. - P. 4628-4631. ↑
- C712.** Kidera S. Shadow region imaging algorithm using array antenna based on aperture synthesis of multiple scattered waves for UWB radars. 2010 IEEE International Geoscience and Remote Sensing Symposium (IGARSS). - Honolulu, HI, 25-30 July 2010. - P. 4055-4058. ↑
- C713.** Xueyang Duan. Electromagnetic scattering from arbitrary random rough surfaces using stabilized extended boundary condition method (SEBCM) for remote sensing of soil moisture. / Xueyang Duan, Moghaddam M. // 2010 IEEE International Geoscience and Remote Sensing Symposium (IGARSS). - Honolulu, HI, 25-30 July 2010. - P. 1386-1389. ↑
- C714.** Yiding Wang. Code sequence selection for SAR radiometric calibration. / Yiding Wang, Yuanshu Li, Zhulei Wang. // 2010 IEEE International Geoscience and Remote Sensing Symposium (IGARSS). - Honolulu, HI, 25-30 July 2010. - P. 209-212. ↑
- C715.** Ping Zhang. 2D uesprit superresolution SAR imaging algorithm. / Ping Zhang, Zhen Li, Quan Chen. // 2010 IEEE International Geoscience and Remote Sensing Symposium (IGARSS). - Honolulu, HI, 25-30 July 2010. - P. 4067-4070. ↑
- C716.** Kusk A. SAR focusing of P-band ice sounding data using back-projection. / Kusk A., Dall J. // 2010 IEEE International Geoscience and Remote Sensing Symposium (IGARSS). - Honolulu, HI, 25-30 July 2010. - P. 4071-4074. ↑
- C717.** Formont P. A test statistic for high resolution polarimetric SAR data classification. / Formont P., Ovarlez

J.-P., Pascal F., Vasile G., Ferro-Famil L. // 2010 IEEE International Geoscience and Remote Sensing Symposium (IGARSS). - Honolulu, HI, 25-30 July 2010. - P. 1871-1874. ↑

**C718.** Xi'ai Cui. Investigating co-seismic deformation of the 2008 Wenchuan earthquake with ALOS SCANSAR interferometric observations. / Xi'ai Cui, Qiming Zeng, Cunren Liang, Jian Jiao. // 2010 IEEE International Geoscience and Remote Sensing Symposium (IGARSS). - Honolulu, HI, 25-30 July 2010. - P. 4612-4615. ↑

**C719.** Correia A.H. Evaluation of the influence of the polarimetric calibration process on the H/A/alpha decomposition. / Correia A.H., da Costa Freitas C., Mura J.C. // 2010 IEEE International Geoscience and Remote Sensing Symposium (IGARSS). - Honolulu, HI, 25-30 July 2010. - P. 2039-2042. ↑

**C720.** Wang R. Analysis and compensation for motion errors in FMCW SAR data. / Wang R., Loffeld O., Nies H., Peters V., Hajgelen M., Essen H. // 2010 IEEE International Geoscience and Remote Sensing Symposium (IGARSS). - Honolulu, HI, 25-30 July 2010. - P. 4075-4078. ↑

**C721.** Bonano M. The extended SBAS technique for generating full resolution ERS/ENVISAT deformation time-series. / Bonano M., Manunta M., Marsella M., Lanari R. // 2010 IEEE International Geoscience and Remote Sensing Symposium (IGARSS). - Honolulu, HI, 25-30 July 2010. - P. 4616-4619. ↑

**C722.** Hambaryan A.K. Multi-frequency and polarimetric measurements of snow microwave reflection and emission by C- and Ku-band, combined scatterometer-radiometer systems. / Hambaryan A.K., Arakelyan A.K., Hambaryan V.K., Karyan V.V., Manukyan M.R., Grigoryan M.L., Hovhannisyan G.G., Arakelyan A.A., Darbinyan S.A. // 2010 IEEE International Geoscience and Remote Sensing Symposium (IGARSS). - Honolulu, HI, 25-30 July 2010. - P. 1733-1736. ↑

**C723.** Kaizhi Wang. Progressive SAR imaging technique. / Kaizhi Wang, Xingzhao Liu, Wenxian Yu, Junli Chen, Guozhong Chen. // 2010 IEEE International Geoscience and Remote Sensing Symposium (IGARSS). - Honolulu, HI, 25-30 July 2010. - P. 4083-4086. ↑

**C724.** Trabal J.M. Evaluation of the self-consistency principle for calibration of the CASA radar network using properties of the observed medium. / Trabal J.M., Chandrasekar V., Gorgucci E., McLaughlin D.J. // 2010 IEEE International Geoscience and Remote Sensing Symposium (IGARSS). - Honolulu, HI, 25-30 July 2010. - P. 4126-4129. ↑

**C725.** Feifeng Liu. A novel range migration algorithm of GEO SAR echo data. / Feifeng Liu, Cheng Hu, Tao Zeng, Teng Long, Lihua Jin. // 2010 IEEE International Geoscience and Remote Sensing Symposium (IGARSS). - Honolulu, HI, 25-30 July 2010. - P. 4656-4659. ↑

**C726.** Jong-Sen Lee. An overview of recent advances in Polarimetric SAR information extraction: Algorithms and applications. / Jong-Sen Lee, Ainsworth T.L. // 2010 IEEE International Geoscience and Remote Sensing Symposium (IGARSS). - Honolulu, HI, 25-30 July 2010. - P. 851-854. ↑

**C727.** Chandrasekar V. CASA dual-doppler system. / Chandrasekar V., Martinez M., Sean Zhang. // 2010 IEEE International Geoscience and Remote Sensing Symposium (IGARSS). - Honolulu, HI, 25-30 July 2010. - P. 4138-4141. ↑

**C728.** Bin Liu. PS-InSAR time series analysis for measuring surface deformation before the L'Aquila earthquake. / Bin Liu, Yi Luo, Jingfa Zhang, Lixia Gong, Wenliang Jiang, Liyan Ren. // 2010 IEEE International Geoscience and Remote Sensing Symposium (IGARSS). - Honolulu, HI, 25-30 July 2010. - P. 4604-4607. ↑

**C729.** McGlinchy J. Extracting structural land cover components using small-footprint waveform lidar data. / McGlinchy J., Van Aardt J., Rhody H., Kerekese J., Ientiluci E., Asner G.P., Knapp D., Mathieu R., Kennedy-Bowdoin T., Erasmus B.F.N., Wessels K., Smit I.P.J., Wu J., Sarrazin D. // 2010 IEEE International Geoscience and Remote Sensing Symposium (IGARSS). - Honolulu, HI, 25-30 July 2010. - P. 1976-1979. ↑

**C730.** Lardeux C. Assessment of compact polarimetry over different tropical environment and dataset. / Lardeux C., Niamen D., Routier J.B., Giraud A., Frison P.L., Pottier E., Rudant J.P. // 2010 IEEE International Geoscience and Remote Sensing Symposium (IGARSS). - Honolulu, HI, 25-30 July 2010. - P. 3279-3282. ↑

**C731.** Hongli Zhao. A study on different PS-like methods for subsidence in Tianjin, China. / Hongli Zhao, Huanhuan Liu, Jinghui Fan, Liu Guang, Jianping Chen, Xiaofang Guo, Peidong Jin, Lu Zhang, Yubao Qiu. // 2010 IEEE International Geoscience and Remote Sensing Symposium (IGARSS). - Honolulu, HI, 25-30 July

2010. - P. 3925-3928. ↑

**C732.** Woo-Kyung Lee. Scansar signal processing and image quality enhancement with fitted-geometry doppler surface. / Woo-Kyung Lee, Jung-Hwan Song. // 2010 IEEE International Geoscience and Remote Sensing Symposium (IGARSS). - Honolulu, HI, 25-30 July 2010. - P. 4063-4066. ↑

**C733.** Allouis T. Assessment of tree and crown heights of a maritime pine forest at plot level using a fullwaveform UltraViolet Lidar prototype. / Allouis T., Durrieu S., Cuesta J., Chazette P., Flamant P.H., Coueron P. // 2010 IEEE International Geoscience and Remote Sensing Symposium (IGARSS). - Honolulu, HI, 25-30 July 2010. - P. 1382-1385. ↑

**C734.** Xiaoxia Huang. Remote sensing applications for petroleum resource exploration in offshore basins of China. / Xiaoxia Huang, Zhenhai Zhu, Hongga Li. // 2010 IEEE International Geoscience and Remote Sensing Symposium (IGARSS). - Honolulu, HI, 25-30 July 2010. - P. 4511-4513. ↑

**C735.** Lim S. A network based attenuation correction system for networked dual polarization radar observations. / Lim S., Chandrasekar V., Wang Y. // 2010 IEEE International Geoscience and Remote Sensing Symposium (IGARSS). - Honolulu, HI, 25-30 July 2010. - P. 2333-2336. ↑

**C736.** Prats P. Taxi: A versatile processing chain for experimental TanDEM-X product evaluation. / Prats P., Rodriguez-Cassola M., Marotti L., Naninni M., Wollstadt S., Schulze D., Tous-Ramon N., Younis M., Krieger G., Reigber A. // 2010 IEEE International Geoscience and Remote Sensing Symposium (IGARSS). - Honolulu, HI, 25-30 July 2010. - P. 4059-4062. ↑

**C737.** Gorgucci E. Retrieval of raindrop shape-size relation using dual polarization radar measurements. / Gorgucci E., Baldini L., Chandrasekar V. // 2010 IEEE International Geoscience and Remote Sensing Symposium (IGARSS). - Honolulu, HI, 25-30 July 2010. - P. 4134-4137. ↑

**C738.** Jie Zhen. GNSS illuminator based high range resolution algorithm in space-surface bistatic SAR. / Jie Zhen, Zhenhua Zhang, Shunjun Wu, Guoman Huang. // 2010 IEEE International Geoscience and Remote Sensing Symposium (IGARSS). - Honolulu, HI, 25-30 July 2010. - P. 4608-4611. ↑

**C739.** Ramongassie S. RADAR and AIS sensors constellation for global maritime surveillance. / Ramongassie S., Taveneau N., Calmettes T., Richard J., Challamel R., Autran O., Foix V., Durand P. // 2010 IEEE International Geoscience and Remote Sensing Symposium (IGARSS). - Honolulu, HI, 25-30 July 2010. - P. 3793-3796. ↑

**C740.** Grosdidier S. Morphological-based source extraction method for HFSW radar ship detection. / Grosdidier S., Baussard A., Khenchaf A. // 2010 IEEE International Geoscience and Remote Sensing Symposium (IGARSS). - Honolulu, HI, 25-30 July 2010. - P. 3708-3711. ↑

**C741.** Lavalley M. Polinsar forestry applications improved by modeling height-dependent temporal decorrelation. / Lavalley M., Simard M., Pottier E., Solimini D. // 2010 IEEE International Geoscience and Remote Sensing Symposium (IGARSS). - Honolulu, HI, 25-30 July 2010. - P. 4772-4775. ↑

**C742.** Pierce L. A dual-frequency SAR mosaic of the Amazon. / Pierce L., Barros O. // 2010 IEEE International Geoscience and Remote Sensing Symposium (IGARSS). - Honolulu, HI, 25-30 July 2010. - P. 4671-4674. ↑

**C743.** Hambaryan A. Multi-frequency and polarimetric measurements of bare and vegetated soils microwave reflection and emission by C- and Ku-band, combined scatterometer-radiometer systems. / Hambaryan A., Arakelyan A., Hambaryan V., Karyan V., Manukyan M., Grigoryan M., Hovhannisyan G., Arakelyan A., Darbinyan S. // 2010 IEEE International Geoscience and Remote Sensing Symposium (IGARSS). - Honolulu, HI, 25-30 July 2010. - P. 4466-4469. ↑

**C744.** Tebaldini S. Polarimetric and structural properties of forest scenarios as imaged by longer wavelength SRS. / Tebaldini S., D'Alessandro M.M., Monti Guarnieri A., Rocca F. // 2010 IEEE International Geoscience and Remote Sensing Symposium (IGARSS). - Honolulu, HI, 25-30 July 2010. - P. 3251-3254. ↑

**C745.** Lideng Wei. Processing for airborne interferometric SAR data with high squint. / Lideng Wei, Songtao Han, Maosheng Xiang. // 2010 IEEE International Geoscience and Remote Sensing Symposium (IGARSS). - Honolulu, HI, 25-30 July 2010. - P. 4668-4670. ↑

- C746.** Xin Tian. Comparison of crop classification capabilities of spaceborne multi-parameter SAR data. / Xin Tian, Erxue Chen, Zengyuan Li, Su Z.B., Feilong Ling, Lina Bai, Fengyu Wang. // 2010 IEEE International Geoscience and Remote Sensing Symposium (IGARSS). - Honolulu, HI, 25-30 July 2010. - P. 359-362. ↑
- C747.** Ahmed R. A biomass estimate over the harvard forest using field measurements with radar and lidar data. / Ahmed R., Siqueira P., Bergen K., Chapman B., Hensley S. // 2010 IEEE International Geoscience and Remote Sensing Symposium (IGARSS). - Honolulu, HI, 25-30 July 2010. - P. 4768-4771. ↑
- C748.** Dazhi Zeng. A high accuracy method for interference fringes suppression in SAR distributed targets' raw data simulation. / Dazhi Zeng, Hanwei Sun, Tao Zeng, Teng Long. // 2010 IEEE International Geoscience and Remote Sensing Symposium (IGARSS). - Honolulu, HI, 25-30 July 2010. - P. 4675-4678. ↑
- C749.** Shah R. Analysis of the correlation properties of digital satellite signals and their applicability in bistatic remote sensing. / Shah R., Garrison J.L., Grant M.S., Katzberg S.J., Geng Tian. // 2010 IEEE International Geoscience and Remote Sensing Symposium (IGARSS). - Honolulu, HI, 25-30 July 2010. - P. 4114-4117. ↑
- C750.** Zhao J.G. A fully polarimetric borehole radar based numerical modelling: Fully polarimetric response to synthetic fractures and "fluid substitution". / Zhao J.G., Sato M. // 2010 IEEE International Geoscience and Remote Sensing Symposium (IGARSS). - Honolulu, HI, 25-30 July 2010. - P. 3929-3932. ↑
- C751.** Rakwatin P. Mapping tropical forest using ALOS PALSAR 50m resolution data with multiscale GLCM analysis. / Rakwatin P., Longepe N., Isoguchi O., Shimada M., Uryu Y. // 2010 IEEE International Geoscience and Remote Sensing Symposium (IGARSS). - Honolulu, HI, 25-30 July 2010. - P. 1234-1237. ↑
- C752.** Marino A. Ship detection with RadarSat-2 Quad-Pol sar data using a notch filter based on perturbation analysis. / Marino A., Walker N., Woodhouse I. // 2010 IEEE International Geoscience and Remote Sensing Symposium (IGARSS). - Honolulu, HI, 25-30 July 2010. - P. 3704-3707. ↑
- C753.** Moser G. Contextual remote-sensing image classification by support vector machines and Markov random fields. / Moser G., Serpico S.B. // 2010 IEEE International Geoscience and Remote Sensing Symposium (IGARSS). - Honolulu, HI, 25-30 July 2010. - P. 3728-3731. ↑
- C754.** Saidi M.N. Pose estimation for ISAR image classification. / Saidi M.N., Toumi A., Khenchaf A., Hoeltzener B., Aboutajdine D. // 2010 IEEE International Geoscience and Remote Sensing Symposium (IGARSS). - Honolulu, HI, 25-30 July 2010. - P. 4620-4623. ↑
- C755.** Williams M.L. Analysis of geosar dual-band InSAR data for peruvian forest. / Williams M.L., Silman M., Saatchi S., Hensley S., Sanford M., Yohannan A., Kofman B., Reis J., Kampes B. // 2010 IEEE International Geoscience and Remote Sensing Symposium (IGARSS). - Honolulu, HI, 25-30 July 2010. - P. 1398-1401. ↑
- C756.** Ikuma T. Predictive quantization of dechirped spotlight-mode SAR raw data in transform domain. / Ikuma T., Naraghi-Pour M., Lewis T. // 2010 IEEE International Geoscience and Remote Sensing Symposium (IGARSS). - Honolulu, HI, 25-30 July 2010. - P. 3789-3792. ↑
- C757.** Shiina T. Z-R relation for snowfall using two small doppler radars and snow particle images. / Shiina T., Kubo M., Muramoto K. // 2010 IEEE International Geoscience and Remote Sensing Symposium (IGARSS). - Honolulu, HI, 25-30 July 2010. - P. 4122-4125. ↑
- C758.** Yamazaki F. Characterization of affected areas of the 2008 Iwate-Miyagi, Japan, earthquake using SAR intensity images. / Yamazaki F., Inoue H., Wen Liu. // 2010 IEEE International Geoscience and Remote Sensing Symposium (IGARSS). - Honolulu, HI, 25-30 July 2010. - P. 4660-4663. ↑
- C759.** Flood B. SAR data collection over rain forests at VHF- and UHF-band. / Flood B., Frojllind P.-O., Gustavsson A., Jonsson T., Larsson B., Lundberg M., Mordin D., Stenstrojm G., Ulander L.M.H. // 2010 IEEE International Geoscience and Remote Sensing Symposium (IGARSS). - Honolulu, HI, 25-30 July 2010. - P. 1394-1397. ↑
- C760.** Vu V.T. Application of the moving target detection by focusing technique in civil traffic monitoring. / Vu V.T., Sjojgren T.K., Pettersson M.I., Marques P.A.C. // 2010 IEEE International Geoscience and Remote Sensing Symposium (IGARSS). - Honolulu, HI, 25-30 July 2010. - P. 4118-4121. ↑
- C761.** Yamada H. Esprit-based scattering power decomposition by using modified volume scattering model. /

Yamada H., Komaya R., Yamaguchi Y., Sato R. // 2010 IEEE International Geoscience and Remote Sensing Symposium (IGARSS). - Honolulu, HI, 25-30 July 2010. - P. 3255-3258. ↑

**C762.** Powell J. Multi-Channel RADAR Depth Sounder (MCRDS) signal processing: A distributed computing approach. / Powell J., Hayden L. // 2010 IEEE International Geoscience and Remote Sensing Symposium (IGARSS). - Honolulu, HI, 25-30 July 2010. - P. 3358-3361. ↑

**C763.** Duk-jin Kim. Application of KOMPSAT-5 data for emergent oil spill monitoring. / Duk-jin Kim, Moon W.M., Ji-Hwan Hwang, Youn-soo Kim. // 2010 IEEE International Geoscience and Remote Sensing Symposium (IGARSS). - Honolulu, HI, 25-30 July 2010. - P. 1254-1257. ↑

**C764.** Singh G. Snow wetness retrieval inversion modeling for C-band and X-band multi-polarization SAR data. / Singh G., Venkataraman G. // 2010 IEEE International Geoscience and Remote Sensing Symposium (IGARSS). - Honolulu, HI, 25-30 July 2010. - P. 4664-4667. ↑

**C765.** Hai Jiang. Random noise SAR based on compressed sensing. / Hai Jiang, Bingchen Zhang, Yueguan Lin, Wen Hong, Yirong Wu, Jin Zhan. // 2010 IEEE International Geoscience and Remote Sensing Symposium (IGARSS). - Honolulu, HI, 25-30 July 2010. - P. 4624-4627. ↑

**C766.** Fang Cao. An improvement for the unsupervised Wishart Freeman classification with fully polarimetric SAR data. / Fang Cao, Wen Hong, Pottier E. // 2010 IEEE International Geoscience and Remote Sensing Symposium (IGARSS). - Honolulu, HI, 25-30 July 2010. - P. 320-322. ↑

**C767.** Fromberg A.F. Deployment of the ASCAT calibration transponders. / Fromberg A.F., Pritchard E.W., Wright N.G., Wilson J.J., Kayal G. // 2010 IEEE International Geoscience and Remote Sensing Symposium (IGARSS). - Honolulu, HI, 25-30 July 2010. - P. 3486-3489. ↑

**C768.** Dazhi Zeng. Effect of the polarization on SISAR imaging and feature recognition in forward scattering radar. / Dazhi Zeng, Xiaoliang Li, Cheng Hu, Teng Long. // 2010 IEEE International Geoscience and Remote Sensing Symposium (IGARSS). - Honolulu, HI, 25-30 July 2010. - P. 1613-1616. ↑

**C769.** Mon-Shieh Yang. Automatic image classification of landslides improved with terrain roughness indices in various kernel sizes. / Mon-Shieh Yang, Ming-Chang Lin, Jin-King Liu, Ming-Chee Wu. // 2010 IEEE International Geoscience and Remote Sensing Symposium (IGARSS). - Honolulu, HI, 25-30 July 2010. - P. 527-529. ↑

**C770.** Schmitt A. Comparison of alternative image representations in the context of SAR change detection. / Schmitt A., Wendleder A., Wessel B., Roth A. // 2010 IEEE International Geoscience and Remote Sensing Symposium (IGARSS). - Honolulu, HI, 25-30 July 2010. - P. 284-287. ↑

**C771.** Le M. Microphysical retrieval from dual frequency precipitation radar board GPM. / Le M., Chandrasekar V., Lim S. // 2010 IEEE International Geoscience and Remote Sensing Symposium (IGARSS). - Honolulu, HI, 25-30 July 2010. - P. 3482-3485. ↑

**C772.** Sartori L.R. Investigations on the full polarimetric PALSAR data to discriminate macrophytes species in the Amazon floodplain wetland. / Sartori L.R., Imai N.N., Mura J.C., de Moraes Novo E.M.L., Silva T.S.F. // 2010 IEEE International Geoscience and Remote Sensing Symposium (IGARSS). - Honolulu, HI, 25-30 July 2010. - P. 413-416. ↑

**C773.** Hamlington B.D. On the feasibility of tsunami detection using satellite-based sea surface roughness measurements. / Hamlington B.D., Leben R.R., Godin O.A., Irisov V.G. // 2010 IEEE International Geoscience and Remote Sensing Symposium (IGARSS). - Honolulu, HI, 25-30 July 2010. - P. 3035-3038. ↑

**C774.** Popescu A. Generic object recognition in high resolution SAR images. / Popescu A., Costache M., Singh J., Datcu M., Schwarz G. // 2010 IEEE International Geoscience and Remote Sensing Symposium (IGARSS). - Honolulu, HI, 25-30 July 2010. - P. 1629-1632. ↑

**C775.** Hoonyol Lee. A ground-based Arc-scanning synthetic aperture radar (ArcSAR) system and focusing algorithms. / Hoonyol Lee, Seong-Jun Cho, Kwang-Eun Kim. // 2010 IEEE International Geoscience and Remote Sensing Symposium (IGARSS). - Honolulu, HI, 25-30 July 2010. - P. 3490-3493. ↑

**C776.** Ghulam A. A filtering approach to improve deformation accuracy using large baseline, low coherence

DInSAR phase images. / Ghulam A., Amer R., Ripperdan R. // 2010 IEEE International Geoscience and Remote Sensing Symposium (IGARSS). - Honolulu, HI, 25-30 July 2010. - P. 3494-3497. ↑

C777. Toumi A. Log-polar and polar image for recognition targets. / Toumi A., Khenchaf A. // 2010 IEEE International Geoscience and Remote Sensing Symposium (IGARSS). - Honolulu, HI, 25-30 July 2010. - P. 1609-1612. ↑

C778. Hansch R. Random Forests for building detection in polarimetric SAR data. / Hansch R., Hellwich O. // 2010 IEEE International Geoscience and Remote Sensing Symposium (IGARSS). - Honolulu, HI, 25-30 July 2010. - P. 460-463. ↑

C779. Ranson K.J. Effects of forest disturbances on forest structural parameters retrieval from lidar waveform data. / Ranson K.J., Sun G. // 2010 IEEE International Geoscience and Remote Sensing Symposium (IGARSS). - Honolulu, HI, 25-30 July 2010. - P. 4370-4373. ↑

C780. Ya-Qiu Jin. Composite scattering from electric-large target over randomly rough surface in numerical approaches. / Ya-Qiu Jin, Feng Xu. // 2010 IEEE International Geoscience and Remote Sensing Symposium (IGARSS). - Honolulu, HI, 25-30 July 2010. - P. 3545-3548. ↑

C781. Notarnicola C. Towards an operational daily soil moisture index derived from combination of MODIS, ASAR and AMSR-E data. / Notarnicola C., Ventura B., Pasolli L., Di Giuseppe F., Zebisch M. // 2010 IEEE International Geoscience and Remote Sensing Symposium (IGARSS). - Honolulu, HI, 25-30 July 2010. - P. 816-819. ↑

C782. Jiancheng Shi. Deriving soil moisture with the combined L-band radar and radiometer measurements. / Jiancheng Shi, Chen K.S., Tsang L., Jackson T., Njoku E., Van Zyl J., O'Neill P., Entekhabi D., Johnson J., Moghaddam M. // 2010 IEEE International Geoscience and Remote Sensing Symposium (IGARSS). - Honolulu, HI, 25-30 July 2010. - P. 812-815. ↑

C783. Pottier E. Recent advances in the development of the open source Toolbox for Polarimetric and Interferometric Polarimetric SAR Data Processing: The PolSARpro v4.1.5 Software. 2010 IEEE International Geoscience and Remote Sensing Symposium (IGARSS). - Honolulu, HI, 25-30 July 2010. - P. 2527-2530. ↑

C784. Gouinaud C. Characterization of ENVISAT multipolarization SAR data with bidimensional statistics. / Gouinaud C., Gouinaud P. // 2010 IEEE International Geoscience and Remote Sensing Symposium (IGARSS). - Honolulu, HI, 25-30 July 2010. - P. 1597-1600. ↑

C785. Yague-Martinez N. Interferometric processing algorithms of TanDEM-X data. / Yague-Martinez N., Rossi C., Lachaise M., Rodriguez-Gonzalez F., Fritz T., Breit H. // 2010 IEEE International Geoscience and Remote Sensing Symposium (IGARSS). - Honolulu, HI, 25-30 July 2010. - P. 3518-3521. ↑

C786. Benson M.L. Extrapolation of LiDAR for forest structure estimation using SAR, InSAR, and optical data. / Benson M.L., Pierce L.E., Bergen K.M., Sarabandi K., Kailai Zhang, Ryan C.E. // 2010 IEEE International Geoscience and Remote Sensing Symposium (IGARSS). - Honolulu, HI, 25-30 July 2010. - P. 1633-1636. ↑

C787. Wakabayashi H. Estimation of sea ice concentration in the Sea of Okhotsk using PALSAR polarimetric data. / Wakabayashi H., Sakai S. // 2010 IEEE International Geoscience and Remote Sensing Symposium (IGARSS). - Honolulu, HI, 25-30 July 2010. - P. 2398-2401. ↑

C788. Lu Zhang. Application of aspect angle normalized polsar images for urban building detection. / Lu Zhang, Huadong Guo, Xinwu Li, Wenxue Fu. // 2010 IEEE International Geoscience and Remote Sensing Symposium (IGARSS). - Honolulu, HI, 25-30 July 2010. - P. 2735-2738. ↑

C789. Mercier G. Progressive change detection in time series of SAR images. 2010 IEEE International Geoscience and Remote Sensing Symposium (IGARSS). - Honolulu, HI, 25-30 July 2010. - P. 3086-3089. ↑

C790. Daqing Ge. Merging multi-track PSI result for land subsidence mapping over very extended area. / Daqing Ge, Ling Zhang, Yan Wang, Xiaofang Guo, Ye Xia. // 2010 IEEE International Geoscience and Remote Sensing Symposium (IGARSS). - Honolulu, HI, 25-30 July 2010. - P. 3522-3525. ↑

C791. Moser G. Unsupervised change detection with very high-resolution SAR images by multiscale analysis and Markov random fields. / Moser G., Serpico S.B. // 2010 IEEE International Geoscience and Remote Sensing

Symposium (IGARSS). - Honolulu, HI, 25-30 July 2010. - P. 3082-3085. ↑

**C792.** Brigui F. Orthogonal polarimetric SAR processor based on signal and interference subspace models. / Brigui F., Thiron-Lefevre L., Ginolhac G., Forster P. // 2010 IEEE International Geoscience and Remote Sensing Symposium (IGARSS). - Honolulu, HI, 25-30 July 2010. - P. 2523-2526. ↑

**C793.** Gunnala S.K. Target detection above rough surfaces in microwave imaging using Compressive Sampling. / Gunnala S.K., Camacho L.M., Tjuatja S. // 2010 IEEE International Geoscience and Remote Sensing Symposium (IGARSS). - Honolulu, HI, 25-30 July 2010. - P. 3498-3501. ↑

**C794.** Sang-Ryool Lee. Overview of KOMPSAT-5 program, mission, and system. 2010 IEEE International Geoscience and Remote Sensing Symposium (IGARSS). - Honolulu, HI, 25-30 July 2010. - P. 797-800. ↑

**C795.** Epov M.I. UWB electromagnetic borehole logging tool. / Epov M.I., Mironov V.L., Muzalevskiy K.V., Yeltsov I.N. // 2010 IEEE International Geoscience and Remote Sensing Symposium (IGARSS). - Honolulu, HI, 25-30 July 2010. - P. 3565-3567. ↑

**C796.** Juneek W.N. Temporal analysis of the magma supply system beneath the Okmok caldera by Interferometric Synthetic Aperture Radar and statistical seismology. / Juneek W.N., Jones W.L., Woods M.T. // 2010 IEEE International Geoscience and Remote Sensing Symposium (IGARSS). - Honolulu, HI, 25-30 July 2010. - P. 1545-1548. ↑

**C797.** Wenming Lin. Development of a signal processing subsystem for a spaceborne rotating, fan-beam scatterometer. / Wenming Lin, Xiaolong Dong, Di Zhu. // 2010 IEEE International Geoscience and Remote Sensing Symposium (IGARSS). - Honolulu, HI, 25-30 July 2010. - P. 4166-4169. ↑

**C798.** Paul S.D. Investigation of cirrus clouds using the calipso lidar data. 2010 IEEE International Geoscience and Remote Sensing Symposium (IGARSS). - Honolulu, HI, 25-30 July 2010. - P. 4142-4145. ↑

**C799.** Sipelgas L. Monitoring environmental conditions in Muuga harbor using Envisat MERIS and ASAR data. / Sipelgas L., Uiboupin R., Raudsepp U. // 2010 IEEE International Geoscience and Remote Sensing Symposium (IGARSS). - Honolulu, HI, 25-30 July 2010. - P. 409-412. ↑

**C800.** Sang-Eun Park. Monitoring of thawing process using envisat asar global mode data. / Sang-Eun Park, Bartsch A., Sabel D., Wagner W. // 2010 IEEE International Geoscience and Remote Sensing Symposium (IGARSS). - Honolulu, HI, 25-30 July 2010. - P. 2031-2034. ↑

**C801.** Salvia M. Monitoring flooded area fraction in floodplains of Paran6 basin using passive and active microwave systems. / Salvia M., Grings F., Perna P., Ferrazzoli P., Rahmoune R., Barber M., Douna V., Karszenbaum H. // 2010 IEEE International Geoscience and Remote Sensing Symposium (IGARSS). - Honolulu, HI, 25-30 July 2010. - P. 142-145. ↑

**C802.** Balaji C. What is the information content of TRMM precipitation radar for determining radiometer observations and vice versa?. / Balaji C., Chaturvedi M., Srinivasa Ramanujam K., Chandrasekar V., Cuong Nguyen, Martinez M. // 2010 IEEE International Geoscience and Remote Sensing Symposium (IGARSS). - Honolulu, HI, 25-30 July 2010. - P. 1899-1902. ↑

**C803.** Hongli Zhao. Detection of land subsidence in Beijing, China, using Interferometric Point Target Analysis technique. / Hongli Zhao, Jinghui Fan, Xiaofang Guo, Jianping Chen, Ye Xia, Daqing Ge, Lu Zhang, Yubao Qiu, Chang Zhong. // 2010 IEEE International Geoscience and Remote Sensing Symposium (IGARSS). - Honolulu, HI, 25-30 July 2010. - P. 1553-1556. ↑

**C804.** Dong-Hyun Kim. KOMPSAT-5 spotlight SAR processor using FSA with calculation of effective velocity. / Dong-Hyun Kim, Jae-Cheol Yoon, Jae-Min Shin, Moon-Gyu Kim. // 2010 IEEE International Geoscience and Remote Sensing Symposium (IGARSS). - Honolulu, HI, 25-30 July 2010. - P. 801-804. ↑

**C805.** Corp L.A. Fusion: A fully ultraportable system for imaging objects in nature. / Corp L.A., Cook B.D., Middleton E.M., Cheng Y., Huemmrich K.F., Campbell P.K.E. // 2010 IEEE International Geoscience and Remote Sensing Symposium (IGARSS). - Honolulu, HI, 25-30 July 2010. - P. 1671-1674. ↑

**C806.** Xiaoqing Chu. A new algorithm for wind speed at low incidence angles using TRMM Precipitation Radar data. / Xiaoqing Chu, Yijun He, Gengxin Chen. // 2010 IEEE International Geoscience and Remote Sensing

Symposium (IGARSS). - Honolulu, HI, 25-30 July 2010. - P. 4162-4165. ↑

**C807.** Maeda T. Approach for volcanic surveillance using satellite-borne microwave radiometer data. / Maeda T., Takano T. // 2010 IEEE International Geoscience and Remote Sensing Symposium (IGARSS). - Honolulu, HI, 25-30 July 2010. - P. 520-522. ↑

**C808.** Ito Y. A study on anomalous signal detection using HMM for ELF electromagnetic wave. / Ito Y., Itai A., Yasukawa H., Takumi I., Hata M. // 2010 IEEE International Geoscience and Remote Sensing Symposium (IGARSS). - Honolulu, HI, 25-30 July 2010. - P. 1601-1604. ↑

**C809.** Monells D. Application of TerraSAR-X data to the monitoring of urban subsidence in the city of Murcia. / Monells D., Centolanza G., Mallorqui J.J., Duque S., Lopez-Dekker P., Tomas R., Herrera G., Lopez-Sanchez J.M., Vicente F., Navarro-Sanchez V.D., Mulas J. // 2010 IEEE International Geoscience and Remote Sensing Symposium (IGARSS). - Honolulu, HI, 25-30 July 2010. - P. 3506-3509. ↑

**C810.** Leilei Kou. Research on interferometric deformation detection for geosynchronous SAR. / Leilei Kou, Xiaoqing Wang, Jinsong Chong, Maosheng Xiang. // 2010 IEEE International Geoscience and Remote Sensing Symposium (IGARSS). - Honolulu, HI, 25-30 July 2010. - P. 3502-3505. ↑

**C811.** Chong-wen Duan. MVM based SAR image processing for ship pose estimation. / Chong-wen Duan, Wei-dong Hu, Xiao-yong Du. // 2010 IEEE International Geoscience and Remote Sensing Symposium (IGARSS). - Honolulu, HI, 25-30 July 2010. - P. 1605-1608. ↑

**C812.** Quinn G.S. Lidar integrated airborne imaging spectroscopy for root disease detection and measurement of foliar chemistry. / Quinn G.S., Niemann K.O., Goodenough D.G. // 2010 IEEE International Geoscience and Remote Sensing Symposium (IGARSS). - Honolulu, HI, 25-30 July 2010. - P. 4385-4388. ↑

**C813.** Bell P.S. Submerged dunes and breakwater embayments mapped using wave inversions of shore-mounted marine X-band radar data. 2010 IEEE International Geoscience and Remote Sensing Symposium (IGARSS). - Honolulu, HI, 25-30 July 2010. - P. 4334-4337. ↑

**C814.** Shin JaeMin. Field test of KOMPSAT-5 Calibration Equipment. / Shin JaeMin, Lee KwangJae, Kim JinHee. // 2010 IEEE International Geoscience and Remote Sensing Symposium (IGARSS). - Honolulu, HI, 25-30 July 2010. - P. 805-807. ↑

**C815.** Xia Ye. High resolution D-INSAR measurement for land subsidence. / Xia Ye, Kaufmann H. // 2010 IEEE International Geoscience and Remote Sensing Symposium (IGARSS). - Honolulu, HI, 25-30 July 2010. - P. 1541-1544. ↑

**C816.** Henke D. Preliminary results of a low-frequency 3D-sar approach for glacier volume mapping. / Henke D., Meier E. // 2010 IEEE International Geoscience and Remote Sensing Symposium (IGARSS). - Honolulu, HI, 25-30 July 2010. - P. 2027-2030. ↑

**C817.** Nieto-Borge J.C. Application of conventional marine radars for measuring ocean wave fields in shallow water conditions. / Nieto-Borge J.C., Mata-Moya D., Jarabo-Amores P., Reichert K., Hessner K. // 2010 IEEE International Geoscience and Remote Sensing Symposium (IGARSS). - Honolulu, HI, 25-30 July 2010. - P. 4338-4341. ↑

**C818.** Villalon-Turrubiates I.E. Multispectral classification of remote sensing imagery for archaeological land use analysis: Prospective study. / Villalon-Turrubiates I.E., Llovera-Torres M.J. // 2010 IEEE International Geoscience and Remote Sensing Symposium (IGARSS). - Honolulu, HI, 25-30 July 2010. - P. 323-326. ↑

**C819.** Sang-Hoon Lee. Directional-adaptive despeckling for high-resolution SAR. 2010 IEEE International Geoscience and Remote Sensing Symposium (IGARSS). - Honolulu, HI, 25-30 July 2010. - P. 808-811. ↑

**C820.** Mishra K.V. Signal analysis and modeling of wind turbine clutter in weather radars. / Mishra K.V., Chandrasekar V. // 2010 IEEE International Geoscience and Remote Sensing Symposium (IGARSS). - Honolulu, HI, 25-30 July 2010. - P. 3561-3564. ↑

**C821.** Scipal K. Triple collocation-A new tool to determine the error structure of global soil moisture products. / Scipal K., Dorigo W., de Jeu R. // 2010 IEEE International Geoscience and Remote Sensing Symposium (IGARSS). - Honolulu, HI, 25-30 July 2010. - P. 4426-4429. ↑

- C822.** Jung Hum Yu. Automatic exclusion of surface deformation in InSAR DEM generation using differential radar interferometry. / Jung Hum Yu, Linlin Ge. // 2010 IEEE International Geoscience and Remote Sensing Symposium (IGARSS). - Honolulu, HI, 25-30 July 2010. - P. 2916-2919. ↑
- C823.** Newell D.A. GPM Microwave Imager design, predicted performance and status. / Newell D.A., Rait G., Ta T., Berdanier B., Draper D., Kubitschek M., Krimchansky S. // 2010 IEEE International Geoscience and Remote Sensing Symposium (IGARSS). - Honolulu, HI, 25-30 July 2010. - P. 546-549. ↑
- C824.** Alparone L. Multiresolution despeckling of VHR SAR images based on MRF segmentation. / Alparone L., Argenti F., Bianchi T., Abbate M., D'Elia C., Mariano P., Meta A. // 2010 IEEE International Geoscience and Remote Sensing Symposium (IGARSS). - Honolulu, HI, 25-30 July 2010. - P. 288-291. ↑
- C825.** Merzouki A. Potential of mapping soil moisture by combining radar backscatter modeling and PolSAR decomposition. / Merzouki A., McNairn H., Pacheco A. // 2010 IEEE International Geoscience and Remote Sensing Symposium (IGARSS). - Honolulu, HI, 25-30 July 2010. - P. 4419-4422. ↑
- C826.** Yanting Wang. Evaluation of system polarization quality for polarimetric SAR imagery and target decomposition. / Yanting Wang, Ainsworth T.L., Jong-Sen Lee. // 2010 IEEE International Geoscience and Remote Sensing Symposium (IGARSS). - Honolulu, HI, 25-30 July 2010. - P. 2043-2046. ↑
- C827.** Zhang C. Imaging algorithm and experimental demonstration of rotating scanning interferometric radiometer. / Zhang C., Liu H., Yan J.Y., Sun W.Y., Zhang S.W., Liu H.G., Wu J. // 2010 IEEE International Geoscience and Remote Sensing Symposium (IGARSS). - Honolulu, HI, 25-30 July 2010. - P. 534-537. ↑
- C828.** Dall'Amico J.T. Comparing data of two airborne L-band radiometers with different spatial resolution over a heterogeneous land surface. / Dall'Amico J.T., Kainulainen J., Loew A., Mauser W. // 2010 IEEE International Geoscience and Remote Sensing Symposium (IGARSS). - Honolulu, HI, 25-30 July 2010. - P. 538-541. ↑
- C829.** Ben Khadra S. The bistatic electromagnetic signature of heterogeneous sea surface: Study of the hydrodynamic phenomena. / Ben Khadra S., Khenchaf A. // 2010 IEEE International Geoscience and Remote Sensing Symposium (IGARSS). - Honolulu, HI, 25-30 July 2010. - P. 3549-3552. ↑
- C830.** Yurchak B.S. Contribution of small-scale correlated fluctuations of the microstructural properties of a spatially extended geophysical target under the assessment of radar backscatter. 2010 IEEE International Geoscience and Remote Sensing Symposium (IGARSS). - Honolulu, HI, 25-30 July 2010. - P. 3557-3560. ↑
- C831.** Nishimoto M. Characteristics of rough surface parameters estimated from measured surface profile of finite length. 2010 IEEE International Geoscience and Remote Sensing Symposium (IGARSS). - Honolulu, HI, 25-30 July 2010. - P. 4436-4439. ↑
- C832.** Tan D.K.P. Target detection performance analysis for airborne passive bistatic radar. / Tan D.K.P., Lesturgie M., Hongbo Sun, Yilong Lu. // 2010 IEEE International Geoscience and Remote Sensing Symposium (IGARSS). - Honolulu, HI, 25-30 July 2010. - P. 3553-3556. ↑
- C833.** Ferro A. Building detection and radar footprint reconstruction from single VHR SAR images. / Ferro A., Brunner D., Bruzzone L. // 2010 IEEE International Geoscience and Remote Sensing Symposium (IGARSS). - Honolulu, HI, 25-30 July 2010. - P. 292-295. ↑
- C834.** Richardson A. Unsupervised nonparametric classification of polarimetric SAR data using the K-nearest neighbor graph. / Richardson A., Goodenough D.G., Chen H., Moa B., Hobart G., Myrvold W. // 2010 IEEE International Geoscience and Remote Sensing Symposium (IGARSS). - Honolulu, HI, 25-30 July 2010. - P. 1867-1870. ↑
- C835.** Hao Liu. Development of a three-element interferometer at 50 56 GHz for Geostationary Interferometric Microwave Sounder (GIMS). / Hao Liu, Ji Wu, Shengwei Zhang, Jingye Yan, Lijie Niu, Cheng Zhang, Bin Li. // 2010 IEEE International Geoscience and Remote Sensing Symposium (IGARSS). - Honolulu, HI, 25-30 July 2010. - P. 554-557. ↑
- C836.** Baade J. High-resolution mapping of fluvial landform change in arid environments using terrasars-X images. / Baade J., Schmullius C. // 2010 IEEE International Geoscience and Remote Sensing Symposium (IGARSS). - Honolulu, HI, 25-30 July 2010. - P. 2159-2162. ↑

- C837.** Patterson C.E. Implementation of a low cost, lightweight X-band antenna with integrated SiGe RF electronics. / Patterson C.E., Thrivikraman T.K., Yepes A.M., Bhattacharya S.K., Cressler J.D., Papapolymerou J. // 2010 IEEE International Geoscience and Remote Sensing Symposium (IGARSS). - Honolulu, HI, 25-30 July 2010. - P. 681-684. ↑
- C838.** Ouchi K. Improvement of ship detection accuracy by sar multi-look cross-correlation technique using adaptive CFAR. / Ouchi K., Seong-In Hwang. // 2010 IEEE International Geoscience and Remote Sensing Symposium (IGARSS). - Honolulu, HI, 25-30 July 2010. - P. 3716-3719. ↑
- C839.** Ohgi N. Japanese hyper-multi spectral mission. / Ohgi N., Iwasaki A., Kawashima T., Inada H. // 2010 IEEE International Geoscience and Remote Sensing Symposium (IGARSS). - Honolulu, HI, 25-30 July 2010. - P. 3756-3759. ↑
- C840.** Hannevik T.N. Automatic ship detection in sar images using aegir. 2010 IEEE International Geoscience and Remote Sensing Symposium (IGARSS). - Honolulu, HI, 25-30 July 2010. - P. 3712-3715. ↑
- C841.** Duque S. Bistatic SAR along track interferometry with multiple fixed receivers. / Duque S., Lopez-Dekker P., Merlano J.C., Mallorqui J.J. // 2010 IEEE International Geoscience and Remote Sensing Symposium (IGARSS). - Honolulu, HI, 25-30 July 2010. - P. 4099-4102. ↑
- C842.** Goykhman Y. Radar retrieval of subsurface parameters for layered media with nonsmooth interfaces. / Goykhman Y., Moghaddam M. // 2010 IEEE International Geoscience and Remote Sensing Symposium (IGARSS). - Honolulu, HI, 25-30 July 2010. - P. 4458-4461. ↑
- C843.** Arakelyan A. Combined active and passive measurements of snow, bare and vegetated soils microwave reflective and emissive characteristics by Ka-band, combined scatterometer-radiometer system. / Arakelyan A., Grigoryan M., Hambaryan A., Arakelyan A. // 2010 IEEE International Geoscience and Remote Sensing Symposium (IGARSS). - Honolulu, HI, 25-30 July 2010. - P. 4462-4465. ↑
- C844.** Romeiser R. A new scalloping filter algorithm for scansar images. / Romeiser R., Horstmann J., Graber H. // 2010 IEEE International Geoscience and Remote Sensing Symposium (IGARSS). - Honolulu, HI, 25-30 July 2010. - P. 4079-4082. ↑
- C845.** Butenuth M. Geometric refinement of road networks using network snakes and SAR images. 2010 IEEE International Geoscience and Remote Sensing Symposium (IGARSS). - Honolulu, HI, 25-30 July 2010. - P. 449-452. ↑
- C846.** Fernandez Diaz J.C. Characterization of full surface roughness in agricultural soils using groundbased LiDAR. / Fernandez Diaz J.C., Judge J., Slatton K.C., Shrestha R., Carter W.E., Bloomquist D. // 2010 IEEE International Geoscience and Remote Sensing Symposium (IGARSS). - Honolulu, HI, 25-30 July 2010. - P. 4442-4445. ↑
- C847.** Adam N. Multi beam joint estimation for persistent scatterer interferometry. / Adam N., Gernhardt S., Eineder M., Bamler R. // 2010 IEEE International Geoscience and Remote Sensing Symposium (IGARSS). - Honolulu, HI, 25-30 July 2010. - P. 4403-4406. ↑
- C848.** Tiangang Yin. Iterative calibration of relative platform position: A new method for SAR baseline estimation. / Tiangang Yin, Christophe E., Soo Chin Liew, Sim Heng Ong. // 2010 IEEE International Geoscience and Remote Sensing Symposium (IGARSS). - Honolulu, HI, 25-30 July 2010. - P. 4407-4410. ↑
- C849.** Lachaise M. Multibaseline gradient ambiguity resolution to support Minimum Cost Flow Phase Unwrapping. / Lachaise M., Bamler R., Gonzalez F.R. // 2010 IEEE International Geoscience and Remote Sensing Symposium (IGARSS). - Honolulu, HI, 25-30 July 2010. - P. 4411-4414. ↑
- C850.** Ratto C. Context-dependent landmine detection with ground-penetrating radar using a Hidden Markov Context Model. / Ratto C., Torriente P., Morton K., Collins L. // 2010 IEEE International Geoscience and Remote Sensing Symposium (IGARSS). - Honolulu, HI, 25-30 July 2010. - P. 4192-4195. ↑
- C851.** Esteban-Fernandez D. Ka-band SAR interferometry studies for the SWOT mission. / Esteban-Fernandez D., Lee-Lueng Fu, Rodriguez E., Brown S., Hodges R. // 2010 IEEE International Geoscience and Remote Sensing Symposium (IGARSS). - Honolulu, HI, 25-30 July 2010. - P. 4401-4402. ↑

- C852.** Reale D. Advanced techniques and new high resolution SAR sensors for monitoring urban areas. / Reale D., Fornaro G., Paucillo A., Zhu X., Adam N., Bamler R. // 2010 IEEE International Geoscience and Remote Sensing Symposium (IGARSS). - Honolulu, HI, 25-30 July 2010. - P. 1800-1803. ↑
- C853.** Buckley J.R. Monitoring grasslands with radarsat 2 quad-pol imagery. / Buckley J.R., Smith A.M. // 2010 IEEE International Geoscience and Remote Sensing Symposium (IGARSS). - Honolulu, HI, 25-30 July 2010. - P. 3090-3093. ↑
- C854.** Sant'Anna S.J.S. Electromagnetic characteristics of simple targets embedded in chiral multilayer structures. / Sant'Anna S.J.S., da S Lacava J.C., Fernandes D. // 2010 IEEE International Geoscience and Remote Sensing Symposium (IGARSS). - Honolulu, HI, 25-30 July 2010. - P. 3031-3034. ↑
- C855.** Alsweiss S. Improved hurricane active/passive simulated wind vector retrievals. / Alsweiss S., Laupattarakasem P., El-Nimri S., Jones W.L., Hristova-Veleva S. // 2010 IEEE International Geoscience and Remote Sensing Symposium (IGARSS). - Honolulu, HI, 25-30 July 2010. - P. 2535-2538. ↑
- C856.** Tebaldini S. Forest structure from longer wavelength SARs. / Tebaldini S., Rocca F. // 2010 IEEE International Geoscience and Remote Sensing Symposium (IGARSS). - Honolulu, HI, 25-30 July 2010. - P. 158-161. ↑
- C857.** Sauber J. DESDynI lidar for solid earth applications. / Sauber J., Hofton M., Bruhn R., Luthcke S., Blair B. // 2010 IEEE International Geoscience and Remote Sensing Symposium (IGARSS). - Honolulu, HI, 25-30 July 2010. - P. 1903-1906. ↑
- C858.** Weissman D.E. Studies of the influence of rainfall upon scatterometer estimates for sea surface stress: Applications to boundary layer parameterization and drag coefficient models within tropical cyclone environments. / Weissman D.E., Winterbottom H.R., Bourassa M.A. // 2010 IEEE International Geoscience and Remote Sensing Symposium (IGARSS). - Honolulu, HI, 25-30 July 2010. - P. 4154-4157. ↑
- C859.** Wen Yang. Semantic segmentation of Polarimetric SAR imagery using Conditional Random Fields. / Wen Yang, Xun Zhang, Lijun Chen, Hong Sun. // 2010 IEEE International Geoscience and Remote Sensing Symposium (IGARSS). - Honolulu, HI, 25-30 July 2010. - P. 1593-1596. ↑
- C860.** Anderson S.J. A MIMO technique for enhanced clutter selectivity in a multiple scattering environment: Application to HF surface wave radar. / Anderson S.J., Anderson W.C. // 2010 International Conference on Electromagnetics in Advanced Applications (ICEAA). - Sydney, NSW, 20-24 Sept. 2010. - P. 133-136. ↑
- C861.** Liming Jiang. Detection of rapid land subsidence of civil constructions with TerraSAR-X interferometry. / Liming Jiang, Hui Lin, Baoqiang Xiang. // 2010 IEEE International Geoscience and Remote Sensing Symposium (IGARSS). - Honolulu, HI, 25-30 July 2010. - P. 3510-3513. ↑
- C862.** Covello F. One-day interferometry results with the COSMO-SkyMed constellation. / Covello F., Battazza F., Coletta A., Battagliere M.L., Bellifemine V., Candela L. // 2010 IEEE International Geoscience and Remote Sensing Symposium (IGARSS). - Honolulu, HI, 25-30 July 2010. - P. 4397-4400. ↑
- C863.** Brcic R. Estimation and compensation of ionospheric delay for SAR interferometry. / Brcic R., Parizzi A., Eineder M., Bamler R., Meyer F. // 2010 IEEE International Geoscience and Remote Sensing Symposium (IGARSS). - Honolulu, HI, 25-30 July 2010. - P. 2908-2911. ↑
- C864.** Borzi. Phase retrieval in SAR interferograms using diffusion and inpainting. / Borzi, A., Di Bisceglie M., Galdi C., Pallotta L., Ullo S.L. // 2010 IEEE International Geoscience and Remote Sensing Symposium (IGARSS). - Honolulu, HI, 25-30 July 2010. - P. 2912-2915. ↑
- C865.** Xuetong Xie. A modified wind vector retrieval algorithm for polarimetric scatterometer. / Xuetong Xie, Mingsen Lin, Zhou Huang, Juhong Zou, Dongxuan Tian, Lixia Liu, Xiaoning Wang, Shiwei Dong. // 2010 IEEE International Geoscience and Remote Sensing Symposium (IGARSS). - Honolulu, HI, 25-30 July 2010. - P. 4184-4187. ↑
- C866.** Caltagirone F. Status, results, potentiality and evolution of COSMO-SkyMed, the Italian Earth Observation constellation for risk management and security. / Caltagirone F., De Luca G., Covello F., Marano G., Angino G., Piemontese M. // 2010 IEEE International Geoscience and Remote Sensing Symposium (IGARSS). - Honolulu, HI, 25-30 July 2010. - P. 4393-4396. ↑

- C867.** Yanfang Dong. Disaster mapping from medium spatial resolution alos palsar images. / Yanfang Dong, Qi Li, Aixia Dou, Xiaoqing Wang. // 2010 IEEE International Geoscience and Remote Sensing Symposium (IGARSS). - Honolulu, HI, 25-30 July 2010. - P. 2167-2170. ↑
- C868.** Gong W. Performance analysis of atmospheric correction in InSAR data based on the Weather Research and Forecasting Model (WRF). / Gong W., Meyer F., Webley P.W., Morton D., Liu S. // 2010 IEEE International Geoscience and Remote Sensing Symposium (IGARSS). - Honolulu, HI, 25-30 July 2010. - P. 2900-2903. ↑
- C869.** Yongfei Mao. The mathematic model of multipath error in airborne interferometric SAR system. / Yongfei Mao, Maosheng Xiang, Lideng Wei, Songtao Han. // 2010 IEEE International Geoscience and Remote Sensing Symposium (IGARSS). - Honolulu, HI, 25-30 July 2010. - P. 2904-2907. ↑
- C870.** O'Neill P. The NASA Soil Moisture Active Passive (SMAP) mission: Overview. / O'Neill P., Entekhabi D., Njoku E., Kellogg K. // 2010 IEEE International Geoscience and Remote Sensing Symposium (IGARSS). - Honolulu, HI, 25-30 July 2010. - P. 3236-3239. ↑
- C871.** Budillon A. Multi-baseline along track SAR interferometric systems for ground moving target indication. / Budillon A., Evangelista A., Pascazio V., Schirizzi G. // 2010 IEEE International Geoscience and Remote Sensing Symposium (IGARSS). - Honolulu, HI, 25-30 July 2010. - P. 2924-2927. ↑
- C872.** Tao Li. Comparison of Beijing-Tianjin Intercity Railway deformation monitoring results between ASAR and PALSAR data. / Tao Li, Zhang Hong, Wang Chao, Tang Yixian. // 2010 IEEE International Geoscience and Remote Sensing Symposium (IGARSS). - Honolulu, HI, 25-30 July 2010. - P. 3514-3517. ↑
- C873.** Hong-yan Shen. Geophysical Characters for Archaeology in the Ancient City of JinYang, China. / Hong-yan Shen, Bing-qiang Yuan. // 2009 International Conference on Information Management, Innovation Management and Industrial Engineering. - Xi'an, 26-27 Dec. 2009. - Vol. 2. - P. 292-297. ↑
- C874.** Dai Yaqiong. Preliminary analysis on characteristics of co-seismic deformation field of the Gkrzk earthquake (Ms6.9) from ascending and descending pass ASAR radar interferometry. / Dai Yaqiong, Hong Shunying, Ren Jinwei, Shen Xuhui. // 2009. APSAR 2009. 2nd Asian-Pacific Conference on Synthetic Aperture Radar. - Xian, Shanxi, 26-30 Oct. 2009. - P. 144-147. ↑
- C875.** Gleich D. Regularization of Complex SAR Images Using Markov Random Fields. / Gleich D., Planinsic P., Kseneman M., Soccorsi M., Datcu M. // 2009. IWSSIP 2009. 16th International Conference on Systems, Signals and Image Processing. - Chalkida, 18-20 June 2009. - P. 1-4. ↑
- C876.** Ling F. Comparison of ALOS PALSAR RVI and Landsat TM NDVI for forest area mapping. / Ling F., Li Z., Chen E., Wang Q. // 2009. APSAR 2009. 2nd Asian-Pacific Conference on Synthetic Aperture Radar. - Xian, Shanxi, 26-30 Oct. 2009. - P. 132-135. ↑
- C877.** Shuyuan Yang. Improvement of Bandelets in cost function and coding strategy for SAR image compression. / Shuyuan Yang, Ruixia Wu, Huixiao Meng, Licheng Jiao. // 2009. APSAR 2009. 2nd Asian-Pacific Conference on Synthetic Aperture Radar. - Xian, Shanxi, 26-30 Oct. 2009. - P. 1132-1135. ↑
- C878.** Lei Yu. Turbo-like Iterative Thresholding for SAR image recovery from compressed measurements. / Lei Yu, Yi Yang, Hong Sun, Chu He. // 2009. APSAR 2009. 2nd Asian-Pacific Conference on Synthetic Aperture Radar. - Xian, Shanxi, 26-30 Oct. 2009. - P. 664-667. ↑
- C879.** Yuan Xinzhe. Application of spaceborne SAR imagery in monitoring green algae. / Yuan Xinzhe, Liu Jianqiang, Xie Chunhua, Zeng Tao, Song Xingai. // 2009. APSAR 2009. 2nd Asian-Pacific Conference on Synthetic Aperture Radar. - Xian, Shanxi, 26-30 Oct. 2009. - P. 129-131. ↑
- C880.** Shouchao Hu. PALSAR interferometry for urban subsidence monitoring: An experiment in Shanghai area. / Shouchao Hu, Jicang Wu, Baosong Ban, Lina Zhang. // 2009. APSAR 2009. 2nd Asian-Pacific Conference on Synthetic Aperture Radar. - Xian, Shanxi, 26-30 Oct. 2009. - P. 140-143. ↑
- C881.** Qisheng He. Relationship between SAR and biomass derived from LiDAR in Mountain areas. / Qisheng He, Chunxiang Cao, Erxue Chen, Feilong Ling, Hao Zhang. // 2009. APSAR 2009. 2nd Asian-Pacific Conference on Synthetic Aperture Radar. - Xian, Shanxi, 26-30 Oct. 2009. - P. 136-139. ↑

- C882.** Guiting Wang. An automatic bridge detection technique for high resolution SAR images. / Guiting Wang, Shan Huang, Licheng Jiao. // 2009. APSAR 2009. 2nd Asian-Pacific Conference on Synthetic Aperture Radar. - Xian, Shanxi, 26-30 Oct. 2009. - P. 498-501. ↑
- C883.** Hong Shun-ying. Precision evaluation and characteristics analysis of the coseismic deformation field of the 12th may 2008 Wenchuan Ms8.0 earthquake. / Hong Shun-ying, Liu Mei, Liu Zhi-rong, Dai Ya-qiong, Shan Xin-jian, Shen Xu-hui, Jing Feng. // 2009. APSAR 2009. 2nd Asian-Pacific Conference on Synthetic Aperture Radar. - Xian, Shanxi, 26-30 Oct. 2009. - P. 148-154. ↑
- C884.** Bian Mingming. Dynamic reconfigurable storage and pretreatment system of SAR signal processing using Nios II architecture. / Bian Mingming, Liu Feng, Xie Yizhuang. // 2009 IET International Radar Conference. - Guillin, China, 20-22 April 2009. - P. 1-4. ↑
- C885.** Deng Shaoping. Segmentation of dual polarized SAR imagery of the west of China based on evidence theory. / Deng Shaoping, Li Pingxiang, Huang Guoman, Zhang Liangpei. // 2009 IET International Radar Conference. - Guillin, China, 20-22 April 2009. - P. 1-4. ↑
- C886.** Cheng Kou. The detection and information compensation of SAR layover based on R-D model. / Cheng Kou, Yang Jie, Shi Lei, Zhao Zheng. // 2009 IET International Radar Conference. - Guillin, China, 20-22 April 2009. - P. 1-3. ↑
- C887.** Lai Xudong. A Flow to Generate DEM from Lidar Data. / Lai Xudong, Zheng Xuedong, Jiang Junwei. // 2009. ICIECS 2009. International Conference on Information Engineering and Computer Science. - Wuhan, 19-20 Dec. 2009. - P. 1-3. ↑
- C888.** Quanye Du. Fast Processing of Airborne LiDAR Data and Imagery. / Quanye Du, Hui Cao, Haitao Ma, Han Hu. // 2009. ICIECS 2009. International Conference on Information Engineering and Computer Science. - Wuhan, 19-20 Dec. 2009. - P. 1-4. ↑
- C889.** Li Nan. Retrieval of Three-Dimensional Wind Field of Typhoon by SVVP Method. / Li Nan, Wei Ming, Pei Xiaofang, Li Luan. // 2009. CiSE 2009. International Conference on Computational Intelligence and Software Engineering. - Wuhan, 11-13 Dec. 2009. - P. 1-4. ↑
- C890.** Molina D.E. Cramer-Rao Bound-Based Evaluation of Texture Extraction from SAR Images. / Molina D.E., Datcu M., Gleich D. // 2009. IWSSIP 2009. 16th International Conference on Systems, Signals and Image Processing. - Chalkida, 18-20 June 2009. - P. 1-4. ↑
- C891.** Popescu A. Damage Assessment Based on SAR Image Analysis: Flood Scenario for Romanian Eastern Carpathian Region. / Popescu A., Patrascu C., Gavat I., Datcu M. // 2009. IWSSIP 2009. 16th International Conference on Systems, Signals and Image Processing. - Chalkida, 18-20 June 2009. - P. 1-5. ↑
- C892.** Kseneman M. Soil Moisture Estimation with TerraSAR-X: With Dubois Empirical Model. / Kseneman M., Gleich D. // 2009. IWSSIP 2009. 16th International Conference on Systems, Signals and Image Processing. - Chalkida, 18-20 June 2009. - P. 1-4. ↑
- C893.** Liu Ru-meng. The application of power density spectrum estimation on synthetic aperture radiometer. / Liu Ru-meng, Chen Wen-xin, Li Hao. // 2009 IET International Radar Conference. - Guillin, China, 20-22 April 2009. - P. 1-4. ↑
- C894.** Wang Ying. Key technology analysis of sub-millimetre wave seeker. / Wang Ying, Zhang Xiaojing, Zhu Huaicheng, Su Hongyan, Yuan Qi. // 2009 IET International Radar Conference. - Guillin, China, 20-22 April 2009. - P. 1-4. ↑
- C895.** Zhang Xiaojing. Research on phase shift in mono-pulse angle tracking system. / Zhang Xiaojing, Su Hongyan, Zhu Huaicheng. // 2009 IET International Radar Conference. - Guillin, China, 20-22 April 2009. - P. 1-4. ↑
- C896.** Haipeng Wang. Statistical analysis to assess building damage in 2008 Wenchuan earthquake from multi-temporal SAR images. / Haipeng Wang, Ya-Qiu Jin. // 2009. APSAR 2009. 2nd Asian-Pacific Conference on Synthetic Aperture Radar. - Xian, Shanxi, 26-30 Oct. 2009. - P. 121-123. ↑
- C897.** Meddeber L. The Practice of an Automatic Registration System Based on Contour Features and

Wavelet Transform for Remote Sensing Images. / Meddeber L., Berrached N.E., Taleb-Ahmed A. // 2009. ICCEE '09. Second International Conference on Computer and Electrical Engineering. - Dubai, 28-30 Dec. 2009. - Vol. 2. - P. 58-63. ↑

C898. Yang Li. Detection scene analysis for high frequency radar. / Yang Li, Ning Zhang, Qiang Yang. // 2009. YC-ICT '09. IEEE Youth Conference on Information, Computing and Telecommunication. - Beijing, 20-21 Sept. 2009. - P. 315-318. ↑

C899. Baboli M. A new wavelet based algorithm for estimating respiratory motion rate using UWB radar. / Baboli M., Ghorashi S.A., Saniei N., Ahmadian A. // 2009. ICBPE '09. International Conference on Biomedical and Pharmaceutical Engineering. - Singapore, 2-4 Dec. 2009. - P. 1-3. ↑

C900. Wang Jian. Research on application of unmanned aerial vehicles borne SAR. / Wang Jian, Liu Jin-mei, Yuan Yuan, Feng Jun. // 2009. APSAR 2009. 2nd Asian-Pacific Conference on Synthetic Aperture Radar. - Xian, Shanxi, 26-30 Oct. 2009. - P. 60-63. ↑

C901. Wang Li-gang. C-Band multi-polarimetric SAR and the flight experiment of land and sea. / Wang Li-gang, Zhang Wei-hua, Xie Chun-hua, Shao Yun, Sun Jian, Zhang Feng-li. // 2009. APSAR 2009. 2nd Asian-Pacific Conference on Synthetic Aperture Radar. - Xian, Shanxi, 26-30 Oct. 2009. - P. 34-38. ↑

C902. Liu Ya-nan. SAR Image Segmentation Based on Immune Genetic Algorithm and Gaussian Mixture Models. / Liu Ya-nan, Guo Yu-tang, Lin Qin, Luo Bin. // 2009. AICI '09. International Conference on Artificial Intelligence and Computational Intelligence. - Shanghai, 7-8 Nov. 2009. - Vol. 1. - P. 434-438. ↑

C903. Guo Ming. Research on Database Storage of Large-Scale Terrestrial LIDAR Data. / Guo Ming, Wang Yanmin, Zhao Youshan, Zhou Junzhao. // 2009. IFCSTA '09. International Forum on Computer Science-Technology and Applications. - Chongqing, 25-27 Dec. 2009. - Vol. 2. - P. 19-23. ↑

C904. Yanovsky F.J. Doppler-polarimetric radar system for recognition of distributed objects. 2009. COMCAS 2009. IEEE International Conference on Microwaves, Communications, Antennas and Electronics Systems. - Tel Aviv, 9-11 Nov. 2009. - P. 1-4. ↑

C905. Arusi R. Linear FM radar operating in the Tera-Hertz regime for concealed objects detection. / Arusi R., Pinhasi Y., Kapilevitch B., Hardon D., Litvak B., Anisimov M. // 2009. COMCAS 2009. IEEE International Conference on Microwaves, Communications, Antennas and Electronics Systems. - Tel Aviv, 9-11 Nov. 2009. - P. 1-4. ↑

C906. Min Han. Design and fabrication of MMW module for 94 GHz radar sensor applications. / Min Han, Dong-sik Ko, Sang-jin Lee, Yong-hyun Baek, Seok-gyu Choi, Sung-wun Moon, Tae-jong Baek, Chang-woo Lee, Yeon-sik Chae, Jin-Koo Rhee. // 2009. APMC 2009. Asia Pacific Microwave Conference. - Singapore, 7-10 Dec. 2009. - P. 1699-1702. ↑

C907. Aris M. Comparison of Reflection and Transmission Method and Metal Back Method Measurement of Dielectric properties of transformer oil using free space microwave measurement system in 8-12 GHz frequency range. / Aris M., Abd Kadir E., Kumar Ghodgaonkar D., Khadri N. // 2009. APMC 2009. Asia Pacific Microwave Conference. - Singapore, 7-10 Dec. 2009. - P. 1609-1612. ↑

C908. Hasan M. Multi-modal Registration of SAR and Optical Satellite Images. / Hasan M., Pickering M.R., Xiuping Jia. // 2009. DICTA '09. Digital Image Computing: Techniques and Applications. - Melbourne, VIC, 1-3 Dec. 2009. - P. 447-453. ↑

C909. Wang Yang. Design and simulation analysis of polarimetric interferometric synthetic aperture radar. / Wang Yang, Zhan Jintong, Ge Jialong, Jiang Kai, Yuan Lihai. // 2009. APSAR 2009. 2nd Asian-Pacific Conference on Synthetic Aperture Radar. - Xian, Shanxi, 26-30 Oct. 2009. - P. 606-609. ↑

C910. Hua Zhong. Road extraction in remote sensing images based on Nonsubsampled Contourlet Transform. / Hua Zhong, Yingtao Feng, Licheng Jiao. // 2009. APSAR 2009. 2nd Asian-Pacific Conference on Synthetic Aperture Radar. - Xian, Shanxi, 26-30 Oct. 2009. - P. 880-883. ↑

C911. Kang Qing. A beam-splitting approach to measuring microwave backscattering coefficient ( $\sigma^\circ$ ) and its application. / Kang Qing, Wang Zhenggang, Zeng Youjun. // 2009. APSAR 2009. 2nd Asian-Pacific Conference on Synthetic Aperture Radar. - Xian, Shanxi, 26-30 Oct. 2009. - P. 896-898. ↑

- C912.** Milne T. Plenary session. 2009. APSAR 2009. 2nd Asian-Pacific Conference on Synthetic Aperture Radar. - Xian, Shanxi, 26-30 Oct. 2009. - P. 1-16. ↑
- C913.** Biao Hou. SAR image retrieval based on Gaussian Mixture Model classification. / Biao Hou, Xu Tang, Licheng Jiao, Shuang Wang. // 2009. APSAR 2009. 2nd Asian-Pacific Conference on Synthetic Aperture Radar. - Xian, Shanxi, 26-30 Oct. 2009. - P. 796-799. ↑
- C914.** He M. Urban change detection using coherence and intensity characteristics of multi-temporal SAR imagery. / He M., He X.F. // 2009. APSAR 2009. 2nd Asian-Pacific Conference on Synthetic Aperture Radar. - Xian, Shanxi, 26-30 Oct. 2009. - P. 840-843. ↑
- C915.** Yanning Cai. Parameter assessment for texture feature quality evaluation in SAR ocean image. / Yanning Cai, Jinsong Chong. // 2009. APSAR 2009. 2nd Asian-Pacific Conference on Synthetic Aperture Radar. - Xian, Shanxi, 26-30 Oct. 2009. - P. 852-855. ↑
- C916.** Zhu Xiao-peng. A MTRC correction algorithm in Bistatic ISAR. / Zhu Xiao-peng, Zhang Qun, Zhu Ren-fei, Li Hong-wei. // 2009. APSAR 2009. 2nd Asian-Pacific Conference on Synthetic Aperture Radar. - Xian, Shanxi, 26-30 Oct. 2009. - P. 977-980. ↑
- C917.** Ren-fei Zhu. Micro-Doppler analysis of vibrating target in bistatic radar. / Ren-fei Zhu, Qun Zhang, Xiao-peng Zhu, Ying Luo. // 2009. APSAR 2009. 2nd Asian-Pacific Conference on Synthetic Aperture Radar. - Xian, Shanxi, 26-30 Oct. 2009. - P. 981-984. ↑
- C918.** Xie Xiaochun. Fast compressive sensing radar imaging based on smoothed l0 norm. / Xie Xiaochun, Zhang Yunhua. // 2009. APSAR 2009. 2nd Asian-Pacific Conference on Synthetic Aperture Radar. - Xian, Shanxi, 26-30 Oct. 2009. - P. 443-446. ↑
- C919.** Junwen Dai. Scattering and image simulation for reconstruction of 3D PEC objects concealed in a dielectric box. / Junwen Dai, Ya-Qiu Jin. // 2009. APSAR 2009. 2nd Asian-Pacific Conference on Synthetic Aperture Radar. - Xian, Shanxi, 26-30 Oct. 2009. - P. 1064-1067. ↑
- C920.** Ya-Qiu Jin. Polarimetric scattering for information retrieval of SAR imagery. 2009. APSAR 2009. 2nd Asian-Pacific Conference on Synthetic Aperture Radar. - Xian, Shanxi, 26-30 Oct. 2009. - P. 750-754. ↑
- C921.** Huang S.Q. A new change detection algorithm for SAR images. / Huang S.Q., Liu D.Z., Cai X.H. // 2009. APSAR 2009. 2nd Asian-Pacific Conference on Synthetic Aperture Radar. - Xian, Shanxi, 26-30 Oct. 2009. - P. 729-732. ↑
- C922.** Biao Xv. The Rapid Generation of DOM for Geophysical Applications. / Biao Xv, Hui Cao, Quanye Du. // 2009. ICIECS 2009. International Conference on Information Engineering and Computer Science. - Wuhan, 19-20 Dec. 2009. - P. 1-4. ↑
- C923.** Fu Peiyi. A Study of Land Subsidence by Radar Remote Sensing at Datong Jurassic & Carboniferous Period Coalfield. / Fu Peiyi, Ge Yonghui, Ma Chao, Jia Xiuming, Shan Xinjian, Li Fangfang, Zhang Xiaoke. // 2009. CISP '09. 2nd International Congress on Image and Signal Processing. - Tianjin, 17-19 Oct. 2009. - P. 1-4. ↑
- C924.** Chen Zhuo. An Improved Automatic Ship Detection Method in SAR Images. 2009. CISP '09. 2nd International Congress on Image and Signal Processing. - Tianjin, 17-19 Oct. 2009. - P. 1-4. ↑
- C925.** Yun Yang. A Novel Deformable Model for Urban Vegetation Detection Using LiDAR Data. / Yun Yang, Ying Lin. // 2009. CISP '09. 2nd International Congress on Image and Signal Processing. - Tianjin, 17-19 Oct. 2009. - P. 1-5. ↑
- C926.** Wang Tao. Forest Reconstruction Using Point Cloud Data of Airborne LIDAR. / Wang Tao, Gong Jianhua. // 2009. MASS '09. International Conference on Management and Service Science. - Wuhan, 20-22 Sept. 2009. - P. 1-4. ↑
- C927.** Zhu Wang. The Design of the Remote Water Quality Monitoring System Based on WSN. / Zhu Wang, Qi Wang, Xiaoqiang Hao. // 2009. WiCom '09. 5th International Conference on Wireless Communications, Networking and Mobile Computing. - Beijing, 24-26 Sept. 2009. - P. 1-4. ↑

- C928.** Wang Dong. Water Objects Extraction from Polarimetric SAR Imagery Based on Sequential Nonlinear Filtering and Independent Component Analysis. / Wang Dong, Qin Ping, Chen Ying-ying. // 2009. CISP '09. 2nd International Congress on Image and Signal Processing. - Tianjin, 17-19 Oct. 2009. - P. 1-5. ↑
- C929.** Huber S. A novel digital beam-forming concept for spaceborne reflector SAR Systems. / Huber S., Younis M., Patyuchenko A., Krieger G. // 2009. EuRAD 2009. European Radar Conference. - Rome, Sept. 30 2009-Oct. 2 2009. - P. 238-241. ↑
- C930.** Lutsenko I.V. Usage of electromagnetic fields of antropogenic irradiation sources for remote sensing of atmosphere. / Lutsenko I.V., Lutsenko V.I., Popov I.V., Sinitsky V.B., Tarnavsky E.V., Anh N.X. // 2009. EuRAD 2009. European Radar Conference. - Rome, Sept. 30 2009-Oct. 2 2009. - P. 545-548. ↑
- C931.** Caltagirone F. Status, results and perspectives of the Italian Earth Observation SAR COSMO-SkyMed. 2009. EuRAD 2009. European Radar Conference. - Rome, Sept. 30 2009-Oct. 2 2009. - P. 330-334. ↑
- C932.** Camps-Valls G. Machine learning in remote sensing data processing. 2009. MLSP 2009. IEEE International Workshop on Machine Learning for Signal Processing. - Grenoble, 1-4 Sept. 2009. - P. 1-6. ↑
- C933.** Glushko D. DDV-novel Doppler-polarimetric technique for remote sensing of precipitation. / Glushko D., Yanovsky F.J. // 2009. EuRAD 2009. European Radar Conference. - Rome, Sept. 30 2009-Oct. 2 2009. - P. 298-301. ↑
- C934.** Sturm C. Evaluation of beam-forming algorithms for automotive OFDM signal based radar. / Sturm C., Reichardt L., Zwick T., Wiesbeck W. // 2009. EuRAD 2009. European Radar Conference. - Rome, Sept. 30 2009-Oct. 2 2009. - P. 141-144. ↑
- C935.** Qing Zhao. Application of ASAR PSI techonology to ground deformation detection in mega-cities of the Pearl River Delta Region in China. / Qing Zhao, Hui Lin, Yuanzhi Zhang, Liming Jiang. // 2009 17th International Conference on Geoinformatics. - Fairfax, VA, 12-14 Aug. 2009. - P. 1-5. ↑
- C936.** Kumari P. Registration of LiDAR data through stable surface matching. / Kumari P., Shrestha R., Carter B. // 2009 17th International Conference on Geoinformatics. - Fairfax, VA, 12-14 Aug. 2009. - P. 1-5. ↑
- C937.** Zhang Yu. Impact analysis and appraisal of Tangjiashan Barrier Lake by spatial information technology. / Zhang Yu, Chen Pengxiao. // 2009 17th International Conference on Geoinformatics. - Fairfax, VA, 12-14 Aug. 2009. - P. 1-5. ↑
- C938.** Yermolov P.P. Sevastopol range for measuring radar, thermal and laser properties of surface ships (1979-1991). / Yermolov P.P., Pustovoytenko V.V. // 2009. CriMiCo 2009. 19th International Crimean Conference Microwave & Telecommunication Technology. - Sevastopol, 14-18 Sept. 2009. - P. 36-39. ↑
- C939.** {no data available}. Title page. 2009. CriMiCo 2009. 19th International Crimean Conference Microwave & Telecommunication Technology. - Sevastopol, 14-18 Sept. 2009. - P. I. ↑
- C940.** Hequn Yang. Development of integrated typhoon remote sensing application system based on .NET and ArcGIS Engine. / Hequn Yang, Yinming Yang, Shengmao Zhang. // 2009 17th International Conference on Geoinformatics. - Fairfax, VA, 12-14 Aug. 2009. - P. 1-5. ↑
- C941.** Ai Wei-hua. Denoising of SAR Images Based on Wavelet Packet. / Ai Wei-hua, Yun-xian Huang, Chao-ling Shen, Xi-Chuan Liu. // 2009. CISP '09. 2nd International Congress on Image and Signal Processing. - Tianjin, 17-19 Oct. 2009. - P. 1-4. ↑
- C942.** Weixing Wang. Design and Implementation of Mobile GeoSpatial Information System for Public Health Emergency. / Weixing Wang, Jianhua Gong, Lihui Zhang, Jinjin Zhang, Fang Liquan, Cao Wuchun. // 2009. WiCom '09. 5th International Conference on Wireless Communications, Networking and Mobile Computing. - Beijing, 24-26 Sept. 2009. - P. 1-4. ↑
- C943.** Wang Ruifu. Calculation and Analysis of Typical Coastal Low-Tide Marks Based on Lidar Data. / Wang Ruifu, Hu Yuling. // 2009. WiCom '09. 5th International Conference on Wireless Communications, Networking and Mobile Computing. - Beijing, 24-26 Sept. 2009. - P. 1-4. ↑
- C944.** Xuejun Cheng. Identification of sand dredges in Yangtze River based on ASAR remote sensing data. /

Xuejun Cheng, Youchuan Wan, Bo Cao. // 2009 17th International Conference on Geoinformatics. - Fairfax, VA, 12-14 Aug. 2009. - P. 1-5. ↑

C945. Mitasova H. New spatial measures of terrain dynamics derived from time series of lidar data. / Mitasova H., Hardin E., Overton M., Harmon R.S. // 2009 17th International Conference on Geoinformatics. - Fairfax, VA, 12-14 Aug. 2009. - P. 1-6. ↑

C946. Jatlaoui M.M. Wireless interrogation techniques for a passive pressure micro-sensor using an EM transducer. / Jatlaoui M.M., Chebila F., Pons P., Aubert H. // 2009. EuMC 2009. European Microwave Conference. - Rome, Sept. 29 2009-Oct. 1 2009. - P. 053-056. ↑

C947. {no data available}. Welcome to EuRAD 2009. 2009. EuRAD 2009. European Radar Conference. - Rome, Italy, Sept. 30 2009-Oct. 2 2009. - P. 1. ↑

C948. Kuzmanic I. Inversion of wavelet coefficients in oil spills detection in radar images for environment risk reduction in Adriatic Sea. / Kuzmanic I., Soda J., Kulenovic Z., Vujovic M. // 2009. ELMAR '09. International Symposium ELMAR. - Zadar, 28-30 Sept. 2009. - P. 33-36. ↑

C949. Radhakrishnan S.R. Lidar measurements on aerosol characteristics at the tropical stations Trivandrum (8.33° N, 77° E) and Gadanki (13.5° N, 79.2° E). / Radhakrishnan S.R., Satyanarayana M., KrishnaKumar V., Pillai V.P.M., Reghunath K. // 2009. ICUMT '09. International Conference on Ultra Modern Telecommunications & Workshops. - St. Petersburg, 12-14 Oct. 2009. - P. 1-4. ↑

C950. Krishnakumar V. Optical properties of cirrus clouds during monsoon over Indian subcontinent. / Krishnakumar V., Satyanarayana M., Mahadevan Pillai V.P., Radhakrishnan S.R., Raghunath K. // 2009. ICUMT '09. International Conference on Ultra Modern Telecommunications & Workshops. - St. Petersburg, 12-14 Oct. 2009. - P. 1-5. ↑

C951. Gebre B.A. Remotely Operated and Autonomous Mapping System (ROAMS). / Gebre B.A., Hao Men, Pochiraju K. // 2009. TePRA 2009. IEEE International Conference on Technologies for Practical Robot Applications. - Woburn, MA, 9-10 Nov. 2009. - P. 173-178. ↑

C952. Marsh J.H. Multi-element arrays for LADAR. 2009. AVFOP '09. IEEE Avionics, Fiber-Optics and Phototonics and Photonics Technology Conference. - San Antonio, TX, 22-24 Sept. 2009. - P. 25-26. ↑

C953. Watkins L.S. Compact high power DPSS laser with very low RIN and phase noise for 1550nm wavelength band. / Watkins L.S., van Leeuwen R., Xu B., Wang Q., Ghosh C. // 2009. AVFOP '09. IEEE Avionics, Fiber-Optics and Phototonics and Photonics Technology Conference. - San Antonio, TX, 22-24 Sept. 2009. - P. 7-8. ↑

C954. Shao Yongshe. Research of the aeroplane intelligent localization methods based on Synthetic Aperture Radar imagery. / Shao Yongshe, Han Yang, Zhang Leiyu. // 2009. ICIS 2009. IEEE International Conference on Intelligent Computing and Intelligent Systems. - Shanghai, 20-22 Nov. 2009. - Vol. 2. - P. 154-157. ↑

C955. Peng Liu. Oil Spill Identification in Marine SAR Images Based on Texture Feature and Fuzzy Logic System. / Peng Liu, Chaofang Zhao. // 2009. FSKD '09. Sixth International Conference on Fuzzy Systems and Knowledge Discovery. - Tianjin, 14-16 Aug. 2009. - Vol. 3. - P. 433-437. ↑

C956. Liu Xiuguo. Application of Two-Pass D-InSAR in Chengdu Region's Deformation Measurement in Wenchuan Earthquake. / Liu Xiuguo, Hu Xie, Li Yongsheng, Gao Wei, Guo Jiyan, Xiao Lin. // 2009. ICIECS 2009. International Conference on Information Engineering and Computer Science. - Wuhan, 19-20 Dec. 2009. - P. 1-4. ↑

C957. Kenney J.D. Precise positioning with wireless sensor nodes: Monitoring natural hazards in all terrains. / Kenney J.D., Poole D.R., Willden G.C., Abbott B.A., Morris A.P., McGinnis R.N., Ferrill D.A. // 2009. SMC 2009. IEEE International Conference on Systems, Man and Cybernetics. - San Antonio, TX, 11-14 Oct. 2009. - P. 722-727. ↑

C958. Sim C.K. Analysis of land cover/use over Penang Island, Malaysia by using ALOS PALSAR data. / Sim C.K., Abdullah K., MatJafri M.Z., Lim H.S. // 2009. IconSpace 2009. International Conference on Space Science and Communication. - Negeri Sembilan, 26-27 Oct. 2009. - P. 209-211. ↑

↑

- C959. Jia Kun. Improvement of classification accuracy integrating C- and X-band synthetic aperture radar data. / Jia Kun, Wu Bingfang, Li Qiangzi, Tian Yichen. // 2009 3rd IEEE International Symposium on Microwave, Antenna, Propagation and EMC Technologies for Wireless Communications. - Beijing, 27-29 Oct. 2009. - P. 340-345. ↑
- C960. Snoeij P. Sentinel 1-the future GMES C-band SAR mission. / Snoeij P., Attema E., Torres R., Levrini G., Croci R., L'Abbate M., Pietropaolo A., Rostan F., Huchler M. // 2009. EuRAD 2009. European Radar Conference. - Rome, Sept. 30 2009-Oct. 2 2009. - P. 21-24. ↑
- C961. Muntzinger M.M. Out-of-sequence measurement processing for an automotive pre-crash application. / Muntzinger M.M., Schroder F., Zuther S., Dietmayer K. // 2009. ITSC '09. 12th International IEEE Conference on Intelligent Transportation Systems. - St. Louis, MO, 4-7 Oct. 2009. - P. 1-6. ↑
- C962. Guo Jianxing. The Study of Image Fusion Method Based on Wavelet-Packet Transform. / Guo Jianxing, Ma Junqiang, Lui Songlin. // 2009. WCSE '09. WRI World Congress on Software Engineering. - Xiamen, 19-21 May 2009. - Vol. 2. - P. 528-531. ↑
- C963. Safian R. Detection of objects inside water exploiting the Brillouin precursors. / Safian R., Mirzaei H., Elhami H. // 2009. EuRAD 2009. European Radar Conference. - Rome, Sept. 30 2009-Oct. 2 2009. - P. 517-520. ↑
- C964. Borgarelli L. Doppler Radar for planetary safe descent and landing. / Borgarelli L., Carbone A., Iorio M., Alberti G. // 2009. EuRAD 2009. European Radar Conference. - Rome, Sept. 30 2009-Oct. 2 2009. - P. 29-32. ↑
- C965. Scarchilli C. Candidate scatterometer concepts for the Post-EPS mission. / Scarchilli C., Di Salvo M., Chung-Chi Lin, Betto M. // 2009. EuRAD 2009. European Radar Conference. - Rome, Sept. 30 2009-Oct. 2 2009. - P. 164-167. ↑
- C966. Otsuka Y. Spatial relationship of F-region field-aligned irregularities and medium-scale traveling ionospheric disturbances observed with the MU radar and all-sky airglow imagers. / Otsuka Y., Shiokawa K., Ogawa T., Yokoyama T., Yamamoto M. // 2009 ICCAS-SICE. - Fukuoka, 18-21 Aug. 2009. - P. 1310-1311. ↑
- C967. Takahashi N. Cloud profiling radar on earthcare satellite. / Takahashi N., Kimura T., Ohno Y., Horie H., Nakatsuka H., Sato K., Sakaide Y., Okada K., Kumagai H. // 2009 ICCAS-SICE. - Fukuoka, 18-21 Aug. 2009. - P. 1328-1332. ↑
- C968. Shimomai T. Performance evaluation of adaptive scan with wide-band noise modulation for spaceborne rain radar based on simulation. / Shimomai T., Adachi K., Kozu T., Hanado H. // 2009 ICCAS-SICE. - Fukuoka, 18-21 Aug. 2009. - P. 1324-1327. ↑
- C969. Li Yong. DEM Extraction from LIDAR Data by Morphological Gradient. / Li Yong, Wu Huayi. // 2009. NCM '09. Fifth International Joint Conference on INC, IMS and IDC. - Seoul, 25-27 Aug. 2009. - P. 1301-1306. ↑
- C970. Kubo M. Visualization of water vapor distribution in the lower atmosphere using two lidars. / Kubo M., Nakamura K., Muramoto K., Ohigashi T., Shinoda T., Fujiyoshi Y. // 2009 ICCAS-SICE. - Fukuoka, 18-21 Aug. 2009. - P. 5445-5450. ↑
- C971. Ebinuma T. Airborne GPS reflectometry from low altitude aircraft. / Ebinuma T., Akio Y., Manandhar D. // 2009 ICCAS-SICE. - Fukuoka, 18-21 Aug. 2009. - P. 3580-3584. ↑
- C972. Lavalie M. Forest parameters inversion using Polarimetric and Interferometric SAR data. / Lavalie M., Solimini D., Pottier E., Desnos Y.-L. // IGARSS 2009 Geoscience and Remote Sensing Symposium, 2009 IEEE International. - Cape Town, 12-17 July 2009. - Vol. 4. - P. IV-129-IV-132-129. ↑
- C973. YuXia Li. Quantitative study of the Eco-water indices based on remote sensing. / YuXia Li, WuNian Yang, Ling Tong, Ji Jian, XingFa Gu. // IGARSS 2009 Geoscience and Remote Sensing Symposium, 2009 IEEE International. - Cape Town, 12-17 July 2009. - Vol. 4. - P. IV-133-IV-136-133. ↑
- C974. Ramos-Perez I. Preliminary results of the Passive Advanced Unit Synthetic Aperture (PAU-SA). / Ramos-Perez I., Bosch-Lluis X., Camps A., Valencia E., Marchan-Hernandez J.F., Rodriguez-Alvarez N., Canales-Contador F. // IGARSS 2009 Geoscience and Remote Sensing Symposium, 2009 IEEE International. -

Cape Town, 12-17 July 2009. - Vol. 4. - P. IV-121-IV-124-121. ↑

**C975.** Calderhead A.I. C-band D-InSAR and field data for calibrating a groundwater flow and land subsidence model. / Calderhead A.I., Martel R., Rivera A., Garfias J., Alasset P.-J. // IGARSS 2009 Geoscience and Remote Sensing Symposium, 2009 IEEE International. - Cape Town, 12-17 July 2009. - Vol. 4. - P. IV-149-IV-152-149. ↑

**C976.** Neumann M. Forest parameter retrieval using a general repeat-pass polarimetric interferometric vegetation model. / Neumann M., Ferro-Famil L., Reigber A. // IGARSS 2009 Geoscience and Remote Sensing Symposium, 2009 IEEE International. - Cape Town, 12-17 July 2009. - Vol. 4. - P. IV-137-IV-140-137. ↑

**C977.** Benson M. Variable wind influence on InSAR imagery of forests. / Benson M., Pierce L., Sarabandi K. // IGARSS 2009 Geoscience and Remote Sensing Symposium, 2009 IEEE International. - Cape Town, 12-17 July 2009. - Vol. 4. - P. IV-141-IV-144-141. ↑

**C978.** Gritzner J.H. Modeling surface-flow characteristics in glaciated landscapes. IGARSS 2009 Geoscience and Remote Sensing Symposium, 2009 IEEE International. - Cape Town, 12-17 July 2009. - Vol. 4. - P. IV-342-IV-345-342. ↑

**C979.** Kropacek J. Parametrization of integrated hydrological model of Nam Co lake catchment on Tibetan Plateau using synergy of SAR and optical data. / Kropacek J., Hochschild V. // IGARSS 2009 Geoscience and Remote Sensing Symposium, 2009 IEEE International. - Cape Town, 12-17 July 2009. - Vol. 4. - P. IV-346-IV-349-346. ↑

**C980.** Hayashi N. Measurement and analysis of paddy field by polarimetric GB-SAR. / Hayashi N., Sato M. // IGARSS 2009 Geoscience and Remote Sensing Symposium, 2009 IEEE International. - Cape Town, 12-17 July 2009. - Vol. 4. - P. IV-358-IV-361-358. ↑

**C981.** Tannous O. Independent component analysis of polarimetric SAR data for separating ground and vegetation components. / Tannous O., Kasilingam D. // IGARSS 2009 Geoscience and Remote Sensing Symposium, 2009 IEEE International. - Cape Town, 12-17 July 2009. - Vol. 4. - P. IV-93-IV-96-93. ↑

**C982.** Yuemin Yue. Developing new spectral indices for karst rocky desertification monitoring in Southwest China. / Yuemin Yue, Kelin Wang, Junsheng Li, Bing Zhang, Bo Liu, Qianjun Jiao, Xiaonan Zhang. // IGARSS 2009 Geoscience and Remote Sensing Symposium, 2009 IEEE International. - Cape Town, 12-17 July 2009. - Vol. 4. - P. IV-318-IV-321-318. ↑

**C983.** Bucini G. Woody cover and heterogeneity in the Savannas of the Kruger National Park, South Africa. / Bucini G., Saatchi S., Hanan N., Boone R.B., Smit I. // IGARSS 2009 Geoscience and Remote Sensing Symposium, 2009 IEEE International. - Cape Town, 12-17 July 2009. - Vol. 4. - P. IV-334-IV-337-334. ↑

**C984.** Quang Huy Nguyen. Hardware-accelerated edge detection for polarimetric synthetic aperture radar data. / Quang Huy Nguyen, Ken Yoong Lee, Myo Tun Aung, Bretschneider T., McLoughlin I. // IGARSS 2009 Geoscience and Remote Sensing Symposium, 2009 IEEE International. - Cape Town, 12-17 July 2009. - Vol. 4. - P. IV-204-IV-207-204. ↑

**C985.** Faruolo M. Real time monitoring of flooded areas by a multi-temporal analysis of optical satellite data. / Faruolo M., Coviello I., Lacava T., Pergola N., Tramutoli V. // IGARSS 2009 Geoscience and Remote Sensing Symposium, 2009 IEEE International. - Cape Town, 12-17 July 2009. - Vol. 4. - P. IV-192-IV-195-192. ↑

**C986.** Angelliaume S. SETHI, the ONERA airborne SAR sensor, and his low frequency capability. / Angelliaume S., Dubois-Fernandez P., Dreuillet Ph., Oriot H., Coulombeix C. // IGARSS 2009 Geoscience and Remote Sensing Symposium, 2009 IEEE International. - Cape Town, 12-17 July 2009. - Vol. 4. - P. IV-177-IV-179-177. ↑

**C987.** Cho M. Integrating remote sensing and ancillary data for regional ecosystem assessment: Eucalyptus grandis agro-system in KwaZulu-Natal, South Africa. / Cho M., van Aardt J., Main R., Majeke B., Ramoelo A., Mathieu R., Norris-Rogers M., Du Plessis M. // IGARSS 2009 Geoscience and Remote Sensing Symposium, 2009 IEEE International. - Cape Town, 12-17 July 2009. - Vol. 4. - P. IV-264-IV-267-264. ↑

**C988.** Robin A. An a-contrario approach for unsupervised change detection in radar images. / Robin A., Mercier G., Moser G., Serpico S. // IGARSS 2009 Geoscience and Remote Sensing Symposium, 2009 IEEE



International. - Cape Town, 12-17 July 2009. - Vol. 4. - P. IV-240-IV-243-240.

**C989.** Severino V. An approach to SAR tomography with limited number of tracks. / Severino V., Nannini M., Reigber A., Scheiber R., Capozzoli A., D'Elia G., Liseno A., Vinetti P. // IGARSS 2009 Geoscience and Remote Sensing Symposium, 2009 IEEE International. - Cape Town, 12-17 July 2009. - Vol. 4. - P. IV-216-IV-219-216.



**C990.** Schneider R.Z. Estimation and correction of ionospheric induced phase errors in SAR images using Coherent Scatterers. / Schneider R.Z., Papathanassiou K. // IGARSS 2009 Geoscience and Remote Sensing Symposium, 2009 IEEE International. - Cape Town, 12-17 July 2009. - Vol. 4. - P. IV-165-IV-168-165.



**C991.** Nonaka T. DEM production utilizing stereo technology of TerraSAR-X data. / Nonaka T., Hayakawa T., Griffiths S., Mercer B. // IGARSS 2009 Geoscience and Remote Sensing Symposium, 2009 IEEE International. - Cape Town, 12-17 July 2009. - Vol. 4. - P. IV-157-IV-160-157.



**C992.** Neumann M. A polarimetric vegetation model to retrieve particle and orientation distribution characteristics. / Neumann M., Ferro-Famil L., Jager M., Reigber A., Pottier E. // IGARSS 2009 Geoscience and Remote Sensing Symposium, 2009 IEEE International. - Cape Town, 12-17 July 2009. - Vol. 4. - P. IV-145-IV-148-145.



**C993.** Jingjuan Liao. Neural network algorithm and backscattering model for biomass estimation of wetland vegetation in Poyang Lake area using Envisat ASAR data. / Jingjuan Liao, Lei Dong, Guozhuang Shen. // IGARSS 2009 Geoscience and Remote Sensing Symposium, 2009 IEEE International. - Cape Town, 12-17 July 2009. - Vol. 4. - P. IV-180-IV-183-180.



**C994.** Sandberg G. Comparison of L- and P-band biomass retrievals based on backscatter from the BioSAR campaign. / Sandberg G., Ulander L.M.H., Fransson J.E.S., Holmgren J., Thuy Le Toan. // IGARSS 2009 Geoscience and Remote Sensing Symposium, 2009 IEEE International. - Cape Town, 12-17 July 2009. - Vol. 4. - P. IV-169-IV-172-169.



**C995.** Williams M.L. Tropical forest biomass recovery using GeoSAR observations. / Williams M.L., Milne T., Tapley I., Reis J.J., Sanford M., Kofman B., Hensley S. // IGARSS 2009 Geoscience and Remote Sensing Symposium, 2009 IEEE International. - Cape Town, 12-17 July 2009. - Vol. 4. - P. IV-173-IV-176-173.



**C996.** Aimin Cai. Study on the influence of drought to crop growth based on SAR remote sensing. / Aimin Cai, Yun Shao, Fengli Zhang, Huaze Gong. // IGARSS 2009 Geoscience and Remote Sensing Symposium, 2009 IEEE International. - Cape Town, 12-17 July 2009. - Vol. 4. - P. IV-382-IV-385-382.



**C997.** Martinez-Espla J.J. A combination of particle filter, matrix pencil and region growing techniques for phase unwrapping in SAR interferometry. / Martinez-Espla J.J., Martinez-Marin T., Lopez-Sanchez J.M., Ballester J.D. // IGARSS 2009 Geoscience and Remote Sensing Symposium, 2009 IEEE International. - Cape Town, 12-17 July 2009. - Vol. 4. - P. IV-542-IV-545-542.



**C998.** Gonzalez F.R. Enhancing complex interferograms by anisotropic diffusion. / Gonzalez F.R., Datcu M. // IGARSS 2009 Geoscience and Remote Sensing Symposium, 2009 IEEE International. - Cape Town, 12-17 July 2009. - Vol. 4. - P. IV-546-IV-549-546.



**C999.** Kwag Y.K. Simulation of dual-channel SAR-GMTI for velocity estimation and compensation. / Kwag Y.K., Jung J.H., Jung C.H. // IGARSS 2009 Geoscience and Remote Sensing Symposium, 2009 IEEE International. - Cape Town, 12-17 July 2009. - Vol. 4. - P. IV-550-IV-553-550.



**C1000.** Chini M. Morphological operators applied to X-band SAR for urban land use classification. / Chini M., Pacifici F., Emery W.J. // IGARSS 2009 Geoscience and Remote Sensing Symposium, 2009 IEEE International. - Cape Town, 12-17 July 2009. - Vol. 4. - P. IV-506-IV-509-506.



**C1001.** Antelo J. Ship detection and recognition in high-resolution satellite images. / Antelo J., Ambrosio G., Gonzalez J., Galindo C. // IGARSS 2009 Geoscience and Remote Sensing Symposium, 2009 IEEE International. - Cape Town, 12-17 July 2009. - Vol. 4. - P. IV-514-IV-517-514.



**C1002.** Sato T. Detection and radiation area estimation of anomalous environmental electromagnetic wave related to earthquake precursor. / Sato T., Takumi I., Hata M., Yasukawa H. // IGARSS 2009 Geoscience and Remote Sensing Symposium, 2009 IEEE International. - Cape Town, 12-17 July 2009. - Vol. 4. - P. IV-518-IV-521-518.



- C1003.** Small D. A revised radiometric normalisation standard for SAR. / Small D., Miranda N., Meier E. // IGARSS 2009 Geoscience and Remote Sensing Symposium, 2009 IEEE International. - Cape Town, 12-17 July 2009. - Vol. 4. - P. IV-566-IV-569-566. ↑
- C1004.** Wang Yanping. Effect of linear array elements spacing on angle imaging performance of downward-looking 3D-SAR. / Wang Yanping, Du Lei, Hong Wen, Wu Yirong, Wei Lideng. // IGARSS 2009 Geoscience and Remote Sensing Symposium, 2009 IEEE International. - Cape Town, 12-17 July 2009. - Vol. 4. - P. IV-570-IV-573-570. ↑
- C1005.** Li Wei. Research on the relationship between satellite attitude stability and interferometric performance. / Li Wei, Li Chunsheng, Chen Jie, Liu Yujing. // IGARSS 2009 Geoscience and Remote Sensing Symposium, 2009 IEEE International. - Cape Town, 12-17 July 2009. - Vol. 4. - P. IV-574-IV-577-574. ↑
- C1006.** Wei Zhang. Interferometric SAR calibration with area calibration site of same height. / Wei Zhang, Maosheng Xiang, Yirong Wu. // IGARSS 2009 Geoscience and Remote Sensing Symposium, 2009 IEEE International. - Cape Town, 12-17 July 2009. - Vol. 4. - P. IV-554-IV-557-554. ↑
- C1007.** Daqing Ge. Large scale land subsidence monitoring with a reduced set of SAR images. / Daqing Ge, Yan Wang, Ling Zhang, Ye Xia, Xiaofang Guo. // IGARSS 2009 Geoscience and Remote Sensing Symposium, 2009 IEEE International. - Cape Town, 12-17 July 2009. - Vol. 4. - P. IV-558-IV-561-558. ↑
- C1008.** Wang Yinbo. Motion measurement errors analysis for the "one-active" LASAR. / Wang Yinbo, Zhang Xiaoling, Li Weihua, Shi Jun. // IGARSS 2009 Geoscience and Remote Sensing Symposium, 2009 IEEE International. - Cape Town, 12-17 July 2009. - Vol. 4. - P. IV-562-IV-565-562. ↑
- C1009.** Duquenoy M. Hyperimage concept: Multidimensional Time-Frequency Analysis applied to SAR imaging. / Duquenoy M., Ovarlez J.P., Ferro-Famil L., Pottier E. // IGARSS 2009 Geoscience and Remote Sensing Symposium, 2009 IEEE International. - Cape Town, 12-17 July 2009. - Vol. 4. - P. IV-414-IV-417-414. ↑
- C1010.** Pasolli E. A pattern recognition system for extracting buried object characteristics in GPR images. / Pasolli E., Melgani F., Donelli M. // IGARSS 2009 Geoscience and Remote Sensing Symposium, 2009 IEEE International. - Cape Town, 12-17 July 2009. - Vol. 4. - P. IV-430-IV-433-430. ↑
- C1011.** Duquenoy M. Supervised classification by neural networks using polarimetric time-frequency signatures. / Duquenoy M., Ovarlez J.R., Morisseau C., Vieillard G., Ferro-Famil L., Pottier E. // IGARSS 2009 Geoscience and Remote Sensing Symposium, 2009 IEEE International. - Cape Town, 12-17 July 2009. - Vol. 4. - P. IV-438-IV-441-438. ↑
- C1012.** Zhifeng Guo. Analysis of the effect of crown structure changes on backscattering coefficient using modeling and SAR data. / Zhifeng Guo, Wenjian Ni, Guoqing Sun. // IGARSS 2009 Geoscience and Remote Sensing Symposium, 2009 IEEE International. - Cape Town, 12-17 July 2009. - Vol. 4. - P. IV-386-IV-389-386. ↑
- C1013.** Wenju He. Urban areas characterization from polarimetric SAR images using Hidden Markov Model. / Wenju He, Jager M., Hellwich O. // IGARSS 2009 Geoscience and Remote Sensing Symposium, 2009 IEEE International. - Cape Town, 12-17 July 2009. - Vol. 4. - P. IV-398-IV-401-398. ↑
- C1014.** Wenju He. Bayesian building extraction from high resolution polarimetric SAR data. / Wenju He, Hellwich O. // IGARSS 2009 Geoscience and Remote Sensing Symposium, 2009 IEEE International. - Cape Town, 12-17 July 2009. - Vol. 4. - P. IV-402-IV-405-402. ↑
- C1015.** Sveinsson J.R. Speckle reduction of SAR images using sure-based adaptive Sigmoid thresholding in the wavelet domain. / Sveinsson J.R., Ulfarsson M.O., Benediktsson J.A. // IGARSS 2009 Geoscience and Remote Sensing Symposium, 2009 IEEE International. - Cape Town, 12-17 July 2009. - Vol. 4. - P. IV-462-IV-465-462. ↑
- C1016.** Lu Zhang. A preliminary study of target contour extraction based on scattering mechanism using polarimetric SAR images. / Lu Zhang, Huadong Guo, Xinwu Li, Qizhong Lin, Yubao Qiu. // IGARSS 2009 Geoscience and Remote Sensing Symposium, 2009 IEEE International. - Cape Town, 12-17 July 2009. - Vol. 4. - P. IV-466-IV-469-466. ↑

- C1017.** Hong-zhong Li. Oil slick spot detection using K-distribution model of the sea background. / Hong-zhong Li, Chao Wang, Hong Zhang, Fan Wu, Jilong Li. // IGARSS 2009 Geoscience and Remote Sensing Symposium, 2009 IEEE International. - Cape Town, 12-17 July 2009. - Vol. 4. - P. IV-470-IV-473-470. ↑
- C1018.** Ito Y. Resolution enhancement of SAR image using a multiframe super resolution technique. IGARSS 2009 Geoscience and Remote Sensing Symposium, 2009 IEEE International. - Cape Town, 12-17 July 2009. - Vol. 4. - P. IV-446-IV-449-446. ↑
- C1019.** Erten E. An accuracy assessment of ML texture tracking algorithm over multitemporal SAR images. / Erten E., Reigber A., Hellwich O., Prats P. // IGARSS 2009 Geoscience and Remote Sensing Symposium, 2009 IEEE International. - Cape Town, 12-17 July 2009. - Vol. 4. - P. IV-454-IV-457-454. ↑
- C1020.** Sveinsson J.R. Speckle reduction of TerraSAR-X imagery using TV segmentation. / Sveinsson J.R., Waske B., Benediktsson J.A. // IGARSS 2009 Geoscience and Remote Sensing Symposium, 2009 IEEE International. - Cape Town, 12-17 July 2009. - Vol. 4. - P. IV-458-IV-461-458. ↑
- C1021.** Li Li. A study on GPP inversion of different ecosystems by remote sensing and impact factors comparison. / Li Li, Chen Liangfu, Gao Yanhua, Liu Qinhua. // IGARSS 2009 Geoscience and Remote Sensing Symposium, 2009 IEEE International. - Cape Town, 12-17 July 2009. - Vol. 4. - P. IV-284-IV-287-284. ↑
- C1022.** Shimizu S. Level 1 algorithm development of spaceborne dual-frequency precipitation radar (DPR) for GPM. / Shimizu S., Yoshida M., Hanado H., Higashiwatoko T. // IGARSS 2009 Geoscience and Remote Sensing Symposium, 2009 IEEE International. - Cape Town, 12-17 July 2009. - Vol. 1. - P. I-212-I-215-212. ↑
- C1023.** Iida Y. A long-term trend observed in TRMM/PR monthly rainfall products and an evaluation of sampling error by a bootstrap method. / Iida Y., Kubota T., Iguchi T., Oki R. // IGARSS 2009 Geoscience and Remote Sensing Symposium, 2009 IEEE International. - Cape Town, 12-17 July 2009. - Vol. 1. - P. I-216-I-219-216. ↑
- C1024.** Uiboupin R. Observation of mesoscale eddies by using SAR data complemented with optical remote sensing and in situ measurements. / Uiboupin R., Laanemets J. // IGARSS 2009 Geoscience and Remote Sensing Symposium, 2009 IEEE International. - Cape Town, 12-17 July 2009. - Vol. 1. - P. I-224-I-227-224. ↑
- C1025.** Sajjad N. Electromagnetic wave scattering from ocean surface at low grazing angles. / Sajjad N., Khenchaf A., Coatanhay A. // IGARSS 2009 Geoscience and Remote Sensing Symposium, 2009 IEEE International. - Cape Town, 12-17 July 2009. - Vol. 1. - P. I-196-I-199-196. ↑
- C1026.** Alqudah A. Improving rainfall estimation from ground based radar measurements using neural networks. / Alqudah A., Yanting Wang, Chandrasekar V. // IGARSS 2009 Geoscience and Remote Sensing Symposium, 2009 IEEE International. - Cape Town, 12-17 July 2009. - Vol. 1. - P. I-200-I-203-200. ↑
- C1027.** Le M. Combined Ku and Ka band observations of precipitation and retrievals for GPM Ground validation. / Le M., Chandrasekar V., Lim S. // IGARSS 2009 Geoscience and Remote Sensing Symposium, 2009 IEEE International. - Cape Town, 12-17 July 2009. - Vol. 1. - P. I-208-I-211-208. ↑
- C1028.** Chretien N. Mapping and monitoring urban growth on wetlands in humid tropical context using earth observation technology: Case study of Mangrove zones around Douala in Cameroon. / Chretien N., Tiafack O., Charly D.N.G. // IGARSS 2009 Geoscience and Remote Sensing Symposium, 2009 IEEE International. - Cape Town, 12-17 July 2009. - Vol. 1. - P. I-120-I-123-120. ↑
- C1029.** Noferini L. A high speed microwave interferometer used for monitoring Stromboli volcano. / Noferini L., Mecatti D., Macaluso G., Pieraccini M., Atzeni C., Ripepe M. // IGARSS 2009 Geoscience and Remote Sensing Symposium, 2009 IEEE International. - Cape Town, 12-17 July 2009. - Vol. 1. - P. I-124-I-127-124. ↑
- C1030.** Wegmuller U. ERS-ENVISAT Tandem cross-interferometry coherence estimation. / Wegmuller U., Santoro M., Werner C., Strozzi T., Wiesmann A. // IGARSS 2009 Geoscience and Remote Sensing Symposium, 2009 IEEE International. - Cape Town, 12-17 July 2009. - Vol. 1. - P. I-128-I-131-128. ↑
- C1031.** Di Wu. Monitoring of Enteromorpha prolifera in Qingdao marine by exploiting the synergy of active and passive remote sensing data. / Di Wu, Bing Zhang, Junsheng Li, Yuanfeng Wu, Hao Zhang, Qian Shen. // IGARSS 2009 Geoscience and Remote Sensing Symposium, 2009 IEEE International. - Cape Town, 12-17 July 2009. - Vol. 1. - P. I-228-I-231-228. ↑

- C1032.** Wimmer W. QA for satellite sea surface temperatures using the ISAR ship-borne radiometric system. / Wimmer W., Robinson I., Donlon C. // IGARSS 2009 Geoscience and Remote Sensing Symposium, 2009 IEEE International. - Cape Town, 12-17 July 2009. - Vol. 1. - P. I-232-I-235-232. ↑
- C1033.** Labbassi K. Remote sensing and geological mapping for a groundwater recharge model in the arid area of Sebt Rbrykine: Doukkala, western Morocco. / Labbassi K., Tajdi A., Er-raji A. // IGARSS 2009 Geoscience and Remote Sensing Symposium, 2009 IEEE International. - Cape Town, 12-17 July 2009. - Vol. 1. - P. I-112-I-115-112. ↑
- C1034.** Lauer C. Bounding the number of relevant objects in automotive environment perception systems. / Lauer C., Herpel T., German R., Pollmer J. // 2009 Sixth International Conference on Networked Sensing Systems (INSS). - Pittsburgh, PA, 17-19 June 2009. - P. 1-8. ↑
- C1035.** Chongbin Xu. General automation test system based on the cooperation of software and hardware. / Chongbin Xu, Zhiwen Zhao, Feng Wang, Ke Xu. // 2009. ICCA 2009. IEEE International Conference on Control and Automation. - Christchurch, 9-11 Dec. 2009. - P. 797-800. ↑
- C1036.** Meddeber L. An automatic registration and mosaicking system based on contour features and wavelet transform for remote sensing images. / Meddeber L., Berrached N.E., Taleb-Ahmed A. // 2009 3rd International Conference on Signals, Circuits and Systems (SCS). - Medenine, 6-8 Nov. 2009. - P. 1-7. ↑
- C1037.** Das S. Classification of convective and stratiform types of rain and their characteristics features at a tropical location. / Das S., Shukla A.K., Maitra A. // 2009. CODEC 2009. 4th International Conference on Computers and Devices for Communication. - Kolkata, 14-16 Dec. 2009. - P. 1-4. ↑
- C1038.** Boerner W.-M. Recent advances in fully polarimetric space-SAR sensor design and its applications. 2009. CODEC 2009. 4th International Conference on Computers and Devices for Communication. - Kolkata, 14-16 Dec. 2009. - P. 1-4. ↑
- C1039.** Bera R. Vehicular communication and safety in realization of intelligent transport system. / Bera R., Mondal D., Sil S., Dhar S., Sur S., Bhaskar D., Sarkar S.K., Kandar D. // 2009. CODEC 2009. 4th International Conference on Computers and Devices for Communication. - Kolkata, 14-16 Dec. 2009. - P. 1-4. ↑
- C1040.** Karantzalos K. Variational model-based 3d building extraction from remote sensing data. / Karantzalos K., Paragios N. // 2009 16th IEEE International Conference on Image Processing (ICIP). - Cairo, 7-10 Nov. 2009. - P. 545-548. ↑
- C1041.** Facciolo G. Geodesic neighborhoods for piecewise affine interpolation of sparse data. / Facciolo G., Caselles V. // 2009 16th IEEE International Conference on Image Processing (ICIP). - Cairo, 7-10 Nov. 2009. - P. 365-368. ↑
- C1042.** Gambardella A. A polarimetric sea surface backscattering model. / Gambardella A., Nunziata F., Migliaccio M. // IGARSS 2009 Geoscience and Remote Sensing Symposium, 2009 IEEE International. - Cape Town, 12-17 July 2009. - Vol. 1. - P. I-192-I-195-192. ↑
- C1043.** Grossi E. MIMO radar waveform design: a divergence-based approach for sequential and fixed-sample size tests. / Grossi E., Lops M. // 2009 3rd IEEE International Workshop on Computational Advances in Multi-Sensor Adaptive Processing (CAMSAP). - Aruba, Dutch Antilles, 13-16 Dec. 2009. - P. 165-168. ↑
- C1044.** Carlberg M. Classifying urban landscape in aerial LiDAR using 3D shape analysis. / Carlberg M., Gao P., Chen G., Zakhor A. // 2009 16th IEEE International Conference on Image Processing (ICIP). - Cairo, 7-10 Nov. 2009. - P. 1701-1704. ↑
- C1045.** Silveira M. Classification of water regions in SAR images using level sets and non-parametric density estimation. / Silveira M., Heleno S. // 2009 16th IEEE International Conference on Image Processing (ICIP). - Cairo, 7-10 Nov. 2009. - P. 1685-1688. ↑
- C1046.** Sato M. High range resolution directional borehole radar for 3-D fracture delineation. / Sato M., Takayama T. // IGARSS 2009 Geoscience and Remote Sensing Symposium, 2009 IEEE International. - Cape Town, 12-17 July 2009. - Vol. 1. - P. I-132-I-135-132. ↑
- C1047.** Bordoni F. Adaptive scan-on-receive based on spatial spectral estimation for high-resolution, wide-

swath Synthetic Aperture Radar. / Bordonì F., Younis M., Varona E.M., Krieger G. // IGARSS 2009 Geoscience and Remote Sensing Symposium, 2009 IEEE International. - Cape Town, 12-17 July 2009. - Vol. 1. - P. I-64-I-67-64. ↑

**C1048.** De Paulis R. Focusing Synthetic Aperture Sonar (SAS) data with the Omega-K technique. / De Paulis R., Prati C., Rocca F., Scirpoli S., Tebaldini S. // IGARSS 2009 Geoscience and Remote Sensing Symposium, 2009 IEEE International. - Cape Town, 12-17 July 2009. - Vol. 1. - P. I-68-I-71-68. ↑

**C1049.** Zaugg E. Coherent multi-frequency-band resolution enhancement for synthetic aperture radar. / Zaugg E., Long D., Edwards M., Margulis A. // IGARSS 2009 Geoscience and Remote Sensing Symposium, 2009 IEEE International. - Cape Town, 12-17 July 2009. - Vol. 1. - P. I-56-I-59-56. ↑

**C1050.** Jelenak Z. A statistical study of wind field distribution within extra-tropical cyclones in North Pacific ocean from 7-years of QuikSCAT wind data. / Jelenak Z., Ahmad K., Sienkiewicz J., Chang P.S. // IGARSS 2009 Geoscience and Remote Sensing Symposium, 2009 IEEE International. - Cape Town, 12-17 July 2009. - Vol. 1. - P. I-104-I-107-104. ↑

**C1051.** Weissman D.E. The combined effect of surface rain and wind on scatterometer observations of surface roughness. / Weissman D.E., Bourassa M.A. // IGARSS 2009 Geoscience and Remote Sensing Symposium, 2009 IEEE International. - Cape Town, 12-17 July 2009. - Vol. 1. - P. I-108-I-111-108. ↑

**C1052.** Bushahab A. UAE mapped attenuation at RF frequencies (UAE-MARF). / Bushahab A., Mubarak K., Dawood A.M., Shubair R. // IGARSS 2009 Geoscience and Remote Sensing Symposium, 2009 IEEE International. - Cape Town, 12-17 July 2009. - Vol. 1. - P. I-92-I-95-92. ↑

**C1053.** Morgenthaler A.W. Modeling and validation of GPR wave scattering with the Semi-Analytic Mode Matching algorithm: Choosing optimal coordinate scattering centers. / Morgenthaler A.W., Rappaport C.M. // IGARSS 2009 Geoscience and Remote Sensing Symposium, 2009 IEEE International. - Cape Town, 12-17 July 2009. - Vol. 1. - P. I-164-I-167-164. ↑

**C1054.** Wahab M. Radar radome and its design considerations. 2009 International Conference on Instrumentation, Communications, Information Technology, and Biomedical Engineering (ICICI-BME). - Bandung, 23-25 Nov. 2009. - P. 1-5. ↑

**C1055.** Gupta S. Remote sensing based season calendar for Indian districts using MODIS data. / Gupta S., Pandit V., Rajan K.S. // IGARSS 2009 Geoscience and Remote Sensing Symposium, 2009 IEEE International. - Cape Town, 12-17 July 2009. - Vol. 4. - P. IV-296-IV-299-296. ↑

**C1056.** Albahkali M. 3D SAR focusing for subsurface point targets. / Albahkali M., Moghaddam M. // IGARSS 2009 Geoscience and Remote Sensing Symposium, 2009 IEEE International. - Cape Town, 12-17 July 2009. - Vol. 1. - P. I-60-I-63-60. ↑

**C1057.** Schwerdt M. Innovative and efficient strategy of calibrating Sentinel-1. / Schwerdt M., Doring B., Zink M., Brautigam B., Schrank D. // IGARSS 2009 Geoscience and Remote Sensing Symposium, 2009 IEEE International. - Cape Town, 12-17 July 2009. - Vol. 1. - P. I-48-I-51-48. ↑

**C1058.** Caorsi S. A neural network electromagnetic approach for GPR pavement diagnostic: A preliminary study. / Caorsi S., Stasolla M. // IGARSS 2009 Geoscience and Remote Sensing Symposium, 2009 IEEE International. - Cape Town, 12-17 July 2009. - Vol. 1. - P. I-168-I-171-168. ↑

**C1059.** Cristallini D. Efficient configurations of SAR sensors for improved range resolution. / Cristallini D., Pastina D., Lombardo P. // IGARSS 2009 Geoscience and Remote Sensing Symposium, 2009 IEEE International. - Cape Town, 12-17 July 2009. - Vol. 1. - P. I-52-I-55-52. ↑

**C1060.** Snoeij P. Analysis of Sentinel-1 mission capabilities. / Snoeij P., Attema E., Pietropaolo A., Mastroddi V., L'Abbate M., Bruno C. // IGARSS 2009 Geoscience and Remote Sensing Symposium, 2009 IEEE International. - Cape Town, 12-17 July 2009. - Vol. 1. - P. I-40-I-43-40. ↑

**C1061.** Snoeij P. FDBAQ a novel encoding scheme for Sentinel-1. / Snoeij P., Attema E., Guarnieri A.M., Rocca F. // IGARSS 2009 Geoscience and Remote Sensing Symposium, 2009 IEEE International. - Cape Town, 12-17 July 2009. - Vol. 1. - P. I-44-I-47-44. ↑

- C1062.** Hanssen R. Sentinel 1: Interferometric applications. / Hanssen R., Rocca F. // IGARSS 2009 Geoscience and Remote Sensing Symposium, 2009 IEEE International. - Cape Town, 12-17 July 2009. - Vol. 1. - P. I-156-I-159-156. ↑
- C1063.** Belli K. 2-1/2 Dimensional bi-static GPR propagation and scattering modeling of roadways and tunnels with projected 2D FDTD. / Belli K., Udall C., Rappaport C., Wadia-Fascetti S. // IGARSS 2009 Geoscience and Remote Sensing Symposium, 2009 IEEE International. - Cape Town, 12-17 July 2009. - Vol. 1. - P. I-172-I-175-172. ↑
- C1064.** Martinez-Lorenzo J.A. Physical limitations on detecting tunnels using Underground Focusing Spotlight Synthetic Aperture Radar. / Martinez-Lorenzo J.A., Rappaport C.M. // IGARSS 2009 Geoscience and Remote Sensing Symposium, 2009 IEEE International. - Cape Town, 12-17 July 2009. - Vol. 1. - P. I-160-I-163-160. ↑
- C1065.** Singhroy V. InSAR monitoring of landslides using RADARSAT. / Singhroy V., Murnaghan K., Zhang Jianlong. // IGARSS 2009 Geoscience and Remote Sensing Symposium, 2009 IEEE International. - Cape Town, 12-17 July 2009. - Vol. 1. - P. I-21-I-24-21. ↑
- C1066.** Musacchio M. ASI-Volcanic Risk System (SRV): A pilot project to develop EO data processing modules and products for volcanic activity monitoring, first results. / Musacchio M., Silvestri M., Buongiorno M.F., Spinetti C., Corradini S., Lombardo V., Merucci L., Sansosti E., Pugnaghi S., Teggi S., Vignoli S., Amodio A., Dini L. // IGARSS 2009 Geoscience and Remote Sensing Symposium, 2009 IEEE International. - Cape Town, 12-17 July 2009. - Vol. 1. - P. I-1-I-4-1. ↑
- C1067.** Doubkova M. The medium resolution soil moisture dataset: Overview of the SHARE ESA DUE TIGER project. / Doubkova M., Bartsch A., Pathe C., Sabel D., Wagner W. // IGARSS 2009 Geoscience and Remote Sensing Symposium, 2009 IEEE International. - Cape Town, 12-17 July 2009. - Vol. 1. - P. I-116-I-119-116. ↑
- C1068.** Attema E. Sentinel-1 mission overview. / Attema E., Davidson M., Snoeij P., Rommen B., Floury N. // IGARSS 2009 Geoscience and Remote Sensing Symposium, 2009 IEEE International. - Cape Town, 12-17 July 2009. - Vol. 1. - P. I-36-I-39-36. ↑
- C1069.** Seker S.S. Light scattering by thin curved dielectric surface and cylinder. / Seker S.S., Apaydin G. // IGARSS 2009 Geoscience and Remote Sensing Symposium, 2009 IEEE International. - Cape Town, 12-17 July 2009. - Vol. 1. - P. I-29-I-32-29. ↑
- C1070.** Joyce K.E. Temperature, color and deformation monitoring of volcanic regions in New Zealand. / Joyce K.E., Samsonov S., Jolly G. // IGARSS 2009 Geoscience and Remote Sensing Symposium, 2009 IEEE International. - Cape Town, 12-17 July 2009. - Vol. 1. - P. I-17-I-20-17. ↑
- C1071.** Qin Dai. ACO algorithm processing multisensor data for urban land cover. / Qin Dai, Jianbo Liu. // 2009 Joint Urban Remote Sensing Event. - Shanghai, 20-22 May 2009. - P. 1-5. ↑
- C1072.** Keqi Zhang. Automatic 3D building reconstruction from airborne LiDAR measurements. / Keqi Zhang, Jianhua Yan, Shu-Ching Chen. // 2009 Joint Urban Remote Sensing Event. - Shanghai, 20-22 May 2009. - P. 1-5. ↑
- C1073.** Chang Liang. InSAR interferogram detail-compensating filtering method based on the stationary wavelet transform. / Chang Liang, He Xiufeng. // 2009 Joint Urban Remote Sensing Event. - Shanghai, 20-22 May 2009. - P. 1-5. ↑
- C1074.** Ferraioli G. Fast InSAR multichannel phase unwrapping for DEM generation. / Ferraioli G., Shabou A., Tupin F., Pascazio V. // 2009 Joint Urban Remote Sensing Event. - Shanghai, 20-22 May 2009. - P. 1-6. ↑
- C1075.** Xiao Xiang Zhu. Space-borne high resolution SAR tomography: experiments in urban environment using TS-X Data. / Xiao Xiang Zhu, Adam N., Brcic R., Bamler R. // 2009 Joint Urban Remote Sensing Event. - Shanghai, 20-22 May 2009. - P. 1-8. ↑
- C1076.** Bailang Yu. An object-based two-stage method for a detailed classification of urban landscape components by integrating airborne LiDAR and color infrared image data: A case study of downtown Houston. / Bailang Yu, Hongxing Liu, Li Zhang, Jianping Wu. // 2009 Joint Urban Remote Sensing Event. - Shanghai, 20-22 May 2009. - P. 1-8. ↑

- C1077.** Bonano M. Advanced interferometric techniques for monitoring urban areas. / Bonano M., Fornaro G., Lanari R., Manunta M., Reale D., Serafino F. // 2009 Joint Urban Remote Sensing Event. - Shanghai, 20-22 May 2009. - P. 1-6. ↑
- C1078.** Hong Chi. Urban dynamic change detection using interferometric SAR in Southeast China. / Hong Chi, Guoqing Sun, Feilong Ling. // 2009 Joint Urban Remote Sensing Event. - Shanghai, 20-22 May 2009. - P. 1-9. ↑
- C1079.** Shilai Cheng. SAR interferometry atmospheric mitigation from GPS water vapor retrieval in Hong Kong. / Shilai Cheng, Hui Lin, Liming Jiang, Fulong Chen, Qing Zhao. // 2009 Joint Urban Remote Sensing Event. - Shanghai, 20-22 May 2009. - P. 1-6. ↑
- C1080.** Wurm M. Urban structuring using multisensoral remote sensing data: By the example of the German cities Cologne and Dresden. / Wurm M., Taubenbock H., Roth A., Dech S. // 2009 Joint Urban Remote Sensing Event. - Shanghai, 20-22 May 2009. - P. 1-8. ↑
- C1081.** Xuexing Chen. Potential and status of high-resolution remote sensing information applied in urban planning in China. / Xuexing Chen, Zhongmei Li, Mingbo Zhang. // 2009 Joint Urban Remote Sensing Event. - Shanghai, 20-22 May 2009. - P. 1-5. ↑
- C1082.** Hernandez J. Point cloud segmentation towards urban ground modeling. / Hernandez J., Marcotegui B. // 2009 Joint Urban Remote Sensing Event. - Shanghai, 20-22 May 2009. - P. 1-5. ↑
- C1083.** Walsh J. The second-order monostatic HF radar cross section incorporating antenna barge motion. / Walsh J., Weimin Huang, Gill E. // 2009. CCECE 09. Canadian Conference on Electrical and Computer Engineering. - St. John's, NL, 3-6 May 2009. - P. 19-22. ↑
- C1084.** McCaughan A. "Biomedical innovation lessons learned during the MCAMS discovery process". 2009. BSEC 2009. First Annual ORNL Biomedical Science & Engineering Conference. - Oak Ridge, TN, 18-19 March 2009. - P. 1-2. ↑
- C1085.** Huang Qihuan. SAR interferometry for long term deformation mapping using SBAS method: A case study in Nanjing area. / Huang Qihuan, He Xiufeng. // 2009 Joint Urban Remote Sensing Event. - Shanghai, 20-22 May 2009. - P. 1-5. ↑
- C1086.** Samad A.M. A comparison of AIRSAR and SPOT imagery for land cover mapping. / Samad A.M., Haron N.S., Karnadi M.S., Maarof I. // 2009. CSPA 2009. 5th International Colloquium on Signal Processing & Its Applications. - Kuala Lumpur, 6-8 March 2009. - P. 93-97. ↑
- C1087.** Zakharov I. Information assessment for polarimetric SAR intensity images. / Zakharov I., Toutin T. // 2009. CWIT 2009. 11th Canadian Workshop on Information Theory. - Ottawa, ON, 13-15 May 2009. - P. 71-74. ↑
- C1088.** Hourui. Orthorectification of TerraSAR-X Images Based on Precise Orbit Information. / Hourui, Tan Zhixiang, Huang Guoman. // 2009. ISA 2009. International Workshop on Intelligent Systems and Applications. - Wuhan, 23-24 May 2009. - P. 1-4. ↑
- C1089.** Wang Xiaojun. Fast evaluation for speckle feature in urban SAR images. / Wang Xiaojun, Meng Cangzeng, Yan Shusheng, Wang Helei, Liu Yang. // 2009 Joint Urban Remote Sensing Event. - Shanghai, 20-22 May 2009. - P. 1-5. ↑
- C1090.** Lei Pang. Three-dimension information extracting from high resolution airborne Synthetic Aperture Radar images. / Lei Pang, Wenli Meng, Hongdong Fan. // 2009 Joint Urban Remote Sensing Event. - Shanghai, 20-22 May 2009. - P. 1-5. ↑
- C1091.** Chen Rong. A modified method for relevance feedback in high-resolution SAR image retrieval system based on SVM. / Chen Rong, Cao Yongfeng, Sun Hong. // 2009 Joint Urban Remote Sensing Event. - Shanghai, 20-22 May 2009. - P. 1-8. ↑
- C1092.** Wegner J.D. Building extraction in urban scenes from high-resolution InSAR data and optical imagery. / Wegner J.D., Soergel U., Thiele A. // 2009 Joint Urban Remote Sensing Event. - Shanghai, 20-22 May 2009. - P. 1-6. ↑

- C1093.** Adam N. Coherent stacking with TerraSAR-X imagery in urban areas. / Adam N., Xiaoxiang Zhu, Bamler R. // 2009 Joint Urban Remote Sensing Event. - Shanghai, 20-22 May 2009. - P. 1-6. ↑
- C1094.** Zhaohui Yang. Automatic recognition of man-made objects in SAR images using support vector machines. / Zhaohui Yang, Qun Su, Yingying Chen. // 2009 Joint Urban Remote Sensing Event. - Shanghai, 20-22 May 2009. - P. 1-5. ↑
- C1095.** Baselice F. DEM reconstruction in urban scenario. / Baselice F., Budillon A., Ferraioli G., Pascazio V. // 2009 Joint Urban Remote Sensing Event. - Shanghai, 20-22 May 2009. - P. 1-5. ↑
- C1096.** Yang Cheng-sheng. Surface subsidence and ground fissures activity monitoring based on D-InSAR: A case of Datong city. / Yang Cheng-sheng, Zhang Qin, Zhao Chao-ying, Qu Wei, Ji Ling-yun, Zhang Jing. // 2009 Joint Urban Remote Sensing Event. - Shanghai, 20-22 May 2009. - P. 1-6. ↑
- C1097.** Jianhua Mao. Building extraction by fusion of LIDAR data and aerial images. / Jianhua Mao, Xuefeng Liu, Qihong Zeng. // 2009 Joint Urban Remote Sensing Event. - Shanghai, 20-22 May 2009. - P. 1-5. ↑
- C1098.** Yuan Feng. Urban DEM generation from airborne Lidar data. / Yuan Feng, Zhang Ji-xian, Zhang Li, Gao Jing-xiang. // 2009 Joint Urban Remote Sensing Event. - Shanghai, 20-22 May 2009. - P. 1-5. ↑
- C1099.** Tooke T.R. Assessment of urban tree shade using fused LIDAR and high spatial resolution imagery. / Tooke T.R., Coops N.C., Voogt J.A. // 2009 Joint Urban Remote Sensing Event. - Shanghai, 20-22 May 2009. - P. 1-6. ↑
- C1100.** Roychowdhury K. Assessing the utility of DMSP/OLS night-time images for characterizing indian urbanization. / Roychowdhury K., Jones S., Arrowsmith C. // 2009 Joint Urban Remote Sensing Event. - Shanghai, 20-22 May 2009. - P. 1-7. ↑
- C1101.** Hangbin Wu. Water feature extraction from aerial-image fused with airborne LIDAR data. / Hangbin Wu, Chun Liu, Yunling Zhang, Weiwei Sun. // 2009 Joint Urban Remote Sensing Event. - Shanghai, 20-22 May 2009. - P. 1-7. ↑
- C1102.** Ye Tian. Road tracking by circular template matching from high resolution remotely sensed imagery. / Ye Tian, Haitao Li, Haiyan Gu, Xiangguo Lin. // 2009 Joint Urban Remote Sensing Event. - Shanghai, 20-22 May 2009. - P. 1-5. ↑
- C1103.** Liu Guang. Mining area subsidence monitoring using multi-band SAR data. / Liu Guang, Guo Huadong, Fan Jinghui, Guo Xiaofang, Perski Z., Yue Huanyin. // 2009 Joint Urban Remote Sensing Event. - Shanghai, 20-22 May 2009. - P. 1-6. ↑
- C1104.** Jianguo He. Monitoring ground subsidence in mining area using spaceborne InSAR technology. / Jianguo He, Guang Liu, Huanyin Yue. // 2009 Joint Urban Remote Sensing Event. - Shanghai, 20-22 May 2009. - P. 1-6. ↑
- C1105.** Daqing Ge. Monitoring urban subsidence with coherent point target SAR interferometry. / Daqing Ge, Yan Wang, Ling Zhang, Yi Wang, Qiong Hu. // 2009 Joint Urban Remote Sensing Event. - Shanghai, 20-22 May 2009. - P. 1-4. ↑
- C1106.** Lei Zhang. Ground settlement monitoring from temporarily persistent scatterers between two SAR acquisitions. / Lei Zhang, Xiaoli Ding, Guangcai Feng, Zhong Lu. // 2009 Joint Urban Remote Sensing Event. - Shanghai, 20-22 May 2009. - P. 1-5. ↑
- C1107.** Weian Wang. A method of deriving features of building from LIDAR point clouds in urban area. / Weian Wang, Bo Zheng, Jue Lu, Jiao Lu, Yi Liu. // 2009 Joint Urban Remote Sensing Event. - Shanghai, 20-22 May 2009. - P. 1-5. ↑
- C1108.** Ying Lin. Non-parametric multiple level set model for efficient image classification in urban areas. / Ying Lin, Yun Yang. // 2009 Joint Urban Remote Sensing Event. - Shanghai, 20-22 May 2009. - P. 1-6. ↑
- C1109.** Gamba P. A detailed comparison between two fast approaches to urban extent extraction in VHR SAR images. / Gamba P., Aldrichi M., Stasolla M., Sirtori E. // 2009 Joint Urban Remote Sensing Event. - Shanghai, 20-22 May 2009. - P. 1-6. ↑

- C1110.** Gamba P. BREC: The Built-up area RECOgnition tool. / Gamba P., Dell'Acqua F., Lisini G. // 2009 Joint Urban Remote Sensing Event. - Shanghai, 20-22 May 2009. - P. 1-5. ↑
- C1111.** Dell'Acqua F. Segment-based urban block outlining in high-resolution SAR images. / Dell'Acqua F., Gamba P., Odasso L., Lisini G. // 2009 Joint Urban Remote Sensing Event. - Shanghai, 20-22 May 2009. - P. 1-6. ↑
- C1112.** Wiman H. Fast compression and access of LiDAR point clouds using wavelets. / Wiman H., Yuchu Qin. // 2009 Joint Urban Remote Sensing Event. - Shanghai, 20-22 May 2009. - P. 1-6. ↑
- C1113.** Yang Fan. The application of remote sensing technology in monitoring environmental disasters of mining cities. / Yang Fan, Shao Yang, Ma Guichen, Qin Zhenzhen. // 2009 Joint Urban Remote Sensing Event. - Shanghai, 20-22 May 2009. - P. 1-5. ↑
- C1114.** Jia Weijie. Automatic registration of SAR and optics image based on multi-features on suburban areas. / Jia Weijie, Zhang Jixian, Yang Jinghui. // 2009 Joint Urban Remote Sensing Event. - Shanghai, 20-22 May 2009. - P. 1-7. ↑
- C1115.** Qing Zhao. Analysis of active ground subsidence zones in Guangzhou city using ASAR Persistent Scatterer Interferometry. / Qing Zhao, Hui Lin, Yuanzhi Zhang, Liming Jiang, Fulong Chen, Shilai Cheng. // 2009 Joint Urban Remote Sensing Event. - Shanghai, 20-22 May 2009. - P. 1-5. ↑
- C1116.** Hui Long. An automatic method on detecting image control points from SAR imagery based on Optical Image Patches. / Hui Long, Kun Fu, Chuanzhao Han. // 2009 Joint Urban Remote Sensing Event. - Shanghai, 20-22 May 2009. - P. 1-4. ↑
- C1117.** Deng Biao. The utilization of SAR remote sensing and GIS technology to delineate urban extent in North China. / Deng Biao, Guo Huadong, Nie Yueping. // 2009 Joint Urban Remote Sensing Event. - Shanghai, 20-22 May 2009. - P. 1-5. ↑
- C1118.** Wen Yang. Supervised land-cover classification of TerraSAR-X imagery over urban areas using extremely randomized clustering forests. / Wen Yang, Tongyuan Zou, Dengxin Dai, Yongmin Shuai. // 2009 Joint Urban Remote Sensing Event. - Shanghai, 20-22 May 2009. - P. 1-6. ↑
- C1119.** Zhou Mei. A classification method for building detection based on LiDAR point clouds. / Zhou Mei, Xia Bing, Su Guozhong, Tang Lingli, Li Chanrong. // 2009 Joint Urban Remote Sensing Event. - Shanghai, 20-22 May 2009. - P. 1-5. ↑
- C1120.** Tanyer-Tigrek F.M. Design of an AMC plane for a unidirectional, low-profile tulip-loop antenna. / Tanyer-Tigrek F.M., Mateos R.M., Craeye C., Lager I.E. // 2009. EuCAP 2009. 3rd European Conference on Antennas and Propagation. - Berlin, 23-27 March 2009. - P. 3139-3142. ↑
- C1121.** Yang Xin. The Global Road Extraction Approach from Synthetic Aperture Radar Images. / Yang Xin, Huang Shunji. // 2009. ICTD 2009. IEEE Circuits and Systems International Conference on Testing and Diagnosis. - Chengdu, 28-29 April 2009. - P. 1-3. ↑
- C1122.** Ding Guo. Wave Simulation of SAR Signal for Two-Dimensions Sea Surface. / Ding Guo, Xingfa Gu, Tao Yu, Xiaoyin Li, Hui Xu, Hongtao Ma. // 2009. ICTD 2009. IEEE Circuits and Systems International Conference on Testing and Diagnosis. - Chengdu, 28-29 April 2009. - P. 1-4. ↑
- C1123.** Akhtar J. Cancellation of range ambiguities with block coding techniques. 2009 IEEE Radar Conference. - Pasadena, CA, 4-8 May 2009. - P. 1-6. ↑
- C1124.** Castillo Atoche A. Systolic array implementations for real time enhancement of remote sensing imaging. / Castillo Atoche A., Aguilar J.O., Castillo J.V. // 2009. SPL. 5th Southern Conference on Programmable Logic. - Sao Carlos, 1-3 April 2009. - P. 59-64. ↑
- C1125.** Wei Shen. Sea Wind Power Energy Evaluation by HF Radar System. / Wei Shen, Biyang We. // 2009. APPEEC 2009. Asia-Pacific Power and Energy Engineering Conference. - Wuhan, 27-31 March 2009. - P. 1-4. ↑
- C1126.** Wei Shen. UHF Radar Designed for Inshore Wave Watcher and Ocean Power Application. / Wei Shen, Biyang Wen, Fan Ding. // 2009. APPEEC 2009. Asia-Pacific Power and Energy Engineering Conference. -

Wuhan, 27-31 March 2009. - P. 1-4. ↑

**C1127.** Podilchak S.K. Radar cross-section modeling of marine vessels in practical oceanic environments for high-frequency surface-wave radar. / Podilchak S.K., Leong H., Solomon R., Antar Y. // 2009 IEEE Radar Conference. - Pasadena, CA, 4-8 May 2009. - P. 1-6. ↑

**C1128.** Uppuluri A.V. Application of passive microwave data in estimating freeze-thaw dates of a small lake. / Uppuluri A.V., Jost R.J., Luecke C., White M.A. // 2009 IEEE Radar Conference. - Pasadena, CA, 4-8 May 2009. - P. 1-5. ↑

**C1129.** Fischman M. Development and integration of the aquarius scatterometer processor/control electronics for achieving high measurement accuracy. / Fischman M., Freedman A., McWatters D., Berkun A., Cheetham C., Chu A., Lee S., Neumann G., Paller M., Tieu B., Wirth J., Wu C. // 2009 IEEE Radar Conference. - Pasadena, CA, 4-8 May 2009. - P. 1-6. ↑

**C1130.** Simpson R.A. Bistatic radar probing of planetary surfaces. / Simpson R.A., Tyler G.L., Hausler B., Patzold M., Asmar S. // 2009 IEEE Radar Conference. - Pasadena, CA, 4-8 May 2009. - P. 1-4. ↑

**C1131.** Chan S. RFI study for the SMAP radar. / Chan S., Spencer M. // 2009 IEEE Radar Conference. - Pasadena, CA, 4-8 May 2009. - P. 1-5. ↑

**C1132.** Williams C.R. Accuracy of reflectivity estimated from profiling radars. 2009 IEEE Radar Conference. - Pasadena, CA, 4-8 May 2009. - P. 1-4. ↑

**C1133.** Schreiber E. First design investigations on a fully-electronic microwave imaging radiometer system. / Schreiber E., Peichl M., Suss H. // 2009 German Microwave Conference. - Munich, 16-18 March 2009. - P. 1-4. ↑

**C1134.** Lucente M. An innovative multimode millimeter wave radar for Moon remote sensing. / Lucente M., Dainelli V., Dionisio C., Noce M. // 2009 IEEE Aerospace conference. - Big Sky, MT, 7-14 March 2009. - P. 1-8. ↑

**C1135.** Calamia M. Comparison and integration of GPS and DInSAR deformation time-series. / Calamia M., Franceschetti G., Lanari R., Casu F., Manzo M. // 2009 IEEE Aerospace conference. - Big Sky, MT, 7-14 March 2009. - P. 1-9. ↑

**C1136.** Zhou Jieping. A Collaboration Mobile System for Epidemiology Investigation in the Wenchuan Earthquake-Stricken Area. / Zhou Jieping, Zhang Lihui, Li Wenhong, Gong Jianhua, Fang Liquan, Cao Wuchun. // 2009. CMC '09. WRI International Conference on Communications and Mobile Computing. - Yunnan, 6-8 Jan. 2009. - Vol. 3. - P. 253-257. ↑

**C1137.** Paichard Y. Orthogonal multicarrier phased coded signal for netted radar systems. 2009 International Waveform Diversity and Design Conference. - Kissimmee, FL, 8-13 Feb. 2009. - P. 234-236. ↑

**C1138.** Paichard Y. A signal level simulator for netted radar waveforms evaluation. / Paichard Y., Brooker M., Inggs M. // 2009 International Waveform Diversity and Design Conference. - Kissimmee, FL, 8-13 Feb. 2009. - P. 278-280. ↑

**C1139.** MacDonald A. Advances in tactical laser radar. 2009 IEEE Aerospace conference. - Big Sky, MT, 7-14 March 2009. - P. 1-10. ↑

**C1140.** Fischman M. Low-noise detector with RFI mitigation capability for the Aquarius L-band scatterometer. / Fischman M., Freedman A., McWatters D., Berkun A., Cheetham C., Chu A., Lee S., Neumann G., Paller M., Tieu B., Wirth J., Wu C. // 2009 IEEE Aerospace conference. - Big Sky, MT, 7-14 March 2009. - P. 1-9. ↑

**C1141.** Shen-Shyang Ho. Automated cyclone tracking using multiple remote satellite data via knowledge transfer. / Shen-Shyang Ho, Talukder A. // 2009 IEEE Aerospace conference. - Big Sky, MT, 7-14 March 2009. - P. 1-7. ↑

**C1142.** Stoker D.S. LIDAR versus satellite-measured optical thickness of a wildfire aerosol. / Stoker D.S., Fathi G., Ionov P., Beck S.M. // 2009 IEEE Aerospace conference. - Big Sky, MT, 7-14 March 2009. - P. 1-6. ↑

**C1143.** Heaps W.S. Precision column CO2 measurement from space using broad band LIDAR. 2009 IEEE

Aerospace conference. - Big Sky, MT, 7-14 March 2009. - P. 1-7. ↑

C1144. Jordan S. Range estimation algorithms comparison in simulated 3-D flash LADAR data. 2009 IEEE Aerospace conference. - Big Sky, MT, 7-14 March 2009. - P. 1-7. ↑

C1145. Capraro G.T. Waveform diversity and knowledge based signal processing in distributed radar. / Capraro G.T., Wicks M.C., Szczepanski W.E. // 2009 IEEE Radar Conference. - Pasadena, CA, 4-8 May 2009. - P. 1-6. ↑

C1146. Plettmeier D. Full polarimetric GPR antenna system aboard the ExoMars rover. / Plettmeier D., Ciarletti V., Hamran S.-E., Corbel C., Cais P., Benedix W.-S., Wolf K., Linke S., Roddecke S. // 2009 IEEE Radar Conference. - Pasadena, CA, 4-8 May 2009. - P. 1-6. ↑

C1147. Johnson W. A study of a potential venus radar topography mission. / Johnson W., Jordan R., Veilleux L., Hodges R., Giersch L. // 2009 IEEE Radar Conference. - Pasadena, CA, 4-8 May 2009. - P. 1-2. ↑

C1148. Prat O.P. Combining a rain microphysical model and observations: Implications for radar rainfall estimation. / Prat O.P., Barros A.P. // 2009 IEEE Radar Conference. - Pasadena, CA, 4-8 May 2009. - P. 1-4. ↑

C1149. Brcic R. Interferometric absolute phase determination with TerraSAR-X wideband SAR data. / Brcic R., Eineder M., Bamler R. // 2009 IEEE Radar Conference. - Pasadena, CA, 4-8 May 2009. - P. 1-6. ↑

C1150. Voo J.K. Recent experiments in Ocean remote sensing with bistatic radar using Navigation Satellite Signals. / Voo J.K., Garrison J.L., Haase J.S., Lulich T.D. // 2009 IEEE Radar Conference. - Pasadena, CA, 4-8 May 2009. - P. 1-6. ↑

C1151. Tanelli S. Next-generation spaceborne Cloud Profiling Radars. / Tanelli S., Durden S.L., Im E., Heymsfield G.M., Racette P., Starr D.O. // 2009 IEEE Radar Conference. - Pasadena, CA, 4-8 May 2009. - P. 1-4. ↑

C1152. Rott H. CoReH2 O-Cold Regions Hydrology High-resolution Observatory. / Rott H., Cline D., Duguay C., Essery R., Haas C., Kern M., Macelloni G., Malnes E., Pulliainen J., Rebhan H., Yueh S. // 2009 IEEE Radar Conference. - Pasadena, CA, 4-8 May 2009. - P. 1-4. ↑

C1153. Werner C. A ground-based real-aperture radar instrument for differential interferometry. / Werner C., Strozzi T., Wiesmann A., Wegmuller U. // 2009 IEEE Radar Conference. - Pasadena, CA, 4-8 May 2009. - P. 1-4. ↑

C1154. Russchenberg H. Integrated atmospheric profiling for satellite communication. 2009. EuCAP 2009. 3rd European Conference on Antennas and Propagation. - Berlin, 23-27 March 2009. - P. 916-919. ↑

C1155. Pathe C. Scatterometer and ScanSAR soil moisture observations of the contiguous United States. / Pathe C., Wagner W., Sabel D., Bartalis Z., Doubkova M., Naeimi V. // 2009 IEEE Radar Conference. - Pasadena, CA, 4-8 May 2009. - P. 1-4. ↑

C1156. Leshkevich G.A. Using satellite radar data to map and monitor variations in Great Lakes ice cover. / Leshkevich G.A., Nghiem S.V. // 2009 IEEE Radar Conference. - Pasadena, CA, 4-8 May 2009. - P. 1-3. ↑

C1157. Blom R.G. The green Sahara: Climate change, hydrologic history and human occupation. / Blom R.G., Farr T.G., Feynmann J., Ruzmaikin A., Paillou P. // 2009 IEEE Radar Conference. - Pasadena, CA, 4-8 May 2009. - P. 1-4. ↑

C1158. Krieger G. The tandem-L mission proposal: Monitoring earth's dynamics with high resolution SAR interferometry. / Krieger G., Hajnsek I., Papathanassiou K., Eineder M., Younis M., De Zan F., Prats P., Huber S., Werner M., Fiedler H., Freeman A., Rosen P., Hensley S., Johnson W., Veilleux L., Grafmueller B., Werninghaus R., Bamler R., Moreira A. // 2009 IEEE Radar Conference. - Pasadena, CA, 4-8 May 2009. - P. 1-6. ↑

C1159. Euillades L. RADARSAT-1 deformation time-series generation by using the SBAS-DInSAR algorithm. / Euillades L., Pepe A., Berardino P., Bonano M., Sansosti E., Lanari R. // 2009 IEEE Radar Conference. - Pasadena, CA, 4-8 May 2009. - P. 1-4. ↑

↑

- C1160.** Heliere F. Cold region hydrology high-resolution observatory (CoReH2 O): A new microwave earth explorer core mission candidate. / Heliere F., Lin C.C., Fois F., Kern M., Thompson A., Bensi P. // 2009 IEEE Radar Conference. - Pasadena, CA, 4-8 May 2009. - P. 1-6. ↑
- C1161.** Baldini L. Ground validation of satellite measurements of precipitation with C-band polarimetric radar. / Baldini L., Gorgucci E., Romaniello V., Chandrasekar V. // 2009 IEEE Radar Conference. - Pasadena, CA, 4-8 May 2009. - P. 1-4. ↑
- C1162.** Weissman D.E. The combined effect of surface rain and wind on scatterometer observations of surface roughness. / Weissman D.E., Bourassa M.A. // 2009 IEEE Radar Conference. - Pasadena, CA, 4-8 May 2009. - P. 1-5. ↑
- C1163.** Krieger G. THE TanDEM-X Mission: Overview and status. / Krieger G., Zink M., Fiedler H., Hajnsek I., Younis M., Huber S., Bachmann M., Gonzalez J.H., Schulze D., Boer J., Werner M., Moreira A. // 2009 IEEE Radar Conference. - Pasadena, CA, 4-8 May 2009. - P. 1-5. ↑
- C1164.** Rodriguez E. A scatterometer for XOVWM, the Extended Ocean Vector Winds Mission. / Rodriguez E., Gaston R.W., Durden S.L., Stiles B., Spencer M., Veilleux L., Hughes R., Fernandez D.E., Chan S., Veleza S., Dunbar R.S. // 2009 IEEE Radar Conference. - Pasadena, CA, 4-8 May 2009. - P. 1-4. ↑
- C1165.** Long D.G. The TropSat mission: An observatory for mesoscale convective system processes in the global tropics. / Long D.G., Milliff R., Rodriguez E. // 2009 IEEE Radar Conference. - Pasadena, CA, 4-8 May 2009. - P. 1-6. ↑
- C1166.** Lehner S. Coastal wind field and sea state measured by TerraSAR-X. / Lehner S., Brusch S., Li X. // 2009 IEEE Radar Conference. - Pasadena, CA, 4-8 May 2009. - P. 1-3. ↑
- C1167.** Fritz J. Simultaneous observations of a tropical cyclone from dual-pol TerraSAR-X and ground-based weather radar. / Fritz J., Chandrasekar V. // 2009 IEEE Radar Conference. - Pasadena, CA, 4-8 May 2009. - P. 1-6. ↑
- C1168.** Heliere F. BIOMASS: A P-band SAR earth explorer core mission candidate. / Heliere F., Lin C.C., Fois F., Davidson M., Thompson A., Bensi P. // 2009 IEEE Radar Conference. - Pasadena, CA, 4-8 May 2009. - P. 1-6. ↑
- C1169.** Wooram Lee. Picosecond pulse generation on CMOS: Design beyond transistor limits. / Wooram Lee, Amoozegar F., Afshari E. // 2009 IEEE Radar Conference. - Pasadena, CA, 4-8 May 2009. - P. 1-6. ↑
- C1170.** Barnes N.P. Tm:germanate fiber laser for planetary water vapor atmospheric profiling. / Barnes N.P., De Young R. // 2009 and 2009 Conference on Quantum electronics and Laser Science Conference. CLEO/QELS 2009. Conference on Lasers and Electro-Optics. - Baltimore, MD, 2-4 June 2009. - P. 1-2. ↑
- C1171.** Khazaal A. SMOS image reconstruction algorithm: Extension of the band limited approach to the fully-polarimetric mode of MIRAS. / Khazaal A., Anterrieu E. // 2009. ACTEA '09. International Conference on Advances in Computational Tools for Engineering Applications. - Zouk Mosbeh, 15-17 July 2009. - P. 180-185. ↑
- C1172.** Xiaoming Zhou. Filter of LIDAR Data Based on Multi-Resolution and Directional Elevation Tolerance. / Xiaoming Zhou, Qiuhe Ma, Ersen Li, Dejin Tang. // 2009. SOPO 2009. Symposium on Photonics and Optoelectronics. - Wuhan, 14-16 Aug. 2009. - P. 1-4. ↑
- C1173.** Dobbs M. A multi-functional fiber laser lidar for Earth Science & Exploration. / Dobbs M., Krabill W., Cisewski M., Harrison F.W., Shum C.K., McGregor D., Neal M., Stokes S. // 2009 and 2009 Conference on Quantum electronics and Laser Science Conference. CLEO/QELS 2009. Conference on Lasers and Electro-Optics. - Baltimore, MD, 2-4 June 2009. - P. 1-2. ↑
- C1174.** Kamali Y. Remote detection of aluminum and trace methane using mobile femtosecond laser system of T&T Lab. / Kamali Y., Daigle J.-F., Simard P.T., Theberge F., Chateaufneuf M., Xu H.L., Azarm A., Chen Y., Marceau C., Sun Z.-D., Bernhardt J., Lessard S.C., Lessard F., Roy G., Dubois J., Chin S.L. // 2009 and 2009 Conference on Quantum electronics and Laser Science Conference. CLEO/QELS 2009. Conference on Lasers and Electro-Optics. - Baltimore, MD, 2-4 June 2009. - P. 1-2. ↑
- C1175.** Abshire J.B. Modified PN codes for laser remote sensing measurements. / Abshire J.B., Xiaoli Sun. //

2009 and 2009 Conference on Quantum electronics and Laser Science Conference. CLEO/QELS 2009. Conference on Lasers and Electro-Optics. - Baltimore, MD, 2-4 June 2009. - P. 1-2. ↑

**C1176.** Anan Fang. Design of Wireless Environmental Monitoring Data Acquisition System Based on Cortex. / Anan Fang, Rihua He. // 2009. PACCS '09. Pacific-Asia Conference on Circuits, Communications and Systems. - Chengdu, 16-17 May 2009. - P. 78-80. ↑

**C1177.** Kaihua Xu. Achieving the Real-time rectification of remote sensing data based on 4S integration in handset. / Kaihua Xu, Puyao Qiao, Yuhua Liu, Jian Cheng. // 2009. ICCSIT 2009. 2nd IEEE International Conference on Computer Science and Information Technology. - Beijing, 8-11 Aug. 2009. - P. 575-579. ↑

**C1178.** Rachmana N. Interpretation target pattern of a buried basic object on Surface Ground Penetrating Radar system. / Rachmana N., Hendrawan, Sugihartono, Suksmono A.B. // 2009. ICEEI '09. International Conference on Electrical Engineering and Informatics. - Selangor, 5-7 Aug. 2009. - Vol. 02. - P. 553-558. ↑

**C1179.** Wong A. SEC: Stochastic Ensemble Consensus Approach to Unsupervised SAR Sea-Ice Segmentation. / Wong A., Clausi D.A., Fieguth P. // 2009. CRV '09. Canadian Conference on Computer and Robot Vision. - Kelowna, BC, 25-27 May 2009. - P. 299-305. ↑

**C1180.** Wong A. IceSynth: An Image Synthesis System for Sea-Ice Segmentation Evaluation. / Wong A., Wen Zhang, Clausi D.A. // 2009. CRV '09. Canadian Conference on Computer and Robot Vision. - Kelowna, BC, 25-27 May 2009. - P. 178-183. ↑

**C1181.** Zhang Zhiyu. SAR Image Processing Based on Fast Discrete Curvelet Transform. / Zhang Zhiyu, Zhang Xiaodan, Zhang Jiulong. // 2009. IFITA '09. International Forum on Information Technology and Applications. - Chengdu, 15-17 May 2009. - Vol. 3. - P. 28-31. ↑

**C1182.** Wu Dan. Application of the Marine Oil Spill Surveillance by Satellite Remote Sensing. / Wu Dan, Shen Jifeng, Zhang Yongzhi, Zhao Pu. // 2009. ESIAT 2009. International Conference on Environmental Science and Information Application Technology. - Wuhan, 4-5 July 2009. - Vol. 1. - P. 505-508. ↑

**C1183.** Wang Xiu-ping. Developments of GNSS Radio Occultation for Sounding Atmosphere. 2009. ESIAT 2009. International Conference on Environmental Science and Information Application Technology. - Wuhan, 4-5 July 2009. - Vol. 1. - P. 653-656. ↑

**C1184.** Klonus S. Performance of evaluation methods in image fusion. / Klonus S., Ehlers M. // 2009. FUSION '09. 12th International Conference on Information Fusion. - Seattle, WA, 6-9 July 2009. - P. 1409-1416. ↑

**C1185.** Wang Zhiyong. Monitoring Co-seismic Deformation Fields of Bam Earthquake Using D-InSAR Technique. / Wang Zhiyong, Zhang Jixian, Huang Guoman. // 2009. ESIAT 2009. International Conference on Environmental Science and Information Application Technology. - Wuhan, 4-5 July 2009. - Vol. 2. - P. 487-490. ↑

**C1186.** Zhiyong Li. Using LiDAR Data Visualization to Investigate Origin of Uphill-Facing Scarps in Mountains, Alaska. / Zhiyong Li, Zuoxun Zeng, Bruhn R.L. // 2009. ESIAT 2009. International Conference on Environmental Science and Information Application Technology. - Wuhan, 4-5 July 2009. - Vol. 1. - P. 84-87. ↑

**C1187.** Long Sichun. Application Study of PS-DInSAR Technique Fusing Multi-metadata in Urban Ground Deformation Survey. / Long Sichun, Li Tao, Liu Jingnan. // 2009. ESIAT 2009. International Conference on Environmental Science and Information Application Technology. - Wuhan, 4-5 July 2009. - Vol. 1. - P. 326-330. ↑

**C1188.** Abshire J.B. Airborne measurements of CO2 column absorption using a pulsed wavelength-scanned laser sounder instrument. / Abshire J.B., Riris H., Hasselbrack B., Allan G., Weaver C., Jianping Mao. // 2009 and 2009 Conference on Quantum electronics and Laser Science Conference. CLEO/QELS 2009. Conference on Lasers and Electro-Optics. - Baltimore, MD, 2-4 June 2009. - P. 1-2. ↑

**C1189.** Dogariu A. Atomic oxygen detection using radar REMPI. / Dogariu A., Michael J., Stockman E., Miles R. // 2009 and 2009 Conference on Quantum electronics and Laser Science Conference. CLEO/QELS 2009. Conference on Lasers and Electro-Optics. - Baltimore, MD, 2-4 June 2009. - P. 1-2. ↑

**C1190.** Buck J.R. Synthetic aperture imaging at optical wavelengths. / Buck J.R., Krause B.W., Malm A., Ryan C.M. // 2009 and 2009 Conference on Quantum electronics and Laser Science Conference. CLEO/QELS 2009.

Conference on Lasers and Electro-Optics. - Baltimore, MD, 2-4 June 2009. - P. 1-2. ↑

**C1191.** Dhar J. Performance enhancement of pulsed solid state power amplifier using Drain Modulation over Gate Modulation. / Dhar J., Arora R.K., Garg S.K., Patel M.K., Bakori B.V. // 2009. ISSCS 2009. International Symposium on Signals, Circuits and Systems. - Iasi, 9-10 July 2009. - P. 1-4. ↑

**C1192.** Poullis C. Automatic reconstruction of cities from remote sensor data. / Poullis C., You S. // 2009. CVPR 2009. IEEE Conference on Computer Vision and Pattern Recognition. - Miami, FL, 20-25 June 2009. - P. 2775-2782. ↑

**C1193.** Luo Peng. A Study on Quantitative Radar Rainfall Measurements by the Method of Set-pair Analysis. / Luo Peng, Song Xingyuan, Tian Wenwen. // 2009. GCIS '09. WRI Global Congress on Intelligent Systems. - Xiamen, 19-21 May 2009. - Vol. 2. - P. 385-388. ↑

**C1194.** Jinhui Lan. New approach of imagery generation and target recognition based on 3D LIDAR data. / Jinhui Lan, Zhuoxun Shen. // 2009. ICEMI '09. 9th International Conference on Electronic Measurement & Instruments. - Beijing, 16-19 Aug. 2009. - P. 1-612-1-616-612. ↑

**C1195.** Zhao Lingjun. Rapid Calculation Research on Water Area Extraction from ASAR Image. / Zhao Lingjun, Ma Yan, Li Guoqing, Yu Wenyang, Zhang Jing. // 2009. GCC '09. Eighth International Conference on Grid and Cooperative Computing. - Lanzhou, Gansu, 27-29 Aug. 2009. - P. 339-343. ↑

**C1196.** Schwarz U. Design and application of dielectrically scaled double-ridged horn antennas for biomedical UWB radar applications. / Schwarz U., Helbig M., Sachs J., Stephan R., Hein M.A. // 2009. ICUWB 2009. IEEE International Conference on Ultra-Wideband. - Vancouver, BC, 9-11 Sept. 2009. - P. 150-154. ↑

**C1197.** Kurz T.H. Close range hyperspectral and lidar data integration for geological outcrop analysis. / Kurz T.H., Buckley S.J., Howell J.A., Schneider D. // 2009. WHISPERS '09. First Workshop on Hyperspectral Image and Signal Processing: Evolution in Remote Sensing. - Grenoble, 26-28 Aug. 2009. - P. 1-4. ↑

**C1198.** Hessner K. High resolution current & bathymetry determined by nautical X-Band radar in shallow waters. / Hessner K., Bell P.S. // OCEANS 2009-EUROPE. - Bremen, 11-14 May 2009. - P. 1-5. ↑

**C1199.** Lurton T. Simulation of the radar observation of a sea patch using the TLM electromagnetic method. / Lurton T., Sintès C., Garelo R. // OCEANS 2009-EUROPE. - Bremen, 11-14 May 2009. - P. 1-7. ↑

**C1200.** Heron M.L. HF radar role in an integrated ocean observing system. / Heron M.L., Prytz A. // OCEANS 2009-EUROPE. - Bremen, 11-14 May 2009. - P. 1-4. ↑

**C1201.** Shiina T. Optical design for in-line typed compact lidar. / Shiina T., Fukuchi T., Asahi I., Sugimoto S., Shimamoto Y., Ninomiya H. // 2009. CLEO/PACIFIC RIM '09. Conference on Lasers & Electro Optics & The Pacific Rim Conference on Lasers and Electro-Optics. - Shanghai, 30-3 Aug. 2009. - P. 1-2. ↑

**C1202.** Sining Li. Simulation of morphological measurement system based on FM-CW. / Sining Li, Min Liu, Wei Lu, Yuhao Guang. // 2009. CLEO/PACIFIC RIM '09. Conference on Lasers & Electro Optics & The Pacific Rim Conference on Lasers and Electro-Optics. - Shanghai, 30-3 Aug. 2009. - P. 1-2. ↑

**C1203.** Dahish A.S. An application of Geographical Information System and Remote Sensing techniques for detection of oil spill. / Dahish A.S., Ahmad A. // 2009 17th International Conference on Geoinformatics. - Fairfax, VA, 12-14 Aug. 2009. - P. 1-4. ↑

**C1204.** Gnyp M.L. Hyperspectral data analysis of nitrogen fertilization effects on winter wheat using spectrometer in North China Plain. / Gnyp M.L., Fei Li, Yuxin Miao, Koppe W., Liangliang Jia, Xinping Chen, Fusuo Zhang, Bareth G. // 2009. WHISPERS '09. First Workshop on Hyperspectral Image and Signal Processing: Evolution in Remote Sensing. - Grenoble, 26-28 Aug. 2009. - P. 1-4. ↑

**C1205.** Niemann K.O. LiDAR-guided analysis of airborne hyperspectral data. / Niemann K.O., Frazer G., Loos R., Visintini F. // 2009. WHISPERS '09. First Workshop on Hyperspectral Image and Signal Processing: Evolution in Remote Sensing. - Grenoble, 26-28 Aug. 2009. - P. 1-4. ↑

**C1206.** Kameyama S. Development of fiber-based CW modulation DIAL system for CO2 monitoring. / Kameyama S., Imaki M., Ueno S., Hirano Y., Sakaizawa D., Kawakami S., Nakajima M. // 2009. CLEO/PACIFIC

RIM '09. Conference on Lasers & Electro Optics & The Pacific Rim Conference on Lasers and Electro-Optics. - Shanghai, 30-3 Aug. 2009. - P. 1. ↑

**C1207.** Marvaldi J. ROSE: development and demonstration of a "Mobile Response Observatory" prototype for subsea environmental monitoring. / Marvaldi J., Legrand J., Masset J.F., Delauney L., Nicot M., Barbot D., Degres Y., Jouannic M., Cabioch F., Guyomarch J., Billand P., Caujan A.M., Hibrat S., Laot C. // OCEANS 2009-EUROPE. - Bremen, 11-14 May 2009. - P. 1-8. ↑

**C1208.** Sedlacek S. Sediment modeling based on radar observed surface hydrodynamics. / Sedlacek S., Ziemer F., Cysewski M. // OCEANS 2009-EUROPE. - Bremen, 11-14 May 2009. - P. 1-5. ↑

**C1209.** Robla S. An approach for tracking oil slicks by using active contours on satellite images. / Robla S., Llata J.R., Torre C., Sarabia E.G. // OCEANS 2009-EUROPE. - Bremen, 11-14 May 2009. - P. 1-8. ↑

**C1210.** Danilo C. Sea surface current retrievals using ASAR WVW acquisitions. / Danilo C., Garello R. // OCEANS 2009-EUROPE. - Bremen, 11-14 May 2009. - P. 1-4. ↑

**C1211.** Kaminski L. Web-based GIS dedicated for marine environment surveillance and monitoring. / Kaminski L., Kulawiak M., Cizmowski W., Chybicki A., Stepnowski A., Orlowski A. // OCEANS 2009-EUROPE. - Bremen, 11-14 May 2009. - P. 1-7. ↑

**C1212.** Boschen F. On the influence of positioning errors on tomography-based sonar imaging systems. / Boschen F., Kummert A., Kraft A. // OCEANS 2009-EUROPE. - Bremen, 11-14 May 2009. - P. 1-6. ↑

**C1213.** Estable S. Detection and classification of offshore artificial objects in TerraSAR-X images: First outcomes of the DeMarine-DEKO project. / Estable S., Teufel F., Petersen L., Knabe S., Saur G., Ullmann T. // OCEANS 2009-EUROPE. - Bremen, 11-14 May 2009. - P. 1-8. ↑

**C1214.** Helzel T. Accuracy and reliability of ocean current and wave monitoring with the coastal radar "WERA". / Helzel T., Petersen L., Mariette V., Thomas N. // OCEANS 2009-EUROPE. - Bremen, 11-14 May 2009. - P. 1-5. ↑

**C1215.** Cococcioni M. Issues and preliminary results in oil spill detection using optical remotely sensed images. / Cococcioni M., Corucci L., Lazzerini B. // OCEANS 2009-EUROPE. - Bremen, 11-14 May 2009. - P. 1-4. ↑

**C1216.** Brusch S. Monitoring river estuaries and coastal areas using TerraSAR-X. / Brusch S., Held P., Lehner S. // OCEANS 2009-EUROPE. - Bremen, 11-14 May 2009. - P. 1-4. ↑

**C1217.** Xiao-Ming Li. Utilization of ASAR wave mode data for shipping safety. / Xiao-Ming Li, Lehner S. // OCEANS 2009-EUROPE. - Bremen, 11-14 May 2009. - P. 1-5. ↑

**C1218.** Romeiser R. High-resolution current measurements from space with TerraSAR-X along-track InSAR. / Romeiser R., Suchandt S., Runge H., Steinbrecher U. // OCEANS 2009-EUROPE. - Bremen, 11-14 May 2009. - P. 1-5. ↑

**C1219.** Gao Wei. Research on Land Use Supervision by Using High Resolution and Fully Polarizations Sar Data. / Gao Wei, Liu Xiuguo, Li Yongsheng, Wang Hongping, Xiao Lin. // 2009. ESIAT 2009. International Conference on Environmental Science and Information Application Technology. - Wuhan, 4-5 July 2009. - Vol. 2. - P. 245-248. ↑

**C1220.** Laneve G. Application of Mathematical Morphology to automatically extract roads on radar images. / Laneve G., Santilli G., Cadau E. // 2009 Joint Urban Remote Sensing Event. - Shanghai, 20-22 May 2009. - P. 1-5. ↑

**C1221.** Zhou Ligu. An investigation of urban water automatic extraction based on texture and imaging knowledge from high resolution SAR images. / Zhou Ligu, Feng Xuezhi, Xiao Pengfeng, Wan wei, Sheng Ye. // 2009 Joint Urban Remote Sensing Event. - Shanghai, 20-22 May 2009. - P. 1-6. ↑

**C1222.** Aldrighi M. Tile mapping of urban area extent in VHR SAR images. / Aldrighi M., Dell'Acqua F., Lisini G. // 2009 Joint Urban Remote Sensing Event. - Shanghai, 20-22 May 2009. - P. 1-5. ↑

- C1223.** Guoyuan Li. Airborne laser scanner point clouds strip adjustment aided by photogrammetry. / Guoyuan Li, Guozhong Su. // 2009 Joint Urban Remote Sensing Event. - Shanghai, 20-22 May 2009. - P. 1-5. ↑
- C1224.** Wang Weian. Geometric processing of QuickBird stereo imagery with high building data in megapolis. / Wang Weian, Qiao Gang. // 2009 Joint Urban Remote Sensing Event. - Shanghai, 20-22 May 2009. - P. 1-9. ↑
- C1225.** Polli D. Low-resolution urban area outlining in satellite SAR images. / Polli D., Dell'Acqua F., Gamba P., Clemenzi S. // 2009 Joint Urban Remote Sensing Event. - Shanghai, 20-22 May 2009. - P. 1-5. ↑
- C1226.** Mingsheng Liao. Post-earthquake landslide detection and early detection of landslide prone areas using SAR. / Mingsheng Liao, Lu Zhang, Balz T. // 2009 Joint Urban Remote Sensing Event. - Shanghai, 20-22 May 2009. - P. 1-5. ↑
- C1227.** Perissin D. Monitoring terrain motion in China by means of spaceborne SAR images. / Perissin D., Teng Wang, Novali F. // 2009 Joint Urban Remote Sensing Event. - Shanghai, 20-22 May 2009. - P. 1-5. ↑
- C1228.** Dell'Acqua F. Steps towards a new technique for automated registration of pre- and post-event images. / Dell'Acqua F., Sacchetti A. // 2009 Joint Urban Remote Sensing Event. - Shanghai, 20-22 May 2009. - P. 1-5. ↑
- C1229.** Jen-Jer Jaw. Data Fusion towards building roof reconstruction based on CSR approach. / Jen-Jer Jaw, Chieh-Chung Cheng. // 2009 Joint Urban Remote Sensing Event. - Shanghai, 20-22 May 2009. - P. 1-9. ↑
- C1230.** Samadzadegan F. Automatic road extraction from LIDAR data based on classifier fusion. / Samadzadegan F., Hahn M., Bigdeli B. // 2009 Joint Urban Remote Sensing Event. - Shanghai, 20-22 May 2009. - P. 1-6. ↑
- C1231.** Samadzadegan F. A multi-agent method for automatic building recognition based on the fusion of Lidar range and intensity data. / Samadzadegan F., Schenk T., Mahmoudi F.T. // 2009 Joint Urban Remote Sensing Event. - Shanghai, 20-22 May 2009. - P. 1-6. ↑
- C1232.** Ting Xiao. Inversion of leaf area index for invasive plant using ENVISAT ASAR. / Ting Xiao, Wen-peng Lin, Neng Chen. // 2009 Joint Urban Remote Sensing Event. - Shanghai, 20-22 May 2009. - P. 1-6. ↑
- C1233.** Haixia He. An approach to urban surface features identification using Pushbroom Hyperspectral Imager. / Haixia He, Bing Zhang, Hao Zhang, Xue Liu, Ru Li. // 2009 Joint Urban Remote Sensing Event. - Shanghai, 20-22 May 2009. - P. 1-6. ↑
- C1234.** Yun Yang. Object-based level set model for building detection in urban area. / Yun Yang, Ying Lin. // 2009 Joint Urban Remote Sensing Event. - Shanghai, 20-22 May 2009. - P. 1-6. ↑
- C1235.** Tu Shangtan. Fuzzy samples retrieval: A method of SAR image retrieval in urban areas. / Tu Shangtan, Sun Hong. // 2009 Joint Urban Remote Sensing Event. - Shanghai, 20-22 May 2009. - P. 1-5. ↑
- C1236.** Wei Yao. Object extraction based on 3D-segmentation of LiDAR data by combining mean shift with normalized cuts: Two examples from urban areas. / Wei Yao, Hinz S., Stilla U. // 2009 Joint Urban Remote Sensing Event. - Shanghai, 20-22 May 2009. - P. 1-6. ↑
- C1237.** Fuan Tsai. Construction and visualization of photo-realistic three-dimensional digital city. / Fuan Tsai, Tea-Ann Teo, Liang-Chien Chen, Szu-Jen Chen. // 2009 Joint Urban Remote Sensing Event. - Shanghai, 20-22 May 2009. - P. 1-7. ↑
- C1238.** Fan Wang. A study of land subsidence with PS-InSAR method based on wavelet phase analysis. / Fan Wang, Zhaoquan Huang, Dengrong Zhang. // 2009 Joint Urban Remote Sensing Event. - Shanghai, 20-22 May 2009. - P. 1-6. ↑
- C1239.** Jia Xu. Statistical characterization and modeling of high resolution COSMO/SkyMed SAR images over urban areas. / Jia Xu, Xiu-feng He, Kang Xu. // 2009 Joint Urban Remote Sensing Event. - Shanghai, 20-22 May 2009. - P. 1-5. ↑
- C1240.** Yamazaki F. Observation of urban heat island using airborne thermal sensors. / Yamazaki F., Murakoshi A., Sekiya N. // 2009 Joint Urban Remote Sensing Event. - Shanghai, 20-22 May 2009. - P. 1-5. ↑

- C1241.** Kukko A. Mobile mapping system and computing methods for modelling of road environment. / Kukko A., Jaakkola A., Lehtomaki M., Kaartinen H., Chen Y. // 2009 Joint Urban Remote Sensing Event. - Shanghai, 20-22 May 2009. - P. 1-6. ↑
- C1242.** Wenbo Wu. Study of residents information extraction in SAR image based on texture features. / Wenbo Wu, Lijing Bu. // 2009 Joint Urban Remote Sensing Event. - Shanghai, 20-22 May 2009. - P. 1-5. ↑
- C1243.** Youquan Zhang. Seasonal displacements in upper-middle alluvial fan of Chaobai River, Beijing, China, observed by the permanent scatterers technique. / Youquan Zhang, Huili gong, Beibei Chen, Na Jiang, Kunchao Lei. // 2009 Joint Urban Remote Sensing Event. - Shanghai, 20-22 May 2009. - P. 1-6. ↑
- C1244.** Yun Shao. Multi-source SAR remote sensing data for emergency monitoring to Wenchuan Earthquake damage assessment. / Yun Shao, Huaze Gong, Shi'Ang Wang, Fengli Zhang, Wei Tian. // 2009 Joint Urban Remote Sensing Event. - Shanghai, 20-22 May 2009. - P. 1-5. ↑
- C1245.** Shenheng Xu. A novel twin-horn feed for multi-beam remote sensing reflector antenna. / Shenheng Xu, Razavi S.F., Rahmat-Samii Y. // 2009. APSURSI 09. IEEE Antennas and Propagation Society International Symposium. - Charleston, SC, 1-5 June 2009. - P. 1-4. ↑
- C1246.** Buddendick H. Radio channel simulations using multiple scattering center models. / Buddendick H., Eibert T.F. // 2009. APSURSI 09. IEEE Antennas and Propagation Society International Symposium. - Charleston, SC, 1-5 June 2009. - P. 1-4. ↑
- C1247.** Sands T.A. Satellite electronic attack of enemy air defenses. 2009. SOUTHEASTCON '09. IEEE Southeastcon. - Atlanta, GA, 5-8 March 2009. - P. 434-438. ↑
- C1248.** Zhao Xiaofeng. Refractivity Estimation from Radar Sea Echos. / Zhao Xiaofeng, Huang Sixun, Sheng Zheng. // 2009. ICIC '09. Second International Conference on Information and Computing Science. - Manchester, 21-22 May 2009. - Vol. 3. - P. 337-340. ↑
- C1249.** Thai T.T. Novel ultrasensitive millimeter-wave pressure transducer utilizing a Si membrane and a stacked-patch configuration. / Thai T.T., DeJean G.R., Tentzeris M.M. // 2009. APSURSI 09. IEEE Antennas and Propagation Society International Symposium. - Charleston, SC, 1-5 June 2009. - P. 1-4. ↑
- C1250.** Yu-Jiun Ren. A dual-polarized cylindrical array antenna for aerial vehicles. / Yu-Jiun Ren, Chi-Hyung Ahn, Ming-Yi Li, Kai Chang. // 2009. APSURSI 09. IEEE Antennas and Propagation Society International Symposium. - Charleston, SC, 1-5 June 2009. - P. 1-4. ↑
- C1251.** Mallat A. CRBS for the Joint Estimation of TOA and AOA in Wideband MISO and MIMO Systems: Comparison with SISO and SIMO Systems. / Mallat A., Vandendorpe L. // 2009. ICC 09. IEEE International Conference on Communications. - Dresden, 14-18 June 2009. - P. 1-6. ↑
- C1252.** Bin Zhang. Low Relative Humidity Layer Observation with Micro Pulse Lidar in Qingdao. / Bin Zhang, Jinjia Guo. // 2009. ESIAT 2009. International Conference on Environmental Science and Information Application Technology. - Wuhan, 4-5 July 2009. - Vol. 3. - P. 520-522. ↑
- C1253.** Jinjia Guo. Meteorological Visibility Measurements by a Micro Pulsed Lidar during the 2006 Qingdao International Sailing Regatta. / Jinjia Guo, Xiaoquan Song, Zhishen Liu, Bin Zhang. // 2009. ESIAT 2009. International Conference on Environmental Science and Information Application Technology. - Wuhan, 4-5 July 2009. - Vol. 3. - P. 606-608. ↑
- C1254.** Perez C. Rain rate retrieval by processing the observations of the 85V and 85H GHz channels of the SSM/I and TMI passive microwave sensors. / Perez C., Mejia C., Mallet C., Crepon M., Badran F., Thiria S. // 2009. IJCNN 2009. International Joint Conference on Neural Networks. - Atlanta, GA, 14-19 June 2009. - P. 511-517. ↑
- C1255.** Canat G. Stimulated Brillouin threshold reduction by core microstructuration in multifilament core fibers. / Canat G., Jetschke S., Lombard L., Unger S., Bourdon P., Kirchhof J., Jolivet V., Vasseur O. // Lasers and Electro-Optics 2009 and the European Quantum Electronics Conference. CLEO Europe-EQEC 2009. European Conference on. - Munich, 14-19 June 2009. - P. 1. ↑
- C1256.** Raybaut M. A novel 2 μm laser source for CO2 DIAL. / Raybaut M., Godard A., Mohamed A.K.,

Lefebvre M., Bohman A., Geiser P., Kaspersen P. // Lasers and Electro-Optics 2009 and the European Quantum Electronics Conference. CLEO Europe-EQEC 2009. European Conference on. - Munich, 14-19 June 2009. - P. 1. ↑

C1257. Rekleitis I. Autonomous planetary exploration using LIDAR data. / Rekleitis I., Bedwani J.-L., Dupuis E. // 2009. ICRA 09. IEEE International Conference on Robotics and Automation. - Kobe, 12-17 May 2009. - P. 3025-3030. ↑

C1258. Slabakova V. Evaluation of QuikSCAT wind vector performance with respect to field measurements for the Bulgarian part of the Black Sea. / Slabakova V., Andreeva N., Eftimova P., Nedkov R. // 2009. RAST '09. 4th International Conference on Recent Advances in Space Technologies. - Istanbul, 11-13 June 2009. - P. 323-327. ↑

C1259. Bayir I. A glimpse to future commercial spy satellite systems. 2009. RAST '09. 4th International Conference on Recent Advances in Space Technologies. - Istanbul, 11-13 June 2009. - P. 370-375. ↑

C1260. Sportouche H. Building extraction and 3D reconstruction in urban areas from high-resolution optical and SAR imagery. / Sportouche H., Tupin F., Denise L. // 2009 Joint Urban Remote Sensing Event. - Shanghai, 20-22 May 2009. - P. 1-11. ↑

C1261. Perissin D. PSInSAR Analysis over the Three Gorges Dam and urban areas in China. / Perissin D., Prati C., Rocca F., Teng Wang. // 2009 Joint Urban Remote Sensing Event. - Shanghai, 20-22 May 2009. - P. 1-5. ↑

C1262. Costantini M. Persistent scatterer pairs (PSP) technique and high resolution SAR interferometry in urban areas. / Costantini M., Minati F., Falco S., Malvarosa F., Trillo F. // 2009 Joint Urban Remote Sensing Event. - Shanghai, 20-22 May 2009. - P. 1. ↑

C1263. Zhou Yong-Shun. Remote Sensing of Human Body by Stepped-Frequency Continuous-Wave. / Zhou Yong-Shun, Kong Lingjiang, Cui Guo-Long, Yang Jian-Yu. // 2009. ICBBE 2009. 3rd International Conference on Bioinformatics and Biomedical Engineering. - Beijing, 11-13 June 2009. - P. 1-4. ↑

C1264. Hernandez C.C. POLARIS: ESA's airborne ice sounding radar front-end design, performance assessment and first results. / Hernandez C.C., Krozer V., Vidkjaer J., Dall J. // 2009. MTT 09. IEEE MTT-S International Microwave Symposium Digest. - Boston, MA, 7-12 June 2009. - P. 393-396. ↑

C1265. Yeary M. An update on multi-channel digital receiver development for the phased array radar at the National Weather Radar Testbed. / Yeary M., Crain J., Zahrai A., Palmer R., Xue M., Yu T.-Y., Zhang G., Zhang Y., Doviak R., Xu Q., Chilson P. // 2009. I2MTC 09. IEEE Instrumentation and Measurement Technology Conference. - Singapore, 5-7 May 2009. - P. 933-937. ↑

C1266. Kaya A. Point Scatterer Model for RCS prediction using ISAR measurements. / Kaya A., Kartal M. // 2009. RAST '09. 4th International Conference on Recent Advances in Space Technologies. - Istanbul, 11-13 June 2009. - P. 422-425. ↑

C1267. Horvath M. Synthetic aperture radar using spread spectrum modulation. / Horvath M., Seller R., Rosner V., Miko G. // 2009. RADIOELEKTRONIKA '09. 19th International Conference Radioelektronika. - Bratislava, 22-23 April 2009. - P. 149-152. ↑

C1268. Ying Zhang. SAR and Infrared Image Fusion Using Nonsubsampled Contourlet Transform. / Ying Zhang, Yanjun Li, Ke Zhang, Hongmei Wang, Meili Li. // 2009. JCAI '09. International Joint Conference on Artificial Intelligence. - Hainan Island, 25-26 April 2009. - P. 398-401. ↑

C1269. Shuo Wang. An internal calibration scheme for polarimetric Synthetic Aperture Radar system. / Shuo Wang, Weidong Yu, Haiming Qi. // IGARSS 2009 Geoscience and Remote Sensing Symposium, 2009 IEEE International. - Cape Town, 12-17 July 2009. - Vol. 4. - P. IV-578-IV-581-578. ↑

C1270. Sivakumar V. CSIR-NLC mobile LIDAR for atmosphere remote sensing. / Sivakumar V., Tesfaye M., Botai J., Moema D., Sharma A., Bollig C., Hannes Rautenbach C.J.D. // IGARSS 2009 Geoscience and Remote Sensing Symposium, 2009 IEEE International. - Cape Town, 12-17 July 2009. - Vol. 2. - P. II-424-II-427-424. ↑

C1271. Wenjian Ni. Characterization of soil surface roughness from terrestrial laser scanner data. / Wenjian Ni,

Guoqing Sun, Zhifeng Guo, Yong Pang. // IGARSS 2009 Geoscience and Remote Sensing Symposium, 2009 IEEE International. - Cape Town, 12-17 July 2009. - Vol. 2. - P. II-428-II-431-428. ↑

**C1272.** Shalei Song. Spectral ratio lidar for objects detection. / Shalei Song, Pingxiang Li, Wei Gong, Liangpei Zhang, Bo Zhu, Lilei Lv, Daoxi Zhang. // IGARSS 2009 Geoscience and Remote Sensing Symposium, 2009 IEEE International. - Cape Town, 12-17 July 2009. - Vol. 2. - P. II-432-II-435-432. ↑

**C1273.** Byeong-pyo Jeong. Estimation of seismic intensity due to the 2008 Wenchuan Earthquake. / Byeong-pyo Jeong, Hosokawa M., Zama S., Takizawa O. // IGARSS 2009 Geoscience and Remote Sensing Symposium, 2009 IEEE International. - Cape Town, 12-17 July 2009. - Vol. 2. - P. II-400-II-403-400. ↑

**C1274.** Wauthier C. The January 2002 eruption of Nyiragongo volcano (DRC) captured by InSAR. / Wauthier C., Cayol W., Kervyn F., d'Oreye N. // IGARSS 2009 Geoscience and Remote Sensing Symposium, 2009 IEEE International. - Cape Town, 12-17 July 2009. - Vol. 2. - P. II-416-II-419-416. ↑

**C1275.** Hosokawa M. Earthquake intensity estimation and damage detection using remote sensing data for global rescue operations. / Hosokawa M., Byeong-pyo Jeong, Takizawa O. // IGARSS 2009 Geoscience and Remote Sensing Symposium, 2009 IEEE International. - Cape Town, 12-17 July 2009. - Vol. 2. - P. II-420-II-423-420. ↑

**C1276.** Nouvel J.F. Radar signal retrodiffusion by water surface. / Nouvel J.F., Souyris J.C. // IGARSS 2009 Geoscience and Remote Sensing Symposium, 2009 IEEE International. - Cape Town, 12-17 July 2009. - Vol. 2. - P. II-483-II-486-483. ↑

**C1277.** Marghany M. Finite difference model for modeling sea surface current from RADARSAT-1 SAR data. IGARSS 2009 Geoscience and Remote Sensing Symposium, 2009 IEEE International. - Cape Town, 12-17 July 2009. - Vol. 2. - P. II-487-II-490-487. ↑

**C1278.** Ding Guo. Sea surface simulation for SAR remote sensing based on the fractal model. / Ding Guo, Xingfa Gu, Tao Yu, Xiaoyin Li, Jingjun Zheng, Hui Xu. // IGARSS 2009 Geoscience and Remote Sensing Symposium, 2009 IEEE International. - Cape Town, 12-17 July 2009. - Vol. 2. - P. II-491-II-494-491. ↑

**C1279.** Zhi Wang. Automated extraction of building geometric features from raw LiDAR data. / Zhi Wang, Li-Xin Wu. // IGARSS 2009 Geoscience and Remote Sensing Symposium, 2009 IEEE International. - Cape Town, 12-17 July 2009. - Vol. 2. - P. II-436-II-439-436. ↑

**C1280.** Berginc G. Simulation of 3D laser systems. / Berginc G., Jouffroy M. // IGARSS 2009 Geoscience and Remote Sensing Symposium, 2009 IEEE International. - Cape Town, 12-17 July 2009. - Vol. 2. - P. II-440-II-443-440. ↑

**C1281.** Marghany M. 3D coastal bathymetry reconstruction using TOPSAR data. IGARSS 2009 Geoscience and Remote Sensing Symposium, 2009 IEEE International. - Cape Town, 12-17 July 2009. - Vol. 2. - P. II-479-II-482-479. ↑

**C1282.** Gorgucci E. Analysis of the mean raindrop shape model for dual polarization radar rainfall estimation. / Gorgucci E., Baldini L. // IGARSS 2009 Geoscience and Remote Sensing Symposium, 2009 IEEE International. - Cape Town, 12-17 July 2009. - Vol. 3. - P. III-113-III-116-113. ↑

**C1283.** Nunziata F. A unified polarimetric approach for SAR sea oil slick observation. / Nunziata F., Gambardella A., Migliaccio M. // IGARSS 2009 Geoscience and Remote Sensing Symposium, 2009 IEEE International. - Cape Town, 12-17 July 2009. - Vol. 2. - P. II-282-II-285-282. ↑

**C1284.** Goo Jun. Spatially adaptive classification of hyperspectral data with Gaussian processes. / Goo Jun, Ghosh J. // IGARSS 2009 Geoscience and Remote Sensing Symposium, 2009 IEEE International. - Cape Town, 12-17 July 2009. - Vol. 2. - P. II-290-II-293-290. ↑

**C1285.** Elsherbini A. Topography of sand covered bedrock using two-frequency airborne interferometric SAR measurements. / Elsherbini A., Sarabandi K. // IGARSS 2009 Geoscience and Remote Sensing Symposium, 2009 IEEE International. - Cape Town, 12-17 July 2009. - Vol. 2. - P. II-250-II-253-250. ↑

**C1286.** Yong-sheng Zhou. Investigation on the applications of decorrelation analysis in Polarimetric SAR Interferometry. / Yong-sheng Zhou, Wen Hong, Fang Cao. // IGARSS 2009 Geoscience and Remote Sensing Symposium, 2009 IEEE International. - Cape Town, 12-17 July 2009. - Vol. 2. - P. II-250-II-253-250. ↑

Symposium, 2009 IEEE International. - Cape Town, 12-17 July 2009. - Vol. 2. - P. II-254-II-257-254. ↑

**C1287.** Berk A. Recent developments in the MODTRAN® atmospheric model and implications for hyperspectral compensation. / Berk A., Acharya P., Anderson G., Gossage B. // IGARSS 2009 Geoscience and Remote Sensing Symposium, 2009 IEEE International. - Cape Town, 12-17 July 2009. - Vol. 2. - P. II-262-II-265-262. ↑

**C1288.** Qulin Tan. Application of SAR remote sensing data to lithological mapping: A case study in railway geological survey. / Qulin Tan, JiaoJiao Gao, Xiaofang Li. // IGARSS 2009 Geoscience and Remote Sensing Symposium, 2009 IEEE International. - Cape Town, 12-17 July 2009. - Vol. 2. - P. II-342-II-344-342. ↑

**C1289.** Yun Shao. Fast extracting and change detection of dammed lakes using high-resolution SAR images: A case study of Tangjiashan Dammed Lake. / Yun Shao, Shiang Wang, Wei Tian, Huaze Gong, Fengli Zhang. // IGARSS 2009 Geoscience and Remote Sensing Symposium, 2009 IEEE International. - Cape Town, 12-17 July 2009. - Vol. 2. - P. II-349-II-352-349. ↑

**C1290.** Daqing Ge. Using permanent scatterer InSAR to detect land subsidence and ground fissures: A case study in Xi'an city. / Daqing Ge, Yan Wang, Ling Zhang, Xiaofang Guo. // IGARSS 2009 Geoscience and Remote Sensing Symposium, 2009 IEEE International. - Cape Town, 12-17 July 2009. - Vol. 2. - P. II-365-II-368-365. ↑

**C1291.** Koskinen J.T. Monitoring of snow cover properties during the spring melting period in forested areas. / Koskinen J.T., Pulliainen J.T., Luojus K.P. // IGARSS 2009 Geoscience and Remote Sensing Symposium, 2009 IEEE International. - Cape Town, 12-17 July 2009. - Vol. 2. - P. II-318-II-321-318. ↑

**C1292.** Martin-Neira M. The PARIS in-orbit demonstrator. / Martin-Neira M., D'Addio S., Buck C., Flouy N., Prieto-Cerdeira R. // IGARSS 2009 Geoscience and Remote Sensing Symposium, 2009 IEEE International. - Cape Town, 12-17 July 2009. - Vol. 2. - P. II-322-II-325-322. ↑

**C1293.** Wu J. Connecting the dots between laser waveforms and herbaceous biomass for assessment of land degradation using small-footprint waveform LiDAR data. / Wu J., van Aardt J.A.N., Asner G.P., Mathieu R., Kennedy-Bowdoin T., Knapp D., Wessels K., Erasmus B.F.N., Smit I. // IGARSS 2009 Geoscience and Remote Sensing Symposium, 2009 IEEE International. - Cape Town, 12-17 July 2009. - Vol. 2. - P. II-334-II-337-334. ↑

**C1294.** Capsoni C. A technique to derive the spatial distribution of rain intensity from NWP data. / Capsoni C., Luini L. // IGARSS 2009 Geoscience and Remote Sensing Symposium, 2009 IEEE International. - Cape Town, 12-17 July 2009. - Vol. 2. - P. II-519-II-522-519. ↑

**C1295.** Seker S.S. A discrete interferometric model for a layer of random medium. / Seker S.S., Lang R.H. // IGARSS 2009 Geoscience and Remote Sensing Symposium, 2009 IEEE International. - Cape Town, 12-17 July 2009. - Vol. 2. - P. II-674-II-677-674. ↑

**C1296.** Zhao Shaojie. The coherent microwave emission of freezing soil: Experimental research and model simulation. / Zhao Shaojie, Zhang Lixin, Zhang Yongpan, Jiang Lingmei, Xing Weipo, Tianjie Z. // IGARSS 2009 Geoscience and Remote Sensing Symposium, 2009 IEEE International. - Cape Town, 12-17 July 2009. - Vol. 2. - P. II-678-II-681-678. ↑

**C1297.** Jie Guang. Synthetic retrieval of aerosol optical depth and surface reflectance using Terra and Aqua platforms in semi-arid regions. / Jie Guang, Yong Xue, Xiaowen Li, Ying Wan, Yingjie Li, Jianwen Ai, Linyan Bai, Linlu Mei. // IGARSS 2009 Geoscience and Remote Sensing Symposium, 2009 IEEE International. - Cape Town, 12-17 July 2009. - Vol. 2. - P. II-694-II-697-694. ↑

**C1298.** Singh G. Snow density estimation using Polarimetric ASAR data. / Singh G., Venkataraman G. // IGARSS 2009 Geoscience and Remote Sensing Symposium, 2009 IEEE International. - Cape Town, 12-17 July 2009. - Vol. 2. - P. II-630-II-633-630. ↑

**C1299.** Deng Mengzhi. Study on tobacco spatial agglomeration pattern based on remote sensing and GIS methods in Henan province, China. / Deng Mengzhi, Wu Daihui, Li Fuxiri, Fan Wenjie. // IGARSS 2009 Geoscience and Remote Sensing Symposium, 2009 IEEE International. - Cape Town, 12-17 July 2009. - Vol. 2. - P. II-646-II-649-646. ↑

**C1300.** Strozzi T. Survey of landslide activity and rockglaciers movement in the Swiss Alps with TerraSAR-X. /

Strozzi T., Wegmuller U., Werner C., Wiesmann A., Delaloye R., Raetz H. // IGARSS 2009 Geoscience and Remote Sensing Symposium, 2009 IEEE International. - Cape Town, 12-17 July 2009. - Vol. 3. - P. III-53-III-56-53. ↑

**C1301.** Viani F. Passive real-time localization through wireless sensor networks. / Viani F., Martinelli M., Ioriatti L., Benedetti M., Massa A. // IGARSS 2009 Geoscience and Remote Sensing Symposium, 2009 IEEE International. - Cape Town, 12-17 July 2009. - Vol. 2. - P. II-718-II-721-718. ↑

**C1302.** Guoqiang Liu. On sensitivity of Kuroshio modeling in the Luzon Strait with ERS-1/2 wind field forcing. / Guoqiang Liu, Yijun He, Hui Shen. // IGARSS 2009 Geoscience and Remote Sensing Symposium, 2009 IEEE International. - Cape Town, 12-17 July 2009. - Vol. 3. - P. III-45-III-48-45. ↑

**C1303.** Joseph A.T. A vegetation correction methodology applied for soil moisture retrieval from C-band radar observations. / Joseph A.T., van der Velde R., O'Neill P.E., Lang R., Gish T. // IGARSS 2009 Geoscience and Remote Sensing Symposium, 2009 IEEE International. - Cape Town, 12-17 July 2009. - Vol. 3. - P. III-49-III-52-49. ↑

**C1304.** Dabrowska-Zielinska K. Microwave satellite data applied for agriculture area-Case study-Poland. / Dabrowska-Zielinska K., Ciolkosz A., Kowalik W., Budzynska M. // IGARSS 2009 Geoscience and Remote Sensing Symposium, 2009 IEEE International. - Cape Town, 12-17 July 2009. - Vol. 2. - P. II-698-II-701-698. ↑

**C1305.** Ventura B. Combined use of Cassini Radar active and passive measurements to characterize Titan morphology. / Ventura B., Casarano D., Notarnicola C., Janssen M., Posa F. // IGARSS 2009 Geoscience and Remote Sensing Symposium, 2009 IEEE International. - Cape Town, 12-17 July 2009. - Vol. 2. - P. II-702-II-705-702. ↑

**C1306.** Zengcan Liu. Study on the backscattering characteristic of typical earth substances in northwest of China. / Zengcan Liu, Chen Yan, Mingquan Jia, Tong Ling, Chunliang Xu. // IGARSS 2009 Geoscience and Remote Sensing Symposium, 2009 IEEE International. - Cape Town, 12-17 July 2009. - Vol. 2. - P. II-710-II-713-710. ↑

**C1307.** Foster J. A new blended snow product using visible, microwave and scatterometer satellite data. / Foster J., Hall D., Eylander J. // IGARSS 2009 Geoscience and Remote Sensing Symposium, 2009 IEEE International. - Cape Town, 12-17 July 2009. - Vol. 2. - P. II-559-II-562-559. ↑

**C1308.** Hayden L. Establishing field and base camp servers for remote sensing of ice sheets in Ilulissat, Greenland. / Hayden L., Powell J.H., Akers E. // IGARSS 2009 Geoscience and Remote Sensing Symposium, 2009 IEEE International. - Cape Town, 12-17 July 2009. - Vol. 2. - P. II-571-II-573-571. ↑

**C1309.** Lei Huang. Derivation of glacier velocity from SAR and optical data with feature tracking. / Lei Huang, Zhen Li. // IGARSS 2009 Geoscience and Remote Sensing Symposium, 2009 IEEE International. - Cape Town, 12-17 July 2009. - Vol. 2. - P. II-574-II-577-574. ↑

**C1310.** Acevo-Herrera R. High-compacted FM-CW SAR for boarding on small UAVs. / Acevo-Herrera R., Aguasca A., Mallorqui J.J., Fabregas X. // IGARSS 2009 Geoscience and Remote Sensing Symposium, 2009 IEEE International. - Cape Town, 12-17 July 2009. - Vol. 2. - P. II-543-II-546-543. ↑

**C1311.** Xiaogang Song. Coseismic surface deformation caused by the Wenchuan M8 earthquake from InSAR data analysis. / Xiaogang Song, Xinjian Shan, Chunyan Qu, Guifang Zhang, Limin Guo, Guohong Zhang. // IGARSS 2009 Geoscience and Remote Sensing Symposium, 2009 IEEE International. - Cape Town, 12-17 July 2009. - Vol. 3. - P. III-69-III-72-69. ↑

**C1312.** Kelly A.C. Constellations: A new paradigm for earth observations. / Kelly A.C., Volz S.M., Yuhas C.L., Case W.F. // IGARSS 2009 Geoscience and Remote Sensing Symposium, 2009 IEEE International. - Cape Town, 12-17 July 2009. - Vol. 3. - P. III-73-III-76-73. ↑

**C1313.** Rousseau L.-P. Potentials of RADARSAT-2 data to monitor freezing/thawing cycles over agricultural lands in Canada. / Rousseau L.-P., Magagi R., Leconte R., Berg A., Toth B. // IGARSS 2009 Geoscience and Remote Sensing Symposium, 2009 IEEE International. - Cape Town, 12-17 July 2009. - Vol. 2. - P. II-598-II-601-598. ↑

**C1314.** Hambaryan A.K. The results of preliminary measurements of snow and water ice microwave reflection

and emission angular dependences at 5, 6GHz. / Hambaryan A.K., Arakelyan A.K., Muradyan H.G., Karyan V.V., Hovhannisyan G.G., Arakelyan A.A., Grigoryan M.L., Hakobyan I.K., Manukyan M.R. // IGARSS 2009 Geoscience and Remote Sensing Symposium, 2009 IEEE International. - Cape Town, 12-17 July 2009. - Vol. 2. - P. II-602-II-605-602. ↑

**C1315.** Xiaojun Yin. Evaluating snow depth in Western China based on passive microwave remote sensing. / Xiaojun Yin, Shi J., Jinyang Du, Jiang Lingmei. // IGARSS 2009 Geoscience and Remote Sensing Symposium, 2009 IEEE International. - Cape Town, 12-17 July 2009. - Vol. 2. - P. II-618-II-621-618. ↑

**C1316.** Zhen Li. The glacier movement estimation and analysis with InSAR in the Qinghai-Tibetan plateau. / Zhen Li, Jianmin Zhou, Bangsen Tian. // IGARSS 2009 Geoscience and Remote Sensing Symposium, 2009 IEEE International. - Cape Town, 12-17 July 2009. - Vol. 2. - P. II-578-II-581-578. ↑

**C1317.** Uiboupin R. Sea ice concentration and type analysis from dual pol Radarsat-2 and Modis images in the Baltic Sea. / Uiboupin R., Sipelgas L., Raudsepp U. // IGARSS 2009 Geoscience and Remote Sensing Symposium, 2009 IEEE International. - Cape Town, 12-17 July 2009. - Vol. 2. - P. II-590-II-593-590. ↑

**C1318.** Blake W. Ground based SAR survey of Basal interface at NEEM drill site. / Blake W., Leuschen C., Laird C., Dahl-Jensen D. // IGARSS 2009 Geoscience and Remote Sensing Symposium, 2009 IEEE International. - Cape Town, 12-17 July 2009. - Vol. 2. - P. II-594-II-597-594. ↑

**C1319.** Duque S. Experimental results with bistatic SAR tomography. / Duque S., Lopez-Dekker P., Mallorqui J.J., Nashashibi A.Y., Patel A.M. // IGARSS 2009 Geoscience and Remote Sensing Symposium, 2009 IEEE International. - Cape Town, 12-17 July 2009. - Vol. 2. - P. II-37-II-40-37. ↑

**C1320.** Yu Ying. Study on bistatic SAR ocean wave imaging mechanism. / Yu Ying, Wang Xiaoqing, Zhu Minhui, Chong Jinsong. // IGARSS 2009 Geoscience and Remote Sensing Symposium, 2009 IEEE International. - Cape Town, 12-17 July 2009. - Vol. 2. - P. II-41-II-44-41. ↑

**C1321.** Xiaolan Qiu. A new calculation method of NuSAR for translational variant bistatic SAR. / Xiaolan Qiu, Donghui Hu, Chibiao Ding. // IGARSS 2009 Geoscience and Remote Sensing Symposium, 2009 IEEE International. - Cape Town, 12-17 July 2009. - Vol. 2. - P. II-45-II-48-45. ↑

**C1322.** Knospe S. Monitoring a tunneling in an urbanized area with Terrasar-X interferometry-Surface deformation measurements and atmospheric error treatment. / Knospe S., Busch W. // IGARSS 2009 Geoscience and Remote Sensing Symposium, 2009 IEEE International. - Cape Town, 12-17 July 2009. - Vol. 2. - P. II-25-II-28-25. ↑

**C1323.** Mermoz S. Investigation of Radarsat-2 and Terrasar-X data for river ice classification. / Mermoz S., Allain S., Bernier M., Pottier E. // IGARSS 2009 Geoscience and Remote Sensing Symposium, 2009 IEEE International. - Cape Town, 12-17 July 2009. - Vol. 2. - P. II-29-II-32-29. ↑

**C1324.** Garrigues S. Multi-thematic exploitation of TerraSAR-X images in the context of the kalideos reference datasets. / Garrigues S., May S., Baghdadi N., Champion I., Froge J.-L., Rabaute T., Durand P., Pourthie N. // IGARSS 2009 Geoscience and Remote Sensing Symposium, 2009 IEEE International. - Cape Town, 12-17 July 2009. - Vol. 2. - P. II-33-II-36-33. ↑

**C1325.** Bin Liu. A fast numerical method for scattering from dielectric rough surfaces. / Bin Liu, Yang Du. // IGARSS 2009 Geoscience and Remote Sensing Symposium, 2009 IEEE International. - Cape Town, 12-17 July 2009. - Vol. 2. - P. II-93-II-96-93. ↑

**C1326.** Yisok Oh. Development of a simple scattering model for vegetation canopies and examination of its validity with scatterometer measurements of green-onion fields. / Yisok Oh, Soon-Gu Kwon. // IGARSS 2009 Geoscience and Remote Sensing Symposium, 2009 IEEE International. - Cape Town, 12-17 July 2009. - Vol. 2. - P. II-101-II-104-101. ↑

**C1327.** McFadden M. Numerical modeling of a spiral-antenna GPR system. / McFadden M., Scott W.R. // IGARSS 2009 Geoscience and Remote Sensing Symposium, 2009 IEEE International. - Cape Town, 12-17 July 2009. - Vol. 2. - P. II-109-II-112-109. ↑

**C1328.** Jie Zhen. A GPS signal based numeric range migration algorithm of space-surface bistatic SAR. / Jie Zhen, Zhenhua Zhang, Shunjun Wu. // IGARSS 2009 Geoscience and Remote Sensing Symposium, 2009 IEEE

International. - Cape Town, 12-17 July 2009. - Vol. 2. - P. II-49-II-52-49. ↑

**C1329.** Zhenhua Zhang. Chirp scaling algorithm for parallel bistatic SAR data processing. / Zhenhua Zhang, Mengdao Xing, Lianghai Li, Jie Zhen, Zheng Bao. // IGARSS 2009 Geoscience and Remote Sensing Symposium, 2009 IEEE International. - Cape Town, 12-17 July 2009. - Vol. 2. - P. II-53-II-56-53. ↑

**C1330.** Yisok Oh. Hybrid of the method of moments/ Monte Carlo technique and a surface scattering model for estimating the radar backscatters OF harvested farm fields. / Yisok Oh, Ji-Hwan Hwang. // IGARSS 2009 Geoscience and Remote Sensing Symposium, 2009 IEEE International. - Cape Town, 12-17 July 2009. - Vol. 2. - P. II-89-II-92-89. ↑

**C1331.** Klein D. Assessment of urban extent and imperviousness of Cape Town using TerraSAR-X and Landsat images. / Klein D., Esch T., Himmler V., Thiel M., Dech S. // IGARSS 2009 Geoscience and Remote Sensing Symposium, 2009 IEEE International. - Cape Town, 12-17 July 2009. - Vol. 3. - P. III-1051-III-1054-1051. ↑

**C1332.** Schneider R.Z. On the accuracy of scatterers LOS rotation estimation procedures in radar polarimetry. IGARSS 2009 Geoscience and Remote Sensing Symposium, 2009 IEEE International. - Cape Town, 12-17 July 2009. - Vol. 3. - P. III-164-III-167-164. ↑

**C1333.** Yijun He. Validation of RADARSAT-2 Polarimetric SAR measurements of ocean waves. / Yijun He, Biao Zhang, Perrie W. // IGARSS 2009 Geoscience and Remote Sensing Symposium, 2009 IEEE International. - Cape Town, 12-17 July 2009. - Vol. 3. - P. III-168-III-171-168. ↑

**C1334.** Di Rosa D. Cross-comparison and validation of MODIS AQUA cloud mask by using CLOUDSAT and CALIPSO datasets. / Di Rosa D., Notarnicola C., Posa F. // IGARSS 2009 Geoscience and Remote Sensing Symposium, 2009 IEEE International. - Cape Town, 12-17 July 2009. - Vol. 3. - P. III-1019-III-1022-1019. ↑

**C1335.** Paradzayi C. Polarimetric analysis over African savanna woodland using ALOS/PALSAR. / Paradzayi C., Annegarn H., Erasmus B., Schmullius C. // IGARSS 2009 Geoscience and Remote Sensing Symposium, 2009 IEEE International. - Cape Town, 12-17 July 2009. - Vol. 3. - P. III-1043-III-1046-1043. ↑

**C1336.** Viergever K.M. Backscatter and interferometry for estimating above-ground biomass of sparse woodland: A case study in Belize. / Viergever K.M., Woodhouse I.H., Marino A., Brolly M., Stuart N. // IGARSS 2009 Geoscience and Remote Sensing Symposium, 2009 IEEE International. - Cape Town, 12-17 July 2009. - Vol. 3. - P. III-1047-III-1050-1047. ↑

**C1337.** Deroin J.-P. Geological mapping in the zone of Chotts, Tunisia, using ALOS sensors. / Deroin J.-P., Dhont D., Jabbour M., Chorowicz J., Fruneau B. // IGARSS 2009 Geoscience and Remote Sensing Symposium, 2009 IEEE International. - Cape Town, 12-17 July 2009. - Vol. 2. - P. II-13-II-16-13. ↑

**C1338.** Suchandt S. Extraction of traffic flows and surface current information using Terrasar-X Along-track interferometry data. / Suchandt S., Runge H., Kotenkov A., Breit H., Steinbrecher U. // IGARSS 2009 Geoscience and Remote Sensing Symposium, 2009 IEEE International. - Cape Town, 12-17 July 2009. - Vol. 2. - P. II-17-II-20-17. ↑
















**C1339.** Romeiser R. Analysis of first Terrasar-X along-track InSAR-derived surface current fields. / Romeiser R., Suchandt S., Runge H., Steinbrecher U. // IGARSS 2009 Geoscience and Remote Sensing Symposium, 2009 IEEE International. - Cape Town, 12-17 July 2009. - Vol. 2. - P. II-21-II-24-21. ↑

**C1340.** Schmitt A. Curvelet-based change detection for man-made objects from SAR images. / Schmitt A., Wessel B., Roth A. // IGARSS 2009 Geoscience and Remote Sensing Symposium, 2009 IEEE International. - Cape Town, 12-17 July 2009. - Vol. 3. - P. III-1059-III-1062-1059. ↑

**C1341.** Holecz F. Synergetic use of multi-temporal ALOS PALSAR and ENVISAT ASAR data for topographic/land cover mapping and monitoring at national scale in Africa. / Holecz F., Barbieri M., Cantone A., Pasquali P., Monaco S. // IGARSS 2009 Geoscience and Remote Sensing Symposium, 2009 IEEE International. - Cape Town, 12-17 July 2009. - Vol. 2. - P. II-5-II-8-5. ↑

**C1342.** Pottier E. Exploitation of ALOS-PALSAR SAR full-polarimetry data to the mapping of an African region. / Pottier E., Ferro-Famil L. // IGARSS 2009 Geoscience and Remote Sensing Symposium, 2009 IEEE International. - Cape Town, 12-17 July 2009. - Vol. 2. - P. II-9-II-12-9. ↑

- C1343.** Nasrabadi N.M. Wiener prediction-based change detection for locating mines in multilook SAR imagery. IGARSS 2009 Geoscience and Remote Sensing Symposium, 2009 IEEE International. - Cape Town, 12-17 July 2009. - Vol. 2. - P. II-113-II-116-113. ↑
- C1344.** Harant O. Preliminary Terrasar-X observations for temperate glaciers on the Chamonix Mont Blanc test site. / Harant O., Fallourd R., Bombrun L., Gay M., Trouve E., Vasile G., Nicolas J.-M. // IGARSS 2009 Geoscience and Remote Sensing Symposium, 2009 IEEE International. - Cape Town, 12-17 July 2009. - Vol. 2. - P. II-218-II-221-218. ↑
- C1345.** Busche T. Comparison of helicopter-borne thin sea ice thickness profiles with polarimetric signatures of dual-pol Terrasar-X data. / Busche T., Hajnsek I., Papathanassiou K., Krumpen T., Rabenstein L., Hoelemann J., Haas C., Willmes S. // IGARSS 2009 Geoscience and Remote Sensing Symposium, 2009 IEEE International. - Cape Town, 12-17 July 2009. - Vol. 2. - P. II-222-II-225-222. ↑
- C1346.** Cuccoli F. Radio base network and tomographic processing for real time estimation of the rainfall rate fields. / Cuccoli F., Facheris L., Gori S. // IGARSS 2009 Geoscience and Remote Sensing Symposium, 2009 IEEE International. - Cape Town, 12-17 July 2009. - Vol. 3. - P. III-121-III-124-121. ↑
- C1347.** Cassells G.F. The use of ALOS PALSAR for supporting sustainable forest use in southern Africa: A case study in Malawi. / Cassells G.F., Woodhouse I.H., Mitchard E.T.A., Tembo M.D. // IGARSS 2009 Geoscience and Remote Sensing Symposium, 2009 IEEE International. - Cape Town, 12-17 July 2009. - Vol. 2. - P. II-206-II-209-206. ↑
- C1348.** Wauthier C. L-band and C-band InSAR studies of African volcanic areas. / Wauthier C., Oyen A.M., Marinkovic P.S., Cayol V., Fernandez, Gonzalez J.P., Hanssen R.F., Kervyn F., d'Oreye N., Shirzaei M., Walter T.R. // IGARSS 2009 Geoscience and Remote Sensing Symposium, 2009 IEEE International. - Cape Town, 12-17 July 2009. - Vol. 2. - P. II-210-II-213-210. ↑
- C1349.** Engelbrecht J. Synthetic aperture radar data employed for soil moisture estimation in the Piketberg region, South Africa. IGARSS 2009 Geoscience and Remote Sensing Symposium, 2009 IEEE International. - Cape Town, 12-17 July 2009. - Vol. 2. - P. II-214-II-217-214. ↑
- C1350.** Walterscheid I. Results and analysis of hybrid bistatic SAR experiments with spaceborne, airborne and stationary sensors. / Walterscheid I., Espeter T., Gierull C., Klare J., Brenner A.R., Ender J.H.G. // IGARSS 2009 Geoscience and Remote Sensing Symposium, 2009 IEEE International. - Cape Town, 12-17 July 2009. - Vol. 2. - P. II-238-II-241-238. ↑
- C1351.** Rodriguez-Cassola M. New processing approach and results for bistatic TerraSAR-X/F-SAR spaceborne-airborne experiments. / Rodriguez-Cassola M., Prats P., Baumgartner S.V., Krieger G., Nottensteiner A., Horn R., Hajnsek I., Moreira A. // IGARSS 2009 Geoscience and Remote Sensing Symposium, 2009 IEEE International. - Cape Town, 12-17 July 2009. - Vol. 2. - P. II-242-II-245-242. ↑
- C1352.** Duque S. Repeat-pass interferometry using a fixed-receiver and ERS-2/ENVISAT as transmitters of opportunity. / Duque S., Lopez-Dekker P., Mallorqui J.J., Merlano J.C. // IGARSS 2009 Geoscience and Remote Sensing Symposium, 2009 IEEE International. - Cape Town, 12-17 July 2009. - Vol. 2. - P. II-246-II-249-246. ↑
- C1353.** Jezek K. TerraSAR-X observations of the recovery glacier system, Antarctica. / Jezek K., Floricioiu D., Farness K., Yague-Martinez N., Eineder M. // IGARSS 2009 Geoscience and Remote Sensing Symposium, 2009 IEEE International. - Cape Town, 12-17 July 2009. - Vol. 2. - P. II-226-II-229-226. ↑
- C1354.** Whitehead K. Determination of variations in glacier surface movements through high resolution interferometry; Bylot Island, Canada. / Whitehead K., Moorman B.J., Wainstein P. // IGARSS 2009 Geoscience and Remote Sensing Symposium, 2009 IEEE International. - Cape Town, 12-17 July 2009. - Vol. 2. - P. II-230-II-233-230. ↑
- C1355.** Henke D. Bistatic experiment with the UWB-CARABAS sensor-First results and prospects of future applications. / Henke D., Barmettler A., Meier E. // IGARSS 2009 Geoscience and Remote Sensing Symposium, 2009 IEEE International. - Cape Town, 12-17 July 2009. - Vol. 2. - P. II-234-II-237-234. ↑
- C1356.** Jinyang Du. Estimation of snow water equivalent using a parameterized snow model. / Jinyang Du, Jiancheng Shi. // IGARSS 2009 Geoscience and Remote Sensing Symposium, 2009 IEEE International. - Cape Town, 12-17 July 2009. - Vol. 2. - P. II-152-II-155-152. ↑

- C1357.** Guner B. Performance analysis of a cross-frequency detector of pulsed sinusoidal RFI in Microwave Radiometry. / Guner B., Johnson J.T., Majurec N. // IGARSS 2009 Geoscience and Remote Sensing Symposium, 2009 IEEE International. - Cape Town, 12-17 July 2009. - Vol. 2. - P. II-166-II-169-166. 
- C1358.** Karvonen J. Sea ice SAR classification based on edge features. / Karvonen J., Hallikainen M. // IGARSS 2009 Geoscience and Remote Sensing Symposium, 2009 IEEE International. - Cape Town, 12-17 July 2009. - Vol. 3. - P. III-129-III-132-129. 
- C1359.** Jenzri H. Contribution of the inter-channel polarimetric coherence for soil classification. / Jenzri H., Abdelfattah R. // IGARSS 2009 Geoscience and Remote Sensing Symposium, 2009 IEEE International. - Cape Town, 12-17 July 2009. - Vol. 2. - P. II-140-II-143-140. 
- C1360.** Rott H. Retrieval of snow parameters from Ku-band and X-band radar backscatter measurements. / Rott H., Heidinger M., Nagler T., Cline D., Yueh S. // IGARSS 2009 Geoscience and Remote Sensing Symposium, 2009 IEEE International. - Cape Town, 12-17 July 2009. - Vol. 2. - P. II-144-II-147-144. 
- C1361.** Xiaolan Xu. Comparison with CLPX II airborne data using DMRT model. / Xiaolan Xu, Ding Liang, Andreadis K.M., Leung Tsang, Josberger E.G. // IGARSS 2009 Geoscience and Remote Sensing Symposium, 2009 IEEE International. - Cape Town, 12-17 July 2009. - Vol. 2. - P. II-148-II-151-148. 
- C1362.** Kirton A. Detailed structural characterisation of the savanna flux site at Skukuza, South Africa. / Kirton A., Scholes B., Verstraete M., Archibald S., Mennell K., Asner G. // IGARSS 2009 Geoscience and Remote Sensing Symposium, 2009 IEEE International. - Cape Town, 12-17 July 2009. - Vol. 2. - P. II-186-II-189-186. 
- C1363.** Mathieu R. Tree cover, tree height and bare soil cover differences along a land use degradation gradient in semi-arid savannas, South Africa. / Mathieu R., Wessels K., Asner G., Knapp D., van Aardt J., Main R., Cho M., Erasmus B., Smit I. // IGARSS 2009 Geoscience and Remote Sensing Symposium, 2009 IEEE International. - Cape Town, 12-17 July 2009. - Vol. 2. - P. II-194-II-197-194. 
- C1364.** Fisher J. Three-dimensional woody vegetation structure across different land-use types and -land-use intensities in a semi-arid savanna. / Fisher J., Erasmus B.F.N., Witkowski E., van Aardt J., Asner G., Kennedy-Bowdoin T., Knapp D., Mathieu R., Wessels K. // IGARSS 2009 Geoscience and Remote Sensing Symposium, 2009 IEEE International. - Cape Town, 12-17 July 2009. - Vol. 2. - P. II-198-II-210-198. 
- C1365.** D'Addio S. Advanced paris altimeter based on delay compensation of Doppler Waveforms. / D'Addio S., Martin-Neira M. // IGARSS 2009 Geoscience and Remote Sensing Symposium, 2009 IEEE International. - Cape Town, 12-17 July 2009. - Vol. 2. - P. II-174-II-177-174. 
- C1366.** Zavorotny V.U. Comparing wind speed retrievals from GPS reflectometry with SFMR surface wind speeds in Hurricane Ike (2008). / Zavorotny V.U., Akos D.M., Walsh E.J. // IGARSS 2009 Geoscience and Remote Sensing Symposium, 2009 IEEE International. - Cape Town, 12-17 July 2009. - Vol. 2. - P. II-178-II-181-178. 
- C1367.** Clarizia M.P. Simulation of GNSS-R returns for delay-DOPPLER analysis of the ocean surface. / Clarizia M.P., Di Bisceglie M., Galdi C., Gommenginger C., Srokosz M. // IGARSS 2009 Geoscience and Remote Sensing Symposium, 2009 IEEE International. - Cape Town, 12-17 July 2009. - Vol. 2. - P. II-182-II-185-182. 
- C1368.** Fengli Zhang. Temporal variation of simulated rice backscattering of S-band HJ-1 SAR. / Fengli Zhang, Kun Lli, Xiaofang Li, Maosong Xu. // IGARSS 2009 Geoscience and Remote Sensing Symposium, 2009 IEEE International. - Cape Town, 12-17 July 2009. - Vol. 2. - P. II-726-II-729-726. 
- C1369.** Gendron M. Automated change detection using Synthetic Aperture Sonar imagery. / Gendron M., Lohrenz M., Dubberley J. // MTS/IEEE Biloxi-Marine Technology for Our Future: Global and Local Challenges OCEANS 2009. - Biloxi, MS, 26-29 Oct. 2009. - P. 1-4. 
- C1370.** Abileah R. Surveying coastal ship traffic with LANDSAT. MTS/IEEE Biloxi-Marine Technology for Our Future: Global and Local Challenges OCEANS 2009. - Biloxi, MS, 26-29 Oct. 2009. - P. 1-6. 
- C1371.** Macon C.L. USACE National Coastal Mapping Program and the next generation of data products. MTS/IEEE Biloxi-Marine Technology for Our Future: Global and Local Challenges OCEANS 2009. - Biloxi, MS, 26-29 Oct. 2009. - P. 1-7. 

- C1372.** Yue Huang. Sub-canopy ground characteristics retrieval of PolinSAR using spectral analysis technique. / Yue Huang, Xinwu Li, Ferro-Famil L., Pottier E., Huadong Guo. // IGARSS 2009 Geoscience and Remote Sensing Symposium, 2009 IEEE International. - Cape Town, 12-17 July 2009. - Vol. 3. - P. III-502-III-505-502. ↑
- C1373.** Flett D. The RADARSAT Constellation Mission: Meeting the government of Canada's needs and requirements. / Flett D., Crevier Y., Girard R. // IGARSS 2009 Geoscience and Remote Sensing Symposium, 2009 IEEE International. - Cape Town, 12-17 July 2009. - Vol. 2. - P. II-910-II-912-910. ↑
- C1374.** Malzone C. Modeling the multidimensional & fiscal impacts of storm surge & sea level rise: A compelling view through a powerful interactive 4D data integration, analysis and visualization tool. / Malzone C., Marcus J., Pauly T. // MTS/IEEE Biloxi-Marine Technology for Our Future: Global and Local Challenges OCEANS 2009. - Biloxi, MS, 26-29 Oct. 2009. - P. 1-7. ↑
- C1375.** Atkinson L.P. HFR surface currents observing system in lower Chesapeake Bay and Virginia coast. / Atkinson L.P., Garner T., Blanco J., Paternostro C., Burke P. // MTS/IEEE Biloxi-Marine Technology for Our Future: Global and Local Challenges OCEANS 2009. - Biloxi, MS, 26-29 Oct. 2009. - P. 1-6. ↑
- C1376.** Waldron D.L. Underwater optical ranging: A hybrid LIDAR-RADAR approach. / Waldron D.L., Mullen L. // MTS/IEEE Biloxi-Marine Technology for Our Future: Global and Local Challenges OCEANS 2009. - Biloxi, MS, 26-29 Oct. 2009. - P. 1-7. ↑
- C1377.** Zelenke B. Evaluating connectivity between marine protected areas using CODAR high-frequency radar. / Zelenke B., Moline M.A., Jones B.H., Ramp S.R., Crawford G.B., Largier J.L., Terrill E.J., Garfield N., Paduan J.D., Washburn L. // MTS/IEEE Biloxi-Marine Technology for Our Future: Global and Local Challenges OCEANS 2009. - Biloxi, MS, 26-29 Oct. 2009. - P. 1-10. ↑
- C1378.** Yinghui Zhao. Target coherence analysis using canonical correlation decomposition for SAS data. / Yinghui Zhao, Wachowski N., Azimi-Sadjadi M.R. // MTS/IEEE Biloxi-Marine Technology for Our Future: Global and Local Challenges OCEANS 2009. - Biloxi, MS, 26-29 Oct. 2009. - P. 1-7. ↑
- C1379.** Alsweiss S. Simulated OVW retrievals in tropical cyclones for the next generation Dual Frequency Scatterometer. / Alsweiss S., Laupattarakasem P., El-Nimri S., Jones W.L., Veleva S., Stiles B.W., Rodriguez E., Gaston R.W. // MTS/IEEE Biloxi-Marine Technology for Our Future: Global and Local Challenges OCEANS 2009. - Biloxi, MS, 26-29 Oct. 2009. - P. 1-4. ↑
- C1380.** Weissman D.E. Coincident observations, with QuikSCAT and ASCAT, of the effects of rain-induced sea surface stress during hurricanes Gustav and Ike. / Weissman D.E., Bourassa M.A. // MTS/IEEE Biloxi-Marine Technology for Our Future: Global and Local Challenges OCEANS 2009. - Biloxi, MS, 26-29 Oct. 2009. - P. 1-10. ↑
- C1381.** Dalponte M. Fusion of hyperspectral and lidar remote sensing data for the estimation of tree stem diameters. / Dalponte M., Bruzzone L., Gianelle D. // IGARSS 2009 Geoscience and Remote Sensing Symposium, 2009 IEEE International. - Cape Town, 12-17 July 2009. - Vol. 2. - P. II-1008-II-1011-1008. ↑
- C1382.** Longepe N. Case studies of frozen ground monitoring using PALSAR/ALOS data. / Longepe N., Tadono T., Shimada M., Pottier E., Allain S. // IGARSS 2009 Geoscience and Remote Sensing Symposium, 2009 IEEE International. - Cape Town, 12-17 July 2009. - Vol. 2. - P. II-1020-II-1023-1020. ↑
- C1383.** Dali J. Polarimetric ice sounding at P-band: First results. IGARSS 2009 Geoscience and Remote Sensing Symposium, 2009 IEEE International. - Cape Town, 12-17 July 2009. - Vol. 2. - P. II-1024-II-1027-1024. ↑
- C1384.** Hopf A.P. CASA Phased Array Radar System description, simulation and products. / Hopf A.P., Salazar J.L., Medina R., Venkatesh V., Knapp E.J., Frasier S.J., McLaughlin D.J. // IGARSS 2009 Geoscience and Remote Sensing Symposium, 2009 IEEE International. - Cape Town, 12-17 July 2009. - Vol. 2. - P. II-968-II-971-968. ↑
- C1385.** Bombrun L. Hierarchical segmentation of Polarimetric SAR images using heterogeneous clutter models. / Bombrun L., Beaulieu J.-M., Vasile G., Ovarlez J.-P., Pascal F., Gay M. // IGARSS 2009 Geoscience and Remote Sensing Symposium, 2009 IEEE International. - Cape Town, 12-17 July 2009. - Vol. 3. - P. III-5-III-8-5. ↑

- C1386.** Singh J. Parametric versus non-parametric complex image analysis. / Singh J., Soccorsi M., Datcu M. // IGARSS 2009 Geoscience and Remote Sensing Symposium, 2009 IEEE International. - Cape Town, 12-17 July 2009. - Vol. 3. - P. III-9-III-12-9. ↑
- C1387.** Marino A. Selectable target detector using the polarization fork. / Marino A., Woodhouse I.H. // IGARSS 2009 Geoscience and Remote Sensing Symposium, 2009 IEEE International. - Cape Town, 12-17 July 2009. - Vol. 3. - P. III-1-III-4-1. ↑
- C1388.** Cerra D. Parameter-free clustering: Application to fawns detection. / Cerra D., Israel M., Datcu M. // IGARSS 2009 Geoscience and Remote Sensing Symposium, 2009 IEEE International. - Cape Town, 12-17 July 2009. - Vol. 3. - P. III-467-III-469-467. ↑
- C1389.** Jingjuan Liao. Surface parameters retrieval from alluvial fan in Ejina area of Inner Mongolia using multi-polarization SAR data. / Jingjuan Liao, Zizhen Pang. // IGARSS 2009 Geoscience and Remote Sensing Symposium, 2009 IEEE International. - Cape Town, 12-17 July 2009. - Vol. 3. - P. III-498-III-501-498. ↑
- C1390.** Floricioiu D. Surface velocity and variations of outlet glaciers of the Patagonia Icefields by means of TerraSAR-X. / Floricioiu D., Eineder M., Rott H., Yague-Martinez N., Nagler T. // IGARSS 2009 Geoscience and Remote Sensing Symposium, 2009 IEEE International. - Cape Town, 12-17 July 2009. - Vol. 2. - P. II-1028-II-1031-1028. ↑
- C1391.** Whitcomb J. Mapping Canadian wetlands using L-band radar satellite imagery S. / Whitcomb J., Moghaddam M., McDonald K., Podest E. // IGARSS 2009 Geoscience and Remote Sensing Symposium, 2009 IEEE International. - Cape Town, 12-17 July 2009. - Vol. 2. - P. II-1032-II-1035-1032. ↑
- C1392.** Broccardo S. Airborne imaging differential optical absorption spectroscopy: Trace-gas measurements from the suburbs to the sub-continent. / Broccardo S., Piketh S., Heue K.-P., Platt U. // IGARSS 2009 Geoscience and Remote Sensing Symposium, 2009 IEEE International. - Cape Town, 12-17 July 2009. - Vol. 2. - P. II-1044-II-1047-1044. ↑
- C1393.** Gras V. A toolbox dedicated to the analysis of airborne SAR sea clutter data. / Gras V., Sintes C.R. // MTS/IEEE Biloxi-Marine Technology for Our Future: Global and Local Challenges OCEANS 2009. - Biloxi, MS, 26-29 Oct. 2009. - P. 1-8. ↑
- C1394.** Essen H. SUMATRA, a W-band SAR for UAV application. / Essen H., Brautigam M., Sommer R., Wahlen A., Johannes W., Wilcke J., Schlechtweg M., Tessmann A. // 2009. RADAR. International Radar Conference-Surveillance for a Safer World. - Bordeaux, 12-16 Oct. 2009. - P. 1-4. ↑
- C1395.** Pandey A. Study of vegetable Okra by microwave remote sensing at X- band. / Pandey A., Prasad R., Rajput N.S. // 2009. ELECTRO '09. International Conference on Emerging Trends in Electronic and Photonic Devices & Systems. - Varanasi, 22-24 Dec. 2009. - P. 211-214. ↑
- C1396.** Nascimento A.D.C. Measuring Synthetic Aperture Radar target differences with stochastic distances. / Nascimento A.D.C., Cintra R.J., Frery A.C. // 2009 IEEE Toronto International Conference Science and Technology for Humanity (TIC-STH). - Toronto, ON, 26-27 Sept. 2009. - P. 587-592. ↑
- C1397.** Truong-Loi M.-L. Compact polarimetry mode at low frequency for vegetation applications. / Truong-Loi M.-L., Dubois-Fernandez P., Freeman A., Pottier E. // 2009. RADAR. International Radar Conference-Surveillance for a Safer World. - Bordeaux, 12-16 Oct. 2009. - P. 1-4. ↑
- C1398.** Kersten P.R. Combining modern spectral estimation with Time-Frequency representation. / Kersten P.R., Jansen R.W., Ainsworth T.L., Toporkov J.V., Sletten M.A. // 2009. RADAR. International Radar Conference-Surveillance for a Safer World. - Bordeaux, 12-16 Oct. 2009. - P. 1-4. ↑
- C1399.** Snoeij P. The Sentinel-1 radar mission: status and performance. / Snoeij P., Attema E., Davidson M., Duesmann B., Floury N., Levrini G., Rommen B., Rosich B. // 2009. RADAR. International Radar Conference-Surveillance for a Safer World. - Bordeaux, 12-16 Oct. 2009. - P. 1-6. ↑
- C1400.** Shaogang Wang. Study on Astronomical Solar Radiation over Rugged Terrain Using DEM Data. 2009 1st International Conference on Information Science and Engineering (ICISE). - Nanjing, 26-28 Dec. 2009. - P. 2184-2187. ↑

- C1401.** Gurram P. Automated 3D object identification using Bayesian networks. / Gurram P., Rhody H., Saber E., Sahin F. // 2009 IEEE Applied Imagery Pattern Recognition Workshop (AIPRW). - Washington, DC, 14-16 Oct. 2009. - P. 1-8. ↑
- C1402.** Maohai Li. GPRS Based Guard Robot Alarm System Design. / Maohai Li, Lining Sun, Qingcheng Huang, Zesu Cai, Songhao Piao. // 2009 Fourth International Conference on Internet Computing for Science and Engineering (ICICSE). - Harbin, 21-22 Dec. 2009. - P. 211-216. ↑
- C1403.** Tiantian Feng. Review and Comparison: Building Extraction Methods Using High-Resolution Images. / Tiantian Feng, Junqiao Zhao. // 2009 Second International Symposium on Information Science and Engineering (ISISE). - Shanghai, 26-28 Dec. 2009. - P. 419-422. ↑
- C1404.** Villalon-Turrubiates I.E. Performance Study of the Robust Bayesian Regularization Technique for Remote Sensing Imaging in Geophysical Applications. / Villalon-Turrubiates I.E., Herrera-Nuez A. // 2009 Mexican International Conference on Computer Science (ENC). - Mexico City, 21-25 Sept. 2009. - P. 3-12. ↑
- C1405.** Ming Wei. Three Dimension Wind Retrieval of Single-Doppler Radar Data with Improved VVP Method. / Ming Wei, Nan Li. // 2009 1st International Conference on Information Science and Engineering (ICISE). - Nanjing, 26-28 Dec. 2009. - P. 5276-5278. ↑
- C1406.** Heron M.L. Bistatic HF ocean radar: Errors and limitations. / Heron M.L., Barbin Y. // MTS/IEEE Biloxi-Marine Technology for Our Future: Global and Local Challenges OCEANS 2009. - Biloxi, MS, 26-29 Oct. 2009. - P. 1-5. ↑
- C1407.** Harlan J. Next generation use of high power and bandwidth in the NE Pacific-A component of the NSF Ocean Observing Initiative. / Harlan J., Kosro P.M., Barletto P. // MTS/IEEE Biloxi-Marine Technology for Our Future: Global and Local Challenges OCEANS 2009. - Biloxi, MS, 26-29 Oct. 2009. - P. 1-8. ↑
- C1408.** Rahmat-Samii Y. A history of reflector antenna development: Past, present and future. / Rahmat-Samii Y., Densmore A. // 2009 SBMO/IEEE MTT-S International Microwave and Optoelectronics Conference (IMOC). - Belem, 3-6 Nov. 2009. - P. 17-23. ↑
- C1409.** Trizna D.B. Coherent microwave marine radars for deterministic wave profile mapping, decameter-scale coastal current mapping and ocean wave spectra measurements. MTS/IEEE Biloxi-Marine Technology for Our Future: Global and Local Challenges OCEANS 2009. - Biloxi, MS, 26-29 Oct. 2009. - P. 1-5. ↑
- C1410.** Trizna D.B. Coherent microwave marine radar measurements of directional ocean wave spectra and mean radial current fields. MTS/IEEE Biloxi-Marine Technology for Our Future: Global and Local Challenges OCEANS 2009. - Biloxi, MS, 26-29 Oct. 2009. - P. 1-8. ↑
- C1411.** Prater J.L. Interferometric measurements using redundant phase centers of synthetic aperture sonars. / Prater J.L., G-Michael T. // MTS/IEEE Biloxi-Marine Technology for Our Future: Global and Local Challenges OCEANS 2009. - Biloxi, MS, 26-29 Oct. 2009. - P. 1-6. ↑
- C1412.** Baque R. The airborne SAR-system: SETHI airborne microwave remote sensing imaging system. / Baque R., Bonin G., Ruault du Plessis O. // 2009. RADAR. International Radar Conference-Surveillance for a Safer World. - Bordeaux, 12-16 Oct. 2009. - P. 1-5. ↑
- C1413.** Sajjad N. Electromagnetic wave scattering from sea and bare soil surfaces based on an improved two-scale model. / Sajjad N., Khenchaf A., Coatanhay A. // 2009. RADAR. International Radar Conference-Surveillance for a Safer World. - Bordeaux, 12-16 Oct. 2009. - P. 1-6. ↑
- C1414.** Grosdidier S. HFSW radar model and evaluation of a multiscale source extraction approach for target detection. / Grosdidier S., Baussard A., Khenchaf A. // 2009. RADAR. International Radar Conference-Surveillance for a Safer World. - Bordeaux, 12-16 Oct. 2009. - P. 1-6. ↑
- C1415.** Boerner W.-M. Recent advances in SAR remote sensing: "Multimodal POLinSAR imaging with applications to remote sensing of the terrestrial covers and the monitoring of environmental stress changes". 2009 Applied Electromagnetics Conference (AEMC). - Kolkata, 14-16 Dec. 2009. - P. 1-8. ↑
- C1416.** Rengarajan S.R. A tutorial on design and analysis of waveguide-fed slot array antennas. 2009 Applied Electromagnetics Conference (AEMC). - Kolkata, 14-16 Dec. 2009. - P. 1-2. ↑

- C1417.** Nouvel J.F. ONERA DRIVE project. 2009. RADAR. International Radar Conference-Surveillance for a Safer World. - Bordeaux, 12-16 Oct. 2009. - P. 1-4. ↑
- C1418.** Eineder M. Scientific requirements and feasibility on an L-band mission dedicated to measure surface deformation. / Eineder M., Friedrich A., Minet C., Bamler R., Flerit F., Hajnsek I. // IGARSS 2009 Geoscience and Remote Sensing Symposium, 2009 IEEE International. - Cape Town, 12-17 July 2009. - Vol. 2. - P. II-789-II-792-789. ↑
- C1419.** De Zan F. Mission design and performance for systematic deformation measurements with a spaceborne SAR system. / De Zan F., Prats P., Krieger G. // IGARSS 2009 Geoscience and Remote Sensing Symposium, 2009 IEEE International. - Cape Town, 12-17 July 2009. - Vol. 2. - P. II-793-II-796-793. ↑
- C1420.** Shimada M. Deformation monitoring using the ALOS/PALSAR. / Shimada M., Miyagi Y. // IGARSS 2009 Geoscience and Remote Sensing Symposium, 2009 IEEE International. - Cape Town, 12-17 July 2009. - Vol. 2. - P. II-797-II-800-797. ↑
- C1421.** Haiyan Li. Improving sea states monitoring of nautical radar using dispersion relation of nonlinear ocean waves. / Haiyan Li, Limin Cui, Zhongfeng Qiu, Shufang Zhang, Yijun He. // IGARSS 2009 Geoscience and Remote Sensing Symposium, 2009 IEEE International. - Cape Town, 12-17 July 2009. - Vol. 3. - P. III-41-III-44-41. ↑
- C1422.** Nirchio F. COSMO-SkyMed contribution in oil spill monitoring of the Mediterranean Sea. / Nirchio F., Pandiscia G., Ruggieri G., Santoleri R., Tataranni F., Giancaspro A., Trivero P., Pinardi N., Masini A., Castellani C. // IGARSS 2009 Geoscience and Remote Sensing Symposium, 2009 IEEE International. - Cape Town, 12-17 July 2009. - Vol. 2. - P. II-781-II-784-781. ↑
- C1423.** Rocca F. 18 Years of interferometry, as seen from POLIMI. IGARSS 2009 Geoscience and Remote Sensing Symposium, 2009 IEEE International. - Cape Town, 12-17 July 2009. - Vol. 2. - P. II-785-II-788-785. ↑
- C1424.** Hochard G. Stable Coherent Area in SAR interferometry. / Hochard G., Binet R., Nicolas J.-M. // IGARSS 2009 Geoscience and Remote Sensing Symposium, 2009 IEEE International. - Cape Town, 12-17 July 2009. - Vol. 2. - P. II-825-II-828-825. ↑
- C1425.** Fritz J. Analyzing radar backscatter of land within the TRMM footprint using high resolution SAR. / Fritz J., Chandrasekar V. // IGARSS 2009 Geoscience and Remote Sensing Symposium, 2009 IEEE International. - Cape Town, 12-17 July 2009. - Vol. 2. - P. II-829-II-832-829. ↑
- C1426.** Yue Huang. 3-D characterization of buildings in a dense urban environment using L-band Pol-InSAR data with irregular baselines. / Yue Huang, Ferro-Famil L. // IGARSS 2009 Geoscience and Remote Sensing Symposium, 2009 IEEE International. - Cape Town, 12-17 July 2009. - Vol. 3. - P. III-29-III-32-29. ↑
- C1427.** Kazumori M. Impact studies of AMSR-E ocean surface wind speed data in NWP at JMA. IGARSS 2009 Geoscience and Remote Sensing Symposium, 2009 IEEE International. - Cape Town, 12-17 July 2009. - Vol. 2. - P. II-801-II-804-801. ↑
- C1428.** Benhmammouch O. Modeling of roughness effects on electromagnetic waves propagation above sea surface using 3D parabolic equation. / Benhmammouch O., Caouen N., Khenchaf A. // IGARSS 2009 Geoscience and Remote Sensing Symposium, 2009 IEEE International. - Cape Town, 12-17 July 2009. - Vol. 2. - P. II-817-II-820-817. ↑
- C1429.** Sobieski P. Comparison between electromagnetic scattering by a rain induced sea surface roughness and field data. / Sobieski P., Craeye C., Bliven L.F. // IGARSS 2009 Geoscience and Remote Sensing Symposium, 2009 IEEE International. - Cape Town, 12-17 July 2009. - Vol. 2. - P. II-821-II-824-821. ↑
- C1430.** Shizhuo Liu. On the value of high-resolution weather models for atmospheric mitigation in SAR interferometry. / Shizhuo Liu, Hanssen R., Mika A. // IGARSS 2009 Geoscience and Remote Sensing Symposium, 2009 IEEE International. - Cape Town, 12-17 July 2009. - Vol. 2. - P. II-749-II-752-749. ↑
- C1431.** Hillman A. RADARSAT-2 initial system operations and performance. / Hillman A., Rolland P., Periard R., Luscombe A., Chabot M., Chen C., Martens N. // IGARSS 2009 Geoscience and Remote Sensing Symposium, 2009 IEEE International. - Cape Town, 12-17 July 2009. - Vol. 2. - P. II-753-II-756-753. ↑

- C1432.** Luscombe A. Image quality and calibration of RADARSAT-2. IGARSS 2009 Geoscience and Remote Sensing Symposium, 2009 IEEE International. - Cape Town, 12-17 July 2009. - Vol. 2. - P. II-757-II-760-757. ↑
- C1433.** Sant'Anna S.J.S. Polarization plane rotation effects on SAR polarimetric attributes. / Sant'Anna S.J.S., da Lacava J.C.S., Fernandes D. // IGARSS 2009 Geoscience and Remote Sensing Symposium, 2009 IEEE International. - Cape Town, 12-17 July 2009. - Vol. 2. - P. II-734-II-737-734. ↑
- C1434.** Xiaofang Li. Microwave scattering behaviour analysis of typical targets with SAR image. / Xiaofang Li, Kun Li, Fengli Zhang, Yun Shao, Qulin Tan. // IGARSS 2009 Geoscience and Remote Sensing Symposium, 2009 IEEE International. - Cape Town, 12-17 July 2009. - Vol. 2. - P. II-738-II-741-738. ↑
- C1435.** Shirokov I.B. Correction of target data taking into consideration the troposphere refractivity. / Shirokov I.B., Gimpilevich Yu.B., Jandieri G.V., Serdyuk I.B. // IGARSS 2009 Geoscience and Remote Sensing Symposium, 2009 IEEE International. - Cape Town, 12-17 July 2009. - Vol. 2. - P. II-745-II-748-745. ↑
- C1436.** Covello F. COSMO-SkyMed mission status: Three out of four satellites in orbit. / Covello F., Battazza F., Coletta A., Manoni G., Valentini G. // IGARSS 2009 Geoscience and Remote Sensing Symposium, 2009 IEEE International. - Cape Town, 12-17 July 2009. - Vol. 2. - P. II-773-II-776-773. ↑
- C1437.** Ciappa A. Sea surface transport derived by frequent revisit time series of COSMO SkyMed SAR data. / Ciappa A., Pietranera L., Coletta A. // IGARSS 2009 Geoscience and Remote Sensing Symposium, 2009 IEEE International. - Cape Town, 12-17 July 2009. - Vol. 2. - P. II-777-II-780-777. ↑
- C1438.** Hwang P.A. Swell influence on ocean surface roughness and radar scattering from the ocean surface. / Hwang P.A., Plant W.J. // IGARSS 2009 Geoscience and Remote Sensing Symposium, 2009 IEEE International. - Cape Town, 12-17 July 2009. - Vol. 3. - P. III-37-III-40-37. ↑
- C1439.** Gruber A. TanDEM-X DEM calibration: Correction of systematic DEM errors by block adjustment. / Gruber A., Wessel B., Huber M. // IGARSS 2009 Geoscience and Remote Sensing Symposium, 2009 IEEE International. - Cape Town, 12-17 July 2009. - Vol. 2. - P. II-761-II-764-761. ↑
- C1440.** Breit H. Processing system and algorithms for the TanDEM-X mission. / Breit H., Fritz T., Eineder M., Bamler R., Lachaise M., Brcic R., Adam N., Yague-Martinez N. // IGARSS 2009 Geoscience and Remote Sensing Symposium, 2009 IEEE International. - Cape Town, 12-17 July 2009. - Vol. 2. - P. II-765-II-768-765. ↑
- C1441.** Huber M. Ensuring globally the TanDEM-X height accuracy: Analysis of the reference data sets ICESat, SRTM and GPS-tracks. / Huber M., Wessel B., Kosmann D., Felbier A., Schwiager V., Habermeyer M., Wendleder A., Roth A. // IGARSS 2009 Geoscience and Remote Sensing Symposium, 2009 IEEE International. - Cape Town, 12-17 July 2009. - Vol. 2. - P. II-769-II-772-769. ↑
- C1442.** Mercer B. 3D topography and forest recovery from an L-BAND single-pass airborne PolInSAR system. / Mercer B., Qiaoping Zhang, Schwaebisch M., Denbina M. // IGARSS 2009 Geoscience and Remote Sensing Symposium, 2009 IEEE International. - Cape Town, 12-17 July 2009. - Vol. 3. - P. III-33-III-36-33. ↑
- C1443.** Santi E. Retrieval of soil moisture with airborne and satellite microwave sensors. / Santi E., Paloscia S., Pampaloni P., Pettinato S., Brogioni M. // IGARSS 2009 Geoscience and Remote Sensing Symposium, 2009 IEEE International. - Cape Town, 12-17 July 2009. - Vol. 2. - P. II-937-II-940-937. ↑
- C1444.** Scheiber R. Extrapolation of airborne polarimetric and interferometric SAR data for validation of bio-geo-retrieval algorithms for future spaceborne SAR missions. / Scheiber R., Seung-Kuk Lee, Papathanassiou K.P., Flouy N. // IGARSS 2009 Geoscience and Remote Sensing Symposium, 2009 IEEE International. - Cape Town, 12-17 July 2009. - Vol. 2. - P. II-941-II-944-941. ↑
- C1445.** Guarnieri A.M. Impact of atmospheric water vapor on the design of a Ku band geosynchronous SAR system. / Guarnieri A.M., Rocca F., Ibars A.B. // IGARSS 2009 Geoscience and Remote Sensing Symposium, 2009 IEEE International. - Cape Town, 12-17 July 2009. - Vol. 2. - P. II-945-II-948-945. ↑
- C1446.** Nitti D.O. Quantitative analysis of stripmap and spotlight SAR interferometry with COSMO-SkyMed constellation. / Nitti D.O., Nutricato R., Bovenga F., Rana F., Conte D., Milillo G., Guerriero L. // IGARSS 2009 Geoscience and Remote Sensing Symposium, 2009 IEEE International. - Cape Town, 12-17 July 2009. - Vol. 2. - P. II-925-II-928-925. ↑

- C1447.** Boni G. The OPERA project: EO-based flood risk management in Italy. / Boni G., Candela L., Castelli F., Dellepiane S., Palandri M., Persi D., Pierdicca N., Rudari R., Serpico S., Siccardi F., Versace C. // IGARSS 2009 Geoscience and Remote Sensing Symposium, 2009 IEEE International. - Cape Town, 12-17 July 2009. - Vol. 2. - P. II-929-II-932-929. ↑
- C1448.** Pierdicca N. Using COSMO-SkyMed data for flood mapping: Some case-studies. / Pierdicca N., Chini M., Pulvirenti L., Candela L., Ferrazzoli P., Guerriero L., Boni G., Siccardi F., Castelli F. // IGARSS 2009 Geoscience and Remote Sensing Symposium, 2009 IEEE International. - Cape Town, 12-17 July 2009. - Vol. 2. - P. II-933-II-936-933. ↑
- C1449.** Chandrasekar V. Attenuation margin requirements in a networked radar system for observation of precipitation. / Chandrasekar V., Willie D., Yanting Wang, Sanghun Lim. // IGARSS 2009 Geoscience and Remote Sensing Symposium, 2009 IEEE International. - Cape Town, 12-17 July 2009. - Vol. 2. - P. II-957-II-959-957. ↑
- C1450.** Tratalba J.M. Differential Reflectivity (ZDR) calibration for CASA radar network using properties of the observed medium. / Tratalba J.M., Chandrasekar V., Gorgucci E., McLaughlin D.J. // IGARSS 2009 Geoscience and Remote Sensing Symposium, 2009 IEEE International. - Cape Town, 12-17 July 2009. - Vol. 2. - P. II-960-II-963-960. ↑
- C1451.** Salazar J.L. Coverage comparison of short range radar networks vs. conventional weather radars: Case study in the northwestern United States. / Salazar J.L., Hopf A., Contreras R.F., Philips B., Knapp E.J., McLaughlin D., Brotzge J., Brewster K. // IGARSS 2009 Geoscience and Remote Sensing Symposium, 2009 IEEE International. - Cape Town, 12-17 July 2009. - Vol. 2. - P. II-964-II-967-964. ↑
- C1452.** Tison C. Analysis of SAR image time-series with a time-frequency method. IGARSS 2009 Geoscience and Remote Sensing Symposium, 2009 IEEE International. - Cape Town, 12-17 July 2009. - Vol. 3. - P. III-13-III-16-13. ↑
- C1453.** Auer S. 3D analysis of scattering effects based on Ray Tracing techniques. / Auer S., Xiaoxiang Zhu, Hinz S., Bamler R. // IGARSS 2009 Geoscience and Remote Sensing Symposium, 2009 IEEE International. - Cape Town, 12-17 July 2009. - Vol. 3. - P. III-17-III-20-17. ↑
- C1454.** Casu F. Satellite ground deformation measurements: An on-demand GRID-InSAR processing system exploiting the SBAS algorithm. / Casu F., Cossu R., Fusco L., Guarino S., Lanari R., Manunta M., Mazzarella G., Sansosti E. // IGARSS 2009 Geoscience and Remote Sensing Symposium, 2009 IEEE International. - Cape Town, 12-17 July 2009. - Vol. 2. - P. II-949-II-952-949. ↑
- C1455.** Basile F. Joint SAR imaging and DEM reconstruction from multichannel layover-affected SAR data. / Basile F., Budillon A., Ferraioli G., Pascasio V. // IGARSS 2009 Geoscience and Remote Sensing Symposium, 2009 IEEE International. - Cape Town, 12-17 July 2009. - Vol. 3. - P. III-25-III-28-25. ↑
- C1456.** Cote S. RADARSAT-1 AND -2 government calibration activities. / Cote S., Srivastava S., Hawkins R., Muir S., Lukowski T. // IGARSS 2009 Geoscience and Remote Sensing Symposium, 2009 IEEE International. - Cape Town, 12-17 July 2009. - Vol. 2. - P. II-890-II-893-890. ↑
- C1457.** Seguin G. RADARSAT constellation, project objectives and status. / Seguin G., Ahmed S. // IGARSS 2009 Geoscience and Remote Sensing Symposium, 2009 IEEE International. - Cape Town, 12-17 July 2009. - Vol. 2. - P. II-894-II-897-894. ↑
- C1458.** Soo Chin Liew. Monitoring turbidity and suspended sediment concentration of coastal and inland waters using satellite data. / Soo Chin Liew, Saengtaksin B., Leong Keong Kwoh. // IGARSS 2009 Geoscience and Remote Sensing Symposium, 2009 IEEE International. - Cape Town, 12-17 July 2009. - Vol. 2. - P. II-837-II-839-837. ↑
- C1459.** Luo J. Evaluation of the single reference image snow-covered area estimation method for the boreal forest zone. / Luo J., Pulliainen J., Metsamäki S. // IGARSS 2009 Geoscience and Remote Sensing Symposium, 2009 IEEE International. - Cape Town, 12-17 July 2009. - Vol. 2. - P. II-867-II-870-867. ↑
- C1460.** Pinheiro M. Tomographic 3D reconstruction from airborne circular SAR. / Pinheiro M., Prats P., Scheiber R., Nannini M., Reigber A. // IGARSS 2009 Geoscience and Remote Sensing Symposium, 2009 IEEE International. - Cape Town, 12-17 July 2009. - Vol. 3. - P. III-21-III-24-21. ↑

- C1461.** Nadai A. Development of X-band airborne polarimetric and interferometric SAR with sub-meter spatial resolution. / Nadai A., Uratsuka S., Umehara T., Matsuoka T., Kobayashi T., Satake M. // IGARSS 2009 Geoscience and Remote Sensing Symposium, 2009 IEEE International. - Cape Town, 12-17 July 2009. - Vol. 2. - P. II-913-II-916-913. ↑
- C1462.** Gonzalez Bonilla M.-J. INTASAR Program. / Gonzalez Bonilla M.-J., Miguel B.G., Cuerda Muoz J.-M., Larranaga Sudupe J.-R., Garcia Rodriguez M. // IGARSS 2009 Geoscience and Remote Sensing Symposium, 2009 IEEE International. - Cape Town, 12-17 July 2009. - Vol. 2. - P. II-917-II-920-917. ↑
- C1463.** Salvi S. Use of Cosmo-Skymed data for seismic risk management in the framework of the ASI-SIGRIS project. / Salvi S., Vignoli S., Serra M., Bosi V. // IGARSS 2009 Geoscience and Remote Sensing Symposium, 2009 IEEE International. - Cape Town, 12-17 July 2009. - Vol. 2. - P. II-921-II-924-921. ↑
- C1464.** McNairn H. TerraSAR-X and RADARSAT-2 for crop classification and acreage estimation. / McNairn H., Shang J., Champagne C., Jiao X. // IGARSS 2009 Geoscience and Remote Sensing Symposium, 2009 IEEE International. - Cape Town, 12-17 July 2009. - Vol. 2. - P. II-898-II-901-898. ↑
- C1465.** Horn R. F-SAR-DLR's new multifrequency polarimetric airborne SAR. / Horn R., Nottensteiner A., Reigber A., Fischer J., Scheiber R. // IGARSS 2009 Geoscience and Remote Sensing Symposium, 2009 IEEE International. - Cape Town, 12-17 July 2009. - Vol. 2. - P. II-902-II-905-902. ↑
- C1466.** Rodriguez M.G. RBX: The new X-band radar from INTA. / Rodriguez M.G., Cores Muradas J.F., Larraaga Sudupe J.R. // IGARSS 2009 Geoscience and Remote Sensing Symposium, 2009 IEEE International. - Cape Town, 12-17 July 2009. - Vol. 2. - P. II-906-II-909-906. ↑
- C1467.** Lombardini F. Full-resolution adaptive differential tomography. IGARSS 2009 Geoscience and Remote Sensing Symposium, 2009 IEEE International. - Cape Town, 12-17 July 2009. - Vol. 3. - P. III-176-III-179-176. ↑
- C1468.** McPherson C.J. Methods of analysis of atmospheric aerosols from future spaceborne high spectral resolution lidar data. / McPherson C.J., Reagan J.A., Ferrare R.A., Hostetler C.A., Hair J.W. // IGARSS 2009 Geoscience and Remote Sensing Symposium, 2009 IEEE International. - Cape Town, 12-17 July 2009. - Vol. 5. - P. V-485-V-488-485. ↑
- C1469.** Martin-Puig C. SAR altimeter retracker performance bound over water surfaces. / Martin-Puig C., Ruffini G. // IGARSS 2009 Geoscience and Remote Sensing Symposium, 2009 IEEE International. - Cape Town, 12-17 July 2009. - Vol. 5. - P. V-449-V-452-449. ↑
- C1470.** Lewis C. A radar suite for ice sheet accumulation measurements and near-surface internal layer mapping. / Lewis C., Patel A., Owen H., Rodriguez-Morales F., Leuschen C., Seguin S.A., Ledford J., Player K., Gogineni S. // IGARSS 2009 Geoscience and Remote Sensing Symposium, 2009 IEEE International. - Cape Town, 12-17 July 2009. - Vol. 5. - P. V-441-V-444-441. ↑
- C1471.** Meyer F.J. Mapping aurora activity with SAR-a case study. / Meyer F.J., Nicoll J., Bristow B. // IGARSS 2009 Geoscience and Remote Sensing Symposium, 2009 IEEE International. - Cape Town, 12-17 July 2009. - Vol. 4. - P. IV-1-IV-4-1. ↑
- C1472.** Lavalley M. Dependence of P-band interferometric height on forest parameters from simulation and observation. / Lavalley M., Williams M.L., Hensley S., Pottier E., Solimini D. // IGARSS 2009 Geoscience and Remote Sensing Symposium, 2009 IEEE International. - Cape Town, 12-17 July 2009. - Vol. 4. - P. IV-5-IV-8-5. ↑
- C1473.** Bevan S.L. Global atmospheric aerosol optical depth retrievals over land and ocean from AATSR. / Bevan S.L., North P., Los S.O., Grey W.M.F. // IGARSS 2009 Geoscience and Remote Sensing Symposium, 2009 IEEE International. - Cape Town, 12-17 July 2009. - Vol. 5. - P. V-481-V-484-481. ↑
- C1474.** Suwa K. Estimation of target motion and 3D target geometry using multistatic ISAR movies. / Suwa K., Wakayama T., Iwamoto M. // IGARSS 2009 Geoscience and Remote Sensing Symposium, 2009 IEEE International. - Cape Town, 12-17 July 2009. - Vol. 5. - P. V-429-V-432-429. ↑
- C1475.** Lopez-Sanchez J.M. Time series of polarimetric and interferometric observations of TerraSAR-X data over rice fields in Spain. / Lopez-Sanchez J.M., Ballester-Berman J.D., Hajnsek I. // IGARSS 2009 Geoscience and Remote Sensing Symposium, 2009 IEEE International. - Cape Town, 12-17 July 2009. - Vol. 5. - P. V-409-

V-412-409. ↑

**C1476.** Cristallini D. Chirp scaling based detection of moving targets in SAR images. / Cristallini D., Lombardo P., Pastina D., Mennella A. // IGARSS 2009 Geoscience and Remote Sensing Symposium, 2009 IEEE International. - Cape Town, 12-17 July 2009. - Vol. 5. - P. V-340-V-343-340. ↑

**C1477.** Le Roy Y. SRAL, a radar altimeter designed to measure a wide range of surface types. / Le Roy Y., Deschaux-Beaume M., Mavrocordatos C., Borde F. // IGARSS 2009 Geoscience and Remote Sensing Symposium, 2009 IEEE International. - Cape Town, 12-17 July 2009. - Vol. 5. - P. V-445-V-448-445. ↑

**C1478.** Xiaoqing Chu. The relationship between radar backscatter cross section and ocean wave parameters at low incidence angles. / Xiaoqing Chu, Yijun He, Gengxin Chen. // IGARSS 2009 Geoscience and Remote Sensing Symposium, 2009 IEEE International. - Cape Town, 12-17 July 2009. - Vol. 5. - P. V-433-V-436-433. ↑

**C1479.** Limin Cui. Measurements of ocean wave spectra with vertical polarization X-band radar image sequences. / Limin Cui, Yijun He. // IGARSS 2009 Geoscience and Remote Sensing Symposium, 2009 IEEE International. - Cape Town, 12-17 July 2009. - Vol. 5. - P. V-437-V-440-437. ↑

**C1480.** Seung-Kuk Lee. Polarimetric SAR interferometry for forest application at P-band: Potentials and challenges. / Seung-Kuk Lee, Kugler F., Papathanassiou K., Hajnsek I. // IGARSS 2009 Geoscience and Remote Sensing Symposium, 2009 IEEE International. - Cape Town, 12-17 July 2009. - Vol. 4. - P. IV-13-IV-16-13. ↑

**C1481.** Tello M. Advances in unsupervised ship detection with multiscale techniques. / Tello M., Lopez-Martinez C., Mallorqui J.J., Tares T., Greidanus H. // IGARSS 2009 Geoscience and Remote Sensing Symposium, 2009 IEEE International. - Cape Town, 12-17 July 2009. - Vol. 4. - P. IV-979-IV-982-979. ↑

**C1482.** Paes R.L. Ship detection in the Brazilian coast using TerraSAR-X SAR images. / Paes R.L., Lorenzetti J.A., Gherardi D.F.M. // IGARSS 2009 Geoscience and Remote Sensing Symposium, 2009 IEEE International. - Cape Town, 12-17 July 2009. - Vol. 4. - P. IV-983-IV-986-983. ↑

**C1483.** Mingsheng Liao. Ship detection from polarimetric sar images. / Mingsheng Liao, Changcheng Wang, Yong Wang, Xiaogang Song. // IGARSS 2009 Geoscience and Remote Sensing Symposium, 2009 IEEE International. - Cape Town, 12-17 July 2009. - Vol. 4. - P. IV-987-IV-990-987. ↑

**C1484.** Caizzzone S. Multifrequency theoretical simulations of backscattering from flooded areas. / Caizzzone S., Ferrazzoli P., Guerriero L., Pierdicca N., Pulvirenti L., Chini M. // IGARSS 2009 Geoscience and Remote Sensing Symposium, 2009 IEEE International. - Cape Town, 12-17 July 2009. - Vol. 4. - P. IV-968-IV-970-968. ↑

**C1485.** Ruijing Sun. Improvement of bare surface soil moisture estimation with L-band dual-polarization radar. / Ruijing Sun, Jiancheng Shi, Jackson T., Kunshan Chen, Yisok Oh. // IGARSS 2009 Geoscience and Remote Sensing Symposium, 2009 IEEE International. - Cape Town, 12-17 July 2009. - Vol. 4. - P. IV-971-IV-974-971. ↑

**C1486.** Margarit G. Operational approach for ship detection and classification. / Margarit G., Mallorqui J. // IGARSS 2009 Geoscience and Remote Sensing Symposium, 2009 IEEE International. - Cape Town, 12-17 July 2009. - Vol. 4. - P. IV-975-IV-978-975. ↑

**C1487.** Strozzi T. Monitoring land subsidence within the Venice Lagoon with SAR interferometry on Trihedral Corner Reflectors. / Strozzi T., Tosi L., Teatini P., Werner C., Wegmuller U. // IGARSS 2009 Geoscience and Remote Sensing Symposium, 2009 IEEE International. - Cape Town, 12-17 July 2009. - Vol. 4. - P. IV-33-IV-36-33. ↑

**C1488.** Dell'Acqua F. Experiences in optical and SAR imagery analysis for damage assessment in the Wuhan, May 2008 earthquake. / Dell'Acqua F., Lisini G., Gamba P. // IGARSS 2009 Geoscience and Remote Sensing Symposium, 2009 IEEE International. - Cape Town, 12-17 July 2009. - Vol. 4. - P. IV-37-IV-40-37. ↑

**C1489.** Wyholt A. Evaluating VHF-band SAR autofocus algorithms using a forest backscatter model. / Wyholt A., Ulander L. // IGARSS 2009 Geoscience and Remote Sensing Symposium, 2009 IEEE International. - Cape Town, 12-17 July 2009. - Vol. 4. - P. IV-9-IV-12-9. ↑

**C1490.** Muoz J.M.C. INTA's developments for UAS and small platforms: QUASAR. / Muoz J.M.C., Bonilla M.J.G., Miguel B.G., Ramon J., Sudupe L., Rodriguez M.G. // IGARSS 2009 Geoscience and Remote Sensing Symposium, 2009 IEEE International. - Cape Town, 12-17 July 2009. - Vol. 4. - P. IV-11-IV-14-11. ↑

Symposium, 2009 IEEE International. - Cape Town, 12-17 July 2009. - Vol. 4. - P. IV-999-IV-1002-999. ↑

**C1491.** Lambers M. GPU-based framework for distributed interactive 3D visualization of multimodal remote sensing data. / Lambers M., Kolb A. // IGARSS 2009 Geoscience and Remote Sensing Symposium, 2009 IEEE International. - Cape Town, 12-17 July 2009. - Vol. 4. - P. IV-57-IV-60-57. ↑

**C1492.** Casu F. SBAS-InSAR analysis of surface deformation at Mauna Loa and Kilauea volcanoes in Hawaii. / Casu F., Lanari R., Sansosti E., Poland M., Miklius A., Solaro G., Tizzani P. // IGARSS 2009 Geoscience and Remote Sensing Symposium, 2009 IEEE International. - Cape Town, 12-17 July 2009. - Vol. 4. - P. IV-41-IV-44-41. ↑

**C1493.** Kumar V. SAR interferometry and Speckle tracking approach for glacier velocity estimation using ERS-1/2 and TerraSAR-X spotlight high resolution data. / Kumar V., Venkataraman G., Rao Y.S. // IGARSS 2009 Geoscience and Remote Sensing Symposium, 2009 IEEE International. - Cape Town, 12-17 July 2009. - Vol. 5. - P. V-332-V-335-332. ↑

**C1494.** Cloude S.R. Polarized point scatterers: An algorithm for detection using ALOS-PALSAR data. IGARSS 2009 Geoscience and Remote Sensing Symposium, 2009 IEEE International. - Cape Town, 12-17 July 2009. - Vol. 5. - P. V-150-V-153-150. ↑

**C1495.** Yamada H. Scattering component decomposition for POL-InSAR dataset and its applications. / Yamada H., Komaya R., Yamaguchi Y., Sato R. // IGARSS 2009 Geoscience and Remote Sensing Symposium, 2009 IEEE International. - Cape Town, 12-17 July 2009. - Vol. 5. - P. V-154-V-157-154. ↑

**C1496.** Ferro-Famil L. Detection and analysis of urban areas using ALOS PALSAR polarimetric data. / Ferro-Famil L., Laval M. // IGARSS 2009 Geoscience and Remote Sensing Symposium, 2009 IEEE International. - Cape Town, 12-17 July 2009. - Vol. 5. - P. V-142-V-145-142. ↑

**C1497.** Lopez-Dekker P. Capon/APES based SAR processing: Practical considerations. / Lopez-Dekker P., Mallorqui J.J. // IGARSS 2009 Geoscience and Remote Sensing Symposium, 2009 IEEE International. - Cape Town, 12-17 July 2009. - Vol. 5. - P. V-168-V-171-168. ↑

**C1498.** Moriyama T. Calibration of spaceborne polarimetric SAR data using a genetic algorithm. IGARSS 2009 Geoscience and Remote Sensing Symposium, 2009 IEEE International. - Cape Town, 12-17 July 2009. - Vol. 5. - P. V-158-V-161-158. ↑

**C1499.** Kui Zhang. A new approach to improve the accuracy of baseline estimation for spaceborne radar interferometry. / Kui Zhang, Ng A.H.-m., Xiaojing Li, Hsing-Chung Chang, Linlin Ge, Rizos C. // IGARSS 2009 Geoscience and Remote Sensing Symposium, 2009 IEEE International. - Cape Town, 12-17 July 2009. - Vol. 5. - P. V-162-V-165-162. ↑

**C1500.** Kuplich T.M. Polarimetric signatures and classification of tropical land covers. / Kuplich T.M., Shimabukuro Y.E., Servello E., Sano E. // IGARSS 2009 Geoscience and Remote Sensing Symposium, 2009 IEEE International. - Cape Town, 12-17 July 2009. - Vol. 5. - P. V-118-V-121-118. ↑

**C1501.** Zhongsheng Xia. Karst forest type discrimination in southwest China using spaceborne polarimetric SAR data. / Zhongsheng Xia, Maosong Xu, Chou Xie, Ridha Touzi, Fengli Zhang, Huazhe Gong, Wei Tian. // IGARSS 2009 Geoscience and Remote Sensing Symposium, 2009 IEEE International. - Cape Town, 12-17 July 2009. - Vol. 5. - P. V-122-V-125-122. ↑

**C1502.** Rosenqvist A. The ALOS PALSAR mosaic over the African continent-A reference baseline dataset for forest- and land cover change monitoring. / Rosenqvist A., De Grandi F. // IGARSS 2009 Geoscience and Remote Sensing Symposium, 2009 IEEE International. - Cape Town, 12-17 July 2009. - Vol. 5. - P. V-115-V-117-115. ↑

**C1503.** Pipia L. Polarimetric coherence optimization for interferometric differential applications. / Pipia L., Fabregas X., Aguasca A., Lopez-Martinez C., Mallorqui J.J. // IGARSS 2009 Geoscience and Remote Sensing Symposium, 2009 IEEE International. - Cape Town, 12-17 July 2009. - Vol. 5. - P. V-146-V-149-146. ↑

**C1504.** Ballester-Berman J.D. Determination of scattering mechanisms inside rice plants by means of PCT and high resolution radar imaging. / Ballester-Berman J.D., Lopez-Sanchez J.M., Sanjuan M.-J. // IGARSS 2009 Geoscience and Remote Sensing Symposium, 2009 IEEE International. - Cape Town, 12-17 July 2009. - Vol. 5. -

P. V-138-V-141-138. ↑

**C1505.** Knuth R. Multisensor SAR analysis for forest monitoring in boreal and tropical forest environments. / Knuth R., Thiel C., Eckardt R., Richter N., Schmulius C. // IGARSS 2009 Geoscience and Remote Sensing Symposium, 2009 IEEE International. - Cape Town, 12-17 July 2009. - Vol. 5. - P. V-126-V-129-126. ↑

**C1506.** Natsuaki R. Local, nonlinear adaptive co-registration of master and slave interferometric SAR complex image data for high quality digital elevation map generation. / Natsuaki R., Hirose A. // IGARSS 2009 Geoscience and Remote Sensing Symposium, 2009 IEEE International. - Cape Town, 12-17 July 2009. - Vol. 5. - P. V-166-V-167-166. ↑

**C1507.** Enjolras V. SWIM: A state of the art multi-incidence beams Ku-band waves scatterometer to go beyond current radar systems. / Enjolras V., Rey L., Cros L., Pouyez S., Amiot T., Tison C., Castillan P. // IGARSS 2009 Geoscience and Remote Sensing Symposium, 2009 IEEE International. - Cape Town, 12-17 July 2009. - Vol. 5. - P. V-316-V-319-316. ↑

**C1508.** Pierdicca N. Atmospheric water vapor effects on spaceborne interferometric SAR imaging: Comparison with ground-based measurements and meteorological model simulations at different scales. / Pierdicca N., Rocca F., Rommen B., Basili P., Bonafoni S., Cimini D., Ciotti P., Consalvi F., Ferretti R., Foster W., Marzano F.S., Mattioli V., Mazzoni A., Montopoli M., Notarpietro R., Padmanabhan S., Perissin D., Pichelli E., Reising S., Sahoo S., Venuti G. // IGARSS 2009 Geoscience and Remote Sensing Symposium, 2009 IEEE International. - Cape Town, 12-17 July 2009. - Vol. 5. - P. V-320-V-323-320. ↑

**C1509.** Praks J. Boreal forest height estimation with SAR interferometry and laser measurements. / Praks J., Hallikainen M., Seppanen J., Hyyppa J. // IGARSS 2009 Geoscience and Remote Sensing Symposium, 2009 IEEE International. - Cape Town, 12-17 July 2009. - Vol. 5. - P. V-308-V-311-308. ↑

**C1510.** Ke Sun. A novel STAP algorithm using sparse recovery technique. / Ke Sun, Hao Zhang, Gang Li, Huadong Meng, Xiqin Wang. // IGARSS 2009 Geoscience and Remote Sensing Symposium, 2009 IEEE International. - Cape Town, 12-17 July 2009. - Vol. 5. - P. V-336-V-339-336. ↑

**C1511.** Gebhardt U. A linear Kalman filter approach for estimation of a vehicle's motion parameters using range-Doppler tracking and road information. / Gebhardt U., Berens P., Holzner J. // IGARSS 2009 Geoscience and Remote Sensing Symposium, 2009 IEEE International. - Cape Town, 12-17 July 2009. - Vol. 5. - P. V-324-V-327-324. ↑

**C1512.** Budillon A. GRLT detection of moving target by along track SAR interferometric systems. / Budillon A., Ciaramello M., Evangelista A., Pascazio V., Schirinz G. // IGARSS 2009 Geoscience and Remote Sensing Symposium, 2009 IEEE International. - Cape Town, 12-17 July 2009. - Vol. 5. - P. V-328-V-331-328. ↑

**C1513.** Cuccoli F. NDSA measurements between two LEO satellites in Ku and K bands for the tropospheric water vapor estimate: Performance evaluation at global scale. / Cuccoli F., Facheris L. // IGARSS 2009 Geoscience and Remote Sensing Symposium, 2009 IEEE International. - Cape Town, 12-17 July 2009. - Vol. 5. - P. V-296-V-299-296. ↑

**C1514.** Pinel N. Rough thin pavement thickness estimation by GPR. / Pinel N., Liu L., Bourlier C., Wang Y., Le Bastard C. // IGARSS 2009 Geoscience and Remote Sensing Symposium, 2009 IEEE International. - Cape Town, 12-17 July 2009. - Vol. 5. - P. V-276-V-279-276. ↑

**C1515.** Prats P. Processing multiple SAR modes with baseband azimuth scaling. / Prats P., Scheiber R., Mittermayer J., Moreira A. // IGARSS 2009 Geoscience and Remote Sensing Symposium, 2009 IEEE International. - Cape Town, 12-17 July 2009. - Vol. 5. - P. V-172-V-175-172. ↑

**C1516.** Tison C. Directional wave spectrum estimation by SWIM instrument on CFOSAT. / Tison C., Amiot T., Bourbier J., Hauser D., Enjolras V., Rey L., Castillan P. // IGARSS 2009 Geoscience and Remote Sensing Symposium, 2009 IEEE International. - Cape Town, 12-17 July 2009. - Vol. 5. - P. V-312-V-315-312. ↑

**C1517.** Sun G. Forest biomass retrieval from lidar and radar. / Sun G., Ranson K.J. // IGARSS 2009 Geoscience and Remote Sensing Symposium, 2009 IEEE International. - Cape Town, 12-17 July 2009. - Vol. 5. - P. V-300-V-303-300. ↑

**C1518.** Zhang Z. Forest parameter mapping based on lidar and SAR data. / Zhang Z., Zhang L., Ni W., Guo

Z., Sun G. // IGARSS 2009 Geoscience and Remote Sensing Symposium, 2009 IEEE International. - Cape Town, 12-17 July 2009. - Vol. 5. - P. V-304-V-307-304. ↑

**C1519.** Pettinato S. An operational algorithm for snow cover mapping in hydrological applications. / Pettinato S., Santi E., Brogioni M., Paloscia S., Pampaloni P. // IGARSS 2009 Geoscience and Remote Sensing Symposium, 2009 IEEE International. - Cape Town, 12-17 July 2009. - Vol. 4. - P. IV-964-IV-967-964. ↑

**C1520.** Ito Y. A web application with visual SAR processor for education. / Ito Y., Teramoto Y., Abe K. // IGARSS 2009 Geoscience and Remote Sensing Symposium, 2009 IEEE International. - Cape Town, 12-17 July 2009. - Vol. 4. - P. IV-645-IV-648-645. ↑

**C1521.** Rivas R. GSOC's Scatterometry GNSS receiver for ocean remote sensing: Design and initial results. / Rivas R., Grillenberger A., Markgraf M. // IGARSS 2009 Geoscience and Remote Sensing Symposium, 2009 IEEE International. - Cape Town, 12-17 July 2009. - Vol. 4. - P. IV-661-IV-664-661. ↑

**C1522.** Migliaccio M. ALOS-PALSAR polarimetric SAR data to observe sea oil slicks. / Migliaccio M., Gambardella A., Nunziata F., Shimada M., Isoguchi O. // IGARSS 2009 Geoscience and Remote Sensing Symposium, 2009 IEEE International. - Cape Town, 12-17 July 2009. - Vol. 4. - P. IV-669-IV-672-669. ↑

**C1523.** Gomez B. Data processing frame for airborne SAR prototype development. / Gomez B., Gonzalez M.J., Cuerda J.M., Cores J.F., Casal N., Gimeno N., Cifuentes P., Arenas A., Lopez A. // IGARSS 2009 Geoscience and Remote Sensing Symposium, 2009 IEEE International. - Cape Town, 12-17 July 2009. - Vol. 4. - P. IV-633-IV-636-633. ↑

**C1524.** Yesheng Gao. Antenna pointing measurement for spaceborne SAR based on sign-MLCC algorithm. / Yesheng Gao, Kaizhi Wang, Xingzhao Liu, Wenxian Yu. // IGARSS 2009 Geoscience and Remote Sensing Symposium, 2009 IEEE International. - Cape Town, 12-17 July 2009. - Vol. 4. - P. IV-637-IV-640-637. ↑

**C1525.** Kawano N. Flood disaster monitoring with ALOS/PALSAR observation. / Kawano N., Shimada M. // IGARSS 2009 Geoscience and Remote Sensing Symposium, 2009 IEEE International. - Cape Town, 12-17 July 2009. - Vol. 4. - P. IV-641-IV-644-641. ↑

**C1526.** Saidi M.N. Automatic target recognition of aircraft models based on ISAR images. / Saidi M.N., Daoudi K., Khenchaf A., Hoeltzner B., Aboutajdine D. // IGARSS 2009 Geoscience and Remote Sensing Symposium, 2009 IEEE International. - Cape Town, 12-17 July 2009. - Vol. 4. - P. IV-685-IV-688-685. ↑

**C1527.** Bovenga F. A first validation experiment for a Multi-Chromatic Analysis (MCA) of SAR data starting from SLC images. / Bovenga F., Giacomazzo V.M., Refice A., Veneziani N., Vitulli R. // IGARSS 2009 Geoscience and Remote Sensing Symposium, 2009 IEEE International. - Cape Town, 12-17 July 2009. - Vol. 4. - P. IV-689-IV-692-689. ↑

**C1528.** Grimaldi C.S.L. Near real time oil spill detection and monitoring using satellite optical data. / Grimaldi C.S.L., Coviello I., Lacava T., Pergola N., Tramutoli V. // IGARSS 2009 Geoscience and Remote Sensing Symposium, 2009 IEEE International. - Cape Town, 12-17 July 2009. - Vol. 4. - P. IV-709-IV-712-709. ↑


**C1529.** Chan-Su Yang. Comparison with L-, C-, and X-band real SAR images and simulation SAR images of spilled oil on sea surface. / Chan-Su Yang, Youn-Seop Kim, Ouchi K., Jae-Ho Na. // IGARSS 2009 Geoscience and Remote Sensing Symposium, 2009 IEEE International. - Cape Town, 12-17 July 2009. - Vol. 4. - P. IV-673-IV-676-673. ↑


**C1530.** Schwarz G. Automated information extraction from high resolution SAR images: TerraSAR-X interpretation applications. / Schwarz G., Soccorsi M., Chaabouni-Chouayakh H., Espinoza D., Cerra D., Rodriguez F., Datcu M. // IGARSS 2009 Geoscience and Remote Sensing Symposium, 2009 IEEE International. - Cape Town, 12-17 July 2009. - Vol. 4. - P. IV-677-IV-680-677. ↑


**C1531.** Ken Yoong Lee. Speckle reduction and edge detection for TerraSAR-X single-look dual-polarization imagery. / Ken Yoong Lee, Bretschneider T.R., Choo Leng Koh. // IGARSS 2009 Geoscience and Remote Sensing Symposium, 2009 IEEE International. - Cape Town, 12-17 July 2009. - Vol. 4. - P. IV-681-IV-684-681. ↑


**C1532.** Donghyun Kim. Spotlight SAR processor by using extended frequency scaling. / Donghyun Kim, Junghoon Keum, Moongyu Kim, Sungwoong Ra. // IGARSS 2009 Geoscience and Remote Sensing


↑


Symposium, 2009 IEEE International. - Cape Town, 12-17 July 2009. - Vol. 4. - P. IV-629-IV-632-629. 


**C1533.** Yanfeng Gu. Kernel regression-based background predicting method for target detection in SAR image. / Yanfeng Gu, Xing Liu, Jinglong Han, Ye Zhang. // IGARSS 2009 Geoscience and Remote Sensing Symposium, 2009 IEEE International. - Cape Town, 12-17 July 2009. - Vol. 4. - P. IV-593-IV-596-593. 


**C1534.** Jung C.H. PSLR estimation considering clutter background from SAR image data. / Jung C.H., Kwag Y.K. // IGARSS 2009 Geoscience and Remote Sensing Symposium, 2009 IEEE International. - Cape Town, 12-17 July 2009. - Vol. 4. - P. IV-597-IV-600-597. 


**C1535.** Dae Man Kim. Combined metal detector and ground-penetrating radar sensor experiments in a variety of soil conditions. / Dae Man Kim, Seok Hwan Kim, Seokjae Lee, Kangwook Kim. // IGARSS 2009 Geoscience and Remote Sensing Symposium, 2009 IEEE International. - Cape Town, 12-17 July 2009. - Vol. 4. - P. IV-601-IV-604-601. 


**C1536.** Matsuoka T. Calibration of the high performance airborne SAR system (Pi-SAR2). / Matsuoka T., Umehara T., Nadai A., Kobayashi T., Satake M., Uratsuka S. // IGARSS 2009 Geoscience and Remote Sensing Symposium, 2009 IEEE International. - Cape Town, 12-17 July 2009. - Vol. 4. - P. IV-582-IV-585-582. 


**C1537.** Ferrer P.J. Transpolarizing trihedral measurement using UPC X-band GB-SAR. / Ferrer P.J., Romeu J., Gonzalez-Arbesu J.M., Aguasca A., Pipia L., Lopez-Martinez C., Fabregas X. // IGARSS 2009 Geoscience and Remote Sensing Symposium, 2009 IEEE International. - Cape Town, 12-17 July 2009. - Vol. 4. - P. IV-586-IV-589-586. 


**C1538.** Mengen C. Accuracy assessment of the first high-resolution IFSAR campaign over the coorong region of South Australia. / Mengen C., Marre F., Dhar T. // IGARSS 2009 Geoscience and Remote Sensing Symposium, 2009 IEEE International. - Cape Town, 12-17 July 2009. - Vol. 4. - P. IV-590-IV-592-590. 


**C1539.** Wang Bingnan. SAR raw signal simulation based on GPU parallel computation. / Wang Bingnan, Zhang Fan, Xiang Maosheng. // IGARSS 2009 Geoscience and Remote Sensing Symposium, 2009 IEEE International. - Cape Town, 12-17 July 2009. - Vol. 4. - P. IV-617-IV-620-617. 

**C1540.** Feng-ming Hu. SAR target recognition based on sub-block statistical features extracted from the Gabor filtered image. / Feng-ming Hu, Xue-hua Fan, Ru-liang Yang. // IGARSS 2009 Geoscience and Remote Sensing Symposium, 2009 IEEE International. - Cape Town, 12-17 July 2009. - Vol. 4. - P. IV-621-IV-624-621. 


**C1541.** Yang Yue. An imaging method and the correction of distortion for Spaceborne-airborne bistatic SAR. / Yang Yue, XiaoLing Zhang, ZiJin Zuo, Yang HaiGuang. // IGARSS 2009 Geoscience and Remote Sensing Symposium, 2009 IEEE International. - Cape Town, 12-17 July 2009. - Vol. 4. - P. IV-625-IV-628-625. 

**C1542.** Li Wei. Anti-jamming techniques for synthetic aperture radar. / Li Wei, Wang Xing-liang, Wang Xian-ming. // IGARSS 2009 Geoscience and Remote Sensing Symposium, 2009 IEEE International. - Cape Town, 12-17 July 2009. - Vol. 4. - P. IV-605-IV-608-605. 

**C1543.** Zhang Yueting. The effects of multi-path scattering on the SAR image of cylinder cavity. / Zhang Yueting, Ding Chibiao, You Hongjian, Qiu Xiaolan. // IGARSS 2009 Geoscience and Remote Sensing Symposium, 2009 IEEE International. - Cape Town, 12-17 July 2009. - Vol. 4. - P. IV-609-IV-612-609. 

**C1544.** Tang Xiaoqing. SAR raw signal simulation accounting for antenna attitude variations. / Tang Xiaoqing, Xiang Maosheng, Wei Lideng, Wu Yirong. // IGARSS 2009 Geoscience and Remote Sensing Symposium, 2009 IEEE International. - Cape Town, 12-17 July 2009. - Vol. 4. - P. IV-613-IV-616-613. 

**C1545.** Mengen C. Sea-clutter analysis at multiple wavelengths (L, C, X) for target-clutter contrast assessment in littoral waters. / Mengen C., Marre F., Dhar T. // IGARSS 2009 Geoscience and Remote Sensing Symposium, 2009 IEEE International. - Cape Town, 12-17 July 2009. - Vol. 4. - P. IV-713-IV-716-713. 

**C1546.** Bonano M. RADARSAT-1 deformation time-series analysis based on the SBAS-DInSAR algorithm. / Bonano M., Pepe A., Euillades L.D., Sansosti E., Berardino P., Lanari R. // IGARSS 2009 Geoscience and Remote Sensing Symposium, 2009 IEEE International. - Cape Town, 12-17 July 2009. - Vol. 4. - P. IV-873-IV-876-873. 

**C1547.** Danklmayer A. Comparison of precipitation effects in space-borne X- and Ka-band SAR imaging. /

Danklmayer A., Chandra M. // IGARSS 2009 Geoscience and Remote Sensing Symposium, 2009 IEEE International. - Cape Town, 12-17 July 2009. - Vol. 4. - P. IV-909-IV-912-909. ↑

C1548. D'Addio S. Modelling and analysis of rain effect on Ka-band single pass InSAR Performance. / D'Addio S., Ludwig M. // IGARSS 2009 Geoscience and Remote Sensing Symposium, 2009 IEEE International. - Cape Town, 12-17 July 2009. - Vol. 4. - P. IV-913-IV-916-913. ↑

C1549. de Macedo K.A.C. Airborne D-InSAR at X-band: Results with the complete repeat-pass processing methodology. / de Macedo K.A.C., Wimmer C., Barbin S.E., Perna S. // IGARSS 2009 Geoscience and Remote Sensing Symposium, 2009 IEEE International. - Cape Town, 12-17 July 2009. - Vol. 4. - P. IV-861-IV-864-861. ↑

C1550. Budillon A. SAR tomography from sparse samples. / Budillon A., Evangelista A., Schirizzi G. // IGARSS 2009 Geoscience and Remote Sensing Symposium, 2009 IEEE International. - Cape Town, 12-17 July 2009. - Vol. 4. - P. IV-865-IV-868-865. ↑

C1551. Xiao Xiang Zhu. Space-borne high resolution tomographic interferometry. / Xiao Xiang Zhu, Adam N., Bamler R. // IGARSS 2009 Geoscience and Remote Sensing Symposium, 2009 IEEE International. - Cape Town, 12-17 July 2009. - Vol. 4. - P. IV-869-IV-872-869. ↑

C1552. Waske B. Fusion of multisource data sets from agricultural areas for improved land cover classification. / Waske B., Benediktsson J.A., Sveinsson J.R. // IGARSS 2009 Geoscience and Remote Sensing Symposium, 2009 IEEE International. - Cape Town, 12-17 July 2009. - Vol. 4. - P. IV-952-IV-955-952. ↑

C1553. Poulain V. Fusion of high resolution optical and SAR images with vector data bases for change detection. / Poulain V., Inglada J., Spigai M., Tournet J.-Y., Marthon P. // IGARSS 2009 Geoscience and Remote Sensing Symposium, 2009 IEEE International. - Cape Town, 12-17 July 2009. - Vol. 4. - P. IV-956-IV-959-956. ↑

C1554. Pierdicca N. High resolution mapping of soil moisture by SAR: Data integration and exploitation of prior information. / Pierdicca N., Pulvirenti L., Bignami C., Ticconi F., Laurenti M. // IGARSS 2009 Geoscience and Remote Sensing Symposium, 2009 IEEE International. - Cape Town, 12-17 July 2009. - Vol. 4. - P. IV-960-IV-963-960. ↑

C1555. Capsoni C. Use of radar images for the development of a propagation oriented space-time rain model. / Capsoni C., Luini L. // IGARSS 2009 Geoscience and Remote Sensing Symposium, 2009 IEEE International. - Cape Town, 12-17 July 2009. - Vol. 4. - P. IV-917-IV-920-917. ↑

C1556. Dubois D. Toward a GUI remote sensing environment built over OTB. / Dubois D., Lepage R., Tanzi T. // IGARSS 2009 Geoscience and Remote Sensing Symposium, 2009 IEEE International. - Cape Town, 12-17 July 2009. - Vol. 4. - P. IV-932-IV-935-932. ↑

C1557. Pottier E. Overview of the PolSARpro V4.0 software. the open source toolbox for polarimetric and interferometric polarimetric SAR data processing. / Pottier E., Ferro-Famil L., Allain S., Cloude S., Hajnsek I., Papathanassiou K., Moreira A., Williams M., Minchella A., Laval M., Desnos Y.-L. // IGARSS 2009 Geoscience and Remote Sensing Symposium, 2009 IEEE International. - Cape Town, 12-17 July 2009. - Vol. 4. - P. IV-936-IV-939-936. ↑

C1558. Touzi R. Multi-resolution target scattering decomposition for urban feature characterization using polarimetric SARs. / Touzi R., Bhattacharya A., Mattar K. // IGARSS 2009 Geoscience and Remote Sensing Symposium, 2009 IEEE International. - Cape Town, 12-17 July 2009. - Vol. 4. - P. IV-857-IV-860-857. ↑

C1559. Moser G. Edge-preserving classification of high-resolution remote-sensing images by Markovian data fusion. / Moser G., Serpico S.B. // IGARSS 2009 Geoscience and Remote Sensing Symposium, 2009 IEEE International. - Cape Town, 12-17 July 2009. - Vol. 4. - P. IV-765-IV-768-765. ↑

C1560. Sportouche H. Building detection by fusion of optical and SAR features in metric resolution data. / Sportouche H., Tupin F., Denise L. // IGARSS 2009 Geoscience and Remote Sensing Symposium, 2009 IEEE International. - Cape Town, 12-17 July 2009. - Vol. 4. - P. IV-769-IV-772-769. ↑

C1561. Atto A.M. General framework on change detection in a sparse domain. / Atto A.M., Mercier G., Pastor D. // IGARSS 2009 Geoscience and Remote Sensing Symposium, 2009 IEEE International. - Cape Town, 12-17 July 2009. - Vol. 4. - P. IV-773-IV-776-773. ↑

July 2009. - Vol. 4. - P. IV-781-IV-784-781.

**C1562.** Cloude S.R. A study of forest vertical structure estimation using coherence tomography coupled to a macro-ecological scattering model. / Cloude S.R., Brolly M., Woodhouse I.H. // IGARSS 2009 Geoscience and Remote Sensing Symposium, 2009 IEEE International. - Cape Town, 12-17 July 2009. - Vol. 4. - P. IV-717-IV-720-717. ↑

**C1563.** Kugler F. Estimation of forest vertical structure parameter by means of multi-baseline Pol-InSAR. / Kugler F., Seung-Kuk Lee, Papathanassiou K.P. // IGARSS 2009 Geoscience and Remote Sensing Symposium, 2009 IEEE International. - Cape Town, 12-17 July 2009. - Vol. 4. - P. IV-721-IV-724-721. ↑

**C1564.** Inglada J. The Orfeo Toolbox remote sensing image processing software. / Inglada J., Christophe E. // IGARSS 2009 Geoscience and Remote Sensing Symposium, 2009 IEEE International. - Cape Town, 12-17 July 2009. - Vol. 4. - P. IV-733-IV-736-733. ↑

**C1565.** Foucher S. An evaluation of PolSAR speckle filters. / Foucher S., Lopez-Martinez C. // IGARSS 2009 Geoscience and Remote Sensing Symposium, 2009 IEEE International. - Cape Town, 12-17 July 2009. - Vol. 4. - P. IV-845-IV-848-845. ↑

**C1566.** Jong-Sen Lee. The effect of orientation angle compensation on polarimetric target decompositions. / Jong-Sen Lee, Ainsworth T.L., Kun-Shan Chen. // IGARSS 2009 Geoscience and Remote Sensing Symposium, 2009 IEEE International. - Cape Town, 12-17 July 2009. - Vol. 4. - P. IV-849-IV-852-849. ↑

**C1567.** Sato R. Analysis and observation of polarimetric scattering behavior in wetland area. / Sato R., Yamaguchi Y., Yamada H. // IGARSS 2009 Geoscience and Remote Sensing Symposium, 2009 IEEE International. - Cape Town, 12-17 July 2009. - Vol. 4. - P. IV-853-IV-856-853. ↑

**C1568.** Jiali Shang. Integration of RADARSAT-2 ScanSAR and AWiFS for operational agricultural land use monitoring over the Canadian prairies. / Jiali Shang, McNairn H., Champagne C., Xianfeng Jiao, Jarvis I., Xiaoyuan Geng. // IGARSS 2009 Geoscience and Remote Sensing Symposium, 2009 IEEE International. - Cape Town, 12-17 July 2009. - Vol. 4. - P. IV-793-IV-796-793. ↑

**C1569.** Sivakumar V. CSIR-NLC mobile LIDAR-first scientific result. / Sivakumar V., Tesfaye M., Moema D., Sharma A., Bollig C. // IGARSS 2009 Geoscience and Remote Sensing Symposium, 2009 IEEE International. - Cape Town, 12-17 July 2009. - Vol. 4. - P. IV-837-IV-840-837. ↑

**C1570.** Chauve A. FullAnalyze: A Research tool for handling, processing and analyzing full-waveform lidar data. / Chauve A., Bretar F., Durrieu S., Pierrot-Deseilligny M., Puech W. // IGARSS 2009 Geoscience and Remote Sensing Symposium, 2009 IEEE International. - Cape Town, 12-17 July 2009. - Vol. 4. - P. IV-841-IV-844-841. ↑

**C1571.** Guida R. SAR monitoring of suburban areas based on an electromagnetic scattering model. / Guida R., Iodice A., Riccio D. // IGARSS 2009 Geoscience and Remote Sensing Symposium, 2009 IEEE International. - Cape Town, 12-17 July 2009. - Vol. 5. - P. V-104-V-107-104. ↑

**C1572.** Wenming Lin. Simulation and optimization of the performance of space-borne radar ocean wave spectrometer. / Wenming Lin, Xiaolong Dong, Yuchi Zhou, Huguang Liu, Jingshan Jiang. // IGARSS 2009 Geoscience and Remote Sensing Symposium, 2009 IEEE International. - Cape Town, 12-17 July 2009. - Vol. 3. - P. III-793-III-796-793. ↑

**C1573.** Nadai A. Polarimetric analysis of the dependency of backscattering from ocean surface on wind direction. / Nadai A., Umehara T., Matsuoka T., Uratsuka S., Kobayashi T., Satake M. // IGARSS 2009 Geoscience and Remote Sensing Symposium, 2009 IEEE International. - Cape Town, 12-17 July 2009. - Vol. 3. - P. III-797-III-800-797. ↑

**C1574.** Soisuvarn S. The development of a C-band Advanced Scatterometer (ASCAT) geophysical model function at NOAA/NESDIS. / Soisuvarn S., Jelenak Z., Chang P.S., Qi Zhu. // IGARSS 2009 Geoscience and Remote Sensing Symposium, 2009 IEEE International. - Cape Town, 12-17 July 2009. - Vol. 3. - P. III-801-III-804-801. ↑

**C1575.** Vesecky J.F. Using HF surface wave radar and the ship Automatic Identification System (AIS) to monitor coastal vessels. / Vesecky J.F., Laws K.E., Paduan J.D. // IGARSS 2009 Geoscience and Remote

Sensing Symposium, 2009 IEEE International. - Cape Town, 12-17 July 2009. - Vol. 3. - P. III-761-III-764-761. ↑

**C1576.** Shimada M. PALSAR CALVAL updated 2009 and change detections at the forest and the Polar regions. / Shimada M., Isoguchi O., Tadono T. // IGARSS 2009 Geoscience and Remote Sensing Symposium, 2009 IEEE International. - Cape Town, 12-17 July 2009. - Vol. 3. - P. III-765-III-768-765. ↑

**C1577.** de Macedo K.A.C. First assessment of the permanent scatterer linear displacement model in airborne InSAR time series. / de Macedo K.A.C., Scheiber R., Moreira A. // IGARSS 2009 Geoscience and Remote Sensing Symposium, 2009 IEEE International. - Cape Town, 12-17 July 2009. - Vol. 3. - P. III-208-III-211-208. ↑

**C1578.** Mityagina M. Surface manifestations of non-tidal internal waves in the north-eastern Black Sea as viewed by satellite sensors. / Mityagina M., Lavrova O. // IGARSS 2009 Geoscience and Remote Sensing Symposium, 2009 IEEE International. - Cape Town, 12-17 July 2009. - Vol. 3. - P. III-196-III-199-196. ↑

**C1579.** Autieri R. Exploiting Markov random fields in Microwave tomography. / Autieri R., D'Urso M., Isernia T., Pascasio V. // IGARSS 2009 Geoscience and Remote Sensing Symposium, 2009 IEEE International. - Cape Town, 12-17 July 2009. - Vol. 3. - P. III-200-III-203-200. ↑

**C1580.** Ruzanski E. Scale decomposition of precipitation patterns and nowcasting in a high-resolution X-band radar network. / Ruzanski E., Yanting Wang, Chandrasekar V. // IGARSS 2009 Geoscience and Remote Sensing Symposium, 2009 IEEE International. - Cape Town, 12-17 July 2009. - Vol. 3. - P. III-837-III-840-837. ↑

**C1581.** Bourassa M.A. Uncertainty in scatterometer derived vorticity. IGARSS 2009 Geoscience and Remote Sensing Symposium, 2009 IEEE International. - Cape Town, 12-17 July 2009. - Vol. 3. - P. III-805-III-808-805. ↑

**C1582.** Chan-Su Yang. Velocity estimation of moving targets on the sea surface by azimuth differentials of simulated-SAR image. / Chan-Su Yang, Youn-Seop Kim, Ouchi K. // IGARSS 2009 Geoscience and Remote Sensing Symposium, 2009 IEEE International. - Cape Town, 12-17 July 2009. - Vol. 3. - P. III-809-III-812-809. ↑

**C1583.** Costes C. Weather hazard interpretation and nowcast by radar. / Costes C., Artis J.-P., Garello R., Mercier G. // IGARSS 2009 Geoscience and Remote Sensing Symposium, 2009 IEEE International. - Cape Town, 12-17 July 2009. - Vol. 3. - P. III-833-III-836-833. ↑

**C1584.** Flampouris S. Observing littoral waves by Doppler radar. / Flampouris S., Seemann J., Ziemer F. // IGARSS 2009 Geoscience and Remote Sensing Symposium, 2009 IEEE International. - Cape Town, 12-17 July 2009. - Vol. 3. - P. III-757-III-760-757. ↑

**C1585.** Tabatabaeenejad A. Comparison of Gaussian and Rayleigh noise models in inversion of subsurface parameters of layered rough surfaces using simulated annealing. / Tabatabaeenejad A., Moghaddam M. // IGARSS 2009 Geoscience and Remote Sensing Symposium, 2009 IEEE International. - Cape Town, 12-17 July 2009. - Vol. 3. - P. III-673-III-676-673. ↑

**C1586.** Elgamel S.A. Target tracking enhancement using a Kalman filter in the presence of interference. / Elgamel S.A., Soraghan J. // IGARSS 2009 Geoscience and Remote Sensing Symposium, 2009 IEEE International. - Cape Town, 12-17 July 2009. - Vol. 3. - P. III-681-III-684-681. ↑

**C1587.** Maximo O.A. Classification of a reference image using auxiliary images. / Maximo O.A., Fernandez D. // IGARSS 2009 Geoscience and Remote Sensing Symposium, 2009 IEEE International. - Cape Town, 12-17 July 2009. - Vol. 3. - P. III-697-III-700-697. ↑

**C1588.** Smith L. Airborne radar depth sounding of fast flowing glaciers. / Smith L., Blake W., Hoch A., Li J., Leuschen C., Gogineni S. // IGARSS 2009 Geoscience and Remote Sensing Symposium, 2009 IEEE International. - Cape Town, 12-17 July 2009. - Vol. 3. - P. III-650-III-653-650. ↑

**C1589.** Tan L. Accuracy improvement of maximum likelihood inversion of forest height with PolInSAR. / Tan L., Ruliang Yang, Weidong Yu. // IGARSS 2009 Geoscience and Remote Sensing Symposium, 2009 IEEE International. - Cape Town, 12-17 July 2009. - Vol. 3. - P. III-654-III-657-654. ↑

**C1590.** Stramondo S. Use of neural networks and SAR interferometry for the automatic retrieval of tectonic parameters. / Stramondo S., Del Frate F., Picchiani M., Schiavon G. // IGARSS 2009 Geoscience and Remote Sensing Symposium, 2009 IEEE International. - Cape Town, 12-17 July 2009. - Vol. 3. - P. III-220-III-223-220. ↑

- C1591.** Gabele M. TerraSAR-X Dual Receive Antenna mode-Channel reconstruction and impact on the GMTI performance. / Gabele M., Brautigam B., Schulze D., Steinbrecher U., Tous-Ramon N., Younis M. // IGARSS 2009 Geoscience and Remote Sensing Symposium, 2009 IEEE International. - Cape Town, 12-17 July 2009. - Vol. 3. - P. III-725-III-728-725. ↑
- C1592.** Pinheiro M. Multi-path correction model for multi-channel airborne SAR. / Pinheiro M., Prats P., Scheiber R., Fischer J. // IGARSS 2009 Geoscience and Remote Sensing Symposium, 2009 IEEE International. - Cape Town, 12-17 July 2009. - Vol. 3. - P. III-729-III-732-729. ↑
- C1593.** Younis M. Digital beam-forming for spaceborne reflector- and planar-antenna SAR-A system performance comparison. / Younis M., Huber S., Patyuchenko A., Bordonì F., Krieger G. // IGARSS 2009 Geoscience and Remote Sensing Symposium, 2009 IEEE International. - Cape Town, 12-17 July 2009. - Vol. 3. - P. III-733-III-736-733. ↑
- C1594.** Wentao An. Three-component decomposition for polarimetric SAR. / Wentao An, Yi Cui, Jiang Yang. // IGARSS 2009 Geoscience and Remote Sensing Symposium, 2009 IEEE International. - Cape Town, 12-17 July 2009. - Vol. 3. - P. III-713-III-716-713. ↑
- C1595.** Mercier G. Statistical characterization of the Sinclair matrix: Application to polarimetric image segmentation. / Mercier G., Frison P.-L. // IGARSS 2009 Geoscience and Remote Sensing Symposium, 2009 IEEE International. - Cape Town, 12-17 July 2009. - Vol. 3. - P. III-717-III-720-717. ↑
- C1596.** Marti-Cardona B. Analysis of ASAR/Envisat polarimetric backscattering characteristics of Doñana national park wetlands. / Marti-Cardona B., Lopez-Martinez C., Dolz-Ripolles J. // IGARSS 2009 Geoscience and Remote Sensing Symposium, 2009 IEEE International. - Cape Town, 12-17 July 2009. - Vol. 3. - P. III-721-III-724-721. ↑
- C1597.** Galvez M.B. Salient features of the radar nodes in the Puerto Rico tropical weather testbed. / Galvez M.B., Colom J., Chandrasekar V., Junyent F., Cruz-Pol S., Rodriguez R. // IGARSS 2009 Geoscience and Remote Sensing Symposium, 2009 IEEE International. - Cape Town, 12-17 July 2009. - Vol. 3. - P. III-841-III-844-841. ↑
- C1598.** Eltoft T. Model-based statistical analysis of PolSAR data. / Eltoft T., Doulgeris A., Anfinson S.N. // IGARSS 2009 Geoscience and Remote Sensing Symposium, 2009 IEEE International. - Cape Town, 12-17 July 2009. - Vol. 3. - P. III-955-III-958-955. ↑
- C1599.** Lopez-Martinez C. PolSAR and PolInSAR model based information estimation. / Lopez-Martinez C., Fabregas X., Pipia L. // IGARSS 2009 Geoscience and Remote Sensing Symposium, 2009 IEEE International. - Cape Town, 12-17 July 2009. - Vol. 3. - P. III-959-III-962-959. ↑
- C1600.** Vasile G. Estimation and segmentation in non-Gaussian POLSAR clutter by SIRV stochastic processes. / Vasile G., Ovarlez J.-P., Pascal F. // IGARSS 2009 Geoscience and Remote Sensing Symposium, 2009 IEEE International. - Cape Town, 12-17 July 2009. - Vol. 3. - P. III-963-III-966-963. ↑
- C1601.** Xiaozhen Ren. A three-dimensional imaging algorithm for tomography SAR. / Xiaozhen Ren, Xiaofei Yin, Ruliang Yang, Weidong Yu. // IGARSS 2009 Geoscience and Remote Sensing Symposium, 2009 IEEE International. - Cape Town, 12-17 July 2009. - Vol. 3. - P. III-184-III-187-184. ↑
- C1602.** Cloude S.R. An assessment of ALOS L-band polarimetry for land-use monitoring in Malawi. / Cloude S.R., Lumsdon P., Cassells G., Woodhouse I.H., Tembo M. // IGARSS 2009 Geoscience and Remote Sensing Symposium, 2009 IEEE International. - Cape Town, 12-17 July 2009. - Vol. 3. - P. III-947-III-950-947. ↑
- C1603.** Whitcomb J. Decadal change in northern wetlands based on differential analysis of JERS and PALSAR data. / Whitcomb J., Moghaddam M., McDonald K., Podest E., Chapman B. // IGARSS 2009 Geoscience and Remote Sensing Symposium, 2009 IEEE International. - Cape Town, 12-17 July 2009. - Vol. 3. - P. III-951-III-954-951. ↑
- C1604.** Hansch R. Semi-supervised learning for classification of polarimetric SAR-data. / Hansch R., Hellwich O. // IGARSS 2009 Geoscience and Remote Sensing Symposium, 2009 IEEE International. - Cape Town, 12-17 July 2009. - Vol. 3. - P. III-987-III-990-987. ↑
- C1605.** Bouvet A. An end-to-end error model for classification methods based on a SAR intensity ratio. /

Bouvet A., Thuy Le Toan. // IGARSS 2009 Geoscience and Remote Sensing Symposium, 2009 IEEE International. - Cape Town, 12-17 July 2009. - Vol. 3. - P. III-991-III-994-991. ↑

**C1606.** De Maio A. Detection of double scatterers in SAR Tomography. / De Maio A., Fornaro G., Pauciuolo A., Reale D. // IGARSS 2009 Geoscience and Remote Sensing Symposium, 2009 IEEE International. - Cape Town, 12-17 July 2009. - Vol. 3. - P. III-172-III-175-172. ↑

**C1607.** Tebaldini S. An algebraic approach to ground-volume decomposition from multi-baseline PolInSAR data. IGARSS 2009 Geoscience and Remote Sensing Symposium, 2009 IEEE International. - Cape Town, 12-17 July 2009. - Vol. 3. - P. III-967-III-970-967. ↑

**C1608.** Ferro-Famil L. Multi-baseline POL-inSAR statistical techniques for the characterization of distributed media. / Ferro-Famil L., Neumann M., Yue Huang. // IGARSS 2009 Geoscience and Remote Sensing Symposium, 2009 IEEE International. - Cape Town, 12-17 July 2009. - Vol. 3. - P. III-971-III-974-971. ↑

**C1609.** Yang-Lang Chang. K-way tree classification based on semi-greedy structure applied to multisource remote sensing images. / Yang-Lang Chang, Zhi-Ming Chen, Jyh-Peng Fang, Wei-Lieh Hsu, Wen-Yew Liang, Tung-Ju Hsieh, Hsuan Ren, Kun-Shan Chen. // IGARSS 2009 Geoscience and Remote Sensing Symposium, 2009 IEEE International. - Cape Town, 12-17 July 2009. - Vol. 3. - P. III-979-III-982-979. ↑

**C1610.** Pincus P.B. Aspects of 3D tomography for multiple-pass spotlight-mode airborne SAR. / Pincus P.B., Preiss M., Gray D.A. // IGARSS 2009 Geoscience and Remote Sensing Symposium, 2009 IEEE International. - Cape Town, 12-17 July 2009. - Vol. 3. - P. III-180-III-183-180. ↑

**C1611.** Bakhanov V.V. Subsatellite experiments in the north-eastern part of the Black Sea. / Bakhanov V.V., Bogatov N.A., Ermoshkin A.V., Zuikova E.M., Kazakov V.I., Kemarskaya O.N., Repina I.A., Titov V.I., Troitskaya Yu.I. // IGARSS 2009 Geoscience and Remote Sensing Symposium, 2009 IEEE International. - Cape Town, 12-17 July 2009. - Vol. 3. - P. III-188-III-191-188. ↑

**C1612.** Mitnik L. Non-linear internal waves in the Banda Sea on satellite synthetic aperture radar and visible images. / Mitnik L., Dubina V. // IGARSS 2009 Geoscience and Remote Sensing Symposium, 2009 IEEE International. - Cape Town, 12-17 July 2009. - Vol. 3. - P. III-192-III-195-192. ↑

**C1613.** Rao Y.S. Classification of polarimetric SAR data over wet and arid regions of India. / Rao Y.S., Turkar V. // IGARSS 2009 Geoscience and Remote Sensing Symposium, 2009 IEEE International. - Cape Town, 12-17 July 2009. - Vol. 3. - P. III-892-III-895-892. ↑

**C1614.** Rodriguez-Alvarez N. Soil moisture and vegetation height retrieval using GNSS-R techniques. / Rodriguez-Alvarez N., Monerris A., Bosch-Lluis X., Camps A., Vall-Llossera M., Marchan-Hernandez J.F., Ramos-Perez I., Valencia E., Martinez-Fernandez J., Sanchez-Martin N., Baroncini-Turricchi G., Perez-Gutierrez C. // IGARSS 2009 Geoscience and Remote Sensing Symposium, 2009 IEEE International. - Cape Town, 12-17 July 2009. - Vol. 3. - P. III-869-III-872-869. ↑

**C1615.** Lehureau G. Combining SAR and optical features in a SVM classifier for man-made structures detection. / Lehureau G., Campedel M., Tupin F., Tison C., Oller G. // IGARSS 2009 Geoscience and Remote Sensing Symposium, 2009 IEEE International. - Cape Town, 12-17 July 2009. - Vol. 3. - P. III-873-III-876-873. ↑

**C1616.** Sato R. Polarimetric scattering feature estimation for accurate vegetation area classification. / Sato R., Yamaguchi Y., Yamada H. // IGARSS 2009 Geoscience and Remote Sensing Symposium, 2009 IEEE International. - Cape Town, 12-17 July 2009. - Vol. 3. - P. III-888-III-891-888. ↑

**C1617.** Lombardini F. Multiple scatterers identification in complex scenarios with adaptive differential tomography. / Lombardini F., Pardini M. // IGARSS 2009 Geoscience and Remote Sensing Symposium, 2009 IEEE International. - Cape Town, 12-17 July 2009. - Vol. 3. - P. III-908-III-911-908. ↑

**C1618.** Doubkova M. On the ability of the ERS scatterometer to detect vegetation properties. / Doubkova M., Naeimi V., Wagner W., Henebry G. // IGARSS 2009 Geoscience and Remote Sensing Symposium, 2009 IEEE International. - Cape Town, 12-17 July 2009. - Vol. 3. - P. III-920-III-923-920. ↑

**C1619.** Isoguchi O. A preliminary study on deforestation monitoring in Sumatra Island by PALSAR. / Isoguchi O., Shimada M., Uryu Y. // IGARSS 2009 Geoscience and Remote Sensing Symposium, 2009 IEEE International. - Cape Town, 12-17 July 2009. - Vol. 3. - P. III-943-III-946-943. ↑

- C1620.** Duk-jin Kim. Investigation of multiple frequency polarimetric SAR signal backscattering from tidal flats. / Duk-jin Kim, Sang-Eun Park, Hyo-Sung Lee, Moon W.M. // IGARSS 2009 Geoscience and Remote Sensing Symposium, 2009 IEEE International. - Cape Town, 12-17 July 2009. - Vol. 3. - P. III-896-III-899-896. ↑
- C1621.** Adam N. Techniques and examples for the 3D reconstruction of complex scattering situations using TerraSAR-X. / Adam N., Xiao Xiang Zhu, Minet C., Liebhart W., Eineder M., Bamler R. // IGARSS 2009 Geoscience and Remote Sensing Symposium, 2009 IEEE International. - Cape Town, 12-17 July 2009. - Vol. 3. - P. III-900-III-903-900. ↑
- C1622.** Costantini M. Method of persistent scatterer pairs (PSP) and high resolution SAR interferometry. / Costantini M., Falco S., Malvarosa F., Minati F., Trillo F. // IGARSS 2009 Geoscience and Remote Sensing Symposium, 2009 IEEE International. - Cape Town, 12-17 July 2009. - Vol. 3. - P. III-904-III-907-904. ↑
- C1623.** Chaabane F. Monitoring slow ground movements around Tunis City by different SAR interferometric measures. / Chaabane F., Elagouni K., Baccouche M., Pourthie N., Tison C., Briole P. // IGARSS 2009 Geoscience and Remote Sensing Symposium, 2009 IEEE International. - Cape Town, 12-17 July 2009. - Vol. 3. - P. III-436-III-439-436. ↑
- C1624.** Hong Chi. Urban dynamic change detection in southeastern China based on interferometric SAR. / Hong Chi, Guoqing Sun, Feilong Ling. // IGARSS 2009 Geoscience and Remote Sensing Symposium, 2009 IEEE International. - Cape Town, 12-17 July 2009. - Vol. 3. - P. III-432-III-435-432. ↑
- C1625.** Hambaryan A.K. Preliminary measurements of bare soil and waved water surface microwave reflection and emission angular dependences at 5, 6GHz. / Hambaryan A.K., Arakelyan A.K., Muradyan H.G., Karyan V.V., Hovhannisyan G.G., Arakelyan A.A., Grigoryan M.L., Hakobyan I.K., Manukyan M.R. // IGARSS 2009 Geoscience and Remote Sensing Symposium, 2009 IEEE International. - Cape Town, 12-17 July 2009. - Vol. 3. - P. III-506-III-509-506. ↑
- C1626.** Dhar T. Multiple Crop Yield prediction using dual-polarimetric TerraSAR-X stripmap imagery. / Dhar T., Gray D., Menges C. // IGARSS 2009 Geoscience and Remote Sensing Symposium, 2009 IEEE International. - Cape Town, 12-17 July 2009. - Vol. 3. - P. III-443-III-446-443. ↑
- C1627.** Crile M.B. Paleoterrain model of the Yamato Marsh, Palm Beach County, Florida. / Crile M.B., Roberts C. // IGARSS 2009 Geoscience and Remote Sensing Symposium, 2009 IEEE International. - Cape Town, 12-17 July 2009. - Vol. 3. - P. III-424-III-427-424. ↑
- C1628.** Del Frate F. Pulse Coupled Neural Network for automatic features extraction from COSMO-SkyMed and TerraSAR-X imagery. / Del Frate F., Licciardi G., Pacifici F., Pratola C., Solimini D. // IGARSS 2009 Geoscience and Remote Sensing Symposium, 2009 IEEE International. - Cape Town, 12-17 July 2009. - Vol. 3. - P. III-384-III-387-384. ↑
- C1629.** Bannerman K. Operational applications of RADARSAT-2 for the environmental monitoring of oil slicks in the Southern Gulf of Mexico. / Bannerman K., Rodriguez M.H., de Miranda F.P., Pedroso E.C., Caceres R.G., Lopez Castillo O. // IGARSS 2009 Geoscience and Remote Sensing Symposium, 2009 IEEE International. - Cape Town, 12-17 July 2009. - Vol. 3. - P. III-381-III-383-381. ↑
- C1630.** Bratsolis E. Unsupervised segmentation of agricultural regions using TerraSAR-X images. IGARSS 2009 Geoscience and Remote Sensing Symposium, 2009 IEEE International. - Cape Town, 12-17 July 2009. - Vol. 3. - P. III-416-III-419-416. ↑
- C1631.** Yuhuan Ren. A study on land cover classification based on HJ-1 CCD image. / Yuhuan Ren, Yalan Liu, Junchuan Fan, Hua Xu, Ling Yi. // IGARSS 2009 Geoscience and Remote Sensing Symposium, 2009 IEEE International. - Cape Town, 12-17 July 2009. - Vol. 3. - P. III-408-III-411-408. ↑
- C1632.** Pantze A. Mapping and monitoring clear-cuts in Swedish forest using ALOS PALSAR satellite images. / Pantze A., Krantz A.H., Fransson J.E.S., Olsson H., Santoro M., Eriksson L.E.B., Ulander L.M.H. // IGARSS 2009 Geoscience and Remote Sensing Symposium, 2009 IEEE International. - Cape Town, 12-17 July 2009. - Vol. 3. - P. III-589-III-592-589. ↑
- C1633.** Wijaya A. Fusion of ALOS Palsar and Landsat ETM data for land cover classification and biomass modeling using non-linear methods. / Wijaya A., Gloaguen R. // IGARSS 2009 Geoscience and Remote Sensing Symposium, 2009 IEEE International. - Cape Town, 12-17 July 2009. - Vol. 3. - P. III-581-III-584-581. ↑

- C1634.** Maosong Xu. Forest type discrimination using polarimetric Radarsat 2 data. / Maosong Xu, Fengli Zhang, Zhongsheng Xia, Chou Xie, Xiaofang Li, Kun Li, Zi Wan, Huaze Gong, Wei Tian. // IGARSS 2009 Geoscience and Remote Sensing Symposium, 2009 IEEE International. - Cape Town, 12-17 July 2009. - Vol. 3. - P. III-601-III-604-601. ↑
- C1635.** Tanase M. Backscatter properties of multitemporal TerraSAR-X data and the effects of influencing factors on burn severity evaluation, in a mediterranean pine forest. / Tanase M., Santoro M., de la Riva J., Perez-Cabello F. // IGARSS 2009 Geoscience and Remote Sensing Symposium, 2009 IEEE International. - Cape Town, 12-17 July 2009. - Vol. 3. - P. III-593-III-596-593. ↑
- C1636.** Shilin Tang. Retrieval of suspended sediment concentration in the Pearl River Estuary from MERIS using support vector machines. / Shilin Tang, Qing Dong, Chuqun Chen, Fenfen Liu, Guangyu Jin. // IGARSS 2009 Geoscience and Remote Sensing Symposium, 2009 IEEE International. - Cape Town, 12-17 July 2009. - Vol. 3. - P. III-239-III-242-239. ↑
- C1637.** Shuguo Wang. Derivation of surface soil moisture using multi-angle ASAR data in the middle stream of Heihe river basin. / Shuguo Wang, Xujun Han, Xin Li, Rui Jin, Hui Lu. // IGARSS 2009 Geoscience and Remote Sensing Symposium, 2009 IEEE International. - Cape Town, 12-17 July 2009. - Vol. 3. - P. III-518-III-521-518. ↑
- C1638.** Gherboudj M. Use of Radarsat-2 images to develop a scaling method of soil moisture over an agricultural area. / Gherboudj M., Magagi R., Berg A., Toth B. // IGARSS 2009 Geoscience and Remote Sensing Symposium, 2009 IEEE International. - Cape Town, 12-17 July 2009. - Vol. 3. - P. III-510-III-513-510. ↑
- C1639.** Yun Shao. Detection subsurface hyper-saline soil in Lop Nur using full-polarimetric SAR data. / Yun Shao, Huaze Gong, Chou Xie, Aimin Cai. // IGARSS 2009 Geoscience and Remote Sensing Symposium, 2009 IEEE International. - Cape Town, 12-17 July 2009. - Vol. 3. - P. III-550-III-553-550. ↑
- C1640.** Huaze Gong. Subsurface microwave remote sensing and scattering modelling on hyper-saline soil: Example of Lop Nur. / Huaze Gong, Yun Shao, Aimin Cai, Chou Xie. // IGARSS 2009 Geoscience and Remote Sensing Symposium, 2009 IEEE International. - Cape Town, 12-17 July 2009. - Vol. 3. - P. III-546-III-549-546. ↑
- C1641.** Long Ma. Research on oil spill identification based on texture features-a case study of "Hebei Spirit" accident. / Long Ma, Ying Li, Baocheng Zhang, Yu Liu, Chao Gao, Shuiming Yu. // IGARSS 2009 Geoscience and Remote Sensing Symposium, 2009 IEEE International. - Cape Town, 12-17 July 2009. - Vol. 3. - P. III-377-III-380-377. ↑
- C1642.** Fornaro G. A new algorithm for the phase unwrapping of interferogram stacks. / Fornaro G., Pauciuolo A., Reale D. // IGARSS 2009 Geoscience and Remote Sensing Symposium, 2009 IEEE International. - Cape Town, 12-17 July 2009. - Vol. 5. - P. V-21-V-24-21. ↑
- C1643.** Gonzalez F.R. Bayesian restoration of interferometric phase through biased anisotropic diffusion. / Gonzalez F.R., Datcu M. // IGARSS 2009 Geoscience and Remote Sensing Symposium, 2009 IEEE International. - Cape Town, 12-17 July 2009. - Vol. 5. - P. V-17-V-20-17. ↑
- C1644.** Chaabane F. InSAR permanent scatterers selection using SAR SVA filtering. / Chaabane F., Sellami M., Nicolas J.-M., Tupin F. // IGARSS 2009 Geoscience and Remote Sensing Symposium, 2009 IEEE International. - Cape Town, 12-17 July 2009. - Vol. 5. - P. V-13-V-16-13. ↑
- C1645.** Hanssen R.F. One-dimensional radar interferometry for line infrastructure. / Hanssen R.F., van Leijen F.J. // IGARSS 2009 Geoscience and Remote Sensing Symposium, 2009 IEEE International. - Cape Town, 12-17 July 2009. - Vol. 5. - P. V-9-V-12-9. ↑
- C1646.** Zheng Xiang. A GPU based time-domain raw signal simulator for interferometric SAR. / Zheng Xiang, Kaizhi Wang, Xingzhao Liu, Wenxian Yu. // IGARSS 2009 Geoscience and Remote Sensing Symposium, 2009 IEEE International. - Cape Town, 12-17 July 2009. - Vol. 5. - P. V-25-V-28-25. ↑
- C1647.** Bijker W. Needs and applications for data mining in large series of remotely sensed images. IGARSS 2009 Geoscience and Remote Sensing Symposium, 2009 IEEE International. - Cape Town, 12-17 July 2009. - Vol. 5. - P. V-92-V-95-92. ↑
- C1648.** Kai Jiang. Damage analysis of 2008 Wenchuan earthquake using SAR images. / Kai Jiang, Chao Wang, Hong Zhang, Wei Chen, Bo Zhang, Yixian Tang, Fan Wu. // IGARSS 2009 Geoscience and Remote

Sensing Symposium, 2009 IEEE International. - Cape Town, 12-17 July 2009. - Vol. 5. - P. V-108-V-111-108. ↑

**C1649.** Reinartz P. Using geometric accuracy of TerraSAR-X data for improvement of direct sensor orientation and ortho-rectification of optical satellite data. / Reinartz P., Muller R., Suri S., Schneider M., Schwind P., Bamler R. // IGARSS 2009 Geoscience and Remote Sensing Symposium, 2009 IEEE International. - Cape Town, 12-17 July 2009. - Vol. 5. - P. V-44-V-47-44. ↑

**C1650.** Toutin T. Calibration of radargrammetric DEMs from RADARSAT-2 high-resolution and fine-quad modes. / Toutin T., Chenier R., Schmitt C., Zakharov I. // IGARSS 2009 Geoscience and Remote Sensing Symposium, 2009 IEEE International. - Cape Town, 12-17 July 2009. - Vol. 5. - P. V-41-V-43-41. ↑

**C1651.** Stasolla M. Fusion of SAR and optical data for urban extent extraction improvement. / Stasolla M., Gamba P. // IGARSS 2009 Geoscience and Remote Sensing Symposium, 2009 IEEE International. - Cape Town, 12-17 July 2009. - Vol. 3. - P. III-330-III-333-330. ↑

**C1652.** Thiel C. Analysis of multi-temporal land observation at C-band. / Thiel C., Cartus O., Eckardt R., Richter N., Schmullius C. // IGARSS 2009 Geoscience and Remote Sensing Symposium, 2009 IEEE International. - Cape Town, 12-17 July 2009. - Vol. 3. - P. III-318-III-321-318. ↑

**C1653.** Al Muhairi A. Exploring the potential of MODIS visible and thermal channels in monitoring and assessing the impact of desalination plant discharges in the Arabian Gulf. / Al Muhairi A., Ghedira H., Al-Ahmad H., Dawood A., Al-Mualla M. // IGARSS 2009 Geoscience and Remote Sensing Symposium, 2009 IEEE International. - Cape Town, 12-17 July 2009. - Vol. 3. - P. III-357-III-360-357. ↑

**C1654.** Pai-Hui Hsu. Land subsidence monitoring and Flood Simulation using multitemporal digital elevation models. / Pai-Hui Hsu, Wen-Ray Su. // IGARSS 2009 Geoscience and Remote Sensing Symposium, 2009 IEEE International. - Cape Town, 12-17 July 2009. - Vol. 3. - P. III-349-III-352-349. ↑

**C1655.** Seppanen J. Soil moisture retrieval from HUT-2D synthetic aperture radiometer data. / Seppanen J., Kainulainen J., Lemmetyinen J., Rautiainen K., Hallikainen M., Makynen M. // IGARSS 2009 Geoscience and Remote Sensing Symposium, 2009 IEEE International. - Cape Town, 12-17 July 2009. - Vol. 3. - P. III-298-III-301-298. ↑

**C1656.** Jagdhuber T. Soil moisture estimation using a multi-angular modified three component polarimetric decomposition. / Jagdhuber T., Hajnsek I., Papathanassiou K.P., Bronstert A. // IGARSS 2009 Geoscience and Remote Sensing Symposium, 2009 IEEE International. - Cape Town, 12-17 July 2009. - Vol. 5. - P. V-5-V-8-5. ↑

**C1657.** Truong-Loi M.-L. Polarimetric analysis from compact-pol measurements: Potential and limitation. / Truong-Loi M.-L., Dubois-Fernandez P., Pottier E., Angelliaume S., Souyris J.-C. // IGARSS 2009 Geoscience and Remote Sensing Symposium, 2009 IEEE International. - Cape Town, 12-17 July 2009. - Vol. 5. - P. V-1-V-4-1. ↑

**C1658.** O'Neill P. Microwave soil moisture retrieval under trees using a modified tau-omega model. / O'Neill P., Lang R., Kurum M., Joseph A., Cosh M., Jackson T. // IGARSS 2009 Geoscience and Remote Sensing Symposium, 2009 IEEE International. - Cape Town, 12-17 July 2009. - Vol. 3. - P. III-290-III-293-290. ↑

**C1659.** Bharadwaj N. Waveform considerations for dual-polarization Doppler weather radar with solid-state transmitters. / Bharadwaj N., Mishra K.V., Chandrasekar V. // IGARSS 2009 Geoscience and Remote Sensing Symposium, 2009 IEEE International. - Cape Town, 12-17 July 2009. - Vol. 3. - P. III-267-III-270-267. ↑

**C1660.** Erturk A.G. Detecting V-Storms using Meteosat Second Generation SEVIRI image and its applications: A case study over Western Turkey. / Erturk A.G., Barbosa H. // IGARSS 2009 Geoscience and Remote Sensing Symposium, 2009 IEEE International. - Cape Town, 12-17 July 2009. - Vol. 3. - P. III-609-III-612-609. ↑

**C1661.** Xichi Hu. Distributed targets detection based on local spectral histograms and agents. / Xichi Hu, Minhui Zhu. // IGARSS 2009 Geoscience and Remote Sensing Symposium, 2009 IEEE International. - Cape Town, 12-17 July 2009. - Vol. 3. - P. III-646-III-649-646. ↑

**C1662.** Yingying Ma. Cloud amount and aerosol characteristic research in the atmosphere over Hubei province, China. / Yingying Ma, Wei Gong, Zhongmin Zhu, Liangpei Zhang, Pingxiang Li. // IGARSS 2009 Geoscience and Remote Sensing Symposium, 2009 IEEE International. - Cape Town, 12-17 July 2009. - Vol. 3. - ↑

P. III-631-III-634-631. ■

**C1663.** Junyent F. Uncertainties in phase and frequency estimation with a magnetron radar: Implication for clear air measurements. / Junyent F., Chandrasekar V., Bharadwaj N. // IGARSS 2009 Geoscience and Remote Sensing Symposium, 2009 IEEE International. - Cape Town, 12-17 July 2009. - Vol. 3. - P. III-613-III-616-613. ↑

---

© В.И. Карнышев, 2011

Тематический реферативный сборник сгенерирован в автоматическом режиме  
с использованием специализированного программного модуля (ПАО ТУСУР)